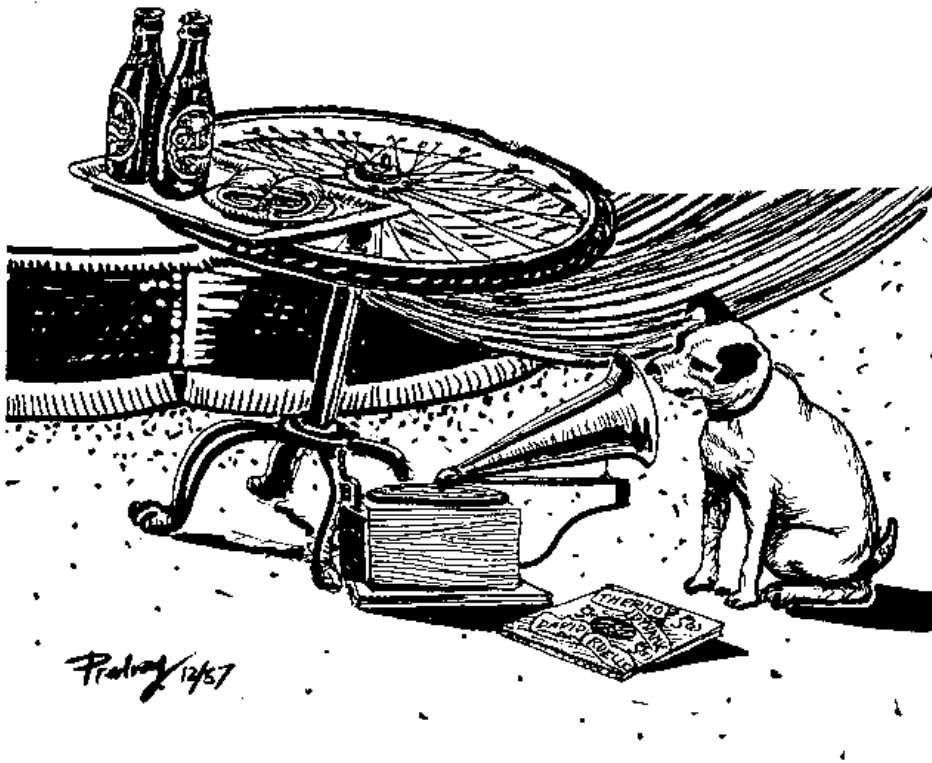


Chaos: Classical and Quantum

I: Deterministic Chaos



Predrag Cvitanović – Roberto Artuso – Ronnie Mainieri – Gregor Tanner –
Gábor Vattay

Contents

Contributors	xi
Acknowledgements	xv
I Geometry of chaos	1
1 Overture	3
1.1 Why ChaosBook?	4
1.2 Chaos ahead	5
1.3 The future as in a mirror	6
1.4 A game of pinball	11
1.5 Chaos for cyclists	15
1.6 Change in time	21
1.7 To statistical mechanics	24
1.8 Chaos: what is it good for?	25
1.9 What is not in ChaosBook	27
résumé 28 commentary 30 guide to exercises 33 exercises 34 references 34	
2 Go with the flow	37
2.1 Dynamical systems	37
2.2 Flows	42
2.3 Computing trajectories	46
résumé 47 commentary 47 exercises 50 references 51	
3 Discrete time dynamics	54
3.1 Poincaré sections	54
3.2 Constructing a Poincaré section	61
3.3 Maps	62
résumé 65 commentary 66 exercises 67 references 67	
4 Local stability	69
4.1 Flows transport neighborhoods	69
4.2 Linear flows	73
4.3 Stability of flows	79
4.4 Neighborhood volume	84
4.5 Stability of maps	86
résumé 89 commentary 90 exercises 91 references 91	

5	Cycle stability	94
5.1	Stability of periodic orbits	94
5.2	Floquet multipliers are invariant	99
5.3	Stability of Poincaré map cycles	101
5.4	There goes the neighborhood	102
	résumé 102 commentary 103 exercises 104 references 104	
6	Get straight	105
6.1	Changing coordinates	105
6.2	Rectification of flows	107
6.3	Collinear helium	108
6.4	Rectification of maps	113
6.5	Rectification of a periodic orbit	114
6.6	Cycle Floquet multipliers are metric invariants	115
	résumé 116 commentary 117 exercises 119 references 119	
7	Hamiltonian dynamics	121
7.1	Hamiltonian flows	122
7.2	Stability of Hamiltonian flows	123
7.3	Symplectic maps	126
7.4	Poincaré invariants	129
	commentary 130 exercises 132 references 132	
8	Billiards	134
8.1	Billiard dynamics	134
8.2	Stability of billiards	136
	résumé 139 commentary 139 exercises 140 references 140	
9	World in a mirror	143
9.1	Discrete symmetries	143
9.2	Symmetries of solutions	151
9.3	Relative periodic orbits	155
9.4	Dynamics reduced to fundamental domain	157
	résumé 160 commentary 161 exercises 163 references 164	
10	Relativity for cyclists	167
10.1	Continuous symmetries	167
10.2	Symmetries of solutions	175
10.3	Stability	181
10.4	Reduced state space	181
10.5	Method of images: Hilbert bases	187
	résumé 189 commentary 191 exercises 193 references 196	
11	Charting the state space	199
11.1	Qualitative dynamics	200
11.2	Stretch and fold	204
11.3	Temporal ordering: itineraries	207
11.4	Spatial ordering	209
11.5	Kneading theory	213

11.6 Symbolic dynamics, basic notions	215
résumé 218 commentary 219 exercises 221 references 222	
12 Stretch, fold, prune	224
12.1 Going global: stable/unstable manifolds	225
12.2 Horseshoes	229
12.3 Symbol plane	233
12.4 Prune danish	236
12.5 Recoding, symmetries, tilings	237
résumé 240 commentary 241 exercises 243 references 244	
13 Fixed points, and how to get them	248
13.1 Where are the cycles?	249
13.2 One-dimensional mappings	253
13.3 Multipoint shooting method	255
13.4 Flows	257
résumé 262 commentary 262 exercises 264 references 266	
II Chaos rules	268
14 Walkabout: Transition graphs	270
14.1 Matrix representations of topological dynamics	270
14.2 Transition graphs: wander from node to node	272
14.3 Transition graphs: stroll from link to link	275
résumé 279 commentary 279 exercises 281 references 281	
15 Counting	283
15.1 How many ways to get there from here?	284
15.2 Topological trace formula	286
15.3 Determinant of a graph	289
15.4 Topological zeta function	293
15.5 Infinite partitions	295
15.6 Shadowing	297
15.7 Counting cycles	298
résumé 302 commentary 303 exercises 304 references 307	
16 Transporting densities	308
16.1 Measures	309
16.2 Perron-Frobenius operator	310
16.3 Why not just leave it to a computer?	312
16.4 Invariant measures	315
16.5 Density evolution for infinitesimal times	318
16.6 Liouville operator	320
résumé 322 commentary 323 exercises 324 references 326	

17 Averaging	328
17.1 Dynamical averaging	328
17.2 Evolution operators	336
17.3 Lyapunov exponents	338
résumé 342 commentary 342 exercises 343 references 344	
18 Trace formulas	347
18.1 A trace formula for maps	348
18.2 A trace formula for flows	353
18.3 An asymptotic trace formula	356
résumé 357 commentary 358 exercises 358 references 359	
19 Spectral determinants	360
19.1 Spectral determinants for maps	360
19.2 Spectral determinant for flows	362
19.3 Dynamical zeta functions	364
19.4 False zeros	368
19.5 Spectral determinants vs. dynamical zeta functions	368
19.6 All too many eigenvalues?	370
résumé 371 commentary 372 exercises 373 references 375	
20 Cycle expansions	377
20.1 Pseudocycles and shadowing	377
20.2 Construction of cycle expansions	380
20.3 Cycle formulas for dynamical averages	384
20.4 Cycle expansions for finite alphabets	387
20.5 Stability ordering of cycle expansions	388
20.6 Dirichlet series	391
résumé 392 commentary 393 exercises 395 references 397	
21 Discrete factorization	399
21.1 Preview	400
21.2 Discrete symmetries	402
21.3 Dynamics in the fundamental domain	403
21.4 Factorizations of dynamical zeta functions	407
21.5 C_2 factorization	409
21.6 D_3 factorization: 3-disk game of pinball	410
résumé 412 commentary 413 exercises 413 references 414	
III Chaos: what to do about it?	416
22 Why cycle?	418
22.1 Escape rates	418
22.2 Natural measure in terms of periodic orbits	420
22.3 Flow conservation sum rules	422
22.4 Correlation functions	423
22.5 Trace formulas vs. level sums	424
résumé 426 commentary 426 exercises 427 references 428	

23 Why does it work?	430
23.1 Linear maps: exact spectra	431
23.2 Evolution operator in a matrix representation	435
23.3 Classical Fredholm theory	438
23.4 Analyticity of spectral determinants	440
23.5 Hyperbolic maps	445
23.6 The physics of eigenvalues and eigenfunctions	447
23.7 Troubles ahead	449
résumé 450 commentary 452 exercises 454 references 454	
24 Intermittency	457
24.1 Intermittency everywhere	458
24.2 Intermittency for pedestrians	461
24.3 Intermittency for cyclists	472
24.4 BER zeta functions	478
résumé 480 commentary 481 exercises 482 references 483	
25 Deterministic diffusion	485
25.1 Diffusion in periodic arrays	486
25.2 Diffusion induced by chains of 1 – <i>dimensional</i> maps	490
25.3 Marginal stability and anomalous diffusion	497
résumé 500 commentary 501 exercises 504 references 504	
26 Turbulence?	506
26.1 Fluttering flame front	507
26.2 Infinite-dimensional flows: Numerics	510
26.3 Visualization	512
26.4 Equilibria of equilibria	513
26.5 Why does a flame front flutter?	515
26.6 Periodic orbits	518
26.7 Intrinsic parametrization	518
26.8 Energy budget	519
résumé 522 commentary 523 exercises 523 references 524	
27 Irrationally winding	526
27.1 Mode locking	527
27.2 Local theory: “Golden mean” renormalization	532
27.3 Global theory: Thermodynamic averaging	534
27.4 Hausdorff dimension of irrational windings	536
27.5 Thermodynamics of Farey tree: Farey model	538
résumé 540 commentary 540 exercises 543 references 544	
IV The rest is noise	547
28 Noise	549
28.1 Deterministic transport	550
28.2 Brownian diffusion	551
28.3 Weak noise	552

28.4 Weak noise approximation	554
résumé 555 commentary 555 exercises 557 references 557	
29 Relaxation for cyclists	560
29.1 Fictitious time relaxation	561
29.2 Discrete iteration relaxation method	566
29.3 Least action method	570
résumé 570 commentary 571 exercises 574 references 574	
V Quantum chaos	577
30 Prologue	579
30.1 Quantum pinball	580
30.2 Quantization of helium	582
commentary 583 references 584	
31 Quantum mechanics, briefly	585
exercises 589	
32 WKB quantization	590
32.1 WKB ansatz	590
32.2 Method of stationary phase	593
32.3 WKB quantization	594
32.4 Beyond the quadratic saddle point	596
résumé 597 commentary 598 exercises 598 references 599	
33 Semiclassical evolution	600
33.1 Hamilton-Jacobi theory	600
33.2 Semiclassical propagator	609
33.3 Semiclassical Green's function	612
résumé 618 commentary 619 exercises 621 references 622	
34 Semiclassical quantization	623
34.1 Trace formula	623
34.2 Semiclassical spectral determinant	629
34.3 One-dof systems	630
34.4 Two-dof systems	631
résumé 632 commentary 633 exercises 635 references 635	
35 Quantum scattering	637
35.1 Density of states	637
35.2 Quantum mechanical scattering matrix	641
35.3 Krein-Friedel-Lloyd formula	642
35.4 Wigner time delay	645
commentary 647 exercises 648 references 648	

36 Chaotic multiscattering	651
36.1 Quantum mechanical scattering matrix	652
36.2 N -scatterer spectral determinant	655
36.3 Semiclassical 1-disk scattering	659
36.4 From quantum cycle to semiclassical cycle	666
36.5 Heisenberg uncertainty	669
commentary 669 references 670	
37 Helium atom	671
37.1 Classical dynamics of collinear helium	672
37.2 Chaos, symbolic dynamics and periodic orbits	673
37.3 Local coordinates, Jacobian matrix	677
37.4 Getting ready	679
37.5 Semiclassical quantization of collinear helium	681
résumé 688 commentary 688 exercises 690 references 691	
38 Diffraction distraction	692
38.1 Quantum eavesdropping	692
38.2 An application	698
résumé 703 commentary 704 exercises 705 references 706	
Epilogue	708
Index	713

Volume www: Appendices on ChaosBook.org

A	A brief history of chaos	732
	A.1 Chaos is born	732
	A.2 Chaos with us	737
	A.3 Death of the Old Quantum Theory	744
	commentary 746 references 747	
B	Linear stability	751
	B.1 Linear algebra	751
	B.2 Eigenvalues and eigenvectors	753
	B.3 Eigenspectra: what to make out of them?	760
	B.4 Stability of Hamiltonian flows	762
	B.5 Monodromy matrix for Hamiltonian flows	763
	exercises 766 references 766	
C	Finding cycles	767
	C.1 Newton-Raphson method	767
	C.2 Hybrid Newton-Raphson / relaxation method	768
D	Symbolic dynamics techniques	771
	D.1 Topological zeta functions for infinite subshifts	771
	D.2 Prime factorization for dynamical itineraries	779
E	Counting itineraries	783
	E.1 Counting curvatures	783
	exercises 784	
F	Implementing evolution	785
	F.1 Koopmania	785
	F.2 Implementing evolution	787
	commentary 790 exercises 790 references 790	
G	Transport of vector fields	792
	G.1 Evolution operator for Lyapunov exponents	792
	G.2 Advection of vector fields by chaotic flows	797
	commentary 801 exercises 801 references 801	
H	Discrete symmetries of dynamics	803
	H.1 Preliminaries and definitions	803
	H.2 Invariants and reducibility	810
	H.3 Lattice derivatives	813
	H.4 Periodic lattices	816
	H.5 Discrete Fourier transforms	818
	H.6 C_{4v} factorization	822
	H.7 C_{2v} factorization	826
	H.8 Hénon map symmetries	829
	commentary 829 exercises 830 references 831	

I	Convergence of spectral determinants	834
I.1	Curvature expansions: geometric picture	834
I.2	On importance of pruning	837
I.3	Ma-the-matical caveats	838
I.4	Estimate of the n th cumulant	839
J	Infinite dimensional operators	841
J.1	Matrix-valued functions	841
J.2	Operator norms	843
J.3	Trace class and Hilbert-Schmidt class	844
J.4	Determinants of trace class operators	846
J.5	Von Koch matrices	849
J.6	Regularization	851
	exercises 853 references 853	
K	Thermodynamic formalism	855
K.1	Rényi entropies	855
K.2	Fractal dimensions	860
	résumé 864 commentary 864 exercises 865 references 865	
L	Statistical mechanics recycled	867
L.1	The thermodynamic limit	867
L.2	Ising models	870
L.3	Fisher droplet model	873
L.4	Scaling functions	878
L.5	Geometrization	881
	résumé 888 commentary 889 exercises 889 references 890	
M	Noise/quantum corrections	892
M.1	Periodic orbits as integrable systems	892
M.2	The Birkhoff normal form	896
M.3	Bohr-Sommerfeld quantization of periodic orbits	897
M.4	Quantum calculation of \hbar corrections	899
	references 905	
S	Solutions	908
T	Projects	1001
T.1	Deterministic diffusion, zig-zag map	1003
	references 1008	
T.2	Deterministic diffusion, sawtooth map	1009

Contributors

No man but a blockhead ever wrote except for money
—Samuel Johnson

This book is a result of collaborative labors of many people over a span of several decades. Coauthors of a chapter or a section are indicated in the byline to the chapter/section title. If you are referring to a specific coauthored section rather than the entire book, cite it as (for example):

C. Chandre, F.K. Diakonov and P. Schmelcher, section “Discrete cyclist relaxation method,” in P. Cvitanović, R. Artuso, R. Mainieri, G. Tanner and G. Vattay, *Chaos: Classical and Quantum* (Niels Bohr Institute, Copenhagen 2008); ChaosBook.org/version12.

Do not cite chapters by their numbers, as those change from version to version. Chapters without a byline are written by Predrag Cvitanović. Friends whose contributions and ideas were invaluable to us but have not contributed written text to this book, are credited in the acknowledgements.

Roberto Artuso

16 Transporting densities	308
18.2 A trace formula for flows	353
22.4 Correlation functions	423
24 Intermittency	457
25 Deterministic diffusion	485

Ronnie Mainieri

2 Flows	37
3.2 The Poincaré section of a flow	61
4 Local stability	69
6.1 Understanding flows	108
11.1 Temporal ordering: itineraries	200
Appendix A: A brief history of chaos	732

Gábor Vattay

Gregor Tanner

24 Intermittency	457
Appendix B.5: Jacobians of Hamiltonian flows	763

Arindam Basu

Rössler flow figures, tables, cycles in chapters 11, 13 and exercise 13.10

Ofer Biham

29.1 Cyclists relaxation method	561
---------------------------------------	-----

Daniel Borrero Oct 23 2008, soluCycles.tex

Solution 13.15

Cristel Chandre

- 29.1 Cyclists relaxation method 561
 29.2 Discrete cyclists relaxation methods 566

Freddy Christiansen

- 13.2 One-dimensional mappings 253
 13.3 Multipoint shooting method 255

Per Dahlqvist

- 24 Intermittency 457
 29.3 Orbit length extremization method for billiards 570

Carl P. Dettmann

- 20.5 Stability ordering of cycle expansions 388

Fotis K. Diakonou

- 29.2 Discrete cyclists relaxation methods 566

G. Bard Ermentrout

- Exercise 5.1

Mitchell J. Feigenbaum

- Appendix B.4: Symplectic invariance 762

Jonathan Halcrow

- Example 3.5: Sections of Lorenz flow 60
 Example 4.7: Stability of Lorenz flow equilibria 81
 Example 4.8: Lorenz flow: Global portrait 83
 Example 9.10: Desymmetrization of Lorenz flow 153
 Example 11.4: Lorenz flow: a 1-dimensional return map 205
 Exercises 9.9 and figure 2.5

Kai T. Hansen

- 11.3 Unimodal map symbolic dynamics 207
 15.5 Topological zeta function for an infinite partition 295
 11.5 Kneading theory 213
 figures throughout the text

Rainer Klages

- Figure 25.5

Yueheng Lan

- Solutions 1.1, 2.1, 2.2, 2.3, 2.4, 2.5, 9.6, 12.6, 11.6, 16.1, 16.2, 16.3, 16.5,
 16.7, 16.10, 17.1 and figures 1.9, 9.2, 9.8 11.5,

Bo Li

- Solutions 31.2, 31.1, 32.1

Joachim Mathiesen

- 17.3 Lyapunov exponents 338

Rössler flow figures, tables, cycles in sect. 17.3 and exercise 13.10

Yamato Matsuoka

Figure 12.4

Radford Mitchell, Jr.

Example 3.6

Rytis Paškauskas

4.5.1 Stability of Poincaré return maps 87

5.3 Stability of Poincaré map cycles 101

Exercises 2.8, 3.1, 4.4 and solution 4.1

Adam Prügel-Bennet

Solutions 1.2, 2.10, 8.1, 19.1, 20.2 23.3, 29.1.

Lamberto Rondoni

16 Transporting densities 308

13.1.1 Cycles from long time series 250

22.2.1 Unstable periodic orbits are dense 421

Table 15.2

Juri Rolf

Solution 23.3

Per E. Rosenqvist

exercises, figures throughout the text

Hans Henrik Rugh

23 Why does it work? 430

Peter Schmelcher

29.2 Discrete cyclists relaxation methods 566

Evangelos Siminos

Example 3.5: Sections of Lorenz flow 60

Example 4.7: Stability of Lorenz flow equilibria 81

Example 4.8: Lorenz flow: Global portrait 83

Example 9.10: Desymmetrization of Lorenz flow 153

Example 11.4: Lorenz flow: a 1-dimensional return map 205

Exercise 9.9

Solution 10.21

Gábor Simon

Rössler flow figures, tables, cycles in chapters 2, 13 and exercise 13.10

Edward A. Spiegel

2 Flows 37

16 Transporting densities 308

Luz V. Vela-Arevalo

7.1 Hamiltonian flows	122
Exercises 7.1, 7.3, 7.5	

R. Wilczak

Figure 10.1, figure 10.4

Exercise 10.26

Solutions 10.1, 10.5, 10.6, 10.7, 10.8, 10.10, 10.14, 10.15, 10.16, 10.17,
10.18, 10.19, 10.20, 10.22, 10.23

Acknowledgements

I feel I never want to write another book. What's the good!
I can eke living on stories and little articles, that don't cost
a tittle of the output a book costs. Why write novels any
more!

—D.H. Lawrence

This book owes its existence to the Niels Bohr Institute's and Nordita's hospitable and nurturing environment, and the private, national and cross-national foundations that have supported the collaborators' research over a span of several decades. P.C. thanks M.J. Feigenbaum of Rockefeller University; D. Ruelle of I.H.E.S., Bures-sur-Yvette; I. Procaccia of the Weizmann Institute; P.H. Damgaard of the Niels Bohr International Academy; G. Mazenko of U. of Chicago James Franck Institute and Argonne National Laboratory; T. Geisel of Max-Planck-Institut für Dynamik und Selbstorganisation, Göttingen; I. Andrić of Rudjer Bošković Institute; P. Hemmer of University of Trondheim; The Max-Planck Institut für Mathematik, Bonn; J. Lowenstein of New York University; Edificio Celi, Milano; Fundação de Faca, Porto Seguro; and Dr. Dj. Cvitanović, Kostrena, for the hospitality during various stages of this work, and the Carlsberg Foundation and Glen P. Robinson for support.

The authors gratefully acknowledge collaborations and/or stimulating discussions with E. Aurell, M. Avila, V. Baladi, B. Brenner, A. de Carvalho, D.J. Driebe, B. Eckhardt, M.J. Feigenbaum, J. Frøjlund, P. Gaspar, P. Gaspard, J. Guckenheimer, G.H. Gunaratne, P. Grassberger, H. Gutowitz, M. Gutzwiller, K.T. Hansen, P.J. Holmes, T. Janssen, R. Klages, Y. Lan, B. Lauritzen, J. Milnor, M. Nordahl, I. Procaccia, J.M. Robbins, P.E. Rosenqvist, D. Ruelle, G. Russberg, M. Sieber, D. Sullivan, N. Søndergaard, T. Tél, C. Tresser, and D. Wintgen.

We thank Dorte Glass for typing parts of the manuscript; D. Borrero, B. Lautrup, J.F. Gibson and D. Viswanath for comments and corrections to the preliminary versions of this text; the M.A. Porter for lengthening the manuscript by the 2013 definite articles hitherto missing; M.V. Berry for the quotation on page 732; H. Fogedby for the quotation on page 440; J. Greensite for the quotation on page 7; Ya.B. Pesin for the remarks quoted on page 747; M.A. Porter for the quotations on page 21 and page 739; E.A. Spiegel for quotation on page 3; and E. Valesco for the quotation on page 25.

F. Haake's heartfelt lament on page 353 was uttered at the end of the first conference presentation of cycle expansions, in 1988. G.P. Morriss advice to students as how to read the introduction to this book, page 6, was offered during a 2002 graduate course in Dresden. K. Huang's C.N. Yang interview quoted on page 315 is available on ChaosBook.org/extras. T.D. Lee remarks on as to who is to blame, page 37 and page 249, as well as M. Shub's helpful technical remark on page 452 came during the Rockefeller University December 2004 "Feigenbaum Fest." Quotes on pages 37, 121, and 312 are taken from a book review by J. Guckenheimer [1].

Who is the 3-legged dog reappearing throughout the book? Long ago, when we were innocent and knew not Borel measurable α to Ω sets, P. Cvitanović asked V. Baladi a question about dynamical zeta functions, who then asked J.-P. Eckmann, who then asked D. Ruelle. The answer was transmitted back: "The master

says: ‘It is holomorphic in a strip.’” Hence His Master’s Voice logo, and the 3-legged dog is us, still eager to fetch the bone. The answer has made it to the book, though not precisely in His Master’s voice. As a matter of fact, the answer *is* the book. We are still chewing on it.

Profound thanks to all the unsung heroes—students and colleagues, too numerous to list here—who have supported this project over many years in many ways, by surviving pilot courses based on this book, by providing invaluable insights, by teaching us, by inspiring us.

Part I

Geometry of chaos

WE START OUT with a recapitulation of the basic notions of dynamics. Our aim is narrow; we keep the exposition focused on prerequisites to the applications to be developed in this text. We assume that the reader is familiar with dynamics on the level of the introductory texts mentioned in remark 1.1, and concentrate here on developing intuition about what a dynamical system can do. It will be a coarse brush sketch—a full description of all possible behaviors of dynamical systems is beyond human ken. While for a novice there is no shortcut through this lengthy detour, a sophisticated traveler might bravely skip this well-trodden territory and embark upon the journey at chapter 15.

The fate has handed you a flow. What are you to do about it?

1. Define your *dynamical system* (\mathcal{M}, f) : the space of its possible states \mathcal{M} , and the law f^t of their evolution in time.
2. Pin it down locally—is there anything about it that is stationary? Try to determine its *equilibria / fixed points* (Chapter 2).
3. Slice it, represent as a map from a section to a section (Chapter 3).
4. Explore the neighborhood by *linearizing* the flow—check the *linear stability* of its equilibria / fixed points, their stability eigen-directions (Chapter 4).
5. Go global: *partition the state space* of 1-dimensional maps. Label the regions by *symbolic dynamics* (Chapter 11).
6. Now venture global distances across the system by continuing eigenvectors into *stable / unstable manifolds*. Their intersections *partition the state space* in a dynamically invariant way (Chapter 12).
7. Guided by this topological partition, compute a set of *periodic orbits* up to a given topological length (Chapter 13).

Along the way you might want to learn about dynamical invariants (chapter 5), nonlinear transformations (chapter 6), classical mechanics (chapter 7), billiards (chapter 8), and discrete (chapter 9) and continuous (chapter 10) symmetries of dynamics.

Chapter 1

Overture

If I have seen less far than other men it is because I have stood behind giants.

—Edoardo Specchio

REREADING classic theoretical physics textbooks leaves a sense that there are holes large enough to steam a Eurostar train through them. Here we learn about harmonic oscillators and Keplerian ellipses - but where is the chapter on chaotic oscillators, the tumbling Hyperion? We have just quantized hydrogen, where is the chapter on the classical 3-body problem and its implications for quantization of helium? We have learned that an instanton is a solution of field-theoretic equations of motion, but shouldn't a strongly nonlinear field theory have turbulent solutions? How are we to think about systems where things fall apart; the center cannot hold; every trajectory is unstable?

This chapter offers a quick survey of the main topics covered in the book. Throughout the book



indicates that the section is on a pedestrian level - you are expected to know/learn this material



indicates that the section is on a somewhat advanced, cyclist level



indicates that the section requires a hearty stomach and is probably best skipped on first reading



fast track points you where to skip to



tells you where to go for more depth on a particular topic

[exercise 1.2] on margin links to an exercise that might clarify a point in the text



indicates that a figure is still missing—you are urged to fetch it

We start out by making promises—we will right wrongs, no longer shall you suffer the slings and arrows of outrageous Science of Perplexity. We relegate a historical overview of the development of chaotic dynamics to appendix **A**, and head straight to the starting line: A pinball game is used to motivate and illustrate most of the concepts to be developed in ChaosBook.

This is a textbook, not a research monograph, and you should be able to follow the thread of the argument without constant excursions to sources. Hence there are no literature references in the text proper, all learned remarks and bibliographical pointers are relegated to the “Commentary” section at the end of each chapter.

1.1 Why ChaosBook?

It seems sometimes that through a preoccupation with science, we acquire a firmer hold over the vicissitudes of life and meet them with greater calm, but in reality we have done no more than to find a way to escape from our sorrows.

—Hermann Minkowski in a letter to David Hilbert

The problem has been with us since Newton’s first frustrating (and unsuccessful) crack at the 3-body problem, lunar dynamics. Nature is rich in systems governed by simple deterministic laws whose asymptotic dynamics are complex beyond belief, systems which are locally unstable (almost) everywhere but globally recurrent. How do we describe their long term dynamics?

The answer turns out to be that we have to evaluate a determinant, take a logarithm. It would hardly merit a learned treatise, were it not for the fact that this determinant that we are to compute is fashioned out of infinitely many infinitely small pieces. The feel is of statistical mechanics, and that is how the problem was solved; in the 1960’s the pieces were counted, and in the 1970’s they were weighted and assembled in a fashion that in beauty and in depth ranks along with thermodynamics, partition functions and path integrals amongst the crown jewels of theoretical physics.

This book is *not* a book about periodic orbits. The red thread throughout the text is the duality between the local, topological, short-time dynamically invariant compact sets (equilibria, periodic orbits, partially hyperbolic invariant tori) and the global long-time evolution of densities of trajectories. Chaotic dynamics is generated by the interplay of locally unstable motions, and the interweaving of their global stable and unstable manifolds. These features are robust and accessible in systems as noisy as slices of rat brains. Poincaré, the first to understand deterministic chaos, already said as much (modulo rat brains). Once this topology

is understood, a powerful theory yields the observable consequences of chaotic dynamics, such as atomic spectra, transport coefficients, gas pressures.

That is what we will focus on in ChaosBook. The book is a self-contained graduate textbook on classical and quantum chaos. Your professor does not know this material, so you are on your own. We will teach you how to evaluate a determinant, take a logarithm—stuff like that. Ideally, this should take 100 pages or so. Well, we fail—so far we have not found a way to traverse this material in less than a semester, or 200-300 page subset of this text. Nothing to be done.

1.2 Chaos ahead

Things fall apart; the centre cannot hold.

—W.B. Yeats: *The Second Coming*

The study of chaotic dynamics is no recent fashion. It did not start with the widespread use of the personal computer. Chaotic systems have been studied for over 200 years. During this time many have contributed, and the field followed no single line of development; rather one sees many interwoven strands of progress.

In retrospect many triumphs of both classical and quantum physics were a stroke of luck: a few integrable problems, such as the harmonic oscillator and the Kepler problem, though ‘non-generic,’ have gotten us very far. The success has lulled us into a habit of expecting simple solutions to simple equations—an expectation tempered by our recently acquired ability to numerically scan the state space of non-integrable dynamical systems. The initial impression might be that all of our analytic tools have failed us, and that the chaotic systems are amenable only to numerical and statistical investigations. Nevertheless, a beautiful theory of deterministic chaos, of predictive quality comparable to that of the traditional perturbation expansions for nearly integrable systems, already exists.

In the traditional approach the integrable motions are used as zeroth-order approximations to physical systems, and weak nonlinearities are then accounted for perturbatively. For strongly nonlinear, non-integrable systems such expansions fail completely; at asymptotic times the dynamics exhibits amazingly rich structure which is not at all apparent in the integrable approximations. However, hidden in this apparent chaos is a rigid skeleton, a self-similar tree of *cycles* (periodic orbits) of increasing lengths. The insight of the modern dynamical systems theory is that the zeroth-order approximations to the harshly chaotic dynamics should be very different from those for the nearly integrable systems: a good starting approximation here is the stretching and folding of baker’s dough, rather than the periodic motion of a harmonic oscillator.

So, what is chaos, and what is to be done about it? To get some feeling for how and why unstable cycles come about, we start by playing a game of pinball. The remainder of the chapter is a quick tour through the material covered in ChaosBook. Do not worry if you do not understand every detail at the first reading—the intention

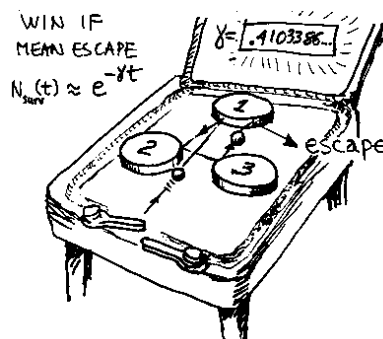


Figure 1.1: A physicist’s bare bones game of pinball.

is to give you a feeling for the main themes of the book. Details will be filled out later. If you want to get a particular point clarified right now, [\[section 1.4\]](#) on the margin points at the appropriate section.

[section 1.4](#)

1.3 The future as in a mirror

All you need to know about chaos is contained in the introduction of [ChaosBook]. However, in order to understand the introduction you will first have to read the rest of the book.

—Gary Morriss

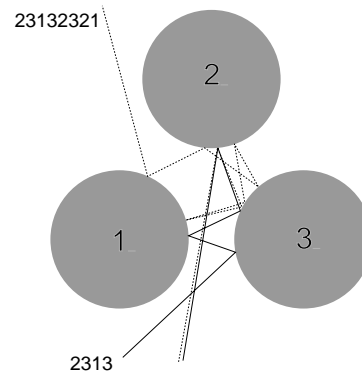
That deterministic dynamics leads to chaos is no surprise to anyone who has tried pool, billiards or snooker—the game is about beating chaos—so we start our story about what chaos is, and what to do about it, with a game of *pinball*. This might seem a trifle, but the game of pinball is to chaotic dynamics what a pendulum is to integrable systems: thinking clearly about what ‘chaos’ in a game of pinball is will help us tackle more difficult problems, such as computing the diffusion constant of a deterministic gas, the drag coefficient of a turbulent boundary layer, or the helium spectrum.

We all have an intuitive feeling for what a ball does as it bounces among the pinball machine’s disks, and only high-school level Euclidean geometry is needed to describe its trajectory. A physicist’s pinball game is the game of pinball stripped to its bare essentials: three equidistantly placed reflecting disks in a plane, [figure 1.1](#). A physicist’s pinball is free, frictionless, point-like, spin-less, perfectly elastic, and noiseless. Point-like pinballs are shot at the disks from random starting positions and angles; they spend some time bouncing between the disks and then escape.

At the beginning of the 18th century Baron Gottfried Wilhelm Leibniz was confident that given the initial conditions one knew everything a deterministic system would do far into the future. He wrote [\[2\]](#), anticipating by a century and a half the oft-quoted Laplace’s “Given for one instant an intelligence which could comprehend all the forces by which nature is animated...”:

That everything is brought forth through an established destiny is just

Figure 1.2: Sensitivity to initial conditions: two pin-balls that start out very close to each other separate exponentially with time.



as certain as that three times three is nine. [...] If, for example, one sphere meets another sphere in free space and if their sizes and their paths and directions before collision are known, we can then foretell and calculate how they will rebound and what course they will take after the impact. Very simple laws are followed which also apply, no matter how many spheres are taken or whether objects are taken other than spheres. From this one sees then that everything proceeds mathematically—that is, infallibly—in the whole wide world, so that if someone could have a sufficient insight into the inner parts of things, and in addition had remembrance and intelligence enough to consider all the circumstances and to take them into account, he would be a prophet and would see the future in the present as in a mirror.

Leibniz chose to illustrate his faith in determinism precisely with the type of physical system that we shall use here as a paradigm of ‘chaos.’ His claim is wrong in a deep and subtle way: a state of a physical system can *never* be specified to infinite precision, and by this we do not mean that eventually the Heisenberg uncertainty principle kicks in. In the classical, deterministic dynamics there is no way to take all the circumstances into account, and a single trajectory cannot be tracked, only a ball of nearby initial points makes physical sense.

1.3.1 What is ‘chaos’?

I accept chaos. I am not sure that it accepts me.

—Bob Dylan, *Bringing It All Back Home*

A deterministic system is a system whose present state is *in principle* fully determined by its initial conditions, in contrast to a stochastic system.

For a stochastic system the initial conditions determine the future only partially, due to noise, or other external circumstances beyond our control: the present state reflects the past initial conditions plus the particular realization of the noise encountered along the way.

A deterministic system with sufficiently complicated dynamics can fool us into regarding it as a stochastic one; disentangling the deterministic from the stochastic is the main challenge in many real-life settings, from stock markets to palpitations of chicken hearts. So, what is ‘chaos’?

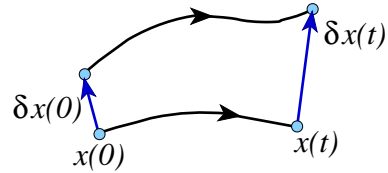


Figure 1.3: Unstable trajectories separate with time.

In a game of pinball, any two trajectories that start out very close to each other separate exponentially with time, and in a finite (and in practice, a very small) number of bounces their separation $\delta \mathbf{x}(t)$ attains the magnitude of L , the characteristic linear extent of the whole system, figure 1.2. This property of *sensitivity to initial conditions* can be quantified as

$$|\delta \mathbf{x}(t)| \approx e^{\lambda t} |\delta \mathbf{x}(0)|$$

where λ , the mean rate of separation of trajectories of the system, is called the *Lyapunov exponent*. For any finite accuracy $\delta x = |\delta \mathbf{x}(0)|$ of the initial data, the dynamics is predictable only up to a finite *Lyapunov time*

section 17.3

$$T_{\text{Lyap}} \approx -\frac{1}{\lambda} \ln |\delta x/L|, \quad (1.1)$$

despite the deterministic and, for Baron Leibniz, infallible simple laws that rule the pinball motion.

A positive Lyapunov exponent does not in itself lead to chaos. One could try to play 1- or 2-disk pinball game, but it would not be much of a game; trajectories would only separate, never to meet again. What is also needed is *mixing*, the coming together again and again of trajectories. While locally the nearby trajectories separate, the interesting dynamics is confined to a globally finite region of the state space and thus the separated trajectories are necessarily folded back and can re-approach each other arbitrarily closely, infinitely many times. For the case at hand there are 2^n topologically distinct n bounce trajectories that originate from a given disk. More generally, the number of distinct trajectories with n bounces can be quantified as

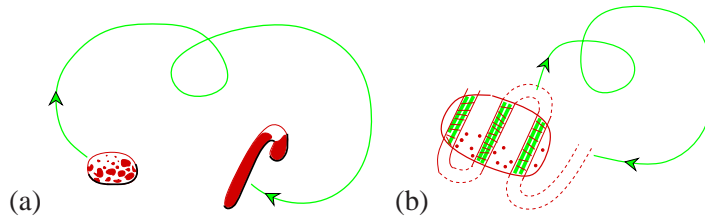
section 15.1

$$N(n) \approx e^{hn}$$

where h , the growth rate of the number of topologically distinct trajectories, is called the “*topological entropy*” ($h = \ln 2$ in the case at hand).

The appellation ‘chaos’ is a confusing misnomer, as in deterministic dynamics there is no chaos in the everyday sense of the word; everything proceeds mathematically—that is, as Baron Leibniz would have it, infallibly. When a physicist says that a certain system exhibits ‘chaos,’ he means that the system obeys deterministic laws of evolution, but that the outcome is highly sensitive to small uncertainties in the specification of the initial state. The word ‘chaos’ has in this

Figure 1.4: Dynamics of a *chaotic* dynamical system is (a) everywhere locally unstable (positive Lyapunov exponent) and (b) globally mixing (positive entropy). (A. Johansen)

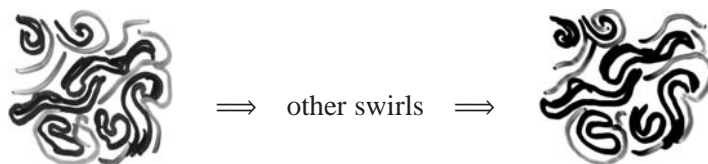


context taken on a narrow technical meaning. If a deterministic system is locally unstable (positive Lyapunov exponent) and globally mixing (positive entropy)—figure 1.4—it is said to be *chaotic*.

While mathematically correct, the definition of chaos as ‘positive Lyapunov + positive entropy’ is useless in practice, as a measurement of these quantities is intrinsically asymptotic and beyond reach for systems observed in nature. More powerful is Poincaré’s vision of chaos as the interplay of local instability (unstable periodic orbits) and global mixing (intertwining of their stable and unstable manifolds). In a chaotic system any open ball of initial conditions, no matter how small, will in finite time overlap with any other finite region and in this sense spread over the extent of the entire asymptotically accessible state space. Once this is grasped, the focus of theory shifts from attempting to predict individual trajectories (which is impossible) to a description of the geometry of the space of possible outcomes, and evaluation of averages over this space. How this is accomplished is what ChaosBook is about.

A definition of ‘turbulence’ is even harder to come by. Intuitively, the word refers to irregular behavior of an infinite-dimensional dynamical system described by deterministic equations of motion—say, a bucket of sloshing water described by the Navier-Stokes equations. But in practice the word ‘turbulence’ tends to refer to messy dynamics which we understand poorly. As soon as a phenomenon is understood better, it is reclaimed and renamed: ‘a route to chaos’, ‘spatiotemporal chaos’, and so on.

In ChaosBook we shall develop a theory of chaotic dynamics for low dimensional attractors visualized as a succession of nearly periodic but unstable motions. In the same spirit, we shall think of turbulence in spatially extended systems in terms of recurrent spatiotemporal patterns. Pictorially, dynamics drives a given spatially extended system (clouds, say) through a repertoire of unstable patterns; as we watch a turbulent system evolve, every so often we catch a glimpse of a familiar pattern:



For any finite spatial resolution, a deterministic flow follows approximately for a finite time an unstable pattern belonging to a finite alphabet of admissible patterns,

and the long term dynamics can be thought of as a walk through the space of such patterns. In ChaosBook we recast this image into mathematics.

1.3.2 When does ‘chaos’ matter?

In dismissing Pollock’s fractals because of their limited magnification range, Jones-Smith and Mathur would also dismiss half the published investigations of physical fractals.

— Richard P. Taylor [4, 5]

When should we be mindful of chaos? The solar system is ‘chaotic’, yet we have no trouble keeping track of the annual motions of planets. The rule of thumb is this; if the Lyapunov time (1.1)—the time by which a state space region initially comparable in size to the observational accuracy extends across the entire accessible state space—is significantly shorter than the observational time, you need to master the theory that will be developed here. That is why the main successes of the theory are in statistical mechanics, quantum mechanics, and questions of long term stability in celestial mechanics.

In science popularizations too much has been made of the impact of ‘chaos theory,’ so a number of caveats are already needed at this point.

At present the theory that will be developed here is in practice applicable only to systems of a low intrinsic *dimension* – the minimum number of coordinates necessary to capture its essential dynamics. If the system is very turbulent (a description of its long time dynamics requires a space of high intrinsic dimension) we are out of luck. Hence insights that the theory offers in elucidating problems of fully developed turbulence, quantum field theory of strong interactions and early cosmology have been modest at best. Even that is a caveat with qualifications. There are applications—such as spatially extended (non-equilibrium) systems, plumber’s turbulent pipes, etc.,—where the few important degrees of freedom can be isolated and studied profitably by methods to be described here.

Thus far the theory has had limited practical success when applied to the very noisy systems so important in the life sciences and in economics. Even though we are often interested in phenomena taking place on time scales much longer than the intrinsic time scale (neuronal inter-burst intervals, cardiac pulses, etc.), disentangling ‘chaotic’ motions from the environmental noise has been very hard.

In 1980’s something happened that might be without parallel; this is an area of science where the advent of cheap computation had actually subtracted from our collective understanding. The computer pictures and numerical plots of fractal science of the 1980’s have overshadowed the deep insights of the 1970’s, and these pictures have since migrated into textbooks. By a regrettable oversight, ChaosBook has none, so ‘Untitled 5’ of figure 1.5 will have to do as the illustration of the power of fractal analysis. Fractal science posits that certain quantities

remark 1.6



Figure 1.5: Katherine Jones-Smith, ‘Untitled 5,’ the drawing used by K. Jones-Smith and R.P. Taylor to test the fractal analysis of Pollock’s drip paintings [6].

(Lyapunov exponents, generalized dimensions, ...) can be estimated on a computer. While some of the numbers so obtained are indeed mathematically sensible characterizations of fractals, they are in no sense observable and measurable on the length-scales and time-scales dominated by chaotic dynamics.

Even though the experimental evidence for the fractal geometry of nature is circumstantial [7], in studies of probabilistically assembled fractal aggregates we know of nothing better than contemplating such quantities. In deterministic systems we can do *much* better.

1.4 A game of pinball

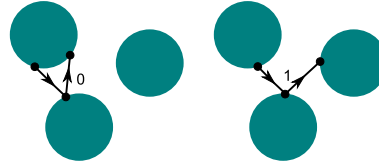
Formulas hamper the understanding.

—S. Smale

We are now going to get down to the brass tacks. Time to fasten your seat belts and turn off all electronic devices. But first, a disclaimer: If you understand the rest of this chapter on the first reading, you either do not need this book, or you are delusional. If you do not understand it, it is not because the people who figured all this out first are smarter than you: the most you can hope for at this stage is to get a flavor of what lies ahead. If a statement in this chapter mystifies/intrigues, fast forward to a section indicated by [\[section ...\]](#) on the margin, read only the parts that you feel you need. Of course, we think that you need to learn ALL of it, or otherwise we would not have included it in ChaosBook in the first place.

Confronted with a potentially chaotic dynamical system, our analysis proceeds in three stages; I. diagnose, II. count, III. measure. First, we determine the intrinsic *dimension* of the system—the minimum number of coordinates necessary to capture its essential dynamics. If the system is very turbulent we are, at present, out of luck. We know only how to deal with the transitional regime

Figure 1.6: Binary labeling of the 3-disk pinball trajectories; a bounce in which the trajectory returns to the preceding disk is labeled 0, and a bounce which results in continuation to the third disk is labeled 1.



between regular motions and chaotic dynamics in a few dimensions. That is still something; even an infinite-dimensional system such as a burning flame front can turn out to have a very few chaotic degrees of freedom. In this regime the chaotic dynamics is restricted to a space of low dimension, the number of relevant parameters is small, and we can proceed to step II; we *count* and *classify* all possible topologically distinct trajectories of the system into a hierarchy whose successive layers require increased precision and patience on the part of the observer. This we shall do in sect. 1.4.2. If successful, we can proceed with step III: investigate the *weights* of the different pieces of the system.

chapter 11
chapter 15

We commence our analysis of the pinball game with steps I, II: diagnose, count. We shall return to step III—measure—in sect. 1.5. The three sections that follow are *highly* technical, they go into the guts of what the book is about. Is today is not your thinking day, skip them, jump straight to sect. 1.7.

chapter 20

1.4.1 Symbolic dynamics

With the game of pinball we are in luck—it is a low dimensional system, free motion in a plane. The motion of a point particle is such that after a collision with one disk it either continues to another disk or it escapes. If we label the three disks by 1, 2 and 3, we can associate every trajectory with an *itinerary*, a sequence of labels indicating the order in which the disks are visited; for example, the two trajectories in figure 1.2 have itineraries `_2313_`, `_23132321_` respectively. Such labeling goes by the name *symbolic dynamics*. As the particle cannot collide two times in succession with the same disk, any two consecutive symbols must differ. This is an example of *pruning*, a rule that forbids certain subsequences of symbols. Deriving pruning rules is in general a difficult problem, but with the game of pinball we are lucky—for well-separated disks there are no further pruning rules.

exercise 1.1
section 2.1

chapter 12

The choice of symbols is in no sense unique. For example, as at each bounce we can either proceed to the next disk or return to the previous disk, the above 3-letter alphabet can be replaced by a binary $\{0, 1\}$ alphabet, figure 1.6. A clever choice of an alphabet will incorporate important features of the dynamics, such as its symmetries.

section 11.6

Suppose you wanted to play a good game of pinball, that is, get the pinball to bounce as many times as you possibly can—what would be a winning strategy? The simplest thing would be to try to aim the pinball so it bounces many times between a pair of disks—if you managed to shoot it so it starts out in the periodic orbit bouncing along the line connecting two disk centers, it would stay there forever. Your game would be just as good if you managed to get it to keep bouncing

Figure 1.7: The 3-disk pinball cycles $\overline{1232}$ and $\overline{121212313}$.

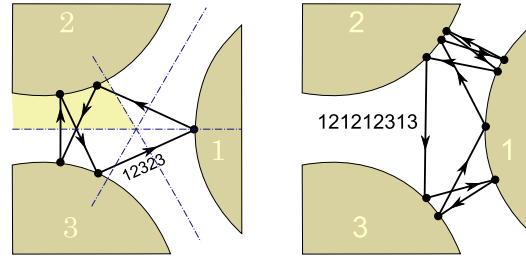
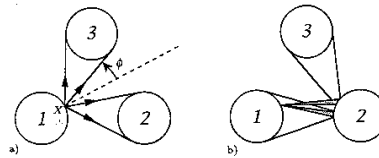


Figure 1.8: (a) A trajectory starting out from disk 1 can either hit another disk or escape. (b) Hitting two disks in a sequence requires a much sharper aim, with initial conditions that hit further consecutive disks nested within each other, as in Fig. 1.9.



between the three disks forever, or place it on any periodic orbit. The only rub is that any such orbit is *unstable*, so you have to aim very accurately in order to stay close to it for a while. So it is pretty clear that if one is interested in playing well, unstable periodic orbits are important—they form the *skeleton* onto which all trajectories trapped for long times cling.

1.4.2 Partitioning with periodic orbits

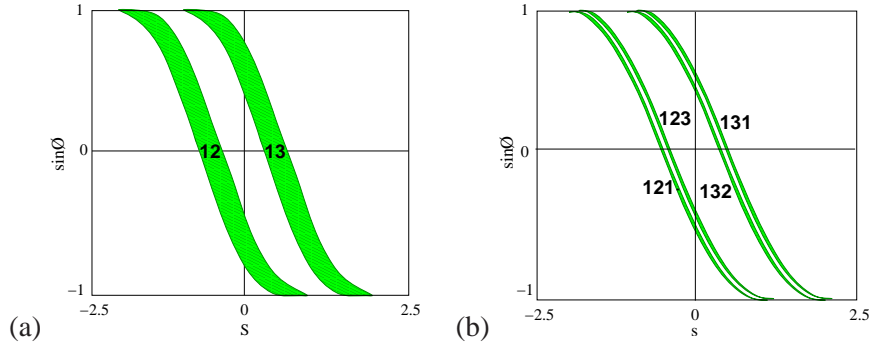
A trajectory is periodic if it returns to its starting position and momentum. We shall sometimes refer to the set of periodic points that belong to a given periodic orbit as a *cycle*.

Short periodic orbits are easily drawn and enumerated—an example is drawn in figure 1.7—but it is rather hard to perceive the systematics of orbits from their configuration space shapes. In mechanics a trajectory is fully and uniquely specified by its position and momentum at a given instant, and no two distinct state space trajectories can intersect. Their projections onto arbitrary subspaces, however, can and do intersect, in rather unilluminating ways. In the pinball example the problem is that we are looking at the projections of a 4-dimensional state space trajectories onto a 2-dimensional subspace, the configuration space. A clearer picture of the dynamics is obtained by constructing a set of state space Poincaré sections.

Suppose that the pinball has just bounced off disk 1. Depending on its position and outgoing angle, it could proceed to either disk 2 or 3. Not much happens in between the bounces—the ball just travels at constant velocity along a straight line—so we can reduce the 4-dimensional flow to a 2-dimensional map P that takes the coordinates of the pinball from one disk edge to another disk edge. The trajectory just after the moment of impact is defined by s_n , the arc-length position of the n th bounce along the billiard wall, and $p_n = p \sin \phi_n$ the momentum component parallel to the billiard wall at the point of impact, see figure 1.9. Such section of a flow is called a *Poincaré section*. In terms of Poincaré sections, the dynamics is reduced to the set of six maps $P_{s_k \leftarrow s_j} : (s_n, p_n) \mapsto (s_{n+1}, p_{n+1})$, with $s \in \{1, 2, 3\}$,

example 3.2

Figure 1.9: The 3-disk game of pinball Poincaré section, trajectories emanating from the disk 1 with $x_0 = (s_0, p_0)$. (a) Strips of initial points \mathcal{M}_{12} , \mathcal{M}_{13} which reach disks 2, 3 in one bounce, respectively. (b) Strips of initial points \mathcal{M}_{121} , \mathcal{M}_{131} , \mathcal{M}_{132} and \mathcal{M}_{123} which reach disks 1, 2, 3 in two bounces, respectively. The Poincaré sections for trajectories originating on the other two disks are obtained by the appropriate relabeling of the strips. Disk radius : center separation ratio a:R = 1:2.5. (Y. Lan)



from the boundary of the disk j to the boundary of the next disk k .

section 8

Next, we mark in the Poincaré section those initial conditions which do not escape in one bounce. There are two strips of survivors, as the trajectories originating from one disk can hit either of the other two disks, or escape without further ado. We label the two strips \mathcal{M}_{12} , \mathcal{M}_{13} . Embedded within them there are four strips \mathcal{M}_{121} , \mathcal{M}_{123} , \mathcal{M}_{131} , \mathcal{M}_{132} of initial conditions that survive for two bounces, and so forth, see figures 1.8 and 1.9. Provided that the disks are sufficiently separated, after n bounces the survivors are divided into 2^n distinct strips: the \mathcal{M}_i th strip consists of all points with itinerary $i = s_1 s_2 s_3 \dots s_n$, $s = \{1, 2, 3\}$. The unstable cycles as a skeleton of chaos are almost visible here: each such patch contains a periodic point $\overline{s_1 s_2 s_3 \dots s_n}$ with the basic block infinitely repeated. Periodic points are skeletal in the sense that as we look further and further, the strips shrink but the periodic points stay put forever.

We see now why it pays to utilize a symbolic dynamics; it provides a navigation chart through chaotic state space. There exists a unique trajectory for every admissible infinite length itinerary, and a unique itinerary labels every trapped trajectory. For example, the only trajectory labeled by $\overline{12}$ is the 2-cycle bouncing along the line connecting the centers of disks 1 and 2; any other trajectory starting out as $12\dots$ either eventually escapes or hits the 3rd disk.

1.4.3 Escape rate

example 17.4

What is a good physical quantity to compute for the game of pinball? Such a system, for which almost any trajectory eventually leaves a finite region (the pinball table) never to return, is said to be open, or a *repeller*. The repeller *escape rate* is an eminently measurable quantity. An example of such a measurement would be an unstable molecular or nuclear state which can be well approximated by a classical potential with the possibility of escape in certain directions. In an experiment many projectiles are injected into a macroscopic ‘black box’ enclosing a microscopic non-confining short-range potential, and their mean escape rate is measured, as in figure 1.1. The numerical experiment might consist of injecting the pinball between the disks in some random direction and asking how many times the pinball bounces on the average before it escapes the region between the disks.

exercise 1.2

For a theorist, a good game of pinball consists in predicting accurately the asymptotic lifetime (or the escape rate) of the pinball. We now show how periodic orbit theory accomplishes this for us. Each step will be so simple that you can follow even at the cursory pace of this overview, and still the result is surprisingly elegant.

Consider figure 1.9 again. In each bounce the initial conditions get thinned out, yielding twice as many thin strips as at the previous bounce. The total area that remains at a given time is the sum of the areas of the strips, so that the fraction of survivors after n bounces, or the *survival probability* is given by

$$\begin{aligned}\hat{\Gamma}_1 &= \frac{|\mathcal{M}_0|}{|\mathcal{M}|} + \frac{|\mathcal{M}_1|}{|\mathcal{M}|}, & \hat{\Gamma}_2 &= \frac{|\mathcal{M}_{00}|}{|\mathcal{M}|} + \frac{|\mathcal{M}_{10}|}{|\mathcal{M}|} + \frac{|\mathcal{M}_{01}|}{|\mathcal{M}|} + \frac{|\mathcal{M}_{11}|}{|\mathcal{M}|}, \\ \hat{\Gamma}_n &= \frac{1}{|\mathcal{M}|} \sum_i^{(n)} |\mathcal{M}_i|,\end{aligned}\tag{1.2}$$

where i is a label of the i th strip, $|\mathcal{M}|$ is the initial area, and $|\mathcal{M}_i|$ is the area of the i th strip of survivors. $i = 01, 10, 11, \dots$ is a label, not a binary number. Since at each bounce one routinely loses about the same fraction of trajectories, one expects the sum (1.2) to fall off exponentially with n and tend to the limit

chapter 22

$$\hat{\Gamma}_{n+1}/\hat{\Gamma}_n = e^{-\gamma_n} \rightarrow e^{-\gamma}.\tag{1.3}$$

The quantity γ is called the *escape rate* from the repeller.

1.5 Chaos for cyclists

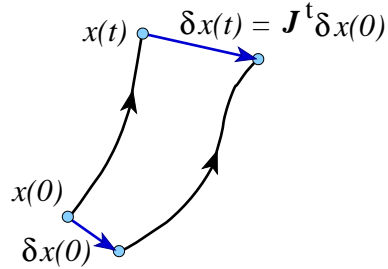
Étant données des équations ... et une solution particulière quelconque de ces équations, on peut toujours trouver une solution périodique (dont la période peut, il est vrai, être très longue), telle que la différence entre les deux solutions soit aussi petite qu'on le veut, pendant un temps aussi long qu'on le veut. D'ailleurs, ce qui nous rend ces solutions périodiques si précieuses, c'est qu'elles sont, pour ainsi dire, la seule brèche par où nous puissions essayer de pénétrer dans une place jusqu'ici réputée inabordable.

—H. Poincaré, *Les méthodes nouvelles de la mécanique céleste*

We shall now show that the escape rate γ can be extracted from a highly convergent *exact* expansion by reformulating the sum (1.2) in terms of unstable periodic orbits.

If, when asked what the 3-disk escape rate is for a disk of radius 1, center-center separation 6, velocity 1, you answer that the continuous time escape rate is roughly $\gamma = 0.4103384077693464893384613078192\dots$, you do not need this book. If you have no clue, hang on.

Figure 1.10: The Jacobian matrix J^t maps an infinitesimal displacement δx at x_0 into a displacement $J^t(x_0)\delta x$ finite time t later.



1.5.1 How big is my neighborhood?

Not only do the periodic points keep track of topological ordering of the strips, but, as we shall now show, they also determine their size. As a trajectory evolves, it carries along and distorts its infinitesimal neighborhood. Let

$$x(t) = f^t(x_0)$$

denote the trajectory of an initial point $x_0 = x(0)$. Expanding $f^t(x_0 + \delta x_0)$ to linear order, the evolution of the distance to a neighboring trajectory $x(t) + \delta x(t)$ is given by the Jacobian matrix J :

$$\delta x_i(t) = \sum_{j=1}^d J^t(x_0)_{ij} \delta x_{0j}, \quad J^t(x_0)_{ij} = \frac{\partial x_i(t)}{\partial x_{0j}}. \quad (1.4)$$

A trajectory of a pinball moving on a flat surface is specified by two position coordinates and the direction of motion, so in this case $d = 3$. Evaluation of a cycle Jacobian matrix is a long exercise - here we just state the result. The Jacobian matrix describes the deformation of an infinitesimal neighborhood of $x(t)$ along the flow; its eigenvectors and eigenvalues give the directions and the corresponding rates of expansion or contraction, figure 1.10. The trajectories that start out in an infinitesimal neighborhood separate along the unstable directions (those whose eigenvalues are greater than unity in magnitude), approach each other along the stable directions (those whose eigenvalues are less than unity in magnitude), and maintain their distance along the marginal directions (those whose eigenvalues equal unity in magnitude).

section 8.2

In our game of pinball the beam of neighboring trajectories is defocused along the unstable eigen-direction of the Jacobian matrix J .

As the heights of the strips in figure 1.9 are effectively constant, we can concentrate on their thickness. If the height is $\approx L$, then the area of the i th strip is $\mathcal{M}_i \approx Ll_i$ for a strip of width l_i .

Each strip i in figure 1.9 contains a periodic point x_i . The finer the intervals, the smaller the variation in flow across them, so the contribution from the strip

of width l_i is well-approximated by the contraction around the periodic point x within the interval,

$$l_i = a_i/|\Lambda_i|, \quad (1.5)$$

where Λ_i is the unstable eigenvalue of the Jacobian matrix $J(x_i)$ evaluated at the i th periodic point for $t = T_p$, the full period (due to the low dimensionality, the Jacobian can have at most one unstable eigenvalue). Only the magnitude of this eigenvalue matters, we can disregard its sign. The prefactors a reflect the overall size of the system and the particular distribution of starting values of x . As the asymptotic trajectories are strongly mixed by bouncing chaotically around the repeller, we expect their distribution to be insensitive to smooth variations in the distribution of initial points.

section 16.4

To proceed with the derivation we need the *hyperbolicity* assumption: for large n the prefactors $a_i \approx O(1)$ are overwhelmed by the exponential growth of Λ_i , so we neglect them. If the hyperbolicity assumption is justified, we can replace $|\mathcal{M}_i| \approx Ll_i$ in (1.2) by $1/|\Lambda_i|$ and consider the sum

section 18.1.1

$$\Gamma_n = \sum_i^{(n)} 1/|\Lambda_i|,$$

where the sum goes over all periodic points of period n . We now define a generating function for sums over all periodic orbits of all lengths:

$$\Gamma(z) = \sum_{n=1}^{\infty} \Gamma_n z^n. \quad (1.6)$$

Recall that for large n the n th level sum (1.2) tends to the limit $\Gamma_n \rightarrow e^{-n\gamma}$, so the escape rate γ is determined by the smallest $z = e^\gamma$ for which (1.6) diverges:

$$\Gamma(z) \approx \sum_{n=1}^{\infty} (ze^{-\gamma})^n = \frac{ze^{-\gamma}}{1 - ze^{-\gamma}}. \quad (1.7)$$

This is the property of $\Gamma(z)$ that motivated its definition. Next, we devise a formula for (1.6) expressing the escape rate in terms of periodic orbits:

$$\begin{aligned} \Gamma(z) &= \sum_{n=1}^{\infty} z^n \sum_i^{(n)} |\Lambda_i|^{-1} \\ &= \frac{z}{|\Lambda_0|} + \frac{z}{|\Lambda_1|} + \frac{z^2}{|\Lambda_{00}|} + \frac{z^2}{|\Lambda_{01}|} + \frac{z^2}{|\Lambda_{10}|} + \frac{z^2}{|\Lambda_{11}|} \\ &\quad + \frac{z^3}{|\Lambda_{000}|} + \frac{z^3}{|\Lambda_{001}|} + \frac{z^3}{|\Lambda_{010}|} + \frac{z^3}{|\Lambda_{100}|} + \dots \end{aligned} \quad (1.8)$$

For sufficiently small z this sum is convergent. The escape rate γ is now given by the leading pole of (1.7), rather than by a numerical extrapolation of a sequence of γ_n extracted from (1.3). As any finite truncation $n < n_{\text{trunc}}$ of (1.8) is a polynomial in z , convergent for any z , finding this pole requires that we know something about Γ_n for any n , and that might be a tall order. section 18.3

We could now proceed to estimate the location of the leading singularity of $\Gamma(z)$ from finite truncations of (1.8) by methods such as Padé approximants. However, as we shall now show, it pays to first perform a simple resummation that converts this divergence into a *zero* of a related function.

1.5.2 Dynamical zeta function

If a trajectory retraces a *prime* cycle r times, its expanding eigenvalue is Λ_p^r . A prime cycle p is a single traversal of the orbit; its label is a non-repeating symbol string of n_p symbols. There is only one prime cycle for each cyclic permutation class. For example, $p = \overline{0011} = \overline{1001} = \overline{1100} = \overline{0110}$ is prime, but $\overline{0101} = \overline{01}$ is not.

By the chain rule for derivatives the stability of a cycle is the same everywhere along the orbit, so each prime cycle of length n_p contributes n_p terms to the sum (1.8). Hence (1.8) can be rewritten as exercise 15.2
section 4.5

$$\Gamma(z) = \sum_p n_p \sum_{r=1}^{\infty} \left(\frac{z^{n_p}}{|\Lambda_p|} \right)^r = \sum_p \frac{n_p t_p}{1 - t_p}, \quad t_p = \frac{z^{n_p}}{|\Lambda_p|} \quad (1.9)$$

where the index p runs through all distinct *prime* cycles. Note that we have resummed the contribution of the cycle p to all times, so truncating the summation up to given p is *not* a finite time $n \leq n_p$ approximation, but an asymptotic, *infinite* time estimate based by approximating stabilities of all cycles by a finite number of the shortest cycles and their repeats. The $n_p z^{n_p}$ factors in (1.9) suggest rewriting the sum as a derivative

$$\Gamma(z) = -z \frac{d}{dz} \sum_p \ln(1 - t_p).$$

Hence $\Gamma(z)$ is a logarithmic derivative of the infinite product

$$1/\zeta(z) = \prod_p (1 - t_p), \quad t_p = \frac{z^{n_p}}{|\Lambda_p|}. \quad (1.10)$$

This function is called the *dynamical zeta function*, in analogy to the Riemann zeta function, which motivates the ‘zeta’ in its definition as $1/\zeta(z)$. This is the prototype formula of periodic orbit theory. The zero of $1/\zeta(z)$ is a pole of $\Gamma(z)$, and the problem of estimating the asymptotic escape rates from finite n sums such as (1.2) is now reduced to a study of the zeros of the dynamical zeta function

(1.10). The escape rate is related by (1.7) to a divergence of $\Gamma(z)$, and $\Gamma(z)$ diverges whenever $1/\zeta(z)$ has a zero.

section 22.1
section 19.4

Easy, you say: “Zeros of (1.10) can be read off the formula, a zero

$$z_p = |\Lambda_p|^{1/n_p}$$

for each term in the product. What’s the problem?” Dead wrong!

1.5.3 Cycle expansions

How are formulas such as (1.10) used? We start by computing the lengths and eigenvalues of the shortest cycles. This usually requires some numerical work, such as the Newton method searches for periodic solutions; we shall assume that the numerics are under control, and that *all* short cycles up to given length have been found. In our pinball example this can be done by elementary geometrical optics. It is very important not to miss any short cycles, as the calculation is as accurate as the shortest cycle dropped—including cycles longer than the shortest omitted does not improve the accuracy (unless exponentially many more cycles are included). The result of such numerics is a table of the shortest cycles, their periods and their stabilities.

chapter 13

section 29.3

Now expand the infinite product (1.10), grouping together the terms of the same total symbol string length

$$\begin{aligned} 1/\zeta &= (1 - t_0)(1 - t_1)(1 - t_{10})(1 - t_{100}) \cdots \\ &= 1 - t_0 - t_1 - [t_{10} - t_1 t_0] - [(t_{100} - t_{10} t_0) + (t_{101} - t_{10} t_1)] \\ &\quad - [(t_{1000} - t_0 t_{100}) + (t_{1110} - t_1 t_{110}) \\ &\quad + (t_{1001} - t_1 t_{001} - t_{101} t_0 + t_{10} t_0 t_1)] - \dots \end{aligned} \tag{1.11}$$

The virtue of the expansion is that the sum of all terms of the same total length n (grouped in brackets above) is a number that is exponentially smaller than a typical term in the sum, for geometrical reasons we explain in the next section.

chapter 20

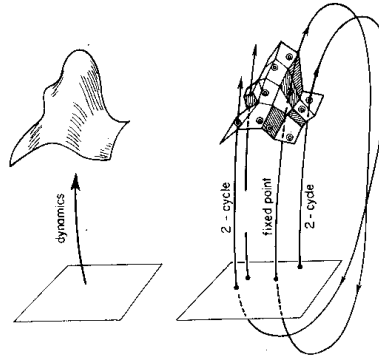
section 20.1

The calculation is now straightforward. We substitute a finite set of the eigenvalues and lengths of the shortest prime cycles into the cycle expansion (1.11), and obtain a polynomial approximation to $1/\zeta$. We then vary z in (1.10) and determine the escape rate γ by finding the smallest $z = e^\gamma$ for which (1.11) vanishes.

1.5.4 Shadowing

When you actually start computing this escape rate, you will find out that the convergence is very impressive: only three input numbers (the two fixed points $\bar{0}$,

Figure 1.11: Approximation to a smooth dynamics (left frame) by the skeleton of periodic points, together with their linearized neighborhoods, (right frame). Indicated are segments of two 1-cycles and a 2-cycle that alternates between the neighborhoods of the two 1-cycles, shadowing first one of the two 1-cycles, and then the other.



$\bar{1}$ and the 2-cycle $\overline{10}$) already yield the pinball escape rate to 3-4 significant digits! We have omitted an infinity of unstable cycles; so why does approximating the dynamics by a finite number of the shortest cycle eigenvalues work so well?

section 20.2.2

The convergence of cycle expansions of dynamical zeta functions is a consequence of the smoothness and analyticity of the underlying flow. Intuitively, one can understand the convergence in terms of the geometrical picture sketched in figure 1.11; the key observation is that the long orbits are *shadowed* by sequences of shorter orbits.

A typical term in (1.11) is a difference of a long cycle $\{ab\}$ minus its shadowing approximation by shorter cycles $\{a\}$ and $\{b\}$

$$t_{ab} - t_a t_b = t_{ab}(1 - t_a t_b / t_{ab}) = t_{ab} \left(1 - \left| \frac{\Lambda_{ab}}{\Lambda_a \Lambda_b} \right| \right), \quad (1.12)$$

where a and b are symbol sequences of the two shorter cycles. If all orbits are weighted equally ($t_p = z^{n_p}$), such combinations cancel exactly; if orbits of similar symbolic dynamics have similar weights, the weights in such combinations almost cancel.

This can be understood in the context of the pinball game as follows. Consider orbits $\bar{0}$, $\bar{1}$ and $\overline{01}$. The first corresponds to bouncing between any two disks while the second corresponds to bouncing successively around all three, tracing out an equilateral triangle. The cycle $\overline{01}$ starts at one disk, say disk 2. It then bounces from disk 3 back to disk 2 then bounces from disk 1 back to disk 2 and so on, so its itinerary is $\underline{2321}$. In terms of the bounce types shown in figure 1.6, the trajectory is alternating between 0 and 1. The incoming and outgoing angles when it executes these bounces are very close to the corresponding angles for 0 and 1 cycles. Also the distances traversed between bounces are similar so that the 2-cycle expanding eigenvalue Λ_{01} is close in magnitude to the product of the 1-cycle eigenvalues $\Lambda_0 \Lambda_1$.

To understand this on a more general level, try to visualize the partition of a chaotic dynamical system's state space in terms of cycle neighborhoods as a tessellation (a tiling) of the dynamical system, with smooth flow approximated by its periodic orbit skeleton, each 'tile' centered on a periodic point, and the scale

of the ‘tile’ determined by the linearization of the flow around the periodic point, as illustrated by figure 1.11.

The orbits that follow the same symbolic dynamics, such as $\{ab\}$ and a ‘pseudo orbit’ $\{a\}\{b\}$, lie close to each other in state space; long shadowing pairs have to start out exponentially close to beat the exponential growth in separation with time. If the weights associated with the orbits are multiplicative along the flow (for example, by the chain rule for products of derivatives) and the flow is smooth, the term in parenthesis in (1.12) falls off exponentially with the cycle length, and therefore the curvature expansions are expected to be highly convergent.

chapter 23

1.6 Change in time

The above derivation of the dynamical zeta function formula for the escape rate has one shortcoming; it estimates the fraction of survivors as a function of the number of pinball bounces, but the physically interesting quantity is the escape rate measured in units of continuous time. For continuous time flows, the escape rate (1.2) is generalized as follows. Define a finite state space region \mathcal{M} such that a trajectory that exits \mathcal{M} never reenters. For example, any pinball that falls off the edge of a pinball table in figure 1.1 is gone forever. Start with a uniform distribution of initial points. The fraction of initial x whose trajectories remain within \mathcal{M} at time t is expected to decay exponentially

$$\Gamma(t) = \frac{\int_{\mathcal{M}} dx dy \delta(y - f^t(x))}{\int_{\mathcal{M}} dx} \rightarrow e^{-\gamma t}.$$

The integral over x starts a trajectory at every $x \in \mathcal{M}$. The integral over y tests whether this trajectory is still in \mathcal{M} at time t . The kernel of this integral

$$\mathcal{L}^t(y, x) = \delta(y - f^t(x)) \quad (1.13)$$

is the Dirac delta function, as for a deterministic flow the initial point x maps into a unique point y at time t . For discrete time, $f^n(x)$ is the n th iterate of the map f . For continuous flows, $f^t(x)$ is the trajectory of the initial point x , and it is appropriate to express the finite time kernel \mathcal{L} in terms of \mathcal{A} , the generator of infinitesimal time translations

$$\mathcal{L}^t = e^{t\mathcal{A}},$$

section 16.6

very much in the way the quantum evolution is generated by the Hamiltonian H , the generator of infinitesimal time quantum transformations.

As the kernel \mathcal{L} is the key to everything that follows, we shall give it a name, and refer to it and its generalizations as the *evolution operator* for a d -dimensional map or a d -dimensional flow.

$$\begin{aligned} \text{tr} \mathcal{L}^t &= \sum_{x_0}^{\infty} e^{-\lambda x_0 t} && \text{MIGHT DIVERGE!} \\ &= \int_V dx \mathcal{L}^t(x, x) \\ &= \sum_p \int_{V_p} dx \mathcal{L}^t(x, x) = \sum_p \sum_{r=1}^{\infty} \frac{\delta(t - rT_p)}{|\det(\mathbf{1} - M_p^r)|} \\ &= \sum_{\text{primes}} \sum_{\text{repeats}} \int_{V_p} dx \mathcal{L}^t(x, x) \end{aligned}$$

Figure 1.12: The trace of an evolution operator is concentrated in tubes around prime cycles, of length T_p and thickness $1/|\Lambda_p|^r$ for the r th repetition of the prime cycle p .

The number of periodic points increases exponentially with the cycle length (in the case at hand, as 2^n). As we have already seen, this exponential proliferation of cycles is not as dangerous as it might seem; as a matter of fact, all our computations will be carried out in the $n \rightarrow \infty$ limit. Though a quick look at long-time density of trajectories might reveal it to be complex beyond belief, this distribution is still generated by a simple deterministic law, and with some luck and insight, our labeling of possible motions will reflect this simplicity. If the rule that gets us from one level of the classification hierarchy to the next does not depend strongly on the level, the resulting hierarchy is approximately self-similar. We now turn such approximate self-similarity to our advantage, by turning it into an operation, the action of the evolution operator, whose iteration encodes the self-similarity.

1.6.1 Trace formula

In physics, when we do not understand something, we give it a name.

—Matthias Neubert

Recasting dynamics in terms of evolution operators changes everything. So far our formulation has been heuristic, but in the evolution operator formalism the escape rate and any other dynamical average are given by exact formulas, extracted from the spectra of evolution operators. The key tools are *trace formulas* and *spectral determinants*.

The trace of an operator is given by the sum of its eigenvalues. The explicit expression (1.13) for $\mathcal{L}^t(x, y)$ enables us to evaluate the trace. Identify y with x and integrate x over the whole state space. The result is an expression for $\text{tr} \mathcal{L}$ as a sum over neighborhoods of prime cycles p and their repetitions

section 18.2

$$\text{tr} \mathcal{L}^t = \sum_p T_p \sum_{r=1}^{\infty} \frac{\delta(t - rT_p)}{|\det(\mathbf{1} - M_p^r)|}, \tag{1.14}$$

where T_p is the period of prime cycle p , and the monodromy matrix M_p is the flow-transverse part of Jacobian matrix J (1.4). This formula has a simple geometrical interpretation sketched in figure 1.12. After the r th return to a Poincaré

section, the initial tube \mathcal{M}_p has been stretched out along the expanding eigen-directions, with the overlap with the initial volume given by $1/|\det(\mathbf{1} - M_p^r)| \rightarrow 1/|\Lambda_p|$, the same weight we obtained heuristically in sect. 1.5.1.

The ‘spiky’ sum (1.14) is disquieting in the way reminiscent of the Poisson resummation formulas of Fourier analysis; the left-hand side is the smooth eigenvalue sum $\text{tr } e^{\mathcal{A}t} = \sum e^{s_\alpha t}$, while the right-hand side equals zero everywhere except for the set $t = rT_p$. A Laplace transform smooths the sum over Dirac delta functions in cycle periods and yields the *trace formula* for the eigenspectrum \mathfrak{s}, s_1, \dots of the classical evolution operator:

chapter 18

$$\int_{0_+}^{\infty} dt e^{-st} \text{tr } \mathcal{L}^t = \text{tr} \frac{1}{s - \mathcal{A}} = \sum_{\alpha=0}^{\infty} \frac{1}{s - s_\alpha} = \sum_p T_p \sum_{r=1}^{\infty} \frac{e^{r(\beta \cdot A_p - sT_p)}}{|\det(\mathbf{1} - M_p^r)|}. \quad (1.15)$$

The beauty of trace formulas lies in the fact that everything on the right-hand-side—prime cycles p , their periods T_p and the eigenvalues of M_p —is an invariant property of the flow, independent of any coordinate choice.

1.6.2 Spectral determinant

The eigenvalues of a linear operator are given by the zeros of the appropriate determinant. One way to evaluate determinants is to expand them in terms of traces, using the identities

exercise 4.1

$$\frac{d}{ds} \ln \det(s - \mathcal{A}) = \text{tr} \frac{d}{ds} \ln(s - \mathcal{A}) = \text{tr} \frac{1}{s - \mathcal{A}}, \quad (1.16)$$

and integrating over s . In this way the *spectral determinant* of an evolution operator becomes related to the traces that we have just computed:

chapter 19

$$\det(s - \mathcal{A}) = \exp \left(- \sum_p \sum_{r=1}^{\infty} \frac{1}{r} \frac{e^{-sT_p r}}{|\det(\mathbf{1} - M_p^r)|} \right). \quad (1.17)$$

The $1/r$ factor is due to the s integration, leading to the replacement $T_p \rightarrow T_p/rT_p$ in the periodic orbit expansion (1.15).

section 19.5

We have now retraced the heuristic derivation of the divergent sum (1.7) and the dynamical zeta function (1.10), but this time with no approximations: formula (1.17) is *exact*. The computation of the zeros of $\det(s - \mathcal{A})$ proceeds very much like the computations of sect. 1.5.3.

1.7 From chaos to statistical mechanics

Under heaven, all is chaos. The situation is excellent!
— Chairman Mao Zedong, a letter to Jiang Qing

The replacement of individual trajectories by evolution operators which propagate densities feels like a bit of mathematical voodoo. Nevertheless, something very radical and deeply foundational has taken place. Understanding the distinction between evolution of individual trajectories and the evolution of the densities of trajectories is key to understanding statistical mechanics—this is the conceptual basis of the second law of thermodynamics, and the origin of irreversibility of the arrow of time for deterministic systems with time-reversible equations of motion: reversibility is attainable for distributions whose measure in the space of density functions goes exponentially to zero with time.

Consider a chaotic flow, such as the stirring of red and white paint by some deterministic machine. *If* we were able to track individual trajectories, the fluid would forever remain a striated combination of pure white and pure red; there would be no pink. What is more, if we reversed the stirring, we would return to the perfect white/red separation. However, that cannot be—in a very few turns of the stirring stick the thickness of the layers goes from centimeters to Ångströms, and the result is irreversibly pink.

A century ago it seemed reasonable to assume that statistical mechanics applies only to systems with very many degrees of freedom. More recent is the realization that much of statistical mechanics follows from chaotic dynamics, and already at the level of a few degrees of freedom the evolution of densities is irreversible. Furthermore, the theory that we shall develop here generalizes notions of ‘measure’ and ‘averaging’ to systems far from equilibrium, and transports us into regions hitherto inaccessible with the tools of equilibrium statistical mechanics.

By going to a description in terms of the asymptotic time evolution operators we give up tracking individual trajectories for long times, but trade in the uncontrollable trajectories for a powerful description of the asymptotic trajectory densities. This will enable us, for example, to give exact formulas for transport coefficients such as the diffusion constants without *any* probabilistic assumptions. The classical Boltzmann equation for evolution of 1-particle density is based on *stosszahlansatz*, neglect of particle correlations prior to, or after a 2-particle collision. It is a very good approximate description of dilute gas dynamics, but a difficult starting point for inclusion of systematic corrections. In the theory developed here, no correlations are neglected - they are all included in the cycle averaging formulas such as the cycle expansion for the diffusion constant $2dD = \lim_{T \rightarrow \infty} \langle x(T)^2 \rangle / T$ of a particle diffusing chaotically across a spatially-periodic array,

chapter 25

section 25.1

$$D = \frac{1}{2d} \frac{1}{\langle T \rangle_\zeta} \sum' (-1)^{k+1} \frac{(\hat{n}_{p_1} + \dots + \hat{n}_{p_k})^2}{|\Lambda_{p_1} \dots \Lambda_{p_k}|}, \quad (1.18)$$

where \hat{n}_p is a translation along one period of a spatially periodic ‘runaway’ trajectory p . Such formulas are *exact*; the issue in their applications is what are the most effective schemes of estimating the infinite cycle sums required for their evaluation. Unlike most statistical mechanics, here there are no phenomenological macroscopic parameters; quantities such as transport coefficients are calculable to any desired accuracy from the microscopic dynamics.

The concepts of equilibrium statistical mechanics do help us, however, to understand the ways in which the simple-minded periodic orbit theory falters. A non-hyperbolicity of the dynamics manifests itself in power-law correlations and even ‘phase transitions.’

chapter 24

1.8 Chaos: what is it good for?

Happy families are all alike; every unhappy family is unhappy in its own way.

— *Anna Karenina*, by Leo Tolstoy

With initial data accuracy $\delta x = |\delta \mathbf{x}(0)|$ and system size L , a trajectory is predictable only up to the *finite* Lyapunov time (1.1), $T_{\text{Lyap}} \approx \lambda^{-1} \ln |L/\delta x|$. Beyond that, chaos rules. And so the most successful applications of ‘chaos theory’ have so far been to problems where observation time is much longer than a typical ‘turnover’ time, such as statistical mechanics, quantum mechanics, and questions of long term stability in celestial mechanics, where the notion of tracking accurately a given state of the system is nonsensical.

So what is chaos good for? *Transport!* Though superficially indistinguishable from the probabilistic random walk diffusion, in low dimensional settings the deterministic diffusion is quite recognizable, through the fractal dependence of the diffusion constant on the system parameters, and perhaps through non-Gaussian relaxation to equilibrium (non-vanishing Burnett coefficients).

Several tabletop experiments that could measure transport on macroscopic scales are sketched in figure 1.13 (each a tabletop, but an expensive tabletop). Figure 1.13 (a) depicts a ‘slanted washboard;’ a particle in a gravity field bouncing down the washboard, losing some energy at each bounce, or a charged particle in a constant electric field trickling across a periodic condensed-matter device. The interplay between chaotic dynamics and energy loss results in a terminal mean velocity/conductance, a function of the washboard slant or external electric field that the periodic theory can predict accurately. Figure 1.13 (b) depicts a ‘cold atom lattice’ of very accurate spatial periodicity, with a dilute cloud of atoms placed onto a standing wave established by strong laser fields. Interaction of gravity with gentle time-periodic jiggling of the EM fields induces a diffusion of the atomic cloud, with a diffusion constant predicted by the periodic orbit theory. Figure 1.13 (c) depicts a tip of an atomic force microscope (AFM) bouncing against a periodic atomic surface moving at a constant velocity. The frictional drag experienced is the interplay of the chaotic bouncing of the tip and the energy loss at each

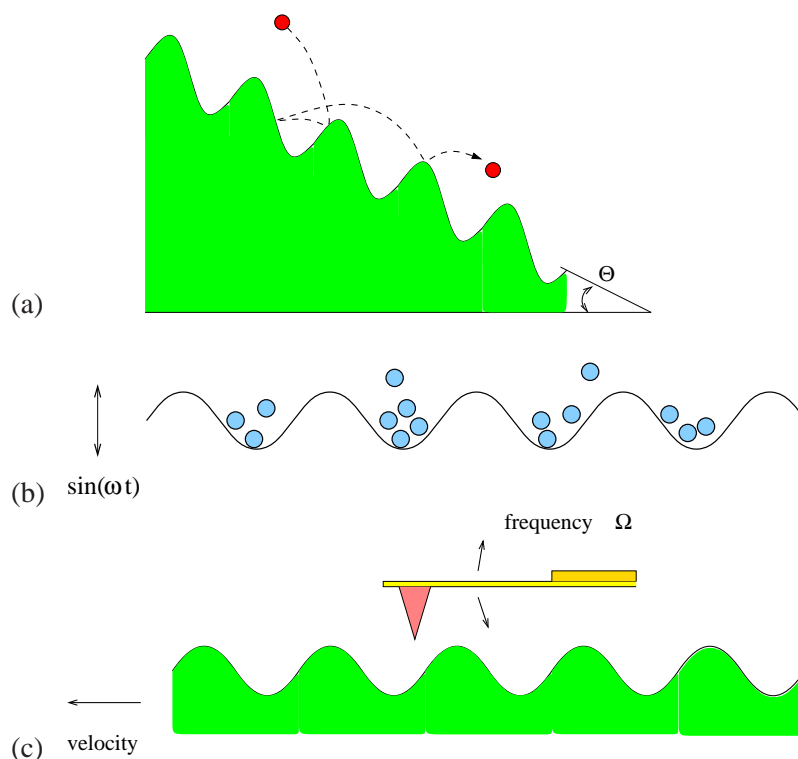


Figure 1.13: (a) Washboard mean velocity, (b) cold atom lattice diffusion, and (c) AFM tip drag force. (Y. Lan)

tip/surface collision, accurately predicted by the periodic orbit theory. None of these experiments have actually been carried out, (save for some numerical experimentation), but are within reach of what can be measured today.

ChaosBook.org/projects

Given microscopic dynamics, periodic orbit theory predicts observable macroscopic transport quantities such as the washboard mean velocity, cold atom lattice diffusion constant, and AFM tip drag force. But the experimental proposal is sexier than that, and goes into the heart of dynamical systems theory.

remark A.1

Smale 1960s theory of the hyperbolic structure of the non-wandering set (AKA ‘horseshoe’) was motivated by his ‘structural stability’ conjecture, which - in non-technical terms - asserts that all trajectories of a chaotic dynamical system deform smoothly under small variations of system parameters.

Why this cannot be true for a system like the washboard in figure 1.13 (a) is easy to see for a cyclist. Take a trajectory which barely grazes the tip of one of the groves. An arbitrarily small change in the washboard slope can result in loss of this collision, change a forward scattering into a backward scattering, and lead to a discontinuous contribution to the mean velocity. You might hold out hope that such events are rare and average out, but not so - a loss of a short cycle leads to a significant change in the cycle-expansion formula for a transport coefficient, such as (1.18).

When we write an equation, it is typically parameterized by a set of parameters by as coupling strengths, and we think of dynamical systems obtained by a smooth variation of a parameter as a ‘family.’ We would expect measurable predictions to also vary smoothly, i.e., be ‘structurally stable.’

But dynamical systems families are ‘families’ only in a name. That the structural stability conjecture turned out to be badly wrong is, however, not a blow for chaotic dynamics. Quite to the contrary, it is actually a virtue, perhaps the most dramatic experimentally measurable prediction of chaotic dynamics.

section 12.2

As long as microscopic periodicity is exact, the prediction is counterintuitive for a physicist - transport coefficients are *not* smooth functions of system parameters, rather they are non-monotonic, *nowhere differentiable* functions. Conversely, if the macroscopic measurement yields a smooth dependence of the transport on system parameters, the periodicity of the microscopic lattice is degraded by impurities, and probabilistic assumptions of traditional statistical mechanics apply. So the proposal is to –by measuring *macroscopic transport*– conductance, diffusion, drag –observe determinism on *nanoscales*, and –for example– determine whether an atomic surface is clean.

section 25.2

The signatures of deterministic chaos are even more baffling to an engineer: a small increase of pressure across a pipe exhibiting turbulent flow does not necessarily lead to an increase in the mean flow; mean flow dependence on pressure drop across the pipe is also a fractal function.

Is this in contradiction with the traditional statistical mechanics? No - deterministic chaos predictions are valid in settings where a few degrees of freedom are important, and chaotic motion time and space scales are commensurate with the external driving and spatial scales. Further degrees of freedom act as noise that smooths out the above fractal effects and restores a smooth functional dependence of transport coefficients on external parameters.

1.9 What is not in ChaosBook

There is only one thing which interests me vitally now, and that is the recording of all that which is omitted in books. Nobody, as far as I can see, is making use of those elements in the air which give direction and motivation to our lives.

— Henry Miller, *Tropic of Cancer*

This book offers everyman a breach into a domain hitherto reputed unreachable, a domain traditionally traversed only by mathematical physicists and mathematicians. What distinguishes it from mathematics is the insistence on computability and numerical convergence of methods offered. A rigorous proof, the end of the story as far as a mathematician is concerned, might state that in a given setting, for times in excess of 10^{32} years, turbulent dynamics settles onto an attractor of dimension less than 600. Such a theorem is of a little use to an honest, hard-working plumber, especially if her hands-on experience is that within the span of a few typical ‘turnaround’ times the dynamics seems to settle on a (transient?) attractor of dimension less than 3. If rigor, magic, fractals or brains is your thing, read remark 1.4 and beyond.

So, no proofs! but lot of hands-on plumbing ahead.

Many a chapter alone could easily grow to a book size if unchecked: the nuts and bolt of the theory include ODEs, PDEs, stochastic ODEs, path integrals, group theory, coding theory, graph theory, ergodic theory, linear operator theory, quantum mechanics, etc.. We include material into the text proper on ‘need-to-know’ basis, relegate technical details to appendices, and give pointers to further reading in the remarks at the end of each chapter.

Résumé

This text is an exposition of the best of all possible theories of deterministic chaos, and the strategy is: 1) count, 2) weigh, 3) add up.

In a chaotic system any open ball of initial conditions, no matter how small, will spread over the entire accessible state space. Hence the theory focuses on describing the geometry of the space of possible outcomes, and evaluating averages over this space, rather than attempting the impossible: precise prediction of individual trajectories. The dynamics of densities of trajectories is described in terms of evolution operators. In the evolution operator formalism the dynamical averages are given by exact formulas, extracted from the spectra of evolution operators. The key tools are *trace formulas* and *spectral determinants*.

The theory of evaluation of the spectra of evolution operators presented here is based on the observation that the motion in dynamical systems of few degrees of freedom is often organized around a few *fundamental* cycles. These short cycles capture the skeletal topology of the motion on a strange attractor/repeller in the sense that any long orbit can approximately be pieced together from the nearby periodic orbits of finite length. This notion is made precise by approximating orbits by prime cycles, and evaluating the associated curvatures. A curvature measures the deviation of a longer cycle from its approximation by shorter cycles; smoothness and the local instability of the flow implies exponential (or faster) fall-off for (almost) all curvatures. Cycle expansions offer an efficient method for evaluating classical and quantum observables.

The critical step in the derivation of the dynamical zeta function was the hyperbolicity assumption, i.e., the assumption of exponential shrinkage of all strips of the pinball repeller. By dropping the a_i prefactors in (1.5), we have given up on any possibility of recovering the precise distribution of starting x (which should anyhow be impossible due to the exponential growth of errors), but in exchange we gain an effective description of the asymptotic behavior of the system. The pleasant surprise of cycle expansions (1.10) is that the infinite time behavior of an unstable system is as easy to determine as the short time behavior.

To keep the exposition simple we have here illustrated the utility of cycles and their curvatures by a pinball game, but topics covered in ChaosBook – unstable flows, Poincaré sections, Smale horseshoes, symbolic dynamics, pruning,

discrete symmetries, periodic orbits, averaging over chaotic sets, evolution operators, dynamical zeta functions, spectral determinants, cycle expansions, quantum trace formulas, zeta functions, and so on to the semiclassical quantization of helium – should give the reader some confidence in the broad sway of the theory. The formalism should work for any average over any chaotic set which satisfies two conditions:

1. the weight associated with the observable under consideration is multiplicative along the trajectory,
2. the set is organized in such a way that the nearby points in the symbolic dynamics have nearby weights.

The theory is applicable to evaluation of a broad class of quantities characterizing chaotic systems, such as the escape rates, Lyapunov exponents, transport coefficients and quantum eigenvalues. A big surprise is that the semi-classical quantum mechanics of systems classically chaotic is very much like the classical mechanics of chaotic systems; both are described by zeta functions and cycle expansions of the same form, with the same dependence on the topology of the classical flow.

But the power of instruction is seldom of much efficacy, except in those happy dispositions where it is almost superfluous.

—Gibbon

Commentary

Remark 1.1 Nonlinear dynamics texts. This text aims to bridge the gap between the physics and mathematics dynamical systems literature. The intended audience is Henri Roux, the perfect physics graduate student with a theoretical bent who does not believe anything he is told. As a complementary presentation we recommend Gaspard’s monograph [8] which covers much of the same ground in a highly readable and scholarly manner.

As far as the prerequisites are concerned—ChaosBook is not an introduction to nonlinear dynamics. Nonlinear science requires a one semester basic course (advanced undergraduate or first year graduate). A good start is the textbook by Strogatz [9], an introduction to the applied mathematician’s visualization of flows, fixed points, manifolds, bifurcations. It is the most accessible introduction to nonlinear dynamics—a book on differential equations in nonlinear disguise, and its broadly chosen examples and many exercises make it a favorite with students. It is not strong on chaos. There the textbook of Alligood, Sauer and Yorke [10] is preferable: an elegant introduction to maps, chaos, period doubling, symbolic dynamics, fractals, dimensions—a good companion to ChaosBook. Introduction more comfortable to physicists is the textbook by Ott [11], with the baker’s map used to illustrate many key techniques in analysis of chaotic systems. Ott is perhaps harder than the above two as first books on nonlinear dynamics. Sprott [12] and Jackson [13] textbooks are very useful compendia of the ’70s and onward ‘chaos’ literature which we, in the spirit of promises made in sect. 1.1, tend to pass over in silence.

An introductory course should give students skills in qualitative and numerical analysis of dynamical systems for short times (trajectories, fixed points, bifurcations) and familiarize them with Cantor sets and symbolic dynamics for chaotic systems. For the dynamical systems material covered here in chapters 2 to 4, as well as for the in-depth study of bifurcation theory we warmly recommend Kuznetsov [14]. A good introduction to numerical experimentation with physically realistic systems is Tufillaro, Abbott, and Reilly [15]. Korsch and Jodl [16] and Nusse and Yorke [17] also emphasize hands-on approach to dynamics. With this, and a graduate level-exposure to statistical mechanics, partial differential equations and quantum mechanics, the stage is set for any of the one-semester advanced courses based on ChaosBook.

Remark 1.2 ChaosBook based courses. The courses taught so far (for a listing, consult ChaosBook.org/courses) start out with the introductory chapters on qualitative dynamics, symbolic dynamics and flows, and then continue in different directions:

Deterministic chaos. Chaotic averaging, evolution operators, trace formulas, zeta functions, cycle expansions, Lyapunov exponents, billiards, transport coefficients, thermodynamic formalism, period doubling, renormalization operators. A graduate level introduction to statistical mechanics from the dynamical point view is given by Dorfman [18]; the Gaspard monograph [8] covers the same ground in more depth. Driebe monograph [19] offers a nice introduction to the problem of irreversibility in dynamics. The role of ‘chaos’

in statistical mechanics is critically dissected by Bricmont in his highly readable essay “*Science of Chaos or Chaos in Science?*” [20].

Spatiotemporal dynamical systems. Partial differential equations for dissipative systems, weak amplitude expansions, normal forms, symmetries and bifurcations, pseudospectral methods, spatiotemporal chaos, turbulence. Holmes, Lumley and Berkooz [21] offer a delightful discussion of why the Kuramoto-Sivashinsky equation deserves study as a staging ground for a dynamical approach to study of turbulence in full-fledged Navier-Stokes boundary shear flows.

Quantum chaos. Semiclassical propagators, density of states, trace formulas, semiclassical spectral determinants, billiards, semiclassical helium, diffraction, creeping, tunneling, higher-order \hbar corrections. For further reading on this topic, consult the quantum chaos part of ChaosBook.org.

Remark 1.3 Periodic orbit theory. This book puts more emphasis on periodic orbit theory than any other current nonlinear dynamics textbook. The role of unstable periodic orbits was already fully appreciated by Poincaré [22, 23], who noted that hidden in the apparent chaos is a rigid skeleton, a tree of *cycles* (periodic orbits) of increasing lengths and self-similar structure, and suggested that the cycles should be the key to chaotic dynamics. Periodic orbits have been at core of much of the mathematical work on the theory of the classical and quantum dynamical systems ever since. We refer the reader to the reprint selection [24] for an overview of some of that literature.

Remark 1.4 If you seek rigor? If you find ChaosBook not rigorous enough, you should turn to the mathematics literature. We recommend Robinson’s advanced graduate level exposition of dynamical systems theory [25] from Smale perspective. The most extensive reference is the treatise by Katok and Hasselblatt [26], an impressive compendium of modern dynamical systems theory. The fundamental papers in this field, all still valuable reading, are Smale [27], Bowen [28] and Sinai [29]. Sinai’s paper is prescient and offers a vision and a program that ties together dynamical systems and statistical mechanics. It is written for readers versed in statistical mechanics. For a dynamical systems exposition, consult Anosov and Sinai [30]. Markov partitions were introduced by Sinai in ref. [31]. The classical text (though certainly not an easy read) on the subject of dynamical zeta functions is Ruelle’s *Statistical Mechanics, Thermodynamic Formalism* [32]. In Ruelle’s monograph transfer operator technique (or the ‘Perron-Frobenius theory’) and Smale’s theory of hyperbolic flows are applied to zeta functions and correlation functions. The status of the theory from Ruelle’s point of view is compactly summarized in his 1995 Pisa lectures [33]. Further excellent mathematical references on thermodynamic formalism are Parry and Pollicott’s monograph [34] with emphasis on the symbolic dynamics aspects of the formalism, and Baladi’s clear and compact reviews of the theory of dynamical zeta functions [35, 36].

Remark 1.5 If you seek magic? ChaosBook resolutely skirts number-theoretical magic such as spaces of constant negative curvature, Poincaré tilings, modular domains, Selberg Zeta functions, Riemann hypothesis, . . . Why? While this beautiful mathematics has been very inspirational, especially in studies of quantum chaos, almost no powerful method in its repertoire survives a transplant to a physical system that you are likely to care about.

Remark 1.6 Sorry, no schmactals! ChaosBook skirts mathematics and empirical practice of fractal analysis, such as Hausdorff and fractal dimensions. Addison's introduction to fractal dimensions [37] offers a well-motivated entry into this field. While in studies of probabilistically assembled fractals such as diffusion limited aggregates (DLA) better measures of 'complexity' are lacking, for deterministic systems there are much better, physically motivated and experimentally measurable quantities (escape rates, diffusion coefficients, spectrum of helium, ...) that we focus on here.

Remark 1.7 Rat brains? If you were wondering while reading this introduction 'what's up with rat brains?', the answer is yes indeed, there is a line of research in neuronal dynamics that focuses on possible unstable periodic states, described for example in refs. [38, 39, 40, 41].

A guide to exercises

God can afford to make mistakes. So can Dada!

—Dadaist Manifesto

The essence of this subject is incommunicable in print; the only way to develop intuition about chaotic dynamics is by computing, and the reader is urged to try to work through the essential exercises. As not to fragment the text, the exercises are indicated by text margin boxes such as the one on this margin, and collected at the end of each chapter. By the end of a (two-semester) course you should have completed at least three small projects: (a) compute everything for a 1-dimensional repeller, (b) compute escape rate for a 3-disk game of pinball, (c) compute a part of the quantum 3-disk game of pinball, or the helium spectrum, or if you are interested in statistical rather than the quantum mechanics, compute a transport coefficient. The essential steps are:

exercise 20.2

- **Dynamics**

1. count prime cycles, exercise 1.1, exercise 9.6, exercise 11.1
2. pinball simulator, exercise 8.1, exercise 13.4
3. pinball stability, exercise 13.7, exercise 13.4
4. pinball periodic orbits, exercise 13.5, exercise 13.6
5. helium integrator, exercise 2.10, exercise 13.11
6. helium periodic orbits, exercise 13.12

- **Averaging, numerical**

1. pinball escape rate, exercise 17.3

- **Averaging, periodic orbits**

1. cycle expansions, exercise 20.1, exercise 20.2
2. pinball escape rate, exercise 20.4, exercise 20.5
3. cycle expansions for averages, exercise 20.1, exercise 22.3
4. cycle expansions for diffusion, exercise 25.1
5. pruning, transition graphs, exercise 15.6
6. desymmetrization exercise 21.1
7. intermittency, phase transitions, exercise 24.6

The exercises that you should do have **underlined titles**. The rest (**smaller type**) are optional. Difficult problems are marked by any number of *** stars. If you solve one of those, it is probably worth a **publication**. Solutions to some of the problems are available on **ChaosBook.org**. A clean solution, a pretty figure, or a nice exercise that you contribute to ChaosBook will be gratefully acknowledged. Often going through a solution is more instructive than reading the chapter that problem is supposed to illustrate.

Exercises

- 1.1. **3-disk symbolic dynamics.** As periodic trajectories will turn out to be our main tool to breach deep into the realm of chaos, it pays to start familiarizing oneself with them now by sketching and counting the few shortest prime cycles (we return to this in sect. 15.4). Show that the 3-disk pinball has $3 \cdot 2^{n-1}$ itineraries of length n . List periodic orbits of lengths 2, 3, 4, 5, \dots . Verify that the shortest 3-disk prime cycles are 12, 13, 23, 123, 132, 1213, 1232, 1323, 12123, \dots . Try to sketch them. (continued in exercise 12.6)
- 1.2. **Sensitivity to initial conditions.** Assume that two pinball trajectories start out parallel, but separated by 1 Ångström, and the disks are of radius $a = 1$ cm and center-to-center separation $R = 6$ cm. Try to estimate in how many bounces the separation will grow to the size of system (assuming that the trajectories have been picked so they remain trapped for at least that long). Estimate the Who's Pinball Wizard's typical score (number of bounces) in a game without cheating, by hook or crook (by the end of chapter 20 you should be in position to make very accurate estimates).

References

- [1.1] J. Guckenheimer, "Piecewise-Smooth Dynamical Systems (*Book Review*)" *SIAM Rev.* **50**, 606 (2008).
- [1.2] G.W. Leibniz, *Von dem Verhängnisse*, in *Hauptschriften zur Grundlegung der Philosophie*, Vol II, , pp. 129-134 (Ernst Cassirer, Leibzig 1906).
- [1.3] T. Li and J. Yorke, "Period 3 implies chaos," *Amer. Math. Monthly* **82**, 985 (1975).
- [1.4] R. P. Taylor, A. P. Micolich and D. Jonas, "Fractal analysis of Pollock's drip paintings," *Nature* **399**, 422 (1999).
- [1.5] K. Jones-Smith and H. Mathur, "Fractal Analysis: Revisiting Pollock's drip paintings," *Nature* **444**, E9 (2006); R. P. Taylor, A. P. Micolich and D. Jonas, "Fractal Analysis: Revisiting Pollock's drip paintings (Reply)," *Nature* **444**, E10 (2006).
- [1.6] R. Kennedy, "The Case of Pollock's Fractals Focuses on Physics," *New York Times* (Dec. 2, 2006).
- [1.7] D. Avnir, O. Biham, D. Lidar and O. Malcai, "Is the Geometry of Nature Fractal?," *Science* **279**, 39 (1998).
- [1.8] P. Gaspard, *Chaos, Scattering and Statistical Mechanics* (Cambridge U. Press, Cambridge 1998).
- [1.9] S.H. Strogatz, *Nonlinear Dynamics and Chaos* (Addison-Wesley, Reading 1994).
- [1.10] K.T. Alligood, T.D. Sauer and J.A. Yorke, *Chaos, an Introduction to Dynamical Systems* (Springer, New York 1996)

- [1.11] E. Ott, *Chaos in Dynamical Systems* (Cambridge U. Press, Cambridge 1993).
- [1.12] J. C. Sprott, *Chaos and Time-Series Analysis* (Oxford Univ. Press, Oxford 2003)
- [1.13] E. Atlee Jackson, *Perspectives of nonlinear dynamics* (Cambridge U. Press, Cambridge 1989).
- [1.14] Y. A. Kuznetsov, *Elements of Applied Bifurcation Theory*, (Springer, New York 2004).
- [1.15] N.B. Tufillaro, T.A. Abbott, and J.P. Reilly, *Experimental Approach to Nonlinear Dynamics and Chaos* (Addison Wesley, Reading MA 1992).
- [1.16] H.J. Korsch and H.-J. Jodl, *Chaos. A Program Collection for the PC*, (Springer, New York 1994).
- [1.17] H.E. Nusse and J.A. Yorke, *Dynamics: Numerical Explorations* (Springer, New York 1997).
- [1.18] J. R. Dorfman, *An Introduction to Chaos in Nonequilibrium Statistical Mechanics* (Cambridge U. Press, Cambridge 1999).
- [1.19] D.J. Driebe, *Fully Chaotic Map and Broken Time Symmetry* (Kluwer, Dordrecht 1999).
- [1.20] J. Bricmont, "Science of Chaos or Chaos in Science?," in: *The Flight from Science and Reason*, P.R. Gross, N. Levitt, and M.W. Lewis, eds., *Annals of the New York Academy of Sciences* **775**; [mp_arc 96-116.ps.gz](#)
- [1.21] P. Holmes, J.L. Lumley and G. Berkooz, *Turbulence, Coherent Structures, Dynamical Systems and Symmetry* (Cambridge U. Press, Cambridge 1996).
- [1.22] H. Poincaré, *Les méthodes nouvelles de la mécanique céleste* (Guthier-Villars, Paris 1892-99)
- [1.23] For a very readable exposition of Poincaré's work and the development of the dynamical systems theory see J. Barrow-Green, *Poincaré and the Three Body Problem*, (Amer. Math. Soc., Providence RI 1997), and F. Diacu and P. Holmes, *Celestial Encounters, The Origins of Chaos and Stability* (Princeton Univ. Press, Princeton NJ 1996).
- [1.24] R.S. MacKay and J.D. Meiss, *Hamiltonian Dynamical Systems* (Adam Hilger, Bristol 1987).
- [1.25] C. Robinson, *Dynamical Systems: Stability, Symbolic Dynamics, and Chaos* (C. R. C. Press, Boca Raton 1999)
- [1.26] A. Katok and B. Hasselblatt, *Introduction to the Modern Theory of Dynamical Systems* (Cambridge U. Press, Cambridge 1995).
- [1.27] S. Smale, "Differentiable Dynamical Systems," *Bull. Am. Math. Soc.* **73**, 747 (1967).

- [1.28] R. Bowen, *Equilibrium states and the ergodic theory of Anosov diffeomorphisms*, Springer Lecture Notes in Math. **470** (1975).
- [1.29] Ya.G. Sinai, “Gibbs measures in ergodic theory,” *Russ. Math. Surveys* **166**, 21 (1972).
- [1.30] D.V. Anosov and Ya.G. Sinai, “Some smooth ergodic systems,” *Russ. Math. Surveys* **22**, 103 (1967).
- [1.31] Ya.G. Sinai, “Construction of Markov partitions,” *Funkts. Analiz i Ego Pril.* **2**, 70 (1968). English translation: *Functional Anal. Appl.* **2**, 245 (1968).
- [1.32] D. Ruelle, *Statistical Mechanics, Thermodynamic Formalism*, (Addison-Wesley, Reading MA 1978).
- [1.33] D. Ruelle, “Functional determinants related to dynamical systems and the thermodynamic formalism,” (Lezioni Fermiane, Pisa), preprint IHES/P/95/30 (March 1995).
- [1.34] W. Parry and M. Pollicott, *Zeta Functions and the Periodic Structure of Hyperbolic Dynamics*, *Astérisque* **187–188** (Société Mathématique de France, Paris 1990).
- [1.35] V. Baladi, “Dynamical zeta functions,” in B. Branner and P. Hjorth, eds., *Real and Complex Dynamical Systems* (Kluwer, Dordrecht 1995).
- [1.36] V. Baladi, *Positive Transfer Operators and Decay of Correlations* (World Scientific, Singapore 2000).
- [1.37] P.S. Addison *Fractals and chaos: an illustrated course*, (Inst. of Physics Publishing, Bristol 1997).
- [1.38] S.J. Schiff, et al. “Controlling chaos in the brain,” *Nature* **370**, 615 (1994).
- [1.39] F. Moss, “Chaos under control,” *Nature* **370**, 596 (1994).
- [1.40] J. Glanz, “Do chaos-control techniques offer hope for epilepsy?” *Science* **265**, 1174 (1994).
- [1.41] J. Glanz, “Mastering the Nonlinear Brain,” *Science* **227**, 1758 (1997).
- [1.42] Henry Miller, *Tropic of Cancer* (Obelisk Press, Paris 1939; Grove Press, New York 1961).

Chapter 2

Go with the flow

Dynamical systems theory includes an extensive body of knowledge about qualitative properties of generic smooth families of vector fields and discrete maps. The theory characterizes structurally stable invariant sets [...] The logic of dynamical systems theory is subtle. The theory abandons the goal of describing the qualitative dynamics of all systems as hopeless and instead restricts its attention to phenomena that are found in selected systems. The subtlety comes in specifying the systems of interest and which dynamical phenomena are to be analyzed.

— John Guckenheimer

(R. Mainieri, P. Cvitanović and E.A. Spiegel)

WE DEFINE a *dynamical system* (M, f) , classify its solutions as equilibria, periodic, and aperiodic, refine the ‘aperiodic’ into wandering and non-wandering sets, decompose the non-wandering into chain-recurrent sets, and illustrate various cases with concrete examples, the Rössler and Lorenz systems.



fast track:
chapter 16, p. 308

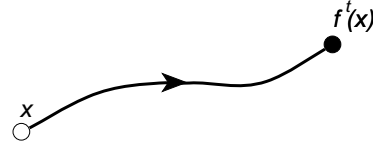
2.1 Dynamical systems

In a dynamical system we observe the world as it evolves with time. We express our observations as numbers and record how they change; given sufficiently detailed information and understanding of the underlying natural laws, we see the future in the present as in a mirror. The motion of the planets against the celestial firmament provides an example. Against the daily motion of the stars from East



section 1.3

Figure 2.1: A trajectory traced out by the evolution rule f^t . Starting from the state space point x , after a time t , the point is at $f^t(x)$.



to West, the planets distinguish themselves by moving among the fixed stars. Ancients discovered that by knowing a sequence of planet's positions—latitudes and longitudes—its future position could be predicted.

For the solar system, tracking the latitude and longitude in the celestial sphere suffices to completely specify the planet's apparent motion. All possible values for positions and velocities of the planets form the *phase space* of the system. More generally, a state of a physical system, at a given instant in time, can be represented by a single point in an abstract space called *state space* \mathcal{M} (mnemonic: curly 'M' for a 'manifold'). As the system changes, so does the *representative point* in state space. We refer to the evolution of such points as *dynamics*, and the function f which specifies where the representative point is at time t as the *evolution rule*.

remark 2.1

If there is a definite rule f that tells us how this representative point moves in \mathcal{M} , the system is said to be deterministic. For a deterministic dynamical system, the evolution rule takes one point of the state space and maps it into exactly one point. However, this is not always possible. For example, knowing the temperature today is not enough to predict the temperature tomorrow; knowing the value of a stock today will not determine its value tomorrow. The state space can be enlarged, in the hope that in a sufficiently large state space it is possible to determine an evolution rule, so we imagine that knowing the state of the atmosphere, measured over many points over the entire planet should be sufficient to determine the temperature tomorrow. Even that is not quite true, and we are less hopeful when it comes to stocks.

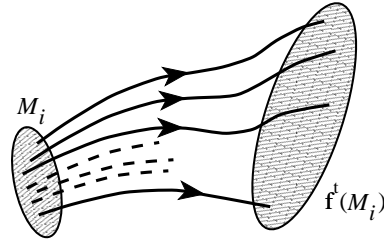
For a deterministic system almost every point has a unique future, so trajectories cannot intersect. We say 'almost' because there might exist a set of measure zero (tips of wedges, cusps, etc.) for which a trajectory is not defined. We may think such sets a nuisance, but it is quite the contrary—they will enable us to partition state space, so that the dynamics can be better understood.

chapter 12

Locally, the state space \mathcal{M} looks like \mathbb{R}^d , meaning that a dynamical evolution is an initial value problem, with d numbers sufficient to determine what will happen time t later. Globally, it may be a more complicated manifold formed by patching together several pieces of \mathbb{R}^d , forming a torus, a cylinder, or some other geometric object. When we need to stress that the dimension d of \mathcal{M} is greater than one, we may refer to the point $x \in \mathcal{M}$ as x_i where $i = 1, 2, 3, \dots, d$. If the dynamics is described by a set of PDEs (partial differential equations), the state space is the infinite dimensional function space. The evolution rule $f : \mathcal{M} \rightarrow \mathcal{M}$ tells us where a point x is in \mathcal{M} after a time interval t .

The pair (\mathcal{M}, f) constitute a *dynamical system*.

Figure 2.2: The evolution rule f^t can be used to map a region M_i of the state space into the region $f^t(M_i)$.



The dynamical systems we will be studying are smooth. This is expressed mathematically by saying that the evolution rule f^t can be differentiated as many times as needed. Its action on a point x is sometimes indicated by $f(x, t)$ to remind us that f is really a function of two variables: the time and a point in state space. Note that time is relative rather than absolute, so only the time interval is necessary. This follows from the fact that a point in state space completely determines all future evolution, and it is not necessary to know anything else. The time parameter can be a real variable ($t \in \mathbb{R}$), in which case the evolution is called a *flow*, or an integer ($t \in \mathbb{Z}$), in which case the evolution advances in discrete steps in time, given by *iteration* of a *map*. The evolution parameter need not be the physical time; for example, a time-stationary solution of a partial differential equation is parameterized by spatial variables. In such situations one talks of a ‘spatial profile’ rather than a ‘flow’.

Nature provides us with innumerable dynamical systems. They manifest themselves through their trajectories: given an initial point x_0 , the evolution rule traces out a sequence of points $x(t) = f^t(x_0)$, the *trajectory* through the point $x_0 = x(0)$. A trajectory is parameterized by the time t and thus belongs to $(f^t(x_0), t) \in \mathcal{M} \times \mathbb{R}$. By extension, we can also talk of the evolution of a region M_i of the state space: just apply f^t to every point in M_i to obtain a new region $f^t(M_i)$, as in figure 2.2.

exercise 2.1

Because f^t is a single-valued function, any point of the trajectory can be used to label the trajectory.

If we mark the trajectory by its initial point x_0 , we are describing it in the *Lagrangian coordinates*.

The subset of points $M_{x_0} \subset \mathcal{M}$ that belong to the infinite-time trajectory of a given point x_0 is called the *orbit* of x_0 ; we shall talk about forward orbits, backward orbits, periodic orbits, etc.. For a flow, an orbit is a smooth continuous curve; for a map, it is a sequence of points. An orbit is a *dynamically invariant* notion. While “trajectory” refers to a state $x(t)$ at time instant t , “orbit” refers to the totality of states that can be reached from x_0 , with state space \mathcal{M} foliated into a union of such orbits (each M_{x_0} labeled by a single point belonging to the set, $x_0 = x(0)$ for example).

2.1.1 A classification of possible motions?

What are the possible trajectories? This is a grand question, and there are many answers, the chapters to follow offering some. Here is the first attempt to classify

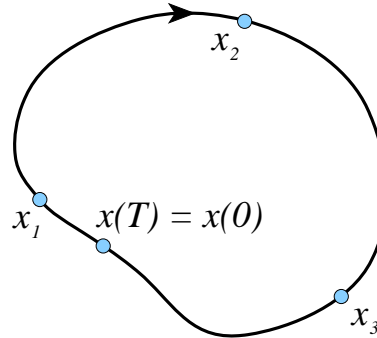


Figure 2.3: A periodic point returns to the initial point after a finite time, $x = f^{T_p}(x)$. Periodic orbit p is the set of periodic points $p = \mathcal{M}_p = \{x_1, x_2, \dots\}$ swept out by the trajectory of any one of them in the finite time T_p .

all possible trajectories:

- stationary: $f^t(x) = x$ for all t
- periodic: $f^t(x) = f^{t+T_p}(x)$ for a given minimum period T_p
- aperiodic: $f^t(x) \neq f^{t'}(x)$ for all $t \neq t'$.

A *periodic orbit* (or a *cycle*) p is the set of points $\mathcal{M}_p \subset \mathcal{M}$ swept out by a trajectory that returns to the initial point in a finite time. We refer to a point on a periodic orbit as a *periodic point*, see figure 2.3. Periodic orbits form a very small subset of the state space, in the same sense that rational numbers are a set of zero measure on the unit interval.

chapter 5

Periodic orbits and equilibrium points are the simplest examples of ‘non-wandering’ invariant sets preserved by dynamics. Dynamics can also preserve higher-dimensional smooth compact invariant manifolds; most commonly encountered are the M -dimensional tori of Hamiltonian dynamics, with notion of periodic motion generalized to quasiperiodic (the superposition of M incommensurate frequencies) motion on a smooth torus, and families of solutions related by a continuous symmetry.

The ancients tried to make sense of all dynamics in terms of periodic motions, epicycles, integrable systems. The embarrassing truth is that for a generic dynamical systems almost all motions are aperiodic. So we refine the classification by dividing aperiodic motions into two subtypes: those that wander off, and those that keep coming back.

A point $x \in \mathcal{M}$ is called a *wandering point*, if there exists an open neighborhood \mathcal{M}_0 of x to which the trajectory never returns

$$f^t(x) \notin \mathcal{M}_0 \quad \text{for all } t > t_{\min}. \tag{2.1}$$

In physics literature, the dynamics of such state is often referred to as *transient*.

Wandering points do not take part in the long-time dynamics, so your first task is to prune them from \mathcal{M} as well as you can. What remains envelops the set of the long-time trajectories, or the *non-wandering set*.

For times much longer than a typical ‘turnover’ time, it makes sense to relax the notion of exact periodicity, and replace it by the notion of *recurrence*. A point is *recurrent* or *non-wandering* if for any open neighborhood \mathcal{M}_0 of x and any time t_{min} there exists a later time t , such that

$$f^t(x) \in \mathcal{M}_0. \quad (2.2)$$

In other words, the trajectory of a non-wandering point reenters the neighborhood \mathcal{M}_0 infinitely often. We shall denote by Ω the *non-wandering set* of f , i.e., the union of all the non-wandering points of \mathcal{M} . The set Ω , the non-wandering set of f , is the key to understanding the long-time behavior of a dynamical system; all calculations undertaken here will be carried out on non-wandering sets.

So much about individual trajectories. What about clouds of initial points? If there exists a connected state space volume that maps into itself under forward evolution (and you can prove that by the method of Lyapunov functionals, or several other methods available in the literature), the flow is globally contracting onto a subset of \mathcal{M} which we shall refer to as the *attractor*. The attractor may be unique, or there can coexist any number of distinct attracting sets, each with its own *basin of attraction*, the set of all points that fall into the attractor under forward evolution. The attractor can be a fixed point, a periodic orbit, aperiodic, or any combination of the above. The most interesting case is that of an aperiodic recurrent attractor, to which we shall refer loosely as a *strange attractor*. We say ‘loosely’, as will soon become apparent that diagnosing and proving existence of a genuine, card-carrying strange attractor is a highly nontrivial undertaking.

example 2.3

Conversely, if we can enclose the non-wandering set Ω by a connected state space volume \mathcal{M}_0 and then show that almost all points within \mathcal{M}_0 , but not in Ω , eventually exit \mathcal{M}_0 , we refer to the non-wandering set Ω as a *repeller*. An example of a repeller is not hard to come by—the pinball game of sect. 1.3 is a simple chaotic repeller.

It would seem, having said that the periodic points are so exceptional that almost all non-wandering points are aperiodic, that we have given up the ancients’ fixation on periodic motions. Nothing could be further from truth. As longer and longer cycles approximate more and more accurately finite segments of aperiodic trajectories, we shall establish control over non-wandering sets by defining them as the closure of the union of all periodic points.

Before we can work out an example of a non-wandering set and get a better grip on what chaotic motion might look like, we need to ponder flows in a little more depth.

2.2 Flows



Knowing the equations and knowing the solution are two different things. Far, far away.

— T.D. Lee

A *flow* is a continuous-time dynamical system. The evolution rule f is a family of mappings of $\mathcal{M} \rightarrow \mathcal{M}$ parameterized by $t \in \mathbb{R}$. Because t represents a time interval, any family of mappings that forms an evolution rule must satisfy:

exercise 2.2

- (a) $f^0(x) = x$ (in 0 time there is no motion)
- (b) $f^t(f^{t'}(x)) = f^{t+t'}(x)$ (the evolution law is the same at all times)
- (c) the mapping $(x, t) \mapsto f^t(x)$ from $\mathcal{M} \times \mathbb{R}$ into \mathcal{M} is continuous.

We shall often find it convenient to represent functional composition by ‘ \circ ’:

appendix H.1

$$f^{t+s} = f^t \circ f^s = f^t(f^s). \quad (2.3)$$

The family of mappings $f^t(x)$ thus forms a continuous (forward semi-) group. Why ‘semi-’group? It may fail to form a group if the dynamics is not reversible, and the rule $f^t(x)$ cannot be used to rerun the dynamics backwards in time, with negative t ; with no reversibility, we cannot define the inverse $f^{-t}(f^t(x)) = f^0(x) = x$, in which case the family of mappings $f^t(x)$ does not form a group. In exceedingly many situations of interest—for times beyond the Lyapunov time, for asymptotic attractors, for dissipative partial differential equations, for systems with noise, for non-invertible maps—the dynamics cannot be run backwards in time, hence, the circumspect emphasis on *semigroups*. On the other hand, there are many settings of physical interest, where dynamics is reversible (such as finite-dimensional Hamiltonian flows), and where the family of evolution maps f^t does form a group.

For infinitesimal times, flows can be defined by differential equations. We write a trajectory as

$$x(t + \tau) = f^{t+\tau}(x_0) = f(f(x_0, t), \tau) \quad (2.4)$$

and express the time derivative of a trajectory at point $x(t)$,

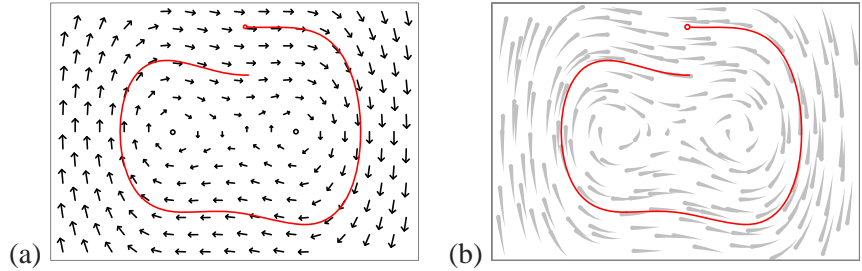
exercise 2.3

$$\left. \frac{dx}{d\tau} \right|_{\tau=0} = \partial_\tau f(f(x_0, t), \tau)|_{\tau=0} = \dot{x}(t). \quad (2.5)$$

as the time derivative of the evolution rule, a vector evaluated at the same point. By considering all possible trajectories, we obtain the vector $\dot{x}(t)$ at any point $x \in \mathcal{M}$. This *vector field* is a (generalized) velocity field:

$$\dot{x}(t) = v(x). \quad (2.6)$$

Figure 2.4: (a) The 2-dimensional vector field for the Duffing system (2.7), together with a short trajectory segment. (b) The flow lines. Each ‘comet’ represents the same time interval of a trajectory, starting at the tail and ending at the head. The longer the comet, the faster the flow in that region.



Newton’s laws, Lagrange’s method, or Hamilton’s method are all familiar procedures for obtaining a set of differential equations for the vector field $v(x)$ that describes the evolution of a mechanical system. Equations of mechanics may appear different in form from (2.6), as they are often involve higher time derivatives, but an equation that is second or higher order in time can always be rewritten as a set of first order equations.

We are concerned here with a much larger world of general flows, mechanical or not, all defined by a time-independent vector field (2.6). At each point of the state space a vector indicates the local direction in which the trajectory evolves. The length of the vector $|v(x)|$ is proportional to the speed at the point x , and the direction and length of $v(x)$ changes from point to point. When the state space is a complicated manifold embedded in \mathbb{R}^d , one can no longer think of the vector field as being embedded in the state space. Instead, we have to imagine that each point x of state space has a different tangent plane TM_x attached to it. The vector field lives in the union of all these tangent planes, a space called the *tangent bundle* TM .

Example 2.1 A 2-dimensional vector field $v(x)$: A simple example of a flow is afforded by the unforced Duffing system

$$\begin{aligned} \dot{x}(t) &= y(t) \\ \dot{y}(t) &= -0.15 y(t) + x(t) - x(t)^3 \end{aligned} \tag{2.7}$$

plotted in figure 2.4. The velocity vectors are drawn superimposed over the configuration coordinates $(x(t), y(t))$ of state space \mathcal{M} , but they belong to a different space, the tangent bundle TM .

$$\text{If } v(x_q) = 0, \tag{2.8}$$

x_q is an *equilibrium point* (also referred to as a *stationary, fixed, critical, invariant, rest, stagnation point, zero of the vector field v, standing wave or steady state* - our usage is ‘equilibrium’ for a flow, ‘fixed point’ for a map), and the trajectory remains forever stuck at x_q . Otherwise the trajectory passing through x_0 at time $t = 0$ can be obtained by integrating the equations (2.6):

$$x(t) = f^t(x_0) = x_0 + \int_0^t d\tau v(x(\tau)), \quad x(0) = x_0. \tag{2.9}$$

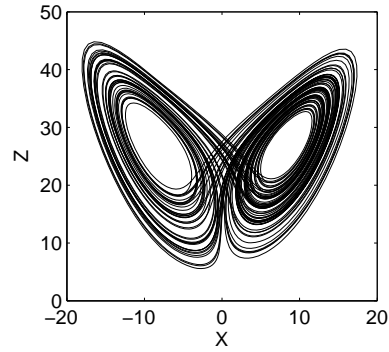


Figure 2.5: Lorenz “butterfly” strange attractor. (J. Halcrow)

We shall consider here only *autonomous* flows, i.e., flows for which the velocity field v_i is *stationary*, not explicitly dependent on time. A non-autonomous system

$$\frac{dy}{d\tau} = w(y, \tau), \tag{2.10}$$

can always be converted into a system where time does not appear explicitly. To do so, extend (‘suspend’) state space to be $(d + 1)$ -dimensional by defining $x = \{y, \tau\}$, with a stationary vector field

exercise 2.4
exercise 2.5

$$v(x) = \begin{bmatrix} w(y, \tau) \\ 1 \end{bmatrix}. \tag{2.11}$$

The new flow $\dot{x} = v(x)$ is autonomous, and the trajectory $y(\tau)$ can be read off $x(t)$ by ignoring the last component of x .

Example 2.2 Lorenz strange attractor: Edward Lorenz arrived at the equation

$$\dot{x} = v(x) = \begin{bmatrix} \dot{x} \\ \dot{y} \\ \dot{z} \end{bmatrix} = \begin{bmatrix} \sigma(y - x) \\ \rho x - y - xz \\ xy - bz \end{bmatrix} \tag{2.12}$$

by a drastic simplification of the Rayleigh-Benard flow. Lorenz fixed $\sigma = 10$, $b = 8/3$, and varied the “Rayleigh number” ρ . For $0 < \rho < 1$ the equilibrium $EQ_0 = (0, 0, 0)$ at the origin is attractive. At $\rho = 1$ it undergoes a pitchfork bifurcation into a pair of equilibria at

remark 2.3

$$x_{EQ_{1,2}} = (\pm \sqrt{b(\rho - 1)}, \pm \sqrt{b(\rho - 1)}, \rho - 1), \tag{2.13}$$

We shall not explore the Lorenz flow dependence on the ρ parameter in what follows, but here is a brief synopsis: the EQ_0 1-dimensional unstable manifold closes into a homoclinic orbit at $\rho = 13.56 \dots$. Beyond that, an infinity of associated periodic orbits are generated, until $\rho = 24.74 \dots$, where $EQ_{1,2}$ undergo a Hopf bifurcation.

All computations that follow will be performed for the Lorenz parameter choice $\sigma = 10, b = 8/3, \rho = 28$. For these parameter values the long-time dynamics is confined to the strange attractor depicted in figure 2.5, and the positions of its equilibria are marked in figure 9.3. (continued in example 3.5)

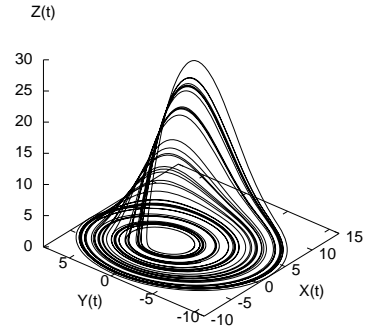


Figure 2.6: A trajectory of the Rössler flow at time $t = 250$. (G. Simon)

Example 2.3 Rössler strange attractor: The Duffing flow of figure 2.4 is bit of a bore—every trajectory ends up in one of the two attractive equilibrium points. Let's construct a flow that does not die out, but exhibits a recurrent dynamics. Start with a harmonic oscillator

$$\dot{x} = -y, \quad \dot{y} = x. \tag{2.14}$$

The solutions are re^{it} , re^{-it} , and the whole x - y plane rotates with constant angular velocity $\dot{\theta} = 1$, period $T = 2\pi$. Now make the system unstable by adding

$$\dot{x} = -y, \quad \dot{y} = x + ay, \quad a > 0, \tag{2.15}$$

or, in radial coordinates, $\dot{r} = ar \sin^2 \theta$, $\dot{\theta} = 1 + (a/2) \sin 2\theta$. The plane is still rotating with the same average angular velocity, but trajectories are now spiraling out. Any flow in the plane either escapes, falls into an attracting equilibrium point, or converges to a limit cycle. Richer dynamics requires at least one more dimension. In order to prevent the trajectory from escaping to ∞ , kick it into 3rd dimension when x reaches some value c by adding

$$\dot{z} = b + z(x - c), \quad c > 0. \tag{2.16}$$

As x crosses c , z shoots upwards exponentially, $z \approx e^{(x-c)t}$. In order to bring it back, start decreasing x by modifying its equation to

$$\dot{x} = -y - z.$$

Large z drives the trajectory toward $x = 0$; there the exponential contraction by e^{-ct} kicks in, and the trajectory drops back toward the x - y plane. This frequently studied example of an autonomous flow is called the Rössler flow

$$\begin{aligned} \dot{x} &= -y - z \\ \dot{y} &= x + ay \\ \dot{z} &= b + z(x - c), \quad a = b = 0.2, \quad c = 5.7 \end{aligned} \tag{2.17}$$

(for definitiveness, we fix the parameters a, b, c in what follows). The system is as simple as they get—it would be linear, were it not for the sole bilinear term zx . Even for so 'simple' a system the nature of long-time solutions is far from obvious. exercise 2.8

There are two repelling equilibrium points (2.8):

$$\begin{aligned} x_{\pm} &= \left(\frac{1}{2} \pm \frac{1}{2} \sqrt{1 - 4ab/c^2}\right)(c, -c/a, c/a) \\ x_- &\approx (ab/c, -b/c, b/c), \quad x_+ \approx (c, -c/a, c/a) \\ (x_-, y_-, z_-) &= (0.0070, -0.0351, 0.0351) \\ (x_+, y_+, z_+) &= (5.6929, -28.464, 28.464) \end{aligned} \tag{2.18}$$

One is close to the origin by construction. The other, some distance away, exists because the equilibrium condition has a 2nd-order nonlinearity.

To see what solutions look like in general, we need to resort to numerical integration. A typical numerically integrated long-time trajectory is sketched in figure 2.6 (see also figure 11.10). Trajectories that start out sufficiently close to the origin seem to converge to a strange attractor. We say 'seem' as there exists no proof that such an attractor is asymptotically aperiodic—it might well be that what we see is but a long transient on a way to an attractive periodic orbit. For now, accept that figure 2.6 and similar figures in what follows are examples of 'strange attractors.' (continued in exercise 2.8 and example 3.4) exercise 3.5
 (R. Paškauskas)

The Rössler flow is the simplest flow which exhibits many of the key aspects of chaotic dynamics; we shall use it and the 3-pinball (see chapter 8) systems throughout ChaosBook to motivate introduction of Poincaré sections, return maps, symbolic dynamics, cycle expansions, and much else. Rössler flow is integrated in exercise 2.7, its equilibria are determined in exercise 2.8, its Poincaré sections constructed in exercise 3.1, and the corresponding return Poincaré map computed in exercise 3.2. Its volume contraction rate is computed in exercise 4.3, its topology investigated in exercise 4.4, the shortest Rössler flow cycles are computed and tabulated in exercise 13.10, and its Lyapunov exponents evaluated in exercise 17.4.



fast track:
chapter 3, p. 54

2.3 Computing trajectories



On two occasions I have been asked [by members of Parliament], 'Pray, Mr. Babbage, if you put into the machine wrong figures, will the right answers come out?' I am not able rightly to apprehend the kind of confusion of ideas that could provoke such a question.

— Charles Babbage

You have not learned dynamics unless you know how to integrate numerically whatever dynamical equations you face. Sooner or later, you need to implement some finite time-step prescription for integration of the equations of motion (2.6). The simplest is the Euler integrator which advances the trajectory by $\delta\tau \times$ velocity at each time step:

$$x_i \rightarrow x_i + v_i(x) \delta\tau. \tag{2.19}$$

This might suffice to get you started, but as soon as you need higher numerical accuracy, you will need something better. There are many excellent reference texts and computer programs that can help you learn how to solve differential equations numerically using sophisticated numerical tools, such as pseudo-spectral methods or implicit methods. If a ‘sophisticated’ integration routine takes days and gobbles up terabits of memory, you are using brain-damaged high level software. Try writing a few lines of your own Runge-Kutta code in some mundane everyday language. While you absolutely need to master the requisite numerical methods, this is neither the time nor the place to expound upon them; how you learn them is your business. And if you have developed some nice routines for solving problems in this text or can point another student to some, let us know.

exercise 2.6

exercise 2.7

exercise 2.9

exercise 2.10

Résumé

Chaotic dynamics with a low-dimensional attractor can be visualized as a succession of nearly periodic but unstable motions. In the same spirit, turbulence in spatially extended systems can be described in terms of recurrent spatiotemporal patterns. Pictorially, dynamics drives a given spatially extended system through a repertoire of unstable patterns; as we watch a turbulent system evolve, every so often we catch a glimpse of a familiar pattern. For any finite spatial resolution and finite time the system follows approximately a pattern belonging to a finite repertoire of possible patterns, and the long-term dynamics can be thought of as a walk through the space of such patterns. Recasting this image into mathematics is the subject of this book.

Commentary

Remark 2.1 ‘State space’ or ‘phase space?’ In this text we denote by the term *state space* the set of admissible states of a general d - or ∞ -dimensional dynamical system, and reserve the term *phase space* to Hamiltonian $2D$ -dimensional state spaces, where D is the number of Hamiltonian degrees of freedom. If the state space is a continuous smooth manifold much of the literature refers to it as ‘phase space,’ but we find the control engineering usage sharper: in the state space (or ‘time-domain’) description of an autonomous physical system, the state of the system is represented as a vector within the ‘state space,’ space whose axes are the state variables, and the set of state variables is related by first-order differential equations. The distinction made here is needed in a text where one treats both general dynamical systems and quantum-mechanical systems. The term ‘phase’ has a precise meaning in wave mechanics, quantum mechanics and dynamics of integrable systems at the heart of Hamilton’s formulation of Newtonian mechanics, while ‘state space’ is more descriptive of the way the notion is used in the general theory of dynamical systems. Further confusion arises when prefix spatio- as in ‘spatiotemporal’ is used in reference to states extended in the (1, 2, or 3-dimensional) physical configuration space. They may exhibit spatial wave-like behaviors, but their *state space* is ∞ -dimensional.

Much of the literature denotes the vector field in a first order differential equation (2.6) by $f(x)$ or $F(x)$ or even $X(x)$, and its integral for time t by the ‘time- t forward map’

$x(x_0, t) = \Phi(x_0, t)$ or $\phi_t(x_0)$ or something else. As we shall treat here maps and flows on equal footing, and need to save Greek letters for matters quantum-mechanical, we reserve the notation $f(x)$ for *maps* such as (2.9), and refer to a state space velocity vector field as $v(x)$. We come to regret this choice very far into the text, only by the time we delve into Navier-Stokes equations.

Remark 2.2 Rössler and Duffing flows. The Duffing system (2.7) arises in the study of electronic circuits [1]. The Rössler flow (2.17) is the simplest flow which exhibits many of the key aspects of chaotic dynamics. It was introduced in ref. [2] as a set of equations describing no particular physical system, but capturing the essence of Lorenz chaos in a simplest imaginable smooth flow. Otto Rössler, a man of classical education, was inspired in this quest by that rarely cited grandfather of chaos, Anaxagoras (456 B.C.). This, and references to earlier work can be found in refs. [3, 4, 5]. We recommend in particular the inimitable Abraham and Shaw illustrated classic [6] for its beautiful sketches of the Rössler and many other flows. Timothy Jones [7] has a number of interesting simulations on a Drexel website.

Remark 2.3 Lorenz equation. The Lorenz equation (2.12) is the most celebrated early illustration of “deterministic chaos” [8] (but not the first - the honor goes to Dame Cartwright [9]). Lorenz’s paper, which can be found in reprint collections refs. [10, 11], is a pleasure to read, and is still one of the best introductions to the physics motivating such models. For a geophysics derivation, see Rothman course notes [12]. The equations, a set of ODEs in \mathbb{R}^3 , exhibit strange attractors [13, 14, 15]. Frøyland [16] has a nice brief discussion of Lorenz flow. Frøyland and Alfsen [17] plot many periodic and heteroclinic orbits of the Lorenz flow; some of the symmetric ones are included in ref. [16]. Guckenheimer-Williams [18] and Afraimovich-Bykov-Shilnikov [19] offer in-depth discussion of the Lorenz equation. The most detailed study of the Lorenz equation was undertaken by Sparrow [20]. For a physical interpretation of ρ as “Rayleigh number.” see Jackson [21] and Seydel [22]. Lorenz truncation to 3 modes is so drastic that the model bears no relation to the geophysical hydrodynamics problem that motivated it. For a detailed pictures of Lorenz invariant manifolds consult Vol II of Jackson [21]. Lorenz attractor is a very thin fractal – as we saw, stable manifold thickness is of order 10^{-4} – whose fractal structure has been accurately resolved by D. Viswanath [23, 24]. If you wander what analytic function theory has to say about Lorenz, check ref. [25]. Refs. [26, 27] might also be of interest. (continued in remark 9.2)

Remark 2.4 Diagnosing chaos. In sect. 1.3.1 we have stated that a deterministic system exhibits ‘chaos’ if its trajectories are locally unstable (positive Lyapunov exponent) and globally mixing (positive entropy). In sect. 17.3 we shall define Lyapunov exponents, and discuss their evaluation, but already at this point it would be handy to have a few quick numerical methods to diagnose chaotic dynamics. Laskar’s *frequency analysis* method [28] is useful for extracting quasi-periodic and weakly chaotic regions of state space in Hamiltonian dynamics with many degrees of freedom. For pointers to other numerical methods, see ref. [29].

Remark 2.5 Dynamical systems software: J.D. Meiss [30] has maintained for many years *Sci.nonlinear FAQ* which is now in part superseded by the SIAM Dynamical Sys-

tems website www.dynamicalsystems.org. The website glossary contains most of Meiss's FAQ plus new ones, and a up-to-date software list [31], with links to DSTool, xpp, AUTO, etc.. Springer on-line *Encyclopaedia of Mathematics* maintains links to dynamical systems software packages on eom.springer.de/D/d130210.htm. Kuznetsov [14] Appendix D.9 gives an exhaustive overview of software available in 2004. (see also remark 12.1)

The exercises that you should do have **underlined titles**. The rest (**smaller type**) are optional. Difficult problems are marked by any number of *** stars.

Exercises

- 2.1. **Trajectories do not intersect.** A trajectory in the state space \mathcal{M} is the set of points one gets by evolving $x \in \mathcal{M}$ forwards and backwards in time:

$$C_x = \{y \in \mathcal{M} : f^t(x) = y \text{ for } t \in \mathbb{R}\}.$$

Show that if two trajectories intersect, then they are the same curve.

- 2.2. **Evolution as a group.** The trajectory evolution f^t is a one-parameter semigroup, where (2.3)

$$f^{t+s} = f^t \circ f^s.$$

Show that it is a commutative semigroup.

In this case, the commutative character of the (semi-)group of evolution functions comes from the commutative character of the time parameter under addition. Can you think of any other (semi-)group replacing time?

- 2.3. **Almost ODE's.**

- Consider the point x on \mathbb{R} evolving according $\dot{x} = e^x$. Is this an ordinary differential equation?
- Is $\dot{x} = x(x(t))$ an ordinary differential equation?
- What about $\dot{x} = x(t+1)$?

- 2.4. **All equilibrium points are fixed points.** Show that a point of a vector field v where the velocity is zero is a fixed point of the dynamics f^t .

- 2.5. **Gradient systems.** Gradient systems (or 'potential problems') are a simple class of dynamical systems for which the velocity field is given by the gradient of an auxiliary function, the 'potential' ϕ

$$\dot{x} = -\nabla\phi(x)$$

where $x \in \mathbb{R}^d$, and ϕ is a function from that space to the reals \mathbb{R} .

- Show that the velocity of the particle is in the direction of most rapid decrease of the function ϕ .
- Show that all extrema of ϕ are fixed points of the flow.

- Show that it takes an infinite amount of time for the system to reach an equilibrium point.

- Show that there are no periodic orbits in gradient systems.

- 2.6. **Runge-Kutta integration.** Implement the fourth-order Runge-Kutta integration formula (see, for example, ref. [32]) for $\dot{x} = v(x)$:

$$\begin{aligned} x_{n+1} &= x_n + \frac{k_1}{6} + \frac{k_2}{3} + \frac{k_3}{3} + \frac{k_4}{6} + O(\delta\tau^5) \\ k_1 &= \delta\tau v(x_n), \quad k_2 = \delta\tau v(x_n + k_1/2) \\ k_3 &= \delta\tau v(x_n + k_2/2) \\ k_4 &= \delta\tau v(x_n + k_3). \end{aligned}$$

If you already know your Runge-Kutta, program what you believe to be a better numerical integration routine, and explain what is better about it.

- 2.7. **Rössler flow.** Use the result of exercise 2.6 or some other integration routine to integrate numerically the Rössler flow (2.17). Does the result look like a 'strange attractor'?

- 2.8. **Equilibria of the Rössler flow.**

- Find all equilibrium points (x_q, y_q, z_q) of the Rössler system (2.17). How many are there?
- Assume that $b = a$. As we shall see, some surprisingly large, and surprisingly small numbers arise in this system. In order to understand their size, introduce parameters

$$\epsilon = a/c, \quad D = 1 - 4\epsilon^2, \quad p^\pm = (1 \pm \sqrt{D})/2.$$

Express all the equilibria in terms of (c, ϵ, D, p^\pm) . Expand equilibria to the first order in ϵ . Note that it makes sense because for $a = b = 0.2, c = 5.7$ in (2.17), $\epsilon \approx 0.03$. (continued as exercise 3.1)

(Rytis Paškauskas)

- 2.9. **Can you integrate me?** Integrating equations numerically is not for the faint of heart. It is not always possible to establish that a set of nonlinear ordinary differential equations has a solution for all times and

there are many cases where the solution only exists for a limited time interval, as, for example, for the equation $\dot{x} = x^2$, $x(0) = 1$.

- (a) For what times do solutions of

$$\dot{x} = x(x(t))$$

exist? Do you need a numerical routine to answer this question?

- (b) Let's test the integrator you wrote in exercise 2.6. The equation $\ddot{x} = -x$ with initial conditions $x(0) = 2$ and $\dot{x} = 0$ has as solution $x(t) = e^{-t}(1 + e^{2t})$. Can your integrator reproduce this solution for the interval $t \in [0, 10]$? Check your solution by plotting the error as compared to the exact result.
- (c) Now we will try something a little harder. The equation is going to be third order

$$\ddot{x} + 0.6\dot{x} + \dot{x} - |x| + 1 = 0,$$

which can be checked—numerically—to be chaotic. As initial conditions we will always use $\ddot{x}(0) = \dot{x}(0) = x(0) = 0$. Can you reproduce the result $x(12) = 0.8462071873$ (all digits are significant)? Even though the equation being integrated is chaotic, the time intervals are not long enough for the exponential separation of trajectories to be noticeable (the exponential growth factor is ≈ 2.4).

- (d) Determine the time interval for which the solution of $\dot{x} = x^2$, $x(0) = 1$ exists.

2.10. **Classical collinear helium dynamics.** In order to apply periodic orbit theory to quantization of helium we

shall need to compute classical periodic orbits of the helium system. In this exercise we commence their evaluation for the collinear helium atom (7.6)

$$H = \frac{1}{2}p_1^2 + \frac{1}{2}p_2^2 - \frac{Z}{r_1} - \frac{Z}{r_2} + \frac{1}{r_1 + r_2}.$$

The nuclear charge for helium is $Z = 2$. Collinear helium has only 3 degrees of freedom and the dynamics can be visualized as a motion in the (r_1, r_2) , $r_i \geq 0$ quadrant. In (r_1, r_2) -coordinates the potential is singular for $r_i \rightarrow 0$ nucleus-electron collisions. These 2-body collisions can be regularized by rescaling the coordinates, with details given in sect. 6.3. In the transformed coordinates (x_1, x_2, p_1, p_2) the Hamiltonian equations of motion take the form

$$\begin{aligned} \dot{P}_1 &= 2Q_1 \left[2 - \frac{P_2^2}{8} - Q_2^2 \left(1 + \frac{Q_2^2}{R^4} \right) \right] \\ \dot{P}_2 &= 2Q_2 \left[2 - \frac{P_1^2}{8} - Q_1^2 \left(1 + \frac{Q_1^2}{R^4} \right) \right] \\ \dot{Q}_1 &= \frac{1}{4}P_1Q_2^2, \quad \dot{Q}_2 = \frac{1}{4}P_2Q_1^2. \end{aligned} \quad (2.20)$$

where $R = (Q_1^2 + Q_2^2)^{1/2}$.

- (a) Integrate the equations of motion by the fourth order Runge-Kutta computer routine of exercise 2.6 (or whatever integration routine you like). A convenient way to visualize the 3-dimensional state space orbit is by projecting it onto the 2-dimensional $(r_1(t), r_2(t))$ plane. (continued as exercise 3.4)

(Gregor Tanner, Per Rosenqvist)

References

- [2.1] G. Duffing, *Erzwungene Schwingungen bei veränderlicher Eigenfrequenz* (Vieweg, Braunschweig 1918).
- [2.2] O. Rössler, "An equation for continuous chaos," *Phys. Lett.* **57A**, 397 (1976).
- [2.3] J. Peinke, J. Parisi, O. E. Rössler, and R. Stoop, *Encounter with Chaos. Self-Organized Hierarchical Complexity in Semiconductor Experiments* (Springer, Berlin 1992).
- [2.4] R. Gilmore and M. Lefranc, *The Topology of Chaos* (Wiley, New York 2002).
- [2.5] J. M. T. Thompson and H. B. Stewart, *Nonlinear Dynamics and Chaos* (Wiley, New York 2002).

- [2.6] R. H. Abraham, C. D. Shaw, *Dynamics—The Geometry of Behavior* (Addison-Wesley, Redwood, Ca, 1992).
- [2.7] T. Jones, *Symmetry of Chaos Animations*, lagrange.physics.drexel.edu/flash.
- [2.8] E. N. Lorenz, “Deterministic nonperiodic flow,” *J. Atmos. Sci.* **20**, 130 (1963).
- [2.9] M. L. Cartwright and J. E. Littlewood, “On nonlinear differential equations of the second order,” *J. London Math. Soc.* **20**, 180 (1945).
- [2.10] P. Cvitanović, ed., *Universality in Chaos*, (Adam Hilger, Bristol 1989).
- [2.11] Bai-Lin Hao, *Chaos II* (World Scientific, Singapore 1990).
- [2.12] D. Rothman, [Nonlinear Dynamics I: Chaos \(MIT OpenCourseWare 2006\)](#).
- [2.13] W. Tucker, “The Lorenz attractor exists,” *C. R. Acad. Sci. Paris Sér. I Math* **328**, 1197 (1999).
- [2.14] W. Tucker, “A rigorous ODE solver and Smale’s 14th problem,” *Found. Comput. Math.* **2**, 53 (2002).
- [2.15] M. Viana, “What’s new on Lorenz strange attractors?” *Math. Intelligencer* **22**, 6 (2000).
- [2.16] J. Frøyland, *Chaos and coherence* (Inst. of Phys. Publ., Bristol 1992).
- [2.17] J. Frøyland and K. H. Alfsen, “Lyapunov-exponent spectra for the Lorenz model,” *Phys. Rev. A* **29**, 2928 (1984).
- [2.18] J. Guckenheimer and R. Williams, “Structural stability of the Lorenz attractor,” *Publ. Math. IHES* **50**, 55 (1979).
- [2.19] V. S. Afraimovich, B. B. Bykov, and L. P. Shilnikov, “On the appearance and the structure of the Lorenz attractor,” *Dokl. Akad. Nauk SSSR* **234**, 336 (1987).
- [2.20] C. Sparrow, *The Lorenz Equations: Bifurcations, Chaos, and Strange Attractors* (Springer-Verlag, Berlin 1982).
- [2.21] E. A. Jackson, *Perspectives of nonlinear dynamics: Vol. 1 and 2* (Cambridge Univ. Press, Cambridge 1989).
- [2.22] R. Seydel, *From equilibrium to chaos: Practical bifurcation and stability analysis* (Elsevier, New York 1988).
- [2.23] D. Viswanath, “Symbolic dynamics and periodic orbits of the Lorenz attractor,” *Nonlinearity* **16**, 1035 (2003).
- [2.24] D. Viswanath, “The fractal property of the Lorenz attractor,” *Physica D* **190**, 115 (2004).

- [2.25] D. Viswanath and S. Şahutoğlu, “Complex singularities and the Lorenz attractor,” *SIAM Review* (2009); [arXiv:0901.4968](https://arxiv.org/abs/0901.4968).
- [2.26] P. Manneville and Y. Pomeau, “Different Ways to Turbulence in Dissipative Systems,” *Physica D* **1**, 219 (1980).
- [2.27] J. B. Laughlin and P. C. Martin, “Transition to Turbulence of a Statically Stressed Fluid,” *Phys. Rev. Lett.* **33**, 1189 (1974).
- [2.28] J. Laskar, “The chaotic behaviour of the solar system: A numerical estimate of the size of the chaotic zones ,” *Icarus* **88**, 266 (1990).
- [2.29] C. Skokos, “Alignment indices: a new, simple method for determining the ordered or chaotic nature of orbits,” *J. Phys A* **34**, 10029 (2001).
- [2.30] J. D. Meiss, *Sci.nonlinear FAQ, Computational Resources*, amath.colorado.edu/faculty/jdm/faq.html.
- [2.31] DSWeb Dynamical Systems Software, www.dynamicalsystems.org.
- [2.32] W. H. Press, B. P. Flannery, S.A. Teukolsky and W.T. Vetterling, *Numerical Recipes* (Cambridge Univ. Press, 1986).

Chapter 3

Discrete time dynamics

(R. Mainieri and P. Cvitanović)

THE TIME PARAMETER in the sect. 2.1 definition of a dynamical system can be either continuous or discrete. Discrete time dynamical systems arise naturally from flows; one can observe the flow at fixed time intervals (by strobing it), or one can record the coordinates of the flow when a special event happens (the Poincaré section method). This triggering event can be as simple as vanishing of one of the coordinates, or as complicated as the flow cutting through a curved hypersurface.

3.1 Poincaré sections

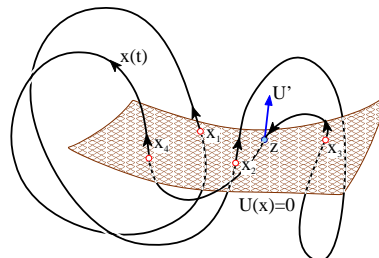


Successive trajectory intersections with a *Poincaré section*, a $(d - 1)$ -dimensional hypersurface or a set of hypersurfaces \mathcal{P} embedded in the d -dimensional state space \mathcal{M} , define the *Poincaré return map* $P(x)$, a $(d - 1)$ -dimensional map of form

$$x' = P(x) = f^{\tau(x)}(x), \quad x', x \in \mathcal{P}. \quad (3.1)$$

Here the *first return function* $\tau(x)$ —sometimes referred to as the *ceiling function*—is the time of flight to the next section for a trajectory starting at x . The choice of

Figure 3.1: A $x(t)$ trajectory that intersects a Poincaré section \mathcal{P} at times t_1, t_2, t_3, t_4 , and closes a cycle (x_1, x_2, x_3, x_4) , $x_k = x(t_k) \in \mathcal{P}$ of topological length 4 with respect to this section. Note that the intersections are not normal to the section, and that the crossing z does not count, as it is in the wrong direction.



the section hypersurface \mathcal{P} is altogether arbitrary. It is rarely possible to define a single section that cuts across all trajectories of interest. In practice one often needs only a local section—a finite hypersurface of codimension 1 intersected by a swarm of trajectories near to the trajectory of interest. The hypersurface can be specified implicitly through a function $U(x)$ that is zero whenever a point x is on the Poincaré section,

$$x \in \mathcal{P} \quad \text{iff} \quad U(x) = 0. \quad (3.2)$$

The gradient of $U(x)$ evaluated at $x \in \mathcal{P}$ serves a two-fold function. First, the flow should pierce the hypersurface \mathcal{P} , rather than being tangent to it. A nearby point $x + \delta x$ is in the hypersurface \mathcal{P} if $U(x + \delta x) = 0$. A nearby point on the trajectory is given by $\delta x = v\delta t$, so a traversal is ensured by the *transversality condition*

$$(v \cdot \partial U) = \sum_{j=1}^d v_j(x) \partial_j U(x) \neq 0, \quad \partial_j U(x) = \frac{\partial}{\partial x_j} U(x), \quad x \in \mathcal{P}. \quad (3.3)$$

Second, the gradient $\partial_j U$ defines the orientation of the hypersurface \mathcal{P} . The flow is oriented as well, and a periodic orbit can pierce \mathcal{P} twice, traversing it in either direction, as in figure 3.1. Hence the definition of Poincaré return map $P(x)$ needs to be supplemented with the orientation condition

$$\begin{aligned} x_{n+1} = P(x_n), \quad U(x_{n+1}) = U(x_n) = 0, \quad n \in \mathbb{Z}^+ \\ \sum_{j=1}^d v_j(x_n) \partial_j U(x_n) > 0. \end{aligned} \quad (3.4)$$

In this way the continuous time t flow $f^t(x)$ is reduced to a discrete time n sequence x_n of successive *oriented* trajectory traversals of \mathcal{P} .

chapter 17

With a sufficiently clever choice of a Poincaré section or a set of sections, any orbit of interest intersects a section. Depending on the application, one might need to convert the discrete time n back to the continuous flow time. This is accomplished by adding up the first return function times $\tau(x_n)$, with the accumulated flight time given by

$$t_{n+1} = t_n + \tau(x_n), \quad t_0 = 0, \quad x_n \in \mathcal{P}. \quad (3.5)$$

Other quantities integrated along the trajectory can be defined in a similar manner, and will need to be evaluated in the process of evaluating dynamical averages.

A few examples may help visualize this.

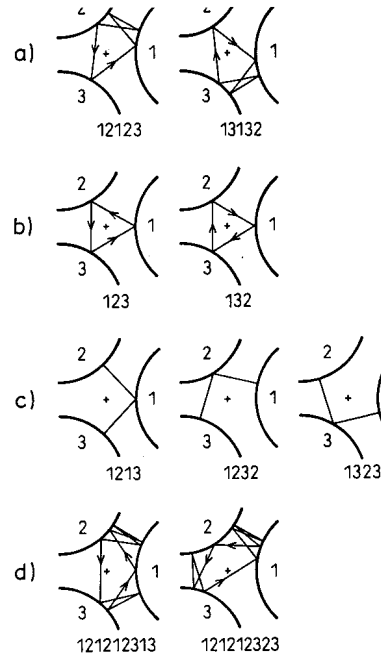


Figure 3.2: Some examples of 3-disk cycles: (a) $\overline{12123}$ and $\overline{13132}$ are mapped into each other by the flip across 1 axis. Similarly (b) $\overline{123}$ and $\overline{132}$ are related by flips, and (c) $\overline{1213}$, $\overline{1232}$ and $\overline{1323}$ by rotations. (d) The cycles $\overline{121212313}$ and $\overline{121212323}$ are related by rotation *and* time reversal. These symmetries are discussed in chapter 9. (From ref. [1])

Example 3.1 Hyperplane \mathcal{P} : The simplest choice of a Poincaré section is a plane \mathcal{P} specified by a point (located at the tip of the vector r_0) and a direction vector a perpendicular to the plane. A point x is in this plane if it satisfies the condition

$$U(x) = (x - r_0) \cdot a = 0. \quad (3.6)$$

Consider a circular periodic orbit centered at r_0 , but not lying in \mathcal{P} . It pierces the hyperplane twice; the $(v \cdot a) > 0$ traversal orientation condition (3.4) ensures that the first return time is the full period of the cycle. (continued in example 12.1)

The above flat hyperplane is an *ad hoc* construct; one Poincaré section rarely suffices to capture all of the dynamics of interest. A more insightful picture of the dynamics is obtained by partitioning the state space into N qualitatively distinct regions $\{\mathcal{M}_1, \mathcal{M}_2, \dots, \mathcal{M}_N\}$ and constructing a Poincaré section \mathcal{P}_s per region. The d -dimensional flow is thus reduced reduced to composition

section 11.1

$$P_{s_n \leftarrow s_{n-1}} \circ \dots \circ P_{s_2 \leftarrow s_1} \circ P_{s_1 \leftarrow s_0}$$

of a set of $(d-1)$ -dimensional maps

$$P_{s_{n+1} \leftarrow s_n} : x_n \mapsto x_{n+1}, \quad s \in \{1, 2, \dots, N\} \quad (3.7)$$

that map the coordinates of Poincaré section \mathcal{P}_{s_n} to those of $\mathcal{P}_{s_{n+1}}$, the next section traversed by a given trajectory.

A return map P_{s_0} from section \mathcal{P}_{s_0} to itself now has a contribution from any admissible (i.e., there exist trajectories that traverse regions $\mathcal{M}_{s_0} \rightarrow \mathcal{M}_{s_1} \rightarrow \dots \rightarrow \mathcal{M}_{s_n} \rightarrow \mathcal{M}_{s_0}$ in the same temporal sequence) periodic sequence of compositions

$$P_{s_0 s_1 \dots s_{n-1}} = P_{s_0 \leftarrow s_{n-1}} \circ \dots \circ P_{s_2 \leftarrow s_1} \circ P_{s_1 \leftarrow s_0} \quad (3.8)$$

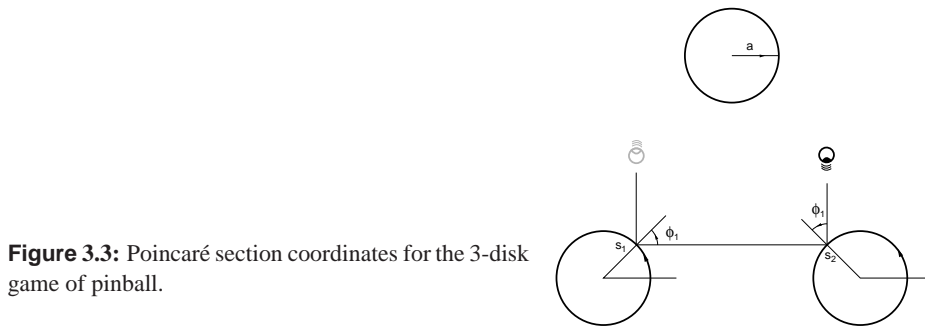


Figure 3.3: Poincaré section coordinates for the 3-disk game of pinball.

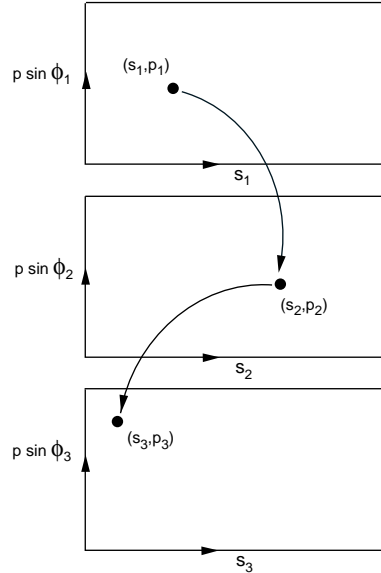


Figure 3.4: Collision sequence $(s_1, p_1) \mapsto (s_2, p_2) \mapsto (s_3, p_3)$ from the boundary of a disk to the boundary of the next disk is coded by the Poincaré sections maps sequence $P_{3 \leftarrow 2} P_{2 \leftarrow 1}$.

The next example offers an unambiguous set of such Poincaré sections which do double duty, providing us both with an exact representation of dynamics in terms of maps, and with a covering symbolic dynamics, a subject that will return to in chapter 11.

Example 3.2 Pinball game, Poincaré dissected. A phase space orbit is fully specified by its position and momentum at a given instant, so no two distinct phase space trajectories can intersect. The configuration space trajectories, however, can and do intersect, in rather unilluminating ways, as e.g. in figure 3.2 (d), and it can be rather hard to perceive the systematics of orbits from their configuration space shapes. The problem is that we are looking at the projections of a 4-dimensional state space trajectories onto a 2-dimensional configuration subspace. A much clearer picture of the dynamics is obtained by constructing a set of state space Poincaré sections.

Suppose that the pinball has just bounced off disk 1. Depending on its position and outgoing angle, it could proceed to either disk 2 or 3. Not much happens in between the bounces—the ball just travels at constant velocity along a straight line—so we can reduce the 4-dimensional flow to a 2-dimensional map $P_{\sigma_k \leftarrow \sigma_j}$ that maps the coordinates (Poincaré section \mathcal{P}_1) of the pinball from one disk edge to another. Just after the moment of impact the trajectory is defined by s_n , the arc-length position of the n th bounce along the billiard wall, and $p_n = p \sin \phi_n$ the momentum component parallel to the billiard wall at the point of impact, figure 3.3. These coordinates (due to Birkhoff) are smart, as they conserve the phase space volume. Trajectories originating from one disk can hit either of the other two disks, or escape without further ado. We label the

survivor state space regions $\mathcal{P}_{12}, \mathcal{P}_{13}$. In terms of the three Poincaré sections, one for each disk, the dynamics is reduced to the set of six maps

$$P_{\sigma_{n+1} \leftarrow \sigma_n} : (s_n, p_n) \mapsto (s_{n+1}, p_{n+1}), \quad \sigma \in \{1, 2, 3\} \tag{3.9}$$

from the boundary of the disk j to the boundary of the next disk k , figure 3.4. The explicit form of this map is easily written down, see sect. 8, but much more economical is the symmetry quotiented version of chapter 9 which replaces the above 6 maps by a return map pair P_0, P_1 . chapter 9

Embedded within $\mathcal{P}_{12}, \mathcal{P}_{13}$ are four strips $\mathcal{P}_{121}, \mathcal{P}_{123}, \mathcal{P}_{131}, \mathcal{P}_{132}$ of initial conditions that survive two bounces, and so forth. Provided that the disks are sufficiently separated, after n bounces the survivors are labeled by 2^n distinct itineraries $\sigma_1 \sigma_2 \sigma_3 \dots \sigma_n$. chapter 8

Billiard dynamics is exceptionally simple - free flight segments, followed by specular reflections at boundaries, thus billiard boundaries are the obvious choice as Poincaré sections. What about smooth, continuous time flows, with no obvious surfaces that would fix the choice of Poincaré sections?

Example 3.3 Pendulum: The phase space of a simple pendulum is 2-dimensional: momentum on the vertical axis and position on the horizontal axis. We choose the Poincaré section to be the positive horizontal axis. Now imagine what happens as a point traces a trajectory through this phase space. As long as the motion is oscillatory, in the pendulum all orbits are loops, so any trajectory will periodically intersect the line, that is the Poincaré section, at one point.

Consider next a pendulum with friction, such as the unforced Duffing system plotted in figure 2.4. Now every trajectory is an inward spiral, and the trajectory will intersect the Poincaré section $y = 0$ at a series of points that get closer and closer to either of the equilibrium points; the Duffing oscillator at rest.

Motion of a pendulum is so simple that you can sketch it yourself on a piece of paper. The next example offers a better illustration of the utility of visualization of dynamics by means of Poincaré sections.

Example 3.4 Rössler flow: (continued from example 2.3) Consider figure 2.6, a typical trajectory of the 3-dimensional Rössler flow (2.17). It wraps around the z axis, so a good choice for a Poincaré section is a plane passing through the z axis. A sequence of such Poincaré sections placed radially at increasing angles with respect to the x axis, figure 3.5, illustrates the 'stretch & fold' action of the Rössler flow, by assembling these sections into a series of snapshots of the flow. A line segment $[A, B]$, traversing the width of the attractor at $y = 0, x > 0$ section, starts out close to the x - y plane, and after the stretching (a) \rightarrow (b) followed by the folding (c) \rightarrow (d), the folded segment returns close to the x - y plane strongly compressed. In one Poincaré return the $[A, B]$ interval is stretched, folded and mapped onto itself, so the flow is expanding. It is also mixing, as in one Poincaré return a point C from the interior of the attractor can map onto the outer edge, while the edge point B lands in the interior.

Once a particular Poincaré section is picked, we can also exhibit the return map (3.1), as in figure 3.6. Cases (a) and (d) are examples of nice 1-to-1 return maps. However, (b) and (c) appear multimodal and non-invertible, artifacts of projection of a 2 - dimensional return map $(R_n, z_n) \rightarrow (R_{n+1}, z_{n+1})$ onto a 1-dimensional subspace $R_n \rightarrow R_{n+1}$. (continued in example 3.6)

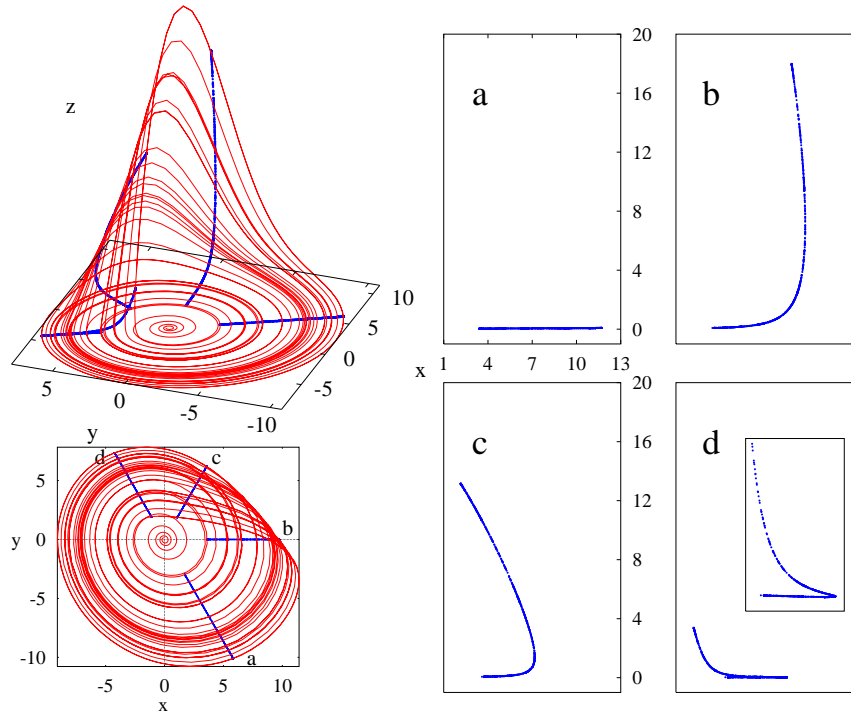


Figure 3.5: (Right:) a sequence of Poincaré sections of the Rössler strange attractor, defined by planes through the z axis, oriented at angles (a) -60° (b) 0° , (c) 60° , (d) 120° , in the x - y plane. (Left:) side and x - y plane view of a typical trajectory with Poincaré sections superimposed. (R. Paškauskas)

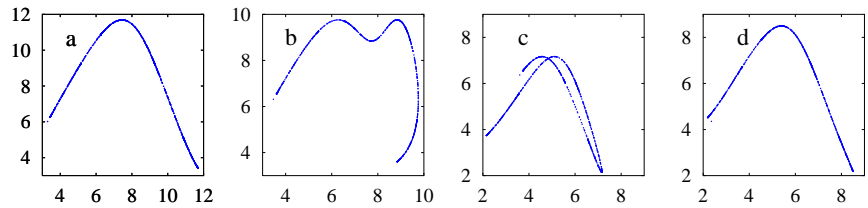


Figure 3.6: Return maps for the $R_n \rightarrow R_{n+1}$ radial distance Poincaré sections of figure 3.5. (R. Paškauskas)



fast track:
sect. 3.3, p. 62

The above examples illustrate why a Poincaré section gives a more informative snapshot of the flow than the full flow portrait. For example, while the full flow portrait of the Rössler flow figure 2.6 gives us no sense of the thickness of the attractor, we see clearly in figure 3.5 Poincaré sections that even though the return map is $2 - dimensional \rightarrow 2 - dimensional$, the flow contraction is so strong that for all practical purposes it renders the return map $1 - dimensional$.

3.1.1 What’s the best Poincaré section?

In practice, picking sections is a dark and painful art, especially for high-dimensional flows where the human visual cortex falls short. It helps to understand why we need them in the first place.

Whenever a system has a continuous symmetry G , any two solutions related by the symmetry are equivalent, so it would be stupid to keep recomputing them

over and over. We would rather replace the whole continuous family of solutions by one.

A smart way to do would be to replace dynamics (M, f) by dynamics on the *quotient state space* $(M/G, \tilde{f})$. We will discuss this in chapter 9, but in general constructing explicit quotient state space flow \tilde{f} appears either difficult, or not appreciated enough to generate much readable literature, or perhaps impossible. So one resorts to method of sections. chapter 9

Time evolution itself is a 1-parameter Abelian Lie group, albeit a highly non-trivial one (otherwise this book would not be much of a doorstop). The invariants of the flow are its infinite-time orbits; particularly useful invariants are compact orbits such as equilibrium points, periodic orbits and tori. For any orbit it suffices to pick a single state space point $x \in \mathcal{M}_p$, the rest of the orbit is generated by the flow and its symmetries.

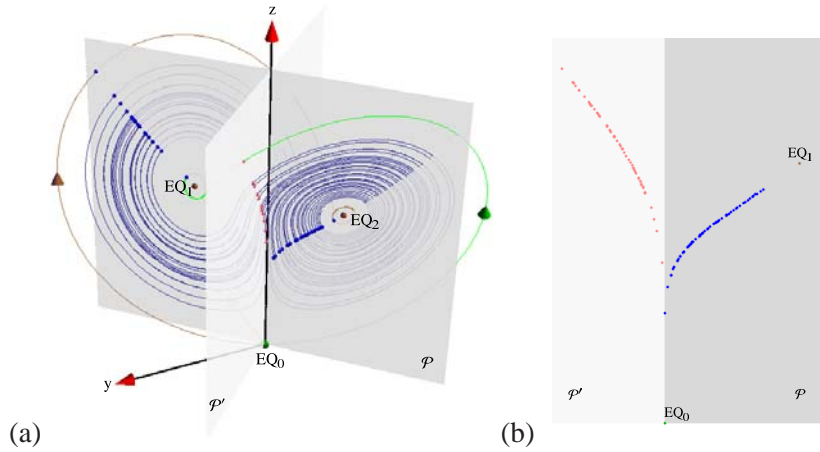
Choice of this one point is utterly arbitrary; in dynamics this is called a “Poincaré section,” and in theoretical physics this goes by the exceptionally uninformative name of “gauge fixing.” The price is that one generates “ghosts,” or, in dynamics, increases the dimensionality of the state space by additional constraints (see sect. 13.4). It is a commonly deployed but inelegant procedure where symmetry is broken for computational convenience, and restored only at the end of the calculation, when all broken pieces are reassembled.

This said, there are a few rules of thumb to follow: (a) You can pick as many sections as convenient. (b) For ease of computation, pick linear sections (3.6) if you can. (c) If equilibria play important role in organizing a flow, pick sections that go through them (see example 3.5). (c) If you have a global discrete or continuous symmetry, pick sections left invariant by the symmetry (see example 9.10). (d) If you are solving a local problem, like finding a periodic orbit, you do not need a global section. Pick a section or a set of (multi-shooting) sections on the fly, requiring only that they are locally transverse to the flow. (e) If you have another rule of thumb dear to you, let us know. chapter 9

Example 3.5 Sections of Lorenz flow: (continued from example 2.2) The plane \mathcal{P} fixed by the $x = y$ diagonal and the z -axis depicted in figure 3.7 is a natural choice of a Poincaré section of the Lorenz flow of figure 2.5, as it contains all three equilibria, $x_{EQ_0} = (0, 0, 0)$ and the (2.13) pair x_{EQ_1}, x_{EQ_2} . A section has to be supplemented with the orientation condition (3.4): here points where flow pierces into the section are marked by dots.

x_{EQ_1}, x_{EQ_2} are centers of out-spirals, and close to them the section to EQ_0 trajectories pass the z -axis either by crossing the section \mathcal{P} or staying on the viewer’s side. We are free to deploy as many sections as we wish: in order to capture the whole flow in this neighborhood we add the second Poincaré section, \mathcal{P}' , through the $y = -x$ diagonal and the z -axis. Together the two sections, figure 3.7(b), capture the whole flow near EQ_0 . In contrast to Rössler sections of figure 3.5, these appear very singular. We explain this singularity in example 4.7, and postpone construction of a Poincaré return map to example 9.10. (E. Siminos and J. Halcrow)

Figure 3.7: (a) Lorenz flow figure 2.5 cut by $y = x$ Poincaré section plane \mathcal{P} through the z axis and both $EQ_{1,2}$ equilibria. Points where flow pierces into section are marked by dots. To aid visualization of the flow near the EQ_0 equilibrium, the flow is cut by the second Poincaré section, \mathcal{P}' , through $y = -x$ and the z axis. (b) Poincaré sections \mathcal{P} and \mathcal{P}' laid side-by-side. The singular nature of these sections close to EQ_0 will be elucidated in example 4.7 and figure 11.8 (b). (E. Siminos)



3.2 Constructing a Poincaré section

For almost any flow of physical interest a Poincaré section is not available in analytic form. We describe now a numerical method for determining a Poincaré section.

Consider the system (2.6) of ordinary differential equations in the vector variable $x = (x_1, x_2, \dots, x_d)$

$$\frac{dx_i}{dt} = v_i(x, t), \tag{3.10}$$

where the flow velocity v is a vector function of the position in state space x and the time t . In general, v cannot be integrated analytically, so we will have to resort to numerical integration to determine the trajectories of the system. Our task is to determine the points at which the numerically integrated trajectory traverses a given hypersurface. The hypersurface will be specified implicitly through a function $U(x)$ that is zero whenever a point x is on the Poincaré section, such as the hyperplane (3.6).

If we use a tiny step size in our numerical integrator, we can observe the value of U as we integrate; its sign will change as the trajectory crosses the hypersurface. The problem with this method is that we have to use a very small integration time step. In order to land exactly on the Poincaré section one often interpolates the intersection point from the two trajectory points on either side of the hypersurface. However, there is a better way.

Let t_a be the time just before U changes sign, and t_b the time just after it changes sign. The method for landing exactly on the Poincaré section will be to convert one of the space coordinates into an integration variable for the part of the trajectory between t_a and t_b . Using

$$\frac{dx_k}{dx_1} \frac{dx_1}{dt} = \frac{dx_k}{dx_1} v_1(x, t) = v_k(x, t) \tag{3.11}$$



remark 3.1

we can rewrite the equations of motion (3.10) as

$$\frac{dt}{dx_1} = \frac{1}{v_1}, \dots, \frac{dx_d}{dx_1} = \frac{v_d}{v_1}. \quad (3.12)$$

Now we use x_1 as the ‘time’ in the integration routine and integrate it from $x_1(t_a)$ to the value of x_1 on the hypersurface, determined by the hypersurface intersection condition (3.6). This is the end point of the integration, with no need for any interpolation or backtracking to the surface of section. The x_1 -axis need not be perpendicular to the Poincaré section; any x_i can be chosen as the integration variable, provided the x_i -axis is not parallel to the Poincaré section at the trajectory intersection point. If the section crossing is transverse (3.3), v_1 cannot vanish in the short segment bracketed by the integration step preceding the section, and the point on the Poincaré section.

Example 3.6 Computation of Rössler flow Poincaré sections. (continued from example 3.4) Poincaré sections of figure 3.5 are defined by the fixing angle $U(x) = \theta - \theta_0 = 0$. Convert Rössler equation (2.17) to cylindrical coordinates:

$$\begin{aligned} \dot{r} &= v_r = -z \cos \theta + ar \sin^2 \theta \\ \dot{\theta} &= v_\theta = 1 + \frac{z}{r} \sin \theta + \frac{a}{2} \sin 2\theta \\ \dot{z} &= v_z = b + z(r \cos \theta - c). \end{aligned} \quad (3.13)$$

In principle one should use the equilibrium x_+ from (2.18) as the origin, and its eigenvectors as the coordinate frame, but here original coordinates suffice, as for parameter values (2.17), and (x_0, y_0, z_0) sufficiently far away from the inner equilibrium, θ increases monotonically with time. Integrate

$$\frac{dr}{d\theta} = v_r/v_\theta, \quad \frac{dt}{d\theta} = 1/v_\theta, \quad \frac{dz}{d\theta} = v_z/v_\theta \quad (3.14)$$

from (r_n, θ_n, z_n) to the next Poincaré section at θ_{n+1} , and switch the integration back to (x, y, z) coordinates. (continued in example 4.1) (Radford Mitchell, Jr.)

3.3 Maps

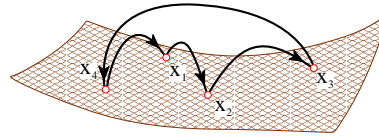


Do it again!
—Isabelle, age 3

Though we have motivated discrete time dynamics by considering sections of a continuous flow, there are many settings in which dynamics is inherently discrete, and naturally described by repeated iterations of the same map

$$f : \mathcal{M} \rightarrow \mathcal{M},$$

Figure 3.8: A flow $x(t)$ of figure 3.1 represented by a Poincaré return map that maps points in the Poincaré section \mathcal{P} as $x_{n+1} = f(x_n)$. In this example the orbit of x_1 is periodic and consists of the four periodic points (x_1, x_2, x_3, x_4) .



or sequences of consecutive applications of a finite set of maps,

$$\{f_A, f_B, \dots, f_Z\} : \mathcal{M} \rightarrow \mathcal{M}, \tag{3.15}$$

for example maps relating different sections among a set of Poincaré sections. The discrete ‘time’ is then an integer, the number of applications of a map. As writing out formulas involving repeated applications of a set of maps explicitly can be awkward, we streamline the notation by denoting a map composition by ‘ \circ ’

$$f_Z(\dots f_B(f_A(x))\dots) = f_Z \circ \dots \circ f_B \circ f_A(x), \tag{3.16}$$

and the n th iterate of map f by

$$f^n(x) = f \circ f^{n-1}(x) = f(f^{n-1}(x)), \quad f^0(x) = x.$$

section 2.1

The *trajectory* of x is now the discrete set of points

$$\{x, f(x), f^2(x), \dots, f^n(x)\},$$

and the *orbit* of x is the subset of all points of \mathcal{M} that can be reached by iterations of f . A *periodic point* (cycle point) x_k belonging to a cycle of period n is a real solution of

$$f^n(x_k) = f(f(\dots f(x_k)\dots)) = x_k, \quad k = 0, 1, 2, \dots, n - 1. \tag{3.17}$$

For example, the orbit of x_1 in figure 3.8 is the 4-cycle (x_1, x_2, x_3, x_4) .

The functional form of such Poincaré return maps P as figure 3.6 can be approximated by tabulating the results of integration of the flow from x to the first Poincaré section return for many $x \in \mathcal{P}$, and constructing a function that interpolates through these points. If we find a good approximation to $P(x)$, we can get rid of numerical integration altogether, by replacing the continuous time trajectory $f^t(x)$ by iteration of the Poincaré return map $P(x)$. Constructing accurate $P(x)$ for a given flow can be tricky, but we can already learn much from approximate Poincaré return maps. Multinomial approximations

$$P_k(x) = a_k + \sum_{j=1}^d b_{kj}x_j + \sum_{i,j=1}^d c_{kij}x_i x_j + \dots, \quad x \in \mathcal{P} \tag{3.18}$$

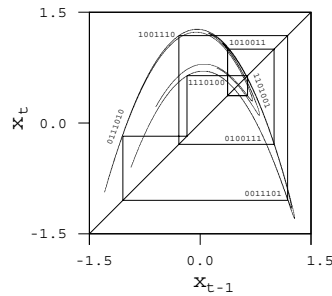


Figure 3.9: The strange attractor and an unstable period 7 cycle of the Hénon map (3.19) with $a = 1.4$, $b = 0.3$. The periodic points in the cycle are connected to guide the eye. (from K.T. Hansen [2])

to Poincaré return maps

$$\begin{pmatrix} x_{1,n+1} \\ x_{2,n+1} \\ \dots \\ x_{d,n+1} \end{pmatrix} = \begin{pmatrix} P_1(x_n) \\ P_2(x_n) \\ \dots \\ P_d(x_n) \end{pmatrix}, \quad x_n, x_{n+1} \in \mathcal{P}$$

motivate the study of model mappings of the plane, such as the Hénon map.

Example 3.7 Hénon map: The map

$$\begin{aligned} x_{n+1} &= 1 - ax_n^2 + by_n \\ y_{n+1} &= x_n \end{aligned} \tag{3.19}$$

is a nonlinear 2-dimensional map most frequently employed in testing various hunches about chaotic dynamics. The Hénon map is sometimes written as a 2-step recurrence relation

$$x_{n+1} = 1 - ax_n^2 + bx_{n-1}. \tag{3.20}$$

An n -step recurrence relation is the discrete-time analogue of an n th order differential equation, and it can always be replaced by a set of n 1-step recurrence relations.

The Hénon map is the simplest map that captures the ‘stretch & fold’ dynamics of return maps such as Rössler’s, figure 3.5. It can be obtained by a truncation of a polynomial approximation (3.18) to a Poincaré return map (3.18) to second order.

A quick sketch of the long-time dynamics of such a mapping (an example is depicted in figure 3.9), is obtained by picking an arbitrary starting point and iterating (3.19) on a computer. We plot here the dynamics in the (x_n, x_{n+1}) plane, rather than in the (x_n, y_n) plane, because we think of the Hénon map as a model return map $x_n \rightarrow x_{n+1}$. As we shall soon see, periodic orbits will be key to understanding the long-time dynamics, so we also plot a typical periodic orbit of such a system, in this case an unstable period 7 cycle. Numerical determination of such cycles will be explained in sect. 29.1, and the periodic point labels 0111010, 1110100, \dots in sect. 12.2. exercise 3.5

Example 3.8 Lozi map: Another example frequently employed is the Lozi map, a linear, ‘tent map’ version of the Hénon map (3.19) given by

$$\begin{aligned}x_{n+1} &= 1 - a|x_n| + by_n \\ y_{n+1} &= x_n.\end{aligned}\tag{3.21}$$

Though not realistic as an approximation to a smooth flow, the Lozi map is a very helpful tool for developing intuition about the topology of a large class of maps of the ‘stretch & fold’ type.

What we get by iterating such maps is—at least qualitatively—not unlike what we get from Poincaré section of flows such as the Rössler flow figure 3.6. For an arbitrary initial point this process might converge to a stable limit cycle, to a strange attractor, to a false attractor (due to roundoff errors), or diverge. In other words, mindless iteration is essentially uncontrollable, and we will need to resort to more thoughtful explorations. As we shall explain in due course, strategies for systematic exploration rely on stable/unstable manifolds, periodic points, saddle-straddle methods and so on.

exercise 3.5

Example 3.9 Parabola: For sufficiently large value of the stretching parameter a , one iteration of the Hénon map (3.19) stretches and folds a region of the (x, y) plane centered around the origin. The parameter a controls the amount of stretching, while the parameter b controls the thickness of the folded image through the ‘1-step memory’ term bx_{n-1} in (3.20). In figure 3.9 the parameter b is rather large, $b = 0.3$, so the attractor is rather thick, with the transverse fractal structure clearly visible. For vanishingly small b the Hénon map reduces to the 1-dimensional quadratic map

$$x_{n+1} = 1 - ax_n^2.\tag{3.22}$$

By setting $b = 0$ we lose determinism, as on reals the inverse of map (3.22) has two preimages $\{x_{n-1}^+, x_{n-1}^-\}$ for most x_n . If Bourbaki is your native dialect: the Hénon map is injective or one-to-one, but the quadratic map is surjective or many-to-one. Still, this 1-dimensional approximation is very instructive. (continued in example 11.5)

exercise 3.6

As we shall see in sect. 11.3, an understanding of 1-dimensional dynamics is indeed the essential prerequisite to unraveling the qualitative dynamics of many higher-dimensional dynamical systems. For this reason many expositions of the theory of dynamical systems commence with a study of 1-dimensional maps. We prefer to stick to flows, as that is where the physics is.

appendix H.8

Résumé

In recurrent dynamics a trajectory exits a region in state space and then reenters it infinitely often, with a finite mean return time. If the orbit is periodic, it returns after a full period. So, on average, nothing much really happens along the trajectory—what is important is behavior of neighboring trajectories transverse to

the flow. This observation motivates a replacement of the continuous time flow by iterative mapping, the Poincaré return map.

The visualization of strange attractors is greatly facilitated by a felicitous choice of Poincaré sections, and the reduction of flows to Poincaré return maps. This observation motivates in turn the study of discrete-time dynamical systems generated by iterations of maps.

A particularly natural application of the Poincaré section method is the reduction of a billiard flow to a boundary-to-boundary return map, described in chapter 8. As we shall show in chapter 6, further simplification of a Poincaré return map, or any nonlinear map, can be attained through rectifying these maps locally by means of smooth conjugacies.

chapter 8
chapter 6

Commentary

Remark 3.1 Determining a Poincaré section. The idea of changing the integration variable from time to one of the coordinates, although simple, avoids the alternative of having to interpolate the numerical solution to determine the intersection. The trick described in sect. 3.2 is due to Hénon [3, 4, 5].

Remark 3.2 Hénon, Lozi maps. The Hénon map is of no particular physical import in and of itself—its significance lies in the fact that it is a minimal normal form for modeling flows near a saddle-node bifurcation, and that it is a prototype of the stretching and folding dynamics that leads to deterministic chaos. It is generic in the sense that it can exhibit arbitrarily complicated symbolic dynamics and mixtures of hyperbolic and non-hyperbolic behaviors. Its construction was motivated by the best known early example of ‘deterministic chaos’, the Lorenz equation, see example 2.2 and remark 2.3.

Hénon’s and Lorenz’s original papers can be found in reprint collections refs. [7, 8]. They are a pleasure to read, and are still the best introduction to the physics motivating such models. The rigorous proof of the existence of Hénon attractor is due to Benedicks and Carleson [9]. A detailed description of the dynamics of the Hénon map is given by Mira and coworkers [10, 11, 12], as well as very many other authors.

The Lozi map [13] is particularly convenient in investigating the symbolic dynamics of 2 – dimensional mappings. Both the Lorenz and Lozi systems are uniformly smooth systems with singularities. The existence of the attractor for the Lozi map was proven by M. Misiurewicz [14], and the existence of the SRB measure was established by L.-S. Young [15].

section 16.1

Remark 3.3 Grasshoppers vs. butterflies. The ‘sensitivity to initial conditions’ was discussed by Maxwell, then 30 years later by Poincaré. In weather prediction, the Lorentz’ ‘Butterfly Effect’ started its journey in 1898, as a ‘Grasshopper Effect’ in a book review by W. S. Franklin [16]. In 1963 Lorenz ascribed a ‘seagull effect’ to an unnamed meteorologist, and in 1972 he repackaged it as the ‘Butterfly Effect’.

Exercises

3.1. Poincaré sections of the Rössler flow.

(continuation of exercise 2.8) Calculate numerically a Poincaré section (or several Poincaré sections) of the Rössler flow. As the Rössler flow state space is $3D$, the flow maps onto a $2D$ Poincaré section. Do you see that in your numerical results? How good an approximation would a replacement of the return map for this section by a 1-dimensional map be? More precisely, estimate the thickness of the strange attractor. (continued as exercise 4.4)

(R. Paškauskas)

3.2. A return Poincaré map for the Rössler flow.

(continuation of exercise 3.1) That Poincaré return maps of figure 3.6 appear multimodal and non-invertible is an artifact of projections of a 2-dimensional return map $(R_n, z_n) \rightarrow (R_{n+1}, z_{n+1})$ onto a 1-dimensional subspace $R_n \rightarrow R_{n+1}$.

Construct a genuine $s_{n+1} = f(s_n)$ return map by parametrizing points on a Poincaré section of the attractor figure 3.5 by a Euclidean length s computed curvilinearly along the attractor section.

This is best done (using methods to be developed in what follows) by a continuation of the unstable manifold of the 1-cycle embedded in the strange attractor, figure 13.2 (b).

(P. Cvitanović)

3.3. Arbitrary Poincaré sections.

We will generalize the construction of Poincaré sections so that they can have any shape, as specified by the equation $U(x) = 0$.

- (a) Start by modifying your integrator so that you can change the coordinates once you get near the Poincaré section. You can do this easily by writing the equations as

$$\frac{dx_k}{ds} = \kappa f_k, \quad (3.23)$$

with $dt/ds = \kappa$, and choosing κ to be 1 or $1/f_1$. This allows one to switch between t and x_1 as the integration 'time'.

- (b) Introduce an extra dimension x_{n+1} into your system and set

$$x_{n+1} = U(x). \quad (3.24)$$

How can this be used to find a Poincaré section?

3.4. Classical collinear helium dynamics.

(continuation of exercise 2.10) Make a Poincaré surface of section by plotting (r_1, p_1) whenever $r_2 = 0$: Note that for $r_2 = 0$, p_2 is already determined by (7.6). Compare your results with figure 6.3 (b).

(Gregor Tanner, Per Rosenqvist)

3.5. Hénon map fixed points.

Show that the two fixed points (x_0, x_0) , (x_1, x_1) of the Hénon map (3.19) are given by

$$x_0 = \frac{-(1-b) - \sqrt{(1-b)^2 + 4a}}{2a},$$

$$x_1 = \frac{-(1-b) + \sqrt{(1-b)^2 + 4a}}{2a}.$$

3.6. Fixed points of maps.

A continuous function F is a contraction of the unit interval if it maps the interval inside itself.

- (a) Use the continuity of F to show that a 1-dimensional contraction F of the interval $[0, 1]$ has at least one fixed point.
- (b) In a uniform (hyperbolic) contraction the slope of F is always smaller than one, $|F'| < 1$. Is the composition of uniform contractions a contraction? Is it uniform?

References

- [3.1] P. Cvitanović, B. Eckhardt, P. E. Rosenqvist, G. Russberg and P. Scherer, "Pinball Scattering," in G. Casati and B. Chirikov, eds., *Quantum Chaos* (Cambridge U. Press, Cambridge 1993).

- [3.2] K.T. Hansen, *Symbolic Dynamics in Chaotic Systems*, Ph.D. thesis (Univ. of Oslo, 1994);
ChaosBook.org/projects/KTHansen/thesis.
- [3.3] M. Hénon, “On the numerical computation of Poincaré maps,” *Physica D* **5**, 412 (1982).
- [3.4] N.B. Tufillaro, T.A. Abbott, and J.P. Reilly, *Experimental Approach to Non-linear Dynamics and Chaos* (Addison Wesley, Reading MA, 1992).
- [3.5] Bai-Lin Hao, *Elementary symbolic dynamics and chaos in dissipative systems* (World Scientific, Singapore, 1989).
- [3.6] M. Hénon, “A two-dimensional mapping with a strange attractor,” *Comm. Math. Phys.* **50**, 69 (1976).
- [3.7] *Universality in Chaos*, P. Cvitanović, ed., (Adam Hilger, Bristol 1989).
- [3.8] Bai-Lin Hao, *Chaos* (World Scientific, Singapore, 1984).
- [3.9] M. Benedicks and L. Carleson, “The dynamics of the Hénon map,” *Ann. of Math.* **133**, 73 (1991).
- [3.10] C. Mira, *Chaotic Dynamics—From one dimensional endomorphism to two dimensional diffeomorphism*, (World Scientific, Singapore, 1987).
- [3.11] I. Gumowski and C. Mira, *Recurrances and Discrete Dynamical Systems* (Springer-Verlag, Berlin 1980).
- [3.12] D. Fournier, H. Kawakami and C. Mira, *C.R. Acad. Sci. Ser. I*, **298**, 253 (1984); **301**, 223 (1985); **301**, 325 (1985).
- [3.13] R. Lozi, “Un attracteur étrange du type attracteur de Hénon,” *J. Phys. (Paris) Colloq.* **39**, 9 (1978).
- [3.14] M. Misiurewicz, “Strange attractors for the Lozi mapping,” *Ann. New York Acad. Sci.* **357**, 348 (1980).
- [3.15] L.-S. Young, “Bowen-Ruelle measures for certain piecewise hyperbolic maps,” *Trans.Amer.Math.Soc.* **287**, 41 (1985).
- [3.16] W. S. Franklin, “New Books,” *Phys. Rev.* **6**, 173 (1898);
see www.ceafinney.com/chaos.
- [3.17] P. Dahlqvist and G. Russberg, “Existence of stable orbits in the x^2y^2 potential,” *Phys. Rev. Lett.* **65**, 2837 (1990).

Chapter 4

Local stability

(R. Mainieri and P. Cvitanović)

SO FAR we have concentrated on description of the trajectory of a single initial point. Our next task is to define and determine the size of a *neighborhood* of $x(t)$. We shall do this by assuming that the flow is locally smooth, and describe the local geometry of the neighborhood by studying the flow linearized around $x(t)$. Nearby points aligned along the stable (contracting) directions remain in the neighborhood of the trajectory $x(t) = f^t(x_0)$; the ones to keep an eye on are the points which leave the neighborhood along the unstable directions. As we shall demonstrate in chapter 18, in hyperbolic systems what matters are the expanding directions. The repercussion are far-reaching: As long as the number of unstable directions is finite, the same theory applies to finite-dimensional ODEs, state space volume preserving Hamiltonian flows, and dissipative, volume contracting infinite-dimensional PDEs.

4.1 Flows transport neighborhoods

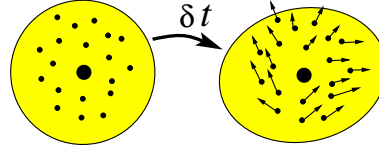


As a swarm of representative points moves along, it carries along and distorts neighborhoods. The deformation of an infinitesimal neighborhood is best understood by considering a trajectory originating near $x_0 = x(0)$ with an initial infinitesimal displacement $\delta x(0)$, and letting the flow transport the displacement $\delta x(t)$ along the trajectory $x(x_0, t) = f^t(x_0)$.

4.1.1 Instantaneous shear

The system of linear *equations of variations* for the displacement of the infinitesimally close neighbor $x + \delta x$ follows from the flow equations (2.6) by Taylor

Figure 4.1: A swarm of neighboring points of $x(t)$ is instantaneously sheared by the action of the stability matrix A - a bit hard to draw.



expanding to linear order

$$\dot{x}_i + \delta \dot{x}_i = v_i(x + \delta x) \approx v_i(x) + \sum_j \frac{\partial v_i}{\partial x_j} \delta x_j.$$

The infinitesimal displacement δx is thus transported along the trajectory $x(x_0, t)$, with time variation given by

$$\frac{d}{dt} \delta x_i(x_0, t) = \sum_j \left. \frac{\partial v_i}{\partial x_j}(x) \right|_{x=x(x_0, t)} \delta x_j(x_0, t). \quad (4.1)$$

As both the displacement and the trajectory depend on the initial point x_0 and the time t , we shall often abbreviate the notation to $x(x_0, t) \rightarrow x(t) \rightarrow x$, $\delta x_i(x_0, t) \rightarrow \delta x_i(t) \rightarrow \delta x$ in what follows. Taken together, the set of equations

$$\dot{x}_i = v_i(x), \quad \delta \dot{x}_i = \sum_j A_{ij}(x) \delta x_j \quad (4.2)$$

governs the dynamics in the tangent bundle $(x, \delta x) \in \mathbf{TM}$ obtained by adjoining the d -dimensional tangent space $\delta x \in TM_x$ to every point $x \in \mathcal{M}$ in the d -dimensional state space $\mathcal{M} \subset \mathbb{R}^d$. The *stability matrix* (velocity gradients matrix)

$$A_{ij}(x) = \frac{\partial v_i(x)}{\partial x_j} \quad (4.3)$$

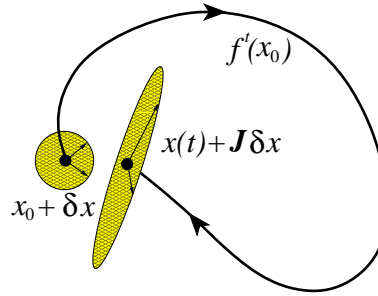
describes the instantaneous rate of shearing of the infinitesimal neighborhood of $x(t)$ by the flow, figure 4.1.

Example 4.1 Rössler and Lorenz flows, linearized: (continued from example 3.6) For the Rössler (2.17) and Lorenz (2.12) flows the stability matrices are, respectively

$$A_{Ross} = \begin{pmatrix} 0 & -1 & -1 \\ 1 & a & 0 \\ z & 0 & x - c \end{pmatrix}, \quad A_{Lor} = \begin{pmatrix} -\sigma & \sigma & 0 \\ \rho - z & -1 & x \\ y & x & -b \end{pmatrix}. \quad (4.4)$$

(continued in example 4.6)

Figure 4.2: The Jacobian matrix J' maps an infinitesimal displacement at x_0 into a displacement rotated and sheared by the linearized flow Jacobian matrix $J'(x_0)$ finite time t later.



4.1.2 Linearized flow

Taylor expanding a *finite time* flow to linear order,

$$f_i^t(x_0 + \delta x) = f_i^t(x_0) + \sum_j \frac{\partial f_i^t(x_0)}{\partial x_{0j}} \delta x_j + \dots, \quad (4.5)$$

one finds that the linearized neighborhood is transported by

$$\delta x(t) = J^t(x_0) \delta x_0, \quad J_{ij}^t(x_0) = \left. \frac{\partial x_i(t)}{\partial x_j} \right|_{x=x_0}. \quad (4.6)$$

This Jacobian matrix is sometimes referred to as the *fundamental solution matrix* or simply *fundamental matrix*, a name inherited from the theory of linear ODEs. It is also sometimes called the *Fréchet derivative* of the nonlinear mapping $f(x)$. It is often denoted Df , but for our needs (we shall have to sort through a plethora of related Jacobian matrices) matrix notation J is more economical. J describes the deformation of an infinitesimal neighborhood at finite time t in the co-moving frame of $x(t)$.

As this is a deformation in the linear approximation, one can think of it as a deformation of an infinitesimal sphere enveloping x_0 into an ellipsoid around $x(t)$, described by the eigenvectors and eigenvalues of the Jacobian matrix of the linearized flow, figure 4.2. Nearby trajectories separate along the *unstable directions*, approach each other along the *stable directions*, and change their distance along the *marginal directions* at a rate slower than exponential, corresponding to the eigenvalues of the Jacobian matrix with magnitude larger than, smaller than, or equal 1. In the literature adjectives *neutral* or *indifferent* are often used instead of ‘marginal,’ (attracting) stable directions are sometimes called ‘asymptotically stable,’ and so on.

One of the preferred directions is what one might expect, the direction of the flow itself. To see that, consider two initial points along a trajectory separated by infinitesimal flight time δt : $\delta x_0 = f^{\delta t}(x_0) - x_0 = v(x_0) \delta t$. By the semigroup property of the flow, $f^{t+\delta t} = f^{\delta t+t}$, where

$$f^{\delta t+t}(x_0) = \int_0^{\delta t+t} d\tau v(x(\tau)) = \delta t v(x(t)) + f^t(x_0).$$

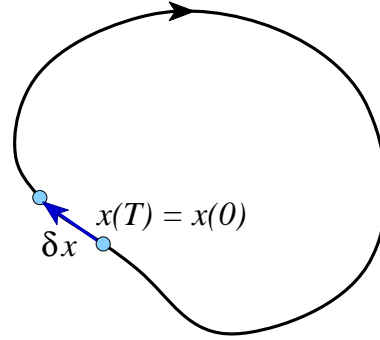


Figure 4.3: Any two points along a periodic orbit p are mapped into themselves after one cycle period T , hence a longitudinal displacement $\delta x = v(x_0)\delta t$ is mapped into itself by the cycle Jacobian matrix J_p .

Expanding both sides of $f^t(f^{\delta t}(x_0)) = f^{\delta t}(f^t(x_0))$, keeping the leading term in δt , and using the definition of the Jacobian matrix (4.6), we observe that $J^t(x_0)$ transports the velocity vector at x_0 to the velocity vector at $x(t)$ at time t :

$$v(x(t)) = J^t(x_0) v(x_0). \quad (4.7)$$

In nomenclature of page 71, the Jacobian matrix maps the initial, Lagrangian coordinate frame into the current, Eulerian coordinate frame.

The velocity at point $x(t)$ in general does not point in the same direction as the velocity at point x_0 , so this is not an eigenvalue condition for J ; the Jacobian matrix computed for an arbitrary segment of an arbitrary trajectory has no invariant meaning.

As the eigenvalues of finite time J have invariant meaning only for periodic orbits, we postpone their interpretation to chapter 5. However, already at this stage we see that if the orbit is periodic, $x(T_p) = x(0)$, at any point along cycle p the velocity v is an eigenvector of the Jacobian matrix $J_p = J^{T_p}$ with a unit eigenvalue,

$$J_p(x) v(x) = v(x), \quad x \in \mathcal{M}_p. \quad (4.8)$$

Two successive points along the cycle separated by δx_0 have the same separation after a completed period $\delta x(T_p) = \delta x_0$, see figure 4.3, hence eigenvalue 1.

As we started by assuming that we know the equations of motion, from (4.3) we also know stability matrix A , the instantaneous rate of shear of an infinitesimal neighborhood $\delta x_i(t)$ of the trajectory $x(t)$. What we do not know is the finite time deformation (4.6).

Our next task is to relate the stability matrix A to Jacobian matrix J . On the level of differential equations the relation follows by taking the time derivative of (4.6) and replacing $\delta \dot{x}$ by (4.2)

$$\delta \dot{x}(t) = J^t \delta x_0 = A \delta x(t) = A J^t \delta x_0.$$

Hence the d^2 matrix elements of Jacobian matrix satisfy the linearized equation (4.1)

$$\frac{d}{dt}J^t(x) = A(x)J^t(x), \quad \text{initial condition } J^0(x) = \mathbf{1}. \quad (4.9)$$

Given a numerical routine for integrating the equations of motion, evaluation of the Jacobian matrix requires minimal additional programming effort; one simply extends the d -dimensional integration routine and integrates concurrently with $f^t(x)$ the d^2 elements of $J^t(x)$.

The qualifier ‘simply’ is perhaps too glib. Integration will work for short finite times, but for exponentially unstable flows one quickly runs into numerical over- and/or underflow problems, so further thought will have to go into implementation this calculation.

So now we know how to compute Jacobian matrix J^t given the stability matrix A , at least when the d^2 extra equations are not too expensive to compute. Mission accomplished.



fast track:
chapter 7, p. 121

And yet... there are mopping up operations left to do. We persist until we derive the integral formula (4.43) for the Jacobian matrix, an analogue of the finite-time ‘Green function’ or ‘path integral’ solutions of other linear problems.

We are interested in smooth, differentiable flows. If a flow is smooth, in a sufficiently small neighborhood it is essentially linear. Hence the next section, which might seem an embarrassment (what is a section on *linear* flows doing in a book on *nonlinear* dynamics?), offers a firm stepping stone on the way to understanding nonlinear flows. If you know your eigenvalues and eigenvectors, you may prefer to fast forward here.



fast track:
sect. 4.3, p. 79

4.2 Linear flows

Diagonalizing the matrix: that’s the key to the whole thing.
— Governor Arnold Schwarzenegger

Linear fields are the simplest vector fields, described by linear differential equations which can be solved explicitly, with solutions that are good for all times.

The state space for linear differential equations is $\mathcal{M} = \mathbb{R}^d$, and the equations of motion (2.6) are written in terms of a vector x and a constant stability matrix A as

$$\dot{x} = v(x) = Ax. \quad (4.10)$$

Solving this equation means finding the state space trajectory

$$x(t) = (x_1(t), x_2(t), \dots, x_d(t))$$

passing through the point x_0 . If $x(t)$ is a solution with $x(0) = x_0$ and $y(t)$ another solution with $y(0) = y_0$, then the linear combination $ax(t) + by(t)$ with $a, b \in \mathbb{R}$ is also a solution, but now starting at the point $ax_0 + by_0$. At any instant in time, the space of solutions is a d -dimensional vector space, which means that one can find a basis of d linearly independent solutions.

How do we solve the linear differential equation (4.10)? If instead of a matrix equation we have a scalar one, $\dot{x} = \lambda x$, the solution is

$$x(t) = e^{t\lambda} x_0. \quad (4.11)$$

In order to solve the d -dimensional matrix case, it is helpful to rederive the solution (4.11) by studying what happens for a short time step δt . If at time $t = 0$ the position is $x(0)$, then

$$\frac{x(\delta t) - x(0)}{\delta t} = \lambda x(0), \quad (4.12)$$

which we iterate m times to obtain Euler's formula for compounding interest

$$x(t) \approx \left(1 + \frac{t}{m}\lambda\right)^m x(0). \quad (4.13)$$

The term in parentheses acts on the initial condition $x(0)$ and evolves it to $x(t)$ by taking m small time steps $\delta t = t/m$. As $m \rightarrow \infty$, the term in parentheses converges to $e^{t\lambda}$. Consider now the matrix version of equation (4.12):

$$\frac{x(\delta t) - x(0)}{\delta t} = Ax(0). \quad (4.14)$$

A representative point x is now a vector in \mathbb{R}^d acted on by the matrix A , as in (4.10). Denoting by $\mathbf{1}$ the identity matrix, and repeating the steps (4.12) and (4.13) we obtain Euler's formula for the exponential of a matrix:

$$x(t) = J^t x(0), \quad J^t = e^{tA} = \lim_{m \rightarrow \infty} \left(\mathbf{1} + \frac{t}{m}A\right)^m. \quad (4.15)$$

We will find this definition the exponential of a matrix helpful in the general case, where the matrix $A = A(x(t))$ varies along a trajectory.

How do we compute the exponential (4.15)?



fast track:
sect. 4.3, p. 79

Example 4.2 Jacobian matrix eigenvalues, diagonalizable case: *Should we be so lucky that $A = A_D$ happens to be a diagonal matrix with eigenvalues $(\lambda^{(1)}, \lambda^{(2)}, \dots, \lambda^{(d)})$, the exponential is simply*

$$J^t = e^{tA_D} = \begin{pmatrix} e^{t\lambda^{(1)}} & \dots & 0 \\ & \ddots & \\ 0 & \dots & e^{t\lambda^{(d)}} \end{pmatrix}. \tag{4.16}$$

Next, suppose that A is diagonalizable and that U is a nonsingular matrix that brings it to a diagonal form $A_D = U^{-1}AU$. Then J can also be brought to a diagonal form (insert factors $\mathbf{1} = UU^{-1}$ between the terms of the product (4.15)):

exercise 4.2

$$J^t = e^{tA} = Ue^{tA_D}U^{-1}. \tag{4.17}$$

The action of both A and J is very simple; the axes of orthogonal coordinate system where A is diagonal are also the eigen-directions of J^t , and under the flow the neighborhood is deformed by a multiplication by an eigenvalue factor for each coordinate axis.

In general J^t is neither diagonal, nor diagonalizable, nor constant along the trajectory. As any matrix, J^t can also be expressed in the singular value decomposition form

$$J = UDV^T \tag{4.18}$$

where D is diagonal, and U, V are orthogonal matrices. The diagonal elements $\sigma_1, \sigma_2, \dots, \sigma_d$ of D are called the *singular values* of J , namely the square root of the eigenvalues of $J^\dagger J$, which is a symmetric, positive semi-definite matrix (and thus admits only real, non-negative eigenvalues). From a geometric point of view, when all singular values are non-zero, J maps the unit sphere into an ellipsoid: the singular values are then the lengths of the semiaxes of this ellipsoid.

Example 4.3 Singular values and geometry of deformations: *Suppose we are in three dimensions, and J is not singular, so that the diagonal elements of D in (4.18) satisfy $\sigma_1 \geq \sigma_2 \geq \sigma_3 > 0$, and consider how J maps the unit ball $S = \{x \in \mathbb{R}^3 \mid x^2 = 1\}$. V is orthogonal (rotation/reflection), so $V^T S$ is still the unit sphere: then D maps S onto ellipsoid $\tilde{S} = \{y \in \mathbb{R}^3 \mid y_1^2/\sigma_1^2 + y_2^2/\sigma_2^2 + y_3^2/\sigma_3^2 = 1\}$ whose principal axes directions - y coordinates - are determined by V . Finally the ellipsoid is further rotated by the orthogonal matrix U . The local directions of stretching and their images under J are called the right-hand and left-hand singular vectors for J and are given by the columns in V and U respectively: it is easy to check that $Jv_k = \sigma_k u_k$, if v_k, u_k are the k -th columns of V and U .*

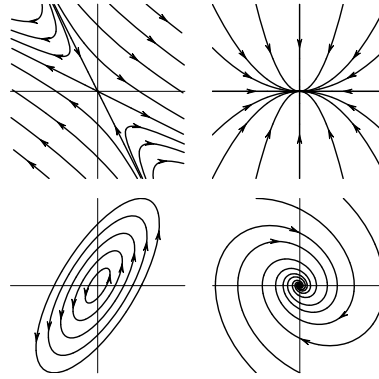
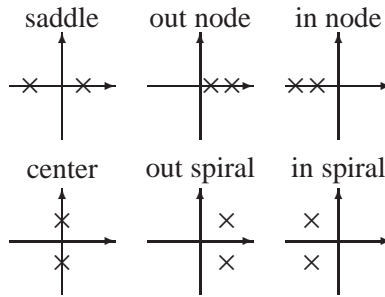


Figure 4.4: Streamlines for several typical 2-dimensional flows: saddle (hyperbolic), in node (attracting), center (elliptic), in spiral.

Figure 4.5: Qualitatively distinct types of exponents of a $[2 \times 2]$ Jacobian matrix.



section 5.1.2

We recapitulate the basic facts of linear algebra in appendix B. A 2-dimensional example serves well to highlight the most important types of linear flows:

Example 4.4 Linear stability of 2-dimensional flows: For a 2-dimensional flow the eigenvalues $\lambda^{(1)}, \lambda^{(2)}$ of A are either real, leading to a linear motion along their eigenvectors, $x_j(t) = x_j(0) \exp(t\lambda^{(j)})$, or a form a complex conjugate pair $\lambda^{(1)} = \mu + i\omega, \lambda^{(2)} = \mu - i\omega$, leading to a circular or spiral motion in the $[x_1, x_2]$ plane.

These two possibilities are refined further into sub-cases depending on the signs of the real part. In the case $\lambda^{(1)} > 0, \lambda^{(2)} < 0$, x_1 grows exponentially with time, and x_2 contracts exponentially. This behavior, called a saddle, is sketched in figure 4.4, as are the remaining possibilities: in/out nodes, inward/outward spirals, and the center. The magnitude of out-spiral $|x(t)|$ diverges exponentially when $\mu > 0$, and in-spiral contracts into $(0, 0)$ when the $\mu < 0$, whereas the phase velocity ω controls its oscillations.

If eigenvalues $\lambda^{(1)} = \lambda^{(2)} = \lambda$ are degenerate, the matrix might have two linearly independent eigenvectors, or only one eigenvector. We distinguish two cases: (a) A can be brought to diagonal form. (b) A can be brought to Jordan form, which (in dimension 2 or higher) has zeros everywhere except for the repeating eigenvalues on the diagonal, and some 1's directly above it. For every such Jordan $[d_\alpha \times d_\alpha]$ block there is only one eigenvector per block.

We sketch the full set of possibilities in figures 4.4 and 4.5, and work out in detail the most important cases in appendix B, example B.3.

4.2.1 Eigenvalues, multipliers - a notational interlude

Throughout this text the symbol Λ_k will always denote the k th *eigenvalue* (in literature sometimes referred to as the *multiplier* or *Floquet multiplier*) of the finite time Jacobian matrix J^t . Symbol $\lambda^{(k)}$ will be reserved for the k th *Floquet* or *characteristic* exponent, or *characteristic value*, with real part $\mu^{(k)}$ and phase $\omega^{(k)}$:

$$\Lambda_k = e^{t\lambda^{(k)}} = e^{t(\mu^{(k)} + i\omega^{(k)})}. \quad (4.19)$$

$J^t(x_0)$ depends on the initial point x_0 and the elapsed time t . For notational brevity we tend to omit this dependence, but in general

$$\Lambda = \Lambda_k = \Lambda_k(x_0, t), \quad \lambda = \lambda^{(k)}(x_0, t), \quad \omega = \omega^{(k)}(x_0, t), \dots \text{ etc.},$$

depend on both the trajectory traversed and the choice of coordinates.

However, as we shall see in sect. 5.2, if the stability matrix A or the Jacobian matrix J is computed on a flow-invariant set \mathcal{M}_p , such as an equilibrium q or a periodic orbit p of period T_p ,

$$A_q = A(x_q), \quad J_p(x) = J^{T_p}(x), \quad x \in \mathcal{M}_p, \quad (4.20)$$

(x is any point on the cycle) its eigenvalues

$$\lambda_q^{(k)} = \lambda^{(k)}(x_q), \quad \Lambda_{p,k} = \Lambda_k(x, T_p)$$

are flow-invariant, independent of the choice of coordinates and the initial point in the cycle p , so we label them by their q or p label.

We number eigenvalues Λ_k in order of decreasing magnitude

$$|\Lambda_1| \geq |\Lambda_2| \geq \dots \geq |\Lambda_d|. \quad (4.21)$$

Since $|\Lambda_j| = e^{t\mu^{(j)}}$, this is the same as labeling by

$$\mu^{(1)} \geq \mu^{(2)} \geq \dots \geq \mu^{(d)}. \quad (4.22)$$

In dynamics the expanding directions, $|\Lambda_e| > 1$, have to be taken care of first, while the contracting directions $|\Lambda_c| < 1$ tend to take care of themselves, hence the ordering by decreasing magnitude is the natural one.



fast track:
sect. 4.3, p. 79

4.2.2 Yes, but how do you really do it?

Economical description of neighborhoods of equilibria and periodic orbits is afforded by projection operators

$$\mathbf{P}_i = \prod_{j \neq i} \frac{\mathbf{M} - \lambda^{(j)} \mathbf{1}}{\lambda^{(i)} - \lambda^{(j)}}, \quad (4.23)$$

where matrix \mathbf{M} is typically either equilibrium stability matrix A , or periodic orbit Jacobian matrix \hat{J} restricted to a Poincaré section, as in (4.56). While usually not phrased in language of projection operators, the requisite linear algebra is standard, and relegated here to appendix B.

Once the distinct non-zero eigenvalues $\{\lambda^{(i)}\}$ are computed, projection operators are polynomials in \mathbf{M} which need no further diagonalizations or orthogonalizations. For each distinct eigenvalue $\lambda^{(i)}$ of \mathbf{M} , the columns/rows of \mathbf{P}_i

$$(\mathbf{M} - \lambda^{(j)} \mathbf{1}) \mathbf{P}_j = \mathbf{P}_j (\mathbf{M} - \lambda^{(j)} \mathbf{1}) = 0, \quad (4.24)$$

are the right/left eigenvectors $\mathbf{e}^{(k)}$, $\mathbf{e}_{(k)}$ of \mathbf{M} which (provided \mathbf{M} is not of Jordan type) span the corresponding linearized subspace, and are a convenient starting seed for tracing out the global unstable/stable manifolds.

Matrices \mathbf{P}_i are *orthogonal* and *complete*:

$$\mathbf{P}_i \mathbf{P}_j = \delta_{ij} \mathbf{P}_j, \quad (\text{no sum on } j), \quad \sum_{i=1}^r \mathbf{P}_i = \mathbf{1}. \quad (4.25)$$

with the dimension of the i th subspace given by $d_i = \text{tr } \mathbf{P}_i$. Completeness relation substituted into $\mathbf{M} = \mathbf{M} \mathbf{1}$ yields

$$\mathbf{M} = \lambda^{(1)} \mathbf{P}_1 + \lambda^{(2)} \mathbf{P}_2 + \cdots + \lambda^{(r)} \mathbf{P}_r. \quad (4.26)$$

As any matrix function $f(\mathbf{M})$ takes the scalar value $f(\lambda^{(i)})$ on the \mathbf{P}_i subspace, $f(\mathbf{M}) \mathbf{P}_i = f(\lambda^{(i)}) \mathbf{P}_i$, it is easily evaluated through its *spectral decomposition*

$$f(\mathbf{M}) = \sum_i f(\lambda^{(i)}) \mathbf{P}_i. \quad (4.27)$$

As \mathbf{M} has only real entries, it will in general have either real eigenvalues (over-damped oscillator, for example), or complex conjugate pairs of eigenvalues (under-damped oscillator, for example). That is not surprising, but also the corresponding eigenvectors can be either real or complex. All coordinates used in

defining the flow are real numbers, so what is the meaning of a *complex* eigenvector?

If two eigenvalues form a complex conjugate pair, $\{\lambda^{(k)}, \lambda^{(k+1)}\} = \{\mu + i\omega, \mu - i\omega\}$, they are in a sense degenerate: while a real $\lambda^{(k)}$ characterizes a motion along a line, a complex $\lambda^{(k)}$ characterizes a spiralling motion in a plane. We determine this plane by replacing the corresponding complex eigenvectors by their real and imaginary parts, $\{\mathbf{e}^{(k)}, \mathbf{e}^{(k+1)}\} \rightarrow \{\text{Re } \mathbf{e}^{(k)}, \text{Im } \mathbf{e}^{(k)}\}$, or, in terms of projection operators:

$$\mathbf{P}_k = \frac{1}{2}(\mathbf{R} + i\mathbf{Q}), \quad \mathbf{P}_{k+1} = \mathbf{P}_k^*,$$

where $\mathbf{R} = \mathbf{P}_k + \mathbf{P}_{k+1}$ is the subspace decomposed by the k th complex eigenvalue pair, and $\mathbf{Q} = (\mathbf{P}_k - \mathbf{P}_{k+1})/i$, both matrices with real elements. Substitution

$$\begin{pmatrix} \mathbf{P}_k \\ \mathbf{P}_{k+1} \end{pmatrix} = \frac{1}{2} \begin{pmatrix} 1 & i \\ 1 & -i \end{pmatrix} \begin{pmatrix} \mathbf{R} \\ \mathbf{Q} \end{pmatrix},$$

brings the $\lambda^{(k)}\mathbf{P}_k + \lambda^{(k+1)}\mathbf{P}_{k+1}$ complex eigenvalue pair in the spectral decomposition (4.26) into the real form,

$$\begin{pmatrix} \mathbf{P}_k & \mathbf{P}_{k+1} \end{pmatrix} \begin{pmatrix} \lambda & 0 \\ 0 & \lambda^* \end{pmatrix} \begin{pmatrix} \mathbf{P}_k \\ \mathbf{P}_{k+1} \end{pmatrix} = \begin{pmatrix} \mathbf{R} & \mathbf{Q} \end{pmatrix} \begin{pmatrix} \mu & -\omega \\ \omega & \mu \end{pmatrix} \begin{pmatrix} \mathbf{R} \\ \mathbf{Q} \end{pmatrix}, \quad (4.28)$$

where we have dropped the superscript $^{(k)}$ for notational brevity.

To summarize, spectrally decomposed matrix \mathbf{M} (4.26) acts along lines on subspaces corresponding to real eigenvalues, and as a $[2 \times 2]$ rotation in a plane on subspaces corresponding to complex eigenvalue pairs.

Now that we have some feeling for the qualitative behavior of eigenvectors and eigenvalues of linear flows, we are ready to return to the nonlinear case.

4.3 Stability of flows



How do you determine the eigenvalues of the finite time local deformation \mathcal{J} for a general nonlinear smooth flow? The Jacobian matrix is computed by integrating the equations of variations (4.2)

$$x(t) = f^t(x_0), \quad \delta x(x_0, t) = J^t(x_0) \delta x(x_0, 0). \quad (4.29)$$

The equations are linear, so we should be able to integrate them—but in order to make sense of the answer, we derive this integral step by step.

4.3.1 Stability of equilibria

For a start, consider the case where x is an equilibrium point (2.8). Expanding around the equilibrium point x_q , using the fact that the stability matrix $A = A(x_q)$ in (4.2) is constant, and integrating,

$$f^t(x) = x_q + e^{At}(x - x_q) + \dots, \tag{4.30}$$

we verify that the simple formula (4.15) applies also to the Jacobian matrix of an equilibrium point,

$$J^t(x_q) = e^{A_q t}, \quad A_q = A(x_q). \tag{4.31}$$

Example 4.5 In-out spirals. Consider an equilibrium whose Floquet exponents $\{\lambda^{(1)}, \lambda^{(2)}\} = \{\mu + i\omega, \mu - i\omega\}$ form a complex conjugate pair. The corresponding complex eigenvectors can be replaced by their real and imaginary parts, $\{e^{(1)}, e^{(2)}\} \rightarrow \{\text{Re } e^{(1)}, \text{Im } e^{(1)}\}$. The 2-dimensional real representation (4.28),

$$\begin{pmatrix} \mu & -\omega \\ \omega & \mu \end{pmatrix} = \mu \begin{pmatrix} 1 & 0 \\ 0 & 1 \end{pmatrix} + \omega \begin{pmatrix} 0 & -1 \\ 1 & 0 \end{pmatrix}$$

consists of the identity and the generator of $SO(2)$ rotations in the $\{\text{Re } e^{(1)}, \text{Im } e^{(1)}\}$ plane. Trajectories $\mathbf{x}(t) = J^t \mathbf{x}(0)$, where (omitting $e^{(3)}, e^{(4)}, \dots$ eigen-directions)

$$J^t = e^{A_q t} = e^{t\mu} \begin{pmatrix} \cos \omega t & -\sin \omega t \\ \sin \omega t & \cos \omega t \end{pmatrix}, \tag{4.32}$$

spiral in/out around $(x, y) = (0, 0)$, see figure 4.4, with the rotation period T , and contraction/expansion radially by the multiplier Λ_{radial} , and by the multiplier Λ_j along the $e^{(j)}$ eigen-direction per a turn of the spiral:

exercise B.1

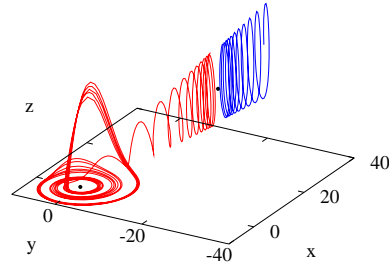
$$T = 2\pi/\omega, \quad \Lambda_{radial} = e^{T\mu}, \quad \Lambda_j = e^{T\mu^{(j)}}. \tag{4.33}$$

We learn that the typical turnover time scale in the neighborhood of the equilibrium $(x, y) = (0, 0)$ is of order $\approx T$ (and not, let us say, $1000 T$, or $10^{-2} T$). Λ_j multipliers give us estimates of strange-set thickness in eigen-directions transverse to the rotation plane.

Example 4.6 Stability of equilibria of the Rössler flow. (continued from example 4.1) The Rössler system (2.17) has two equilibrium points (2.18), the inner equilibrium (x_-, y_-, z_-) , and the outer equilibrium point (x^+, y^+, z^+) . Together with their exponents (eigenvalues of the stability matrix) the two equilibria yield quite detailed information about the flow. Figure 4.6 shows two trajectories which start in the neighborhood of the outer '+' equilibrium. Trajectories to the right of the equilibrium point '+' escape, and those to the left spiral toward the inner equilibrium point '-', where they seem to wander chaotically for all times. The stable manifold of outer equilibrium point thus serves as the attraction basin boundary. Consider now the numerical values for eigenvalues of the two equilibria

exercise 4.4
exercise 2.8

Figure 4.6: Two trajectories of the Rössler flow initiated in the neighborhood of the ‘+’ or ‘outer’ equilibrium point (2.18). (R. Paškauskas)



$$\begin{aligned} (\mu_-^{(1)}, \mu_-^{(2)} \pm i \omega_-^{(2)}) &= (-5.686, \quad 0.0970 \pm i 0.9951) \\ (\mu_+^{(1)}, \mu_+^{(2)} \pm i \omega_+^{(2)}) &= (0.1929, \quad -4.596 \times 10^{-6} \pm i 5.428) \end{aligned} \quad (4.34)$$

Outer equilibrium: The $\mu_+^{(2)} \pm i \omega_+^{(2)}$ complex eigenvalue pair implies that that neighborhood of the outer equilibrium point rotates with angular period $T_+ \approx |2\pi/\omega_+^{(2)}| = 1.1575$. The multiplier by which a trajectory that starts near the ‘+’ equilibrium point contracts in the stable manifold plane is the excruciatingly slow $\Lambda_2^+ \approx \exp(\mu_+^{(2)} T_+) = 0.9999947$ per rotation. For each period the point of the stable manifold moves away along the unstable eigen-direction by factor $\Lambda_1^+ \approx \exp(\mu_+^{(1)} T_+) = 1.2497$. Hence the slow spiraling on both sides of the ‘+’ equilibrium point.

Inner equilibrium: The $\mu_-^{(2)} \pm i \omega_-^{(2)}$ complex eigenvalue pair tells us that neighborhood of the ‘-’ equilibrium point rotates with angular period $T_- \approx |2\pi/\omega_-^{(2)}| = 6.313$, slightly faster than the harmonic oscillator estimate in (2.14). The multiplier by which a trajectory that starts near the ‘-’ equilibrium point spirals away per one rotation is $\Lambda_{\text{radial}} \approx \exp(\mu_-^{(2)} T_-) = 1.84$. The $\mu_-^{(1)}$ eigenvalue is essentially the z expansion correcting parameter c introduced in (2.16). For each Poincaré section return, the trajectory is contracted into the stable manifold by the amazing factor of $\Lambda_1 \approx \exp(\mu_-^{(1)} T_-) = 10^{-15.6}$ (!).

Suppose you start with a 1 mm interval pointing in the Λ_1 eigen-direction. After one Poincaré return the interval is of order of 10^{-4} fermi, the furthest we will get into subnuclear structure in this book. Of course, from the mathematical point of view, the flow is reversible, and the Poincaré return map is invertible. (continued in example 11.3) (R. Paškauskas)

Example 4.7 Stability of Lorenz flow equilibria: (continued from example 4.1) A glance at figure 3.7 suggests that the flow is organized by its 3 equilibria, so lets have a closer look at their stable/unstable manifolds.

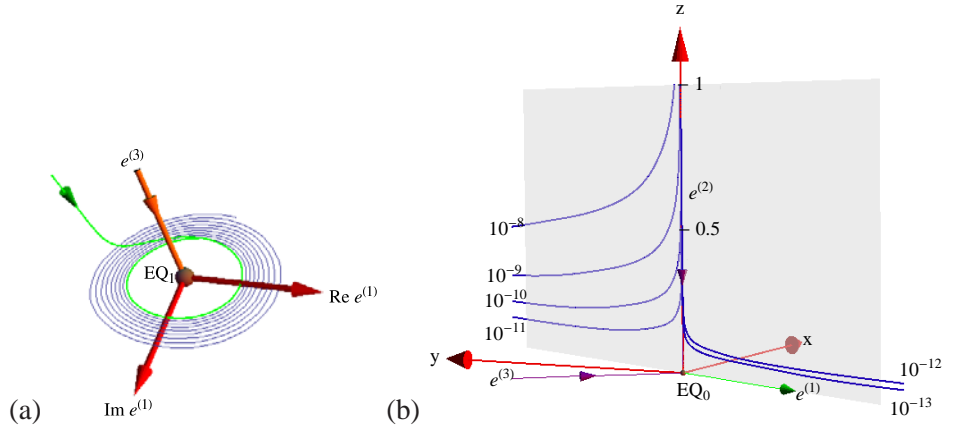
The E_{Q_0} equilibrium stability matrix (4.4) evaluated at $x_{E_{Q_0}} = (0, 0, 0)$ is block-diagonal. The z -axis is an eigenvector with a contracting eigenvalue $\lambda^{(2)} = -b$. From (4.48) it follows that all $[x, y]$ areas shrink at rate $-(\sigma + 1)$. Indeed, the $[x, y]$ submatrix remark 9.10

$$A^- = \begin{pmatrix} -\sigma & \sigma \\ \rho & -1 \end{pmatrix} \quad (4.35)$$

has a real expanding/contracting eigenvalue pair $\lambda^{(1,3)} = -(\sigma + 1)/2 \pm \sqrt{(\sigma - 1)^2/4 + \rho\sigma}$, with the right eigenvectors $e^{(1)}, e^{(3)}$ in the $[x, y]$ plane, given by (either) column of the projection operator

$$P_i = \frac{A^- - \lambda^{(j)} \mathbf{1}}{\lambda^{(i)} - \lambda^{(j)}} = \frac{1}{\lambda^{(i)} - \lambda^{(j)}} \begin{pmatrix} -\sigma - \lambda^{(j)} & \sigma \\ \rho & -1 - \lambda^{(j)} \end{pmatrix}, \quad i \neq j \in \{1, 3\}. \quad (4.36)$$

Figure 4.7: (a) A perspective view of the linearized Lorenz flow near EQ_1 equilibrium, see figure 3.7 (a). The unstable eigenplane of EQ_1 is spanned by $\text{Re } \mathbf{e}^{(1)}$ and $\text{Im } \mathbf{e}^{(1)}$. The stable eigenvector $\mathbf{e}^{(3)}$. (b) Lorenz flow near the EQ_0 equilibrium: unstable eigenvector $\mathbf{e}^{(1)}$, stable eigenvectors $\mathbf{e}^{(2)}$, $\mathbf{e}^{(3)}$. Trajectories initiated at distances $10^{-8} \dots 10^{-12}$, 10^{-13} away from the z -axis exit finite distance from EQ_0 along the $(\mathbf{e}^{(1)}, \mathbf{e}^{(2)})$ eigenplane. Due to the strong $\lambda^{(1)}$ expansion, the EQ_0 equilibrium is, for all practical purposes, unreachable, and the $EQ_1 \rightarrow EQ_0$ heteroclinic connection never observed in simulations such as figure 2.5. (E. Siminos; continued in figure 11.8.)



$EQ_{1,2}$ equilibria have no symmetry, so their eigenvalues are given by the roots of a cubic equation, the secular determinant $\det(A - \lambda \mathbf{1}) = 0$:

$$\lambda^3 + \lambda^2(\sigma + b + 1) + \lambda b(\sigma + \rho) + 2\sigma b(\rho - 1) = 0. \quad (4.37)$$

For $\rho > 24.74$, $EQ_{1,2}$ have one stable real eigenvalue and one unstable complex conjugate pair, leading to a spiral-out instability and the strange attractor depicted in figure 2.5.

As all numerical plots of the Lorenz flow are here carried out for the Lorenz parameter choice $\sigma = 10, b = 8/3, \rho = 28$, we note the values of these eigenvalues for future reference,

$$\begin{aligned} EQ_0 : (\lambda^{(1)}, \lambda^{(2)}, \lambda^{(3)}) &= (11.83, -2.666, -22.83) \\ EQ_1 : (\mu^{(1)} \pm i \omega^{(1)}, \lambda^{(3)}) &= (0.094 \pm i 10.19, -13.85), \end{aligned} \quad (4.38)$$

as well as the rotation period $T_{EQ_1} = 2\pi/\omega^{(1)}$ about EQ_1 , and the associated expansion/contraction multipliers $\Lambda^{(i)} = \exp(\mu^{(i)} T_{EQ_1})$ per a spiral-out turn:

$$T_{EQ_1} = 0.6163, \quad (\Lambda^{(1)}, \Lambda^{(3)}) = (1.060, 1.957 \times 10^{-4}). \quad (4.39)$$

We learn that the typical turnover time scale in this problem is of order $T \approx T_{EQ_1} \approx 1$ (and not, let us say, 1000, or 10^{-2}). Combined with the contraction rate (4.48), this tells us that the Lorenz flow strongly contracts state space volumes, by factor of $\approx 10^{-4}$ per mean turnover time.

In the EQ_1 neighborhood the unstable manifold trajectories slowly spiral out, with very small radial per-turn expansion multiplier $\Lambda^{(1)} \approx 1.06$, and very strong contraction multiplier $\Lambda^{(3)} \approx 10^{-4}$ onto the unstable manifold, figure 4.7 (a). This contraction confines, for all practical purposes, the Lorenz attractor to a 2-dimensional surface evident in the section figure 3.7.

In the $x_{EQ_0} = (0, 0, 0)$ equilibrium neighborhood the extremely strong $\lambda^{(3)} \approx -23$ contraction along the $\mathbf{e}^{(3)}$ direction confines the hyperbolic dynamics near EQ_0 to the plane spanned by the unstable eigenvector $\mathbf{e}^{(1)}$, with $\lambda^{(1)} \approx 12$, and the slowest contraction rate eigenvector $\mathbf{e}^{(2)}$ along the z -axis, with $\lambda^{(2)} \approx -3$. In this plane the strong expansion along $\mathbf{e}^{(1)}$ overwhelms the slow $\lambda^{(2)} \approx -3$ contraction down the z -axis, making it extremely unlikely for a random trajectory to approach EQ_0 , figure 4.7 (b). Thus linearization suffices to describe analytically the singular dip in the Poincaré sections of figure 3.7, and the empirical scarcity of trajectories close to EQ_0 . (continued in example 4.9)

(E. Siminos and J. Halcrow)

Example 4.8 Lorenz flow: Global portrait. (continued from example 4.7) As the EQ_1 unstable manifold spirals out, the strip that starts out in the section above EQ_1 in figure 3.7 cuts across the z -axis invariant subspace. This strip necessarily contains a heteroclinic orbit that hits the z -axis head on, and in infinite time (but exponentially fast) descends all the way to EQ_0 .

How? As in the neighborhood of the EQ_0 equilibrium the dynamics is linear (see figure 4.7 (a)), there is no need to integrate numerically the final segment of the heteroclinic connection - it is sufficient to bring a trajectory a small distance away from EQ_0 , continue analytically to a small distance beyond EQ_0 , then resume the numerical integration.

What happens next? Trajectories to the left of z -axis shoot off along the $e^{(1)}$ direction, and those to the right along $-e^{(1)}$. As along the $e^{(1)}$ direction $xy > 0$, the nonlinear term in the \dot{z} equation (2.12) bends both branches of the EQ_0 unstable manifold $W^u(EQ_0)$ upwards. Then ... - never mind. Best to postpone the completion of this narrative to example 9.10, where the discrete symmetry of Lorenz flow will help us streamline the analysis. As we shall show, what we already know about the 3 equilibria and their stable/unstable manifolds suffices to completely pin down the topology of Lorenz flow. (continued in example 9.10)

(E. Siminos and J. Halcrow)

4.3.2 Stability of trajectories

Next, consider the case of a general, non-stationary trajectory $x(t)$. The exponential of a constant matrix can be defined either by its Taylor series expansion, or in terms of the Euler limit (4.15):

$$e^{tA} = \sum_{k=0}^{\infty} \frac{t^k}{k!} A^k \tag{4.40}$$

$$= \lim_{m \rightarrow \infty} \left(\mathbf{1} + \frac{t}{m} A \right)^m . \tag{4.41}$$

Taylor expanding is fine if A is a constant matrix. However, only the second, tax-accountant's discrete step definition of an exponential is appropriate for the task at hand, as for a dynamical system the local rate of neighborhood distortion $A(x)$ depends on where we are along the trajectory. The linearized neighborhood is multiplicatively deformed along the flow, and the m discrete time step approximation to J^t is therefore given by a generalization of the Euler product (4.41):

$$\begin{aligned} J^t &= \lim_{m \rightarrow \infty} \prod_{n=m}^1 (\mathbf{1} + \delta t A(x_n)) = \lim_{m \rightarrow \infty} \prod_{n=m}^1 e^{\delta t A(x_n)} \\ &= \lim_{m \rightarrow \infty} e^{\delta t A(x_n)} e^{\delta t A(x_{m-1})} \dots e^{\delta t A(x_2)} e^{\delta t A(x_1)} , \end{aligned} \tag{4.42}$$

where $\delta t = (t - t_0)/m$, and $x_n = x(t_0 + n\delta t)$. Slightly perverse indexing of the products indicates that the successive infinitesimal deformation are applied by

multiplying from the left. The two formulas for J agree to leading order in δt , and the $m \rightarrow \infty$ limit of this procedure is the integral

$$J_{ij}^t(x_0) = \left[\mathbf{T} e^{\int_0^t d\tau A(x(\tau))} \right]_{ij}, \quad (4.43)$$

where \mathbf{T} stands for time-ordered integration, *defined* as the continuum limit of the successive left multiplications (4.42). This integral formula for J is the main conceptual result of this chapter.

exercise 4.5

It makes evident important properties of Jacobian matrices, such as that they are multiplicative along the flow,

$$J^{t+t'}(x) = J^{t'}(x') J^t(x), \quad \text{where } x' = f^{t'}(x), \quad (4.44)$$

an immediate consequence of time-ordered product structure of (4.42). However, in practice J is evaluated by integrating (4.9) along with the ODEs that define a particular flow.



in depth:
sect. 17.3, p. 338

4.4 Neighborhood volume



section 17.3
remark 17.3

Consider a small state space volume $\Delta V = d^d x$ centered around the point x_0 at time $t = 0$. The volume $\Delta V'$ around the point $x' = x(t)$ time t later is

$$\Delta V' = \frac{\Delta V'}{\Delta V} \Delta V = \left| \det \frac{\partial x'}{\partial x} \right| \Delta V = |\det J(x_0)^t| \Delta V, \quad (4.45)$$

so the $|\det J|$ is the ratio of the initial and the final volumes. The determinant $\det J^t(x_0) = \prod_{i=1}^d \Lambda_i(x_0, t)$ is the product of the Floquet multipliers. We shall refer to this determinant as the *Jacobian* of the flow. This Jacobian is easily evaluated. Take the time derivative, use the J evolution equation (4.9) and the matrix identity $\ln \det J = \text{tr} \ln J$:

exercise 4.1

$$\frac{d}{dt} \ln \Delta V(t) = \frac{d}{dt} \ln \det J = \text{tr} \frac{d}{dt} \ln J = \text{tr} \frac{1}{J} \dot{J} = \text{tr} A = \partial_i v_i.$$

(Here, as elsewhere in this book, a repeated index implies summation.) Integrate both sides to obtain the time evolution of an infinitesimal volume

$$\det J^t(x_0) = \exp \left[\int_0^t d\tau \text{tr} \mathbf{A}(x(\tau)) \right] = \exp \left[\int_0^t d\tau \partial_i v_i(x(\tau)) \right]. \quad (4.46)$$

As the divergence $\partial_i v_i$ is a scalar quantity, the integral in the exponent (4.43) needs *no time ordering*. So all we need to do is evaluate the time average

$$\begin{aligned} \overline{\partial_i v_i} &= \lim_{t \rightarrow \infty} \frac{1}{t} \int_0^t d\tau \sum_{i=1}^d A_{ii}(x(\tau)) \\ &= \frac{1}{t} \ln \left| \prod_{i=1}^d \Lambda_i(x_0, t) \right| = \sum_{i=1}^d \lambda^{(i)}(x_0, t) \end{aligned} \quad (4.47)$$

along the trajectory. If the flow is not singular (for example, the trajectory does not run head-on into the Coulomb $1/r$ singularity), the stability matrix elements are bounded everywhere, $|A_{ij}| < M$, and so is the trace $\sum_i A_{ii}$. The time integral in (4.46) grows at most linearly with t , hence $\overline{\partial_i v_i}$ is bounded for all times, and numerical estimates of the $t \rightarrow \infty$ limit in (4.47) are not marred by any blowups.

Example 4.9 Lorenz flow state space contraction: (continued from example 4.7) It follows from (4.4) and (4.47) that Lorenz flow is volume contracting,

$$\partial_i v_i = \sum_{i=1}^3 \lambda^{(i)}(x, t) = -\sigma - b - 1, \quad (4.48)$$

at a constant, coordinate- and ρ -independent rate, set by Lorenz to $\partial_i v_i = -13.66$. As for periodic orbits and for long time averages there is no contraction/expansion along the flow, $\lambda^{(l)} = 0$, and the sum of $\lambda^{(i)}$ is constant by (4.48), there is only one independent exponent $\lambda^{(i)}$ to compute. (continued in example 4.8)

Even if we were to insist on extracting $\overline{\partial_i v_i}$ from (4.42) by first multiplying Jacobian matrices along the flow, and then taking the logarithm, we can avoid exponential blowups in J' by using the multiplicative structure (4.44), $\det J'^{t+t'}(x_0) = \det J'(x') \det J^t(x_0)$ to restart with $J^0(x') = \mathbf{1}$ whenever the eigenvalues of $J(x_0)$ start getting out of hand. In numerical evaluations of Lyapunov exponents, $\lambda = \lim_{t \rightarrow \infty} \mu^{(i)}(x_0, t)$, the sum rule (4.47) can serve as a helpful check on the accuracy of the computation.

section 17.3

The divergence $\partial_i v_i$ characterizes the behavior of a state space volume in the infinitesimal neighborhood of the trajectory. If $\partial_i v_i < 0$, the flow is *locally contracting*, and the trajectory might be falling into an attractor. If $\partial_i v_i(x) < 0$, for all $x \in \mathcal{M}$, the flow is *globally contracting*, and the dimension of the attractor is necessarily smaller than the dimension of state space \mathcal{M} . If $\partial_i v_i = 0$, the flow preserves state space volume and $\det J = \mathbf{1}$. A flow with this property is called *incompressible*. An important class of such flows are the Hamiltonian flows considered in sect. 7.2.

But before we can get to that, Henri Roux, the perfect student and always alert, pipes up. He does not like our definition of the Jacobian matrix in terms of the time-ordered exponential (4.43). Depending on the signs of multipliers, the left hand side of (4.46) can be either positive or negative. But the right hand side is an exponential of a real number, and that can only be positive. What gives? As we shall see much later on in this text, in discussion of topological indices arising in semiclassical quantization, this is not at all a dumb question.

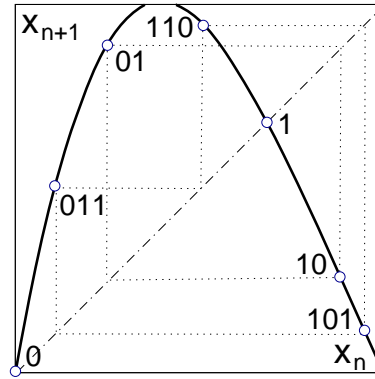


Figure 4.8: A unimodal map, together with fixed points 0, 1, 2-cycle 01 and 3-cycle 011.

4.5 Stability of maps



The transformation of an infinitesimal neighborhood of a trajectory under the iteration of a map follows from Taylor expanding the iterated mapping at finite time n to linear order, as in (4.5). The linearized neighborhood is transported by the Jacobian matrix evaluated at a discrete set of times $n = 1, 2, \dots$,

$$M_{ij}^n(x_0) = \left. \frac{\partial f_i^n(x)}{\partial x_j} \right|_{x=x_0}. \tag{4.49}$$

In case of a periodic orbit, $f^n(x) = x$, we shall refer to this Jacobian matrix as the *monodromy* matrix. Derivative notation $M^f(x_0) \rightarrow Df^f(x_0)$ is frequently employed in the literature. As in the continuous case, we denote by Λ_k the k th *eigenvalue* or multiplier of the finite time Jacobian matrix $M^n(x_0)$, and by $\mu^{(k)}$ the real part of k th *eigen-exponent*

$$\Lambda_{\pm} = e^{n(\mu \pm i\omega)}, \quad |\Lambda| = e^{n\mu}.$$

For complex eigenvalue pairs the phase ω describes the rotation velocity in the plane defined by the corresponding pair of eigenvectors, with one period of rotation given by

$$T = 2\pi/\omega. \tag{4.50}$$

Example 4.10 Stability of a 1-dimensional map: Consider the orbit $\{\dots, x_{-1}, x_0, x_1, x_2, \dots\}$ of a 1-dimensional map $x_{n+1} = f(x_n)$. Since point x_n is carried into point x_{n+1} , in studying linear stability (and higher derivatives) of the map it is often convenient to deploy a local coordinate systems z_a centered on the orbit points x_a , together with a notation for the map, its derivative, and, by the chain rule, the derivative of the k th iterate f^k evaluated at the point x_a ,

$$\begin{aligned} x &= x_a + z_a, & f_a(z_a) &= f(x_a + z_a) \\ f'_a &= f'(x_a) \\ \Lambda(x_0, k) &= f_a^{k'} = f'_{a+k-1} \cdots f'_{a+1} f'_a, & k &\geq 2. \end{aligned} \tag{4.51}$$

Here a is the label of point x_a , and the label $a+1$ is a shorthand for the next point b on the orbit of x_a , $x_b = x_{a+1} = f(x_a)$. For example, a period-3 periodic point in figure 4.8 might have label $a = 011$, and by $x_{110} = f(x_{011})$ the next point label is $b = 110$.

The 1-step product formula for the stability of the n th iterate of a d -dimensional map

$$\begin{aligned} M^n(x_0) &= M(x_{n-1}) \cdots M(x_1)M(x_0), \\ M(x)_{kl} &= \frac{\partial}{\partial x_l} f_k(x), \quad x_m = f^m(x_0) \end{aligned} \tag{4.52}$$

follows from the chain rule for matrix derivatives

$$\frac{\partial}{\partial x_i} f_j(f(x)) = \sum_{k=1}^d \frac{\partial}{\partial y_k} f_j(y) \Big|_{y=f(x)} \frac{\partial}{\partial x_i} f_k(x).$$

If you prefer to think of a discrete time dynamics as a sequence of Poincaré section returns, then (4.52) follows from (4.44): Jacobian matrices are multiplicative along the flow.

exercise 17.1

Example 4.11 Hénon map Jacobian matrix: For the Hénon map (3.19) the Jacobian matrix for the n th iterate of the map is

$$M^n(x_0) = \prod_{m=n}^1 \begin{pmatrix} -2ax_m & b \\ 1 & 0 \end{pmatrix}, \quad x_m = f_1^m(x_0, y_0). \tag{4.53}$$

The determinant of the Hénon one time step Jacobian matrix (4.53) is constant,

$$\det M = \Lambda_1 \Lambda_2 = -b \tag{4.54}$$

so in this case only one eigenvalue $\Lambda_1 = -b/\Lambda_2$ needs to be determined. This is not an accident; a constant Jacobian was one of desiderata that led Hénon to construct a map of this particular form.



fast track:
chapter 7, p. 121

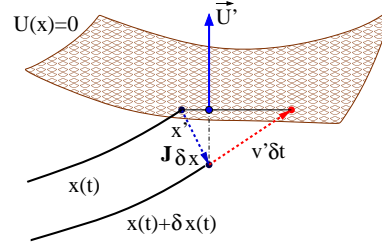
4.5.1 Stability of Poincaré return maps

(R. Paškauskas and P. Cvitanović)



We now relate the linear stability of the Poincaré return map $P : \mathcal{P} \rightarrow \mathcal{P}$ defined in sect. 3.1 to the stability of the continuous time flow in the full state space.

Figure 4.9: If $x(t)$ intersects the Poincaré section \mathcal{P} at time τ , the nearby $x(t) + \delta x(t)$ trajectory intersects it time $\tau + \delta t$ later. As $(U' \cdot v' \delta t) = -(U' \cdot J \delta x)$, the difference in arrival times is given by $\delta t = -(U' \cdot J \delta x)/(U' \cdot v')$.



The hypersurface \mathcal{P} can be specified implicitly through a function $U(x)$ that is zero whenever a point x is on the Poincaré section. A nearby point $x + \delta x$ is in the hypersurface \mathcal{P} if $U(x + \delta x) = 0$, and the same is true for variations around the first return point $x' = x(\tau)$, so expanding $U(x')$ to linear order in variation δx restricted to the Poincaré section leads to the condition

$$\sum_{i=1}^{d+1} \frac{\partial U(x')}{\partial x_i} \frac{dx'_i}{dx_j} \Big|_{\mathcal{P}} = 0. \quad (4.55)$$

In what follows $U_i = \partial_i U$ is the gradient of U defined in (3.3), unprimed quantities refer to the starting point $x = x_0 \in \mathcal{P}$, $v = v(x_0)$, and the primed quantities to the first return: $x' = x(\tau)$, $v' = v(x')$, $U' = U(x')$. For brevity we shall also denote the full state space Jacobian matrix at the first return by $J = \mathcal{F}(x_0)$. Both the first return x' and the time of flight to the next Poincaré section $\tau(x)$ depend on the starting point x , so the Jacobian matrix

$$\hat{J}(x)_{ij} = \frac{dx'_i}{dx_j} \Big|_{\mathcal{P}} \quad (4.56)$$

with both initial and the final variation constrained to the Poincaré section hypersurface \mathcal{P} is related to the continuous flow Jacobian matrix by

$$\frac{dx'_i}{dx_j} \Big|_{\mathcal{P}} = \frac{\partial x'_i}{\partial x_j} + \frac{dx'_i}{d\tau} \frac{d\tau}{dx_j} = J_{ij} + v'_i \frac{d\tau}{dx_j}.$$

The return time variation $d\tau/dx$, figure 4.9, is eliminated by substituting this expression into the constraint (4.55),

$$0 = \partial_i U' J_{ij} + (v' \cdot \partial U') \frac{d\tau}{dx_j},$$

yielding the projection of the full space $(d+1)$ -dimensional Jacobian matrix to the Poincaré map d -dimensional Jacobian matrix:

$$\hat{J}_{ij} = \left(\delta_{ik} - \frac{v'_i \partial_k U'}{(v' \cdot \partial U')} \right) J_{kj}. \quad (4.57)$$

Substituting (4.7) we verify that the initial velocity $v(x)$ is a zero-eigenvector of \hat{J}

$$\hat{J}v = 0, \quad (4.58)$$

so the Poincaré section eliminates variations parallel to v , and \hat{J} is a rank d matrix, i.e., one less than the dimension of the continuous time flow.

Résumé

A neighborhood of a trajectory deforms as it is transported by a flow. In the linear approximation, the stability matrix A describes the shearing/compression/expansion of an infinitesimal neighborhood in an infinitesimal time step. The deformation after a finite time t is described by the Jacobian matrix

$$J^t(x_0) = \mathbf{T}e^{\int_0^t d\tau A(x(\tau))},$$

where \mathbf{T} stands for the time-ordered integration, defined multiplicatively along the trajectory. For discrete time maps this is multiplication by time step Jacobian matrix M along the n points $x_0, x_1, x_2, \dots, x_{n-1}$ on the trajectory of x_0 ,

$$M^n(x_0) = M(x_{n-1})M(x_{n-2}) \cdots M(x_1)M(x_0),$$

with $M(x)$ the single discrete time step Jacobian matrix. In ChaosBook Λ_k denotes the k th *eigenvalue* of the finite time Jacobian matrix $J^t(x_0)$, and $\mu^{(k)}$ the real part of k th *eigen-exponent*

$$|\Lambda| = e^{n\mu}, \quad \Lambda_{\pm} = e^{n(\mu \pm i\omega)}.$$

For complex eigenvalue pairs the ‘angular velocity’ ω describes rotational motion in the plane spanned by the real and imaginary parts of the corresponding pair of eigenvectors.

The eigenvalues and eigen-directions of the Jacobian matrix describe the deformation of an initial infinitesimal cloud of neighboring trajectories into a distorted cloud a finite time t later. Nearby trajectories separate exponentially along unstable eigen-directions, approach each other along stable directions, and change slowly (algebraically) their distance along marginal directions. The Jacobian matrix J^t is in general neither symmetric, nor diagonalizable by a rotation, nor do its (left or right) eigenvectors define an orthonormal coordinate frame. Furthermore, although the Jacobian matrices are multiplicative along the flow, in dimensions higher than one their eigenvalues in general are not. This lack of multiplicativity has important repercussions for both classical and quantum dynamics.

Commentary

Remark 4.1 Linear flows. The subject of linear algebra generates innumerable tomes of its own; in sect. 4.2 we only sketch, and in appendix B recapitulate a few facts that our narrative relies on: a useful reference book is [1]. The basic facts are presented at length in many textbooks. The standard references that exhaustively enumerate and explain all possible cases are Hirsch and Smale [2] and Arnol'd [3]. A quick overview is given by Izhikevich [4]; for different notions of orbit stability see Holmes and Shea-Brown [5]. For ChaosBook purposes, we enjoyed the discussion in chapter 2 Meiss [6], chapter 1 of Perko [7] and chapters 3 and 5 of Glendinning [8] the most.

The construction of projection operators given here is taken from refs. [9, 10]. Who wrote this down first we do not know, lineage certainly goes all the way back to Lagrange polynomials [11], but projection operators tend to get drowned in sea of algebraic details. Halmos [12] is a good early reference - but we like Harter's exposition [13, 14, 15] best, for its multitude of specific examples and physical illustrations.

The nomenclature tends to be a bit confusing. In referring to velocity gradients matrix A defined in (4.3) as the "stability matrix" we follow Tabor [16]. Sometimes A , which describes the instantaneous shear of the trajectory point $x(x_0, t)$ is referred to as the 'Jacobian matrix,' a particularly unfortunate usage when one considers linearized stability of an equilibrium point (4.31). What Jacobi had in mind in his 1841 fundamental paper [17] on the determinants today known as 'jacobians' were transformations between different coordinate frames. These are dimensionless quantities, while dimensionally A_{ij} is 1/[time]. More unfortunate still is referring to $J^t = e^{tA}$ as an 'evolution operator,' which here (see sect. 17.2) refers to something altogether different. In this book Jacobian matrix J^t always refers to (4.6), the linearized deformation after a finite time t , either for a continuous time flow, or a discrete time mapping.

Remark 4.2 Matrix decompositions of Jacobian matrix. Though singular values decomposition provides geometrical insights into how tangent dynamics acts, many popular algorithms for asymptotic stability analysis (recovering Lyapunov spectrum) employ another standard matrix decomposition: the QR scheme [1], through which a nonsingular matrix A is (uniquely) written as a product of an orthogonal and an upper triangular matrix $A = QR$. This can be thought as a Gram-Schmidt decomposition of the column vectors of A (which are linearly independent as A is nonsingular). The geometric meaning of QR decomposition is that the volume of the d -dimensional parallelepiped spanned by the column vectors of A has a volume coinciding with the product of the diagonal elements of the triangular matrix R , whose role is thus pivotal in algorithms computing Lyapunov spectra [20, 21, 22].

Remark 4.3 Routh-Hurwitz criterion for stability of a fixed point. For a criterion that matrix has roots with negative real parts, see Routh-Hurwitz criterion [18, 19] on the coefficients of the characteristic polynomial. The criterion provides a necessary condition that a fixed point is stable, and determines the numbers of stable/unstable eigenvalues of a fixed point.

Exercises

4.1. **Trace-log of a matrix.** Prove that

$$\det M = e^{\text{tr} \ln M}.$$

for an arbitrary nonsingular finite dimensional matrix M , $\det M \neq 0$.

4.2. **Stability, diagonal case.** Verify the relation (4.17)

$$J^t = e^{tA} = \mathbf{U}^{-1} e^{tA_D} \mathbf{U}, \quad A_D = \mathbf{U} \mathbf{A} \mathbf{U}^{-1}.$$

4.3. **State space volume contraction.**

- (a) Compute the Rössler flow volume contraction rate at the equilibria.
- (b) Study numerically the instantaneous $\partial_i v_i$ along a typical trajectory on the Rössler attractor; color-code the points on the trajectory by the sign (and perhaps the magnitude) of $\partial_i v_i$. If you see regions of local expansion, explain them.
- (c) (optional) color-code the points on the trajectory by the sign (and perhaps the magnitude) of $\partial_i v_i - \partial_i v_i$.
- (d) Compute numerically the average contraction rate (4.47) along a typical trajectory on the Rössler attractor. Plot it as a function of time.
- (e) Argue on basis of your results that this attractor is of dimension smaller than the state space $d = 3$.
- (f) (optional) Start some trajectories on the escape side of the outer equilibrium, color-code the points on the trajectory. Is the flow volume contracting?

(continued in exercise 20.12)

4.4. **Topology of the Rössler flow.** (continuation of exercise 3.1)

- (a) Show that equation $|\det(A - \lambda \mathbf{1})| = 0$ for Rössler flow in the notation of exercise 2.8 can be written as

$$\lambda^3 + \lambda^2 c (p^\mp - \epsilon) + \lambda (p^\pm / \epsilon + 1 - c^2 \epsilon p^\mp) \mp c \sqrt{D} = 0 \quad (4.59)$$

(b) Solve (4.59) for eigenvalues λ^\pm for each equilibrium as an expansion in powers of ϵ . Derive

$$\begin{aligned} \lambda_1^- &= -c + \epsilon c / (c^2 + 1) + o(\epsilon) \\ \lambda_2^- &= \epsilon c^3 / [2(c^2 + 1)] + o(\epsilon^2) \\ \theta_2^- &= 1 + \epsilon / [2(c^2 + 1)] + o(\epsilon) \\ \lambda_1^+ &= c\epsilon(1 - \epsilon) + o(\epsilon^3) \\ \lambda_2^+ &= -\epsilon^5 c^2 / 2 + o(\epsilon^6) \\ \theta_2^+ &= \sqrt{1 + 1/\epsilon} (1 + o(\epsilon)) \end{aligned} \quad (4.60)$$

Compare with exact eigenvalues. What are dynamical implications of the extravagant value of λ_1^- ? (continued as exercise 13.10)

(R. Paškauskas)

4.5. **Time-ordered exponentials.** Given a time dependent matrix $V(t)$ check that the time-ordered exponential

$$\mathcal{U}(t) = \mathbf{T} e^{\int_0^t d\tau V(\tau)}$$

may be written as

$$\mathcal{U}(t) = \sum_{m=0}^{\infty} \int_0^t dt_1 \int_0^{t_1} dt_2 \cdots \int_0^{t_{m-1}} dt_m V(t_1) \cdots V(t_m)$$

and verify, by using this representation, that $\mathcal{U}(t)$ satisfies the equation

$$\dot{\mathcal{U}}(t) = V(t)\mathcal{U}(t),$$

with the initial condition $\mathcal{U}(0) = 1$.

4.6. **A contracting baker's map.** Consider a contracting (or 'dissipative') baker's map, acting on a unit square $[0, 1]^2 = [0, 1] \times [0, 1]$, defined by

$$\begin{pmatrix} x_{n+1} \\ y_{n+1} \end{pmatrix} = \begin{pmatrix} x_n/3 \\ 2y_n \end{pmatrix} \quad y_n \leq 1/2$$

$$\begin{pmatrix} x_{n+1} \\ y_{n+1} \end{pmatrix} = \begin{pmatrix} x_n/3 + 1/2 \\ 2y_n - 1 \end{pmatrix} \quad y_n > 1/2.$$

This map shrinks strips by a factor of 1/3 in the x -direction, and then stretches (and folds) them by a factor of 2 in the y -direction.

By how much does the state space volume contract for one iteration of the map?

References

- [4.1] C.D. Meyer, *Matrix Analysis and Applied Linear Algebra*, (SIAM, Philadelphia 2001).
- [4.2] M. W. Hirsch and S. Smale, *Differential Equations, Dynamical Systems, and Linear Algebra*, (Academic Press, San Diego 1974).
- [4.3] V.I. Arnold, *Ordinary Differential Equations*, (Mit Press, Cambridge 1978).
- [4.4] E. M. Izhikevich, “Equilibrium,”
www.scholarpedia.org/article/Equilibrium.
- [4.5] P. Holmes and E. T. Shea-Brown, “Stability,”
www.scholarpedia.org/article/Stability.
- [4.6] J. D. Meiss, *Differential Dynamical Systems* (SIAM, Philadelphia 2007).
- [4.7] L. Perko, *Differential Equations and Dynamical Systems* (Springer-Verlag, New York 1991).
- [4.8] P. Glendinning, *Stability, Instability, and Chaos* (Cambridge Univ. Press, Cambridge 1994).
- [4.9] P. Cvitanović, “Group theory for Feynman diagrams in non-Abelian gauge theories,” *Phys. Rev. D* **14**, 1536 (1976).
- [4.10] P. Cvitanović, “Classical and exceptional Lie algebras as invariance algebras,” Oxford preprint 40/77 (June 1977, unpublished); available on ChaosBook.org/refs.
- [4.11] K. Hoffman and R. Kunze, *Linear Algebra* (Prentice-Hall, Englewood Cliffs, NJ 1971), Chapter 6.
- [4.12] P. R. Halmos, *Finite-dimensional vector spaces* (D. Van Nostrand, Princeton, 1958).
- [4.13] W. G. Harter, *J. Math. Phys.* **10**, 4 (1969).
- [4.14] W. G. Harter and N. Dos Santos, “Double-group theory on the half-shell and the two-level system. I. Rotation and half-integral spin states,” *Am. J. Phys.* **46**, 251 (1978).
- [4.15] W. G. Harter, *Principles of Symmetry, Dynamics, and Spectroscopy* (Wiley, New York 1974).
- [4.16] M. Tabor, Sect 1.4 “Linear stability analysis,” in *Chaos and Integrability in Nonlinear Dynamics: An Introduction* (Wiley, New York 1989), pp. 20-31.
- [4.17] C. G. J. Jacobi, “De functionibus alternantibus earumque divisione per productum e differentiis elementorum conflatum,” in *Collected Works*, Vol. 22, 439; *J. Reine Angew. Math. (Crelle)* (1841).
- [4.18] wikipedia.org, “*Routh-Hurwitz stability criterion*.”

- [4.19] G. Meinsma, “Elementary proof of the [Routh-Hurwitz test](#),” *Systems and Control Letters* **25** 237 (1995).
- [4.20] G. Benettin, L. Galgani, A. Giorgilli and J.-M. Strelcyn, “Lyapunov characteristic exponents for smooth dynamical systems; a method for computing all of them. Part 1: Theory,” *Meccanica* **15**, 9 (1980).
- [4.21] K. Ramasubramanian and M.S. Sriram, “A comparative study of computation of Lyapunov spectra with different algorithms,” *Physica D* **139**, 72 (2000).
- [4.22] C. Skokos, “The Lyapunov characteristic exponents and their computation,” [arXiv:0811.0882](#).

Chapter 5

Cycle stability

THOPOLOGICAL FEATURES of a dynamical system –singularities, periodic orbits, and the ways in which the orbits intertwine– are invariant under a general continuous change of coordinates. Surprisingly, there also exist quantities that depend on the notion of metric distance between points, but nevertheless do not change value under a smooth change of coordinates. Local quantities such as the eigenvalues of equilibria and periodic orbits, and global quantities such as Lyapunov exponents, metric entropy, and fractal dimensions are examples of properties of dynamical systems independent of coordinate choice.

We now turn to the first, local class of such invariants, linear stability of periodic orbits of flows and maps. This will give us metric information about local dynamics. If you already know that the eigenvalues of periodic orbits are invariants of a flow, skip this chapter.



fast track:
chapter 7, p. 121

5.1 Stability of periodic orbits



As noted on page 40, a trajectory can be stationary, periodic or aperiodic. For chaotic systems almost all trajectories are aperiodic—nevertheless, equilibria and periodic orbits turn out to be the key to unraveling chaotic dynamics. Here we note a few of the properties that make them so precious to a theorist.

An obvious virtue of periodic orbits is that they are *topological* invariants: a fixed point remains a fixed point for any choice of coordinates, and similarly a periodic orbit remains periodic in any representation of the dynamics. Any reparametrization of a dynamical system that preserves its topology has to preserve topological relations between periodic orbits, such as their relative inter-windings

and knots. So the mere existence of periodic orbits suffices to partially organize the spatial layout of a non-wandering set. No less important, as we shall now show, is the fact that cycle eigenvalues are *metric* invariants: they determine the relative sizes of neighborhoods in a non-wandering set.

We start by noting that due to the multiplicative structure (4.44) of Jacobian matrices, the Jacobian matrix for the r th repeat of a prime cycle p of period T_p is

$$J^{rT_p}(x) = J^{T_p}(f^{(r-1)T_p}(x)) \cdots J^{T_p}(f^{T_p}(x)) J^{T_p}(x) = J_p(x)^r, \quad (5.1)$$

where $J_p(x) = J^{T_p}(x)$ is the Jacobian matrix for a single traversal of the prime cycle p , $x \in \mathcal{M}_p$ is any point on the cycle, and $f^{rT_p}(x) = x$ as $f^t(x)$ returns to x every multiple of the period T_p . Hence, it suffices to restrict our considerations to the stability of prime cycles.



fast track:
sect. 5.2, p. 99

5.1.1 Floquet vectors

When dealing with periodic orbits, some of the quantities already introduced inherit names from the Floquet theory of differential equations with time-periodic coefficients. Consider the equation of variations (4.2) evaluated on a periodic orbit p ,

$$\dot{\delta x} = A(t) \delta x, \quad A(t) = A(x(t)) = A(t + T_p). \quad (5.2)$$

The T_p periodicity of the stability matrix implies that if $\delta x(t)$ is a solution of (5.2) then also $\delta x(t + T_p)$ satisfies the same equation: moreover the two solutions are related by (4.6)

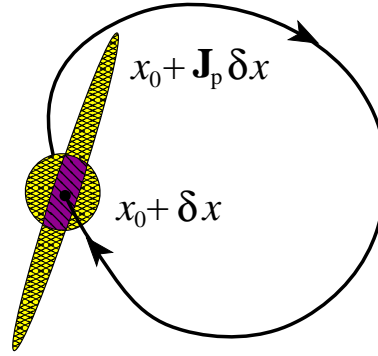
$$\delta x(t + T_p) = J_p(x) \delta x(t). \quad (5.3)$$

Even though the Jacobian matrix $J_p(x)$ depends upon x (the ‘starting’ point of the periodic orbit), we shall show in sect. 5.2 that its eigenvalues do not, so we may write for its eigenvectors $\mathbf{e}^{(j)}$ (sometimes referred to as ‘covariant Lyapunov vectors,’ or, for periodic orbits, as ‘Floquet vectors’)

$$J_p(x) \mathbf{e}^{(j)}(x) = \Lambda_{p,j} \mathbf{e}^{(j)}(x), \quad \Lambda_{p,j} = \sigma_p^{(j)} e^{i\lambda_p^{(j)} T_p}. \quad (5.4)$$

where $\lambda_p^{(j)} = \mu_p^{(j)} \pm i\omega_p^{(j)}$ and $\sigma_p^{(j)}$ are independent of x . When $\Lambda_{p,j}$ is real, we do care about $\sigma_p^{(j)} = \Lambda_{p,j}/|\Lambda_{p,j}| \in \{+1, -1\}$, the sign of the j th Floquet multiplier.

Figure 5.1: For a prime cycle p , Floquet matrix J_p returns an infinitesimal spherical neighborhood of $x_0 \in \mathcal{M}_p$ stretched into an ellipsoid, with overlap ratio along the eigdirection $\mathbf{e}^{(i)}$ of $J_p(x)$ given by the Floquet multiplier $|\Lambda_{p,i}|$. These ratios are invariant under smooth nonlinear reparametrizations of state space coordinates, and are intrinsic property of cycle p .



If $\sigma_p^{(j)} = -1$ and $\lambda_p^{(j)} \neq 0$, the corresponding eigen-direction is said to be *inverse hyperbolic*. Keeping track of this by case-by-case enumeration is an unnecessary nuisance, so most of our formulas will be stated in terms of the Floquet multipliers Λ_j rather than in the terms of the multiplier signs $\sigma^{(j)}$, exponents $\mu^{(j)}$ and phases $\omega^{(j)}$. section 7.2

Expand δx in the (5.4) eigenbasis, $\delta x(t) = \sum \delta x_j(t) \mathbf{e}^{(j)}$, $\mathbf{e}^{(j)} = \mathbf{e}^{(j)}(x(0))$. Taking into account (5.3), we get that $\delta x_j(t)$ is multiplied by $\Lambda_{p,j}$ per each period

$$\delta x(t + T_p) = \sum_j \delta x_j(t + T_p) \mathbf{e}^{(j)} = \sum_j \Lambda_{p,j} \delta x_j(t) \mathbf{e}^{(j)}.$$

We can absorb this exponential growth / contraction by rewriting the coefficients $\delta x_j(t)$ as

$$\delta x_j(t) = e^{\lambda_p^{(j)} t} u_j(t), \quad u_j(0) = \delta x_j(0),$$

with $u_j(t)$ periodic with period T_p . Thus each solution of the equation of variations (4.2) may be expressed in the Floquet form

$$\delta x(t) = \sum_j e^{\lambda_p^{(j)} t} u_j(t) \mathbf{e}^{(j)}, \quad u_j(t + T_p) = u_j(t). \quad (5.5)$$

The continuous time t appearing in (5.5) does not imply that eigenvalues of the Jacobian matrix enjoy any multiplicative property for $t \neq rT_p$: $\lambda_p^{(j)} = \mu_p^{(j)} \pm i\omega_p^{(j)}$ refer to a full traversal of the periodic orbit. Indeed, while $u_j(t)$ describes the variation of $\delta x(t)$ with respect to the stationary eigen-frame fixed by eigenvectors at the point $x(0)$, the object of real interest is the co-moving eigen-frame defined below in (5.13).

5.1.2 Floquet matrix eigenvalues and exponents

The time-dependent T -periodic vector fields, such as the flow linearized around the periodic orbit, are described by Floquet theory. Hence from now on we shall

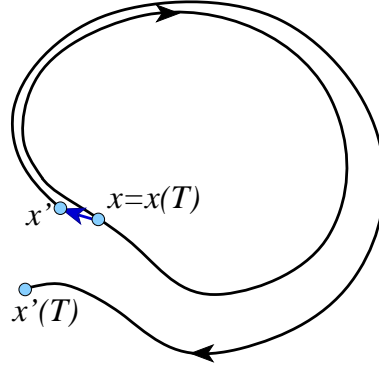


Figure 5.2: An unstable periodic orbit repels every neighboring trajectory $x'(t)$, except those on its center and unstable manifolds.

refer to a Jacobian matrix evaluated on a periodic orbit as a Floquet matrix, to its eigenvalues $\Lambda_{p,j}$ as Floquet multipliers (5.4), and to $\lambda_p^{(j)} = \mu_p^{(j)} + i\omega_p^{(j)}$ as Floquet or characteristic exponents. We sort the *Floquet multipliers* $\{\Lambda_{p,1}, \Lambda_{p,2}, \dots, \Lambda_{p,d}\}$ of the $[d \times d]$ Floquet matrix J_p evaluated on the p -cycle into sets $\{e, m, c\}$

$$\begin{aligned} \text{expanding:} & \quad \{\Lambda\}_e = \{\Lambda_{p,j} : |\Lambda_{p,j}| > 1\} \\ \text{marginal:} & \quad \{\Lambda\}_m = \{\Lambda_{p,j} : |\Lambda_{p,j}| = 1\} \\ \text{contracting:} & \quad \{\Lambda\}_c = \{\Lambda_{p,j} : |\Lambda_{p,j}| < 1\}. \end{aligned} \tag{5.6}$$

and denote by Λ_p (no j th eigenvalue index) the product of *expanding* Floquet multipliers

$$\Lambda_p = \prod_e \Lambda_{p,e}. \tag{5.7}$$

As J_p is a real matrix, complex eigenvalues always come in complex conjugate pairs, $\Lambda_{p,i+1} = \Lambda_{p,i}^*$, so the product (5.7) is always real.

The stretching/contraction rates per unit time are given by the real parts of Floquet exponents

$$\mu_p^{(i)} = \frac{1}{T_p} \ln |\Lambda_{p,i}|. \tag{5.8}$$

The factor $1/T_p$ in the definition of the Floquet exponents is motivated by its form for the linear dynamical systems, for example (4.16), as well as the fact that exponents so defined can be interpreted as Lyapunov exponents (17.33) evaluated on the prime cycle p . As in the three cases of (5.6), we sort the Floquet exponents $\lambda = \mu \pm i\omega$ into three sets

section 17.3

$$\begin{aligned} \text{expanding:} & \quad \{\lambda\}_e = \{\lambda_p^{(i)} : \mu_p^{(i)} > 0\} \\ \text{marginal:} & \quad \{\lambda\}_m = \{\lambda_p^{(i)} : \mu_p^{(i)} = 0\} \\ \text{contracting:} & \quad \{\lambda\}_c = \{\lambda_p^{(i)} : \mu_p^{(i)} < 0\}. \end{aligned} \tag{5.9}$$

A periodic orbit p of a d -dimensional flow or a map is *stable* if real parts of all of its Floquet exponents (other than the vanishing longitudinal exponent, explained in sect. 5.2.1) are strictly negative, $\mu_p^{(i)} < 0$. The region of system parameter values for which a periodic orbit p is stable is called the *stability window* of p . The set \mathcal{M}_p of initial points that are asymptotically attracted to p as $t \rightarrow +\infty$ (for a fixed set of system parameter values) is called the *basin of attraction* of p . If *all* Floquet exponents (other than the vanishing longitudinal exponent) are strictly positive, $\mu^{(i)} \geq \mu_{min} > 0$, the cycle is *repelling*, and unstable to any perturbation. If some are strictly positive, and rest strictly negative, $-\mu^{(i)} \geq \mu_{min} > 0$, the cycle is said to be *hyperbolic* or a *saddle*, and unstable to perturbations outside its stable manifold. Repelling and hyperbolic cycles are unstable to generic perturbations, and thus said to be *unstable*, see figure 5.2. If all $\mu^{(i)} = 0$, the orbit is said to be *elliptic*, and if $\mu^{(i)} = 0$ for a subset of exponents (other than the longitudinal one), the orbit is said to be *partially hyperbolic*. Such orbits proliferate in Hamiltonian flows.

section 7.3

If *all* Floquet exponents (other than the vanishing longitudinal exponent) of *all* periodic orbits of a flow are strictly bounded away from zero, the flow is said to be *hyperbolic*. Otherwise the flow is said to be *nonhyperbolic*.

Example 5.1 Stability of cycles of 1-dimensional maps: The stability of a prime cycle p of a 1-dimensional map follows from the chain rule (4.51) for stability of the n_p th iterate of the map

$$\Lambda_p = \frac{d}{dx_0} f^{n_p}(x_0) = \prod_{m=0}^{n_p-1} f'(x_m), \quad x_m = f^m(x_0). \quad (5.10)$$

Λ_p is a property of the cycle, not the initial periodic point, as taking any periodic point in the p cycle as the initial one yields the same Λ_p .

A critical point x_c is a value of x for which the mapping $f(x)$ has vanishing derivative, $f'(x_c) = 0$. A periodic orbit of a 1-dimensional map is stable if

$$|\Lambda_p| = |f'(x_{n_p})f'(x_{n_p-1}) \cdots f'(x_2)f'(x_1)| < 1,$$

and superstable if the orbit includes a critical point, so that the above product vanishes. For a stable periodic orbit of period n the slope Λ_p of the n th iterate $f^n(x)$ evaluated on a periodic point x (fixed point of the n th iterate) lies between -1 and 1 . If $|\Lambda_p| > 1$, p -cycle is unstable.

Example 5.2 Stability of cycles for maps: No matter what method we use to determine the unstable cycles, the theory to be developed here requires that their Floquet multipliers be evaluated as well. For maps a Floquet matrix is easily evaluated by picking any periodic point as a starting point, running once around a prime cycle, and multiplying the individual periodic point Jacobian matrices according to (4.52). For example, the Floquet matrix M_p for a Hénon map (3.19) prime cycle p of length n_p is given by (4.53),

$$M_p(x_0) = \prod_{k=n_p}^1 \begin{pmatrix} -2ax_k & b \\ 1 & 0 \end{pmatrix}, \quad x_k \in \mathcal{M}_p,$$

and the Floquet matrix M_p for a 2-dimensional billiard prime cycle p of length n_p

$$M_p = (-1)^{n_p} \prod_{k=n_p}^1 \begin{pmatrix} 1 & \tau_k \\ 0 & 1 \end{pmatrix} \begin{pmatrix} 1 & 0 \\ r_k & 1 \end{pmatrix}$$

follows from (8.11) of chapter 8 below. The decreasing order in the indices of the products in above formulas is a reminder that the successive time steps correspond to multiplication from the left, $M_p(x_1) = M(x_{n_p}) \cdots M(x_1)$. We shall compute Floquet multipliers of Hénon map cycles once we learn how to find their periodic orbits, see exercise 13.13.

5.2 Floquet multipliers are invariant



The 1-dimensional map Floquet multiplier (5.10) is a product of derivatives over all points around the cycle, and is therefore independent of which periodic point is chosen as the initial one. In higher dimensions the form of the Floquet matrix $J_p(x_0)$ in (5.1) does depend on the choice of coordinates and the initial point $x_0 \in \mathcal{M}_p$. Nevertheless, as we shall now show, the cycle Floquet multipliers are intrinsic property of a cycle in any dimension. Consider the i th eigenvalue, eigenvector pair $(\Lambda_{p,i}, \mathbf{e}^{(i)})$ computed from J_p evaluated at a periodic point x ,

$$J_p(x) \mathbf{e}^{(i)}(x) = \Lambda_{p,i} \mathbf{e}^{(i)}(x), \quad x \in \mathcal{M}_p. \quad (5.11)$$

Consider another point on the cycle at time t later, $x' = f^t(x)$ whose Floquet matrix is $J_p(x')$. By the group property (4.44), $J^{T_{p+t}} = J^{t+T_p}$, and the Jacobian matrix at x' can be written either as

$$J^{T_{p+t}}(x) = J^{T_p}(x') J^t(x) = J_p(x') J^t(x),$$

or $J^t(x) J_p(x)$. Multiplying (5.11) by $J^t(x)$, we find that the Floquet matrix evaluated at x' has the same Floquet multiplier,

$$J_p(x') \mathbf{e}^{(i)}(x') = \Lambda_{p,i} \mathbf{e}^{(i)}(x'), \quad \mathbf{e}^{(i)}(x') = J^t(x) \mathbf{e}^{(i)}(x), \quad (5.12)$$

but with the eigenvector $\mathbf{e}^{(i)}$ transported along the flow $x \rightarrow x'$ to $\mathbf{e}^{(i)}(x') = J^t(x) \mathbf{e}^{(i)}(x)$. Hence, in the spirit of the Floquet theory (5.5) one can define time-periodic unit eigenvectors (in a co-moving 'Lagrangian frame')

$$\mathbf{e}^{(j)}(t) = e^{-\lambda_p^{(j)} t} J^t(x) \mathbf{e}^{(j)}(0), \quad \mathbf{e}^{(j)}(t) = \mathbf{e}^{(j)}(x(t)), \quad x(t) \in \mathcal{M}_p. \quad (5.13)$$

J_p evaluated anywhere along the cycle has the same set of Floquet multipliers $\{\Lambda_{p,1}, \Lambda_{p,2}, \dots, 1, \dots, \Lambda_{p,d-1}\}$. As quantities such as $\text{tr } J_p(x)$, $\det J_p(x)$ depend

only on the eigenvalues of $J_p(x)$ and not on the starting point x , in expressions such as $\det(\mathbf{1} - J_p^r(x))$ we may omit reference to x ,

$$\det(\mathbf{1} - J_p^r) = \det(\mathbf{1} - J_p^r(x)) \quad \text{for any } x \in \mathcal{M}_p. \quad (5.14)$$

We postpone the proof that the cycle Floquet multipliers are smooth conjugacy invariants of the flow to sect. 6.6.

5.2.1 Marginal eigenvalues

The presence of marginal eigenvalues signals either a continuous symmetry of the flow (which one should immediately exploit to simplify the problem), or a non-hyperbolicity of a flow (a source of much pain, hard to avoid). In that case (typical of parameter values for which bifurcations occur) one has to go beyond linear stability, deal with Jordan type subspaces (see example 4.4), and sub-exponential growth rates, such as t^α .

chapter 24
exercise 5.1

For flow-invariant solutions such as periodic orbits, the time evolution is itself a continuous symmetry, hence a periodic orbit of a flow always has a *marginal Floquet multiplier*:

As $J^t(x)$ transports the velocity field $v(x)$ by (4.7), after a complete period

$$J_p(x) v(x) = v(x), \quad (5.15)$$

so for a periodic orbit of a *flow* the local velocity field is always has an eigenvector $\mathbf{e}^{(\parallel)}(x) = v(x)$ with the unit Floquet multiplier,

$$\Lambda_{p,\parallel} = 1, \quad \lambda_p^{(\parallel)} = 0. \quad (5.16)$$

exercise 6.3

The continuous invariance that gives rise to this marginal Floquet multiplier is the invariance of a cycle (the set \mathcal{M}_p) under a translation of its points along the cycle: two points on the cycle (see figure 4.3) initially distance δx apart, $x'(0) - x(0) = \delta x(0)$, are separated by the exactly same δx after a full period T_p . As we shall see in sect. 5.3, this marginal stability direction can be eliminated by cutting the cycle by a Poincaré section and eliminating the continuous flow Floquet matrix in favor of the Floquet matrix of the Poincaré return map.

If the flow is governed by a time-independent Hamiltonian, the energy is conserved, and that leads to an additional marginal Floquet multiplier (we shall show in sect. 7.3 that due to the symplectic invariance (7.19) real eigenvalues come in pairs). Further marginal eigenvalues arise in presence of continuous symmetries, as discussed in chapter 10 below.

5.3 Stability of Poincaré map cycles



(R. Paškauskas and P. Cvitanović)

If a continuous flow periodic orbit p pierces the Poincaré section \mathcal{P} once, the section point is a fixed point of the Poincaré return map P with stability (4.57)

$$\hat{J}_{ij} = \left(\delta_{ik} - \frac{v_i U_k}{(v \cdot U)} \right) J_{kj}, \quad (5.17)$$

with all primes dropped, as the initial and the final points coincide, $x' = f^{T_p}(x) = x$. If the periodic orbit p pierces the Poincaré section n times, the same observation applies to the n th iterate of P .

We have already established in (4.58) that the velocity $v(x)$ is a zero eigenvector of the Poincaré section Floquet matrix, $\hat{J}v = 0$. Consider next $(\Lambda_{p,\alpha}, \mathbf{e}^{(\alpha)})$, the full state space α th (eigenvalue, eigenvector) pair (5.11), evaluated at a periodic point on a Poincaré section,

$$J(x) \mathbf{e}^{(\alpha)}(x) = \Lambda_\alpha \mathbf{e}^{(\alpha)}(x), \quad x \in \mathcal{P}. \quad (5.18)$$

Multiplying (5.17) by $\mathbf{e}^{(\alpha)}$ and inserting (5.18), we find that the full state space Floquet matrix and the Poincaré section Floquet matrix \hat{J} have the same Floquet multiplier

$$\hat{J}(x) \hat{\mathbf{e}}^{(\alpha)}(x) = \Lambda_\alpha \hat{\mathbf{e}}^{(\alpha)}(x), \quad x \in \mathcal{P}, \quad (5.19)$$

where $\hat{\mathbf{e}}^{(\alpha)}$ is a projection of the full state space eigenvector onto the Poincaré section:

$$(\hat{\mathbf{e}}^{(\alpha)})_i = \left(\delta_{ik} - \frac{v_i U_k}{(v \cdot U)} \right) (\mathbf{e}^{(\alpha)})_k. \quad (5.20)$$

Hence, \hat{J}_p evaluated on any Poincaré section point along the cycle p has the same set of Floquet multipliers $\{\Lambda_{p,1}, \Lambda_{p,2}, \dots, \Lambda_{p,d}\}$ as the full state space Floquet matrix J_p , except for the marginal unit Floquet multiplier (5.16).

As established in (4.58), due to the continuous symmetry (time invariance) \hat{J}_p is a rank $d-1$ matrix. We shall refer to any such rank $[(d-1-N) \times (d-1-N)]$ submatrix with $N-1$ continuous symmetries quotiented out as the *monodromy matrix* M_p (from Greek *mono-* = alone, single, and *dromo* = run, racecourse, meaning a single run around the stadium). Quotienting continuous symmetries is discussed in chapter 10 below.

5.4 There goes the neighborhood



In what follows, our task will be to determine the size of a *neighborhood* of $x(t)$, and that is why we care about the Floquet multipliers, and especially the unstable (expanding) ones. Nearby points aligned along the stable (contracting) directions remain in the neighborhood of the trajectory $x(t) = f^t(x_0)$; the ones to keep an eye on are the points which leave the neighborhood along the unstable directions. The sub-volume $|\mathcal{M}_t| = \prod_i^e \Delta x_i$ of the set of points which get no further away from $f^t(x_0)$ than L , the typical size of the system, is fixed by the condition that $\Delta x_i \Lambda_i = O(L)$ in each expanding direction i . Hence the neighborhood size scales as $\propto 1/|\Lambda_p|$ where Λ_p is the product of expanding Floquet multipliers (5.7) only; contracting ones play a secondary role.

So the dynamically important information is carried by the expanding sub-volume, not the total volume computed so easily in (4.47). That is also the reason why the dissipative and the Hamiltonian chaotic flows are much more alike than one would have naively expected for ‘compressible’ vs. ‘incompressible’ flows. In hyperbolic systems what matters are the expanding directions. Whether the contracting eigenvalues are inverses of the expanding ones or not is of secondary importance. As long as the number of unstable directions is finite, the same theory applies both to the finite-dimensional ODEs and infinite-dimensional PDEs.

Résumé

Periodic orbits play a central role in any invariant characterization of the dynamics, because (a) their existence and inter-relations are a *topological*, coordinate-independent property of the dynamics, and (b) their Floquet multipliers form an infinite set of *metric invariants*: The Floquet multipliers of a periodic orbit remain invariant under any smooth nonlinear change of coordinates $f \rightarrow h \circ f \circ h^{-1}$. Let us summarize the linearized flow notation used throughout the ChaosBook.

section 6.6

Differential formulation, flows:

$$\dot{x} = v, \quad \delta \dot{x} = A \delta x$$

governs the dynamics in the tangent bundle $(x, \delta x) \in \mathbf{TM}$ obtained by adjoining the d -dimensional tangent space $\delta x \in T\mathcal{M}_x$ to every point $x \in \mathcal{M}$ in the d -dimensional state space $\mathcal{M} \subset \mathbb{R}^d$. The *stability matrix* $A = \partial v / \partial x$ describes the instantaneous rate of shearing of the infinitesimal neighborhood of $x(t)$ by the flow.

Finite time formulation, maps: A discrete sets of trajectory points $\{x_0, x_1, \dots, x_n, \dots\} \in \mathcal{M}$ can be generated by composing finite-time maps, either given as $x_{n+1} = f(x_n)$, or obtained by integrating the dynamical equations

$$x_{n+1} = f(x_n) = x_n + \int_{t_n}^{t_{n+1}} d\tau v(x(\tau)), \quad (5.21)$$

for a discrete sequence of times $\{t_0, t_1, \dots, t_n, \dots\}$, specified by some criterion such as strobing or Poincaré sections. In the discrete time formulation the dynamics in the tangent bundle $(x, \delta x) \in \mathbf{TM}$ is governed by

$$x_{n+1} = f(x_n), \quad \delta x_{n+1} = J(x_n) \delta x_n, \quad J(x_n) = J^{t_{n+1}-t_n}(x_n),$$

where $J(x_n) = \partial x_{n+1} / \partial x_n = \int d\tau \exp(A \tau)$ is the Jacobian matrix.

Stability of invariant solutions: The linear stability of an equilibrium $v(x_E Q) = 0$ is described by the eigenvalues and eigenvectors $\{\lambda^{(j)}, \mathbf{e}^{(j)}\}$ of the stability matrix A evaluated at the equilibrium point, and the linear stability of a periodic orbit $f^T(x) = x, x \in \mathcal{M}_p$,

$$J_p(x) \mathbf{e}^{(j)}(x) = \Lambda_{p,j} \mathbf{e}^{(j)}(x), \quad \Lambda_{p,j} = \sigma_p^{(j)} e^{\lambda_p^{(j)} T_p},$$

by its Floquet multipliers, vectors and exponents $\{\Lambda_j, \mathbf{e}^{(j)}\}$, where $\lambda_p^{(j)} = \mu_p^{(j)} \pm i\omega_p^{(j)}$. For every continuous symmetry there is a marginal eigen-direction, with $\Lambda_{p,j} = 1, \lambda_p^{(j)} = 0$. With all $1 + N$ continuous symmetries quotiented out (Poincaré sections for time, slices for continuous symmetries of dynamics, see sect. 10.4) linear stability of a periodic orbit (and, more generally, of a partially hyperbolic torus) is described by the $[(d-1-N) \times (d-1-N)]$ monodromy matrix, all of whose Floquet multipliers $|\Lambda_{p,j}| \neq 1$ are generically strictly hyperbolic,

$$M_p(x) \mathbf{e}^{(j)}(x) = \Lambda_{p,j} \mathbf{e}^{(j)}(x), \quad x \in \mathcal{M}_p / G.$$

We shall show in chapter 11 that extending the linearized stability hyperbolic eigen-directions into stable and unstable manifolds yields important global information about the topological organization of state space. What matters most are the expanding directions. The physically important information is carried by the unstable manifold, and the expanding sub-volume characterized by the product of expanding Floquet multipliers of J_p . As long as the number of unstable directions is finite, the theory can be applied to flows of arbitrarily high dimension.



in depth:
appendix B, p. 751



fast track:
chapter 9, p. 143

Commentary

Remark 5.1 Floquet theory. Study of time-dependent and T -periodic vector fields is a classical subject in the theory of differential equations [1, 2]. In physics literature Floquet exponents often assume different names according to the context where the theory is applied: they are called Bloch phases in the discussion of Schrödinger equation with a periodic potential [3], or quasi-momenta in the quantum theory of time-periodic Hamiltonians.

Exercises

5.1. A limit cycle with analytic Floquet exponent.

There are only two examples of nonlinear flows for which the Floquet multipliers can be evaluated analytically. Both are cheats. One example is the 2 – dimensional flow

$$\begin{aligned}\dot{q} &= p + q(1 - q^2 - p^2) \\ \dot{p} &= -q + p(1 - q^2 - p^2).\end{aligned}$$

Determine all periodic solutions of this flow, and determine analytically their Floquet exponents. Hint: go to polar coordinates $(q, p) = (r \cos \theta, r \sin \theta)$. G. Bard

Ermentrout

5.2. **The other example of a limit cycle with analytic Floquet exponent.** What is the other example of a nonlinear flow for which the Floquet multipliers can be evaluated analytically? Hint: email G.B. Ermentrout.

5.3. **Yet another example of a limit cycle with analytic Floquet exponent.** Prove G.B. Ermentrout wrong by solving a third example (or more) of a nonlinear flow for which the Floquet multipliers can be evaluated analytically.

References

- [5.1] G. Floquet, “Sur les equations differentielles lineaires à coefficients periodique,” *Ann. Ecole Norm. Ser. 2*, **12**, 47 (1883).
- [5.2] E. L. Ince, *Ordinary Differential Equations* (Dover, New York 1953).
- [5.3] N. W. Ashcroft and N. D. Mermin, *Solid State Physics* (Holt, Rinehart and Winston, New York 1976).

Chapter 6

Get straight

We owe it to a book to withhold judgment until we reach page 100.

—Henrietta McNutt, George Johnson’s seventh-grade English teacher

A HAMILTONIAN SYSTEM is said to be ‘integrable’ if one can find a change of coordinates to an action-angle coordinate frame where the phase space dynamics is described by motion on circles, one circle for each degree of freedom. In the same spirit, a natural description of a hyperbolic, unstable flow would be attained if one found a change of coordinates into a frame where the stable/unstable manifolds are straight lines, and the flow is along hyperbolas. Achieving this globally for anything but a handful of contrived examples is too much to hope for. Still, as we shall now show, we can make some headway on straightening out the flow locally.



Even though such nonlinear coordinate transformations are very important, especially in celestial mechanics, we shall not necessarily use them much in what follows, so you can safely skip this chapter on the first reading. Except, perhaps, you might want to convince yourself that cycle stabilities are indeed metric invariants of flows (sect. 6.6), and you might like transformations that turn a Keplerian ellipse into a harmonic oscillator (example 6.2) and regularize the 2-body Coulomb collisions (sect. 6.3) in classical helium.



fast track:
chapter 7, p. 121

6.1 Changing coordinates

Problems are handed down to us in many shapes and forms, and they are not always expressed in the most convenient way. In order to simplify a given problem,

one may stretch, rotate, bend and mix the coordinates, but in doing so, the vector field will also change. The vector field lives in a (hyper)plane tangent to state space and changing the coordinates of state space affects the coordinates of the tangent space as well, in a way that we will now describe.

Denote by h the *conjugation function* which maps the coordinates of the initial state space \mathcal{M} into the reparameterized state space $\mathcal{M}' = h(\mathcal{M})$, with a point $x \in \mathcal{M}$ related to a point $y \in \mathcal{M}'$ by

$$y = h(x) = (y_1(x), y_2(x), \dots, y_d(x)).$$

The change of coordinates must be one-to-one and span both \mathcal{M} and \mathcal{M}' , so given any point y we can go back to $x = h^{-1}(y)$. For smooth flows the reparameterized dynamics should support the same number of derivatives as the initial one. If h is a (piecewise) analytic function, we refer to h as a *smooth conjugacy*.

The evolution rule $g^t(y_0)$ on \mathcal{M}' can be computed from the evolution rule $f^t(x_0)$ on \mathcal{M} by taking the initial point $y_0 \in \mathcal{M}'$, going back to \mathcal{M} , evolving, and then mapping the final point $x(t)$ back to \mathcal{M}' :

$$y(t) = g^t(y_0) = h \circ f^t \circ h^{-1}(y_0). \tag{6.1}$$

Here ‘ \circ ’ stands for functional composition $h \circ f(x) = h(f(x))$, so (6.1) is a shorthand for $y(t) = h(f^t(h^{-1}(y_0)))$.

The vector field $\dot{x} = v(x)$ in \mathcal{M} , locally tangent to the flow f^t , is related to the flow by differentiation (2.5) along the trajectory. The vector field $\dot{y} = w(y)$ in \mathcal{M}' , locally tangent to g^t follows by the chain rule:

exercise 6.2

$$\begin{aligned} w(y) &= \left. \frac{dg^t}{dt}(y) \right|_{t=0} = \left. \frac{d}{dt} (h \circ f^t \circ h^{-1}(y)) \right|_{t=0} \\ &= h'(h^{-1}(y)) v(h^{-1}(y)) = h'(x) v(x). \end{aligned} \tag{6.2}$$

In order to rewrite the right-hand side as a function of y , note that the ∂_y differentiation of $h(h^{-1}(y)) = y$ implies

$$\left. \frac{\partial h}{\partial x} \right|_x \cdot \left. \frac{\partial h^{-1}}{\partial y} \right|_y = 1 \quad \rightarrow \quad \frac{\partial h}{\partial x}(x) = \left[\frac{\partial h^{-1}}{\partial y}(y) \right]^{-1}, \tag{6.3}$$

so the equations of motion in the transformed coordinates, with the indices reinstated, are

$$\dot{y}_i = w_i(y) = \left[\frac{\partial h^{-1}}{\partial y}(y) \right]_{ij}^{-1} v_j(h^{-1}(y)). \tag{6.4}$$

Imagine that the state space is a rubber sheet with the flow lines drawn on it. A coordinate change h corresponds to pulling and tugging on the rubber sheet smoothly, without cutting, gluing, or self-intersections of the distorted rubber sheet. Trajectories that are closed loops in \mathcal{M} will remain closed loops in the new manifold \mathcal{M}' , but their shapes will change. Globally h deforms the rubber sheet in a highly nonlinear manner, but locally it simply rescales and shears the tangent field by the Jacobian matrix $\partial_j h_i$, hence the simple transformation law (6.2) for the velocity fields.

The time itself is a parametrization of points along flow lines, and it can also be reparameterized, $s = s(t)$, with the attendant modification of (6.4). An example is the 2-body collision regularization of the helium Hamiltonian (7.6), to be undertaken in sect. 6.3 below.



fast track:
sect. 6.6, p. 115

6.2 Rectification of flows

A profitable way to exploit invariance of dynamics under smooth conjugacies is to use it to pick out the simplest possible representative of an equivalence class. In general and globally these are just words, as we have no clue how to pick such ‘canonical’ representative, but for smooth flows we can always do it locally and for sufficiently short time, by appealing to the *rectification theorem*, a fundamental theorem of ordinary differential equations. The theorem assures us that there exists a solution (at least for a short time interval) and what the solution looks like. The rectification theorem holds in the neighborhood of points of the vector field $v(x)$ that are not singular, that is, everywhere except for the equilibrium points (2.8), and points at which v is infinite. According to the theorem, in a small neighborhood of a non-singular point there exists a change of coordinates $y = h(x)$ such that $\dot{x} = v(x)$ in the new, *canonical* coordinates takes form

$$\begin{aligned} \dot{y}_1 &= \dot{y}_2 = \cdots = \dot{y}_{d-1} = 0 \\ \dot{y}_d &= 1, \end{aligned} \tag{6.5}$$

with unit velocity flow along y_d , and no flow along any of the remaining directions. This is an example of a one-parameter Lie group of transformations, with finite time τ action

$$\begin{aligned} y'_i &= y_i, & i &= 1, 2, \dots, d-1 \\ y'_d &= y_d + \tau. \end{aligned}$$

exercise 9.8
exercise 6.1

Example 6.1 Harmonic oscillator, rectified: As a simple example of global rectification of a flow consider the harmonic oscillator

$$\dot{q} = p, \quad \dot{p} = -q. \quad (6.6)$$

The trajectories $x(t) = (q(t), p(t))$ circle around the origin, so a fair guess is that the system would have a simpler representation in polar coordinates $y = (r, \theta)$:

$$h^{-1} : \begin{cases} q &= h_1^{-1}(r, \theta) = r \cos \theta \\ p &= h_2^{-1}(r, \theta) = r \sin \theta \end{cases}. \quad (6.7)$$

The Jacobian matrix of the transformation is

$$h' = \begin{pmatrix} \cos \theta & \sin \theta \\ -\frac{\sin \theta}{r} & \frac{\cos \theta}{r} \end{pmatrix} \quad (6.8)$$

resulting in (6.4) of rectified form

exercise 5.1

$$\begin{pmatrix} \dot{r} \\ \dot{\theta} \end{pmatrix} = \begin{pmatrix} \cos \theta & \sin \theta \\ -\frac{\sin \theta}{r} & \frac{\cos \theta}{r} \end{pmatrix} \begin{pmatrix} \dot{q} \\ \dot{p} \end{pmatrix} = \begin{pmatrix} 0 \\ -1 \end{pmatrix}. \quad (6.9)$$

In the new coordinates the radial coordinate r is constant, and the angular coordinate θ wraps around a cylinder with constant angular velocity. There is a subtle point in this change of coordinates: the domain of the map h^{-1} is not the plane \mathbb{R}^2 , but rather the plane minus the origin. We had mapped a plane into a cylinder, and coordinate transformations should not change the topology of the space in which the dynamics takes place; the coordinate transformation is not defined on the equilibrium point $x = (0, 0)$, or $r = 0$.

6.3 Collinear helium

(G. Tanner)

So far much has been said about 1-dimensional maps, game of pinball and other curious but rather idealized dynamical systems. If you have become impatient and started wondering what good are the methods learned so far in solving real life physical problems, good news are here. We will apply here concepts of nonlinear dynamics to nothing less than the helium, a dreaded three-body Coulomb problem.

Can we really jump from three static disks directly to three charged particles moving under the influence of their mutually attracting or repelling forces? It turns out, we can, but we have to do it with care. The full problem is indeed not accessible in all its detail, but we are able to analyze a somewhat simpler subsystem—collinear helium. This system plays an important role in the classical and quantum dynamics of the full three-body problem.

The classical helium system consists of two electrons of mass m_e and charge $-e$ moving about a positively charged nucleus of mass m_{he} and charge $+2e$.

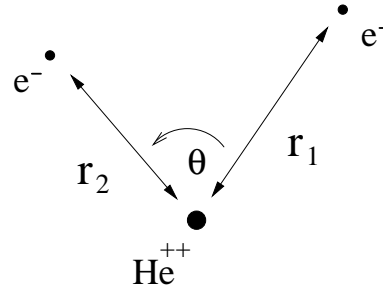


Figure 6.1: Coordinates for the helium three body problem in the plane.

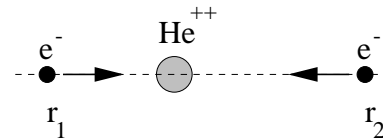


Figure 6.2: Collinear helium, with the two electrons on opposite sides of the nucleus.

The helium electron-nucleus mass ratio $m_{he}/m_e = 1836$ is so large that we may work in the infinite nucleus mass approximation $m_{he} = \infty$, fixing the nucleus at the origin. Finite nucleus mass effects can be taken into account without any substantial difficulty. We are now left with two electrons moving in three spatial dimensions around the origin. The total angular momentum of the combined electron system is still conserved. In the special case of angular momentum $L = 0$, the electrons move in a fixed plane containing the nucleus. The three body problem can then be written in terms of three independent coordinates only, the electron-nucleus distances r_1 and r_2 and the inter-electron angle Θ , see figure 6.1.

This looks like something we can lay our hands on; the problem has been reduced to three degrees of freedom, six phase space coordinates in all, and the total energy is conserved. But let us go one step further; the electrons are attracted by the nucleus but repelled by each other. They will tend to stay as far away from each other as possible, preferably on opposite sides of the nucleus. It is thus worth having a closer look at the situation where the three particles are all on a line with the nucleus being somewhere between the two electrons. If we, in addition, let the electrons have momenta pointing towards the nucleus as in figure 6.2, then there is no force acting on the electrons perpendicular to the common interparticle axis. That is, if we start the classical system on the dynamical subspace $\Theta = \pi, \frac{d}{dt}\Theta = 0$, the three particles will remain in this *collinear configuration* for all times.

6.3.1 Scaling

In what follows we will restrict the dynamics to this collinear subspace. It is a system of two degrees of freedom with the Hamiltonian

$$H = \frac{1}{2m_e} (p_1^2 + p_2^2) - \frac{2e^2}{r_1} - \frac{2e^2}{r_2} + \frac{e^2}{r_1 + r_2} = E, \quad (6.10)$$

where E is the total energy. As the dynamics is restricted to the fixed energy shell, the four phase space coordinates are not independent; the energy shell dependence

can be made explicit by writing

$$(r_1, r_2, p_1, p_2) \rightarrow (r_1(E), r_2(E), p_1(E), p_2(E)).$$

We will first consider the dependence of the dynamics on the energy E . A simple analysis of potential versus kinetic energy tells us that if the energy is positive both electrons can escape to $r_i \rightarrow \infty$, $i = 1, 2$. More interestingly, a single electron can still escape even if E is negative, carrying away an unlimited amount of kinetic energy, as the total energy of the remaining inner electron has no lower bound. Not only that, but one electron *will* escape eventually for almost all starting conditions. The overall dynamics thus depends critically on whether $E > 0$ or $E < 0$. But how does the dynamics change otherwise with varying energy? Fortunately, not at all. Helium dynamics remains invariant under a change of energy up to a simple scaling transformation; a solution of the equations of motion at a fixed energy $E_0 = -1$ can be transformed into a solution at an arbitrary energy $E < 0$ by scaling the coordinates as

$$r_i(E) = \frac{e^2}{(-E)} r_i, \quad p_i(E) = \sqrt{-m_e E} p_i, \quad i = 1, 2,$$

together with a time transformation $t(E) = e^2 m_e^{1/2} (-E)^{-3/2} t$. We include the electron mass and charge in the scaling transformation in order to obtain a non-dimensionalized Hamiltonian of the form

$$H = \frac{p_1^2}{2} + \frac{p_2^2}{2} - \frac{2}{r_1} - \frac{2}{r_2} + \frac{1}{r_1 + r_2} = -1. \quad (6.11)$$

The case of negative energies chosen here is the most interesting one for us. It exhibits chaos, unstable periodic orbits and is responsible for the bound states and resonances of the quantum problem.

6.3.2 Regularization of two-body collisions

Next, we have a closer look at the singularities in the Hamiltonian (6.11). Whenever two bodies come close to each other, accelerations become large, numerical routines require lots of small steps, and numerical precision suffers. No numerical routine will get us through the singularity itself, and in collinear helium electrons have no option but to collide with the nucleus. Hence a *regularization* of the differential equations of motions is a necessary prerequisite to any numerical work on such problems, both in celestial mechanics (where a spaceship executes close approaches both at the start and its destination) and in quantum mechanics (where much of semiclassical physics is dominated by returning classical orbits that probe the quantum wave function at the nucleus).

There is a fundamental difference between two-body collisions $r_1 = 0$ or $r_2 = 0$, and the triple collision $r_1 = r_2 = 0$. Two-body collisions can be regularized, with the singularities in equations of motion removed by a suitable coordinate transformation together with a time transformation preserving the Hamiltonian structure of the equations. Such regularization is not possible for the triple collision, and solutions of the differential equations can not be continued through the singularity at the origin. As we shall see, the chaos in collinear helium originates from this singularity of triple collisions.

A regularization of the two-body collisions is achieved by means of the Kustaanheimo–Stiefel (KS) transformation, which consists of a coordinate dependent time transformation which stretches the time scale near the origin, and a canonical transformation of the phase space coordinates. In order to motivate the method, we apply it first to the 1-dimensional Kepler problem

$$H = \frac{1}{2}p^2 - \frac{2}{x} = E. \quad (6.12)$$

Example 6.2 Keplerian ellipse, rectified: *To warm up, consider the $E = 0$ case, starting at $x = 0$ at $t = 0$. Even though the equations of motion are singular at the initial point, we can immediately integrate*

$$\frac{1}{2}\dot{x}^2 - \frac{2}{x} = 0$$

by means of separation of variables

$$\sqrt{x}dx = \sqrt{2}dt, \quad x = (3t)^{\frac{2}{3}}, \quad (6.13)$$

and observe that the solution is not singular. The aim of regularization is to compensate for the infinite acceleration at the origin by introducing a fictitious time, in terms of which the passage through the origin is smooth.

A time transformation $dt = f(q, p)d\tau$ for a system described by a Hamiltonian $H(q, p) = E$ leaves the Hamiltonian structure of the equations of motion unaltered, if the Hamiltonian itself is transformed into $\mathcal{H}(q, p) = f(q, p)(H(q, p) - E)$. For the 1-dimensional Coulomb problem with (6.12) we choose the time transformation $dt = xd\tau$ which lifts the $|x| \rightarrow 0$ singularity in (6.12) and leads to a new Hamiltonian

$$\mathcal{H} = \frac{1}{2}xp^2 - 2 - Ex = 0. \quad (6.14)$$

The solution (6.13) is now parameterized by the fictitious time $d\tau$ through a pair of equations

$$x = \tau^2, \quad t = \frac{1}{3}\tau^3.$$

The equations of motion are, however, still singular as $x \rightarrow 0$:

$$\frac{d^2x}{d\tau^2} = -\frac{1}{2x} \frac{dx}{d\tau} + xE.$$

Appearance of the square root in (6.13) now suggests a canonical transformation of form

$$x = Q^2, \quad p = \frac{P}{2Q} \quad (6.15)$$

which maps the Kepler problem into that of a harmonic oscillator with Hamiltonian

$$H(Q, P) = \frac{1}{8}P^2 - EQ^2 = 2, \quad (6.16)$$

with all singularities completely removed.

We now apply this method to collinear helium. The basic idea is that one seeks a higher-dimensional generalization of the ‘square root removal’ trick (6.15), by introducing a new vector Q with property $r = |Q|^2$. In this simple 1-dimensional example the KS transformation can be implemented by

$$r_1 = Q_1^2, \quad r_2 = Q_2^2, \quad p_1 = \frac{P_1}{2Q_1}, \quad p_2 = \frac{P_2}{2Q_2} \quad (6.17)$$

and reparameterization of time by $d\tau = dt/r_1 r_2$. The singular behavior in the original momenta at r_1 or $r_2 = 0$ is again compensated by stretching the time scale at these points. The Hamiltonian structure of the equations of motions with respect to the new time τ is conserved, if we consider the Hamiltonian

$$H_{ko} = \frac{1}{8}(Q_2^2 P_1^2 + Q_1^2 P_2^2) - 2R_{12}^2 + Q_1^2 Q_2^2 (-E + 1/R_{12}^2) = 0 \quad (6.18)$$

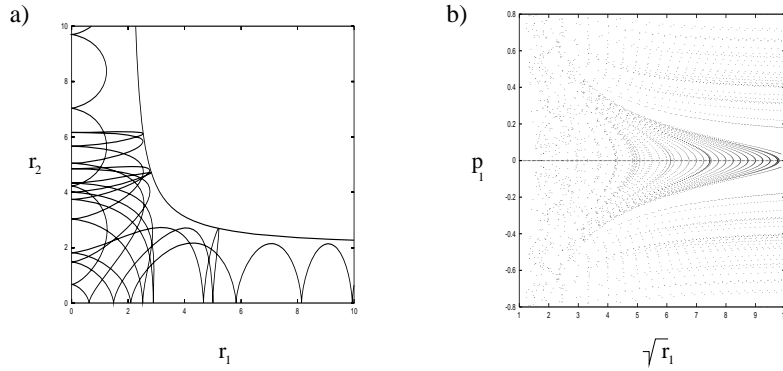
with $R_{12} = (Q_1^2 + Q_2^2)^{1/2}$, and we will take $E = -1$ in what follows. The equations of motion now have the form

$$\begin{aligned} \dot{P}_1 &= 2Q_1 \left[2 - \frac{P_2^2}{8} - Q_2^2 \left(1 + \frac{Q_2^2}{R_{12}^4} \right) \right]; & \dot{Q}_1 &= \frac{1}{4} P_1 Q_2^2 \\ \dot{P}_2 &= 2Q_2 \left[2 - \frac{P_1^2}{8} - Q_1^2 \left(1 + \frac{Q_1^2}{R_{12}^4} \right) \right]; & \dot{Q}_2 &= \frac{1}{4} P_2 Q_1^2. \end{aligned} \quad (6.19)$$

Individual electron–nucleus collisions at $r_1 = Q_1^2 = 0$ or $r_2 = Q_2^2 = 0$ no longer pose a problem to a numerical integration routine. The equations (6.19) are singular only at the triple collision $R_{12} = 0$, i.e., when both electrons hit the nucleus at the same time.

The new coordinates and the Hamiltonian (6.18) are very useful when calculating trajectories for collinear helium; they are, however, less intuitive as a visualization of the three-body dynamics. We will therefore refer to the old coordinates r_1, r_2 when discussing the dynamics and the periodic orbits.

Figure 6.3: (a) A typical trajectory in the $[r_1, r_2]$ plane; the trajectory enters here along the r_1 axis and escapes to infinity along the r_2 axis; (b) Poincaré map ($r_2=0$) for collinear helium. Strong chaos prevails for small r_1 near the nucleus.



To summarize, we have brought a 3-body problem into a form where the 2-body collisions have been transformed away, and the phase space trajectories computable numerically. To appreciate the full beauty of what has been attained, you have to fast-forward to quantum chaos part of ChaosBook.org; we are already ‘almost’ ready to quantize helium by semiclassical methods.



fast track:
chapter 5, p. 94

6.4 Rectification of maps



In sect. 6.2 we had argued that nonlinear coordinate transformations can be profitably employed to simplify the representation of a flow. We shall now apply the same idea to nonlinear maps, and determine a smooth nonlinear change of coordinates that flattens out the vicinity of a fixed point and makes the map *linear* in an open neighborhood. In its simplest form the idea can be implemented only for an isolated nondegenerate fixed point (otherwise are needed in the normal form expansion around the point), and only in a finite neighborhood of a point, as the conjugating function in general has a finite radius of convergence. In sect.6.5 we will extend the method to periodic orbits.

6.4.1 Rectification of a fixed point in one dimension

exercise 6.3

Consider a 1-dimensional map $x_{n+1} = f(x_n)$ with a fixed point at $x = 0$, with stability $\Lambda = f'(0)$. If $|\Lambda| \neq 1$, one can determine term-by-term the power series for a smooth conjugation $h(x)$ centered at the fixed point, $h(0) = 0$, that flattens out the neighborhood of the fixed point

$$f(x) = h^{-1}(\Lambda h(x)) \tag{6.20}$$

and replaces the nonlinear map $f(x)$ by a *linear* map $y_{n+1} = \Lambda y_n$.

To compute the conjugation h we use the functional equation $h^{-1}(\Lambda x) = f(h^{-1}(x))$ and the expansions

$$\begin{aligned} f(x) &= \Lambda x + x^2 f_2 + x^3 f_3 + \dots \\ h^{-1}(x) &= x + x^2 h_2 + x^3 h_3 + \dots \end{aligned} \quad (6.21)$$

Equating the coefficients of x^k on both sides of the functional equation yields h_k order by order as a function of f_2, f_3, \dots . If $h(x)$ is a conjugation, so is any scaling $h(bx)$ of the function for a real number b . Hence the value of $h(0)$ is not determined by the functional equation (6.20); it is convenient to set $h'(0) = 1$.

The algebra is not particularly illuminating and best left to computers. In any case, for the time being we will not use much beyond the first, linear term in these expansions.

Here we have assumed $\Lambda \neq 1$. If the fixed point has first $k-1$ derivatives vanishing, the conjugacy is to the k th normal form.

In several dimensions, Λ is replaced by the Jacobian matrix, and one has to check that the eigenvalues M are non-resonant, that is, there is no integer linear relation between the Floquet exponents (5.8).

remark 6.3

6.5 Rectification of a periodic orbit

In sect. 6.4.1 we have constructed the conjugation function for a fixed point. Here we turn to the problem of constructing it for periodic orbits. Each point around the cycle has a differently distorted neighborhood, with differing second and higher order derivatives, so we need to compute a different conjugation function h_a at each periodic point x_a . We expand the map f around each periodic point along the cycle,

$$y_a(\phi) = f_a(\phi) - x_{a+1} = \phi f_{a,1} + \phi^2 f_{a,2} + \dots \quad (6.22)$$

where x_a is a point on the cycle, $f_a(\phi) = f(x_a + \phi)$ is centered on the periodic orbit, and the index k in $f_{a,k}$ refers to the k th order in the expansion (6.21).

For a periodic orbit the conjugation formula (6.20) generalizes to

$$f_a(\phi) = h_{a+1}^{-1}(f'_a(0)h_a(\phi)), \quad a = 1, 2, \dots, n,$$

point by point. The conjugation functions h_a are obtained in the same way as before, by equating coefficients of the expansion (6.21), and assuming that the



cycle Floquet multiplier $\Lambda = \prod_{a=0}^{n-1} f'(x_a)$ is not marginal, $|\Lambda| \neq 1$. The explicit expressions for h_a in terms of f are obtained by iterating around the whole cycle,

$$f^n(x_a + \phi) = h_a^{-1}(\Lambda h_a(\phi)) + x_a. \quad (6.23)$$

evaluated at each periodic point a . Again we have the freedom to set $h_a(0) = 1$ for all a . remark 6.2

6.5.1 Repeats of cycles

We have traded in our initial nonlinear map f for a (locally) linear map Λy and an equally complicated conjugation function h . What is gained by rewriting the map f in terms of the conjugacy function h ? Once the neighborhood of a fixed point is linearized, the repeats of it are trivialized; from the conjugation formula (6.21) one can compute the derivatives of a function composed with itself r times:

$$f^r(x) = h^{-1}(\Lambda^r h(x)).$$

One can already discern the form of the expansion for arbitrary repeats; the answer will depend on the conjugacy function $h(x)$ computed for a *single* repeat, and all the dependence on the repeat number will be carried by factors polynomial in Λ^r , a considerable simplification. The beauty of the idea is difficult to gauge at this stage—an appreciation only sets in when one starts computing perturbative corrections, be it in celestial mechanics (where the method was born), be it the quantum or stochastic corrections to ‘semiclassical’ approximations.

6.6 Cycle Floquet multipliers are metric invariants



In sect. 5.2 we have established that for a given flow the cycle Floquet multipliers are intrinsic to a given cycle, independent of the starting point along the cycle. Now we can prove a much stronger statement; cycle Floquet multipliers are *smooth conjugacy* or *metric invariants* of the flow, the same in *any* representation of the dynamical system.

That the cycle Floquet multipliers are an invariant property of the given dynamical system follows from elementary considerations of sect. 6.1: If the same dynamics is given by a map f in x coordinates, and a map g in the $y = h(x)$ coordinates, then f and g (or any other good representation) are related by (6.4), a reparameterization and a coordinate transformation $g = h \circ f \circ h^{-1}$. As both f and g are arbitrary representations of the dynamical system, the explicit form of the conjugacy h is of no interest, only the properties invariant under any transformation h are of general import. Furthermore, a good representation should not mutilate the data; h must be a *smooth conjugacy* which maps nearby periodic

points of f into nearby periodic points of g . This smoothness guarantees that the cycles are not only topological invariants, but that their linearized neighborhoods are also metrically invariant. For a fixed point $f(x) = x$ of a 1-dimensional map this follows from the chain rule for derivatives,

$$\begin{aligned} g'(y) &= h'(f \circ h^{-1}(y))f'(h^{-1}(y))\frac{1}{h'(x)} \\ &= h'(x)f'(x)\frac{1}{h'(x)} = f'(x). \end{aligned} \tag{6.24}$$

In d dimensions the relationship between the maps in different coordinate representations is again $g \circ h = h \circ f$. We now make the matrix structure of relation (6.3) explicit:

$$\Gamma_{ik}(x) = \left. \frac{\partial h_i}{\partial x_k} \right|_x \quad \text{and} \quad \Gamma_{ik}^{-1}(x) = \left. \frac{\partial h_i^{-1}}{\partial y_k} \right|_{h(x)},$$

i.e., $\Gamma_{ik}(x)$ is the matrix inverse of $\Gamma_{ik}^{-1}(x)$. The chain rule now relates M' , the Jacobian matrix of the map g to the Jacobian matrix of map f :

$$M'_{ij}(h(x)) = \Gamma_{ik}(f(x))M_{kl}(x)\Gamma_{lj}^{-1}(x). \tag{6.25}$$

If x is a fixed point then (6.25) is a *similarity* transformation and thus preserves eigenvalues: it is easy to verify that in the case of period n_p cycle again $M'^{n_p}(h(x))$ and $M^{n_p}(x)$ are related by a similarity transformation (note that this is not true for $M^r(x)$ with $r \neq n_p$). As stability of a flow can always be reduced to stability of a Poincaré section return map, a Floquet multiplier of any cycle, for a flow or a map in arbitrary dimension, is a metric invariant of the dynamical system.

exercise 6.3



in depth:
appendix B.4, p. 762

Résumé

Dynamics (\mathcal{M}, f) is invariant under the group of all smooth conjugacies

$$(\mathcal{M}, f) \rightarrow (\mathcal{M}', g) = (h(\mathcal{M}), h \circ f \circ h^{-1}).$$

This invariance can be used to (i) find a simplified representation for the flow and (ii) identify a set of invariants, numbers computed within a particular choice of (\mathcal{M}, f) , but invariant under all $\mathcal{M} \rightarrow h(\mathcal{M})$ smooth conjugacies.

The $2D$ -dimensional phase space of an integrable Hamiltonian system of D degrees of freedom is fully foliated by D -tori. In the same spirit, for a uniformly hyperbolic, chaotic dynamical system one would like to change into a coordinate frame where the stable/unstable manifolds form a set of transversally intersecting hyper-planes, with the flow everywhere locally hyperbolic. That cannot be achieved in general: Fully globally integrable and fully globally chaotic flows are a very small subset of all possible flows, a ‘set of measure zero’ in the world of all dynamical systems.

What we *really* care about is developing invariant notions of what a given dynamical system is. The totality of smooth one-to-one nonlinear coordinate transformations h which map all trajectories of a given dynamical system (\mathcal{M}, f) onto all trajectories of dynamical systems (\mathcal{M}, g^t) gives us a huge equivalence class, much larger than the equivalence classes familiar from the theory of linear transformations, such as the rotation group $O(d)$ or the Galilean group of all rotations and translations in \mathbb{R}^d . In the theory of Lie groups, the full invariant specification of an object is given by a finite set of Casimir invariants. What a good full set of invariants for a group of general nonlinear smooth conjugacies might be is not known, but the set of all periodic orbits and their Floquet multipliers will turn out to be a good start.

Commentary

Remark 6.1 Rectification of flows. See Section 2.2.5 of ref. [10] for a pedagogical introduction to smooth coordinate reparameterizations. Explicit examples of transformations into canonical coordinates for a group of scalings and a group of rotations are worked out.

Remark 6.2 Rectification of maps. The methods outlined above are standard in the analysis of fixed points and construction of normal forms for bifurcations, see for example ref. [26, 35, 2, 3, 4, 5, 6, 7, 11]. The geometry underlying such methods is pretty, and we enjoyed reading, for example, Percival and Richards [8], chaps. 2 and 4 of Ozorio de Almeida’s monograph [9], and, as always, Arnol’d [1].

Recursive formulas for evaluation of derivatives needed to evaluate (6.21) are given, for example, in Appendix A of ref. [9]. Section 10.6 of ref. [11] describes in detail the smooth conjugacy that relates the Ulam map (11.5) to the tent map (11.4). For ‘negative Schwartzian derivatives,’ families of conjugacies of Ulam-type maps, associated Lyapunov exponents, continuous measures and further pointers to literature, see ref. [12].

Remark 6.3 A resonance condition. In the hyperbolic case there is a resonance condition that must be satisfied: none of the Floquet exponents may be related by ratios of integers. That is, if $\Lambda_{p,1}, \Lambda_{p,2}, \dots, \Lambda_{p,d}$ are the Floquet multipliers of the Jacobian matrix, then they are in resonance if there exist integers n_1, \dots, n_d such that

$$(\Lambda_{p,1})^{n_1} (\Lambda_{p,2})^{n_2} \cdots (\Lambda_{p,d})^{n_d} = 1.$$

If there is resonance, then one may get corrections to the basic conjugation formulas in the form of monomials in the variables of the map. (R. Mainieri)

Exercises

6.1. **Harmonic oscillator in polar coordinates:** Given a harmonic oscillator (6.6) that follows $\dot{p} = -q$ and $\dot{q} = p$, use (6.8) to rewrite the system in polar coordinates (6.7) and find equations for r and θ .

1. Show that the 1-dimensional state space of the rewritten system is the quotient space $\mathcal{M}/\text{SO}(2)$.
2. Construct a Poincaré section of the quotiented flow.

6.2. **Coordinate transformations.** Changing coordinates is conceptually simple, but can become confusing when carried out in detail. The difficulty arises from confusing functional relationships, such as $x(t) = h^{-1}(y(t))$ with numerical relationships, such as $w(y) = h'(x)v(x)$. Working through an example will clear this up.

- (a) The differential equation in the \mathcal{M} space is $\dot{x} = \{2x_1, x_2\}$ and the change of coordinates from \mathcal{M} to \mathcal{M}' is $h(x_1, x_2) = \{2x_1 + x_2, x_1 - x_2\}$. Solve for $x(t)$. Find h^{-1} .
- (b) Show that in the transformed space \mathcal{M}' , the differential equation is

$$\frac{d}{dt} \begin{bmatrix} y_1 \\ y_2 \end{bmatrix} = \frac{1}{3} \begin{bmatrix} 5y_1 + 2y_2 \\ y_1 + 4y_2 \end{bmatrix}.$$

Solve this system. Does it match the solution in the \mathcal{M} space?

6.3. **Linearization for maps.** Let $f : C \rightarrow C$ be a map from the complex numbers into themselves, with a fixed point at the origin and analytic there. By manipulating power series, find the first few terms of the map h that conjugates f to αz , that is,

$$f(z) = h^{-1}(\alpha h(z)).$$

There are conditions on the derivative of f at the origin to assure that the conjugation is always possible. Can you formulate these conditions by examining the series?

(difficulty: medium)

(R. Mainieri)

6.4. **Ulam and tent maps.** Show that the smooth conjugacy (6.1)

$$\begin{aligned} g(y_0) &= h \circ f \circ h^{-1}(y_0) \\ y &= h(x) = \sin^2(\pi x/2), \end{aligned}$$

conjugates the tent map $f(x) = 1 - 2|x - 1/2|$ into the Ulam map $g(y) = 4y(1-y)$. (continued as exercise 13.1)

References

- [6.1] V.I. Arnol'd, *Ordinary Differential Equations* (Springer-Verlag, New York 1992).
- [6.2] C. L. Siegel. Iteration of analytic functions. *Ann. Math.*, 43:607–612, 1942.
- [6.3] J. Moser. *Ann. Scuola Norm. Super. Pisa*, 20:265–315, 1966; 20:499–535, 1966.
- [6.4] S. Sternberg. *Amer. J. Math.*, 79:809, 1957; 80:623, 1958; 81:578, 1959.
- [6.5] K.-T. Chen. *Amer. J. Math.*, 85:693–722, 1963.
- [6.6] G.R. Belitskiĭ. *Russian Math. Surveys*, 31:107–177, 1978.
- [6.7] A.D. Brjuno. *Trans. Moscow Math. Soc.*, 25:131–288, 1971; 26:199–238, 1972.
- [6.8] I. Percival and D. Richards, *Introduction to Dynamics* (Cambridge Univ. Press, Cambridge 1982).

- [6.9] A.M. Ozorio de Almeida, *Hamiltonian Systems: Chaos and Quantization* (Cambridge Univ. Press, Cambridge 1988).
- [6.10] G. W. Bluman and S. Kumei, *Symmetries and Differential Equations* (Springer, New York 1989).
- [6.11] H.-O. Peitgen, H. Jürgens and D. Saupe, *Chaos and Fractals* (Springer-Verlag, Berlin 1992).
- [6.12] J. M. Aguirregabiria, “Robust chaos with variable Lyapunov exponent in smooth one-dimensional maps,” [arXiv:0810.3781](https://arxiv.org/abs/0810.3781).

Chapter 7

Hamiltonian dynamics

Conservative mechanical systems have equations of motion that are symplectic and can be expressed in Hamiltonian form. The generic properties within the class of symplectic vector fields are quite different from those within the class of all smooth vector fields: the system always has a first integral (“energy”) and a preserved volume, and equilibrium points can never be asymptotically stable in their energy level.

— John Guckenheimer

YOU MIGHT THINK that the strangeness of contracting flows, flows such as the Rössler flow of figure 2.6 is of concern only to chemists or biomedical engineers or the weathermen; physicists do Hamiltonian dynamics, right? Now, that’s full of chaos, too! While it is easier to visualize aperiodic dynamics when a flow is contracting onto a lower-dimensional attracting set, there are plenty examples of chaotic flows that do preserve the full symplectic invariance of Hamiltonian dynamics. The whole story started in fact with Poincaré’s restricted 3-body problem, a realization that chaos rules also in general (non-Hamiltonian) flows came much later.

Here we briefly review parts of classical dynamics that we will need later on; symplectic invariance, canonical transformations, and stability of Hamiltonian flows. If your eventual destination are applications such as chaos in quantum and/or semiconductor systems, read this chapter. If you work in neuroscience or fluid dynamics, skip this chapter, continue reading with the billiard dynamics of chapter 8 which requires no incantations of symplectic pairs or loxodromic quartets.



fast track:
chapter 7, p. 121

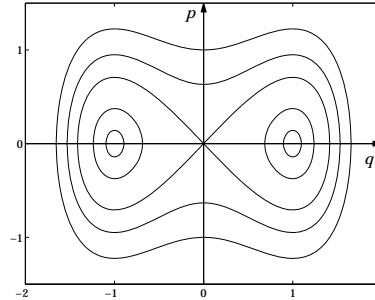


Figure 7.1: Phase plane of the unforced, undamped Duffing oscillator. The trajectories lie on level sets of the Hamiltonian (7.4).

7.1 Hamiltonian flows

(P. Cvitanović and L.V. Vela-Arevalo)

An important class of flows are Hamiltonian flows, given by a Hamiltonian $H(q, p)$ together with the Hamilton's equations of motion

appendix B
remark 2.1

$$\dot{q}_i = \frac{\partial H}{\partial p_i}, \quad \dot{p}_i = -\frac{\partial H}{\partial q_i}, \quad (7.1)$$

with the $2D$ phase space coordinates x split into the configuration space coordinates and the conjugate momenta of a Hamiltonian system with D degrees of freedom (dof):

$$x = (\mathbf{q}, \mathbf{p}), \quad \mathbf{q} = (q_1, q_2, \dots, q_D), \quad \mathbf{p} = (p_1, p_2, \dots, p_D). \quad (7.2)$$

The energy, or the value of the Hamiltonian function at the state space point $x = (\mathbf{q}, \mathbf{p})$ is constant along the trajectory $x(t)$,

$$\begin{aligned} \frac{d}{dt}H(\mathbf{q}(t), \mathbf{p}(t)) &= \frac{\partial H}{\partial q_i} \dot{q}_i(t) + \frac{\partial H}{\partial p_i} \dot{p}_i(t) \\ &= \frac{\partial H}{\partial q_i} \frac{\partial H}{\partial p_i} - \frac{\partial H}{\partial p_i} \frac{\partial H}{\partial q_i} = 0, \end{aligned} \quad (7.3)$$

so the trajectories lie on surfaces of constant energy, or *level sets* of the Hamiltonian $\{(q, p) : H(q, p) = E\}$. For 1-dof Hamiltonian systems this is basically the whole story.

Example 7.1 Unforced undamped Duffing oscillator: When the damping term is removed from the Duffing oscillator (2.7), the system can be written in Hamiltonian form with the Hamiltonian

$$H(q, p) = \frac{p^2}{2} - \frac{q^2}{2} + \frac{q^4}{4}. \quad (7.4)$$

This is a 1-dof Hamiltonian system, with a 2-dimensional state space, the plane (q, p) . The Hamilton's equations (7.1) are

$$\dot{q} = p, \quad \dot{p} = q - q^3. \quad (7.5)$$

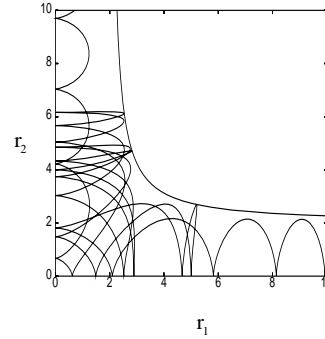


Figure 7.2: A typical collinear helium trajectory in the $[r_1, r_2]$ plane; the trajectory enters along the r_1 -axis and then, like almost every other trajectory, after a few bounces escapes to infinity, in this case along the r_2 -axis.

For 1-dof systems, the ‘surfaces’ of constant energy (7.3) are simply curves in the phase plane (q, p) , and the dynamics is very simple: the curves of constant energy are the trajectories, as shown in figure 7.1.

Thus all 1-dof systems are *integrable*, in the sense that the entire phase plane is foliated by curves of constant energy, either periodic – as is the case for the harmonic oscillator (a ‘bound state’)—or open (a ‘scattering trajectory’). Add one more degree of freedom, and chaos breaks loose.

example 6.1

Example 7.2 Collinear helium: In the quantum chaos part of ChaosBook.org we shall apply the periodic orbit theory to the quantization of helium. In particular, we will study collinear helium, a doubly charged nucleus with two electrons arranged on a line, an electron on each side of the nucleus. The Hamiltonian for this system is

$$H = \frac{1}{2}p_1^2 + \frac{1}{2}p_2^2 - \frac{2}{r_1} - \frac{2}{r_2} + \frac{1}{r_1 + r_2}. \tag{7.6}$$

Collinear helium has 2 dof, and thus a 4-dimensional phase space \mathcal{M} , which energy conservation reduces to 3 dimensions. The dynamics can be projected onto the 2-dimensional configuration plane, the (r_1, r_2) , $r_i \geq 0$ quadrant, figure 7.2. It looks messy, and, indeed, it will turn out to be no less chaotic than a pinball bouncing between three disks. As always, a Poincaré section will be more informative than this rather arbitrary projection of the flow.

Note an important property of Hamiltonian flows: if the Hamilton equations (7.1) are rewritten in the 2D phase space form $\dot{x}_i = v_i(x)$, the divergence of the velocity field v vanishes, namely the flow is incompressible. The symplectic invariance requirements are actually more stringent than just the phase space volume conservation, as we shall see in the next section.

7.2 Stability of Hamiltonian flows

Hamiltonian flows offer an illustration of the ways in which an invariance of equations of motion can affect the dynamics. In the case at hand, the *symplectic invariance* will reduce the number of independent Floquet multipliers by a factor of 2 or 4.

7.2.1 Canonical transformations

The equations of motion for a time-independent, D -dof Hamiltonian (7.1) can be written

$$\dot{x}_i = \omega_{ij} H_j(x), \quad \omega = \begin{pmatrix} 0 & \mathbf{I} \\ -\mathbf{I} & 0 \end{pmatrix}, \quad H_j(x) = \frac{\partial}{\partial x_j} H(x), \quad (7.7)$$

where $x = (\mathbf{q}, \mathbf{p}) \in \mathcal{M}$ is a phase space point, $H_k = \partial_k H$ is the column vector of partial derivatives of H , \mathbf{I} is the $[D \times D]$ unit matrix, and ω the $[2D \times 2D]$ symplectic form

$$\omega^T = -\omega, \quad \omega^2 = -\mathbf{1}. \quad (7.8)$$

The evolution of J^t (4.6) is again determined by the stability matrix A , (4.9):

$$\frac{d}{dt} J^t(x) = A(x) J^t(x), \quad A_{ij}(x) = \omega_{ik} H_{kj}(x), \quad (7.9)$$

where the matrix of second derivatives $H_{kn} = \partial_k \partial_n H$ is called the *Hessian matrix*. From the symmetry of H_{kn} it follows that

$$A^T \omega + \omega A = 0. \quad (7.10)$$

This is the defining property for infinitesimal generators of *symplectic* (or canonical) transformations, transformations which leave the symplectic form ω invariant.

Symplectic matrices are by definition linear transformations that leave the (antisymmetric) quadratic form $x_i \omega_{ij} y_j$ invariant. This immediately implies that any symplectic matrix satisfies

$$Q^T \omega Q = \omega, \quad (7.11)$$

and – when Q is close to the identity $Q = \mathbf{1} + \delta t A$ – it follows that that A must satisfy (7.10).

Consider now a smooth nonlinear change of variables of form $y_i = h_i(x)$, and define a new function $K(x) = H(h(x))$. Under which conditions does K generate a Hamiltonian flow? In what follows we will use the notation $\tilde{\partial}_j = \partial / \partial y_j$: by employing the chain rule we have that

$$\omega_{ij} \partial_j K = \omega_{ij} \tilde{\partial}_l H \frac{\partial h_l}{\partial x_j} \quad (7.12)$$

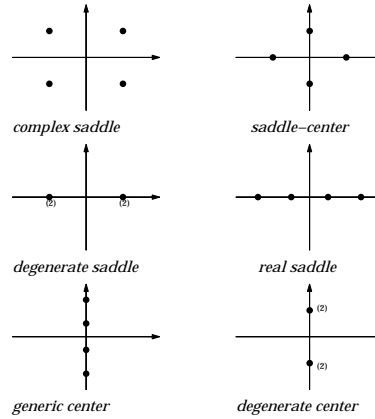


Figure 7.3: Stability exponents of a Hamiltonian equilibrium point, 2-dof.

(Here, as elsewhere in this book, a repeated index implies summation.) By virtue of (7.1) $\tilde{\delta}_l H = -\omega_{lm} \dot{y}_m$, so that, again by employing the chain rule, we obtain

$$\omega_{ij} \partial_j K = -\omega_{ij} \frac{\partial h_l}{\partial x_j} \omega_{lm} \frac{\partial h_m}{\partial x_n} \dot{x}_n \tag{7.13}$$

The right hand side simplifies to \dot{x}_i (yielding Hamiltonian structure) only if

$$-\omega_{ij} \frac{\partial h_l}{\partial x_j} \omega_{lm} \frac{\partial h_m}{\partial x_n} = \delta_{in} \tag{7.14}$$

or, in compact notation, by defining $(\partial h)_{ij} = \frac{\partial h_i}{\partial x_j}$

$$-\omega(\partial h)^T \omega(\partial h) = \mathbf{1} \tag{7.15}$$

which is equivalent to the requirement that ∂h is symplectic. h is then called a *canonical transformation*. We care about canonical transformations for two reasons. First (and this is a dark art), if the canonical transformation h is very cleverly chosen, the flow in new coordinates might be considerably simpler than the original flow. Second, Hamiltonian flows themselves are a prime example of canonical transformations.

example 6.1

Example 7.3 Hamiltonian flows are canonical: For Hamiltonian flows it follows from (7.10) that $\frac{d}{dt}(J^T \omega J) = 0$, and since at the initial time $J^0(x_0) = \mathbf{1}$, Jacobian matrix is a symplectic transformation (7.11). This equality is valid for all times, so a Hamiltonian flow $f^t(x)$ is a canonical transformation, with the linearization $\partial_x f^t(x)$ a symplectic transformation (7.11): For notational brevity here we have suppressed the dependence on time and the initial point, $J = J^t(x_0)$. By elementary properties of determinants it follows from (7.11) that Hamiltonian flows are phase space volume preserving:

$$|\det J| = 1. \tag{7.16}$$

Actually it turns out that for symplectic matrices (on any field) one always has $\det J = +1$.

7.2.2 Stability of equilibria of Hamiltonian flows

For an equilibrium point x_q the stability matrix A is constant. Its eigenvalues describe the linear stability of the equilibrium point. A is the matrix (7.10) with real matrix elements, so its eigenvalues (the Floquet exponents of (4.31)) are either real or come in complex pairs. In the case of Hamiltonian flows, it follows from (7.10) that the characteristic polynomial of A for an equilibrium x_q satisfies

section 4.3.1
exercise 7.4
exercise 7.5

$$\begin{aligned} \det(A - \lambda \mathbf{1}) &= \det(\omega^{-1}(A - \lambda \mathbf{1})\omega) = \det(-\omega A \omega - \lambda \mathbf{1}) \\ &= \det(A^T + \lambda \mathbf{1}) = \det(A + \lambda \mathbf{1}). \end{aligned} \quad (7.17)$$

That is, the symplectic invariance implies in addition that if λ is an eigenvalue, then $-\lambda$, λ^* and $-\lambda^*$ are also eigenvalues. Distinct symmetry classes of the Floquet exponents of an equilibrium point in a 2-dof system are displayed in figure 7.3. It is worth noting that while the linear stability of equilibria in a Hamiltonian system always respects this symmetry, the nonlinear stability can be completely different.

7.3 Symplectic maps

A Floquet multiplier $\Lambda = \Lambda(x_0, t)$ associated to a trajectory is an eigenvalue of the Jacobian matrix J . As J is symplectic, (7.11) implies that

$$J^{-1} = -\omega J^T \omega, \quad (7.18)$$

so the characteristic polynomial is reflexive, namely it satisfies

$$\begin{aligned} \det(J - \Lambda \mathbf{1}) &= \det(J^T - \Lambda \mathbf{1}) = \det(-\omega J^T \omega - \Lambda \mathbf{1}) \\ &= \det(J^{-1} - \Lambda \mathbf{1}) = \det(J^{-1}) \det(\mathbf{1} - \Lambda J) \\ &= \Lambda^{2D} \det(J - \Lambda^{-1} \mathbf{1}). \end{aligned} \quad (7.19)$$

Hence if Λ is an eigenvalue of J , so are $1/\Lambda$, Λ^* and $1/\Lambda^*$. Real eigenvalues always come paired as Λ , $1/\Lambda$. The Liouville conservation of phase space volumes (7.16) is an immediate consequence of this pairing up of eigenvalues. The complex eigenvalues come in pairs Λ , Λ^* , $|\Lambda| = 1$, or in loxodromic quartets Λ , $1/\Lambda$, Λ^* and $1/\Lambda^*$. These possibilities are illustrated in figure 7.4.

Example 7.4 Hamiltonian Hénon map, reversibility: By (4.54) the Hénon map (3.19) for $b = -1$ value is the simplest 2 – dimensional orientation preserving area-preserving map, often studied to better understand topology and symmetries of Poincaré sections of 2 dof Hamiltonian flows. We find it convenient to multiply (3.20)

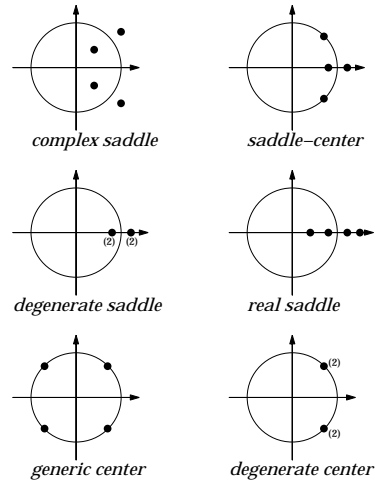


Figure 7.4: Stability of a symplectic map in \mathbb{R}^4 .

by a and absorb the a factor into x in order to bring the Hénon map for the $b = -1$ parameter value into the form

$$x_{i+1} + x_{i-1} = a - x_i^2, \quad i = 1, \dots, n_p, \tag{7.20}$$

The 2-dimensional Hénon map for $b = -1$ parameter value

$$\begin{aligned} x_{n+1} &= a - x_n^2 - y_n \\ y_{n+1} &= x_n. \end{aligned} \tag{7.21}$$

is Hamiltonian (symplectic) in the sense that it preserves area in the $[x, y]$ plane.

For definitiveness, in numerical calculations in examples to follow we shall fix (arbitrarily) the stretching parameter value to $a = 6$, a value large enough to guarantee that all roots of $0 = f^n(x) - x$ (periodic points) are real.

exercise 8.6

Example 7.5 2-dimensional symplectic maps: In the 2-dimensional case the eigenvalues (5.6) depend only on $\text{tr } M^t$

$$\Lambda_{1,2} = \frac{1}{2} \left(\text{tr } M^t \pm \sqrt{(\text{tr } M^t - 2)(\text{tr } M^t + 2)} \right). \tag{7.22}$$

The trajectory is elliptic if the stability residue $|\text{tr } M^t| - 2 \leq 0$, with complex eigenvalues $\Lambda_1 = e^{i\theta t}$, $\Lambda_2 = \Lambda_1^* = e^{-i\theta t}$. If $|\text{tr } M^t| - 2 > 0$, λ is real, and the trajectory is either

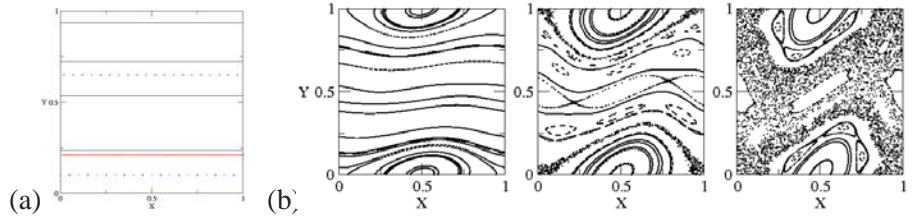
$$\text{hyperbolic} \quad \Lambda_1 = e^{\lambda t}, \quad \Lambda_2 = e^{-\lambda t}, \quad \text{or} \tag{7.23}$$

$$\text{inverse hyperbolic} \quad \Lambda_1 = -e^{\lambda t}, \quad \Lambda_2 = -e^{-\lambda t}. \tag{7.24}$$

Example 7.6 Standard map. Given a smooth function $g(x)$, the map

$$\begin{aligned} x_{n+1} &= x_n + y_{n+1} \\ y_{n+1} &= y_n + g(x_n) \end{aligned} \tag{7.25}$$

Figure 7.5: Phase portrait for the standard map for (a) $k = 0$: symbols denote periodic orbits, full lines represent quasiperiodic orbits. (b) $k = 0.3$, $k = 0.85$ and $k = 1.4$: each plot consists of 20 random initial conditions, each iterated 400 times.



is an area-preserving map. The corresponding n th iterate Jacobian matrix (4.49) is

$$M^n(x_0, y_0) = \prod_{k=0}^{n-1} \begin{pmatrix} 1 + g'(x_k) & 1 \\ g'(x_k) & 1 \end{pmatrix}. \quad (7.26)$$

The map preserves areas, $\det M = 1$, and one can easily check that M is symplectic. In particular, one can consider x on the unit circle, and y as the conjugate angular momentum, with a function g periodic with period 1. The phase space of the map is thus the cylinder $S_1 \times \mathbf{R}$ (S_1 stands for the 1-torus, which is fancy way to say “circle”): by taking (7.25) mod 1 the map can be reduced on the 2-torus S_2 .

The standard map corresponds to the choice $g(x) = k/2\pi \sin(2\pi x)$. When $k = 0$, $y_{n+1} = y_n = y_0$, so that angular momentum is conserved, and the angle x rotates with uniform velocity

$$x_{n+1} = x_n + y_0 = x_0 + (n + 1)y_0 \pmod{1}.$$

The choice of y_0 determines the nature of the motion (in the sense of sect. 2.1.1): for $y_0 = 0$ we have that every point on the $y_0 = 0$ line is stationary, for $y_0 = p/q$ the motion is periodic, and for irrational y_0 any choice of x_0 leads to a quasiperiodic motion (see figure 7.5 (a)).

Despite the simple structure of the standard map, a complete description of its dynamics for arbitrary values of the nonlinear parameter k is fairly complex: this can be appreciated by looking at phase portraits of the map for different k values: when k is very small the phase space looks very much like a slightly distorted version of figure 7.5 (a), while, when k is sufficiently large, single trajectories wander erratically on a large fraction of the phase space, as in figure 7.5 (b).

This gives a glimpse of the typical scenario of transition to chaos for Hamiltonian systems.

Note that the map (7.25) provides a stroboscopic view of the flow generated by a (time-dependent) Hamiltonian

$$H(x, y; t) = \frac{1}{2}y^2 + G(x)\delta_1(t) \quad (7.27)$$

where δ_1 denotes the periodic delta function

$$\delta_1(t) = \sum_{m=-\infty}^{\infty} \delta(t - m) \quad (7.28)$$

and

$$G'(x) = -g(x). \quad (7.29)$$

Important features of this map, including transition to global chaos (destruction of the last invariant torus), may be tackled by detailed investigation of the stability of

periodic orbits. A family of periodic orbits of period Q already present in the $k = 0$ rotation maps can be labeled by its winding number P/Q . The Greene residue describes the stability of a P/Q -cycle:

$$R_{P/Q} = \frac{1}{4} (2 - \text{tr } M_{P/Q}) . \tag{7.30}$$

If $R_{P/Q} \in (0, 1)$ the orbit is elliptic, for $R_{P/Q} > 1$ the orbit is hyperbolic orbits, and for $R_{P/Q} < 0$ inverse hyperbolic.

For $k = 0$ all points on the $y_0 = P/Q$ line are periodic with period Q , winding number P/Q and marginal stability $R_{P/Q} = 0$. As soon as $k > 0$, only a $2Q$ of such orbits survive, according to Poincaré-Birkhoff theorem: half of them elliptic, and half hyperbolic. If we further vary k in such a way that the residue of the elliptic Q -cycle goes through 1, a bifurcation takes place, and two or more periodic orbits of higher period are generated.

7.4 Poincaré invariants

Let C be a region in phase space and $V(0)$ its volume. Denoting the flow of the Hamiltonian system by $f^t(x)$, the volume of C after a time t is $V(t) = f^t(C)$, and using (7.16) we derive the *Liouville theorem*:

$$\begin{aligned} V(t) &= \int_{f^t(C)} dx = \int_C \left| \det \frac{\partial f^t(x')}{\partial x} \right| dx' \\ &= \int_C \det(J) dx' = \int_C dx' = V(0), \end{aligned} \tag{7.31}$$

Hamiltonian flows preserve phase space volumes.

The symplectic structure of Hamilton's equations buys us much more than the 'incompressibility,' or the phase space volume conservation. Consider the symplectic product of two infinitesimal vectors

$$\begin{aligned} (\delta x, \delta \hat{x}) &= \delta x^T \omega \delta \hat{x} = \delta p_i \delta \hat{q}_i - \delta q_i \delta \hat{p}_i \\ &= \sum_{i=1}^D \{ \text{oriented area in the } (q_i, p_i) \text{ plane} \} . \end{aligned} \tag{7.32}$$

Time t later we have

$$(\delta x', \delta \hat{x}') = \delta x'^T J^T \omega J \delta \hat{x} = \delta x^T \omega \delta \hat{x} .$$

This has the following geometrical meaning. We imagine there is a reference phase space point. We then define two other points infinitesimally close so that the vectors δx and $\delta \hat{x}$ describe their displacements relative to the reference point.

Under the dynamics, the three points are mapped to three new points which are still infinitesimally close to one another. The meaning of the above expression is that the area of the parallelepiped spanned by the three final points is the same as that spanned by the initial points. The integral (Stokes theorem) version of this infinitesimal area invariance states that for Hamiltonian flows the D oriented areas \mathcal{V}_i bounded by D loops $\Omega\mathcal{V}_i$, one per each (q_i, p_i) plane, are separately conserved:

$$\int_{\mathcal{V}} dp \wedge dq = \oint_{\Omega\mathcal{V}} p \cdot dq = \text{invariant} . \quad (7.33)$$

Morally a Hamiltonian flow is really D -dimensional, even though its phase space is $2D$ -dimensional. Hence for Hamiltonian flows one emphasizes D , the number of the degrees of freedom.



in depth:
appendix B.4, p. 762

Commentary

Remark 7.1 Hamiltonian dynamics literature. If you are reading this book, in theory you already know everything that is in this chapter. In practice you do not. Try this: Put your right hand on your heart and say: “I understand why nature prefers symplectic geometry.” Honest? Out there there are about 2 centuries of accumulated literature on Hamilton, Lagrange, Jacobi etc. formulation of mechanics, some of it excellent. In context of what we will need here, we make a very subjective recommendation—we enjoyed reading Percival and Richards [1] and Ozorio de Almeida [2].

Remark 7.2 Symplectic. The term symplectic—Greek for twining or plaiting together—was introduced into mathematics by Hermann Weyl. ‘Canonical’ lineage is church-doctrinal: Greek ‘kanon,’ referring to a reed used for measurement, came to mean in Latin a rule or a standard.

Remark 7.3 The sign convention of ω . The overall sign of ω , the symplectic invariant in (7.7), is set by the convention that the Hamilton’s principal function (for energy conserving flows) is given by $R(q, q', t) = \int_q^{q'} p_i dq_i - Et$. With this sign convention the action along a classical path is minimal, and the kinetic energy of a free particle is positive.

Remark 7.4 Symmetries of the symbol square. For a more detailed discussion of symmetry lines see refs. [3, 4, 5, 6, 7]. It is an open question (see remark 21.2) as to how time reversal symmetry can be exploited for reductions of cycle expansions. For example, the fundamental domain symbolic dynamics for reflection symmetric systems is discussed in some detail in sect. 21.5, but how does one recode from time-reversal symmetric symbol sequences to desymmetrized 1/2 state space symbols?

Remark 7.5 Standard map. Standard maps model free rotators under the influence of short periodic pulses, as can be physically implemented, for instance, by pulsed optical lattices in cold atoms physics. On the theoretical side, standard maps exhibit a number of important features: small k values provide an example of *KAM* perturbative regime (see ref. [10]), while for larger k chaotic deterministic transport is observed [8, 9]; the transition to global chaos also presents remarkable universality features [3, 11, 6]. Also the quantum counterpart of this model has been widely investigated, being the first example where phenomena like quantum dynamical localization have been observed [12]. Stability residue was introduced by Greene [11]. For some hands-on experience of the standard map, download Meiss simulation code [13].

Remark 7.6 Loxodromic quartets. For symplectic flows, real eigenvalues always come paired as Λ , $1/\Lambda$, and complex eigenvalues come either in Λ , Λ^* pairs, $|\Lambda| = 1$, or Λ , $1/\Lambda$, Λ^* , $1/\Lambda^*$ loxodromic quartets. As most maps studied in introductory nonlinear dynamics are $2d$, you have perhaps never seen a loxodromic quartet. How likely are we to run into such things in higher dimensions? According to a very extensive study of periodic orbits of a driven billiard with a four dimensional phase space, carried in ref. [17], the three kinds of eigenvalues occur with about the same likelihood.

Exercises

7.1. **Complex nonlinear Schrödinger equation.** Consider the complex nonlinear Schrödinger equation in one spatial dimension [15]:

$$i \frac{\partial \phi}{\partial t} + \frac{\partial^2 \phi}{\partial x^2} + \beta \phi |\phi|^2 = 0, \quad \beta \neq 0.$$

(a) Show that the function $\psi : \mathbb{R} \rightarrow \mathbb{C}$ defining the traveling wave solution $\phi(x, t) = \psi(x - ct)$ for $c > 0$ satisfies a second-order complex differential equation equivalent to a Hamiltonian system in \mathbb{R}^4 relative to the noncanonical symplectic form whose matrix is given by

$$w_c = \begin{bmatrix} 0 & 0 & 1 & 0 \\ 0 & 0 & 0 & 1 \\ -1 & 0 & 0 & -c \\ 0 & -1 & c & 0 \end{bmatrix}.$$

(b) Analyze the equilibria of the resulting Hamiltonian system in \mathbb{R}^4 and determine their linear stability properties.

(c) Let $\psi(s) = e^{ics/2} a(s)$ for a real function $a(s)$ and determine a second order equation for $a(s)$. Show that the resulting equation is Hamiltonian and has heteroclinic orbits for $\beta < 0$. Find them.

(d) Find ‘soliton’ solutions for the complex nonlinear Schrödinger equation.

(Luz V. Vela-Arevalo)

7.2. **Symplectic group/algebra**

Show that if a matrix C satisfies (7.10), then $\exp(sC)$ is a symplectic matrix.

7.3. **When is a linear transformation canonical?**

(a) Let A be a $[n \times n]$ invertible matrix. Show that the map $\phi : \mathbb{R}^{2n} \rightarrow \mathbb{R}^{2n}$ given by $(\mathbf{q}, \mathbf{p}) \mapsto (A\mathbf{q}, (A^{-1})^T \mathbf{p})$ is a canonical transformation.

(b) If \mathbf{R} is a rotation in \mathbb{R}^3 , show that the map $(\mathbf{q}, \mathbf{p}) \mapsto (\mathbf{R}\mathbf{q}, \mathbf{R}\mathbf{p})$ is a canonical transformation.

(Luz V. Vela-Arevalo)

7.4. **Determinants of symplectic matrices.** Show that the determinant of a symplectic matrix is +1, by going through the following steps:

- use (7.19) to prove that for eigenvalue pairs each member has the same multiplicity (the same holds for quartet members),
- prove that the *joint* multiplicity of $\lambda = \pm 1$ is even,
- show that the multiplicities of $\lambda = 1$ and $\lambda = -1$ cannot be both odd. (Hint: write

$$P(\lambda) = (\lambda - 1)^{2m+1} (\lambda + 1)^{2l+1} Q(\lambda)$$

and show that $Q(1) = 0$).

7.5. **Cherry’s example.** What follows refs. [14, 16] is mostly a reading exercise, about a Hamiltonian system that is *linearly stable* but *nonlinearly unstable*. Consider the Hamiltonian system on \mathbb{R}^4 given by

$$H = \frac{1}{2}(q_1^2 + p_1^2) - (q_2^2 + p_2^2) + \frac{1}{2}p_2(p_1^2 - q_1^2) - q_1 q_2 p_1.$$

- Show that this system has an equilibrium at the origin, which is linearly stable. (The linearized system consists of two uncoupled oscillators with frequencies in ratios 2:1).
- Convince yourself that the following is a family of solutions parameterize by a constant τ :

$$q_1 = -\sqrt{2} \frac{\cos(t - \tau)}{t - \tau}, \quad q_2 = \frac{\cos 2(t - \tau)}{t - \tau},$$

$$p_1 = \sqrt{2} \frac{\sin(t - \tau)}{t - \tau}, \quad p_2 = \frac{\sin 2(t - \tau)}{t - \tau}.$$

These solutions clearly blow up in finite time; however they start at $t = 0$ at a distance $\sqrt{3}/\tau$ from the origin, so by choosing τ large, we can find solutions starting arbitrarily close to the origin, yet going to infinity in a finite time, so the origin is *nonlinearly unstable*.

(Luz V. Vela-Arevalo)

References

- [7.1] I. Percival and D. Richards, *Introduction to dynamics* (Cambridge Univ. Press, Cambridge 1982).
- [7.2] A.M. Ozorio de Almeida, *Hamiltonian systems: Chaos and quantization* (Cambridge Univ. Press, Cambridge 1988).
- [7.3] J.M. Greene, “A method for determining a stochastic transition,” *J. Math. Phys.* **20**, 1183 (1979).
- [7.4] C. Mira, *Chaotic dynamics—From one dimensional endomorphism to two dimensional diffeomorphism* (World Scientific, Singapore, 1987).
- [7.5] P.H. Richter, H.-J. Scholz and A. Wittek, “A breathing chaos,” *Nonlinearity* **1**, 45 (1990).
- [7.6] S.J. Shenker and L.P. Kadanoff, “Critical behavior of a KAM surface: I. Empirical results,” *J.Stat.Phys.* **27**, 631 (1982).
- [7.7] J.M. Greene, R.S. MacKay, F. Vivaldi and M.J. Feigenbaum, “Universal behaviour in families of area-preserving maps,” *Physica D* **3**, 468 (1981).
- [7.8] B.V. Chirikov, “A universal instability of many-dimensional oscillator system,” *Phys. Rep.* **52**, 265 (1979).
- [7.9] J.D. Meiss, “Symplectic maps, variational principles, and transport,” *Rev. Mod. Phys.* **64**, 795 (1992).
- [7.10] J.V. José and E.J. Salatan, *Classical dynamics - A contemporary approach* (Cambridge Univ. Press, Cambridge 1998).
- [7.11] J.M. Greene, “Two-dimensional measure-preserving mappings,” *J. Math. Phys.* **9**, 760 (1968).
- [7.12] G. Casati and B.V. Chirikov, *Quantum chaos: Between order and disorder* (Cambridge Univ. Press, Cambridge 1995).
- [7.13] J.D. Meiss, “Visual explorations of dynamics: The standard map,”
[arXiv:0801.0883](https://arxiv.org/abs/0801.0883).
- [7.14] T.M. Cherry, “Some examples of trajectories defined by differential equations of a generalized dynamical type,” *Trans. Camb. Phil. Soc.* **XXIII**, 165 (1925).
- [7.15] J. E. Marsden and T. S. Ratiu, *Introduction to mechanics and symmetry* (Springer, New York, 1994).
- [7.16] K.R. Meyer, “Counter-examples in dynamical systems via normal form theory,” *SIAM Review* **28**, 41 (1986).
- [7.17] F. Lenz, C. Petri, F.N.R. Koch, F.K. Diakonov and P. Schmelcher, “Evolutionary phase space in driven elliptical billiards,”
[arXiv:0904.3636](https://arxiv.org/abs/0904.3636).

Chapter 8

Billiards

THE DYNAMICS that we have the best intuitive grasp on, and find easiest to grapple with both numerically and conceptually, is the dynamics of billiards. For billiards, discrete time is altogether natural; a particle moving through a billiard suffers a sequence of instantaneous kicks, and executes simple motion in between, so there is no need to contrive a Poincaré section. We have already used this system in sect. 1.3 as the intuitively most accessible example of chaos. Here we define billiard dynamics more precisely, anticipating the applications to come.

8.1 Billiard dynamics

A billiard is defined by a connected region $Q \subset \mathbb{R}^D$, with boundary $\partial Q \subset \mathbb{R}^{D-1}$ separating Q from its complement $\mathbb{R}^D \setminus Q$. The region Q can consist of one compact, finite volume component (in which case the billiard phase space is bounded, as for the stadium billiard of figure 8.1), or can be infinite in extent, with its complement $\mathbb{R}^D \setminus Q$ consisting of one or several finite or infinite volume components (in which case the phase space is open, as for the 3-disk pinball game in figure 1.1). In what follows we shall most often restrict our attention to *planar billiards*.

A point particle of mass m and momentum $p_n = mv_n$ moves freely within the billiard, along a straight line, until it encounters the boundary. There it reflects specularly (*specular* = mirrorlike), with no change in the tangential component of momentum, and instantaneous reversal of the momentum component normal to the boundary,

$$p' = p - 2(p \cdot \hat{n})\hat{n}, \quad (8.1)$$

with \hat{n} the unit vector normal to the boundary ∂Q at the collision point. The angle of incidence equals the angle of reflection, as illustrated in figure 8.2. A billiard is

Figure 8.1: The stadium billiard is a 2-dimensional domain bounded by two semi-circles of radius $d = 1$ connected by two straight walls of length $2a$. At the points where the straight walls meet the semi-circles, the curvature of the border changes discontinuously; these are the only singular points of the flow. The length a is the only parameter.

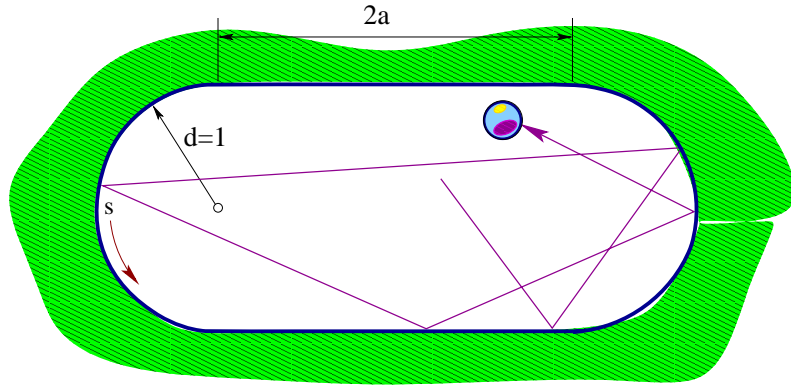
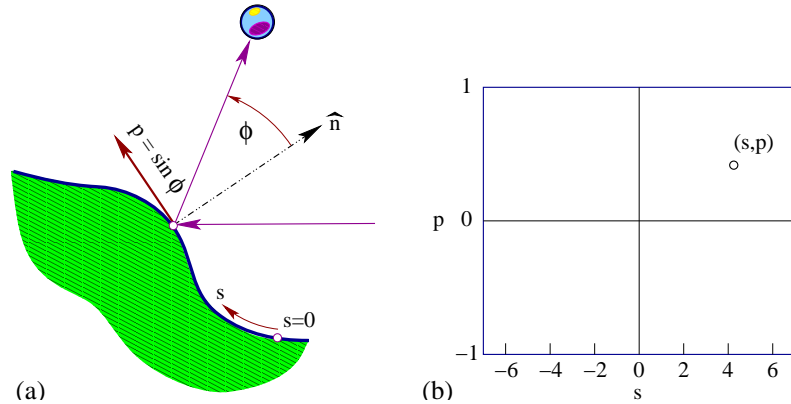


Figure 8.2: (a) A planar billiard trajectory is fixed by specifying the perimeter length parametrized by s and the outgoing trajectory angle ϕ , both measured counterclockwise with respect to the outward normal \hat{n} . (b) The Birkhoff phase space coordinate pair (s, p) fully specifies the trajectory, where $p = |p| \sin \phi$ is the momentum component tangential to the boundary. As the pinball kinetic energy is conserved in elastic scattering, the pinball mass and the magnitude of the pinball momentum are customarily set to $m = |p| = 1$.



a Hamiltonian system with a $2D$ -dimensional phase space $x = (q, p)$ and potential $V(q) = 0$ for $q \in Q$, $V(q) = \infty$ for $q \in \partial Q$.

remark 2.1

A billiard flow has a natural Poincaré section defined by Birkhoff coordinates s_n , the arc length position of the n th bounce measured along the billiard boundary, and $p_n = |p| \sin \phi_n$, the momentum component parallel to the boundary, where ϕ_n is the angle between the outgoing trajectory and the normal to the boundary. We measure both the arc length s , and the parallel momentum p counterclockwise relative to the outward normal (see figure 8.2 as well as figure 3.3). In $D = 2$, the Poincaré section is a cylinder (topologically an annulus), figure 8.3, where the parallel momentum p ranges for $-|p|$ to $|p|$, and the s coordinate is cyclic along each connected component of ∂Q . The volume in the full phase space is preserved by the Liouville theorem (7.31). The Birkhoff coordinates $x = (s, p) \in \mathcal{P}$, are the natural choice, because with them the Poincaré return map preserves the phase space volume of the (s, p) parameterized Poincaré section (a perfectly good coordinate set (s, ϕ) does not do that).

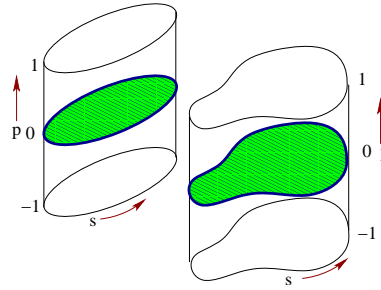
exercise 8.6
section 8.2

Without loss of generality we set $m = |v| = |p| = 1$. Poincaré section condition eliminates one dimension, and the energy conservation $|p| = 1$ eliminates another, so the Poincaré section return map P is $(2D - 2)$ -dimensional.

The dynamics is given by the Poincaré return map

$$P : (s_n, p_n) \mapsto (s_{n+1}, p_{n+1}) \tag{8.2}$$

Figure 8.3: In $D = 2$ the billiard Poincaré section is a cylinder, with the parallel momentum p ranging over $p \in \{-1, 1\}$, and with the s coordinate is cyclic along each connected component of ∂Q . The rectangle figure 8.2(b) is such cylinder unfolded, with periodic boundary conditions glueing together the left and the right edge of the rectangle.



from the n th collision to the $(n + 1)$ st collision. The discrete time dynamics map P is equivalent to the Hamiltonian flow (7.1) in the sense that both describe the same full trajectory. Let t_n denote the instant of n th collision. Then the position of the pinball $\in Q$ at time $t_n + \tau \leq t_{n+1}$ is given by $2D - 2$ Poincaré section coordinates $(s_n, p_n) \in \mathcal{P}$ together with τ , the distance reached by the pinball along the n th section of its trajectory (as we have set the pinball velocity to 1, the time of flight equals the distance traversed).

Example 8.1 3-disk game of pinball: In case of bounces off a circular disk, the position coordinate $s = r\theta$ is given by angle $\theta \in [0, 2\pi]$. For example, for the 3-disk game of pinball of figure 1.6 and figure 3.3 we have two types of collisions:

exercise 8.1

$$P_0 : \begin{cases} \phi' = -\phi + 2 \arcsin p \\ p' = -p + \frac{a}{R} \sin \phi' \end{cases} \quad \text{back-reflection} \quad (8.3)$$

$$P_1 : \begin{cases} \phi' = \phi - 2 \arcsin p + 2\pi/3 \\ p' = p - \frac{a}{R} \sin \phi' \end{cases} \quad \text{reflect to 3rd disk.} \quad (8.4)$$

Here $a =$ radius of a disk, and $R =$ center-to-center separation. Actually, as in this example we are computing intersections of circles and straight lines, nothing more than high-school geometry is required. There is no need to compute arcsin - one only needs to compute one square root per each reflection, and the simulations can be very fast.

exercise 8.2

Trajectory of the pinball in the 3-disk billiard is generated by a series of P_0 's and P_1 's. At each step one has to check whether the trajectory intersects the desired disk (and no disk in-between). With minor modifications, the above formulas are valid for any smooth billiard as long as we replace a by the local curvature of the boundary at the point of collision.

8.2 Stability of billiards

We turn next to the question of local stability of discrete time billiard systems. Infinitesimal equations of variations (4.2) do not apply, but the multiplicative structure (4.44) of the finite-time Jacobian matrices does. As they are more physical than most maps studied by dynamicists, let us work out the billiard stability in some detail.

On the face of it, a plane billiard phase space is 4-dimensional. However, one dimension can be eliminated by energy conservation, and the other by the fact that the magnitude of the velocity is constant. We shall now show how going to a local frame of motion leads to a $[2 \times 2]$ Jacobian matrix.

Consider a 2-dimensional billiard with phase space coordinates $x = (q_1, q_2, p_1, p_2)$. Let t_k be the instant of the k th collision of the pinball with the billiard boundary, and $t_k^\pm = t_k \pm \epsilon$, ϵ positive and infinitesimal. With the mass and the velocity equal to 1, the momentum direction can be specified by angle θ : $x = (q_1, q_2, \sin \theta, \cos \theta)$. Now parametrize the 2 – dimensional neighborhood of a trajectory segment by $\delta x = (\delta z, \delta \theta)$, where

$$\delta z = \delta q_1 \cos \theta - \delta q_2 \sin \theta, \quad (8.5)$$

$\delta \theta$ is the variation in the direction of the pinball motion. Due to energy conservation, there is no need to keep track of δq_{\parallel} , variation along the flow, as that remains constant. $(\delta q_1, \delta q_2)$ is the coordinate variation transverse to the k th segment of the flow. From the Hamilton's equations of motion for a free particle, $dq_i/dt = p_i$, $dp_i/dt = 0$, we obtain the equations of motion (4.1) for the linearized neighborhood

$$\frac{d}{dt} \delta \theta = 0, \quad \frac{d}{dt} \delta z = \delta \theta. \quad (8.6)$$

Let $\delta \theta_k = \delta \theta(t_k^+)$ and $\delta z_k = \delta z(t_k^+)$ be the local coordinates immediately after the k th collision, and $\delta \theta_k^- = \delta \theta(t_k^-)$, $\delta z_k^- = \delta z(t_k^-)$ immediately before. Integrating the free flight from t_{k-1}^+ to t_k^- we obtain

$$\begin{aligned} \delta z_k^- &= \delta z_{k-1} + \tau_k \delta \theta_{k-1}, & \tau_k &= t_k - t_{k-1} \\ \delta \theta_k^- &= \delta \theta_{k-1}, \end{aligned} \quad (8.7)$$

and the Jacobian matrix (4.43) for the k th free flight segment is

$$M_T(x_k) = \begin{pmatrix} 1 & \tau_k \\ 0 & 1 \end{pmatrix}. \quad (8.8)$$

At incidence angle ϕ_k (the angle between the outgoing particle and the outgoing normal to the billiard edge), the incoming transverse variation δz_k^- projects onto an arc on the billiard boundary of length $\delta z_k^- / \cos \phi_k$. The corresponding incidence angle variation $\delta \phi_k = \delta z_k^- / \rho_k \cos \phi_k$, $\rho_k =$ local radius of curvature, increases the angular spread to

$$\begin{aligned} \delta z_k &= -\delta z_k^- \\ \delta \theta_k &= -\delta \theta_k^- - \frac{2}{\rho_k \cos \phi_k} \delta z_k^-, \end{aligned} \quad (8.9)$$

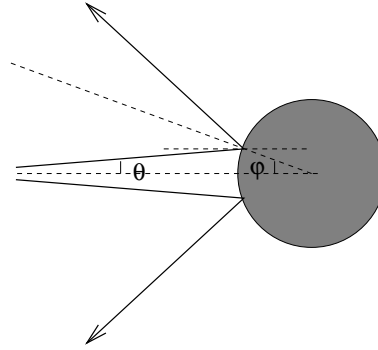


Figure 8.4: Defocusing of a beam of nearby trajectories at a billiard collision. (A. Wirzba)

so the Jacobian matrix associated with the reflection is

$$M_R(x_k) = -\begin{pmatrix} 1 & 0 \\ r_k & 1 \end{pmatrix}, \quad r_k = \frac{2}{\rho_k \cos \phi_k}. \quad (8.10)$$

The full Jacobian matrix for n_p consecutive bounces describes a beam of trajectories defocused by M_T along the free flight (the τ_k terms below) and defocused/refocused at reflections by M_R (the r_k terms below)

exercise 8.4

$$M_p = (-1)^{n_p} \prod_{k=n_p}^1 \begin{pmatrix} 1 & \tau_k \\ 0 & 1 \end{pmatrix} \begin{pmatrix} 1 & 0 \\ r_k & 1 \end{pmatrix}, \quad (8.11)$$

where τ_k is the flight time of the k th free-flight segment of the orbit, $\eta_k = 2/\rho_k \cos \phi_k$ is the defocusing due to the k th reflection, and ρ_k is the radius of curvature of the billiard boundary at the k th scattering point (for our 3-disk game of pinball, $\rho = 1$). As the billiard dynamics is phase space volume preserving, $\det M = 1$, and the eigenvalues are given by (7.22).

This is an example of the Jacobian matrix chain rule (4.52) for discrete time systems (the Hénon map stability (4.53) is another example). Stability of every flight segment or reflection taken alone is a shear with two unit eigenvalues,

$$\det M_T = \det \begin{pmatrix} 1 & \tau_k \\ 0 & 1 \end{pmatrix}, \quad \det M_R = \det \begin{pmatrix} 1 & 0 \\ r_k & 1 \end{pmatrix}, \quad (8.12)$$

but acting in concert in the intervowen sequence (8.11) they can lead to a hyperbolic deformation of the infinitesimal neighborhood of a billiard trajectory.

exercise 13.7

As a concrete application, consider the 3-disk pinball system of sect. 1.3. Analytic expressions for the lengths and eigenvalues of $\overline{0}$, $\overline{1}$ and $\overline{10}$ cycles follow from elementary geometrical considerations. Longer cycles require numerical evaluation by methods such as those described in chapter 13.

exercise 13.8
exercise 8.3
chapter 13

Résumé

A particular natural application of the Poincaré section method is the reduction of a billiard flow to a boundary-to-boundary return map.

Commentary

Remark 8.1 Billiards. The 3-disk game of pinball is to chaotic dynamics what a pendulum is to integrable systems; the simplest physical example that captures the essence of chaos. Another contender for the title of the ‘harmonic oscillator of chaos’ is the baker’s map which is used as the red thread through Ott’s introduction to chaotic dynamics [11]. The baker’s map is the simplest reversible dynamical system which is hyperbolic and has positive entropy. We will not have much use for the baker’s map here, as due to its piecewise linearity it is so nongeneric that it misses all of the subtleties of cycle expansions curvature corrections that will be central to this treatise.

chapter 20

That the 3-disk game of pinball is a quintessential example of deterministic chaos appears to have been first noted by B. Eckhardt [1]. The model was studied in depth classically, semiclassically and quantum mechanically by P. Gaspard and S.A. Rice [3], and used by P. Cvitanović and B. Eckhardt [4] to demonstrate applicability of cycle expansions to quantum mechanical problems. It has been used to study the higher order \hbar corrections to the Gutzwiller quantization by P. Gaspard and D. Alonso Ramirez [5], construct semiclassical evolution operators and entire spectral determinants by P. Cvitanović and G. Vattay [6], and incorporate the diffraction effects into the periodic orbit theory by G. Vattay, A. Wirzba and P.E. Rosenqvist [7]. Gaspard’s monograph [8], which we warmly recommend, utilizes the 3-disk system in much more depth than will be attained here. For further links check ChaosBook.org.

A pinball game does miss a number of important aspects of chaotic dynamics: generic bifurcations in smooth flows, the interplay between regions of stability and regions of chaos, intermittency phenomena, and the renormalization theory of the ‘border of order’ between these regions. To study these we shall have to face up to much harder challenge, dynamics of smooth flows.

Nevertheless, pinball scattering is relevant to smooth potentials. The game of pinball may be thought of as the infinite potential wall limit of a smooth potential, and pinball symbolic dynamics can serve as a *covering* symbolic dynamics in smooth potentials. One may start with the infinite wall limit and adiabatically relax an unstable cycle onto the corresponding one for the potential under investigation. If things go well, the cycle will remain unstable and isolated, no new orbits (unaccounted for by the pinball symbolic dynamics) will be born, and the lost orbits will be accounted for by a set of pruning rules. The validity of this adiabatic approach has to be checked carefully in each application, as things can easily go wrong; for example, near a bifurcation the same naive symbol string assignments can refer to a whole island of distinct periodic orbits.

section 29.1

Remark 8.2 Stability analysis. The chapter 1 of Gaspard monograph [8] is recommended reading if you are interested in Hamiltonian flows, and billiards in particular. A. Wirzba has generalized the stability analysis of sect. 8.2 to scattering off 3-dimensional spheres (follow the links in ChaosBook.org/extras). A clear discussion of linear stability for the general d -dimensional case is given in Gaspard [8], sect. 1.4.

Exercises

- 8.1. **A pinball simulator.** Implement the disk \rightarrow disk maps to compute a trajectory of a pinball for a given starting point, and a given $R:a = (\text{center-to-center distance}):(\text{disk radius})$ ratio for a 3-disk system. As this requires only computation of intersections of lines and circles together with specular reflections, implementation should be within reach of a high-school student. Please start working on this program now; it will be continually expanded in chapters to come, incorporating the Jacobian calculations, Newton root-finding, and so on. Fast code will use elementary geometry (only one $\sqrt{\dots}$ per iteration, rest are multiplications) and eschew trigonometric functions. Provide a graphic display of the trajectories and of the Poincaré section iterates. To be able to compare with the numerical results of coming chapters, work with $R:a = 6$ and/or 2.5 values. Draw the correct versions of figure 1.9 or figure 12.3 for $R:a = 2.5$ and/or 6.
- 8.2. **Trapped orbits.** Shoot 100,000 trajectories from one of the disks, and trace out the strips of figure 1.9 for various $R:a$ by color coding the initial points in the Poincaré section by the number of bounces preceding their escape. Try also $R:a = 6:1$, though that might be too thin and require some magnification. The initial conditions can be randomly chosen, but need not - actually a clearer picture is obtained by systematic scan through regions of interest.
- 8.3. **Pinball stability.** Add to your exercise 8.1 pinball simulator a routine that computes the $[2 \times 2]$ Jacobian matrix. To be able to compare with the numerical results of coming chapters, work with $R:a = 6$ and/or 2.5 values.
- 8.4. **Stadium billiard.** Consider the *Bunimovich stadium* [9, 10] defined in figure 8.1. The Jacobian matrix associated with the reflection is given by (8.10). Here we

take $\rho_k = -1$ for the semicircle sections of the boundary, and $\cos \phi_k$ remains constant for all bounces in a rotation sequence. The time of flight between two semicircle bounces is $\tau_k = 2 \cos \phi_k$. The Jacobian matrix of one semicircle reflection followed by the flight to the next bounce is

$$\begin{aligned} \mathbf{J} &= (-1) \begin{pmatrix} 1 & 2 \cos \phi_k \\ 0 & 1 \end{pmatrix} \begin{pmatrix} 1 & 0 \\ -2/\cos \phi_k & 1 \end{pmatrix} \\ &= (-1) \begin{pmatrix} -3 & 2 \cos \phi_k \\ 2/\cos \phi_k & 1 \end{pmatrix}. \end{aligned}$$

A free flight must always be followed by $k = 1, 2, 3, \dots$ bounces along a semicircle, hence the natural symbolic dynamics for this problem is *nary*, with the corresponding Jacobian matrix given by shear (*ie.* the eigenvalues remain equal to 1 throughout the whole rotation), and k bounces inside a circle lead to

$$\mathbf{J}^k = (-1)^k \begin{pmatrix} -2k - 1 & 2k \cos \phi \\ 2k/\cos \phi & 2k - 1 \end{pmatrix}. \quad (8.13)$$

The Jacobian matrix of a cycle p of length n_p is given by

$$\mathbf{J}_p = (-1)^{\sum n_k} \prod_{k=1}^{n_p} \begin{pmatrix} 1 & \tau_k \\ 0 & 1 \end{pmatrix} \begin{pmatrix} 1 & 0 \\ n_k r_k & 1 \end{pmatrix}. \quad (8.14)$$

Adopt your pinball simulator to the stadium billiard.

- 8.5. **A test of your pinball simulator.** Test your exercise 8.3 pinball simulator by computing numerically cycle stabilities by tracking distances to nearby orbits. Compare your result with the exact analytic formulas of exercise 13.7 and 13.8.
- 8.6. **Birkhoff coordinates.** Prove that the Birkhoff coordinates are phase space volume preserving.

References

- [8.1] B. Eckhardt, *Fractal properties of scattering singularities*, *J. Phys. A* **20**, 5971 (1987).
- [8.2] G.D. Birkhoff, *Acta Math.* **50**, 359 (1927), reprinted in ref. [24].

- [8.3] P. Gaspard and S.A. Rice, *J. Chem. Phys.* **90**, 2225 (1989); **90**, 2242 (1989); **90**, 2255 (1989).
- [8.4] P. Cvitanović and B. Eckhardt, “Periodic-orbit quantization of chaotic system,” *Phys. Rev. Lett.* **63**, 823 (1989).
- [8.5] P. Gaspard and D. Alonso Ramirez, *Phys. Rev. A* **45**, 8383 (1992).
- [8.6] P. Cvitanović and G. Vattay, *Phys. Rev. Lett.* **71**, 4138 (1993).
- [8.7] G. Vattay, A. Wirzba and P.E. Rosenqvist, *Phys. Rev. Lett.* **73**, 2304 (1994).
- [8.8] Ya.G. Sinai, *Usp. Mat. Nauk* **25**, 141 (1970).
- [8.9] L.A. Bunimovich, *Funct. Anal. Appl.* **8**, 254 (1974).
- [8.10] L.A. Bunimovich, *Comm. Math. Phys.* **65**, 295 (1979).
- [8.11] L. Bunimovich and Ya.G. Sinai, *Markov Partition for Dispersed Billiard*, *Comm. Math. Phys.* **78**, 247 (1980); **78**, 479 (1980); *Erratum, ibid.* **107**, 357 (1986).
- [8.12] R. Bridges, “The spin of a bouncing ‘superball,’” *Phys. Educ.* **26**, 350 (1991); www.iop.org/EJ/abstract/0031-9120/26/6/003
- [8.13] H. Lamba, “Chaotic, regular and unbounded behaviour in the elastic impact oscillator;” [arXiv:chao-dyn/9310004](https://arxiv.org/abs/9310004).
- [8.14] S.W. Shaw and P.J. Holmes, *Phys. Rev. Lett.* **51**, 623 (1983).
- [8.15] C.R. de Oliveira and P.S. Goncalves, “Bifurcations and chaos for the quasiperiodic bouncing ball,” *Phys. Rev. E* **56**, 4868 (1997).
- [8.16] E. Cataldo and R. Sampaio, “A Brief Review and a New Treatment for Rigid Bodies Collision Models,” *J. Braz. Soc. Mech. Sci.* **23** (2001).
- [8.17] J. M. T. Thompson and R. Ghaffari. *Phys. Lett. A* **91**, 5 (1982).
- [8.18] J.M.T. Thompson, A.R. Bokaian and R. Ghaffari. *J. Energy Resources Technology (Trans ASME)*, **106**, 191-198 (1984).
- [8.19] E. Fermi. *Phys. Rev.* **75**, 1169 (1949).
- [8.20] J. P. Cleveland, B. Anczykowski, i A. E. Schmid, and V. B. Elings. *Appl. Phys. Lett.* **72**, 2613 (1998).
- [8.21] G. A. Tomlinson, *Philos. Mag* **7**, 905 (1929).
- [8.22] T. Gyalog and H. Thomas, *Z. Phys. Lett. B* **104**, 669 (1997).
- [8.23] J. Berg and G. A. D. Briggs. *Phys. Rev. B* **55**, 14899 (1997).
- [8.24] J. Guckenheimer, P. J. Holmes. *J. Sound Vib.* **84**, 173 (1982).
- [8.25] J. M. Luck, Anita Mehta *Phys. Rev. E* **48**, 3988 (1993).

- [8.26] A. Valance, D. Bideau. *Phys. Rev. E* **57**, 1886 (1998).
- [8.27] S.M. Hammel, J.A. Yorke, and C. Grebogi. *J. Complexity* **3**, 136 (1987).
- [8.28] L. Małyś, R. Klages. *Physica D* **187**, 165 (2004).

Chapter 9

World in a mirror

A detour of a thousand pages starts with a single misstep.
—Chairman Miaw

DYNAMICAL SYSTEMS often come equipped with symmetries, such as the reflection and rotation symmetries of various potentials. In this chapter we study quotienting of discrete symmetries, and in the next chapter we study symmetry reduction for continuous symmetries. We look at individual orbits, and the ways they are interrelated by symmetries. This sets the stage for a discussion of how symmetries affect global densities of trajectories, and the factorization of spectral determinants to be undertaken in chapter 21.

As we shall show here and in chapter 21, discrete symmetries simplify the dynamics in a rather beautiful way: If dynamics is invariant under a set of discrete symmetries G , the state space \mathcal{M} is tiled by a set of symmetry-related tiles, and the dynamics can be reduced to dynamics within one such tile, the *fundamental domain* \mathcal{M}/G . In presence of a symmetry the notion of a prime periodic orbit has to be reexamined: a set of symmetry-related full state space cycles is replaced by often much shorter *relative periodic orbit*, the shortest segment of the full state space cycle which tiles the cycle and all of its copies under the action of the group. Furthermore, the group operations that relate distinct tiles do double duty as letters of an alphabet which assigns symbolic itineraries to trajectories.

section 11.1

Familiarity with basic group-theoretic notions is assumed, with details relegated to appendix H.1. The erudite reader might prefer to skip the lengthy group-theoretic overture and go directly to $C_2 = D_1$ example 9.7, example 9.10, and $C_{3v} = D_3$ example 9.12, backtrack as needed.

9.1 Discrete symmetries

Normal is just a setting on a washing machine.
—Borgette, Borgo's daughter



We show that a symmetry equates multiplets of equivalent orbits, or ‘stratifies’ the state space into equivalence classes, each class a ‘group orbit.’ We start by defining a finite (discrete) group, its state space representations, and what we mean by a *symmetry* (*invariance* or *equivariance*) of a dynamical system. As is always the problem with ‘gruppenpest’ (read appendix A.2.3) way too many abstract notions have to be defined before an intelligent conversation can take place. Perhaps best to skim through this section on the first reading, then return to it later as needed.

Definition: A **finite group** consists of a set of elements

$$G = \{e, g_2, \dots, g_n\} \quad (9.1)$$

and a group multiplication rule $g_j \circ g_i$ (often abbreviated as $g_j g_i$), satisfying

1. Closure: If $g_i, g_j \in G$, then $g_j \circ g_i \in G$
2. Associativity: $g_k \circ (g_j \circ g_i) = (g_k \circ g_j) \circ g_i$
3. Identity e : $g \circ e = e \circ g = g$ for all $g \in G$
4. Inverse g^{-1} : For every $g \in G$, there exists a unique element $h = g^{-1} \in G$ such that $h \circ g = g \circ h = e$.

$|G| = n$, the number of elements, is called the *order* of the group.

Example 9.1 Discrete groups of order 2 on \mathbb{R}^3 . Three types of discrete group of order 2 can arise by linear action on our 3-dimensional Euclidian space \mathbb{R}^3 :

$$\begin{aligned} \text{reflections: } \sigma(x, y, z) &= (x, y, -z) \\ \text{rotations: } C^{1/2}(x, y, z) &= (-x, -y, z) \\ \text{inversions: } P(x, y, z) &= (-x, -y, -z). \end{aligned} \quad (9.2)$$

σ is a reflection (or an inversion) through the $[x, y]$ plane. $C^{1/2}$ is $[x, y]$ -plane, constant z rotation by π about the z -axis (or an inversion thorough the z -axis). P is an inversion (or parity operation) through the point $(0, 0, 0)$. Singly, each operation generates a group of order 2: $D_1 = \{e, \sigma\}$, $C_2 = \{e, C^{1/2}\}$, and $D_1 = \{e, P\}$. Together, they form the dihedral group $D_2 = \{e, \sigma, C^{1/2}, P\}$ of order 4. (continued in example 9.2)

Definition: Coordinate transformations. Consider a map $x' = f(x)$, $x, f(x) \in \mathcal{M}$. An *active* linear coordinate transformation Mx corresponds to a non-singular $[d \times d]$ matrix M that maps the vector $x \in \mathcal{M}$ onto another vector $Mx \in \mathcal{M}$. The corresponding *passive* coordinate transformation $f(x) \rightarrow M^{-1}f(x)$ changes the coordinate system with respect to which the vector $f(x) \in \mathcal{M}$ is measured. Together, a passive and active coordinate transformations yield the map in the transformed coordinates:

$$\hat{f}(x) = M^{-1}f(Mx). \quad (9.3)$$

Definition: Matrix representation. Linear action of a discrete group G element g on states $x \in \mathcal{M}$ is given by a finite non-singular $[d \times d]$ matrix g , the *matrix representation* of element $g \in G$. We shall denote by ‘ g ’ both the abstract group element and its matrix representation.

If the coordinate transformation g belongs to a linear non-singular representation of a discrete finite group G , for any element $g \in G$ there exists a number $m \leq |G|$ such that

$$g^m \equiv \underbrace{g \circ g \circ \dots \circ g}_{m \text{ times}} = e \quad \rightarrow \quad |\det g| = 1. \quad (9.4)$$

As the modulus of its determinant is unity, $\det g$ is an m th root of 1.

Example 9.2 Discrete operations on \mathbb{R}^3 . (continued from example 9.1) The matrix representation of reflections, rotations and inversions defined by (9.2) is

$$\sigma = \begin{pmatrix} 1 & 0 & 0 \\ 0 & 1 & 0 \\ 0 & 0 & -1 \end{pmatrix}, \quad C^{1/2} = \begin{pmatrix} -1 & 0 & 0 \\ 0 & -1 & 0 \\ 0 & 0 & 1 \end{pmatrix}, \quad P = \begin{pmatrix} -1 & 0 & 0 \\ 0 & -1 & 0 \\ 0 & 0 & -1 \end{pmatrix}, \quad (9.5)$$

with $\det C^{1/2} = 1$, $\det \sigma = \det P = -1$; that is why we refer to $C^{1/2}$ as a rotation, and σ , P as inversions. (continued in example 9.4)

Definition: Symmetry of a dynamical system. A group G is a *symmetry* of the dynamics if for every solution $f(x) \in \mathcal{M}$ and $g \in G$, $gf(x)$ is also a solution.

Another way to state this: A dynamical system (\mathcal{M}, f) is *invariant* (or *G-equivariant*) under a symmetry group G if the time evolution $f : \mathcal{M} \rightarrow \mathcal{M}$ (a discrete time map f , or the continuous flow f^t map from the d -dimensional manifold \mathcal{M} into itself) commutes with all actions of G ,

$$f(gx) = gf(x), \quad (9.6)$$

or, in the language of physicists: The ‘law of motion’ is invariant, i.e., retains its form in any symmetry-group related coordinate frame (9.3),

$$f(x) = g^{-1}f(gx), \quad (9.7)$$

for any state $x \in \mathcal{M}$ and any finite non-singular $[d \times d]$ matrix representation g of element $g \in G$. Why ‘equivariant?’ A function $h(x)$ is said to be *G-invariant* if $h(x) = h(gx)$ for all $g \in G$. The group actions map the solution $f : \mathcal{M} \rightarrow \mathcal{M}$ into different (but equivalent) solutions $gf(x)$, hence the invariance condition $f(x) = g^{-1}f(gx)$ appropriate to vectors (and, more generally, tensors).

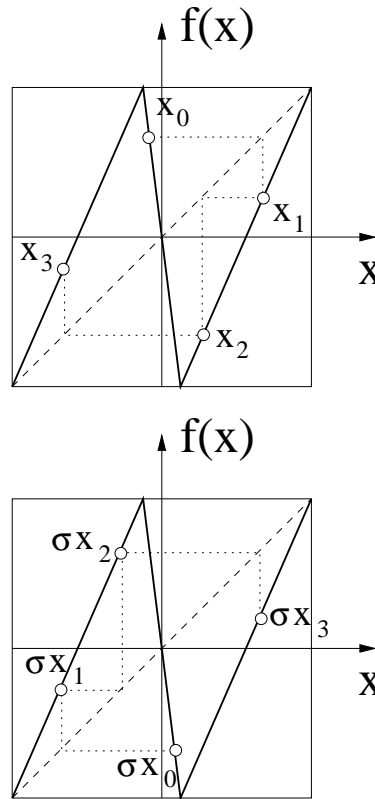


Figure 9.1: The bimodal Ulam sawtooth map with the D_1 symmetry $f(-x) = -f(x)$. If the trajectory $x_0 \rightarrow x_1 \rightarrow x_2 \rightarrow \dots$ is a solution, so is its reflection $\sigma x_0 \rightarrow \sigma x_1 \rightarrow \sigma x_2 \rightarrow \dots$. (continued in figure 9.2)

The full set of such solutions is G -invariant, but the flow that generates them is said to be G -equivariant. It is obvious from the context, but for verbal emphasis applied mathematicians like to distinguish the two cases by *in/equi*-variant. The distinction is helpful in distinguishing the dynamics written in the original, equivariant coordinates from the dynamics rewritten in terms of *invariant* coordinates, see sects. 9.1.2 and 10.4.

exercise 9.7

Example 9.3 A reflection symmetric 1d map. Consider a 1d map f with reflection symmetry $f(-x) = -f(x)$, such as the bimodal ‘sawtooth’ map of figure 9.1, piecewise-linear on the state space $M = [-1, 1]$, a compact 1-dimensional line interval, split into three regions $M = M_L \cup M_C \cup M_R$. Denote the reflection operation by $\sigma x = -x$. The 2-element group $G = \{e, \sigma\}$ goes by many names, such as Z_2 or C_2 . Here we shall refer to it as D_1 , dihedral group generated by a single reflection. The G -equivariance of the map implies that if $\{x_n\}$ is a trajectory, then also $\{\sigma x_n\}$ is a symmetry-equivalent trajectory because $\sigma x_{n+1} = \sigma f(x_n) = f(\sigma x_n)$ (continued in example 9.7)

Example 9.4 Equivariance of the Lorenz flow. (continued from example 9.2) The vector field in Lorenz equations (2.12) is equivariant under the action of cyclic group $C_2 = \{e, C^{1/2}\}$ acting on \mathbb{R}^3 by a π rotation about the z axis,

$$C^{1/2}(x, y, z) = (-x, -y, z).$$

(continued in example 9.10)

Example 9.5 Discrete symmetries of the plane Couette flow. The plane Couette flow is a fluid flow bounded by two countermoving planes, in a cell periodic in streamwise and spanwise directions. The Navier-Stokes equations for the plane Couette flow have two discrete symmetries: rotation by π in the (streamwise,spanwise) plane, and rotation by π in the (streamwise,wall-normal) plane. That is why there are some equilibria (as opposed to relative equilibria) and some periodic orbit solutions. They belong to discrete symmetry subspaces. (continued in example 10.4)

9.1.1 Subgroups, orbits, subspaces

A solution tends to exhibit less symmetry than the dynamical equations of motion. The symmetry of a solution is thus a subgroup of the symmetry group of dynamics. This section makes this statement precise by setting up the group-theoretic notions needed in what follows. The reader might prefer to skip to sect.9.2, backtrack as needed.

Definition: Subgroup, coset. Let $H = \{e, b_2, b_3, \dots, b_h\} \subseteq G$ be a subgroup of order $h = |H|$. The set of h elements $\{c, cb_2, cb_3, \dots, cb_h\}$, $c \in G$ but not in H , is called left *coset* cH . For a given subgroup H the group elements are partitioned into H and $m - 1$ cosets, where $m = |G|/|H|$. The cosets cannot be subgroups, since they do not include the identity element.

Definition: Class. An element $b \in G$ is *conjugate* to a if $b = c a c^{-1}$ where c is some other group element. If b and c are both conjugate to a , they are conjugate to each other. Application of all conjugations separates the set of group elements into mutually not-conjugate subsets called *classes*, *types* or *conjugacy classes*. The identity e is always in the class $\{e\}$ of its own. This is the only class which is a subgroup, all other classes lack the identity element.

exercise 9.3

exercise 9.5

Physical importance of classes is clear from (9.7), the way coordinate transformations act on mappings: action of elements of a class (say reflections, or rotations) is equivalent up to a redefinition of the coordinate frame.

Definition: Invariant subgroup. A subgroup $H \subseteq G$ is an *invariant* subgroup or *normal divisor* if it consists of complete classes. Class is complete if no conjugation takes an element of the class out of H .

H divides G into H and $m - 1$ cosets, each of order $|H|$. Think of action of H within each coset as identifying its $|H|$ elements as equivalent. This leads to the notion of G/H as the *factor group* or *quotient group* G/H of G , with respect to the *normal divisor* (or invariant subgroup) H . Its order is $m = |G|/|H|$, and its multiplication table can be worked out from the G multiplication table class by class, with the subgroup H playing the role of identity. G/H is *homeomorphic* to G , with $|H|$ elements in a class of G represented by a single element in G/H .

So far we have discussed the structure of a group as an abstract entity. Now we switch gears and describe the action of the group on the state space of a dynamical system of interest. This is the key step; if a set of solutions is equivalent by symmetry (a circle, let's say), we would like to represent it by a single solution (cut the circle at a point, or rewrite the dynamics in an 'reduced state space,' where the circle of solutions is represented by a single point).

Definition: Orbit. The subset $\mathcal{M}_{x_0} \subset \mathcal{M}$ traversed by the infinite-time trajectory of a given point x_0 is called the *orbit* (or a *solution*) $x(t) = f^t(x_{Init})$. An orbit is a *dynamically invariant* notion: it refers to the set of all states that can be reached in time from x_0 , thus as a set it is invariant under time evolution. The full state space \mathcal{M} is foliated (stratified) into a union of such orbits. We label a generic orbit \mathcal{M}_{x_0} by any point belonging to it, $x_0 = x(0)$ for example.

A generic orbit might be ergodic, unstable and essentially uncontrollable. The ChaosBook strategy is to populate the state space by a hierarchy of orbits which are *compact invariant sets* (equilibria, periodic orbits, invariant tori, ...), each computable in a finite time. They are a set of zero Lebesgue measure, but dense on the non-wandering set, and are to a generic orbit what fractions are to normal numbers on the unit interval. Orbits which are compact invariant sets we label by whatever alphabet we find convenient in a given context: point $EQ = x_{EQ} = \mathcal{M}_{EQ}$ for an equilibrium, 1-dimensional loop $p = \mathcal{M}_p$ for a prime periodic orbit p , etc. (note also discussion on page 190, and the distinction between trajectory and orbit made in sect. 2.1; a trajectory is a finite-time segment of an orbit).

Definition: Group orbit. The set of points gx generated by all actions of the group G on the state space point x is called the *group orbit* or *G-orbit* \mathcal{M}_x . If G is a symmetry, intrinsic properties of an equilibrium (such as stability eigenvalues) or a cycle p (period, Floquet multipliers) evaluated anywhere along its G -orbit are the same.

A symmetry thus reduces the number of inequivalent solutions \mathcal{M}_{x_0} . So we also need to describe the symmetry of a *solution*, as opposed to (9.7), the symmetry of the *system*. We start by defining the notions of *reduced state space*, of *isotropy* of a state space point, and of *stabilizer* of an orbit.

Definition: Reduced state space. The action of group G partitions the state space \mathcal{M} into a union of group orbits. This set of group orbits, denoted \mathcal{M}/G , has many names: *reduced state space*, *quotient space* or any of the names listed on page 181.

Reduction of the dynamical state space is discussed in sect. 9.4 for discrete symmetries, and in sect. 10.4 for continuous symmetries.

Definition: Isotropy subgroup. The maximal set of group actions which maps a state space point x into itself,

$$G_x = \{g \in G : gx = x\}, \quad (9.8)$$

is called the *isotropy group* or *little group* of x .

We also need a notion of *set-wise* invariance, as opposed to the *point-wise* invariance under G_x .

exercise 9.2

Definition: Stabilizer. We shall sometimes refer to the subset of nontrivial group actions $G_p \subseteq G$ on state space points within a compact set \mathcal{M}_p , which leave no point fixed but leave the set invariant, as the *stabilizer* G_p of \mathcal{M}_p ,

$$G_p = \{g \in G_p : gx \in \mathcal{M}_p, gx \neq x \text{ for } g \neq e\}, \quad (9.9)$$

and reserve the notion of ‘isotropy’ of a set \mathcal{M}_p for the subgroup G_p that leaves each point in it fixed.

Saying that G_p is the symmetry of the solution p , or that the orbit \mathcal{M}_p is ‘ G_p -invariant,’ accomplishes as much without confusing you with all these names (see remark 9.1). In what follows we shall speak freely and say things like “the symmetry of the periodic orbit p is $C_2 = \{e, R\}$,” rather than bandy about ‘stabilizers’ and such.

The splitting of a group G into an stabilizer G_p and $m - 1$ cosets cG_p relates an orbit \mathcal{M}_p to $m - 1$ other distinct orbits $c\mathcal{M}_p$. All of them have equivalent stabilizers, or, more precisely, the points on the same group orbit have *conjugate stabilizers*:

exercise 9.4

$$G_{c_p} = c G_p c^{-1}. \quad (9.10)$$

If G_p is the stabilizer of orbit \mathcal{M}_p , elements of the coset space $g \in G/G_p$ generate the $m_p - 1$ distinct copies of \mathcal{M}_p , so for discrete groups the multiplicity of orbit p is $m_p = |G|/|G_p|$.

Definition: Fixed-point subspace \mathcal{M}_H of a subgroup or a ‘centralizer’ $H \subset G$, G a symmetry of dynamics, is the set of all state space points left *H-fixed*, *point-wise* invariant under subgroup action

$$\mathcal{M}_H = \text{Fix}(H) = \{x \in \mathcal{M} : hx = x \text{ for all } h \in H\}. \quad (9.11)$$

Points in state space subspace \mathcal{M}_G which are fixed points of the full group action are called *invariant points*,

$$\mathcal{M}_G = \text{Fix}(G) = \{x \in \mathcal{M} : gx = x \text{ for all } g \in G\}. \quad (9.12)$$

Definition: Flow invariant subspace. A typical point in \mathcal{M}_H moves with time, but, due to equivariance (9.6), its trajectory $x(t) = f^t(x)$ remains within $f(\mathcal{M}_H) \subseteq \mathcal{M}_H$ for all times,

$$hf^t(x) = f^t(hx) = f^t(x), \quad h \in H, \quad (9.13)$$

i.e., belong to a *flow invariant subspace*. This suggests a systematic approach to seeking compact invariant solutions. The larger the symmetry subgroup, the smaller \mathcal{M}_H , easing the numerical searches, so start with the largest subgroups H first.

We can often decompose the state space into smaller subspaces, with group acting within each ‘chunk’ separately:

Definition: Invariant subspace. $\mathcal{M}_\alpha \subset \mathcal{M}$ is an *invariant* subspace if

$$\{ \mathcal{M}_\alpha : gx \in \mathcal{M}_\alpha \text{ for all } g \in G \text{ and } x \in \mathcal{M}_\alpha \}. \quad (9.14)$$

$\{0\}$ and \mathcal{M} are always invariant subspaces. So is any $\text{Fix}(H)$ which is point-wise invariant under action of G .

Definition: Irreducible subspace. A space \mathcal{M}_α whose only invariant subspaces are $\{0\}$ and \mathcal{M}_α is called *irreducible*.

9.1.2 Invariant bases

Physical laws should have the same form in symmetry-equivalent coordinate frames, so they are often formulated in terms of functions (Hamiltonians, Lagrangians, ...) invariant under a given set of symmetries.

Example 9.6 Polynomials invariant under discrete operations on \mathbb{R}^3 . (continued from example 9.1) σ is a reflection through the $[x, y]$ plane. Any $\{e, \sigma\}$ -invariant function can be expressed in the polynomial basis $\{u_1, u_2, u_3\} = \{x, y, z^2\}$.

$C^{1/2}$ is a $[x, y]$ -plane rotation by π about the z -axis. Any $\{e, C^{1/2}\}$ -invariant function can be expressed in the polynomial basis $\{u_1, u_2, u_3, u_4\} = \{x^2, xy, y^2, z\}$, with one syzygy between the basis polynomials, $(x^2)(y^2) - (xy)^2 = 0$.

P is an inversion through the point $(0, 0, 0)$. Any $\{e, P\}$ -invariant function can be expressed in the polynomial basis $\{u_1, \dots, u_6\} = \{x^2, y^2, z^2, xy, xz, yz\}$, with three syzygies between the basis polynomials, $(x^2)(y^2) - (xy)^2 = 0$, and its 2 permutations.

For the D_2 dihedral group $G = \{e, \sigma, C^{1/2}, P\}$ the G -invariant polynomial basis is $\{u_1, u_2, u_3, u_4\} = \{x^2, y^2, z^2, xy\}$, with one syzygy, $(x^2)(y^2) - (xy)^2 = 0$. (continued in example 10.13)

The key result of the representation theory of invariant functions is:

Hilbert-Weyl theorem. For a compact group G there exists a finite G -invariant homogenous polynomial basis $\{u_1, u_2, \dots, u_m\}$, $m \geq d$, such that any G -invariant polynomial can be written as a multinomial

$$h(x) = p(u_1(x), u_2(x), \dots, u_m(x)), \quad x \in \mathcal{M}. \quad (9.15)$$

These polynomials are linearly independent, but can be functionally dependent through nonlinear relations called *syzygies*.

In practice, explicit construction of G -invariant basis can be a laborious undertaking, and we will not take this path except for a few simple low-dimensional cases, such as the 5-dimensional example of sect. 10.5. We prefer to apply the symmetry to the system as given, rather than undertake a series of nonlinear coordinate transformations that the theorem suggests. (What ‘compact’ in the above refers to will become clearer after we have discussed continuous symmetries. For now, it suffices to know that any finite discrete group is ‘compact’.)

exercise 9.1

9.2 Symmetries of solutions

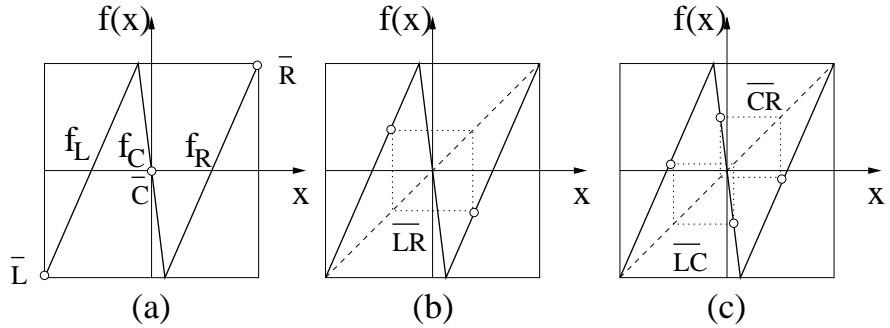
The solutions of an equivariant system can satisfy all of the system’s symmetries, a proper subgroup of them, or have no symmetry at all. For a generic ergodic orbit $f^t(x)$ the trajectory and any of its images under action of $g \in G$ are distinct with probability one, $f^t(x) \cap g f^{t'}(x) = \emptyset$ for all t, t' . For example, a typical turbulent trajectory of plane Couette flow has no symmetry beyond the identity, so its symmetry group is the trivial $\{e\}$. For compact invariant sets, such as fixed points and periodic orbits the situation is very different. For example, the symmetry of the laminar solution of the plane Couette flow is the full symmetry of its Navier-Stokes equations. In between we find solutions whose symmetries are subgroups of the full symmetry of the defining equations.

The key concept in the classification of dynamical orbits is the concept of their symmetry (*isotropy* or *stabilizer*). We note three types of solutions: (i) fully asymmetric a , (ii) G_p set-wise invariant cycles s built by repeats of relative cycle segments \tilde{s} , and (iii) isotropy subgroup $G_E Q$ -invariant equilibria or point-wise G_p -fixed cycles b .

Definition: Asymmetric orbits. An equilibrium or periodic orbit is not symmetric if $\{x_a\} \cap \{g x_a\} = \emptyset$ for any $g \in G$, where $\{x_a\}$ is the set of periodic points belonging to the cycle a . Thus $g \in G$ generate $|G|$ distinct orbits with the same number of points and the same stability properties.

A string of unmotivated definitions (no less than an unmotivated definition of strings) has a way of making trite mysterious, so let’s switch gears again: develop a feeling for why they are needed by first working out the simplest, 1-dimensional example with a single reflection symmetry.

Figure 9.2: The D_1 -equivariant bimodal sawtooth map of figure 9.1 has three types of periodic orbits: (a) D_1 -fixed fixed point \bar{C} , asymmetric fixed points pair $\{\bar{L}, \bar{R}\}$. (b) D_1 -symmetric (setwise invariant) 2-cycle \bar{LR} . (c) Asymmetric 2-cycles pair $\{\bar{LC}, \bar{CR}\}$. (continued in figure 9.8) (Y. Lan)



Example 9.7 Group D_1 - a reflection symmetric 1d map: Consider the bimodal ‘sawtooth’ map of example 9.3, with the state space $M = [-1, 1]$ split into three regions $M = \{M_L, M_C, M_R\}$ which we label with a 3-letter alphabet L (eft), C (enter), and R (ight). The symbolic dynamics is complete ternary dynamics, with any sequence of letters $\mathcal{A} = \{L, C, R\}$ corresponding to an admissible trajectory (‘complete’ means no additional grammar rules required, see example 11.6 below). The D_1 -equivariance of the map, $D_1 = \{e, \sigma\}$, implies that if $\{x_n\}$ is a trajectory, so is $\{\sigma x_n\}$.

Asymmetric cycles. σ maps a cycle a into the reflected cycle σa , with the same period and the same stability properties, see figure 9.2 (c).

Definition: G_p -symmetric cycles. A cycle p is G_p -symmetric (set-wise symmetric, self-dual) if the action of elements of G_p on the set of periodic points \mathcal{M}_p reproduces the set. The set of group elements with this property form the stabilizer G_p of the cycle s . $g \in G_p$ acts as a shift in time, mapping the periodic point $x \in \mathcal{M}_p$ into $f^{T_p/|G_p|}(x)$.

Example 9.8 D_1 -symmetric cycles: For D_1 the period of a set-wise symmetric cycle is even ($n_s = 2n_{\bar{s}}$), and the mirror image of the x_s periodic point is reached by traversing the relative periodic orbit segment \bar{s} of length $n_{\bar{s}}$, $f^{n_{\bar{s}}}(x_s) = \sigma x_s$, see figure 9.2 (b).

Definition: G_p -fixed orbits: An equilibrium x_q or a compact solution p is point-wise or G_p -fixed if it lies in the invariant points subspace $\text{Fix}(G_p)$, $gx_q = x_q$ for all $g \in G_p$. A solution that is G -invariant under all group G operations has multiplicity 1. Stability of such solutions will have to be examined with care, as they lie on the boundaries of domains related by the action of the symmetry group.

Example 9.9 Group D_1 -invariant cycles: In the example at hand there is only one G -invariant (point-wise invariant) orbit, the fixed point \bar{C} at the origin, see figure 9.2 (a). We shall continue analysis of this system in example 9.13, and work out the symbolic dynamics of such reflection symmetric systems in example 12.5.

As reflection symmetry is the only discrete symmetry that a map of the interval can have, this example completes the group-theoretic analysis of 1-dimensional maps. Consider next a 3-dimensional flow with a symmetry.

exercise 9.7
 exercise 9.8
 exercise 9.9

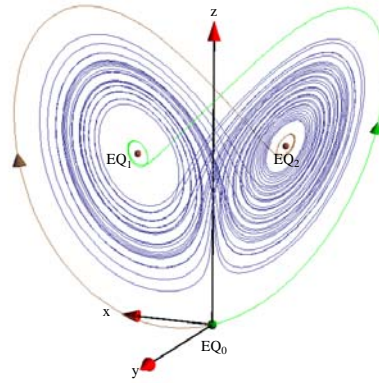


Figure 9.3: Lorenz attractor of figure 3.7, the full state space coordinates $[x, y, z]$, with the unstable manifold orbits $W^u(EQ_0)$. (Green) is a continuation of the unstable $e^{(1)}$ of EQ_0 , and (brown) is its π -rotated symmetric partner. Compare with figure 9.4. (E. Siminos)

Example 9.10 Desymmetrization of Lorenz flow: (continuation of example 9.4) Lorenz equation (2.12) is invariant under the action of order-2 group $C_2 = \{e, C^{1/2}\}$, where $C^{1/2}$ is $[x, y]$ -plane, constant z half-cycle rotation by π about the z -axis:

$$(x, y, z) \rightarrow C^{1/2}(x, y, z) = (-x, -y, z). \quad (9.16)$$

$(C^{1/2})^2 = 1$ condition decomposes the state space into two linearly irreducible subspaces $\mathcal{M} = \mathcal{M}^+ \oplus \mathcal{M}^-$, the z -axis \mathcal{M}^+ and the $[x, y]$ plane \mathcal{M}^- , with projection operators onto the two subspaces given by (see sect. 4.2.2)

$$\mathbf{P}^+ = \frac{1}{2}(1 + C^{1/2}) = \begin{pmatrix} 0 & 0 & 0 \\ 0 & 0 & 0 \\ 0 & 0 & 1 \end{pmatrix}, \quad \mathbf{P}^- = \frac{1}{2}(1 - C^{1/2}) = \begin{pmatrix} 1 & 0 & 0 \\ 0 & 1 & 0 \\ 0 & 0 & 0 \end{pmatrix}. \quad (9.17)$$

As the flow is C_2 -invariant, so is its linearization $\dot{x} = Ax$. Evaluated at EQ_0 , A commutes with $C^{1/2}$, and, as we have already seen in example 4.7, the EQ_0 stability matrix decomposes into $[x, y]$ and z blocks.

The 1-dimensional \mathcal{M}^+ subspace is the fixed-point subspace of C_2 , with the z -axis points left fixed (i.e., point-wise invariant) under the group action

$$\mathcal{M}^+ = \text{Fix}(C_2) = \{x \in \mathcal{M} : g x = x \text{ for } g \in \{e, C^{1/2}\}\}. \quad (9.18)$$

A C_2 -fixed point $x(t)$ in $\text{Fix}(C_2)$ moves with time, but according to (9.13) remains within $x(t) \subseteq \text{Fix}(C_2)$ for all times; the subspace $\mathcal{M}^+ = \text{Fix}(C_2)$ is flow invariant. In case at hand this jargon is a bit of an overkill: clearly for $(x, y, z) = (0, 0, z)$ the full state space Lorenz equation (2.12) is reduced to the exponential contraction to the EQ_0 equilibrium,

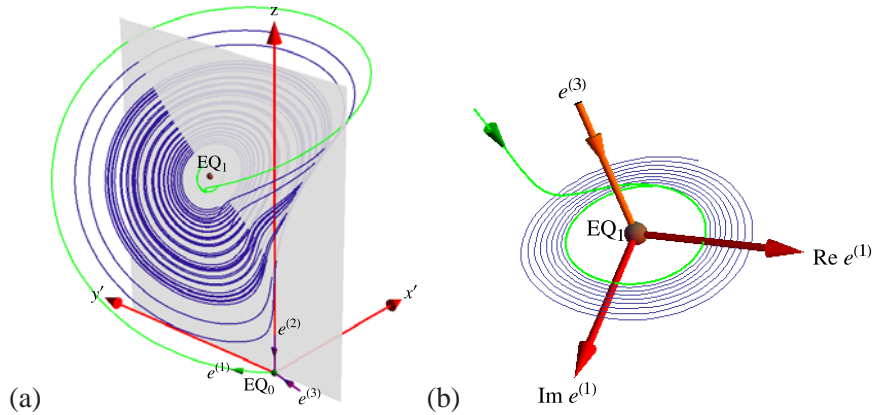
$$\dot{z} = -b z. \quad (9.19)$$

However, for flows in higher-dimensional state spaces the flow-invariant \mathcal{M}_α subspaces can each be high-dimensional, with interesting dynamics of its own. Even in this simple case this subspace plays an important role as a topological obstruction, with the number of windings of a trajectory around it providing a natural symbolic dynamics.

The \mathcal{M}^- subspace is, however, not flow-invariant, as the nonlinear terms $\dot{z} = xy - bz$ in the Lorenz equation (2.12) send all initial conditions within $\mathcal{M}^- = (x(0), y(0), 0)$ into the full, $z(t) \neq 0$ state space $\mathcal{M}/\mathcal{M}^+$. The $C^{1/2}$ symmetry is nevertheless very useful.

By taking as a Poincaré section any $C^{1/2}$ -invariant, infinite-extent, non-self-intersecting surface that contains the z axis, the state space is divided into a half-space fundamental domain $\tilde{\mathcal{M}} = \mathcal{M}/C_2$ and its 180° rotation $C^{1/2}\tilde{\mathcal{M}}$. An example is afforded

Figure 9.4: (a) Lorenz attractor plotted in $[x', y', z]$, the doubled-polar angle coordinates (9.20), with points related by π -rotation in the $[x, y]$ plane identified. Stable eigenvectors of EQ_0 : $e^{(3)}$ and $e^{(2)}$, along the z axis (9.19). Unstable manifold orbit $W^u(EQ_0)$ (green) is a continuation of the unstable $e^{(1)}$ of EQ_0 . (b) Blow-up of the region near EQ_1 : The unstable eigenplane of EQ_1 defined by $\text{Re } e^{(2)}$ and $\text{Im } e^{(2)}$, the stable eigenvector $e^{(3)}$. The descent of the EQ_0 unstable manifold (green) defines the innermost edge of the strange attractor. As it is clear from (a), it also defines its outermost edge. (E. Siminos)



by the \mathcal{P} plane section of the Lorenz flow in figure 3.7. Take the fundamental domain $\tilde{\mathcal{M}}$ to be the half-space between the viewer and \mathcal{P} . Then the full Lorenz flow is captured by re-injecting back into $\tilde{\mathcal{M}}$ any trajectory that exits it, by a rotation of π around the z axis.

As any such $C^{1/2}$ -invariant section does the job, a choice of a ‘fundamental domain’ is here largely matter of taste. For purposes of visualization it is convenient to make the double-cover nature of the full state space by $\tilde{\mathcal{M}}$ explicit, through any state space redefinition that maps a pair of points related by symmetry into a single point. In case at hand, this can be easily accomplished by expressing (x, y) in polar coordinates $(x, y) = (r \cos \theta, r \sin \theta)$, and then plotting the flow in the ‘doubled-polar angle representation.’

$$(x', y') = (r \cos 2\theta, r \sin 2\theta) = ((x^2 - y^2)/r, 2xy/r), \tag{9.20}$$

as in figure 9.4(a). In contrast to the original G -equivariant coordinates $[x, y, z]$, the Lorenz flow expressed in the new coordinates $[x', y', z]$ is G -invariant, see example 9.6. In this representation the $\tilde{\mathcal{M}} = \mathcal{M}/C_2$ fundamental domain flow is a smooth, continuous flow, with (any choice of) the fundamental domain stretched out to seamlessly cover the entire $[x', y']$ plane. (continued in example 11.4)

(E. Siminos and J. Halcrow)

Note: nonlinear coordinate transformations such as the doubled-polar angle representation (9.20) are *not* required to implement the symmetry quotienting \mathcal{M}/G . Here they are deployed only as a visualization aid that might help the reader disentangle 2-dimensional projections of higher-dimensional flows. All numerical calculations can still be carried in the initial, full state space formulation of a flow, with symmetry-related points identified by *linear* symmetry transformations.

The next example is a non-Abelian symmetry group, with elements that do not commute, illustrated by the 3-disk game of pinball, example 9.12 and example 9.14.



in depth:
appendix H, p. 803

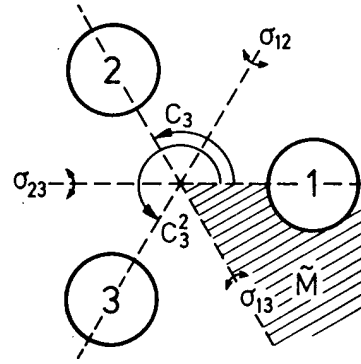


Figure 9.5: The symmetries of three disks on an equilateral triangle. The fundamental domain is indicated by the shaded wedge.

9.3 Relative periodic orbits



We show that a symmetry reduces computation of periodic orbits to repeats of shorter, ‘relative periodic orbit’ segments.

Invariance of a flow under a symmetry means that the group action image of a cycle is again a cycle, with the same period and stability. The new orbit may be topologically distinct (in which case it contributes to the multiplicity of the cycle) or it may be the same cycle.

A cycle p is G_p -symmetric under symmetry operation $g \in G_p$ if the operation acts on it as a shift in time, advancing a cycle point to a cycle point on the symmetry related segment. The cycle p can thus be subdivided into m_p repeats of a *relative periodic orbit segment*, ‘prime’ in the sense that the full state space cycle is built from its repeats. Thus in presence of a symmetry the notion of a periodic orbit is replaced by the notion of the shortest segment of the full state space cycle which tiles the cycle under the action of the group. In what follows we refer to this segment as a *relative periodic orbit segment* (in the literature sometime referred to as a *short periodic orbit*).

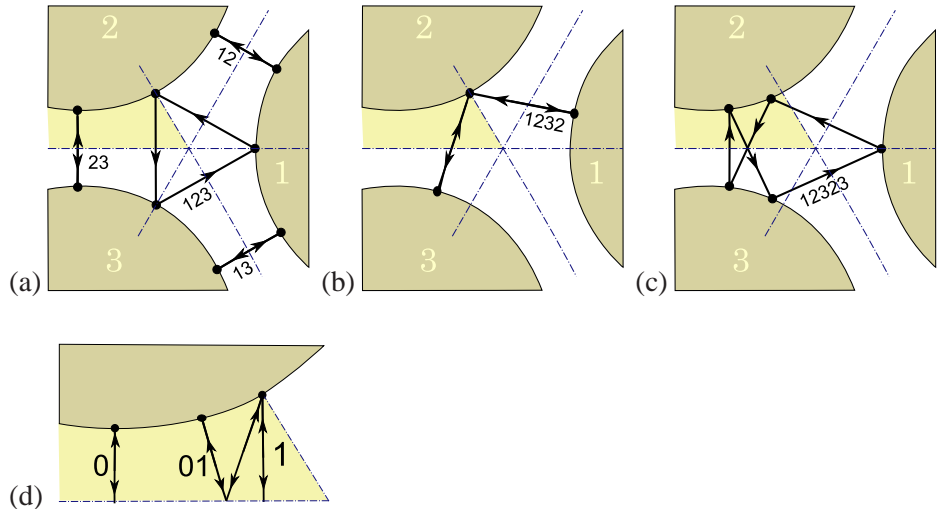
Relative periodic orbits (or *equivariant periodic orbits*) are orbits $x(t)$ in state space \mathcal{M} which exactly recur

$$x(t) = g x(t + T) \tag{9.21}$$

for the shortest fixed *relative period* T and a fixed group action $g \in G_p$. This group action is referred to as a ‘phase,’ or a ‘shift.’ For a discrete group by (9.4) $g^m = e$ for some finite m , so the corresponding full state space orbit is periodic with period mT .

The period of the full orbit is given by the $m_p \times$ (period of the relative periodic orbit), $n_{\bar{p}} = n_p / |G_p|$, and the i th Floquet multiplier $\Lambda_{\bar{p},i}$ is given by $\Lambda_{\bar{p},i}^{m_p}$ of the relative periodic orbit. The elements of the quotient space $b \in G/G_p$ generate the copies bp , so the multiplicity of the full state space cycle p is $m_p = |G|/|G_p|$.

Figure 9.6: The 3-disk pinball cycles: (a) $\overline{12}$, $\overline{13}$, $\overline{23}$, $\overline{123}$; the clockwise $\overline{132}$ not drawn. (b) Cycle $\overline{1232}$; the symmetry related $\overline{1213}$ and $\overline{1323}$ not drawn. (c) $\overline{12323}$; $\overline{12123}$, $\overline{12132}$, $\overline{12313}$, $\overline{13131}$ and $\overline{13232}$ not drawn. (d) The fundamental domain, i.e., the $1/6$ th wedge indicated in (a), consisting of a section of a disk, two segments of symmetry axes acting as straight mirror walls, and the escape gap to the left. The above 14 full-space cycles restricted to the fundamental domain and re-coded in binary reduce to the two fixed points $\overline{0}$, $\overline{1}$, 2-cycle $\overline{10}$, and 5-cycle $\overline{00111}$ (not drawn). See figure 9.9 for the $\overline{001}$ cycle.



Example 9.11 Relative periodic orbits of Lorenz flow: (continuation of example 9.10) The relation between the full state space periodic orbits, and the fundamental domain (9.20) reduced relative periodic orbits of the Lorenz flow: an asymmetric full state space cycle pair p, Rp maps into a single cycle \tilde{p} in the fundamental domain, and any self-dual cycle $p = Rp = \tilde{p}R\tilde{p}$ is a repeat of a relative periodic orbit \tilde{p} .

Next illustration of these ideas brings in the noncommutative group structure: the example of sect. 1.3, symmetries of a 3-disk game of pinball.

exercise 9.5

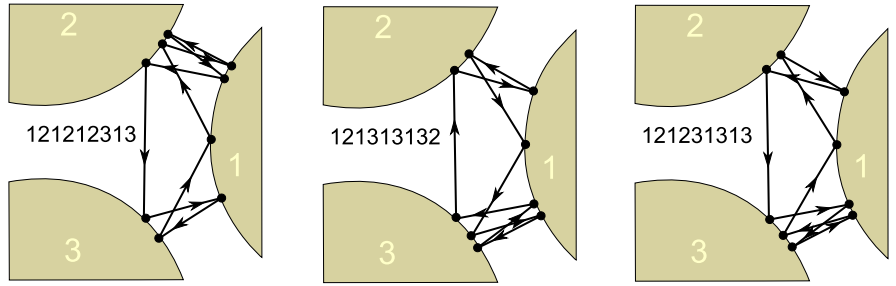
Example 9.12 $C_{3v} = D_3$ invariance - 3-disk game of pinball: As the three disks in figure 9.5 are equidistantly spaced, our game of pinball has a sixfold symmetry. The symmetry group of relabeling the 3 disks is the permutation group S_3 ; however, it is more instructive to think of this group geometrically, as C_{3v} (dihedral group D_3), the group of order $|G| = 6$ consisting of the identity element e , three reflections across axes $\{\sigma_{12}, \sigma_{23}, \sigma_{13}\}$, and two rotations by $\pm 2\pi/3$ and $4\pi/3$ denoted $\{C^{1/3}, C^{2/3}\}$. Applying an element (identity, rotation by $\pm 2\pi/3$, or one of the three possible reflections) of this symmetry group to a trajectory yields another trajectory. For instance, σ_{23} , the flip across the symmetry axis going through disk 1 interchanges the symbols 2 and 3; it maps the cycle $\overline{12123}$ into $\overline{13132}$, figure 9.6 (c). Cycles $\overline{12}$, $\overline{23}$, and $\overline{13}$ in figure 9.6 (a) are related to each other by rotation by $\pm 2\pi/3$, or, equivalently, by a relabeling of the disks.

The nontrivial subgroups of D_3 are $D_1 = \{e, \sigma\}$, consisting of the identity and any one of the reflections, of order 2, and $C_3 = \{e, C^{1/3}, C^{2/3}\}$, of order 3, so possible cycle multiplicities are $|G|/|G_p| = 1, 2, 3$ or 6. Only the fixed point at the origin has full symmetry $G_p = G$. Such equilibria exist for smooth potentials, but not for the 3-disk billiard.

The C_3 subgroup $G_p = \{e, C^{1/3}, C^{2/3}\}$ invariance is exemplified by 2 cycles $\overline{123}$ and $\overline{132}$ which are invariant under rotations by $2\pi/3$ and $4\pi/3$, but are mapped into each other by any reflection, figure 9.7 (a), and have multiplicity $|G|/|G_p| = 2$.

The C_v type of a subgroup is exemplified by the invariances of $\tilde{p} = \overline{1213}$. This cycle is invariant under reflection $\sigma_{23}\{\overline{1213}\} = \overline{1312} = \overline{1213}$, so the invariant subgroup is $G_{\tilde{p}} = \{e, \sigma_{23}\}$, with multiplicity is $m_{\tilde{p}} = |G|/|G_p| = 3$; the cycles in this class, $\overline{1213}$, $\overline{1232}$ and $\overline{1323}$, are related by $2\pi/3$ rotations, figure 9.7 (b).

Figure 9.7: Cycle $\overline{121212313}$ has multiplicity 6; shown here is $\overline{121313132} = \sigma_{23}\overline{121212313}$. However, $\overline{121231313}$ which has the same stability and period is related to $\overline{121313132}$ by time reversal, but not by any C_{3v} symmetry.



A cycle of no symmetry, such as $\overline{12123}$, has $G_p = \{e\}$ and contributes in all six copies (the remaining cycles in the class are $\overline{12132}$, $\overline{12313}$, $\overline{12323}$, $\overline{13132}$ and $\overline{13232}$), figure 9.7 (c).

Besides the above spatial symmetries, for Hamiltonian systems cycles may be related by time reversal symmetry. An example are the cycles $\overline{121212313}$ and $\overline{313212121} = \overline{121213132}$ which have the same periods and stabilities, but are related by no space symmetry, see figure 9.7. (continued in example 9.14)

9.4 Dynamics reduced to fundamental domain

I submit my total lack of apprehension of fundamental concepts.

—John F. Gibson



So far we have used symmetry to effect a reduction in the number of independent cycles, by separating them into equivalence classes. The next step achieves much more: it replaces each class by a single (typically shorter) prime cycle segment.

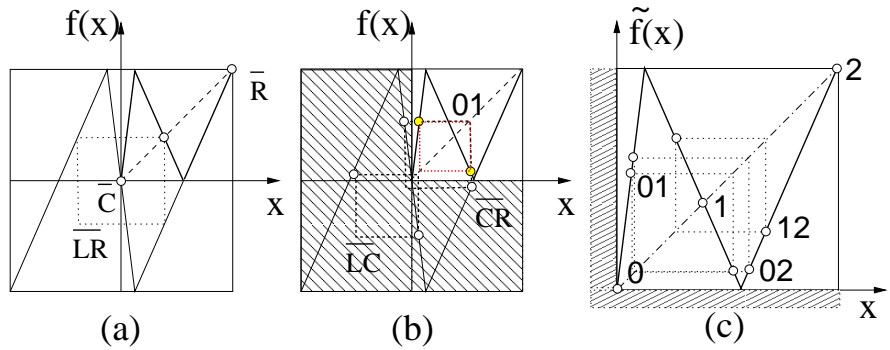
1. Discrete symmetry tessellates the state space into copies of a fundamental domain, and thus induces a natural partition of state space. The state space is completely tiled by a *fundamental domain* and its symmetry images: If the dynamics is invariant under a discrete symmetry, the state space \mathcal{M} can be completely tiled by the fundamental domain $\tilde{\mathcal{M}}$ and its images $\tilde{\mathcal{M}}_a = a\tilde{\mathcal{M}}$, $\tilde{\mathcal{M}}_b = b\tilde{\mathcal{M}}$, ... under the action of the symmetry group $G = \{e, a, b, \dots\}$,

$$\mathcal{M} = \tilde{\mathcal{M}} \cup \tilde{\mathcal{M}}_a \cup \tilde{\mathcal{M}}_b \dots \cup \tilde{\mathcal{M}}_{|G|} = \tilde{\mathcal{M}} \cup a\tilde{\mathcal{M}} \cup b\tilde{\mathcal{M}} \dots \quad (9.22)$$

2. Discrete symmetries can be used to restrict all computations to a *fundamental domain* $\tilde{\mathcal{M}} = \mathcal{M}/G$, i.e., the reduced state space quotient of the full state space \mathcal{M} by the group actions of G .

Now we can use the invariance condition (9.6) to move the starting point x into the fundamental domain $x = a\tilde{x}$, and then use the relation $a^{-1}b = h^{-1}$ to also relate the endpoint $y \in \tilde{\mathcal{M}}_b$ to its image in the fundamental domain $\tilde{\mathcal{M}}$. While the global trajectory runs over the full space \mathcal{M} , the restricted trajectory is brought back into the fundamental domain $\tilde{\mathcal{M}}$ any

Figure 9.8: The bimodal Ulam sawtooth map of figure 9.2 with the D_1 symmetry $f(-x) = -f(x)$ restricted to the fundamental domain. $f(x)$ is indicated by the thin line, and fundamental domain map $\tilde{f}(\tilde{x})$ by the thick line. (a) Boundary fixed point \bar{C} is the fixed point $\bar{0}$. The asymmetric fixed point pair $\{\bar{L}, \bar{R}\}$ is reduced to the fixed point $\bar{2}$, and the full state space symmetric 2-cycle \bar{LR} is reduced to the fixed point $\bar{1}$. (b) The asymmetric 2-cycle pair $\{\bar{LC}, \bar{CR}\}$ is reduced to 2-cycle 01 . (c) All fundamental domain fixed points and 2-cycles. (Y. Lan)



time it exits into an adjoining tile; the two trajectories are related by the symmetry operation h which maps the global endpoint into its fundamental domain image.

3. Cycle multiplicities induced by the symmetry are removed by *desymmetrization*, reduction of the full dynamics to the dynamics on a *fundamental domain*. Each symmetry-related set of global cycles p corresponds to precisely one fundamental domain (or relative) cycle \tilde{p} . Conversely, each fundamental domain cycle \tilde{p} traces out a segment of the global cycle p , with the end point of the cycle \tilde{p} mapped into the irreducible segment of p with the group element $h_{\tilde{p}}$. The relative periodic orbits in the full space, folded back into the fundamental domain, are periodic orbits.
4. The group elements $G = \{e, g_2, \dots, g_{|G|}\}$ which map the fundamental domain $\tilde{\mathcal{M}}$ into its copies $g\tilde{\mathcal{M}}$, serve also as letters of a symbolic dynamics alphabet.

For a symmetry reduction in presence of continuous symmetries, see sect.10.4.

exercise 9.6

Example 9.13 Group D_1 and reduction to the fundamental domain. Consider again the reflection-symmetric bimodal Ulam sawtooth map $f(-x) = -f(x)$ of example 9.7, with symmetry group $D_1 = \{e, \sigma\}$. The state space $\mathcal{M} = [-1, 1]$ can be tiled by half-line $\tilde{\mathcal{M}} = [0, 1]$, and $\sigma\tilde{\mathcal{M}} = [-1, 0]$, its image under a reflection across $x = 0$ point. The dynamics can then be restricted to the fundamental domain $\tilde{x}_k \in \tilde{\mathcal{M}} = [0, 1]$; every time a trajectory leaves this interval, it is mapped back using σ .

In figure 9.8 the fundamental domain map $\tilde{f}(\tilde{x})$ is obtained by reflecting $x < 0$ segments of the global map $f(x)$ into the upper right quadrant. \tilde{f} is also bimodal and piecewise-linear, with $\tilde{\mathcal{M}} = [0, 1]$ split into three regions $\tilde{\mathcal{M}} = \{\tilde{\mathcal{M}}_0, \tilde{\mathcal{M}}_1, \tilde{\mathcal{M}}_2\}$ which we label with a 3-letter alphabet $\tilde{\mathcal{A}} = \{0, 1, 2\}$. The symbolic dynamics is again complete ternary dynamics, with any sequence of letters $\{0, 1, 2\}$ admissible.

However, the interpretation of the ‘desymmetrized’ dynamics is quite different - the multiplicity of every periodic orbit is now 1, and relative periodic segments of the full state space dynamics are all periodic orbits in the fundamental domain. Consider figure 9.8:

In (a) the boundary fixed point \bar{C} is also the fixed point $\bar{0}$. In this case the set of points invariant under group action of D_1 , $\tilde{\mathcal{M}} \cap \sigma\tilde{\mathcal{M}}$, is just this fixed point $x = 0$, the reflection symmetry point.

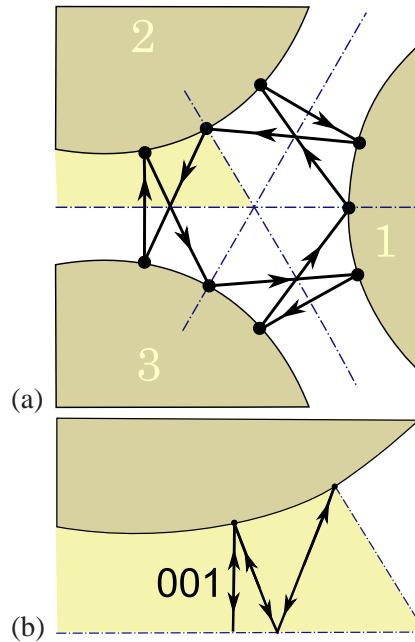


Figure 9.9: (a) The pair of full-space 9-cycles, the counter-clockwise $\overline{121232313}$ and the clockwise $\overline{131323212}$ correspond to (b) one fundamental domain 3-cycle $\overline{001}$.

The asymmetric fixed point pair $\{\overline{L}, \overline{R}\}$ is reduced to the fixed point $\overline{2}$, and the full state space symmetric 2-cycle \overline{LR} is reduced to the fixed point $\overline{1}$. The asymmetric 2-cycle pair $\{\overline{LC}, \overline{CR}\}$ is reduced to the 2-cycle $\overline{01}$. Finally, the symmetric 4-cycle \overline{LCRC} is reduced to the 2-cycle $\overline{02}$. This completes the conversion from the full state space for all fundamental domain fixed points and 2-cycles, figure 9.8 (c).

Example 9.14 3-disk game of pinball in the fundamental domain

If the dynamics is equivariant under interchanges of disks, the absolute disk labels $\epsilon_i = 1, 2, \dots, N$ can be replaced by the symmetry-invariant relative disk \rightarrow disk increments g_i , where g_i is the discrete group element that maps disk $i-1$ into disk i . For 3-disk system g_i is either reflection σ back to initial disk (symbol '0') or $2\pi/3$ rotation by C to the next disk (symbol '1'). An immediate gain arising from symmetry invariant relabeling is that N -disk symbolic dynamics becomes $(N-1)$ -nary, with no restrictions on the admissible sequences.

An irreducible segment corresponds to a periodic orbit in the fundamental domain, a one-sixth slice of the full 3-disk system, with the symmetry axes acting as reflecting mirrors (see figure 9.6(d)). A set of orbits related in the full space by discrete symmetries maps onto a single fundamental domain orbit. The reduction to the fundamental domain desymmetrizes the dynamics and removes all global discrete symmetry-induced degeneracies: rotationally symmetric global orbits (such as the 3-cycles $\overline{123}$ and $\overline{132}$) have multiplicity 2, reflection symmetric ones (such as the 2-cycles $\overline{12}$, $\overline{13}$ and $\overline{23}$) have multiplicity 3, and global orbits with no symmetry are 6-fold degenerate. Table 12.2 lists some of the shortest binary symbols strings, together with the corresponding full 3-disk symbol sequences and orbit symmetries. Some examples of such orbits are shown in figures 9.7 and 9.9. (continued in example 12.7)

Résumé

If a dynamical system (\mathcal{M}, f) has a symmetry G , the symmetry should be deployed to ‘quotient’ the state space to \mathcal{M}/G , i.e., identify all symmetry-equivalent $x \in \mathcal{M}$ on a group orbit. The main result of this chapter can be stated as follows:

In presence of a discrete symmetry G , associated with each full state space cycle p is the group of its symmetries $G_p \subseteq G$ of order $1 \leq |G_p| \leq |G|$, whose elements leave the set \mathcal{M}_p invariant. The elements of G_p act on p as time shifts, tiling it with $|G_p|$ copies of its shortest invariant segment, the relative periodic orbit \tilde{p} . The elements of the coset $b \in G/G_p$ generate $m_p = |G|/|G_p|$ equivalent copies of p .

Once you grasp the relation between the full state space \mathcal{M} and the desymmetrized, G -quotiented reduced state space \mathcal{M}/G , you will find the life as a fundamentalist so much simpler that you will never return to your full state space confused ways of yesteryear. The reduction to the fundamental domain $\tilde{\mathcal{M}} = \mathcal{M}/G$ simplifies symbolic dynamics and eliminates symmetry-induced degeneracies. For the short orbits the labor saving is dramatic. For example, for the 3-disk game of pinball there are 256 periodic points of length 8, but reduction to the fundamental domain non-degenerate prime cycles reduces this number to 30. In the next chapter continuous symmetries will induce relative periodic orbits that never close a periodic orbit, and in the chapter 25 they will tile the infinite periodic state space, and reduce calculation of diffusion constant in an infinite domain to a calculation on a compact torus.

Commentary

Remark 9.1 Literature. We found Tinkham [1] the most enjoyable as a no-nonsense, the user friendliest introduction to the basic concepts. For a summary of the theory of discrete groups see, for example, ref. [2]. Chapter 3 of Rebecca Hoyle [3] is a very student-friendly overview of the group theory a nonlinear dynamicist might need, with exception of the quotienting, reduction of dynamics to a fundamental domain, which is not discussed at all. We found sites such as en.wikipedia.org/wiki/Quotient_group helpful. Curiously, we have not read any of the group theory books that Hoyle recommends as background reading, which just confirms that there are way too many group theory books out there. For example, one that you will not find useful at all is ref. [4]. The reason is presumably that in the 20th century physics (which motivated much of the work on the modern group theory) the focus is on the linear representations used in quantum mechanics, crystallography and quantum field theory. We shall need these techniques in Chapter 21, where we reduce the linear action of evolution operators to irreducible subspaces. However, here we are looking at nonlinear dynamics, and the emphasis is on the symmetries of orbits, their reduced state space sisters, and the isotypic decomposition of their linear stability matrices.

appendix A.2.3

In ChaosBook we focus on chaotic dynamics, and skirt the theory of bifurcations, the landscape between the boredom of regular motions and the thrills of chaos. Chapter 4 of Rebecca Hoyle [3] is a student-friendly introduction to the treatment of bifurcations in presence of symmetries, worked out in full detail and generality in monographs by Golubitsky, Stewart and Schaeffer [5], Golubitsky and Stewart [6] and Chossat and Lauterbach [7]. Term ‘stabilizer’ is used, for example, by Broer *et al.* [8] to refer to a periodic orbit with Z_2 symmetry; they say that the relative or pre-periodic segment is in this case called a ‘short periodic orbit.’ In Efstathiou [9] a subgroup of ‘short periodic orbit’ symmetries is referred to as a ‘nontrivial isotropy group or stabilizer.’ (continued in remark 10.1)

Remark 9.2 Symmetries of the Lorenz equation: (continued from remark 2.3) After having studied example 9.10 you will appreciate why ChaosBook.org starts out with the symmetry-less Rössler flow (2.17), instead of the better known Lorenz flow (2.12). Indeed, getting rid of symmetry was one of Rössler’s motivations. He threw the baby out with the water; for Lorenz flow dimensionalities of stable/unstable manifolds make possible a robust heteroclinic connection absent from Rössler flow, with unstable manifold of an equilibrium flowing into the stable manifold of another equilibrium. How such connections are forced upon us is best grasped by perusing the chapter 13 ‘Heteroclinic tangles’ of the inimitable Abraham and Shaw illustrated classic [10]. Their beautiful hand-drawn sketches elucidate the origin of heteroclinic connections in the Lorenz flow (and its high-dimensional Navier-Stokes relatives) better than any computer simulation. Miranda and Stone [11] were first to quotient the C_2 symmetry and explicitly construct the desymmetrized, ‘proto-Lorenz system,’ by a nonlinear coordinate transformation into the Hilbert-Weyl polynomial basis invariant under the action of the symmetry group [12]. For in-depth discussion of symmetry-reduced (‘images’) and symmetry-extended (‘covers’) topology, symbolic dynamics, periodic orbits, invariant polynomial bases etc., of Lorenz, Rössler and many other low-dimensional systems there is no better reference than the Gilmore and Letellier monograph [13]. They interpret [14] the proto-Lorenz and its ‘double cover’ Lorenz as ‘intensities’ being the squares of ‘amplitudes,’ and call

quotiented flows such as (Lorenz)/ C_2 ‘images.’ Our ‘doubled-polar angle’ visualization figure 11.8 is a proto-Lorenz in disguise; we, however, integrate the flow and construct Poincaré sections and return maps in the original Lorenz $[x, y, z]$ coordinates, without any nonlinear coordinate transformations. The Poincaré return map figure 11.9 is reminiscent in shape both of the one given by Lorenz in his original paper, and the one plotted in a radial coordinate by Gilmore and Letellier. Nevertheless, it is profoundly different: our return maps are from unstable manifold \rightarrow itself, and thus intrinsic and coordinate independent. In this we follow ref. [15]. This construction is necessary for high-dimensional flows in order to avoid problems such as double-valuedness of return map projections on arbitrary 1-dimensional coordinates encountered already in the Rössler example of figure 3.6. More importantly, as we know the embedding of the unstable manifold into the full state space, a periodic point of our return map *is* - regardless of the length of the cycle - the periodic point in the full state space, so no additional Newton searches are needed. In homage to Lorenz, we note that his return map was already symmetry-reduced: as z belongs to the symmetry invariant $\text{Fix}(G)$ subspace, one can replace dynamics in the full space by \dot{z}, \ddot{z}, \dots . That is G -invariant by construction [13].

Remark 9.3 Examples of systems with discrete symmetries. Almost any flow of interest is symmetric in some way or other: the list of examples is endless, we list here a handful that we found interesting. One has a C_2 symmetry in the Lorenz system (remark 2.3), the Ising model, and in the 3-dimensional anisotropic Kepler potential [16, 17, 18], a $D_4 = C_{4v}$ symmetry in quartic oscillators [19, 20], in the pure x^2y^2 potential [21, 22] and in hydrogen in a magnetic field [23], and a $D_2 = C_{2v} = V_4 = C_2 \times C_2$ symmetry in the stadium billiard [24]. A very nice nontrivial desymmetrization is carried out in ref. [25]. An example of a system with $D_3 = C_{3v}$ symmetry is provided by the motion of a particle in the Hénon-Heiles potential [26, 27, 28, 29]

$$V(r, \theta) = \frac{1}{2}r^2 + \frac{1}{3}r^3 \sin(3\theta) .$$

Our 3-disk coding is insufficient for this system because of the existence of elliptic islands and because the three orbits that run along the symmetry axis cannot be labeled in our code. As these orbits run along the boundary of the fundamental domain, they require the special treatment. A partial classification of the 67 possible symmetries of solutions of the plane Couette flow of example 9.5, and their reduction 5 conjugate classes is given in ref. [30].

Exercises

9.1. **Polynomials invariant under discrete operations on \mathbb{R}^3 .** Prove that the $\{e, \sigma\}$, $\{e, C^{1/2}\}$, $\{e, P\}$ and $\{e, \sigma, C^{1/2}, P\}$ -invariant polynomial basis and syzygies are those listed in example 9.6.

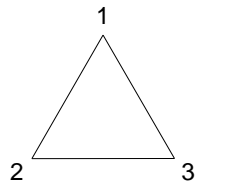
9.2. $G_x \subset G$. Prove that the set G_x as defined in (9.8) is a subgroup of G .

9.3. **Transitivity of conjugation.** Assume that $g_1, g_2, g_3 \in G$ and both g_1 and g_2 are conjugate to g_3 . Prove that g_1 is conjugate to g_2 .

9.4. **Isotropy subgroup of gx .** Prove that for $g \in G$, x and gx have conjugate isotropy subgroups:

$$G_{gx} = g G_x g^{-1}$$

9.5. **D_3 : symmetries of an equilateral triangle.** Consider group $D_3 \cong C_{3v}$, the symmetry group of an equilateral triangle:



- (a) List the group elements and the corresponding geometric operations
- (b) Find the subgroups of the group D_3 .
- (c) Find the classes of D_3 and the number of elements in them, guided by the geometric interpretation of group elements. Verify your answer using the definition of a class.
- (d) List the conjugacy classes of subgroups of D_3 .

9.6. **Reduction of 3-disk symbolic dynamics to binary.** (continued from exercise 1.1)

- (a) Verify that the 3-disk cycles $\{\overline{12}, \overline{13}, \overline{23}\}$, $\{\overline{123}, \overline{132}\}$, $\{\overline{1213} + 2 \text{ perms.}\}$, $\{\overline{121232313} + 5 \text{ perms.}\}$, $\{\overline{121323} + 2 \text{ perms.}\}$, \dots , correspond to the fundamental domain cycles $\overline{0}, \overline{1}, \overline{01}, \overline{001}, \overline{011}, \dots$ respectively.
- (b) Check the reduction for short cycles in table 12.2 by drawing them both in the full 3-disk system and in the fundamental domain, as in figure 9.9.

(c) Optional: Can you see how the group elements listed in table 12.2 relate irreducible segments to the fundamental domain periodic orbits?

(continued in exercise 12.6)

9.7. **C_2 -equivariance of Lorenz system.** Verify that the vector field in Lorenz equations (2.12)

$$\dot{x} = v(x) = \begin{bmatrix} \dot{x} \\ \dot{y} \\ \dot{z} \end{bmatrix} = \begin{bmatrix} \sigma(y - x) \\ \rho x - y - xz \\ xy - bz \end{bmatrix} \quad (9.23)$$

is equivariant under the action of cyclic group $C_2 = \{e, C^{1/2}\}$ acting on \mathbb{R}^3 by a π rotation about the z axis,

$$C^{1/2}(x, y, z) = (-x, -y, z),$$

as claimed in example 9.4. (continued in exercise 9.8)

9.8. **Lorenz system in polar coordinates: group theory.** Use (6.7), (6.8) to rewrite the Lorenz equation (9.23) in polar coordinates (r, θ, z) , where $(x, y) = (r \cos \theta, r \sin \theta)$.

1. Show that in the polar coordinates Lorenz flow takes form

$$\begin{aligned} \dot{r} &= \frac{r}{2} (-\sigma - 1 + (\sigma + \rho - z) \sin 2\theta + (1 - \sigma) \cos 2\theta) \\ \dot{\theta} &= \frac{1}{2} (-\sigma + \rho - z + (\sigma - 1) \sin 2\theta + (\sigma + \rho - z) \cos 2\theta) \\ \dot{z} &= -bz + \frac{r^2}{2} \sin 2\theta. \end{aligned} \quad (9.24)$$

- 2. Argue that the transformation to polar coordinates is invertible almost everywhere. Where does the inverse not exist? What is group-theoretically special about the subspace on which the inverse not exist?
- 3. Show that this is the $(\text{Lorenz})/C_2$ quotient map for the Lorenz flow, i.e., that it identifies points related by the π rotation in the $[x, y]$ plane.
- 4. Rewrite (9.23) in the invariant polynomial basis of example 9.6 and exercise 9.24.
- 5. Show that a periodic orbit of the Lorenz flow in polar representation (9.24) is either a periodic orbit or a relative periodic orbit (9.21) of the Lorenz flow in the (x, y, z) representation.

By going to polar coordinates we have quotiented out the π -rotation $(x, y, z) \rightarrow (-x, -y, z)$ symmetry of the Lorenz equations, and constructed an explicit representation of the desymmetrized Lorenz flow.

9.9. **Proto-Lorenz system.** Here we quotient out the C_2 symmetry by constructing an explicit “intensity” representation of the desymmetrized Lorenz flow, following Miranda and Stone [11].

1. Rewrite the Lorenz equation (2.12) in terms of variables

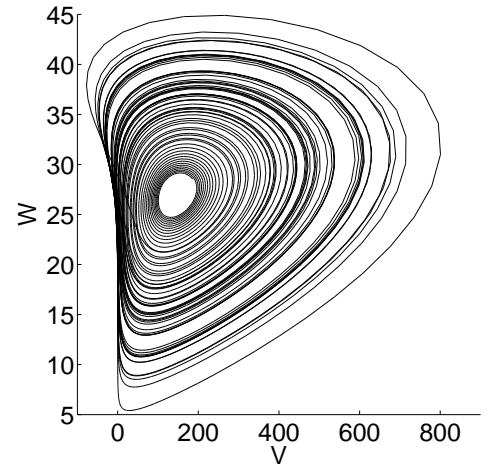
$$(u, v, z) = (x^2 - y^2, 2xy, z), \quad (9.25)$$

show that it takes form

$$\begin{bmatrix} \dot{u} \\ \dot{v} \\ \dot{z} \end{bmatrix} = \begin{bmatrix} -(\sigma + 1)u + (\sigma - r)v + (1 - \sigma)N + vz \\ (r - \sigma)u - (\sigma + 1)v + (r + \sigma)N - uz - uN \\ v/2 - bz \end{bmatrix}$$

$$N = \sqrt{u^2 + v^2}.$$

2. Show that this is the $(\text{Lorenz})/C_2$ quotient map for the Lorenz flow, i.e., that it identifies points related by the π rotation (9.16).
3. Show that (9.25) is invertible. Where does the inverse not exist?
4. Compute the equilibria of proto-Lorenz and their stabilities. Compare with the equilibria of the Lorenz flow.
5. Plot the strange attractor both in the original form (2.12) and in the proto-Lorenz form (9.26)



for the Lorenz parameter values $\sigma = 10, b = 8/3, \rho = 28$. Topologically, does it resemble more the Lorenz, or the Rössler attractor, or neither? (plot by J. Halcrow)

Show that a periodic orbit of the proto-Lorenz is either a periodic orbit or a relative periodic orbit of the Lorenz flow.

- 9.26 Show that if a periodic orbit of the proto-Lorenz is also periodic orbit of the Lorenz flow, their Floquet multipliers are the same. How do the Floquet multipliers of relative periodic orbits of the Lorenz flow relate to the Floquet multipliers of the proto-Lorenz?
- 9 What does the volume contraction formula (4.48) look like now? Interpret.
10. Show that the coordinate change (9.25) is the same as rewriting (9.24) in variables

$$(u, v) = (r^2 \cos 2\theta, r^2 \sin 2\theta),$$
 i.e., squaring a complex number $z = x + iy, z^2 = u + iv$.
11. How is (9.26) related to the invariant polynomial basis of example 9.6 and exercise 9.24?

References

[9.1] M. Tinkham, *Group Theory and Quantum Mechanics* (Dover, New York, 2003).

[9.2] S. G. Johnson, Topics in applied mathematics, MIT course 18.325, 2005.

[9.3] R. Hoyle, *Pattern Formation: An Introduction to Methods* (Cambridge Univ. Press, Cambridge, 2006).

- [9.4] P. Cvitanović, *Group Theory - Birdtracks, Lie's, and Exceptional Magic* (Princeton Univ. Press, Princeton, NJ, 2008), birdtracks.eu.
- [9.5] M. Golubitsky, I. Stewart, and D. G. Schaeffer, *Singularities and Groups in Bifurcation Theory, vol. II* (Springer, New York, 1988).
- [9.6] M. Golubitsky and I. Stewart, *The Symmetry Perspective* (Birkhäuser, Boston, 2002).
- [9.7] P. Chossat and R. Lauterbach, *Methods in Equivariant Bifurcations and Dynamical Systems* (World Scientific, Singapore, 2000).
- [9.8] H. W. Broer, I. Hoveijn, G. A. Lunter, and G. Vegter, *Bifurcations in Hamiltonian Systems: Computing Singularities by Gröbner Bases* (Springer, New York, 2003).
- [9.9] K. Efstathiou, *Metamorphoses of Hamiltonian systems with symmetries* (Springer, New York, 2005).
- [9.10] R. H. Abraham and C. D. Shaw, *Dynamics - The Geometry of Behavior* (Wesley, Reading, MA, 1992).
- [9.11] R. Miranda and E. Stone, The proto-Lorenz system, *Phys. Letters A* **178**, 105 (1993).
- [9.12] D. A. Cox, J. B. Little, and D. O'Shea, *Ideals, Varieties and Algorithms* (Springer, New York, 1996).
- [9.13] R. Gilmore and C. Letellier, *The Symmetry of Chaos* (Oxford Univ. Press, Oxford, 2007).
- [9.14] C. Letellier and R. Gilmore, Covering dynamical systems: Two-fold covers, *Phys. Rev. E* **63**, 016206 (2001).
- [9.15] F. Christiansen, P. Cvitanović, and V. Putkaradze, Spatiotemporal chaos in terms of unstable recurrent patterns, *Nonlinearity* **10**, 55 (1997), [arXiv:chao-dyn/9606016](https://arxiv.org/abs/chao-dyn/9606016).
- [9.16] M. C. Gutzwiller, The quantization of a classically ergodic system, *Physica D* **5**, 183 (1982).
- [9.17] G. Tanner and D. Wintgen, Quantization of chaotic systems, *CHAOS* **2**, 53 (1992).
- [9.18] P. Cvitanović and F. Christiansen, Periodic orbit quantization of the anisotropic Kepler problem, *CHAOS* **2**, 61 (1992).
- [9.19] G. H. B. Eckhardt and E. Pollak, *Phys. Rev. A* **39**, 3776 (1989).
- [9.20] C. C. Martens, R. L. Waterland, and W. P. Reinhardt, *J. Chem. Phys.* **90**, 2328 (1989).
- [9.21] S. G. Matanyan, G. K. Savvidy, and N. G. Ter-Arutyunyan-Savvidy, *Sov. Phys. JETP* **53**, 421 (1981).

- [9.22] A. Carnegie and I. C. Percival, *J. Phys. A* **17**, 801 (1984).
- [9.23] B. Eckhardt and D. Wintgen, Symbolic description of periodic orbits for the quadratic Zeeman effect, *J. Phys. B* **23**, 355 (1990).
- [9.24] J. M. Robbins, Discrete symmetries in periodic-orbit theory, *Phys. Rev. A* **40**, 2128 (1989).
- [9.25] N. Balasz and A. Voros, Chaos on the pseudosphere, *Phys. Rep.* **143**, 109 (1986).
- [9.26] M. Hénon and C. Heiles, The applicability of the third integral of motion: Some numerical experiments, *Astron. J.* **69**, 73 (1964).
- [9.27] C. Jung and H. J. Scholz, *J. Phys. A* **20**, 3607 (1987).
- [9.28] C. Jung and P. Richter, *J. Phys. A* **23**, 2847 (1990).
- [9.29] B. Lauritzen, Discrete symmetries and the periodic-orbit expansions, *Phys. Rev. A* **43**, 603 (1991).
- [9.30] J. F. Gibson, J. Halcrow, and P. Cvitanović, Equilibrium and traveling-wave solutions of plane Couette flow, *J. Fluid Mech.* **638**, 243 (2009), [arXiv:0808.3375](https://arxiv.org/abs/0808.3375).

Chapter 10

Relativity for cyclists



WHAT IF THE LAWS OF MOTION retain their form for a family of coordinate frames related by *continuous* symmetries? The notion of ‘fundamental domain’ is of no use here. If the symmetry is continuous, the dynamical system should be reduced to a lower-dimensional, desymmetrized system, with ‘ignorable’ coordinates eliminated (but not forgotten).

We shall describe here two ways of reducing a continuous symmetry. In the ‘method of slices’ or ‘moving frames’ of sect. 10.4 we slice the state space in such a way that an entire class of symmetry-equivalent points is represented by a single point. In the Hilbert polynomial basis approach of sect. 10.5 we replace the equivariant dynamics by the dynamics rewritten in terms of invariant coordinates. In either approach we retain the option of computing in the original coordinates, and then, when done, projecting the solution onto the symmetry reduced state space.

Instead of writing yet **another tome on group theory**, in what follows we continue to serve group theoretic nuggets on need-to-know basis, through a series of pedestrian examples (but take a slightly higher, cyclist road in the text proper).

10.1 Continuous symmetries

First of all, why worry about continuous symmetries? Here is an example of the effect a continuous symmetry has on dynamics (for physics background, see [exercise 10.1](#) [exercise 10.2](#) remark 10.2).

Example 10.1 Complex Lorenz flow: Consider a complex generalization of Lorenz equations (2.12),

$$\begin{aligned}\dot{x} &= -\sigma x + \sigma y, & \dot{y} &= (\rho - z)x - ay \\ \dot{z} &= (xy^* + x^*y)/2 - bz,\end{aligned}\tag{10.1}$$

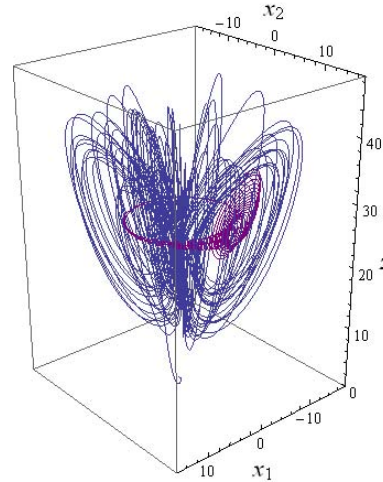


Figure 10.1: A typical $\{x_1, x_2, z\}$ trajectory of the complex Lorenz flow, with a short trajectory of figure 10.4 whose initial point is close to the relative equilibrium TW_1 superimposed. See also figure 10.7. (R. Wilczak)

where x, y are complex variables, z is real, while the parameters σ, b are real and $\rho = \rho_1 + i\rho_2, a = 1 - ie$ are complex. Recast in real variables, this is a set of five coupled ODEs

$$\begin{aligned}
 \dot{x}_1 &= -\sigma x_1 + \sigma y_1 \\
 \dot{x}_2 &= -\sigma x_2 + \sigma y_2 \\
 \dot{y}_1 &= (\rho_1 - z)x_1 - \rho_2 x_2 - y_1 - ey_2 \\
 \dot{y}_2 &= \rho_2 x_1 + (\rho_1 - z)x_2 + ey_1 - y_2 \\
 \dot{z} &= -bz + x_1 y_1 + x_2 y_2.
 \end{aligned}
 \tag{10.2}$$

In all numerical examples that follow, the parameters will be set to $\rho_1 = 28, \rho_2 = 0, b = 8/3, \sigma = 10, e = 1/10$, unless explicitly stated otherwise. As we shall show in example 10.7, this is a dynamical system with a continuous (but no discrete) symmetry. Figure 10.1 offers a visualization of its typical long-time dynamics. It is a mess. In the rest of this chapter we shall investigate various ways of ‘quotienting’ its $SO(2)$ symmetry, and reducing the dynamics to a 4-dimensional reduced state space. As we shall show here, the dynamics has a nice ‘stretch & fold’ action, but that is totally masked by the continuous symmetry drifts. We shall not rest until we attain the simplicity of figure 10.12, and the bliss of 1-dimensional return map of figure 10.14.

In a presence of a continuous symmetry an orbit can explore the manifold swept by combined action of the dynamics and the symmetry induced drifts. Further problems arise when we try to determine whether an orbit shadows another orbit (see the figure 13.1 for a sketch of a close pass to a periodic orbit), or develop symbolic dynamics (partition the state space, as in chapter 11): here a 1-dimensional trajectory is replaced by a $(N+1)$ -dimensional ‘sausage,’ a dimension for each continuous symmetry (N being the total number of parameters specifying the continuous transformation, and ‘1’ for the time parameter t). How are we to measure distances between such objects? We shall develop here more illuminating visualizations of such flow than figure 10.1, learn how to ‘quotient’ their symmetries, and offer computationally straightforward methods of reducing the dynamics to lower-dimensional, reduced state spaces. The methods should also be applicable to high-dimensional flows, such as translationally invariant fluid flows bounded by pipes or planes (see example 10.4).

But first, a lightning review of the theory of Lie groups. The group-theoretical concepts of sect. 9.1 apply to compact continuous groups as well, and will not be repeated here. All the group theory that we shall need is in principle contained in the *Peter-Weyl theorem*, and its corollaries: A compact Lie group G is completely reducible, its representations are fully reducible, every compact Lie group is a closed subgroup of a unitary group $U(n)$ for some n , and every continuous, unitary, irreducible representation of a compact Lie group is finite dimensional.

Example 10.2 Special orthogonal group $SO(2)$ is a group of length-preserving rotations in a plane. ‘Special’ refers to requirement that $\det g = 1$, in contradistinction to the orthogonal group $O(n)$ which allows for $\det g = \pm 1$. A group element can be parameterized by angle θ , with the group multiplication law $g(\theta')g(\theta) = g(\theta' + \theta)$, and its action on smooth periodic functions $u(\theta + 2\pi) = u(\theta)$ generated by

$$g(\theta') = e^{\theta' \mathbf{T}}, \quad \mathbf{T} = \frac{d}{d\theta}. \quad (10.3)$$

Expand the exponential, apply it to a differentiable function $u(\theta)$, and you will recognize a Taylor series. So $g(\theta')$ shifts the coordinate by θ' , $g(\theta') u(\theta) = u(\theta' + \theta)$.

Example 10.3 Translation group: Differential operator \mathbf{T} in (10.3) is reminiscent of the generator of translations. Indeed, for a constant velocity field $v(x) = c \cdot \mathbf{T}$ the time evolution is nothing but a translation by (time \times velocity):

$$e^{-\tau c \cdot \mathbf{T}} u(x) = e^{-\tau c \cdot \frac{d}{dx}} u(x) = u(x - \tau c). \quad (10.4)$$

As x is a point in the Euclidean \mathbb{R}^d space, the group is not compact. In general, a sequence of time steps in time evolution always forms an Abelian Lie group, albeit never as trivial as this free ballistic motion.

If the group actions consist of N rotations which commute, for example act on an N -dimensional cell with periodic boundary conditions, the group is an Abelian group that acts on a torus T^N .

Example 10.4 Continuous symmetries of the plane Couette flow. (continued from example 9.5) The plane Couette flow is a Navier-Stokes flow bounded by two countermoving planes, in a cell periodic in streamwise and spanwise directions. Every solution of Navier-Stokes equations belongs, by the $SO(2) \times SO(2)$ symmetry, to a 2-torus T^2 of equivalent solutions. Furthermore these tori are interrelated by a discrete D_2 group of spanwise and streamwise flips of the flow cell. (continued in example 10.10)

Let G be a group, and $g\mathcal{M} \rightarrow \mathcal{M}$ a group action on the state space \mathcal{M} . The $[d \times d]$ matrices g acting on vectors in the d -dimensional state space \mathcal{M} form a linear representation of the group G . If the action of every element g of a group G commutes with the flow

$$gv(x) = v(gx), \quad gf^\tau(x) = f^\tau(gx), \quad (10.5)$$

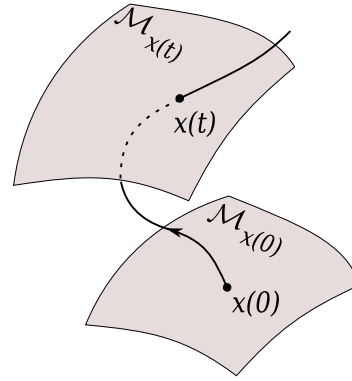


Figure 10.2: The group orbit $\mathcal{M}_{x(0)}$ of state space point $x(0)$, and the group orbit $\mathcal{M}_{x(t)}$ reached by the trajectory $x(t)$ time t later. Any point on the manifold $\mathcal{M}_{x(t)}$ is physically equivalent to any other.

G is a symmetry of the dynamics, and, as in (9.6), the dynamics is said to be invariant under G , or G -equivariant.

In order to explore the implications of equivariance for the solutions of dynamical equations, we start by examining the way a compact Lie group acts on state space \mathcal{M} . For any $x \in \mathcal{M}$, the *group orbit* \mathcal{M}_x of x is the set of all group actions (see page 148 and figure 10.2)

$$\mathcal{M}_x = \{g x \mid g \in G\}. \quad (10.6)$$

As we saw in example 10.3, the time evolution itself is a noncompact 1-parameter Lie group. Thus the time evolution and the continuous symmetries can be considered on the same Lie group footing. For a given state space point x a symmetry group of N continuous transformations together with the evolution in time sweeps out, in general, a smooth $(N+1)$ -dimensional manifold of equivalent solutions (if the solution has a nontrivial symmetry, the manifold may have a dimension less than $N + 1$). For solutions p for which the group orbit of x_p is periodic in time T_p , the group orbit sweeps out a *compact* invariant manifold \mathcal{M}_p . The simplest example is the $N = 0$, no symmetry case, where the invariant manifold \mathcal{M}_p is the 1-torus traced out by a periodic trajectory p . If \mathcal{M} is a smooth C^∞ manifold, and G is compact and acts smoothly on \mathcal{M} , the reduced state space can be realized as a ‘stratified manifold,’ meaning that each group orbit (a ‘stratum’) is represented by a point in the reduced state space, see sect. 10.4. Generalizing the description of a non-wandering set of sect. 2.1.1, we say that for flows with continuous symmetries the non-wandering set Ω of dynamics (2.2) is the closure of the set of compact invariant manifolds \mathcal{M}_p . Without symmetries, we visualize the non-wandering set as a set of points; in presence of a continuous symmetry, each such ‘point’ is a group orbit.

10.1.1 Lie groups for pedestrians

[...] which is an expression of consecration of ‘angular momentum.’

— Mason A. Porter’s student

Definition: A Lie group is a topological group G such that (i) G has the structure of a smooth differential manifold, and (ii) the composition map $G \times G \rightarrow G : (g, h) \rightarrow gh^{-1}$ is smooth, i.e., \mathbb{C}^∞ differentiable.

Do not be mystified by this definition. Mathematicians also have to make a living. Historically, the theory of compact Lie groups that we will deploy here emerged as a generalization of the theory of $SO(2)$ rotations, i.e., Fourier analysis. By a ‘smooth differential manifold’ one means objects like the circle of angles that parameterize continuous rotations in a plane, example 10.2, or the manifold swept by the three Euler angles that parameterize $SO(3)$ rotations.

An element of a compact Lie group continuously connected to identity can be written as

$$g(\theta) = e^{\theta \cdot \mathbf{T}}, \quad \theta \cdot \mathbf{T} = \sum \theta_a \mathbf{T}_a, \quad a = 1, 2, \dots, N, \quad (10.7)$$

where $\theta \cdot \mathbf{T}$ is a *Lie algebra* element, and θ_a are the parameters of the transformation. Repeated indices are summed throughout this chapter, and the dot product refers to a sum over Lie algebra generators. The Euclidian product of two vectors x, y will be indicated by x -transpose times y , i.e., $x^T y = \sum_i^d x_i y_i$. Unitary transformations $\exp(\theta \cdot \mathbf{T})$ are generated by sequences of infinitesimal steps of form

$$g(\delta\theta) \simeq 1 + \delta\theta \cdot \mathbf{T}, \quad \delta\theta \in \mathbb{R}^N, \quad |\delta\theta| \ll 1, \quad (10.8)$$

where \mathbf{T}_a , the *generators* of infinitesimal transformations, are a set of linearly independent $[d \times d]$ anti-hermitian matrices, $(\mathbf{T}_a)^\dagger = -\mathbf{T}_a$, acting linearly on the d -dimensional state space \mathcal{M} . In order to streamline the exposition, we postpone discussion of combining continuous coordinate transformations with the discrete ones to sect. 10.2.1.

exercise 10.3

For continuous groups the Lie algebra, i.e., the set of N generators \mathbf{T}_a of infinitesimal transformations, takes the role that the $|G|$ group elements play in the theory of discrete groups. The flow field at the state space point x induced by the action of the group is given by the set of N *tangent fields*

$$t_a(x)_i = (\mathbf{T}_a)_{ij} x_j. \quad (10.9)$$

Any representation of a compact Lie group G is fully reducible, and invariant tensors constructed by contractions of \mathbf{T}_a are useful for identifying irreducible representations. The simplest such invariant is

$$\mathbf{T}^T \cdot \mathbf{T} = \sum_\alpha C_2^{(\alpha)} \mathbf{1}^{(\alpha)}, \quad (10.10)$$

where $C_2^{(\alpha)}$ is the quadratic Casimir for irreducible representation labeled α , and $\mathbf{1}^{(\alpha)}$ is the identity on the α -irreducible subspace, 0 elsewhere. The dot product of two tangent fields is thus a sum weighted by Casimirs,

$$t(x)^T \cdot t(x') = \sum_{\alpha} C_2^{(\alpha)} x_i \delta_{ij}^{(\alpha)} x'_j. \quad (10.11)$$

Example 10.5 *SO(2) irreducible representations:* (continued from example 10.2) Expand a smooth periodic function $u(\theta + 2\pi) = u(\theta)$ as a Fourier series

$$u(\theta) = \sum_{m=0}^{\infty} (u_1^{(m)} \cos m\theta + u_2^{(m)} \sin m\theta). \quad (10.12)$$

The matrix representation of the $SO(2)$ action (10.3) on the m th Fourier coefficient pair $(u_1^{(m)}, u_2^{(m)})$ is

$$g^{(m)}(\theta') = \begin{pmatrix} \cos m\theta' & \sin m\theta' \\ -\sin m\theta' & \cos m\theta' \end{pmatrix}, \quad (10.13)$$

with the Lie group generator

$$\mathbf{T}^{(m)} = \begin{pmatrix} 0 & m \\ -m & 0 \end{pmatrix}. \quad (10.14)$$

The $SO(2)$ group tangent (10.9) to state space point $u(\theta)$ on the m th invariant subspace is

$$t^{(m)}(u) = \begin{pmatrix} m u_2^{(m)} \\ -m u_1^{(m)} \end{pmatrix}. \quad (10.15)$$

The L^2 norm of $t(u)$ is weighted by the $SO(2)$ quadratic Casimir (10.10), $C_2^{(m)} = m^2$,

$$\oint \frac{d\theta}{2\pi} (\mathbf{T}u(\theta))^T \mathbf{T}u(2\pi - \theta) = \sum_{m=1}^{\infty} m^2 (u_1^{(m)2} + u_2^{(m)2}), \quad (10.16)$$

and converges only for sufficiently smooth $u(\theta)$. What does that mean? We saw in (10.4) that \mathbf{T} generates translations, and by (10.14) the velocity of the m th Fourier mode is m times higher than for the $m = 1$ component. If $|u^{(m)}|$ does not fall off faster than $1/m$, the action of $SO(2)$ is overwhelmed by the high Fourier modes.

Example 10.6 *SO(2) rotations for complex Lorenz equations:* Substituting the Lie algebra generator

$$\mathbf{T} = \begin{pmatrix} 0 & 1 & 0 & 0 & 0 \\ -1 & 0 & 0 & 0 & 0 \\ 0 & 0 & 0 & 1 & 0 \\ 0 & 0 & -1 & 0 & 0 \\ 0 & 0 & 0 & 0 & 0 \end{pmatrix} \quad (10.17)$$

acting on a 5-dimensional space (10.2) into (10.7) yields a finite angle $SO(2)$ rotation:

$$g(\theta) = \begin{pmatrix} \cos \theta & \sin \theta & 0 & 0 & 0 \\ -\sin \theta & \cos \theta & 0 & 0 & 0 \\ 0 & 0 & \cos \theta & \sin \theta & 0 \\ 0 & 0 & -\sin \theta & \cos \theta & 0 \\ 0 & 0 & 0 & 0 & 1 \end{pmatrix}. \tag{10.18}$$

From (10.14) we see that the action of $SO(2)$ on the complex Lorenz equations state space decomposes into $m = 0$ G -invariant subspace (z -axis) and $m = 1$ subspace with multiplicity 2.

The generator \mathbf{T} is indeed anti-hermitian, $\mathbf{T}^\dagger = -\mathbf{T}$, and the group is compact, its elements parametrized by $\theta \bmod 2\pi$. Locally, at $x \in \mathcal{M}$, the infinitesimal action of the group is given by the group tangent field $t(x) = \mathbf{T}x = (x_2, -x_1, y_2, -y_1, 0)$. In other words, the flow induced by the group action is normal to the radial direction in the (x_1, x_2) and (y_1, y_2) planes, while the z -axis is left invariant.



fast track:
sect. 10.2, p. 175

10.1.2 Lie groups for cyclists

Here comes all of the theory of Lie groups in one quick serving. You will live even if you do not digest this section, or, to spell it out; skip this section unless you already know the theory of Lie algebras.



The $[d \times d]$ matrices g acting on vectors in the state space \mathcal{M} form a linear representation of the group G . Tensors transform as

$$h'_{ij}{}^k = g_i{}^{i'} g_j{}^{j'} g^k{}_{k'} h_{i'j'}{}^{k'}. \tag{10.19}$$

A multilinear function $h(\bar{q}, \bar{r}, \dots, s)$ is an invariant function if (and only if) for any transformation $g \in G$ and for any set of vectors q, r, s, \dots it is unchanged by the coordinate transformation

$$h(\bar{g}q, \bar{g}r, \dots, gs) = h(\bar{q}, \bar{r}, \dots, s) = h_{ab\dots}{}^{\dots c} q^a r^b \dots s_c. \tag{10.20}$$

Examples of such invariant functions are the length $r(x)^2 = \delta_i^j x^i x_j$ and the volume $V(x, y, z) = \epsilon^{ijk} x_i y_j z_k$. Substitute the infinitesimal form of group action (10.8) into (10.19), keep the linear terms. In the index-notation longhand, the Lie algebra generator acts on each index separately,

$$(\mathbf{T}_a)_i{}^{i'} h_{i'j\dots}{}^{k\dots} + (\mathbf{T}_a)_j{}^{j'} h_{ij'\dots}{}^{k\dots} - (\mathbf{T}_a)_k{}^{k'} h_{ij\dots}{}^{k'\dots} + \dots = 0. \tag{10.21}$$

Hence the tensor $h_{ij\dots}{}^{k\dots}$ is invariant if $\mathbf{T}_a h = 0$, i.e., the N generators \mathbf{T}_a ‘annihilate’ it.

As one does not want the symmetry rules to change at every step, the generators \mathbf{T}_a , $a = 1, 2, \dots, N$, are themselves invariant tensors:

$$(\mathbf{T}_a)^i_j = g^i_{i'} g_j^{j'} g_{aa'} (\mathbf{T}_{a'})^{i'}_{j'}, \quad (10.22)$$

where $g_{ab} = [e^{-i\theta \cdot C}]_{ab}$ is the adjoint $[N \times N]$ matrix representation of $g \in G$. The $[d \times d]$ matrices \mathbf{T}_a are in general non-commuting, and from (10.21) it follows that they close N -element *Lie algebra*

$$[\mathbf{T}_a, \mathbf{T}_b] = \mathbf{T}_a \mathbf{T}_b - \mathbf{T}_b \mathbf{T}_a = -C_{abc} \mathbf{T}_c, \quad a, b, c = 1, 2, \dots, N,$$

where the fully antisymmetric adjoint representation hermitian generators

$$[C_c]_{ab} = C_{abc} = -C_{bac} = -C_{acb}$$

are the *structure constants* of the Lie algebra.

As we will not use non-Abelian Lie groups in this chapter, we omit the derivation of the Jacobi relation between C_{abc} 's, and you can safely ignore all this talk of tensors and Lie algebra commutators as far as the pedestrian applications at hand are concerned.

10.1.3 Equivariance under infinitesimal transformations

A flow $\dot{x} = v(x)$ is G -equivariant (10.5) if

exercise 10.5
exercise 10.6

$$v(x) = g^{-1} v(gx), \quad \text{for all } g \in G. \quad (10.23)$$

For an infinitesimal transformation (10.8) the G -equivariance condition becomes

$$v(x) = (1 - \theta \cdot \mathbf{T}) v(x + \theta \cdot \mathbf{T}x) + \dots = v(x) - \theta \cdot \mathbf{T}v(x) + \frac{dv}{dx} \theta \cdot \mathbf{T}x + \dots$$

The $v(x)$ cancel, and θ_a are arbitrary. Denote the *group flow tangent field* at x by $t_a(x)_i = (\mathbf{T}_a)_i^j x_j$. Thus the infinitesimal, Lie algebra G -equivariance condition is

$$t_a(v) - A(x) t_a(x) = 0, \quad (10.24)$$

where $A = \partial v / \partial x$ is the stability matrix (4.3). If case you find such learned remarks helpful: the left-hand side of (10.24) is the *Lie derivative* of the dynamical

flow field v along the direction of the infinitesimal group-rotation induced flow $t_a(x) = \mathbf{T}_a x$,

$$\mathcal{L}_{t_a} v = \left(\mathbf{T}_a - \frac{\partial}{\partial y} (\mathbf{T}_a x) \right) v(y) \Big|_{y=x} . \tag{10.25}$$

The equivariance condition (10.24) states that the two flows, one induced by the dynamical vector field v , and the other by the group tangent field t , commute if their Lie derivatives (or the ‘Lie brackets’ or ‘Poisson brackets’) vanish.

exercise 10.7
exercise 10.8
exercise 10.9

Example 10.7 Equivariance of complex Lorenz flow: That complex Lorenz flow (10.2) is equivariant under $SO(2)$ rotations (10.18) can be checked by substituting the Lie algebra generator (10.17) and the stability matrix (4.3) for complex Lorenz flow (10.2),

$$A = \begin{pmatrix} -\sigma & 0 & \sigma & 0 & 0 \\ 0 & -\sigma & 0 & \sigma & 0 \\ \rho_1 - z & -\rho_2 & -1 & -e & -x_1 \\ \rho_2 & \rho_1 - z & e & -1 & -x_2 \\ y_1 & y_2 & x_1 & x_2 & -b \end{pmatrix}, \tag{10.26}$$

into the equivariance condition (10.24). Considering that $t(v)$ depends on the full set of equations (10.2), and $A(x)$ is only its linearization, this is not an entirely trivial statement. For the parameter values (10.2) the flow is strongly volume contracting (4.47),

$$\partial_i v_i = \sum_{i=1}^5 \lambda_i(x, t) = -b - 2(\sigma + 1) = -24 - 2/3, \tag{10.27}$$

at a coordinate-, ρ - and e -independent constant rate.

Checking equivariance as a Lie algebra condition (10.24) is easier than checking it for global, finite angle rotations (10.23).

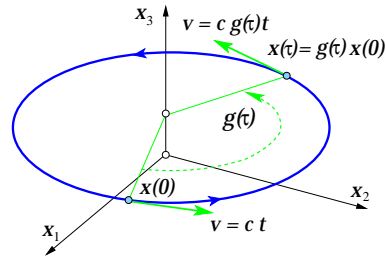
10.2 Symmetries of solutions

Let $v(x)$ be the dynamical flow, and f^τ the trajectory or ‘time- τ forward map’ of an initial point x_0 ,

$$\frac{dx}{dt} = v(x), \quad x(\tau) = f^\tau(x_0) = x_0 + \int_0^\tau d\tau' v(x(\tau')). \tag{10.28}$$

As discussed in sect. 9.2, solutions $x(\tau)$ can be classified by their symmetries. Generic trajectories have no symmetry, but recurrent solutions often do. The simplest solutions are the *equilibria* or *steady* solutions (2.8).

Figure 10.3: (a) A *relative equilibrium orbit* starts out at some point $x(0)$, with the dynamical flow field $v(x) = c \cdot t(x)$ pointing along the group tangent space. For the $SO(2)$ symmetry depicted here, the flow traces out the group orbit of $x(0)$ in time $T = 2\pi/c$. (b) An *equilibrium* lives either in the fixed $\text{Fix}(G)$ subspace (x_3 axis in this sketch), or on a group orbit as the one depicted here, but with zero angular velocity c . In that case the circle (in general, N -torus) depicts a continuous family of fixed equilibria, related only by the group action.



Definition: Equilibrium $x_{EQ} \in \mathcal{M}_{EQ}$ is a fixed, time-invariant solution,

$$\begin{aligned} v(x_{EQ}) &= 0, \\ x(x_{EQ}, \tau) &= x_{EQ} + \int_0^\tau d\tau' v(x(\tau')) = x_{EQ}. \end{aligned} \tag{10.29}$$

An *equilibrium* with full symmetry,

$$g x_{EQ} = x_{EQ} \quad \text{for all } g \in G,$$

lies, by definition, in $\text{Fix}(G)$ subspace (9.11), for example the x_3 axis in figure 10.3 (a). The multiplicity of such solution is one. An equilibrium x_{EQ} with symmetry G_{EQ} smaller than the full group G belongs to a group orbit G/G_{EQ} . If G is finite there are $|G|/|G_{EQ}|$ equilibria in the group orbit, and if G is continuous then the group orbit of x is a continuous family of equilibria of dimension $\dim G - \dim G_{EQ}$. For example, if the angular velocity c in figure 10.3 (b) equals zero, the group orbit consists of a circle of (dynamically static) equivalent equilibria.

exercise 10.10
exercise 10.11

Definition: Relative equilibrium solution $x_{TW}(\tau) \in \mathcal{M}_{TW}$: the dynamical flow field points along the group tangent field, with constant ‘angular’ velocity c , and the trajectory stays on the group orbit, see figure 10.3 (a):

$$\begin{aligned} v(x) &= c \cdot t(x), \quad x \in \mathcal{M}_{TW} \\ x(\tau) &= g(-\tau c) x(0) = e^{-\tau c \cdot \mathbf{T}} x(0). \end{aligned} \tag{10.30}$$

exercise 10.12
exercise 10.13
exercise 10.14
exercise 10.15
exercise 10.16
exercise 10.17
exercise 10.18

A *traveling wave*

$$x(\tau) = g(-c\tau) x_{TW} = x_{TW} - c\tau, \quad c \in \mathbb{R}^d \tag{10.31}$$

is a special type of a relative equilibrium of equivariant evolution equations, where the action is given by translation (10.4), $g(y) x(0) = x(0) + y$. A *rotating wave* is

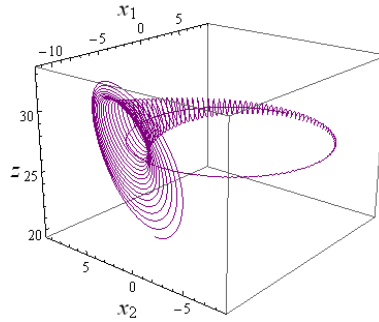


Figure 10.4: $\{x_1, x_2, z\}$ plot of the complex Lorenz flow with initial point close to TW_1 . In figure 10.1 this relative equilibrium is superimposed over the strange attractor. (R. Wilczak)

another special case of relative equilibrium, with the action is given by angular rotation. By equivariance, all points on the group orbit are equivalent, the magnitude of the velocity c is same everywhere along the orbit, so a ‘traveling wave’ moves at a constant speed. For an $N > 1$ trajectory traces out a line within the group orbit. As the c_a components are generically not in rational ratios, the trajectory explores the N -dimensional group orbit (10.6) quasi-periodically. In other words, the group orbit $g(\tau)x(0)$ coincides with the dynamical orbit $x(\tau) \in \mathcal{M}_{TW}$ and is thus flow invariant.

Example 10.8 A relative equilibrium: For complex Lorenz equations and our canonical parameter values of (10.2) a computation yields the relative equilibrium TW_1 with a representative group orbit point

$$(x_1, x_2, y_1, 0, z)_{TW_1} = (8.48492, 0.0771356, 8.48562, 0, 26.9999), \quad (10.32)$$

and angular velocity $c_{TW_1} = 1/11$. This corresponds to period $T_{TW_1} = 2\pi/c \approx 69$, so a simulation has to be run up to time of order of at least 70 for the strange attractor in figure 10.1 to start filling in.

Figure 10.4 shows the complex Lorenz flow with the initial point (10.32) on the relative equilibrium TW_1 . It starts out by drifting in a circle around the z -axis, but as the numerical errors accumulate, the trajectory spirals out.

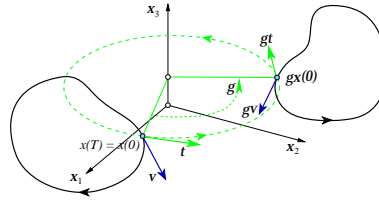
Calculation of the relative equilibrium stability reveals that it is spiral-out unstable, with the very short period $T_{spiral} = 0.6163$. This is the typical time scale for fast oscillations visible in figure 10.1, with some 100 turns for one circumambulation of the TW_1 orbit. In that time an initial deviation from x_{TW_1} is multiplied by the factor $\Lambda_{radial} \approx 500$. It would be sweet if we could eliminate the drift time scale ≈ 70 and focus just on the fast time scale of ≈ 0.6 . That we will attain by reformulating the dynamics in a reduced state space.

Definition: Periodic orbit. Let x be a periodic point on the periodic orbit p of period T ,

$$f^T(x) = x, \quad x \in \mathcal{M}_p.$$

By equivariance, $g x$ is another periodic point, with the orbits of x and $g x$ either identical or disjoint.

Figure 10.5: A periodic orbit starts out at $x(0)$ with the dynamical v and group tangent t flows pointing in different directions, and returns after time T_p to the initial point $x(0) = x(T_p)$. The group orbit of $x(0)$ sweeps out a $(1+N)$ -dimensional torus, a continuous family of equivalent periodic orbits, two of which are sketched here. For $SO(2)$ this is topologically a 2-torus.



If gx lands on the same orbit, g is an element of periodic orbit’s symmetry group G_p . If the symmetry group is the full group G , we are back to (10.30), i.e., the periodic orbit is the group orbit traced out by a relative equilibrium. The other option is that the isotropy group is discrete, the orbit segment $\{x, gx\}$ is pre-periodic (or eventually periodic), $x(0) = g_p x(T_p)$, where T_p is a fraction of the full period, $T_p = T/m$, and thus

$$\begin{aligned} x(0) &= g_p x(T_p), & x \in \mathcal{M}_p, & & g_p \in G_p \\ x(0) &= g_p^m x(m T_p) = x(T) = x(0). \end{aligned} \tag{10.33}$$

If the periodic solutions are disjoint, as in figure 10.5, their multiplicity (if G is finite, see sect. 9.1), or the dimension of the manifold swept under the group action (if G is continuous) can be determined by applications of $g \in G$. They form a family of conjugate solutions (9.10),

$$\mathcal{M}_{g_p} = g \mathcal{M}_p g^{-1}. \tag{10.34}$$

Definition: Relative periodic orbit p is an orbit \mathcal{M}_p in state space \mathcal{M} which exactly recurs

$$x_p(0) = g_p x_p(T_p), \quad x_p(\tau) \in \mathcal{M}_p, \tag{10.35}$$

at a fixed *relative period* T_p , but shifted by a fixed group action g_p which brings the endpoint $x_p(T_p)$ back into the initial point $x_p(0)$, see figure 10.6. The group action g_p parameters $\theta = (\theta_1, \theta_2, \dots, \theta_N)$ are referred to as “phases,” or “shifts.” In contrast to the pre-periodic (10.33), the phase here are irrational, and the trajectory sweeps out ergodically the group orbit without ever closing into a periodic orbit. For dynamical systems with only continuous (no discrete) symmetries, the parameters $\{\theta_1, \dots, \theta_N\}$ are real numbers, ratios π/θ_j are almost never rational, likelihood of finding a periodic orbit for such system is zero, and such relative periodic orbits are almost never eventually periodic.

Relative periodic orbits are to periodic solutions what relative equilibria (traveling waves) are to equilibria (steady solutions). Equilibria satisfy $f^x(x) - x = 0$ and relative equilibria satisfy $f^x(x) - g(\tau)x = 0$ for any τ . In a co-moving frame,

Figure 10.6: A relative periodic orbit starts out at $x(0)$ with the dynamical v and group tangent t flows pointing in different directions, and returns to the group orbit of $x(0)$ after time T_p at $x(T_p) = g_p x(0)$, a rotation of the initial point by g_p . For flows with continuous symmetry a generic relative periodic orbit (not pre-periodic to a periodic orbit) fills out ergodically what is topologically a torus, as in figure 10.5; if you are able to draw such a thing, kindly send us the figure. As illustrated by figure 10.8 (a) this might be a project for Lucas Films.

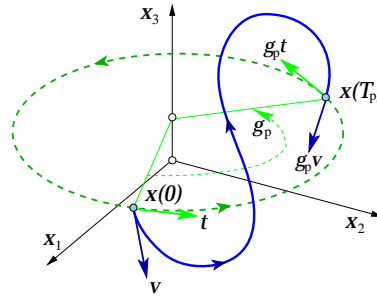
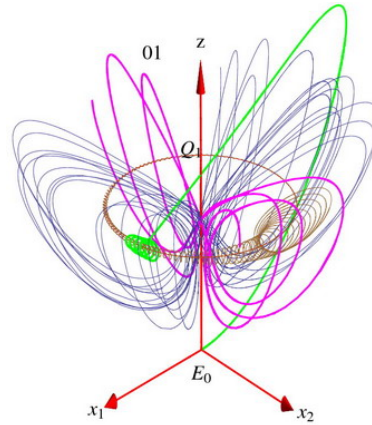


Figure 10.7: (Figure 10.1 continued) A group portrait of the complex Lorenz equations state space dynamics. Plotted are relative equilibrium TW_1 (red), its unstable manifold (brown), equilibrium EQ_0 , one trajectory from the group orbit of its unstable manifold (green), 3 repetitions of relative periodic orbit $\overline{01}$ (magenta) and a generic orbit (blue). (E. Siminos)



i.e., frame moving along the group orbit with velocity $v(x) = c \cdot t(x)$, the relative equilibrium appears as an equilibrium. Similarly, a relative periodic orbit is periodic in its mean velocity $c_p = \theta_p/T_p$ co-moving frame (see figure 10.8), but in the stationary frame its trajectory is quasiperiodic. A co-moving frame is helpful in visualizing a single ‘relative’ orbit, but useless for viewing collections of orbits, as each one drifts with its own angular velocity. Visualization of all relative periodic orbits as periodic orbits we attain only by global symmetry reductions, to be undertaken in sect. 10.4.

Example 10.9 Complex Lorenz flow with relative periodic orbit: Figure 10.7 is a group portrait of the complex Lorenz equations state space dynamics, with several important players posing against a generic orbit in the background.

The unstable manifold of relative equilibrium TW_1 is characterized by a 2-dimensional complex eigenvector pair, so its group orbit is a 3-dimensional. Only one representative trajectory on it is plotted in the figure. The unstable manifold of equilibrium EQ_0 has one expanding eigenvalue, but its group orbit is a cone originating at EQ_0 . Only one representative trajectory on this cone is shown in the figure. It lands close to TW_1 , and then spirals out along its unstable manifold. 3 repetitions of a short relative periodic orbit $\overline{01}$ are drawn. The trajectory fills out ergodically a 2-dimensional orbit M_{01} . The assignment of its symbolic dynamics label will be possible only after the symmetry reduction, see figure 10.14 and figure 11.9.

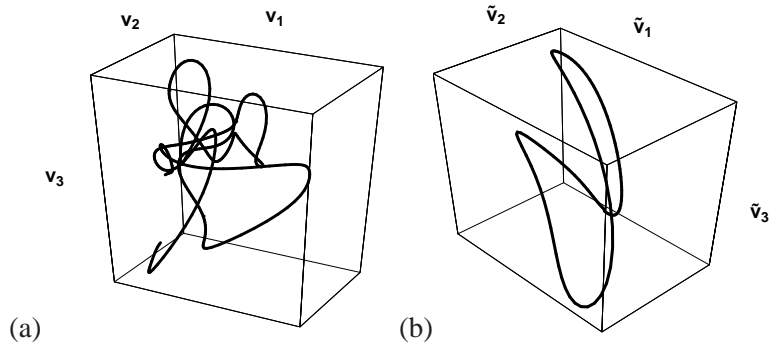


Figure 10.8: A relative periodic orbit of Kuramoto-Sivashinsky flow projected on (a) the stationary state space coordinate frame $\{v_1, v_2, v_3\}$, traced for four periods T_p ; (b) the co-moving $\{\tilde{v}_1, \tilde{v}_2, \tilde{v}_3\}$ coordinate frame, moving with the mean angular velocity $c_p = \theta_p/T_p$. (from ref. [1])

10.2.1 Discrete and continuous symmetries together

We expect to see relative periodic orbits because a trajectory that starts on and returns to a given torus of a symmetry equivalent solutions is unlikely to intersect it at the initial point, unless forced to do so by a discrete symmetry. This we will make explicit in sect. 10.4, where relative periodic orbits will be viewed as periodic orbits of the reduced dynamics.

If, in addition to a continuous symmetry, one has a discrete symmetry which is not its subgroup, one does expect equilibria and periodic orbits. However, a relative periodic orbit can be pre-periodic if it is equivariant under a discrete symmetry, as in (10.33): If $g^m = 1$ is of finite order m , then the corresponding orbit is periodic with period mT_p . If g is not of a finite order, a relative periodic orbit is periodic only after a shift by g_p , as in (10.35). Morally, as it will be shown in chapter 21, such orbit is the true ‘prime’ orbit, i.e., the shortest segment that under action of G tiles the entire invariant submanifold \mathcal{M}_p .

Example 10.10 Relative orbits in the plane Couette flow. (continued from example 10.4) Translational symmetry allows for relative equilibria (traveling waves), characterized by a fixed profile Eulerian velocity $u_{TW}(x)$ moving with constant velocity c , i.e.

$$u(x, \tau) = u_{TW}(x - c\tau). \tag{10.36}$$

As the plane Couette flow is bounded by two counter-moving planes, it is easy to see where the relative equilibrium (traveling wave) solutions come from. A relative equilibrium solution hugs close to one of the walls and drifts with it with constant velocity, slower than the wall, while maintaining its shape. A relative periodic solution is a solution that recurs at time T_p with exactly the same disposition of the Eulerian velocity fields over the entire cell, but shifted by a 2-dimensional (streamwise, spanwise) translation g_p . By discrete symmetries these solutions come in counter-traveling pairs $u_q(x - c\tau)$, $-u_q(-x + c\tau)$: for example, for each one drifting along with the upper wall, there is a counter-moving one drifting along with the lower wall. Discrete symmetries also imply existence of strictly stationary solutions, or ‘standing waves.’ For example, a solution with velocity fields antisymmetric under reflection through the midplane has equal flow velocities in opposite directions, and is thus an equilibrium stationary in time.

chapter 21

10.3 Stability



A spatial derivative of the equivariance condition (10.5) yields the matrix equivariance condition satisfied by the stability matrix (stated here both for the finite group actions, and for the infinitesimal, Lie algebra generators):

$$gA(x)g^{-1} = A(gx), \quad [\mathbf{T}_a, A] = \frac{\partial A}{\partial x} t_a(x). \quad (10.37)$$

exercise 10.19
exercise 10.20

For a flow within the fixed $\text{Fix}(G)$ subspace, $t(x)$ vanishes, and the symmetry imposes strong conditions on the perturbations out of the $\text{Fix}(G)$ subspace. As in this subspace stability matrix A commutes with the Lie algebra generators \mathbf{T} , the spectrum of its eigenvalues and eigenvectors is decomposed into irreducible representations of the symmetry group. This we have already observed for the EQ_0 of the Lorenz flow in example 9.10.

A infinitesimal symmetry group transformation maps the initial and the end point of a finite trajectory into a nearby, slightly rotated equivalent points, so we expect the perturbations along to group orbit to be marginal, with unit eigenvalues. The argument is akin to (4.7), the proof of marginality of perturbations along a periodic orbit. Consider two nearby initial points separated by an N -dimensional infinitesimal group transformation (10.8): $\delta x_0 = g(\delta\theta)x_0 - x_0 = \delta\theta \cdot \mathbf{T}x_0 = \delta\theta \cdot t(x_0)$. By the commutativity of the group with the flow, $g(\delta\theta)f^\tau(x_0) = f^\tau(g(\delta\theta)x_0)$. Expanding both sides, keeping the leading term in $\delta\theta$, and using the definition of the Jacobian matrix (4.6), we observe that $J^\tau(x_0)$ transports the N -dimensional group tangent space at $x(0)$ to the rotated tangent space at $x(\tau)$ at time τ :

$$t_a(\tau) = J^\tau(x_0) t_a(0), \quad t_a(\tau) = \mathbf{T}_a x(\tau). \quad (10.38)$$

For a relative periodic orbit, $g_p x(T_p) = x(0)$, at any point along cycle p the group tangent vector $t_a(\tau)$ is an eigenvector of the Jacobian matrix with an eigenvalue of unit magnitude,

$$J_p t_a(x) = t_a(x), \quad J_p(x) = g_p J^{T_p}(x), \quad x \in \mathcal{M}_p. \quad (10.39)$$

Two successive points along the cycle separated by $\delta x_0 = \delta\theta \cdot t(\tau)$ have the same separation after a completed period $\delta x(T_p) = g_p \delta x_0$, hence eigenvalue of magnitude 1. In presence of an N -dimensional Lie symmetry group, N eigenvalues equal unity.

10.4 Reduced state space

Given Lie group G acting smoothly on a C^∞ manifold \mathcal{M} , the *reduced state space* \mathcal{M}/G is the set of equivalence classes, each class a group orbit. In the literature

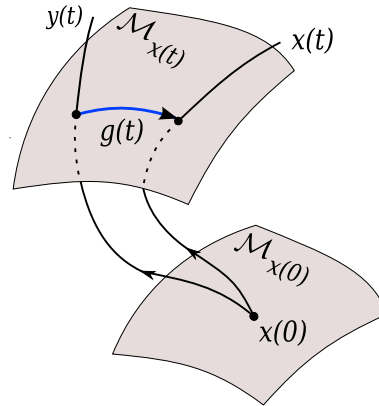


Figure 10.9: Two trajectories $x(t)$, $y(t)$ are equivalent up to a group rotation $g(t)$ as long as they belong to the same group orbit $\mathcal{M}_{x(t)}$.

this space is often rediscovered, and thus has many names - it is alternatively called ‘desymmetrized state space,’ ‘orbit space,’ ‘quotient space,’ or ‘image space,’ obtained by mapping equivariant dynamics to invariant dynamics by methods such as ‘moving frames,’ ‘cross sections,’ ‘slices,’ ‘freezing,’ ‘Hilbert bases,’ ‘quotienting,’ or ‘desymmetrization’

remark 10.1

Symmetry reduction replaces a dynamical system (\mathcal{M}, f) with a symmetry by a ‘desymmetrized’ system $(\bar{\mathcal{M}}, \bar{f})$, a system where each group orbit is replaced by a point, and the action of the group is trivial, $gy = y$ for all $y \in \bar{\mathcal{M}}$, $g \in G$. The reduced state space $\bar{\mathcal{M}}$ is sometimes called the ‘quotient space’ \mathcal{M}/G because the symmetry has been ‘divided out.’ For a discrete symmetry, the reduced state space \mathcal{M}/G is given by the fundamental domain of sect. 9.4. In presence of a continuous symmetry, the reduction to \mathcal{M}/G amounts to a change of coordinates where the ‘ignorable angles’ $\{\theta_1, \dots, \theta_N\}$ that parameterize N group translations can be separated out.

We start our discussion of symmetry reduction by considering the finite-rotations *method of moving frames*, and its differential formulation, the *method of slices*.

10.4.1 Go with the flow: method of moving frames

The idea: As the symmetries commute with dynamics, we can evolve a solution $x(\tau)$ for as long as we like, and then rotate it to any equivalent point (see figure 10.9) on its group orbit,

$$x(\tau) = g(\tau)y(\tau), \tag{10.40}$$

any time and any way we like. In the ‘method of slices’ one point on each group orbit is picked as the reduced state space representative of the equivalence class, by slicing across the group orbits by a fixed hypersurface. We start by describing how the method works for a finite segment of the full state space trajectory.

Split up the integration into a sequence of finite time steps, each followed by a rigid coordinate frame rotation (‘moving frame’) such that the next segment’s initial point is in the *slice* fixed by a point y .

Figure 10.10: Slice \bar{M} is a Poincaré section (10.41) for group orbits (indicated by dotted lines here). The full state space trajectory $x(t)$ and the reduced state space trajectory $y(t)$ belong to the same group orbit $\mathcal{M}_{x(t)}$ and are equivalent up to a group rotation $g(t)$ (10.40).

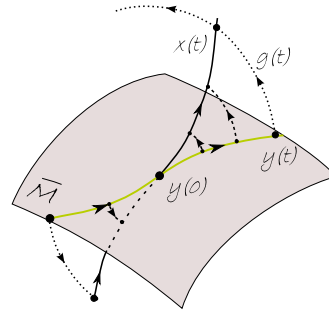
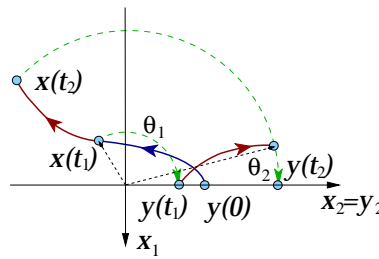


Figure 10.11: Method of moving frames for a flow $SO(2)$ -equivariant under (10.18) with slice through $y' = (0, 1, 0, 0, 0)$, group tangent $t' = (1, 0, 0, 0, 0)$. The clockwise orientation condition restricts the slice to half-hyperplane $y_1 = 0, y_2 > 0$. A trajectory started on the slice at $y(0)$, evolves to a state space point with a non-zero $x_1(t_1)$. Compute the polar angle θ_1 of $x(t_1)$ in the (x_1, x_2) plane. The entire state space is then rotated (hence ‘moving frame’) clockwise by θ_1 to $y(t_1) = g(-\theta_1)x(t_1)$, so that the equivalent point on the circle lies on the slice, $y_1(t_1) = 0$. Thus after every finite time step followed by a rotation the trajectory restarts from the $y_1(t_k) = 0$ reduced state space.



Definition: Slice. Let G act regularly on a d -dimensional manifold \mathcal{M} , i.e., with all group orbits N -dimensional. A *slice* through point y' is a $(d-N)$ -dimensional submanifold \bar{M} such that all group orbits in an open neighborhood of the slice-defining point y' intersect \bar{M} transversally and only once (see figure 10.10).

The simplest *slice condition* defines a slice as a $(d-N)$ -dimensional hyperplane \bar{M} normal to the N group rotation tangents t'_a at point y' :

$$(y - y')^T t'_a = 0, \quad t'_a = t_a(y') = \mathbf{T}_a y'. \quad (10.41)$$

In other words, ‘slice’ is a Poincaré section (3.6) for group orbits. The G -invariant subspaces are always within the slice, as $\mathbf{T}_a x = 0$ for x in an invariant subspace, see (10.21). Each ‘big circle’ –group orbit tangent to t'_a – intersects the hyperplane exactly twice, with the two solutions separated by π . As for a Poincaré section (3.4), we add an orientation condition, and select the intersection with the clockwise rotation angle into the slice.

Definition: Moving frame. Assume that for a given $x \in \mathcal{M}$ and a given slice \bar{M} there exists a unique group element $g = g(x)$ that rotates x into the slice, $gx = y \in \bar{M}$. The map that associates to a state space point x a Lie group action $g(x)$ is called a *moving frame*.

As $y'^T t'_a = 0$ by the antisymmetry of \mathbf{T}_a , the slice condition (10.41) fixes θ for a given x by

$$0 = y'^T t'_a = x^T g(\theta)^T t'_a, \quad (10.42)$$

exercise 6.1
exercise 10.21

where g^T denotes the transpose of g . The method of moving frames is a post-processing method; trajectories are computed in the full state space, then rotated into the slice whenever desired, with the slice condition easily implemented. The slice group tangent t' is a given vector, and $g(\theta)x$ is another vector, linear in x and a function of group parameters θ . Rotation parameters θ are determined numerically, by a Newton method, through the slice condition (10.42).

exercise 10.22

Figure 10.11 illustrates the method of moving frames for an $SO(2)$ slice normal to the x_2 axis. Looks innocent, except there is nothing to prevent a trajectory from going thorough $(x_1, x_2) = (0, 0)$, and what θ is one to use then? We can always chose a finite time step that hops over this singularity, but in the continuous time formulation we will not be so lucky.

How does one pick a slice point y' ? A generic point y' not in an invariant subspace (on the complex Lorenz equations z axis, for example) should suffice to fix a slice. The rules of thumb are much like the ones for picking Poincaré sections, sect. 3.1.1. The intuitive idea is perhaps best visualized in the context of fluid flows. Suppose the flow exhibits an unstable coherent structure that – approximately– recurs often at different spatial dispositions. One can fit a ‘template’ to one recurrence of such structure, and describe other recurrences as its translations. A well chosen slice point belongs to such dynamically important equivalence class (i.e. group orbit). A slice is locally isomorphic to M/G , in an open neighborhood of y' . As is the case for the dynamical Poincaré sections, in general a single slice does not suffice to reduce $M \rightarrow M/G$ globally.

The Euclidian product of two vectors x, y is indicated in (10.41) by x -transpose times y , i.e., $x^T y = \sum_i^d x_i y_i$. More general bilinear norms $\langle x, y \rangle$ can be used, as long as they are G -invariant, i.e., constant on each irreducible subspace. An example is the quadratic Casimir (10.11).

Note: method of moving frames has nothing in common with the co-moving frames, such as the one illustrated in figure 10.8. Each relative periodic orbit has its own co-moving frame. In the method of moving frames (or the method of slices) one fixes a stationary slice, and rotates all solutions back into the slice.

Example 10.11 An $SO(2)$ moving frame: (continued from example 10.2) *The $SO(2)$ action $(y_1, y_2) = (x_1 \cos \theta - x_2 \sin \theta, x_1 \sin \theta + x_2 \cos \theta)$ is regular on $\mathbb{R}^2 \setminus \{0\}$. Thus we can define a slice as a ‘hyperplane’ (here a mere line), through $y' = (0, 1)$, with group tangent $t' = (0, 1)$, and ensure uniqueness by clockwise rotation into positive x_2 axis. Hence the reduced state space is the half-line $x_1 = 0, y_2 = x_2 > 0$. The slice condition $y_1 = 0$ yields the explicit formula for the moving frame parameter*

$$\theta(x_1, x_2) = \tan^{-1}(x_1/x_2), \tag{10.43}$$

i.e., the angle which rotates the point (x_1, x_2) back to the slice, taking care that \tan^{-1} distinguishes (x_1, x_2) plane quadrants correctly. As $SO(2)$ preserves lengths, $x_1^2 + x_2^2 = y_1^2 + y_2^2$, and the group-orbit point in the slice is an $SO(2)$ -invariant,

$$y_2 = \sqrt{x_1^2 + x_2^2}. \tag{10.44}$$

The example is a bit trivial. If dynamics is in plane and $SO(2)$ equivariant, the solutions can only be circles of radius $\sqrt{x_1^2 + x_2^2}$, so this is the “rectification” of the harmonic oscillator by a change to polar coordinates, example 6.1. Still, it illustrates the sense in which the method of moving frames yields group invariants. (E. Siminos)

10.4.2 Dynamics within a slice

I made a wrong mistake.
—Yogi Berra

The choice of finite time steps in the preceding sections was arbitrary, so it is tempting to see what happens if the steps are taken infinitesimal. As we shall see, we do get a flow restricted to the slice, but at a price.

By equivariance one can always write the full state space trajectory as $x(\tau) = g(\tau) y(\tau)$, where the $(d-N)$ -dimensional reduced state space trajectory $y(\tau)$ is to be fixed by some condition, and $g(\tau)$ is then the corresponding curve on the N -dimensional group manifold of the group action that rotates y into x at time τ . The time derivative is then $\dot{x} = v(gy) = \dot{g}y + g\dot{y}$, with the reduced state space velocity field given by $u = dy/dt$. Rewriting this as $u = g^{-1}v(gy) - g^{-1}\dot{g}y$ and using the equivariance condition (10.23) leads to

$$u = v - g^{-1}\dot{g}y.$$

The Lie group element (10.7) and its time derivative describe the group tangent flow

$$g^{-1}\dot{g} = g^{-1}\frac{d}{dt}e^{\theta \cdot \mathbf{T}} = \dot{\theta} \cdot \mathbf{T}.$$

This is the group tangent velocity $g^{-1}\dot{g}y = \dot{\theta} \cdot t(y)$ evaluated at the point y , i.e., with $g = 1$. The flow in the $(d-N)$ directions transverse to the group flow is now obtained by subtracting the flow along the group tangent direction,

$$u(y) = v(y) - \dot{\theta}(y) \cdot t(y), \quad u = dy/dt, \quad (10.45)$$

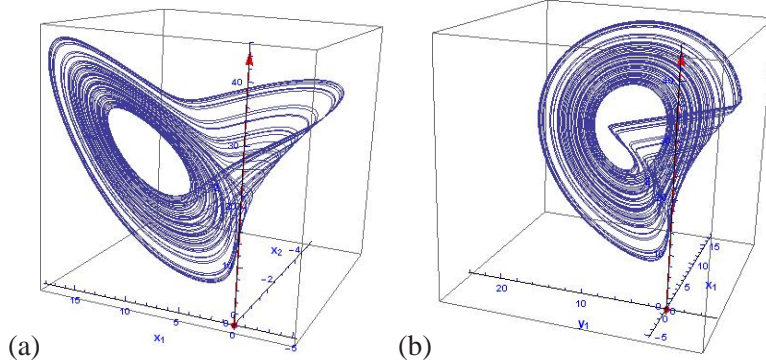
for any factorization of the flow of form $x(\tau) = g(\tau)y(\tau)$. To integrate these equations we first have to fix a particular flow factorization by imposing conditions on $y(\tau)$, and then integrate phases $\theta(\tau)$ on a given reduced state space trajectory $y(\tau)$.

exercise 10.23
exercise 10.24

Here we demand that the reduced state space is confined to a hyperplane slice. Substituting (10.45) into the time derivative of the fixed slice condition (10.42),

$$u(y)^T t'_a = v(y)^T t'_a - \dot{\theta}_a \cdot t(y)^T t'_a = 0,$$

Figure 10.12: Method of moving frames, slice fixed by a point on the complex Lorenz equations relative equilibrium group orbit, $y' = x_{TW_1}$. (a) The strange attractor of figure 10.1 in the reduced state space of (10.47), $\{x_1, x_2, z\}$ projection. (b) $\{x_2, y_2, z\}$ projection. The reduced state space complex Lorenz flow strange attractor of figure 10.1 now exhibits a discontinuity due to the vanishing denominator in (10.48).



yields the equation for the group phases flow $\dot{\theta}$ for the slice fixed by y' , together with the reduced state space \bar{M} flow $u(y)$:

$$\dot{\theta}_a(y) = \frac{v(y)^T t'_a}{t(y)^T \cdot t'} \tag{10.46}$$

$$u(y) = v(y) - \dot{\theta}(y) \cdot t(y), \quad y \in \bar{M}. \tag{10.47}$$

Each group orbit $\mathcal{M}_x = \{g \cdot x \mid g \in G\}$ is an equivalence class; method of slices represents the class by its single slice intersection point y . By construction $\bar{u}^T t' = 0$, and the motion stays in the $(d-N)$ -dimensional slice. We have thus replaced the original dynamical system $\{\mathcal{M}, f\}$ by a reduced system $\{\bar{M}, \bar{f}\}$.

In the pattern recognition and ‘template fitting’ settings (10.46) is called the ‘reconstruction equation.’ Integrated together, the reduced state space trajectory (10.47) and $g(\tau) = \exp\{\theta(\tau) \cdot \mathbf{T}\}$, the integrated phase (10.46), reconstruct the full state space trajectory $x(\tau) = g(\tau) y(\tau)$ from the reduced state space trajectory $y(\tau)$, so no information about the flow is lost in the process of symmetry reduction.

exercise 10.25
exercise 10.26

Example 10.12 A slice for complex Lorenz flow. (continuation of example 10.6) Here we can use the fact that

$$t(y)^T \cdot t' = \bar{x}^T \mathbf{T}^T \cdot \mathbf{T} y' = \bar{x}_1 x'_1 + \bar{x}_2 x'_2 + \bar{y}_1 y'_1 + \bar{y}_2 y'_2$$

is the dot-product restricted to the $m = 1$ 4-dimensional representation of $SO(2)$. A generic y' can be brought to form $y' = (0, 1, y'_1, y'_2, z)$ by a rotation and rescaling. Then $\mathbf{T} y' = (1, 0, y'_2, -y'_1, 0)$, and

$$\frac{v(\bar{x}) \cdot t'}{t(\bar{x}) \cdot t'} = -\frac{v_1 + v_3 y'_2 - v_4 y'_1}{\bar{x}_2 + \bar{y}_1 y'_1 + \bar{y}_2 y'_2}. \tag{10.48}$$

A long time trajectory of (10.47) with y' on the relative equilibrium TW_1 group orbit is shown in figure 10.12. As initial condition we chose the initial point (10.32) on the unstable manifold of TW_1 , rotated back to the slice by angle θ as prescribed by (10.42). We show the part of the trajectory for $t \in [70, 100]$. The relative equilibrium TW_1 , now an equilibrium of the reduced state space dynamics, organizes the flow into a Rössler type attractor (see figure 2.6). The denominator in (10.46) vanishes and the phase velocity $\dot{\theta}(y)$ diverges whenever the direction of group action on the reduced state space point

is perpendicular to the direction of group action on the slicepoint y' . While the reduced state space flow appears continuous in the $\{x_1, x_2, z\}$ projection, figure 10.12 (a), this singularity manifests itself as a discontinuity in the $\{x_2, y_2, z\}$ projection, figure 10.12 (b). The reduced state space complex Lorenz flow strange attractor of figure 10.1 now exhibits a discontinuity whenever the trajectory crosses this -dimensional subspace.

Slice flow equations (10.47) and (10.46) are pretty, but there is a trouble in the paradise. The slice flow encounters singularities in subsets of state space, with phase velocity $\dot{\theta}$ divergent whenever the denominator in (10.48) changes sign, see $\{x_2, y_2, z\}$ projection of figure 10.12 (b). Hence a single slice does not in general suffice to cover \mathcal{M}/G globally.

10.5 Method of images: Hilbert bases

(E. Siminos and P. Cvitanović)

Erudite reader might wander: why all this slicing and dicing, when the problem of symmetry reduction had been solved by Hilbert and Weyl nearly a century ago? Indeed, the most common approach to symmetry reduction is by means of a Hilbert invariant polynomial bases (9.15), motivated intuitively by existence of such nonlinear invariants as the rotationally-invariant length $r^2 = x_1^2 + x_2^2 + \dots + x_d^2$, or, in Hamiltonian dynamics, the energy function. One trades in the equivariant state space coordinates $\{x_1, x_2, \dots, x_d\}$ for a non-unique set of $m \geq d$ polynomials $\{u_1, u_2, \dots, u_m\}$ invariant under the action of the symmetry group. These polynomials are linearly independent, but functionally dependent through $m - d + N$ relations called *syzygies*.

Example 10.13 An $SO(2)$ Hilbert basis: (continued from example 9.6) The Hilbert basis

$$\begin{aligned} u_1 &= x_1^2 + x_2^2, & u_2 &= y_1^2 + y_2^2, \\ u_3 &= x_1 y_2 - x_2 y_1, & u_4 &= x_1 y_1 + x_2 y_2, \\ u_5 &= z. \end{aligned} \tag{10.49}$$

is invariant under the $SO(2)$ action on a 5-dimensional state space (10.18). That implies, in particular, that the image of the full state space relative equilibrium TW_{11} group orbit of figure 10.4 is the stationary equilibrium point EQ_1 , see figure 10.13. The polynomials are linearly independent, but related through one syzygy,

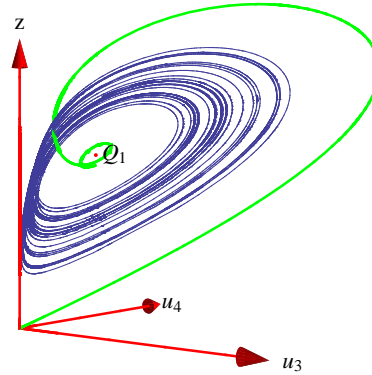
$$u_1 u_2 - u_3^2 - u_4^2 = 0, \tag{10.50}$$

yielding a 4-dimensional $\mathcal{M}/SO(2)$ reduced state space, a symmetry-invariant representation of the 5-dimensional $SO(2)$ equivariant dynamics. (continued in example 10.14)

The dynamical equations follow from the chain rule

$$\dot{u}_i = \frac{\partial u_i}{\partial x_j} \dot{x}_j, \tag{10.51}$$

Figure 10.13: Invariant ‘image’ of complex Lorenz equations dynamics, figure 10.1, projected onto the invariant polynomials basis (10.49). Note the unstable manifold connection from the equilibrium E_{Q_0} at the origin to the strange attractor controlled by the rotation around relative equilibrium E_{Q_1} (the reduced state space image of TW_1); as in the Lorenz flow figure 3.7, natural measure close to E_{Q_0} is vanishingly small but non-zero.



upon substitution $\{x_1, x_2, \dots, x_d\} \rightarrow \{u_1, u_2, \dots, u_m\}$. One can either rewrite the dynamics in this basis or plot the ‘image’ of solutions computed in the original, equivariant basis in terms of these invariant polynomials.

Example 10.14 Complex Lorenz equations in a Hilbert basis: (continuation of example 10.13) Substitution of (10.2) and (10.49) into (10.51) yields complex Lorenz equations in terms of invariant polynomials:

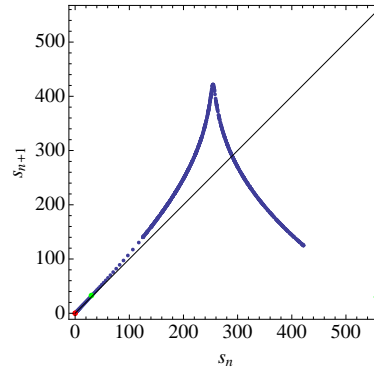
$$\begin{aligned}
 \dot{u}_1 &= 2\sigma(u_3 - u_1) \\
 \dot{u}_2 &= -2u_2 - 2u_3(u_5 - \rho_1) \\
 \dot{u}_3 &= \sigma u_2 - (\sigma - 1)u_3 - e u_4 + u_1(\rho_1 - u_5) \\
 \dot{u}_4 &= e u_3 - (\sigma + 1)u_4 \\
 \dot{u}_5 &= u_3 - b u_5.
 \end{aligned}
 \tag{10.52}$$

As far as visualization goes, we need neither construct nor integrate the invariant dynamics (10.52). It suffices to integrate the original, unreduced flow of Figure 10.1, but plot the solution in the image space, i.e., u_i invariant, Hilbert polynomial coordinates, as in figure 10.13. A drawback of such polynomial projections is that the folding mechanism is harder to view since the dynamics is squeezed near the z -axis.

Reducing dimensionality of a dynamical system by elimination of variables through inclusion of syzygies such as (10.50) introduces singularities. Such elimination of variables, however, is not needed for visualization purposes; syzygies merely guarantee that the dynamics takes place on a submanifold in the projection on the $\{u_1, u_2, \dots, u_m\}$ coordinates. However, when one *reconstructs* the dynamics in the original space \mathcal{M} from its image \mathcal{M}/G , the transformations have singularities at the fixed-point subspaces of the isotropy subgroups in \mathcal{M} .

Nevertheless we can now easily identify a suitable Poincaré section, guided by the Lorenz flow examples of chapter 9, as one that contains the z -axis and the image of the relative equilibrium TW_1 , here defined by the condition $u_1 = u_4$. As in example 11.4, we construct the first return map using as coordinate the Euclidean arclength along the intersection of the unstable manifold of TW_1 with the Poincaré surface of section, see figure 10.14. Thus the goals set into the introduction to this chapter are attained: we have reduced the messy strange attractor of figure 10.1 to a 1-dimensional return map. As will be explained in

Figure 10.14: Return map to the Poincaré section $u_1 = u_4$ for complex Lorenz equations projected on invariant polynomials (10.49). The return map coordinate is the Euclidean arclength distance from TW_1 , measured along the Poincaré section of its spiral-out unstable manifold, as for the Lorenz flow return map of example 11.4.



example 11.4 for the Lorenz attractor, we now have the symbolic dynamics and can compute as many relative periodic orbits of the complex Lorenz flow as we wish, missing none.

What limits the utility of Hilbert basis methods are not such singularities, but rather the fact that the algebra needed to determine a Hilbert basis becomes computationally prohibitive as the dimension of the system or of the group increases. Moreover, even if such basis were available, rewriting the equations in an invariant polynomial basis seems impractical, so Hilbert basis computations appear not feasible beyond state space dimension of order ten. When our goal is to quotient continuous symmetries of high-dimensional flows, such as the Navier-Stokes flows, we need a more practical, workable framework. The method of moving frames of sect. 10.4 is one such minimalist alternative.

Résumé

The message: If a dynamical systems has a symmetry, use it! Here we have described how, and offered two approaches to continuous symmetry reduction. In the *method of slices* one fixes a ‘slice’ $(y - y')^T t' = 0$, a hyperplane normal to the group tangent t' that cuts across group orbits in the neighborhood of the slice-fixing point y' . Each class of symmetry-equivalent points is represented by a single point, with the symmetry-reduced dynamics in the reduced state space \mathcal{M}/G given by (10.47):

$$u = v - \dot{\theta} \cdot t, \quad \dot{\theta} = (v \cdot t') / (t \cdot t').$$

In practice one runs the dynamics in the full state space, and post-processes the trajectory by the method of moving frames. In the *Hilbert polynomial basis* approach one transforms the equivariant state space coordinates into invariant ones, by a nonlinear coordinate transformation

$$\{x_1, x_2, \dots, x_d\} \rightarrow \{u_1, u_2, \dots, u_m\},$$

and study the invariant ‘image’ of dynamics (10.51) rewritten in terms of invariant coordinates.

In practice, continuous symmetry reduction is considerably more involved than the discrete symmetry reduction to a fundamental domain of chapter 9. Slices are only local sections of group orbits, and Hilbert polynomials are non-unique and difficult to compute for high-dimensional flows. However, there is no need to actually recast the dynamics in the new coordinates: either approach can be used as a visualization tool, with all computations carried out in the original coordinates, and then, when done, projecting the solutions onto the symmetry reduced state space by post-processing the data. The trick is to construct a good set of symmetry invariant Poincaré sections (see sect. 3.1), and that is always a dark art, with or without a symmetry.

In sect. 2.1.1 we made an attempt to classify ‘all possible motions:’ (1) equilibria, (2) periodic orbits, (3) everything else. Now one can discern in the fog of dynamics an outline of a more serious classification - long time dynamics takes place on the closure of a set of all invariant compact sets preserved by the dynamics, and those are: (1) 0-dimensional equilibria \mathcal{M}_{EQ} , (2) 1-dimensional periodic orbits \mathcal{M}_p , (3) global symmetry induced N -dimensional relative equilibria \mathcal{M}_{TW} , (4) $(N+1)$ -dimensional relative periodic orbits \mathcal{M}_p , (5) terra incognita. We have some inklings of the ‘terra incognita:’ for example, symplectic symmetry induces existence of KAM-tori, and in general dynamical settings we encounter *partially hyperbolic invariant tori*, isolated tori that are consequences of dynamics, not of a global symmetry. They are harder to compute than anything we have attempted so far, as they cannot be represented by a single relative periodic orbit, but require a numerical computation of full $(N+1)$ -dimensional compact invariant sets and their infinite-dimensional linearized Jacobian matrices, marginal in $(N+1)$ dimensions, and hyperbolic in the rest.

We conclude with a few general observations: Higher dimensional dynamics requires study of compact invariant sets of higher dimension than 0-dimensional equilibria and 1-dimensional periodic orbits studied so far. We expect, for example, partially hyperbolic invariant tori to play important role. In this chapter we have focused on the simplest example of such compact invariant sets, where invariant tori are a robust consequence of a global continuous symmetry of the dynamics. The direct product structure of a global symmetry that commutes with the flow enables us to reduce the dynamics to a desymmetrized $(d-1-N)$ -dimensional reduced state space \mathcal{M}/G .

Relative equilibria and relative periodic orbits are the hallmark of systems with continuous symmetry. Amusingly, in this extension of ‘periodic orbit’ theory from unstable 1-dimensional closed periodic orbits to unstable $(N+1)$ -dimensional compact manifolds \mathcal{M}_p invariant under continuous symmetries, there are either no or proportionally few periodic orbits. In presence of a continuous symmetry, likelihood of finding a periodic orbit is *zero*. Relative periodic orbits are almost never eventually periodic, i.e., they almost never lie on periodic trajectories in the full state space, so looking for periodic orbits in systems with continuous symmetries is a fool’s errand.

However, dynamical systems are often equivariant under a combination of continuous symmetries and discrete coordinate transformations of chapter 9, for example the orthogonal group $O(n)$. In presence of discrete symmetries relative periodic orbits within discrete symmetry-invariant subspaces are eventually periodic. Atypical as they are (no generic chaotic orbit can ever enter these discrete invariant subspaces) they will be important for periodic orbit theory, as there the shortest orbits dominate, and they tend to be the most symmetric solutions.

chapter 21

Commentary

Remark 10.1 A brief history of relativity, or, ‘Desymmetrization and its discontents’ (after [Civilization and its discontents](#); continued from remark 9.1): The literature on symmetries in dynamical systems is immense, most of it deliriously unintelligible. Would it kill them to say ‘symmetry group of orbit \mathcal{M}_p ’ instead of carrying on about ‘isotropies, quotients, factors, normalizers, centralizers and stabilizers?’ For the dynamical systems applications at hand we need only basic results, on the level of any standard group theory textbook [2]. Chapter 2. of ref. [3] offers a pedagogical introduction to Lie groups of transformations, and Nakahara [4] to Lie derivatives and brackets. The presentation given here is in part based on Siminos thesis [29] and ref. [30]. The reader is referred to the monographs of Golubitsky and Stewart [42], Hoyle [44], Olver [45], Bredon [19], and Krupa [46] for more depth and rigor than would be wise to wade into here.

The relative equilibria and relative periodic solutions are related to equilibria and periodic solutions respectively of dynamics reduced by the symmetries. They appear in many physical situations, such as motion of rigid bodies, gravitational N -body problems, molecules, nonlinear waves, spiralling patterns and turbulence. According to Cushman, Bates [5] and Yoder [6], C. Huygens [7] understood the relative equilibria of a spherical pendulum many years before publishing them in 1673. A reduction of the translation symmetry was obtained by fixing the center of mass at the origin or, considering a configuration as an element of the disposition space $\mathbb{R}^D/(1, \dots, 1)\mathbb{R}$ by Jacobi. According to Chenciner [8, 10], the first attempt to find (relative) periodic solutions of the N -body problem by was the 1896 short note by Poincaré [9], in the context of the 3-body problem. Relative equilibria of the N -body problem (known in this context as the Lagrange points, stationary in the co-rotating frame) are circular motions in the inertial frame, and relative periodic orbits correspond to quasiperiodic motions in the inertial frame. Relative equilibria can exist in a rotating frame, and are called central configurations. For relative periodic orbits in celestial mechanics see also ref. [11]. Striking application of relative periodic orbits has been the discovery of “choreographies” of N -body problems [12, 13, 14].

The notion of a *moving frame* as a map from a manifold to a Lie group was introduced by Cartan [33], and the factorization (10.40) is stated (without reference) on p. 31 of Anosov and Arnol’d [34]. We follow Fels and Olver who view the method as an alternative to the Gröbner bases methods (here called ‘Hilbert bases’) to compute functionally independent fundamental invariant bases for general group actions, with no explicit connection to dynamics, differential equations or symmetry reduction. ‘Fundamental’ here means that they can be used to generate all other invariants. Olver’s monograph [45] is pedagogical, but does not describe the original Cartan’s method. Fels and Olver papers [40, 41] are lengthy and technical. They refer to Cartan’s method as method of ‘moving frames’ and view it as a special and less rigorous case of their ‘moving coframe’ method. The name ‘moving coframes’ arises through the use of Maurer-Cartan form which is a coframe on the Lie group G , i.e., they form a pointwise basis for the cotangent

space. In refs. [29, 30] the invariant bases generated by the moving frame method are used as a basis to project a full state space trajectory to the slice (i.e., the M/G reduced state space).

The basic idea of the ‘method of slices’ is intuitive; for example, it is stated without attribution as the problem 1. of Sect. 6.2 of Arnol’d *Ordinary Differential Equations* [32]. It is reinvented often,

HaMe98

Derivation of sect. 10.4.2 follows Rowley and Marsden [37] who, in the pattern recognition and ‘template fitting’ settings, call (10.46) the ‘reconstruction equation’ [36, 35].

For the definition of ‘slice’ see, for example, Chossat and Lauterbach [39]. Briefly, a submanifold $\mathcal{M}_{y'}$ containing y' is called a *slice* through y' if it is invariant under isotropy $G_{y'}(\mathcal{M}_{y'}) = \mathcal{M}_{y'}$. If y' is a fixed point of G , then slice is invariant under the whole group. The slice theorem is explained, for example, in [Encyclopaedia of Mathematics](#). Slices tend to be discussed in contexts much more difficult than our application - symplectic groups, sections in absence of global charts, non-compact Lie groups. We follow refs. [35] in referring to a local group-orbit section as a ‘slice.’ Refs. [19, 16] and others refer to global group-orbit sections as ‘cross-sections,’ a term that we rather avoid, as it already has a different and well established meaning in physics. Duistermaat and Kolk [15] refer to ‘slices,’ but the usage goes back at least to Guillemin and Sternberg [16] in 1984, Palais [18] in 1961 and Mastow [17] in 1957. Bredon [19] discusses both cross-sections and slices. Guillemin and Sternberg [16] define the ‘cross-section,’ but emphasize that finding it is very rare: “existence of a global section is a very stringent condition on a group action. The notion of ‘slice’ is weaker but has a much broader range of existence.”

The Gilmore and Lettelier monograph [21] offers a very clear, detailed and user friendly discussion of symmetry reduction by means of Hilbert polynomial bases (do not look for ‘Hilbert’ in the index, though). The determination of a Hilbert basis appears computationally prohibitive for state space dimensions larger than ten [38, 39], and rewriting the equations of motions in invariant polynomial bases appears impractical for high-dimensional flows.

Sect. 10.1.2 ‘Lie groups for cyclists’ is bit of a joke in more ways than one. First, ‘cyclist,’ ‘pedestrian’ throughout ChaosBook.org refer jokingly both to the title of Lipkin’s *Lie groups for pedestrians* [22] and to our preoccupations with [actual cycling](#). Lipkin’s ‘pedestrian’ is fluent in Quantum Field Theory, but wobbly on Dynkin diagrams. More to the point, it’s impossible to dispose of Lie groups in a page of text. As a counterdote to the 1-page summary of sect. 10.1.2, consider reading Gilmore’s monograph [20] which offers a quirky, personal and enjoyable distillation of a lifetime of pondering Lie groups. As seems to be the case with any textbook on Lie groups, it will not help you with the problem at hand, but it is the only place you can learn both what Galois actually did when he invented the theory of finite groups in 1830, and what, inspired by Galois, Lie actually did in his 1874 study of symmetries of ODEs. Gilmore also explains many things that we pass over in silence here, such as matrix groups, group manifolds, and compact groups.

Remark 10.2 Complex Lorenz equations (10.1) were introduced by Gibbon and McGuinness [24, 25] as a low-dimensional model of baroclinic instability in the atmosphere. They are a generalization of Lorenz equations (2.12). Ning and Haken [26] have shown that equations isomorphic to complex Lorenz equations also appear as a truncation of Maxwell-Bloch equations describing a single mode, detuned, ring laser. They set

$e + \rho_2 = 0$ so that a detuned equilibrium exists. Bakasov and Abraham [27] criticize this choice as being “degenerate” (the choice of Ning and Haken leads to non-generic bifurcations) and show that one can use complex Lorenz equations with $\rho_2 = 0$ and $e \neq 0$ to describe detuned lasers. Here we are not interested in the physical applications of these equations; rather, we study them as a simple example of a dynamical system with continuous (but no discrete) symmetries, with a view of testing methods of reducing the dynamics to a lower-dimensional reduced state space. Complex Lorenz flow examples and exercises in this chapter are based on E. Siminos thesis [29] and R. Wilczak project report [31].

(E. Siminos)

(E. Siminos and P. Cvitanović)



Exercises

10.1. **Visualizations of the 5-dimensional complex Lorenz flow:** Plot complex Lorenz flow projected on any three of the five $\{x_1, x_2, y_1, y_2, z\}$ axes. Experiment with different visualizations.

10.2. **An SO(2)-equivariant flow with two Fourier modes:** Complex Lorenz equations (10.1) of Gibbon and McGuinness [24] have a degenerate 4-dimensional subspace, with SO(2) acting only in its lowest non-trivial representation. Here is a possible model, still 5-dimensional, but with SO(2) acting in the two lowest representations. Such models arise as truncations of Fourier-basis representations of PDEs on periodic domains. In the complex form, the simplest such modification of complex Lorenz equations may be the “2-mode” system

$$\begin{aligned} \dot{x} &= -\sigma x + \sigma x^* y \\ \dot{y} &= (r - z)x^2 - ay \\ \dot{z} &= \frac{1}{2}(x^2 y^* + x^{*2} y) - bz, \end{aligned} \tag{10.53}$$

where $x, y, r = r_1 + ir_2, a = 1 + ie$ are complex and z, b, σ are real. Rewritten in terms of real variables $x = x_1 + ix_2, y = y_1 + iy_2$ this is a 5-dimensional first order ODE system

$$\begin{aligned} \dot{x}_1 &= -\sigma x_1 + \sigma y_1 \\ \dot{x}_2 &= -\sigma x_2 + \sigma y_2 \\ \dot{y}_1 &= (\rho_1 - z)x_1^2 - r_2 x_2 - y_1 - ey_2 \\ \dot{y}_2 &= \\ \dot{z} &= -bz + x_1 y_1 + x_2 y_2. \end{aligned} \tag{10.54}$$

Verify (10.54) by substituting $x = x_1 + ix_2, y = y_1 + iy_2, r = r_1 + ir_2, a = 1 + ie$ into the complex 2-mode equations (10.53).

10.3. **SO(2) rotations in a plane:** Show by exponentiation (10.7) that the SO(2) Lie algebra element \mathbf{T} generates rotation g in a plane,

$$\begin{aligned} g(\theta) &= e^{\mathbf{T}\theta} = \cos \theta \begin{pmatrix} 1 & 0 \\ 0 & 1 \end{pmatrix} + \sin \theta \begin{pmatrix} 0 & 1 \\ -1 & 0 \end{pmatrix} \\ &= \begin{pmatrix} \cos \theta & \sin \theta \\ -\sin \theta & \cos \theta \end{pmatrix}. \end{aligned} \tag{10.55}$$

10.4. **Invariance under fractional rotations.** Argue that if the isotropy group of the velocity field $v(x)$ is the discrete subgroup C_m of SO(2) rotations about an axis (let’s say the ‘z-axis’),

$$C^{1/m} v(x) = v(C^{1/m} x) = v(x), \quad (C^{1/m})^m = e,$$

the only non-zero components of Fourier-transformed equations of motion are a_{jm} for $j = 1, 2, \dots$. Argue that the Fourier representation is then the quotient map of the dynamics, \mathcal{M}/C_m . (Hint: this sounds much fancier than what is - think first of how it applies to the Lorenz system and the 3-disk pinball.)

10.5. **U(1) equivariance of complex Lorenz equations for finite angles:** Show that the vector field in complex Lorenz equations (10.1) is equivariant under the unitary group U(1) acting on $\mathbb{R}^5 \cong \mathbb{C}^2 \times \mathbb{R}$ by

$$g(\theta)(x, y, z) = (e^{i\theta} x, e^{i\theta} y, z), \quad \theta \in [0, 2\pi]. \tag{10.56}$$

(E. Siminos)

10.6. **SO(2) equivariance of complex Lorenz equations for finite angles:** Show that complex Lorenz equations (10.2) are equivariant under rotation for finite angles.

10.7. **Stability matrix of complex Lorenz flow:** Compute the stability matrix (10.26) for complex Lorenz equations (10.2).


10.8. **Rotational equivariance, infinitesimal angles.** Show that complex Lorenz equations are equivariant under infinitesimal SO(2) rotations.

10.9. **Discover the equivariance of a given flow:**



Suppose you were given complex Lorenz equations, but nobody told you they are SO(2) equivariant. More generally, you might encounter a flow without realizing that it has a continuous symmetry - how would you discover it?

10.10. **Equilibria of complex Lorenz equations:** Find all equilibria of complex Lorenz equations. Hint: Equilibria come either in the fixed Fix (G) subspace, or on a group orbit.

10.11. **Equilibria of complex Lorenz equations:**  In exercise 10.10 we found only one equilibrium of complex Lorenz equations. The Ning and Haken [26] version of complex Lorenz equations (a truncation of Maxwell-Bloch equations describing a single mode ring laser) sets $e + \rho_2 = 0$ so that a detuned equilibrium exists. Test your routines on 2 cases: (a) $e = 0, \rho_2 = 0$. As discussed by Siminos [29], reality of parameters a, ρ in (10.1) implies existence of a discrete C_2 symmetry. (b) $e + \rho_2 = 0, e \neq 0$. You might want to compare results with those of Ning and Haken.

10.12. **Complex Lorenz equations in polar coordinates.** Rewrite complex Lorenz equations from Cartesian to polar coordinates, using $(x_1, x_2, y_1, y_2, z) =$

$$(r_1 \cos \theta_1, r_1 \sin \theta_1, r_2 \cos \theta_2, r_2 \sin \theta_2, z), \quad (10.57)$$

where $r_1 \geq 0, r_2 \geq 0$. Show that in polar coordinates the equations take form

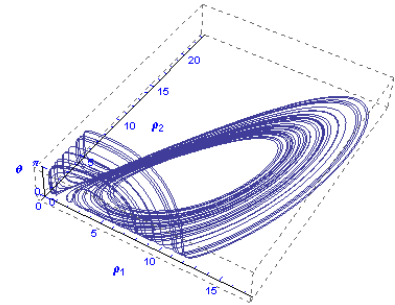
$$\begin{pmatrix} \dot{r}_1 \\ \dot{\theta}_1 \\ \dot{r}_2 \\ \dot{\theta}_2 \\ \dot{z} \end{pmatrix} = \begin{pmatrix} -\sigma(r_1 - r_2 \cos \theta) \\ -\sigma \frac{r_2}{r_1} \sin \theta \\ -r_2 + r_1((\rho_1 - z) \cos \theta - \rho_2 \sin \theta) \\ e + \frac{r_1}{r_2}((\rho_1 - z) \sin \theta + \rho_2 \cos \theta) \\ -bz + r_1 r_2 \cos \theta \end{pmatrix},$$

We know from classical mechanics that for translationally or rotationally invariant flows the relative distance is invariant (that is why one speaks of ‘relative’ equilibria), hence we introduce a variable $\theta = \theta_1 - \theta_2$. θ_1 and θ_2 change in time, but at the relative equilibria the difference between them is constant. Show that this new

variable allows us to rewrite the complex Lorenz equations as 4 coupled polar coordinates equations:

$$\begin{pmatrix} \dot{r}_1 \\ \dot{r}_2 \\ \dot{\theta} \\ \dot{z} \end{pmatrix} = \begin{pmatrix} -\sigma(r_1 - r_2 \cos \theta) \\ -r_2 + (\rho_1 - z)r_1 \cos \theta \\ -e - \left(\sigma \frac{r_2}{r_1} + (\rho_1 - z) \frac{r_1}{r_2}\right) \sin \theta \\ -bz + r_1 r_2 \cos \theta \end{pmatrix} \quad (10.58)$$

where we have set $\rho_2 = 0$. Plot a long-time solution of these equations and show that the polar representation introduces singularities into what initially was a smooth flow:



We shall encounter the same problem in implementing the $x_1 = 0$ moving frames slice). A polar coordinates $\{r_1, r_2, \theta\}$ plot of the complex Lorenz flow strange attractor. θ is very small until the trajectory approaches either $r_1 \rightarrow 0$ or $r_2 \rightarrow 0$, where Mathematica continues through the singularity by a rapid change of θ by π . The the fixed Fix (G) subspace $(r_1, r_2, \theta, z) = (0, 0, \theta, z)$ separates the two folds of the attractor.

10.13. **Visualizations of the complex Lorenz flow in polar coordinates:** Plot complex Lorenz flow projected on any three of the $\{r_1, r_2, \theta, z\}$ coordinates. Experiment with different visualizations. The flow (10.58) is singular as $r_j \rightarrow 0$, with angle θ_j going through a rapid change there: is that a problem? Does it make sense to insist on $r_1 \geq 0, r_2 \geq 0$, or should one let them have either sign in order that the θ trajectory be continuous?

10.14. **Computing the relative equilibrium TW_1 :** Find the relative equilibria of the complex Lorenz equations by finding the equilibria of the system in polar coordinates (10.58). Show that

(a) The relative equilibrium (hereafter referred to [29] as TW_1) is given by

$$(r_1, r_2, \theta, z) = \left(\sqrt{b(\rho_1 - d)}, \sqrt{bd(\rho_1 - d)}, \cos^{-1}(1/\sqrt{d}), \rho_1 - d \right), \quad (10.59)$$

where $d = 1 + e^2/(\sigma + 1)^2$,

- (b) The angular velocity of relative equilibrium TW_1 is

$$\dot{\theta}_i = \sigma e / (\sigma + 1), \tag{10.60}$$

with the period $T_{TW_1} = 2\pi(\sigma + 1)/\sigma e$.

- 10.15. **Relative equilibrium TW_1 in polar coordinates:** Plot the equilibrium TW_1 in polar coordinates.
- 10.16. **Relative equilibrium TW_1 in Cartesian coordinates:** Show that for our parameter values,

$$\begin{aligned} x_{TW_1} &= (x_1, x_2, y_1, y_2, z) \\ &= (8.4849, 0.077135, 8.4856, 0, 26.999), \end{aligned} \tag{10.61}$$

is a point on the TW_1 orbit. Plot the relative equilibrium TW_1 in Cartesian coordinates.

- 10.17. **Eigenvalues and eigenvectors of TW_1 stability matrix:** Compute the eigenvalues and eigenvectors of the stability matrix (10.26) evaluated at TW_1 and using the (10.2) parameter values, in (a) Cartesian coordinates, (b) polar coordinates.

- 10.18. **The eigen-system of TW_1 stability matrix in polar coordinates:** Plot the eigenvectors of A at TW_1 in polar coordinates, as well as the complex Lorenz flow at values very near TW_1 .

- 10.19. **Eigenvalues and eigenvectors of EQ_0 stability matrix:** Find the eigenvalues and the eigenvectors of the stability matrix A (10.26) at $EQ_0 = (0, 0, 0, 0, 0)$ determined in exercise 10.10. ChaosBook convention is to order eigenvalues from most positive (unstable) to the most negative. Follow that. Replace complex eigenvectors by the real, imaginary parts, as that is what you actually use.

- 10.20. **The eigen-system of the stability matrix at EQ_0 :** Plot the eigenvectors of A at EQ_0 and the complex Lorenz flow at values very close to EQ_0 .

- 10.21. **SO(2) or harmonic oscillator slice:** Construct a moving frame slice for action of SO(2) on \mathbb{R}^2

$$(x, y) \mapsto (x \cos \theta - y \sin \theta, x \sin \theta + y \cos \theta)$$

by, for instance, the positive y axis: $x = 0, y > 0$. Write out explicitly the group transformations that bring any point back to the slice. What invariant is preserved by this construction? (E. Siminos)

- 10.22. **State space reduction by a slice, finite time segments:** Replace integration of the complex Lorenz equations by a sequence of finite time steps, each followed by a rotation such that the next segment initial point is in the slice $y_2 = 0, y_1 > 0$.

- 10.23. **State space reduction by a slice, ODE formulation:** Reconsider (10.22) in the sequence of infinitesimal time steps limit, each followed by an infinitesimal rotation such that the next segment initial point is in the slice $y_2 = 0, y_1 > 0$. Derive the corresponding $4d$ reduced state space ODE for the complex Lorenz flow. Here is a way to do it, bit different from the derivation given in sect. 10.4.2.

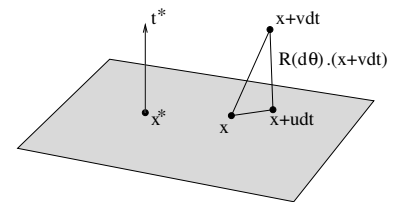
Infinitesimal time version of the moving frames symmetry reduction is attained by taking small time steps in figure 10.11 and dropping the higher order terms. For infinitesimal $d\theta$ we set $\sin d\theta \approx d\theta, \cos d\theta \approx 1, g(d\theta) \approx 1 + d\theta \mathbf{T}$, and the condition (10.41) for rotating an infinitesimal time evolution step $dx = v dt$ back into the slice

$$\begin{aligned} 0 &= (y + dx) \cdot g(d\theta)^T \mathbf{T}y' \\ &\approx (y + dt v) \cdot (1 + d\theta \mathbf{T})^T \mathbf{T}y' \\ &\approx dt v \cdot \mathbf{T}y' + d\theta y \cdot \mathbf{T}^T \mathbf{T}y' \end{aligned}$$

yields

$$d\theta \approx -\frac{v \cdot \mathbf{T}y'}{y \cdot \mathbf{T}^T \mathbf{T}y'} dt. \tag{10.62}$$

Let $u(y)$ be the vector field that generates the flow in the reduced state space. According to



in the limit that $g(d\theta) \approx 1 + d\theta \mathbf{T}$ the infinitesimal time step under u is connected to the time step under v by

$$y + u dt = (1 + d\theta \mathbf{T}) \cdot (y + v dt).$$

Dropping second order terms, dividing through with dt

$$u = v + \frac{d\theta}{dt} \mathbf{T}y,$$

and substituting (10.62) gives the reduced state space equations (10.47):

$$\dot{x} = v - \frac{(v \cdot \mathbf{T}y')}{(y \cdot y')_4} \mathbf{T}y, \tag{10.63}$$

where we have used the fact that $-x \cdot \mathbf{T} \mathbf{T}x^* = (x \cdot x^*)_4 = x_1 x_1^* + x_2 x_2^* + y_1 y_1^* + y_2 y_2^*$ is the dot-product restricted to the 4-dimensional representation of SO(2). By construction, the motion stays in the $(d-1)$ -dimensional slice.

- 10.24. **Accumulated phase shift:** Derive the $1d$ equation (10.46) for the accumulated phase shift θ associated with the 4-dimensional reduced state space ODE of exercise 10.23.

- 10.25. **The moving frame flow stays in the reduced state space:** Show that the flow (10.63) stays in a $(d-1)$ -dimensional slice.
- 10.26. **State space reduction by a relative equilibrium TW_1 cross-section:** Replace integration of the complex Lorenz equations by a sequence of short time steps, each followed by a rotation such that the next segment initial

point is in the relative equilibrium TW_1 cross-section

$$(y - y_{TW_1}) \cdot t_{TW_1} = 0, \quad t_{TW_1} = \mathbf{T}y_{TW_1}, \quad (10.64)$$

where for any x , $y = g(\theta) \cdot x$ is the rotation that lies in the cross-section. Check figure 10.12 by long-time integration of (10.63).

References

- [10.1] P. Cvitanović, R. L. Davidchack and E. Siminos, “State space geometry of a spatio-temporally chaotic Kuramoto-Sivashinsky flow,” *SIAM J. Applied Dynam. Systems* (2009); [arXiv:0709.2944](https://arxiv.org/abs/0709.2944).
- [10.2] M. Hamermesh, *Group theory and its application to physical problems* (Addison-Wesley, Reading, 1962).
- [10.3] G. W. Bluman and S. Kumei, *Symmetries and differential equations* (Springer, New York 1989).
- [10.4] M. Nakahara, *Geometry, topology and physics* (Inst. of Physics Publ., Bristol, 1990).
- [10.5] R. H. Cushman and L. M. Bates, *Global aspects of classical integrable systems*, p. 402 (Birkhäuser, Basel 1997).
- [10.6] J. G. Yoder, *Unrolling time: Christiaan Huygens and the mathematization of nature* (Cambridge Univ. Press, Cambridge 1988).
- [10.7] C. Huygens, *L’Horloge à pendule* (Swets & Zeitlinger, Amsterdam 1673, 1967).
- [10.8] A. Albouy and A. Chenciner, “Le problème des n corps et les distances mutuelles,” *Invent. Math.* **31**, 151 (1998).
- [10.9] H. Poincaré, “Sur les solutions périodiques et le principe de moindre action,” *C.R.A.S.* **123**, 915 (1896).
- [10.10] A. Chenciner, “Symmetries and ‘simple’ solutions of the classical N -body problem,” in *Proceedings ICMP03* (2003).
- [10.11] R. Broucke, “On relative periodic solutions of the planar general three-body problem,” *Celestial Mechanics and Dynamical Astronomy* **12**, 439 (1975).
- [10.12] A. Chenciner and R. Montgomery, “A remarkable solution of the 3-body problem in the case of equal masses,” *Ann. Math.* **152**, 881 (2000).
- [10.13] A. Chenciner, J. Gerver, R. Montgomery and C. Simó, “Simple choreographic motions of N -bodies: A preliminary study,” pp. 287-308 in P. Newton, P. Holmes and A. Weinstein, eds., *Geometry, mechanics and dynamics* (Springer, New York 2002).

- [10.14] C. McCord, J. Montaldi, M. Roberts and L. Sbano, “Relative periodic orbits of symmetric Lagrangian systems,” pp. 482-493, in Freddy Dumortier and et.al., eds., *Proceedings of Equadiff 2003* (2004).
- [10.15] J. J. Duistermaat and J. A. C. Kolk, *Lie groups* (Springer, New York 2000).
- [10.16] V. Guillemin and S. Sternberg, *Symplectic techniques in physics* (Cambridge Univ. Press, Cambridge 1990).
- [10.17] G. D. Mostow, “Equivariant embeddings in Euclidean space,” *Ann. Math.* **65**, 432 (1957).
- [10.18] R. S. Palais, “On the existence of slices for actions of non-compact Lie groups,” *Ann. Math.* **73**, 295 (1961).
- [10.19] G. Bredon, *Introduction to compact transformation groups*, (Academic Press, New York 1972).
- [10.20] R. Gilmore, *Lie groups, physics, and geometry* (Cambridge Univ. Press, Cambridge 2008).
- [10.21] R. Gilmore and C. Letellier, *The symmetry of chaos* (Oxford U. Press, Oxford 2007).
- [10.22] H. J. Lipkin, *Lie groups for pedestrians* (North-Holland, Amsterdam 1966).
- [10.23] T. Hawkins, *Emergence of the theory of Lie groups: An essay in the history of mathematics, 1869-1926* (Springer, New York 2000).
- [10.24] J. Gibbon and M. McGuinness, “The real and complex Lorenz equations in rotating fluids and lasers,” *Physica D* **5**, 108 (1982).
- [10.25] A. Fowler, J. Gibbon and M. McGuinness, “The complex Lorenz equations,” *Physica D* **4**, 139 (1982).
- [10.26] C.-z. Ning and H. Haken, “Detuned lasers and the complex Lorenz equations: Subcritical and supercritical Hopf bifurcations,” *Phys. Rev.* **41**, 3826 (1990).
- [10.27] A. A. Bakasov and N. B. Abraham, “Laser second threshold: Its exact analytical dependence on detuning and relaxation rates,” *Phys. Rev. A* **48**, 1633 (1993).
- [10.28] N. B. Abraham, U. A. Allen, E. Peterson, A. Vicens, R. Vilaseca, V. Espinosa and G. L. Lippi, “Structural similarities and differences among attractors and their intensity maps in the laser-Lorenz model,” *Optics Comm.* **117**, 367 (1995).
- [10.29] E. Siminos, *Recurrent spatio-temporal structures in presence of continuous symmetries*, Ph.D. thesis (Georgia Inst. of Tech. 2009);
ChaosBook.org/projects/theses.html.

- [10.30] E. Siminos and P. Cvitanović, “Continuous symmetry reduction and return maps for high dimensional flows,” *Physica D*, (2010).
- [10.31] R. Wilczak, *Reducing the state-space of the complex Lorenz flow*, NSF REU summer 2009 project, U. of Chicago (2009); ChaosBook.org/projects/Wilczak/blog.pdf.
- [10.32] V.I. Arnol’d, *Ordinary differential equations* (Springer-Verlag, New York 1992).
- [10.33] É. Cartan, “La méthode du repère mobile, la théorie des groupes continus, et les espaces généralisés,” *Exposés de Géométrie* **5** (1935).
- [10.34] D. V. Anosov and V. I. Arnol’d, *Dynamical systems I: Ordinary Differential Equations and Smooth Dynamical Systems* (Springer, 1988).
- [10.35] C. W. Rowley and J. E. Marsden, “Reconstruction equations and the Karhunen-Loève expansion for systems with symmetry,” *Physica D* **142**, 1 (2000).
- [10.36] J. E. Marsden and T. S. Ratiu, *Introduction to mechanics and symmetry* (Springer, New York, 1994).
- [10.37] C. W. Rowley, I. G. Kevrekidis, J. E. Marsden and K. Lust, “Reduction and reconstruction for self-similar dynamical systems,” *Nonlinearity* **16**, 1257 (2003).
- [10.38] K. Gatermann, *Computer algebra methods for equivariant dynamical systems* (Springer-Verlag, New York 2000).
- [10.39] P. Chossat and R. Lauterbach, *Methods in equivariant bifurcations and dynamical systems* (World Scientific, Singapore 2000).
- [10.40] M. Fels and P. J. Olver, “Moving coframes: I. a practical algorithm,” *Acta Appl. Math.* **51**, 161 (1998).
- [10.41] M. Fels and P. J. Olver, “Moving coframes: II. regularization and theoretical foundations,” *Acta Appl. Math.* **55**, 127 (1999).
- [10.42] M. Golubitsky and I. Stewart, *The symmetry perspective* (Birkhäuser, Boston 2002).
- [10.43] M. Golubitsky, I. Stewart and D. G. Schaeffer, *Singularities and groups in bifurcation theory, vol. II* (Springer-Verlag, New York 1988).
- [10.44] R. Hoyle, *Pattern formation: An introduction to methods* (Cambridge Univ. Press, Cambridge 2006).
- [10.45] P. J. Olver, *Classical invariant theory* (Cambridge Univ. Press, Cambridge 1999).
- [10.46] M. Krupa, “Bifurcations of relative equilibria,” *SIAM J. Math. Anal.* **21**, 1453 (1990).
- [10.47] D. Viswanath, “Recurrent motions within plane Couette turbulence,” *J. Fluid Mech.* **580**, 339 (2007); [arXiv:physics/0604062](https://arxiv.org/abs/physics/0604062).

Chapter 11

Charting the state space

The classification of the constituents of a chaos, nothing less is here essayed.

—Herman Melville, *Moby Dick*, chapter 32

IN THIS CHAPTER and the next we learn how to *partition* state space in a topologically invariant way, and *name* topologically distinct orbits.

We start in sect. 11.1 with a simple and intuitive example, a 3-disk game of pinball. The qualitative dynamics of stretching/shrinking strips of surviving state space regions enables us to partition the state space and assign *symbolic dynamics* itineraries to trajectories. For the 3-disk game of pinball all possible symbol sequences enumerate all possible orbits.

In sect. 11.2 we use Rössler and Lorenz flows to motivate modeling of higher-dimensional flows by iteration of 1-dimensional maps. For these two flows the 1-dimensional maps capture essentially all of the higher-dimensional flow dynamics, both qualitatively and quantitatively. 1-dimensional maps suffice to explain the two key aspects of qualitative dynamics; *temporal ordering*, or *itinerary* with which a trajectory visits state space regions (sect. 11.3), and the *spatial ordering* between trajectory points (sect. 11.4), which is the key to determining the admissibility of an orbit with a prescribed itinerary. In a generic dynamical system not every symbol sequence is realized as a dynamical trajectory; as one looks further and further, one discovers more and more ‘pruning’ rules which prohibit families of itineraries. For 1-dimensional ‘stretch & fold’ maps the *kneading theory* (sect. 11.5) provides the definitive answer as to which temporal itineraries are *admissible* as trajectories of the dynamical system. Finally, sect. 11.6 is meant serve as a guide to the basic concepts of symbolic dynamics.

Deceptively simple, this subject can get very difficult very quickly, so in this chapter we do the first, 1-dimensional pass at a pedestrian level, postponing the discussion of higher-dimensional, cyclist level issues to chapter 12.

Even though by inclination you might only care about the serious stuff, like

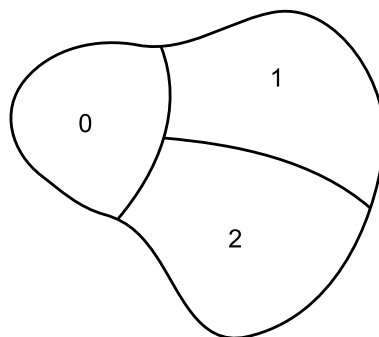


Figure 11.1: A coarse partition of M into regions M_0 , M_1 , and M_2 , labeled by ternary alphabet $\mathcal{A} = \{1, 2, 3\}$.

Rydberg atoms or mesoscopic devices, and resent wasting time on formal things, this chapter and chapters 14 and 15 are good for you. Study them.

11.1 Qualitative dynamics



(R. Mainieri and P. Cvitanović)

What can a flow do to points in state space? This is a very difficult question to answer because we have assumed very little about the evolution function f ; continuity, and differentiability a sufficient number of times. Trying to make sense of this question is one of the basic concerns in the study of dynamical systems. The first answer was inspired by the motion of the planets: they appear to repeat their motion through the firmament, so the ancients' attempts to describe dynamical systems were to think of them as periodic.

However, periodicity is almost never quite exact. What one tends to observe is *recurrence*. A recurrence of a point x_0 of a dynamical system is a return of that point to a neighborhood of where it started. How close the point x_0 must return is up to us: we can choose a volume of any size and shape, and call it the neighborhood M_0 , as long as it encloses x_0 . For chaotic dynamical systems, the evolution might bring the point back to the starting neighborhood infinitely often. That is, the set

$$\{y \in M_0 : y = f^t(x_0), \quad t > t_0\} \quad (11.1)$$

will in general have an infinity of recurrent episodes.

To observe a recurrence we must look at neighborhoods of points. This suggests another way of describing how points move in state space, the important first step on the way to a theory of dynamical systems: qualitative, topological dynamics, or *symbolic dynamics*. As the subject can get quite technical, a summary of the basic notions and definitions of symbolic dynamics is relegated to sect. 11.6; check that section and references cited in remark 11.1 whenever you run into baffling jargon.

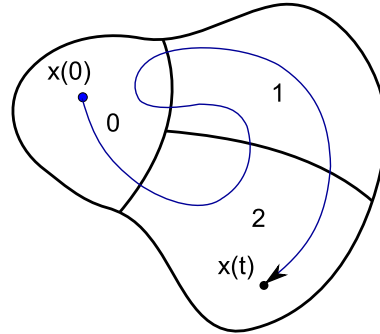


Figure 11.2: A trajectory with itinerary 021012.

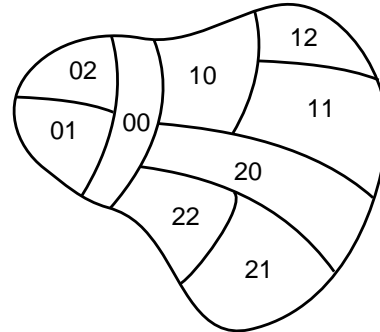


Figure 11.3: A 1-step memory refinement of the partition of figure 11.1, with each region M_i subdivided into M_{i_0} , M_{i_1} , and M_{i_2} , labeled by nine ‘words’ $\{00, 01, 02, \dots, 21, 22\}$.

We start by dividing the state space up into regions M_A, M_B, \dots, M_Z , as in figure 11.1. This can be done in many ways, not all equally clever. Any such division of state space into distinct regions constitutes a *partition*, and we associate with each region (sometimes referred to as a *state*) a symbol s from an N -letter *alphabet* or *state set* $\mathcal{A} = \{A, B, C, \dots, Z\}$. As the state evolves, different regions will be visited. The visitation sequence - forthwith referred to as the *itinerary* - can be represented by the letters of the alphabet \mathcal{A} . If, as in the example sketched in figure 11.2, the state space is divided into three regions M_0, M_1 , and M_2 , the ‘letters’ are the integers $\{0, 1, 2\}$, and the itinerary for the trajectory sketched in the figure is $0 \mapsto 2 \mapsto 1 \mapsto 0 \mapsto 1 \mapsto 2 \mapsto \dots$.

Example 11.1 3-disk symbolic dynamics: Consider the motion of a free point particle in a plane with 3 elastically reflecting convex disks, figure 11.4. After a collision with a disk a particle either continues to another disk or escapes, so a trajectory can be labeled by the disk sequence. Sets of configuration space pinball trajectories of figure 11.4 become quickly hard to disentangle. As we shall see in what follows, their state space visualization in terms of Poincaré sections $\mathcal{P} = [s, p]$ (figure 11.5, see also figure 3.4) is much more powerful. (continued in example 11.2) exercise 1.1

In general only a subset of points in M_B reaches M_A . This observation offers a systematic way to refine a partition by introducing *m-step memory*: the region $M_{s_m \dots s_1 s_0}$ consists of the subset of points of M_{s_0} whose trajectory for the next m time steps will be $s_0 \mapsto s_1 \mapsto \dots \mapsto s_m$, see figure 11.3.

Example 11.2 3-disk state space partition: (continued from example 11.1) At each bounce a cone of initially nearby trajectories defocuses (see figures 1.8 and 11.4), and in order to attain a desired longer and longer itinerary of bounces the strip of initial

Figure 11.4: Two pinballs that start out very close to each other exhibit the same qualitative dynamics $_2313_$ for the first three bounces, but due to the exponentially growing separation of trajectories with time, follow different itineraries thereafter: one escapes after $_2313_$, the other one escapes after $_23132321_$. (Notation $_2313_$ is explained in sect. 11.6.)

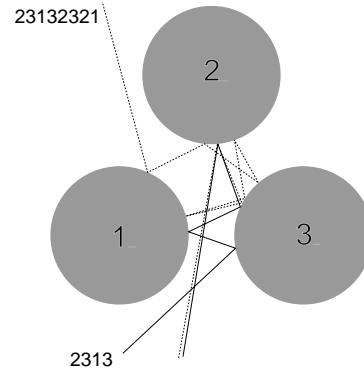
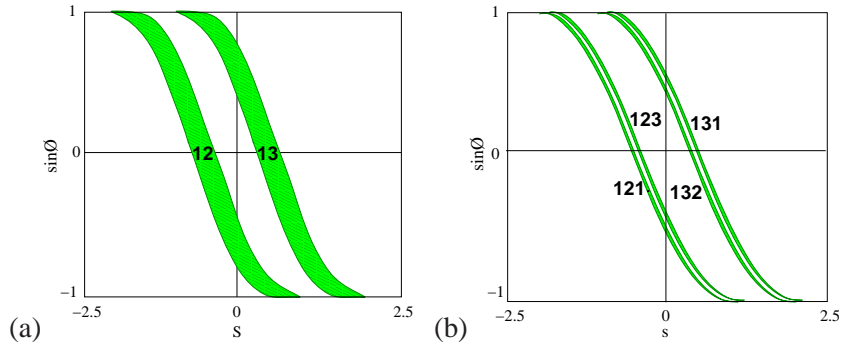


Figure 11.5: The 3-disk game of pinball Poincaré section, trajectories emanating from the disk 1 with $x = (\text{arclength, parallel momentum}) = (s, p)$, where $p = \sin \theta$. (a) Strips of initial points \mathcal{M}_{12} , \mathcal{M}_{13} which reach disks 2, 3 in one bounce, respectively. (b) 1-step memory refinement of partition (see figure 11.3): strips of initial points \mathcal{M}_{121} , \mathcal{M}_{131} , \mathcal{M}_{132} and \mathcal{M}_{123} which reach disks 1, 2, 3 in two bounces, respectively. Disk radius : center separation ratio $a:R = 1:2.5$. (Y. Lan)



points $x_0 = (s_0, p_0)$ has to be specified with exponentially finer precision, nested within the initial state space strips drawn in figure 11.5. (continued in example 12.2)

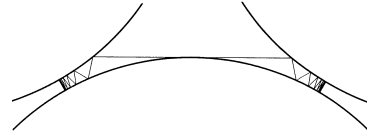
If there is no way to reach partition \mathcal{M}_i from partition \mathcal{M}_j , and conversely, partition \mathcal{M}_j from partition \mathcal{M}_i , the state space consists of at least two disconnected pieces, and we can analyze it piece by piece. An interesting partition should be dynamically connected, i.e., one should be able to go from any region \mathcal{M}_i to any other region \mathcal{M}_j in a finite number of steps. A dynamical system with such a partition is said to be *metrically indecomposable*.

In general one also encounters transient regions - regions to which the dynamics does not return to once they are exited. Hence we have to distinguish between (uninteresting to us) wandering trajectories that never return to the initial neighborhood, and the non-wandering set (2.2) of the *recurrent* trajectories.

However, knowing that a point from \mathcal{M}_i reaches $\{\mathcal{M}_j, \dots, \mathcal{M}_k\}$ in one step is not quite good enough. We would be happier if we knew that the map of the entire initial region $f(\mathcal{M}_i)$ overlaps nicely with the entire \mathcal{M}_j ; otherwise we have to subpartition \mathcal{M}_j into the subset $f(\mathcal{M}_i)$ and the remainder, and often we will find ourselves partitioning *ad infinitum*, a difficult topic that we shall return to sect. 12.4.

Such considerations motivate the notion of a *Markov partition*, a partition for which no memory of preceding steps is required to fix the transitions allowed in the next step. *Finite Markov partitions* can be generated by *expanding d*-dimensional iterated mappings $f : \mathcal{M} \rightarrow \mathcal{M}$, if \mathcal{M} can be divided into N regions

Figure 11.6: For the 3-disk game of pinball no itineraries are pruned as long as the inter-disk spacing exceeds $R : a > 2.04821419\dots$ (from K.T. Hansen [20])



$\{\mathcal{M}_0, \mathcal{M}_1, \dots, \mathcal{M}_{N-1}\}$ such that in one step points from an initial region \mathcal{M}_i either fully cover a region \mathcal{M}_j , or miss it altogether,

$$\text{either } \mathcal{M}_j \cap f(\mathcal{M}_i) = \emptyset \text{ or } \mathcal{M}_j \subset f(\mathcal{M}_i). \tag{11.2}$$

Whether such partitions can be found is not clear at all - the borders need to be lower-dimensional sets invariant under dynamics, and there is no guarantee that these are topologically simple objects. However, the game of pinball (and many other non-wandering repeller sets) is especially nice: the issue of determining the partition borders does not arise, as the survivors live on disconnected pieces of the state space, separated by a chasm of escaping trajectories.

The itinerary of a billiard trajectory is finite for a scattering trajectory, coming in from infinity and escaping after a finite number of collisions, infinite for a trapped trajectory, and infinitely repeating for a periodic orbit. A finite length trajectory is not uniquely specified by its finite itinerary, but an isolated unstable cycle is: its itinerary is an infinitely repeating block of symbols. For hyperbolic flows the intersection of the future and past itineraries, the bi-infinite itinerary $S^-.S^+ = \dots s_{-2}s_{-1}s_0.s_1s_2s_3\dots$ specifies a unique orbit. Almost all infinite length trajectories (orbits) are aperiodic. Still, the longer the trajectory is, the closer to it is a periodic orbit whose itinerary shadows the trajectory for its whole length: think of the state space as the unit interval, aperiodic orbits as normal numbers, and periodic ones as fractions whose denominators correspond to cycle periods, as is literally the case for the Farey map (20.31).

Determining whether the symbolic dynamics is complete (as is the case for sufficiently separated disks, see figure 11.6), pruned (for example, for touching or overlapping disks), or only a first coarse-graining of the topology (as, for example, for smooth potentials with islands of stability) requires a case-by-case investigation, a discussion we postpone until sect. 11.5 and chapter 12. For now we assume that the disks are sufficiently separated that there is no additional pruning beyond the prohibition of self-bounces.

Inspecting figure 11.5 we see that the relative ordering of regions with differing finite itineraries is a qualitative, topological property of the flow. This observation motivates searches for simple, ‘canonical’ partitions which exhibit in a simple manner the spatial ordering common to entire classes of topologically similar nonlinear flows.

11.2 From d -dimensional flows to 1-dimensional maps

Symbolic dynamics for the 3-disk game of pinball is so straightforward that one may altogether fail to see the connection between the topology of hyperbolic flows and their symbolic dynamics. This is brought out more clearly by the 1-dimensional visualization of ‘stretch & fold’ flows to which we turn now.

We construct here the return maps (3.4) for two iconic flows, the Rössler and the Lorenz, in order to show how ODEs in higher dimensions can be modeled by low-dimensional maps. In the examples at hand the strong dissipation happens to render the dynamics essentially 1-dimensional, both qualitatively and quantitatively. However, as we shall show in chapter 12, strong dissipation is not essential -the hyperbolicity is- so the method applies to Hamiltonian (symplectic areas preserving) flows as well. The key idea is to replace the original, arbitrarily concocted coordinates by intrinsic, dynamically invariant curvilinear coordinates erected on neighborhoods of unstable manifolds.



fast track:
sect. 11.3, p. 207

Suppose concentrations of certain chemical reactants worry you, or the variations in the Chicago temperature, humidity, pressure and winds affect your mood. Such quantities vary within some fixed range, and so do their rates of change. Even if we are studying an open system such as the 3-disk pinball game, we tend to be interested in a finite region around the disks and ignore the escapees. So a typical dynamical system that we care about is *bounded*. If the price to keep going is high - for example, we try to stir up some tar, and observe it come to a dead stop the moment we cease our labors - the dynamics tends to settle into a simple state. However, as the resistance to change decreases - the tar is heated up and we are more vigorous in our stirring - the dynamics becomes unstable.

Example 11.3 Rössler attractor return map: Stretch & fold. (continued from example 4.6) In the Rössler flow (2.17) of example 3.4 we sketched the attractor by running a long chaotic trajectory, and noted that the attractor of figure 3.5 is very thin. For Rössler flow an interval transverse to the attractor is stretched, folded and fiercely pressed back. The attractor is ‘fractal,’ but for all practical purposes the return map is 1-dimensional; your printer will need a resolution better than 10^{13} dots per inch to start resolving its structure. We had attempted to describe this ‘stretch & fold’ flow by a 1-dimensional return map, but the maps that we plotted in figure 3.6 were disquieting; they did not appear to be a 1-to-1 maps. This apparent non-invertibility is an artifact of projection of a 2 – dimensional return map $(R_n, z_n) \rightarrow (R_{n+1}, z_{n+1})$ onto the 1-dimensional subspace $R_n \rightarrow R_{n+1}$. Now that we understand equilibria and their linear stability, let’s do this right.

The key idea is to measure arclength distances along the unstable manifold of the x_- equilibrium point, as in figure 11.7 (a). Luck is with us; figure 11.7 (b) return map $s_{n+1} = P(s_n)$ looks much like a parabola of example 3.9, so we shall take the unimodal map symbolic dynamics, sect. 11.3, as our guess for the covering symbolic dynamics. (continued in example 11.11)

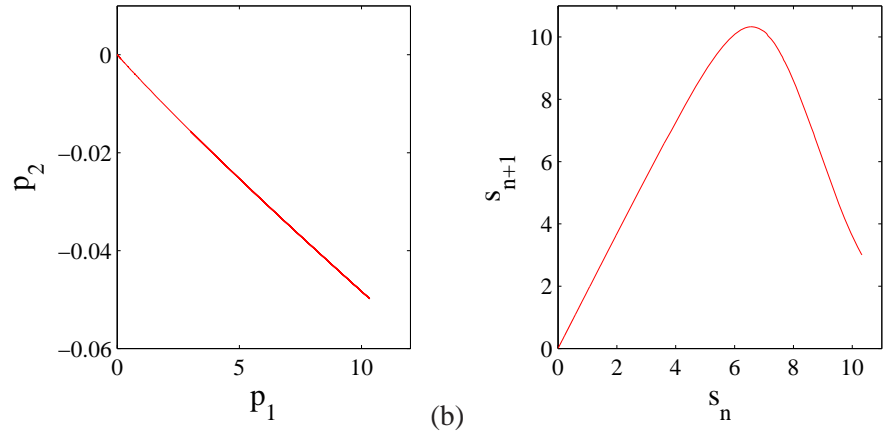


Figure 11.7: (a) $x = 0, y > 0$ Poincaré section of the x_- unstable manifold, Rössler flow figure 2.6. (p_1, p_2) are measured with the origin placed at x_- . (b) $s \rightarrow P(s)$ return map, where s is the arc-length distance measured along the unstable manifold of equilibrium point x_- . (A. Basu and J. Newman)

You get the idea - Rössler flow winds around the stable manifold of the ‘central’ equilibrium, stretches and folds, and the dynamics on the Poincaré section of the flow can be reduced to a 1-dimensional map. The next example is similar, but the folding mechanism is very different: the unstable manifold of one of the equilibria collides with the stable manifold of the other one, forcing a robust *heteroclinic connection* between the two.



fast track:
sect. 11.3, p. 207

11.2.1 Heteroclinic connections

In general, two manifolds can intersect in a stable way if the sum of their dimensions is greater than or equal to the dimension of the state space, hence an unstable manifold of dimension k is likely to intersect a stable manifold whose codimension in state space is less than or equal to k (i.e., robustly with respect to small changes of system parameters). Trajectories that leave a fixed point along its unstable manifold and reach another fixed point along its stable manifold are called *heteroclinic* if the two fixed points are distinct or *homoclinic* if the initial and the final point are the same point. Whether the two manifolds actually intersect is a subtle question that is central to the issue of “structural stability” of ergodic dynamical systems.

remark 11.3

Example 11.4 Lorenz flow: Stretch & crease. We now deploy the symmetry of Lorenz flow to streamline and complete analysis of the Lorenz strange attractor commenced in example 9.10. There we showed that the dihedral $D_1 = \{e, R\}$ symmetry identifies the two equilibria E_{Q_1} and E_{Q_2} , and the traditional ‘two-eared’ Lorenz flow figure 2.5 is replaced by the ‘single-eared’ flow of figure 9.4 (a). Furthermore, symmetry identifies two sides of any plane through the z axis, replacing a full-space Poincaré section plane by a half-plane, and the two directions of a full-space eigenvector of E_{Q_0} by a one-sided eigenvector, see figure 9.4 (a).

Example 4.8 explained the genesis of the $x_{E_{Q_1}}$ equilibrium unstable manifold, its orientation and thickness, its collision with the z -axis, and its heteroclinic connec-

Figure 11.8: (a) A Poincaré section of the Lorenz flow in the doubled-polar angle representation, figure 9.4, given by the $[y', z]$ plane that contains the z -axis and the equilibrium EQ_1 . x' axis points toward the viewer. (b) The Poincaré section of the Lorenz flow by the section Crossings *into* the section are marked red (solid) and crossings *out* of the section are marked blue (dashed). Outermost points of both in- and out-sections are given by the EQ_0 unstable manifold $W^u(EQ_0)$ intersection: (E. Siminos)

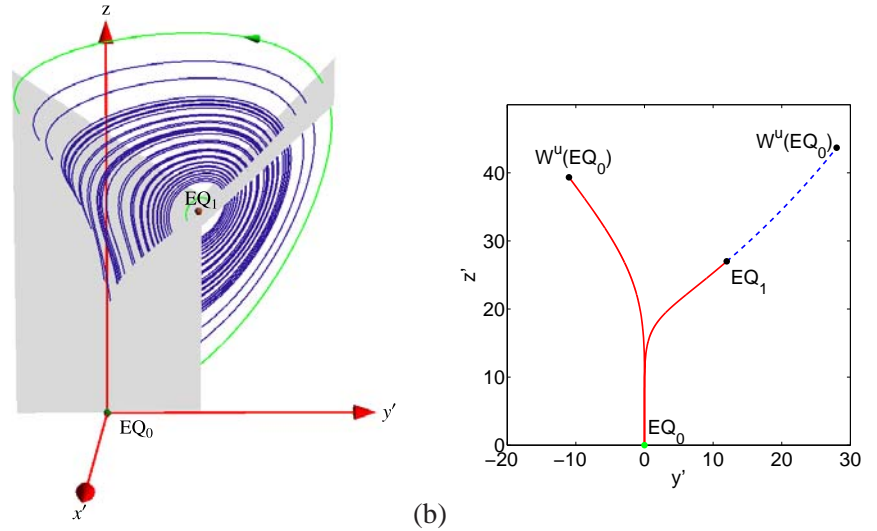
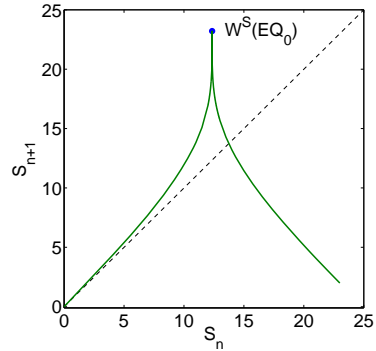


Figure 11.9: The Poincaré return map $s_{n+1} = P(s_n)$ parameterized by Euclidean arclength s measured along the EQ_1 unstable manifold, from x_{EQ_1} to $W^u(EQ_0)$ section point, uppermost right point of the blue (dashed) segment in figure 11.8 (b). The critical point (the ‘crease’) of the map is given by the section of the heteroclinic orbit $W^s(EQ_0)$ that descends all the way to EQ_0 , in infinite time and with infinite slope. (E. Siminos)



tion to the $x_{EQ_0} = (0, 0, 0)$ equilibrium. All that remains is to describe how the EQ_0 neighborhood connects back to the EQ_1 unstable manifold.

Figure 9.4 and figure 11.8(a) show clearly how the Lorenz dynamics is pieced together from the 2 equilibria and their unstable manifolds: Having completed the descent to EQ_0 , the infinitesimal neighborhood of the heteroclinic $EQ_1 \rightarrow EQ_0$ trajectory is ejected along the unstable manifold of EQ_0 and is re-injected into the unstable manifold of EQ_1 . Both sides of the narrow strip enclosing the EQ_0 unstable manifold lie above it, and they get folded onto each other with a knife-edge crease (contracted exponentially for infinite time to the EQ_0 heteroclinic point), with the heteroclinic out-trajectory defining the outer edge of the strange attractor. This leads to the folding of the outer branch of the Lorenz strange attractor, illustrated in figure 11.8 (b), with the outermost edge following the unstable manifold of EQ_0 .

Now the stage is set for construction of Poincaré sections and associated Poincaré return maps. There are two natural choices; the section at EQ_0 , lower part of figure 11.8 (b), and the section (blue) above EQ_1 . The first section, together with the blowup of the EQ_0 neighborhood, figure 4.7 (b), illustrates clearly the scarcity of trajectories (vanishing natural measure) in the neighborhood of EQ_0 . The flat section above EQ_1 (which is, believe it or not, a smooth conjugacy by the flow of the knife-sharp section at EQ_0) is more convenient for our purposes. Its return map (3.4) is given by figure 11.9.

The rest is straight sailing: to accuracy 10^{-4} the return map is unimodal, its critical point's forward trajectory yields the kneading sequence (11.13), and the admissible binary sequences, so any number of periodic points can be accurately determined from

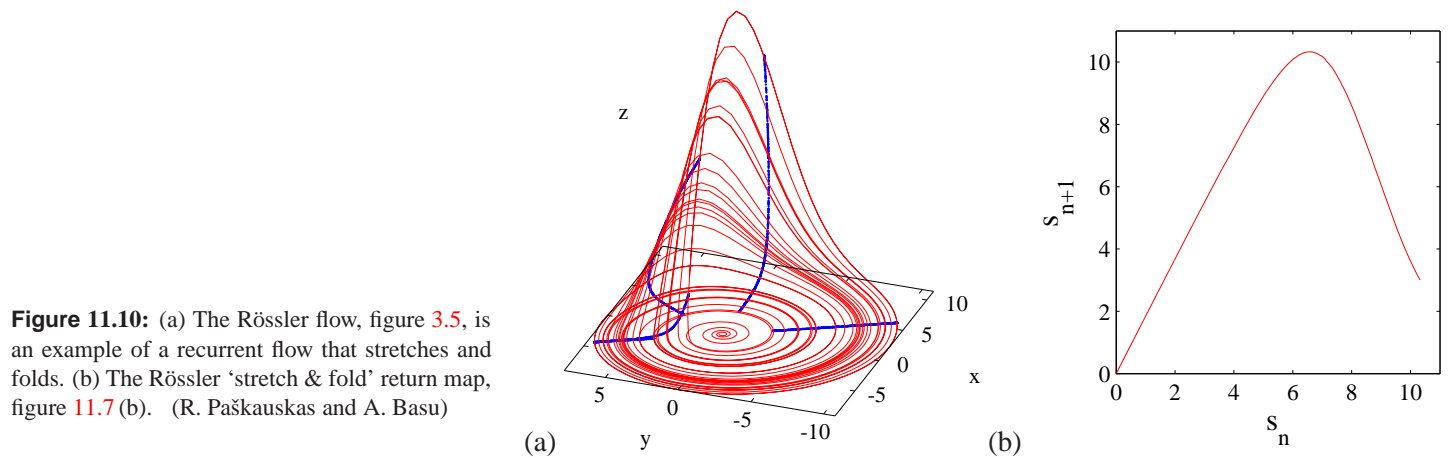


Figure 11.10: (a) The Rössler flow, figure 3.5, is an example of a recurrent flow that stretches and folds. (b) The Rössler ‘stretch & fold’ return map, figure 11.7 (b). (R. Paškauskas and A. Basu)

this 1-dimensional return map, and the 3-dimensional cycles then verified by integrating the Lorenz differential equations (2.12). As already observed by Lorenz, such a map is everywhere expanding on the strange attractor, so it is no wonder mathematicians can here make the ergodicity rigorous.

section 20.5
(E. Siminos and J. Halcrow)

What have we learned from the above two exemplary 3-dimensional flows? If a flow is locally unstable but globally bounded, any open ball of initial points will be stretched out and then folded back. If the equilibria are hyperbolic, the trajectories will be attracted along some eigen-directions and ejected along others. The unstable manifold of one equilibrium can avoid stable manifolds of other equilibria, as is the case for Rössler, or slice them head on, as is the case for Lorenz. A typical trajectory wanders through state space, alternatively attracted into equilibria neighborhoods, and then ejected again. What is important is the motion along the unstable manifolds – that is where $1d$ maps come from.

At this juncture we proceed to show how this works on the simplest example: unimodal mappings of the interval. The erudite reader may skim through this chapter and then take a more demanding path, via the Smale horseshoes of chapter 12. Unimodal maps are easier, but physically less compelling. The Smale horseshoes offer the high road, more complicated, but the right tool to generalize what we learned from the 3-disk dynamics, and begin analysis of general dynamical systems. It is up to you - unimodal maps suffice to get quickly to the heart of this treatise.

11.3 Temporal ordering: itineraries

In this section we learn how to *name* topologically distinct trajectories for the simple, but instructive case; 1-dimensional maps of an interval.

The simplest mapping of this type is *unimodal*; interval is stretched and folded only once, with at most two points mapping into a point in the refolded inter-

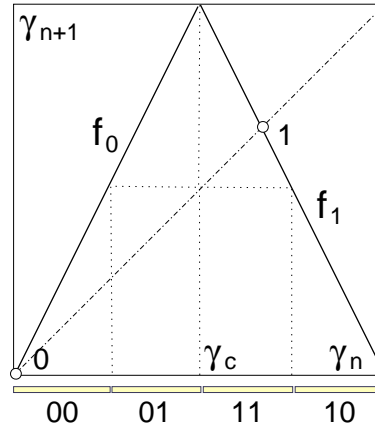


Figure 11.11: The full tent map (11.4) partition $\{\mathcal{M}_{00}, \mathcal{M}_{01}, \mathcal{M}_{11}, \mathcal{M}_{10}\}$ together with the fixed points x_0, x_1 .

val, as in the Rössler return map figure 11.10(b). A unimodal map $f(x)$ is a 1-dimensional function $\mathbb{R} \rightarrow \mathbb{R}$ defined on an interval $\mathcal{M} \in \mathbb{R}$ with a monotonically increasing (or decreasing) branch, a *critical point* (or interval) x_c for which $f(x_c)$ attains the maximum (minimum) value, followed by a monotonically decreasing (increasing) branch. *Uni*-modal means that the map is a 1-humped map with one critical point within interval \mathcal{M} . *Multi*-modal maps, with several critical points within interval \mathcal{M} , can be described with a straight-forward generalization of the methods we describe next.

Example 11.5 Unimodal maps: (continued from example 3.9) The simplest examples of unimodal maps are the quadratic map

$$f(x) = Ax(1 - x), \quad x \in \mathcal{M} = [0, 1] \tag{11.3}$$

and numerically computed return maps such as figure 11.10(b). Such dynamical systems are irreversible (the inverse of f is double-valued), but, as we shall show in sect. 12.2, they may nevertheless serve as effective descriptions of invertible 2-dimensional hyperbolic flows. For the unimodal map such as figure 11.12 a Markov partition of the unit interval \mathcal{M} is given by the two intervals $\{\mathcal{M}_0, \mathcal{M}_1\}$. (continued in example 11.6)

Example 11.6 Full tent map, Ulam map: (continued from example 11.5) The simplest examples of unimodal maps with complete binary symbolic dynamics are the full tent map, figure 11.11,

$$f(\gamma) = 1 - 2|\gamma - 1/2|, \quad \gamma \in \mathcal{M} = [0, 1], \tag{11.4}$$

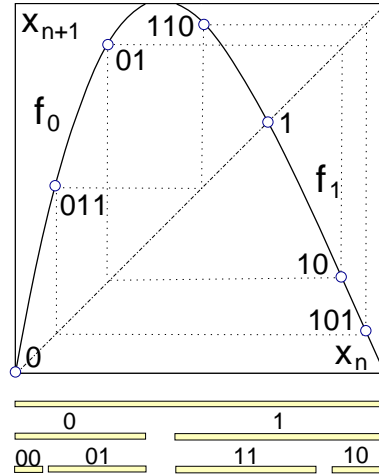
the Ulam map (quadratic map (11.3) with $A = 4$)

$$f(x) = 4x(1 - x), \quad x \in \mathcal{M} = [0, 1], \tag{11.5}$$

exercise 6.4

and the repelling unimodal maps such as figure 11.12. For unimodal maps the Markov partition of the unit interval \mathcal{M} is given by intervals $\{\mathcal{M}_0, \mathcal{M}_1\}$. We refer to (11.4) as the complete tent map because its symbolic dynamics is complete binary: as both $f(\mathcal{M}_0)$ and $f(\mathcal{M}_1)$ fully cover $\mathcal{M} = \{\mathcal{M}_0, \mathcal{M}_1\}$, all binary sequences are realized as admissible itineraries.

Figure 11.12: A unimodal repeller with the survivor intervals after 1 and 2 iterations. Intervals marked $s_1 s_2 \cdots s_n$ consist of points that do not escape in n iterations, and follow the itinerary $S^+ = s_1 s_2 \cdots s_n$. Note that the spatial ordering does not respect the binary ordering; for example $x_{00} < x_{01} < x_{11} < x_{10}$. Also indicated: the fixed points $\underline{0}$, $\underline{1}$, the 2-cycle $\underline{01}$, and the 3-cycle $\underline{011}$.



For $1d$ maps the *critical value* denotes either the maximum or the minimum value of $f(x)$ on the defining interval; we assume here that it is a maximum, $f(x_c) \geq f(x)$ for all $x \in \mathcal{M}$. The critical point x_c that yields the critical value $f(x_c)$ belongs neither to the left nor to the right partition \mathcal{M} , and is denoted by its own symbol $s = C$. As we shall see, its images and preimages serve as partition boundary points.

The trajectory x_1, x_2, x_3, \dots of the initial point x_0 is given by the iteration $x_{n+1} = f(x_n)$. Iterating f and checking whether the point lands to the left or to the right of x_c generates a *temporally* ordered topological itinerary (11.17) for a given trajectory,

$$s_n = \begin{cases} 1 & \text{if } x_n > x_c \\ C & \text{if } x_n = x_c \\ 0 & \text{if } x_n < x_c \end{cases} \quad (11.6)$$

We refer to $S^+(x_0) = .s_1 s_2 s_3 \cdots$ as the *future itinerary*. Our next task is to answer the reverse problem: given an itinerary, what is the *spatial* ordering of points that belong to the corresponding state space trajectory?

11.4 Spatial ordering

Tired of being harassed by your professors? Finish, get a job, do combinatorics your own way, while you still know everything.

—Professor Gatto Nero

Suppose you have succeeded in constructing a covering symbolic dynamics, such as the one we constructed for a well-separated 3-disk system. Now start moving the disks toward each other. At some critical separation (see figure 11.6) a disk will start blocking families of trajectories traversing the other two disks. The order in which trajectories disappear is determined by their relative ordering in

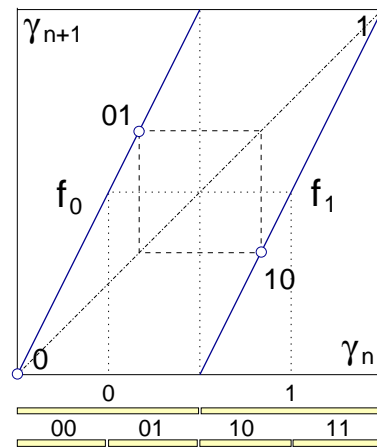


Figure 11.13: The $n = 2$, 4-intervals state space partition for the Bernoulli shift map (11.7), together with the fixed points $\bar{0}$, $\bar{1}$ and the 2-cycle $\overline{01}$.

space; the ones closest to the intervening disk will be pruned first. Determining inadmissible itineraries requires that we relate the spatial ordering of trajectories to their time ordered itineraries.

exercise 12.7

The easiest point of departure is to start out by working out this relation for the symbolic dynamics of 1-dimensional mappings. As it appears impossible to present this material without getting bogged down in a sea of 0's, 1's and subscripted subscripts, we announce the main result before embarking upon its derivation:

section 11.5

The admissibility criterion (sect. 11.5) eliminates *all* itineraries that cannot occur for a given unimodal map.

Example 11.7 Bernoulli shift map state space partition. First, an easy example: the Bernoulli shift map, figure 11.13,

$$b(\gamma) = \begin{cases} b_0(\gamma) = 2\gamma, & \gamma \in \mathcal{M}_0 = [0, 1/2) \\ b_1(\gamma) = 2\gamma - 1, & \gamma \in \mathcal{M}_1 = [1/2, 1] \end{cases}, \quad (11.7)$$

models the 50-50% probability of a coin toss. It maps the unit interval onto itself, with fixed points $\gamma_0 = 0$, $\gamma_1 = 1$. The closely related doubling map acts on the circle

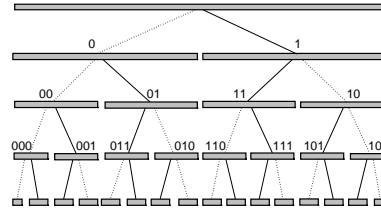
$$x \mapsto 2x \pmod{1}, \quad x \in [0, 1] \quad (11.8)$$

and consequently has only one fixed point, $x_0 = 0 = 1 \pmod{1}$. The Bernoulli map is called a 'shift' map, as a multiplication by 2 acts on the binary representation of $\gamma = .s_1s_2s_3\dots$ by shifting its digits, $b(\gamma) = .s_2s_3\dots$. The n th preimages $b^{-n}(\gamma)$ of the critical point $\gamma_c = 1/2$ partition the state space into 2^n subintervals, each labeled by the first n binary digits of points $\gamma = .s_1s_2s_3\dots$ within the subinterval: figure 11.13 illustrates such 4-intervals state space partition $\{\mathcal{M}_{00}, \mathcal{M}_{01}, \mathcal{M}_{11}, \mathcal{M}_{10}\}$ for $n = 2$.

Consider a map $f(x)$ topologically conjugate (two monotonically increasing branches) to the Bernoulli shift, with the forward orbit of x generating the itinerary $s_1s_2s_3\dots$. Convert this itinerary into Bernoulli map point $\gamma = .s_1s_2s_3\dots$. These values can now be used to spatially order points with different temporal itineraries: if $\gamma < \gamma'$, then $x < x'$.

Suppose we have already computed all $(n - 1)$ -cycles of $f(x)$, and would now like to compute the cycle $p = s_1s_2s_3\dots s_n$ of period n . Mark γ values on the unit interval

Figure 11.14: Alternating binary tree relates the itinerary labeling of the unimodal map intervals, figure 11.12, to their spatial ordering. Dotted line stands for 0, full line for 1; the binary sub-tree whose root is a full line (symbol 1) reverses the orientation, due to the orientation reversing fold in figures 11.10 and 11.12. See also figure 14.4.



for all known periodic points of the Bernoulli shift map, and then insert in between them $\gamma_{\sigma^k p}, k = 0, 1, \dots, n_p - 1$ corresponding to periodic points of cycle p . In the dynamical state space they will be bracketed by corresponding cycle points x_j from cycles already computed, and thus the knowledge of the topological ordering of all cycle points provides us with robust initial guesses for periodic-orbit searches for any map with 2 monotonically increasing branches. (continued in example 23.5)

For the Bernoulli shift converting itineraries into a topological ordering is easy; the binary expansion of coordinate γ is also its temporary itinerary. The tent map (11.4), figure 11.11 is a bit harder. It consists of two straight segments joined at $x = 1/2$. The symbol s_n defined in (11.6) equals 0 if the function increases, and 1 if the function decreases. Iteration forward in time generates the time itinerary. More importantly, the piecewise linearity of the map makes the converse possible: determine analytically an initial point given its itinerary, a property that we now use to define a topological coordinatization common to all unimodal maps.

Here we have to face the fundamental problem of pedagogy: combinatorics cannot be taught. The best one can do is to state the answer, and then hope that you will figure it out by yourself.

The tent map point $\gamma(S^+)$ with future itinerary S^+ is given by converting the sequence of s_n 's into a binary number by the following algorithm:

$$w_{n+1} = \begin{cases} w_n & \text{if } s_{n+1} = 0 \\ 1 - w_n & \text{if } s_{n+1} = 1 \end{cases}, \quad w_1 = s_1$$

$$\gamma(S^+) = 0.w_1w_2w_3\dots = \sum_{n=1}^{\infty} w_n/2^n. \tag{11.9}$$

This follows by inspection from the binary tree of figure 11.14. Once you figure this out, feel free to complain that the way the rule is stated here is incomprehensible, and show us how you did it better. exercise 11.4

Example 11.8 Converting γ to S^+ : γ whose itinerary is $S^+ = 0110000\dots$ is given by the binary number $\gamma = .0110000\dots$. Conversely, the itinerary of $\gamma = .01$ is $s_1 = 0$, $f(\gamma) = .1 \rightarrow s_2 = 1$, $f^2(\gamma) = f(.1) = 1 \rightarrow s_3 = 1$, etc.. Orbit that starts out as a finite block followed by infinite repeats of another block $p = S_p = (s_1s_2s_3\dots s_n)^\infty$ is said to be heteroclinic to the cycle p . An orbit that starts out as $p^i n f t y$ followed by a finite block followed

We refer to $\gamma(S^+)$ as the *(future) topological coordinate*. w_i 's are the digits in the binary expansion of the starting point γ for the full tent map (11.4). In the left half-interval the map $f(x)$ acts by multiplication by 2, while in the right half-interval the map acts as a flip as well as multiplication by 2, reversing the ordering, and generating in the process the sequence of s_i 's from the binary digits w_n .

The mapping $x_0 \rightarrow S^+(x_0) \rightarrow \gamma_0 = \gamma(S^+)$ is a *topological conjugacy* which maps the trajectory of an initial point x_0 under iteration of a given unimodal map to that initial point γ for which the trajectory of the 'canonical' unimodal map, the full tent map (11.4), has the same itinerary. The virtue of this conjugacy is that $\gamma(S^+)$ *preserves the ordering* for any unimodal map in the sense that if $\bar{x} > x$, then $\bar{\gamma} > \gamma$.

Example 11.9 Periodic orbits of unimodal maps. Let

$$f(x) = \begin{cases} f_0(x) & \text{if } x < x_c \\ f_1(x) & \text{if } x > x_c \end{cases}, \tag{11.10}$$

and assume that all periodic orbits are unstable, i.e., the stability $\Lambda_p = f_a^{k_t}$ (see (4.51)) satisfies $|\Lambda_p| > 1$. Then the periodic point $x_{s_1 s_2 s_3 \dots s_n}$ is the only fixed point of the unique composition (3.17) of n maps

$$f_{s_n} \circ \dots \circ f_{s_2} \circ f_{s_1}(x_{s_1 s_2 s_3 \dots s_n}) = x_{s_1 s_2 s_3 \dots s_n} \tag{11.11}$$

(note that successive maps, applied from the left, correspond to later times, i.e., later symbols in the itinerary).

The n th iterate of a unimodal map has at most 2^n monotone segments, and therefore there will be 2^n or fewer periodic points of length n . For the full tent map (11.4) it has exactly 2^n periodic points. A periodic orbit p of length n corresponds to an infinite repetition of a length $n = n_p$ symbol string block, customarily indicated by a line over the string: $p = S_p = (s_1 s_2 s_3 \dots s_n)^\infty = \overline{s_1 s_2 s_3 \dots s_n}$. As all itineraries are infinite, we shall adopt convention that a finite string itinerary $p = s_1 s_2 s_3 \dots s_n$ stands for infinite repetition of a finite block, and routinely omit the overline. A cycle p is called prime if its itinerary S cannot be written as a repetition of a shorter block S' . If the itinerary of x_0 is $p = s_1 s_2 s_3 \dots s_n$, its cyclic permutation $\sigma^k p = \overline{s_k s_{k+1} \dots s_n s_1 \dots s_{k-1}}$ corresponds to the point x_{k-1} in the same cycle. section 12.2

Example 11.10 Periodic points of the full tent map. Each cycle p is a set of n_p rational-valued full tent map periodic points γ . It follows from (11.9) that if the repeating string $s_1 s_2 \dots s_n$ contains an odd number of '1's, the string of well ordered symbols $w_1 w_2 \dots w_{2n}$ has to be of the double length before it repeats itself. The cycle-point γ is a geometrical sum which we can rewrite as the odd-denominator fraction

$$\gamma(\overline{s_1 s_2 \dots s_n}) = \frac{2^{2n}}{2^{2n} - 1} \sum_{t=1}^{2n} w_t / 2^t \tag{11.12}$$

Using this we can calculate the $\hat{\gamma}_p = \hat{\gamma}(S_p)$ for all short cycles. For orbits up to length 5 this is done in table 11.1.

S	$\hat{\gamma}(S)$	S	$\hat{\gamma}(S)$
$\overline{0}$	$.0 = 0$	$\overline{10111}$	$.11010 = 26/31$
$\overline{1}$	$.10 = 2/3$	$\overline{10110}$	$.1101100100 = 28/33$
$\overline{10}$	$.1100 = 4/5$	$\overline{10010}$	$.11100 = 28/31$
$\overline{101}$	$.1110 = 6/7$	$\overline{10011}$	$.1110100010 = 10/11$
$\overline{100}$	$.111000 = 8/9$	$\overline{10001}$	$.11110 = 30/31$
$\overline{1011}$	$.11010010 = 14/17$	$\overline{10000}$	$.1111100000 = 32/33$
$\overline{1001}$	$.11110 = 14/15$		
$\overline{1000}$	$.11110000 = 16/17$		

Table 11.1: The maximal values of unimodal map cycles up to length 5. (K.T. Hansen)

Critical points are special - they define the boundary between intervals, i.e., interval is split into 0 [left part], x_c [critical point] and 1 [right part]. For the dike map and the repeller figure 11.12 x_c is the whole interval of points along the flat top of the map, but usually it is a point. As illustrated by figures 11.11 and 11.13, for a unimodal map the preimages $f^{-n}(x_c)$ of the critical point x_c serve as partition boundary points. But not all preimages—one has to ensure that they are within the set of all admissible orbits by checking them against the kneading sequence of the map.

11.5 Kneading theory

(K.T. Hansen and P. Cvitanović)

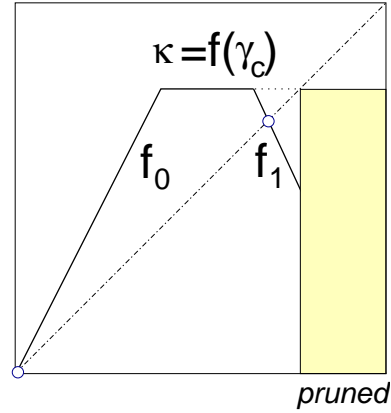
The main motivation for being mindful of spatial ordering of temporal itineraries is that this spatial ordering provides us with criteria that separate inadmissible orbits from those realizable by the dynamics. For 1-dimensional mappings the *kneading theory* provides a precise and definitive criterion of admissibility.

If the parameter in the quadratic map (11.3) is $A > 4$, then the iterates of the critical point x_c diverge for $n \rightarrow \infty$, and any sequence S^+ composed of letters $s_i = \{0, 1\}$ is admissible, and any value of $0 \leq \gamma < 1$ corresponds to an admissible orbit in the non-wandering set of the map. The corresponding repeller is a complete binary labeled Cantor set, the $n \rightarrow \infty$ limit of the n th level covering intervals sketched in figure 11.12.

For $A < 4$ only a subset of the points in the interval $\gamma \in [0, 1]$ corresponds to admissible orbits. The forbidden symbolic values are determined by observing that the largest x_n value in an orbit $x_1 \rightarrow x_2 \rightarrow x_3 \rightarrow \dots$ has to be smaller than or equal to the image of the critical point, *the critical value* $f(x_c)$. Let $K = S^+(x_c)$ be the itinerary of the critical point x_c , denoted the *kneading sequence* of the map. The corresponding topological coordinate is called the *kneading value*

$$\kappa = \gamma(K) = \gamma(S^+(x_c)). \tag{11.13}$$

Figure 11.15: The ‘dike’ map obtained by slicing of the top portion of the tent map in figure 11.11. Any orbit that visits the primary pruning interval $(\kappa, 1]$ is inadmissible. The admissible orbits form the Cantor set obtained by removing from the unit interval the primary pruning interval and all its iterates. Any admissible orbit has the same topological coordinate and itinerary as the corresponding tent map figure 11.11 orbit.



The ‘canonical’ map that has the same kneading sequence K (11.13) as $f(x)$ is the dike map, figure 11.15,

$$f(\gamma) = \begin{cases} f_0(\gamma) = 2\gamma & \gamma \in \mathcal{M}_0 = [0, \kappa/2) \\ f_c(\gamma) = \kappa & \gamma \in \mathcal{M}_c = [\kappa/2, 1 - \kappa/2] \\ f_1(\gamma) = 2(1 - \gamma) & \gamma \in \mathcal{M}_1 = (1 - \kappa/2, 1] \end{cases}, \quad (11.14)$$

obtained by slicing off all $\gamma(S^+(x_0)) > \kappa$. The dike map is the full tent map figure 11.11 with the top sliced off. It is convenient for coding the symbolic dynamics, as those γ values that survive the pruning are the same as for the full tent map figure 11.11, and are easily converted into admissible itineraries by (11.9).

If $\gamma(S^+) > \gamma(K)$, the point x whose itinerary is S^+ would exceed the critical value, $x > f(x_c)$, and hence cannot be an admissible orbit. Let

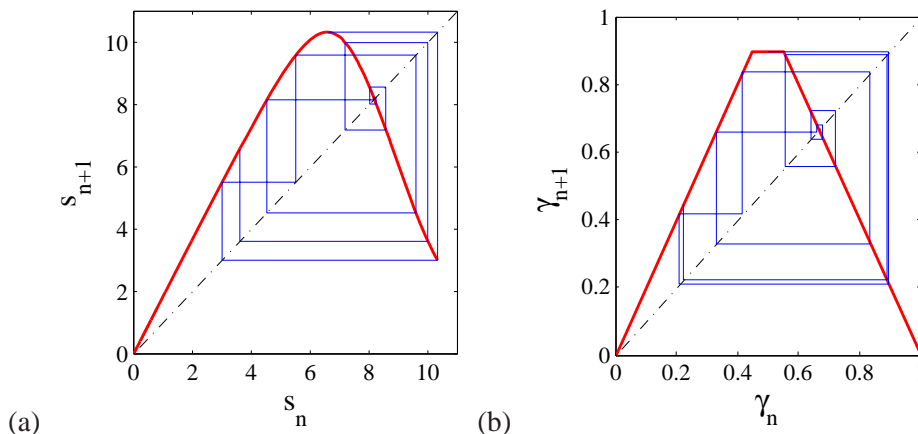
$$\hat{\gamma}(S^+) = \sup_m \gamma(\sigma^m(S^+)) \quad (11.15)$$

be the *maximal value*, the highest topological coordinate reached by the orbit $x_1 \rightarrow x_2 \rightarrow x_3 \rightarrow \dots$, where σ is the shift (11.20), $\sigma(\dots s_{-2}s_{-1}s_0.s_1s_2s_3 \dots) = \dots s_{-2}s_{-1}s_0.s_1s_2s_3 \dots$. We shall call the interval $(\kappa, 1]$ the *primary pruned interval*. The orbit S^+ is inadmissible if γ of any shifted sequence of S^+ falls into this interval.

Criterion of admissibility: Let κ be the kneading value of the critical point, and $\hat{\gamma}(S^+)$ be the maximal value of the orbit S^+ . Then the orbit S^+ is admissible if and only if $\hat{\gamma}(S^+) \leq \kappa$.

While a unimodal map may depend on many arbitrarily chosen parameters, its dynamics determines the unique kneading value κ . We shall call κ the *topological parameter* of the map. Unlike the parameters of the original dynamical system, the topological parameter has no reason to be either smooth or continuous. The jumps in κ as a function of the map parameter such as A in (11.3) correspond to inadmissible values of the topological parameter. Each jump in κ corresponds to a stability window associated with a stable cycle of a smooth unimodal map. For

Figure 11.16: (a) Web diagram generated by the trajectory of the critical point the unimodal Rössler return map of figure 11.7 (b). (b) The web diagram for the corresponding ‘canonical’ dike map (11.14) with the same kneading sequence. (A. Basu and J. Newman)



the quadratic map (11.3) κ increases monotonically with the parameter A , but for a general unimodal map such monotonicity need not hold.

Example 11.11 Rössler return map web diagram: (continuation of example 11.2) The arclength distance along the unstable manifold of the x_- equilibrium point return map, figure 11.7 (b), generates the kneading sequence (11.13) as the itinerary of the critical point plotted in figure 11.16 (a).

For further details of unimodal dynamics, the reader is referred to appendix D.1. As we shall see in sect. 12.4, for higher dimensional maps and flows there is no single parameter that orders dynamics monotonically; as a matter of fact, there is an infinity of parameters that need adjustment for a given symbolic dynamics. This difficult subject is beyond our current ambition horizon.



fast track:
chapter 12, p. 224

11.6 Symbolic dynamics, basic notions

(Mathematics) is considered a specialized dialect of the natural language and its functioning as a special case of speech.

— Yuri I. Manin [1]

In this section we collect the basic notions and definitions of symbolic dynamics. The reader might prefer to skim through this material on first reading, return to it later as the need arises.



Shifts. We associate with every initial point $x_0 \in \mathcal{M}$ the *future itinerary*, a sequence of symbols $S^+(x_0) = s_1 s_2 s_3 \dots$ which indicates the order in which the

regions are visited. If the trajectory x_1, x_2, x_3, \dots of the initial point x_0 is generated by

$$x_{n+1} = f(x_n), \tag{11.16}$$

then the itinerary is given by the symbol sequence

$$s_n = s \quad \text{if} \quad x_n \in \mathcal{M}_s. \tag{11.17}$$

Similarly, the *past itinerary* $S^-(x_0) = \dots s_{-2}s_{-1}s_0$ describes the history of x_0 , the order in which the regions were visited before arriving to the point x_0 . To each point x_0 in the dynamical space we thus associate a bi-infinite itinerary

$$S(x_0) = (s_k)_{k \in \mathbb{Z}} = S^- \cdot S^+ = \dots s_{-2}s_{-1}s_0 \cdot s_1s_2s_3 \dots. \tag{11.18}$$

The itinerary will be finite for a scattering trajectory, entering and then escaping \mathcal{M} after a finite time, infinite for a trapped trajectory, and infinitely repeating for a periodic trajectory.

The set of all bi-infinite itineraries that can be formed from the letters of the alphabet \mathcal{A} is called the *full shift* (or *topological Markov chain*)

$$\mathcal{A}^{\mathbb{Z}} = \{(s_k)_{k \in \mathbb{Z}} : s_k \in \mathcal{A} \text{ for all } k \in \mathbb{Z}\}. \tag{11.19}$$

The jargon is not thrilling, but this is how professional dynamicists talk to each other. We will stick to plain English to the extent possible.

We refer to this set of all conceivable itineraries as the *covering* symbolic dynamics. The name *shift* is descriptive of the way the dynamics acts on these sequences. As is clear from the definition (11.17), a forward iteration $x \rightarrow x' = f(x)$ shifts the entire itinerary to the left through the ‘decimal point.’ This operation, denoted by the shift operator σ ,

$$\sigma(\dots s_{-2}s_{-1}s_0 \cdot s_1s_2s_3 \dots) = \dots s_{-2}s_{-1}s_0s_1 \cdot s_2s_3 \dots, \tag{11.20}$$

demoting the current partition label s_1 from the future S^+ to the ‘has been’ itinerary S^- . The inverse shift σ^{-1} shifts the entire itinerary one step to the right.

A finite sequence $b = s_k s_{k+1} \dots s_{k+n_b-1}$ of symbols from \mathcal{A} is called a *block* of length n_b . If the symbols outside of the block remain unspecified, we denote to the totality of orbits that share this block by $_ \cdot s_k s_{k+1} \dots s_{k+n_b-1} _$

A state space orbit is *periodic* if it returns to its initial point after a finite time; in the shift space the orbit is periodic if its itinerary is an infinitely repeating block

p^∞ . We shall refer to the set of periodic points \mathcal{M}_p that belong to a given periodic orbit as a *cycle*

$$p = \overline{s_1 s_2 \cdots s_{n_p}} = \{x_{s_1 s_2 \cdots s_{n_p}}, x_{s_2 \cdots s_{n_p} s_1}, \cdots, x_{s_{n_p} s_1 \cdots s_{n_p-1}}\}. \quad (11.21)$$

By its definition, a cycle is invariant under cyclic permutations of the symbols in the repeating block. A bar over a finite block of symbols denotes a periodic itinerary with infinitely repeating basic block; we shall omit the bar whenever it is clear from the context that the orbit is periodic. Each *periodic point* is labeled by the first n_p steps of its future itinerary. For example, the 2nd periodic point is labeled by

$$x_{s_2 \cdots s_{n_p} s_1} = \overline{x_{s_2 \cdots s_{n_p} s_1} s_2 \cdots s_{n_p} s_1}.$$

This - a bit strained - notation is meant to indicate that the symbol block repeats both in the past and in the future. It is helpful for determining spatial ordering of cycles of 2D-hyperbolic maps, to be undertaken in sect. 12.3.1.

A *prime cycle* p of length n_p is a single traversal of the orbit; its label is a block of n_p symbols that cannot be written as a repeat of a shorter block (in literature such cycle is sometimes called *primitive*; we shall refer to it as ‘prime’ throughout this text).

Partitions. A partition is called *generating* if every infinite symbol sequence corresponds to a distinct point in the state space. Finite Markov partition (11.2) is an example. Constructing a generating partition for a given system is a difficult problem. In examples to follow we shall concentrate on cases which allow finite partitions, but in practice almost any generating partition of interest is infinite.

A partition too coarse, coarser than, for example, a Markov partition, would assign the same symbol sequence to distinct dynamical trajectories. To avoid that, we often find it convenient to work with partitions finer than strictly necessary. Ideally the dynamics in the refined partition assigns a unique infinite itinerary $\cdots s_{-2} s_{-1} s_0 \cdot s_1 s_2 s_3 \cdots$ to each distinct orbit, but there might exist full shift symbol sequences (11.19) which are not realized as orbits; such sequences are called *inadmissible*, and we say that the symbolic dynamics is *pruned*. The word is suggested by ‘pruning’ of branches corresponding to forbidden sequences for symbolic dynamics organized hierarchically into a tree structure, as explained in chapter 14.

A mapping $f : \mathcal{M} \rightarrow \mathcal{M}$ together with a partition \mathcal{A} induces *topological dynamics* (Σ, σ) , where the *subshift*

$$\Sigma = \{(s_k)_{k \in \mathbb{Z}}\}, \quad (11.22)$$

is the set of all *admissible* (i.e., ‘pruned’) infinite itineraries, and $\sigma : \Sigma \rightarrow \Sigma$ is the shift operator (11.20). The designation ‘subshift’ comes from the fact that

$\Sigma \subset \mathcal{A}^{\mathbb{Z}}$ is the subset of the full shift (11.19). One of our principal tasks in developing symbolic dynamics of dynamical systems that occur in nature will be to determine Σ , the set of all bi-infinite itineraries S that are actually realized by the given dynamical system.

Pruning. If the dynamics is pruned, the alphabet must be supplemented by a *grammar*, a set of pruning rules. After the inadmissible sequences have been pruned, it is often convenient to parse the symbolic strings into words of variable length - this is called *coding*. Suppose that the grammar can be stated as a finite number of pruning rules, each forbidding a block of finite length,

$$\mathcal{G} = \{b_1, b_2, \dots, b_k\}, \quad (11.23)$$

where a *pruning block* b is a sequence of symbols $b = s_1 s_2 \dots s_{n_b}$, $s \in \mathcal{A}$, of finite length n_b . In this case we can always construct a finite Markov partition (11.2) by replacing finite length words of the original partition by letters of a new alphabet. In particular, if the longest forbidden block is of length $M + 1$, we say that the symbolic dynamics is a shift of finite type with M -step memory. In that case we can *recode* the symbolic dynamics in terms of a new alphabet, with each new letter given by an admissible block of at most length M .

A topological dynamical system (Σ, σ) for which all admissible itineraries are generated by a finite transition matrix (14.1)

$$\Sigma = \{(s_k)_{k \in \mathbb{Z}} : T_{s_k s_{k+1}} = 1 \text{ for all } k\} \quad (11.24)$$

is called a subshift of *finite type*.



in depth:
chapter 12, p. 224

Résumé

From our initial chapters 2 to 4 fixation on things local: a representative point, a short-time trajectory, a neighborhood, in this chapter we have made a courageous leap and gone global.

The main lesson is that - if one intends to go thoughtfully about globalization - one should trust the dynamics itself, and let it partition the state space, by means of its (topologically invariant) unstable manifolds. This works if every equilibrium and periodic orbit is unstable, so one exits its local neighborhood via its unstable manifold. We delineate the segment of the unstable manifold between the fixed point and the point where the nonlinearity of the dynamics folds back on itself as the primary segment, and measure location of nearby state space points by

arclengths measured along this (curvilinear) segment. For 1-dimensional maps the folding point is the critical point, and easy to determine. In higher dimensions, the situation is not so clear - we shall discuss that in chapter 12.

Trajectories exit a neighborhood of an equilibrium or periodic point along unstable directions, and fall along stable manifolds towards other fixed points, until they again are repelled along their unstable manifolds. Such sequences of visitations can be described by *symbolic dynamics*. As we shall show in chapter 14, they are encoded by transition matrices / transition graphs, and approximated dynamically by sequences of unstable manifold \rightarrow unstable manifold maps, or, in case of a return to the initial neighborhood, by return maps $s \rightarrow f(s)$.

As ‘kneading theory’ of sect. 11.5 illustrates, not all conceivable symbol sequences are actually realized (*admissible*). The identification of all inadmissible or *pruned* sequences is in general not possible. However, the theory to be developed here relies on exhaustive enumeration of all admissible itineraries up to a given topological length; chapters 12 and 15 describe several strategies for accomplishing this for physically realistic goals.

Commentary

Remark 11.1 Symbolic dynamics. For a brief history of symbolic dynamics, from J. Hadamard in 1898 onward, see notes to chapter 1 of Kitchens monograph [2], a very clear and enjoyable mathematical introduction to topics discussed here. Diacu and Holmes [3] provide an excellent survey of symbolic dynamics applied to celestial mechanics. For a compact survey of symbolic dynamics techniques, consult sects. 3.2 and 8.3 of Robinson [4]. The binary labeling of the once-folding map periodic points was introduced by Myrberg [5] for 1-dimensional maps, and its utility to 2-dimensional maps has been emphasized in refs. [6, 7]. For 1-dimensional maps it is now customary to use the *R-L* notation of Metropolis, Stein and Stein [8, 9], indicating that the point x_n lies either to the left or to the right of the critical point in figure 11.12. The symbolic dynamics of such mappings has been extensively studied by means of the Smale horseshoes, see for example ref. [10]. Using letters rather than numerals in symbol dynamics alphabets probably reflects good taste. We prefer numerals for their computational convenience, as they speed up conversions of itineraries into the topological coordinates (δ, γ) introduced in sect. 12.3.1. The alternating binary ordering of figure 11.14 is related to the Gray codes of computer science [11].

Remark 11.2 Kneading theory. The admissible itineraries are studied, for example, in refs. [12, 8, 10, 13]. We follow here the Milnor-Thurston exposition [14]. They study the topological zeta function for piecewise monotone maps of the interval, and show that for the finite subshift case it can be expressed in terms of a finite dimensional *kneading determinant*. As the kneading determinant is essentially the topological zeta function introduced in sect. 15.4, we do not discuss it here. Baladi and Ruelle have reworked this theory in a series of papers [15, 16, 17, 18]. See also P. Dahlqvist’s appendix D.1.

Remark 11.3 Heteroclinic connections. For sketches of heteroclinic connections in the nonlinear setting, see Abraham and Shaw illustrated classic [19]. Section 5 of ref. [20] makes elegant use of stable manifold co-dimension counts and of invariant subspaces implied by discrete symmetries of the underlying PDE to deduce the existence of a heteroclinic connection.

Exercises

- 11.1. **Binary symbolic dynamics.** Verify that the shortest prime binary cycles of the unimodal repeller of figure 11.12 are $\overline{0}, \overline{1}, \overline{01}, \overline{001}, \overline{011}, \dots$. Compare with table 15.1. Try to sketch them in the graph of the unimodal function $f(x)$; compare ordering of the periodic points with figure 11.14. The point is that while overlaid on each other the longer cycles look like a hopeless jumble, the periodic points are clearly and logically ordered by the alternating binary tree.
- 11.2. **Generating prime cycles.** Write a program that generates all binary prime cycles up to given finite length.
- 11.3. **A contracting baker's map.** Consider a contracting (or "dissipative") baker's defined in exercise 4.6. The symbolic dynamics encoding of trajectories is realized via symbols 0 ($y \leq 1/2$) and 1 ($y > 1/2$). Consider the observable $a(x, y) = x$. Verify that for any periodic orbit $p = (\epsilon_1 \dots \epsilon_{n_p}), \epsilon_i \in \{0, 1\}$

$$A_p = \frac{3}{4} \sum_{j=1}^{n_p} \delta_{j,1}.$$

- 11.4. **Unimodal map symbolic dynamics.** Show that the tent map point $\gamma(S^+)$ with future itinerary S^+ is given by converting the sequence of s_n 's into a binary number by the algorithm (11.9). This follows by inspection from the binary tree of figure 11.14.
- 11.5. **Unimodal map kneading value.** Consider the 1 - dimensional quadratic map

$$f(x) = Ax(1 - x), \quad A = 3.8. \quad (11.25)$$

- (a) (easy) Plot (11.25), and the first 4-8 (whatever looks better) iterates of the critical point $x_c = 1/2$.
- (b) (hard) Draw corresponding intervals of the partition of the unit interval as levels of a Cantor set, as in the symbolic dynamics partition of figure 11.12. Note, however, that some of the intervals of figure 11.12 do not appear in this case - they are *pruned*.
- (c) (easy) Check numerically that $K = S^+(x_c)$, kneading sequence (the itinerary of the critical point (11.13)) is

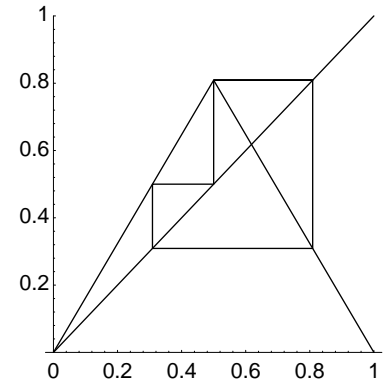
$$K = 101101111011011110101111011110\dots$$

As the orbits of a chaotic map are exponentially unstable, so many digits seem too good to be true - recheck this sequence using arbitrary precision arithmetics.

- (d) (medium) The tent map point $\gamma(S^+)$ with future itinerary S^+ is given by converting the sequence of s_n 's into a binary number by the algorithm (11.9). List the corresponding kneading value (11.13) sequence $\kappa = \gamma(K)$ to the same number of digits as K .
- (e) (hard) Plot the dike map, figure 11.15, with the same kneading sequence K as $f(x)$. The dike map is obtained by slicing off all $\gamma(S^+(x_0)) > \kappa$, from the full tent map figure 11.11, see (11.14).

How this kneading sequence is converted into a series of pruning rules is a dark art, relegated to sect. 15.5.

- 11.6. **"Golden mean" pruned map.** Consider a symmetrical tent map on the unit interval such that its highest point belongs to a 3-cycle:



- (a) Find the value $|\Lambda|$ for the slope (the two different slopes $\pm\Lambda$ just differ by a sign) where the maximum at $1/2$ is part of a 3-cycle, as in the figure.
- (b) Show that no orbit of this map can visit the region $x > (1 + \sqrt{5})/4$ more than once. Verify that once an orbit exceeds $x > (\sqrt{5}-1)/4$, it does not reenter the region $x < (\sqrt{5}-1)/4$.
- (c) If an orbit is in the interval $(\sqrt{5}-1)/4 < x < 1/2$, where will it be on the next iteration?
- (d) If the symbolic dynamics is such that for $x < 1/2$ we use the symbol 0 and for $x > 1/2$ we use the symbol 1, show that no periodic orbit will have the substring $_00_$ in it.
- (e) On the second thought, is there a periodic orbit that violates the above $_00_$ pruning rule?

For continuation, see exercise 15.7 and exercise 19.2. See also exercise 15.6 and exercise 15.8.

- 11.7. **Binary 3-step transition matrix.** Construct $[8 \times 8]$ binary 3-step transition matrix analogous to the 2-step transition matrix (14.10). Convince yourself that the number of terms of contributing to $\text{tr } T^n$ is independent of the memory length, and that this $[2^m \times 2^m]$ trace is well defined in the infinite memory limit $m \rightarrow \infty$.
- 11.8. **Full tent map periodic points.** This exercise is easy: just making sure you know how to go back and forth between spatial and temporal ordering of trajectory points.
- (a) derive (11.12)
- (b) compute the five periodic points of cycle $\overline{10011}$
- (c) compute the five periodic points of cycle $\overline{10000}$
- (d) (optional) plot the above two cycles on the graph of the full tent map.
- (continued in exercise 13.15)

References

- [11.1] Yuri I. Manin, *Mathematics as Metaphor: Selected Essays*, (Amer. Math. Soc., Providence RI 2007).
- [11.2] B.P. Kitchens, *Symbolic dynamics: one-sided, two-sided, and countable state Markov shifts* (Springer, Berlin 1998).
- [11.3] F. Diacu and P. Holmes, *Celestial Encounters, The Origins of Chaos and Stability* (Princeton Univ. Press, Princeton NJ 1996).
- [11.4] C. Robinson, *Dynamical Systems: Stability, Symbolic Dynamics, and Chaos* (C. R. C. Press, Boca Raton 1999)
- [11.5] P.J. Myrberg, *Ann. Acad. Sc. Fenn., Ser. A*, **256**, 1 (1958); **259**, 1 (1958).
- [11.6] C. Mira, *Chaotic Dynamics—From one dimensional endomorphism to two dimensional diffeomorphism*, (World Scientific, Singapore, 1987).
- [11.7] D. Fournier, H. Kawakami and C. Mira, *C.R. Acad. Sci. Ser. I*, **298**, 253 (1984); **301**, 223 (1985); **301**, 325 (1985).
- [11.8] N. Metropolis, M.L. Stein and P.R. Stein, “On Finite Limit Sets for Transformations on the Unit Interval,” *J. Comb. Theo.* **15**, 25 (1973).
- [11.9] P. Collet and J.P. Eckmann, *Iterated Maps on the Interval as Dynamical Systems* (Birkhauser, Boston 1980).
- [11.10] J. Guckenheimer and P. Holmes, *Non-linear Oscillations, Dynamical Systems and Bifurcations of Vector Fields* (Springer, New York, 1986).
- [11.11] W.H. Press, B.P. Flannery, S.A. Teukolsky and W.T. Vetterling, *Numerical Recipes* (Cambridge Univ. Press, 1986).
- [11.12] A.N. Sarkovskii, “Coexistence of cycles of a continuous map of a line into itself,” *Ukrainian Math. J.* **16**, 61 (1964).
- [11.13] R.L. Devaney, *An Introduction to Chaotic Dynamical Systems* (Addison-Wesley, Reading MA, 1987).

- [11.14] J. Milnor and W. Thurston, "On iterated maps of the interval," in A. Dold and B. Eckmann, eds., *Dynamical Systems, Proceedings, U. of Maryland 1986-87, Lec. Notes in Math.* **1342**, 465 (Springer, Berlin 1988).
- [11.15] V. Baladi and D. Ruelle, "An extension of the theorem of Milnor and Thurston on the zeta functions of interval maps," *Ergodic Theory Dynamical Systems* **14**, 621 (1994).
- [11.16] V. Baladi, "Infinite kneading matrices and weighted zeta functions of interval maps," *J. Functional Analysis* **128**, 226 (1995).
- [11.17] D. Ruelle, "Sharp determinants for smooth interval maps," in F. Ledrappier, J. Lewowicz, and S. Newhouse, eds., *Proceedings of Montevideo Conference 1995* (Addison-Wesley, Harlow 1996).
- [11.18] V. Baladi and D. Ruelle, "Sharp determinants," *Invent. Math.* **123**, 553 (1996).
- [11.19] Abraham, R. H. and Shaw, C. D., *Dynamics - The geometry of behavior* (Addison-Wesley, Reading, MA 1992).
- [11.20] I.G. Kevrekidis, B. Nicolaenko and J.C. Scovel, "Back in the saddle again: a computer assisted study of the Kuramoto-Sivashinsky equation," *SIAM J. Applied Math.* **50**, 760 (1990).
- [11.21] G. 't Hooft and M. Veltman, *DIAGRAMMAR, CERN report 73/9*, (1973); reprinted in *Particle interactions at very high energies, NATO Adv. Study Inst. Series, Sect. B*, vol. **4B**, 177; www.phys.uu.nl/~thoof/gthpub.html.

Chapter 12

Stretch, fold, prune

I.1. Introduction to conjugacy problems for diffeomorphisms. This is a survey article on the area of global analysis defined by differentiable dynamical systems or equivalently the action (differentiable) of a Lie group G on a manifold M . Here $\text{Diff}(M)$ is the group of all diffeomorphisms of M and a diffeomorphism is a differentiable map with a differentiable inverse. (...) Our problem is to study the global structure, i.e., all of the orbits of M .

—Stephen Smale, *Differentiable Dynamical Systems*

WE HAVE LEARNED that the Rössler attractor is very thin, but otherwise the return maps that we found were disquieting – figure 3.6 did not appear to be a one-to-one map. This apparent loss of invertibility is an artifact of projection of higher-dimensional return maps onto their lower-dimensional subspaces. As the choice of a lower-dimensional subspace is arbitrary, the resulting snapshots of return maps look rather arbitrary, too. Such observations beg a question: Does there exist a natural, intrinsic coordinate system in which we should plot a return map?

We shall argue in sect. 12.1 that the answer is yes: The intrinsic coordinates are given by the stable/unstable manifolds, and a return map should be plotted as a map from the unstable manifold back onto the immediate neighborhood of the unstable manifold. In chapter 5 we established that Floquet multipliers of periodic orbits are (local) dynamical invariants. Here we shall show that every equilibrium point and every periodic orbit carries with it stable and unstable manifolds which provide topologically invariant *global* foliation of the state space. They will enable us to partition the state space in a dynamically invariant way, and assign symbolic dynamics itineraries to trajectories.

The topology of stretching and folding fixes the relative spatial ordering of trajectories, and separates the admissible and inadmissible itineraries. We illustrate how this works on Hénon map example 12.3. Determining which symbol sequences are absent, or ‘pruned’ is a formidable problem when viewed in the state

space, $[x_1, x_2, \dots, x_d]$ coordinates. It is equivalent to the problem of determining the location of all homoclinic tangencies, or all turning points of the Hénon attractor. They are dense on the attractor, and show no self-similar structure in the state space coordinates. However, in the ‘danish pastry’ representation of sect. 12.3 (and the ‘pruned danish,’ in American vernacular, of sect. 12.4), the pruning problem is visualized as crisply as the New York subway map; any itinerary which strays into the ‘pruned region’ is banned.

The level is distinctly cyclist, in distinction to the pedestrian tempo of the preceding chapter. Skip most of this chapter unless you really need to get into nitty-gritty details of symbolic dynamics.



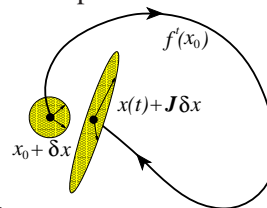
fast track:
chapter 13, p. 248

12.1 Going global: stable/unstable manifolds

The complexity of this figure will be striking, and I shall not even try to draw it.

— H. Poincaré, on his discovery of homoclinic tangles, *Les méthodes nouvelles de la mécanique céleste*

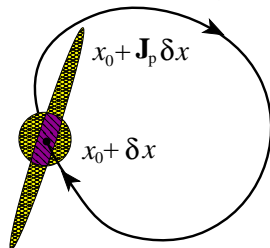
The Jacobian matrix J^t transports an infinitesimal neighborhood, its eigenvalues and eigen-directions describing deformation of an initial infinitesimal sphere of



neighboring trajectories into an ellipsoid time t later, as in figure 4.2.

Nearby trajectories separate exponentially along the unstable directions, approach each other along the stable directions, and creep along the marginal directions.

The fixed point q Jacobian matrix $J(x)$ eigenvectors (5.12) form a rectilinear coordinate frame in which the flow into, out of, or encircling the fixed point is



linear in the sense of sect. 4.2.

The continuations of the span of the local stable, unstable eigen-directions into global curvilinear invariant manifolds are called the *stable*, respectively *unstable manifolds*. They consist of all points which march into the fixed point forward,

respectively backward in time

$$\begin{aligned} W^s &= \{x \in \mathcal{M} : f^t(x) - x_q \rightarrow 0 \text{ as } t \rightarrow \infty\} \\ W^u &= \{x \in \mathcal{M} : f^{-t}(x) - x_q \rightarrow 0 \text{ as } t \rightarrow \infty\}. \end{aligned} \quad (12.1)$$

Eigenvectors $\mathbf{e}^{(i)}$ of the monodromy matrix $J(x)$ play a special role - on them the action of the dynamics is the linear multiplication by Λ_i (for a real eigenvector) along 1 - dimensional invariant curve $W_{(i)}^{u,s}$ or spiral in/out action in a 2-D surface (for a complex pair). For $t \rightarrow \pm\infty$ a finite segment on $W_{(c)}^s$, respectively $W_{(e)}^u$ converges to the linearized map eigenvector $\mathbf{e}^{(c)}$, respectively $\mathbf{e}^{(e)}$, where $^{(c)}$, $^{(e)}$ stand respectively for ‘contracting,’ ‘expanding.’ In this sense each eigenvector defines a (curvilinear) axis of the stable, respectively unstable manifold.

Actual construction of these manifolds is the converse of their definition (12.1): one starts with an arbitrarily small segment of a fixed point eigenvector and lets evolution stretch it into a finite segment of the associated manifold. As a periodic point x on cycle p is a fixed point of $f^{T_p}(x)$, the fixed point discussion that follows applies equally well to equilibria and periodic orbits.

Expanding real and positive Floquet multiplier. Consider i th expanding eigenvalue, eigenvector pair $(\Lambda_i, \mathbf{e}^{(i)})$ computed from $J = J_p(x)$ evaluated at a fixed point x ,

$$J(x)\mathbf{e}^{(i)}(x) = \Lambda_i\mathbf{e}^{(i)}(x), \quad x \in \mathcal{M}_p, \quad \Lambda_i > 1. \quad (12.2)$$

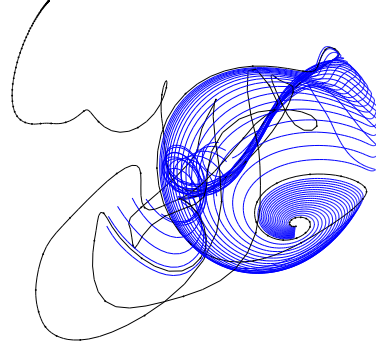
Take an infinitesimal eigenvector $\mathbf{e}^{(i)}(x)$, $\|\mathbf{e}^{(i)}(x)\| = \varepsilon \ll 1$, and its return $\Lambda_i\mathbf{e}^{(i)}(x)$ after one period T_p . Sprinkle the straight interval between $[\varepsilon, \Lambda_i\varepsilon] \subset W_{(i)}^u$ with a large number of points $x^{(k)}$, for example equidistantly spaced on logarithmic scale between $\ln \varepsilon$ and $\ln \Lambda_i + \ln \varepsilon$. The successive returns of these points $f^{T_p}(x^{(k)})$, $f^{2T_p}(x^{(k)})$, \dots , $f^{mT_p}(x^{(k)})$ trace out the 1d curve $W_{(i)}^u$ within the unstable manifold. As separations between points tend to grow exponentially, every so often one needs to interpolate new starting points between the rarified ones. Repeat for $-\mathbf{e}^{(i)}(x)$.

Contracting real and positive Floquet multiplier. Reverse the action of the map backwards in time. This turns a contracting direction into an expanding one, tracing out the curvilinear stable manifold $W_{(i)}^s$ as a continuation of $\mathbf{e}^{(i)}$.

Expanding/contracting real negative Floquet multiplier. As above, but every even iterate $f^{2T_p}(x^{(k)})$, $f^{4T_p}(x^{(k)})$, $f^{6T_p}(x^{(k)})$ continues in the direction $\mathbf{e}^{(i)}$, every odd one in the direction $-\mathbf{e}^{(i)}$.

Complex Floquet multiplier pair, expanding/contracting. The complex Floquet multiplier pair $\{\Lambda_j, \Lambda_{j+1} = \Lambda_j^*\}$ has Floquet exponents (5.9) of form $\lambda^{(j)} = \mu^{(j)} \pm i\omega^{(j)}$, with the sign of $\mu^{(k,j)} \neq 0$ determining whether the linear neighborhood is out / in spiralling. The orthogonal pair of real eigenvectors $\{\text{Re } \mathbf{e}^{(j)}, \text{Im } \mathbf{e}^{(j)}\}$

Figure 12.1: A $2d$ unstable manifold obtained by continuation from the linearized neighborhood of a complex eigenvalue pair of an unstable equilibrium of plane Couette flow, a projection from a 61,506-dimensional state space ODE truncation of the (∞ -dimensional) Navier-Stokes PDE. (J.F. Gibson, 8 Nov. 2005 blog entry [62])



spans a plane, as in (4.28). $T = 2\pi/\omega^{(j)}$ is the time of one turn of the spiral, $J^T \text{Re } \mathbf{e}^{(j)}(x) = |\Lambda_j| \text{Re } \mathbf{e}^{(j)}(x)$. As in the real cases above, sprinkle the straight interval between $[\varepsilon, |\Lambda_j|\varepsilon]$ along $\text{Re } \mathbf{e}^{(j)}(x)$ with a large number of points $x^{(k)}$. The flow will now trace out the $2d$ invariant manifold as an out / in spiralling strip. Two low-dimensional examples are the unstable manifolds of the Lorenz flow, figure 11.8 (a), and the Rössler flow, figure 11.10 (a). For a highly non-trivial example, see figure 12.1.

The unstable manifolds of a flow are d_u -dimensional. Taken together with the marginally stable direction along the flow, they are rather hard to visualize. A more insightful visualization is offered by $(d-1)$ -dimensional Poincaré sections (3.2) with the marginal flow direction eliminated (see also sect. 3.1.1). Stable, unstable manifolds for maps are defined by

$$\begin{aligned}\hat{W}^s &= \{x \in \mathcal{P} : P^n(x) - x_q \rightarrow 0 \text{ as } n \rightarrow \infty\} \\ \hat{W}^u &= \{x \in \mathcal{P} : P^{-n}(x) - x_q \rightarrow 0 \text{ as } n \rightarrow \infty\},\end{aligned}\quad (12.3)$$

where $P(x)$ is the $(d-1)$ -dimensional return map (3.1). In what follows, all invariant manifolds W^u, W^s will be restricted to their Poincaré sections \hat{W}^u, \hat{W}^s .

Example 12.1 A section at a fixed point with a complex Floquet multiplier pair: (continued from example 3.1) The simplest choice of a Poincaré section for a fixed (or periodic) point x_q with a complex Floquet multiplier pair is the plane \mathcal{P} specified by the fixed point (located at the tip of the vector x_q) and the eigenvector $\text{Im } \mathbf{e}^{(k)}$ perpendicular to the plane. A point x is in the section \mathcal{P} if it satisfies the condition

$$(x - x_q) \cdot \text{Im } \mathbf{e}^{(k)} = 0. \quad (12.4)$$

In the neighborhood of x_q the spiral out/in motion is in the $\{\text{Re } \mathbf{e}^{(k)}, \text{Im } \mathbf{e}^{(k)}\}$ plane, and thus guaranteed to be cut by the Poincaré section \mathcal{P} normal to $\mathbf{e}^{(k)}$.

In general the full state space eigenvectors do not lie in a Poincaré section; the eigenvectors $\hat{\mathbf{e}}^{(j)}$ tangent to the section are given by (5.20). Furthermore, while in the linear neighborhood of fixed point x the trajectories return with approximate periodicity T_p , this is not the case for the globally continued manifolds; $\tau(x)$, or the first return times (3.1) differ, and the $\hat{W}_{(j)}^u$ restricted to the Poincaré section is

obtained by continuing trajectories of the points from the full state space curve $W_{(j)}^u$ to the section \mathcal{P} .

For long times the unstable manifolds wander throughout the connected ergodic component, and are no more informative than an ergodic trajectory. For example, the line with equitemporal knots in figure 12.1 starts out on a smoothly curved neighborhood of the equilibrium, but after a ‘turbulent’ episode decays into an attractive equilibrium point. The trick is to stop continuing an invariant manifold while the going is still good.



fast track:
sect. 12.2, p. 229

Learning where to stop is a bit of a technical exercise, the reader might prefer to skip next section on the first reading.

12.1.1 Parametrization of invariant manifolds



As the flow is nonlinear, there is no ‘natural’ linear basis to represent it. Wistful hopes like ‘POD modes,’ ‘Karhunen-Loève,’ and other linear changes of bases do not cut it. The invariant manifolds are curved, and their coordinatizations are of necessity curvilinear, just as the maps of our globe are, but infinitely foliated and thus much harder to chart.

Let us illustrate this by parameterizing a $1d$ slice of an unstable manifold by its arclength. Sprinkle evenly points $\{x^{(1)}, x^{(2)}, \dots, x^{(N-1)}\}$ between the equilibrium point $x_q = x^{(0)}$ and point $x = x^{(N)}$, along the $1d$ unstable manifold continuation $x^{(k)} \in \hat{W}_{(j)}^u$ of the unstable $\hat{e}^{(j)}$ eigendirection (we shall omit the eigendirection label (j) in what follows). Then the arclength from equilibrium point $x_q = x^{(0)}$ to $x = x^{(N)}$ is given by

$$s^2 = \lim_{N \rightarrow \infty} \sum_{k=1}^N g_{ij} dx_i^{(k)} dx_j^{(k)}, \quad dx_i^{(k)} = x_i^{(k)} - x_i^{(k-1)}. \quad (12.5)$$

For the lack of a better idea (perhaps the dynamically determined $g = \mathcal{F}^T J$ would be a more natural metric?) let us measure arclength in the Euclidian metric, $g_j = \delta_{ij}$, so

$$s = \lim_{N \rightarrow \infty} \left(\sum_{k=1}^N (dx^{(k)})^2 \right)^{1/2}. \quad (12.6)$$

By definition $f^{\tau(x)}(x) \in \hat{W}_{(j)}^u$, so $f^t(x)$ induces a $1d$ map $s(s_0, \tau) = s(f^{\tau(x_0)}(x_0))$.

Turning points are points on the unstable manifold for which the local unstable manifold curvature diverges for forward iterates of the map, i.e., points at which the manifold folds back onto itself arbitrarily sharply. For our purposes, approximate turning points suffice. The $1d$ curve $\hat{W}_{(j)}^u$ starts out linear at x_q , then gently curves until—under the influence of other unstable equilibria and/or periodic orbits—it folds back sharply at ‘turning points’ and then nearly retraces itself. This is likely to happen if there is only one unstable direction, as we saw in the Rössler attractor example 11.3, but if there are several, the ‘turning point’ might get stretched out in the non-leading expanding directions.

The trick is to figure out a good *base segment* to the nearest turning point $L = [0, s_b]$, and after the foldback assign to $s(x, t) > s_b$ the nearest point s on the base segment. If the stable manifold contraction is strong, the 2nd coordinate connecting $s(x, t) \rightarrow s$ can be neglected. We saw in example 11.3 how this works. You might, by nature and temperament, take the dark view: Rössler has helpful properties, namely insanely strong contraction along a 1-dimensional stable direction, that are not present in real problems, such as turbulence in a plane Couette flow, and thus the lessons of chapter 11 of no use when it comes to real plumbing. For this reason, both of the training examples to come, the billiards and the Hénon map are of Hamiltonian, phase space preserving type, and thus as far from being insanely contracting as possible. Yet, to a thoughtful reader, they unfold themselves as pages of a book.

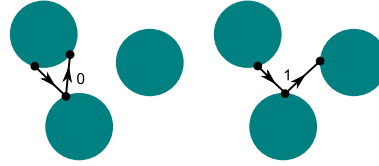
Assign to each d -dimensional point $\hat{x} \in L_q$ a coordinate $s = s(\hat{x})$ whose value is the Euclidean arclength (12.5) to x_q measured along the 1-dimensional \mathcal{P}_q section of the x_q unstable manifold. Next, for a nearby point $\hat{x}_0 \notin L_q$ determine the point $\hat{x}_1 \in L_q$ which minimizes the Euclidean distance $(\hat{x}_0 - \hat{x}_1)^2$, and assign arc length coordinate value $s_0 = s(\hat{x}_1)$ to \hat{x}_0 . In this way, an approximate 1-dimensional intrinsic coordinate system is built along the unstable manifold. This parametrization is useful if the non-wandering set is sufficiently thin that its perpendicular extent can be neglected, with every point on the non-wandering set assigned the nearest point on the base segment L_q .

Armed with this intrinsic curvilinear coordinate parametrization, we are now in a position to construct a 1-dimensional model of the dynamics on the non-wandering set. If \hat{x}_n is the n th Poincaré section of a trajectory in neighborhood of x_q , and s_n is the corresponding curvilinear coordinate, then $s_{n+1} = f^{t_n}(s_n)$ models the full state space dynamics $\hat{x}_n \rightarrow \hat{x}_{n+1}$. We approximate $f(s_n)$ by a smooth, continuous 1-dimensional map $f : L_q \rightarrow L_q$ by taking $\hat{x}_n \in L_q$, and assigning to \hat{x}_{n+1} the nearest base segment point $s_{n+1} = s(\hat{x}_{n+1})$.

12.2 Horseshoes

If you find yourself mystified by Smale’s article abstract quoted on page 229, about ‘the action (differentiable) of a Lie group G on a manifold M ,’ time has come to bring Smale to everyman. If you still remain mystified by the end of this chapter, reading chapter 16 might help; for example, the Liouville operators

Figure 12.2: Binary labeling of trajectories of the symmetric 3-disk pinball; a bounce in which the trajectory returns to the preceding disk is labeled 0, and a bounce which results in continuation to the third disk is labeled 1.



form a Lie group of symplectic, or canonical transformations acting on the (p, q) manifold.

If a flow is locally unstable but globally bounded, any open ball of initial points will be stretched out and then folded. An example is a 3-dimensional invertible flow sketched in figure 11.10 which returns a Poincaré section of the flow folded into a ‘horseshoe’ (we shall belabor this in figure 12.4). We now offer two examples of locally unstable but globally bounded flows which return an initial area stretched and folded into a ‘horseshoe,’ such that the initial area is intersected at most twice. We shall refer to such mappings with at most 2^i transverse self-intersections at the n th iteration as the *once-folding* maps.

exercise 12.1

The first example is the 3-disk game of pinball figure 11.5, which, for sufficiently separated disks (see figure 11.6), is an example of a complete Smale horseshoe. We start by exploiting its symmetry to simplify it, and then partition its state space by its stable / unstable manifolds.

Example 12.2 Recoding 3-disk dynamics in binary. (continued from example 11.2) *The $\mathcal{A} = \{1, 2, 3\}$ symbolic dynamics for 3-disk system is neither unique, nor necessarily the smartest one - before proceeding it pays to quotient the symmetries of the dynamics in order to obtain a more efficient description. We do this in a quick way here, and redo it in more detail in sect. 12.5.*

As the three disks are equidistantly spaced, the disk labels are arbitrary; what is important is how a trajectory evolves as it hits subsequent disks, not what label the starting disk had. We exploit this symmetry by recoding, in this case replacing the absolute disk labels by relative symbols, indicating the type of the collision. For the 3-disk game of pinball there are two topologically distinct kinds of collisions, figure 12.2:

$$s_i = \begin{cases} 0 & : \text{ pinball returns to the disk it came from} \\ 1 & : \text{ pinball continues to the third disk.} \end{cases} \quad (12.7)$$

exercise 11.1

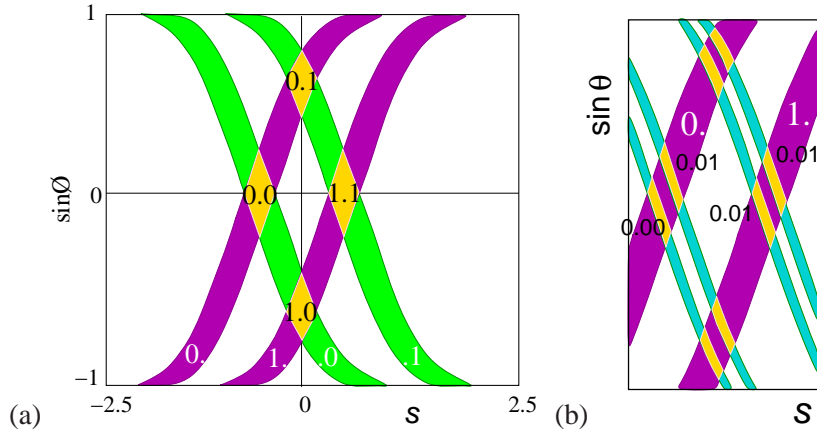
exercise 12.6

In the binary recoding of the 3-disk symbolic dynamics the prohibition of self-bounces is automatic. If the disks are sufficiently far apart there are no further restrictions on symbols, the symbolic dynamics is complete, and all binary sequences (see table 15.1) are admissible.

exercise 11.2

It is intuitively clear that as we go backward in time (reverse the velocity vector), we also need increasingly precise specification of $x_0 = (s_0, p_0)$ in order to follow a given past itinerary. Another way to look at the survivors after two bounces is to plot \mathcal{M}_{s_1, s_2} , the intersection of \mathcal{M}_{s_2} with the strips \mathcal{M}_{s_1} , obtained by time reversal (the velocity changes sign $\sin \phi \rightarrow -\sin \phi$). \mathcal{M}_{s_1, s_2} , figure 12.3 (a), is a ‘rectangle’ of nearby trajectories which have arrived from disk s_1 and are heading for disk s_2 . (continued in example 12.6)

Figure 12.3: The 3-disk game of pinball of figure 11.5, generated by starting from disk 1, preceded by disk 2, coded in binary, as in figure 12.2. (a) Strips $\mathcal{M}_{s_i,j}$ which have survived a bounce in the past and will survive a bounce in the future. (b) Iteration corresponds to the decimal point shift; for example, all points in the rectangle [1.01] map into the rectangles [0.10], [0.11] in one iteration.



The 3-disk repeller does not really look like a ‘horseshoe;’ the ‘fold’ is cut out of the picture by allowing the pinballs that fly between the disks to fall off the table and escape. Next example captures the ‘stretch & fold’ horseshoe dynamics of return maps such as Rössler’s, figure 3.5.

Example 12.3 A Hénon repeller complete horseshoe: (continued from example 3.7) Consider 2-dimensional Hénon map

exercise 3.5

$$(x_{n+1}, y_{n+1}) = (1 - ax_n^2 + by_n, x_n). \tag{12.8}$$

If you start with a small ball of initial points centered around the fixed point x_0 , and iterate the map, the ball will be stretched and squashed along the unstable manifold W_0^u . Iterated backward in time,

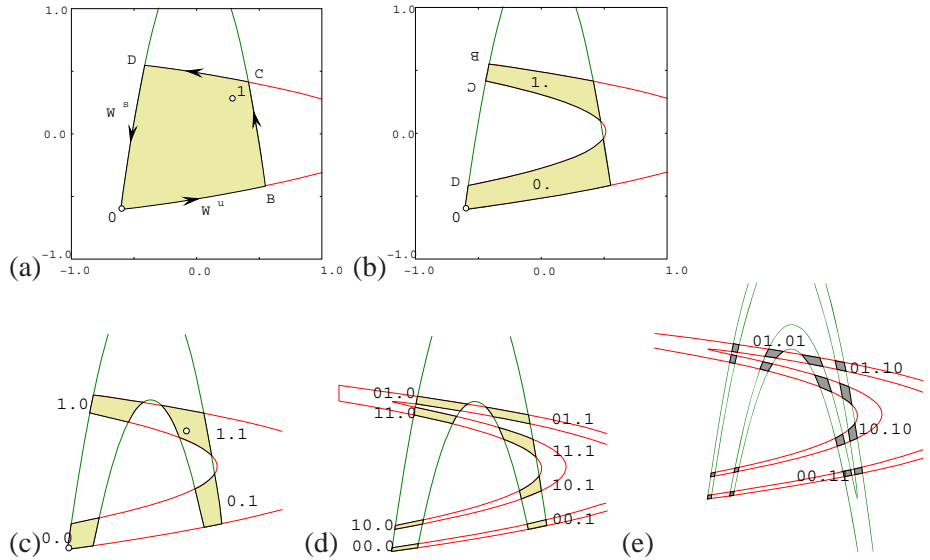
$$(x_{n-1}, y_{n-1}) = (y_n, -b^{-1}(1 - ay_n^2 - x_n)), \tag{12.9}$$

this small ball of initial points traces out the stable manifold W_0^s . Their intersections enclose the region \mathcal{M} , figure 12.4(a). Any point outside W_0^s border of \mathcal{M} escapes to infinity forward in time, while –by time reversal– any point outside W_0^u border arrives from infinity back in paste. In this way the unstable - stable manifolds define topologically, invariant and optimal initial region \mathcal{M} ; all orbits that stay confined for all times are confined to \mathcal{M} .

The Hénon map models qualitatively the Poincaré section return map of figure 11.10. For $b = 0$ the Hénon map reduces to the parabola (11.3), and, as shown in sects. 3.3 and 29.1, for $b \neq 0$ it is kind of a fattened parabola; by construction, it takes a rectangular initial area and returns it bent as a horseshoe. Parameter a controls the amount of stretching, while the parameter b controls the amount of compression of the folded horseshoe. For definitiveness, fix the parameter values to $a = 6$, $b = -1$; the map is then strongly stretching but area preserving, the furthest away from the strongly dissipative examples discussed in sect. 11.2. The map is quadratic, so it has 2 fixed points $x_0 = f(x_0)$, $x_1 = f(x_1)$ indicated in figure 12.4(a). For the parameter values at hand, they are both unstable.

Iterated one step forward, the region \mathcal{M} is stretched and folded into a Smale horseshoe drawn in figure 12.4(b). Label the two forward intersections $f(\mathcal{M}) \cap \mathcal{M}$ by \mathcal{M}_s , with $s \in \{0, 1\}$. The horseshoe consists of the two strips $\mathcal{M}_0, \mathcal{M}_1$, and the bent segment that lies entirely outside the W_0^s line. As all points in this segment escape to infinity under forward iteration, this region can safely be cut out and thrown away.

Figure 12.4: The Hénon map (12.8) for $a = 6, b = -1$: fixed point $\bar{0}$ with segments of its stable, unstable manifolds W^s, W^u , and fixed point $\bar{1}$. (a) Their intersection bounds the region $\mathcal{M} = 0BCD$ which contains the non-wandering set Ω . (b) The intersection of the forward image $f(\mathcal{M})$ with \mathcal{M} consists of two (future) strips $\mathcal{M}_0, \mathcal{M}_1$, with points BCD brought closer to fixed point $\bar{0}$ by the stable manifold contraction. (c) The intersection of the forward image $f(\mathcal{M})$ with the backward backward $f^{-1}(\mathcal{M})$ is a four-region cover of Ω . (d) The intersection of the twice-folded forward horseshoe $f^2(\mathcal{M})$ with backward horseshoe $f^{-1}(\mathcal{M})$. (e) The intersection of $f^2(\mathcal{M})$ with $f^{-2}(\mathcal{M})$ is a 16-region cover of Ω . Iteration yields the complete Smale horseshoe non-wandering set Ω , i.e., the union of all non-wandering points of f , with every forward fold intersecting every backward fold. (P. Cvitanović and Y. Matsuoka)



Iterated one step backwards, the region \mathcal{M} is again stretched and folded into a horseshoe, figure 12.4(c). As stability and instability are interchanged under time reversal, this horseshoe is transverse to the forward one. Again the points in the horseshoe bend wander off to infinity as $n \rightarrow -\infty$, and we are left with the two (past) strips $\mathcal{M}_0, \mathcal{M}_1$. Iterating two steps forward we obtain the four strips $\mathcal{M}_{11}, \mathcal{M}_{01}, \mathcal{M}_{00}, \mathcal{M}_{10}$, and iterating backwards we obtain the four strips $\mathcal{M}_{00}, \mathcal{M}_{01}, \mathcal{M}_{11}, \mathcal{M}_{10}$ transverse to the forward ones just as for 3-disk pinball game figure 12.2. Iterating three steps forward we get an 8 strips, and so on ad infinitum. (continued in example 12.4)

What is the significance of the subscript such as $_{.011}$ which labels the \mathcal{M}_{011} future strip? The two strips $\mathcal{M}_0, \mathcal{M}_1$ partition the state space into two regions labeled by the two-letter alphabet $\mathcal{A} = \{0, 1\}$. $S^+ = .011$ is the *future itinerary* for all $x \in \mathcal{M}_{011}$. Likewise, for the past strips all $x \in \mathcal{M}_{s_{-m} \dots s_{-1} s_0}$ have the *past itinerary* $S^- = s_{-m} \dots s_{-1} s_0$. Which partition we use to present pictorially the regions that do not escape in m iterations is a matter of taste, as the backward strips are the preimages of the forward ones

$$\mathcal{M}_0 = f(\mathcal{M}_{.0}), \quad \mathcal{M}_1 = f(\mathcal{M}_{.1}).$$

Ω , the non-wandering set (2.2) of \mathcal{M} , is the union of all points whose forward and backward trajectories remain trapped for all time, given by the intersections of all images and preimages of \mathcal{M} :

$$\Omega = \left\{ x : x \in \lim_{m,n \rightarrow \infty} f^m(\mathcal{M}) \cap f^{-n}(\mathcal{M}) \right\}. \quad (12.10)$$

Two important properties of the Smale horseshoe are that it has a *complete binary symbolic dynamics* and that it is *structurally stable*.

For a *complete* Smale horseshoe every forward fold $f^n(\mathcal{M})$ intersects transversally every backward fold $f^{-m}(\mathcal{M})$, so a unique bi-infinite binary sequence can be

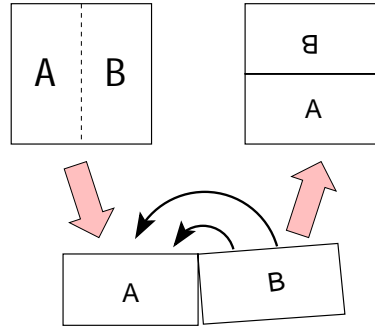


Figure 12.5: Kneading orientation preserving danish pastry: mimic the horseshoe dynamics of figure 12.6 by: (1) squash the unit square by factor 1/2, (2) stretch it by factor 2, and (3) fold the right half back over the left half.

associated to every element of the non-wandering set. A point $x \in \Omega$ is labeled by the intersection of its past and future itineraries $S(x) = \cdots s_2 s_1 s_0 \cdot s_1 s_2 \cdots$, where $s_n = s$ if $f^n(x) \in M_s$, $s \in \{0, 1\}$ and $n \in \mathbb{Z}$.

remark A.1

The system is said to be *structurally stable* if all intersections of forward and backward iterates of M remain transverse for sufficiently small perturbations $f \rightarrow f + \delta$ of the flow, for example, for slight displacements of the disks in the pinball problem, or sufficiently small variations of the Hénon map parameters a, b . While structural stability is exceedingly desirable, it is also exceedingly rare. About this, more later.

section 1.8

section 25.2

12.3 Symbol plane

Consider a system for which you have succeeded in constructing a covering symbolic dynamics, such as a well-separated 3-disk system. Now start moving the disks toward each other. At some critical separation a disk will start blocking families of trajectories traversing the other two disks. The order in which trajectories disappear is determined by their relative ordering in space; the ones closest to the intervening disk will be pruned first. Determining inadmissible itineraries requires that we relate the spatial ordering of trajectories to their time ordered itineraries.

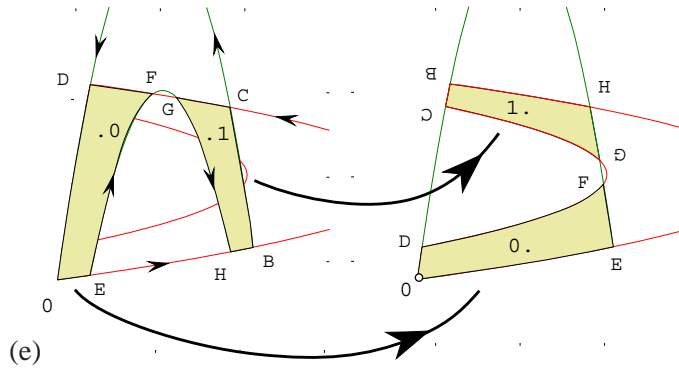
exercise 12.7

So far we have rules that, given a state space partition, generate a *temporally* ordered itinerary for a given trajectory. Our next task is the converse: given a set of itineraries, what is the *spatial* ordering of corresponding points along the trajectories? In answering this question we will be aided by Smale’s visualization of the relation between the topology of a flow and its symbolic dynamics by means of ‘horseshoes,’ such as figure 12.4.

12.3.1 Kneading danish pastry

The danish pastry transformation, the simplest baker’s transformation appropriate to Hénon type mappings, yields a binary coordinatization of all possible periodic points.

Figure 12.6: The dynamics maps two (past) strips $\mathcal{M}_0, \mathcal{M}_1$ into two (future) strips $\mathcal{M}_0, \mathcal{M}_1$. The corners are labeled to aid visualization. Note that the $BCGH$ strip is rotated by 180 degrees. (P. Cvitanović and Y. Matsuoka)



The symbolic dynamics of once-folding map is given by the danish pastry transformation. This generates both the longitudinal and transverse alternating binary tree. The longitudinal coordinate is given by the head of a symbolic sequence; the transverse coordinate is given by the tail of the symbolic sequence. The dynamics on this space is given by symbol shift permutations; volume preserving, with 2 expansion and 1/2 contraction.

For a better visualization of 2-dimensional non-wandering sets, fatten the intersection regions until they completely cover a unit square, as in figure 12.7. We shall refer to such a ‘map’ of the topology of a given ‘stretch & fold’ dynamical system as the *symbol square*. The symbol square is a topologically accurate representation of the non-wandering set and serves as a street map for labeling its pieces. Finite memory of m steps and finite foresight of n steps partitions the symbol square into *rectangles* $[s_{-m+1} \cdots s_0.s_1s_2 \cdots s_n]$, such as those of figure 12.6. In the binary dynamics symbol square the size of such rectangle is $2^m \times 2^{-n}$; it corresponds to a region of the dynamical state space which contains all points that share common n future and m past symbols. This region maps in a nontrivial way in the state space, but in the symbol square its dynamics is exceedingly simple; all of its points are mapped by the decimal point shift (11.20)

exercise 12.2
exercise 12.3

$$\sigma(\cdots s_{-2}s_{-1}s_0.s_1s_2s_3 \cdots) = \cdots s_{-2}s_{-1}s_0s_1.s_2s_3 \cdots, \quad (12.11)$$

Example 12.4 A Hénon repeller subshift: (continued from example 12.3) The Hénon map acts on the binary partition as a shift map. Figure 12.6 illustrates action $f(\mathcal{M}_0) = \mathcal{M}_0$. The square $[01.01]$ gets mapped into the rectangles $\sigma[01.01] = [10.1] = \{[10.10], [10.11]\}$, see figure 12.4 (e). Further examples can be gleaned from figure 12.4.

As the horseshoe mapping is a simple repetitive operation, we expect a simple relation between the symbolic dynamics labeling of the horseshoe strips, and their relative placement. The symbol square points $\gamma(S^+)$ with future itinerary S^+ are constructed by converting the sequence of s_n 's into a binary number by the algorithm (11.9). This follows by inspection from figure 12.9. In order to understand this relation between the topology of horseshoes and their symbolic dynamics, it might be helpful to backtrace to sect. 11.4 and work through and understand first the symbolic dynamics of 1-dimensional unimodal mappings.

Figure 12.7: Kneading danish pastry: symbol square representation of an orientation preserving once-folding map obtained by fattening the Smale horseshoe intersections of (a) figure 12.6 (b) figure 12.4 into a unit square. Also indicated: the fixed points $\bar{0}$, $\bar{1}$ and the 2-cycle points $\{0\bar{1}, \bar{1}0\}$. In the symbol square the dynamics maps rectangles into rectangles by a decimal point shift.

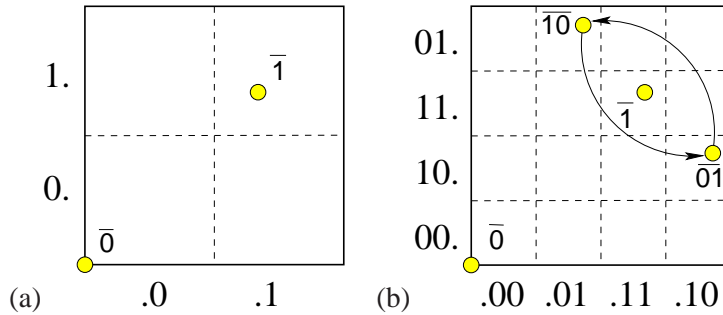
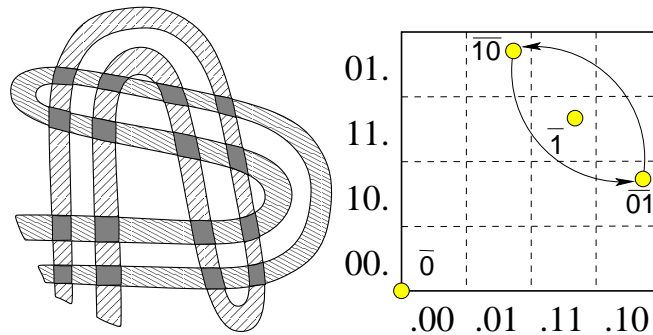


Figure 12.8: Kneading orientation preserving danish pastry: symbol square representation of an orientation preserving once-folding map obtained by fattening the intersections of two forward iterates / two backward iterates of Smale horseshoe into a unit square.



Under backward iteration the roles of 0 and 1 symbols are interchanged; \mathcal{M}_b^1 has the same orientation as \mathcal{M} , while \mathcal{M}_f^1 has the opposite orientation. We assign to an *orientation preserving* once-folding map the *past topological coordinate* $\delta = \delta(S^-)$ by the algorithm:

exercise 12.4

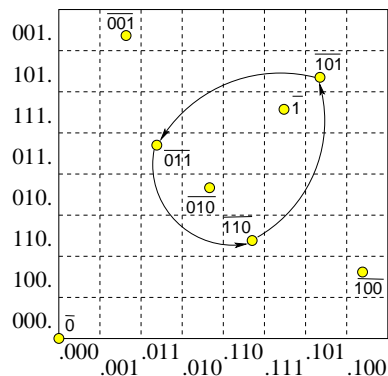
$$w_{n-1} = \begin{cases} w_n & \text{if } s_n = 0 \\ 1 - w_n & \text{if } s_n = 1 \end{cases}, \quad w_0 = s_0$$

$$\delta(S^-) = 0.w_0w_{-1}w_{-2}\dots = \sum_{n=1}^{\infty} w_{1-n}/2^n. \tag{12.12}$$

Such formulas are best derived by solitary contemplation of the action of a folding map, in the same way we derived the future topological coordinate (11.9).

The coordinate pair (δ, γ) associates a point (x, y) in the state space Cantor set of figure 12.4 to a point in the symbol square of figure 12.9, preserving the

Figure 12.9: Kneading danish pastry: symbol square representation of an orientation preserving once-folding map obtained by fattening the Smale horseshoe intersections of figure 12.4 (e) into a unit square. Also indicated: the fixed points $\bar{0}$, $\bar{1}$, and the 3-cycle points $\{011, 110, 101\}$. In the symbol square the dynamics maps rectangles into rectangles by a decimal point shift.



topological ordering. The symbol square $[\delta, \gamma]$ serves as a topologically faithful representation of the non-wandering set of any once-folding map, and aids us in partitioning the set and ordering the partitions for any flow of this type.



fast track:
chapter 13, p. 248

12.4 Prune danish

Anyone know where I can get a good prune danish in Charlotte? I mean a real NY Jewish bakery kind of prune danish!

— Googled

In general, not all possible symbol sequences are realized as physical trajectories. Trying to get from ‘here’ to ‘there’ we might find that a short path is excluded by some obstacle, such as a disk that blocks the path, or a potential ridge. In order to enumerate orbits correctly, we need to *prune* the inadmissible symbol sequences, i.e., describe the grammar of the admissible itineraries.

The complete Smale horseshoe dynamics discussed so far is rather straightforward, and sets the stage for situations that resembles more the real life. A generic once-folding map does not yield a complete horseshoe; some of the horseshoe pieces might be *pruned*, i.e., not realized for particular parameter values of the mapping. In 1 dimension, the criterion for whether a given symbolic sequence is realized by a given unimodal map is easily formulated; any orbit that strays to the right of the value computable from the *kneading sequence* (the orbit of the critical point (11.13)) is pruned. This is a topological statement, independent of a particular unimodal map. Our objective is to generalize this notion to 2 – dimensional once-folding maps.

Adjust the parameters of a once-folding map so that the intersection of the backward and forward folds is still transverse, but no longer complete, as in figure 12.10 (a). The utility of the symbol square lies in the fact that the surviving, admissible itineraries still maintain the same relative spatial ordering as for the complete case.

In the example of figure 12.10 the rectangles $[10.1]$, $[11.1]$ have been pruned, and consequently *any* trajectory containing blocks $b_1 = 101$, $b_2 = 111$ is pruned, the symbol dynamics is a subshift of finite type (11.24). We refer to the border of this primary pruned region as the *pruning front*; another example of a pruning front is drawn in figure 12.11 (b). We call it a ‘front’ as it can be visualized as a border between admissible and inadmissible; any trajectory whose points would fall to the right of the front in figure 12.11 is inadmissible, i.e., pruned. The pruning front is a complete description of the symbolic dynamics of once-folding maps. For now we need this only as a concrete illustration of how pruning rules arise.

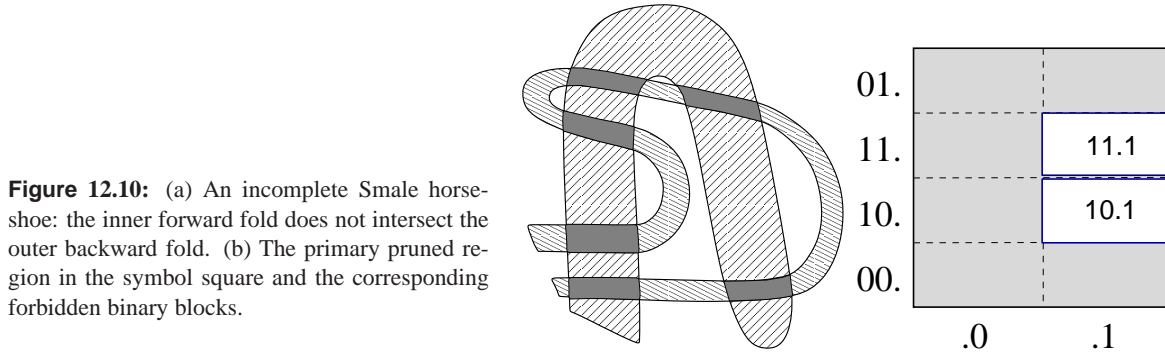


Figure 12.10: (a) An incomplete Smale horseshoe: the inner forward fold does not intersect the outer backward fold. (b) The primary pruned region in the symbol square and the corresponding forbidden binary blocks.

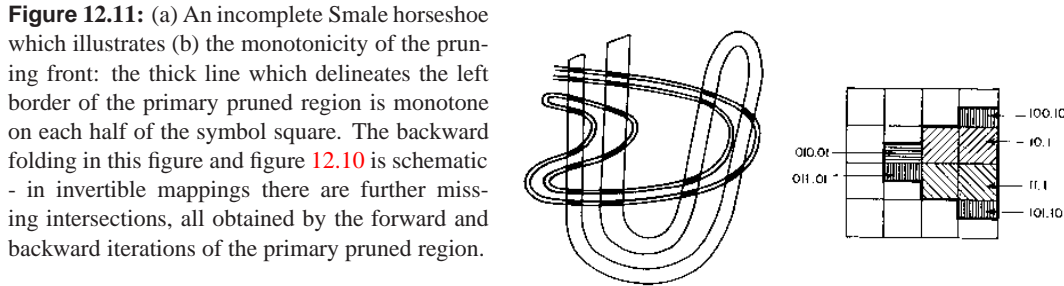




Figure 12.11: (a) An incomplete Smale horseshoe which illustrates (b) the monotonicity of the pruning front: the thick line which delineates the left border of the primary pruned region is monotone on each half of the symbol square. The backward folding in this figure and figure 12.10 is schematic - in invertible mappings there are further missing intersections, all obtained by the forward and backward iterations of the primary pruned region.

In the example at hand there are total of two forbidden blocks 101, 111, so for now we concentrate on this kind of pruning because it is particularly clean and simple.

 fast track:
chapter 13, p. 248

Though a useful tool, Markov partitioning is not without drawbacks. One glaring shortcoming is that Markov partitions are not unique: any of many different partitions might do the job. The C_2 - and D_3 -equivariant systems that we discuss next offers a simple illustration of different Markov partitioning strategies for the same dynamical system.

12.5 Recoding, symmetries, tilings

 In chapter 9 we made a claim that if there is a symmetry of dynamics, we must use it. Here we shall show how to use it, on two concrete examples, and in chapter 21 we shall be handsomely rewarded for our labors. First, the simplest example of equivariance, a single ‘reflection’ C_2 group of example 9.13.

Example 12.5 C_2 recoded: Assume that each orbit is uniquely labeled by an infinite string $\{s_i\}$, $s_i \in \{+, -\}$ and that the dynamics is C_2 -equivariant under the $+ \leftrightarrow -$ interchange. Periodic orbits separate into two classes, the self-dual configurations $+-$, $++--$, $+-+-$, $+-+-$, $+-+-$, $+-+-$, \dots , with multiplicity $m_p = 1$, and the pairs $+$, $-$, $++-$, $--+$, \dots , with multiplicity $m_p = 2$. For example, as there is no absolute distinction exercise 9.6

Table 12.1: Correspondence between the C_2 symmetry reduced cycles \tilde{p} and the full state space periodic orbits p , together with their multiplicities m_p . Also listed are the two shortest cycles (length 6) related by time reversal, but distinct under C_2 .

\tilde{p}	p	m_p
1	+	2
0	-+	1
01	-- ++	1
001	-++	2
011	--- +++	1
0001	-+-- +-++	1
0011	-+++	2
0111	---- ++++	1
00001	-+-+-	2
00011	-+---- +-+++	1
00101	-++-- +- -++	1
00111	-+---- +-+++	1
01011	--+++	2
01111	----- +++++	1
001011	-++---- +- -+++	1
001101	-+++-- +- - -++	1

between the ‘left’ or the ‘right’ lobe of the Lorenz attractor, figure 3.7 (a), the Floquet multipliers satisfy $\Lambda_+ = \Lambda_-$, $\Lambda_{++-} = \Lambda_{+--}$, and so on.

exercise 21.5

The symmetry reduced labeling $\rho_i \in \{0, 1\}$ is related to the full state space labeling $s_i \in \{+, -\}$ by

$$\begin{aligned} \text{If } s_i &= s_{i-1} \text{ then } \rho_i = 1 \\ \text{If } s_i &\neq s_{i-1} \text{ then } \rho_i = 0 \end{aligned} \tag{12.13}$$

For example, the fixed point $\overline{+} = \dots + + + \dots$ maps into $\dots 111 \dots = \overline{1}$, and so does the fixed point $\overline{-}$. The 2-cycle $\overline{+-} = \dots - + - + \dots$ maps into fixed point $\dots 000 \dots = \overline{0}$, and the 4-cycle $\overline{+-+-} = \dots - - + + - - + + \dots$ maps into 2-cycle $\dots 0101 \dots = \overline{01}$. A list of such reductions is given in table 12.1.

Next, let us take the old pinball game and ‘quotient’ the state space by the symmetry, or ‘desymmetrize.’ As the three disks are equidistantly spaced, our game of pinball has a sixfold symmetry. For instance, the cycles $\overline{12}$, $\overline{23}$, and $\overline{13}$ in figure 12.12 are related to each other by rotation by $\pm 2\pi/3$ or, equivalently, by a relabeling of the disks. We exploit this symmetry by recoding, as in (12.7).

exercise 11.1

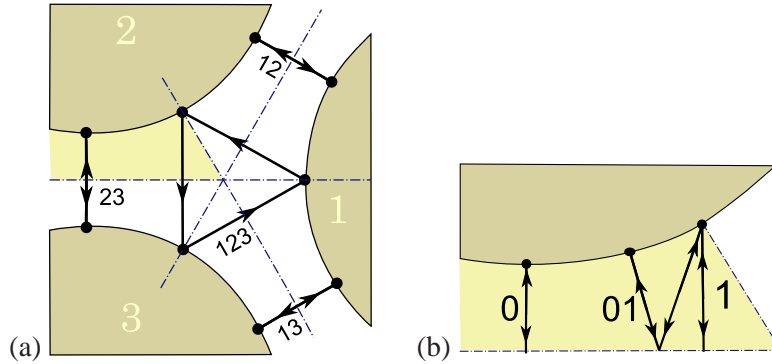
exercise 12.6

Example 12.6 Recoding ternary symbolic dynamics in binary: Given a ternary sequence and labels of 2 preceding disks, rule (12.7) fixes the subsequent binary symbols. Here we list an arbitrary ternary itinerary, and the corresponding binary sequence:

$$\begin{aligned} \text{ternary} &: 3 \ 1 \ 2 \ 1 \ 3 \ 1 \ 2 \ 3 \ 2 \ 1 \ 2 \ 3 \ 1 \ 3 \ 2 \ 3 \\ \text{binary} &: \cdot \ 1 \ 0 \ 1 \ 0 \ 1 \ 1 \ 0 \ 1 \ 0 \ 1 \ 1 \ 0 \ 1 \ 0 \end{aligned} \tag{12.14}$$

The first 2 disks initialize the trajectory and its direction; $3 \mapsto 1 \mapsto 2 \mapsto \dots$. Due to the 3-disk symmetry the six distinct 3-disk sequences initialized by 12, 13, 21, 23, 31, 32 respectively have the same weights, the same size state space partitions, and are coded by a single binary sequence. (continued in example 12.7)

Figure 12.12: The 3-disk game of pinball with the disk radius : center separation ratio $a:R = 1:2.5$. (a) 2-cycles $\overline{12}$, $\overline{13}$, $\overline{23}$, and 3-cycles $\overline{123}$ and $\overline{132}$ (not drawn). (b) The fundamental domain, i.e., the small 1/6th wedge indicated in (a), consisting of a section of a disk, two segments of symmetry axes acting as straight mirror walls, and an escape gap. The above five cycles restricted to the fundamental domain are the two fixed points $\overline{0}$, $\overline{1}$. See figure 9.6 for cycle $\overline{10}$ and further examples.



exercise 12.7
exercise 14.2

Binary symbolic dynamics has two immediate advantages over the ternary one; the prohibition of self-bounces is automatic, and the coding utilizes the symmetry of the 3-disk pinball game in an elegant manner.

exercise 11.2

The 3-disk game of pinball is tiled by six copies of the *fundamental domain*, a one-sixth slice of the full 3-disk system, with the symmetry axes acting as reflecting mirrors, see figure 12.12 (b). Every global 3-disk trajectory has a corresponding fundamental domain mirror trajectory obtained by replacing every crossing of a symmetry axis by a reflection. Depending on the symmetry of the full state space trajectory, a repeating binary alphabet block corresponds either to the full periodic orbit or to a relative periodic orbit (examples are shown in figure 12.12 and table 12.2). A relative periodic orbit corresponds to a periodic orbit in the fundamental domain.

Table 12.2 lists some of the shortest binary periodic orbits, together with the corresponding full 3-disk symbol sequences and orbit symmetries. For a number of deep reasons that will be elucidated in chapter 21, life is much simpler in the fundamental domain than in the full system, so whenever possible our computations will be carried out in the fundamental domain.

Example 12.7 D_3 recoded - 3-disk game of pinball: (continued from example 12.6) The D_3 recoding can be worked out by a glance at figure 12.12 (a) (continuation of example 9.14). For the symmetric 3-disk game of pinball the fundamental domain is bounded by a disk segment and the two adjacent sections of the symmetry axes that act as mirrors (see figure 12.12 (b)). The three symmetry axes divide the space into six copies of the fundamental domain. Any trajectory on the full space can be pieced together from bounces in the fundamental domain, with symmetry axes replaced by flat mirror reflections. The binary $\{0, 1\}$ reduction of the ternary three disk $\{1, 2, 3\}$ labels has a simple geometric interpretation, figure 12.2: a collision of type 0 reflects the projectile to the disk it comes from (back-scatter), whereas after a collision of type 1 projectile continues to the third disk. For example, $\overline{23} = \dots 232323 \dots$ maps into $\dots 000 \dots = \overline{0}$ (and so do $\overline{12}$ and $\overline{13}$), $\overline{123} = \dots 12312 \dots$ maps into $\dots 111 \dots = \overline{1}$ (and so does $\overline{132}$), and so forth. Such reductions for short cycles are given in table 12.2, figure 12.12 and figure 9.7.

Table 12.2: D_3 correspondence between the binary labeled fundamental domain prime cycles \tilde{p} and the full 3-disk ternary labeled cycles p , together with the D_3 transformation that maps the end point of the \tilde{p} cycle into the irreducible segment of the p cycle, see sect. 9.12. Breaks in the above ternary sequences mark repeats of the irreducible segment; for example, the full space 12-cycle 1212 3131 2323 consists of 1212 and its symmetry related segments 3131, 2323. The multiplicity of p cycle is $m_p = 6n_{\tilde{p}}/n_p$. The shortest pair of fundamental domain cycles related by time reversal (but no spatial symmetry) are the 6-cycles $\overline{001011}$ and $\overline{001101}$.

\tilde{p}	p	$\mathbf{g}_{\tilde{p}}$	\tilde{p}	p	$\mathbf{g}_{\tilde{p}}$
0	1 2	σ_{12}	000001	121212 131313	σ_{23}
1	1 2 3	C	000011	121212 313131 232323	C^2
01	12 13	σ_{23}	000101	121213	e
001	121 232 313	C	000111	121213 212123	σ_{12}
011	121 323	σ_{13}	001011	121232 131323	σ_{23}
0001	1212 1313	σ_{23}	001101	121231 323213	σ_{13}
0011	1212 3131 2323	C^2	001111	121231 232312 313123	C
0111	1213 2123	σ_{12}	010111	121312 313231 232123	C^2
00001	12121 23232 31313	C	011111	121321 323123	σ_{13}
00011	12121 32323	σ_{13}	0000001	1212121 2323232 3131313	C
00101	12123 21213	σ_{12}	0000011	1212121 3232323	σ_{13}
00111	12123	e	0000101	1212123 2121213	σ_{12}
01011	12131 23212 31323	C	0000111	1212123	e
01111	12132 13123	σ_{23}

Résumé

In the preceding and this chapter we start with a d -dimensional state space and end with a 1-dimensional return map description of the dynamics. The arc-length parametrization of the unstable manifold maintains the 1-to-1 relation of the full d -dimensional state space dynamics and its 1-dimensional return-map representation. To high accuracy *no information about the flow is lost* by its 1-dimensional return map description. We explain why Lorenz equilibria are heteroclinically connected (it is not due to the symmetry), and how to generate all periodic orbits of Lorenz flow up to given length. This we do, in contrast to the rest of the thesis, without any group-theoretical jargon to blind you with.

For 1-dimensional maps the folding point is the critical point, and easy to determine. In higher dimensions, the situation is not so clear - one can attempt to determine the (fractal set of) folding points by looking at their higher iterates - due to the contraction along stable manifolds, the fold gets to be exponentially sharper at each iterate. In practice this set is essentially uncontrollable for the same reason the flow itself is chaotic - exponential growth of errors. We prefer to determine a folding point by bracketing it by longer and longer cycles which can be determined accurately using variational methods of chapter 29, irrespective of their period.

For a generic dynamical system a subshift of finite type is the exception rather than the rule. Its symbolic dynamics can be arbitrarily complex; even for the logistic map the grammar is finite only for special parameter values. Only some repelling sets (like our game of pinball) and a few purely mathematical constructs (called Anosov flows) are structurally stable - for most systems of inter-

est an infinitesimal perturbation of the flow destroys and/or creates an infinity of trajectories, and specification of the grammar requires determination of pruning blocks of arbitrary length. The repercussions are dramatic and counterintuitive; for example, the transport coefficients such as the deterministic diffusion constant of sect. 25.2 are emphatically *not* smooth functions of the system parameters. Importance of symbolic dynamics is often grossly unappreciated; as we shall see in chapters 20 and 23, the existence of a finite grammar is the crucial prerequisite for construction of zeta functions with nice analyticity properties. This generic lack of structural stability is what makes nonlinear dynamics so hard.

section 25.2

The conceptually simpler finite subshift Smale horseshoes suffice to motivate most of the key concepts that we shall need for time being. Our strategy is akin to bounding a real number by a sequence of rational approximants; we converge toward the non-wandering set under investigation by a sequence of self-similar Cantor sets. The rule that everything to one side of the pruning front is forbidden might be striking in its simplicity: instead of pruning a Cantor set embedded within some larger Cantor set, the pruning front cleanly cuts out a *compact* region in the symbol square, and that is all - there are no additional pruning rules. A ‘self-similar’ Cantor set (in the sense in which we use the word here) is a Cantor set equipped with a *subshift of finite type* symbol dynamics, i.e., the corresponding grammar can be stated as a finite number of pruning rules, each forbidding a finite subsequence $_s_1 s_2 \dots s_n _$. Here the notation $_s_1 s_2 \dots s_n _$ stands for n consecutive symbols s_1, s_2, \dots, s_n , preceded and followed by arbitrary symbol strings.

The symbol square is a useful tool in transforming topological pruning into pruning rules for inadmissible sequences; those are implemented by constructing transition matrices and/or graphs, see chapters 14 and 15.

Commentary

Remark 12.1 Stable/unstable manifolds. For pretty hand-drawn pictures of invariant manifolds, see Abraham and Shaw [10]. Construction of invariant manifolds by map iteration is described in Simo [35]. Fixed point stable / unstable manifolds and their homoclinic and heteroclinic intersections can be computed using DsTool [59, 60, 61]. Unstable manifold turning points were utilized in refs. [13, 2, 32, 33, 34] to partition state space and prune inadmissible symbol sequences. The arclength parameterized return maps were introduced by Christiansen *et al.* [63], and utilized in ref. [37]. Even though no dynamical system has been studied more exhaustively than the Lorenz equations, the analysis of sect. 11.2 is new. The desymmetrization follows Gilmore and Lettelier [13], but the key new idea is taken from Christiansen *et al.* [63]: the arc-length parametrization of the unstable manifold maintains the 1-to-1 relation of the *full* d -dimensional state space dynamics and its 1-dimensional return-map representation, in contrast to 1-dimensional *projections* of the $(d-1)$ -dimensional Poincaré section return maps previously deployed in the literature. In other words, to high accuracy *no information about the flow is lost* by its 1-dimensional return map description.

Remark 12.2 Smale horseshoe. S. Smale understood clearly that the crucial ingredient in the description of a chaotic flow is the topology of its non-wandering set, and he

provided us with the simplest visualization of such sets as intersections of Smale horse-shoes. In retrospect, much of the material covered here can already be found in Smale's fundamental paper [27], but an engineer or a scientist who has run into a chaotic time series in his laboratory might not know that he is investigating the action (differentiable) of a Lie group G on a manifold M , and that the Lefschetz trace formula is the way to go.

Remark 12.3 Pruning fronts. The 'partition conjecture' is due to Grassberger and Kantz [3]. The notion of a pruning front and the 'pruning-front conjecture' was formulated by Cvitanović *et al.* [13], and developed by K.T. Hansen for a number of dynamical systems in his Ph.D. thesis [20] and a series of papers [21]-[25]. The 'multimodal map approximation' is described in the K.T. Hansen thesis [20]. Hansen's thesis is still the most accessible exposition of the pruning theory and its applications. Detailed studies of pruning fronts are carried out in refs. [14, 16, 15]; ref. [5] is the most detailed study carried out so far. The rigorous theory of pruning fronts has been developed by Y. Ishii [17, 18] for the Lozi map, and A. de Carvalho [19] in a very general setting. Beyond the orbit pruning and its infinity of admissible unstable orbits, an attractor of Hénon type may also own an infinity of attractive orbits coexisting with the strange attractor [64, 65]. We offer heuristic arguments and numerical evidence that the coexistence of attractive orbits does not destroy the strange attractor/repeller, which is also in this case described by the 2 – dimensional danish pastry plot.

Exercises

12.1. **A Smale horseshoe.** The Hénon map of example 3.7

$$\begin{bmatrix} x' \\ y' \end{bmatrix} = \begin{bmatrix} 1 - ax^2 + by \\ x \end{bmatrix} \quad (12.15)$$

maps the $[x, y]$ plane into itself - it was constructed by Hénon [6] in order to mimic the Poincaré section of once-folding map induced by a flow like the one sketched in figure 11.10. For definitiveness fix the parameters to $a = 6, b = -1$.

- Draw a rectangle in the (x, y) plane such that its n th iterate by the Hénon map intersects the rectangle 2^n times.
- Construct the inverse of the (12.15).
- Iterate the rectangle back in the time; how many intersections are there between the n forward and m backward iterates of the rectangle?
- Use the above information about the intersections to guess the (x, y) coordinates for the two fixed points, a 2-periodic point, and points on the two distinct 3-cycles from table 15.1. The exact periodic points are computed in exercise 13.13.

12.2. **Kneading Danish pastry.** Write down the $(x, y) \rightarrow (x, y)$ mapping that implements the baker's map

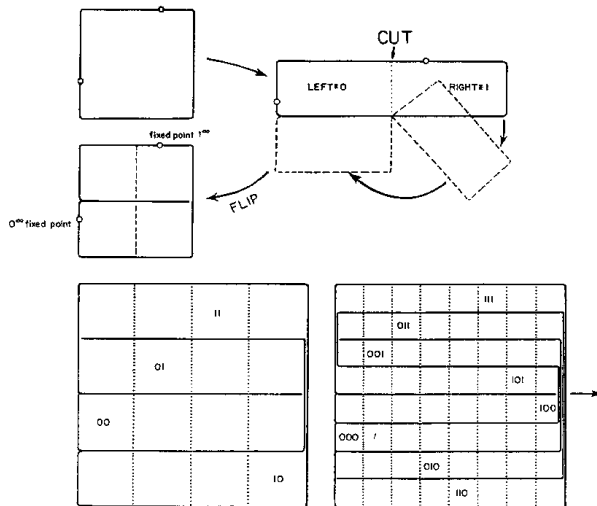


FIG. 4. Iterative construction of the symbol plane.

Figure: Kneading danish pastry: symbol square representation of an orientation reversing once-folding map obtained by fattening the Smale horseshoe intersections

of figure 12.4 into a unit square. In the symbol square the dynamics maps rectangles into rectangles by a decimal point shift. together with the inverse mapping.

Sketch a few rectangles in symbol square and their forward and backward images. (Hint: the mapping is very much like the tent map (11.4)).

12.3. **Kneading danish without flipping.** The baker's map of exercise 12.2 includes a flip - a map of this type is called an orientation reversing once-folding map. Write down the $(x, y) \rightarrow (x, y)$ mapping that implements an orientation preserving baker's map (no flip; Jacobian determinant = 1). Sketch and label the first few folds of the symbol square.

12.4. **Orientation reversing once-folding map.** By adding a reflection around the vertical axis to the horseshoe map g we get the orientation reversing map \tilde{g} shown in the second Figure above. \tilde{Q}_0 and \tilde{Q}_1 are oriented as Q_0 and Q_1 , so the definition of the future topological coordinate γ is identical to the γ for the orientation preserving horseshoe. The inverse intersections \tilde{Q}_0^{-1} and \tilde{Q}_1^{-1} are oriented so that \tilde{Q}_0^{-1} is opposite to Q_0 , while \tilde{Q}_1^{-1} has the same orientation as Q_1 . Check that the past topological coordinate δ is given by

$$w_{n-1} = \begin{cases} 1 - w_n & \text{if } s_n = 0 \\ w_n & \text{if } s_n = 1 \end{cases}, \quad w_0 = s_0$$

$$\delta(x) = 0.w_0w_{-1}w_{-2}\dots = \sum_{n=1}^{\infty} w_{1-n}/2^n \quad (12.16)$$

12.5. **Infinite symbolic dynamics.** Let σ be a function that returns zero or one for every infinite binary string: $\sigma : \{0, 1\}^{\mathbb{N}} \rightarrow \{0, 1\}$. Its value is represented by $\sigma(\epsilon_1, \epsilon_2, \dots)$ where the ϵ_i are either 0 or 1. We will now define an operator \mathcal{T} that acts on observables on the space of binary strings. A function a is an observable if it has bounded variation, that is, if

$$\|a\| = \sup_{\{\epsilon_i\}} |a(\epsilon_1, \epsilon_2, \dots)| < \infty.$$

For these functions

$$\begin{aligned} \mathcal{T}a(\epsilon_1, \epsilon_2, \dots) &= a(0, \epsilon_1, \epsilon_2, \dots)\sigma(0, \epsilon_1, \epsilon_2, \dots) \\ &\quad + a(1, \epsilon_1, \epsilon_2, \dots)\sigma(1, \epsilon_1, \epsilon_2, \dots). \end{aligned}$$

- (a) (easy) Consider a finite version T_n of the operator \mathcal{T} :

$$T_n a(\epsilon_1, \epsilon_2, \dots, \epsilon_{1,n}) = \\ a(0, \epsilon_1, \epsilon_2, \dots, \epsilon_{n-1})\sigma(0, \epsilon_1, \epsilon_2, \dots, \epsilon_{n-1}) + \\ a(1, \epsilon_1, \epsilon_2, \dots, \epsilon_{n-1})\sigma(1, \epsilon_1, \epsilon_2, \dots, \epsilon_{n-1}).$$

Show that T_n is a $2^n \times 2^n$ matrix. Show that its trace is bounded by a number independent of n .

- (b) (medium) With the operator norm induced by the function norm, show that \mathcal{T} is a bounded operator.
 (c) (hard) Show that \mathcal{T} is not trace class.

- 12.6. **3-disk fundamental domain cycles.** (continued from exercise 9.6) Try to sketch $\overline{0}, \overline{1}, \overline{01}, \overline{001}, \overline{011}, \dots$.

in the fundamental domain, and interpret the symbols $\{0, 1\}$ by relating them to topologically distinct types of collisions. Compare with table 12.2. Then try to sketch the location of periodic points in the Poincaré section of the billiard flow. The point of this exercise is that while in the configuration space longer cycles look like a hopeless jumble, in the Poincaré section they are clearly and logically ordered. The Poincaré section is always to be preferred to projections of a flow onto the configuration space coordinates, or any other subset of state space coordinates which does not respect the topological organization of the flow.

- 12.7. **3-disk pruning.** (Not easy) Show that for 3-disk game of pinball the pruning of orbits starts at $R : a = 2.04821419\dots$, figure 11.6. (K.T. Hansen)

References

- [12.1] E. Hopf, *Ergodentheorie* (Chelsea Publ. Co., New York 1948).
- [12.2] T. Bedford, M.S. Keane and C. Series, eds., *Ergodic Theory, Symbolic Dynamics and Hyperbolic Spaces* (Oxford Univ. Press, Oxford, 1991).
- [12.3] M.S. Keane, *Ergodic theory and subshifts of finite type*, in ref. [2].
- [12.4] B. Kitchens, "Symbolic dynamics, group automorphisms and Markov partition," in *Real and Complex Dynamical Systems*, B. Branner and P. Hjorth, ed. (Kluwer, Dordrecht, 1995).
- [12.5] R. Bowen, "Markov partitions for Axiom A diffeomorphisms," *Amer. J. Math.* **92**, 725 (1970).
- [12.6] D. Ruelle, *Transactions of the A.M.S.* **185**, 237 (197?).
- [12.7] R. Bowen, *Periodic orbits for hyperbolic flows*, *Amer. J. Math.* **94**, 1-30 (1972).
- [12.8] R. Bowen, *Symbolic dynamics for hyperbolic flows*, *Amer. J. Math.* **95**, 429-460 (1973).
- [12.9] R. Bowen and O.E. Lanford, "Zeta functions of restrictions," pp. 43-49 in *Proceeding of the Global Analysis* (A.M.S., Providence 1968).
- [12.10] V.M. Alekseev and M.V. Jakobson, "Symbolic dynamics and hyperbolic dynamical systems," *Phys. Reports* **75**, 287 (1981).
- [12.11] A. Manning, "Axiom A diffeomorphisms have rational zeta function," *Bull. London Math. Soc.* **3**, 215 (1971).
- [12.12] W. Thurston, "On the geometry and dynamics of diffeomorphisms of surfaces," *Bull. Amer. Math. Soc.* **19**, 417 (1988).

- [12.13] P. Cvitanović, G.H. Gunaratne and I. Procaccia, *Phys. Rev. A* **38**, 1503 (1988).
- [12.14] G. D'Alessandro, P. Grassberger, S. Isola and A. Politi, "On the topology of the Hénon Map," *J. Phys. A* **23**, 5285 (1990).
- [12.15] F. Giovannini and A. Politi, "Generating partitions in Hénon-type maps," *Phys. Lett. A* **161**, 333 (1992);
- [12.16] G. D'Alessandro, S. Isola and A. Politi, "Geometric properties of the pruning front," *Prog. Theor. Phys.* **86**, 1149 (1991).
- [12.17] Y. Ishii, "Towards the kneading theory for Lozi attractors. I. Critical sets and pruning fronts," Kyoto Univ. Math. Dept. preprint (Feb. 1994).
- [12.18] Y. Ishii, "Towards a kneading theory for Lozi mappings. II. A solution of the pruning front conjecture and the first tangency problem," *Nonlinearity* **10**, 731 (1997).
- [12.19] A. de Carvalho, Ph.D. thesis, CUNY New York 1995; "Pruning fronts and the formation of horseshoes," preprint (1997).
- [12.20] K.T. Hansen, *Symbolic Dynamics in Chaotic Systems*, Ph.D. thesis (Univ. of Oslo, 1994);
ChaosBook.org/projects/KTHansen/thesis.
- [12.21] K.T. Hansen, *CHAOS* **2**, 71 (1992).
- [12.22] K.T. Hansen, *Nonlinearity* **5**.
- [12.23] K.T. Hansen, *Nonlinearity* **5**.
- [12.24] P. Cvitanović and K.T. Hansen, "Symbolic dynamics and Markov partitions for the stadium billiard," *J. Stat. Phys.*, (accepted 1996, revised version still not resubmitted); [arXiv:chao-dyn/9502005](https://arxiv.org/abs/chao-dyn/9502005).
- [12.25] K.T. Hansen, *Symbolic dynamics IV; a unique partition of maps of Hénon type*, in preparation.
- [12.26] Fa-Geng Xie and Bai-Lin Hao, "Counting the number of periods in one-dimensional maps with multiple critical points," *Physica A* **202**, 237 (1994).
- [12.27] V. Franceschini and L. Russo, *J. Stat. Phys.* **25**, 757 (1981).
- [12.28] M. Benedicks and L. Carleson, *Ann. of Math.*, **122**, 1 (1985).
- [12.29] M. Benedicks and L. Carleson, *IXth Int. Congr. on Mathematical Physics*, in B. Simon *et al.*, eds., p. 489 (Adam Hilger, Bristol, 1989).
- [12.30] M. Benedicks and L. Carleson, *Ann. of Math.* **133**, 73 (1991).
- [12.31] G. D'Alessandro and A. Politi, "Hierarchical approach to complexity ...," *Phys. Rev. Lett.* **64**, 1609 (1990).

- [12.32] F. Christiansen and A. Politi, “A generating partition for the standard map,” *Phys. Rev. E* **51**, 3811 (1995); [arXiv:chao-dyn/9411005](#).
- [12.33] F. Christiansen and A. Politi, “Symbolic encoding in symplectic maps,” *Nonlinearity* **9**, 1623 (1996).
- [12.34] F. Christiansen and A. Politi, “Guidelines for the construction of a generating partition in the standard map,” *Physica D* **109**, 32 (1997).
- [12.35] C. Simo, “On the analytical and numerical approximation of invariant manifolds,” in D. Baenest and C. Froeschlé, *Les Méthodes Modernes de la Mécanique Céleste* (Goutelas 1989), p. 285.
- [12.36] C. Simo, in *Dynamics and Mission Design Near Libration Points*, Vol. 1-4, (World Sci. Pub., Monograph Ser. Math., 2000-2001).
- [12.37] Y. Lan and P. Cvitanović, “Unstable recurrent patterns in Kuramoto-Sivashinsky dynamics,” *Phys. Rev. E* **78**, 026208 (2004); [arXiv:0804.2474](#).
- [12.38] T. Hall, “Fat one-dimensional representatives of pseudo-Anosov isotopy classes with minimal periodic orbit structure,” *Nonlinearity* **7**, 367 (1994).
- [12.39] P. Cvitanović and K.T. Hansen, “Symbolic dynamics of the wedge billiard,” Niels Bohr Inst. preprint, unpublished (Nov. 1992)
- [12.40] P. Cvitanović and K.T. Hansen, “Bifurcation structures in maps of Hénon type,” *Nonlinearity* **11**, 1233 (1998).
- [12.41] R.W. Easton, “Trellises formed by stable and unstable manifolds in plane,” *Trans. Am. Math. Soc.* **294**, 2 (1986).
- [12.42] V. Rom-Kedar, “Transport rates of a class of two-dimensional maps and flows,” *Physica D* **43**, 229 (1990).
- [12.43] V. Daniels, M. Vallières and J-M. Yuan, “Chaotic scattering on a double well: Periodic orbits, symbolic dynamics, and scaling,” *Chaos* **3**, 475 (1993).
- [12.44] P.H. Richter, H.-J. Scholz and A. Wittek, “A Breathing Chaos,” *Nonlinearity* **1**, 45 (1990).
- [12.45] F. Hofbauer, “Periodic points for piecewise monotone transformations,” *Ergod. The. and Dynam. Sys.* **5**, 237 (1985).
- [12.46] F. Hofbauer, “Piecewise invertible dynamical systems,” *Prob. Th. Rel. Fields* **72**, 359 (1986).
- [12.47] K.T. Hansen, “Pruning of orbits in 4-disk and hyperbola billiards,” *CHAOS* **2**, 71 (1992).
- [12.48] G. Troll, “A devil’s staircase into chaotic scattering,” *Physica D* **50**, 276 (1991)
- [12.49] P. Grassberger, “Toward a quantitative theory of self-generated complexity,” *Int. J. Theor. Phys* **25**, 907 (1986).

- [12.50] D.L. Rod, *J. Diff. Equ.* **14**, 129 (1973).
- [12.51] R.C. Churchill, G. Pecelli and D.L. Rod, *J. Diff. Equ.* **17**, 329 (1975).
- [12.52] R.C. Churchill, G. Pecelli and D.L. Rod, in G. Casati and J. Ford, eds., *Como Conf. Proc. on Stochastic Behavior in Classical and Quantum Hamiltonian Systems* (Springer, Berlin 1976).
- [12.53] R. Mainieri, Ph.D. thesis, New York Univ. (1990); *Phys. Rev. A* **45**, 3580 (1992)
- [12.54] M.J. Giannoni and D. Ullmo, “Coding chaotic billiards: I. Non-compact billiards on a negative curvature manifold,” *Physica D* **41**, 371 (1990).
- [12.55] D. Ullmo and M.J. Giannoni, “Coding chaotic billiards: II. Compact billiards defined on the pseudosphere,” *Physica D* **84**, 329 (1995).
- [12.56] H. Solari, M. Natiello and G.B. Mindlin, “Nonlinear Physics and its Mathematical Tools,” (IOP Publishing Ltd., Bristol, 1996).
- [12.57] R. Gilmore, “Topological analysis of chaotic time series data,” *Revs. Mod. Phys.* **70**, 1455 (1998).
- [12.58] E. Hille, *Analytic function theory II*, (Ginn and Co., Boston 1962).
- [12.59] A. Back, J. Guckenheimer, M. R. Myers, F. J. Wicklin and P. A. Worfolk, “DsTool: Computer assisted exploration of dynamical systems,” *Notices of the AMS* **39**, 303 (1992).
- [12.60] B. Krauskopf and H. M. Osinga, “Investigating torus bifurcations in the forced Van der Pol oscillator,” pp. 199–208 in E. Doedel and L. Tuckerman, eds., *Numerical Methods for Bifurcation Problems and Large-Scale Dynamical Systems, The IMA Volumes in Mathematics and its Applications* **119** (Springer-Verlag, New York 2000).
- [12.61] J. P. England, B. Krauskopf and H. M. Osinga, “Computing one-dimensional stable and unstable sets of planar maps without the inverse,” *J. Applied Dynam. Systems* **3**, 161 (2004).
- [12.62] J. F. Gibson, J. Halcrow, and P. Cvitanović, “Visualizing the geometry of state-space in plane Couette flow,” *J. Fluid Mech.* **611**, 107 (2008); [arXiv:0705.3957](https://arxiv.org/abs/0705.3957).
- [12.63] F. Christiansen, P. Cvitanović and V. Putkaradze, “Hopf’s last hope: spatiotemporal chaos in terms of unstable recurrent patterns,” *Nonlinearity* **10**, 55 (1997); [arXiv:chao-dyn/9606016](https://arxiv.org/abs/chao-dyn/9606016).
- [12.64] S.E. Newhouse, *Topology* **13**, 9 (1974).
- [12.65] S.E. Newhouse, *Publ. Math. IHES* **50**, 101 (1979).

Chapter 13

Fixed points, and how to get them

HAVING SET UP the dynamical context, now we turn to the key and unavoidable piece of numerics in this subject; search for the solutions (x, T) , $x \in \mathbb{R}^d$, $T \in \mathbb{R}$ of the *periodic orbit condition*

$$f^{t+T}(x) = f^t(x), \quad T > 0 \quad (13.1)$$

for a given flow or mapping.

In chapters 18 and 19 we will establish that spectra of evolution operators can be extracted from periodic orbit sums:

$$\sum (\text{spectral eigenvalues}) = \sum (\text{periodic orbits}) .$$

Hence, periodic orbits are the necessary ingredient for evaluation of spectra of evolution operators. We need to know what periodic orbits can exist, and the symbolic dynamics developed so far is an invaluable tool toward this end.

Sadly, searching for periodic orbits will never become as popular as a week on Côte d'Azur, or publishing yet another log-log plot in *Phys. Rev. Letters*. This chapter is intended as a hands-on guide to extraction of periodic orbits, and should be skipped on first reading - you can return to it whenever the need for finding actual cycles arises. A serious cyclist will want to also learn about the variational methods to find cycles, chapter 29. They are particularly useful when little is understood about the topology of a flow, such as in high-dimensional periodic orbit searches.

chapter 29



fast track:
chapter 15, p. 283

A *prime cycle* p of period T_p is a single traversal of the periodic orbit, so our task will be to find a periodic point $x \in \mathcal{M}_p$ and the shortest time T_p for which (13.1) has a solution. A periodic point of a flow f^t which crosses a Poincaré section n times is a fixed point of the P^n iterate of P , the return map (3.1), hence we shall refer to all cycles as “fixed points” in this chapter. By cyclic invariance, Floquet multipliers and the period of the cycle are independent of the choice of the initial point, so it will suffice to solve (13.1) at a single periodic point. section 5.2

If the cycle is an attracting limit cycle with a sizable basin of attraction, it can be found by integrating the flow for sufficiently long time. If the cycle is unstable, simple integration forward in time will not reveal it, and methods to be described here need to be deployed. In essence, any method for finding a cycle is based on devising a new dynamical system which possesses the same cycle, but for which this cycle is attractive. Beyond that, there is a great freedom in constructing such systems, and many different methods are used in practice.

Due to the exponential divergence of nearby trajectories in chaotic dynamical systems, fixed point searches based on direct solution of the fixed-point condition (13.1) as an initial value problem can be numerically very unstable. Methods that start with initial guesses for a number of points along the cycle, such as the multipoint shooting method described here in sect. 13.3, and the variational methods of chapter 29, are considerably more robust and safer. chapter 29

A prerequisite for any exhaustive cycle search is a good understanding of the topology of the flow: a preliminary step to any serious periodic orbit calculation is preparation of a list of all distinct admissible prime periodic symbol sequences, such as the list given in table 15.1. The relations between the temporal symbol sequences and the spatial layout of the topologically distinct regions of the state space discussed in chapters 11 and 12 should enable us to guess location of a series of periodic points along a cycle. Armed with such informed guess we proceed to improve it by methods such as the Newton-Raphson iteration; we show how this works by applying the Newton method to 1- and d -dimensional maps. But first, where are the cycles?

13.1 Where are the cycles?

Q: What if you choose a really bad initial condition and it doesn't converge? A: Well then you only have yourself to blame.

— T.D. Lee

The simplest and conceptually easiest setting for guessing where the cycles are is the case of planar billiards. The Maupertuis principle of least action here dictates that the physical trajectories extremize the length of an approximate orbit that visits a desired sequence of boundary bounces.

Example 13.1 Periodic orbits of billiards. Consider how this works for 3-disk pinball game of sect. 12.5. Label the three disks by 1, 2 and 3, and associate to every section 12.5
section 1.4

trajectory an itinerary, a sequence of labels indicating the order in which the disks are visited, as in figure 3.2. Given the itinerary, you can construct a guess trajectory by taking a point on the boundary of each disk in the sequence, and connecting them by straight lines. Imagine that this is a rubber band wrapped through 3 rings, and shake the band until it shrinks into the physical trajectory, the rubber band of shortest length.

Extremization of a cycle length requires variation of n bounce positions s_i . The computational problem is to find the extremum values of cycle length $L(s)$ where $s = (s_1, \dots, s_n)$, a task that we postpone to sect. 29.3. As an example, the short periods and stabilities of 3-disk cycles computed this way are listed table 29.3, and some examples are plotted in figure 3.2. It's a no brainer, and millions of such cycles have been computed. exercise 29.2
exercise 13.13

If we were only so lucky. Real life finds us staring at something like Yang-Mills or Navier-Stokes equations, utterly clueless. What to do?

One, there is always mindless computation. In practice one might be satisfied with any rampaging robot that finds “the most important” cycles. Ergodic exploration of recurrences that we turn to next sometimes perform admirably well.

13.1.1 Cycles from long time series

Two wrongs don't make a right, but three lefts do.
—Appliance guru

(L. Rondoni and P. Cvitanović)

The equilibria and periodic orbits (with the exception of sinks and stable limit cycles) are never seen in simulations and experiments because they are unstable. Nevertheless, one does observe close passes to the least unstable equilibria and periodic orbits, as in figure 13.1. Ergodic exploration by long-time trajectories (or long-lived transients, in case of strange repellers) can uncover state space regions of low velocity, or finite time recurrences. In addition, such trajectories preferentially sample the natural measure of the ‘turbulent’ flow, and by initiating searches within the state space concentrations of natural measure bias the search toward the dynamically important invariant solutions. remark 13.1
section 16.1

The search consists of following a long trajectory in state space, and looking for close returns of the trajectory to itself, see figure 13.1. Whenever the trajectory almost closes in a loop (within a given tolerance), another point of this near miss of a cycle can be taken as an initial condition. Supplemented by a Newton routine described below, a sequence of improved initial conditions may indeed rapidly lead to closing a cycle. The method preferentially finds the least unstable orbits, while missing the more unstable ones that contribute little to the cycle expansions.

This blind search is seriously flawed: in contrast to the 3-disk example 13.1, it is not systematic, it gives no insight into organization of the ergodic sets, and can easily miss very important cycles. Foundations to a systematic exploration of ergodic state space are laid in chapters 11 and 12, but are a bit of work to implement.

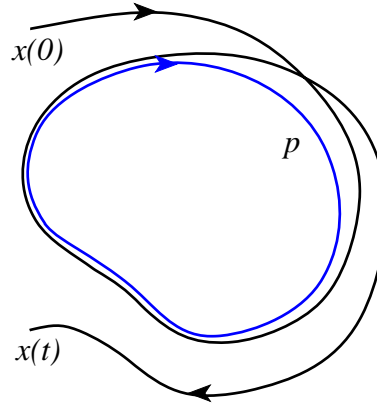


Figure 13.1: An ergodic trajectory can shadow an unstable periodic orbit p for a finite time.

13.1.2 Cycles found by thinking

Thinking is extra price.

—Dicho Colombiano

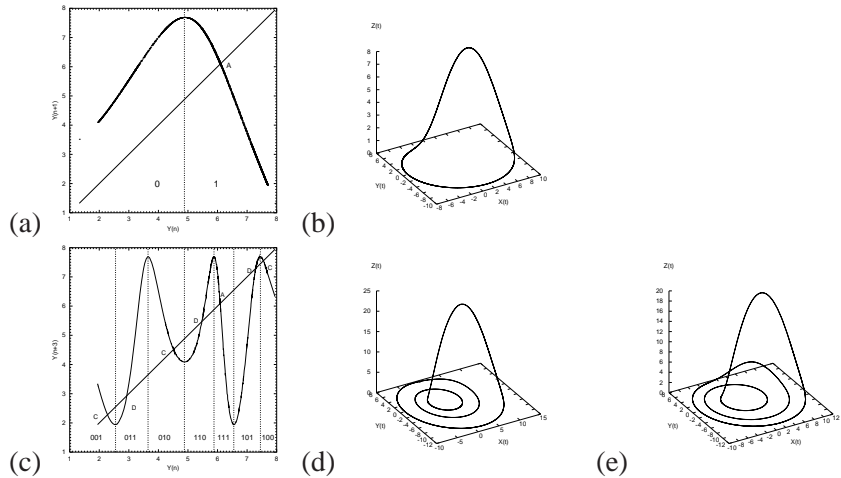
A systematic charting out of state space starts out by a hunt for equilibrium points. If the equations of motion are a finite set of ODEs, setting the velocity field $v(x)$ in (2.6) to zero reduces search for equilibria to a search for zeros of a set of algebraic equations. We should be able, in principle, to enumerate and determine all real and complex zeros in such cases, e.g. the Lorenz example 2.2 and the Rössler example 2.3. If the equations of motion and the boundary conditions are invariant under some symmetry, some equilibria can be determined by symmetry considerations: if a function is e.g. antisymmetric, it must vanish at origin, e.g. the Lorenz $EQ_0 = (0, 0, 0)$ equilibrium.

As to other equilibria: if you have no better idea, create a state space grid, about 50 x_k across \mathcal{M} in each dimension, and compute the velocity field $v_k = v(x_k)$ at each grid point; a few million v_k values are easily stored. Plot x_k for which $|v_k|^2 < \epsilon$, $\epsilon \ll |v_{max}|^2$ but sufficiently large that a few thousand x_k are plotted. If the velocity field varies smoothly across the state space, the regions $|v_k|^2 < \epsilon$ isolate the (candidate) equilibria. Start a Newton iteration with the smallest $|v_k|^2$ point within each region. Barring exceptionally fast variations in $v(x)$ this should yield all equilibrium points.

For ODEs equilibria are fixed points of algebraic sets of equations, but steady states of PDEs such as the Navier-Stokes flow are themselves solutions of ODEs or PDEs, and much harder to determine.

Equilibria—by definition—do not move, so they cannot be “turbulent.” What makes them dynamically important are their stable/unstable manifolds. A chaotic trajectory can be thought of as a sequence of near visitations of equilibria. Typically such neighborhoods have many stable, contracting directions and a handful of unstable directions. Our strategy will be to generalize the billiard Poincaré section maps $P_{s_{n+1} \leftarrow s_n}$ of example 3.2 to maps from a section of the unstable manifold of equilibrium s_n to the section of unstable manifold of equilibrium s_{n+1} , and thus reduce the continuous time flow to a sequence of maps. These Poincaré section

Figure 13.2: (a) $y \rightarrow P_1(y, z)$ return map for $x = 0, y > 0$ Poincaré section of the Rössler flow figure 2.6. (b) The $\bar{1}$ -cycle found by taking the fixed point $y_{k+n} = y_k$ together with the fixed point of the $z \rightarrow z$ return map (not shown) an initial guess $(0, y^{(0)}, z^{(0)})$ for the Newton-Raphson search. (c) $y_{k+3} = P_1^3(y_k, z_k)$, the third iterate of Poincaré return map (3.1) together with the corresponding plot for $z_{k+3} = P_2^3(y_k, z_k)$, is used to pick starting guesses for the Newton-Raphson searches for the two 3-cycles: (d) the $\overline{001}$ cycle, and (e) the $\overline{011}$ cycle. (G. Simon)



maps do double duty, providing us both with an exact representation of dynamics in terms of maps, and with a covering symbolic dynamics.

We showed in the Lorenz flow example 11.4 how to reduce the 3-dimensional Lorenz flow to a 1-dimensional return map. In the Rössler flow example 2.3 we sketched the attractor by running a long chaotic trajectory, and noted that the attractor is very thin, but otherwise the return maps that we plotted were disquieting – figure 3.6 did not appear to be a 1-to-1 map. In the next example we show how to use such information to approximately locate cycles. In the remainder of this chapter and in chapter 29 we shall learn how to turn such guesses into highly accurate cycles.

Example 13.2 Rössler attractor. Run a long simulation of the Rössler flow f^t , plot a Poincaré section, as in figure 3.5, and extract the corresponding Poincaré return map P , as in figure 3.6. Luck is with us; figure 13.2(a) return map $y \rightarrow P_1(y, z)$ looks much like a parabola, so we take the unimodal map symbolic dynamics, sect. 11.3, as our guess for the covering dynamics. Strictly speaking, the attractor is “fractal,” but for all practical purposes the return map is 1-dimensional; your printer will need a resolution better than 10^{14} dots per inch to start resolving its structure.

Periodic points of a prime cycle p of cycle length n_p for the $x = 0, y > 0$ Poincaré section of the Rössler flow figure 2.6 are fixed points $(y, z) = P^{n_p}(y, z)$ of the n th Poincaré return map.

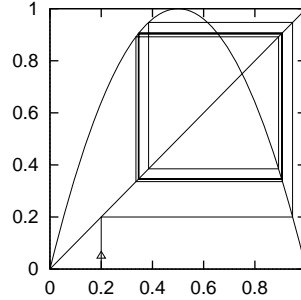
Using the fixed point $y_{k+1} = y_k$ in figure 13.2(a) together with the simultaneous fixed point of the $z \rightarrow P_1(y, z)$ return map (not shown) as a starting guess $(0, y^{(0)}, z^{(0)})$ for the Newton-Raphson search for the cycle p with symbolic dynamics label $\bar{1}$, we find the cycle figure 13.2(b) with the Poincaré section point $(0, y_p, z_p)$, period T_p , expanding, marginal, contracting Floquet multipliers $(\Lambda_{p,e}, \Lambda_{p,m}, \Lambda_{p,c})$, and Lyapunov exponents $(\lambda_{p,e}, \lambda_{p,m}, \lambda_{p,c})$:

exercise 13.10

$$\begin{aligned}
 \bar{1}\text{-cycle:} \quad (x, y, z) &= (0, 6.09176832, 1.2997319) \\
 T_1 &= 5.88108845586 \\
 (\Lambda_{1,e}, \Lambda_{1,m}, \Lambda_{1,c}) &= (-2.40395353, 1 + 10^{-14}, -1.29 \times 10^{-14}) \\
 (\lambda_{1,e}, \lambda_{1,m}, \lambda_{1,c}) &= (0.149141556, 10^{-14}, -5.44).
 \end{aligned}
 \tag{13.2}$$

The Newton-Raphson method that we used is described in sect. 13.4.

Figure 13.3: The inverse time path to the $\overline{01}$ -cycle of the logistic map $f(x) = 4x(1 - x)$ from an initial guess of $x = 0.2$. At each inverse iteration we chose the 0, respectively 1 branch.



As an example of a search for longer cycles, we use $y_{k+3} = P_1^3(y_k, z_k)$, the third iterate of Poincaré return map (3.1) plotted in figure 13.2(c), together with a corresponding plot for $z_{k+3} = f^3(y_k, z_k)$, to pick starting guesses for the Newton-Raphson searches for the two 3-cycles plotted in figure 13.2(d), (e). For a listing of the short cycles of the Rössler flow, consult exercise 13.10.

The numerical evidence suggests (but a proof is lacking) that all cycles that comprise the strange attractor of the Rössler flow are hyperbolic, each with an expanding eigenvalue $|\Lambda_e| > 1$, a contracting eigenvalue $|\Lambda_c| < 1$, and a marginal eigenvalue $|\Lambda_m| = 1$ corresponding to displacements along the direction of the flow.

For the Rössler flow the contracting eigenvalues turn out to be insanely contracting, a factor of e^{-32} per one par-course of the attractor, so their numerical determination is quite difficult. Fortunately, they are irrelevant; for all practical purposes the strange attractor of the Rössler flow is 1-dimensional, a very good realization of a horseshoe template. (G. Simon and P. Cvitanović)

13.2 One-dimensional mappings

(F. Christiansen)

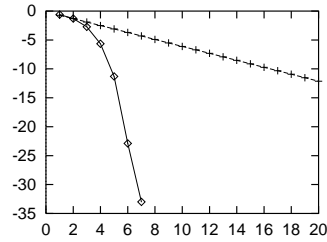
13.2.1 Inverse iteration

Let us first consider a very simple method to find unstable cycles of a 1-dimensional map such as the logistic map. Unstable cycles of 1 – dimensional maps are attracting cycles of the inverse map. The inverse map is not single valued, so at each backward iteration we have a choice of branch to make. By choosing branch according to the symbolic dynamics of the cycle we are trying to find, we will automatically converge to the desired cycle. The rate of convergence is given by the stability of the cycle, i.e., the convergence is exponentially fast. Figure 13.3 shows such path to the $\overline{01}$ -cycle of the logistic map.

exercise 13.13

The method of inverse iteration is fine for finding cycles for 1-d maps and some 2 – dimensional systems such as the repeller of exercise 13.13. It is not particularly fast, especially if the inverse map is not known analytically. However, it completely fails for higher dimensional systems where we have both stable and unstable directions. Inverse iteration will exchange these, but we will still be left

Figure 13.4: Convergence of Newton method (\diamond) vs. inverse iteration (+). The error after n iterations searching for the $\overline{01}$ -cycle of the logistic map $f(x) = 4x(1 - x)$ with an initial starting guess of $x_1 = 0.2, x_2 = 0.8$. y-axis is \log_{10} of the error. The difference between the exponential convergence of the inverse iteration method and the super-exponential convergence of Newton method is dramatic.



with both stable and unstable directions. The best strategy is to directly attack the problem of finding solutions of $f^n(x) = x$.

13.2.2 Newton method

Newton method for determining a zero x^* of a function $F(x)$ of one variable is based on a linearization around a starting guess x_0 :

$$F(x) \approx F(x_0) + F'(x_0)(x - x_0). \tag{13.3}$$

An approximate solution x_1 of $F(x) = 0$ is

$$x_1 = x_0 - F(x_0)/F'(x_0). \tag{13.4}$$

The approximate solution can then be used as a new starting guess in an iterative process. A fixed point of a map f is a solution to $F(x) = x - f(x) = 0$. We determine x by iterating

$$\begin{aligned} x_m &= g(x_{m-1}) = x_{m-1} - F(x_{m-1})/F'(x_{m-1}) \\ &= x_{m-1} - \frac{1}{1 - f'(x_{m-1})}(x_{m-1} - f(x_{m-1})). \end{aligned} \tag{13.5}$$

Provided that the fixed point is not marginally stable, $f'(x) \neq 1$ at the fixed point x , a fixed point of f is a super-stable fixed point of the Newton-Raphson map g , $g'(x) = 0$, and with a sufficiently good initial guess, the Newton-Raphson iteration will converge super-exponentially fast.

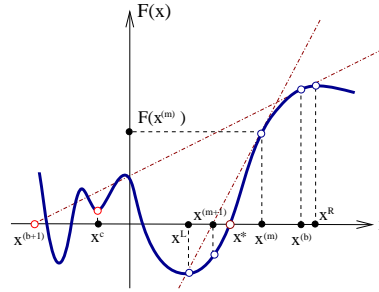
To illustrate the efficiency of the Newton method we compare it to the inverse iteration method in figure 13.4. Newton method wins hands down: the number of significant digits of the accuracy of x estimate doubles with each iteration.

In order to avoid jumping too far from the desired x^* (see figure 13.5), one often initiates the search by the *damped Newton method*,

$$\Delta x_m = x_{m+1} - x_m = -\frac{F(x_m)}{F'(x_m)} \Delta\tau, \quad 0 < \Delta\tau \leq 1,$$

takes small $\Delta\tau$ steps at the beginning, reinstating to the full $\Delta\tau = 1$ jumps only when sufficiently close to the desired x^* .

Figure 13.5: Newton method: bad initial guess $x^{(b)}$ leads to the Newton estimate $x^{(b+1)}$ far away from the desired zero of $F(x)$. Sequence $\dots, x^{(m)}, x^{(m+1)}, \dots$, starting with a good guess converges super-exponentially to x^* . The method diverges if it iterates into the basin of attraction of a local minimum x^c .



13.3 Multipoint shooting method

(F. Christiansen)

Periodic orbits of length n are fixed points of f^n so in principle we could use the simple Newton method described above to find them. However, this is not an optimal strategy. f^n will be a highly oscillating function with perhaps as many as 2^n or more closely spaced fixed points, and finding a specific periodic point, for example one with a given symbolic sequence, requires a *very* good starting guess. For binary symbolic dynamics we must expect to improve the accuracy of our initial guesses by at least a factor of 2^n to find orbits of length n . A better alternative is the *multipoint shooting method*. While it might very hard to give a precise initial point guess for a long periodic orbit, if our guesses are informed by a good state space partition, a rough guess for each point along the desired trajectory might suffice, as for the individual short trajectory segments the errors have no time to explode exponentially. And, indeed, in chapter 11 we have developed a qualitative theory of how these cycle points are laid out topologically.

A cycle of length n is a zero of the n -dimensional vector function F :

$$F(x) = F \begin{pmatrix} x_1 \\ x_2 \\ \vdots \\ x_n \end{pmatrix} = \begin{pmatrix} x_1 - f(x_n) \\ x_2 - f(x_1) \\ \dots \\ x_n - f(x_{n-1}) \end{pmatrix}.$$

The relations between the temporal symbol sequences and the spatial layout of the topologically distinct regions of the state space discussed in chapter 11 enable us to guess location of a series of periodic points along a cycle. Armed with such informed initial guesses we can initiate a Newton-Raphson iteration. The iteration in the Newton method now takes the form of

$$\frac{d}{dx} F(x)(x' - x) = -F(x), \tag{13.6}$$

where $\frac{d}{dx}F(x)$ is an $[n \times n]$ matrix:

$$\frac{d}{dx}F(x) = \begin{pmatrix} 1 & & & & -f'(x_n) \\ -f'(x_1) & 1 & & & \\ & \dots & & & \\ & & 1 & & \\ & & & \dots & \\ & & & & 1 \\ -f'(x_{n-1}) & & & & 1 \end{pmatrix}. \quad (13.7)$$

This matrix can easily be inverted numerically by first eliminating the elements below the diagonal. This creates non-zero elements in the n th column. We eliminate these and are done.

Example 13.3 Newton inversion for a 3-cycle. *Let us illustrate how this works step by step for a 3-cycle. The initial setup for a Newton step is:*

$$\begin{pmatrix} 1 & 0 & -f'(x_3) \\ -f'(x_1) & 1 & 0 \\ 0 & -f'(x_2) & 1 \end{pmatrix} \begin{pmatrix} \Delta x_1 \\ \Delta x_2 \\ \Delta x_3 \end{pmatrix} = - \begin{pmatrix} F_1 \\ F_2 \\ F_3 \end{pmatrix},$$

where $\Delta x_i = x'_i - x_i$ is the correction to our initial guess x_i , and $F_i = x_i - f(x_{i-1})$ is the error at i th periodic point. Eliminate the sub-diagonal elements by adding $f'(x_1)$ times the first row to the second row, then adding $f'(x_2)$ times the second row to the third row:

$$\begin{pmatrix} 1 & 0 & -f'(x_3) \\ 0 & 1 & -f'(x_1)f'(x_3) \\ 0 & 0 & 1 - f'(x_2)f'(x_1)f'(x_3) \end{pmatrix} \begin{pmatrix} \Delta x_1 \\ \Delta x_2 \\ \Delta x_3 \end{pmatrix} = - \begin{pmatrix} F_1 \\ F_2 + f'(x_1)F_1 \\ F_3 + f'(x_2)F_2 + f'(x_2)f'(x_1)F_1 \end{pmatrix}.$$

The next step is to invert the last element in the diagonal, i.e., divide the third row by $1 - f'(x_2)f'(x_1)f'(x_3)$. If this element is zero at the periodic orbit this step cannot work. As $f'(x_2)f'(x_1)f'(x_3)$ is the stability of the cycle (when the Newton iteration has converged), this is not a good method to find marginally stable cycles. We now have

$$\begin{pmatrix} 1 & 0 & -f'(x_3) \\ 0 & 1 & -f'(x_1)f'(x_3) \\ 0 & 0 & 1 \end{pmatrix} \begin{pmatrix} \Delta x_1 \\ \Delta x_2 \\ \Delta x_3 \end{pmatrix} = - \begin{pmatrix} F_1 \\ F_2 + f'(x_1)F_1 \\ \frac{F_3 + f'(x_2)F_2 + f'(x_2)f'(x_1)F_1}{1 - f'(x_2)f'(x_1)f'(x_3)} \end{pmatrix}.$$

Finally we add $f'(x_3)$ times the third row to the first row and $f'(x_1)f'(x_3)$ times the third row to the second row. The left hand side matrix is now the unit matrix, the right hand side is an explicit formula for the corrections to our initial guess. We have gone through one Newton iteration.

When one sets up the Newton iteration on the computer it is not necessary to write the left hand side as a matrix. All one needs is a vector containing the $f'(x_i)$'s, a vector containing the n 'th column, i.e., the cumulative product of the $f'(x_i)$'s, and a vector containing the right hand side. After the iteration the vector containing the right hand side should be the correction to the initial guess.

exercise 13.1

13.3.1 d -dimensional mappings



Armed with clever initial guesses, informed by symbolic dynamics, we can easily extend the Newton-Raphson iteration method to d -dimensional mappings. In this case $f'(x_i)$ is a $[d \times d]$ matrix, and $\frac{d}{dx}F(x)$ is an $[nd \times nd]$ matrix. In each of the steps that we went through above we are then manipulating d rows of the left hand side matrix. (Remember that matrices do not commute - always multiply from the left.) In the inversion of the n th element of the diagonal we are inverting a $[d \times d]$ matrix $(1 - \prod f'(x_i))$ which can be done if none of the eigenvalues of $\prod f'(x_i)$ equals 1, i.e., if the cycle has no marginally stable eigen-directions.

Example 13.4 Newton method for time delay maps. Some d -dimensional mappings (such as the Hénon map (3.19)) can be written as 1-dimensional time delay mappings of the form

$$f(x_i) = f(x_{i-1}, x_{i-2}, \dots, x_{i-d}). \tag{13.8}$$

In this case $\frac{d}{dx}F(x)$ is an $[n \times n]$ matrix as in the case of usual 1-dimensional maps but with non-zero matrix elements on d off-diagonals. In the elimination of these off-diagonal elements the last d columns of the matrix will become non-zero and in the final cleaning of the diagonal we will need to invert a $[d \times d]$ matrix. In this respect, nothing is gained numerically by looking at such maps as 1-dimensional time delay maps.

13.4 Flows

(R. Paškauskas and P. Cvitanović)

For a continuous time flow the periodic orbit Floquet multiplier (5.16) along the flow direction of necessity equals unity; the separation of any two points along a cycle remains unchanged after a completion of the cycle. More unit Floquet multipliers arise if the flow satisfies conservation laws, such as the symplectic invariance for Hamiltonian flows, or the dynamics is equivariant under a continuous symmetry transformation.

section 5.2.1

section 10.3

Let us apply the Newton method of (13.4) to search for periodic orbits with unit Floquet multipliers, starting with the case of a *continuous time flow*. Assume that the periodic orbit condition (13.1) holds for $x + \Delta x$ and $T + \Delta t$, with the initial guesses x and T close to the desired solution, i.e., with $|\Delta x|, \Delta t$ small. The Newton setup (13.4)

$$\begin{aligned} 0 &= x + \Delta x - f^{T+\Delta t}(x + \Delta x) \\ &\approx x - f^T(x) + (1 - J(x)) \cdot \Delta x - v(f^T(x))\Delta t \end{aligned} \tag{13.9}$$

suffers from two shortcomings. First, we now need to solve not only for the periodic point x , but for the period T as well. Second, the marginal, unit Floquet

multiplier (5.16) along the flow direction (arising from the time-translation invariance of a periodic orbit) renders the factor $(1 - J)$ in (13.5) non-invertible: if x is close to the solution, $f^T(x) \approx x$, then $J(x) \cdot v(x) = v(f^T(x)) \approx v(x)$. If Δx is parallel to the velocity vector, the derivative term $(1 - J) \cdot \Delta x \approx 0$, and it becomes harder to invert $(1 - J)$ as the iterations approach the solution.

As a periodic orbit p is a 1-dimensional set of points invariant under dynamics, Newton guess is not improved by picking Δx such that the new point lies on the orbit of the initial one, so we need to constrain the variation Δx to directions transverse to the flow, by requiring, for example, that

$$v(x) \cdot \Delta x = 0. \quad (13.10)$$

Combining this constraint with the variational condition (13.9) we obtain a Newton setup for flows, best displayed in the matrix form:

$$\begin{pmatrix} 1 - J(x) & v(x) \\ v(x) & 0 \end{pmatrix} \begin{pmatrix} \Delta x \\ \Delta t \end{pmatrix} = - \begin{pmatrix} x - f(x) \\ 0 \end{pmatrix} \quad (13.11)$$

This illustrates the general strategy for determining periodic orbits in presence of continuous symmetries - for each symmetry, break the invariance by a constraint, and compute the value of the corresponding continuous parameter (here the period T) by iterating the enlarged set of Newton equations. Constraining the variations to transverse ones thus fixes both of Newton's shortcomings: it breaks the time-translation invariance, and the period T can be read off once the fixed point has been found (hence we omit the superscript in f^T for the remainder of this discussion).

More generally, the Poincaré surface of section technique of sect. 3.1 turns the periodic orbit search into a fixed point search on a suitably defined surface of section, with a neighboring point variation Δx with respect to a reference point x constrained to *stay* on the surface manifold (3.2),

$$U(x + \Delta x) = U(x) = 0. \quad (13.12)$$

The price to pay are constraints imposed by the section: in order to *stay* on the surface, arbitrary variation Δx is not allowed.

Example 13.5 A hyperplane Poincaré section. *Let us for the sake of simplicity assume that the Poincaré surface of section is a (hyper)-plane, i.e., it is given by the linear condition (3.6)*

$$(x - x_0) \cdot a = 0, \quad (13.13)$$

where a is a vector normal to the Poincaré section and x_0 is any point in the Poincaré section. The Newton setup is then (derived as (13.11))

$$\begin{pmatrix} 1 - J & v(x) \\ a & 0 \end{pmatrix} \begin{pmatrix} x' - x \\ \Delta t \end{pmatrix} = \begin{pmatrix} -F(x) \\ 0 \end{pmatrix}. \quad (13.14)$$

The last row in this equation ensures that x will be in the surface of section, and the addition of $v(x)\Delta t$, a small vector along the direction of the flow, ensures that such an x can be found, at least if x is sufficiently close to a fixed point of f .

To illustrate how addition of the extra constraint resolves the problem of $(1 - J)$ non-invertability, let us take a particularly simple example; consider a 3-d flow with the $(x, y, 0)$ -plane as Poincaré section, $a = (0, 0, 1)$. Let all trajectories cross the Poincaré section perpendicularly, i.e., with $v = (0, 0, v_z)$, which means that the marginally stable direction is also perpendicular to the Poincaré section. Furthermore, let the unstable direction be parallel to the x -axis and the stable direction be parallel to the y -axis. The Newton setup is now

$$\begin{pmatrix} 1 - \Lambda_u & 0 & 0 & 0 \\ 0 & 1 - \Lambda_s & 0 & 0 \\ 0 & 0 & 0 & v_z \\ 0 & 0 & 1 & 0 \end{pmatrix} \begin{pmatrix} \delta_x \\ \delta_y \\ \delta_z \\ \delta\tau \end{pmatrix} = \begin{pmatrix} -F_x \\ -F_y \\ -F_z \\ 0 \end{pmatrix}. \quad (13.15)$$

If you consider only the upper-left $[3 \times 3]$ matrix (which we started out with, prior to adding the constraint (13.13)) then this matrix is not invertible and the equation does not have a unique solution. However, the full $[4 \times 4]$ matrix is invertible, as $\det(\cdot) = -v_z \det(1 - M_\perp)$, where M_\perp is the $[2 \times 2]$ monodromy matrix for a surface of section transverse to the orbit, see sect. 5.3. (F. Christiansen)

13.4.1 Cost function

It pays to think in terms of a *cost* (or *error*) function $I(\Delta x) = (x + \Delta x - f(x + \Delta x))^2 / 2$. Periodic orbit condition (13.1) corresponds both to a zero of $I(\Delta x)$, and of its first Δx variation. Expand $I(\Delta x)$ to the second order in Δx , $\tilde{I} \approx \tilde{\Delta x}^2 / 2 + (x - f(x)) \cdot \tilde{\Delta x} + (x - f(x))^2 / 2$, where $\tilde{\Delta x} = (1 - J(x))\Delta x$. To find an extremum, we set the derivative with respect to $\tilde{\Delta x}$ to zero. As the term $(x - f(x))^2 / 2$ is a constant under Δx variation, let us define an unconstrained *cost function*

$$I_0(\tilde{\Delta x}) = \frac{1}{2} \tilde{\Delta x} \cdot \tilde{\Delta x} + (x - f(x)) \cdot \tilde{\Delta x}, \quad (13.16)$$

Setting the derivative of this function

$$\frac{\partial I_0(\tilde{\Delta x})}{\partial \tilde{\Delta x}} = \tilde{\Delta x} + x - f(x) = (1 - J(x)) \cdot \Delta x + x - f(x) \quad (13.17)$$

to zero recovers the Newton setup (13.4)

Next, we need to enforce the constraint that curbs the directions in which Δx can point. Lagrange multipliers come to help.

A *local surface of section* can be constructed when $f(x)$ is “near” the initial point x . A natural choice is a hyperplane perpendicular to the velocity vector $v(x)$. The reference point x_0 in (13.13) is x itself, and the surface of section condition

is $U(x + \Delta x) = v(x) \cdot \Delta x = 0$. Introduce a Lagrange multiplier λ , and assembled a cost function with the constraint:

$$I_1(\tilde{\Delta}x, \lambda) = \frac{1}{2}\tilde{\Delta}x \cdot \tilde{\Delta}x + [x - f(x)] \cdot \tilde{\Delta}x + \lambda v(x) \cdot \tilde{\Delta}x. \quad (13.18)$$

Now we differentiate $I_1(\Delta x, \lambda)$ with respect to each argument and set the derivatives to zero. We recover the Newton setup (13.11), with the Lagrange multiplier $\lambda = \Delta t$ interpreted as the time increment needed to place $f(x)$ onto the section, $f(x) \rightarrow f(x) + v(f(x))\Delta t$.

A *global surface of section* is a fixed surface $U(x + \Delta x) - U(x_0) \approx \partial U(x)\Delta x + U(x) - U(x_0)$ that hopefully transects all or a significant portion of recurrent parts of the flow. It is not as ‘natural’ as the local section (13.10), but hard to avoid in practice, and one is interested not only in the fixed point itself, but in the global reach of its unstable manifold as well. The simplest choice is a hyperplane (13.13). The cost function and the variational equations are then

example 13.5

$$I_2(\Delta x, \lambda) = \frac{1}{2}\Delta x[1 - J(x)]\Delta x + (x - f(x)) \Delta x + \lambda(\partial U(x)\Delta x + U(x) - U(x_0)), \quad (13.19)$$

$$\begin{pmatrix} 1 - J(x) & \partial U(x) \\ \partial U(x) & 0 \end{pmatrix} \begin{pmatrix} \Delta x \\ \lambda \end{pmatrix} = - \begin{pmatrix} x - f(x) \\ U(x) - U(x_0) \end{pmatrix} \quad (13.20)$$

Further *continuous symmetries* can be handled in the same fashion. Suppose, for example, that we are searching for periodic orbits of a Hamiltonian flow. There, periodic orbits not only have the time-translation symmetry, but energy-translation symmetry as well. What is energy-translation symmetry? If there exists a periodic orbit at x with energy $H(x) = E$, and period T , it is very likely that it belongs to a family of orbits $(x + \epsilon\Delta x(E), T + \epsilon\Delta t(E))$ continuous under variation of E . As with the time-translation symmetry, this implies a unit Floquet multiplier: indeed, we know from sect. 7.3 that symplectic eigenvalues come in pairs, so unit multiplier in the time direction implies a unit multiplier in its dual, the energy direction, $(\Lambda_t, \Lambda_E, \dots) = (1, 1, \dots)$. But extending the number of constraints is no longer a problem: add more Lagrange multipliers. Consider the following system

$$I_3(\Delta x, \lambda_1, \lambda_2) = \Delta x[1 - J(x)]\Delta x/2 + (x - f(x)) \Delta x + \lambda_1 (U(x + \Delta x) - U(x_0)) + \lambda_2 (H(x + \Delta x) - E_0) \quad (13.21)$$

$$\begin{pmatrix} 1 - J(x) & \partial U(x) & \partial H(x) \\ \partial U(x) & 0 & 0 \\ \partial H(x) & 0 & 0 \end{pmatrix} \begin{pmatrix} \Delta x \\ \lambda_1 \\ \lambda_2 \end{pmatrix} = - \begin{pmatrix} x - f(x) \\ U(x) - U(x_0) \\ H(x) - E_0 \end{pmatrix} \quad (13.22)$$

This is the Newton iteration setup for how to search for a periodic orbit of a Hamiltonian flow with a global surface of section $U(x) = U(x_0)$ and fixed energy E_0 .

Note that these instructions do not put every iteration on a surface $U(x) = U(x_0)$ and energy $H(x) = E_0$, unless the surface is a plane $U(x) = a \cdot (x - x_0)$, but instead assure that the iterations will gradually approach (provided they converge) to the surfaces.

For periodic orbits multi-point shooting generalizes in the same way as (13.7), but with n additional equations – one for each point on a Poincaré section. The Newton setup looks like this

$$\begin{pmatrix} 1 & & & & -J_n \\ -J_1 & 1 & & & \\ & \dots & \dots & & \\ & & \dots & 1 & \\ & & & \dots & 1 \\ \hline & a & & & -J_{n-1} & 1 \\ & & & \dots & & \\ & & & & & a \end{pmatrix} \begin{pmatrix} v_1 \\ \vdots \\ v_n \\ \hline 0 \\ \vdots \\ 0 \end{pmatrix} \begin{pmatrix} \Delta x_1 \\ \Delta x_2 \\ \vdots \\ \Delta x_n \\ \Delta t_1 \\ \vdots \\ \Delta t_n \end{pmatrix} = \begin{pmatrix} -F_1 \\ -F_2 \\ \vdots \\ -F_n \\ 0 \\ \vdots \\ 0 \end{pmatrix}.$$

Solving this equation resembles the corresponding task for maps. However, in the process we will need to invert an $[(d + 1)n \times (d + 1)n]$ matrix rather than a $[d \times d]$ matrix.

13.4.2 How good is my orbit?

Provided we understand the topology of the flow, multi-shooting methods and their variational cousins of chapter 29 enable us to compute periodic orbits of arbitrary length. A notion that errors somehow grow exponentially with the cycle length at Lyapunov exponent rate cannot be right. So how do we characterize the accuracy of an orbit of arbitrary length?

The numerical round-off errors along a trajectory are uncorrelated and act as noise, so the errors $(x(t + \Delta t) - f^{\Delta t}(x(t)))^2$ are expected to accumulate as the sum of squares of uncorrelated steps, linearly with time. Hence the accumulated numerical noise along an orbit sliced by N intermediate sections separated by $\Delta t_k = t_{k+1} - t_k \sim T_p/N$ can be characterized by an effective diffusion constant

$$D_p = \frac{1}{2(d_e + 1)} \sum_{k=1}^N \frac{1}{\Delta t_k} (x_{k+1} - f^{\Delta t_k}(x_k))^2. \tag{13.23}$$

For hyperbolic flows errors are exponentially amplified along unstable and contracted along stable eigen-directions, so $d_e + 1$ stands for the number of unstable directions of the flow together with the single marginal direction along the flow. An honest calculation requires an honest error estimate. If you are computing a large set of periodic orbits p , list D_p along with T_p and other properties of cycles.

Résumé

There is no general computational algorithm that is guaranteed to find all solutions (up to a given period T_{\max}) to the periodic orbit condition

$$f^{t+T}(x) = f^t(x), \quad T > 0$$

for a general flow or mapping. Due to the exponential divergence of nearby trajectories in chaotic dynamical systems, direct solution of the periodic orbit condition can be numerically very unstable.

A prerequisite for a systematic and complete cycle search is a good (but hard to come by) understanding of the topology of the flow. Usually one starts by - possibly analytic - determination of the equilibria of the flow. Their locations, stabilities, stability eigenvectors and invariant manifolds offer skeletal information about the topology of the flow. Next step is numerical long-time evolution of “typical” trajectories of the dynamical system under investigation. Such numerical experiments build up the “natural measure,” and reveal regions most frequently visited. The periodic orbit searches can then be initialized by taking nearly recurring orbit segments and deforming them into a closed orbits. With a sufficiently good initial guess the Newton-Raphson formula

section 16.4.1

$$\begin{pmatrix} 1 - J & v(x) \\ a & 0 \end{pmatrix} \begin{pmatrix} \delta x \\ \delta T \end{pmatrix} = \begin{pmatrix} f(x) - x \\ 0 \end{pmatrix}$$

yields improved estimate $x' = x + \delta x$, $T' = T + \delta T$. Iteration then yields the period T and the location of a periodic point x_p in the Poincaré surface $(x_p - x_0) \cdot a = 0$, where a is a vector normal to the Poincaré section at x_0 .

The problem one faces with high-dimensional flows is that their topology is hard to visualize, and that even with a decent starting guess for a point on a periodic orbit, methods like the Newton-Raphson method are likely to fail. Methods that start with initial guesses for a number of points along the cycle, such as the multipoint shooting method of sect. 13.3, are more robust. The relaxation (or variational) methods take this strategy to its logical extreme, and start by a guess of not a few points along a periodic orbit, but a guess of the entire orbit. As these methods are intimately related to variational principles and path integrals, we postpone their introduction to chapter 29.

chapter 29

Commentary

Remark 13.1 Close recurrence searches. For low-dimensional maps of flows (for high-dimensional flows, forget about it) picking initial guesses for periodic orbits from close recurrences of a long ergodic trajectory seems like an obvious idea. Nevertheless,

ref. [1] is frequently cited. Such methods have been deployed by many, among them G. Tanner, L. Rondoni, G. Morris, C.P. Dettmann, and R.L. Davidchack [2, 14, 15, 10, 11] (see also sect. 20.5). Sometimes one can determine most of the admissible itineraries and their weights without working too hard, but method comes with no guarantee.

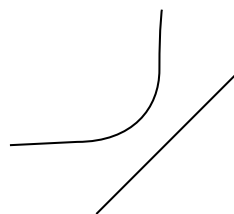
Remark 13.2 Piecewise linear maps. The Lozi map (3.21) is linear, and 100,000's of cycles can be easily computed by $[2 \times 2]$ matrix multiplication and inversion.

Remark 13.3 Cycles, searches, and symmetries. A few comments about the role of symmetries in actual extraction of cycles. In the N -disk billiard example, a fundamental domain is a sliver of the N -disk configuration space delineated by a pair of adjoining symmetry axes. The flow may further be reduced to a return map on a Poincaré surface of section. While in principle any Poincaré surface of section will do, a natural choice in the present context are crossings of symmetry axes, see example 7.6. In actual numerical integrations only the last crossing of a symmetry line needs to be determined. The cycle is run in global coordinates and the group elements associated with the crossings of symmetry lines are recorded; integration is terminated when the orbit closes in the fundamental domain. Periodic orbits with non-trivial symmetry subgroups are particularly easy to find since their points lie on crossings of symmetry lines, see example 7.6.

Remark 13.4 Newton gone wild. Skowronek and Gora [23] offer an interesting discussion of Newton iterations gone wild while searching for roots of polynomials as simple as $x^2 + 1 = 0$.

Exercises

- 13.1. **Cycles of the Ulam map.** Test your cycle-searching routines by computing a bunch of short cycles and their stabilities for the Ulam map $f(x) = 4x(1 - x)$.
- 13.2. **Cycles stabilities for the Ulam map, exact.** In exercise 13.1 you should have observed that the numerical results for the cycle Floquet multipliers (4.51) are exceptionally simple: the Floquet multiplier of the $x_0 = 0$ fixed point is 4, while the eigenvalue of any other n -cycle is $\pm 2^n$. Prove this. (Hint: the Ulam map can be conjugated to the tent map (11.4). This problem is perhaps too hard, but give it a try - the answer is in many introductory books on nonlinear dynamics.)
- 13.3. **Stability of billiard cycles.** Compute stabilities of few simple cycles.
- (a) A simple scattering billiard is the two-disk billiard. It consists of a disk of radius one centered at the origin and another disk of unit radius located at $L + 2$. Find all periodic orbits for this system and compute their stabilities. (You might have done this already in exercise 1.2; at least now you will be able to see where you went wrong when you knew nothing about cycles and their extraction.)
 - (b) Find all periodic orbits and stabilities for a billiard ball bouncing between the diagonal $y = x$ and one of the hyperbola branches $y = -1/x$.



- 13.4. **Cycle stability.** Add to the pinball simulator of exercise 8.1 a routine that evaluates the expanding eigenvalue for a given cycle.
- 13.5. **Pinball cycles.** Determine the stability and length of all fundamental domain prime cycles of the binary symbol string lengths up to 5 (or longer) for $R : a = 6$ 3-disk pinball.
- 13.6. **Newton-Raphson method.** Implement the Newton-Raphson method in 2 - dimensional and apply it to determination of pinball cycles.

- 13.7. **Fundamental domain fixed points.** Use the formula (8.11) for billiard Jacobian matrix to compute the periods T_p and the expanding eigenvalues Λ_p of the fundamental domain $\bar{0}$ (the 2-cycle of the complete 3-disk space) and $\bar{1}$ (the 3-cycle of the complete 3-disk space) fixed points:

$$\begin{array}{c|cc} & T_p & \Lambda_p \\ \hline \bar{0}: & R - 2 & R - 1 + R\sqrt{1 - 2/R} \\ \bar{1}: & R - \sqrt{3} & -\frac{2R}{\sqrt{3}} + 1 - \frac{2R}{\sqrt{3}}\sqrt{1 - \sqrt{3}/R} \end{array} \quad (13.24)$$

We have set the disk radius to $a = 1$.

- 13.8. **Fundamental domain 2-cycle.** Verify that for the $\bar{10}$ -cycle the cycle length and the trace of the Jacobian matrix are given by

$$\begin{aligned} L_{10} &= 2\sqrt{R^2 - \sqrt{3}R + 1} - 2, \\ \text{tr } \mathbf{J}_{10} &= \Lambda_{10} + 1/\Lambda_{10} \\ &= 2L_{10} + 2 + \frac{1}{2} \frac{L_{10}(L_{10} + 2)^2}{\sqrt{3}R/2 - 1}. \end{aligned} \quad (13.25)$$

The $\bar{10}$ -cycle is drawn in figure 12.12. The unstable eigenvalue Λ_{10} follows from (7.22).

- 13.9. **A test of your pinball simulator: $\bar{10}$ -cycle.** Test your exercise 8.3 pinball simulator stability evaluation by checking numerically the exact analytic $\bar{10}$ -cycle stability formula (13.25).
- 13.10. **Rössler flow cycles.** (continuation of exercise 4.4) Determine all cycles for the Rössler flow (2.17), as well as their stabilities, up to
- (a) 3 Poincaré sections returns
 - (b) (optional) 5 Poincaré sections returns (Hint: implement (13.14), the multipoint shooting methods for flows; you can cross-check your shortest cycles against the ones listed in the table.)

Table: The Rössler flow (2.17): The itinerary p , a periodic point $x_p = (0, y_p, z_p)$ and the expanding eigenvalue Λ_p for all cycles up to the topological length 7. (J. Mathiesen, G. Simon, A. Basu)

n_p	p	y_p	z_p	Λ_e
1	1	6.091768	1.299732	-2.403953
2	01	3.915804	3.692833	-3.512007
3	001	2.278281	7.416481	-2.341923
	011	2.932877	5.670806	5.344908
4	0111	3.466759	4.506218	-16.69674
5	01011	4.162799	3.303903	-23.19958
	01111	3.278914	4.890452	36.88633
6	001011	2.122094	7.886173	-6.857665
	010111	4.059211	3.462266	61.64909
	011111	3.361494	4.718206	-92.08255
7	0101011	3.842769	3.815494	77.76110
	0110111	3.025957	5.451444	-95.18388
	0101111	4.102256	3.395644	-142.2380
	0111111	3.327986	4.787463	218.0284

- 13.11. **Cycle stability, helium.** Add to the helium integrator of exercise 2.10 a routine that evaluates the expanding eigenvalue for a given cycle.
- 13.12. **Collinear helium cycles.** Determine the stability and length of all fundamental domain prime cycles up to symbol sequence length 5 or longer for collinear helium of figure 7.2.
- 13.13. **Uniqueness of unstable cycles***.** Prove that there exists only one 3-disk prime cycle for a given finite admissible prime cycle symbol string. Hints: look at the Poincaré section mappings; can you show that there is exponential contraction to a unique periodic point with a given itinerary? Exercise 29.1 might be helpful in this effort.
- 13.14. **Inverse iteration method for a Hamiltonian repeller.**

Table: All periodic orbits up to 6 bounces for the Hamiltonian Hénon mapping (13.26) with $a = 6$. Listed are the cycle itinerary, its expanding eigenvalue Λ_p , and its “center of mass.” The “center of mass” is listed because it turns out the “center of mass” is often a simple rational or a quadratic irrational.

p	Λ_p	$\sum x_{p,i}$
0	0.715168×10^1	-0.607625
1	-0.295285×10^1	0.274292
10	-0.989898×10^1	0.333333
100	-0.131907×10^3	-0.206011
110	0.558970×10^2	0.539345
1000	-0.104430×10^4	-0.816497
1100	0.577998×10^4	0.000000
1110	-0.103688×10^3	0.816497
10000	-0.760653×10^4	-1.426032
11000	0.444552×10^4	-0.606654
10100	0.770202×10^3	0.151375
11100	-0.710688×10^3	0.248463
11010	-0.589499×10^3	0.870695
11110	0.390994×10^3	1.095485
100000	-0.545745×10^5	-2.034134
110000	0.322221×10^5	-1.215250
101000	0.513762×10^4	-0.450662
111000	-0.478461×10^4	-0.366025
110100	-0.639400×10^4	0.333333
101100	-0.639400×10^4	0.333333
111100	0.390194×10^4	0.548583
111010	0.109491×10^4	1.151463
111110	-0.104338×10^4	1.366025

Consider the Hénon map (3.19) for area-preserving (“Hamiltonian”) parameter value $b = -1$. The coordinates of a periodic orbit of length n_p satisfy the equation

$$x_{p,i+1} + x_{p,i-1} = 1 - ax_{p,i}^2, \quad i = 1, \dots, n_p, \quad (13.26)$$

with the periodic boundary condition $x_{p,0} = x_{p,n_p}$. Verify that the itineraries and the stabilities of the short periodic orbits for the Hénon repeller (13.26) at $a = 6$ are as listed above.

Hint: you can use any cycle-searching routine you wish, but for the complete repeller case (all binary sequences are realized), the cycles can be evaluated simply by inverse iteration, using the inverse of (13.26)

$$x''_{p,i} = S_{p,i} \sqrt{\frac{1 - x'_{p,i+1} - x'_{p,i-1}}{a}}, \quad i = 1, \dots, n_p.$$

Here $S_{p,i}$ are the signs of the corresponding periodic point coordinates, $S_{p,i} = x_{p,i}/|x_{p,i}|$. (G. Vattay)

- 13.15. **Ulam map periodic points.** (continued from exercise 11.8)
- (a) compute the five periodic points of cycle $\overline{10011}$ for the Ulam map (11.5) $f(x) = 4x(1 - x)$. using your Newton or other routine.
 - (b) compute the five periodic points of cycle $\overline{10000}$
 - (c) plot the above two cycles on the graph of the Ulam map, verify that their topological ordering is as in the ‘canonical’ full tent map exercise 11.8.
 - (d) (optional) This works only for the Ulam map: compute periodic points by conjugating the full tent map periodic points of exercise 11.8 using exercise 6.4.
- 13.16. **Newton setups for flows.**
- (a) We have formulated three Newton setups for flows: the ‘local’ setup (13.11), the ‘hyperplane’ setup (13.14), and the ‘global’ setup (13.20). Derive (13.20) and verify that if the surface of section is a hyperplane, it reduces to (13.14). (Hint: it is not inconceivable that (13.14) is wrong as it stands.)
 - (b) (optional) Derive (13.22), the Newton setup for Hamiltonian flows.
- 13.17. **“Center of mass” puzzle**.** Why is the “center of mass,” tabulated in exercise 13.14, often a rational number?

References

- [13.1] D. Auerbach, P. Cvitanović, J.-P. Eckmann, G.H. Gunaratne and I. Procaccia, *Phys. Rev. Lett.* **58**, 2387 (1987).
- [13.2] M. Baranger and K.T.R. Davies *Ann. Physics* **177**, 330 (1987).
- [13.3] B.D. Mestel and I. Percival, *Physica D* **24**, 172 (1987); Q. Chen, J.D. Meiss and I. Percival, *Physica D* **29**, 143 (1987).
- [13.4] find Helleman et all Fourier series methods
- [13.5] J.M. Greene, *J. Math. Phys.* **20**, 1183 (1979)
- [13.6] H.E. Nusse and J. Yorke, “A procedure for finding numerical trajectories on chaotic saddles” *Physica D* **36**, 137 (1989).
- [13.7] D.P. Lathrop and E.J. Kostelich, “Characterization of an experimental strange attractor by periodic orbits”
- [13.8] T. E. Huston, K.T.R. Davies and M. Baranger *Chaos* **2**, 215 (1991).
- [13.9] M. Brack, R. K. Bhaduri, J. Law and M. V. N. Murthy, *Phys. Rev. Lett.* **70**, 568 (1993).
- [13.10] J. J. Crofts and R. L. Davidchack, “Efficient detection of periodic orbits in chaotic systems by stabilising transformations;” [arXiv:nlin.CD/0502013](https://arxiv.org/abs/nlin.CD/0502013).
- [13.11] J. J. Crofts and R. L. Davidchack, “On the use of stabilizing transformations for detecting unstable periodic orbits in high-dimensional flows,” *Chaos* **19** (2009).
- [13.12] C. Polymilis, G. Servizi, Ch. Skokos, G. Turchetti, and M. N. Vrahatis, “Locating periodic orbits by Topological Degree theory;” [arXiv:nlin.CD/0211044](https://arxiv.org/abs/nlin.CD/0211044).
- [13.13] B. Doyon and L. J. Dubé, “On Jacobian matrices for flows,” *CHAOS* **15**, 013108 (2005).
- [13.14] S.C. Farantos, “Exploring Molecular Vibrational Motions with Periodic Orbits,” *Int. Rev. Phys. Chem.* **15**, 345 (1996);
tccc.iesl.forth.gr/~farantos,
tccc.iesl.forth.gr/articles/review/review1.ps.gz.
- [13.15] S.C. Farantos, “POMULT: A Program for Computing Periodic Orbits in Hamiltonian Systems Based on Multiple Shooting Algorithms,” *Computer Phys. Comm.* **108**, 240 (1998);
esperia.iesl.forth.gr/~farantos/articles/po_cpc/po_ccp.ps.
- [13.16] M. Baranger, K.T.R. Davies and J.H. Mahoney, “The calculation of periodic trajectories,” *Ann. Phys.* **186**, 95 (1988).

- [13.17] K.T.R. Davies, T.E. Huston and M. Baranger, “Calculations of periodic trajectories for the Henon-Heiles Hamiltonian using the monodromy method,” *CHAOS* **2**, 215 (1992).
- [13.18] N.S. Simonović, “Calculations of periodic orbits: The monodromy method and application to regularized systems,” *CHAOS* **9**, 854 (1999).
- [13.19] N.S. Simonović, “Calculations of Periodic Orbits for Hamiltonian Systems with Regularizable Singularities,” *Few-Body-Systems* **32**, 183 (2003).
- [13.20] Z. Gills, C. Iwata, R. Roy, I.B. Schwartz and I. Triandaf, “Tracking Unstable Steady States: Extending the Stability Regime of a Multimode Laser System,” *Phys. Rev. Lett.* **69**, 3169 (1992).
- [13.21] N.J. Balmforth, P. Cvitanović, G.R. Ierley, E.A. Spiegel and G. Vattay, “Advection of vector fields by chaotic flows,” *Stochastic Processes in Astrophysics, Annals of New York Academy of Sciences* **706**, 148 (1993); [preprint](#).
- [13.22] A. Endler and J.A.C. Gallas, “Rational reductions of sums of orbital coordinates for a Hamiltonian repeller,” (2005).
- [13.23] L. Skowronek and P. F. Gora, “Chaos in Newtonian iterations: Searching for zeros which are not there,” *Acta Phys. Polonica B* **38**, 1909 (2007); [arXiv:nlin.CD/0703061](#).

Part II

Chaos rules

QUADRACY: all these cycles, but what to do with them? What you have now is a topologically invariant road map of the state space, with the chaotic region pinned down by a rigid skeleton, a tree of *cycles* (periodic orbits) of increasing lengths and self-similar structure. In chapter 15 we shall turn this topological dynamics into a multiplicative operation on the state space partitions by means of transition matrices of chapter 14, the simplest examples of evolution operators. This will enable us to *count* the distinct orbits, and in the process touch upon all the main themes of this book, going the whole distance from diagnosing chaotic dynamics to computing zeta functions.

1. Partition the state space and describe all allowed ways of getting from ‘here’ to ‘there’ by means of transition graphs (transition matrices). These generate the totality of admissible itineraries. (Chapter 14)
2. Learn to count (Chapter 15)
3. Learn how to measure what’s important (Chapter 16)
4. Learn how to evolve the measure, compute averages (Chapter 17)
5. Learn what a ‘Fourier transform’ is for a nonlinear world, not a circle (Chapter 18),
6. and how the short-time / long-time duality is encoded by spectral determinant expression for evolution operator spectrum in terms of periodic orbits. (Chapter 19)
7. Learn how use short period cycles to describe chaotic world at times much beyond the Lyapunov time (Chapter 20).

Next ponder how symmetries simplify spectral determinants (chapter 21), develop some feeling for the traces of evolution operators (chapter 22), why all this works (chapter 23), when does it not work (chapter 24), what does it have to do with foundations of statistical mechanics (chapter 25) and turbulence (chapter 24).

Chapter 14

Walkabout: Transition graphs

I think I'll go on a walkabout
find out what it's all about [...] take a ride to the other side
—Red Hot Chili Peppers, 'Walkabout'

IN CHAPTERS 11 AND 12 we learned that invariant manifolds partition the state space in invariant way, and how to name distinct orbits. We have established and related the *temporally* and *spatially* ordered topological dynamics for a class of 'stretch & fold' dynamical systems, and discussed pruning of inadmissible trajectories.

Here we shall use these results to generate the totality of admissible itineraries. This task will be particularly easy for repellers with complete Smale horseshoes and for subshifts of finite type, for which the admissible itineraries are generated by finite transition matrices, and the topological dynamics can be visualized by means of finite transition graphs. We shall then turn topological dynamics into a linear multiplicative operation on the state space partitions by means of transition matrices, the simplest examples of 'evolution operators.' They will enable us – in chapter 15 – to *count* the distinct orbits.

14.1 Matrix representations of topological dynamics



The allowed transitions between the regions of a partition $\{\mathcal{M}_1, \mathcal{M}_2, \dots, \mathcal{M}_m\}$ are encoded in the $[m \times m]$ -dimensional transition matrix whose elements take values

$$T_{ij} = \begin{cases} 1 & \text{if the transition } \mathcal{M}_j \rightarrow \mathcal{M}_i \text{ is possible} \\ 0 & \text{otherwise.} \end{cases} \quad (14.1)$$

The transition matrix is an explicit linear representation of topological dynamics. If the partition is a dynamically invariant partition constructed from stable/unstable manifolds, it encodes the topological dynamics as an invariant law

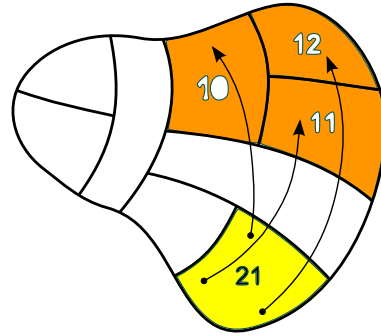


Figure 14.1: Points from the region \mathcal{M}_{21} reach regions $\{\mathcal{M}_{10}, \mathcal{M}_{11}, \mathcal{M}_{12}\}$, and no other regions, in one time step. Labeling exemplifies the ‘shift map’ of example 11.7 and (11.20).

of motion, with the allowed transitions at any instant independent of the trajectory history, requiring no memory.

Several related matrices as well will be needed in what follows. Often it is convenient to distinguish between two or more paths connecting the same two regions; that is encoded by the *adjacency* matrix with non-negative integer entries,

$$A_{ij} = \begin{cases} k & \text{if a transition } \mathcal{M}_j \rightarrow \mathcal{M}_i \text{ is possible in } k \text{ ways} \\ 0 & \text{otherwise.} \end{cases} \quad (14.2)$$

More generally, we shall encounter $[m \times m]$ matrices which assign different real or complex weights to different transitions,

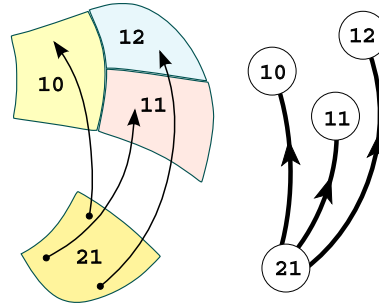
$$L_{ij} = \begin{cases} L_{ij} \in \mathbb{R} \text{ or } \mathbb{C} & \text{if } \mathcal{M}_j \rightarrow \mathcal{M}_i \text{ is allowed} \\ 0 & \text{otherwise.} \end{cases} \quad (14.3)$$

As in statistical physics, we shall refer to these as *transfer* matrices.

\mathcal{M}_i is *accessible* from \mathcal{M}_j in k steps if $(L^k)_{ij} \neq 0$. A matrix L is called *reducible* if there exists one or more index pairs $\{i, j\}$ such that $(L^k)_{ij} = 0$ for all k , otherwise the matrix is *irreducible*. This means that a trajectory starting in any partition region eventually reaches all of the partition regions, i.e., the partition is dynamically transitive or indecomposable, as assumed in (2.2). The notion of topological *transitivity* is crucial in ergodic theory: a mapping is transitive if it has a dense orbit. If that is not the case, state space decomposes into disconnected pieces, each of which can be analyzed separately by a separate irreducible matrix. Region \mathcal{M}_i is said to be *transient* if no trajectory returns to it. Region \mathcal{M}_j is said to be *absorbing* if no trajectory leaves it, $L_{jj} \neq 0$, $L_{ij} = 0$ for all $i \neq j$. Hence it suffices to restrict our considerations to irreducible matrices.

If L has strictly positive entries, $L_{ij} > 0$, the matrix is called *positive*; if $L_{ij} \geq 0$, the matrix is called *non-negative*. Matrix L is said to be *eventually positive* or *Perron-Frobenius* if L^k is positive for some power k (as a consequence, the matrix is transitive as well). A non-negative matrix whose columns conserve probability, $\sum_i L_{ij} = 1$, is called *Markov, probability or stochastic* matrix.

Figure 14.2: Topological dynamics: shrink each state space partition region figure 14.1 to a *node*, and indicate the possibility of reaching a region by a *directed link*. The links stand for transition matrix elements $T_{10,21} = T_{11,21} = T_{12,21} = 1$; remaining $T_{ij,21} = 0$.



Example 14.1 Markov chain. The Google PageRank of a webpage is computed by a Markov chain, with a rather large Markov matrix M .

A subshift (11.22) of finite type is a *topological dynamical system* (Σ, σ) , where the shift σ acts on the space of all admissible itineraries (s_k)

$$\Sigma = \{(s_k)_{k \in \mathbb{Z}} : T_{s_{k+1}s_k} = 1 \text{ for all } k\}, \quad s_k \in \{a, b, c, \dots, z\}. \quad (14.4)$$

The task of generating the totality of admissible itineraries is particularly easy for subshifts of finite type, for which the admissible itineraries are generated by finite transition matrices, and the topological dynamics can be visualized by means of finite transition graphs.

14.2 Transition graphs: wander from node to node

Let us abstract from a state space partition such as figure 14.1 its topological essence: indicate a partition region \mathcal{M}_a by a *node*, and indicate the possibility of reaching the region \mathcal{M}_b , $L_{ba} \neq 0$ by a *directed link*, as in figure 14.2. Do this for all nodes. The result is a *transition graph*.

A *transition graph* (or *digraph*, or simply ‘*graph*’) consists of a set of *nodes* (or *vertices*, or *states*), one for each letter in the alphabet $\mathcal{A} = \{a, b, c, \dots, z\}$, connected by a set of directed *links* (*edges*, *arcs*, *arrows*). A directed link starts out from node j and terminates at node i whenever the matrix element (14.3) takes value $L_{ij} \neq 0$. A link connects two nodes, or originates and terminates on the same node (a ‘self-loop’). For example, if a partition includes regions labeled $\{\dots, \mathcal{M}_{101}, \mathcal{M}_{110}, \dots\}$, the transition matrix element connecting the two is drawn as $L_{101,110} = \textcircled{101} \leftarrow \textcircled{110}$, whereas $L_{0,0} = \textcircled{0} \leftarrow \textcircled{0}$. Here a dotted link indicates that the shift $\sigma(x_{011\dots}) = x_{11\dots}$ involves symbol 0, and a full one a shift $\sigma(x_{110\dots}) = x_{10\dots}$ that involves 1. A $j \rightarrow \dots \rightarrow k$ *walk* (*path*, *itinerary*) traverses a connected set of directed links, starting at node j and ending at node k . A *loop* (*periodic orbit*, *cycle*) is a walk that ends at the starting node (which can be any node along the loop), for example

$$t_{011} = L_{110,011}L_{011,101}L_{101,110} = \begin{array}{c} \textcircled{101} \\ \downarrow \\ \textcircled{011} \\ \uparrow \\ \textcircled{110} \\ \leftarrow \\ \textcircled{101} \end{array} . \quad (14.5)$$

Our convention for ordering indices is that the successive steps in a visitation sequence $j \rightarrow i \rightarrow k$ are generated by matrix multiplication from the left, $T_{kj} = \sum T_{ki}T_{ij}$. Two graphs are *isomorphic* if one can be obtained from the other by relabeling links and nodes. As we are interested in recurrent (transitive, indecomposable) dynamics, we restrict our attention to *irreducible* or *strongly connected* graphs, i.e., graphs for which there is a path from any node to any other node.

A transition graph describes compactly the ways in which the state space regions map into each other, accounts for finite memory effects in dynamics, and generates the totality of admissible trajectories as the set of all possible walks along its links.

Construction of a good transition graph is, like combinatorics, unexplainable. The only way to learn is by some diagrammatic gymnastics, so we work our way through a sequence of exercises in lieu of plethora of baffling definitions.

Example 14.2 Full binary shift. Consider a full shift on two-state partition $\mathcal{A} = \{0, 1\}$, with no pruning restrictions. The transition matrix and the corresponding transition graph are

$$T = \begin{pmatrix} 1 & 1 \\ 1 & 1 \end{pmatrix} = \text{graph} \tag{14.6}$$

Dotted links correspond to shifts originating in region 0, and the full ones to shifts originating in 1. The admissible itineraries are generated as walks on this transition graph. (continued in example 14.8)

Example 14.3 Complete N-ary dynamics: If all transition matrix entries equal unity (one can reach any region from any other region in one step),

$$T_c = \begin{pmatrix} 1 & 1 & \dots & 1 \\ 1 & 1 & \dots & 1 \\ \vdots & \vdots & \ddots & \vdots \\ 1 & 1 & \dots & 1 \end{pmatrix}, \tag{14.7}$$

the symbolic dynamics is called complete, or a full shift. The corresponding transition graph is obvious, but a bit tedious to draw for arbitrary N .

Example 14.4 Pruning rules for a 3-disk alphabet: As the disks are convex, there can be no two consecutive reflections off the same disk, hence the covering symbolic dynamics consists of all sequences which include no symbol repetitions 11, 22, 33. This is a finite set of finite length pruning rules, hence, the dynamics is a subshift of finite type (see (11.23) for definition), with the transition matrix / graph given by

$$T = \begin{pmatrix} 0 & 1 & 1 \\ 1 & 0 & 1 \\ 1 & 1 & 0 \end{pmatrix} = \text{graph} \tag{14.8}$$

The complete unrestricted symbolic dynamics is too simple to be illuminating, so we turn next to the simplest example of pruned symbolic dynamics, the finite subshift obtained by prohibition of repeats of one of the symbols, let us say $_11_$. This situation arises, for example, in studies of the circle maps, where this kind of symbolic dynamics describes “golden mean” rotations.

exercise 15.6
exercise 15.8

Example 14.5 ‘Golden mean’ pruning. Consider a subshift on two-state partition $\mathcal{A} = \{0, 1\}$, with the simplest grammar \mathcal{G} possible, a single pruned block $b = _11_$ (consecutive repeat of symbol 1 is inadmissible): the state M_0 maps both onto M_0 and M_1 , but the state M_1 maps only onto M_0 . The transition matrix and the corresponding transition graph are

$$T = \begin{pmatrix} 1 & 1 \\ 1 & 0 \end{pmatrix} = \text{graph} \quad (14.9)$$

Admissible itineraries correspond to walks on this finite transition graph. (continued in example 14.9)

In the complete N -ary symbolic dynamics case (see example 14.3) the choice of the next symbol requires no memory of the previous ones. However, any further refinement of the state space partition requires finite memory.

Example 14.6 Finite memory transition graphs. For the binary labeled repeller with complete binary symbolic dynamics, we might chose to partition the state space into four regions $\{M_{00}, M_{01}, M_{10}, M_{11}\}$, a 1-step refinement of the initial partition $\{M_0, M_1\}$. Such partitions are drawn in figure 12.3, as well as figure 1.9. Topologically f acts as a left shift (12.11), and its action on the rectangle $[_01]$ is to move the decimal point to the right, to $[0.1]$, forget the past, $[_1]$, and land in either of the two rectangles $[_10], [_11]$. Filling in the matrix elements for the other three initial states we obtain the 1-step memory transition matrix/graph acting on the 4-regions partition

exercise 11.7

$$T = \begin{pmatrix} T_{00,00} & 0 & T_{00,10} & 0 \\ T_{01,00} & 0 & T_{01,10} & 0 \\ 0 & T_{10,01} & 0 & T_{10,11} \\ 0 & T_{11,01} & 0 & T_{11,11} \end{pmatrix} = \text{graph} \quad (14.10)$$

(continued in example 15.7)

By the same token, for M -step memory the only nonvanishing matrix elements are of the form $T_{s_1 s_2 \dots s_{M+1}, s_0 s_1 \dots s_M}$, $s_{M+1} \in \{0, 1\}$. This is a sparse matrix, as the only non vanishing entries in the $a = s_0 s_1 \dots s_M$ column of T_{ba} are in the rows $b = s_1 \dots s_M 0$ and $b = s_1 \dots s_M 1$. If we increase the number of steps remembered, the transition matrix grows large quickly, as the N -ary dynamics with M -step memory requires an $[N^{M+1} \times N^{M+1}]$ matrix. Since the matrix is very sparse, it pays to find a compact representation for T . Such representation is afforded by transition graphs, which are not only compact, but also give us an intuitive picture of the topological dynamics.

exercise 15.1

Figure 14.3: Transition graph (graph whose links correspond to the nonzero elements of a transition matrix T_{ba}) describes which regions b can be reached from the region a in one time step. The 7 nodes correspond to the 7 regions of the partition (14.11). The links represent non-vanishing transition matrix elements, such as $T_{101,110} = \overset{\circ}{101} \leftarrow \overset{\circ}{110}$. Dotted links correspond to a shift by symbol 0, and the full ones by symbol 1.

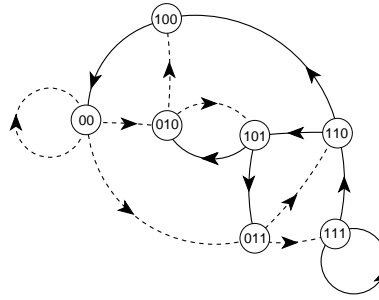
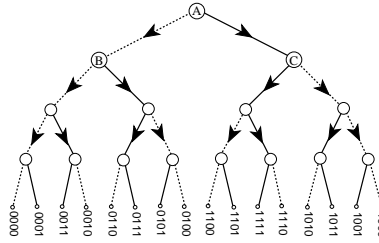


Figure 14.4: The self-similarity of the complete binary symbolic dynamics represented by a binary tree: trees originating in nodes B, C, \dots (actually - any node) are the same as the tree originating in node A . Level $m = 4$ partition is labeled by 16 binary strings, coded by dotted (0) and full (1) links read down the tree, starting from A . See also figure 11.14.



Example 14.7 A 7-state transition graph. Consider a state space partitioned into 7 regions

$$\{\mathcal{M}_{00}, \mathcal{M}_{011}, \mathcal{M}_{010}, \mathcal{M}_{110}, \mathcal{M}_{111}, \mathcal{M}_{101}, \mathcal{M}_{100}\}. \tag{14.11}$$

Let the evolution in time map the regions into each other by acting on the labels as shift (12.11): $\mathcal{M}_{011} \rightarrow \{\mathcal{M}_{110}, \mathcal{M}_{111}\}$, $\mathcal{M}_{00} \rightarrow \{\mathcal{M}_{00}, \mathcal{M}_{011}, \mathcal{M}_{010}\} \dots$, with nonvanishing $L_{110,011}, L_{011,00}, \dots$. This is compactly summarized by the transition graph of figure 14.3. (continued as example 15.6)

14.3 Transition graphs: stroll from link to link

exercise 15.1

What do finite graphs have to do with infinitely long trajectories? To understand the main idea, let us construct a graph that enumerates all possible itineraries for the case of complete binary symbolic dynamics. In this construction the nodes will be unlabeled, links labeled, signifying different kinds of transitions.

Example 14.8 Complete binary topological dynamics. Mark a dot ‘.’ on a piece of paper. Draw two short lines out of the dot, end each with a dot. The full line will signify that the first symbol in an itinerary is ‘1,’ and the dotted line will signify ‘0.’ Repeat the procedure for each of the two new dots, and then for the four dots, and so on. The result is the binary tree of figure 14.4. Starting at the top node, the tree enumerates exhaustively all distinct finite itineraries of lengths $n = 1, 2, 3, \dots$

$$\begin{aligned} &\{0, 1\} \quad \{00, 01, 10, 11\} \\ &\{000, 001, 010, 011, 100, 101, 111, 110\} \dots \end{aligned}$$

The $n = 4$ nodes in figure 14.4 correspond to the 16 distinct binary strings of length 4, and so on. By habit we have drawn the tree as the alternating binary tree of figure 11.14, but that has no significance as far as enumeration of itineraries is concerned

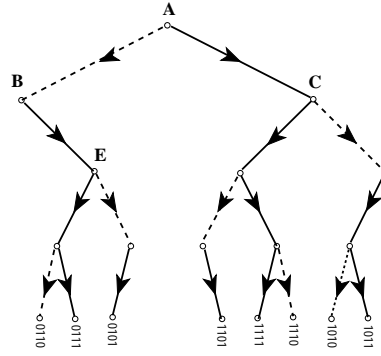


Figure 14.5: The self-similarity of the $_00_$ pruned binary tree: trees originating from nodes C and E are the same as the entire tree.

- a binary tree with labels in the natural order, as increasing binary ‘decimals’ would serve just as well.

The trouble with an infinite tree is that it does not fit on a piece of paper. On the other hand, we are not doing much - at each node we are turning either left or right. Hence all nodes are equivalent. In other words, the tree is self-similar; the trees originating in nodes B and C are themselves copies of the entire tree. The result of identifying $B = A$, $C = A$ is a single node, 2-link transition graph with adjacency matrix figure 14.2

$$A = (2) = \begin{array}{c} \circlearrowleft \\ \circlearrowright \\ \text{A=B=C} \end{array} \quad (14.12)$$

An itinerary generated by the binary tree figure 14.4, no matter how long, corresponds to a walk on this graph.

This is the most compact encoding of the complete binary symbolic dynamics. Any number of more complicated transition graphs such as the 2-node (14.6) and the 4-node (14.10) graphs generate all itineraries as well, and might be sometimes preferable.

exercise 15.6
exercise 15.5

We turn next to the simplest example of pruned symbolic dynamics, the finite subshift obtained by prohibition of repeats of one of the symbols, let us say $_00_$.

Example 14.9 ‘Golden mean’ pruning. (a link-to-link version of example 14.5) Now the admissible itineraries are enumerated by the pruned binary tree of figure 14.5. Identification of nodes $A = C = E$ leads to the finite 2-node, 3-links transition graph

$$T = \begin{pmatrix} 0 & 1 \\ 1 & 1 \end{pmatrix} = \begin{array}{c} \circlearrowleft \\ \text{B} \\ \circlearrowright \\ \text{A=C=E} \end{array} \quad (14.13)$$

As 0 is always followed by 1, the walks on this graph generate only the admissible itineraries. This is the same graph as the 2-node graph (14.9). (continued in example 15.4)

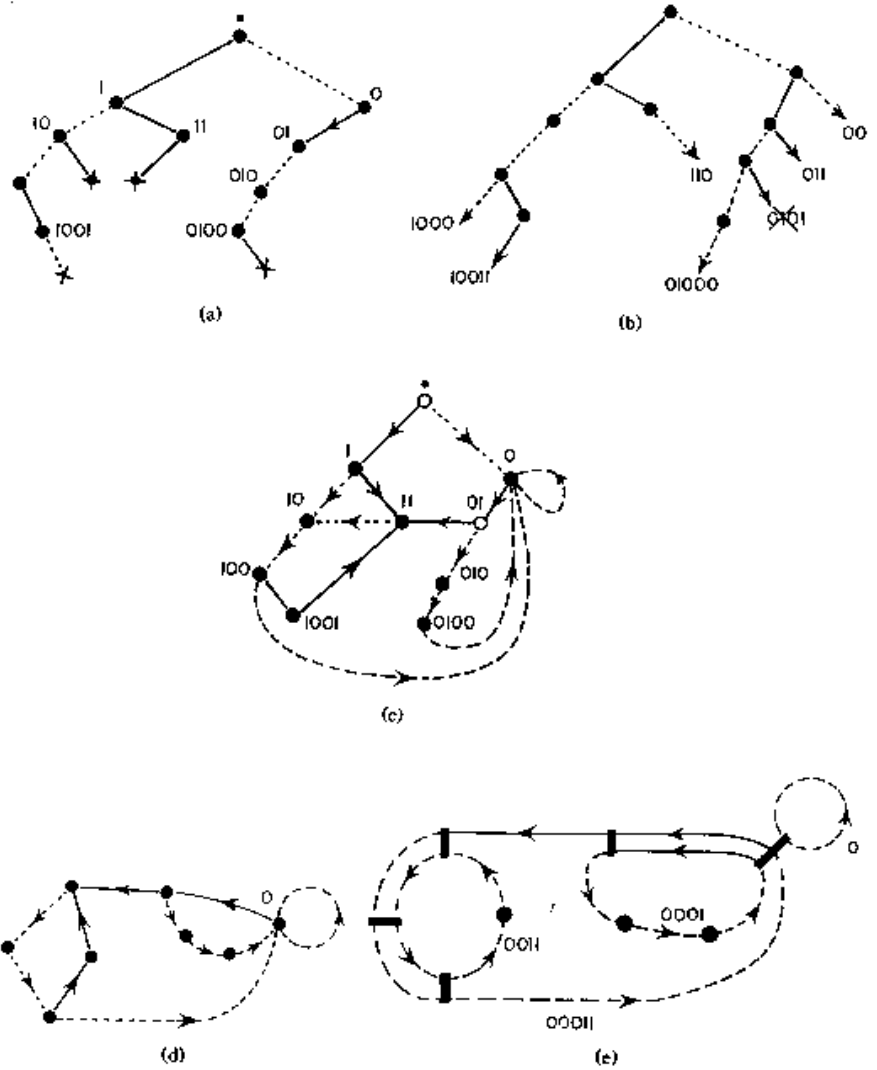


Figure 14.6: Conversion of the pruning front of figure 12.11 (b) into a finite transition graph. (a) Starting with the initial node “·”, delineate all pruning blocks on the binary tree. A solid line stands for “1” and a dashed line for “0”. The ends of forbidden strings are marked with \times . Label all internal nodes by reading the bits connecting “·”, the base of the tree, to the node. (b) Indicate all admissible starting blocks by arrows. (c) Recursively drop the leading bits in the admissible blocks; if the truncated string corresponds to an internal node in (a), connect them. (d) Delete the transient, non-circulating nodes; all admissible sequences are generated as walks on this finite transition graph. (e) Identify all distinct loops and construct the determinant (15.20).

14.3.1 Converting pruning blocks into transition graphs



Suppose now that, by hook or crook, you have been so lucky fishing for pruning rules that you now know the grammar (11.23) in terms of a finite set of pruning blocks $\mathcal{G} = \{b_1, b_2, \dots, b_k\}$, of lengths $\leq m$. Our task is to generate all admissible itineraries. What to do?

We have already seen the main ingredients of a general algorithm: (1) transition graph encodes self-similarities of the tree of all itineraries, and (2) if we have a pruning block of length m , we need to descend m levels before we can start identifying the self-similar sub-trees.

Finite grammar transition graph algorithm.

1. Starting with the root of the tree, delineate all branches that correspond to all pruning blocks; implement the pruning by removing the last node in each

pruning block (marked 'x' in figure 14.6 (a)).

2. Label all nodes internal to pruning blocks by the itinerary connecting the root point to the internal node, figure 14.6 (b). Why? So far we have pruned forbidden branches by looking m_b steps into future for a given pruning block, let's say $b = 10110$. However, the blocks with a right combination of past and future [1.0110], [10.110], [101.10] and [1011.0] are also pruned. In other words, any node whose near past coincides with the beginning of a pruning block is potentially dangerous - a branch further down the tree might get pruned.
3. Add to each internal node all remaining branches allowed by the alphabet, and label them, figure 14.6 (c). Why? Each one of them is the beginning point of an infinite tree, a tree that should be similar to another one originating closer to the root of the whole tree.
4. Pick one of the free external nodes closest to the root of the entire tree, forget the most distant symbol in its past. Does the truncated itinerary correspond to an internal node? If yes, identify the two nodes. If not, forget the next symbol in the past, repeat. If no such truncated past corresponds to any internal node, identify with the root of the tree.

This is a little bit abstract, so let's say the free external node in question is [1010.]. Three time steps back the past is [010.]. That is not dangerous, as no pruning block in this example starts with 0. Now forget the third step in the past: [10.] is dangerous, as that is the start of the pruning block [10.110]. Hence the free external node [1010.] should be identified with the internal node [10.].

5. Repeat until all free nodes have been tied back into the internal nodes.
6. Clean up: check whether every node can be reached from every other node. Remove the transient nodes, i.e., the nodes to which dynamics never returns.
7. The result is a transition graph. There is no guarantee that this is the smartest, most compact transition graph possible for given pruning (if you have a better algorithm, teach us), but walks around it do generate all admissible itineraries, and nothing else.

Example 14.10 Heavy pruning.

We complete this training by examples by implementing the pruning of figure 12.11 (b). The pruning blocks are

$$[100.10], [10.1], [010.01], [011.01], [11.1], [101.10]. \quad (14.14)$$

Blocks 01101, 10110 contain the forbidden block 101, so they are redundant as pruning rules. Draw the pruning tree as a section of a binary tree with 0 and 1 branches and label each internal node by the sequence of 0's and 1's connecting it to the root of the tree (figure 14.6 (a)). These nodes are the potentially dangerous nodes - beginnings of blocks that might end up pruned. Add the side branches to those nodes (figure 14.6 (b)).

As we continue down such branches we have to check whether the pruning imposes constraints on the sequences so generated: we do this by knocking off the leading bits and checking whether the shortened strings coincide with any of the internal pruning tree nodes: $00 \rightarrow 0$; $110 \rightarrow 10$; $011 \rightarrow 11$; $0101 \rightarrow 101$ (pruned); $1000 \rightarrow 00 \rightarrow 00 \rightarrow 0$; $10011 \rightarrow 0011 \rightarrow 011 \rightarrow 11$; $01000 \rightarrow 0$.

The trees originating in identified nodes are identical, so the tree is “self-similar.” Now connect the side branches to the corresponding nodes, figure 14.6 (d). Nodes “.” and 1 are transient nodes; no sequence returns to them, and as you are interested here only in infinitely recurrent sequences, delete them. The result is the finite transition graph of figure 14.6 (d); the admissible bi-infinite symbol sequences are generated as all possible walks on this graph.

Résumé

The set of all admissible itineraries is encoded multiplicatively by transition matrices, diagrammatically by transition graphs. Pruning rules for inadmissible sequences are implemented by constructing corresponding transition matrices and/or transition graphs.

Commentary

Remark 14.1 Transition graphs. We enjoyed studying Lind and Marcus [1] introduction to symbolic dynamics and transition graphs. Finite transition graphs or finite automata are discussed in refs. [2, 3, 4]. They belong to the category of regular languages. Transition graphs for unimodal maps are discussed in refs. [8, 9, 10]. (see also remark 11.1)

Remark 14.2 Inflating transition graphs. In the above examples the symbolic dynamics has been encoded by labeling links in the transition graph. Alternatively one can encode the dynamics by labeling the nodes, as in example 14.6, where the 4 nodes refer to 4 Markov partition regions $\{\mathcal{M}_{00}, \mathcal{M}_{01}, \mathcal{M}_{10}, \mathcal{M}_{11}\}$, and the 8 links to the 8 non-zero entries in the 2-step memory transition matrix (14.10).

Remark 14.3 The unbearable growth of transition graphs. A construction of finite Markov partitions is described in refs. [11, 12], as well as in the innumerable many other references.

If two regions in a Markov partition are not disjoint but share a boundary, the boundary trajectories require special treatment in order to avoid overcounting, see sect. 21.3.1. If the image of a trial partition region cuts across only a part of another trial region and thus violates the Markov partition condition (11.2), a further refinement of the partition is needed to distinguish distinct trajectories.

The finite transition graph construction sketched above is not necessarily the minimal one; for example, the transition graph of figure 14.6 does not generate only the “fundamental” cycles (see chapter 20), but shadowed cycles as well, such as t_{00011} in (15.20). For methods of reduction to a minimal graph, consult refs. [8, 49, 9]. Furthermore, when one implements the time reversed dynamics by the same algorithm, one usually gets a graph of a very different topology even though both graphs generate the same admissible sequences, and have the same determinant. The algorithm described here makes some sense for 1 – *dimensional* dynamics, but is unnatural for 2 – *dimensional* maps whose dynamics it treats as 1-dimensional. In practice, generic pruning grows longer and longer, and more plentiful pruning rules. For generic flows the refinements might never stop, and almost always we might have to deal with infinite Markov partitions, such as those that will be discussed in sect. 15.5. Not only do the transition graphs get more and more unwieldy, they have the unpleasant property that every time we add a new rule, the graph has to be constructed from scratch, and it might look very different from the previous one, even though it leads to a minute modification of the topological entropy. The most determined effort to construct such graphs may be the one of ref. [14]. Still, this seems to be the best technology available, unless the reader alerts us to something superior.

Exercises

- 14.1. **Time reversibility.**** Hamiltonian flows are time reversible. Does that mean that their transition graphs are symmetric in all node \rightarrow node links, their transition matrices are adjacency matrices, symmetric and diagonalizable, and that they have only real eigenvalues?
- 14.2. **Alphabet $\{0,1\}$, prune $_1000_$, $_00100_$, $_01100_$.** This example is motivated by the pruning front description of the symbolic dynamics for the Hénon-type map-remark 12.3.
- step 1.** $_1000_$ prunes all cycles with a $_000_$ subsequence with the exception of the fixed point $\bar{0}$; hence we factor out $(1 - t_0)$ explicitly, and prune $_000_$ from the rest. This means that x_0 is an isolated fixed point - no cycle stays in its vicinity for more than 2 iterations. In the notation of sect. 14.3.1, the alphabet is $\{1, 2, 3; \bar{0}\}$,

and the remaining pruning rules have to be rewritten in terms of symbols $2=10, 3=100$:

step 2. alphabet $\{1, 2, 3; \bar{0}\}$, prune $_33_$, $_213_$, $_313_$. This means that the 3-cycle $\bar{3} = \overline{100}$ is pruned and no long cycles stay close enough to it for a single $_100_$ repeat. As in example 1?!, prohibition of $_33_$ is implemented by dropping the symbol “3” and extending the alphabet by the allowed blocks $13, 23$:

step 3. alphabet $\{1, 2, \underline{13}, \underline{23}; \bar{0}\}$, prune $_213_$, $_2313_$, $_1313_$, where $\underline{13} = 13, \underline{23} = 23$ are now used as single letters. Pruning of the repetitions $_1313_$ (the 4-cycle $\overline{13} = \overline{1100}$ is pruned) yields the

result: alphabet $\{1, 2, \underline{23}, \underline{113}; \bar{0}\}$, unrestricted 4-ary dynamics. The other remaining possible blocks $_213_$, $_2313_$ are forbidden by the rules of step 3.

References

- [14.1] D.A. Lind and B. Marcus, *An introduction to symbolic dynamics and coding* (Cambridge Univ. Press, Cambridge 1995).
- [14.2] A. Salomaa, *Formal languages* (Academic Press, San Diego 1973).
- [14.3] J.E. Hopcroft and J.D. Ullman, *Introduction to automata theory, languages, and computation* (Addison-Wesley, Reading MA 1979).
- [14.4] D.M. Cvetković, M. Doob and H. Sachs, *Spectra of graphs* (Academic Press, New York 1980).
- [14.5] C.J. Puccia and R. Levins, *Qualitative modeling of complex systems: An introduction to loop analysis and time averaging* (Harvard Univ. Press, Cambridge MA 1986).
- [14.6] E.D. Sontag, *Mathematical control theory: Deterministic finite dimensional systems* (Springer, New York 1998).
- [14.7] J. Bang-Jensen and G. Gutin, *Digraphs: Theory, algorithms and applications* (Springer, London 2002).
- [14.8] P. Grassberger, “On the symbolic dynamics of the one-humped map of the interval” *Z. Naturforsch. A* **43**, 671 (1988).
- [14.9] P. Grassberger, R. Badii and A. Politi, “Scaling laws for invariant measures on hyperbolic and nonhyperbolic attractors,” *J. Stat. Phys.* **51**, 135 (1988).

- [14.10] S. Isola and A. Politi, "Universal encoding for unimodal maps," *J. Stat. Phys.* **61**, 259 (1990).
- [14.11] A. Boyarski and M. Skarowsky, *Trans. Am. Math. Soc.* **225**, 243 (1979); A. Boyarski, *J. Stat. Phys.* **50**, 213 (1988).
- [14.12] C.S. Hsu, M.C. Kim, *Phys. Rev. A* **31**, 3253 (1985); N. Balmforth, E.A. Spiegel, C. Tresser, *Phys. Rev. Lett.* **72**, 80 (1994).

Chapter 15

Counting

I'm gonna close my eyes
And count to ten
I'm gonna close my eyes
And when I open them again
Everything will make sense to me then

—Tina Dico, 'Count To Ten'

WE ARE NOW in a position to apply the periodic orbit theory to the first and the easiest problem in theory of chaotic systems: cycle counting. This is the simplest illustration of the *raison d'être* of periodic orbit theory; we derive a duality transformation that relates *local* information - in this case the next admissible symbol in a symbol sequence - to *global* averages, in this case the mean rate of growth of the number of cycles with increasing cycle period. In chapter 14 we have transformed, by means of the transition matrices / graphs, the topological dynamics of chapter 11 into a multiplicative operation. Here we show that the n th power of a transition matrix counts all itineraries of length n . The asymptotic growth rate of the number of admissible itineraries is therefore given by the leading eigenvalue of the transition matrix; the leading eigenvalue is in turn given by the leading zero of the characteristic determinant of the transition matrix, which is - in this context - called the *topological zeta function*.

For flows with finite transition graphs this determinant is a finite *topological polynomial* which can be read off the graph. However, (a) even something as humble as the quadratic map generically requires an infinite partition (sect. 15.5), but (b) the finite partition approximants converge exponentially fast.

The method goes well beyond the problem at hand, and forms the core of the entire treatise, making tangible the abstract notion of “spectral determinants” yet to come.

15.1 How many ways to get there from here?

In the 3-disk system of example 11.1 the number of admissible trajectories doubles with every iterate: there are $K_n = 3 \cdot 2^n$ distinct itineraries of length n . If disks are too close and a subset of trajectories is pruned, this is only an upper bound and explicit formulas might be hard to discover, but we still might be able to establish a lower exponential bound of the form $K_n \geq Ce^{n\hat{h}}$. Bounded exponentially by $3e^{n \ln 2} \geq K_n \geq Ce^{n\hat{h}}$, the number of trajectories must grow exponentially as a function of the itinerary length, with rate given by the *topological entropy*:

$$h = \lim_{n \rightarrow \infty} \frac{1}{n} \ln K_n . \tag{15.1}$$

We shall now relate this quantity to the spectrum of the transition matrix, with the growth rate of the number of topologically distinct trajectories given by the leading eigenvalue of the transition matrix.

The transition matrix element $T_{ij} \in \{0, 1\}$ in (14.1) indicates whether the transition from the starting partition j into partition i in one step is allowed or not, and the (i, j) element of the transition matrix iterated n times

exercise 15.1

$$(T^n)_{ij} = \sum_{k_1, k_2, \dots, k_{n-1}} T_{ik_1} T_{k_1 k_2} \dots T_{k_{n-1} j} \tag{15.2}$$

receives a contribution 1 from every admissible sequence of transitions, so $(T^n)_{ij}$ is the number of admissible n symbol itineraries starting with j and ending with i .

Example 15.1 3-disk itinerary counting. The $(T^2)_{13} = T_{12}T_{23} = 1$ element of T^2 for the 3-disk transition matrix (14.8)

$$\begin{pmatrix} 0 & 1 & 1 \\ 1 & 0 & 1 \\ 1 & 1 & 0 \end{pmatrix}^2 = \begin{pmatrix} 2 & 1 & 1 \\ 1 & 2 & 1 \\ 1 & 1 & 2 \end{pmatrix} . \tag{15.3}$$

corresponds to path $3 \rightarrow 2 \rightarrow 1$, the only 2-step path from 3 to 1, while $(T^2)_{33} = T_{31}T_{13} + T_{32}T_{23} = 2$ counts the two returning, periodic paths $\overline{31}$ and $\overline{32}$. Note that the trace $\text{tr } T^2 = (T^2)_{11} + (T^2)_{22} + (T^2)_{33} = 2T_{13}T_{31} + 2T_{21}T_{12} + 2T_{32}T_{23}$ has a contribution from each 2-cycle $\overline{12}$, $\overline{13}$, $\overline{23}$ twice, one contribution from each periodic point.

The total number of admissible itineraries of n symbols is

$$K_n = \sum_{ij} (T^n)_{ij} = (1, 1, \dots, 1) T^n \begin{pmatrix} 1 \\ 1 \\ \vdots \\ 1 \end{pmatrix} . \tag{15.4}$$

We can also count the number of prime cycles and pruned periodic points, but in order not to break up the flow of the argument, we relegate these pretty results to sect. 15.7. Recommended reading if you ever have to compute lots of cycles.

A finite $[N \times N]$ matrix T has eigenvalues $\{\lambda_0, \lambda_1, \dots, \lambda_{m-1}\}$ and (right) eigenvectors $\{\varphi_0, \varphi_1, \dots, \varphi_{m-1}\}$ satisfying $T\varphi_\alpha = \lambda_\alpha\varphi_\alpha$. Expressing the initial vector in (15.4) in this basis (which might be incomplete, with $m \leq N$ eigenvectors),

$$T^n \begin{pmatrix} 1 \\ 1 \\ \vdots \\ 1 \end{pmatrix} = T^n \sum_{\alpha=0}^{m-1} b_\alpha \varphi_\alpha = \sum_{\alpha=0}^{m-1} b_\alpha \lambda_\alpha^n \varphi_\alpha,$$

and contracting with $(1, 1, \dots, 1)$, we obtain

$$K_n = \sum_{\alpha=0}^{m-1} c_\alpha \lambda_\alpha^n.$$

exercise 15.3

The constants c_α depend on the choice of initial and final partitions: In this example we are sandwiching T^n between the vector $(1, 1, \dots, 1)$ and its transpose, but any other pair of vectors would do, as long as they are not orthogonal to the leading eigenvector φ_0 . In an experiment the vector $(1, 1, \dots, 1)$ would be replaced by a description of the initial state, and the right vector would describe the measurement time n later.

Perron theorem states that a Perron-Frobenius matrix has a nondegenerate (isolated) positive real eigenvalue $\lambda_0 > 1$ (with a positive eigenvector) which exceeds the moduli of all other eigenvalues. Therefore as n increases, the sum is dominated by the leading eigenvalue of the transition matrix, $\lambda_0 > |\text{Re } \lambda_\alpha|$, $\alpha = 1, 2, \dots, m - 1$, and the topological entropy (15.1) is given by

$$\begin{aligned} h &= \lim_{n \rightarrow \infty} \frac{1}{n} \ln c_0 \lambda_0^n \left[1 + \frac{c_1}{c_0} \left(\frac{\lambda_1}{\lambda_0} \right)^n + \dots \right] \\ &= \ln \lambda_0 + \lim_{n \rightarrow \infty} \left[\frac{\ln c_0}{n} + \frac{1}{n} \frac{c_1}{c_0} \left(\frac{\lambda_1}{\lambda_0} \right)^n + \dots \right] \\ &= \ln \lambda_0. \end{aligned} \tag{15.5}$$

What have we learned? The transition matrix T is a one-step, *short time* operator, advancing the trajectory from one partition to the next admissible partition. Its eigenvalues describe the rate of growth of the total number of trajectories at the *asymptotic times*. Instead of painstakingly counting K_1, K_2, K_3, \dots and estimating (15.1) from a slope of a log-linear plot, we have the *exact* topological entropy if we can compute the leading eigenvalue of the transition matrix T . This is reminiscent of the way free energy is computed from transfer matrices for 1-dimensional lattice models with finite range interactions. Historically, it is this analogy with statistical mechanics that led to introduction of evolution operator methods into the theory of chaotic systems.

15.2 Topological trace formula

There are two standard ways of computing eigenvalues of a matrix - by evaluating the trace $\text{tr } T^n = \sum \lambda_\alpha^n$, or by evaluating the determinant $\det(1 - zT)$. We start by evaluating the trace of transition matrices. The main lesson will be that the trace receives contributions only from itineraries that return to the initial partition, i.e., periodic orbits.

Consider an M -step memory transition matrix, like the 1-step memory example (14.10). The trace of the transition matrix counts the number of partitions that map into themselves. More generally, each closed walk through n concatenated entries of T contributes to $\text{tr } T^n$ the product (15.2) of the matrix entries along the walk. Each step in such a walk shifts the symbolic string by one symbol; the trace ensures that the walk closes on a periodic string c . Define t_c to be the *local trace*, the product of matrix elements along a cycle c , each term being multiplied by a book keeping variable z . In chapters that follow, the ‘local trace’ t_c will take a continuum of values, so for the remainder of this chapter we stick to the ‘ t_c ’ notation rather than to the 0 or z^n values specific to the counting problem.

The quantity $z^n \text{tr } T^n$ is then the sum of t_c for all cycles of period n . The t_c = (product of matrix elements along cycle c is manifestly cyclically invariant, $t_{100} = t_{010} = t_{001}$, so a prime cycle p of period n_p contributes n_p times, once for each periodic point along its orbit. For the purposes of periodic orbit counting, the local trace takes values

$$t_p = \begin{cases} z^{n_p} & \text{if } p \text{ is an admissible cycle} \\ 0 & \text{otherwise,} \end{cases} \tag{15.6}$$

i.e., (setting $z = 1$) the local trace is $t_p = 1$ if the cycle is admissible, and $t_p = 0$ otherwise.

Example 15.2 Traces for binary symbolic dynamics. For example, for the $[8 \times 8]$ transition matrix $T_{s_1 s_2 s_3, s_0 s_1 s_2}$ version of (14.10), or any refined partition $[2^n \times 2^n]$ transition matrix, n arbitrarily large, the periodic point $\overline{100}$ contributes $t_{100} = z^3 T_{100,010} T_{010,001} T_{001,100}$ to $z^3 \text{tr } T^3$. This product is manifestly cyclically invariant, $t_{100} = t_{010} = t_{001}$, so a prime cycle $p = \overline{100}$ of period 3 contributes 3 times, once for each periodic point along its orbit.

exercise 11.7

For the binary labeled non-wandering set the first few traces are given by (consult tables 15.1 and 15.2)

$$\begin{aligned} z \text{tr } T &= t_0 + t_1, \\ z^2 \text{tr } T^2 &= t_0^2 + t_1^2 + 2t_{10}, \\ z^3 \text{tr } T^3 &= t_0^3 + t_1^3 + 3t_{100} + 3t_{101}, \\ z^4 \text{tr } T^4 &= t_0^4 + t_1^4 + 2t_{10}^2 + 4t_{1000} + 4t_{1001} + 4t_{1011}. \end{aligned} \tag{15.7}$$

In the binary case the trace picks up only two contributions on the diagonal, $T_{0 \dots 0, 0 \dots 0} + T_{1 \dots 1, 1 \dots 1}$, no matter how much memory we assume. We can even take infinite memory

Table 15.1: Prime cycles for the binary symbolic dynamics up to length 9. The numbers of prime cycles are given in table 15.3.

n_p	p	n_p	p	n_p	p	n_p	p	n_p	p
1	0	7	0001001	8	00001111	9	000001101	9	001001111
	1		0000111		00010111		000010011		001010111
2	01		0001011		00011011		000010101		001011011
3	001		0001101		00011101		000011001		001011101
	011		0010011		00100111		000100011		001100111
4	0001		0010101		00101011		000100101		001101011
	0011		0001111		00101101		000101001		001101101
	0111		0010111		00110101		000001111		001110101
5	00001		0011011		00011111		000010111		010101011
	00011		0011101		00101111		000011011		000111111
	00101		0101011		00110111		000011101		001011111
	00111		0011111		00111011		000100111		001101111
	01011		0101111		00111101		000101011		001110111
	01111		0110111		01010111		000101101		001111011
6	000001		0111111		01011011		000110011		001111101
	000011	8	00000001		00111111		000110101		010101111
	000101		00000011		01011111		000111001		010110111
	000111		00000101		01101111		001001011		010111011
	001011		00001001		01111111		001001101		001111111
	001101		00000111	9	000000001		001010011		010111111
	001111		00001011		000000011		001010101		011011111
	010111		00001101		000000101		000011111		011101111
	011111		00010011		000001001		000101111		011111111
7	0000001		00010101		000010001		000110111		
	0000011		00011001		000000111		000111011		
	0000101		00100101		000001011		000111101		

Table 15.2: The total numbers N_n of periodic points of period n for binary symbolic dynamics. The numbers of contributing prime cycles illustrates the preponderance of long prime cycles of period n over the repeats of shorter cycles of periods n_p , where $n = rn_p$. Further enumerations of binary prime cycles are given in tables 15.1 and 15.3. (L. Rondoni)

n	N_n	# of prime cycles of period n_p									
		1	2	3	4	5	6	7	8	9	10
1	2	2									
2	4	2	1								
3	8	2		2							
4	16	2	1		3						
5	32	2				6					
6	64	2	1	2			9				
7	128	2						18			
8	256	2	1		3				30		
9	512	2		2						56	
10	1024	2	1			6					99

$M \rightarrow \infty$, in which case the contributing partitions are shrunk to the fixed points, $\text{tr } T = T_{\bar{0},\bar{0}} + T_{\bar{1},\bar{1}}$.

If there are no restrictions on symbols, the symbolic dynamics is complete, and all binary sequences are admissible (or allowable) itineraries. As this type of symbolic dynamics pops up frequently, we list the shortest binary prime cycles in table 15.1. exercise 11.2

Hence $\text{tr } T^n = N_n$ counts the number of *admissible periodic points* of period n . The n th order trace (15.7) picks up contributions from all repeats of prime cycles, with each cycle contributing n_p periodic points, so N_n , the total number of periodic points of period n is given by

$$z^n N_n = z^n \text{tr } T^n = \sum_{n_p | n} n_p t_p^{n/n_p} = \sum_p n_p \sum_{r=1}^{\infty} \delta_{n, n_p r} t_p^r. \tag{15.8}$$

Here $m|n$ means that m is a divisor of n . An example is the periodic orbit counting in table 15.2.

In order to get rid of the awkward divisibility constraint $n = n_p r$ in the above sum, we introduce the generating function for numbers of periodic points

$$\sum_{n=1}^{\infty} z^n N_n = \text{tr} \frac{zT}{1 - zT}. \tag{15.9}$$

The right hand side is the geometric series sum of $N_n = \text{tr } T^n$. Substituting (15.8) into the left hand side, and replacing the right hand side by the eigenvalue sum $\text{tr } T^n = \sum \lambda_\alpha^n$, we obtain our first example of a trace formula, the *topological trace formula*

$$\sum_{\alpha=0} \frac{z \lambda_\alpha}{1 - z \lambda_\alpha} = \sum_p \frac{n_p t_p}{1 - t_p}. \tag{15.10}$$

A trace formula relates the spectrum of eigenvalues of an operator - here the transition matrix - to the spectrum of periodic orbits of a dynamical system. It is a statement of duality between the short-time, local information - in this case the next admissible symbol in a symbol sequence - to long-time, global averages, in this case the mean rate of growth of the number of cycles with increasing cycle period.

The z^n sum in (15.9) is a discrete version of the Laplace transform (see sect. 18.1.2), and the resolvent on the left hand side is the antecedent of the more sophisticated trace formulas (18.10) and (18.23). We shall now use this result to compute the spectral determinant of the transition matrix.

15.3 Determinant of a graph

Our next task is to determine the zeros of the *spectral determinant* of an $[m \times m]$ transition matrix

$$\det(1 - zT) = \prod_{\alpha=0}^{m-1} (1 - z\lambda_\alpha). \tag{15.11}$$

We could now proceed to diagonalize T on a computer, and get this over with. It pays, however, to dissect $\det(1 - zT)$ with some care; understanding this computation in detail will be the key to understanding the cycle expansion computations of chapter 20 for arbitrary dynamical averages. For T a finite matrix, (15.11) is just the characteristic polynomial for T . However, we shall be able to compute this object even when the dimension of T and other such operators becomes infinite, and for that reason we prefer to refer to (15.11) loosely as the “spectral determinant.”

There are various definitions of the determinant of a matrix; we will view the determinant as a sum over all possible permutation cycles composed of the traces $\text{tr } T^k$, in the spirit of the determinant–trace relation (1.16):

exercise 4.1

$$\begin{aligned} \det(1 - zT) &= \exp(\text{tr } \ln(1 - zT)) = \exp\left(-\sum_{n=1}^{\infty} \frac{z^n}{n} \text{tr } T^n\right) \\ &= 1 - z \text{tr } T - \frac{z^2}{2} ((\text{tr } T)^2 - \text{tr } T^2) - \dots \end{aligned} \tag{15.12}$$

This is sometimes called a *cumulant* expansion. Formally, the right hand is a Taylor series in z about $z = 0$. If T is an $[m \times m]$ finite matrix, then the characteristic polynomial is at most of order m . In that case the coefficients of z^n must vanish *exactly* for $n > m$.

We now proceed to relate the determinant in (15.12) to the corresponding transition graph of chapter 14: toward this end, we start with the usual textbook expression for a determinant as the sum of products of all permutations

$$\det M = \sum_{\{\pi\}} (-1)^\pi M_{1,\pi_1} M_{2,\pi_2} \cdots M_{m,\pi_m} \tag{15.13}$$

where $M = 1 - zT$ is a $[m \times m]$ matrix, $\{\pi\}$ denotes the set of permutations of m symbols, π_k is the permutation π applied to k , and $(-1)^\pi = \pm 1$ is the parity of permutation π . The right hand side of (15.13) yields a polynomial in T of order m in z : a contribution of order n in z picks up $m - n$ unit factors along the diagonal, the remaining matrix elements yielding

$$(-z)^n (-1)^\pi T_{s_1 \pi s_1} \cdots T_{s_n \pi s_n} \tag{15.14}$$

where π is the permutation of the subset of n distinct symbols $s_1 \cdots s_n$ indexing T matrix elements. As in (15.7), we refer to any combination $t_c = T_{s_1 s_k} T_{s_3 s_2} \cdots T_{s_2 s_1}$, for a given itinerary $c = s_1 s_2 \cdots s_k$, as the *local trace* associated with a closed loop c on the transition graph. Each term of the form (15.14) may be factored in terms of local traces $t_{c_1} t_{c_2} \cdots t_{c_k}$, that is loops on the transition graph. These loops are non-intersecting, as each node may only be reached by *one* link, and they are indeed loops, as if a node is reached by a link, it has to be the starting point of another *single* link, as each s_j must appear exactly *once* as a row and column index.

So the general structure is clear, a little more thinking is only required to get the sign of a generic contribution. We consider only the case of loops of length 1 and 2, and leave to the reader the task of generalizing the result by induction. Consider first a term in which only loops of unit length appear in (15.14), i.e., only the diagonal elements of T are picked up. We have $k = m$ loops and an even permutation π so the sign is given by $(-1)^k$, where k is the number of loops. Now take the case in which we have i single loops and j loops of length $n = 2j + i$. The parity of the permutation gives $(-1)^j$ and the first factor in (15.14) gives $(-1)^n = (-1)^{2j+i}$. So once again these terms combine to $(-1)^k$, where $k = i + j$ is the number of loops. Let f be the maximal number of non-intersecting loops. We may summarize our findings as follows:

exercise 15.4

The characteristic polynomial of a transition matrix is given by the sum of all possible partitions π of the corresponding transition graph into products of k non-intersecting loops, with each loop trace t_p carrying a minus sign:

$$\det(1 - zT) = \sum_{k=0}^f \sum_{\pi} (-1)^k t_{p_1} \cdots t_{p_k} \tag{15.15}$$

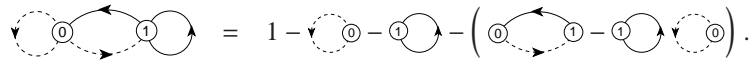
Any self-intersecting loop is *shadowed* by a product of two loops that share the intersection point. As both the long loop t_{ab} and its shadow $t_a t_b$ in the case at hand carry the same weight $z^{n_a+n_b}$, the cancelation is exact, and the loop expansion (15.15) is finite. In the case that the local traces count prime cycles (15.6), $t_p = 0$ or z^n , we refer to $\det(1 - zT)$ as the *topological polynomial*.

We refer to the set of all non-self-intersecting loops $\{t_{p_1}, t_{p_2}, \cdots t_{p_f}\}$ as the *fundamental cycles* (for an explicit example, see the loop expansion of example 15.6). This is not a very good definition, as transition graphs are not unique –the most we know is that for a given finite-grammar language, there exist transition graph(s) with the minimal number of loops. Regardless of how cleverly a transition graph is constructed, it is always true that for any finite transition graph the number of fundamental cycles f is finite. If the graph has m nodes, no fundamental cycle is of period longer than m , as any longer cycle is of necessity self-intersecting.

The above loop expansion of a determinant in terms of traces is most easily grasped by working through a few examples. The complete binary dynamics transition graph of figure 14.4 is a little bit too simple, but let us start humbly and consider it anyway.

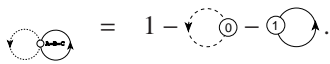
Example 15.3 Topological polynomial for complete binary dynamics: (continuation of example 14.2) There are only two non-intersecting loops, yielding

$$\det(1 - zT) = 1 - t_0 - t_1 - (t_{01} - t_0t_1) = 1 - 2z \tag{15.16}$$



Due to the symmetry under $0 \leftrightarrow 1$ interchange, this is a redundant graph (the 2-cycle t_{01} is exactly shadowed by the 1-cycles). Another way to see is that itineraries are labeled by the $\{0, 1\}$ links, node labels can be omitted. As both nodes have 2 in-links and 2 out-links, they can be identified, and a more economical presentation is in terms of the $[1 \times 1]$ adjacency matrix (14.12)

$$\det(1 - zA) = 1 - t_0 - t_1 = 1 - 2z \tag{15.17}$$



The leading (and only) zero of this characteristic polynomial yields the topological entropy $e^h = 2$. As there are $K_n = 2^n$ binary strings of length N , this comes as no surprise.

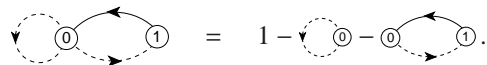
Similarly, for the complete symbolic dynamics of N symbols the transition graph has one node and N links, yielding

$$\det(1 - zT) = 1 - Nz, \tag{15.18}$$

which gives the topological entropy $h = \ln N$.

Example 15.4 Golden mean pruning: The “golden mean” pruning of example 14.5 has one grammar rule: the substring $_{11}$ is forbidden. The corresponding transition graph non-intersecting loops are of length 1 and 2, so the topological polynomial is given by exercise 15.5

$$\det(1 - zT) = 1 - t_0 - t_{01} = 1 - z - z^2 \tag{15.19}$$



The leading root of this polynomial is the golden mean, so the entropy (15.5) is the logarithm of the golden mean, $h = \ln \frac{1+\sqrt{5}}{2}$.



fast track:
sect. 15.4, p. 293

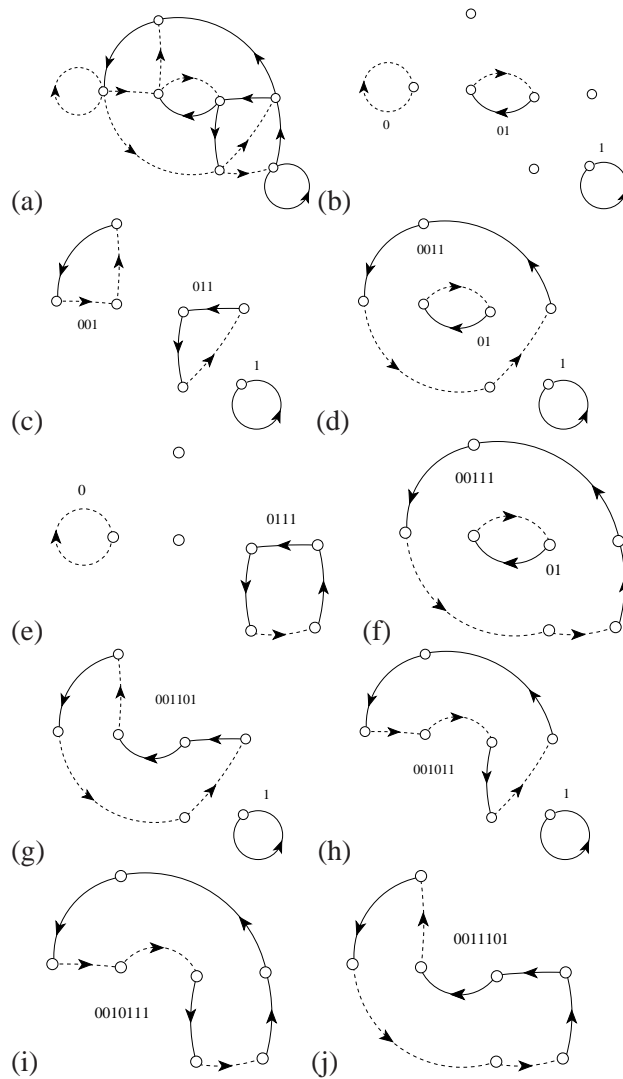


Figure 15.1: (a) The region labels in the nodes of transition graph figure 14.3 can be omitted, as the links alone keep track of the symbolic dynamics. (b)-(j) The fundamental cycles (15.23) for the transition graph (a), i.e., the set of its non-self-intersecting loops. Each loop represents a local trace t_p , as in (14.5).

Example 15.5 Nontrivial pruning: The non-self-intersecting loops of the transition graph of figure 14.6 (d) are indicated in figure 14.6 (e). The determinant can be written down by inspection, as the sum of all possible partitions of the graph into products of non-intersecting loops, with each loop carrying a minus sign:

$$\det(1 - zT) = 1 - t_0 - t_{0011} - t_{0001} - t_{00011} + t_0 t_{0011} + t_{0011} t_{0001} . \tag{15.20}$$

With $t_p = z^{n_p}$, where n_p is the period of the p -cycle, the smallest root of

$$0 = 1 - z - 2z^4 + z^8 \tag{15.21}$$

yields the topological entropy $h = -\ln z$, $z = 0.658779 \dots$, $h = 0.417367 \dots$, significantly smaller than the entropy of the covering symbolic dynamics, the complete binary shift with topological entropy $h = \ln 2 = 0.693 \dots$

exercise 15.9

Example 15.6 Loop expansion of a transition graph. (continued from example 14.7) Consider a state space covered by 7 neighborhoods (14.11), with the topological time evolution given by the transition graph of figure 14.3.

The determinant $\det(1 - zT)$ of the transition graph in figure 14.3 can be read off the graph, and expanded as a polynomial in z , with coefficients given by products of non-intersecting loops (traces of powers of T) of the transition graph figure 15.1:

$$\begin{aligned} \det(1 - zT) &= 1 - (t_0 + t_1)z - (t_{01} - t_0t_1)z^2 - (t_{001} + t_{011} - t_{01}t_0 - t_{01}t_1)z^3 \\ &\quad - (t_{0011} + t_{0111} - t_{001}t_1 - t_{011}t_0 - t_{011}t_1 + t_{01}t_0t_1)z^4 \\ &\quad - (t_{00111} - t_{0111}t_0 - t_{0011}t_1 + t_{011}t_0t_1)z^5 \\ &\quad - (t_{001011} + t_{001101} - t_{0011}t_{01} - t_{001}t_{011})z^6 \\ &\quad - (t_{0010111} + t_{0011101} - t_{001011}t_1 - t_{001101}t_1 - t_{00111}t_{01} + t_{0011}t_{01}t_1 + t_{001}t_{011}t_1)z^7. \end{aligned} \tag{15.22}$$

Twelve cycles up to period 7 are fundamental cycles:

$$\overline{0}, \overline{1}, \overline{01}, \overline{001}, \overline{011}, \overline{0011}, \overline{0111}, \overline{00111}, \overline{001011}, \overline{001101}, \overline{0010111}, \overline{0011101}, \tag{15.23}$$

out of the total of 41 prime cycles (listed in table 15.1) up to cycle period 7. The topological polynomial $t_p \rightarrow z^{n_p}$

$$1/\zeta_{top}(z) = 1 - 2z + z^7$$

is interesting; the shadowing fails first at the cycle length $n = 7$, so the topological entropy is only a bit smaller than the binary $h = \ln 2$. Not exactly obvious from the partition (14.11).

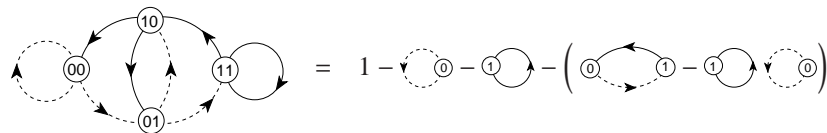
15.4 Topological zeta function

What happens if there is no finite-memory transition matrix, if the transition graph is infinite? If we are never sure that looking further into the future will reveal no further forbidden blocks? There is still a way to define the determinant, and this idea is central to the whole treatise: the determinant is then defined by its *cumulant* expansion (15.12)

exercise 4.1

$$\det(1 - zT) = 1 - \sum_{n=1}^{\infty} \hat{c}_n z^n. \tag{15.24}$$

Example 15.7 Complete binary $\det(1 - zT)$ expansion. (continuation of example 14.6) consider the loop expansion of the binary 1-step memory transition graph (14.10)



$$\begin{aligned} &= 1 - \text{loop}(0) - \text{loop}(1) - (\text{loop}(0,1) - \text{loop}(1,0)) \\ &= 1 - t_0 - t_1 - [(t_{01} - t_1t_0)] - [(t_{001} - t_{01}t_0) + (t_{011} - t_{01}t_1)] \\ &\quad - [(t_{0001} - t_0t_{001}) + (t_{0111} - t_{011}t_1) \\ &\quad \quad + (t_{0011} - t_{001}t_1 - t_0t_{011} + t_0t_{01}t_1)] \\ &= 1 - \sum_f t_f - \sum_n \hat{c}_n = 1 - 2z. \end{aligned} \tag{15.25}$$

For finite dimensional matrices the expansion is a finite polynomial, and (15.24) is an identity; however, for infinite dimensional operators the cumulant expansion coefficients \hat{c}_n define the determinant.

Let us now evaluate the determinant in terms of traces for an arbitrary transition matrix. In order to obtain an expression for the spectral determinant (15.11) in terms of cycles, substitute (15.8) into (15.24) and sum over the repeats of prime cycles using $\ln(1 - x) = -\sum_r x^r/r$,

$$\begin{aligned} \det(1 - zT) &= \exp\left(-\sum_p \sum_{r=1}^{\infty} \frac{t_p^r}{r}\right) = \exp\left(\sum_p \ln(1 - t_p)\right) \\ &= \prod_p (1 - t_p), \end{aligned} \tag{15.26}$$

where for the topological entropy the weight assigned to a prime cycle p of period n_p is $t_p = z^{n_p}$ if the cycle is admissible, or $t_p = 0$ if it is pruned. This determinant is called the *topological* or the *Artin-Mazur* zeta function, conventionally denoted by

$$1/\zeta_{\text{top}}(z) = \prod_p (1 - z^{n_p}) = 1 - \sum_{n=1} \hat{c}_n z^n. \tag{15.27}$$

Counting cycles amounts to giving each admissible prime cycle p weight $t_p = z^{n_p}$ and expanding the Euler product (15.27) as a power series in z . As the precise expression for the coefficients \hat{c}_n in terms of local traces t_p is more general than the current application to counting, we shall postpone its derivation to chapter 20.

The topological entropy h can now be determined from the leading zero $z = e^{-h}$ of the topological zeta function. For a finite $[m \times m]$ transition matrix, the number of terms in the characteristic equation (15.15) is finite, and we refer to this expansion as the *topological polynomial* of order $\leq m$. The utility of defining the determinant by its cumulant expansion is that it works even when the partition is infinite, $m \rightarrow \infty$; an example is given in sect. 15.5, and many more later on.



fast track:
sect. 15.5, p. 295

15.4.1 Topological zeta function for flows



We now apply the method that we shall use in deriving (18.23) to the problem of deriving the topological zeta functions for flows. The time-weighted density of prime cycles of period t is

$$\Gamma(t) = \sum_p \sum_{r=1} T_p \delta(t - rT_p). \tag{15.28}$$

The Laplace transform smooths the sum over Dirac delta spikes (see (18.22)) and yields the *topological trace formula*

$$\sum_p \sum_{r=1}^{\infty} T_p \int_{0_+}^{\infty} dt e^{-st} \delta(t - rT_p) = \sum_p T_p \sum_{r=1}^{\infty} e^{-sT_p r} \tag{15.29}$$

and the *topological zeta function* for flows:

$$1/\zeta_{\text{top}}(s) = \prod_p (1 - e^{-sT_p}), \tag{15.30}$$

related to the trace formula by

$$\sum_p T_p \sum_{r=1}^{\infty} e^{-sT_p r} = -\frac{\partial}{\partial s} \ln 1/\zeta_{\text{top}}(s).$$

This is the continuous time version of the discrete time topological zeta function (15.27) for maps; its leading zero $s = -h$ yields the topological entropy for a flow.

15.5 Topological zeta function for an infinite partition

(K.T. Hansen and P. Cvitanović)



To understand the need for topological zeta function (15.24), we turn a dynamical system with (as far as we know - there is no proof) an infinite partition, or an infinity of ever-longer pruning rules. Consider the 1 – *dimensional* quadratic map (11.3)

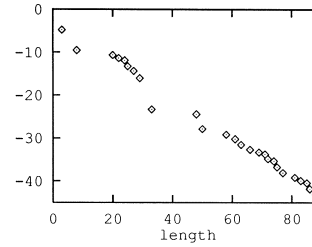
$$f(x) = Ax(1 - x), \quad A = 3.8.$$

Numerically the kneading sequence (the itinerary of the critical point $x = 1/2$ (11.13)) is

$$K = 1011011110110111101011110111110\dots$$

where the symbolic dynamics is defined by the partition of figure 11.12. How this kneading sequence is converted into a series of pruning rules is a dark art. For the moment it suffices to state the result, to give you a feeling for what a “typical” infinite partition topological zeta function looks like. For example, approximating the dynamics by a transition graph corresponding to a repeller of the period 29

Figure 15.2: The logarithm $\ln |z_0^{(n)} - z_0|$ of the difference between the leading zero of the n -th polynomial approximation to topological zeta function and our best estimate (15.33), as a function of order of the polynomial n (the topological zeta function evaluated for the closest value of A to $A = 3.8$ for which the quadratic map has a stable cycle of period n). (from K.T. Hansen [20])



attractive cycle close to the $A = 3.8$ strange attractor yields a transition graph with 29 nodes and the characteristic polynomial

$$\begin{aligned}
 1/\zeta_{\text{top}}^{(29)} = & 1 - z^1 - z^2 + z^3 - z^4 - z^5 + z^6 - z^7 + z^8 - z^9 - z^{10} \\
 & + z^{11} - z^{12} - z^{13} + z^{14} - z^{15} + z^{16} - z^{17} - z^{18} + z^{19} + z^{20} \\
 & - z^{21} + z^{22} - z^{23} + z^{24} + z^{25} - z^{26} + z^{27} - z^{28}. \quad (15.31)
 \end{aligned}$$

The smallest real root of this approximate topological zeta function is

exercise 15.20

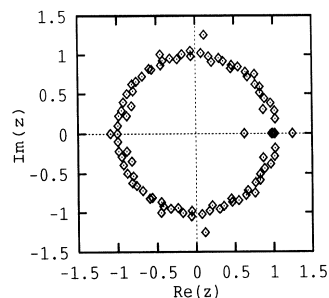
$$z = 0.62616120\dots \quad (15.32)$$

Constructing finite transition graphs of increasing length corresponding to $A \rightarrow 3.8$ we find polynomials with better and better estimates for the topological entropy. For the closest stable period 90 orbit we obtain our best estimate of the topological entropy of the repeller:

$$h = -\ln 0.62616130424685\dots = 0.46814726655867\dots \quad (15.33)$$

Figure 15.2 illustrates the convergence of the truncation approximations to the topological zeta function as a plot of the logarithm of the difference between the zero of a polynomial and our best estimate (15.33), plotted as a function of the period of the stable periodic orbit. The error of the estimate (15.32) is expected to be of order $z^{29} \approx e^{-14}$ because going from period 28 to a longer truncation typically yields combinations of loops with 29 and more nodes giving terms $\pm z^{29}$ and of higher order in the polynomial. Hence the convergence is exponential, with an exponent of $-0.47 = -h$, the topological entropy itself. In figure 15.3 we plot the zeroes of the polynomial approximation to the topological zeta function obtained by accounting for all forbidden strings of length 90 or less. The leading zero giving the topological entropy is the point closest to the origin. Most of the other zeroes are close to the unit circle; we conclude that for infinite state space partitions the topological zeta function has a unit circle as the radius of convergence. The convergence is controlled by the ratio of the leading to the next-to-leading eigenvalues, which is in this case indeed $\lambda_1/\lambda_0 = 1/e^h = e^{-h}$.

Figure 15.3: The 90 zeroes of the topological zeta function for the quadratic map for $A = 3.8$ approximated by the nearest topological zeta function with a stable cycle of length 90. (from K.T. Hansen [20])



15.6 Shadowing

The topological zeta function is a pretty function, but the infinite product (15.26) should make you pause. For finite transition matrices the left hand side is a determinant of a finite matrix, therefore a finite polynomial; so why is the right hand side an infinite product over the infinitely many prime periodic orbits of all periods?

The way in which this infinite product rearranges itself into a finite polynomial is instructive, and crucial for all that follows. You can already take a peek at the full cycle expansion (20.7) of chapter 20; all cycles beyond the fundamental t_0 and t_1 appear in the shadowing combinations such as

$$t_{s_1 s_2 \dots s_n} - t_{s_1 s_2 \dots s_m} t_{s_{m+1} \dots s_n} .$$

For subshifts of finite type such shadowing combinations cancel *exactly*, if we are counting cycles as we do in (15.16) and (15.25), or if the dynamics is piecewise linear, as in exercise 19.3. As we argue in sect. 1.5.4, for nice hyperbolic flows whose symbolic dynamics is a subshift of finite type, the shadowing combinations *almost* cancel, and the spectral determinant is dominated by the fundamental cycles from (15.15), with longer cycles contributing only small “curvature” corrections.

These exact or nearly exact cancelations depend on the flow being smooth and the symbolic dynamics being a subshift of finite type. If the dynamics requires an infinite state space partition, with pruning rules for blocks of increasing length, most of the shadowing combinations still cancel, but the few corresponding to new forbidden blocks do not, leading to a finite radius of convergence for the spectral determinant, as depicted in figure 15.3.

One striking aspect of the pruned cycle expansion (15.31) compared to the trace formulas such as (15.9) is that coefficients are not growing exponentially - indeed they all remain of order 1, so instead having a radius of convergence e^{-h} , in the example at hand the topological zeta function has the unit circle as the radius of convergence. In other words, exponentiating the spectral problem from a trace formula to a spectral determinant as in (15.24) increases the *analyticity domain*:

the pole in the trace (15.10) at $z = e^{-h}$ is promoted to a smooth zero of the spectral determinant with a larger radius of convergence.

This sensitive dependence of spectral determinants on whether or not the symbolic dynamics is a subshift of finite type is bad news. If the system is generic and not structurally stable (see sect. 12.2), a smooth parameter variation is in no sense a smooth variation of topological dynamics - infinities of periodic orbits are created or destroyed, and transition graphs go from being finite to infinite and back. That will imply that the global averages that we intend to compute are generically nowhere differentiable functions of the system parameters, and averaging over families of dynamical systems can be a highly nontrivial enterprise; a simple illustration is the parameter dependence of the diffusion constant computed in a remark in chapter 25.

You might well ask: What is wrong with computing the entropy from (15.1)? Does all this theory buy us anything? An answer: If we count K_n level by level, we ignore the self-similarity of the pruned tree - examine for example figure 14.5, or the cycle expansion of (15.35) - and the finite estimates of $h_n = \ln K_n/n$ converge nonuniformly to h , and on top of that with a slow rate of convergence, $|h - h_n| \approx O(1/n)$ as in (15.5). The determinant (15.11) is much smarter, as by construction it encodes the self-similarity of the dynamics, and yields the asymptotic value of h with no need for any finite n extrapolations.



fast track:
sect. 16, p. 308

15.7 Counting cycles



In what follows, we shall occasionally need to compute all cycles up to topological period n , so it is important to know their exact number. The formulas are fun to derive, but a bit technical for plumber on the street, and probably best skipped on the first reading.

15.7.1 Counting periodic points

The number of periodic points of period n is denoted N_n . It can be computed from (15.24) and (15.9) as a logarithmic derivative of the topological zeta function

$$\begin{aligned} \sum_{n=1}^{\infty} N_n z^n &= \operatorname{tr} \left(-z \frac{d}{dz} \ln(1 - zT) \right) = -z \frac{d}{dz} \ln \det(1 - zT) \\ &= \frac{-z \frac{d}{dz} (1/\zeta_{\text{top}})}{1/\zeta_{\text{top}}}. \end{aligned} \quad (15.34)$$

Table 15.3: Number of prime cycles for various alphabets and grammars up to period 10. The first column gives the cycle period, the second gives the formula (15.37) for the number of prime cycles for complete N -symbol dynamics, and columns three through five give the numbers of prime cycles for $N = 2, 3$ and 4.

n	$M_n(N)$	$M_n(2)$	$M_n(3)$	$M_n(4)$
1	N	2	3	4
2	$N(N - 1)/2$	1	3	6
3	$N(N^2 - 1)/3$	2	8	20
4	$N^2(N^2 - 1)/4$	3	18	60
5	$(N^5 - N)/5$	6	48	204
6	$(N^6 - N^3 - N^2 + N)/6$	9	116	670
7	$(N^7 - N)/7$	18	312	2340
8	$N^4(N^4 - 1)/8$	30	810	8160
9	$N^3(N^6 - 1)/9$	56	2184	29120
10	$(N^{10} - N^5 - N^2 + N)/10$	99	5880	104754

Observe that the trace formula (15.10) diverges at $z \rightarrow e^{-h}$, because the denominator has a simple zero there.

Example 15.8 Complete N -ary dynamics: To check formula (15.34) for the finite-grammar situation, consider the complete N -ary dynamics (14.7) for which the number of periodic points of period n is simply $\text{tr } T_c^n = N^n$. Substituting

$$\sum_{n=1}^{\infty} \frac{z^n}{n} \text{tr } T_c^n = \sum_{n=1}^{\infty} \frac{(zN)^n}{n} = -\ln(1 - zN),$$

into (15.24) we verify (15.18). The logarithmic derivative formula (15.34) in this case does not buy us much either, it simply recovers

$$\sum_{n=1}^{\infty} N_n z^n = \frac{Nz}{1 - Nz}.$$

Example 15.9 Nontrivial pruned dynamics: Consider the pruning of figure 14.6 (e). Substituting (15.34) we obtain

$$\sum_{n=1}^{\infty} N_n z^n = \frac{z + 8z^4 - 8z^8}{1 - z - 2z^4 + z^8}. \tag{15.35}$$

The topological zeta function is not merely a tool for extracting the asymptotic growth of N_n ; it actually yields the exact numbers of periodic points. In case at hand it yields a nontrivial recursive formula $N_1 = N_2 = N_3 = 1$, $N_n = 2n + 1$ for $n = 4, 5, 6, 7, 8$, and $N_n = N_{n-1} + 2N_{n-4} - N_{n-8}$ for $n > 8$.

15.7.2 Counting prime cycles

Having calculated the number of periodic points, our next objective is to evaluate the number of *prime* cycles M_n for a dynamical system whose symbolic dynamics is built from N symbols. The problem of finding M_n is classical in combinatorics (counting necklaces made out of n beads of N different kinds) and is easily solved. There are N^n possible distinct strings of length n composed of N letters. These N^n strings include all M_d prime d -cycles whose period d equals or divides n . A prime cycle is a non-repeating symbol string: for example, $p = \overline{011} = \overline{101} = \overline{110} = \dots 011011 \dots$ is prime, but $\overline{0101} = 010101 \dots = \overline{01}$ is not. A prime d -cycle contributes d strings to the sum of all possible strings, one for each cyclic permutation. The total number of possible periodic symbol sequences of period n is therefore related to the number of prime cycles by

$$N_n = \sum_{d|n} dM_d, \tag{15.36}$$

where N_n equals $\text{tr } T^n$. The number of prime cycles can be computed recursively

$$M_n = \frac{1}{n} \left(N_n - \sum_{d|n, d < n} dM_d \right),$$

or by the *Möbius inversion formula*


$$M_n = n^{-1} \sum_{d|n} \mu\left(\frac{n}{d}\right) N_d. \tag{15.37}$$

exercise 15.10

where the Möbius function $\mu(1) = 1$, $\mu(n) = 0$ if n has a squared factor, and $\mu(p_1 p_2 \dots p_k) = (-1)^k$ if all prime factors are different.

We list the number of prime cycles up to period 10 for 2-, 3- and 4-letter complete symbolic dynamics in table 15.3, obtained by Möbius inversion (15.37).

exercise 15.11

Example 15.10 Counting N -disk periodic points:  A simple example of pruning is the exclusion of “self-bounces” in the N -disk game of pinball. The number of points that are mapped back onto themselves after n iterations is given by $N_n = \text{tr } T^n$. The pruning of self-bounces eliminates the diagonal entries, $T_{N\text{-disk}} = T_c - \mathbf{1}$, so the number of the N -disk periodic points is

$$N_n = \text{tr } T_{N\text{-disk}}^n = (N - 1)^n + (-1)^n(N - 1). \tag{15.38}$$

Here T_c is the complete symbolic dynamics transition matrix (14.7). For the N -disk pruned case (15.38), Möbius inversion (15.37) yields

$$\begin{aligned} M_n^{N\text{-disk}} &= \frac{1}{n} \sum_{d|n} \mu\left(\frac{n}{d}\right) (N - 1)^d + \frac{N - 1}{n} \sum_{d|n} \mu\left(\frac{n}{d}\right) (-1)^d \\ &= M_n^{(N-1)} \quad \text{for } n > 2. \end{aligned} \tag{15.39}$$

Table 15.4: List of 3-disk prime cycles up to period 10. Here n is the cycle period, M_n is the number of prime cycles, N_n is the number of periodic points, and S_n the number of distinct prime cycles under D_3 symmetry (see chapter 21 for further details). Column 3 also indicates the splitting of N_n into contributions from orbits of periods that divide n . The prefactors in the fifth column indicate the degeneracy m_p of the cycle; for example, 3·12 stands for the three prime cycles $\overline{12}$, $\overline{13}$ and $\overline{23}$ related by $2\pi/3$ rotations. Among symmetry-related cycles, a representative \hat{p} which is lexically lowest is listed. The cycles of period 9 grouped with parentheses are related by time reversal symmetry, but not by any D_3 transformation.

n	M_n	N_n	S_n	$m_p \cdot \hat{p}$
1	0	0	0	
2	3	6=3·2	1	3·12
3	2	6=2·3	1	2·123
4	3	18=3·2+3·4	1	3·1213
5	6	30=6·5	1	6·12123
6	9	66=3·2+2·3+9·6	2	6·121213 + 3·121323
7	18	126=18·7	3	6·1212123 + 6·1212313 + 6·1213123
8	30	258=3·2+3·4+30·8	6	6·12121213 + 3·12121313 + 6·12121323 + 6·12123123 + 6·12123213 + 3·12132123
9	56	510=2·3+56·9	10	6·121212123 + 6·(121212313 + 121212323) + 6·(121213123 + 121213213) + 6·121231323 + 6·(121231213 + 121232123) + 2·121232313 + 6·121321323
10	99	1022	18	

There are no fixed points, so $M_1^{N-disk} = 0$. The number of periodic points of period 2 is $N^2 - N$, hence there are $M_2^{N-disk} = N(N - 1)/2$ prime cycles of period 2; for periods $n > 2$, the number of prime cycles is the same as for the complete $(N - 1)$ -ary dynamics of table 15.3.

Example 15.11 Pruning individual cycles:



Consider the 3-disk game of pinball. The prohibition of repeating a symbol affects counting only for the fixed points and the 2-cycles. Everything else is the same as counting for a complete binary dynamics (15.39). To obtain the topological zeta function, just divide out the binary 1- and 2-cycles $(1 - zt_0)(1 - zt_1)(1 - z^2t_{01})$ and multiply with the correct 3-disk 2-cycles $(1 - z^2t_{12})(1 - z^2t_{13})(1 - z^2t_{23})$:

exercise 15.14

exercise 15.15

$$\begin{aligned}
 1/\zeta_{3-disk} &= (1 - 2z) \frac{(1 - z^2)^3}{(1 - z)^2(1 - z^2)} \\
 &= (1 - 2z)(1 + z)^2 = 1 - 3z^2 - 2z^3.
 \end{aligned}
 \tag{15.40}$$

The factorization reflects the underlying 3-disk symmetry; we shall rederive it in (21.25). As we shall see in chapter 21, symmetries lead to factorizations of topological polynomials and topological zeta functions.

Example 15.12 Alphabet $\{a, cb^k; \bar{b}\}$: (continuation of exercise 15.16) In the cycle counting case, the dynamics in terms of $a \rightarrow z, cb^k \rightarrow z + z^2 + z^3 + \dots = z/(1 - z)$ is a complete binary dynamics with the explicit fixed point factor $(1 - t_b) = (1 - z)$:

exercise 15.19

$$1/\zeta_{top} = (1 - z) \left(1 - z - \frac{z}{1 - z} \right) = 1 - 3z + z^2.$$

Table 15.5: The 4-disk prime cycles up to period 8. The symbols is the same as shown in table 15.4. Orbits related by time reversal symmetry (but no C_{4v} symmetry) already appear at cycle period 5. Cycles of period 7 and 8 have been omitted.

n	M_n	N_n	S_n	$m_p \cdot \hat{p}$
1	0	0	0	
2	6	12=6·2	2	4·12 + 2·13
3	8	24=8·3	1	8·123
4	18	84=6·2+18·4	4	8·1213 + 4·1214 + 2·1234 + 4·1243
5	48	240=48·5	6	8·(12123 + 12124) + 8·12313 + 8·(12134 + 12143) + 8·12413
6	116	732=6·2+8·3+116·6	17	8·121213 + 8·121214 + 8·121234 + 8·121243 + 8·121313 + 8·121314 + 4·121323 + 8·(121324 + 121423) + 4·121343 + 8·121424 + 4·121434 + 8·123124 + 8·123134 + 4·123143 + 4·124213 + 8·124243
7	312	2184	39	
8	810	6564	108	

Résumé

The main result of this chapter is the cycle expansion (15.27) of the topological zeta function (i.e., the spectral determinant of the transition matrix):

$$1/\zeta_{\text{top}}(z) = 1 - \sum_{k=1} \hat{c}_k z^k .$$

For subshifts of finite type, the transition matrix is finite, and the topological zeta function is a finite polynomial evaluated by the loop expansion (15.15) of $\det(1 - zT)$. For infinite grammars the topological zeta function is defined by its cycle expansion. The topological entropy h is given by the leading zero $z = e^{-h}$. This expression for the entropy is *exact*; in contrast to the initial definition (15.1), no $n \rightarrow \infty$ extrapolations of $\ln K_n/n$ are required.

What have we accomplished? We have related the number of topologically distinct paths from one state space region to another region to the leading eigenvalue of the transition matrix T . The spectrum of T is given by topological zeta function, a certain sum over traces $\text{tr } T^n$, and in this way the periodic orbit theory has entered the arena through the trace formula (15.10), already at the level of the topological dynamics.

The main lesson of learning how to count well, a lesson that will be constantly reaffirmed, is that while trace formulas are a conceptually essential step in deriving and understanding periodic orbit theory, the spectral determinant is the right object to use in actual computations. Instead of summing all of the exponentially many periodic points required by trace formulas at each level of truncation, spectral determinants incorporate only the small incremental corrections to what is already known - and that makes them a more powerful tool for computations.

Contrary to claims one all too often encounters in the literature, “exponential proliferation of trajectories” is not the problem; what limits the convergence of cycle expansions is the proliferation of the grammar rules, or the “algorithmic complexity,” as illustrated by sect. 15.5, and figure 15.3 in particular. Nice, finite grammar leads to nice, discrete spectrum; infinite grammar leads to analyticity walls in the complex spectral plane.

Historically, these topological zeta functions were the inspiration for applying the transfer matrix methods of statistical mechanics to the problem of computation of dynamical averages for chaotic flows. The key result was the dynamical zeta function to be derived in chapter 18, a weighted generalization of the topological zeta function.

Commentary

Remark 15.1 Artin-Mazur zeta functions. Motivated by A. Weil’s zeta function for the Frobenius map [8], Artin and Mazur [11] introduced the zeta function (15.27) that counts periodic points for diffeomorphisms (see also ref. [9] for their evaluation for maps of the interval). Smale [10] conjectured rationality of the zeta functions for Axiom A diffeomorphisms, later proved by Guckenheimer [11] and Manning [12]. See remark 19.4 on page 373 for more zeta function history.

Remark 15.2 “Entropy.” The ease with which the topological entropy can be motivated obscures the fact that our construction does not lead to an invariant characterization of the dynamics, as the choice of symbolic dynamics is largely arbitrary: the same caveat applies to other entropies. In order to obtain invariant characterizations we will have to work harder. Mathematicians like to define the (impossible to evaluate) supremum over all possible partitions. The key point that eliminates the need for such searches is the existence of *generators*, i.e., partitions that under the dynamics are able to probe the whole state space on arbitrarily small scales. A generator is a finite partition $\mathcal{M} = \{M_1 \dots M_N\}$ with the following property: consider the partition built upon all possible intersections of sets $f^n(M_i)$, where f is dynamical evolution and n takes all possible integer values (positive as well as negative), then the closure of such a partition coincides with the ‘algebra of all measurable sets.’ For a thorough (and readable) discussion of generators and how they allow a computation of the Kolmogorov entropy, see ref. [1].

Remark 15.3 Perron-Frobenius matrices. For a proof of the Perron theorem on the leading eigenvalue see ref. [26]. Appendix A4.1 of ref. [2] offers a clear discussion of the spectrum of the transition matrix.

Remark 15.4 Determinant of a graph. Many textbooks offer derivations of the loop expansions of characteristic polynomials for transition matrices and their transition graphs, see for example refs. [3, 4, 5].

Remark 15.5 Ordering periodic orbit expansions. In sect. 20.5 we will introduce an alternative way of hierarchically organizing cumulant expansions, in which the order is dictated by stability rather than cycle period: such a procedure may be better suited to perform computations when the symbolic dynamics is not well understood.

Remark 15.6 T is not trace class. Note to the erudite reader: the transition matrix T (in the infinite partition limit (15.24)) is *not* trace class. Still the trace is well defined in the $n \rightarrow \infty$ limit.

Remark 15.7 Counting prime cycles. Duval has an efficient algorithm for generating Lyndon words (non-periodic necklaces, i.e., prime cycle itineraries).



Exercises

15.1. A transition matrix for 3-disk pinball.

- a) Draw the transition graph corresponding to the 3-disk ternary symbolic dynamics, and write down the corresponding transition matrix corresponding to the graph. Show that iteration of the transition matrix results in two coupled linear difference equations, - one for the diagonal and one for the off diagonal elements. (Hint: relate $\text{tr} T^n$ to $\text{tr} T^{n-1} + \dots$)
- b) Solve the above difference equation and obtain the number of periodic orbits of length n . Compare your result with table 15.4.
- c) Find the eigenvalues of the transition matrix \mathbf{T} for the 3-disk system with ternary symbolic dynamics and calculate the topological entropy. Compare this to the topological entropy obtained from the binary symbolic dynamics $\{0, 1\}$.

15.2. **3-disk prime cycle counting.** A *prime cycle* p of length n_p is a single traversal of the orbit; its label is a non-repeating symbol string of n_p symbols. For example, $\overline{12}$ is prime, but $\overline{2121}$ is not, since it is $\overline{21} = \overline{12}$ repeated.

Verify that a 3-disk pinball has 3, 2, 3, 6, 9, ... prime cycles of length 2, 3, 4, 5, 6, ...

15.3. **Sum of A_{ij} is like a trace.** Let A be a matrix with eigenvalues λ_k . Show that

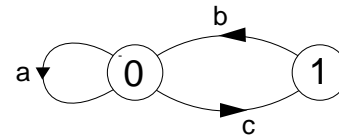
$$\Gamma_n := \sum_{i,j} [A^n]_{ij} = \sum_k c_k \lambda_k^n.$$

- (a) Under what conditions do $\ln |\text{tr} A^n|$ and $\ln |\Gamma_n|$ have the same asymptotic behavior as $n \rightarrow \infty$, i.e., their ratio converges to one?
- (b) Do eigenvalues λ_k need to be distinct, $\lambda_k \neq \lambda_l$ for $k \neq l$? How would a degeneracy $\lambda_k = \lambda_l$ affect your argument for (a)?

15.4. **Loop expansions.** Prove by induction the sign rule in the determinant expansion (15.15):

$$\det(1 - z\mathbf{T}) = \sum_{k \geq 0} \sum_{p_1 + \dots + p_k} (-1)^k t_{p_1} t_{p_2} \dots t_{p_k}.$$

15.5. **Transition matrix and cycle counting.** Suppose you are given the transition graph



This diagram can be encoded by a matrix T , where the entry T_{ij} means that there is a link connecting node i to node j . The value of the entry is the weight of the link.

- a) Walks on the graph are given a weight that is the product of the weights of all links crossed by the walk. Convince yourself that the transition matrix for this graph is:

$$T = \begin{bmatrix} a & c \\ b & 0 \end{bmatrix}.$$

- b) Enumerate all the walks of length three on the transition graph. Now compute T^3 and look at the entries. Is there any relation between the terms in T^3 and all the walks?
- c) Show that T_{ij}^n is the number of walks from point i to point j in n steps. (Hint: one might use the method of induction.)
- d) Estimate the number K_n of walks of length n for this simple transition graph.
- e) The topological entropy h measures the rate of exponential growth of the total number of walks K_n as a function of n . What is the topological entropy for this transition graph?

15.6. **Alphabet {0,1}, prune 00_.** The transition graph example 14.9 implements this pruning rule which implies that “0” must always be bracketed by “1”s; in terms of a new symbol $2 := 10$, the dynamics becomes unrestricted symbolic dynamics with with binary alphabet $\{1,2\}$. The cycle expansion (15.15) becomes

$$\begin{aligned} 1/\zeta &= (1 - t_1)(1 - t_2)(1 - t_{12})(1 - t_{112}) \dots \\ &= 1 - t_1 - t_2 - (t_{12} - t_1 t_2) \\ &\quad - (t_{112} - t_{12} t_1) - (t_{122} - t_{12} t_2) \dots \end{aligned} \tag{15.41}$$

In the original binary alphabet this corresponds to:

$$\begin{aligned} 1/\zeta &= 1 - t_1 - t_{10} - (t_{110} - t_1 t_{10}) \\ &\quad - (t_{1110} - t_{110} t_1) - (t_{11010} - t_{110} t_{10}) \dots \end{aligned} \tag{15.42}$$

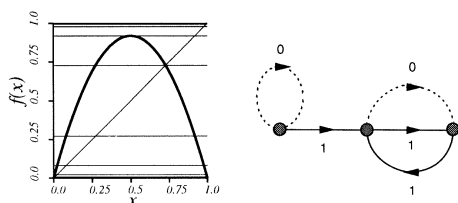
This symbolic dynamics describes, for example, circle maps with the golden mean winding number. For unimodal maps this symbolic dynamics is realized by the tent map of exercise 11.6.

15.7. **“Golden mean” pruned map.** (continuation of exercise 11.6) Show that the total number of periodic orbits of length n for the “golden mean” tent map is

$$\frac{(1 + \sqrt{5})^n + (1 - \sqrt{5})^n}{2^n}.$$

Continued in exercise 19.2. See also exercise 15.8.

15.8. **A unimodal map with golden mean pruning.** Consider the unimodal map



for which the critical point maps into the right hand fixed point in three iterations, $S^+ = 100\bar{1}$. Show that the admissible itineraries are generated by the above transition graph, with transient neighborhood of $\bar{0}$ fixed point, and $_00_$ pruned from the recurrent set. (K.T. Hansen)

15.9. **Glitches in shadowing.** (medium difficulty) Note that the combination t_{00011} minus the “shadow” $t_0 t_{0011}$ in (15.20) cancels exactly, and does not contribute to the topological zeta function (15.21). Are you able to construct a smaller transition graph than figure 14.6 (e)?

15.10. **Whence Möbius function?** To understand the origin of the Möbius function (15.37), consider the function

$$f(n) = \sum_{d|n} g(d) \tag{15.43}$$

where $d|n$ stands for sum over all divisors d of n . Invert recursively this infinite tower of equations and derive the Möbius inversion formula

$$g(n) = \sum_{d|n} \mu(n/d) f(d). \tag{15.44}$$

15.11. **Counting prime binary cycles.** In order to get comfortable with Möbius inversion reproduce the results of the second column of table 15.3.

Write a program that determines the number of prime cycles of length n . You might want to have this program later on to be sure that you have missed no 3-pinball prime cycles.

15.12. **Counting subsets of cycles.** The techniques developed above can be generalized to counting subsets of cycles. Consider the simplest example of a dynamical system with a complete binary tree, a repeller map (11.4) with two straight branches, which we label 0 and 1. Every cycle weight for such map factorizes, with a factor t_0 for each 0, and factor t_1 for each 1 in its symbol string. Prove that the transition matrix traces (15.7) collapse to $tr(T^k) = (t_0 + t_1)^k$, and $1/\zeta$ is simply

$$\prod_p (1 - t_p) = 1 - t_0 - t_1 \tag{15.45}$$

Substituting (15.45) into the identity

$$\prod_p (1 + t_p) = \prod_p \frac{1 - t_p^2}{1 - t_p}$$

we obtain

$$\begin{aligned} \prod_p (1 + t_p) &= \frac{1 - t_0^2 - t_1^2}{1 - t_0 - t_1} \\ &= 1 + t_0 + t_1 + \frac{2t_0 t_1}{1 - t_0 - t_1} \\ &= 1 + t_0 + t_1 \\ &\quad + \sum_{n=2}^{\infty} \sum_{k=1}^{n-1} 2 \binom{n-2}{k-1} t_0^k t_1^{n-k}. \end{aligned}$$

Hence for $n \geq 2$ the number of terms in the cumulant expansion with k 0's and $n - k$ 1's in their symbol sequences is $2 \binom{n-2}{k-1}$.

In order to count the number of prime cycles in each such subset we denote with $M_{n,k}$ ($n = 1, 2, \dots$; $k = \{0, 1\}$ for $n = 1$; $k = 1, \dots, n - 1$ for $n \geq 2$) the number of prime n -cycles whose labels contain k zeros. Show that

$$M_{1,0} = M_{1,1} = 1, \quad n \geq 2, k = 1, \dots, n - 1$$

$$nM_{n,k} = \sum_{m|\frac{n}{k}} \mu(m) \binom{n/m}{k/m}$$

where the sum is over all m which divide both n and k . (continued as exercise 20.7)

15.13. **Logarithmic periodicity of $\ln N_n$.** (medium difficulty) Plot $(\ln N_n, nh)$ for a system with a nontrivial finite transition graph. Do you see any periodicity? If yes, why?

15.14. **Symmetric 4-disk pinball topological zeta function.** Show that the 4-disk pinball topological zeta function (the pruning affects only the fixed points and the 2-cycles) is given by

$$1/\zeta_{\text{top}}^{4\text{-disk}} = (1 - 3z) \frac{(1 - z^2)^6}{(1 - z)^3(1 - z^2)^3}$$

$$= (1 - 3z)(1 + z)^3$$

$$= 1 - 6z^2 - 8z^3 - 3z^4. \quad (15.46)$$

15.15. **Symmetric N -disk pinball topological zeta function.** Show that for an N -disk pinball, the topological zeta function is given by

$$1/\zeta_{\text{top}}^{N\text{-disk}} = (1 - (N - 1)z) \times \frac{(1 - z^2)^{N(N-1)/2}}{(1 - z)^{N-1}(1 - z^2)^{(N-1)(N-2)/2}}$$

$$= (1 - (N - 1)z)(1 + z)^{N-1}. \quad (15.47)$$

The topological zeta function has a root $z^{-1} = N - 1$, as we already know it should from (15.38) or (15.18). We shall see in sect. 21.4 that the other roots reflect the symmetry factorizations of zeta functions.

15.16. **Alphabet $\{a, b, c\}$, prune $ab_.$** Write down the topological zeta function for this pruning rule.

15.17. **Alphabet $\{0,1\}$, prune n repeats of "0" $000 \dots 00_.$** This is equivalent to the n symbol alphabet $\{1, 2, \dots, n\}$ unrestricted symbolic dynamics, with symbols corresponding to the possible $10 \dots 00$ block lengths: $2:=10,$

$3:=100, \dots, n:=100 \dots 00$. Show that the cycle expansion (15.15) becomes

$$1/\zeta = 1 - t_1 - t_2 \dots - t_n - (t_{12} - t_1 t_2) \dots - (t_{1n} - t_1 t_n) \dots$$

15.18. **Alphabet $\{0,1\}$, prune $1000_., 00100_., 01100_.$** Show that the topological zeta function is given by

$$1/\zeta = (1 - t_0)(1 - t_1 - t_2 - t_{23} - t_{113}) \quad (15.48)$$

with the unrestricted 4-letter alphabet $\{1, 2, \underline{23}, \underline{113}\}$. Here 2 and 3 refer to 10 and 100 respectively, as in exercise 15.17.

15.19. **Alphabet $\{0,1\}$, prune $1000_., 00100_., 01100_., 10011_.$** (This grammar arises from Hénon map pruning, see remark 12.3.) The first three pruning rules were incorporated in the preceding exercise.

(a) Show that the last pruning rule $10011_.$ leads (in a way similar to exercise 15.18) to the alphabet $\{\underline{21^k}, \underline{23}, \underline{21^k 113}; \bar{1}, \bar{0}\}$, and the cycle expansion

$$1/\zeta = (1 - t_0)(1 - t_1 - t_2 - t_{23} + t_1 t_{23} - t_{2113}). \quad (15.49)$$

Note that this says that 1, 23, 2, 2113 are the fundamental cycles; not all cycles up to length 7 are needed, only 2113.

(b) Show that the topological zeta function is

$$1/\zeta_{\text{top}} = (1 - z)(1 - z - z^2 - z^5 + z^6 - z^7) \quad (15.50)$$

and that it yields the entropy $h = 0.522737642 \dots$

15.20. **Alphabet $\{0,1\}$, prune only the fixed point $\bar{0}$.** This is equivalent to the infinite alphabet $\{1, 2, 3, 4, \dots\}$ unrestricted symbolic dynamics. The prime cycles are labeled by all non-repeating sequences of integers, ordered lexically: $t_n, n > 0$; $t_{mn}, t_{mnn}, \dots, n > m > 0$; $t_{mnr}, r > n > m > 0, \dots$ (see sect. 24.3). Now the number of fundamental cycles is infinite as well:

$$1/\zeta = 1 - \sum_{n>0} t_n - \sum_{n>m>0} (t_{mn} - t_n t_m)$$

$$- \sum_{n>m>0} (t_{mnn} - t_m t_{nn})$$

$$- \sum_{n>m>0} (t_{mnn} - t_{mn} t_n) \quad (15.51)$$

$$- \sum_{r>n>m>0} (t_{mnr} + t_{mnr} - t_{mn} t_r$$

$$- t_{mr} t_n - t_m t_{nr} + t_m t_n t_r) \dots$$

. As shown in table 24.1, this grammar plays an important role in description of fixed points of marginal stability.

References

- [15.1] V.I. Arnold and A. Avez, “Ergodic Problems of Classical Mechanics,” *Addison-Wesley, Redwood City* (1989).
- [15.2] J. Zinn-Justin, “Quantum Field Theory and Critical Phenomena,” *Clarendon Press, Oxford* (1996).
- [15.3] A. Salomaa, “Formal Languages,” *Academic Press, San Diego* (1973).
- [15.4] J.E. Hopcroft and J.D. Ullman, “Introduction to Automata Theory, Languages and Computation,” *Addison-Wesley, Reading Ma* (1979).
- [15.5] D.M. Cvektović, M. Doob and H. Sachs, “Spectra of Graphs,” *Academic Press, New York* (1980).
- [15.6] J. Riordan, *An Introduction to Combinatorial Analysis*, (Wiley, New York 1958) ; E.N. Gilbert and J. Riordan, *Illinois J.Math* **5**, 657 (1961).
- [15.7] K.M. Brucks, *Adv. Appl. Math.* **8**, 434 (1987).
- [15.8] A. Weil, *Bull.Am.Math.Soc.* **55**, 497 (1949).
- [15.9] J. Milnor and W. Thurston, “On iterated maps of the interval,” in A. Dold and B. Eckmann, eds., *Dynamical Systems, Proceedings, U. of Maryland 1986-87, Lec. Notes in Math.* **1342**, 465 (Springer, Berlin 1988).
- [15.10] S. Smale, *Ann. Math.*, **74**, 199 (1961).
- [15.11] J. Guckenheimer, *Invent. Math.* **39**, 165 (1977).
- [15.12] A. Manning, *Bull. London Math. Soc.* **3**, 215 (1971).
- [15.13] A.L. Kholodenko, “Designing new apartment buildings for strings and conformal field theories. First steps,” [arXiv:hep-th/0312294](https://arxiv.org/abs/hep-th/0312294)
- [15.14] P. Dahlqvist, *On the effect of pruning on the singularity structure of zeta functions*, *J. Math. Phys.* **38**, 4273 (1997).

Chapter 16

Transporting densities

Paulina: I'll draw the curtain:
My lord's almost so far transported that
He'll think anon it lives.

—W. Shakespeare: *The Winter's Tale*

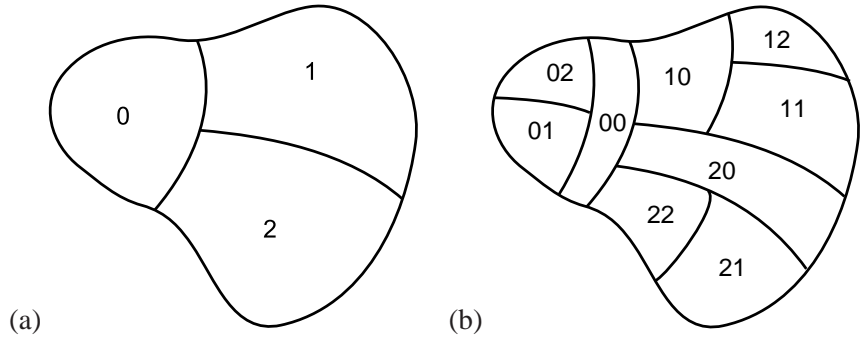
(P. Cvitanović, R. Artuso, L. Rondoni, and E.A. Spiegel)

IN CHAPTERS 2, 3, 7 and 8 we learned how to track an individual trajectory, and saw that such a trajectory can be very complicated. In chapter 4 we studied a small neighborhood of a trajectory and learned that such neighborhood can grow exponentially with time, making the concept of tracking an individual trajectory for long times a purely mathematical idealization.

While the trajectory of an individual representative point may be highly convoluted, as we shall see, the density of these points might evolve in a manner that is relatively smooth. The evolution of the density of representative points is for this reason (and other that will emerge in due course) of great interest. So are the behaviors of other properties carried by the evolving swarm of representative points.

We shall now show that the global evolution of the density of representative points is conveniently formulated in terms of linear action of evolution operators. We shall also show that the important, long-time “natural” invariant densities are unspeakably unfriendly and essentially uncomputable everywhere singular functions with support on fractal sets. Hence, in chapter 17 we rethink what is it that the theory needs to predict (“expectation values” of “observables”), relate these to the eigenvalues of evolution operators, and in chapters 18 to 20 show how to compute these without ever having to compute a “natural” invariant density ρ .

Figure 16.1: (a) First level of partitioning: A coarse partition of \mathcal{M} into regions \mathcal{M}_0 , \mathcal{M}_1 , and \mathcal{M}_2 . (b) $n = 2$ level of partitioning: A refinement of the above partition, with each region \mathcal{M}_i subdivided into \mathcal{M}_{i0} , \mathcal{M}_{i1} , and \mathcal{M}_{i2} .



16.1 Measures

Do I then measure, O my God, and know not what I measure?

—St. Augustine, *The confessions of Saint Augustine*

A fundamental concept in the description of dynamics of a chaotic system is that of *measure*, which we denote by $d\mu(x) = \rho(x)dx$. An intuitive way to define and construct a physically meaningful measure is by a process of *coarse-graining*. Consider a sequence $1, 2, \dots, n, \dots$ of increasingly refined partitions of state space, figure 16.1, into regions \mathcal{M}_i defined by the characteristic function

$$\chi_i(x) = \begin{cases} 1 & \text{if } x \in \mathcal{M}_i, \\ 0 & \text{otherwise.} \end{cases} \quad (16.1)$$

A coarse-grained measure is obtained by assigning the “mass,” or the fraction of trajectories contained in the i th region $\mathcal{M}_i \subset \mathcal{M}$ at the n th level of partitioning of the state space:

$$\Delta\mu_i = \int_{\mathcal{M}} d\mu(x)\chi_i(x) = \int_{\mathcal{M}_i} d\mu(x) = \int_{\mathcal{M}_i} dx\rho(x). \quad (16.2)$$

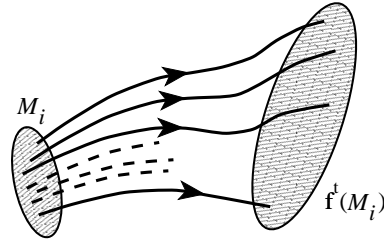
The function $\rho(x) = \rho(x, t)$ denotes the *density* of representative points in state space at time t . This density can be (and in chaotic dynamics, often is) an arbitrarily ugly function, and it may display remarkable singularities; for instance, there may exist directions along which the measure is singular with respect to the Lebesgue measure (namely the uniform measure on the state space). We shall assume that the measure is normalized

$$\sum_i^{(n)} \Delta\mu_i = 1, \quad (16.3)$$

where the sum is over subregions i at the n th level of partitioning. The infinitesimal measure $\rho(x)dx$ can be thought of as an infinitely refined partition limit of $\Delta\mu_i = |\mathcal{M}_i|\rho(x_i)$, $x_i \in \mathcal{M}_i$, with normalization

$$\int_{\mathcal{M}} dx\rho(x) = 1. \quad (16.4)$$

Figure 16.2: The evolution rule f^t can be used to map a region M_i of the state space into the region $f^t(M_i)$.



Here $|M_i|$ is the volume of region M_i , and all $|M_i| \rightarrow 0$ as $n \rightarrow \infty$.

So far, any arbitrary sequence of partitions will do. What are intelligent ways of partitioning state space? We already know the answer from chapter 11, but let us anyway develop some intuition about how the dynamics transports densities.

chapter 11

16.2 Perron-Frobenius operator

Given a density, the question arises as to what it might evolve into with time. Consider a swarm of representative points making up the measure contained in a region M_i at time $t = 0$. As the flow evolves, this region is carried into $f^t(M_i)$, as in figure 16.2. No trajectory is created or destroyed, so the conservation of representative points requires that

$$\int_{f^t(M_i)} dx \rho(x, t) = \int_{M_i} dx_0 \rho(x_0, 0).$$

Transform the integration variable in the expression on the left hand side to the initial points $x_0 = f^{-t}(x)$,

$$\int_{M_i} dx_0 \rho(f^t(x_0), t) |\det J^t(x_0)| = \int_{M_i} dx_0 \rho(x_0, 0).$$

The density changes with time as the inverse of the Jacobian (4.46)

$$\rho(x, t) = \frac{\rho(x_0, 0)}{|\det J^t(x_0)|}, \quad x = f^t(x_0), \tag{16.5}$$

which makes sense: the density varies inversely with the infinitesimal volume occupied by the trajectories of the flow.

The relation (16.5) is linear in ρ , so the manner in which a flow transports densities may be recast into the language of operators, by writing

exercise 16.1

$$\rho(x, t) = (\mathcal{L}^t \circ \rho)(x) = \int_{\mathcal{M}} dx_0 \delta(x - f^t(x_0)) \rho(x_0, 0). \tag{16.6}$$

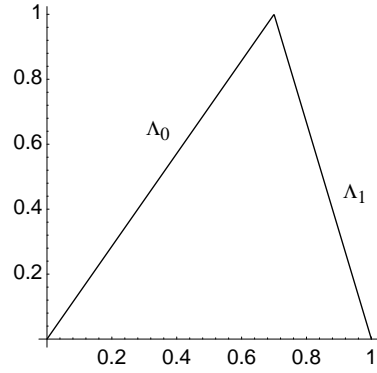


Figure 16.3: A piecewise-linear skew ‘full tent map’ (16.11) ($\Lambda_0 = 4/3, \Lambda_1 = -4$).

Let us check this formula. As long as the zero is not smack on the border of $\partial\mathcal{M}$, integrating Dirac delta functions is easy: $\int_{\mathcal{M}} dx \delta(x) = 1$ if $0 \in \mathcal{M}$, zero otherwise. The integral over a 1-dimensional Dirac delta function picks up the Jacobian of its argument evaluated at all of its zeros:

$$\int dx \delta(h(x)) = \sum_{\{x:h(x)=0\}} \frac{1}{|h'(x)|}, \tag{16.7}$$

and in d dimensions the denominator is replaced by

$$\begin{aligned} \int dx \delta(h(x)) &= \int dx \delta(h(x)) = \sum_j \int_{\mathcal{M}_j} dx \delta(h(x)) = \sum_{\{x:h(x)=0\}} \frac{1}{\left| \det \frac{\partial h(x)}{\partial x} \right|}. \end{aligned} \tag{16.8}$$

Now you can check that (16.6) is just a rewrite of (16.5):

exercise 16.2

$$\begin{aligned} (\mathcal{L}^t \circ \rho)(x) &= \sum_{x_0=f^{-t}(x)} \frac{\rho(x_0)}{|f^{t'}(x_0)|} && \text{(1-dimensional)} \\ &= \sum_{x_0=f^{-t}(x)} \frac{\rho(x_0)}{|\det J^t(x_0)|} && \text{(d-dimensional)}. \end{aligned} \tag{16.9}$$

For a deterministic, invertible flow x has only one preimage x_0 ; allowing for multiple preimages also takes account of noninvertible mappings such as the ‘stretch & fold’ maps of the interval, to be discussed briefly in the next example, and in more detail in sect. 11.3.

We shall refer to the integral operator with singular kernel (16.6) as the *Perron-Frobenius operator*:

exercise 16.3
example 23.7

$$\mathcal{L}^t(x, y) = \delta(x - f^t(y)). \tag{16.10}$$

If you do not like the word “kernel” you might prefer to think of $\mathcal{L}^t(x, y)$ as a matrix with indices x, y , and index summation in matrix multiplication replaced by an integral over y , $(\mathcal{L}^t \circ \rho)(x) = \int dy \mathcal{L}^t(x, y)\rho(y)$. (In the next example Perron-Frobenius operator is a matrix, and (16.14) illustrates a matrix approximation to the Perron-Frobenius operator.) The Perron-Frobenius operator assembles the density $\rho(x, t)$ at time t by going back in time to the density $\rho(x_0, 0)$ at time $t = 0$.

remark 19.4

Example 16.1 Perron-Frobenius operator for a piecewise-linear map: Assume the expanding 1 – dimensional map $f(x)$ of figure 16.3, a piecewise-linear 2–branch map with slopes $\Lambda_0 > 1$ and $\Lambda_1 = -\Lambda_0/(\Lambda_0 - 1) < -1$:

exercise 16.7

$$f(x) = \begin{cases} f_0(x) = \Lambda_0 x, & x \in \mathcal{M}_0 = [0, 1/\Lambda_0] \\ f_1(x) = \Lambda_1(1 - x), & x \in \mathcal{M}_1 = (1/\Lambda_0, 1] \end{cases} \quad (16.11)$$

Both $f(\mathcal{M}_0)$ and $f(\mathcal{M}_1)$ map onto the entire unit interval $\mathcal{M} = [0, 1]$. We shall refer to any unimodal map whose critical point maps onto the “left” unstable fixed point x_0 as the “Ulam” map. Assume a piecewise constant density

$$\rho(x) = \begin{cases} \rho_0 & \text{if } x \in \mathcal{M}_0 \\ \rho_1 & \text{if } x \in \mathcal{M}_1 \end{cases} \quad (16.12)$$

As can be easily checked using (16.9), the Perron-Frobenius operator acts on this piecewise constant function as a [2x2] Markov matrix \mathbf{L} with matrix elements

exercise 16.1

exercise 16.5

$$\begin{pmatrix} \rho_0 \\ \rho_1 \end{pmatrix} \rightarrow \mathbf{L}\rho = \begin{pmatrix} \frac{1}{|\Lambda_0|} & \frac{1}{|\Lambda_1|} \\ \frac{1}{|\Lambda_0|} & \frac{1}{|\Lambda_1|} \end{pmatrix} \begin{pmatrix} \rho_0 \\ \rho_1 \end{pmatrix}, \quad (16.13)$$

stretching both ρ_0 and ρ_1 over the whole unit interval Λ . In this example the density is constant after one iteration, so \mathbf{L} has only a unit eigenvalue $e^{s_0} = 1/|\Lambda_0| + 1/|\Lambda_1| = 1$, with constant density eigenvector $\rho_0 = \rho_1$. The quantities $1/|\Lambda_0|, 1/|\Lambda_1|$ are, respectively, the fractions of state space taken up by the $|\mathcal{M}_0|, |\mathcal{M}_1|$ intervals. This simple explicit matrix representation of the Perron-Frobenius operator is a consequence of the piecewise linearity of f , and the restriction of the densities ρ to the space of piecewise constant functions. The example gives a flavor of the enterprise upon which we are about to embark in this book, but the full story is much subtler: in general, there will exist no such finite-dimensional representation for the Perron-Frobenius operator. (continued in example 17.4)



fast track:
sect. 16.4, p. 315

16.3 Why not just leave it to a computer?

Another subtlety in the [dynamical systems] theory is that topological and measure-theoretic concepts of genericity lead to different results.

— John Guckenheimer

BRUTO INSENSITIVO METHOD:

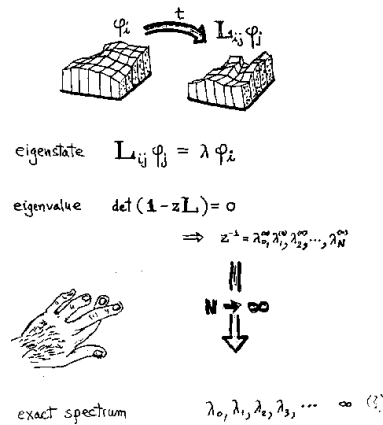


Figure 16.4: State space discretization approach to computing averages.

(R. Artuso and P. Cvitanović)

To a student with a practical bent the above Example 16.1 suggests a strategy for constructing evolution operators for smooth maps, as limits of partitions of state space into regions \mathcal{M}_i , with a piecewise-linear approximations f_i to the dynamics in each region, but that would be too naive; much of the physically interesting spectrum would be missed. As we shall see, the choice of function space for ρ is crucial, and the physically motivated choice is a space of smooth functions, rather than the space of piecewise constant functions.



chapter 23

All of the insight gained in this chapter and in what is to follow is nothing but an elegant way of thinking of the evolution operator, \mathcal{L} , as a matrix (this point of view will be further elaborated in chapter 23). There are many textbook methods of approximating an operator \mathcal{L} by sequences of finite matrix approximations \mathcal{L} , but in what follows the great achievement will be that we shall avoid constructing any matrix approximation to \mathcal{L} altogether. Why a new method? Why not just run it on a computer, as many do with such relish in diagonalizing quantum Hamiltonians?

The simplest possible way of introducing a state space discretization, figure 16.4, is to partition the state space \mathcal{M} with a non-overlapping collection of sets \mathcal{M}_i , $i = 1, \dots, N$, and to consider densities (16.2) piecewise constant on each \mathcal{M}_i :

$$\rho(x) = \sum_{i=1}^N \rho_i \frac{\chi_i(x)}{|\mathcal{M}_i|}$$

where $\chi_i(x)$ is the characteristic function (16.1) of the set \mathcal{M}_i . This piecewise constant density is a coarse grained presentation of a fine grained density $\hat{\rho}(x)$, with (16.2)

$$\rho_i = \int_{\mathcal{M}_i} dx \hat{\rho}(x).$$

The Perron-Frobenius operator does not preserve the piecewise constant form, but we may reapply coarse graining to the evolved measure

$$\begin{aligned}\rho'_i &= \int_{\mathcal{M}_i} dx (\mathcal{L} \circ \rho)(x) \\ &= \sum_{j=1}^N \frac{\rho_j}{|\mathcal{M}_j|} \int_{\mathcal{M}_i} dx \int_{\mathcal{M}_j} dy \delta(x - f(y)),\end{aligned}$$

or

$$\rho'_i = \sum_{j=1}^N \rho_j \frac{|\mathcal{M}_j \cap f^{-1}(\mathcal{M}_i)|}{|\mathcal{M}_j|}.$$

In this way

$$\mathbf{L}_{ij} = \frac{|\mathcal{M}_i \cap f^{-1}(\mathcal{M}_j)|}{|\mathcal{M}_i|}, \quad \rho' = \rho \mathbf{L} \quad (16.14)$$

is a matrix approximation to the Perron-Frobenius operator, and its leading left eigenvector is a piecewise constant approximation to the invariant measure. It is an old idea of Ulam that such an approximation for the Perron-Frobenius operator is a meaningful one.

remark 16.3

The problem with such state space discretization approaches is that they are blind, the grid knows not what parts of the state space are more or less important. This observation motivated the development of the invariant partitions of chaotic systems undertaken in chapter 11, we exploited the intrinsic topology of a flow to give us both an invariant partition of the state space and a measure of the partition volumes, in the spirit of figure 1.11.

Furthermore, a piecewise constant ρ belongs to an unphysical function space, and with such approximations one is plagued by numerical artifacts such as spurious eigenvalues. In chapter 23 we shall employ a more refined approach to extracting spectra, by expanding the initial and final densities ρ, ρ' in some basis $\varphi_0, \varphi_1, \varphi_2, \dots$ (orthogonal polynomials, let us say), and replacing $\mathcal{L}(y, x)$ by its φ_α basis representation $\mathbf{L}_{\alpha\beta} = \langle \varphi_\alpha | \mathcal{L} | \varphi_\beta \rangle$. The art is then the subtle art of finding a “good” basis for which finite truncations of $\mathbf{L}_{\alpha\beta}$ give accurate estimates of the eigenvalues of \mathcal{L} .

chapter 23

Regardless of how sophisticated the choice of basis might be, the basic problem cannot be avoided - as illustrated by the natural measure for the Hénon map (3.19) sketched in figure 16.5, eigenfunctions of \mathcal{L} are complicated, singular functions concentrated on fractal sets, and in general cannot be represented by a nice basis set of smooth functions. We shall resort to matrix representations of \mathcal{L} and the φ_α basis approach only insofar this helps us prove that the spectrum that we

compute is indeed the correct one, and that finite periodic orbit truncations do converge.



in depth:
chapter 1, p. 3

16.4 Invariant measures

A *stationary* or *invariant density* is a density left unchanged by the flow

$$\rho(x, t) = \rho(x, 0) = \rho(x). \quad (16.15)$$

Conversely, if such a density exists, the transformation $f^t(x)$ is said to be *measure-preserving*. As we are given deterministic dynamics and our goal is the computation of asymptotic averages of observables, our task is to identify interesting invariant measures for a given $f^t(x)$. Invariant measures remain unaffected by dynamics, so they are fixed points (in the infinite-dimensional function space of ρ densities) of the Perron-Frobenius operator (16.10), with the unit eigenvalue:

exercise 16.3

$$\mathcal{L}^t \rho(x) = \int_{\mathcal{M}} dy \delta(x - f^t(y)) \rho(y) = \rho(x). \quad (16.16)$$

In general, depending on the choice of $f^t(x)$ and the function space for $\rho(x)$, there may be no, one, or many solutions of the eigenfunction condition (16.16). For instance, a singular measure $d\mu(x) = \delta(x - x_q)dx$ concentrated on an equilibrium point $x_q = f^t(x_q)$, or any linear combination of such measures, each concentrated on a different equilibrium point, is stationary. There are thus infinitely many stationary measures that can be constructed. Almost all of them are unnatural in the sense that the slightest perturbation will destroy them.

From a physical point of view, there is no way to prepare initial densities which are singular, so we shall focus on measures which are limits of transformations experienced by an initial smooth distribution $\rho(x)$ under the action of f ,

$$\rho_0(x) = \lim_{t \rightarrow \infty} \int_{\mathcal{M}} dy \delta(x - f^t(y)) \rho(y, 0), \quad \int_{\mathcal{M}} dy \rho(y, 0) = 1. \quad (16.17)$$

Intuitively, the “natural” measure should be the measure that is the least sensitive to the (in practice unavoidable) external noise, no matter how weak.

16.4.1 Natural measure

Huang: Chen-Ning, do you think ergodic theory gives us useful insight into the foundation of statistical mechanics?

Yang: I don't think so.

—Kerson Huang, *C.N. Yang interview*

In computer experiments, as the Hénon example of figure 16.5, the long time evolution of many “typical” initial conditions leads to the same asymptotic distribution. Hence the *natural* (also called equilibrium measure, SRB measure, Sinai-Bowen-Ruelle measure, physical measure, invariant density, natural density, or even “natural invariant”) is defined as the limit

exercise 16.8
exercise 16.9

$$\bar{\rho}_{x_0}(y) = \begin{cases} \lim_{t \rightarrow \infty} \frac{1}{t} \int_0^t d\tau \delta(y - f^\tau(x_0)) & \text{flows} \\ \lim_{n \rightarrow \infty} \frac{1}{n} \sum_{k=0}^{n-1} \delta(y - f^k(x_0)) & \text{maps,} \end{cases} \quad (16.18)$$

where x_0 is a generic initial point. Generated by the action of f , the natural measure satisfies the stationarity condition (16.16) and is thus invariant by construction.

Staring at an average over infinitely many Dirac deltas is not a prospect we cherish. From a computational point of view, the natural measure is the visitation frequency defined by coarse-graining, integrating (16.18) over the \mathcal{M}_i region

$$\Delta \bar{\mu}_i = \lim_{t \rightarrow \infty} \frac{t_i}{t}, \quad (16.19)$$

where t_i is the accumulated time that a trajectory of total duration t spends in the \mathcal{M}_i region, with the initial point x_0 picked from some smooth density $\rho(x)$.

Let $a = a(x)$ be any *observable*. In the mathematical literature $a(x)$ is a function belonging to some function space, for instance the space of integrable functions L^1 , that associates to each point in state space a number or a set of numbers. In physical applications the observable $a(x)$ is necessarily a smooth function. The observable reports on some property of the dynamical system. Several examples will be given in sect. 17.1.

The *space average* of the observable a with respect to a measure ρ is given by the d -dimensional integral over the state space \mathcal{M} :

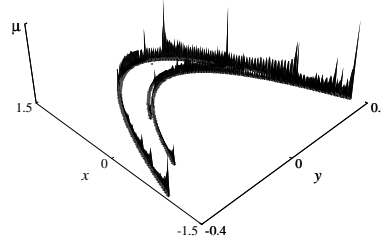
$$\begin{aligned} \langle a \rangle_\rho &= \frac{1}{|\rho_{\mathcal{M}}|} \int_{\mathcal{M}} dx \rho(x) a(x) \\ |\rho_{\mathcal{M}}| &= \int_{\mathcal{M}} dx \rho(x) = \text{mass in } \mathcal{M}. \end{aligned} \quad (16.20)$$

For now we assume that the state space \mathcal{M} has a finite dimension and a finite volume. By definition, $\langle a \rangle_\rho$ is a function(al) of ρ . For $\rho = \rho_0$ natural measure we shall drop the subscript in the definition of the space average; $\langle a \rangle_\rho = \langle a \rangle$.

Inserting the right-hand-side of (16.18) into (16.20), we see that the natural measure corresponds to a *time average* of the observable a along a trajectory of the initial point x_0 ,

$$\bar{a}_{x_0} = \lim_{t \rightarrow \infty} \frac{1}{t} \int_0^t d\tau a(f^\tau(x_0)). \quad (16.21)$$

Figure 16.5: Natural measure (16.19) for the Hénon map (3.19) strange attractor at parameter values $(a, b) = (1.4, 0.3)$. See figure 3.9 for a sketch of the attractor without the natural measure binning. (Courtesy of J.-P. Eckmann)



Analysis of the above asymptotic time limit is the central problem of ergodic theory. The *Birkhoff ergodic theorem* asserts that if an invariant measure ρ exists, the limit $\overline{a(x_0)}$ for the time average (16.21) exists for (almost) all initial x_0 . Still, Birkhoff theorem says nothing about the dependence on x_0 of time averages $\overline{a_{x_0}}$ (or, equivalently, that the construction of natural measures (16.18) leads to a “single” density, independent of x_0). This leads to one of the possible definitions of an *ergodic* evolution: f is ergodic if for any integrable observable a in (16.21) the limit function is constant. If a flow enjoys such a property the time averages coincide (apart from a set of ρ measure 0) with space averages

remark 16.1
appendix A

$$\lim_{t \rightarrow \infty} \frac{1}{t} \int_0^t d\tau a(f^\tau(x_0)) = \langle a \rangle . \tag{16.22}$$

For future reference, we note a further property that is stronger than ergodicity: if the space average of a product of any two variables decorrelates with time,

$$\lim_{t \rightarrow \infty} \langle a(x)b(f^t(x)) \rangle = \langle a \rangle \langle b \rangle , \tag{16.23}$$

section 22.4

the dynamical system is said to be *mixing*. The terminology may be understood better once we consider as the pair of observables in (16.23) characteristic functions of two sets \mathcal{A} and \mathcal{B} : then (16.23) may be written as

$$\lim_{t \rightarrow \infty} \frac{\mu(\mathcal{A} \cap f^t(\mathcal{B}))}{\mu(\mathcal{A})} = \mu(\mathcal{B})$$

so that the set \mathcal{B} spreads “uniformly” over the whole state space as t increases. Mixing is a fundamental notion in characterizing statistical behavior for dynamical systems: suppose we start with an arbitrary smooth nonequilibrium distribution $\rho(x)v(x)$: the after time t the average of an observable a is given by

$$\int_{\mathcal{M}} dx \rho(x)v(f^t(x))a(x)$$

and this tends to the equilibrium average $\langle a \rangle_\rho$ if f is mixing.

Example 16.2 The Hénon attractor natural measure: A numerical calculation of the natural measure (16.19) for the Hénon attractor (3.19) is given by the histogram

in figure 16.5. The state space is partitioned into many equal-size areas M_i , and the coarse grained measure (16.19) is computed by a long-time iteration of the Hénon map, and represented by the height of the column over area M_i . What we see is a typical invariant measure - a complicated, singular function concentrated on a fractal set.

If an invariant measure is quite singular (for instance a Dirac δ concentrated on a fixed point or a cycle), its existence is most likely of no physical import; no smooth initial density will converge to this measure if its neighborhood is repelling. In practice the average (16.18) is problematic and often hard to control, as generic dynamical systems are neither uniformly hyperbolic nor structurally stable: it is not known whether even the simplest model of a strange attractor, the Hénon attractor of figure 16.5, is “strange,” or merely a transient to a very long stable cycle.

exercise 17.1

16.4.2 Determinism vs. stochasticity

While dynamics can lead to very singular ρ 's, in any physical setting we cannot do better than to measure ρ averaged over some region \mathcal{M} ; the coarse-graining is not an approximation but a physical necessity. One is free to think of a measure as a probability density, as long as one keeps in mind the distinction between deterministic and stochastic flows. In deterministic evolution the evolution kernels are not probabilistic; the density of trajectories is transported *deterministically*. What this distinction means will become apparent later: for deterministic flows our trace and determinant formulas will be *exact*, while for quantum and stochastic flows they will only be the leading saddle point (stationary phase, steepest descent) approximations.

chapter 19

Clearly, while deceptively easy to define, measures spell trouble. The good news is that if you hang on, you will *never need to compute them*, at least not in this book. How so? The evolution operators to which we next turn, and the trace and determinant formulas to which they will lead us, will assign the correct weights to desired averages without recourse to any explicit computation of the coarse-grained measure $\Delta\rho_i$.

16.5 Density evolution for infinitesimal times

Consider the evolution of a smooth density $\rho(x) = \rho(x, 0)$ under an infinitesimal step $\delta\tau$, by expanding the action of $\mathcal{L}^{\delta\tau}$ to linear order in $\delta\tau$:

$$\begin{aligned} \mathcal{L}^{\delta\tau}\rho(y) &= \int_{\mathcal{M}} dx \delta(y - f^{\delta\tau}(x))\rho(x) \\ &= \int_{\mathcal{M}} dx \delta(y - x - \delta\tau v(x))\rho(x) \\ &= \frac{\rho(y - \delta\tau v(y))}{\left| \det \left(1 + \delta\tau \frac{\partial v(y)}{\partial x} \right) \right|} = \frac{\rho(y) - \delta\tau v_i(y)\partial_i\rho(y)}{1 + \delta\tau \sum_{i=1}^d \partial_i v_i(y)} \end{aligned}$$

$$\rho(x, \delta\tau) = \rho(x, 0) - \delta\tau \frac{\partial}{\partial x} (v(x)\rho(x, 0)). \quad (16.24)$$

Here we have used the infinitesimal form of the flow (2.6), the Dirac delta Jacobian (16.9), and the $\ln \det = \text{tr} \ln$ relation. By the Einstein summation convention, repeated indices imply summation, $v_i(y)\partial_i = \sum_{i=1}^d v_i(y)\partial_i$. Moving $\rho(y, 0)$ to the left hand side and dividing by $\delta\tau$, we discover that the rate of the deformation of ρ under the infinitesimal action of the Perron-Frobenius operator is nothing but the *continuity equation* for the density:

exercise 4.1

$$\partial_t \rho + \partial \cdot (\rho v) = 0. \quad (16.25)$$

The family of Perron-Frobenius operators $\{\mathcal{L}^t\}_{t \in \mathbb{R}_+}$ forms a semigroup parameterized by time

- (a) $\mathcal{L}^0 = I$
- (b) $\mathcal{L}^t \mathcal{L}^{t'} = \mathcal{L}^{t+t'} \quad t, t' \geq 0$ (semigroup property) .

From (16.24), time evolution by an infinitesimal step $\delta\tau$ forward in time is generated by

$$\mathcal{A}\rho(x) = + \lim_{\delta\tau \rightarrow 0^+} \frac{1}{\delta\tau} (\mathcal{L}^{\delta\tau} - I)\rho(x) = -\partial_i (v_i(x)\rho(x)). \quad (16.26)$$

We shall refer to

$$\mathcal{A} = -\partial \cdot v + \sum_i^d v_i(x)\partial_i \quad (16.27)$$

as the time evolution *generator*. If the flow is finite-dimensional and invertible, \mathcal{A} is a generator of a full-fledged group. The left hand side of (16.26) is the definition of time derivative, so the evolution equation for $\rho(x)$ is

$$\left(\frac{\partial}{\partial t} - \mathcal{A} \right) \rho(x) = 0. \quad (16.28)$$

The finite time Perron-Frobenius operator (16.10) can be formally expressed by exponentiating the time evolution generator \mathcal{A} as

$$\mathcal{L}^t = e^{t\mathcal{A}}. \quad (16.29)$$

The generator \mathcal{A} is reminiscent of the generator of translations. Indeed, for a constant velocity field dynamical evolution is nothing but a translation by (time \times velocity):

exercise 16.10

$$e^{-tv} \frac{\partial}{\partial x} a(x) = a(x - tv). \quad (16.30)$$

16.5.1 Resolvent of \mathcal{L}

Here we limit ourselves to a brief remark about the notion of the “spectrum” of a linear operator.

The Perron-Frobenius operator \mathcal{L} acts multiplicatively in time, so it is reasonable to suppose that there exist constants $M > 0, \beta \geq 0$ such that $\|\mathcal{L}\| \leq Me^{t\beta}$ for all $t \geq 0$. What does that mean? The operator norm is defined in the same spirit in which one defines matrix norms: We are assuming that no value of $\mathcal{L}\rho(x)$ grows faster than exponentially for any choice of function $\rho(x)$, so that the fastest possible growth can be bounded by $e^{t\beta}$, a reasonable expectation in the light of the simplest example studied so far, the exact escape rate (17.20). If that is so, multiplying \mathcal{L}^t by $e^{-t\beta}$ we construct a new operator $e^{-t\beta} \mathcal{L}^t = e^{t(\mathcal{A}-\beta)}$ which decays exponentially for large t , $\|e^{t(\mathcal{A}-\beta)}\| \leq M$. We say that $e^{-t\beta} \mathcal{L}^t$ is an element of a *bounded* semigroup with generator $\mathcal{A} - \beta I$. Given this bound, it follows by the Laplace transform

$$\int_0^\infty dt e^{-st} \mathcal{L}^t = \frac{1}{s - \mathcal{A}}, \quad \text{Re } s > \beta, \tag{16.31}$$

that the *resolvent* operator $(s - \mathcal{A})^{-1}$ is bounded (“resolvent” = able to cause separation into constituents)

$$\left\| \frac{1}{s - \mathcal{A}} \right\| \leq \int_0^\infty dt e^{-st} M e^{t\beta} = \frac{M}{s - \beta}.$$

If one is interested in the spectrum of \mathcal{L} , as we will be, the resolvent operator is a natural object to study; it has no time dependence, and it is bounded. The main lesson of this brief aside is that for continuous time flows, the Laplace transform is the tool that brings down the generator in (16.29) into the resolvent form (16.31) and enables us to study its spectrum.

16.6 Liouville operator



A case of special interest is the Hamiltonian or symplectic flow defined by Hamilton’s equations of motion (7.1). A reader versed in quantum mechanics will have observed by now that with replacement $\mathcal{A} \rightarrow -\frac{i}{\hbar} \hat{H}$, where \hat{H} is the quantum Hamiltonian operator, (16.28) looks rather like the time dependent Schrödinger equation, so this is probably the right moment to figure out what all this means in the case of Hamiltonian flows.

The Hamilton’s evolution equations (7.1) for any time-independent quantity $Q = Q(q, p)$ are given by

$$\frac{dQ}{dt} = \frac{\partial Q}{\partial q_i} \frac{dq_i}{dt} + \frac{\partial Q}{\partial p_i} \frac{dp_i}{dt} = \frac{\partial H}{\partial p_i} \frac{\partial Q}{\partial q_i} - \frac{\partial Q}{\partial p_i} \frac{\partial H}{\partial q_i}. \tag{16.32}$$

As equations with this structure arise frequently for symplectic flows, it is convenient to introduce a notation for them, the *Poisson bracket*

remark 16.4

$$\{A, B\} = \frac{\partial A}{\partial p_i} \frac{\partial B}{\partial q_i} - \frac{\partial A}{\partial q_i} \frac{\partial B}{\partial p_i}. \quad (16.33)$$

In terms of Poisson brackets the time evolution equation (16.32) takes the compact form

$$\frac{dQ}{dt} = \{H, Q\}. \quad (16.34)$$

The full state space flow velocity is $\dot{x} = v = (\dot{q}, \dot{p})$, where the dot signifies time derivative.

The discussion of sect. 16.5 applies to any deterministic flow. If the density itself is a material invariant, combining

$$\partial_t I + v \cdot \partial I = 0.$$

and (16.25) we conclude that $\partial_i v_i = 0$ and $\det J^{(x_0)} = 1$. An example of such incompressible flow is the Hamiltonian flow of sect. 7.2. For incompressible flows the continuity equation (16.25) becomes a statement of conservation of the state space volume (see sect. 7.2), or the *Liouville theorem*

$$\partial_t \rho + v_i \partial_i \rho = 0. \quad (16.35)$$

Hamilton's equations (7.1) imply that the flow is incompressible, $\partial_i v_i = 0$, so for Hamiltonian flows the equation for ρ reduces to the *continuity equation* for the phase space density:

$$\partial_t \rho + \partial_i (\rho v_i) = 0, \quad i = 1, 2, \dots, D. \quad (16.36)$$

Consider the evolution of the phase space density ρ of an ensemble of noninteracting particles; the particles are conserved, so

$$\frac{d}{dt} \rho(q, p, t) = \left(\frac{\partial}{\partial t} + \dot{q}_i \frac{\partial}{\partial q_i} + \dot{p}_i \frac{\partial}{\partial p_i} \right) \rho(q, p, t) = 0.$$

Inserting Hamilton's equations (7.1) we obtain the *Liouville equation*, a special case of (16.28):

$$\frac{\partial}{\partial t} \rho(q, p, t) = -\mathcal{A} \rho(q, p, t) = \{H, \rho(q, p, t)\}, \quad (16.37)$$

where $\{ , \}$ is the Poisson bracket (16.33). The generator of the flow (16.27) is in this case a generator of infinitesimal symplectic transformations,

$$\mathcal{A} = \dot{q}_i \frac{\partial}{\partial q_i} + \dot{p}_i \frac{\partial}{\partial p_i} = \frac{\partial H}{\partial p_i} \frac{\partial}{\partial q_i} - \frac{\partial H}{\partial q_i} \frac{\partial}{\partial p_i}. \quad (16.38)$$

For example, for separable Hamiltonians of form $H = p^2/2m + V(q)$, the equations of motion are

$$\dot{q}_i = \frac{p_i}{m}, \quad \dot{p}_i = -\frac{\partial V(q)}{\partial q_i}. \quad (16.39)$$

and the action of the generator

exercise 16.11

$$\mathcal{A} = -\frac{p_i}{m} \frac{\partial}{\partial q_i} + \partial_i V(q) \frac{\partial}{\partial p_i}. \quad (16.40)$$

can be interpreted as a translation (16.30) in configuration space, followed by acceleration by force $\partial V(q)$ in the momentum space.

The time evolution generator (16.27) for the case of symplectic flows is called the *Liouville operator*. You might have encountered it in statistical mechanics, while discussing what ergodicity means for 10^{23} hard balls. Here its action will be very tangible; we shall apply the Liouville operator to systems as small as 1 or 2 hard balls and to our surprise learn that this suffices to already get a bit of a grip on foundations of the nonequilibrium statistical mechanics.

Résumé

In physically realistic settings the initial state of a system can be specified only to a finite precision. If the dynamics is chaotic, it is not possible to calculate accurately the long time trajectory of a given initial point. Depending on the desired precision, and given a deterministic law of evolution, the state of the system can then be tracked for a finite time.

The study of long-time dynamics thus requires trading in the evolution of a single state space point for the evolution of a *measure*, or the *density* of representative points in state space, acted upon by an *evolution operator*. Essentially this means trading in *nonlinear* dynamical equations on a finite dimensional space $x = (x_1, x_2 \cdots x_d)$ for a *linear* equation on an infinite dimensional vector space of density functions $\rho(x)$. For finite times and for maps such densities are evolved by the *Perron-Frobenius operator*,

$$\rho(x, t) = (\mathcal{L}^t \circ \rho)(x),$$

and in a differential formulation they satisfy the *continuity equation*:

$$\partial_t \rho + \partial \cdot (\rho v) = 0.$$

The most physical of stationary measures is the natural measure, a measure robust under perturbations by weak noise.

Reformulated this way, classical dynamics takes on a distinctly quantum-mechanical flavor. If the Lyapunov time (1.1), the time after which the notion of an individual deterministic trajectory loses meaning, is much shorter than the observation time, the “sharp” observables are those dual to time, the eigenvalues of evolution operators. This is very much the same situation as in quantum mechanics; as atomic time scales are so short, what is measured is the energy, the quantum-mechanical observable dual to the time. For long times the dynamics is described in terms of stationary measures, i.e., fixed points of the appropriate evolution operators. Both in classical and quantum mechanics one has a choice of implementing dynamical evolution on densities (“Schrödinger picture,” sect.16.5) or on observables (“Heisenberg picture,” sect. 17.2 and chapter 18).

In what follows we shall find the second formulation more convenient, but the alternative is worth keeping in mind when posing and solving invariant density problems. However, as classical evolution operators are not unitary, their eigenstates can be quite singular and difficult to work with. In what follows we shall learn how to avoid dealing with these eigenstates altogether. As a matter of fact, what follows will be a labor of radical deconstruction; after having argued so strenuously here that only smooth measures are “natural,” we shall merrily proceed to erect the whole edifice of our theory on periodic orbits, i.e., objects that are δ -functions in state space. The trick is that each comes with an interval, its neighborhood – periodic points only serve to pin these intervals, just as the millimeter marks on a measuring rod partition continuum into intervals.

Commentary

Remark 16.1 Ergodic theory: An overview of ergodic theory is outside the scope of this book: the interested reader may find it useful to consult refs. [1, 3, 4, 5]. The existence of time average (16.21) is the basic result of ergodic theory, known as the Birkhoff theorem, see for example refs. [1, 25], or the statement of theorem 7.3.1 in ref. [12]. The natural measure (16.19) of sect. 16.4.1 is often referred to as the SRB or Sinai-Ruelle-Bowen measure [29, 28, 32].

There is much literature on explicit form of natural measure for special classes of 1-dimensional maps [19, 14, 15] - J. M. Aguirregabiria [16], for example, discusses several families of maps with known smooth measure, and behavior of measure under smooth conjugacies. As no such explicit formulas exist for higher dimensions and general dynamical systems, we do not discuss such measures here.

Remark 16.2 Time evolution as a Lie group: Time evolution of sect. 16.5 is an example of a 1-parameter Lie group. Consult, for example, chapter 2. of ref. [13] for a clear and pedagogical introduction to Lie groups of transformations. For a discussion of the bounded semigroups of page 320 see, for example, Marsden and Hughes [6].

Remark 16.3 Discretization of the Perron-Frobenius operator It is an old idea of Ulam [18] that such an approximation for the Perron-Frobenius operator is a meaningful one. The piecewise-linear approximation of the Perron-Frobenius operator (16.14) has been shown to reproduce the spectrum for expanding maps, once finer and finer Markov partitions are used [19, 23, 20]. The subtle point of choosing a state space partitioning for a “generic case” is discussed in ref. [21, 22].

Remark 16.4 The sign convention of the Poisson bracket: The Poisson bracket is antisymmetric in its arguments and there is a freedom to define it with either sign convention. When such freedom exists, it is certain that both conventions are in use and this is no exception. In some texts [8, 7] you will see the right hand side of (16.33) defined as $\{B, A\}$ so that (16.34) is $\frac{dQ}{dt} = \{Q, H\}$. Other equally reputable texts [24] employ the convention used here. Landau and Lifshitz [8] denote a Poisson bracket by $[A, B]$, notation that we reserve here for the quantum-mechanical commutator. As long as one is consistent, there should be no problem.

Remark 16.5 “Anon it lives”? “Anon it lives” refers to a statue of King Leontes’s wife, Hermione, who died in a fit of grief after he unjustly accused her of infidelity. Twenty years later, the servant Paulina shows Leontes this statue of Hermione. When he repents, the statue comes to life. Or perhaps Hermione actually lived and Paulina has kept her hidden all these years. The text of the play seems deliberately ambiguous. It is probably a parable for the resurrection of Christ. (John F. Gibson)

Exercises

16.1. **Integrating over Dirac delta functions.** Let us verify a few of the properties of the delta function and check (16.9), as well as the formulas (16.7) and (16.8) to be used later.

(a) If $f : \mathbb{R}^d \rightarrow \mathbb{R}^d$, show that

$$\int_{\mathbb{R}^d} dx \delta(f(x)) = \sum_{x \in f^{-1}(0)} \frac{1}{|\det \partial_x f|}.$$

(b) The delta function can be approximated by a se-

quence of Gaussians

$$\int dx \delta(x) f(x) = \lim_{\sigma \rightarrow 0} \int dx \frac{e^{-\frac{x^2}{2\sigma}}}{\sqrt{2\pi\sigma}} f(x).$$

Use this approximation to see whether the formal expression

$$\int_{\mathbb{R}} dx \delta(x^2)$$

makes sense.

16.2. **Derivatives of Dirac delta functions.** Consider $\delta^{(k)}(x) = \frac{\partial^k}{\partial x^k} \delta(x)$.

Using integration by parts, determine the value of

$$\int_{\mathbb{R}} dx \delta'(y) \quad , \quad \text{where } y = f(x) - x \quad (16.41)$$

$$\int dx \delta^{(2)}(y) = \sum_{\{x:y(x)=0\}} \frac{1}{|y'|} \left\{ 3 \frac{(y'')^2}{(y')^4} - \frac{y'''}{(y')^3} \right\}$$

$$\int dx b(x) \delta^{(2)}(y) = \sum_{\{x:y(x)=0\}} \frac{1}{|y'|} \left\{ \frac{b''}{(y')^2} - \frac{b'y''}{(y')^3} + b \left(3 \frac{(y'')^2}{(y')^4} - \frac{y'''}{(y')^3} \right) \right\} \quad (16.43)$$

These formulas are useful for computing effects of weak noise on deterministic dynamics [9].

16.3. **\mathcal{L}^t generates a semigroup.** Check that the Perron-Frobenius operator has the semigroup property,

$$\int_M dz \mathcal{L}^{t_2}(y, z) \mathcal{L}^{t_1}(z, x) = \mathcal{L}^{t_2+t_1}(y, x), \quad t_1, t_2 \geq 0. \quad (16.44)$$

As the flows in which we tend to be interested are invertible, the \mathcal{L} 's that we will use often do form a group, with $t_1, t_2 \in \mathbb{R}$.

16.4. **Escape rate of the tent map.**

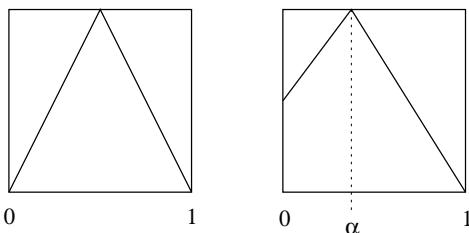
- (a) Calculate by numerical experimentation the log of the fraction of trajectories remaining trapped in the interval $[0, 1]$ for the tent map

$$f(x) = a(1 - 2|x - 0.5|)$$

for several values of a .

- (b) Determine analytically the a dependence of the escape rate $\gamma(a)$.
- (c) Compare your results for (a) and (b).

16.5. **Invariant measure.** We will compute the invariant measure for two different piecewise linear maps.



- (a) Verify the matrix \mathcal{L} representation (17.19).
- (b) The maximum value of the first map is 1. Compute an invariant measure for this map.
- (c) Compute the leading eigenvalue of \mathcal{L} for this map.

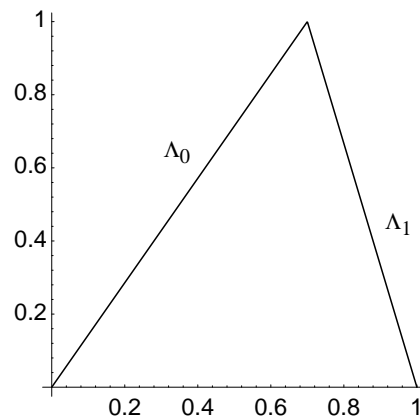
(d) For this map there is an infinite number of invariant measures, but only one of them will be found when one carries out a numerical simulation. Determine that measure, and explain why your choice is the natural measure for this map.

(e) In the second map the maximum occurs at $\alpha = (3 - \sqrt{5})/2$ and the slopes are $\pm(\sqrt{5} + 1)/2$. Find the natural measure for this map. Show that it is piecewise linear and that the ratio of its two values is $(\sqrt{5} + 1)/2$.

(medium difficulty)

16.6. **Escape rate for a flow conserving map.** Adjust Λ_0, Λ_1 in (17.17) so that the gap between the intervals $\mathcal{M}_0, \mathcal{M}_1$ vanishes. Show that the escape rate equals zero in this situation.

16.7. **Eigenvalues of the Perron-Frobenius operator for the skew full tent map.** Show that for the skew full tent map



$$f(x) = \begin{cases} f_0(x) = \Lambda_0 x, & x \in \mathcal{M}_0 = [0, 1/\Lambda_0] \\ f_1(x) = \frac{\Lambda_0}{\Lambda_0 - 1}(1 - x), & x \in \mathcal{M}_1 = (1/\Lambda_0, 1] \end{cases}$$

the eigenvalues are available analytically, compute the first few.

16.8. **“Kissing disks”**** (continuation of exercises 8.1 and 8.2). Close off the escape by setting $R = 2$, and look in real time at the density of the Poincaré section iterates for a trajectory with a randomly chosen initial condition. Does it look uniform? Should it be uniform? (Hint - phase space volumes are preserved for Hamiltonian flows by the Liouville theorem). Do you notice the trajectories that loiter near special regions of phase space for long times? These exemplify “intermittency,” a bit of unpleasantness to which we shall return in chapter 24.

16.9. **Invariant measure for the Gauss map.** Consider the Gauss map:

$$f(x) = \begin{cases} \frac{1}{x} - \left[\frac{1}{x} \right] & x \neq 0 \\ 0 & x = 0 \end{cases} \quad (16.46)$$

where $[\]$ denotes the integer part.

(a) Verify that the density

$$\rho(x) = \frac{1}{\log 2} \frac{1}{1+x}$$

is an invariant measure for the map.

(b) Is it the natural measure?

16.10. **\mathcal{A} as a generator of translations.** Verify that for a constant velocity field the evolution generator \mathcal{A} in

(16.30) is the generator of translations,

$$e^{tv \frac{\partial}{\partial x}} a(x) = a(x + tv).$$

16.11. **Incompressible flows.** Show that (16.9) implies that $\rho_0(x) = 1$ is an eigenfunction of a volume-preserving flow with eigenvalue $s_0 = 0$. In particular, this implies that the natural measure of hyperbolic and mixing Hamiltonian flows is uniform. Compare this results with the numerical experiment of exercise 16.8.

References

- [16.1] Ya.G. Sinai, *Introduction to Ergodic Theory* ((Princeton Univ. Press, Princeton, New Jersey 1994).
- [16.2] A. Katok and B. Hasselblatt, *Introduction to the Modern Theory of Dynamical Systems*, (Cambridge University Press, Cambridge 1995).
- [16.3] I.P. Cornfeld, S.V. Fomin and Ya.G. Sinai, *Ergodic Theory* (Springer, Berlin, 1982)
- [16.4] V.I. Arnold and A. Avez, *Ergodic Problems of Classical Mechanics* (Addison-Wesley, Amsterdam, 1988)
- [16.5] M. Pollicott and M. Yuri, *Dynamical Systems and Ergodic Theory* (Cambridge University Press, Cambridge, 1998)
- [16.6] J.E. Marsden and T.J.R. Hughes, *Mathematical Foundations of Elasticity* (Prentice-Hall, Englewood Cliffs, New Jersey 1983)
- [16.7] H. Goldstein, *Classical Mechanics* (Addison-Wesley, Reading, 1980).
- [16.8] L.D. Landau and E.M. Lifshitz, *Mechanics* (Pergamon, London, 1959).
- [16.9] P. Cvitanović, C.P. Dettmann, R. Mainieri and G. Vattay, *Trace formulas for stochastic evolution operators: Weak noise perturbation theory*, *J. Stat. Phys.* **93**, 981 (1998); [arXiv:chao-dyn/9807034](https://arxiv.org/abs/9807034).
- [16.10] P. Cvitanović, C.P. Dettmann, R. Mainieri and G. Vattay, *Trace formulas for stochastic evolution operators: Smooth conjugation method*, *Nonlinearity* **12**, 939 (1999); [arXiv:chao-dyn/9811003](https://arxiv.org/abs/9811003).
- [16.11] P. Cvitanović, C.P. Dettmann, G. Palla, N. Sørensgård and G. Vattay, *Spectrum of stochastic evolution operators: Local matrix representation approach*, *Phys. Rev.* **E 60**, 3936 (1999); [arXiv:chao-dyn/9904027](https://arxiv.org/abs/9904027).
- [16.12] A. Lasota and M.C. Mackey, *Chaos, Fractals and Noise* (Springer, New York 1994).

- [16.13] G. W. Bluman and S. Kumei, *Symmetries and Differential Equations* (Springer, New York 1989).
- [16.14] L. Billings and E.M. Bolt, “Invariant densities for skew tent maps,” *Chaos Solitons and Fractals* **12**, 365 (2001);
see also www.mathstat.concordia.ca/pg/bilbollt.html.
- [16.15] J.-R. Luévano and E. Pia, *The Schröder functional equation and its relation to the invariant measures of chaotic maps*; [arXiv:0907.3765](https://arxiv.org/abs/0907.3765).
- [16.16] J. M. Aguirregabiria, *Robust chaos with prescribed natural invariant measure and Lyapunov exponent*; [arXiv:0907.3790](https://arxiv.org/abs/0907.3790).
- [16.17] G.D. Birkhoff, *Collected Math. Papers*, Vol. **II** (Amer. Math. Soc., Providence RI 1950).
- [16.18] S. M. Ulam, *A Collection of Mathematical Problems* (Interscience Publishers, New York, 1960).
- [16.19] G. Froyland, *Commun. Math. Phys.* **189**, 237 (1997).
- [16.20] G. Froyland, *Discrete and Continuous Dynamical Systems* **17**, 671 (2007).
- [16.21] G. Froyland, *Nonlinearity* **12**, 79 (1999).
- [16.22] G. Froyland, “Extracting dynamical behaviour via Markov models,” in A. Mees (ed.) *Nonlinear dynamics and statistics: Proceedings Newton Institute, Cambridge 1998* (Birkhäuser, Boston 2000);
math-www.uni-paderborn.de/froyland.
- [16.23] M. Dellnitz, G. Froyland and S. Sertl, *Nonlinearity* **13**, 1171 (2000).
- [16.24] M.C. Gutzwiller, *Chaos in Classical and Quantum Mechanics* (Springer, New York 1990).
- [16.25] A. Katok and B. Hasselblatt, *Introduction to the Modern Theory of Dynamical Systems* (Cambridge U. Press, Cambridge 1995).

Chapter 17

Averaging

For it, the mystic evolution;
Not the right only justified
– what we call evil also justified.

—Walt Whitman,
Leaves of Grass: Song of the Universal

WE DISCUSS FIRST the necessity of studying the averages of observables in chaotic dynamics. A time average of an observable is computed by integrating its value along a trajectory. The integral along trajectory can be split into a sum of over integrals evaluated on trajectory segments; if exponentiated, this yields a *multiplicative* weight for successive trajectory segments. This elementary observation will enable us to recast the formulas for averages in a multiplicative form that motivates the introduction of evolution operators and further formal developments to come. The main result is that any *dynamical* average measurable in a chaotic system can be extracted from the spectrum of an appropriately constructed evolution operator. In order to keep our toes closer to the ground, in sect. 17.3 we try out the formalism on the first quantitative diagnosis that a system's got chaos, Lyapunov exponents.

17.1 Dynamical averaging

In chaotic dynamics detailed prediction is impossible, as any finitely specified initial condition, no matter how precise, will fill out the entire accessible state space after a finite Lyapunov time (1.1). Hence for chaotic dynamics one cannot follow individual trajectories for a long time; what is attainable is a description of the geometry of the set of possible outcomes, and evaluation of long time averages. Examples of such averages are transport coefficients for chaotic dynamical flows, such as escape rate, mean drift and diffusion rate; power spectra; and a host of mathematical constructs such as generalized dimensions, entropies and Lyapunov

exponents. Here we outline how such averages are evaluated within the evolution operator framework. The key idea is to replace the expectation values of observables by the expectation values of generating functionals. This associates an evolution operator with a given observable, and relates the expectation value of the observable to the leading eigenvalue of the evolution operator.

17.1.1 Time averages

Let $a = a(x)$ be any *observable*, a function that associates to each point in state space a number, a vector, or a tensor. The observable reports on a property of the dynamical system. It is a device, such as a thermometer or laser Doppler velocitometer. The device itself does not change during the measurement. The velocity field $a_i(x) = v_i(x)$ is an example of a vector observable; the length of this vector, or perhaps a temperature measured in an experiment at instant τ are examples of scalar observables. We define the *integrated observable* A as the time integral of the observable a evaluated along the trajectory of the initial point x_0 ,

$$A^t(x_0) = \int_0^t d\tau a(f^\tau(x_0)). \quad (17.1)$$

If the dynamics is given by an iterated mapping and the time is discrete, $t \rightarrow n$, the integrated observable is given by

$$A^n(x_0) = \sum_{k=0}^{n-1} a(f^k(x_0)) \quad (17.2)$$

(we suppress possible vectorial indices for the time being).

Example 17.1 Integrated observables. If the observable is the velocity, $a_i(x) = v_i(x)$, its time integral $A_i^t(x_0)$ is the trajectory $A_i^t(x_0) = x_i(t)$.

For Hamiltonian flows the action associated with a trajectory $x(t) = [q(t), p(t)]$ passing through a phase space point $x_0 = [q(0), p(0)]$ is:

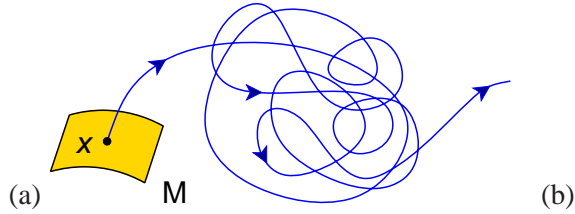
$$A^t(x_0) = \int_0^t d\tau \dot{\mathbf{q}}(\tau) \cdot \mathbf{p}(\tau). \quad (17.3)$$

The *time average* of the observable along a orbit is defined by

$$\overline{a(x_0)} = \lim_{t \rightarrow \infty} \frac{1}{t} A^t(x_0). \quad (17.4)$$

If a does not behave too wildly as a function of time – for example, if $a(x)$ is the Chicago temperature, bounded between $-80^\circ F$ and $+130^\circ F$ for all times – $A^t(x_0)$

Figure 17.1: (a) A typical chaotic trajectory explores the phase space with the long time visitation frequency building up the natural measure $\rho_0(x)$. (b) time average evaluated along an atypical trajectory such as a periodic orbit fails to explore the entire accessible state space. (A. Johansen)



is expected to grow not faster than t , and the limit (17.4) exists. For an example of a time average - the Lyapunov exponent - see sect. 17.3.

The time average depends on the orbit, but not on the initial point on that orbit: if we start at a later state space point $f^T(x_0)$ we get a couple of extra finite contributions that vanish in the $t \rightarrow \infty$ limit:

$$\begin{aligned} \overline{a(f^T(x_0))} &= \lim_{t \rightarrow \infty} \frac{1}{t} \int_T^{t+T} d\tau a(f^\tau(x_0)) \\ &= \overline{a(x_0)} - \lim_{t \rightarrow \infty} \frac{1}{t} \left(\int_0^T d\tau a(f^\tau(x_0)) - \int_t^{t+T} d\tau a(f^\tau(x_0)) \right) \\ &= \overline{a(x_0)}. \end{aligned}$$

The integrated observable $A^t(x_0)$ and the time average $\overline{a(x_0)}$ take a particularly simple form when evaluated on a periodic orbit. Define

exercise 4.6

$$A_p = \begin{cases} a_p T_p = \int_0^{T_p} d\tau a(f^\tau(x_0)) & \text{for a flow} \\ a_p n_p = \sum_{i=1}^{n_p} a(f^i(x_0)) & \text{for a map} \end{cases}, \quad x_0 \in \mathcal{M}_p, \quad (17.5)$$

where p is a prime cycle, T_p is its period, and n_p is its discrete time period in the case of iterated map dynamics. A_p is a loop integral of the observable along a single traversal of a prime cycle p , so it is an intrinsic property of the cycle, independent of the starting point $x_0 \in \mathcal{M}_p$. (If the observable a is not a scalar but a vector or matrix we might have to be more careful in defining an average which is independent of the starting point on the cycle). If the trajectory retraces itself r times, we just obtain A_p repeated r times. Evaluation of the asymptotic time average (17.4) requires therefore only a single traversal of the cycle:

$$a_p = A_p / T_p. \quad (17.6)$$

However, $\overline{a(x_0)}$ is in general a wild function of x_0 ; for a hyperbolic system it takes the same value $\langle a \rangle$ for almost all initial x_0 , but a different value (17.6) on any periodic orbit, i.e., on a dense set of points (figure 17.1 (b)).

Example 17.2 Deterministic diffusion. *The phase space of an open system such as the Sinai gas (an infinite 2-dimensional periodic array of scattering disks, see sect. 25.1) is dense with initial points that correspond to periodic runaway trajectories. The mean distance squared traversed by any such trajectory grows as $x(t)^2 \sim t^2$, and its contribution to the diffusion rate $D \propto x(t)^2/t$, (17.4) evaluated with $a(x) = x(t)^2$, diverges. Seemingly there is a paradox; even though intuition says the typical motion should be diffusive, we have an infinity of ballistic trajectories. (continued in example 17.3)*

For chaotic dynamical systems, this paradox is resolved by robust averaging, i.e., averaging also over the initial x , and worrying about the measure of the “pathological” trajectories.

17.1.2 Space averages

The *space average* of a quantity a that may depend on the point x of state space \mathcal{M} and on the time t is given by the d -dimensional integral over the d coordinates of the dynamical system:

$$\begin{aligned}\langle a \rangle(t) &= \frac{1}{|\mathcal{M}|} \int_{\mathcal{M}} dx a(f^t(x)) \\ |\mathcal{M}| &= \int_{\mathcal{M}} dx = \text{volume of } \mathcal{M}.\end{aligned}\quad (17.7)$$

The space \mathcal{M} is assumed to have finite volume (open systems like the 3-disk game of pinball are discussed in sect. 17.1.3).

What is it we *really* do in experiments? We cannot measure the time average (17.4), as there is no way to prepare a single initial condition with infinite precision. The best we can do is to prepare some initial density $\rho(x)$ perhaps concentrated on some small (but always finite) neighborhood, so one should abandon the uniform space average (17.7), and consider instead

$$\langle a \rangle_{\rho}(t) = \frac{1}{|\mathcal{M}|} \int_{\mathcal{M}} dx \rho(x) a(f^t(x)). \quad (17.8)$$

For the ergodic and mixing systems that we shall consider here *any* smooth initial density will tend to the asymptotic natural measure $t \rightarrow \infty$ limit $\rho(x, t) \rightarrow \rho_0(x)$, so we can just as well take the initial $\rho(x) = \text{const.}$ and define the *expectation value* $\langle a \rangle$ of an observable a to be the asymptotic time and space average over the state space \mathcal{M}

$$\langle a \rangle = \frac{1}{|\mathcal{M}|} \int_{\mathcal{M}} dx \overline{a(x)} = \lim_{t \rightarrow \infty} \frac{1}{|\mathcal{M}|} \int_{\mathcal{M}} dx \frac{1}{t} \int_0^t d\tau a(f^{\tau}(x)). \quad (17.9)$$

We use the same $\langle \cdot \cdot \cdot \rangle$ notation as for the space average (17.7), and distinguish the two by the presence of the time variable in the argument: if the quantity $\langle a \rangle(t)$

being averaged depends on time, then it is a space average, if it does not, it is the expectation value $\langle a \rangle$.

The expectation value is a space average of time averages, with every $x \in \mathcal{M}$ used as a starting point of a time average. The advantage of averaging over space is that it smears over the starting points which were problematic for the time average (like the periodic points). While easy to define, the expectation value $\langle a \rangle$ turns out not to be particularly tractable in practice. Here comes a simple idea that is the basis of all that follows: Such averages are more conveniently studied by investigating instead of $\langle a \rangle$ the space averages of form

$$\langle e^{\beta \cdot A^t} \rangle = \frac{1}{|\mathcal{M}|} \int_{\mathcal{M}} dx e^{\beta \cdot A^t(x)}. \quad (17.10)$$

In the present context β is an auxiliary variable of no physical significance whose role is to enable us to recover the desired space average by differentiation,

$$\langle A^t \rangle = \left. \frac{\partial}{\partial \beta} \langle e^{\beta \cdot A^t} \rangle \right|_{\beta=0}.$$

In most applications β is a scalar, but if the observable is a d -dimensional vector $a_i(x) \in \mathbb{R}^d$, so is $\beta \in \mathbb{R}^d$; if the observable is a $d \times d$ tensor, β is also a rank-2 tensor, and so on. Here we will mostly limit the considerations to scalar values of β .

If the limit $\overline{a(x_0)}$ for the time average (17.4) exists for “almost all” initial x_0 and the system is ergodic and mixing (in the sense of sect. 1.3.1), we expect the time average along almost all trajectories to tend to the same value \bar{a} , and the integrated observable A^t to tend to $t\bar{a}$. The space average (17.10) is an integral over exponentials, and such integral also grows exponentially with time. So as $t \rightarrow \infty$ we would expect the space average of $\exp(\beta \cdot A^t(x))$ to grow exponentially with time

$$\langle e^{\beta \cdot A^t} \rangle \rightarrow (\text{const}) e^{ts(\beta)},$$

and its rate of growth to be given by the limit

$$s(\beta) = \lim_{t \rightarrow \infty} \frac{1}{t} \ln \langle e^{\beta \cdot A^t} \rangle. \quad (17.11)$$

Now we understand one reason for why it is smarter to compute $\langle \exp(\beta \cdot A^t) \rangle$ rather than $\langle a \rangle$: the expectation value of the observable (17.9) and the moments of the integrated observable (17.1) can be computed by evaluating the derivatives of

$s(\beta)$

$$\begin{aligned} \left. \frac{\partial s}{\partial \beta} \right|_{\beta=0} &= \lim_{t \rightarrow \infty} \frac{1}{t} \langle A^t \rangle = \langle a \rangle, \\ \left. \frac{\partial^2 s}{\partial \beta^2} \right|_{\beta=0} &= \lim_{t \rightarrow \infty} \frac{1}{t} (\langle A^t A^t \rangle - \langle A^t \rangle \langle A^t \rangle) \\ &= \lim_{t \rightarrow \infty} \frac{1}{t} \langle (A^t - t \langle a \rangle)^2 \rangle, \end{aligned} \tag{17.12}$$

and so forth. We have written out the formulas for a scalar observable; the vector case is worked out in the exercise 17.2. If we can compute the function $s(\beta)$, we have the desired expectation value without having to estimate any infinite time limits from finite time data. exercise 17.2

Suppose we could evaluate $s(\beta)$ and its derivatives. What are such formulas good for? A typical application is to the problem of determining transport coefficients from underlying deterministic dynamics.

Example 17.3 Deterministic diffusion. *(continued from example 17.2) Consider a point particle scattering elastically off a d -dimensional array of scatterers. If the scatterers are sufficiently large to block any infinite length free flights, the particle will diffuse chaotically, and the transport coefficient of interest is the diffusion constant $\langle x(t)^2 \rangle \approx 4Dt$. In contrast to D estimated numerically from trajectories $x(t)$ for finite but large t , the above formulas yield the asymptotic D without any extrapolations to the $t \rightarrow \infty$ limit. For example, for $a_i = v_i$ and zero mean drift $\langle v_i \rangle = 0$, in d dimensions the diffusion constant is given by the curvature of $s(\beta)$ at $\beta = 0$,*

section 25.1

$$D = \lim_{t \rightarrow \infty} \frac{1}{2dt} \langle x(t)^2 \rangle = \frac{1}{2d} \sum_{i=1}^d \left. \frac{\partial^2 s}{\partial \beta_i^2} \right|_{\beta=0}, \tag{17.13}$$

so if we can evaluate derivatives of $s(\beta)$, we can compute transport coefficients that characterize deterministic diffusion. As we shall see in chapter 25, periodic orbit theory yields an explicit closed form expression for D .



fast track:
sect. 17.2, p. 336

17.1.3 Averaging in open systems



If the \mathcal{M} is a compact region or set of regions to which the dynamics is confined for all times, (17.9) is a sensible definition of the expectation value. However, if the trajectories can exit \mathcal{M} without ever returning,

$$\int_{\mathcal{M}} dy \delta(y - f^t(x_0)) = 0 \quad \text{for } t > t_{exit}, \quad x_0 \in \mathcal{M},$$

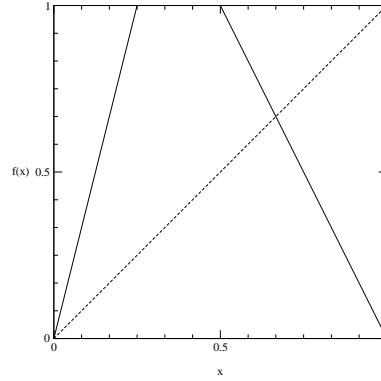


Figure 17.2: A piecewise-linear repeller (17.17): All trajectories that land in the gap between the f_0 and f_1 branches escape ($\Lambda_0 = 4$, $\Lambda_1 = -2$).

we might be in trouble. In particular, for a repeller the trajectory $f^t(x_0)$ will eventually leave the region \mathcal{M} , unless the initial point x_0 is on the repeller, so the identity

$$\int_{\mathcal{M}} dy \delta(y - f^t(x_0)) = 1, \quad t > 0, \quad \text{iff } x_0 \in \text{non-wandering set} \quad (17.14)$$

might apply only to a fractal subset of initial points a set of zero Lebesgue measure (non-wandering sets defined in sect. 2.1.1). Clearly, for open systems we need to modify the definition of the expectation value to restrict it to the dynamics on the non-wandering set, the set of trajectories which are confined for all times.

Note by \mathcal{M} a state space region that encloses all interesting initial points, say the 3-disk Poincaré section constructed from the disk boundaries and all possible incidence angles, and denote by $|\mathcal{M}|$ the volume of \mathcal{M} . The volume of the state space containing all trajectories which start out within the state space region \mathcal{M} and recur within that region at the time t

$$|\mathcal{M}(t)| = \int_{\mathcal{M}} dx dy \delta(y - f^t(x)) \sim |\mathcal{M}| e^{-\gamma t} \quad (17.15)$$

is expected to decrease exponentially, with the escape rate γ . The integral over x takes care of all possible initial points; the integral over y checks whether their trajectories are still within \mathcal{M} by the time t . For example, any trajectory that falls off the pinball table in figure 1.1 is gone for good.

section 1.4.3

section 22.1

The non-wandering set can be very difficult object to describe; but for any finite time we can construct a normalized measure from the finite-time covering volume (17.15), by redefining the space average (17.10) as

$$\langle e^{\beta \cdot A^t} \rangle = \int_{\mathcal{M}} dx \frac{1}{|\mathcal{M}(t)|} e^{\beta \cdot A^t(x)} \sim \frac{1}{|\mathcal{M}|} \int_{\mathcal{M}} dx e^{\beta \cdot A^t(x) + \gamma t}. \quad (17.16)$$

in order to compensate for the exponential decrease of the number of surviving trajectories in an open system with the exponentially growing factor $e^{\gamma t}$. What

does this mean? Once we have computed γ we can replenish the density lost to escaping trajectories, by pumping in $e^{\gamma t}$ in such a way that the overall measure is correctly normalized at all times, $\langle 1 \rangle = 1$.

Example 17.4 A piecewise-linear repeller: (continuation of example 16.1) What is gained by reformulating the dynamics in terms of “operators?” We start by considering a simple example in which the operator is a $[2 \times 2]$ matrix. Assume the expanding 1-dimensional map $f(x)$ of figure 17.2, a piecewise-linear 2-branch repeller with slopes $\Lambda_0 > 1$ and $\Lambda_1 < -1$:

$$f(x) = \begin{cases} f_0 = \Lambda_0 x & \text{if } x \in \mathcal{M}_0 = [0, 1/\Lambda_0] \\ f_1 = \Lambda_1(x - 1) & \text{if } x \in \mathcal{M}_1 = [1 + 1/\Lambda_1, 1] \end{cases} . \quad (17.17)$$

Both $f(\mathcal{M}_0)$ and $f(\mathcal{M}_1)$ map onto the entire unit interval $\mathcal{M} = [0, 1]$. Assume a piecewise constant density

$$\rho(x) = \begin{cases} \rho_0 & \text{if } x \in \mathcal{M}_0 \\ \rho_1 & \text{if } x \in \mathcal{M}_1 \end{cases} . \quad (17.18)$$

There is no need to define $\rho(x)$ in the gap between \mathcal{M}_0 and \mathcal{M}_1 , as any point that lands in the gap escapes.

The physical motivation for studying this kind of mapping is the pinball game: f is the simplest model for the pinball escape, figure 1.8, with f_0 and f_1 modelling its two strips of survivors.

As can be easily checked using (16.9), the Perron-Frobenius operator acts on this piecewise constant function as a $[2 \times 2]$ “transfer” matrix with matrix elements

$$\begin{pmatrix} \rho_0 \\ \rho_1 \end{pmatrix} \rightarrow \mathcal{L}\rho = \begin{pmatrix} \frac{1}{|\Lambda_0|} & \frac{1}{|\Lambda_1|} \\ \frac{1}{|\Lambda_0|} & \frac{1}{|\Lambda_1|} \end{pmatrix} \begin{pmatrix} \rho_0 \\ \rho_1 \end{pmatrix} , \quad (17.19)$$

exercise 16.1
exercise 16.5

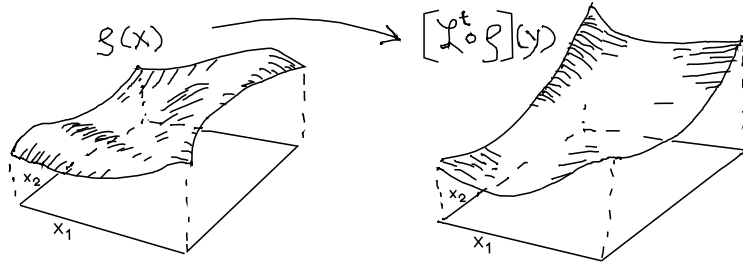
stretching both ρ_0 and ρ_1 over the whole unit interval Λ , and decreasing the density at every iteration. In this example the density is constant after one iteration, so \mathcal{L} has only one non-zero eigenvalue $e^{s_0} = 1/|\Lambda_0| + 1/|\Lambda_1|$, with constant density eigenvector $\rho_0 = \rho_1$. The quantities $1/|\Lambda_0|$, $1/|\Lambda_1|$ are, respectively, the sizes of the $|\mathcal{M}_0|$, $|\mathcal{M}_1|$ intervals, so the exact escape rate (1.3) – the log of the fraction of survivors at each iteration for this linear repeller – is given by the sole eigenvalue of \mathcal{L} :

$$\gamma = -s_0 = -\ln(1/|\Lambda_0| + 1/|\Lambda_1|) . \quad (17.20)$$

Voila! Here is the rationale for introducing operators – in one time step we have solved the problem of evaluating escape rates at infinite time. This simple explicit matrix representation of the Perron-Frobenius operator is a consequence of the piecewise linearity of f , and the restriction of the densities ρ to the space of piecewise constant functions. The example gives a flavor of the enterprise upon which we are about to embark in this book, but the full story is much subtler: in general, there will exist no such finite-dimensional representation for the Perron-Frobenius operator. (continued in example 23.5)

We now turn to the problem of evaluating $\langle e^{\beta \cdot A^t} \rangle$.

Figure 17.3: Space averaging pieces together the time average computed along the $t \rightarrow \infty$ orbit of figure 17.1 by a space average over infinitely many short t trajectory segments starting at all initial points at once.



17.2 Evolution operators

The above simple shift of focus, from studying $\langle a \rangle$ to studying $\langle \exp(\beta \cdot A^t) \rangle$ is the key to all that follows. Make the dependence on the flow explicit by rewriting this quantity as

$$\langle e^{\beta \cdot A^t} \rangle = \frac{1}{|\mathcal{M}|} \int_{\mathcal{M}} dx \int_{\mathcal{M}} dy \delta(y - f^t(x)) e^{\beta \cdot A^t(x)}. \quad (17.21)$$

Here $\delta(y - f^t(x))$ is the Dirac delta function: for a deterministic flow an initial point x maps into a unique point y at time t . Formally, all we have done above is to insert the identity

$$1 = \int_{\mathcal{M}} dy \delta(y - f^t(x)), \quad (17.22)$$

into (17.10) to make explicit the fact that we are averaging only over the trajectories that remain in \mathcal{M} for all times. However, having made this substitution we have replaced the study of individual trajectories $f^t(x)$ by the study of the evolution of density of *the totality* of initial conditions. Instead of trying to extract a temporal average from an arbitrarily long trajectory which explores the phase space ergodically, we can now probe the entire state space with short (and controllable) finite time pieces of trajectories originating from every point in \mathcal{M} .

As a matter of fact (and that is why we went to the trouble of defining the generator (16.27) of infinitesimal transformations of densities) *infinitesimally* short time evolution induced by the generator \mathcal{A} of (16.27) suffices to determine the spectrum and eigenvalues of \mathcal{L}^t .

We shall refer to the kernel of the operation (17.21) as the *evolution operator*

$$\mathcal{L}^t(y, x) = \delta(y - f^t(x)) e^{\beta \cdot A^t(x)}. \quad (17.23)$$

The simplest example is the $\beta = 0$ case, i.e., the Perron-Frobenius operator introduced in sect. 16.2. Another example - designed to deliver the Lyapunov exponent

- will be the evolution operator (17.36). The action of the evolution operator on a function ϕ is given by

$$(\mathcal{L}^t \phi)(y) = \int_{\mathcal{M}} dx \delta(y - f^t(x)) e^{\beta \cdot A^t(x)} \phi(x). \tag{17.24}$$

In terms of the evolution operator, the space average of the generating function (17.21) is given by

$$\langle e^{\beta \cdot A^t} \rangle = \frac{1}{|\mathcal{M}|} \int_{\mathcal{M}} dx \int_{\mathcal{M}} dy \phi(y) \mathcal{L}^t(y, x) \phi(x).$$

where $\phi(x)$ is the constant function $\phi(x) = 1$. If the linear operator \mathcal{L} can be thought of as a matrix, high powers of a matrix are dominated by its fastest growing matrix elements, and the limit (17.11)

$$s(\beta) = \lim_{t \rightarrow \infty} \frac{1}{t} \ln \langle \mathcal{L}^t \rangle.$$

yields the leading eigenvalue of $\mathfrak{s}_0(\beta)$, and, through it, all desired expectation values (17.12).

The evolution operator is different for different observables, as its definition depends on the choice of the integrated observable A in the exponential. Its job is deliver to us the expectation value of a , but before showing that it accomplishes that, we need to verify the semigroup property of evolution operators.

By its definition, the integral over the observable a is additive along the trajectory

$$\begin{aligned} \begin{array}{c} \text{x(0)} \curvearrowright \text{x(t+2)} \\ \text{A}^{t_1+t_2}(x_0) \end{array} &= \begin{array}{c} \text{x(0)} \curvearrowright \text{x(t_1)} \\ \text{A}^{t_1}(x_0) \end{array} + \begin{array}{c} \text{x(t_1)} \curvearrowright \text{x(t_1+t_2)} \\ \text{A}^{t_2}(f^{t_1}(x_0)) \end{array} \\ &= \int_0^{t_1} d\tau a(f^\tau(x)) + \int_{t_1}^{t_1+t_2} d\tau a(f^\tau(x)) \\ &= \text{A}^{t_1}(x_0) + \text{A}^{t_2}(f^{t_1}(x_0)). \end{aligned}$$

exercise 16.3

As $A^t(x)$ is additive along the trajectory, the evolution operator generates a semigroup

section 16.5

$$\mathcal{L}^{t_1+t_2}(y, x) = \int_{\mathcal{M}} dz \mathcal{L}^{t_2}(y, z) \mathcal{L}^{t_1}(z, x), \tag{17.25}$$

as is easily checked by substitution

$$\mathcal{L}^{t_2} \mathcal{L}^{t_1} a(y) = \int_{\mathcal{M}} dx \delta(y - f^{t_2}(x)) e^{\beta \cdot A^{t_2}(x)} (\mathcal{L}^{t_1} a)(x) = \mathcal{L}^{t_1+t_2} a(y).$$

This semigroup property is the main reason why (17.21) is preferable to (17.9) as a starting point for evaluation of dynamical averages: it recasts averaging in form of operators multiplicative along the flow.

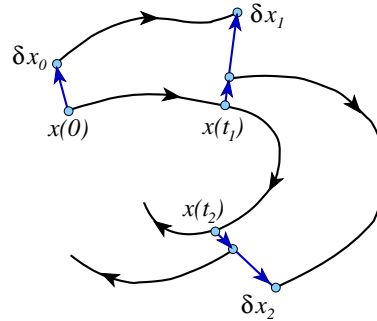


Figure 17.4: A long-time numerical calculation of the leading Lyapunov exponent requires rescaling the distance in order to keep the nearby trajectory separation within the linearized flow range.

17.3 Lyapunov exponents

(J. Mathiesen and P. Cvitanović)

Let us apply the newly acquired tools to the fundamental diagnostics in this subject: Is a given system “chaotic”? And if so, how chaotic? If all points in a neighborhood of a trajectory converge toward the same trajectory, the attractor is a fixed point or a limit cycle. However, if the attractor is strange, any two trajectories

example 2.3

section 1.3.1

$$x(t) = f^t(x_0) \quad \text{and} \quad x(t) + \delta x(t) = f^t(x_0 + \delta x_0) \tag{17.26}$$

that start out very close to each other separate exponentially with time, and in a finite time their separation attains the size of the accessible state space. This *sensitivity to initial conditions* can be quantified as

$$|\delta x(t)| \approx e^{\lambda t} |\delta x_0| \tag{17.27}$$

where λ , the mean rate of separation of trajectories of the system, is called the *Lyapunov exponent*.

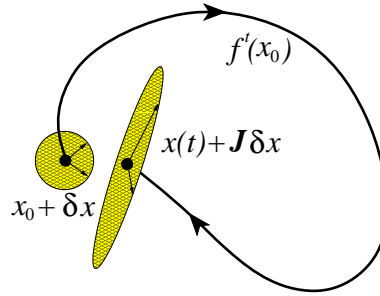
17.3.1 Lyapunov exponent as a time average

We can start out with a small δx and try to estimate λ from (17.27), but now that we have quantified the notion of linear stability in chapter 4 and defined the dynamical time averages in sect. 17.1.1, we can do better. The problem with measuring the growth rate of the distance between two points is that as the points separate, the measurement is less and less a local measurement. In study of experimental time series this might be the only option, but if we have the equations of motion, a better way is to measure the growth rate of vectors transverse to a given orbit.

The mean growth rate of the distance $|\delta x(t)|/|\delta x_0|$ between neighboring trajectories (17.27) is given by the *Lyapunov exponent*

$$\lambda = \lim_{t \rightarrow \infty} \frac{1}{t} \ln |\delta x(t)|/|\delta x_0| \tag{17.28}$$

Figure 17.5: The symmetric matrix $\mathbf{J} = (J^t)^T J^t$ maps a swarm of initial points in an infinitesimal spherical neighborhood of x_0 into a cigar-shaped neighborhood finite time t later, with semiaxes determined by the local stretching/shrinking $|\Lambda_i|$, but local individual trajectory rotations by the complex phase of J^t ignored.



(For notational brevity we shall often suppress the dependence of quantities such as $\lambda = \lambda(x_0)$, $\delta x(t) = \delta x(x_0, t)$ on the initial point x_0 and the time t). One can take (17.28) as is, take a small initial separation δx_0 , track distance between two nearby trajectories until $|\delta x(t_1)|$ gets significantly bigger, then record $t_1 \lambda_1 = \ln(|\delta x(t_1)|/|\delta x_0|)$, rescale $\delta x(t_1)$ by factor $|\delta x_0|/|\delta x(t_1)|$, and continue add infinitum, as in figure 17.4, with the leading Lyapunov exponent given by

$$\lambda = \lim_{t \rightarrow \infty} \frac{1}{t} \sum_i t_i \lambda_i. \tag{17.29}$$

However, we can do better. Given the equations of motion, for infinitesimal δx we know the $\delta x_i(t)/\delta x_j(0)$ ratio exactly, as this is by definition the Jacobian matrix (4.43)

$$\lim_{\delta x(0) \rightarrow 0} \frac{\delta x_i(t)}{\delta x_j(0)} = \frac{\partial x_i(t)}{\partial x_j(0)} = J^t_{ij}(x_0),$$

so the leading Lyapunov exponent can be computed from the linear approximation (4.29)

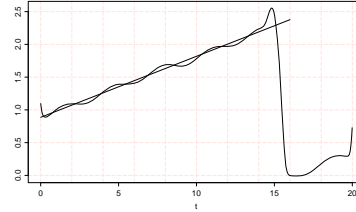
$$\overline{\lambda(x_0)} = \lim_{t \rightarrow \infty} \frac{1}{t} \ln \frac{|J^t(x_0)\delta x_0|}{|\delta x_0|} = \lim_{t \rightarrow \infty} \frac{1}{2t} \ln (\hat{n}^T (J^t)^T J^t \hat{n}). \tag{17.30}$$

In this formula the scale of the initial separation drops out, only its orientation given by the initial orientation unit vector $\hat{n} = \delta x_0/|\delta x_0|$ matters. The eigenvalues of J are either real or come in complex conjugate pairs. As J is in general not symmetric and not diagonalizable, it is more convenient to work with the symmetric and diagonalizable matrix $\mathbf{M} = (J^t)^T J^t$, with real positive eigenvalues $\{|\Lambda_1|^2 \geq \dots \geq |\Lambda_d|^2\}$, and a complete orthonormal set of eigenvectors of $\{u_1, \dots, u_d\}$. Expanding the initial orientation $\hat{n} = \sum(\hat{n} \cdot u_i)u_i$ in the $\mathbf{M}u_i = |\Lambda_i|^2 u_i$ eigenbasis, we have

$$\hat{n}^T \mathbf{M} \hat{n} = \sum_{i=1}^d (\hat{n} \cdot u_i)^2 |\Lambda_i|^2 = (\hat{n} \cdot u_1)^2 e^{2\mu_1 t} (1 + O(e^{-2(\mu_1 - \mu_2)t})), \tag{17.31}$$

where $t\mu_i = \ln |\Lambda_i(x_0, t)|$, with real parts of characteristic exponents (4.19) ordered by $\mu_1 > \mu_2 \geq \mu_3 \dots$. For long times the largest Lyapunov exponent dominates

Figure 17.6: A numerical estimate of the leading Lyapunov exponent for the Rössler flow (2.17) from the dominant expanding eigenvalue formula (17.30). The leading Lyapunov exponent $\lambda \approx 0.09$ is positive, so numerics supports the hypothesis that the Rössler attractor is strange. (J. Mathiesen)



exponentially (17.30), provided the orientation \hat{n} of the initial separation was not chosen perpendicular to the dominant expanding eigen-direction u_1 . The Lyapunov exponent is the time average

$$\begin{aligned} \overline{\lambda(x_0)} &= \lim_{t \rightarrow \infty} \frac{1}{t} \left\{ \ln |\hat{n} \cdot u_1| + \ln |\Lambda_1(x_0, t)| + O(e^{-2(\lambda_1 - \lambda_2)t}) \right\} \\ &= \lim_{t \rightarrow \infty} \frac{1}{t} \ln |\Lambda_1(x_0, t)|, \end{aligned} \tag{17.32}$$

where $\Lambda_1(x_0, t)$ is the leading eigenvalue of $J^t(x_0)$. By choosing the initial displacement such that \hat{n} is normal to the first $(i-1)$ eigen-directions we can define not only the leading, but all Lyapunov exponents as well:

$$\overline{\lambda_i(x_0)} = \lim_{t \rightarrow \infty} \frac{1}{t} \ln |\Lambda_i(x_0, t)|, \quad i = 1, 2, \dots, d. \tag{17.33}$$

The leading Lyapunov exponent now follows from the Jacobian matrix by numerical integration of (4.9).

The equations can be integrated accurately for a finite time, hence the infinite time limit of (17.30) can be only estimated from plots of $\frac{1}{2} \ln(\hat{n}^T \mathbf{M} \hat{n})$ as function of time, such as figure 17.6 for the Rössler flow (2.17).

As the local expansion and contraction rates vary along the flow, the temporal dependence exhibits small and large humps. The sudden fall to a low level is caused by a close passage to a folding point of the attractor, an illustration of why numerical evaluation of the Lyapunov exponents, and proving the very existence of a strange attractor is a very difficult problem. The approximately monotone part of the curve can be used (at your own peril) to estimate the leading Lyapunov exponent by a straight line fit.

As we can already see, we are courting difficulties if we try to calculate the Lyapunov exponent by using the definition (17.32) directly. First of all, the state space is dense with atypical trajectories; for example, if x_0 happened to lie on a periodic orbit p , $\overline{\lambda}$ would be simply $\ln |\Lambda_p|/T_p$, a local property of cycle p , not a global property of the dynamical system. Furthermore, even if x_0 happens to be a “generic” state space point, it is still not obvious that $\ln |\Lambda(x_0, t)|/t$ should be converging to anything in particular. In a Hamiltonian system with coexisting elliptic islands and chaotic regions, a chaotic trajectory gets captured in the neighborhood of an elliptic island every so often and can stay there for arbitrarily long time; as

there the orbit is nearly stable, during such episode $\ln |\Lambda(x_0, t)|/t$ can dip arbitrarily close to 0^+ . For state space volume non-preserving flows the trajectory can traverse locally contracting regions, and $\ln |\Lambda(x_0, t)|/t$ can occasionally go negative; even worse, one never knows whether the asymptotic attractor is periodic or “strange,” so any finite estimate of $\bar{\lambda}$ might be dead wrong.

exercise 17.1

17.3.2 Evolution operator evaluation of Lyapunov exponents

A cure to these problems was offered in sect. 17.2. We shall now replace time averaging along a single orbit by action of a multiplicative evolution operator on the entire state space, and extract the Lyapunov exponent from its leading eigenvalue. If the chaotic motion fills the whole state space, we are indeed computing the asymptotic Lyapunov exponent. If the chaotic motion is transient, leading eventually to some long attractive cycle, our Lyapunov exponent, computed on non-wandering set, will characterize the chaotic transient; this is actually what any experiment would measure, as even very small amount of external noise will suffice to destabilize a long stable cycle with a minute immediate basin of attraction.

Example 17.5 Lyapunov exponent, discrete time 1-dimensional dynamics. Due to the chain rule (4.52) for the derivative of an iterated map, the stability of a 1 – dimensional mapping is multiplicative along the flow, so the integral (17.1) of the observable $a(x) = \ln |f'(x)|$, the local trajectory divergence rate, evaluated along the trajectory of x_0 is additive:

$$A^n(x_0) = \ln |f^{n'}(x_0)| = \sum_{k=0}^{n-1} \ln |f'(x_k)|. \tag{17.34}$$

The Lyapunov exponent is then the expectation value (17.9) given by a spatial integral (17.8) weighted by the natural measure

$$\lambda = \langle \ln |f'(x)| \rangle = \int_{\mathcal{M}} dx \rho_0(x) \ln |f'(x)|. \tag{17.35}$$

The associated (discrete time) evolution operator (17.23) is

$$\mathcal{L}(y, x) = \delta(y - f(x)) e^{\beta \ln |f'(x)|}. \tag{17.36}$$

Here we have restricted our considerations to 1 – d maps, as for higher-dimensional flows only the Jacobian matrices are multiplicative, not the individual eigenvalues. Construction of the evolution operator for evaluation of the Lyapunov spectra in the general case requires more cleverness than warranted at this stage in the narrative: an extension of the evolution equations to a flow in the tangent space.

All that remains is to determine the value of the Lyapunov exponent

$$\lambda = \langle \ln |f'(x)| \rangle = \left. \frac{\partial s(\beta)}{\partial \beta} \right|_{\beta=0} = s'(0) \tag{17.37}$$

from (17.12), the derivative of the leading eigenvalue $s_0(\beta)$ of the evolution operator (17.36).

example 20.1

The only question is: how?

Résumé

The expectation value $\langle a \rangle$ of an observable $a(x)$ measured $A^t(x) = \int_0^t d\tau a(x(\tau))$ and averaged along the flow $x \rightarrow f^t(x)$ is given by the derivative

$$\langle a \rangle = \left. \frac{\partial s}{\partial \beta} \right|_{\beta=0}$$

of the leading eigenvalue $e^{s(\beta)}$ of the corresponding evolution operator \mathcal{L}^t .

Instead of using the Perron-Frobenius operator (16.10) whose leading eigenfunction, the natural measure, once computed, yields expectation value (16.20) of any observable $a(x)$, we construct a specific, hand-tailored evolution operator \mathcal{L} for each and every observable. However, by time we arrive to chapter 20, the scaffolding will be removed, both \mathcal{L} 's and their eigenfunctions will be gone, and only the explicit and exact periodic orbit formulas for expectation values of observables will remain.

chapter 20

The next question is: how do we evaluate the eigenvalues of \mathcal{L} ? We saw in example 17.4, in the case of piecewise-linear dynamical systems, that these operators reduce to finite matrices, but for generic smooth flows, they are infinite-dimensional linear operators, and finding smart ways of computing their eigenvalues requires some thought. In chapter 11 we undertook the first step, and replaced the *ad hoc* partitioning (16.14) by the intrinsic, topologically invariant partitioning. In chapter 15 we applied this information to our first application of the evolution operator formalism, evaluation of the topological entropy, the growth rate of the number of topologically distinct orbits. This small victory will be refashioned in chapters 18 and 19 into a systematic method for computing eigenvalues of evolution operators in terms of periodic orbits.

Commentary

Remark 17.1 “Pressure.” The quantity $\langle \exp(\beta \cdot A^t) \rangle$ is called a “partition function” by Ruelle [1]. Mathematicians decorate it with considerably more Greek and Gothic letters than is the case in this treatise. Ruelle [1] and Bowen [2] had given name “pressure” $P(a)$ to $s(\beta)$ (where a is the observable introduced here in sect. 17.1.1), defined by the “large system” limit (17.11). As we shall apply the theory also to computation of the physical gas pressure exerted on the walls of a container by a bouncing particle, we prefer to refer to $s(\beta)$ as simply the leading eigenvalue of the evolution operator introduced in sect. 16.5.

The “convexity” properties such as $P(a) \leq P(|a|)$ will be pretty obvious consequence of the definition (17.11). In the case that \mathcal{L} is the Perron-Frobenius operator (16.10), the eigenvalues $\{s_0(\beta), s_1(\beta), \dots\}$ are called the *Ruelle-Pollicott resonances* [3, 4, 5], with the leading one, $s(\beta) = s_0(\beta)$ being the one of main physical interest. In order to aid the reader in digesting the mathematics literature, we shall try to point out the notational correspondences whenever appropriate. The rigorous formalism is replete with lims, sups, infs, Ω -sets which are not really essential to understanding of the theory, and are avoided in this presentation.

Remark 17.2 Microcanonical ensemble. In statistical mechanics the space average (17.7) performed over the Hamiltonian system constant energy surface invariant measure $\rho(x)dx = dqdp \delta(H(q, p) - E)$ of volume $\omega(E) = \int_{\mathcal{M}} dqdp \delta(H(q, p) - E)$

$$\langle a(t) \rangle = \frac{1}{\omega(E)} \int_{\mathcal{M}} dqdp \delta(H(q, p) - E) a(q, p, t) \quad (17.38)$$

is called the *microcanonical ensemble average*.

Remark 17.3 Lyapunov exponents. The Multiplicative Ergodic Theorem of Oseledec [6] states that the limits (17.30–17.33) exist for almost all points x_0 and all tangent vectors \hat{n} . There are at most d distinct values of λ as we let \hat{n} range over the tangent space. These are the Lyapunov exponents [8] $\lambda_i(x_0)$.

We are doubtful of the utility of Lyapunov exponents as means of predicting any observables of physical significance, but that is the minority position - in the literature one encounters many provocative speculations, especially in the context of foundations of statistical mechanics (“hydrodynamic” modes) and the existence of a Lyapunov spectrum in the thermodynamic limit of spatiotemporal chaotic systems.

There is much literature on numerical computation of the Lyapunov exponents, see for example refs. [14, 15, 17]. For early numerical methods to compute Lyapunov vectors, see refs. [16, 17]. The drawback of the Gram-Schmidt method is that the vectors so constructed are orthogonal by fiat, whereas the stable / unstable eigenvectors of the Jacobian matrix are in general not orthogonal. Hence the Gram-Schmidt vectors are not covariant, i.e., the linearized dynamics does not transport them into the eigenvectors of the Jacobian matrix computed further downstream. For computation of covariant Lyapunov vectors, see refs. [18, 20].

Remark 17.4 State space discretization. Ref. [21] discusses numerical discretizations of state space, and construction of Perron-Frobenius operators as stochastic matrices, or directed weighted graphs, as coarse-grained models of the global dynamics, with transport rates between state space partitions computed using this matrix of transition probabilities; a rigorous discussion of some of the former features is included in ref. [22].

Exercises

17.1. **How unstable is the Hénon attractor?**

- (a) Evaluate numerically the Lyapunov exponent λ by iterating some 100,000 times or so the Hénon map

$$\begin{bmatrix} x' \\ y' \end{bmatrix} = \begin{bmatrix} 1 - ax^2 + y \\ bx \end{bmatrix}$$

for $a = 1.4, b = 0.3$.

- (b) Would you describe the result as a 'strange attractor'? Why?
- (c) How robust is the Lyapunov exponent for the Hénon attractor? Evaluate numerically the Lyapunov exponent by iterating the Hénon map for $a = 1.39945219, b = 0.3$. How much do you trust now your result for the part (a) of this exercise?
- (d) Re-examine this computation by plotting the iterates, and erasing the plotted points every 1000 iterates or so. Keep at it until the 'strange' attractor vanishes like the smile of the Cheshire cat. What replaces it? Do a few numerical experiments to estimate the length of typical transient before the dynamics settles into this long-time attractor.
- (e) Use your Newton search routine to confirm existence of this attractor. Compute its Lyapunov exponent, compare with your numerical result from above. What is the itinerary of the attractor.
- (f) Would you describe the result as a 'strange attractor'? Do you still have confidence in claims such as the one made for the part (b) of this exercise?

17.2. **Expectation value of a vector observable.**

Check and extend the expectation value formulas (17.12) by evaluating the derivatives of $s(\beta)$ up to 4-th order for the space average $\langle \exp(\beta \cdot A^t) \rangle$ with a_i a vector quantity:

- (a)

$$\left. \frac{\partial s}{\partial \beta_i} \right|_{\beta=0} = \lim_{t \rightarrow \infty} \frac{1}{t} \langle A_i^t \rangle = \langle a_i \rangle, \quad (17.39)$$

- (b)

$$\begin{aligned} \left. \frac{\partial^2 s}{\partial \beta_i \partial \beta_j} \right|_{\beta=0} &= \lim_{t \rightarrow \infty} \frac{1}{t} \left(\langle A_i^t A_j^t \rangle - \langle A_i^t \rangle \langle A_j^t \rangle \right) \\ &= \lim_{t \rightarrow \infty} \frac{1}{t} \langle (A_i^t - t \langle a_i \rangle)(A_j^t - t \langle a_j \rangle) \rangle. \end{aligned}$$

Note that the formalism is smart: it automatically yields the *variance* from the mean, rather than simply the 2nd moment $\langle a^2 \rangle$.

- (c) compute the third derivative of $s(\beta)$.
- (d) compute the fourth derivative assuming that the mean in (17.39) vanishes, $\langle a_i \rangle = 0$. The 4-th order moment formula

$$K(t) = \frac{\langle x^4(t) \rangle}{\langle x^2(t) \rangle^2} - 3 \quad (17.40)$$

that you have derived is known as *kurtosis*: it measures a deviation from what the 4-th order moment would be were the distribution a pure Gaussian (see (25.22) for a concrete example). If the observable is a vector, the kurtosis $K(t)$ is given by

$$\frac{\sum_{ij} \left[\langle A_i A_i A_j A_j \rangle + 2 \left(\langle A_i A_j \rangle \langle A_j A_i \rangle - \langle A_i A_i \rangle \langle A_j A_j \rangle \right) \right]}{\left(\sum_i \langle A_i A_i \rangle \right)^2}$$

17.3. **Pinball escape rate from numerical simulation*.**

Estimate the escape rate for $R : a = 6$ 3-disk pinball by shooting 100,000 randomly initiated pinballs into the 3-disk system and plotting the logarithm of the number of trapped orbits as function of time. For comparison, a numerical simulation of ref. [3] yields $\gamma = .410 \dots$

17.4. **Rössler attractor Lyapunov exponents.**

- (a) Evaluate numerically the expanding Lyapunov exponent λ_e of the Rössler attractor (2.17).
- (b) Plot your own version of figure 17.6. Do not worry if it looks different, as long as you understand why your plot looks the way it does. (Remember the nonuniform contraction/expansion of figure 4.3.)
- (c) Give your best estimate of λ_e . The literature gives surprisingly inaccurate estimates - see whether you can do better.
- (d) Estimate the contracting Lyapunov exponent λ_c . Even though it is much smaller than λ_e , a glance at the stability matrix (4.4) suggests that you can probably get it by integrating the infinitesimal volume along a long-time trajectory, as in (4.47).

References

[17.1] D. Ruelle, *Bull. Amer. Math. Soc.* **78**, 988 (1972).

- [17.2] R. Bowen, *Equilibrium states and the ergodic theory of Anosov diffeomorphisms*, Springer Lect. Notes on Math. **470** (1975).
- [17.3] D. Ruelle, “The thermodynamical formalism for expanding maps,” *J. Diff. Geo.* **25**, 117 (1987).
- [17.4] M. Pollicott, “On the rate of mixing of Axiom A flows,” *Invent. Math.* **81**, 413 (1985).
- [17.5] D. Ruelle, *J. Diff. Geo.* **25**, 99 (1987).
- [17.6] V. I. Oseledec, *Trans. Moscow Math. Soc.* **19**, 197 (1968).
- [17.7] M. Pollicott, *Lectures on Ergodic Theory and Pesin Theory in Compact Manifolds*, (Cambridge Univ. Press, Cambridge 1993).
- [17.8] A. M. Lyapunov, *General problem of stability of motion*, Ann.Math. Studies **17** (1949) (Princeton Univ. Press).
- [17.9] Ya.B. Pesin, *Uspekhi Mat. Nauk* **32**, 55 (1977), [*Russian Math. Surveys* **32**, 55 (1977)]
- [17.10] Ya.B. Pesin, *Dynamical systems with generalized hyperbolic attractors: hyperbolic, ergodic and topological properties*, *Ergodic Theory and Dynamical Systems*, **12**, 123 (1992).
- [17.11] Ya.B. Pesin, *Func. Anal. Applic.* **8**, 263 (1974).
- [17.12] A. Katok, *Lyapunov exponents, entropy and periodic orbits for diffeomorphisms*, *Publ. Math. IHES* **51**, 137 (1980).
- [17.13] D. Bessis, G. Paladin, G. Turchetti and S. Vaienti, *Generalized Dimensions, Entropies and Lyapunov Exponents from the Pressure Function for Strange Sets*, *J. Stat. Phys.* **51**, 109 (1988).
- [17.14] A. Wolf, J.B. Swift, et al., “Determining Lyapunov Exponents from a Time Series,” *Physica D* **16**, 285 (1985).
- [17.15] J.-P. Eckmann, S.O. Kamphorst, et al., “Lyapunov exponents from time series,” *Phys. Rev. A* **34**, 4971 (1986).
- [17.16] I. Shimada and T. Nagashima, *Prog. Theor. Phys.* **61**, 1605 (1979).
- [17.17] G. Benettin, L. Galgani, A. Giorgilli and J.-M. Strelcyn, “Lyapunov characteristic exponents for smooth dynamical systems and for Hamiltonian systems: a method for computing all of them. Part 1: Theory,” *Meccanica* **15**, 9 (1980); “Part 2: Numerical Application,” *Meccanica* **15**, 21 (1980).
- [17.18] F. Ginelli, P. Poggi, A. Turchi, H. Chaté, R. Livi and A. Politi, “Characterizing dynamics with covariant Lyapunov vectors,” *Phys Rev Lett* **99**, 130601 (2007); [arXiv:0706.0510](https://arxiv.org/abs/0706.0510).
- [17.19] C. Skokos, “The Lyapunov Characteristic Exponents and their computation,” [arXiv:0811.0882](https://arxiv.org/abs/0811.0882).

- [17.20] A. Politi, A. Torcini and S. Lepri, *J. Phys. IV* **8**, 263 (1998).
- [17.21] M. Dellnitz, O. Junge, W.S. Koon, F. Lekien, M.W. Lo, J.E. Marsden, K. Padberg, R. Preis, S.D. Ross, and B. Thiere, "Transport in Dynamical Astronomy and Multibody Problems," *Internat. J. Bifur. Chaos* **15**, 699 (2005); www.cds.caltech.edu/~koon/papers
- [17.22] G. Froyland, "Computer-assisted bounds for the rate of decay of correlations," *Commun.Math.Phys.* **189**, 237 (1997); C. Liverani, "Rigorous numerical investigation of the statistical properties of piecewise expanding maps. A feasibility study," *Nonlinearity* **14**, 463 (2001).
- [17.23] P. Cvitanović, "Chaos for cyclists," in E. Moss, ed., *Noise and chaos in nonlinear dynamical systems* (Cambridge Univ. Press, Cambridge 1989).
- [17.24] P. Cvitanović, "The power of chaos," in J.H. Kim and J. Stringer, eds., *Applied Chaos*, (John Wiley & Sons, New York 1992).
- [17.25] P. Cvitanović, ed., *Periodic Orbit Theory - theme issue, CHAOS* **2**, 1-158 (1992).
- [17.26] P. Cvitanović, "Dynamical averaging in terms of periodic orbits," *Physica D* **83**, 109 (1995).

Chapter 18

Trace formulas

The trace formula is not a formula, it is an idea.

—Martin Gutzwiller

DYNAMICS IS POSED in terms of local equations, but the ergodic averages require global information. How can we use a local description of a flow to learn something about the global behavior? In chapter 17 we have related global averages to the eigenvalues of appropriate evolution operators. Here we show that the traces of evolution operators can be evaluated as integrals over Dirac delta functions, and in this way the spectra of evolution operators become related to periodic orbits. If there is one idea that one should learn about chaotic dynamics, it happens in this chapter, and it is this: there is a fundamental local \leftrightarrow global duality which says that

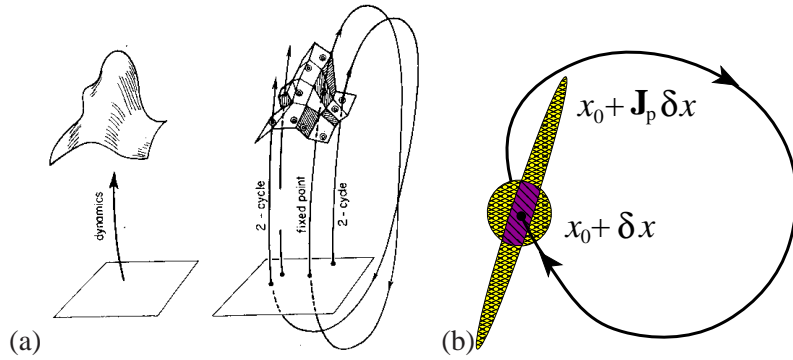
the spectrum of eigenvalues is dual to the spectrum of periodic orbits

For dynamics on the circle, this is called Fourier analysis; for dynamics on well-tiled manifolds, Selberg traces and zetas; and for generic nonlinear dynamical systems the duality is embodied in the trace formulas that we will now derive. These objects are to dynamics what partition functions are to statistical mechanics.

The above phrasing is a bit too highfalutin, so it perhaps pays to go again through the quick sketch of sects. 1.5 and 1.6. We have a state space that we would like to tessellate by periodic orbits, one short orbit per neighborhood, as in figure 18.1 (a). How big is the neighborhood of a given cycle?

Along stable directions neighbors of the periodic orbit get closer with time, so we only have to keep track of those who are moving away along the unstable directions. The fraction of those who remain in the neighborhood for one recurrence time T_p is given by the overlap ratio along the initial sphere and the returning ellipsoid, figure 18.1 (b), and along the expanding eigen-direction $\mathbf{e}^{(i)}$ of $J_p(x)$ this is given by the expanding Floquet multiplier $1/|\Lambda_{p,i}|$. A bit more

Figure 18.1: (a) Smooth dynamics tessellated by the skeleton of periodic points, together with their linearized neighborhoods. (b) Jacobian matrix J_p maps spherical neighborhood of $x_0 \rightarrow$ ellipsoidal neighborhood time T_p later, with the overlap ratio along the expanding eigdirection $e^{(i)}$ of $J_p(x)$ given by the expanding eigenvalue $1/|\Lambda_{p,i}|$.



thinking leads to the conclusion that one also cares about how long it takes to return (the long returns contributing less to the time averages), so the weight t_p of the p -neighborhood $t_p = e^{-sT_p}/|\Lambda_p|$ decreases exponentially both with the shortest recurrence period and the product (5.7) of expanding Floquet multipliers $\Lambda_p = \prod_e \Lambda_{p,e}$. With emphasis on *expanding* - the flow could be a 60,000-dimensional dissipative flow, and still the neighborhood is defined by the handful of expanding eigen-directions. Now the long-time average of a physical observable -let us say power D dissipated by viscous friction of a fluid flowing through a pipe- can be estimated by its mean value (17.6) D_p/T_p computed on each neighborhood, and weighted by the above estimate

$$\langle D \rangle \approx \sum_p \frac{D_p}{T_p} \frac{e^{-sT_p}}{|\Lambda_p|}.$$

Wrong in detail, this estimate is the crux of many a *Phys. Rev. Letter*, and in its essence the key result of this chapter, the ‘trace formula.’ Here we redo the argument in a bit greater depth, and derive the correct formula (20.20) for a long time average $\langle D \rangle$ as a weighted sum over periodic orbits. It will take three chapters, but it is worth it - the reward is an *exact* (i.e., not heuristic) and highly convergent and controllable formula for computing averages over chaotic flows.

18.1 A trace formula for maps

Our extraction of the spectrum of \mathcal{L} commences with the evaluation of the trace. As the case of discrete time mappings is somewhat simpler, we first derive the trace formula for maps, and then, in sect. 18.2, for flows. The final formula (18.23) covers both cases.

To compute an expectation value using (17.21) we have to integrate over all the values of the kernel $\mathcal{L}^n(x, y)$. Were \mathcal{L}^n a matrix sum over its matrix elements would be dominated by the leading eigenvalue as $n \rightarrow \infty$ (we went through the argument in some detail in sect. 15.1). As the trace of \mathcal{L}^n is also dominated by the leading eigenvalue as $n \rightarrow \infty$, we might just as well look at the trace for which we have a very explicit formula

exercise 15.3

$$\mathrm{tr} \mathcal{L}^n = \int dx \mathcal{L}^n(x, x) = \int dx \delta(x - f^n(x)) e^{\beta \cdot A^n(x)}. \quad (18.1)$$

On the other hand, by its matrix motivated definition, the trace is the sum over eigenvalues,

$$\mathrm{tr} \mathcal{L}^n = \sum_{\alpha=0}^{\infty} e^{s_{\alpha} n}. \quad (18.2)$$

We find it convenient to write the eigenvalues as exponents $e^{s_{\alpha}}$ rather than as multipliers λ_{α} , and we assume that spectrum of \mathcal{L} is discrete, s_0, s_1, s_2, \dots , ordered so that $\mathrm{Re} s_{\alpha} \geq \mathrm{Re} s_{\alpha+1}$.

For the time being we choose not to worry about convergence of such sums, ignore the question of what function space the eigenfunctions belong to, and compute the eigenvalue spectrum without constructing any explicit eigenfunctions. We shall revisit these issues in more depth in chapter 23, and discuss how lack of hyperbolicity leads to continuous spectra in chapter 24.

18.1.1 Hyperbolicity assumption

We have learned in sect. 16.2 how to evaluate the delta-function integral (18.1).

section 16.2

According to (16.8) the trace (18.1) picks up a contribution whenever $x - f^n(x) = 0$, i.e., whenever x belongs to a periodic orbit. For reasons which we will explain in sect. 18.2, it is wisest to start by focusing on discrete time systems. The contribution of an isolated prime cycle p of period n_p for a map f can be evaluated by restricting the integration to an infinitesimal open neighborhood \mathcal{M}_p around the cycle,

$$\begin{aligned} \mathrm{tr}_p \mathcal{L}^{n_p} &= \int_{\mathcal{M}_p} dx \delta(x - f^{n_p}(x)) \\ &= \frac{n_p}{|\det(\mathbf{1} - M_p)|} = n_p \prod_{i=1}^d \frac{1}{|1 - \Lambda_{p,i}|}. \end{aligned} \quad (18.3)$$

For the time being we set here and in (16.9) the observable $e^{\beta A_p} = 1$. Periodic orbit Jacobian matrix M_p is also known as the *monodromy matrix*, and its eigenvalues $\Lambda_{p,1}, \Lambda_{p,2}, \dots, \Lambda_{p,d}$ as the Floquet multipliers.

section 5.1.2

We sort the eigenvalues $\Lambda_{p,1}, \Lambda_{p,2}, \dots, \Lambda_{p,d}$ of the p -cycle $[d \times d]$ monodromy matrix M_p into expanding, marginal and contracting sets $\{e, m, c\}$, as in (5.6). As the integral (18.3) can be evaluated only if M_p has no eigenvalue of unit magnitude, we assume that no eigenvalue is marginal (we shall show in sect. 18.2 that the longitudinal $\Lambda_{p,d+1} = 1$ eigenvalue for flows can be eliminated by restricting

the consideration to the transverse monodromy matrix M_p), and factorize the trace (18.3) into a product over the expanding and the contracting eigenvalues

$$\left| \det(\mathbf{1} - M_p) \right|^{-1} = \frac{1}{|\Lambda_p|} \prod_e \frac{1}{1 - 1/\Lambda_{p,e}} \prod_c \frac{1}{1 - \Lambda_{p,c}}, \quad (18.4)$$

where $\Lambda_p = \prod_e \Lambda_{p,e}$ is the product of expanding eigenvalues. Both $\Lambda_{p,c}$ and $1/\Lambda_{p,e}$ are smaller than 1 in absolute value, and as they are either real or come in complex conjugate pairs we are allowed to drop the absolute value brackets $|\cdots|$ in the above products.

The *hyperbolicity assumption* requires that the stabilities of all cycles included in the trace sums be exponentially bounded away from unity:

$$\begin{aligned} |\Lambda_{p,e}| &> e^{\lambda_e T_p} && \text{any } p, \text{ any expanding } |\Lambda_{p,e}| > 1 \\ |\Lambda_{p,c}| &< e^{-\lambda_c T_p} && \text{any } p, \text{ any contracting } |\Lambda_{p,c}| < 1, \end{aligned} \quad (18.5)$$

where $\lambda_e, \lambda_c > 0$ are strictly positive bounds on the expanding, contracting cycle Lyapunov exponents. If a dynamical system satisfies the hyperbolicity assumption (for example, the well separated 3-disk system clearly does), the \mathcal{L} spectrum will be relatively easy to control. If the expansion/contraction is slower than exponential, let us say $|\Lambda_{p,i}| \sim T_p^2$, the system may exhibit “phase transitions,” and the analysis is much harder - we shall discuss this in chapter 24.

Example 18.1 Elliptic stability. *Elliptic stability, i.e., a pair of purely imaginary exponents $\Lambda_m = e^{\pm i\theta}$ is excluded by the hyperbolicity assumption. While the contribution of a single repeat of a cycle*

$$\frac{1}{(1 - e^{i\theta})(1 - e^{-i\theta})} = \frac{1}{2(1 - \cos \theta)} \quad (18.6)$$

does not make (16.9) diverge, if $\Lambda_m = e^{i2\pi p/r}$ is r th root of unity, $1/|\det(\mathbf{1} - M_p^r)|$ diverges. For a generic θ repeats $\cos(r\theta)$ behave badly and by ergodicity $1 - \cos(r\theta)$ is arbitrarily small, $1 - \cos(r\theta) < \epsilon$, infinitely often. This goes by the name of “small divisor problem,” and requires a separate treatment.

It follows from (18.4) that for long times, $t = rT_p \rightarrow \infty$, only the product of expanding eigenvalues matters, $|\det(\mathbf{1} - M_p^r)| \rightarrow |\Lambda_p|^r$. We shall use this fact to motivate the construction of dynamical zeta functions in sect. 19.3. However, for evaluation of the full spectrum the exact cycle weight (18.3) has to be kept.

18.1.2 A classical trace formula for maps

If the evolution is given by a discrete time mapping, and all periodic points have Floquet multipliers $|\Lambda_{p,i}| \neq 1$ strictly bounded away from unity, the trace \mathcal{L}^n is

given by the sum over all *periodic points* i of period n :

$$\text{tr } \mathcal{L}^n = \int dx \mathcal{L}^n(x, x) = \sum_{x_i \in \text{Fix } f^n} \frac{e^{\beta \cdot A_i}}{|\det(\mathbf{1} - M^n(x_i))|}. \quad (18.7)$$

Here $\text{Fix } f^n = \{x : f^n(x) = x\}$ is the set of all periodic points of period n , and A_i is the observable (17.5) evaluated over n discrete time steps along the cycle to which the periodic point x_i belongs. The weight follows from the properties of the Dirac delta function (16.8) by taking the determinant of $\partial_i(x_j - f^n(x)_j)$. If a trajectory retraces itself r times, its monodromy matrix is M_p^r , where M_p is the $[d \times d]$ monodromy matrix (4.6) evaluated along a single traversal of the prime cycle p . As we saw in (17.5), the integrated observable A^n is additive along the cycle: If a prime cycle p trajectory retraces itself r times, $n = rn_p$, we obtain A_p repeated r times, $A_i = A^n(x_i) = rA_p$, $x_i \in \mathcal{M}_p$.

A prime cycle is a single traversal of the orbit, and its label is a non-repeating symbol string. There is only one prime cycle for each cyclic permutation class. For example, the four periodic points $\overline{0011} = \overline{1001} = \overline{1100} = \overline{0110}$ belong to the same prime cycle $p = 0011$ of length 4. As both the stability of a cycle and the weight A_p are the same everywhere along the orbit, each prime cycle of length n_p contributes n_p terms to the sum, one for each periodic point. Hence (18.7) can be rewritten as a sum over all prime cycles and their repeats

chapter 11

$$\text{tr } \mathcal{L}^n = \sum_p n_p \sum_{r=1}^{\infty} \frac{e^{r\beta \cdot A_p}}{|\det(\mathbf{1} - M_p^r)|} \delta_{n, n_p r}, \quad (18.8)$$

with the Kronecker delta $\delta_{n, n_p r}$ projecting out the periodic contributions of total period n . This constraint is awkward, and will be more awkward still for the continuous time flows, where it would yield a series of Dirac delta spikes. In both cases a Laplace transform rids us of the time periodicity constraint.

In the sum over all cycle periods,

$$\sum_{n=1}^{\infty} z^n \text{tr } \mathcal{L}^n = \text{tr} \frac{z\mathcal{L}}{1 - z\mathcal{L}} = \sum_p n_p \sum_{r=1}^{\infty} \frac{z^{n_p r} e^{r\beta \cdot A_p}}{|\det(\mathbf{1} - M_p^r)|}, \quad (18.9)$$

the constraint $\delta_{n, n_p r}$ is replaced by weight z^n . Such discrete time Laplace transform of $\text{tr } \mathcal{L}^n$ is usually referred to as a “generating function.” Why this transform? We are actually not interested in evaluating the sum (18.8) for any particular fixed period n ; what we are interested in is the long time $n \rightarrow \infty$ behavior. The transform trades in the large time n behavior for the small z behavior. Expressing the trace as in (18.2), in terms of the sum of the eigenvalues of \mathcal{L} , we obtain the *trace formula for maps*:

$$\sum_{\alpha=0}^{\infty} \frac{ze^{s_\alpha}}{1 - ze^{s_\alpha}} = \sum_p n_p \sum_{r=1}^{\infty} \frac{z^{n_p r} e^{r\beta \cdot A_p}}{|\det(\mathbf{1} - M_p^r)|}. \quad (18.10)$$

This is our second example of the duality between the spectrum of eigenvalues and the spectrum of periodic orbits, announced in the introduction to this chapter. (The first example was the topological trace formula (15.10).)



fast track:
sect. 18.2, p. 353

Example 18.2 A trace formula for transfer operators: For a piecewise-linear map (17.17), we can explicitly evaluate the trace formula. By the piecewise linearity and the chain rule $\Lambda_p = \Lambda_0^{n_0} \Lambda_1^{n_1}$, where the cycle p contains n_0 symbols 0 and n_1 symbols 1, the trace (18.7) reduces to

$$\text{tr } \mathcal{L}^n = \sum_{m=0}^n \binom{n}{m} \frac{1}{|1 - \Lambda_0^m \Lambda_1^{n-m}|} = \sum_{k=0}^{\infty} \left(\frac{1}{|\Lambda_0| \Lambda_0^k} + \frac{1}{|\Lambda_1| \Lambda_1^k} \right)^n, \tag{18.11}$$

with eigenvalues

$$e^{sk} = \frac{1}{|\Lambda_0| \Lambda_0^k} + \frac{1}{|\Lambda_1| \Lambda_1^k}. \tag{18.12}$$

As the simplest example of spectrum for such dynamical system, consider the symmetric piecewise-linear 2-branch repeller (17.17) for which $\Lambda = \Lambda_1 = -\Lambda_0$. In this case all odd eigenvalues vanish, and the even eigenvalues are given by $e^{sk} = 2/\Lambda^{k+1}$, k even. exercise 16.7

Asymptotically the spectrum (18.12) is dominated by the lesser of the two fixed point slopes $\Lambda = \Lambda_0$ (if $|\Lambda_0| < |\Lambda_1|$, otherwise $\Lambda = \Lambda_1$), and the eigenvalues e^{sk} fall off exponentially as $1/\Lambda^k$, dominated by the single less unstable fixed-point. example 23.1

For $k = 0$ this is in agreement with the explicit transfer matrix (17.19) eigenvalues (17.20). The alert reader should experience anxiety at this point. Is it not true that we have already written down explicitly the transfer operator in (17.19), and that it is clear by inspection that it has only one eigenvalue $e^{s_0} = 1/|\Lambda_0| + 1/|\Lambda_1|$? The example at hand is one of the simplest illustrations of necessity of defining the space that the operator acts on in order to define the spectrum. The transfer operator (17.19) is the correct operator on the space of functions piecewise constant on the state space partition $\{\mathcal{M}_0, \mathcal{M}_1\}$; on this space the operator indeed has only the eigenvalue e^{s_0} . As we shall see in example 23.1, the full spectrum (18.12) corresponds to the action of the transfer operator on the space of real analytic functions.

The Perron-Frobenius operator trace formula for the piecewise-linear map (17.17) follows from (18.9)

$$\text{tr } \frac{z\mathcal{L}}{1 - z\mathcal{L}} = \frac{z \left(\frac{1}{|\Lambda_0 - 1|} + \frac{1}{|\Lambda_1 - 1|} \right)}{1 - z \left(\frac{1}{|\Lambda_0 - 1|} + \frac{1}{|\Lambda_1 - 1|} \right)}, \tag{18.13}$$

verifying the trace formula (18.10).

18.2 A trace formula for flows

Amazing! I did not understand a single word.

—Fritz Haake

(R. Artuso and P. Cvitanović)

Our extraction of the spectrum of \mathcal{L}^t commences with the evaluation of the trace

$$\mathrm{tr} \mathcal{L}^t = \mathrm{tr} e^{\mathcal{A}t} = \int dx \mathcal{L}^t(x, x) = \int dx \delta(x - f^t(x)) e^{\beta \cdot \mathcal{A}^t(x)}. \quad (18.14)$$

We are not interested in any particular time t , but into the long-time behavior as $t \rightarrow \infty$, so we need to transform the trace from the “time domain” into the “frequency domain.” A generic flow is a semi-flow defined forward in time, so the appropriate transform is a Laplace rather than Fourier.

For a continuous time flow, the Laplace transform of an evolution operator yields the resolvent (16.31). This is a delicate step, since the evolution operator becomes the identity in the $t \rightarrow 0^+$ limit. In order to make sense of the trace we regularize the Laplace transform by a lower cutoff ϵ smaller than the period of any periodic orbit, and write

$$\int_{\epsilon}^{\infty} dt e^{-st} \mathrm{tr} \mathcal{L}^t = \mathrm{tr} \frac{e^{-(s-\mathcal{A})\epsilon}}{s - \mathcal{A}} = \sum_{\alpha=0}^{\infty} \frac{e^{-(s-s_{\alpha})\epsilon}}{s - s_{\alpha}}, \quad (18.15)$$

where \mathcal{A} is the generator of the semigroup of dynamical evolution, see sect. 16.5. Our task is to evaluate $\mathrm{tr} \mathcal{L}^t$ from its explicit state space representation.

18.2.1 Integration along the flow

As any pair of nearby points on a cycle returns to itself exactly at each cycle period, the eigenvalue of the Jacobian matrix corresponding to the eigenvector along the flow necessarily equals unity for all periodic orbits. Hence for flows the trace integral $\mathrm{tr} \mathcal{L}^t$ requires a separate treatment for the longitudinal direction. To evaluate the contribution of an isolated prime cycle p of period T_p , restrict the integration to an infinitesimally thin tube \mathcal{M}_p enveloping the cycle (see figure 1.12), and consider a local coordinate system with a longitudinal coordinate dx_{\parallel} along the direction of the flow, and $d-1$ transverse coordinates x_{\perp} ,

section 5.2.1

$$\mathrm{tr}_p \mathcal{L}^t = \int_{\mathcal{M}_p} dx_{\perp} dx_{\parallel} \delta(x_{\perp} - f_{\perp}^t(x)) \delta(x_{\parallel} - f_{\parallel}^t(x_{\parallel})). \quad (18.16)$$

(we set $\beta = 0$ in the $\exp(\beta \cdot A^t)$ weight for the time being). Pick a point on the prime cycle p , and let

$$v(x_{||}) = \left(\sum_{i=1}^d v_i(x)^2 \right)^{1/2} \quad (18.17)$$

be the magnitude of the tangential velocity at any point $x = (x_{||}, 0, \dots, 0)$ on the cycle p . The velocity $v(x)$ must be strictly positive, as otherwise the orbit would stagnate for infinite time at $v(x) = 0$ points, and that would get us nowhere.

As $0 \leq \tau < T_p$, the trajectory $x_{||}(\tau) = f^\tau(x_p)$ sweeps out the entire cycle, and for larger times $x_{||}$ is a cyclic variable of periodicity T_p ,

$$x_{||}(\tau) = x_{||}(\tau + rT_p) \quad r = 1, 2, \dots \quad (18.18)$$

We parametrize both the longitudinal coordinate $x_{||}(\tau)$ and the velocity $v(\tau) = v(x_{||}(\tau))$ by the flight time τ , and rewrite the integral along the periodic orbit as

$$\oint_p dx_{||} \delta(x_{||} - f^t(x_{||})) = \oint_p d\tau v(\tau) \delta(x_{||}(\tau) - x_{||}(\tau + t)). \quad (18.19)$$

By the periodicity condition (18.18) the Dirac δ function picks up contributions for $t = rT_p$, so the Laplace transform can be split as

$$\begin{aligned} \int_0^\infty dt e^{-st} \delta(x_{||}(\tau) - x_{||}(\tau + t)) &= \sum_{r=1}^\infty e^{-sT_p r} I_r \\ I_r &= \int_{-\epsilon}^\epsilon dt e^{-st} \delta(x_{||}(\tau) - x_{||}(\tau + rT_p + t)). \end{aligned}$$

Taylor expanding and applying the periodicity condition (18.18), we have $x_{||}(\tau + rT_p + t) = x_{||}(\tau) + v(\tau)t + \dots$,

$$I_r = \int_{-\epsilon}^\epsilon dt e^{-st} \delta(x_{||}(\tau) - x_{||}(\tau + rT_p + t)) = \frac{1}{v(\tau)},$$

so the remaining integral (18.19) over τ is simply the cycle period $\oint_p d\tau = T_p$. The contribution of the longitudinal integral to the Laplace transform is thus

$$\int_0^\infty dt e^{-st} \oint_p dx_{||} \delta(x_{||} - f^t(x_{||})) = T_p \sum_{r=1}^\infty e^{-sT_p r}. \quad (18.20)$$

This integration is a prototype of what needs to be done for each marginal direction, whenever existence of a conserved quantity (energy in Hamiltonian flows, angular momentum, translational invariance, etc.) implies existence of a smooth manifold of equivalent (equivariant) solutions of dynamical equations.

18.2.2 Stability in the transverse directions

Think of the $\tau = 0$ point in above integrals along the cycle p as a choice of a particular Poincaré section. As we have shown in sect. 5.3, the transverse Floquet multipliers do not depend on the choice of a Poincaré section, so ignoring the dependence on $x_{||}(\tau)$ in evaluating the transverse integral in (18.16) is justified. For the transverse integration variables the Jacobian matrix is defined in a reduced Poincaré surface of section \mathcal{P} of fixed $x_{||}$. Linearization of the periodic flow transverse to the orbit yields

$$\int_{\mathcal{P}} dx_{\perp} \delta(x_{\perp} - f_{\perp}^{rT_p}(x)) = \frac{1}{|\det(\mathbf{1} - M_p^r)|}, \quad (18.21)$$

where M_p is the p -cycle $[d-1 \times d-1]$ transverse monodromy matrix. As in (18.5) we have to assume hyperbolicity, i.e., that the magnitudes of all transverse eigenvalues are bounded away from unity.

Substitution (18.20), (18.21) in (18.16) leads to an expression for $\text{tr } \mathcal{L}^t$ as a sum over all prime cycles p and their repetitions

$$\int_{\epsilon}^{\infty} dt e^{-st} \text{tr } \mathcal{L}^t = \sum_p T_p \sum_{r=1}^{\infty} \frac{e^{r(\beta \cdot A_p - sT_p)}}{|\det(\mathbf{1} - M_p^r)|}. \quad (18.22)$$

The $\epsilon \rightarrow 0$ limit of the two expressions for the resolvent, (18.15) and (18.22), now yields the *classical trace formula for flows*

$$\sum_{\alpha=0}^{\infty} \frac{1}{s - s_{\alpha}} = \sum_p T_p \sum_{r=1}^{\infty} \frac{e^{r(\beta \cdot A_p - sT_p)}}{|\det(\mathbf{1} - M_p^r)|}. \quad (18.23)$$

exercise 18.1

(If you are worried about the convergence of the resolvent sum, keep the ϵ regularization.)

This formula is still another example of the duality between the (local) cycles and (global) eigenvalues. If T_p takes only integer values, we can replace $e^{-s} \rightarrow z$ throughout, so the trace formula for maps (18.10) is a special case of the trace formula for flows. The relation between the continuous and discrete time cases can be summarized as follows:

$$\begin{aligned} T_p &\leftrightarrow n_p \\ e^{-s} &\leftrightarrow z \\ e^{t\mathcal{A}} &\leftrightarrow \mathcal{L}^n. \end{aligned} \quad (18.24)$$

We could now proceed to estimate the location of the leading singularity of $\text{tr}(s - \mathcal{A})^{-1}$ by extrapolating finite cycle length truncations of (18.23) by methods

such as Padé approximants. However, it pays to first perform a simple resummation which converts this divergence of a trace into a *zero* of a spectral determinant. We shall do this in sect. 19.2, but first a brief refresher of how all this relates to the formula for escape rate (1.8) offered in the introduction might help digest the material.



fast track:
sect. 19, p. 360

18.3 An asymptotic trace formula



In order to illuminate the manipulations of sect. 18.1 and relate them to something we already possess intuition about, we now rederive the heuristic sum of sect. 1.5.1 from the exact trace formula (18.10). The Laplace transforms (18.10) or (18.23) are designed to capture the time $\rightarrow \infty$ asymptotic behavior of the trace sums. By the hyperbolicity assumption (18.5), for $t = T_p r$ large the cycle weight approaches

$$\left| \det(\mathbf{1} - M_p^r) \right| \rightarrow |\Lambda_p|^r, \tag{18.25}$$

where Λ_p is the product of the expanding eigenvalues of M_p . Denote the corresponding approximation to the n th trace (18.7) by

$$\Gamma_n = \sum_i^{(n)} \frac{1}{|\Lambda_i|}, \tag{18.26}$$

and denote the approximate trace formula obtained by replacing the cycle weights $\left| \det(\mathbf{1} - M_p^r) \right|$ by $|\Lambda_p|^r$ in (18.10) by $\Gamma(z)$. Equivalently, think of this as a replacement of the evolution operator (17.23) by a transfer operator (as in example 18.2). For concreteness consider a dynamical system whose symbolic dynamics is complete binary, for example the 3-disk system figure 1.6. In this case distinct periodic points that contribute to the n th periodic points sum (18.8) are labeled by all admissible itineraries composed of sequences of letters $s \in \{0, 1\}$:

$$\begin{aligned} \Gamma(z) &= \sum_{n=1}^{\infty} z^n \Gamma_n = \sum_{n=1}^{\infty} z^n \sum_{x_i \in \text{Fix} f^n} \frac{e^{\beta \cdot A^n(x_i)}}{|\Lambda_i|} \\ &= z \left\{ \frac{e^{\beta \cdot A_0}}{|\Lambda_0|} + \frac{e^{\beta \cdot A_1}}{|\Lambda_1|} \right\} + z^2 \left\{ \frac{e^{2\beta \cdot A_0}}{|\Lambda_0|^2} + \frac{e^{\beta \cdot A_{01}}}{|\Lambda_{01}|} + \frac{e^{\beta \cdot A_{10}}}{|\Lambda_{10}|} + \frac{e^{2\beta \cdot A_1}}{|\Lambda_1|^2} \right\} \\ &\quad + z^3 \left\{ \frac{e^{3\beta \cdot A_0}}{|\Lambda_0|^3} + \frac{e^{\beta \cdot A_{001}}}{|\Lambda_{001}|} + \frac{e^{\beta \cdot A_{010}}}{|\Lambda_{010}|} + \frac{e^{\beta \cdot A_{100}}}{|\Lambda_{100}|} + \dots \right\} \end{aligned} \tag{18.27}$$

Both the cycle averages A_i and the stabilities Λ_i are the same for all points $x_i \in \mathcal{M}_p$ in a cycle p . Summing over repeats of all prime cycles we obtain

$$\Gamma(z) = \sum_p \frac{n_p t_p}{1 - t_p}, \quad t_p = z^{n_p} e^{\beta \cdot A_p} / |\Lambda_p|. \quad (18.28)$$

This is precisely our initial heuristic estimate (1.9). Note that we could not perform such sum over r in the exact trace formula (18.10) as $|\det(\mathbf{1} - M_p^r)| \neq |\det(\mathbf{1} - M_p)|^r$; the correct way to resum the exact trace formulas is to first expand the factors $1/|1 - \Lambda_{p,i}|$, as we shall do in (19.9).

section 19.2

If the weights $e^{\beta A^n(x)}$ are multiplicative along the flow, and the flow is hyperbolic, for given β the magnitude of each $|e^{\beta A^n(x_i)} / \Lambda_i|$ term is bounded by some constant M^n . The total number of cycles grows as 2^n (or as e^{hn} , $h =$ topological entropy, in general), and the sum is convergent for z sufficiently small, $|z| < 1/2M$. For large n the n th level sum (18.7) tends to the leading \mathcal{L}^n eigenvalue e^{ns_0} . Summing this asymptotic estimate level by level

$$\Gamma(z) \approx \sum_{n=1}^{\infty} (ze^{s_0})^n = \frac{ze^{s_0}}{1 - ze^{s_0}} \quad (18.29)$$

we see that we should be able to determine s_0 by determining the smallest value of $z = e^{-s_0}$ for which the cycle expansion (18.28) diverges.

If one is interested only in the leading eigenvalue of \mathcal{L} , it suffices to consider the approximate trace $\Gamma(z)$. We will use this fact in sect. 19.3 to motivate the introduction of dynamical zeta functions (19.14), and in sect. 19.5 we shall give the exact relation between the exact and the approximate trace formulas.

Résumé

The description of a chaotic dynamical system in terms of cycles can be visualized as a tessellation of the dynamical system, figure 18.1, with a smooth flow approximated by its *periodic orbit skeleton*, each region \mathcal{M}_i centered on a periodic point x_i of the topological length n , and the size of the region determined by the linearization of the flow around the periodic point. The integral over such topologically partitioned state space yields the *classical trace formula*

$$\sum_{\alpha=0}^{\infty} \frac{1}{s - s_{\alpha}} = \sum_p T_p \sum_{r=1}^{\infty} \frac{e^{r(\beta \cdot A_p - s T_p)}}{|\det(\mathbf{1} - M_p^r)|}.$$

Now that we have a trace formula, we might ask for what is it good? As it stands, it is little more than a scary divergent formula which relates the unspeakable infinity

of global eigenvalues to the unthinkable infinity of local unstable cycles. However, it is a good stepping stone on the way to construction of spectral determinants (to which we turn next), and a first hint that when the going is good, the theory might turn out to be convergent beyond our wildest dreams (chapter 23). In order to implement such formulas, we will have to determine “all” prime cycles. The first step is topological: enumeration of all admissible cycles undertaken in chapter 12. The more onerous enterprise of actually computing the cycles we first approach traditionally, as a numerical task in chapter 13, and then more boldly as a part and parcel of variational foundations of classical and quantum dynamics in chapter 29.

Commentary

Remark 18.1 Who’s done it? Continuous time flow traces weighted by cycle periods were introduced by Bowen [1] who treated them as Poincaré section suspensions weighted by the “time ceiling” function (3.5). They were used by Parry and Pollicott [2].

Remark 18.2 Flat and sharp traces. In the above formal derivation of trace formulas we cared very little whether our sums were well posed. In the Fredholm theory traces like (18.14) require compact operators with continuous function kernels. This is not the case for our Dirac delta evolution operators: nevertheless, there is a large class of dynamical systems for which our results may be shown to be perfectly legal. In the mathematical literature expressions like (18.7) are called *flat* traces (see the review [4] and chapter 23). Other names for traces appear as well: for instance, in the context of 1 – dimensional mappings, *sharp* traces refer to generalizations of (18.7) where contributions of periodic points are weighted by the Lefschetz sign ± 1 , reflecting whether the periodic point sits on a branch of n th iterate of the map which crosses the diagonal starting from below or starting from above [10]. Such traces are connected to the theory of kneading invariants (see ref. [4] and references therein). Traces weighted by ± 1 sign of the derivative of the fixed point have been used to study the period doubling repeller, leading to high precision estimates of the Feigenbaum constant δ , refs. [5, 6, 6].

Exercises

18.1. $t \rightarrow 0_+$ **regularization of eigenvalue sums**.** In taking the Laplace transform (18.23) we have ignored the $t \rightarrow 0_+$ divergence, as we do not know how to regularize the delta function kernel in this limit. In the quantum (or heat kernel) case this limit gives rise to the Weyl or Thomas-Fermi mean eigenvalue spacing. Regularize the divergent sum in (18.23) and assign to such volume

term some interesting role in the theory of classical resonance spectra. E-mail the solution to the authors.

18.2. **General weights.** (easy) Let f^t be a flow and \mathcal{L}^t the operator

$$\mathcal{L}^t g(x) = \int dy \delta(x - f^t(y)) w(t, y) g(y)$$

where w is a weight function. In this problem we will try and determine some of the properties w must satisfy.

- (a) Compute $\mathcal{L}^s \mathcal{L}^t g(x)$ to show that

$$w(s, f^t(x))w(t, x) = w(t + s, x).$$

- (b) Restrict t and s to be integers and show that the

most general form of w is

$$w(n, x) = g(x)g(f(x))g(f^2(x)) \cdots g(f^{n-1}(x)),$$

for some g that can be multiplied. Could g be a function from $\mathbb{R}^{n_1} \mapsto \mathbb{R}^{n_2}$? ($n_i \in \mathbb{N}$.)

References

- [18.1] R. Bowen, *Equilibrium states and the ergodic theory of Anosov diffeomorphisms*, Springer Lecture Notes in Math. **470** (1975).
- [18.2] W. Parry and M. Pollicott, *Zeta Functions and the periodic Structure of Hyperbolic Dynamics*, *Astérisque* **187–188** (Société Mathématique de France, Paris 1990).
- [18.3] P. Cvitanović and B. Eckhardt, *J. Phys.* **A 24**, L237 (1991).
- [18.4] V. Baladi and D. Ruelle, *Ergodic Theory Dynamical Systems* **14**, 621 (1994).
- [18.5] R. Artuso, E. Aurell and P. Cvitanović, *Nonlinearity* **3**, 325 (1990); 361 (1990).
- [18.6] M. Pollicott, *J. Stat. Phys.* **62**, 257 (1991).

Chapter 19

Spectral determinants

“It seems very pretty,” she said when she had finished it, “but it’s rather hard to understand!” (You see she didn’t like to confess, even to herself, that she couldn’t make it out at all.) “Somehow it seems to fill my head with ideas — only I don’t exactly know what they are!”

—Lewis Carroll, *Through the Looking Glass*

THE PROBLEM with the trace formulas (18.10), (18.23) and (18.28) is that they diverge at $z = e^{-s_0}$, respectively $s = s_0$, i.e., precisely where one would like to use them. While this does not prevent numerical estimation of some “thermodynamic” averages for iterated mappings, in the case of the Gutzwiller trace formula this leads to a perplexing observation that crude estimates of the radius of convergence seem to put the entire physical spectrum out of reach. We shall now cure this problem by thinking, at no extra computational cost; while traces and determinants are formally equivalent, determinants are the tool of choice when it comes to computing spectra. Determinants tend to have larger analyticity domains because if $\text{tr } \mathcal{L}/(1 - z\mathcal{L}) = -\frac{d}{dz} \ln \det(1 - z\mathcal{L})$ diverges at a particular value of z , then $\det(1 - z\mathcal{L})$ might have an isolated zero there, and a zero of a function is easier to determine numerically than its poles.

chapter 23

19.1 Spectral determinants for maps

The eigenvalues z_k of a linear operator are given by the zeros of the determinant

$$\det(1 - z\mathcal{L}) = \prod_k (1 - z/z_k). \quad (19.1)$$

For finite matrices this is the characteristic determinant; for operators this is the Hadamard representation of the *spectral determinant* (sparing the reader from

pondering possible regularization factors). Consider first the case of maps, for which the evolution operator advances the densities by integer steps in time. In this case we can use the formal matrix identity

exercise 4.1

$$\ln \det(1 - M) = \operatorname{tr} \ln(1 - M) = - \sum_{n=1}^{\infty} \frac{1}{n} \operatorname{tr} M^n, \tag{19.2}$$

to relate the spectral determinant of an evolution operator for a map to its traces (18.8), and hence to periodic orbits:

$$\begin{aligned} \det(1 - z\mathcal{L}) &= \exp\left(- \sum_n \frac{z^n}{n} \operatorname{tr} \mathcal{L}^n\right) \\ &= \exp\left(- \sum_p \sum_{r=1}^{\infty} \frac{1}{r} \frac{z^{n_p r} e^{r\beta \cdot A_p}}{|\det(\mathbf{1} - M_p^r)|}\right). \end{aligned} \tag{19.3}$$

Going the other way, the trace formula (18.10) can be recovered from the spectral determinant by taking a derivative

$$\operatorname{tr} \frac{z\mathcal{L}}{1 - z\mathcal{L}} = -z \frac{d}{dz} \ln \det(1 - z\mathcal{L}). \tag{19.4}$$



fast track:
sect. 19.2, p. 362

Example 19.1 Spectral determinants of transfer operators:



For a piecewise-linear map (17.17) with a finite Markov partition, an explicit formula for the spectral determinant follows by substituting the trace formula (18.11) into (19.3):

$$\det(1 - z\mathcal{L}) = \prod_{k=0}^{\infty} \left(1 - \frac{t_0}{\Lambda_0^k} - \frac{t_1}{\Lambda_1^k}\right), \tag{19.5}$$

where $t_s = z/|\Lambda_s|$. The eigenvalues are necessarily the same as in (18.12), which we already determined from the trace formula (18.10).

The exponential spacing of eigenvalues guarantees that the spectral determinant (19.5) is an entire function. It is this property that generalizes to piecewise smooth flows with finite Markov partitions, and singles out spectral determinants rather than the trace formulas or dynamical zeta functions as the tool of choice for evaluation of spectra.

19.2 Spectral determinant for flows

... an analogue of the [Artin-Mazur] zeta function for diffeomorphisms seems quite remote for flows. However we will mention a wild idea in this direction. [...] define $l(\gamma)$ to be the minimal period of γ [...] then define formally (another zeta function!) $Z(s)$ to be the infinite product

$$Z(s) = \prod_{\gamma \in \Gamma} \prod_{k=0}^{\infty} (1 - [\exp l(\gamma)]^{-s-k}).$$

—Stephen Smale, *Differentiable Dynamical Systems*

We write the formula for the spectral determinant for flows by analogy to (19.3)

$$\det(s - \mathcal{A}) = \exp \left(- \sum_p \sum_{r=1}^{\infty} \frac{1}{r} \frac{e^{r(\beta \cdot A_p - s T_p)}}{|\det(\mathbf{1} - M_p^r)|} \right), \tag{19.6}$$

and then check that the trace formula (18.23) is the logarithmic derivative of the spectral determinant

$$\text{tr} \frac{1}{s - \mathcal{A}} = \frac{d}{ds} \ln \det(s - \mathcal{A}). \tag{19.7}$$

With z set to $z = e^{-s}$ as in (18.24), the spectral determinant (19.6) has the same form for both maps and flows. We refer to (19.6) as *spectral determinant*, as the spectrum of the operator \mathcal{A} is given by the zeros of

$$\det(s - \mathcal{A}) = 0. \tag{19.8}$$

We now note that the r sum in (19.6) is close in form to the expansion of a logarithm. This observation enables us to recast the spectral determinant into an infinite product over periodic orbits as follows:

Let M_p be the p -cycle $[d \times d]$ transverse Jacobian matrix, with eigenvalues $\Lambda_{p,1}, \Lambda_{p,2}, \dots, \Lambda_{p,d}$. Expanding the expanding eigenvalue factors $1/(1 - 1/\Lambda_{p,e})$ and the contracting eigenvalue factors $1/(1 - \Lambda_{p,c})$ in (18.4) as geometric series, substituting back into (19.6), and resumming the logarithms, we find that the spectral determinant is formally given by the infinite product

$$\det(s - \mathcal{A}) = \prod_{k_1=0}^{\infty} \dots \prod_{l_c=0}^{\infty} \frac{1}{\zeta_{k_1 \dots l_c}}$$

$$1/\zeta_{k_1 \dots l_c} = \prod_p \left(1 - t_p \frac{\Lambda_{p,e+1}^{l_1} \Lambda_{p,e+2}^{l_2} \dots \Lambda_{p,d}^{l_c}}{\Lambda_{p,1}^{k_1} \Lambda_{p,2}^{k_2} \dots \Lambda_{p,e}^{k_e}} \right) \tag{19.9}$$

$$t_p = t_p(z, s, \beta) = \frac{1}{|\Lambda_p|} e^{\beta \cdot A_p - s T_p} z^{n_p}. \tag{19.10}$$

In such formulas t_p is a weight associated with the p cycle (letter t refers to the “local trace” evaluated along the p cycle trajectory), and the index p runs through all distinct prime cycles. Why the factor z^{t_p} ? It is associated with the trace formula (18.10) for maps, whereas the factor e^{-sT_p} is specific to the continuous time trace formul (18.23); according to (18.24) we should use either one or the other. But we have learned in sect. 3.1 that flows can be represented either by their continuous-time trajectories, or by their topological time Poincaré section return maps. In cases when we have good control over the topology of the flow, it is often convenient to insert the z^{t_p} factor into cycle weights, as a formal parameter which keeps track of the topological cycle lengths. These factors will assist us in expanding zeta functions and determinants, eventually we shall set $z = 1$. The subscripts e, c indicate that there are e expanding eigenvalues, and c contracting eigenvalues. The observable whose average we wish to compute contributes through the $A^t(x)$ term in the p cycle multiplicative weight $e^{\beta A_p}$. By its definition (17.1), the weight for maps is a product along the periodic points

chapter 20

$$e^{A_p} = \prod_{j=0}^{n_p-1} e^{a(f^j(x_p))},$$

and the weight for flows is an exponential of the integral (17.5) along the cycle

$$e^{A_p} = \exp\left(\int_0^{T_p} a(x(\tau))d\tau\right).$$

This formula is correct for scalar weighting functions; more general matrix valued weights require a time-ordering prescription as in the Jacobian matrix of sect.4.1.

Example 19.2 Expanding 1–dimensional map:  For expanding 1–dimensional mappings the spectral determinant (19.9) takes the form

$$\det(1 - z\mathcal{L}) = \prod_p \prod_{k=0}^{\infty} (1 - t_p/\Lambda_p^k), \quad t_p = \frac{e^{\beta A_p}}{|\Lambda_p|} z^{n_p}. \tag{19.11}$$

Example 19.3 Two-degree of freedom Hamiltonian flows: For a 2-degree of freedom Hamiltonian flows the energy conservation eliminates on phase space variable, and restriction to a Poincaré section eliminates the marginal longitudinal eigenvalue $\Lambda = 1$, so a periodic orbit of 2-degree of freedom hyperbolic Hamiltonian flow has one expanding transverse eigenvalue Λ , $|\Lambda| > 1$, and one contracting transverse eigenvalue $1/\Lambda$. The weight in (18.4) is expanded as follows:

$$\frac{1}{|\det(\mathbf{1} - M_p^r)|} = \frac{1}{|\Lambda|^r (1 - 1/\Lambda_p^r)^2} = \frac{1}{|\Lambda|^r} \sum_{k=0}^{\infty} \frac{k+1}{\Lambda_p^{kr}}. \tag{19.12}$$

The spectral determinant exponent can be resummed,

$$-\sum_{r=1}^{\infty} \frac{1}{r} \frac{e^{(\beta A_p - s T_p)r}}{|\det(\mathbf{1} - M_p^r)|} = \sum_{k=0}^{\infty} (k+1) \log \left(1 - \frac{e^{\beta A_p - s T_p}}{|\Lambda_p| \Lambda_p^k} \right),$$

and the spectral determinant for a 2-dimensional hyperbolic Hamiltonian flow rewritten as an infinite product over prime cycles

$$\det(s - \mathcal{A}) = \prod_p \prod_{k=0}^{\infty} \left(1 - t_p / \Lambda_p^k \right)^{k+1}. \tag{19.13}$$

exercise 23.4

Now we are finally poised to deal with the problem posed at the beginning of chapter 18; how do we actually evaluate the averages introduced in sect. 17.1? The eigenvalues of the dynamical averaging evolution operator are given by the values of s for which the spectral determinant (19.6) of the evolution operator (17.23) vanishes. If we can compute the leading eigenvalue $s_0(\beta)$ and its derivatives, we are done. Unfortunately, the infinite product formula (19.9) is no more than a shorthand notation for the periodic orbit weights contributing to the spectral determinant; more work will be needed to bring such formulas into a tractable form. This shall be accomplished in chapter 20, but here it is natural to introduce still another variant of a determinant, the dynamical zeta function.

19.3 Dynamical zeta functions

It follows from sect. 18.1.1 that if one is interested only in the leading eigenvalue of \mathcal{L}^t , the size of the p cycle neighborhood can be approximated by $1/|\Lambda_p|^r$, the dominant term in the $rT_p = t \rightarrow \infty$ limit, where $\Lambda_p = \prod_e \Lambda_{p,e}$ is the product of the expanding eigenvalues of the Jacobian matrix M_p . With this replacement the spectral determinant (19.6) is replaced by the *dynamical zeta function*

$$1/\zeta = \exp \left(- \sum_p \sum_{r=1}^{\infty} \frac{1}{r} t_p^r \right) \tag{19.14}$$

that we have already derived heuristically in sect. 1.5.2. Resumming the logarithms using $\sum_r t_p^r / r = -\ln(1 - t_p)$ we obtain the *Euler product representation* of the dynamical zeta function:

$$1/\zeta = \prod_p (1 - t_p). \tag{19.15}$$

In order to simplify the notation, we usually omit the explicit dependence of $1/\zeta$, t_p on z, s, β whenever the dependence is clear from the context.

The approximate trace formula (18.28) plays the same role *vis-à-vis* the dynamical zeta function (19.7)

$$\Gamma(s) = \frac{d}{ds} \ln \zeta^{-1} = \sum_p \frac{T_p t_p}{1 - t_p}, \tag{19.16}$$

as the exact trace formula (18.23) plays *vis-à-vis* the spectral determinant (19.6). The heuristically derived dynamical zeta function of sect. 1.5.2 now re-emerges as the $1/\zeta_{0\dots 0}(z)$ part of the *exact* spectral determinant; other factors in the infinite product (19.9) affect the non-leading eigenvalues of \mathcal{L} .

In summary, the dynamical zeta function (19.15) associated with the flow $f^t(x)$ is defined as the product over all prime cycles p . The quantities, T_p , n_p and Λ_p , denote the period, topological length and product of the expanding Floquet multipliers of prime cycle p , A_p is the integrated observable $a(x)$ evaluated on a single traversal of cycle p (see (17.5)), s is a variable dual to the time t , z is dual to the discrete “topological” time n , and $t_p(z, s, \beta)$ denotes the local trace over the cycle p . We have included the factor z^{n_p} in the definition of the cycle weight in order to keep track of the number of times a cycle traverses the surface of section. The dynamical zeta function is useful because the term

$$1/\zeta(s) = 0 \tag{19.17}$$

when $s = s_0$. Here s_0 is the leading eigenvalue of $\mathcal{L}^t = e^{tA}$, which is often all that is necessary for application of this equation. The above argument completes our derivation of the trace and determinant formulas for classical chaotic flows. In chapters that follow we shall make these formulas tangible by working out a series of simple examples.

The remainder of this chapter offers examples of zeta functions.



fast track:
chapter 20, p. 377

19.3.1 A contour integral formulation



The following observation is sometimes useful, in particular for zeta functions with richer analytic structure than just zeros and poles, as in the case of intermittency (chapter 24): Γ_n , the trace sum (18.26), can be expressed in terms of the dynamical zeta function (19.15)

$$1/\zeta(z) = \prod_p \left(1 - \frac{z^{n_p}}{|\Lambda_p|} \right). \tag{19.18}$$

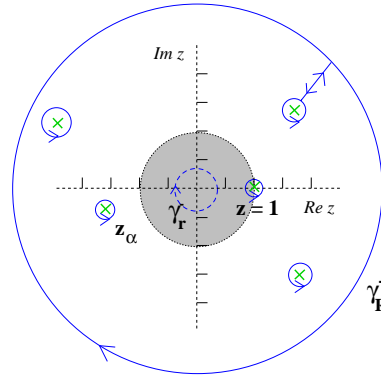


Figure 19.1: The survival probability Γ_n can be split into contributions from poles (x) and zeros (o) between the small and the large circle and a contribution from the large circle.

as a contour integral

$$\Gamma_n = \frac{1}{2\pi i} \oint_{\gamma_r} z^{-n} \left(\frac{d}{dz} \log \zeta^{-1}(z) \right) dz, \tag{19.19}$$

exercise 19.7

where a small contour γ_r encircles the origin in negative (clockwise) direction. If the contour is small enough, i.e., it lies inside the unit circle $|z| = 1$, we may write the logarithmic derivative of $\zeta^{-1}(z)$ as a convergent sum over all periodic orbits. Integrals and sums can be interchanged, the integrals can be solved term by term, and the trace formula (18.26) is recovered. For hyperbolic maps, cycle expansions or other techniques provide an analytical continuation of the dynamical zeta function beyond the leading zero; we may therefore deform the original contour into a larger circle with radius R which encircles both poles and zeros of $\zeta^{-1}(z)$, as depicted in figure 19.1. Residue calculus turns this into a sum over the zeros z_α and poles z_β of the dynamical zeta function, that is

chapter 20

$$\Gamma_n = \sum_{|z_\alpha| < R}^{\text{zeros}} \frac{1}{z_\alpha^n} - \sum_{|z_\beta| < R}^{\text{poles}} \frac{1}{z_\beta^n} + \frac{1}{2\pi i} \oint_{\gamma_R} dz z^{-n} \frac{d}{dz} \log \zeta^{-1}, \tag{19.20}$$

where the last term gives a contribution from a large circle γ_R . It would be a miracle if you still remembered this, but in sect. 1.4.3 we interpreted Γ_n as fraction of survivors after n bounces, and defined the escape rate γ as the rate of the find exponential decay of Γ_n . We now see that this exponential decay is dominated by the leading zero or pole of $\zeta^{-1}(z)$.

19.3.2 Dynamical zeta functions for transfer operators



Ruelle's original dynamical zeta function was a generalization of the topological zeta function (15.27) to a function that assigns different weights to different cycles:

chapter 15

$$\zeta(z) = \exp \sum_{n=1}^{\infty} \frac{z^n}{n} \left(\sum_{x_i \in \text{Fix } f^n} \text{tr} \prod_{j=0}^{n-1} g(f^j(x_i)) \right).$$

exercise 18.2

Here we sum over all periodic points x_i of period n , and $g(x)$ is any (matrix valued) weighting function, where the weight evaluated multiplicatively along the trajectory of x_i .

By the chain rule (4.51) the stability of any n -cycle of a 1 – dimensional map is given by $\Lambda_p = \prod_{j=1}^n f'(x_j)$, so the 1 – dimensional map cycle stability is the simplest example of a multiplicative cycle weight $g(x_i) = 1/|f'(x_i)|$, and indeed - via the Perron-Frobenius evolution operator (16.9) - the historical motivation for Ruelle’s more abstract construction.

In particular, for a piecewise-linear map with a finite Markov partition such as the map of example 16.1, the dynamical zeta function is given by a finite polynomial, a straightforward generalization of the topological transition matrix determinant (14.1). As explained in sect. 15.3, for a finite $[N \times N]$ dimensional matrix the determinant is given by

$$\prod_p (1 - t_p) = \sum_{n=1}^N z^n c_n,$$

where c_n is given by the sum over all non-self-intersecting closed paths of length n together with products of all non-intersecting closed paths of total length n .

Example 19.4 A piecewise linear repeller: Due to piecewise linearity, the stability of any n -cycle of the piecewise linear repeller (17.17) factorizes as $\Lambda_{s_1 s_2 \dots s_n} = \Lambda_0^m \Lambda_1^{n-m}$, where m is the total number of times the letter $s_j = 0$ appears in the p symbol sequence, so the traces in the sum (18.28) take the particularly simple form

$$\text{tr } T^n = \Gamma_n = \left(\frac{1}{|\Lambda_0|} + \frac{1}{|\Lambda_1|} \right)^n.$$

The dynamical zeta function (19.14) evaluated by resumming the traces,

exercise 19.3

$$1/\zeta(z) = 1 - z/|\Lambda_0| - z/|\Lambda_1|, \tag{19.21}$$

is indeed the determinant $\det(1 - zT)$ of the transfer operator (17.19), which is almost as simple as the topological zeta function (15.34).

chapter 15

More generally, piecewise-linear approximations to dynamical systems yield polynomial or rational polynomial cycle expansions, provided that the symbolic dynamics is a subshift of finite type.

We see that the exponential proliferation of cycles so dreaded by quantum chaologists is a bogus anxiety; we are dealing with exponentially many cycles of increasing length and instability, but all that really matters in this example are the stabilities of the two fixed points. Clearly the information carried by the infinity of longer cycles is highly redundant; we shall learn in chapter 20 how to exploit this redundancy systematically.

19.4 False zeros

Compare (19.21) with the Euler product (19.15). For simplicity consider two equal scales, $|\Lambda_0| = |\Lambda_1| = e^\lambda$. Our task is to determine the leading zero $z = e^\gamma$ of the Euler product. It is a novice error to assume that the infinite Euler product (19.15) vanishes whenever one of its factors vanishes. If that were true, each factor $(1 - z^{n_p}/|\Lambda_p|)$ would yield

$$0 = 1 - e^{n_p(\gamma - \lambda_p)}, \quad (19.22)$$

so the escape rate γ would equal the Floquet exponent of a repulsive cycle, one eigenvalue $\gamma = \gamma_p$ for each prime cycle p . This is false! The exponentially growing number of cycles with growing period conspires to shift the zeros of the infinite product. The correct formula follows from (19.21)

$$0 = 1 - e^{\gamma - \lambda + h}, \quad h = \ln 2. \quad (19.23)$$

This particular formula for the escape rate is a special case of a general relation between escape rates, Lyapunov exponents and entropies that is not yet included into this book. Physically this means that the escape induced by the repulsion by each unstable fixed point is diminished by the rate of backscatter from other repelling regions, i.e., the entropy h ; the positive entropy of orbits shifts the “false zeros” $z = e^{\lambda_p}$ of the Euler product (19.15) to the true zero $z = e^{\lambda - h}$.

19.5 Spectral determinants vs. dynamical zeta functions

In sect. 19.3 we derived the dynamical zeta function as an approximation to the spectral determinant. Here we relate dynamical zeta functions to spectral determinants *exactly*, by showing that a dynamical zeta function can be expressed as a ratio of products of spectral determinants.

The elementary identity for d -dimensional matrices

$$1 = \frac{1}{\det(1 - M)} \sum_{k=0}^d (-1)^k \text{tr}(\wedge^k M), \quad (19.24)$$

inserted into the exponential representation (19.14) of the dynamical zeta function, relates the dynamical zeta function to *weighted* spectral determinants.

Example 19.5 Dynamical zeta function in terms of determinants, 1 – dimensional maps: For 1 – dimensional maps the identity

$$1 = \frac{1}{(1 - 1/\Lambda)} - \frac{1}{\Lambda} \frac{1}{(1 - 1/\Lambda)}$$

substituted into (19.14) yields an expression for the dynamical zeta function for 1 – dimensional maps as a ratio of two spectral determinants

$$1/\zeta = \frac{\det(1 - z\mathcal{L})}{\det(1 - z\mathcal{L}_{(1)})} \quad (19.25)$$

where the cycle weight in $\mathcal{L}_{(1)}$ is given by replacement $t_p \rightarrow t_p/\Lambda_p$. As we shall see in chapter 23, this establishes that for nice hyperbolic flows $1/\zeta$ is meromorphic, with poles given by the zeros of $\det(1 - z\mathcal{L}_{(1)})$. The dynamical zeta function and the spectral determinant have the same zeros, although in exceptional circumstances some zeros of $\det(1 - z\mathcal{L}_{(1)})$ might be cancelled by coincident zeros of $\det(1 - z\mathcal{L}_{(1)})$. Hence even though we have derived the dynamical zeta function in sect. 19.3 as an “approximation” to the spectral determinant, the two contain the same spectral information.

Example 19.6 Dynamical zeta function in terms of determinants, 2 – dimensional Hamiltonian maps: For 2-dimensional Hamiltonian flows the above identity yields

$$\frac{1}{|\Lambda|} = \frac{1}{|\Lambda|(1 - 1/\Lambda)^2} (1 - 2/\Lambda + 1/\Lambda^2),$$

so

$$1/\zeta = \frac{\det(1 - z\mathcal{L}) \det(1 - z\mathcal{L}_{(2)})}{\det(1 - z\mathcal{L}_{(1)})}. \quad (19.26)$$

This establishes that for nice 2 – dimensional hyperbolic flows the dynamical zeta function is meromorphic.

Example 19.7 Dynamical zeta functions for 2 – dimensional Hamiltonian flows: The relation (19.26) is not particularly useful for our purposes. Instead we insert the identity

$$1 = \frac{1}{(1 - 1/\Lambda)^2} - \frac{2}{\Lambda} \frac{1}{(1 - 1/\Lambda)^2} + \frac{1}{\Lambda^2} \frac{1}{(1 - 1/\Lambda)^2}$$

into the exponential representation (19.14) of $1/\zeta_k$, and obtain

$$1/\zeta_k = \frac{\det(1 - z\mathcal{L}_{(k)}) \det(1 - z\mathcal{L}_{(k+2)})}{\det(1 - z\mathcal{L}_{(k+1)})^2}. \quad (19.27)$$

Even though we have no guarantee that $\det(1 - z\mathcal{L}_{(k)})$ are entire, we do know that the upper bound on the leading zeros of $\det(1 - z\mathcal{L}_{(k+1)})$ lies strictly below the leading zeros of $\det(1 - z\mathcal{L}_{(k)})$, and therefore we expect that for 2-dimensional Hamiltonian flows the dynamical zeta function $1/\zeta_k$ generically has a double leading pole coinciding with the leading zero of the $\det(1 - z\mathcal{L}_{(k+1)})$ spectral determinant. This might fail if the poles and leading eigenvalues come in wrong order, but we have not encountered such situations in our numerical investigations. This result can also be stated as follows: the theorem establishes that the spectral determinant (19.13) is entire, and also implies that the poles in $1/\zeta_k$ must have the right multiplicities to cancel in the $\det(1 - z\mathcal{L}) = \prod 1/\zeta_k^{k+1}$ product.

Figure 19.2: A game of pinball consisting of two disks of equal size in a plane, with its only periodic orbit (A. Wirzba).

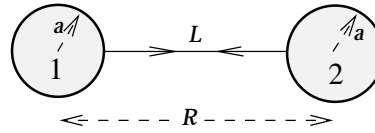
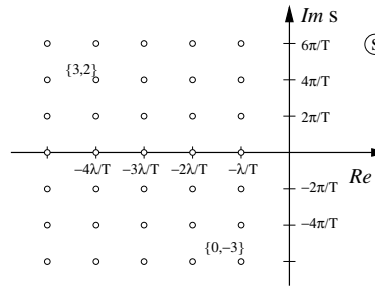


Figure 19.3: The classical resonances $\alpha = \{k, n\}$ (19.28) for a 2-disk game of pinball.



19.6 All too many eigenvalues?



What does the 2-dimensional hyperbolic Hamiltonian flow spectral determinant (19.13) tell us? Consider one of the simplest conceivable hyperbolic flows: the game of pinball of figure 19.2 consisting of two disks of equal size in a plane. There is only one periodic orbit, with the period T and expanding eigenvalue Λ given by elementary considerations (see exercise 13.7), and the resonances $\det(s_\alpha - \mathcal{A}) = 0, \alpha = \{k, n\}$ plotted in figure 19.3:

$$s_\alpha = -(k + 1)\lambda + n\frac{2\pi i}{T}, \quad n \in \mathbb{Z}, k \in \mathbb{Z}_+, \quad \text{multiplicity } k + 1, \quad (19.28)$$

can be read off the spectral determinant (19.13) for a single unstable cycle:

$$\det(s - \mathcal{A}) = \prod_{k=0}^{\infty} \left(1 - e^{-sT} / |\Lambda| \Lambda^k\right)^{k+1}. \quad (19.29)$$

In the above $\lambda = \ln |\Lambda| / T$ is the cycle Lyapunov exponent. For an open system, the real part of the eigenvalue s_α gives the decay rate of α th eigenstate, and the imaginary part gives the “node number” of the eigenstate. The negative real part of s_α indicates that the resonance is unstable, and the decay rate in this simple case (zero entropy) equals the cycle Lyapunov exponent.

Rapidly decaying eigenstates with large negative $\text{Re } s_\alpha$ are not a problem, but as there are eigenvalues arbitrarily far in the imaginary direction, this might seem like all too many eigenvalues. However, they are necessary - we can check this by explicit computation of the right hand side of (18.23), the trace formula for flows:

$$\begin{aligned} \sum_{\alpha=0}^{\infty} e^{s_\alpha t} &= \sum_{k=0}^{\infty} \sum_{n=-\infty}^{\infty} (k + 1) e^{-(k+1)\lambda t + i2\pi n t / T} \\ &= \sum_{k=0}^{\infty} (k + 1) \left(\frac{1}{|\Lambda| \Lambda^k}\right)^{t/T} \sum_{n=-\infty}^{\infty} e^{i2\pi n t / T} \end{aligned}$$

$$\begin{aligned}
 &= \sum_{k=0}^{\infty} \frac{k+1}{|\Lambda|^r \Lambda^{kr}} \sum_{r=-\infty}^{\infty} \delta(r - t/T) \\
 &= T \sum_{r=-\infty}^{\infty} \frac{\delta(t - rT)}{|\Lambda|^r (1 - 1/\Lambda^r)^2}.
 \end{aligned} \tag{19.30}$$

Hence, the two sides of the trace formula (18.23) are verified. The formula is fine for $t > 0$; for $t \rightarrow 0_+$, however, sides are divergent and need regularization.

The reason why such sums do not occur for maps is that for discrete time we work with the variable $z = e^s$, so an infinite strip along $\text{Im } s$ maps into an annulus in the complex z plane, and the Dirac delta sum in the above is replaced by the Kronecker delta sum in (18.8). In the case at hand there is only one time scale T , and we could just as well replace s by the variable $z = e^{-sT}$. In general, a continuous time flow has an infinity of irrationally related cycle periods, and the resonance arrays are more irregular, cf. figure 20.1.

Résumé

The eigenvalues of evolution operators are given by the zeros of corresponding determinants, and one way to evaluate determinants is to expand them in terms of traces, using the matrix identity $\log \det = \text{tr } \log$. Traces of evolution operators can be evaluated as integrals over Dirac delta functions, and in this way the spectra of evolution operators are related to periodic orbits. The spectral problem is now recast into a problem of determining zeros of either the *spectral determinant*

$$\det(s - \mathcal{A}) = \exp \left(- \sum_p \sum_{r=1}^{\infty} \frac{1}{r} \frac{e^{\beta \cdot A_p - s T_p} r}{|\det(\mathbf{1} - M_p^r)|} \right),$$

or the leading zeros of the *dynamical zeta function*

$$1/\zeta = \prod_p (1 - t_p), \quad t_p = \frac{1}{|\Lambda_p|} e^{\beta \cdot A_p - s T_p}.$$

The spectral determinant is the tool of choice in actual calculations, as it has superior convergence properties (this will be discussed in chapter 23 and is illustrated, for example, by table 20.2). In practice both spectral determinants and dynamical zeta functions are preferable to trace formulas because they yield the eigenvalues more readily; the main difference is that while a trace diverges at an eigenvalue and requires extrapolation methods, determinants vanish at s corresponding to an eigenvalue s_α , and are analytic in s in an open neighborhood of s_α .

The critical step in the derivation of the periodic orbit formulas for spectral determinants and dynamical zeta functions is the hyperbolicity assumption (18.5)

that no cycle stability eigenvalue is marginal, $|\Lambda_{p,i}| \neq 1$. By dropping the prefactors in (1.5), we have given up on any possibility of recovering the precise distribution of the initial x (return to the past is rendered moot by the chaotic mixing and the exponential growth of errors), but in exchange we gain an effective description of the asymptotic behavior of the system. The pleasant surprise (to be demonstrated in chapter 20) is that the infinite time behavior of an unstable system turns out to be as easy to determine as its short time behavior.

Commentary

Remark 19.1 Piecewise monotone maps. A partial list of cases for which the transfer operator is well defined: the expanding Hölder case, weighted subshifts of finite type, expanding differentiable case, see Bowen [28]; expanding holomorphic case, see Ruelle [9]; piecewise monotone maps of the interval, see Hofbauer and Keller [13] and Baladi and Keller [16].

Remark 19.2 Smale's wild idea. Smale's wild idea quoted on page 362 was technically wrong because 1) the Selberg zeta function yields the spectrum of a quantum mechanical Laplacian rather than the classical resonances, 2) the spectral determinant weights are different from what Smale conjectured, as the individual cycle weights also depend on the stability of the cycle, 3) the formula is not dimensionally correct, as k is an integer and s represents inverse time. Only for spaces of constant negative curvature do all cycles have the same Lyapunov exponent $\lambda = \ln |\Lambda_p|/T_p$. In this case, one can normalize time so that $\lambda = 1$, and the factors e^{-sT_p}/Λ_p^k in (19.9) simplify to $s^{-(s+k)T_p}$, as intuited in Smale's quote on page 362 (where $l(\gamma)$ is the cycle period denoted here by T_p). Nevertheless, Smale's intuition was remarkably on the target.

Remark 19.3 Is this a generalization of the Fourier analysis? Fourier analysis is a theory of the space \leftrightarrow eigenfunction duality for dynamics on a circle. The way in which periodic orbit theory generalizes Fourier analysis to nonlinear flows is discussed in ref. [3], a very readable introduction to the Selberg Zeta function.

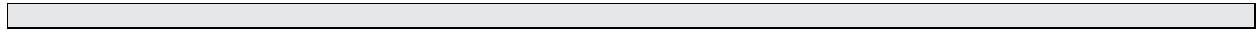
Remark 19.4 Zeta functions, antecedents. For a function to be deserving of the appellation "zeta function," one expects it to have an Euler product representation (19.15), and perhaps also satisfy a functional equation. Various kinds of zeta functions are reviewed in refs. [6, 7, 8]. Historical antecedents of the dynamical zeta function are the fixed-point counting functions introduced by Weil [9], Lefschetz [10] and Artin and Mazur [11], and the determinants of transfer operators of statistical mechanics [29].

In his review article Smale [27] already intuited, by analogy to the Selberg Zeta function, that the spectral determinant is the right generalization for continuous time flows. In dynamical systems theory, dynamical zeta functions arise naturally only for piecewise linear mappings; for smooth flows the natural object for the study of classical and quantal spectra are the spectral determinants. Ruelle derived the relation (19.3) between spectral

determinants and dynamical zeta functions, but since he was motivated by the Artin-Mazur zeta function (15.27) and the statistical mechanics analogy, he did not consider the spectral determinant to be a more natural object than the dynamical zeta function. This has been put right in papers on “flat traces” [18, 23].

The nomenclature has not settled down yet; what we call evolution operators here is elsewhere called transfer operators [32], Perron-Frobenius operators [4] and/or Ruelle-Araki operators.

Here we refer to kernels such as (17.23) as evolution operators. We follow Ruelle in usage of the term “dynamical zeta function,” but elsewhere in the literature the function (19.15) is often called the Ruelle zeta function. Ruelle [33] points out that the corresponding transfer operator T was never considered by either Perron or Frobenius; a more appropriate designation would be the Ruelle-Araki operator. Determinants similar to or identical with our spectral determinants are sometimes called Selberg Zetas, Selberg-Smale zetas [8], functional determinants, Fredholm determinants, or even - to maximize confusion - dynamical zeta functions [12]. A Fredholm determinant is a notion that applies only to trace class operators - as we consider here a somewhat wider class of operators, we prefer to refer to their determinants loosely as “spectral determinants.”



Exercises

19.1. Escape rate for a 1 – dimensional repeller, numerically.

Consider the quadratic map

$$f(x) = Ax(1 - x) \tag{19.31}$$

on the unit interval. The trajectory of a point starting in the unit interval either stays in the interval forever or after some iterate leaves the interval and diverges to minus infinity. Estimate numerically the escape rate (22.8), the rate of exponential decay of the measure of points remaining in the unit interval, for either $A = 9/2$ or $A = 6$. Remember to compare your numerical estimate with the solution of the continuation of this exercise, exercise 20.2.

19.2. Spectrum of the “golden mean” pruned map.

(medium - exercise 15.7 continued)

- (a) Determine an expression for $\text{tr } \mathcal{L}^n$, the trace of powers of the Perron-Frobenius operator (16.10) acting on the space of real analytic functions for the tent map of exercise 15.7.
- (b) Show that the spectral determinant for the Perron-Frobenius operator is

$$\det(1 - z\mathcal{L}) = \tag{19.32}$$

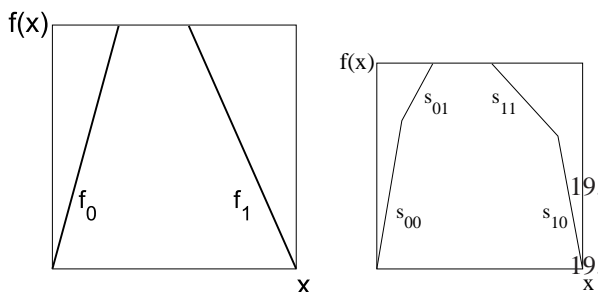
$$\prod_{k \text{ even}} \left(1 - \frac{z}{\Lambda^{k+1}} - \frac{z^2}{\Lambda^{2k+2}} \right) \times \prod_{k \text{ odd}} \left(1 + \frac{z}{\Lambda^{k+1}} + \frac{z^2}{\Lambda^{2k+2}} \right).$$

19.3. Dynamical zeta functions. (easy)

- (a) Evaluate in closed form the dynamical zeta function

$$1/\zeta(z) = \prod_p \left(1 - \frac{z^{n_p}}{|\Lambda_p|} \right)$$

for the piecewise-linear map (17.17) with the left branch slope Λ_0 , the right branch slope Λ_1 .



- (b) What if there are four different slopes $s_{00}, s_{01}, s_{10},$ and s_{11} instead of just two, with the preimages of the gap adjusted so that junctions of branches s_{00}, s_{01} and s_{11}, s_{10} map in the gap in one iteration? What would the dynamical zeta function be?

19.4. Dynamical zeta functions from transition graphs.

Extend sect. 15.3 to evaluation of dynamical zeta functions for piecewise linear maps with finite transition graphs. This generalizes the results of exercise 19.3.

19.5. Zeros of infinite products. Determination of the quantities of interest by periodic orbits involves working with infinite product formulas.

- (a) Consider the infinite product

$$F(z) = \prod_{k=0}^{\infty} (1 + f_k(z))$$

where the functions f_k are “sufficiently nice.” This infinite product can be converted into an infinite sum by the use of a logarithm. Use the properties of infinite sums to develop a sensible definition of infinite products.

- (b) If z^* is a root of the function F , show that the infinite product diverges when evaluated at z^* .
 (c) How does one compute a root of a function represented as an infinite product?
 (d) Let p be all prime cycles of the binary alphabet $\{0, 1\}$. Apply your definition of $F(z)$ to the infinite product

$$F(z) = \prod_p \left(1 - \frac{z^{n_p}}{\Lambda^{n_p}}\right)$$

- (e) Are the roots of the factors in the above product the zeros of $F(z)$?

(Per Rosenqvist)

19.6. Dynamical zeta functions as ratios of spectral determinants. (medium) Show that the zeta function

$$1/\zeta(z) = \exp\left(-\sum_p \sum_{r=1}^{\infty} \frac{1}{r} \frac{z^{n_p}}{|\Lambda_p|^r}\right)$$

can be written as the ratio

$$1/\zeta(z) = \det(1 - z\mathcal{L}_{(0)})/\det(1 - z\mathcal{L}_{(1)}),$$

where $\det(1 - z\mathcal{L}_{(s)}) = \prod_p \prod_{k=0}^{\infty} (1 - z^{n_p}/|\Lambda_p|\Lambda_p^{k+s})$.

19.7. Contour integral for survival probability. Perform explicitly the contour integral appearing in (19.19).

19.8. Dynamical zeta function for maps. In this problem we will compare the dynamical zeta function and the spectral determinant. Compute the exact dynamical zeta function for the skew full tent map (16.45)

$$1/\zeta(z) = \prod_{p \in P} \left(1 - \frac{z^{n_p}}{|\Lambda_p|}\right).$$

What are its roots? Do they agree with those computed in exercise 16.7?

19.9. Dynamical zeta functions for Hamiltonian maps. Starting from

$$1/\zeta(s) = \exp\left(-\sum_p \sum_{r=1}^{\infty} \frac{1}{r} t_p^r\right)$$

for a 2-dimensional Hamiltonian map. Using the equality

$$1 = \frac{1}{(1 - 1/\Lambda)^2} (1 - 2/\Lambda + 1/\Lambda^2),$$

show that

$$1/\zeta = \det(1 - \mathcal{L}) \det(1 - \mathcal{L}_{(2)})/\det(1 - \mathcal{L}_{(1)})^2.$$

In this expression $\det(1 - z\mathcal{L}_{(k)})$ is the expansion one gets by replacing $t_p \rightarrow t_p/\Lambda_p^k$ in the spectral determinant.

19.10. Riemann ζ function. The Riemann ζ function is defined as the sum

$$\zeta(s) = \sum_{n=1}^{\infty} \frac{1}{n^s}, \quad s \in \mathbb{C}.$$

- (a) Use factorization into primes to derive the Euler product representation

$$\zeta(s) = \prod_p \frac{1}{1 - p^{-s}}.$$

The dynamical zeta function exercise 19.15 is called a “zeta” function because it shares the form of the Euler product representation with the Riemann zeta function.

- (b) (Not trivial:) For which complex values of s is the Riemann zeta sum convergent?
 (c) Are the zeros of the terms in the product, $s = -\ln p$, also the zeros of the Riemann ζ function? If not, why not?

- 19.11. **Finite truncations.** (easy) Suppose we have a 1-dimensional system with complete binary dynamics, where the stability of each orbit is given by a simple multiplicative rule:

$$\Lambda_p = \Lambda_0^{n_{p,0}} \Lambda_1^{n_{p,1}}, \quad n_{p,0} = \#0 \text{ in } p, \quad n_{p,1} = \#1 \text{ in } p,$$

so that, for example, $\Lambda_{00101} = \Lambda_0^3 \Lambda_1^2$.

- (a) Compute the dynamical zeta function for this system; perhaps by creating a transfer matrix analogous to (17.19), with the right weights.

- (b) Compute the finite p truncations of the cycle expansion, i.e. take the product only over the p up to given length with $n_p \leq N$, and expand as a series in z

$$\prod_p \left(1 - \frac{z^{n_p}}{|\Lambda_p|} \right).$$

Do they agree? If not, how does the disagreement depend on the truncation length N ?

References

- [19.1] D. Ruelle, *Statistical Mechanics, Thermodynamic Formalism* (Addison-Wesley, Reading MA, 1978)
- [19.2] M. Pollicott, "Meromorphic extensions of generalised zeta functions," *Invent. Math.* **85**, 147 (1986).
- [19.3] H.P. McKean, *Comm. Pure and Appl. Math.* **25**, 225 (1972); **27**, 134 (1974).
- [19.4] Y. Oono and Y. Takahashi, *Progr. Theor. Phys* **63**, 1804 (1980); S.-J. Chang and J. Wright, *Phys. Rev. A* **23**, 1419 (1981); Y. Takahashi and Y. Oono, *Progr. Theor. Phys* **71**, 851 (1984).
- [19.5] P. Cvitanović, P.E. Rosenqvist, H.H. Rugh, and G. Vattay, "A Fredholm determinant for semi-classical quantization," *CHAOS* **3**, 619 (1993).
- [19.6] A. Voros, in: *Zeta Functions in Geometry* (Proceedings, Tokyo 1990), eds. N. Kurokawa and T. Sunada, *Advanced Studies in Pure Mathematics* **21**, Math. Soc. Japan, Kinokuniya, Tokyo (1992), p.327-358.
- [19.7] Kiyosi Itô, ed., *Encyclopedic Dictionary of Mathematics*, (MIT Press, Cambridge, 1987).
- [19.8] N.E. Hurt, "Zeta functions and periodic orbit theory: A review," *Results in Mathematics* **23**, 55 (Birkhäuser, Basel 1993).
- [19.9] A. Weil, "Numbers of solutions of equations in finite fields," *Bull. Am. Math. Soc.* **55**, 497 (1949).
- [19.10] D. Fried, "Lefschetz formula for flows," *The Lefschetz centennial conference, Contemp. Math.* **58**, 19 (1987).
- [19.11] E. Artin and B. Mazur, *Annals. Math.* **81**, 82 (1965)
- [19.12] M. Sieber and F. Steiner, *Phys. Lett. A* **148**, 415 (1990).
- [19.13] F. Hofbauer and G. Keller, "Ergodic properties of invariant measures for piecewise monotonic transformations," *Math. Z.* **180**, 119 (1982).

- [19.14] G. Keller, "On the rate of convergence to equilibrium in one-dimensional systems," *Comm. Math. Phys.* **96**, 181 (1984).
- [19.15] F. Hofbauer and G. Keller, "Zeta-functions and transfer-operators for piecewise linear transformations," *J. reine angew. Math.* **352**, 100 (1984).
- [19.16] V. Baladi and G. Keller, "Zeta functions and transfer operators for piecewise monotone transformations," *Comm. Math. Phys.* **127**, 459 (1990).

Chapter 20

Cycle expansions

Recycle... It's the Law!

—Poster, New York City Department of Sanitation

THE EULER PRODUCT representations of spectral determinants (19.9) and dynamical zeta functions (19.15) are really only a shorthand notation - the zeros of the individual factors are *not* the zeros of the zeta function, and convergence of such objects is far from obvious. Now we shall give meaning to the dynamical zeta functions and spectral determinants by expanding them as cycle expansions, series representations ordered by increasing topological cycle length, with products in (19.9), (19.15) expanded as sums over *pseudocycles*, products of t_p 's. The zeros of correctly truncated cycle expansions yield the desired eigenvalues, and the expectation values of observables are given by the cycle averaging formulas obtained from the partial derivatives of dynamical zeta functions (or spectral determinants).

20.1 Pseudocycles and shadowing

How are periodic orbit formulas such as (19.15) evaluated? We start by computing the lengths and Floquet multipliers of the shortest cycles. This always requires numerical work, such as the Newton method searches for periodic solutions; we shall assume that the numerics is under control, and that *all* short cycles up to a given (topological) length have been found. Examples of the data required for application of periodic orbit formulas are the lists of cycles given in table 29.3 and exercise 13.14. It is important not to miss any short cycles, as the calculation is as accurate as the shortest cycle dropped - including cycles longer than the shortest omitted does not improve the accuracy (more precisely, improves it, but painfully slowly).

Expand the dynamical zeta function (19.15) as a formal power series,

$$1/\zeta = \prod_p (1 - t_p) = 1 - \sum'_{\{p_1 p_2 \dots p_k\}} (-1)^{k+1} t_{p_1} t_{p_2} \dots t_{p_k} \quad (20.1)$$

where the prime on the sum indicates that the sum is over all distinct non-repeating combinations of prime cycles. As we shall frequently use such sums, let us denote by $t_\pi = (-1)^{k+1} t_{p_1} t_{p_2} \dots t_{p_k}$ an element of the set of all distinct products of the prime cycle weights t_p . The formal power series (20.1) is now compactly written as

$$1/\zeta = 1 - \sum'_{\pi} t_\pi. \quad (20.2)$$

For $k > 1$, t_π are weights of *pseudocycles*; they are sequences of shorter cycles that shadow a cycle with the symbol sequence $p_1 p_2 \dots p_k$ along segments p_1, p_2, \dots, p_k . \sum' denotes the restricted sum, for which any given prime cycle p contributes at most once to a given pseudocycle weight t_π .

The pseudocycle weight, i.e., the product of weights (19.10) of prime cycles comprising the pseudocycle,

$$t_\pi = (-1)^{k+1} \frac{1}{|\Lambda_\pi|} e^{\beta A_\pi - s T_\pi} z^{n_\pi}, \quad (20.3)$$

depends on the pseudocycle topological length n_π , integrated observable A_π , period T_π , and stability Λ_π

$$\begin{aligned} n_\pi &= n_{p_1} + \dots + n_{p_k}, & T_\pi &= T_{p_1} + \dots + T_{p_k} \\ A_\pi &= A_{p_1} + \dots + A_{p_k}, & \Lambda_\pi &= \Lambda_{p_1} \Lambda_{p_2} \dots \Lambda_{p_k}. \end{aligned} \quad (20.4)$$

Throughout this text, the terms “periodic orbit” and “cycle” are used interchangeably; while “periodic orbit” is more precise, “cycle” (which has many other uses in mathematics) is easier on the ear than “pseudo-periodic-orbit.” While in Soviet times acronyms were a rage (and in France they remain so), we shy away from acronyms such as UPOs (Unstable Periodic Orbits).

20.1.1 Curvature expansions

The simplest example is the pseudocycle sum for a system described by a complete binary symbolic dynamics. In this case the Euler product (19.15) is given by

$$\begin{aligned} 1/\zeta &= (1 - t_0)(1 - t_1)(1 - t_{01})(1 - t_{001})(1 - t_{011}) \\ &\quad (1 - t_{0001})(1 - t_{0011})(1 - t_{0111})(1 - t_{00001})(1 - t_{00011}) \\ &\quad (1 - t_{00101})(1 - t_{00111})(1 - t_{01011})(1 - t_{01111}) \dots \end{aligned} \quad (20.5)$$

(see table 15.1), and the first few terms of the expansion (20.2) ordered by increasing total pseudocycle length are:

$$\begin{aligned}
 1/\zeta &= 1 - t_0 - t_1 - t_{01} - t_{001} - t_{011} - t_{0001} - t_{0011} - t_{0111} - \dots \\
 &\quad + t_0 t_1 + t_0 t_{01} + t_{01} t_1 + t_0 t_{001} + t_0 t_{011} + t_{001} t_1 + t_{011} t_1 \\
 &\quad - t_0 t_{01} t_1 - \dots
 \end{aligned}
 \tag{20.6}$$

We refer to such series representation of a dynamical zeta function or a spectral determinant, expanded as a sum over pseudocycles, and ordered by increasing cycle length and instability, as a *cycle expansion*.

The next step is the key step: regroup the terms into the dominant *fundamental* contributions t_f and the decreasing *curvature* corrections \hat{c}_n , each \hat{c}_n split into prime cycles p of length $n_p=n$ grouped together with pseudocycles whose full itineraries build up the itinerary of p . For the binary case this regrouping is given by

$$\begin{aligned}
 1/\zeta &= 1 - t_0 - t_1 - [(t_{01} - t_1 t_0)] - [(t_{001} - t_{01} t_0) + (t_{011} - t_{01} t_1)] \\
 &\quad - [(t_{0001} - t_0 t_{001}) + (t_{0111} - t_{011} t_1) \\
 &\quad \quad + (t_{0011} - t_{001} t_1 - t_0 t_{011} + t_0 t_{01} t_1)] - \dots \\
 &= 1 - \sum_f t_f - \sum_n \hat{c}_n .
 \end{aligned}
 \tag{20.7}$$

All terms in this expansion up to length $n_p = 6$ are given in table 20.1. We refer to such regrouped series as *curvature expansions*.

Such separation into “fundamental” and “curvature” parts of cycle expansions is possible *only* for dynamical systems whose symbolic dynamics has finite grammar. The fundamental cycles t_0, t_1 have no shorter approximants; they are the “building blocks” of the dynamics in the sense that all longer orbits can be approximately pieced together from them. The fundamental part of a cycle expansion is given by the sum of the products of all non-intersecting loops of the associated transition graph. The terms grouped in brackets are the curvature corrections; the terms grouped in parenthesis are combinations of longer cycles and corresponding sequences of “shadowing” pseudocycles. If all orbits are weighted equally ($t_p = z^{n_p}$), such combinations cancel exactly, and the dynamical zeta function reduces to the topological polynomial (15.27). If the flow is continuous and smooth, orbits of similar symbolic dynamics will traverse the same neighborhoods and will have similar weights, and the weights in such combinations will almost cancel. The utility of cycle expansions of dynamical zeta functions and spectral determinants, in contrast to direct averages over periodic orbits such as the trace formulas discussed in sect. 22.5, lies precisely in this organization into nearly canceling combinations: cycle expansions are dominated by short cycles, with long cycles giving exponentially decaying corrections.

section 15.3
section 20.4

In the case where we know of no finite grammar symbolic dynamics that would help us organize the cycles, the best thing to use is a *stability cutoff* which

Table 20.1: The binary curvature expansion (20.7) up to length 6, listed in such way that the sum of terms along the p th horizontal line is the curvature \hat{c}_p associated with a prime cycle p , or a combination of prime cycles such as the $t_{100101} + t_{100110}$ pair.

- t_0			
- t_1			
- t_{10}	+ $t_1 t_0$		
- t_{100}	+ $t_{10} t_0$		
- t_{101}	+ $t_{10} t_1$		
- t_{1000}	+ $t_{100} t_0$		
- t_{1001}	+ $t_{100} t_1$	+ $t_{101} t_0$	- $t_1 t_{10} t_0$
- t_{1011}	+ $t_{101} t_1$		
- t_{10000}	+ $t_{1000} t_0$		
- t_{10001}	+ $t_{1001} t_0$	+ $t_{1000} t_1$	- $t_0 t_{100} t_1$
- t_{10010}	+ $t_{100} t_{10}$		
- t_{10101}	+ $t_{101} t_{10}$		
- t_{10011}	+ $t_{1011} t_0$	+ $t_{1001} t_1$	- $t_0 t_{101} t_1$
- t_{10111}	+ $t_{1011} t_1$		
- t_{100000}	+ $t_{10000} t_0$		
- t_{100001}	+ $t_{10001} t_0$	+ $t_{10000} t_1$	- $t_0 t_{1000} t_1$
- t_{100010}	+ $t_{10010} t_0$	+ $t_{1000} t_{10}$	- $t_0 t_{100} t_{10}$
- t_{100011}	+ $t_{10011} t_0$	+ $t_{10001} t_1$	- $t_0 t_{1001} t_1$
- t_{100101}	- t_{100110}	+ $t_{10010} t_1$	+ $t_{10110} t_0$
	+ $t_{10} t_{1001}$	+ $t_{100} t_{101}$	- $t_0 t_{10} t_{101} - t_1 t_{10} t_{100}$
- t_{101110}	+ $t_{10110} t_1$	+ $t_{1011} t_{10}$	- $t_1 t_{101} t_{10}$
- t_{100111}	+ $t_{10011} t_1$	+ $t_{10111} t_0$	- $t_0 t_{1011} t_1$
- t_{101111}	+ $t_{10111} t_1$		

we shall discuss in sect. 20.5. The idea is to truncate the cycle expansion by including only the pseudocycles such that $|\Lambda_{p_1} \cdots \Lambda_{p_k}| \leq \Lambda_{\max}$, with the cutoff Λ_{\max} equal to or greater than the most unstable Λ_p in the data set.

20.2 Construction of cycle expansions

20.2.1 Evaluation of dynamical zeta functions

Cycle expansions of dynamical zeta functions are evaluated numerically by first computing the weights $t_p = t_p(\beta, s)$ of all prime cycles p of topological length $n_p \leq N$ for given fixed β and s . Denote by subscript (i) the i th prime cycle computed, ordered by the topological length $n_{(i)} \leq n_{(i+1)}$. The dynamical zeta function $1/\zeta_N$ truncated to the $n_p \leq N$ cycles is computed recursively, by multiplying

$$1/\zeta_{(i)} = 1/\zeta_{(i-1)}(1 - t_{(i)}z^{n_{(i)}}), \tag{20.8}$$

and truncating the expansion at each step to a finite polynomial in z^n , $n \leq N$. The result is the N th order polynomial approximation

$$1/\zeta_N = 1 - \sum_{n=1}^N c_n z^n. \tag{20.9}$$

In other words, a cycle expansion is a Taylor expansion in the dummy variable z raised to the topological cycle length. If both the number of cycles and their in-

dividual weights grow not faster than exponentially with the cycle length, and we multiply the weight of each cycle p by a factor z^{np} , the cycle expansion converges for sufficiently small $|z|$.

If the dynamics is given by iterated mapping, the leading zero of (20.9) as function of z yields the leading eigenvalue of the appropriate evolution operator. For continuous time flows, z is a dummy variable that we set to $z = 1$, and the leading eigenvalue of the evolution operator is given by the leading zero of (20.9) as function of s .

20.2.2 Evaluation of traces, spectral determinants

Due to the lack of factorization of the full pseudocycle weight,

$$\det(\mathbf{1} - M_{p_1 p_2}) \neq \det(\mathbf{1} - M_{p_1}) \det(\mathbf{1} - M_{p_2}),$$

the cycle expansions for the spectral determinant (19.9) are somewhat less transparent than is the case for the dynamical zeta functions.

We commence the cycle expansion evaluation of a spectral determinant by computing recursively the trace formula (18.10) truncated to all prime cycles p and their repeats such that $n_p r \leq N$:

$$\begin{aligned} \operatorname{tr} \frac{z\mathcal{L}}{1-z\mathcal{L}} \Big|_{(i)} &= \operatorname{tr} \frac{z\mathcal{L}}{1-z\mathcal{L}} \Big|_{(i-1)} + n_{(i)} \sum_{r=1}^{n_{(i)} r \leq N} \frac{e^{\beta \cdot A_{(i)} - s T_{(i)} r}}{\left| \prod (1 - \Lambda_{(i),j}^r) \right|} z^{n_{(i)} r} \\ \operatorname{tr} \frac{z\mathcal{L}}{1-z\mathcal{L}} \Big|_N &= \sum_{n=1}^N C_n z^n, \quad C_n = \operatorname{tr} \mathcal{L}^n. \end{aligned} \quad (20.10)$$

This is done numerically: the periodic orbit data set consists of the list of the cycle periods T_p , the cycle Floquet multipliers $\Lambda_{p,1}, \Lambda_{p,2}, \dots, \Lambda_{p,d}$, and the cycle averages of the observable A_p for all prime cycles p such that $n_p \leq N$. The coefficient of $z^{n_p r}$ is then evaluated numerically for the given (β, s) parameter values. Now that we have an expansion for the trace formula (18.9) as a power series, we compute the N th order approximation to the spectral determinant (19.3),

$$\det(1 - z\mathcal{L})|_N = 1 - \sum_{n=1}^N Q_n z^n, \quad Q_n = n\text{th cumulant}, \quad (20.11)$$

as follows. The logarithmic derivative relation (19.4) yields

$$\begin{aligned} \left(\operatorname{tr} \frac{z\mathcal{L}}{1-z\mathcal{L}} \right) \det(1 - z\mathcal{L}) &= -z \frac{d}{dz} \det(1 - z\mathcal{L}) \\ (C_1 z + C_2 z^2 + \dots)(1 - Q_1 z - Q_2 z^2 - \dots) &= Q_1 z + 2Q_2 z^2 + 3Q_3 z^3 \dots \end{aligned}$$

Table 20.2: 3-disk repeller escape rates computed from the cycle expansions of the spectral determinant (19.6) and the dynamical zeta function (19.15), as function of the maximal cycle length N . The first column indicates the disk-disk center separation to disk radius ratio $R:a$, the second column gives the maximal cycle length used, and the third the estimate of the classical escape rate from the fundamental domain spectral determinant cycle expansion. As for larger disk-disk separations the dynamics is more uniform, the convergence is better for $R:a = 6$ than for $R:a = 3$. For comparison, the fourth column lists a few estimates from the fundamental domain dynamical zeta function cycle expansion (20.7), and the fifth from the full 3-disk cycle expansion (20.36). The convergence of the fundamental domain dynamical zeta function is significantly slower than the convergence of the corresponding spectral determinant, and the full (unfactorized) 3-disk dynamical zeta function has still poorer convergence. (P.E. Rosenqvist.)

$R:a$	N	$\det(s - \mathcal{A})$	$1/\zeta(s)$	$1/\zeta(s)_{3\text{-disk}}$
6	1	0.39	0.407	
	2	0.4105	0.41028	0.435
	3	0.410338	0.410336	0.4049
	4	0.4103384074	0.4103383	0.40945
	5	0.4103384077696	0.4103384	0.410367
	6	0.410338407769346482	0.4103383	0.410338
	7	0.4103384077693464892		0.4103396
	8	0.410338407769346489338468		
	9	0.4103384077693464893384613074		
	10	0.4103384077693464893384613078192		
3	1	0.41		
	2	0.72		
	3	0.675		
	4	0.67797		
	5	0.677921		
	6	0.6779227		
	7	0.6779226894		
	8	0.6779226896002		
	9	0.677922689599532		
	10	0.67792268959953606		

so the n th order term of the spectral determinant cycle (or in this case, the cumulant) expansion is given recursively by the trace formula expansion coefficients

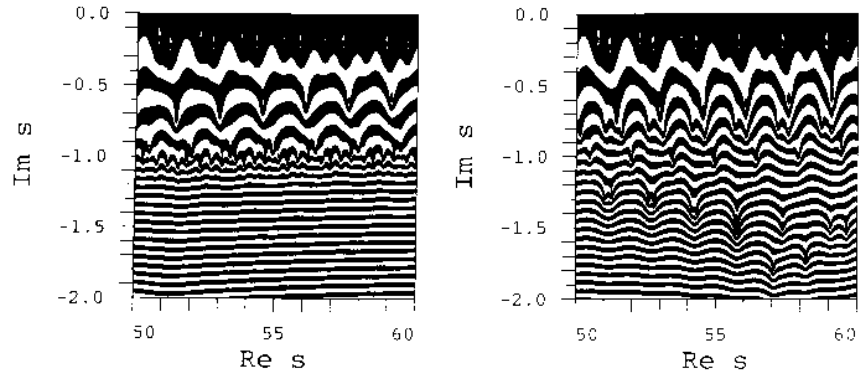
$$Q_n = \frac{1}{n} (C_n - C_{n-1}Q_1 - \dots - C_1Q_{n-1}), \quad Q_1 = C_1. \tag{20.12}$$

Given the trace formula (20.10) truncated to z^N , we now also have the spectral determinant truncated to z^N .

The same program can also be reused to compute the dynamical zeta function cycle expansion (20.9), by replacing $\prod (1 - \Lambda_{(i,j)}^r)$ in (20.10) by the product of expanding eigenvalues $\Lambda_{(i)} = \prod_e \Lambda_{(i),e}$ (see sect. 19.3).

The calculation of the leading eigenvalue of a given continuous flow evolution operator is now straightforward. After the prime cycles and the pseudocycles have been grouped into subsets of equal topological length, the dummy variable can be set equal to $z = 1$. With $z = 1$, expansion (20.11) is the cycle expansion for (19.6), the spectral determinant $\det(s - \mathcal{A})$. We vary s in cycle weights, and determine the eigenvalue s_α by finding $s = s_\alpha$ for which (20.11) vanishes. As an example, the convergence of a leading eigenvalue for a nice hyperbolic system is illustrated in table 20.2 by the listing of pinball escape rate γ estimates computed from truncations of (20.7) and (20.11) to different maximal cycle lengths.

Figure 20.1: Examples of the complex s plane scans: contour plots of the logarithm of the absolute values of (a) $1/\zeta(s)$, (b) spectral determinant $\det(s - \mathcal{A})$ for the 3-disk system, separation $a : R = 6$, A_1 subspace are evaluated numerically. The eigenvalues of the evolution operator \mathcal{L} are given by the centers of elliptic neighborhoods of the rapidly narrowing rings. While the dynamical zeta function is analytic on a strip $\text{Im } s \geq -1$, the spectral determinant is entire and reveals further families of zeros. (P.E. Rosenqvist)



The pleasant surprise is that the coefficients in these cycle expansions can be proven to fall off exponentially or even faster, due to analyticity of $\det(s - \mathcal{A})$ or $1/\zeta(s)$ for s values well beyond those for which the corresponding trace formula diverges.

chapter 23

20.2.3 Newton algorithm for determination of the evolution operator eigenvalues

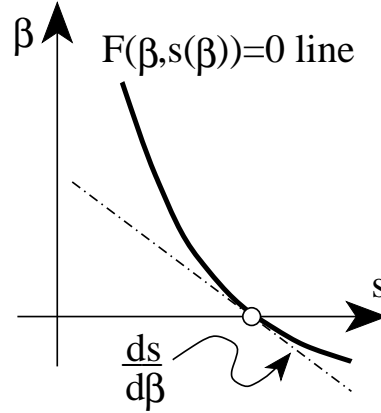


The cycle expansions of spectral determinants yield the eigenvalues of the evolution operator beyond the leading one. A convenient way to search for these is by plotting either the absolute magnitude $\ln |\det(s - \mathcal{A})|$ or the phase of spectral determinants and dynamical zeta functions as functions of the complex variable s . The eye is guided to the zeros of spectral determinants and dynamical zeta functions by means of complex s plane contour plots, with different intervals of the absolute value of the function under investigation assigned different colors; zeros emerge as centers of elliptic neighborhoods of rapidly changing colors. Detailed scans of the whole area of the complex s plane under investigation and searches for the zeros of spectral determinants, figure 20.1, reveal complicated patterns of resonances even for something so simple as the 3-disk game of pinball. With a good starting guess (such as a location of a zero suggested by the complex s scan of figure 20.1), a zero $1/\zeta(s) = 0$ can now be easily determined by standard numerical methods, such as the iterative Newton algorithm (13.4), with the m th Newton estimate given by

$$s_{m+1} = s_m - \left(\zeta(s_m) \frac{\partial}{\partial s} \zeta^{-1}(s_m) \right)^{-1} = s_m - \frac{1/\zeta(s_m)}{\langle T \rangle_\zeta}. \quad (20.13)$$

The denominator $\langle T \rangle_\zeta$ required for the Newton iteration is given below, by the cycle expansion (20.22). We need to evaluate it anyhow, as $\langle T \rangle_\zeta$ enters our cycle averaging formulas.

Figure 20.2: The eigenvalue condition is satisfied on the curve $F = 0$ the (β, s) plane. The expectation value of the observable (17.12) is given by the slope of the curve.



20.3 Cycle formulas for dynamical averages

The eigenvalue condition in any of the three forms that we have given so far - the level sum (22.18), the dynamical zeta function (20.2), the spectral determinant (20.11):

$$1 = \sum_i^{(n)} t_i, \quad t_i = t_i(\beta, s(\beta)), \quad n_i = n, \quad (20.14)$$

$$0 = 1 - \sum_{\pi}' t_{\pi}, \quad t_{\pi} = t_{\pi}(z, \beta, s(\beta)) \quad (20.15)$$

$$0 = 1 - \sum_{n=1}^{\infty} Q_n, \quad Q_n = Q_n(\beta, s(\beta)), \quad (20.16)$$

is an implicit equation for the eigenvalue $s = s(\beta)$ of form $F(\beta, s(\beta)) = 0$. The eigenvalue $s = s(\beta)$ as a function of β is sketched in figure 20.2; the eigenvalue condition is satisfied on the curve $F = 0$. The cycle averaging formulas for the slope and the curvature of $s(\beta)$ are obtained as in (17.12) by taking derivatives of the eigenvalue condition. Evaluated along $F = 0$, the first derivative leads to

$$\begin{aligned} 0 &= \frac{d}{d\beta} F(\beta, s(\beta)) \\ &= \frac{\partial F}{\partial \beta} + \frac{ds}{d\beta} \frac{\partial F}{\partial s} \Big|_{s=s(\beta)} \implies \frac{ds}{d\beta} = -\frac{\partial F}{\partial \beta} / \frac{\partial F}{\partial s}, \end{aligned} \quad (20.17)$$

and the second derivative of $F(\beta, s(\beta)) = 0$ yields

$$\frac{d^2 s}{d\beta^2} = -\left[\frac{\partial^2 F}{\partial \beta^2} + 2 \frac{ds}{d\beta} \frac{\partial^2 F}{\partial \beta \partial s} + \left(\frac{ds}{d\beta} \right)^2 \frac{\partial^2 F}{\partial s^2} \right] / \frac{\partial F}{\partial s}. \quad (20.18)$$

Denoting by

$$\langle A \rangle_F = -\frac{\partial F}{\partial \beta} \Big|_{\beta, s=s(\beta)}, \quad \langle T \rangle_F = \frac{\partial F}{\partial s} \Big|_{\beta, s=s(\beta)},$$

$$\langle (A - \langle A \rangle)^2 \rangle_F = \left. \frac{\partial^2 F}{\partial \beta^2} \right|_{\beta, s=s(\beta)} \quad (20.19)$$

respectively the mean cycle expectation value of A , the mean cycle period, and the second derivative of F computed for $F(\beta, s(\beta)) = 0$, we obtain the cycle averaging formulas for the expectation value of the observable (17.12), and its variance:

$$\langle a \rangle = \frac{\langle A \rangle_F}{\langle T \rangle_F} \quad (20.20)$$

$$\langle (a - \langle a \rangle)^2 \rangle = \frac{1}{\langle T \rangle_F} \langle (A - \langle A \rangle)^2 \rangle_F . \quad (20.21)$$

These formulas are the central result of the periodic orbit theory. As we shall now show, for each choice of the eigenvalue condition function $F(\beta, s)$ in (22.18), (20.2) and (20.11), the above quantities have explicit cycle expansions.

20.3.1 Dynamical zeta function cycle expansions

For the dynamical zeta function condition (20.15), the cycle averaging formulas (20.17), (20.21) require evaluation of the derivatives of dynamical zeta function at a given eigenvalue. Substituting the cycle expansion (20.2) for dynamical zeta function we obtain

$$\begin{aligned} \langle A \rangle_\zeta &:= -\frac{\partial}{\partial \beta} \frac{1}{\zeta} = \sum' A_\pi t_\pi \\ \langle T \rangle_\zeta &:= \frac{\partial}{\partial s} \frac{1}{\zeta} = \sum' T_\pi t_\pi, \quad \langle n \rangle_\zeta := -z \frac{\partial}{\partial z} \frac{1}{\zeta} = \sum' n_\pi t_\pi, \end{aligned} \quad (20.22)$$

where the subscript in $\langle \cdot \cdot \rangle_\zeta$ stands for the dynamical zeta function average over prime cycles, A_π , T_π , and n_π are evaluated on pseudocycles (20.4), and pseudocycle weights $t_\pi = t_\pi(z, \beta, s(\beta))$ are evaluated at the eigenvalue $s(\beta)$. In most applications $\beta = 0$, and $s(\beta)$ of interest is typically the leading eigenvalue $s_0 = s_0(0)$ of the evolution generator \mathcal{A} .

For bounded flows the leading eigenvalue (the escape rate) vanishes, $s(0) = 0$, the exponent $\beta A_\pi - s T_\pi$ in (20.3) vanishes, so the cycle expansions take a simple form

$$\langle A \rangle_\zeta = \sum'_\pi (-1)^{k+1} \frac{A_{p_1} + A_{p_2} \cdots + A_{p_k}}{|\Lambda_{p_1} \cdots \Lambda_{p_k}|}, \quad (20.23)$$

and similarly for $\langle T \rangle_\zeta$, $\langle n \rangle_\zeta$. For example, for the complete binary symbolic dynamics the mean cycle period $\langle T \rangle_\zeta$ is given by

$$\begin{aligned} \langle T \rangle_\zeta &= \frac{T_0}{|\Lambda_0|} + \frac{T_1}{|\Lambda_1|} + \left(\frac{T_{01}}{|\Lambda_{01}|} - \frac{T_0 + T_1}{|\Lambda_0 \Lambda_1|} \right) \\ &+ \left(\frac{T_{001}}{|\Lambda_{001}|} - \frac{T_{01} + T_0}{|\Lambda_{01} \Lambda_0|} \right) + \left(\frac{T_{011}}{|\Lambda_{011}|} - \frac{T_{01} + T_1}{|\Lambda_{01} \Lambda_1|} \right) + \dots \end{aligned} \quad (20.24)$$

Note that the cycle expansions for averages are grouped into the same shadowing combinations as the dynamical zeta function cycle expansion (20.7), with nearby pseudocycles nearly cancelling each other.

The cycle averaging formulas for the expectation value of the observable $\langle a \rangle$ follow by substitution into (20.21). Assuming zero mean drift $\langle a \rangle = 0$, the cycle expansion (20.11) for the variance $\langle (A - \langle A \rangle)^2 \rangle_\zeta$ is given by

$$\langle A^2 \rangle_\zeta = \sum' (-1)^{k+1} \frac{(A_{p_1} + A_{p_2} \cdots + A_{p_k})^2}{|\Lambda_{p_1} \cdots \Lambda_{p_k}|}. \quad (20.25)$$

20.3.2 Spectral determinant cycle expansions

The dynamical zeta function cycle expansions have a particularly simple structure, with the shadowing apparent already by a term-by-term inspection of table 20.2. For “nice” hyperbolic systems the shadowing ensures exponential convergence of the dynamical zeta function cycle expansions. This, however, is not the best achievable convergence. As has been explained in chapter 23, for such systems the spectral determinant constructed from the same cycle data base is entire, and its cycle expansion converges faster than exponentially. In practice, the best convergence is attained by the spectral determinant cycle expansion (20.16) and its derivatives. The $\partial/\partial s$, $\partial/\partial \beta$ derivatives are in this case computed recursively, by taking derivatives of the spectral determinant cycle expansion contributions (20.12) and (20.10).

The cycle averaging formulas are exact, and highly convergent for nice hyperbolic dynamical systems. An example of its utility is the cycle expansion formula for the Lyapunov exponent of example 20.1. Further applications of cycle expansions will be discussed in chapter 22.

20.3.3 Continuous vs. discrete mean return time

Sometimes it is convenient to compute an expectation value along a flow, in continuous time, and sometimes it might be easier to compute it in discrete time, from a Poincaré return map. Return times (3.1) might vary wildly, and it is not at all clear that the continuous and discrete time averages are related in any simple way. The relationship turns out to be both elegantly simple, and totally general.

exercise 20.14

The mean cycle period $\langle T \rangle_\zeta$ fixes the normalization of the unit of time; it can be interpreted as the average near recurrence or the average first return time. For example, if we have evaluated a billiard expectation value $\langle a \rangle$ in terms of continuous time, and would like to also have the corresponding average $\langle a \rangle_{\text{dscr}}$ measured in discrete time, given by the number of reflections off billiard walls, the two averages are related by

$$\langle a \rangle_{\text{dscr}} = \langle a \rangle \langle T \rangle_\zeta / \langle n \rangle_\zeta, \quad (20.26)$$

where $\langle n \rangle_\zeta$ the average of the number of bounces n_p along the cycle p is given by is (20.22).

Example 20.1 Cycle expansion formula for Lyapunov exponents:

In sect. 17.3 we defined the Lyapunov exponent for a 1 – dimensional mapping, related it to the leading eigenvalue of an evolution operator and promised to evaluate it. Now we are finally in position to deliver on our promise.

The cycle averaging formula (20.23) yields an exact explicit expression for the Lyapunov exponent in terms of prime cycles:

$$\lambda = \frac{1}{\langle n \rangle_\zeta} \sum' (-1)^{k+1} \frac{\log |\Lambda_{p_1}| + \dots + \log |\Lambda_{p_k}|}{|\Lambda_{p_1} \cdots \Lambda_{p_k}|} . \tag{20.27}$$

For a repeller, the $1/|\Lambda_p|$ weights are replaced by normalized measure (22.10) $\exp(\gamma n_p)/|\Lambda_p|$, where γ is the escape rate.

We state without proof that for 2 – dimensional Hamiltonian flows such as our game of pinball there is only one expanding eigenvalue and (20.27) applies as it stands. However, in dimensions higher than one, a correct calculation of Lyapunov exponents requires a bit of sophistication.

20.4 Cycle expansions for finite alphabets



A finite transition graph like the one given in figure 14.6 (d) is a compact encoding of the transition matrix for a given subshift. It is a sparse matrix, and the associated determinant (15.20) can be written down by inspection: it is the sum of all possible partitions of the graph into products of non-intersecting loops, with each loop carrying a minus sign:

$$\det (1 - T) = 1 - t_0 - t_{0011} - t_{0001} - t_{00011} + t_0 t_{0011} + t_{0011} t_{0001} \tag{20.28}$$

The simplest application of this determinant is to the evaluation of the topological entropy; if we set $t_p = z^{n_p}$, where n_p is the length of the p -cycle, the determinant reduces to the topological polynomial (15.21).

The determinant (20.28) is exact for the finite graph figure 14.6 (e), as well as for the associated finite-dimensional transfer operator of example 17.4. For the associated (infinite dimensional) evolution operator, it is the beginning of the cycle expansion of the corresponding dynamical zeta function:

$$\begin{aligned} 1/\zeta = & 1 - t_0 - t_{0011} - t_{0001} + t_{0001} t_{0011} \\ & -(t_{00011} - t_0 t_{0011} + \dots \text{curvatures}) \dots \end{aligned} \tag{20.29}$$

The cycles $\overline{0}$, $\overline{0001}$ and $\overline{0011}$ are the *fundamental* cycles introduced in (20.7); they are not shadowed by any combinations of shorter cycles, and are the basic building blocks of the dynamics. All other cycles appear together with their shadows (for example, the $t_{00011} - t_{0011}$ combination) and yield exponentially small corrections for hyperbolic systems.

For the cycle counting purposes both t_{ab} and the pseudocycle combination $t_{a+b} = t_a t_b$ in (20.2) have the same weight $z^{n_a+n_b}$, so all curvature combinations $t_{ab} - t_a t_b$ vanish exactly, and the topological polynomial (15.27) offers a quick way of checking the fundamental part of a cycle expansion.

Since for finite grammars the topological zeta functions reduce to polynomials, we are assured that there are just a few fundamental cycles and that all long cycles can be grouped into curvature combinations. For example, the fundamental cycles in exercise 9.6 are the three 2-cycles which bounce back and forth between two disks and the two 3-cycles which visit every disk. It is only after these fundamental cycles have been included that a cycle expansion is expected to start converging smoothly, i.e., only for n larger than the lengths of the fundamental cycles are the curvatures \hat{c}_n (in expansion (20.7)), a measure of the deviations between long orbits and their short cycle approximants, expected to fall off rapidly with n .

20.5 Stability ordering of cycle expansions

There is never a second chance. Most often there is not even the first chance.

—John Wilkins

(C.P. Dettmann and P. Cvitanović)

Most dynamical systems of interest have no finite grammar, so at any order in z a cycle expansion may contain unmatched terms which do not fit neatly into the almost cancelling curvature corrections. Similarly, for intermittent systems that we shall discuss in chapter 24, curvature corrections are in general not small, so again the cycle expansions may converge slowly. For such systems schemes which collect the pseudocycle terms according to some criterion other than the topology of the flow may converge more quickly than expansions based on the topological length.

All chaotic systems exhibit some degree of shadowing, and a good truncation criterion should do its best to respect the shadowing at least approximately. If a long cycle is shadowed by two or more shorter cycles and the flow is smooth, the period and the action will be additive in sense that the period of the longer cycle is approximately the sum of the shorter cycle periods. Similarly, stability is multiplicative, so shadowing is approximately preserved by including all terms with pseudocycle stability

$$\left| \Lambda_{p_1} \cdots \Lambda_{p_k} \right| \leq \Lambda_{\max} \quad (20.30)$$

and ignoring all more unstable pseudocycles.

Two such schemes for ordering cycle expansions which approximately respect shadowing are truncations by the pseudocycle period (or action) and the stability ordering that we shall discuss here. In these schemes a dynamical zeta function or a spectral determinant is expanded keeping all terms for which the period, action or stability for a combination of cycles (pseudocycle) is less than a given cutoff.

The two settings in which the stability ordering may be preferable to the ordering by topological cycle length are the cases of bad grammar and of intermittency.

20.5.1 Stability ordering for bad grammars

For generic flows it is often not clear what partition of the state space generates the “optimal” symbolic dynamics. Stability ordering does not require understanding dynamics in such detail: if you can find the cycles, you can use stability ordered cycle expansions. Stability truncation is thus easier to implement for a generic dynamical system than the curvature expansions (20.7) which rely on finite subshift approximations to a given flow.

Cycles can be detected numerically by searching a long trajectory for near recurrences. The long trajectory method for detecting cycles preferentially finds the least unstable cycles, regardless of their topological length. Another practical advantage of the method (in contrast to Newton method searches) is that it only finds cycles in a given connected ergodic component of state space, ignoring isolated cycles or other ergodic regions elsewhere in the state space.

Why should stability ordered cycle expansion of a dynamical zeta function converge better than the rude trace formula (22.9)? The argument has essentially already been laid out in sect. 15.6: in truncations that respect shadowing most of the pseudocycles appear in shadowing combinations and nearly cancel, while only the relatively small subset affected by the longer and longer pruning rules is not shadowed. So the error is typically of the order of $1/\Lambda$, smaller by factor e^{hT} than the trace formula (22.9) error, where h is the entropy and T typical cycle length for cycles of stability Λ .

20.5.2 Smoothing



The breaking of exact shadowing cancellations deserves further comment. Partial shadowing which may be present can be (partially) restored by smoothing the stability ordered cycle expansions by replacing the $1/\Lambda$ weight for each term with pseudocycle stability $\Lambda = \Lambda_{p_1} \cdots \Lambda_{p_k}$ by $f(\Lambda)/\Lambda$. Here, $f(\Lambda)$ is a monotonically decreasing function from $f(0) = 1$ to $f(\Lambda_{\max}) = 0$. No smoothing corresponds to a step function.

A typical “shadowing error” induced by the cutoff is due to two pseudocycles of stability Λ separated by $\Delta\Lambda$, and whose contribution is of opposite signs. Ignoring possible weighting factors the magnitude of the resulting term is of order $1/\Lambda - 1/(\Lambda + \Delta\Lambda) \approx \Delta\Lambda/\Lambda^2$. With smoothing there is an extra term of the form $f'(\Lambda)\Delta\Lambda/\Lambda$, which we want to minimise. A reasonable guess might be to keep $f'(\Lambda)/\Lambda$ constant and as small as possible, that is

$$f(\Lambda) = 1 - \left(\frac{\Lambda}{\Lambda_{\max}} \right)^2$$

The results of a stability ordered expansion (20.30) should always be tested for robustness by varying the cutoff Λ_{\max} . If this introduces significant variations, smoothing is probably necessary.

20.5.3 Stability ordering for intermittent flows



Longer but less unstable cycles can give larger contributions to a cycle expansion than short but highly unstable cycles. In such situation truncation by length may require an exponentially large number of very unstable cycles before a significant longer cycle is first included in the expansion. This situation is best illustrated by intermittent maps that we shall study in detail in chapter 24, the simplest of which is the Farey map

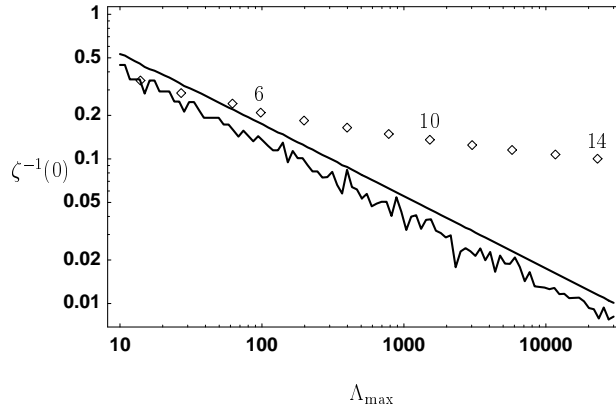
$$f(x) = \begin{cases} f_0 = x/(1-x) & 0 \leq x \leq 1/2 \\ f_1 = (1-x)/x & 1/2 \leq x \leq 1 \end{cases}, \quad (20.31)$$

a map which will reappear in the intermittency chapter 24.

For this map the symbolic dynamics is of complete binary type, so lack of shadowing is not due to lack of a finite grammar, but rather to the intermittency caused by the existence of the marginal fixed point $x_0 = 0$, for which the stability equals $\Lambda_0 = 1$. This fixed point does not participate directly in the dynamics and is omitted from cycle expansions. Its presence is felt in the stabilities of neighboring cycles with n consecutive repeats of the symbol 0’s whose stability falls off only as $\Lambda \sim n^2$, in contrast to the most unstable cycles with n consecutive 1’s which are exponentially unstable, $|\Lambda_{01^n}| \sim [(\sqrt{5} + 1)/2]^n$.

The symbolic dynamics is of complete binary type. A quick count in the style of sect. 15.7.2 leads to a total of 74,248,450 prime cycles of length 30 or less, not including the marginal point $x_0 = 0$. Evaluating a cycle expansion to this order would be no mean computational feat. However, the least unstable cycle omitted has stability of roughly $\Lambda_{10^{30}} \sim 30^2 = 900$, and so amounts to a 0.1% correction. The situation may be much worse than this estimate suggests, because the next, 10^{31} cycle contributes a similar amount, and could easily reinforce the error. Adding up all such omitted terms, we arrive at an estimated error of about 3%,

Figure 20.3: Comparison of cycle expansion truncation schemes for the Farey map (20.31); the deviation of the truncated cycles expansion for $|1/\zeta_N(0)|$ from the exact flow conservation value $1/\zeta(0) = 0$ is a measure of the accuracy of the truncation. The jagged line is logarithm of the stability ordering truncation error; the smooth line is smoothed according to sect. 20.5.2; the diamonds indicate the error due the topological length truncation, with the maximal cycle length N shown. They are placed along the stability cutoff axis at points determined by the condition that the total number of cycles is the same for both truncation schemes.



for a cycle-length truncated cycle expansion based on more than 10^9 pseudocycle terms! On the other hand, truncating by stability at say $\Lambda_{max} = 3000$, only 409 prime cycles suffice to attain the same accuracy of about 3% error, figure 20.3.

As the Farey map maps the unit interval onto itself, the leading eigenvalue of the Perron-Frobenius operator should equal $s_0 = 0$, so $1/\zeta(0) = 0$. Deviation from this exact result serves as an indication of the convergence of a given cycle expansion. The errors of different truncation schemes are indicated in figure 20.3. We see that topological length truncation schemes are hopelessly bad in this case; stability length truncations are somewhat better, but still rather bad. In simple cases like this one, where intermittency is caused by a single marginal fixed point, the convergence can be improved by going to infinite alphabets.

20.6 Dirichlet series

The most patient reader will thank me for compressing so much nonsense and falsehood into a few lines.

—Gibbon



A Dirichlet series is defined as

$$f(s) = \sum_{j=1}^{\infty} a_j e^{-\lambda_j s} \tag{20.32}$$

where s, a_j are complex numbers, and $\{\lambda_j\}$ is a monotonically increasing series of real numbers $\lambda_1 < \lambda_2 < \dots < \lambda_j < \dots$. A classical example of a Dirichlet series is the Riemann zeta function for which $a_j = 1, \lambda_j = \ln j$. In the present context, formal series over individual pseudocycles such as (20.2) ordered by the increasing pseudocycle periods are often Dirichlet series. For example, for the pseudocycle weight (20.3), the Dirichlet series is obtained by ordering pseudocycle-

cles by increasing periods $\lambda_\pi = T_{p_1} + T_{p_2} + \dots + T_{p_k}$, with the coefficients

$$a_\pi = \frac{e^{\beta \cdot (A_{p_1} + A_{p_2} + \dots + A_{p_k})}}{|\Lambda_{p_1} \Lambda_{p_2} \dots \Lambda_{p_k}|} d_\pi,$$

where d_π is a degeneracy factor, in the case that d_π pseudocycles have the same weight.

If the series $\sum |a_j|$ diverges, the Dirichlet series is absolutely convergent for $\text{Re } s > \sigma_a$ and conditionally convergent for $\text{Re } s > \sigma_c$, where σ_a is the *abscissa of absolute convergence*

$$\sigma_a = \lim_{N \rightarrow \infty} \sup \frac{1}{\lambda_N} \ln \sum_{j=1}^N |a_j|, \quad (20.33)$$

and σ_c is the *abscissa of conditional convergence*

$$\sigma_c = \lim_{N \rightarrow \infty} \sup \frac{1}{\lambda_N} \ln \left| \sum_{j=1}^N a_j \right|. \quad (20.34)$$

We shall encounter another example of a Dirichlet series in the semiclassical quantization, the quantum chaos part of ChaosBook.org.

Résumé

A *cycle expansion* is a series representation of a dynamical zeta function, trace formula or a spectral determinant, with products in (19.15) expanded as sums over *pseudocycles*, products of the prime cycle weights t_p .

If a flow is hyperbolic and has a topology of a Smale horseshoe (a subshift of finite type), the dynamical zeta functions are holomorphic, the spectral determinants are entire, and the spectrum of the evolution operator is discrete. The situation is considerably more reassuring than what practitioners of quantum chaos fear; there is no “abscissa of absolute convergence” and no “entropy barrier,” the exponential proliferation of cycles is no problem, spectral determinants are entire and converge everywhere, and the topology dictates the choice of cycles to be used in cycle expansion truncations.

In that case, the basic observation is that the motion in dynamical systems of few degrees of freedom is in this case organized around a few *fundamental* cycles, with the cycle expansion of the Euler product

$$1/\zeta = 1 - \sum_f t_f - \sum_n \hat{c}_n,$$

regrouped into dominant *fundamental* contributions t_f and decreasing *curvature* corrections \hat{c}_n . The fundamental cycles t_f have no shorter approximants; they are the “building blocks” of the dynamics in the sense that all longer orbits can be approximately pieced together from them. A typical curvature contribution to \hat{c}_n is a *difference* of a long cycle $\{ab\}$ minus its shadowing approximation by shorter cycles $\{a\}$ and $\{b\}$:

$$t_{ab} - t_a t_b = t_{ab}(1 - t_a t_b / t_{ab})$$

The orbits that follow the same symbolic dynamics, such as $\{ab\}$ and a “pseudocycle” $\{a\}\{b\}$, lie close to each other, have similar weights, and for longer and longer orbits the curvature corrections fall off rapidly. Indeed, for systems that satisfy the “axiom A” requirements, such as the 3-disk billiard, curvature expansions converge very well.

Once a set of the shortest cycles has been found, and the cycle periods, stabilities and integrated observable computed, the cycle averaging formulas such as the ones associated with the dynamical zeta function

$$\begin{aligned} \langle a \rangle &= \langle A \rangle_\zeta / \langle T \rangle_\zeta \\ \langle A \rangle_\zeta &= -\frac{\partial}{\partial \beta} \frac{1}{\zeta} = \sum' A_\pi t_\pi, & \langle T \rangle_\zeta &= \frac{\partial}{\partial s} \frac{1}{\zeta} = \sum' T_\pi t_\pi \end{aligned}$$

yield the expectation value (the chaotic, ergodic average over the non-wandering set) of the observable $a(x)$.

Commentary

Remark 20.1 Pseudocycle expansions. Bowen’s introduction of shadowing ϵ -pseudoorbits [28] was a significant contribution to Smale’s theory. Expression “pseudoorbits” seems to have been introduced in the Parry and Pollicott’s 1983 paper [16]. Following them M. Berry [9] had used the expression “pseudoorbits” in his 1986 paper on Riemann zeta and quantum chaos. Cycle and curvature expansions of dynamical zeta functions and spectral determinants were introduced in refs. [10, 2]. Some literature [12] refers to the pseudoorbits as “composite orbits,” and to the cycle expansions as “Dirichlet series” (see also remark 20.6 and sect. 20.6).

Remark 20.2 Cumulant expansion. To a statistical mechanician the curvature expansions are very reminiscent of cumulant expansions. Indeed, (20.12) is the standard Plemelj-Smithies cumulant formula for the Fredholm determinant. The difference is that in cycle expansions each Q_n coefficient is expressed as a sum over exponentially many cycles.

Remark 20.3 Exponential growth of the number of cycles. Going from $N_n \approx N^n$ periodic points of length n to M_n prime cycles reduces the number of computations from N_n to $M_n \approx N^{n-1}/n$. Use of discrete symmetries (chapter 21) reduces the number of n th level terms by another factor. While the reformulation of the theory from the trace (18.28) to the cycle expansion (20.7) thus does not eliminate the exponential growth in the number of cycles, in practice only the shortest cycles are used, and for them the computational labor saving can be significant.

Remark 20.4 Shadowing cycle-by-cycle. A glance at the low order curvatures in the table 20.1 leads to the temptation of associating curvatures to individual cycles, such as $\hat{c}_{0001} = t_{0001} - t_0 t_{001}$. Such combinations tend to be numerically small (see for example ref. [3], table 1). However, splitting \hat{c}_n into individual cycle curvatures is not possible in general [12]; the first example of such ambiguity in the binary cycle expansion is given by the $t_{100101}, t_{100110} 0 \leftrightarrow 1$ symmetric pair of 6-cycles; the counterterm $t_{001} t_{011}$ in table 20.1 is shared by the two cycles.

Remark 20.5 Stability ordering. The stability ordering was introduced by Dahlqvist and Russberg [13] in a study of chaotic dynamics for the $(x^2 y^2)^{1/a}$ potential. The presentation here runs along the lines of Dettmann and Morriss [14] for the Lorentz gas which is hyperbolic but the symbolic dynamics is highly pruned, and Dettmann and Cvitanović [15] for a family of intermittent maps. In the applications discussed in the above papers, the stability ordering yields a considerable improvement over the topological length ordering. In quantum chaos applications cycle expansion cancelations are affected by the phases of pseudocycles (their actions), hence *period ordering* rather than stability is frequently employed.

Remark 20.6 Are cycle expansions Dirichlet series?

Even though some literature [12] refers to cycle expansions as “Dirichlet series,” they are not Dirichlet series. Cycle expansions collect contributions of individual cycles into groups that correspond to the coefficients in cumulant expansions of spectral determinants, and the convergence of cycle expansions is controlled by general properties of spectral determinants. Dirichlet series order cycles by their periods or actions, and are only conditionally convergent in regions of interest. The abscissa of absolute convergence is in this context called the “entropy barrier”; contrary to the frequently voiced anxieties, this number does not necessarily has much to do with the actual convergence of the theory.

Exercises

20.1. **Cycle expansions.** Write programs that implement *binary* symbolic dynamics cycle expansions for (a) dynamical zeta functions, (b) spectral determinants. Combined with the cycles computed for a 2-branch repeller or a 3-disk system they will be useful in problem that follow.

20.2. **Escape rate for a 1 – dimensional repeller.** (continuation of exercise 19.1 - easy, but long)
Consider again the quadratic map (19.31)

$$f(x) = Ax(1 - x)$$

on the unit interval, for definitiveness take either $A = 9/2$ or $A = 6$. Describing the itinerary of any trajectory by the binary alphabet $\{0, 1\}$ ('0' if the iterate is in the first half of the interval and '1' if is in the second half), we have a repeller with a complete binary symbolic dynamics.

- (a) Sketch the graph of f and determine its two fixed points $\bar{0}$ and $\bar{1}$, together with their stabilities.
- (b) Sketch the two branches of f^{-1} . Determine all the prime cycles up to topological length 4 using your pocket calculator and backwards iteration of f (see sect. 13.2.1).
- (c) Determine the leading zero of the zeta function (19.15) using the weights $t_p = z^{n_p}/|\Lambda_p|$ where Λ_p is the stability of the p cycle.
- (d) Show that for $A = 9/2$ the escape rate of the repeller is 0.361509... using the spectral determinant, with the same cycle weight. If you have taken $A = 6$, the escape rate is in 0.83149298..., as shown in solution 20.2. Compare the coefficients of the spectral determinant and the zeta function cycle expansions. Which expansion converges faster?

(Per Rosenqvist)

20.3. **Escape rate for the Ulam map.** (Medium; repeat of exercise 13.1) We will try to compute the escape rate for the Ulam map (11.5)

$$f(x) = 4x(1 - x),$$

using the method of cycle expansions. The answer should be zero, as nothing escapes.

- (a) Compute a few of the stabilities for this map. Show that $\Lambda_0 = 4$, $\Lambda_1 = -2$, $\Lambda_{01} = -4$, $\Lambda_{001} = -8$ and $\Lambda_{011} = 8$.

(b) Show that

$$\Lambda_{\epsilon_1 \dots \epsilon_n} = \pm 2^n$$

and determine a rule for the sign.

(c) (hard) Compute the dynamical zeta function for this system

$$\zeta^{-1} = 1 - t_0 - t_1 - (t_{01} - t_0 t_1) - \dots$$

You might note that the convergence as function of the truncation cycle length is slow. Try to fix that by treating the $\Lambda_0 = 4$ cycle separately. (continued as exercise 20.13)

20.4. **Pinball escape rate, semi-analytical.** Estimate the 3-disk pinball escape rate for $R : a = 6$ by substituting analytical cycle stabilities and periods (exercise 13.7 and exercise 13.8) into the appropriate binary cycle expansion. Compare with the numerical estimate exercise 17.3.

20.5. **Pinball escape rate, from numerical cycles.** Compute the escape rate for $R : a = 6$ 3-disk pinball by substituting list of numerically computed cycle stabilities of exercise 13.5 into the binary cycle expansion.

20.6. **Pinball resonances, in the complex plane.** Plot the logarithm of the absolute value of the dynamical zeta function and/or the spectral determinant cycle expansion (20.5) as contour plots in the complex s plane. Do you find zeros other than the one corresponding to the complex one? Do you see evidence for a finite radius of convergence for either cycle expansion?

20.7. **Counting the 3-disk pseudocycles.** (continuation of exercise 15.12.) Verify that the number of terms in the 3-disk pinball curvature expansion (20.35) is given by

$$\begin{aligned} \prod_p (1 + t_p) &= \frac{1 - 3z^4 - 2z^6}{1 - 3z^2 - 2z^3} \\ &= 1 + 3z^2 + 2z^3 + \frac{z^4(6 + 12z + 2z^2)}{1 - 3z^2 - 2z^3} \\ &= 1 + 3z^2 + 2z^3 + 6z^4 + 12z^5 \\ &\quad + 20z^6 + 48z^7 + 84z^8 + 184z^9 + \dots \end{aligned}$$

This means that, for example, c_6 has a total of 20 terms, in agreement with the explicit 3-disk cycle expansion (20.36).

20.8. **3-disk unfactorized zeta cycle expansions.** Check that the curvature expansion (20.2) for the 3-disk pinball, assuming no symmetries between disks, is given by

$$\begin{aligned}
 1/\zeta &= (1 - z^2 t_{12})(1 - z^2 t_{13})(1 - z^2 t_{23}) \\
 &\quad (1 - z^3 t_{123})(1 - z^3 t_{132})(1 - z^4 t_{1213}) \\
 &\quad (1 - z^4 t_{1232})(1 - z^4 t_{1323})(1 - z^5 t_{12123}) \cdots \\
 &= 1 - z^2 t_{12} - z^2 t_{23} - z^2 t_{31} - z^3 (t_{123} + t_{132}) \\
 &\quad - z^4 [(t_{1213} - t_{12} t_{13}) + (t_{1232} - t_{12} t_{23}) \\
 &\quad + (t_{1323} - t_{13} t_{23})] \quad (20.35) \\
 &\quad - z^5 [(t_{12123} - t_{12} t_{123}) + \cdots] - \cdots
 \end{aligned}$$

The symmetrically arranged 3-disk pinball cycle expansion of the Euler product (20.2) (see table 15.5 and figure 9.5) is given by:

$$\begin{aligned}
 1/\zeta &= (1 - z^2 t_{12})^3 (1 - z^3 t_{123})^2 (1 - z^4 t_{1213})^3 \\
 &\quad (1 - z^5 t_{12123})^6 (1 - z^6 t_{121213})^6 \quad 20.10. \\
 &\quad (1 - z^6 t_{121323})^3 \cdots \quad (20.36) \\
 &= 1 - 3z^2 t_{12} - 2z^3 t_{123} - 3z^4 (t_{1213} - t_{12}^2) \\
 &\quad - 6z^5 (t_{12123} - t_{12} t_{123}) \\
 &\quad - z^6 (6 t_{121213} + 3 t_{121323} + t_{12}^3 - 9 t_{12} t_{1213} - t_{123}^2) \\
 &\quad - 6z^7 (t_{1212123} + t_{1212313} + t_{1213123} + t_{12}^2 t_{123} \\
 &\quad - 3 t_{12} t_{12123} - t_{123} t_{1213}) \\
 &\quad - 3z^8 (2 t_{12121213} + t_{12121313} + 2 t_{12121323} \\
 &\quad + 2 t_{12123123} + 2 t_{12123213} + t_{12132123} \\
 &\quad + 3 t_{12}^2 t_{1213} + t_{12} t_{123}^2 - 6 t_{12} t_{121213} \\
 &\quad - 3 t_{12} t_{121323} - 4 t_{123} t_{12123} - t_{123}^2) - \cdots
 \end{aligned}$$

Remark 20.7 Unsymmetrized cycle expansions. The above 3-disk cycle expansions might be useful for cross-checking purposes, but, as we shall see in chapter 21, they are not recommended for actual computations, as the factorized zeta functions yield much better convergence.

20.9. **4-disk unfactorized dynamical zeta function cycle expansions.** For the symmetrically arranged 4-disk pinball the symmetry group is C_{4v} , of order 8. The degenerate cycles can have multiplicities 2, 4 or 8 (see table 15.3):

$$\begin{aligned}
 1/\zeta &= (1 - z^2 t_{12})^4 (1 - z^2 t_{13})^2 (1 - z^3 t_{123})^8 \\
 &\quad (1 - z^4 t_{1213})^8 (1 - z^4 t_{1214})^4 (1 - z^4 t_{1234})^2 \\
 &\quad (1 - z^4 t_{1243})^4 (1 - z^5 t_{12123})^8 (1 - z^5 t_{12124})^8 \quad 20.11. \\
 &\quad (1 - z^5 t_{12134})^8 (1 - z^5 t_{12143})^8 \\
 &\quad (1 - z^5 t_{12313})^8 (1 - z^5 t_{12413})^8 \cdots \quad (20.37)
 \end{aligned}$$

and the cycle expansion is given by

$$\begin{aligned}
 1/\zeta &= 1 - z^2 (4 t_{12} + 2 t_{13}) - 8z^3 t_{123} \\
 &\quad - z^4 (8 t_{1213} + 4 t_{1214} + 2 t_{1234} + 4 t_{1243} \\
 &\quad - 6 t_{12}^2 - t_{13}^2 - 8 t_{12} t_{13}) \\
 &\quad - 8z^5 (t_{12123} + t_{12124} + t_{12134} + t_{12143} + t_{12313} \\
 &\quad + t_{12413} - 4 t_{12} t_{123} - 2 t_{13} t_{123}) \\
 &\quad - 4z^6 (2 S_8 + S_4 + t_{12}^3 + 3 t_{12}^2 t_{13} + t_{12} t_{13}^2 \\
 &\quad - 8 t_{12} t_{1213} - 4 t_{12} t_{1214} \\
 &\quad - 2 t_{12} t_{1234} - 4 t_{12} t_{1243} \\
 &\quad - 4 t_{13} t_{1213} - 2 t_{13} t_{1214} - t_{13} t_{1234} \\
 &\quad - 2 t_{13} t_{1243} - 7 t_{123}^2) - \cdots
 \end{aligned}$$

where in the coefficient to z^6 the abbreviations S_8 and S_4 stand for the sums over the weights of the 12 orbits with multiplicity 8 and the 5 orbits of multiplicity 4, respectively; the orbits are listed in table 15.5.

Tail resummations. A simple illustration of such tail resummation is the ζ function for the Ulam map (11.5) for which the cycle structure is exceptionally simple: the eigenvalue of the $x_0 = 0$ fixed point is 4, while the eigenvalue of any other n -cycle is $\pm 2^n$. Typical cycle weights used in thermodynamic averaging are $t_0 = 4^z$, $t_1 = t = 2^z$, $t_p = t^{np}$ for $p \neq 0$. The simplicity of the cycle eigenvalues enables us to evaluate the ζ function by a simple trick: we note that if the value of any n -cycle eigenvalue were t^n , (19.21) would yield $1/\zeta = 1 - 2t$. There is only one cycle, the x_0 fixed point, that has a different weight $(1 - t_0)$, so we factor it out, multiply the rest by $(1 - t)/(1 - t)$, and obtain a rational ζ function

$$1/\zeta(z) = \frac{(1 - 2t)(1 - t_0)}{(1 - t)} \quad (20.38)$$

Consider how we would have detected the pole at $z = 1/t$ without the above trick. As the $\bar{0}$ fixed point is isolated in its stability, we would have kept the factor $(1 - t_0)$ in (20.7) unexpanded, and noted that all curvature combinations in (20.7) which include the t_0 factor are unbalanced, so that the cycle expansion is an infinite series:

$$\prod_p (1 - t_p) = (1 - t_0)(1 - t - t^2 - t^3 - t^4 - \dots) \quad (20.39)$$

(we shall return to such infinite series in chapter 24). The geometric series in the brackets sums up to (20.38). Had we expanded the $(1 - t_0)$ factor, we would have noted that the ratio of the successive curvatures is exactly $c_{n+1}/c_n = t$; summing we would recover the rational ζ function (20.38).

20.11. Escape rate for the Rössler flow. (continuation of exercise 13.10) Try to compute the escape rate for the Rössler flow (2.17) using the method of cycle expansions. The answer should be zero, as nothing escapes.

Ideally you should already have computed the cycles and have an approximate grammar, but failing that you can cheat a bit and peak into exercise 13.10.

- 20.12. **State space volume contraction, recycled.** (continuation of exercise 4.3) The plot of instantaneous state space volume contraction as a function of time in exercise 4.3 (d) illustrates one problem of time-averaging in chaotic flows - the observable might vary wildly across each recurrence to a given Poincaré section. Evaluated on a given short cycle, the average is crisp and arbitrarily accurate. Recompute $\langle \partial \cdot v \rangle$ by means of cycle expansion, study its convergence. $1/t$ convergence of mindless time-averaging is now replaced by exponential convergence in the cycle length.
- 20.13. **Ulam map is conjugate to the tent map.** (continuation of exercise 20.3 / repeat of exercise 6.4 and exercise 13.2; requires real smarts, unless you look it up) Explain the magically simple form of cycle stabilities of

exercise 20.3 by constructing an explicit smooth conjugacy (6.1)

$$g^t(y_0) = h \circ f^t \circ h^{-1}(y_0)$$

that conjugates the Ulam map (11.5) into the tent map (11.4).

- 20.14. **Continuous vs. discrete mean return time.** Show that the expectation value $\langle a \rangle$ time-averaged over continuous time flow is related to the corresponding average $\langle a \rangle_{\text{dscr}}$ measured in discrete time (e.g., Poincaré section returns) by (20.26):

$$\langle a \rangle_{\text{dscr}} = \langle a \rangle \langle T \rangle_{\zeta} / \langle n \rangle_{\zeta} . \quad (20.40)$$

(Hint: consider the form of their cycle expansions.) The mean discrete period $\langle n \rangle_{\zeta}$ averaged over cycles, and the mean continuous time period $\langle T \rangle_{\zeta}$ need to be evaluated only once, thereafter one can compute either $\langle a \rangle$ or $\langle a \rangle_{\text{dscr}}$, whichever is more convenient.

References

- [20.1] P. Cvitanović, *Phys. Rev. Lett.* **61**, 2729 (1988).
- [20.2] R. Artuso, E. Aurell and P. Cvitanović, "Recycling of strange sets I: Cycle expansions," *Nonlinearity* **3**, 325 (1990).
- [20.3] R. Artuso, E. Aurell and P. Cvitanović, "Recycling of strange sets II: Applications," *Nonlinearity* **3**, 361 (1990).
- [20.4] S. Grossmann and S. Thomae, *Z. Naturforsch.* **32 a**, 1353 (1977); reprinted in ref. [5].
- [20.5] *Universality in Chaos*, P. Cvitanović, ed., (Adam Hilger, Bristol 1989).
- [20.6] F. Christiansen, P. Cvitanović and H.H. Rugh, *J. Phys A* **23**, L713 (1990).
- [20.7] J. Plemelj, "Zur Theorie der Fredholmschen Funktionalgleichung," *Monat. Math. Phys.* **15**, 93 (1909).
- [20.8] F. Smithies, "The Fredholm theory of integral equations," *Duke Math.* **8**, 107 (1941).
- [20.9] M.V. Berry, in *Quantum Chaos and Statistical Nuclear Physics*, ed. T.H. Seligman and H. Nishioka, *Lecture Notes in Physics* **263**, 1 (Springer, Berlin, 1986).
- [20.10] P. Cvitanović, "Invariant measurements of strange sets in terms of cycles," *Phys. Rev. Lett.* **61**, 2729 (1988).
- [20.11] B. Eckhardt and G. Russberg, *Phys. Rev.* **E 47**, 1578 (1993).

- [20.12] E. Aurell, ‘Convergence of Dynamical Zeta Functions,’ *J. Stat. Phys.* **58**, 967 (1990).
- [20.13] P. Dahlgvist and G. Russberg, ‘Periodic orbit quantization of bound chaotic systems,’ *J. Phys. A* **24**, 4763 (1991); P. Dahlgvist *J. Phys. A* **27**, 763 (1994).
- [20.14] C. P. Dettmann and G. P. Morriss, *Phys. Rev. Lett.* **78**, 4201 (1997).
- [20.15] C. P. Dettmann and P. Cvitanović, *Cycle expansions for intermittent diffusion Phys. Rev. E* **56**, 6687 (1997); [arXiv:chao-dyn/9708011](https://arxiv.org/abs/chao-dyn/9708011).
- [20.16] W. Parry and M. Pollicott, *Ann. Math.* **118**, 573 (1983).

Chapter 21

Discrete factorization

No endeavor that is worthwhile is simple in prospect; if it is right, it will be simple in retrospect.

—Edward Teller

THE UTILITY of discrete symmetries in reducing spectrum calculations is familiar from quantum mechanics. Here we show that the classical spectral determinants factor in essentially the same way as the quantum ones. In the process we 1.) learn that the classical dynamics, once recast into the language of evolution operators, is much closer to quantum mechanics than is apparent in the Newtonian, ODE formulation (linear evolution operators/PDEs, group-theoretical spectral decompositions, . . .), 2.) that once the symmetry group is quotiented out, the dynamics simplifies, and 3.) it's a triple home run: simpler symbolic dynamics, fewer cycles needed, much better convergence of cycle expansions. Once you master this, going back is unthinkable.

The main result of this chapter can be stated as follows:

If the dynamics possesses a discrete symmetry, the contribution of a cycle p of multiplicity m_p to a dynamical zeta function factorizes into a product over the d_α -dimensional irreducible representations D_α of the symmetry group,

$$(1 - t_p)^{m_p} = \prod_{\alpha} \det \left(1 - D_{\alpha}(h_{\tilde{p}})t_{\tilde{p}} \right)^{d_{\alpha}}, \quad t_p = t_{\tilde{p}}^{g/m_p},$$

where $t_{\tilde{p}}$ is the cycle weight evaluated on the relative periodic orbit \tilde{p} , $g = |G|$ is the order of the group, $h_{\tilde{p}}$ is the group element relating the fundamental domain cycle \tilde{p} to a segment of the full space cycle p , and m_p is the multiplicity of the p cycle. As dynamical zeta functions have particularly simple cycle expansions, a geometrical shadowing interpretation of their convergence, and suffice for determination of leading eigenvalues, we shall use them to explain the group-theoretic factorizations; the full spectral determinants can be factorized using the same techniques. p -cycle into a cycle weight t_p .

This chapter is meant to serve as a detailed guide to the computation of dynamical zeta functions and spectral determinants for systems with discrete symmetries. Familiarity with basic group-theoretic notions is assumed, with the definitions relegated to appendix H.1. We develop here the cycle expansions for factorized determinants, and exemplify them by working two cases of physical interest: $C_2 = D_1$, $C_{3v} = D_3$ symmetries. $C_{2v} = D_2 \times D_2$ and $C_{4v} = D_4$ symmetries are discussed in appendix H.

21.1 Preview

As we saw in chapter 9, discrete symmetries relate classes of periodic orbits and reduce dynamics to a fundamental domain. Such symmetries simplify and improve the cycle expansions in a rather beautiful way; in classical dynamics, just as in quantum mechanics, the symmetrized subspaces can be probed by linear operators of different symmetries. If a linear operator commutes with the symmetry, it can be block-diagonalized, and, as we shall now show, the associated spectral determinants and dynamical zeta functions factorize.

21.1.1 Reflection symmetric 1-d maps

Consider f , a map on the interval with reflection symmetry $f(-x) = -f(x)$. A simple example is the piecewise-linear sawtooth map of figure 9.2. Denote the reflection operation by $Rx = -x$. The symmetry of the map implies that if $\{x_n\}$ is a trajectory, than also $\{Rx_n\}$ is a trajectory because $Rx_{n+1} = Rf(x_n) = f(Rx_n)$. The dynamics can be restricted to a fundamental domain, in this case to one half of the original interval; every time a trajectory leaves this interval, it can be mapped back using R . Furthermore, the evolution operator commutes with R , $\mathcal{L}(y, x) = \mathcal{L}(Ry, Rx)$. R satisfies $R^2 = \mathbf{e}$ and can be used to decompose the state space into mutually orthogonal symmetric and antisymmetric subspaces by means of projection operators

$$\begin{aligned} P_{A_1} &= \frac{1}{2}(\mathbf{e} + R), & P_{A_2} &= \frac{1}{2}(\mathbf{e} - R), \\ \mathcal{L}_{A_1}(y, x) &= P_{A_1}\mathcal{L}(y, x) = \frac{1}{2}(\mathcal{L}(y, x) + \mathcal{L}(-y, x)), \\ \mathcal{L}_{A_2}(y, x) &= P_{A_2}\mathcal{L}(y, x) = \frac{1}{2}(\mathcal{L}(y, x) - \mathcal{L}(-y, x)). \end{aligned} \quad (21.1)$$

To compute the traces of the symmetrization and antisymmetrization projection operators (21.1), we have to distinguish three kinds of cycles: asymmetric cycles a , symmetric cycles s built by repeats of irreducible segments \tilde{s} , and boundary cycles b . Now we show that the spectral determinant can be written as the product over the three kinds of cycles: $\det(1 - \mathcal{L}) = \det(1 - \mathcal{L})_a \det(1 - \mathcal{L})_{\tilde{s}} \det(1 - \mathcal{L})_b$.

Asymmetric cycles: A periodic orbits is not symmetric if $\{x_a\} \cap \{Rx_a\} = \emptyset$, where $\{x_a\}$ is the set of periodic points belonging to the cycle a . Thus R generates a second orbit with the same number of points and the same stability properties. Both orbits give the same contribution to the first term and no contribution to the second term in (21.1); as they are degenerate, the prefactor 1/2 cancels. Resumming as in the derivation of (19.15) we find that asymmetric orbits yield the same contribution to the symmetric and the antisymmetric subspaces:

$$\det(1 - \mathcal{L}_{\pm})_a = \prod_a \prod_{k=0}^{\infty} \left(1 - \frac{t_a}{\Lambda_a^k}\right), \quad t_a = \frac{z^{n_a}}{|\Lambda_a|}.$$

Symmetric cycles: A cycle s is reflection symmetric if operating with R on the set of periodic points reproduces the set. The period of a symmetric cycle is always even ($n_s = 2n_{\tilde{s}}$) and the mirror image of the x_s periodic point is reached by traversing the irreducible segment \tilde{s} of length $n_{\tilde{s}}$, $f^{n_{\tilde{s}}}(x_s) = Rx_s$. $\delta(x - f^n(x))$ picks up $2n_{\tilde{s}}$ contributions for every even traversal, $n = rn_{\tilde{s}}$, r even, and $\delta(x + f^n(x))$ for every odd traversal, $n = rn_{\tilde{s}}$, r odd. Absorb the group-theoretic prefactor in the Floquet multiplier by defining the stability computed for a segment of length $n_{\tilde{s}}$,

$$\Lambda_{\tilde{s}} = - \left. \frac{\partial f^{n_{\tilde{s}}}(x)}{\partial x} \right|_{x=x_s}.$$

Restricting the integration to the infinitesimal neighborhood $\mathcal{M}_{\tilde{s}}$ of the s cycle, we obtain the contribution to $\text{tr } \mathcal{L}_{\pm}^n$:

$$\begin{aligned} z^n \text{tr } \mathcal{L}_{\pm}^n &\rightarrow \int_{\mathcal{M}_{\tilde{s}}} dx z^n \frac{1}{2} (\delta(x - f^n(x)) \pm \delta(x + f^n(x))) \\ &= n_{\tilde{s}} \left(\sum_{r=2}^{\text{even}} \delta_{n, rn_{\tilde{s}}} \frac{t_{\tilde{s}}^r}{1 - 1/\Lambda_{\tilde{s}}^r} \pm \sum_{r=1}^{\text{odd}} \delta_{n, rn_{\tilde{s}}} \frac{t_{\tilde{s}}^r}{1 - 1/\Lambda_{\tilde{s}}^r} \right) \\ &= n_{\tilde{s}} \sum_{r=1}^{\infty} \delta_{n, rn_{\tilde{s}}} \frac{(\pm t_{\tilde{s}})^r}{1 - 1/\Lambda_{\tilde{s}}^r}. \end{aligned}$$

Substituting all symmetric cycles s into $\det(1 - \mathcal{L}_{\pm})$ and resumming we obtain:

$$\det(1 - \mathcal{L}_{\pm})_{\tilde{s}} = \prod_{\tilde{s}} \prod_{k=0}^{\infty} \left(1 \mp \frac{t_{\tilde{s}}}{\Lambda_{\tilde{s}}^k}\right)$$

Boundary cycles: In the example at hand there is only one cycle which is neither symmetric nor antisymmetric, but lies on the boundary of the fundamental domain, the fixed point at the origin. Such cycle contributes simultaneously to both

$\delta(x - f^n(x))$ and $\delta(x + f^n(x))$:

$$\begin{aligned} z^n \operatorname{tr} \mathcal{L}_\pm^n &\rightarrow \int_{\mathcal{M}_b} dx z^n \frac{1}{2} (\delta(x - f^n(x)) \pm \delta(x + f^n(x))) \\ &= \sum_{r=1}^{\infty} \delta_{n,r} t_b^r \frac{1}{2} \left(\frac{1}{1 - 1/\Lambda_b^r} \pm \frac{1}{1 + 1/\Lambda_b^r} \right) \\ z^n \operatorname{tr} \mathcal{L}_+^n &\rightarrow \sum_{r=1}^{\infty} \delta_{n,r} \frac{t_b^r}{1 - 1/\Lambda_b^{2r}}; \quad z^n \operatorname{tr} \mathcal{L}_-^n \rightarrow \sum_{r=1}^{\infty} \delta_{n,r} \frac{1}{\Lambda_b^r} \frac{t_b^r}{1 - 1/\Lambda_b^{2r}}. \end{aligned}$$

Boundary orbit contributions to the factorized spectral determinants follow by resummation:

$$\det(1 - \mathcal{L}_+)_b = \prod_{k=0}^{\infty} \left(1 - \frac{t_b}{\Lambda_b^{2k}} \right), \quad \det(1 - \mathcal{L}_-)_b = \prod_{k=0}^{\infty} \left(1 - \frac{t_b}{\Lambda_b^{2k+1}} \right)$$

Only the even derivatives contribute to the symmetric subspace, and only the odd ones to the antisymmetric subspace, because the orbit lies on the boundary.

Finally, the symmetry reduced spectral determinants follow by collecting the above results:

$$\begin{aligned} F_+(z) &= \prod_a \prod_{k=0}^{\infty} \left(1 - \frac{t_a}{\Lambda_a^k} \right) \prod_{\bar{s}} \prod_{k=0}^{\infty} \left(1 - \frac{t_{\bar{s}}}{\Lambda_{\bar{s}}^k} \right) \prod_{k=0}^{\infty} \left(1 - \frac{t_b}{\Lambda_b^{2k}} \right) \\ F_-(z) &= \prod_a \prod_{k=0}^{\infty} \left(1 - \frac{t_a}{\Lambda_a^k} \right) \prod_{\bar{s}} \prod_{k=0}^{\infty} \left(1 + \frac{t_{\bar{s}}}{\Lambda_{\bar{s}}^k} \right) \prod_{k=0}^{\infty} \left(1 - \frac{t_b}{\Lambda_b^{2k+1}} \right) \end{aligned} \quad (21.2)$$

We shall work out the symbolic dynamics of such reflection symmetric systems in some detail in sect. 21.5. As reflection symmetry is essentially the only discrete symmetry that a map of the interval can have, this example completes the group-theoretic factorization of determinants and zeta functions for 1 - dimensional maps. We now turn to discussion of the general case.

exercise 21.1

21.2 Discrete symmetries

A dynamical system is invariant under a symmetry group $G = \{e, g, \dots, g_{|G|}\}$ if the equations of motion are invariant under all symmetries $g \in G$. For a map $x_{n+1} = f(x_n)$ and the evolution operator $\mathcal{L}(y, x)$ defined by (17.23) this means

$$\begin{aligned} f(x) &= \mathbf{g}^{-1} f(\mathbf{g}x) \\ \mathcal{L}(y, x) &= \mathcal{L}(\mathbf{g}y, \mathbf{g}x). \end{aligned} \quad (21.3)$$

Bold face letters for group elements indicate a suitable representation on state space. For example, if a 2-dimensional map has the symmetry $x_1 \rightarrow -x_1, x_2 \rightarrow -x_2$, the symmetry group G consists of the identity and C , a rotation by π around the origin. The map f must then commute with rotations by π , $f(Rx) = \mathbf{C}f(x)$, with R given by the $[2 \times 2]$ matrix

$$R = \begin{pmatrix} -1 & 0 \\ 0 & -1 \end{pmatrix}. \quad (21.4)$$

R satisfies $R^2 = e$ and can be used to decompose the state space into mutually orthogonal symmetric and antisymmetric subspaces by means of projection operators (21.1). More generally the projection operator onto the α irreducible subspace of dimension d_α is given by $P_\alpha = (d_\alpha/|G|) \sum \chi_\alpha(h) \mathbf{h}^{-1}$, where $\chi_\alpha(h) = \text{tr } D_\alpha(h)$ are the group characters, and the transfer operator \mathcal{L} splits into a sum of inequivalent irreducible subspace contributions $\sum_\alpha \text{tr } \mathcal{L}_\alpha$,

$$\mathcal{L}_\alpha(y, x) = \frac{d_\alpha}{|G|} \sum_{h \in G} \chi_\alpha(h) \mathcal{L}(\mathbf{h}^{-1}y, x). \quad (21.5)$$

The prefactor d_α in the above reflects the fact that a d_α -dimensional representation occurs d_α times.

21.2.1 Cycle degeneracies

Taking into account these degeneracies, the Euler product (19.15) takes the form

$$\prod_p (1 - t_p) = \prod_{\hat{p}} (1 - t_{\hat{p}})^{m_{\hat{p}}}. \quad (21.6)$$

The Euler product (19.15) for the D_3 symmetric 3-disk problem is given in (20.36).

21.3 Dynamics in the fundamental domain

If the dynamics is invariant under a discrete symmetry, the state space M can be completely tiled by the fundamental domain \tilde{M} and its images $a\tilde{M}, b\tilde{M}, \dots$ under the action of the symmetry group $G = \{e, a, b, \dots\}$,

$$M = \sum_{a \in G} M_a = \sum_{a \in G} a\tilde{M}.$$

In the above example (21.4) with symmetry group $G = \{e, C\}$, the state space $M = \{x_1-x_2 \text{ plane}\}$ can be tiled by a fundamental domain $\tilde{M} = \{\text{half-plane } x_1 \geq 0\}$, and $\mathbf{C}\tilde{M} = \{\text{half-plane } x_1 \leq 0\}$, its image under rotation by π .

If the space M is decomposed into g tiles, a function $\phi(x)$ over M splits into a g -dimensional vector $\phi_a(x)$ defined by $\phi_a(x) = \phi(x)$ if $x \in M_a$, $\phi_a(x) = 0$ otherwise. Let $h = ab^{-1}$ conflicts with be the symmetry operation that maps the endpoint domain M_b into the starting point domain M_a , and let $D(h)_{ba}$, the left regular representation, be the $[g \times g]$ matrix whose b, a -th entry equals unity if $a = hb$ and zero otherwise; $D(h)_{ba} = \delta_{bh,a}$. Since the symmetries act on state space as well, the operation h enters in two guises: as a $[g \times g]$ matrix $D(h)$ which simply permutes the domain labels, and as a $[d \times d]$ matrix representation \mathbf{h} of a discrete symmetry operation on the d state space coordinates. For instance, in the above example (21.4) $h \in C_2$ and $D(h)$ can be either the identity or the interchange of the two domain labels,

$$D(e) = \begin{pmatrix} 1 & 0 \\ 0 & 1 \end{pmatrix}, \quad D(C) = \begin{pmatrix} 0 & 1 \\ 1 & 0 \end{pmatrix}. \quad (21.7)$$

Note that $D(h)$ is a permutation matrix, mapping a tile M_a into a different tile $M_{ha} \neq M_a$ if $h \neq e$. Consequently only $D(e)$ has diagonal elements, and $\text{tr } D(h) = g\delta_{h,e}$. However, the state space transformation $\mathbf{h} \neq \mathbf{e}$ leaves invariant sets of *boundary* points; for example, under reflection σ across a symmetry axis, the axis itself remains invariant. The boundary periodic orbits that belong to such pointwise invariant sets will require special care in $\text{tr } \mathcal{L}$ evaluations.

One can associate to the evolution operator (17.23) a $[g \times g]$ matrix evolution operator defined by

$$\mathcal{L}_{ba}(y, x) = D(h)_{ba} \mathcal{L}(y, x),$$

if $x \in M_a$ and $y \in M_b$, and zero otherwise. Now we can use the invariance condition (21.3) to move the starting point x into the fundamental domain $x = \mathbf{a}\tilde{x}$, $\mathcal{L}(y, x) = \mathcal{L}(\mathbf{a}^{-1}y, \tilde{x})$, and then use the relation $\mathbf{a}^{-1}b = h^{-1}$ to also relate the endpoint y to its image in the fundamental domain, $\tilde{\mathcal{L}}(\tilde{y}, \tilde{x}) := \mathcal{L}(\mathbf{h}^{-1}\tilde{y}, \tilde{x})$. With this operator which is restricted to the fundamental domain, the global dynamics reduces to

$$\mathcal{L}_{ba}(y, x) = D(h)_{ba} \tilde{\mathcal{L}}(\tilde{y}, \tilde{x}).$$

While the global trajectory runs over the full space M , the restricted trajectory is brought back into the fundamental domain \tilde{M} any time it crosses into adjoining tiles; the two trajectories are related by the symmetry operation h which maps the global endpoint into its fundamental domain image.

Now the traces (19.3) required for the evaluation of the eigenvalues of the transfer operator can be evaluated on the fundamental domain alone

$$\text{tr } \mathcal{L} = \int_M dx \mathcal{L}(x, x) = \int_{\tilde{M}} d\tilde{x} \sum_h \text{tr } D(h) \mathcal{L}(\mathbf{h}^{-1}\tilde{x}, \tilde{x}) \quad (21.8)$$

The fundamental domain integral $\int d\tilde{x} \mathcal{L}(\mathbf{h}^{-1}\tilde{x}, \tilde{x})$ picks up a contribution from every global cycle (for which $h = e$), but it also picks up contributions from shorter segments of global cycles. The permutation matrix $D(h)$ guarantees by the identity $\text{tr } D(h) = 0, h \neq e$, that only those repeats of the fundamental domain cycles \tilde{p} that correspond to complete global cycles p contribute. Compare, for example, the contributions of the $\overline{12}$ and $\overline{0}$ cycles of figure 12.12. $\text{tr } D(h)\tilde{\mathcal{L}}$ does not get a contribution from the $\overline{0}$ cycle, as the symmetry operation that maps the first half of the $\overline{12}$ into the fundamental domain is a reflection, and $\text{tr } D(\sigma) = 0$. In contrast, $\sigma^2 = e, \text{tr } D(\sigma^2) = 6$ insures that the repeat of the fundamental domain fixed point $\text{tr} (D(h)\tilde{\mathcal{L}})^2 = 6t_0^2$, gives the correct contribution to the global trace $\text{tr } \mathcal{L}^2 = 3 \cdot 2t_{12}$.

Let p be the full orbit, \tilde{p} the orbit in the fundamental domain and $h_{\tilde{p}}$ an element of \mathcal{H}_p , the symmetry group of p . Restricting the volume integrations to the infinitesimal neighborhoods of the cycles p and \tilde{p} , respectively, and performing the standard resummations, we obtain the identity

$$(1 - t_p)^{m_p} = \det (1 - D(h_{\tilde{p}})t_{\tilde{p}}) , \quad (21.9)$$

valid cycle by cycle in the Euler products (19.15) for $\det (1 - \mathcal{L})$. Here “det” refers to the $[g \times g]$ matrix representation $D(h_{\tilde{p}})$; as we shall see, this determinant can be evaluated in terms of standard characters, and no explicit representation of $D(h_{\tilde{p}})$ is needed. Finally, if a cycle p is invariant under the symmetry subgroup $\mathcal{H}_{\tilde{p}} \subseteq G$ of order h_p , its weight can be written as a repetition of a fundamental domain cycle

$$t_p = t_{\tilde{p}}^{h_p} \quad (21.10)$$

computed on the irreducible segment that corresponds to a fundamental domain cycle. For example, in figure 12.12 we see by inspection that $t_{12} = t_0^2$ and $t_{123} = t_1^3$.

21.3.1 Boundary orbits

Before we can turn to a presentation of the factorizations of dynamical zeta functions for the different symmetries we have to discuss an effect that arises for orbits that run on a symmetry line that borders a fundamental domain. In our 3-disk example, no such orbits are possible, but they exist in other systems, such as in

the bounded region of the Hénon-Heiles potential and in 1-d maps. For the symmetrical 4-disk billiard, there are in principle two kinds of such orbits, one kind bouncing back and forth between two diagonally opposed disks and the other kind moving along the other axis of reflection symmetry; the latter exists for bounded systems only. While there are typically very few boundary orbits, they tend to be among the shortest orbits, and their neglect can seriously degrade the convergence of cycle expansions, as those are dominated by the shortest cycles.

While such orbits are invariant under some symmetry operations, their neighborhoods are not. This affects the Jacobian matrix M_p of the linearization perpendicular to the orbit and thus the eigenvalues. Typically, *e.g.* if the symmetry is a reflection, some eigenvalues of M_p change sign. This means that instead of a weight $1/\det(\mathbf{1} - M_p)$ as for a regular orbit, boundary cycles also pick up contributions of form $1/\det(\mathbf{1} - \mathbf{h}M_p)$, where \mathbf{h} is a symmetry operation that leaves the orbit pointwise invariant; see for example sect. 21.1.1.

Consequences for the dynamical zeta function factorizations are that sometimes a boundary orbit does not contribute. A derivation of a dynamical zeta function (19.15) from a determinant like (19.9) usually starts with an expansion of the determinants of the Jacobian. The leading order terms just contain the product of the expanding eigenvalues and lead to the dynamical zeta function (19.15). Next to leading order terms contain products of expanding and contracting eigenvalues and are sensitive to their signs. Clearly, the weights t_p in the dynamical zeta function will then be affected by reflections in the Poincaré surface of section perpendicular to the orbit. In all our applications it was possible to implement these effects by the following simple prescription.

If an orbit is invariant under a little group $\mathcal{H}_p = \{e, b_2, \dots, b_h\}$, then the corresponding group element in (21.9) will be replaced by a projector. If the weights are insensitive to the signs of the eigenvalues, then this projector is

$$g_p = \frac{1}{h} \sum_{i=1}^h b_i. \quad (21.11)$$

In the cases that we have considered, the change of sign may be taken into account by defining a sign function $\epsilon_p(g) = \pm 1$, with the “-” sign if the symmetry element g flips the neighborhood. Then (21.11) is replaced by

$$g_p = \frac{1}{h} \sum_{i=1}^h \epsilon(b_i) b_i. \quad (21.12)$$

We have illustrated the above in sect. 21.1.1 by working out the full factorization for the 1-dimensional reflection symmetric maps.

21.4 Factorizations of dynamical zeta functions

In chapter 9 we have shown that a discrete symmetry induces degeneracies among periodic orbits and decomposes periodic orbits into repetitions of irreducible segments; this reduction to a fundamental domain furthermore leads to a convenient symbolic dynamics compatible with the symmetry, and, most importantly, to a factorization of dynamical zeta functions. This we now develop, first in a general setting and then for specific examples.

21.4.1 Factorizations of dynamical dynamical zeta functions

According to (21.9) and (21.10), the contribution of a degenerate class of global cycles (cycle p with multiplicity $m_p = g/h_p$) to a dynamical zeta function is given by the corresponding fundamental domain cycle \tilde{p} :

$$(1 - t_{\tilde{p}}^{h_p})^{g/h_p} = \det \left(1 - D(h_{\tilde{p}})t_{\tilde{p}} \right) \quad (21.13)$$

Let $D(h) = \bigoplus_{\alpha} d_{\alpha} D_{\alpha}(h)$ be the decomposition of the matrix representation $D(h)$ into the d_{α} dimensional irreducible representations α of a finite group G . Such decompositions are block-diagonal, so the corresponding contribution to the Euler product (19.9) factorizes as

$$\det (1 - D(h)t) = \prod_{\alpha} \det (1 - D_{\alpha}(h)t)^{d_{\alpha}} , \quad (21.14)$$

where now the product extends over all distinct d_{α} -dimensional irreducible representations, each contributing d_{α} times. For the cycle expansion purposes, it has been convenient to emphasize that the group-theoretic factorization can be effected cycle by cycle, as in (21.13); but from the transfer operator point of view, the key observation is that the symmetry reduces the transfer operator to a block diagonal form; this block diagonalization implies that the dynamical zeta functions (19.15) factorize as

$$\frac{1}{\zeta} = \prod_{\alpha} \frac{1}{\zeta_{\alpha}^{d_{\alpha}}} , \quad \frac{1}{\zeta_{\alpha}} = \prod_{\tilde{p}} \det \left(1 - D_{\alpha}(h_{\tilde{p}})t_{\tilde{p}} \right) . \quad (21.15)$$

Determinants of d -dimensional irreducible representations can be evaluated using the expansion of determinants in terms of traces,

$$\begin{aligned} \det (1 + M) &= 1 + \operatorname{tr} M + \frac{1}{2} \left((\operatorname{tr} M)^2 - \operatorname{tr} M^2 \right) \\ &+ \frac{1}{6} \left((\operatorname{tr} M)^3 - 3 (\operatorname{tr} M) (\operatorname{tr} M^2) + 2 \operatorname{tr} M^3 \right) \\ &+ \cdots + \frac{1}{d!} \left((\operatorname{tr} M)^d - \cdots \right) , \end{aligned} \quad (21.16)$$

and each factor in (21.14) can be evaluated by looking up the characters $\chi_\alpha(h) = \text{tr } D_\alpha(h)$ in standard tables [17]. In terms of characters, we have for the 1-dimensional representations

$$\det(1 - D_\alpha(h)t) = 1 - \chi_\alpha(h)t ,$$

for the 2-dimensional representations

$$\det(1 - D_\alpha(h)t) = 1 - \chi_\alpha(h)t + \frac{1}{2}(\chi_\alpha(h)^2 - \chi_\alpha(h^2))t^2 ,$$

and so forth.

In the fully symmetric subspace $\text{tr } D_{A_1}(h) = 1$ for all orbits; hence a straightforward fundamental domain computation (with no group theory weights) always yields a part of the full spectrum. In practice this is the most interesting subspectrum, as it contains the leading eigenvalue of the transfer operator.

exercise 21.2

21.4.2 Factorizations of spectral determinants

Factorization of the full spectral determinant (19.3) proceeds in essentially the same manner as the factorization of dynamical zeta functions outlined above. By (21.5) and (21.8) the trace of the transfer operator \mathcal{L} splits into the sum of inequivalent irreducible subspace contributions $\sum_\alpha \text{tr } \mathcal{L}_\alpha$, with

$$\text{tr } \mathcal{L}_\alpha = d_\alpha \sum_{h \in G} \chi_\alpha(h) \int_{\tilde{M}} d\tilde{x} \mathcal{L}(\mathbf{h}^{-1}\tilde{x}, \tilde{x}) .$$

This leads by standard manipulations to the factorization of (19.9) into

$$\begin{aligned} F(z) &= \prod_{\alpha} F_{\alpha}(z)^{d_{\alpha}} \\ F_{\alpha}(z) &= \exp \left(- \sum_{\tilde{p}} \sum_{r=1}^{\infty} \frac{1}{r} \frac{\chi_{\alpha}(h_{\tilde{p}}^r) z^{n_{\tilde{p}} r}}{|\det(\mathbf{1} - \tilde{M}_{\tilde{p}}^r)|} \right) , \end{aligned} \quad (21.17)$$

where $\tilde{M}_{\tilde{p}} = \mathbf{h}_{\tilde{p}} M_{\tilde{p}}$ is the fundamental domain Jacobian. Boundary orbits require special treatment, discussed in sect. 21.3.1, with examples given in the next section as well as in the specific factorizations discussed below.

The factorizations (21.15), (21.17) are the central formulas of this chapter. We now work out the group theory factorizations of cycle expansions of dynamical zeta functions for the cases of C_2 and D_3 symmetries. The cases of the D_2 , D_4 symmetries are worked out in appendix H below.

21.5 C_2 factorization

As the simplest example of implementing the above scheme consider the C_2 symmetry. For our purposes, all that we need to know here is that each orbit or configuration is uniquely labeled by an infinite string $\{s_i\}$, $s_i = +, -$ and that the dynamics is invariant under the $+ \leftrightarrow -$ interchange, i.e., it is C_2 symmetric. The C_2 symmetry cycles separate into two classes, the self-dual configurations $+-, ++--$, $+++----$, $+--+-+--$, \dots , with multiplicity $m_p = 1$, and the asymmetric configurations $+, -, ++-, --+, \dots$, with multiplicity $m_p = 2$. For example, as there is no absolute distinction between the “up” and the “down” spins, or the “left” or the “right” lobe, $t_+ = t_-$, $t_{+-} = t_{-+}$, and so on.

exercise 21.5

The symmetry reduced labeling $\rho_i \in \{0, 1\}$ is related to the standard $s_i \in \{+, -\}$ Ising spin labeling by

$$\begin{aligned} \text{If } s_i &= s_{i-1} \text{ then } \rho_i = 1 \\ \text{If } s_i &\neq s_{i-1} \text{ then } \rho_i = 0 \end{aligned} \tag{21.18}$$

For example, $\overline{+} = \dots + + + \dots$ maps into $\dots 111 \dots = \overline{1}$ (and so does $\overline{-}$), $\overline{-+} = \dots - + - + \dots$ maps into $\dots 000 \dots = \overline{0}$, $\overline{-+ + -} = \dots - - + + - - + + \dots$ maps into $\dots 0101 \dots = \overline{01}$, and so forth. A list of such reductions is given in table 12.1.

Depending on the maximal symmetry group \mathcal{H}_p that leaves an orbit p invariant (see sects. 21.2 and 21.3 as well as sect. 21.1.1), the contributions to the dynamical zeta function factor as

$$\begin{aligned} \mathcal{H}_p = \{e\} : \quad & A_1 \quad A_2 \\ (1 - t_{\bar{p}})^2 &= (1 - t_{\bar{p}})(1 - t_{\bar{p}}) \\ \mathcal{H}_p = \{e, \sigma\} : \quad & (1 - t_{\bar{p}})^2 = (1 - t_{\bar{p}})(1 + t_{\bar{p}}), \end{aligned} \tag{21.19}$$

For example:

$$\begin{aligned} \mathcal{H}_{++-} = \{e\} : \quad & (1 - t_{++-})^2 = (1 - t_{001})(1 - t_{001}) \\ \mathcal{H}_{+-} = \{e, \sigma\} : \quad & (1 - t_{+-}) = (1 - t_0)(1 + t_0), \quad t_{+-} = t_0^2 \end{aligned}$$

This yields two binary cycle expansions. The A_1 subspace dynamical zeta function is given by the standard binary expansion (20.7). The antisymmetric A_2 subspace dynamical zeta function ζ_{A_2} differs from ζ_{A_1} only by a minus sign for cycles with an odd number of 0's:

$$\begin{aligned} 1/\zeta_{A_2} &= (1 + t_0)(1 - t_1)(1 + t_{10})(1 - t_{100})(1 + t_{101})(1 + t_{1000}) \\ &\quad (1 - t_{1001})(1 + t_{1011})(1 - t_{10000})(1 + t_{10001}) \\ &\quad (1 + t_{10010})(1 - t_{10011})(1 - t_{10101})(1 + t_{10111}) \dots \\ &= 1 + t_0 - t_1 + (t_{10} - t_1 t_0) - (t_{100} - t_{10} t_0) + (t_{101} - t_{10} t_1) \\ &\quad - (t_{1001} - t_1 t_{001} - t_{101} t_0 + t_{10} t_0 t_1) - \dots \end{aligned} \tag{21.20}$$

Note that the group theory factors do not destroy the curvature corrections (the cycles and pseudo cycles are still arranged into shadowing combinations).

If the system under consideration has a boundary orbit (*cf.* sect.21.3.1) with group-theoretic factor $\mathbf{h}_p = (\mathbf{e} + \sigma)/2$, the boundary orbit does not contribute to the antisymmetric subspace

$$\text{boundary: } (1 - t_p) = \begin{matrix} A_1 & A_2 \\ (1 - t_{\bar{p}})(1 - 0t_{\bar{p}}) \end{matrix} \quad (21.21)$$

This is the $1/\zeta$ part of the boundary orbit factorization of sect.21.1.1.

21.6 D_3 factorization: 3-disk game of pinball

The next example, the D_3 symmetry, can be worked out by a glance at figure 12.12 (a). For the symmetric 3-disk game of pinball the fundamental domain is bounded by a disk segment and the two adjacent sections of the symmetry axes that act as mirrors (see figure 12.12 (b)). The three symmetry axes divide the space into six copies of the fundamental domain. Any trajectory on the full space can be pieced together from bounces in the fundamental domain, with symmetry axes replaced by flat mirror reflections. The binary $\{0, 1\}$ reduction of the ternary three disk $\{1, 2, 3\}$ labels has a simple geometric interpretation: a collision of type 0 reflects the projectile to the disk it comes from (back-scatter), whereas after a collision of type 1 projectile continues to the third disk. For example, $\overline{23} = \dots 232323 \dots$ maps into $\dots 000 \dots = \overline{0}$ (and so do $\overline{12}$ and $\overline{13}$), $\overline{123} = \dots 12312 \dots$ maps into $\dots 111 \dots = \overline{1}$ (and so does $\overline{132}$), and so forth. A list of such reductions for short cycles is given in table 12.2.

D_3 has two 1-dimensional irreducible representations, symmetric and anti-symmetric under reflections, denoted A_1 and A_2 , and a pair of degenerate 2-dimensional representations of mixed symmetry, denoted E . The contribution of an orbit with symmetry g to the $1/\zeta$ Euler product (21.14) factorizes according to

$$\det(1 - D(h)t) = (1 - \chi_{A_1}(h)t)(1 - \chi_{A_2}(h)t)(1 - \chi_E(h)t + \chi_{A_2}(h)t^2)^2 \quad (21.22)$$

with the three factors contributing to the D_3 irreducible representations A_1 , A_2 and E , respectively, and the 3-disk dynamical zeta function factorizes into $\zeta = \zeta_{A_1} \zeta_{A_2} \zeta_E^2$. Substituting the D_3 characters [17]

D_3	A_1	A_2	E
e	1	1	2
C, C^2	1	1	-1
σ_v	1	-1	0

into (21.22), we obtain for the three classes of possible orbit symmetries (indicated in the first column)

$$\begin{array}{rcl}
 \mathbf{h}_{\bar{p}} & & A_1 \quad A_2 \quad E \\
 e : & (1 - t_{\bar{p}})^6 & = (1 - t_{\bar{p}})(1 - t_{\bar{p}})(1 - 2t_{\bar{p}} + t_{\bar{p}}^2)^2 \\
 C, C^2 : & (1 - t_{\bar{p}}^3)^2 & = (1 - t_{\bar{p}})(1 - t_{\bar{p}})(1 + t_{\bar{p}} + t_{\bar{p}}^2)^2 \\
 \sigma_v : & (1 - t_{\bar{p}}^2)^3 & = (1 - t_{\bar{p}})(1 + t_{\bar{p}})(1 + 0t_{\bar{p}} - t_{\bar{p}}^2)^2.
 \end{array} \tag{21.23}$$

where σ_v stands for any one of the three reflections.

The Euler product (19.15) on each irreducible subspace follows from the factorization (21.23). On the symmetric A_1 subspace the ζ_{A_1} is given by the standard binary curvature expansion (20.7). The antisymmetric A_2 subspace ζ_{A_2} differs from ζ_{A_1} only by a minus sign for cycles with an odd number of 0's, and is given in (21.20). For the mixed-symmetry subspace E the curvature expansion is given by

$$\begin{aligned}
 1/\zeta_E &= (1 + zt_1 + z^2t_1^2)(1 - z^2t_0^2)(1 + z^3t_{100} + z^6t_{100}^2)(1 - z^4t_{10}^2) \\
 &\quad (1 + z^4t_{1001} + z^8t_{1001}^2)(1 + z^5t_{10000} + z^{10}t_{10000}^2) \\
 &\quad (1 + z^5t_{10101} + z^{10}t_{10101}^2)(1 - z^5t_{10011})^2 \dots \\
 &= 1 + zt_1 + z^2(t_1^2 - t_0^2) + z^3(t_{001} - t_1t_0^2) \\
 &\quad + z^4 [t_{0011} + (t_{001} - t_1t_0^2)t_1 - t_{01}^2] \\
 &\quad + z^5 [t_{00001} + t_{01011} - 2t_{00111} + (t_{0011} - t_{01}^2)t_1 + (t_1^2 - t_0^2)t_{100}] \dots
 \end{aligned} \tag{21.24}$$

We have reinserted the powers of z in order to group together cycles and pseudocycles of the same length. Note that the factorized cycle expansions retain the curvature form; long cycles are still shadowed by (somewhat less obvious) combinations of pseudocycles.

Referring back to the topological polynomial (15.40) obtained by setting $t_p = 1$, we see that its factorization is a consequence of the D_3 factorization of the ζ function:

$$1/\zeta_{A_1} = 1 - 2z, \quad 1/\zeta_{A_2} = 1, \quad 1/\zeta_E = 1 + z, \tag{21.25}$$

as obtained from (20.7), (21.20) and (21.24) for $t_p = 1$.

Their symmetry is $K = \{\mathbf{e}, \sigma\}$, so according to (21.11), they pick up the group-theoretic factor $\mathbf{h}_p = (\mathbf{e} + \sigma)/2$. If there is no sign change in t_p , then evaluation of $\det(1 - \frac{\mathbf{e} + \sigma}{2}t_{\bar{p}})$ yields

$$\text{boundary: } (1 - t_p)^3 = (1 - t_{\bar{p}})(1 - 0t_{\bar{p}})(1 - t_{\bar{p}})^2, \quad t_p = t_{\bar{p}}. \tag{21.26}$$

However, if the cycle weight changes sign under reflection, $t_{\sigma\bar{p}} = -t_{\bar{p}}$, the boundary orbit does not contribute to the subspace symmetric under reflection across the orbit;

$$\text{boundary: } (1 - t_p)^3 = \overset{A_1}{(1 - 0t_{\bar{p}})} \overset{A_2}{(1 - t_{\bar{p}})} \overset{E}{(1 - t_{\bar{p}})^2}, \quad t_p = t_{\bar{p}}. \quad (21.27)$$

Résumé

If a dynamical system has a discrete symmetry, the symmetry should be exploited; much is gained, both in understanding of the spectra and ease of their evaluation. Once this is appreciated, it is hard to conceive of a calculation without factorization; it would correspond to quantum mechanical calculations without wave-function symmetrizations.

While the reformulation of the chaotic spectroscopy from the trace sums to the cycle expansions does not reduce the exponential growth in number of cycles with the cycle length, in practice only the short orbits are used, and for them the labor saving is dramatic. For example, for the 3-disk game of pinball there are 256 periodic points of length 8, but reduction to the fundamental domain non-degenerate prime cycles reduces the number of the distinct cycles of length 8 to 30.

In addition, cycle expansions of the symmetry reduced dynamical zeta functions converge dramatically faster than the unfactorized dynamical zeta functions. One reason is that the unfactorized dynamical zeta function has many closely spaced zeros and zeros of multiplicity higher than one; since the cycle expansion is a polynomial expansion in topological cycle length, accommodating such behavior requires many terms. The dynamical zeta functions on separate subspaces have more evenly and widely spaced zeros, are smoother, do not have symmetry-induced multiple zeros, and fewer cycle expansion terms (short cycle truncations) suffice to determine them. Furthermore, the cycles in the fundamental domain sample state space more densely than in the full space. For example, for the 3-disk problem, there are 9 distinct (symmetry unrelated) cycles of length 7 or less in full space, corresponding to 47 distinct periodic points. In the fundamental domain, we have 8 (distinct) periodic orbits up to length 4 and thus 22 different periodic points in 1/6-th the state space, i.e., an increase in density by a factor 3 with the same numerical effort.

We emphasize that the symmetry factorization (21.23) of the dynamical zeta function is *intrinsic* to the classical dynamics, and not a special property of quantal spectra. The factorization is not restricted to the Hamiltonian systems, or only to the configuration space symmetries; for example, the discrete symmetry can be a symmetry of the Hamiltonian phase space [4]. In conclusion, the manifold advantages of the symmetry reduced dynamics should thus be obvious; full state space cycle expansions, such as those of exercise 20.8, are useful only for cross-checking purposes.

Commentary

Remark 21.1 Symmetry reductions in periodic orbit theory. This chapter is based on a collaborative effort with B. Eckhardt, ref. [1]. The group-theoretic factorizations of dynamical zeta functions that we develop here were first introduced and applied in ref. [2]. They are closely related to the symmetrizations introduced by Gutzwiller [3] in the context of the semiclassical periodic orbit trace formulas, put into more general group-theoretic context by Robbins [4], whose exposition, together with Lauritzen's [5] treatment of the boundary orbits, has influenced the presentation given here. The symmetry reduced trace formula for a finite symmetry group $G = \{e, g_2, \dots, g_{|G|}\}$ with $|G|$ group elements, where the integral over Haar measure is replaced by a finite group discrete sum $|G|^{-1} \sum_{g \in G} = 1$, was derived in ref. [1]. A related group-theoretic decomposition in context of hyperbolic billiards was utilized in ref. [6], and for the Selberg's zeta function in ref. [7]. One of its loftier antecedents is the Artin factorization formula of algebraic number theory, which expresses the zeta-function of a finite extension of a given field as a product of L -functions over all irreducible representations of the corresponding Galois group.

The techniques of this chapter have been applied to computations of the 3-disk classical and quantum spectra in refs. [8, 9], and to a "Zeeman effect" pinball and the x^2y^2 potentials in ref. [10]. In a larger perspective, the factorizations developed above are special cases of a general approach to exploiting the group-theoretic invariances in spectra computations, such as those used in enumeration of periodic geodesics [6, 11, 12] for hyperbolic billiards [13] and Selberg zeta functions [14].

Remark 21.2 Other symmetries. In addition to the symmetries exploited here, time reversal symmetry and a variety of other non-trivial discrete symmetries can induce further relations among orbits; we shall point out several of examples of cycle degeneracies under time reversal. We do not know whether such symmetries can be exploited for further improvements of cycle expansions.

Exercises

21.1. **Sawtooth map desymmetrization.** Work out the some of the shortest global cycles of different symmetries and fundamental domain cycles for the sawtooth map of figure 9.2. Compute the dynamical zeta function and the spectral determinant of the Perron-Frobenius operator for this map; check explicitly the factorization (21.2).

21.2. **2 – dimensional asymmetric representation.** The above expressions can sometimes be simplified further using standard group-theoretical methods. For example, the $\frac{1}{2}((\text{tr } M)^2 - \text{tr } M^2)$ term in (21.16) is the trace of the

antisymmetric part of the $M \times M$ Kronecker product. Show that if α is a 2-dimensional representation, this is the A_2 antisymmetric representation, and

$$2\text{-dim: } \det(1 - D_\alpha(h)t) = 1 - \chi_\alpha(h)t + \chi_{A_2}(h)t^2. \quad (21.28)$$

21.3. **Characters of D_3 .** (continued from exercise 9.5) $D_3 \cong C_{3v}$, the group of symmetries of an equilateral triangle: has three irreducible representations, two one-dimensional and the other one of multiplicity 2.

(a) All finite discrete groups are isomorphic to a per-

mutation group or one of its subgroups, and elements of the permutation group can be expressed as cycles. Express the elements of the group D_3 as cycles. For example, one of the rotations is (123), meaning that vertex 1 maps to 2, $2 \rightarrow 3$, and $3 \rightarrow 1$.

- (b) Use your representation from exercise 9.5 to compute the D_3 character table.
- (c) Use a more elegant method from the group-theory literature to verify your D_3 character table.
- (d) Two D_3 irreducible representations are one dimensional and the third one of multiplicity 2 is formed by $[2 \times 2]$ matrices. Find the matrices for all six group elements in this representation.

(Hint: get yourself a good textbook, like Hamermesh [2] or Tinkham [15], and read up on classes and characters.)

21.4. 3-disk desymmetrization.

- a) Work out the 3-disk symmetry factorization for the 0 and 1 cycles, i.e. which symmetry do they have, what is the degeneracy in full space and how do they factorize (how do they look in the A_1 , A_2 and the E representations).
- b) Find the shortest cycle with no symmetries and factorize it as in a)
- c) Find the shortest cycle that has the property that its time reversal is not described by the same symbolic dynamics.

- d) Compute the dynamical zeta functions and the spectral determinants (symbolically) in the three representations; check the factorizations (21.15) and (21.17).

(Per Rosenqvist)

21.5. **C_2 factorizations: the Lorenz and Ising systems.** In the Lorenz system the labels + and - stand for the left or the right lobe of the attractor and the symmetry is a rotation by π around the z -axis. Similarly, the Ising Hamiltonian (in the absence of an external magnetic field) is invariant under spin flip. Work out the factorizations for some of the short cycles in either system.

21.6. **Ising model.** The Ising model with two states $\epsilon_i = \{+, -\}$ per site, periodic boundary condition, and Hamiltonian

$$H(\epsilon) = -J \sum_i \delta_{\epsilon_i, \epsilon_{i+1}},$$

is invariant under spin-flip: $+ \leftrightarrow -$. Take advantage of that symmetry and factorize the dynamical zeta function for the model, i.e., find all the periodic orbits that contribute to each factor and their weights.

21.7. **One orbit contribution.** If p is an orbit in the fundamental domain with symmetry h , show that it contributes to the spectral determinant with a factor

$$\det \left(1 - D(h) \frac{t_p}{\lambda_p^k} \right),$$

where $D(h)$ is the representation of h in the regular representation of the group.

References

- [21.1] P. Cvitanović and B. Eckhardt, "Symmetry decomposition of chaotic dynamics," *Nonlinearity* **6**, 277 (1993).
- [21.2] P. Cvitanović and B. Eckhardt, "Periodic-orbit quantization of chaotic system," *Phys. Rev. Lett.* **63**, 823 (1989).
- [21.3] M.C. Gutzwiller, "The quantization of a classically ergodic system," *Physica D* **5**, 183 (1982).
- [21.4] J.M. Robbins, "Semiclassical trace formulas in the presence of continuous symmetries," *Phys. Rev. A* **40**, 2128 (1989).
- [21.5] B. Lauritzen, Discrete symmetries and the periodic-orbit expansions, *Phys. Rev. A* **43** 603, (1991).

- [21.6] N. Balasz and A. Voros, "Chaos on the pseudosphere," *Phys. Rep.* **143**, 109 (1986).
- [21.7] A. B. Venkov and P. G. Zograf, "Analogues of Artin's factorization formulas in the spectral theory of automorphic functions associated with induced representations of Fuchsian groups," *Math. USSR* **21**, 435 (1983).
- [21.8] P. Cvitanović, B. Eckhardt, P. E. Rosenqvist, G. Russberg and P. Scherer, "Pinball Scattering," in G. Casati and B. Chirikov, eds., *Quantum Chaos* (Cambridge U. Press, Cambridge 1993).
- [21.9] P. Scherer, *Quantenzustände eines klassisch chaotischen Billards*, Ph.D. thesis, Univ. Köln (Berichte des Forschungszentrums Jülich 2554, ISSN 0366-0885, Jülich, 1991).
- [21.10] P. Dahlqvist and G. Russberg, "Periodic orbit quantization of bound chaotic systems," *J. Phys. A* **24**, 4763 (1991); P. Dahlqvist *J. Phys. A* **27**, 763 (1994).
- [21.11] H.P. McKean, *Comm. Pure and Appl. Math.* **25**, 225 (1972); **27**, 134 (1974).
- [21.12] M. Sieber and F. Steiner, *Phys. Lett. A* **148**, 415 (1990).
- [21.13] M. C. Gutzwiller, *J. Math. Phys.* **8**, 1979 (1967); **10**, 1004 (1969); **11**, 1791 (1970); **12**, 343 (1971).
- [21.14] M. C. Gutzwiller, *Chaos in Classical and Quantum Mechanics* (Springer, New York 1990).
- [21.15] M. Tinkham, *Group theory and quantum mechanics* (McGraw-Hill, New York 1964).
- [21.16] J.M. Robbins, S.C. Creagh and R.G. Littlejohn, *Phys. Rev.* **A39**, 2838 (1989); **A41**, 6052 (1990).
- [21.17] M. Hamermesh, *Group Theory and its Application to Physical Problems* (Addison-Wesley, Reading, 1962).

Part III

Chaos: what to do about it?

WHAT YOU KNOW NOW is to partition topologically and invariantly the state space, compute a hierarchy of cycles, compute spectral determinants and their eigenvalues. What next?

1. Why cycle? (Chapter 22)
2. Why does it work? (Chapter 23)
3. When does it not work? (Chapter 24)
4. When does it work? Deterministic diffusion and foundations of 'far from equilibrium' statistical mechanics (Chapter 25)
5. What does it have to do with turbulence? (Chapter 26).

Chapter 22

Why cycle?

“Progress was a labyrinth ... people plunging blindly in and then rushing wildly back, shouting that they had found it ... the invisible king the élan vital the principle of evolution ... writing a book, starting a war, founding a school...”

—F. Scott Fitzgerald, *This Side of Paradise*

IN THE PRECEDING CHAPTERS we have moved rather briskly through the evolution operator formalism. Here we slow down in order to develop some fingertip feeling for the traces of evolution operators.

22.1 Escape rates

We start by verifying the claim (17.11) that for a nice hyperbolic flow the trace of the evolution operator grows exponentially with time. Consider again the game of pinball of figure 1.1. Designate by \mathcal{M} a state space region that encloses the three disks, say the surface of the table \times all pinball directions. The fraction of initial points whose trajectories start out within the state space region \mathcal{M} and recur within that region at the time t is given by

$$\hat{\Gamma}_{\mathcal{M}}(t) = \frac{1}{|\mathcal{M}|} \int \int_{\mathcal{M}} dx dy \delta(y - f^t(x)). \quad (22.1)$$

This quantity is eminently measurable and physically interesting in a variety of problems spanning nuclear physics to celestial mechanics. The integral over x takes care of all possible initial pinballs; the integral over y checks whether they are still within \mathcal{M} by the time t . If the dynamics is bounded, and \mathcal{M} envelops the entire accessible state space, $\hat{\Gamma}_{\mathcal{M}}(t) = 1$ for all t . However, if trajectories exit \mathcal{M} the recurrence fraction decreases with time. For example, any trajectory that falls off the pinball table in figure 1.1 is gone for good.

These observations can be made more concrete by examining the pinball phase space of figure 1.9. With each pinball bounce the initial conditions that survive get thinned out, each strip yielding two thinner strips within it. The total fraction of survivors (1.2) after n bounces is given by

$$\hat{\Gamma}_n = \frac{1}{|\mathcal{M}|} \sum_i^{(n)} |\mathcal{M}_i|, \quad (22.2)$$

where i is a binary label of the i th strip, and $|\mathcal{M}_i|$ is the area of the i th strip. The phase space volume is preserved by the flow, so the strips of survivors are contracted along the stable eigen-directions, and ejected along the unstable eigen-directions. As a crude estimate of the number of survivors in the i th strip, assume that the spreading of a ray of trajectories per bounce is given by a factor Λ , the mean value of the expanding eigenvalue of the corresponding Jacobian matrix of the flow, and replace $|\mathcal{M}_i|$ by the phase space strip width estimate $|\mathcal{M}_i|/|\mathcal{M}| \sim 1/\Lambda_i$. This estimate of a size of a neighborhood (given already on p.97) is right in spirit, but not without drawbacks. One problem is that in general the eigenvalues of a Jacobian matrix for a finite segment of a trajectory have no invariant meaning; they depend on the choice of coordinates. However, we saw in chapter 18 that the sizes of neighborhoods are determined by Floquet multipliers of periodic points, and those are invariant under smooth coordinate transformations.

In the approximation $\hat{\Gamma}_n$ receives 2^n contributions of equal size

$$\hat{\Gamma}_1 \sim \frac{1}{\Lambda} + \frac{1}{\Lambda}, \dots, \quad \hat{\Gamma}_n \sim \frac{2^n}{\Lambda^n} = e^{-n(\lambda-h)} = e^{-n\gamma}, \quad (22.3)$$

up to pre-exponential factors. We see here the interplay of the two key ingredients of chaos first alluded to in sect. 1.3.1: the escape rate γ equals local expansion rate (the Lyapunov exponent $\lambda = \ln \Lambda$), minus the rate of global reinjection back into the system (the topological entropy $h = \ln 2$).

As at each bounce one loses routinely the same fraction of trajectories, one expects the sum (22.2) to fall off exponentially with n . More precisely, by the hyperbolicity assumption of sect. 18.1.1 the expanding eigenvalue of the Jacobian matrix of the flow is exponentially bounded from both above and below,

$$1 < |\Lambda_{min}| \leq |\Lambda(x)| \leq |\Lambda_{max}|, \quad (22.4)$$

and the area of each strip in (22.2) is bounded by $|\Lambda_{max}^{-n}| \leq |\mathcal{M}_i| \leq |\Lambda_{min}^{-n}|$. Replacing $|\mathcal{M}_i|$ in (22.2) by its over (under) estimates in terms of $|\Lambda_{max}|$, $|\Lambda_{min}|$ immediately leads to exponential bounds $(2/|\Lambda_{max}|)^n \leq \hat{\Gamma}_n \leq (2/|\Lambda_{min}|)^n$, i.e.,

$$\ln |\Lambda_{max}| - \ln 2 \geq -\frac{1}{n} \ln \hat{\Gamma}_n \geq \ln |\Lambda_{min}| - \ln 2. \quad (22.5)$$

The argument based on (22.5) establishes only that the sequence $\gamma_n = -\frac{1}{n} \ln \Gamma_n$ has a lower and an upper bound for any n . In order to prove that γ_n converge to the limit γ , we first show that for hyperbolic systems the sum over survivor intervals (22.2) can be replaced by the sum over periodic orbit stabilities. By (22.4) the size of \mathcal{M}_i strip can be bounded by the stability Λ_i of i th periodic point:

$$C_1 \frac{1}{|\Lambda_i|} < \frac{|\mathcal{M}_i|}{|\mathcal{M}|} < C_2 \frac{1}{|\Lambda_i|}, \quad (22.6)$$

for any periodic point i of period n , with constants C_j dependent on the dynamical system but independent of n . The meaning of these bounds is that for longer and longer cycles in a system of bounded hyperbolicity, the shrinking of the i th strip is better and better approximated by the derivatives evaluated on the periodic point within the strip. Hence the survival probability can be bounded close to the periodic point stability sum

$$\hat{C}_1 \Gamma_n < \sum_i^{(n)} \frac{|\mathcal{M}_i|}{|\mathcal{M}|} < \hat{C}_2 \Gamma_n, \quad (22.7)$$

where $\Gamma_n = \sum_i^{(n)} 1/|\Lambda_i|$ is the asymptotic trace sum (18.26). In this way we have established that for hyperbolic systems the survival probability sum (22.2) can be replaced by the periodic orbit sum (18.26).

exercise 22.1
exercise 16.4

We conclude that for hyperbolic, locally unstable flows the fraction (22.1) of initial x whose trajectories remain trapped within \mathcal{M} up to time t is expected to decay exponentially,

$$\Gamma_{\mathcal{M}}(t) \propto e^{-\gamma t},$$

where γ is the asymptotic *escape rate* defined by

$$\gamma = - \lim_{t \rightarrow \infty} \frac{1}{t} \ln \Gamma_{\mathcal{M}}(t). \quad (22.8)$$

22.2 Natural measure in terms of periodic orbits

We now refine the reasoning of sect. 22.1. Consider the trace (18.7) in the asymptotic limit (18.25):

$$\text{tr } \mathcal{L}^n = \int dx \delta(x - f^n(x)) e^{\beta A^n(x)} \approx \sum_i^{(n)} \frac{e^{\beta A^n(x_i)}}{|\Lambda_i|}.$$

The factor $1/|\Lambda_i|$ was interpreted in (22.2) as the area of the i th phase space strip. Hence $\text{tr } \mathcal{L}^n$ is a discretization of the integral $\int dx e^{\beta A^n(x)}$ approximated by a tessellation into strips centered on periodic points x_i , figure 1.11, with the volume of the i th neighborhood given by estimate $|\mathcal{M}_i| \sim 1/|\Lambda_i|$, and $e^{\beta A^n(x)}$ estimated by $e^{\beta A^n(x_i)}$, its value at the i th periodic point. If the symbolic dynamics is a complete, any rectangle $[s_{-m} \cdots s_0.s_1 s_2 \cdots s_n]$ of sect. 12.3.1 always contains the periodic point $\overline{s_{-m} \cdots s_0.s_1 s_2 \cdots s_n}$; hence even though the periodic points are of measure zero (just like rationals in the unit interval), they are dense on the non-wandering set. Equipped with a measure for the associated rectangle, periodic orbits suffice to cover the entire non-wandering set. The average of $e^{\beta A^n}$ evaluated on the non-wandering set is therefore given by the trace, properly normalized so $\langle 1 \rangle = 1$:

$$\langle e^{\beta A^n} \rangle_n \approx \frac{\sum_i^{(n)} e^{\beta A^n(x_i)} / |\Lambda_i|}{\sum_i^{(n)} 1 / |\Lambda_i|} = \sum_i^{(n)} \mu_i e^{\beta A^n(x_i)}. \quad (22.9)$$

Here μ_i is the *normalized natural measure*

$$\sum_i^{(n)} \mu_i = 1, \quad \mu_i = e^{\beta A^n(x_i)} / |\Lambda_i|, \quad (22.10)$$

correct both for the closed systems as well as the open systems of sect. 17.1.3.

Unlike brute numerical slicing of the integration space into an arbitrary lattice (for a critique, see sect. 16.3), the periodic orbit theory is smart, as it automatically partitions integrals by the intrinsic topology of the flow, and assigns to each tile the invariant natural measure μ_i .

22.2.1 Unstable periodic orbits are dense

(L. Rondoni and P. Cvitanović)

Our goal in sect. 17.1 was to evaluate the space and time averaged expectation value (17.9). An average over all periodic orbits can accomplish the job only if the periodic orbits fully explore the asymptotically accessible state space.

Why should the unstable periodic points end up being dense? The cycles are intuitively expected to be *dense* because on a connected chaotic set a typical trajectory is expected to behave ergodically, and pass infinitely many times arbitrarily close to any point on the set, including the initial point of the trajectory itself. The argument is more or less the following. Take a partition of \mathcal{M} in arbitrarily small regions, and consider particles that start out in region \mathcal{M}_i , and return to it in n steps after some peregrination in state space. In particular, a particle might return a little to the left of its original position, while a close neighbor might return a little to the right of its original position. By assumption, the flow is continuous, so generically one expects to be able to gently move the initial point in such a

way that the trajectory returns precisely to the initial point, i.e., one expects a periodic point of period n in cell i . As we diminish the size of regions \mathcal{M}_i , aiming a trajectory that returns to \mathcal{M}_i becomes increasingly difficult. Therefore, we are guaranteed that unstable orbits of larger and larger period are densely interspersed in the asymptotic non-wandering set.

The above argument is heuristic, by no means guaranteed to work, and it must be checked for the particular system at hand. A variety of ergodic but insufficiently mixing counter-examples can be constructed - the most familiar being a quasiperiodic motion on a torus.

22.3 Flow conservation sum rules

If the dynamical system is bounded, all trajectories remain confined for all times, escape rate (22.8) vanishes $\gamma = -s_0 = 0$, and the leading eigenvalue of the Perron-Frobenius operator (16.10) is simply $\exp(-t\gamma) = 1$. Conservation of material flow thus implies that for bound flows cycle expansions of dynamical zeta functions and spectral determinants satisfy exact *flow conservation* sum rules:

$$\begin{aligned} 1/\zeta(0,0) &= 1 + \sum_{\pi}' \frac{(-1)^k}{|\Lambda_{p_1} \cdots \Lambda_{p_k}|} = 0 \\ F(0,0) &= 1 - \sum_{n=1}^{\infty} c_n(0,0) = 0 \end{aligned} \tag{22.11}$$

obtained by setting $s = 0$ in (20.15), (20.16) cycle weights $t_p = e^{-sT_p}/|\Lambda_p| \rightarrow 1/|\Lambda_p|$. These sum rules depend neither on the cycle periods T_p nor on the observable $a(x)$ under investigation, but only on the cycle stabilities $\Lambda_{p,1}, \Lambda_{p,2}, \dots, \Lambda_{p,d}$, and their significance is purely geometric: they are a measure of how well periodic orbits tessellate the state space. Conservation of material flow provides the first and very useful test of the quality of finite cycle length truncations, and is something that you should always check first when constructing a cycle expansion for a bounded flow.

The trace formula version of the flow conservation flow sum rule comes in two varieties, one for the maps, and another for the flows. By flow conservation the leading eigenvalue is $s_0 = 0$, and for maps (20.14) yields

$$\text{tr } \mathcal{L}^n = \sum_{i \in \text{Fix } f^n} \frac{1}{|\det(\mathbf{1} - M^n(x_i))|} = 1 + e^{s_1 n} + \dots \tag{22.12}$$

For flows one can apply this rule by grouping together cycles from $t = T$ to $t = T + \Delta T$

$$\frac{1}{\Delta T} \sum_{\substack{T \leq r T_p \leq T + \Delta T \\ p,r}} \frac{T_p}{|\det(\mathbf{1} - M_p^r)|} = \frac{1}{\Delta T} \int_T^{T+\Delta T} dt (1 + e^{s_1 t} + \dots)$$

$$= 1 + \frac{1}{\Delta T} \sum_{\alpha=1}^{\infty} \frac{e^{s_{\alpha} T}}{s_{\alpha}} (e^{s_{\alpha} \Delta T} - 1) \approx 1 + e^{s_1 T} + \dots \quad (22.13)$$

As is usual for the fixed level trace sums, the convergence of (22.12) is controlled by the gap between the leading and the next-to-leading eigenvalues of the evolution operator.

22.4 Correlation functions

The *time correlation function* $C_{AB}(t)$ of two observables A and B along the trajectory $x(t) = f^t(x_0)$ is defined as

$$C_{AB}(t; x_0) = \lim_{T \rightarrow \infty} \frac{1}{T} \int_0^T d\tau A(x(\tau+t))B(x(\tau)), \quad x_0 = x(0). \quad (22.14)$$

If the system is ergodic, with invariant continuous measure $\rho_0(x)dx$, then correlation functions do not depend on x_0 (apart from a set of zero measure), and may be computed by a state space average as well

$$C_{AB}(t) = \int_{\mathcal{M}} dx_0 \rho_0(x_0) A(f^t(x_0)) B(x_0). \quad (22.15)$$

For a chaotic system we expect that time evolution will lose the information contained in the initial conditions, so that $C_{AB}(t)$ will approach the *uncorrelated* limit $\langle A \rangle \cdot \langle B \rangle$. As a matter of fact the asymptotic decay of correlation functions

$$\hat{C}_{AB} := C_{AB} - \langle A \rangle \langle B \rangle \quad (22.16)$$

for any pair of observables coincides with the definition of *mixing*, a fundamental property in ergodic theory. We now assume $\langle B \rangle = 0$ (otherwise we may define a new observable by $B(x) - \langle B \rangle$). Our purpose is now to connect the asymptotic behavior of correlation functions with the spectrum of the Perron-Frobenius operator \mathcal{L} . We can write (22.15) as

$$\tilde{C}_{AB}(t) = \int_{\mathcal{M}} dx \int_{\mathcal{M}} dy A(y) B(x) \rho_0(x) \delta(y - f^t(x)),$$

and recover the evolution operator

$$\tilde{C}_{AB}(t) = \int_{\mathcal{M}} dx \int_{\mathcal{M}} dy A(y) \mathcal{L}^t(y, x) B(x) \rho_0(x)$$

We recall that in sect. 16.1 we showed that $\rho(x)$ is the eigenvector of \mathcal{L} corresponding to probability conservation

$$\int_{\mathcal{M}} dy \mathcal{L}^t(x, y) \rho(y) = \rho(x).$$

Now, we can expand the x dependent part in terms of the eigenbasis of \mathcal{L} :

$$B(x) \rho_0(x) = \sum_{\alpha=0}^{\infty} c_{\alpha} \rho_{\alpha}(x),$$

where $\rho_0(x)$ is the natural measure. Since the average of the left hand side is zero the coefficient c_0 must vanish. The action of \mathcal{L} then can be written as

$$\tilde{C}_{AB}(t) = \sum_{\alpha \neq 0} e^{-s_{\alpha} t} c_{\alpha} \int_{\mathcal{M}} dy A(y) \rho_{\alpha}(y). \quad (22.17)$$

exercise 22.2

We see immediately that if the spectrum has a *gap*, i.e., if the second largest leading eigenvalue is isolated from the largest eigenvalue ($s_0 = 0$) then (22.17) implies *exponential* decay of correlations

$$\tilde{C}_{AB}(t) \sim e^{-\nu t}.$$

The correlation decay rate $\nu = s_1$ then depends only on intrinsic properties of the dynamical system (the position of the next-to-leading eigenvalue of the Perron-Frobenius operator), while the choice of a particular observable influences only the prefactor.

Correlation functions are often accessible from time series measurable in laboratory experiments and numerical simulations: moreover they are linked to transport exponents.

22.5 Trace formulas vs. level sums



Trace formulas (18.10) and (18.23) diverge precisely where one would like to use them, at s equal to eigenvalues s_{χ} . Instead, one can proceed as follows; according to (18.27) the “level” sums (all symbol strings of length n) are asymptotically going like $e^{s_0 n}$

$$\sum_{i \in \text{Fix} f^n} \frac{e^{\beta A^n(x_i)}}{|\Lambda_i|} \rightarrow e^{s_0 n},$$

so an n th order estimate $s_{(n)}$ of the leading eigenvalue is given by

$$1 = \sum_{i \in \text{Fix} f^n} \frac{e^{\beta A^n(x_i)} e^{-s_{(n)} n}}{|\Lambda_i|} \tag{22.18}$$

which generates a “normalized measure.” The difficulty with estimating this $n \rightarrow \infty$ limit is at least twofold:

1. due to the exponential growth in number of intervals, and the exponential decrease in attainable accuracy, the maximal n attainable experimentally or numerically is in practice of order of something between 5 to 20.

2. the pre-asymptotic sequence of finite estimates $s_{(n)}$ is not unique, because the sums Γ_n depend on how we define the escape region, and because in general the areas \mathcal{M}_i in the sum (22.2) should be weighted by the density of initial conditions x_0 . For example, an overall measuring unit rescaling $\mathcal{M}_i \rightarrow \alpha \mathcal{M}_i$ introduces $1/n$ corrections in $s_{(n)}$ defined by the log of the sum (22.8): $s_{(n)} \rightarrow s_{(n)} - \ln \alpha/n$. This can be partially fixed by defining a level average

$$\langle e^{\beta A(s)} \rangle_{(n)} := \sum_{i \in \text{Fix} f^n} \frac{e^{\beta A^n(x_i)} e^{s n}}{|\Lambda_i|} \tag{22.19}$$

and requiring that the ratios of successive levels satisfy

$$1 = \frac{\langle e^{\beta A(s_{(n)})} \rangle_{(n+1)}}{\langle e^{\beta A(s_{(n)})} \rangle_{(n)}}.$$

This avoids the worst problem with the formula (22.18), the inevitable $1/n$ corrections due to its lack of rescaling invariance. However, even though much published pondering of “chaos” relies on it, there is no need for such gymnastics: the dynamical zeta functions and spectral determinants are already invariant not only under linear rescalings, but under *all* smooth nonlinear conjugacies $x \rightarrow h(x)$, and require no $n \rightarrow \infty$ extrapolations to asymptotic times. Comparing with the cycle expansions (20.7) we see what the difference is; while in the level sum approach we keep increasing exponentially the number of terms with no reference to the fact that most are already known from shorter estimates, in the cycle expansions short terms dominate, longer ones enter only as exponentially small corrections.

The beauty of the trace formulas is that they are coordinatization independent: both $|\det(\mathbf{1} - M_p)| = |\det(\mathbf{1} - M^{T_p}(x))|$ and $e^{\beta A_p} = e^{\beta A^{T_p}(x)}$ contribution to the cycle weight t_p are independent of the starting periodic point point x . For the Jacobian matrix M_p this follows from the chain rule for derivatives, and for $e^{\beta A_p}$ from the fact that the integral over $e^{\beta A^t(x)}$ is evaluated along a closed loop. In addition, $|\det(\mathbf{1} - M_p)|$ is invariant under smooth coordinate transformations.

Résumé

We conclude this chapter by a general comment on the relation of the finite trace sums such as (22.2) to the spectral determinants and dynamical zeta functions. One might be tempted to believe that given a deterministic rule, a sum like (22.2) could be evaluated to any desired precision. For short finite times this is indeed true: every region \mathcal{M}_i in (22.2) can be accurately delineated, and there is no need for fancy theory. However, if the dynamics is unstable, local variations in initial conditions grow exponentially and in finite time attain the size of the system. The difficulty with estimating the $n \rightarrow \infty$ limit from (22.2) is then at least twofold:

1. due to the exponential growth in number of intervals, and the exponential decrease in attainable accuracy, the maximal n attainable experimentally or numerically is in practice of order of something between 5 to 20;

2. the pre-asymptotic sequence of finite estimates γ_n is not unique, because the sums $\hat{\Gamma}_n$ depend on how we define the escape region, and because in general the areas $|\mathcal{M}_i|$ in the sum (22.2) should be weighted by the density of initial x_0 .

In contrast, the dynamical zeta functions and spectral determinants are invariant under *all* smooth nonlinear conjugacies $x \rightarrow h(x)$, not only linear rescalings, and require no $n \rightarrow \infty$ extrapolations.

Commentary

Remark 22.1 Nonhyperbolic measures. $\mu_i = 1/|\Lambda_i|$ is the natural measure only for the strictly hyperbolic systems. For non-hyperbolic systems, the measure might develop cusps. For example, for Ulam type maps (unimodal maps with quadratic critical point mapped onto the “left” unstable fixed point x_0 , discussed in more detail in chapter 24), the measure develops a square-root singularity on the $\bar{0}$ cycle:

$$\mu_0 = \frac{1}{|\Lambda_0|^{1/2}}. \quad (22.20)$$

The thermodynamics averages are still expected to converge in the “hyperbolic” phase where the positive entropy of unstable orbits dominates over the marginal orbits, but they fail in the “non-hyperbolic” phase. The general case remains unclear [13, 2, 3, 5].

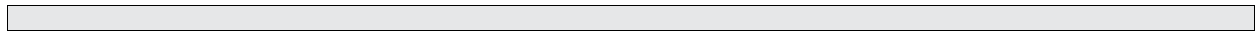
Remark 22.2 Trace formula periodic orbit averaging. The cycle averaging formulas are not the first thing that one would intuitively write down; the approximate trace formulas are more accessibly heuristically. The trace formula averaging (22.13) seems to have been discussed for the first time by Hannay and Ozorio de Almeida [8, 9]. Another novelty of the cycle averaging formulas and one of their main virtues, in contrast to the explicit analytic results such as those of ref. [4], is that their evaluation *does not* require any explicit construction of the (coordinate dependent) eigenfunctions of the Perron-Frobenius operator (i.e., the natural measure ρ_0).

Remark 22.3 Role of noise in dynamical systems. In any physical application the dynamics is always accompanied by additional external noise. The noise can be characterized by its strength σ and distribution. Lyapunov exponents, correlation decay and dynamo rate can be defined in this case the same way as in the deterministic case. You might fear that noise completely destroys the results derived here. However, one can show that the deterministic formulas remain valid to accuracy comparable with noise width if the noise level is small. A small level of noise even helps as it makes the dynamics more ergodic, with deterministically non-communicating parts of the state space now weakly connected due to the noise, making periodic orbit theory applicable to non-ergodic systems. For small amplitude noise one can expand

$$\bar{a} = \bar{a}_0 + \bar{a}_1\sigma^2 + \bar{a}_2\sigma^4 + \dots,$$

around the deterministic averages a_0 . The expansion coefficients $\bar{a}_1, \bar{a}_2, \dots$ can also be expressed via periodic orbit formulas. The calculation of these coefficients is one of the challenges facing periodic orbit theory, discussed in refs. [9, 10, 11].

Remark 22.4 Escape rates. A lucid introduction to escape from repellers is given by Kadanoff and Tang [9]. For a review of transient chaos see refs. [10, 12]. The ζ -function formulation is given by Ruelle [13] and W. Parry and M. Pollicott [14] and discussed in ref. [15]. Altmann and Tel [16] give a detailed study of escape rates, with citations to more recent literature.



Exercises

22.1. Escape rate of the logistic map.

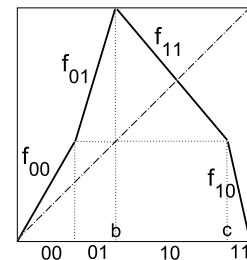
- (a) Calculate the fraction of trajectories remaining trapped in the interval $[0, 1]$ for the logistic map

$$f(x) = A(1 - (2x - 1)^2), \quad (22.21)$$

and determine the A dependence of the escape rate $\gamma(A)$ numerically.

- (b) Work out a numerical method for calculating the lengths of intervals of trajectories remaining stuck for n iterations of the map.
- (c) What is your expectation about the A dependence near the critical value $A_c = 1$?

22.2. Four-scale map correlation decay rate. Consider the piecewise-linear map



$$f(x) = \begin{cases} f_{00} = \Lambda_0 x \\ f_{01} = s_{01}(x - b) + 1 \\ f_{11} = \Lambda_1(x - b) + 1 \\ f_{10} = s_{10}(x - 1) \end{cases}$$

with a 4-interval state space Markov partition

$$\begin{aligned} \mathcal{M} &= \{\mathcal{M}_{00}, \mathcal{M}_{01}, \mathcal{M}_{10}, \mathcal{M}_{11}\} \\ &= \{[0, b/\Lambda_0], (b/\Lambda_0, b][b, c][c, 1]\}. \end{aligned}$$

- (a) compute s_{01}, s_{10}, c .

- (b) Show that the 2-cycle Floquet multiplier does not depend on b ,

$$\Lambda_{01} = s_{01} s_{10} = -\frac{\Lambda_0 \Lambda_1}{(\Lambda_0 - 1)(\Lambda_1 + 1)}.$$

- (c) Write down the $[2 \times 2]$ Perron-Frobenius operator acting on the space of densities piecewise constant over the four partitions.
- (d) Construct the corresponding transition graph.
- (e) Write down the corresponding spectral determinant.
- (f) Show that the escape rate vanishes, $\gamma = -\ln(z_0) = 0$.
- (g) Determine the spectrum of the Perron-Frobenius operator on the space of densities piecewise constant over the four partitions. Show that the second largest eigenvalue of the is $\frac{1}{z_1} = -1 + \frac{1}{\Lambda_0} - \frac{1}{\Lambda_1}$.
- (h) Is this value consistent with the tent map value previously computed in exercise 16.4 (with the appropriate choice of $\{\Lambda_0, \Lambda_1, c\}$).
- (i) (optional) Is this next-to leading eigenvalue still correct if the Perron-Frobenius operator acts on the space of analytic functions?

22.3. **Lyapunov exponents for 1-dimensional maps.** Extend your cycle expansion programs so that the first and the second moments of observables can be computed. Use it to compute the Lyapunov exponent for some or all of the following maps:

- (a) the piecewise-linear skew tent, flow conserving map

$$f(x) = \begin{cases} \Lambda_0 x & \text{if } 0 \leq x < \Lambda_0^{-1}, \\ \Lambda_1(1-x) & \text{if } \Lambda_0^{-1} \leq x \leq 1. \end{cases},$$

$$\Lambda_1 = \Lambda_0 / (\Lambda_0 - 1).$$

- (b) the Ulam map $f(x) = 4x(1-x)$.
- (c) the skew Ulam map

$$f(x) = \Lambda_0 x(1-x)(1-bx), \quad (22.22)$$

$1/\Lambda_0 = x_c(1-x_c)(1-bx_c)$. In our numerical work we fix (arbitrarily, the value chosen in ref. [3]) $b = 0.6$, so

$$f(x) = 0.1218 x(1-x)(1-0.6x)$$

with a peak $f(x_c) = 1$ at $x_c = 0.7$.

- (d) the repeller of $f(x) = Ax(1-x)$, for either $A = 9/2$ or $A = 6$ (this is a continuation of exercise 20.2).
- (e) for the 2-branch flow conserving map

$$\begin{aligned} f_0(x) &= \frac{1}{2h} \left(h - p + \sqrt{(h-p)^2 + 4hx} \right) \\ f_1(x) &= \frac{1}{2h} (h + p - 1) \\ &+ \frac{1}{2h} \sqrt{(h+p-1)^2 + 4h(x-p)}, \end{aligned} \quad (22.23)$$

with a 2-interval state space Markov partition $\mathcal{M} = \{\mathcal{M}_0, \mathcal{M}_1\} = \{[0, p], (p, 1]\}$. This is a non-linear perturbation of the $h = 0$ Bernoulli shift map (23.6); the first 15 eigenvalues of the Perron-Frobenius operator are listed in ref. [1] for $p = 0.8, h = 0.1$. Use these parameter values when computing the Lyapunov exponent.

Cases (a) and (b) can be computed analytically; cases (c), (d) and (e) require numerical computation of cycle stabilities. Just to see whether the theory is worth the trouble, also cross check your cycle expansions results for cases (c) and (d) with Lyapunov exponent computed by direct numerical averaging along trajectories of randomly chosen initial points:

- (f) trajectory-trajectory separation (17.27) (hint: rescale δx every so often, to avoid numerical overflows),
- (g) iterated stability (17.32).

How good is the numerical accuracy compared with the periodic orbit theory predictions?

References

[22.1] F. Christiansen, G. Paladin and H.H. Rugh, *Phys. Rev. Lett.* **65**, 2087 (1990).

[22.2] A. Politi, R. Badii and P. Grassberger, *J. Phys. A* **15**, L763 (1988); P. Grassberger, R. Badii and A. Politi, "Scaling laws for invariant measures on hyperbolic and nonhyperbolic attractors," *J. Stat. Phys.* **51**, 135 (1988).

[22.3] E. Ott, C. Grebogi and J.A. Yorke, *Phys. Lett. A* **135**, 343 (1989).

- [22.4] C. Grebogi, E. Ott and J.A. Yorke, *Phys. Rev. A* **36**, 3522 (1987).
- [22.5] C. Grebogi, E. Ott and J. Yorke, *Physica D* **7**, 181 (1983).
- [22.6] C. Grebogi, E. Ott and J.A. Yorke, *Phys. Rev. A* **36**, 3522 (1987).
- [22.7] C. Grebogi, E. Ott and J. Yorke, “Unstable periodic orbits and the dimension of multifractal chaotic attractors,” *Phys. Rev. A* **37**, 1711 (1988).
- [22.8] J. H. Hannay and A. M. Ozorio de Almeida, *J. Phys. A* **17**, 3429, (1984).
- [22.9] L. Kadanoff and C. Tang, *Escape from strange repellers*, *Proc. Natl. Acad. Sci. USA*, **81**, 1276 (1984).
- [22.10] T. Tél, “On the organization of transient chaos: Application to irregular scattering,” in Bai-lin Hao, ed., *Directions in Chaos*, vol. 3, (World Scientific, Singapore 1988) p. 149,
- [22.11] T. Tél, *J. Phys.* **A22**, L691 (1989).
- [22.12] S. Bleher, C. Grebogi and J.A. Yorke, *Physica* **46D**, 87 (1990),
- [22.13] D. Ruelle, *J. Stat. Phys.* **44**, 281 (1986).
- [22.14] W. Parry and M. Pollicott, *Ann. Math.* **118**, 573 (1983).
- [22.15] P. Cvitanović, “Invariant measurements of strange sets in terms of cycles,” *Phys. Rev. Lett.* **61**, 2729 (1988).
- [22.16] E.G. Altmann and T. Tél, “Poincare recurrences and transient chaos in leaked systems,” (2008); [arXiv:0808.3785](https://arxiv.org/abs/0808.3785).

Chapter 23

Why does it work?

Bloch: “Space is the field of linear operators.”

Heisenberg: “Nonsense, space is blue and birds fly through it.”

—Felix Bloch, *Heisenberg and the early days of quantum mechanics*

(R. Artuso, H.H. Rugh and P. Cvitanović)

AS WE SHALL SEE, the trace formulas and spectral determinants work well, sometimes very well. The question is: Why? And it still is. The heuristic manipulations of chapters 18 and 6 were naive and reckless, as we are facing infinite-dimensional vector spaces and singular integral kernels.

We now outline the key ingredients of proofs that put the trace and determinant formulas on solid footing. This requires taking a closer look at the evolution operators from a mathematical point of view, since up to now we have talked about eigenvalues without any reference to what kind of a function space the corresponding eigenfunctions belong to. We shall restrict our considerations to the spectral properties of the Perron-Frobenius operator for maps, as proofs for more general evolution operators follow along the same lines. What we refer to as a “the set of eigenvalues” acquires meaning only within a precisely specified functional setting: this sets the stage for a discussion of the analyticity properties of spectral determinants. In example 23.1 we compute explicitly the eigenspectrum for the three analytically tractable piecewise linear examples. In sect. 23.3 we review the basic facts of the classical Fredholm theory of integral equations. The program is sketched in sect. 23.4, motivated by an explicit study of eigenspectrum of the Bernoulli shift map, and in sect. 23.5 generalized to piecewise real-analytic hyperbolic maps acting on appropriate densities. We show on a very simple example that the spectrum is quite sensitive to the regularity properties of the functions considered.

For expanding and hyperbolic finite-subshift maps analyticity leads to a very strong result; not only do the determinants have better analyticity properties than

the trace formulas, but the spectral determinants are singled out as entire functions in the complex s plane.

remark 23.1

The goal of this chapter is not to provide an exhaustive review of the rigorous theory of the Perron-Frobenius operators and their spectral determinants, but rather to give you a feeling for how our heuristic considerations can be put on a firm basis. The mathematics underpinning the theory is both hard and profound.

If you are primarily interested in applications of the periodic orbit theory, you should skip this chapter on the first reading.



fast track:
chapter 13, p. 248

23.1 Linear maps: exact spectra

We start gently; in example 23.1 we work out the *exact* eigenvalues and eigenfunctions of the Perron-Frobenius operator for the simplest example of unstable, expanding dynamics, a linear 1 – dimensional map with one unstable fixed point. . Ref. [6] shows that this can be carried over to d -dimensions. Not only that, but in example 23.5 we compute the exact spectrum for the simplest example of a dynamical system with an *infinity* of unstable periodic orbits, the Bernoulli shift.

Example 23.1 The simplest eigenspectrum - a single fixed point: *In order to get some feeling for the determinants defined so formally in sect. 19.2, let us work out a trivial example: a repeller with only one expanding linear branch*

$$f(x) = \Lambda x, \quad |\Lambda| > 1,$$

and only one fixed point $x_q = 0$. The action of the Perron-Frobenius operator (16.10) is

$$\mathcal{L}\phi(y) = \int dx \delta(y - \Lambda x) \phi(x) = \frac{1}{|\Lambda|} \phi(y/\Lambda). \quad (23.1)$$

From this one immediately gets that the monomials y^k are eigenfunctions:

$$\mathcal{L}y^k = \frac{1}{|\Lambda|\Lambda^k} y^k, \quad k = 0, 1, 2, \dots \quad (23.2)$$

What are these eigenfunctions? Think of eigenfunctions of the Schrödinger equation: k labels the k th eigenfunction x^k in the same spirit in which the number of nodes labels the k th quantum-mechanical eigenfunction. A quantum-mechanical amplitude with more nodes has more variability, hence a higher kinetic energy. Analogously, for a Perron-Frobenius operator, a higher k eigenvalue $1/|\Lambda|\Lambda^k$ is getting exponentially smaller because densities that vary more rapidly decay more rapidly under the expanding action of the map.

Example 23.2 The trace formula for a single fixed point: The eigenvalues Λ^{-k-1} fall off exponentially with k , so the trace of \mathcal{L} is a convergent sum

$$\mathrm{tr} \mathcal{L} = \frac{1}{|\Lambda|} \sum_{k=0}^{\infty} \Lambda^{-k} = \frac{1}{|\Lambda|(1 - \Lambda^{-1})} = \frac{1}{|f(0)' - 1|},$$

in agreement with (18.7). A similar result follows for powers of \mathcal{L} , yielding the single-fixed point version of the trace formula for maps (18.10):

$$\sum_{k=0}^{\infty} \frac{ze^{s_k}}{1 - ze^{s_k}} = \sum_{r=1}^{\infty} \frac{z^r}{|1 - \Lambda^r|}, \quad e^{s_k} = \frac{1}{|\Lambda|\Lambda^k}. \quad (23.3)$$

The left hand side of (23.3) is a meromorphic function, with the leading zero at $z = |\Lambda|$. So what?

Example 23.3 Meromorphic functions and exponential convergence: As an illustration of how exponential convergence of a truncated series is related to analytic properties of functions, consider, as the simplest possible example of a meromorphic function, the ratio

$$h(z) = \frac{z - a}{z - b}$$

with a, b real and positive and $a < b$. Within the spectral radius $|z| < b$ the function h can be represented by the power series

$$h(z) = \sum_{k=0}^{\infty} \sigma_k z^k,$$

where $\sigma_0 = a/b$, and the higher order coefficients are given by $\sigma_j = (a - b)/b^{j+1}$. Consider now the truncation of order N of the power series

$$h_N(z) = \sum_{k=0}^N \sigma_k z^k = \frac{a}{b} + \frac{z(a - b)(1 - z^N/b^N)}{b^2(1 - z/b)}.$$

Let \hat{z}_N be the solution of the truncated series $h_N(\hat{z}_N) = 0$. To estimate the distance between a and \hat{z}_N it is sufficient to calculate $h_N(a)$. It is of order $(a/b)^{N+1}$, so finite order estimates converge exponentially to the asymptotic value.

This example shows that: (1) an estimate of the leading pole (the leading eigenvalue of \mathcal{L}) from a finite truncation of a trace formula converges exponentially, and (2) the non-leading eigenvalues of \mathcal{L} lie outside of the radius of convergence of the trace formula and cannot be computed by means of such cycle expansion. However, as we shall now see, the whole spectrum is reachable at no extra effort, by computing it from a determinant rather than a trace.

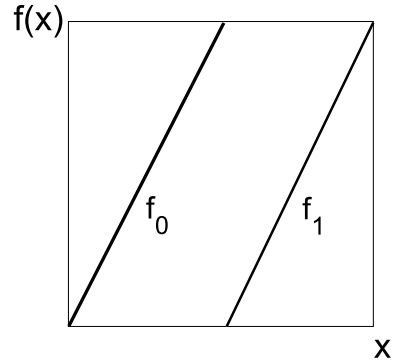


Figure 23.1: The Bernoulli shift map.

Example 23.4 The spectral determinant for a single fixed point: The spectral determinant (19.3) follows from the trace formulas of example 23.2:

$$\det(1 - z\mathcal{L}) = \prod_{k=0}^{\infty} \left(1 - \frac{z}{|\Lambda|\Lambda^k}\right) = \sum_{n=0}^{\infty} (-t)^n Q_n, \quad t = \frac{z}{|\Lambda|}, \quad (23.4)$$

where the cummulants Q_n are given explicitly by the Euler formula

exercise 23.3

$$Q_n = \frac{1}{1 - \Lambda^{-1}} \frac{\Lambda^{-1}}{1 - \Lambda^{-2}} \cdots \frac{\Lambda^{-n+1}}{1 - \Lambda^{-n}}. \quad (23.5)$$

The main lesson to glean from this simple example is that the cummulants Q_n decay asymptotically *faster* than exponentially, as $\Lambda^{-n(n-1)/2}$. For example, if we approximate series such as (23.4) by the first 10 terms, the error in the estimate of the leading zero is $\approx 1/\Lambda^{50}$!

So far all is well for a rather boring example, a dynamical system with a single repelling fixed point. What about chaos? Systems where the number of unstable cycles increases exponentially with their length? We now turn to the simplest example of a dynamical system with an infinity of unstable periodic orbits.

Example 23.5 Eigenfunction of Bernoulli shift map. (continued from example 11.7) The Bernoulli shift map figure 23.1

$$f(x) = \begin{cases} f_0(x) = 2x, & x \in I_0 = [0, 1/2) \\ f_1(x) = 2x - 1, & x \in I_1 = (1/2, 1] \end{cases} \quad (23.6)$$

models the 50-50% probability of a coin toss. The associated Perron-Frobenius operator (16.9) assembles $\rho(y)$ from its two preimages

$$\mathcal{L}\rho(y) = \frac{1}{2}\rho\left(\frac{y}{2}\right) + \frac{1}{2}\rho\left(\frac{y+1}{2}\right). \quad (23.7)$$

For this simple example the eigenfunctions can be written down explicitly: they coincide, up to constant prefactors, with the Bernoulli polynomials $B_n(x)$. These polynomials are generated by the Taylor expansion of the generating function

$$\mathcal{G}(x, t) = \frac{te^{xt}}{e^t - 1} = \sum_{k=0}^{\infty} B_k(x) \frac{t^k}{k!}, \quad B_0(x) = 1, \quad B_1(x) = x - \frac{1}{2}, \dots$$

The Perron-Frobenius operator (23.7) acts on the generating function \mathcal{G} as

$$\mathcal{L}\mathcal{G}(x, t) = \frac{1}{2} \left(\frac{te^{xt/2}}{e^t - 1} + \frac{te^{t/2}e^{xt/2}}{e^t - 1} \right) = \frac{t}{2} \frac{e^{xt/2}}{e^{t/2} - 1} = \sum_{k=1}^{\infty} B_k(x) \frac{(t/2)^k}{k!},$$

hence each $B_k(x)$ is an eigenfunction of \mathcal{L} with eigenvalue $1/2^k$.

The full operator has two components corresponding to the two branches. For the n times iterated operator we have a full binary shift, and for each of the 2^n branches the above calculations carry over, yielding the same trace $(2^n - 1)^{-1}$ for every cycle on length n . Without further ado we substitute everything back and obtain the determinant,

$$\det(1 - z\mathcal{L}) = \exp \left(- \sum_{n=1}^{\infty} \frac{z^n}{n} \frac{2^n}{2^n - 1} \right) = \prod_{k=0}^{\infty} \left(1 - \frac{z}{2^k} \right), \tag{23.8}$$

verifying that the Bernoulli polynomials are eigenfunctions with eigenvalues $1, 1/2, \dots, 1/2^n, \dots$.

The Bernoulli map spectrum looks reminiscent of the single fixed-point spectrum (23.2), with the difference that the leading eigenvalue here is 1, rather than $1/|\Lambda|$. The difference is significant: the single fixed-point map is a repeller, with escape rate (1.7) given by the \mathcal{L} leading eigenvalue $\gamma = \ln |\Lambda|$, while there is no escape in the case of the Bernoulli map. As already noted in discussion of the relation (19.23), for bound systems the local expansion rate (here $\ln |\Lambda| = \ln 2$) is balanced by the entropy (here $\ln 2$, the log of the number of preimages F_s), yielding zero escape rate.

section 19.4

So far we have demonstrated that our periodic orbit formulas are correct for two piecewise linear maps in 1 dimension, one with a single fixed point, and one with a full binary shift chaotic dynamics. For a single fixed point, eigenfunctions are monomials in x . For the chaotic example, they are orthogonal polynomials on the unit interval. What about higher dimensions? We check our formulas on a 2 – dimensional hyperbolic map next.

Example 23.6 The simplest of 2 – dimensional maps - a single hyperbolic fixed point: We start by considering a very simple linear hyperbolic map with a single hyperbolic fixed point,

$$f(x) = (f_1(x_1, x_2), f_2(x_1, x_2)) = (\Lambda_s x_1, \Lambda_u x_2), \quad 0 < |\Lambda_s| < 1, \quad |\Lambda_u| > 1.$$

The Perron-Frobenius operator (16.10) acts on the 2 – dimensional density functions as

$$\mathcal{L}\rho(x_1, x_2) = \frac{1}{|\Lambda_s \Lambda_u|} \rho(x_1/\Lambda_s, x_2/\Lambda_u) \tag{23.9}$$

What are good eigenfunctions? Cribbing the 1 – dimensional eigenfunctions for the stable, contracting x_1 direction from example 23.1 is not a good idea, as under the iteration of \mathcal{L} the high terms in a Taylor expansion of $\rho(x_1, x_2)$ in the x_1 variable would get multiplied by exponentially exploding eigenvalues $1/\Lambda_s^k$. This makes sense, as in

the contracting directions hyperbolic dynamics crunches up initial densities, instead of smoothing them. So we guess instead that the eigenfunctions are of form

$$\varphi_{k_1 k_2}(x_1, x_2) = x_2^{k_2} / x_1^{k_1+1}, \quad k_1, k_2 = 0, 1, 2, \dots, \quad (23.10)$$

a mixture of the Laurent series in the contraction x_1 direction, and the Taylor series in the expanding direction, the x_2 variable. The action of Perron-Frobenius operator on this set of basis functions

$$\mathcal{L}\varphi_{k_1 k_2}(x_1, x_2) = \frac{\sigma}{|\Lambda_u|} \frac{\Lambda_s^{k_1}}{\Lambda_u^{k_2}} \varphi_{k_1 k_2}(x_1, x_2), \quad \sigma = \Lambda_s / |\Lambda_s|$$

is smoothing, with the higher k_1, k_2 eigenvalues decaying exponentially faster, by $\Lambda_s^{k_1} / \Lambda_u^{k_2+1}$ factor in the eigenvalue. One verifies by an explicit calculation (undoing the geometric series expansions to lead to (19.9)) that the trace of \mathcal{L} indeed equals $1/|\det(\mathbf{1} - M)| = 1/|(1 - \Lambda_u)(1 - \Lambda_s)|$, from which it follows that all our trace and spectral determinant formulas apply. The argument applies to any hyperbolic map linearized around the fixed point of form $f(x_1, \dots, x_d) = (\Lambda_1 x_1, \Lambda_2 x_2, \dots, \Lambda_d x_d)$.

So far we have checked the trace and spectral determinant formulas derived heuristically in chapters 18 and 19, but only for the case of 1 – dimensional and 2 – dimensional linear maps. But for infinite-dimensional vector spaces this game is fraught with dangers, and we have already been misled by piecewise linear examples into spectral confusions: contrast the spectra of example 16.1 and example 17.4 with the spectrum computed in example 18.2.

We show next that the above results do carry over to a sizable class of piecewise analytic expanding maps.

23.2 Evolution operator in a matrix representation

The standard, and for numerical purposes sometimes very effective way to look at operators is through their matrix representations. Evolution operators are moving density functions defined over some state space, and as in general we can implement this only numerically, the temptation is to discretize the state space as in sect. 16.3. The problem with such state space discretization approaches is that they sometimes yield plainly wrong spectra (compare example 17.4 with the result of example 18.2), so we have to think through carefully what is it that we really measure.

An expanding map $f(x)$ takes an initial smooth density $\phi_n(x)$, defined on a subinterval, stretches it out and overlays it over a larger interval, resulting in a new, smoother density $\phi_{n+1}(x)$. Repetition of this process smoothes the initial density, so it is natural to represent densities $\phi_n(x)$ by their Taylor series. Expanding

$$\phi_n(y) = \sum_{k=0}^{\infty} \phi_n^{(k)}(0) \frac{y^k}{k!}, \quad \phi_{n+1}(y)_k = \sum_{\ell=0}^{\infty} \phi_{n+1}^{(\ell)}(0) \frac{y^\ell}{\ell!},$$

$$\phi_{n+1}^{(\ell)}(0) = \int dx \delta^{(\ell)}(y - f(x)) \phi_n(x) \Big|_{y=0}, \quad x = f^{-1}(0),$$

and substitute the two Taylor series into (16.6):

$$\phi_{n+1}(y) = (\mathcal{L}\phi_n)(y) = \int_{\mathcal{M}} dx \delta(y - f(x)) \phi_n(x).$$

The matrix elements follow by evaluating the integral

$$\mathbf{L}_{\ell k} = \frac{\partial^\ell}{\partial y^\ell} \int dx \mathcal{L}(y, x) \frac{x^k}{k!} \Big|_{y=0}. \quad (23.11)$$

we obtain a matrix representation of the evolution operator

$$\int dx \mathcal{L}(y, x) \frac{x^k}{k!} = \sum_{k'} \frac{y^{k'}}{k'!} \mathbf{L}_{k'k}, \quad k, k' = 0, 1, 2, \dots$$

which maps the x^k component of the density of trajectories $\phi_n(x)$ into the $y^{k'}$ component of the density $\phi_{n+1}(y)$ one time step later, with $y = f(x)$.

We already have some practice with evaluating derivatives $\delta^{(\ell)}(y) = \frac{\partial^\ell}{\partial y^\ell} \delta(y)$ from sect. 16.2. This yields a representation of the evolution operator centered on the fixed point, evaluated recursively in terms of derivatives of the map f :

$$\begin{aligned} (\mathbf{L})_{\ell k} &= \int dx \delta^{(\ell)}(x - f(x)) \frac{x^k}{k!} \Big|_{x=f(x)} \\ &= \frac{1}{|f'|} \left(\frac{d}{dx} \frac{1}{f'(x)} \right)^\ell \frac{x^k}{k!} \Big|_{x=f(x)}. \end{aligned} \quad (23.12)$$

The matrix elements vanish for $\ell < k$, so \mathbf{L} is a lower triangular matrix. The diagonal and the successive off-diagonal matrix elements are easily evaluated iteratively by computer algebra

$$\mathbf{L}_{kk} = \frac{1}{|\Lambda|\Lambda^k}, \quad \mathbf{L}_{k+1,k} = -\frac{(k+2)!f''}{2k!|\Lambda|\Lambda^{k+2}}, \quad \dots$$

For chaotic systems the map is expanding, $|\Lambda| > 1$. Hence the diagonal terms drop off exponentially, as $1/|\Lambda|^{k+1}$, the terms below the diagonal fall off even faster, and truncating \mathbf{L} to a finite matrix introduces only exponentially small errors.

The trace formula (23.3) takes now a matrix form

$$\text{tr} \frac{z\mathcal{L}}{1 - z\mathcal{L}} = \text{tr} \frac{\mathbf{L}}{1 - z\mathbf{L}}. \quad (23.13)$$

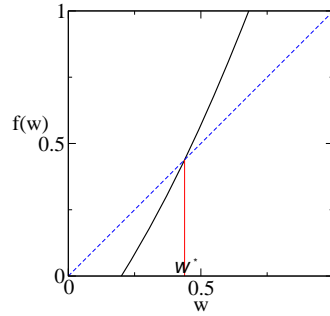


Figure 23.2: A nonlinear one-branch repeller with a single fixed point w_q .

In order to illustrate how this works, we work out a few examples.

In example 23.7 we show that these results carry over to any analytic single-branch 1 – dimensional repeller. Further examples motivate the steps that lead to a proof that spectral determinants for general analytic 1 – dimensional expanding maps, and - in sect. 23.5, for 1 – dimensional hyperbolic mappings - are also entire functions.

Example 23.7 Perron-Frobenius operator in a matrix representation: As in example 23.1, we start with a map with a single fixed point, but this time with a nonlinear piecewise analytic map f with a nonlinear inverse $F = f^{-1}$, sign of the derivative $\sigma = \sigma(F') = F'/|F'|$, and the Perron-Frobenius operator acting on densities analytic in an open domain enclosing the fixed point $x = w_q$,

$$\mathcal{L}\phi(y) = \int dx \delta(y - f(x)) \phi(x) = \sigma F'(y) \phi(F(y)).$$

Assume that F is a contraction of the unit disk in the complex plane, i.e.,

$$|F(z)| < \theta < 1 \text{ and } |F'(z)| < C < \infty \text{ for } |z| < 1, \tag{23.14}$$

and expand ϕ in a polynomial basis with the Cauchy integral formula

$$\phi(z) = \sum_{n=0}^{\infty} z^n \phi_n = \oint \frac{dw}{2\pi i} \frac{\phi(w)}{w - z}, \quad \phi_n = \oint \frac{dw}{2\pi i} \frac{\phi(w)}{w^{n+1}}$$

Combining this with (23.22), we see that in this basis Perron-Frobenius operator \mathcal{L} is represented by the matrix

$$\mathcal{L}\phi(w) = \sum_{m,n} w^m L_{mn} \phi_n, \quad L_{mn} = \oint \frac{dw}{2\pi i} \frac{\sigma F'(w)(F(w))^n}{w^{m+1}}. \tag{23.15}$$

Taking the trace and summing we get:

$$\text{tr } \mathcal{L} = \sum_{n \geq 0} L_{nn} = \oint \frac{dw}{2\pi i} \frac{\sigma F'(w)}{w - F(w)}.$$

This integral has but one simple pole at the unique fixed point $w^* = F(w^*) = f(w^*)$. Hence

$$\text{tr } \mathcal{L} = \frac{\sigma F'(w^*)}{1 - F'(w^*)} = \frac{1}{|f'(w^*) - 1|}.$$

exercise 23.6

This super-exponential decay of cummulants Q_k ensures that for a repeller consisting of a single repelling point the spectral determinant (23.4) is *entire* in the complex z plane.

In retrospect, the matrix representation method for solving the density evolution problems is eminently sensible — after all, that is the way one solves a close relative to classical density evolution equations, the Schrödinger equation. *When* available, matrix representations for \mathcal{L} enable us to compute many more orders of cumulant expansions of spectral determinants and many more eigenvalues of evolution operators than the cycle expansions approach.

Now, if the spectral determinant is entire, formulas such as (19.25) imply that the dynamical zeta function is a meromorphic function. The practical import of this observation is that it guarantees that finite order estimates of zeroes of dynamical zeta functions and spectral determinants converge exponentially, or - in cases such as (23.4) - super-exponentially to the exact values, and so the cycle expansions to be discussed in chapter 20 represent a *true perturbative* approach to chaotic dynamics.

Before turning to specifics we summarize a few facts about classical theory of integral equations, something you might prefer to skip on first reading. The purpose of this exercise is to understand that the Fredholm theory, a theory that works so well for the Hilbert spaces of quantum mechanics does not necessarily work for deterministic dynamics - the ergodic theory is much harder.



fast track:
sect. 23.4, p. 440

23.3 Classical Fredholm theory

He who would valiant be 'gainst all disaster
Let him in constancy follow the Master.
—John Bunyan, *Pilgrim's Progress*



The Perron-Frobenius operator

$$\mathcal{L}\phi(x) = \int dy \delta(x - f(y)) \phi(y)$$

has the same appearance as a classical Fredholm integral operator

$$\mathcal{K}\varphi(x) = \int_{\mathcal{M}} dy \mathcal{K}(x, y) \varphi(y), \quad (23.16)$$

and one is tempted to resort too classical Fredholm theory in order to establish analyticity properties of spectral determinants. This path to enlightenment is

blocked by the singular nature of the kernel, which is a distribution, whereas the standard theory of integral equations usually concerns itself with regular kernels $\mathcal{K}(x, y) \in L^2(\mathcal{M}^2)$. Here we briefly recall some steps of Fredholm theory, before working out the example of example 23.5.

The general form of Fredholm integral equations of the second kind is

$$\varphi(x) = \int_{\mathcal{M}} dy \mathcal{K}(x, y) \varphi(y) + \xi(x) \quad (23.17)$$

where $\xi(x)$ is a given function in $L^2(\mathcal{M})$ and the kernel $\mathcal{K}(x, y) \in L^2(\mathcal{M}^2)$ (Hilbert-Schmidt condition). The natural object to study is then the linear integral operator (23.16), acting on the Hilbert space $L^2(\mathcal{M})$: the fundamental property that follows from the $L^2(Q)$ nature of the kernel is that such an operator is *compact*, that is close to a finite rank operator. A compact operator has the property that for every $\delta > 0$ only a *finite* number of linearly independent eigenvectors exist corresponding to eigenvalues whose absolute value exceeds δ , so we immediately realize (figure 23.5) that much work is needed to bring Perron-Frobenius operators into this picture.

We rewrite (23.17) in the form

$$\mathcal{T}\varphi = \xi, \quad \mathcal{T} = \mathbf{1} - \mathcal{K}. \quad (23.18)$$

The Fredholm alternative is now applied to this situation as follows: the equation $\mathcal{T}\varphi = \xi$ has a unique solution for every $\xi \in L^2(\mathcal{M})$ **or** there exists a non-zero solution of $\mathcal{T}\varphi_0 = 0$, with an eigenvector of \mathcal{K} corresponding to the eigenvalue 1. The theory remains the same if instead of \mathcal{T} we consider the operator $\mathcal{T}_\lambda = \mathbf{1} - \lambda\mathcal{K}$ with $\lambda \neq 0$. As \mathcal{K} is a compact operator there is at most a denumerable set of λ for which the second part of the Fredholm alternative holds: apart from this set the inverse operator $(\mathbf{1} - \lambda\mathcal{T})^{-1}$ exists and is bounded (in the operator sense). When λ is sufficiently small we may look for a perturbative expression for such an inverse, as a geometric series

$$(\mathbf{1} - \lambda\mathcal{K})^{-1} = \mathbf{1} + \lambda\mathcal{K} + \lambda^2\mathcal{K}^2 + \dots = \mathbf{1} + \lambda\mathcal{W}, \quad (23.19)$$

where \mathcal{K}^n is a compact integral operator with kernel

$$\mathcal{K}^n(x, y) = \int_{\mathcal{M}^{n-1}} dz_1 \dots dz_{n-1} \mathcal{K}(x, z_1) \dots \mathcal{K}(z_{n-1}, y),$$

and \mathcal{W} is also compact, as it is given by the convergent sum of compact operators. The problem with (23.19) is that the series has a finite radius of convergence, while apart from a denumerable set of λ 's the inverse operator is well defined.

A fundamental result in the theory of integral equations consists in rewriting the resolving kernel \mathcal{W} as a ratio of two *analytic* functions of λ

$$\mathcal{W}(x, y) = \frac{\mathcal{D}(x, y; \lambda)}{D(\lambda)}.$$

If we introduce the notation

$$\mathcal{K} \begin{pmatrix} x_1 \dots x_n \\ y_1 \dots y_n \end{pmatrix} = \begin{vmatrix} \mathcal{K}(x_1, y_1) & \dots & \mathcal{K}(x_1, y_n) \\ \dots & \dots & \dots \\ \mathcal{K}(x_n, y_1) & \dots & \mathcal{K}(x_n, y_n) \end{vmatrix}$$

we may write the explicit expressions

$$\begin{aligned} D(\lambda) &= 1 + \sum_{n=1}^{\infty} (-1)^n \frac{\lambda^n}{n!} \int_{\mathcal{M}^n} dz_1 \dots dz_n \mathcal{K} \begin{pmatrix} z_1 \dots z_n \\ z_1 \dots z_n \end{pmatrix} \\ &= \exp \left(- \sum_{m=1}^{\infty} \frac{\lambda^m}{m} \text{tr} \mathcal{K}^m \right) \tag{23.20} \\ \mathcal{D}(x, y; \lambda) &= \mathcal{K} \begin{pmatrix} x \\ y \end{pmatrix} + \sum_{n=1}^{\infty} \frac{(-\lambda)^n}{n!} \int_{\mathcal{M}^n} dz_1 \dots dz_n \mathcal{K} \begin{pmatrix} x & z_1 & \dots & z_n \\ y & z_1 & \dots & z_n \end{pmatrix} \end{aligned}$$

The quantity $D(\lambda)$ is known as the Fredholm determinant (see (19.24)): it is an entire analytic function of λ , and $D(\lambda) = 0$ if and only if $1/\lambda$ is an eigenvalue of \mathcal{K} .

Worth emphasizing again: the Fredholm theory is based on the compactness of the integral operator, i.e., on the functional properties (summability) of its kernel. As the Perron-Frobenius operator is not compact, there is a bit of wishful thinking involved here.

23.4 Analyticity of spectral determinants

They savored the strange warm glow of being much more ignorant than ordinary people, who were only ignorant of ordinary things.

—Terry Pratchett

Spaces of functions integrable L^1 , or square-integrable L^2 on interval $[0, 1]$ are mapped into themselves by the Perron-Frobenius operator, and in both cases the constant function $\phi_0 \equiv 1$ is an eigenfunction with eigenvalue 1. If we focus our attention on L^1 we also have a family of L^1 eigenfunctions,

$$\phi_\theta(y) = \sum_{k \neq 0} \exp(2\pi iky) \frac{1}{|k|^\theta} \tag{23.21}$$

with complex eigenvalue $2^{-\theta}$, parameterized by complex θ with $\text{Re } \theta > 0$. By varying θ one realizes that such eigenvalues fill out the entire unit disk. Such *essential spectrum*, the case $k = 0$ of figure 23.5, hides all fine details of the spectrum.

What’s going on? Spaces L^1 and L^2 contain arbitrarily ugly functions, allowing any singularity as long as it is (square) integrable - and there is no way that expanding dynamics can smooth a kinky function with a non-differentiable singularity, let’s say a discontinuous step, and that is why the eigenspectrum is dense rather than discrete. Mathematicians love to wallow in this kind of muck, but there is no way to prepare a nowhere differentiable L^1 initial density in a laboratory. The only thing we can prepare and measure are piecewise smooth (real-analytic) density functions.

For a bounded linear operator \mathcal{A} on a Banach space Ω , the spectral radius is the smallest positive number ρ_{spec} such that the spectrum is inside the disk of radius ρ_{spec} , while the essential spectral radius is the smallest positive number ρ_{ess} such that outside the disk of radius ρ_{ess} the spectrum consists only of isolated eigenvalues of finite multiplicity (see figure 23.5).

exercise 23.5

We may shrink the essential spectrum by letting the Perron-Frobenius operator act on a space of smoother functions, exactly as in the one-branch repeller case of sect. 23.1. We thus consider a smaller space, $\mathbb{C}^{k+\alpha}$, the space of k times differentiable functions whose k ’th derivatives are Hölder continuous with an exponent $0 < \alpha \leq 1$: the expansion property guarantees that such a space is mapped into itself by the Perron-Frobenius operator. In the strip $0 < \text{Re } \theta < k + \alpha$ most ϕ_θ will cease to be eigenfunctions in the space $\mathbb{C}^{k+\alpha}$; the function ϕ_n survives only for integer valued $\theta = n$. In this way we arrive at a finite set of *isolated* eigenvalues $1, 2^{-1}, \dots, 2^{-k}$, and an essential spectral radius $\rho_{ess} = 2^{-(k+\alpha)}$.

We follow a simpler path and restrict the function space even further, namely to a space of analytic functions, i.e., functions for which the Taylor expansion is convergent at each point of the interval $[0, 1]$. With this choice things turn out easy and elegant. To be more specific, let ϕ be a holomorphic and bounded function on the disk $D = B(0, R)$ of radius $R > 0$ centered at the origin. Our Perron-Frobenius operator preserves the space of such functions provided $(1 + R)/2 < R$ so all we need is to choose $R > 1$. If $F_s, s \in \{0, 1\}$, denotes the s inverse branch of the Bernoulli shift (23.6), the corresponding action of the Perron-Frobenius operator is given by $\mathcal{L}_s h(y) = \sigma F'_s(y) h \circ F_s(y)$, using the Cauchy integral formula along the ∂D boundary contour:

$$\mathcal{L}_s h(y) = \sigma \oint \frac{dw}{2\pi i} \frac{h(w)F'_s(y)}{w - F_s(y)}. \tag{23.22}$$

For reasons that will be made clear later we have introduced a sign $\sigma = \pm 1$ of the given real branch $|F'(y)| = \sigma F'(y)$. For both branches of the Bernoulli shift $s = 1$, but in general one is not allowed to take absolute values as this could destroy analyticity. In the above formula one may also replace the domain D by *any*

domain containing $[0, 1]$ such that the inverse branches maps the closure of D into the interior of D . Why? simply because the kernel remains non-singular under this condition, i.e., $w - F(y) \neq 0$ whenever $w \in \partial D$ and $y \in \text{Cl } D$. The problem is now reduced to the standard theory for Fredholm determinants, sect. 23.3. The integral kernel is no longer singular, traces and determinants are well-defined, and we can evaluate the trace of \mathcal{L}_F by means of the Cauchy contour integral formula:

$$\text{tr } \mathcal{L}_F = \oint \frac{dw}{2\pi i} \frac{\sigma F'(w)}{w - F(w)}.$$

Elementary complex analysis shows that since F maps the closure of D into its own interior, F has a unique (real-valued) fixed point x^* with a multiplier strictly smaller than one in absolute value. Residue calculus therefore yields

exercise 23.6

$$\text{tr } \mathcal{L}_F = \frac{\sigma F'(x^*)}{1 - F'(x^*)} = \frac{1}{|f'(x^*) - 1|},$$

justifying our previous *ad hoc* calculations of traces using Dirac delta functions.

Example 23.8 Perron-Frobenius operator in a matrix representation: As in example 23.1, we start with a map with a single fixed point, but this time with a nonlinear piecewise analytic map f with a nonlinear inverse $F = f^{-1}$, sign of the derivative $\sigma = \sigma(F') = F'/|F'|$

$$\mathcal{L}\phi(z) = \int dx \delta(z - f(x)) \phi(x) = \sigma F'(z) \phi(F(z)).$$

Assume that F is a contraction of the unit disk, i.e.,

$$|F(z)| < \theta < 1 \quad \text{and} \quad |F'(z)| < C < \infty \quad \text{for} \quad |z| < 1, \quad (23.23)$$

and expand ϕ in a polynomial basis by means of the Cauchy formula

$$\phi(z) = \sum_{n \geq 0} z^n \phi_n = \oint \frac{dw}{2\pi i} \frac{\phi(w)}{w - z}, \quad \phi_n = \oint \frac{dw}{2\pi i} \frac{\phi(w)}{w^{n+1}}$$

Combining this with (23.22), we see that in this basis \mathcal{L} is represented by the matrix

$$\mathcal{L}\phi(w) = \sum_{m,n} w^m L_{mn} \phi_n, \quad L_{mn} = \oint \frac{dw}{2\pi i} \frac{\sigma F'(w)(F(w))^n}{w^{m+1}}. \quad (23.24)$$

Taking the trace and summing we get:

$$\text{tr } \mathcal{L} = \sum_{n \geq 0} L_{nn} = \oint \frac{dw}{2\pi i} \frac{\sigma F'(w)}{w - F(w)}.$$

This integral has but one simple pole at the unique fixed point $w^* = F(w^*) = f(w^*)$. Hence

$$\text{tr } \mathcal{L} = \frac{\sigma F'(w^*)}{1 - F'(w^*)} = \frac{1}{|f'(w^*) - 1|}.$$

We worked out a very specific example, yet our conclusions can be generalized, provided a number of restrictive requirements are met by the dynamical system under investigation:

exercise 23.6

- 1) the evolution operator is *multiplicative* along the flow,
- 2) the symbolic dynamics is a *finite subshift*,
- 3) all cycle eigenvalues are *hyperbolic* (exponentially bounded in magnitude away from 1),
- 4) the map (or the flow) is *real analytic*, i.e., it has a piecewise analytic continuation to a complex extension of the state space.

These assumptions are romantic expectations not satisfied by the dynamical systems that we actually desire to understand. Still, they are not devoid of physical interest; for example, nice repellers like our 3-disk game of pinball do satisfy the above requirements.

Properties 1 and 2 enable us to represent the evolution operator as a finite matrix in an appropriate basis; properties 3 and 4 enable us to bound the size of the matrix elements and control the eigenvalues. To see what can go wrong, consider the following examples:

Property 1 is violated for flows in 3 or more dimensions by the following weighted evolution operator

$$\mathcal{L}^t(y, x) = |\Lambda^t(x)|^\beta \delta(y - f^t(x)) ,$$

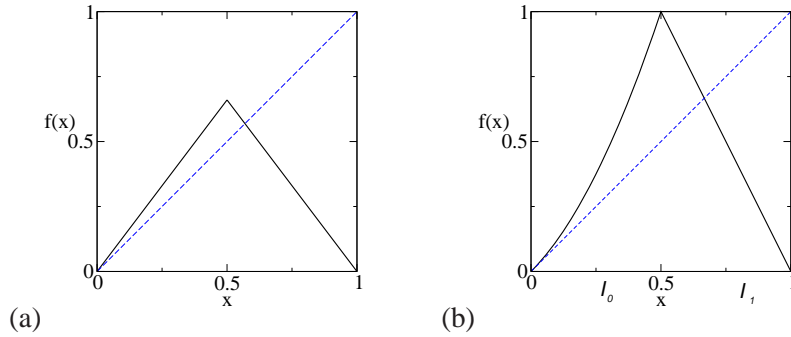
where $\Lambda^t(x)$ is an eigenvalue of the Jacobian matrix transverse to the flow. Semi-classical quantum mechanics suggest operators of this form with $\beta = 1/2$. The problem with such operators arises from the fact that when considering the Jacobian matrices $J_{ab} = J_a J_b$ for two successive trajectory segments a and b , the corresponding eigenvalues are in general *not* multiplicative, $\Lambda_{ab} \neq \Lambda_a \Lambda_b$ (unless a, b are iterates of the same prime cycle p , so $J_a J_b = J_p^{a+b}$). Consequently, this evolution operator is not multiplicative along the trajectory. The theorems require that the evolution be represented as a matrix in an appropriate polynomial basis, and thus cannot be applied to non-multiplicative kernels, i.e., kernels that do not satisfy the semi-group property $\mathcal{L}^s \mathcal{L}^t = \mathcal{L}^{s+t}$.

Property 2 is violated by the 1 – dimensional tent map (see figure 23.3 (a))

$$f(x) = \alpha(1 - |1 - 2x|), \quad 1/2 < \alpha < 1 .$$

All cycle eigenvalues are hyperbolic, but in general the critical point $x_c = 1/2$ is not a pre-periodic point, so there is no finite Markov partition and the symbolic dynamics does not have a finite grammar (see sect. 12.4 for definitions). In practice, this means that while the leading eigenvalue of \mathcal{L} might be computable,

Figure 23.3: (a) A (hyperbolic) tent map without a finite Markov partition. (b) A Markov map with a marginal fixed point.



the rest of the spectrum is very hard to control; as the parameter α is varied, the non-leading zeros of the spectral determinant move wildly about.

Property 3 is violated by the map (see figure 23.3 (b))

$$f(x) = \begin{cases} x + 2x^2 & , \quad x \in I_0 = [0, \frac{1}{2}] \\ 2 - 2x & , \quad x \in I_1 = [\frac{1}{2}, 1] \end{cases} .$$

Here the interval $[0, 1]$ has a Markov partition into two subintervals I_0 and I_1 , and f is monotone on each. However, the fixed point at $x = 0$ has marginal stability $\Lambda_0 = 1$, and violates condition 3. This type of map is called “intermittent” and necessitates much extra work. The problem is that the dynamics in the neighborhood of a marginal fixed point is very slow, with correlations decaying as power laws rather than exponentially. We will discuss such flows in chapter 24.

Property 4 is required as the heuristic approach of chapter 18 faces two major hurdles:

1. The trace (18.8) is not well defined because the integral kernel is singular.
2. The existence and properties of eigenvalues are by no means clear.

Actually, property 4 is quite restrictive, but we need it in the present approach, so that the Banach space of analytic functions in a disk is preserved by the Perron-Frobenius operator.

In attempting to generalize the results, we encounter several problems. First, in higher dimensions life is not as simple. Multi-dimensional residue calculus is at our disposal but in general requires that we find poly-domains (direct product of domains in each coordinate) and this need not be the case. Second, and perhaps somewhat surprisingly, the ‘counting of periodic orbits’ presents a difficult problem. For example, instead of the Bernoulli shift consider the doubling map (11.8) of the circle, $x \mapsto 2x \bmod 1$, $x \in R/Z$. Compared to the shift on the interval $[0, 1]$ the only difference is that the endpoints 0 and 1 are now glued together. Because these endpoints are fixed points of the map, the number of cycles of length

n decreases by 1. The determinant becomes:

$$\det(1 - z\mathcal{L}) = \exp\left(-\sum_{n=1}^{\infty} \frac{z^n}{n} \frac{2^n - 1}{2^n - 1}\right) = 1 - z. \quad (23.25)$$

The value $z = 1$ still comes from the constant eigenfunction, but the Bernoulli polynomials no longer contribute to the spectrum (as they are not periodic). Proofs of these facts, however, are difficult if one sticks to the space of analytic functions.

Third, our Cauchy formulas *a priori* work only when considering purely expanding maps. When stable and unstable directions co-exist we have to resort to stranger function spaces, as shown in the next section.

23.5 Hyperbolic maps

I can give you a definition of a Banach space, but I do not know what that means.

—Federico Bonnetto, *Banach space*

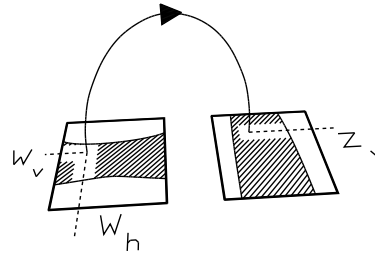
(H.H. Rugh)

Proceeding to hyperbolic systems, one faces the following paradox: If f is an area-preserving hyperbolic and real-analytic map of, for example, a 2-dimensional torus then the Perron-Frobenius operator is unitary on the space of L^2 functions, and its spectrum is confined to the unit circle. On the other hand, when we compute determinants we find eigenvalues scattered around inside the unit disk. Thinking back to the Bernoulli shift example 23.5 one would like to imagine these eigenvalues as popping up from the L^2 spectrum by shrinking the function space. Shrinking the space, however, can only make the spectrum smaller so this is obviously not what happens. Instead one needs to introduce a ‘mixed’ function space where in the unstable direction one resorts to analytic functions, as before, but in the stable direction one instead considers a ‘dual space’ of distributions on analytic functions. Such a space is neither included in nor includes L^2 and we have thus resolved the paradox. However, it still remains to be seen how traces and determinants are calculated.

The linear hyperbolic fixed point example 23.6 is somewhat misleading, as we have made explicit use of a map that acts independently along the stable and unstable directions. For a more general hyperbolic map, there is no way to implement such direct product structure, and the whole argument falls apart. Here comes an idea; use the analyticity of the map to rewrite the Perron-Frobenius operator acting as follows (where σ denotes the sign of the derivative in the unstable direction):

$$\mathcal{L}h(z_1, z_2) = \oint \oint \frac{\sigma h(w_1, w_2)}{(z_1 - f_1(w_1, w_2))(f_2(w_1, w_2) - z_2)} \frac{dw_1}{2\pi i} \frac{dw_2}{2\pi i}. \quad (23.26)$$

Figure 23.4: For an analytic hyperbolic map, specifying the contracting coordinate w_h at the initial rectangle and the expanding coordinate z_v at the image rectangle defines a unique trajectory between the two rectangles. In particular, w_v and z_h (not shown) are uniquely specified.



Here the function ϕ should belong to a space of functions analytic respectively *outside* a disk and *inside* a disk in the first and the second coordinates; with the additional property that the function decays to zero as the first coordinate tends to infinity. The contour integrals are along the boundaries of these disks. It is an exercise in multi-dimensional residue calculus to verify that for the above linear example this expression reduces to (23.9). Such operators form the building blocks in the calculation of traces and determinants. One can prove the following:

Theorem: *The spectral determinant for 2-dimensional hyperbolic analytic maps is entire.*

remark 23.8

The proof, apart from the Markov property that is the same as for the purely expanding case, relies heavily on the analyticity of the map in the explicit construction of the function space. The idea is to view the hyperbolicity as a cross product of a contracting map in forward time and another contracting map in backward time. In this case the Markov property introduced above has to be elaborated a bit. Instead of dividing the state space into intervals, one divides it into rectangles. The rectangles should be viewed as a direct product of intervals (say horizontal and vertical), such that the forward map is contracting in, for example, the horizontal direction, while the inverse map is contracting in the vertical direction. For Axiom A systems (see remark 23.8) one may choose coordinate axes close to the stable/unstable manifolds of the map. With the state space divided into N rectangles $\{\mathcal{M}_1, \mathcal{M}_2, \dots, \mathcal{M}_N\}$, $\mathcal{M}_i = I_i^h \times I_i^v$ one needs a complex extension $D_i^h \times D_i^v$, with which the hyperbolicity condition (which simultaneously guarantees the Markov property) can be formulated as follows:

Analytic hyperbolic property: Either $f(\mathcal{M}_i) \cap \text{Int}(\mathcal{M}_j) = \emptyset$, or for each pair $w_h \in \text{Cl}(D_i^h)$, $z_v \in \text{Cl}(D_j^v)$ there exist unique analytic functions of w_h, z_v : $w_v = w_v(w_h, z_v) \in \text{Int}(D_i^v)$, $z_h = z_h(w_h, z_v) \in \text{Int}(D_j^h)$, such that $f(w_h, w_v) = (z_h, z_v)$. Furthermore, if $w_h \in I_i^h$ and $z_v \in I_j^v$, then $w_v \in I_i^v$ and $z_h \in I_j^h$ (see figure 23.4).

In plain English, this means for the iterated map that one replaces the coordinates z_h, z_v at time n by the contracting pair z_h, w_v , where w_v is the contracting coordinate at time $n + 1$ for the ‘partial’ inverse map.

In two dimensions the operator in (23.26) acts on functions analytic outside D_i^h in the horizontal direction (and tending to zero at infinity) and inside D_i^v in the vertical direction. The contour integrals are precisely along the boundaries of these domains.

A map f satisfying the above condition is called *analytic hyperbolic* and the theorem states that the associated spectral determinant is entire, and that the trace formula (18.8) is correct.

Examples of analytic hyperbolic maps are provided by small analytic perturbations of the cat map, the 3-disk repeller, and the 2 – dimensional baker’s map.

23.6 The physics of eigenvalues and eigenfunctions



We appreciate by now that any honest attempt to look at the spectral properties of the Perron-Frobenius operator involves hard mathematics, but the effort is rewarded by the fact that we are finally able to control the analyticity properties of dynamical zeta functions and spectral determinants, and thus substantiate the claim that these objects provide a powerful and well-founded perturbation theory.

Often (see chapter 17) physically important part of the spectrum is just the leading eigenvalue, which gives us the escape rate from a repeller, or, for a general evolution operator, formulas for expectation values of observables and their higher moments. Also the eigenfunction associated to the leading eigenvalue has a physical interpretation (see chapter 16): it is the density of the natural measures, with singular measures ruled out by the proper choice of the function space. This conclusion is in accord with the generalized Perron-Frobenius theorem for evolution operators. In the finite dimensional setting, such a theorem is formulated as follows:

remark 23.7

- **Perron-Frobenius theorem:** Let L_{ij} be a nonnegative matrix, such that some n exists for which $(L^n)_{ij} > 0 \forall i, j$: then
 1. The maximal modulus eigenvalue is non-degenerate real, and positive
 2. The corresponding eigenvector (defined up to a constant) has nonnegative coordinates

We may ask what physical information is contained in eigenvalues beyond the leading one: suppose that we have a probability conserving system (so that the dominant eigenvalue is 1), for which the essential spectral radius satisfies $0 < \rho_{ess} < \theta < 1$ on some Banach space \mathcal{B} . Denote by \mathbf{P} the projection corresponding to the part of the spectrum inside a disk of radius θ . We denote by $\lambda_1, \lambda_2, \dots, \lambda_M$ the eigenvalues outside of this disk, ordered by the size of their absolute value, with $\lambda_1 = 1$. Then we have the following decomposition

$$\mathcal{L}\varphi = \sum_{i=1}^M \lambda_i \psi_i L_i \psi_i^* \varphi + \mathbf{P}\mathcal{L}\varphi \quad (23.27)$$

when L_i are (finite) matrices in Jordan canonical form ($L_0 = 0$ is a $[1 \times 1]$ matrix, as λ_0 is simple, due to the Perron-Frobenius theorem), whereas ψ_i is a row vector

whose elements form a basis on the eigenspace corresponding to λ_i , and ψ_i^* is a column vector of elements of \mathcal{B}^* (the dual space of linear functionals over \mathcal{B}) spanning the eigenspace of \mathcal{L}^* corresponding to λ_i . For iterates of the Perron-Frobenius operator, (23.27) becomes

$$\mathcal{L}^n \varphi = \sum_{i=1}^M \lambda_i^n \psi_i L_i^n \psi_i^* \varphi + \mathbf{P} \mathcal{L}^n \varphi. \quad (23.28)$$

If we now consider, for example, correlation between initial φ evolved n steps and final ξ ,

$$\langle \xi | \mathcal{L}^n | \varphi \rangle = \int_{\mathcal{M}} dy \xi(y) (\mathcal{L}^n \varphi)(y) = \int_{\mathcal{M}} dw (\xi \circ f^n)(w) \varphi(w), \quad (23.29)$$

it follows that

$$\langle \xi | \mathcal{L}^n | \varphi \rangle = \lambda_1^n \omega_1(\xi, \varphi) + \sum_{i=2}^L \lambda_i^n \omega_i^{(n)}(\xi, \varphi) + O(\theta^n), \quad (23.30)$$

where

$$\omega_i^{(n)}(\xi, \varphi) = \int_{\mathcal{M}} dy \xi(y) \psi_i L_i^n \psi_i^* \varphi.$$

The eigenvalues beyond the leading one provide two pieces of information: they rule the convergence of expressions containing high powers of the evolution operator to leading order (the λ_1 contribution). Moreover if $\omega_1(\xi, \varphi) = 0$ then (23.29) defines a correlation function: as each term in (23.30) vanishes exponentially in the $n \rightarrow \infty$ limit, the eigenvalues $\lambda_2, \dots, \lambda_M$ determine the exponential decay of correlations for our dynamical system. The prefactors ω depend on the choice of functions, whereas the exponential decay rates (given by logarithms of λ_i) do not: the correlation spectrum is thus a *universal* property of the dynamics (once we fix the overall functional space on which the Perron-Frobenius operator acts).

exercise 23.7

Example 23.9 Bernoulli shift eigenfunctions: Let us revisit the Bernoulli shift example (23.6) on the space of analytic functions on a disk: apart from the origin we have only simple eigenvalues $\lambda_k = 2^{-k}$, $k = 0, 1, \dots$. The eigenvalue $\lambda_0 = 1$ corresponds to probability conservation: the corresponding eigenfunction $B_0(x) = 1$ indicates that the natural measure has a constant density over the unit interval. If we now take any analytic function $\eta(x)$ with zero average (with respect to the Lebesgue measure), it follows that $\omega_1(\eta, \eta) = 0$, and from (23.30) the asymptotic decay of the correlation function is (unless also $\omega_1(\eta, \eta) = 0$)

$$C_{\eta, \eta}(n) \sim \exp(-n \log 2). \quad (23.31)$$

Thus, $-\log \lambda_1$ gives the exponential decay rate of correlations (with a prefactor that depends on the choice of the function). Actually the Bernoulli shift case may be treated exactly, as for analytic functions we can employ the Euler-MacLaurin summation formula

$$\eta(z) = \int_0^1 dw \eta(w) + \sum_{m=1}^{\infty} \frac{\eta^{(m-1)}(1) - \eta^{(m-1)}(0)}{m!} B_m(z). \quad (23.32)$$

As we are considering functions with zero average, we have from (23.29) and the fact that Bernoulli polynomials are eigenvectors of the Perron-Frobenius operator that

$$C_{\eta,\eta}(n) = \sum_{m=1}^{\infty} \frac{(2^{-m})^n (\eta^{(m)}(1) - \eta^{(m)}(0))}{m!} \int_0^1 dz \eta(z) B_m(z).$$

The decomposition (23.32) is also useful in realizing that the linear functionals ψ_i^* are singular objects: if we write it as

$$\eta(z) = \sum_{m=0}^{\infty} B_m(z) \psi_m^*[\eta],$$

we see that these functionals are of the form

$$\psi_i^*[\varepsilon] = \int_0^1 dw \Psi_i(w) \varepsilon(w),$$

where

$$\Psi_i(w) = \frac{(-1)^{i-1}}{i!} \left(\delta^{(i-1)}(w-1) - \delta^{(i-1)}(w) \right), \quad (23.33)$$

when $i \geq 1$ and $\Psi_0(w) = 1$. This representation is only meaningful when the function ε is analytic in neighborhoods of $w, w-1$.

23.7 Troubles ahead

The above discussion confirms that for a series of examples of increasing generality formal manipulations with traces and determinants are justified: the Perron-Frobenius operator has isolated eigenvalues, the trace formulas are explicitly verified, and the spectral determinant is an entire function whose zeroes yield the eigenvalues. Real life is harder, as we may appreciate through the following considerations:

- Our discussion tacitly assumed something that is physically entirely reasonable: our evolution operator is acting on the space of analytic functions, i.e., we are allowed to represent the initial density $\rho(x)$ by its Taylor expansions in the neighborhoods of periodic points. This is however far from being the only possible choice: mathematicians often work with the function space

exercise 23.1

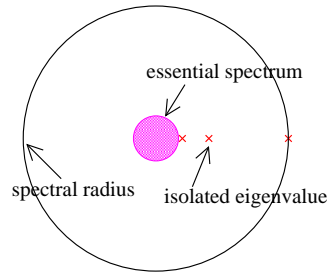


Figure 23.5: Spectrum of the Perron-Frobenius operator acting on the space of $\mathbb{C}^{k+\alpha}$ Hölder-continuous functions: only k isolated eigenvalues remain between the spectral radius, and the essential spectral radius which bounds the “essential,” continuous spectrum.

$\mathbb{C}^{k+\alpha}$, i.e., the space of k times differentiable functions whose k 'th derivatives are Hölder continuous with an exponent $0 < \alpha \leq 1$: then every y^η with $\text{Re } \eta > k$ is an eigenfunction of the Perron-Frobenius operator and we have

$$\mathcal{L}y^\eta = \frac{1}{|\Lambda|\Lambda^\eta}y^\eta, \quad \eta \in \mathbb{C}.$$

This spectrum differs markedly from the analytic case: only a small number of isolated eigenvalues remain, enclosed between the spectral radius and a smaller disk of radius $1/|\Lambda|^{k+1}$, see figure 23.5. In literature the radius of this disk is called the *essential spectral radius*.

In sect. 23.4 we discussed this point further, with the aid of a less trivial 1 – dimensional example. The physical point of view is complementary to the standard setting of ergodic theory, where many chaotic properties of a dynamical system are encoded by the presence of a *continuous* spectrum, used to prove asymptotic decay of correlations in the space of L^2 square-integrable functions.

exercise 23.2

- A deceptively innocent assumption is hidden beneath much that was discussed so far: that (23.1) maps a given function space into itself. The *expanding* property of the map guarantees that: if $f(x)$ is smooth in a domain D then $f(x/\Lambda)$ is smooth on a *larger* domain, provided $|\Lambda| > 1$. For higher-dimensional hyperbolic flows this is not the case, and, as we saw in sect. 23.5, extensions of the results obtained for expanding 1 – dimensional maps are highly nontrivial.
- It is not at all clear that the above analysis of a simple one-branch, one fixed point repeller can be extended to dynamical systems with Cantor sets of periodic points: we showed this in sect. 23.4.

Résumé

Examples of analytic eigenfunctions for 1 – dimensional maps are seductive, and make the problem of evaluating ergodic averages appear easy; just integrate over the desired observable weighted by the natural measure, right? No, generic natural

measure sits on a fractal set and is singular everywhere. The point of this book is that you never need to construct the natural measure, cycle expansions will do that job.

A theory of evaluation of dynamical averages by means of trace formulas and spectral determinants requires a deep understanding of their analyticity and convergence. We worked here through a series of examples:

1. exact spectrum (but for a single fixed point of a linear map)
2. exact spectrum for a locally analytic map, matrix representation
3. rigorous proof of existence of discrete spectrum for 2 – *dimensional* hyperbolic maps

In the case of especially well-behaved “Axiom A” systems, where both the symbolic dynamics and hyperbolicity are under control, it is possible to treat traces and determinants in a rigorous fashion, and strong results about the analyticity properties of dynamical zeta functions and spectral determinants outlined above follow.

Most systems of interest are *not* of the “axiom A” category; they are neither purely hyperbolic nor (as we have seen in chapters 11 and 12) do they have finite grammar. The importance of symbolic dynamics is generally grossly unappreciated; the crucial ingredient for nice analyticity properties of zeta functions is the existence of a finite grammar (coupled with uniform hyperbolicity).

The dynamical systems which are *really* interesting - for example, smooth bounded Hamiltonian potentials - are presumably never fully chaotic, and the central question remains: How do we attack this problem in a systematic and controllable fashion?

Theorem: Conjecture 3 with technical hypothesis is true in a lot of cases.

— M. Shub

Commentary

Remark 23.1 Surveys of rigorous theory. We recommend the references listed in remark 1.1 for an introduction to the mathematical literature on this subject. For a physicist, Driebe's monograph [19] might be the most accessible introduction into mathematics discussed briefly in this chapter. There are a number of reviews of the mathematical approach to dynamical zeta functions and spectral determinants, with pointers to the original references, such as refs. [1, 2]. An alternative approach to spectral properties of the Perron-Frobenius operator is given in ref. [3].

Ergodic theory, as presented by Sinai [14] and others, tempts one to describe the densities on which the evolution operator acts in terms of either integrable or square-integrable functions. For our purposes, as we have already seen, this space is not suitable. An introduction to ergodic theory is given by Sinai, Kornfeld and Fomin [15]; more advanced old-fashioned presentations are Walters [12] and Denker, Grillenberger and Sigmund [16]; and a more formal one is given by Peterson [17]. W. Tucker [28, 29, 30] has proven rigorously via interval arithmetic that the Lorentz attractor is strange for the original parameters, and has a long stable periodic orbit for the slightly different parameters.

Remark 23.2 Fredholm theory. Our brief summary of Fredholm theory is based on the exposition of ref. [4]. A technical introduction of the theory from an operator point of view is given in ref. [5]. The theory is presented in a more general form in ref. [6].

Remark 23.3 Bernoulli shift. For a more in-depth discussion, consult chapter 3 of ref. [19]. The extension of Fredholm theory to the case of Bernoulli shift on $\mathbb{C}^{k+\alpha}$ (in which the Perron-Frobenius operator is *not* compact – technically it is only *quasi-compact*. That is, the essential spectral radius is strictly smaller than the spectral radius) has been given by Ruelle [7]: a concise and readable statement of the results is contained in ref. [8]. We see from (23.31) that for the Bernoulli shift the exponential decay rate of correlations coincides with the Lyapunov exponent: while such an identity holds for a number of systems, it is by no means a general result, and there exist explicit counterexamples.

Remark 23.4 Hyperbolic dynamics. When dealing with hyperbolic systems one might try to reduce to the expanding case by projecting the dynamics along the unstable directions. As mentioned in the text this can be quite involved technically, as such unstable foliations are not characterized by strong smoothness properties. For such an approach, see ref. [3].

Remark 23.5 Spectral determinants for smooth flows. The theorem on page 445 also applies to hyperbolic analytic maps in d dimensions and smooth hyperbolic analytic flows in $(d + 1)$ dimensions, provided that the flow can be reduced to a piecewise

analytic map by a suspension on a Poincaré section, complemented by an analytic “ceiling” function (3.5) that accounts for a variation in the section return times. For example, if we take as the ceiling function $g(x) = e^{sT(x)}$, where $T(x)$ is the next Poincaré section time for a trajectory starting at x , we reproduce the flow spectral determinant (19.13). Proofs are beyond the scope of this chapter.

Remark 23.6 Explicit diagonalization. For 1–dimensional repellers a diagonalization of an explicit truncated L_{mn} matrix evaluated in a judiciously chosen basis may yield many more eigenvalues than a cycle expansion (see refs. [10, 11]). The reasons why one persists in using periodic orbit theory are partially aesthetic and partially pragmatic. The explicit calculation of L_{mn} demands an explicit choice of a basis and is thus non-invariant, in contrast to cycle expansions which utilize only the invariant information of the flow. In addition, we usually do not know how to construct L_{mn} for a realistic high-dimensional flow, such as the hyperbolic 3-disk game of pinball flow of sect. 1.3, whereas periodic orbit theory is true in higher dimensions and straightforward to apply.

Remark 23.7 Perron-Frobenius theorem. A proof of the Perron-Frobenius theorem may be found in ref. [12]. For positive transfer operators, this theorem has been generalized by Ruelle [13].

Remark 23.8 Axiom A systems. The proofs in sect. 23.5 follow the thesis work of H.H. Rugh [9, 18, 19]. For a mathematical introduction to the subject, consult the excellent review by V. Baladi [1]. It would take us too far afield to give and explain the definition of Axiom A systems (see refs. [27, 28]). Axiom A implies, however, the existence of a Markov partition of the state space from which the properties 2 and 3 assumed on page 434 follow.

Remark 23.9 Left eigenfunctions. We shall never use an explicit form of left eigenfunctions, corresponding to highly singular kernels like (23.33). Many details have been elaborated in a number of papers, such as ref. [20], with a daring physical interpretation.

Remark 23.10 Ulam’s idea. The approximation of Perron-Frobenius operator defined by (16.14) has been shown to reproduce the spectrum for expanding maps, once finer and finer Markov partitions are used [21]. The subtle point of choosing a state space partitioning for a “generic case” is discussed in ref. [22].

Exercises

- 23.1. **What space does \mathcal{L} act on?** Show that (23.2) is a complete basis on the space of analytic functions on a disk (and thus that we found the *complete* set of eigenvalues).
- 23.2. **What space does \mathcal{L} act on?** What can be said about the spectrum of (23.1) on $L^1[0, 1]$? Compare the result with figure 23.5.
- 23.3. **Euler formula.** Derive the Euler formula (23.5), $|u| < 1$:

$$\begin{aligned} \prod_{k=0}^{\infty} (1 + tu^k) &= 1 + \frac{t}{1-u} + \frac{t^2 u}{(1-u)(1-u^2)} \\ &\quad + \frac{t^3 u^3}{(1-u)(1-u^2)(1-u^3)} \cdots \\ &= \sum_{k=0}^{\infty} t^k \frac{u^{\frac{k(k-1)}{2}}}{(1-u) \cdots (1-u^k)}. \end{aligned}$$

- 23.4. **2 – dimensional product expansion**.** We conjecture that the expansion corresponding to exercise 23.3 is in the 2 – dimensional case given by

$$\prod_{k=0}^{\infty} (1 + tu^k)^{k+1}$$

$$\begin{aligned} &= \sum_{k=0}^{\infty} \frac{F_k(u)}{(1-u)^2(1-u^2)^2 \cdots (1-u^k)^2} t^k \\ &= 1 + \frac{1}{(1-u)^2} t + \frac{2u}{(1-u)^2(1-u^2)^2} t^2 \\ &\quad + \frac{u^2(1+4u+u^2)}{(1-u)^2(1-u^2)^2(1-u^3)^2} t^3 + \cdots \end{aligned}$$

$F_k(u)$ is a polynomial in u , and the coefficients fall off asymptotically as $C_n \approx u^{n^{3/2}}$. Verify; if you have a proof to all orders, e-mail it to the authors. (See also solution 23.3).

- 23.5. **Bernoulli shift on L spaces.** Check that the family (23.21) belongs to $L^1([0, 1])$. What can be said about the essential spectral radius on $L^2([0, 1])$? A useful reference is [24].
- 23.6. **Cauchy integrals.** Rework all complex analysis steps used in the Bernoulli shift example on analytic functions on a disk.
- 23.7. **Escape rate.** Consider the escape rate from a strange repeller: find a choice of trial functions ξ and φ such that (23.29) gives the fraction on particles surviving after n iterations, if their initial density distribution is $\rho_0(x)$. Discuss the behavior of such an expression in the long time limit.

References

[23.1] V. Baladi, *A brief introduction to dynamical zeta functions*, in: DMV-Seminar 27, *Classical Nonintegrability, Quantum Chaos*, A. Knauf and Ya.G. Sinai (eds), (Birkhäuser, Boston 1997).

[23.2] M. Pollicott, *Periodic orbits and zeta functions*, 1999 AMS Summer Institute on *Smooth ergodic theory and applications*, Seattle (1999), To appear *Proc. Symposia Pure Applied Math., AMS*.

[23.3] M. Viana, *Stochastic dynamics of deterministic systems*, (Col. Bras. de Matemática, Rio de Janeiro, 1997)

[23.4] A.N. Kolmogorov and S.V. Fomin, *Elements of the theory of functions and functional analysis* (Dover, 1999).

[23.5] R.G. Douglas, *Banach algebra techniques in operator theory* (Springer, New York, 1998).

- [23.6] A. Grothendieck, *La théorie de Fredholm*, *Bull. Soc. Math. France* **84**, 319 (1956).
- [23.7] D. Ruelle, “An extension of the theory of Fredholm determinants,” *Inst. Hautes Études Sci. Publ. Math.* **72**, 175-193 (1990).
- [23.8] V. Baladi, *Dynamical zeta functions*, in B. Branner and P. Hjorth, eds., *Proceedings of the NATO ASI Real and Complex Dynamical Systems* (1993), (Kluwer Academic Publishers, Dordrecht, 1995)
- [23.9] D. Ruelle, “Zeta-Functions for Expanding Maps and Anosov Flows,” *Inv. Math.* **34**, 231-242 (1976).
- [23.10] F. Christiansen, P. Cvitanović and H.H. Rugh, *J. Phys A* **23**, L713 (1990).
- [23.11] D. Alonso, D. MacKernan, P. Gaspard and G. Nicolis, *Phys. Rev.* **E54**, 2474 (1996).
- [23.12] P. Walters, *An introduction to ergodic theory* (Springer, New York 1982).
- [23.13] D. Ruelle, *Commun. Math. Phys.* **9**, 267 (1968).
- [23.14] Ya. G. Sinai, *Topics in ergodic theory* (Princeton Univ. Press, Princeton 1994).
- [23.15] I. Kornfeld, S. Fomin and Ya. Sinai, *Ergodic Theory* (Springer, New York 1982).
- [23.16] M. Denker, C. Grillenberger and K. Sigmund, *Ergodic theory on compact spaces* (Springer Lecture Notes in Math. **470**, 1975).
- [23.17] K. Peterson, *Ergodic theory* (Cambridge Univ. Press, Cambridge 1983).
- [23.18] D. Fried, “The Zeta functions of Ruelle and Selberg I,” *Ann. Scient. Éc. Norm. Sup.* **19**, 491 (1986).
- [23.19] H.H. Rugh, “The Correlation Spectrum for Hyperbolic Analytic Maps,” *Nonlinearity* **5**, 1237 (1992).
- [23.20] H.H. Hasegawa and W.C. Saphir, *Phys. Rev.* **A46**, 7401 (1992).
- [23.21] G. Froyland, *Commun. Math. Phys.* **189**, 237 (1997).
- [23.22] G. Froyland, “Extracting dynamical behaviour via Markov models,” in A. Mees, ed., *Nonlinear dynamics and statistics: Proceedings Newton Institute, Cambridge 1998* (Birkhäuser, Boston 2000); math-www.uni-paderborn.de/froyland.
- [23.23] V. Baladi, A. Kitaev, D. Ruelle and S. Semmes, “Sharp determinants and kneading operators for holomorphic maps,” IHES preprint (1995).
- [23.24] A. Zygmund, *Trigonometric series* (Cambridge Univ. Press, Cambridge 1959).
- [23.25] J.D. Crawford and J.R. Cary, *Physica* **D6**, 223 (1983)

- [23.26] P. Collet and S. Isola, *Commun.Math.Phys.* **139**, 551 (1991)
- [23.27] F. Christiansen, S. Isola, G. Paladin and H.H. Rugh, *J. Phys. A* **23**, L1301 (1990).
- [23.28] W. Tucker, “The Lorenz attractor exists,” *C. R. Acad. Sci. Paris Sér. I Math* **328**, 1197 (1999).
- [23.29] W. Tucker, “A rigorous ODE solver and Smale’s 14th problem,” *Found. Comput. Math.* **2**, 53 (2002).
- [23.30] M. Viana, “What’s new on Lorenz strange attractors?” *Math. Intelligencer* **22**, 6 (2000).

Chapter 24

Intermittency

Sometimes They Come Back

—Stephen King

(R. Artuso, P. Dahlqvist, G. Tanner and P. Cvitanović)

IN THE THEORY of chaotic dynamics developed so far we assumed that the evolution operators have discrete spectra $\{z_0, z_1, z_2, \dots\}$ given by the zeros of

$$1/\zeta(z) = (\dots) \prod_k (1 - z/z_k).$$

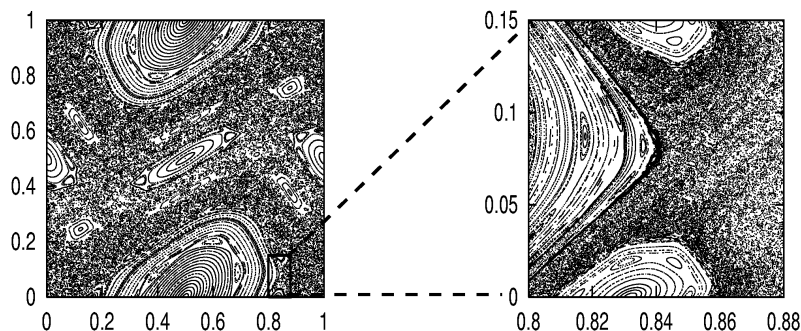
The assumption was based on the tacit premise that the dynamics is everywhere exponentially unstable. Real life is nothing like that - state spaces are generically infinitely interwoven patterns of stable and unstable behaviors. The stable (in the case of Hamiltonian flows, integrable) orbits do not communicate with the ergodic components of the phase space, and can be treated by classical methods. In general, one is able to treat the dynamics near stable orbits as well as chaotic components of the phase space dynamics well within a periodic orbit approach. Problems occur at the borderline between chaos and regular dynamics where marginally stable orbits and manifolds present difficulties and still unresolved challenges.

We shall use the simplest example of such behavior - intermittency in 1-dimensional maps - to illustrate effects of marginal stability. The main message will be that spectra of evolution operators are no longer discrete, dynamical zeta functions exhibit branch cuts of the form

$$1/\zeta(z) = (\dots) + (1 - z)^\alpha (\dots),$$

and correlations decay no longer exponentially, but as power laws.

Figure 24.1: Typical phase space for an area-preserving map with mixed phase space dynamics; here the standard map for $k = 1.2$.



24.1 Intermittency everywhere

In many fluid dynamics experiments one observes transitions from regular behaviors to behaviors where long time intervals of regular behavior (“laminar phases”) are interrupted by fast irregular bursts. The closer the parameter is to the onset of such bursts, the longer are the intervals of regular behavior. The distributions of laminar phase intervals are well described by power laws.

This phenomenon is called *intermittency*, and it is a very general aspect of dynamics, a shadow cast by non-hyperbolic, marginally stable state space regions. Complete hyperbolicity assumed in (18.5) is the exception rather than the rule, and for almost any dynamical system of interest (dynamics in smooth potentials, billiards with smooth walls, the infinite horizon Lorentz gas, etc.) one encounters mixed state spaces with islands of stability coexisting with hyperbolic regions, see figure 24.1 and example 7.6. Wherever stable islands are interspersed with chaotic regions, trajectories which come close to the stable islands can stay ‘glued’ for arbitrarily long times. These intervals of regular motion are interrupted by irregular bursts as the trajectory is re-injected into the chaotic part of the phase space. How the trajectories are precisely ‘glued’ to the marginally stable region is often hard to describe. What coarsely looks like a border of an island will under magnification dissolve into infinities of island chains of decreasing sizes, broken tori and bifurcating orbits, as illustrated in figure 24.1.

Intermittency is due to the existence of fixed points and cycles of marginal stability (5.6), or (in studies of the onset of intermittency) to the proximity of a nearly marginal complex or unstable orbits. In Hamiltonian systems intermittency goes hand in hand with the existence of (marginally stable) KAM tori. In more general settings, the existence of marginal or nearly marginal orbits is due to incomplete intersections of stable and unstable manifolds in a Smale horseshoe type dynamics (see figure 12.11). Following the stretching and folding of the invariant manifolds in time one will inevitably find state space points at which the stable and unstable manifolds are almost or exactly tangential to each other, implying non-exponential separation of nearby points in state space or, in other words, marginal stability. Under small parameter perturbations such neighborhoods undergo tangent bifurcations - a stable/unstable pair of periodic orbits is destroyed or created by coalescing into a marginal orbit, so the pruning which we shall encounter in chapter 12, and the intermittency discussed here are two sides of the same coin.

section 12.4

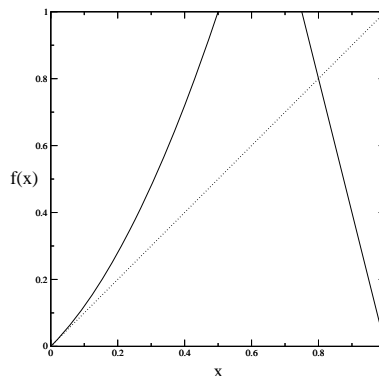


Figure 24.2: A complete binary repeller with a marginal fixed point.

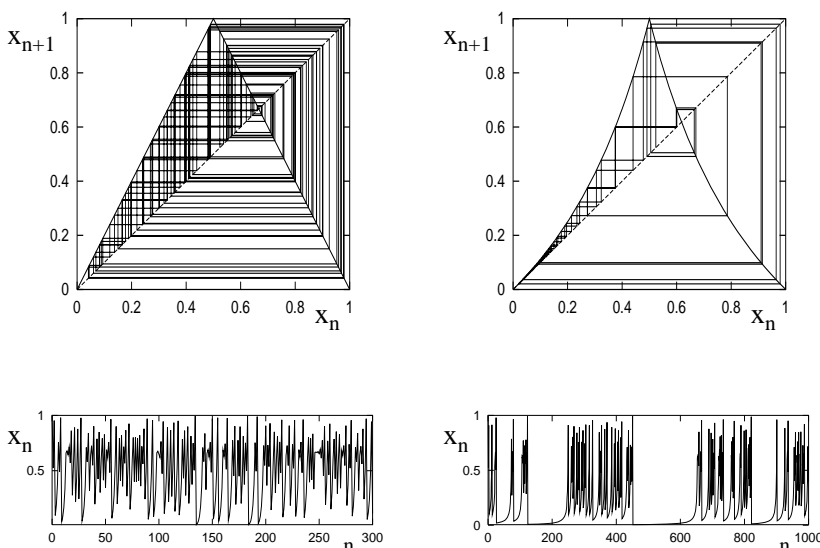


Figure 24.3: (a) A tent map trajectory. (b) A Farey map trajectory.

How to deal with the full complexity of a typical Hamiltonian system with mixed phase space is a very difficult, still open problem. Nevertheless, it is possible to learn quite a bit about intermittency by considering rather simple examples. Here we shall restrict our considerations to 1-dimensional maps which in the neighborhood of a single marginally stable fixed point at $x=0$ take the form

$$x \mapsto f(x) = x + O(x^{1+s}), \tag{24.1}$$

and are expanding everywhere else. Such a map may allow for escape, like the map shown in figure 24.2 or the dynamics may be bounded, like the Farey map (20.31)

$$x \mapsto f(x) = \begin{cases} x/(1-x) & x \in [0, 1/2[\\ (1-x)/x & x \in [1/2, 1] \end{cases}$$

introduced in sect. 20.5.

Figure 24.3 compares a trajectory of the tent map (11.4) side by side with a trajectory of the Farey map. In a stark contrast to the uniformly chaotic trajectory of the tent map, the Farey map trajectory alternates intermittently between slow regular motion close to the marginally stable fixed point, and chaotic bursts.

section 20.5.3

The presence of marginal stability has striking dynamical consequences: correlation decay may exhibit long range power law asymptotic behavior and diffusion processes can assume anomalous character. Escape from a repeller of the form figure 24.2 may be algebraic rather than exponential. In long time explorations of the dynamics intermittency manifests itself by enhancement of natural measure in the proximity of marginally stable cycles.

The questions we shall address here are: how does marginal stability affect zeta functions or spectral determinants? And, can we deduce power law decays of correlations from cycle expansions?

In example 23.5 we saw that marginal stability violates one of the conditions which ensure that the spectral determinant is an entire function. Already the simple fact that the cycle weight $1/|1 - \Lambda_p^r|$ in the trace (18.3) or the spectral determinant (19.3) diverges for marginal orbits with $|\Lambda_p| = 1$ tells us that we have to treat these orbits with care.

In the following we will incorporate marginal stability orbits into cycle-expansions in a systematic manner. To get to know the difficulties lying ahead, we will start in sect. 24.2 with a piecewise linear map, with the asymptotics (24.1). We will construct a dynamical zeta function in the usual way without worrying too much about its justification and show that it has a branch cut singularity. We will calculate the rate of escape from our piecewise linear map and find that it is characterized by decay, rather than exponential decay, a power law. We will show that dynamical zeta functions in the presence of marginal stability can still be written in terms of periodic orbits, exactly as in chapters 17 and 22, with one exception: the marginally stable orbits have to be explicitly excluded. This innocent looking step has far reaching consequences; it forces us to change the symbolic dynamics from a finite to an infinite alphabet, and entails a reorganization of the order of summations in cycle expansions, sect. 24.2.4.

Branch cuts are typical also for smooth intermittent maps with isolated marginally stable fixed points and cycles. In sect. 24.3, we discuss the cycle expansions and curvature combinations for zeta functions of smooth maps tailored to intermittency. The knowledge of the type of singularity one encounters enables us to develop the efficient resummation method presented in sect. 24.3.1.

Finally, in sect. 24.4, we discuss a probabilistic approach to intermittency that yields approximate dynamical zeta functions and provides valuable information about more complicated systems, such as billiards.

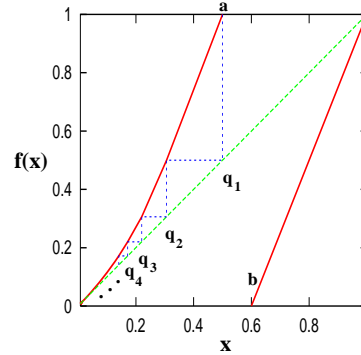


Figure 24.4: A piecewise linear intermittent map of (24.2) type: more specifically, the map piecewise linear over intervals (24.8) of the toy example studied below, $a = .5$, $b = .6$, $s = 1.0$.

24.2 Intermittency for pedestrians

Intermittency does not only present us with a large repertoire of interesting dynamics, it is also at the root of many sorrows such as slow convergence of cycle expansions. In order to get to know the kind of problems which arise when studying dynamical zeta functions in the presence of marginal stability we will consider an artfully concocted piecewise linear model first. From there we will move on to the more general case of smooth intermittant maps, sect. 24.3.

24.2.1 A toy map

The Bernoulli shift map (23.6) is an idealized, but highly instructive, example of a hyperbolic map. To study intermittency we will now construct a likewise piecewise linear model, an intermittent map stripped down to its bare essentials.

Consider a map $x \mapsto f(x)$ on the unit interval $\mathcal{M} = [0, 1]$ with two monotone branches

$$f(x) = \begin{cases} f_0(x) & \text{for } x \in \mathcal{M}_0 = [0, a] \\ f_1(x) & \text{for } x \in \mathcal{M}_1 = [b, 1] \end{cases} \quad (24.2)$$

The two branches are assumed complete, that is $f_0(\mathcal{M}_0) = f_1(\mathcal{M}_1) = \mathcal{M}$. The map allows escape if $a < b$ and is bounded if $a = b$ (see figure 24.2 and figure 24.4). We take the right branch to be expanding and linear:

$$f_1(x) = \frac{1}{1-b}(x-b).$$

Next, we will construct the left branch in a way, which will allow us to model the intermittent behavior (24.1) near the origin. We chose a monotonically decreasing sequence of points q_n in $[0, a]$ with $q_1 = a$ and $q_n \rightarrow 0$ as $n \rightarrow \infty$. This sequence defines a partition of the left interval \mathcal{M}_0 into an infinite number of connected intervals \mathcal{M}_n , $n \geq 2$ with

$$\mathcal{M}_n =]q_n, q_{n-1}] \quad \text{and} \quad \mathcal{M}_0 = \bigcup_{n=2}^{\infty} \mathcal{M}_n. \quad (24.3)$$

The map $f_0(x)$ is now specified by the following requirements

- $f_0(x)$ is continuous.
- $f_0(x)$ is linear on the intervals \mathcal{M}_n for $n \geq 2$.
- $f_0(q_n) = q_{n-1}$, that is $\mathcal{M}_n = f_0^{-n+1}([a, 1])$.

This fixes the map for any given sequence $\{q_n\}$. The last condition ensures the existence of a simple Markov partition. The slopes of the various linear segments are

$$\begin{aligned} f'_0(x) &= \frac{f_0(q_{n-1}) - f_0(q_n)}{q_{n-1} - q_n} = \frac{|\mathcal{M}_{n-1}|}{|\mathcal{M}_n|} && \text{for } x \in \mathcal{M}_n, n \geq 3 \\ f'_0(x) &= \frac{f_0(q_1) - f_0(q_2)}{q_1 - q_2} = \frac{1-a}{|\mathcal{M}_2|} && \text{for } x \in \mathcal{M}_2 \\ f'_0(x) &= \frac{1}{1-b} = \frac{|\mathcal{M}|}{|\mathcal{M}_1|} && \text{for } x \in \mathcal{M}_1 \end{aligned} \quad (24.4)$$

with $|\mathcal{M}_n| = q_{n-1} - q_n$ for $n \geq 2$. Note that we do not require as yet that the map exhibit intermittent behavior.

We will see that the family of periodic orbits with code 10^n plays a key role for intermittent maps of the form (24.1). An orbit 10^n enters the intervals $\mathcal{M}_1 \rightarrow \mathcal{M}_{n+1} \rightarrow \mathcal{M}_n \rightarrow \dots \rightarrow \mathcal{M}_2$ successively and the family approaches the marginal stable fixed point at $x = 0$ for $n \rightarrow \infty$. The stability of a cycle 10^n for $n \geq 1$ is given by the chain rule (4.51),

$$\Lambda_{10^n} = f'_0(x_{n+1})f'_0(x_n) \dots f'_0(x_2)f'_1(x_1) = \frac{1}{|\mathcal{M}_{n+1}|} \frac{1-a}{1-b}, \quad (24.5)$$

with $x_i \in \mathcal{M}_i$.

The properties of the map (24.2) are completely determined by the sequence $\{q_n\}$. By choosing $q_n = 2^{-n}$, for example, we recover the uniformly hyperbolic Bernoulli shift map (23.6). An intermittent map of the form (24.3) having the asymptotic behavior (24.1) can be constructed by choosing an algebraically decaying sequence $\{q_n\}$ behaving asymptotically like

$$q_n \sim \frac{1}{n^{1/s}}, \quad (24.6)$$

where s is the intermittency exponent in (24.1). Such a partition leads to intervals whose length decreases asymptotically like a power-law, that is,

$$|\mathcal{M}_n| \sim \frac{1}{n^{1+1/s}}. \quad (24.7)$$

As can be seen from (24.5), the Floquet multipliers of periodic orbit families approaching the marginal fixed point, such as the 10^l family increase in turn only algebraically with the cycle length.

It may now seem natural to construct an intermittent toy map in terms of a partition $|\mathcal{M}_n| = 1/n^{1+1/s}$, that is, a partition which follows (24.7) exactly. Such a choice leads to a dynamical zeta function which can be written in terms of so-called Jonquière functions (or polylogarithms) which arise naturally also in the context of the Farey map (20.31), and the anomalous diffusion of sect. 25.3. We will, however, not go along this route here; instead, we will engage in a bit of reverse engineering and construct a less obvious partition which will simplify the algebra considerably later without losing any of the key features typical for intermittent systems. We fix the intermittent toy map by specifying the intervals \mathcal{M}_n in terms of Gamma functions according to

remark 25.7

$$|\mathcal{M}_n| = C \frac{\Gamma(n + m - 1/s - 1)}{\Gamma(n + m)} \quad \text{for } n \geq 2, \quad (24.8)$$

where $m = [1/s]$ denotes the integer part of $1/s$ and C is a normalization constant fixed by the condition $\sum_{n=2}^{\infty} |\mathcal{M}_n| = q_1 = a$, that is,

$$C = a \left[\sum_{n=m+1}^{\infty} \frac{\Gamma(n - 1/s)}{\Gamma(n + 1)} \right]^{-1}. \quad (24.9)$$

Using Stirling's formula for the Gamma function

$$\Gamma(z) \sim e^{-z} z^{z-1/2} \sqrt{2\pi} (1 + 1/12z + \dots),$$

we verify that the intervals decay asymptotically like $n^{-(1+1/s)}$, as required by the condition (24.7).

Next, let us write down the dynamical zeta function of the toy map in terms of its periodic orbits, that is

$$1/\zeta(z) = \prod_p \left(1 - \frac{z^{n_p}}{|\Lambda_p|} \right)$$

One may be tempted to expand the dynamical zeta function in terms of the binary symbolic dynamics of the map; we saw, however, in sect. 20.5 that such cycle expansion converges extremely slowly. The shadowing mechanism between orbits and pseudo-orbits fails for orbits of the form 10^l with stabilities given by (24.5), due to the marginal stability of the fixed point $\bar{0}$. It is therefore advantageous to choose as the fundamental cycles the family of orbits with code 10^l or, equivalently, switch from the finite (binary) alphabet to an infinite alphabet given by

$$10^{n-1} \rightarrow n.$$

Due to the piecewise-linear form of the map which maps intervals \mathcal{M}_n exactly onto \mathcal{M}_{n-1} , all periodic orbits entering the left branch at least twice are canceled exactly by pseudo cycles, and the cycle expanded dynamical zeta function depends only on the fundamental series 1, 10, 100, ...:

$$\begin{aligned} 1/\zeta(z) &= \prod_{p \neq 0} \left(1 - \frac{z^{10^p}}{|\Lambda_p|}\right) = 1 - \sum_{n=1}^{\infty} \frac{z^n}{|\Lambda_{10^{n-1}}|} \\ &= 1 - (1-b)z - C \frac{1-b}{1-a} \sum_{n=2}^{\infty} \frac{\Gamma(n+m-1/s-1)}{\Gamma(n+m)} z^n. \end{aligned} \quad (24.10)$$

The fundamental term (20.7) consists here of an infinite sum over algebraically decaying cycle weights. The sum is divergent for $|z| \geq 1$. We will see that this behavior is due to a branch cut of $1/\zeta$ starting at $z = 1$. We need to find analytic continuations of sums over algebraically decreasing terms in (24.10). Note also that we omitted the fixed point $\bar{0}$ in the above Euler product; we will discuss this point as well as a proper derivation of the zeta function in more detail in sect. 24.2.4.

24.2.2 Branch cuts

Starting from the dynamical zeta function (24.10), we first have to worry about finding an analytical continuation of the sum for $|z| \geq 1$. We do, however, get this part for free here due to the particular choice of interval lengths made in (24.8). The sum over ratios of Gamma functions in (24.10) can be evaluated analytically by using the following identities valid for $1/s = \alpha > 0$ (the famed binomial theorem in disguise),

- α non-integer

$$(1-z)^\alpha = \sum_{n=0}^{\infty} \frac{\Gamma(n-\alpha)}{\Gamma(-\alpha)\Gamma(n+1)} z^n \quad (24.11)$$

- α integer

$$\begin{aligned} (1-z)^\alpha \log(1-z) &= \sum_{n=1}^{\alpha} (-1)^n c_n z^n \\ &+ (-1)^{\alpha+1} \alpha! \sum_{n=\alpha+1}^{\infty} \frac{(n-\alpha-1)!}{n!} z^n \end{aligned} \quad (24.12)$$

with

$$c_n = \binom{\alpha}{n} \sum_{k=0}^{n-1} \frac{1}{\alpha-k}.$$

In order to simplify the notation, we restrict the intermittency parameter to the range $1 \leq 1/s < 2$ with $[1/s] = m = 1$. All what follows can easily be generalized to arbitrary $s > 0$ using equations (24.11) and (24.12). The infinite sum in (24.10) can now be evaluated with the help of (24.11) or (24.12), that is,

$$\sum_{n=2}^{\infty} \frac{\Gamma(n - 1/s)}{\Gamma(n + 1)} z^n = \begin{cases} \Gamma(-\frac{1}{s}) \left[(1 - z)^{1/s} - 1 + \frac{1}{s}z \right] & \text{for } 1 < 1/s < 2; \\ (1 - z) \log(1 - z) + z & \text{for } s = 1. \end{cases}$$

The normalization constant C in (24.8) can be evaluated explicitly using (24.9) and the dynamical zeta function can be given in closed form. We obtain for $1 < 1/s < 2$

$$1/\zeta(z) = 1 - (1 - b)z - \frac{a}{1/s - 1} \frac{1 - b}{1 - a} \left((1 - z)^{1/s} - 1 + \frac{1}{s}z \right). \quad (24.13)$$

and for $s = 1$,

$$1/\zeta(z) = 1 - (1 - b)z - a \frac{1 - b}{1 - a} ((1 - z) \log(1 - z) + z). \quad (24.14)$$

It now becomes clear why the particular choice of intervals \mathcal{M}_h made in the last section is useful; by summing over the infinite family of periodic orbits $\mathcal{O}1$ explicitly, we have found the desired analytical continuation for the dynamical zeta function for $|z| \geq 1$. The function has a branch cut starting at the branch point $z = 1$ and running along the positive real axis. That means, the dynamical zeta function takes on different values when approaching the positive real axis for $\text{Re } z > 1$ from above and below. The dynamical zeta function for general $s > 0$ takes on the form

$$1/\zeta(z) = 1 - (1 - b)z - \frac{a}{g_s(1)} \frac{1 - b}{1 - a} \frac{1}{z^{m-1}} \left((1 - z)^{1/s} - g_s(z) \right) \quad (24.15)$$

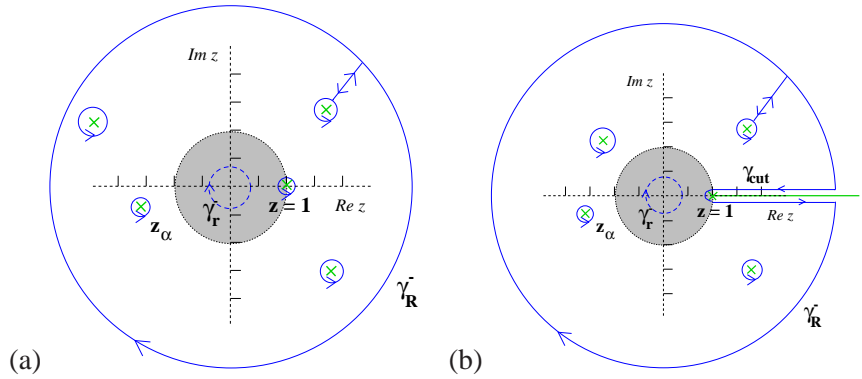
for non-integer s with $m = [1/s]$ and

$$1/\zeta(z) = 1 - (1 - b)z - \frac{a}{g_m(1)} \frac{1 - b}{1 - a} \frac{1}{z^{m-1}} \left((1 - z)^m \log(1 - z) - g_m(z) \right) \quad (24.16)$$

for $1/s = m$ integer and $g_s(z)$ are polynomials of order $m = [1/s]$ which can be deduced from (24.11) or (24.12). We thus find algebraic branch cuts for non integer intermittency exponents $1/s$ and logarithmic branch cuts for $1/s$ integer. We will see in sect. 24.3 that branch cuts of that form are generic for 1-dimensional intermittent maps.

Branch cuts are the all important new feature of dynamical zeta functions due to intermittency. So, how do we calculate averages or escape rates of the dynamics of the map from a dynamical zeta function with branch cuts? We take ‘a learning by doing’ approach and calculate the escape from our toy map for $a < b$.

Figure 24.5: The survival probability Γ_n calculated by contour integration; integrating (24.17) inside the domain of convergence $|z| < 1$ (shaded area) of $1/\zeta(z)$ in periodic orbit representation yields (18.26). A deformation of the contour γ_r^- (dashed line) to a larger circle γ_R^- gives contributions from the poles and zeros (x) of $1/\zeta(z)$ between the two circles. These are the only contributions for hyperbolic maps (a), for intermittent systems additional contributions arise, given by the contour γ_{cut} running along the branch cut (b).



24.2.3 Escape rate

Our starting point for the calculation of the fraction of survivors after n time steps, is the integral representation (19.19)

$$\Gamma_n = \frac{1}{2\pi i} \oint_{\gamma_r^-} z^{-n} \left(\frac{d}{dz} \log \zeta^{-1}(z) \right) dz, \tag{24.17}$$

where the contour encircles the origin in the clockwise direction. If the contour lies inside the unit circle $|z| = 1$, we may expand the logarithmic derivative of $\zeta^{-1}(z)$ as a convergent sum over all periodic orbits. Integrals and sums can be interchanged, the integrals can be solved term by term, and the formula (18.26) is recovered. For hyperbolic maps, cycle expansion methods or other techniques may provide an analytic extension of the dynamical zeta function beyond the leading zero; we may therefore deform the original contour into a larger circle with radius R which encircles both poles and zeros of $\zeta^{-1}(z)$, see figure 24.5 (a). Residue calculus turns this into a sum over the zeros z_α and poles z_β of the dynamical zeta function, that is

$$\Gamma_n = \sum_{|z_\alpha| < R}^{\text{zeros}} \frac{1}{z_\alpha^n} - \sum_{|z_\beta| < R}^{\text{poles}} \frac{1}{z_\beta^n} + \frac{1}{2\pi i} \oint_{\gamma_R^-} dz z^{-n} \frac{d}{dz} \log \zeta^{-1}, \tag{24.18}$$

where the last term gives a contribution from a large circle γ_R^- . We thus find exponential decay of Γ_n dominated by the leading zero or pole of $\zeta^{-1}(z)$.

Things change considerably in the intermittent case. The point $z = 1$ is a branch cut singularity and there exists no Taylor series expansion of ζ^{-1} around $z = 1$. Second, the path deformation that led us to (24.18) requires more care, as it must not cross the branch cut. When expanding the contour to large $|z|$ values, we have to deform it along the branch $\text{Re}(z) \geq 1, \text{Im}(z) = 0$ encircling the branch cut in anti-clockwise direction, see figure 24.5 (b). We will denote the detour around the cut as γ_{cut} . We may write symbolically

$$\oint_{\gamma_r} = \sum^{\text{zeros}} - \sum^{\text{poles}} + \oint_{\gamma_R} + \oint_{\gamma_{cut}}$$

where the sums include only the zeros and the poles in the area enclosed by the contours. The asymptotics is controlled by the zero, pole or cut closest to the origin.

Let us now go back to our intermittent toy map. The asymptotics of the survival probability of the map is here governed by the behavior of the integrand $\frac{d}{dz} \log \zeta^{-1}$ in (24.17) at the branch point $z = 1$. We restrict ourselves again to the case $1 < 1/s < 2$ first and write the dynamical zeta function (24.13) in the form

$$1/\zeta(z) = a_0 + a_1(1 - z) + b_0(1 - z)^{1/s} \equiv G(1 - z)$$

and

$$a_0 = \frac{b - a}{1 - a}, \quad b_0 = \frac{a}{1 - 1/s} \frac{1 - b}{1 - a}.$$

Setting $u = 1 - z$, we need to evaluate

$$\frac{1}{2\pi i} \oint_{\gamma_{cut}} (1 - u)^{-n} \frac{d}{du} \log G(u) du \quad (24.19)$$

where γ_{cut} goes around the cut (i.e., the negative u axis). Expanding the integrand $\frac{d}{du} \log G(u) = G'(u)/G(u)$ in powers of u and $u^{1/s}$ at $u = 0$, one obtains

$$\frac{d}{du} \log G(u) = \frac{a_1}{a_0} + \frac{1}{s} \frac{b_0}{a_0} u^{1/s-1} + O(u). \quad (24.20)$$

The integrals along the cut may be evaluated using the general formula

$$\frac{1}{2\pi i} \oint_{\gamma_{cut}} u^\alpha (1 - u)^{-n} du = \frac{\Gamma(n - \alpha - 1)}{\Gamma(n)\Gamma(-\alpha)} \sim \frac{1}{n^{\alpha+1}} (1 + O(1/n)) \quad (24.21)$$

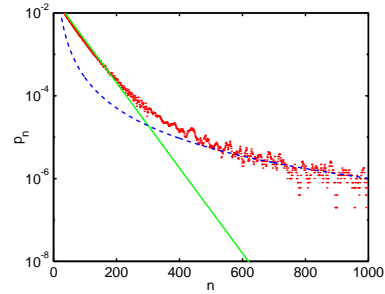
which can be obtained by deforming the contour back to a loop around the point $u = 1$, now in positive (anti-clockwise) direction. The contour integral then picks up the $(n-1)$ st term in the Taylor expansion of the function u^α at $u = 1$, cf. (24.11). For the continuous time case the corresponding formula is

$$\frac{1}{2\pi i} \oint_{\gamma_{cut}} z^\alpha e^{zt} dz = \frac{1}{\Gamma(-\alpha)} t^{\alpha+1}. \quad (24.22)$$

Plugging (24.20) into (24.19) and using (24.21) we get the asymptotic result

$$\Gamma_n \sim \frac{b_0}{a_0} \frac{1}{s} \frac{1}{\Gamma(1 - 1/s)} \frac{1}{n^{1/s}} = \frac{a}{s - 1} \frac{1 - b}{b - a} \frac{1}{\Gamma(1 - 1/s)} \frac{1}{n^{1/s}}. \quad (24.23)$$

Figure 24.6: The asymptotic escape from an intermittent repeller is a power law. Normally it is preceded by an exponential, which can be related to zeros close to the cut but beyond the branch point $z = 1$, as in figure 24.5 (b).



We see that, asymptotically, the escape from an intermittent repeller is described by power law decay rather than the exponential decay we are familiar with for hyperbolic maps; a numerical simulation of the power-law escape from an intermittent repeller is shown in figure 24.6.

For general non-integer $1/s > 0$, we write

$$1/\zeta(z) = A(u) + (u)^{1/s} B(u) \equiv G(u)$$

with $u = 1 - z$ and $A(u)$, $B(u)$ are functions analytic in a disc of radius 1 around $u = 0$. The leading terms in the Taylor series expansions of $A(u)$ and $B(u)$ are

$$a_0 = \frac{b - a}{1 - a}, \quad b_0 = \frac{a}{g_s(1)} \frac{1 - b}{1 - a},$$

see (24.15). Expanding $\frac{d}{du} \log G(u)$ around $u = 0$, one again obtains leading order contributions according to (24.20) and the general result follows immediately using (24.21), that is,

$$\Gamma_n \sim \frac{a}{sg_s(1)} \frac{1 - b}{b - a} \frac{1}{\Gamma(1 - 1/s)} \frac{1}{n^{1/s}}. \tag{24.24}$$

Applying the same arguments for integer intermittency exponents $1/s = m$, one obtains

$$\Gamma_n \sim (-1)^{m+1} \frac{a}{sg_m(1)} \frac{1 - b}{b - a} \frac{m!}{n^m}. \tag{24.25}$$

So far, we have considered the survival probability for a repeller, that is we assumed $a < b$. The formulas (24.24) and (24.25) do obviously not apply for the case $a = b$, that is, for the bounded map. The coefficient $a_0 = (b - a)/(1 - a)$ in the series representation of $G(u)$ is zero, and the expansion of the logarithmic derivative of $G(u)$ (24.20) is no longer valid. We get instead

$$\frac{d}{du} \log G(u) = \begin{cases} \frac{1}{u} \left(1 + O(u^{1/s-1}) \right) & s < 1 \\ \frac{1}{u} \left(\frac{1}{s} + O(u^{1-1/s}) \right) & s > 1 \end{cases},$$

assuming non-integer $1/s$ for convenience. One obtains for the survival probability.

$$\Gamma_n \sim \begin{cases} 1 + O(n^{1-1/s}) & s < 1 \\ 1/s + O(n^{1/s-1}) & s > 1 \end{cases} .$$

For $s > 1$, this is what we expect. There is no escape, so the survival probability is equal to 1, which we get as an asymptotic result here. The result for $s > 1$ is somewhat more worrying. It says that Γ_n defined as sum over the instabilities of the periodic orbits as in (22.12) does not tend to unity for large n . However, the case $s > 1$ is in many senses anomalous. For instance, the invariant density cannot be normalized. It is therefore not reasonable to expect that periodic orbit theories will work without complications.

24.2.4 Why does it work (anyway)?

Due to the piecewise linear nature of the map constructed in the previous section, we had the nice property that interval lengths did exactly coincide with the inverse of the stability of periodic orbits of the system, that is

$$|\mathcal{M}_n| = 1/|\Lambda_{10}|^{n-1} .$$

There is thus no problem in replacing the survival probability Γ_n given by (1.2), (22.2), that is the fraction of state space \mathcal{M} surviving n iterations of the map,

$$\Gamma_n = \frac{1}{|\mathcal{M}|} \sum_i^{(n)} |\mathcal{M}_i| .$$

by a sum over periodic orbits of the form (18.26). The only orbit to worry about is the marginal fixed point $\bar{0}$ itself which we excluded from the zeta function (24.10).

For smooth intermittent maps, things are less clear and the fact that we had to prune the marginal fixed point is a warning sign that interval estimates by periodic orbit stabilities might go horribly wrong. The derivation of the survival probability in terms of cycle stabilities in chapter 22 did indeed rely heavily on a hyperbolicity assumption which is clearly not fulfilled for intermittent maps. We therefore have to carefully reconsider this derivation in order to show that periodic orbit formulas are actually valid for intermittent systems in the first place.

We will for simplicity consider maps, which have a finite number of say s branches defined on intervals \mathcal{M}_s and we assume that the map maps each interval \mathcal{M}_s onto \mathcal{M} , that is $f(\mathcal{M}_s) = \mathcal{M}$. This ensures the existence of a complete symbolic dynamics - just to make things easy (see figure 24.2).

The generating partition is composed of the domains \mathcal{M}_i . The n th level partition $\mathcal{C}^{(n)} = \{\mathcal{M}_i\}$ can be constructed iteratively. Here i 's are words $i = s_2 s_2 \dots s_n$ of length n , and the intervals \mathcal{M}_i are constructed recursively

$$\mathcal{M}_{sj} = f_s^{-1}(\mathcal{M}_j), \tag{24.26}$$

where sj is the concatenation of letter s with word j of length $n_j < n$.

In what follows we will concentrate on the survival probability Γ_n , postponing other quantities of interest, such as averages, to later considerations. In establishing the equivalence of the survival probability and the periodic orbit formula for the escape rate for hyperbolic systems we have assumed that the map is expanding, with a minimal expansion rate $|f'(x)| \geq \Lambda_{\min} > 1$. This enabled us to bound the size of every survivor strip \mathcal{M}_i by (22.6), the stability Λ_i of the periodic orbit i within the \mathcal{M}_i , and bound the survival probability by the periodic orbit sum (22.7).

The bound (22.6)

$$C_1 \frac{1}{|\Lambda_i|} < \frac{|\mathcal{M}_i|}{|\mathcal{M}|} < C_2 \frac{1}{|\Lambda_i|}$$

relies on hyperbolicity, and is thus indeed violated for intermittent systems. The problem is that now there is no lower bound on the expansion rate, the minimal expansion rate is $\Lambda_{\min} = 1$. The survivor strip \mathcal{M}_{0^n} which includes the marginal fixed point is thus completely overestimated by $1/|\Lambda_{0^n}| = 1$ which is constant for all n .

exercise 19.7

However, bounding survival probability strip by strip is not what is required for establishing the bound (22.7). For intermittent systems a somewhat weaker bound can be established, saying that the average size of intervals *along a periodic orbit* can be bounded close to the stability of the periodic orbit for all but the interval \mathcal{M}_{0^n} . The weaker bound applies to averaging over each prime cycle p separately

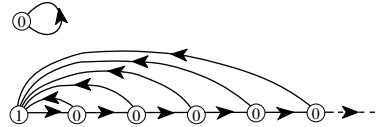
$$C_1 \frac{1}{|\Lambda_p|} < \frac{1}{n_p} \sum_{i \in p} \frac{|\mathcal{M}_i|}{|\mathcal{M}|} < C_2 \frac{1}{|\Lambda_p|}, \tag{24.27}$$

where the word i represents a code of the periodic orbit p and all its cyclic permutations. It can be shown that one can find positive constants C_1, C_2 independent of p . Summing over all periodic orbits leads then again to (22.7).

To study averages of multiplicative weights we follow sect. 17.1 and introduce a state space observable $a(x)$ and the integrated quantity

$$A^n(x) = \sum_{k=0}^{n-1} a(f^k(x)).$$

Figure 24.7: Transition graph corresponding to the alphabet $\{0^{k-1}1; \bar{0}, k \geq 1\}$



This leads us to introduce the generating function (17.10)

$$\langle e^{\beta A^n(x)} \rangle,$$

where $\langle . \rangle$ denote some averaging over the distribution of initial points, which we choose to be uniform (rather than the *a priori* unknown invariant density). Again, all we have to show is, that constants C_1, C_2 exist, such that

$$C_1 \frac{e^{\beta A_p}}{|\Lambda_p|} < \frac{1}{n_p} \sum_{i \in p} \frac{1}{|\mathcal{M}|} \int_{\mathcal{M}_Q} e^{\beta A^n(x)} dx < C_2 \frac{e^{\beta A_p}}{|\Lambda_p|}, \tag{24.28}$$

is valid for all p . After performing the above average one gets

$$C_1 \Gamma_n(\beta) < \frac{1}{|\mathcal{M}|} \int_{\mathcal{M}} e^{\beta A(x,n)} dx < C_2 \Gamma_n(\beta), \tag{24.29}$$

with

$$\Gamma_n(\beta) = \sum_p^n \frac{e^{\beta A_p}}{|\Lambda_p|}. \tag{24.30}$$

and a dynamical zeta function can be derived. In the intermittent case one can expect that the bound (24.28) holds using an averaging argument similar to the one discussed in (24.27). This justifies the use of dynamical zeta functions for intermittent systems.

One lesson we should have learned so far is that the natural alphabet to use is not $\{0, 1\}$ but rather the infinite alphabet $\{0^{k-1}1; \bar{0}; k \geq 1\}$. The symbol $\bar{0}$ occurs unaccompanied by any 1's only in the $\bar{0}$ marginal fixed point which is disconnected from the rest of the transition graph, see figure 24.7.

chapter 12

What happens if we remove a single prime cycle from a dynamical zeta function? In the hyperbolic case such a removal introduces a pole in the $1/\zeta$ and slows down the convergence of cycle expansions. The heuristic interpretation of such a pole is that for a subshift of finite type removal of a single prime cycle leads to unbalancing of cancellations within the infinity of shadowing pairs. Nevertheless, removal of a single prime cycle is an exponentially small perturbation of the trace sums, and the asymptotics of the associated trace formulas is unaffected.

chapter 23

In the intermittent case, the fixed point $\bar{0}$ does not provide any shadowing, and a statement such as

$$\Lambda_{1.0^{k+1}} \approx \Lambda_{1.0^k} \Lambda_0,$$

is meaningless. It seems therefore sensible to take out the factor $(1 - \delta) = 1 - z$ from the product representation of the dynamical zeta function (19.15), that is, to consider a pruned dynamical zeta function $1/\zeta_{inter}(z)$ defined by

$$1/\zeta(z) = (1 - z)1/\zeta_{inter}(z).$$

We saw in the last sections, that the zeta function $1/\zeta_{inter}(z)$ has all the nice properties we know from the hyperbolic case, that is, we can find a cycle expansion with - in the toy model case - vanishing curvature contributions and we can calculate dynamical properties like escape after having understood, how to handle the branch cut. But you might still be worried about leaving out the extra factor $1 - z$ all together. It turns out, that this is not only a matter of convenience, omitting the marginal $\bar{0}$ cycle is a dire necessity. The cycle weight $\Lambda_0^n = 1$ overestimates the corresponding interval length of \mathcal{M}_0^n in the partition of the phase space \mathcal{M} by an increasing amount thus leading to wrong results when calculating escape. By leaving out the $\bar{0}$ cycle (and thus also the \mathcal{M}_0^n contribution), we are guaranteed to get at least the right asymptotical behavior.

Note also, that if we are working with the spectral determinant (19.3), given in product form as

$$\det(1 - z\mathcal{L}) = \prod_p \prod_{m=0}^{\infty} \left(1 - \frac{z^{n_p}}{|\Lambda_p| \Lambda_p^m} \right),$$

for intermittent maps the marginal stable cycle has to be excluded. It introduces an (unphysical) essential singularity at $z = 1$ due the presence of a factor $(1 - z)^\infty$ stemming from the $\bar{0}$ cycle.

24.3 Intermittency for cyclists

Admittedly, the toy map is what is says - a toy model. The piece wise linearity of the map led to exact cancellations of the curvature contributions leaving only the fundamental terms. There are still infinitely many orbits included in the fundamental term, but the cycle weights were chosen in such a way that the zeta function could be written in closed form. For a smooth intermittent map this all will not be the case in general; still, we will argue that we have already seen almost all the fundamentally new features due to intermittency. What remains are technicalities - not necessarily easy to handle, but nothing very surprise any more.

In the following we will sketch, how to make cycle expansion techniques work for general 1-dimensional maps with a single isolated marginal fixed point. To keep the notation simple, we will consider two-branch maps with a complete binary symbolic dynamics as for example the Farey map, figure 24.3, or the repeller depicted in figure 24.2. We again assume that the behavior near the fixed point is given by (24.1). This implies that the stability of a family of periodic orbits approaching the marginally stable orbit, as for example the family 10^n , will increase only algebraically, that is we find again for large n

$$\frac{1}{\Lambda_{10^n}} \sim \frac{1}{n^{1+1/s}},$$

where s denotes the intermittency exponent.

When considering zeta functions or trace formulas, we again have to take out the marginal orbit $\bar{0}$; periodic orbit contributions of the form t_{n1} are now unbalanced and we arrive at a cycle expansion in terms of infinitely many fundamental terms as for our toy map. This corresponds to moving from our binary symbolic dynamics to an infinite symbolic dynamics by making the identification

$$10^{n-1} \rightarrow n; \quad 10^{n-1}10^{m-1} \rightarrow nm; \quad 10^{n-1}10^{m-1}10^{k-1} \rightarrow nmk; \dots$$

see also table 24.1. The topological length of the orbit is thus no longer determined by the iterations of our two-branch map, but by the number of times the cycle goes from the right to the left branch. Equivalently, one may define a new map, for which all the iterations on the left branch are done in one step. Such a map is called an *induced map* and the topological length of orbits in the infinite alphabet corresponds to the iterations of this induced map.

exercise 12.1

For generic intermittent maps, curvature contributions in the cycle expanded zeta function will not vanish exactly. The most natural way to organize the cycle expansion is to collect orbits and pseudo orbits of the same topological length with respect to the infinite alphabet. Denoting cycle weights in the new alphabet as $t_{nm\dots} = t_{10^{n-1}10^{m-1}\dots}$, one obtains

$$\begin{aligned} \zeta^{-1} &= \prod_{p \neq 0} (1 - t_p) = 1 - \sum_{n=1}^{\infty} c_n e & (24.31) \\ &= 1 - \sum_{n=1}^{\infty} t_n - \sum_{m=1}^{\infty} \sum_{n=1}^{\infty} \frac{1}{2} (t_{mn} - t_m t_n) \\ &\quad - \sum_{k=1}^{\infty} \sum_{m=1}^{\infty} \sum_{n=1}^{\infty} \left(\frac{1}{3} t_{kmn} - \frac{1}{2} t_{km} t_n + \frac{1}{6} t_k t_m t_n \right) - \sum_{l=1}^{\infty} \sum_{k=1}^{\infty} \sum_{m=1}^{\infty} \sum_{n=1}^{\infty} \dots \end{aligned}$$

The first sum is the fundamental term, which we have already seen in the toy model, (24.10). The curvature terms c_n in the expansion are now e -fold infinite sums where the prefactors take care of double counting of prime periodic orbits.

Table 24.1: Infinite alphabet versus the original binary alphabet for the shortest periodic orbit families. Repetitions of prime cycles ($11 = 1^2, 0101 = 01^2, \dots$) and their cyclic repeats ($110 = 101, 1110 = 1101, \dots$) are accounted for by cancelations and combination factors in the cycle expansion (24.31).

∞ – alphabet		binary alphabet				
		$n = 1$	$n = 2$	$n = 3$	$n = 4$	$n = 5$
1-cycles	n	1	10	100	1000	10000
2-cycles	mn					
	$1n$	11	110	1100	11000	110000
	$2n$	101	0101	10100	101000	1010000
	$3n$	1001	10010	100100	1001000	10010000
	$4n$	10001	100010	1000100	10001000	100010000
3-cycles	kmn					
	$11n$	111	1110	11100	111000	1110000
	$12n$	1101	11010	110100	1101000	11010000
	$13n$	11001	110010	1100100	11001000	110010000
	$21n$	1011	10110	101100	1011000	10110000
	$22n$	10101	101010	1010100	10101000	101010000
	$23n$	101001	1010010	10100100	101001000	1010010000
	$31n$	10011	100110	1001100	10011000	100110000
	$32n$	100101	1001010	10010100	100101000	1001010000
	$33n$	1001001	10010010	100100100	1001001000	10010010000

Let us consider the fundamental term first. For generic intermittent maps, we can not expect to obtain an analytic expression for the infinite sum of the form

$$f(z) = \sum_{n=0}^{\infty} h_n z^n. \tag{24.32}$$

with algebraically decreasing coefficients

$$h_n \sim \frac{1}{n^\alpha} \text{ with } \alpha > 0$$

To evaluate the sum, we face the same problem as for our toy map: the power series diverges for $z > 1$, that is, exactly in the ‘interesting’ region where poles, zeros or branch cuts of the zeta function are to be expected. By carefully subtracting the asymptotic behavior with the help of (24.11) or (24.12), one can in general construct an analytic continuation of $f(z)$ around $z = 1$ of the form

$$\begin{aligned} f(z) &\sim A(z) + (1 - z)^{\alpha-1} B(z) && \alpha \notin \mathbb{N} \\ f(z) &\sim A(z) + (1 - z)^{\alpha-1} \ln(1 - z) && \alpha \in \mathbb{N}, \end{aligned} \tag{24.33}$$

where $A(z)$ and $B(z)$ are functions analytic in a disc around $z = 1$. We thus again find that the zeta function (24.31) has a branch cut along the real axis $\text{Re } z \geq 1$.

From here on we can switch to auto-pilot and derive algebraic escape, decay of correlation and all the rest. We find in particular that the asymptotic behavior derived in (24.24) and (24.25) is a general result, that is, the survival probability is given asymptotically by

$$\Gamma_n \sim C \frac{1}{n^{1/s}} \quad (24.34)$$

for all 1-dimensional maps of the form (24.1). We have to work a bit harder if we want more detailed information like the prefactor C , exponential precursors given by zeros or poles of the dynamical zeta function or higher order corrections. This information is buried in the functions $A(z)$ and $B(z)$ or more generally in the analytically continued zeta function. To get this analytic continuation, one may follow either of the two different strategies which we will sketch next.

24.3.1 Resummation

One way to get information about the zeta function near the branch cut is to derive the leading coefficients in the Taylor series of the functions $A(z)$ and $B(z)$ in (24.33) at $z = 1$. This can be done in principle, if the coefficients h_j in sums like (24.32) are known (as for our toy model). One then considers a resummation of the form

$$\sum_{j=0}^{\infty} h_j z^j = \sum_{j=0}^{\infty} a_j (1-z)^j + (1-z)^{\alpha-1} \sum_{j=0}^{\infty} b_j (1-z)^j, \quad (24.35)$$

and the coefficients a_j and b_j are obtained in terms of the h_j 's by expanding $(1-z)^j$ and $(1-z)^{j+\alpha-1}$ on the right hand side around $z = 0$ using (24.11) and equating the coefficients.

In practical calculations one often has only a finite number of coefficients h_j , $0 \leq j \leq N$, which may have been obtained by finding periodic orbits and their stabilities numerically. One can still design a resummation scheme for the computation of the coefficients a_j and b_j in (24.35). We replace the infinite sums in (24.35) by finite sums of increasing degrees n_a and n_b , and require that

$$\sum_{i=0}^{n_a} a_i (1-z)^i + (1-z)^{\alpha-1} \sum_{i=0}^{n_b} b_i (1-z)^i = \sum_{i=0}^N h_i z^i + O(z^{N+1}). \quad (24.36)$$

One proceeds again by expanding the right hand side around $z = 0$, skipping all powers z^{N+1} and higher, and then equating coefficients. It is natural to require that $|n_b + \alpha - 1 - n_a| < 1$, so that the maximal powers of the two sums in (24.36) are adjacent. If one chooses $n_a + n_b + 2 = N + 1$, then, for each cutoff length N , the integers n_a and n_b are uniquely determined from a linear system of equations. The

price we pay is that the so obtained coefficients depend on the cutoff N . One can now study convergence of the coefficients a_j , and b_j , with respect to increasing values of N , or various quantities derived from a_j and b_j . Note that the leading coefficients a_0 and b_0 determine the prefactor C in (24.34), cf. (24.23). The resummed expression can also be used to compute zeros, inside or outside the radius of convergence of the cycle expansion $\sum h_j z^j$.

The scheme outlined in this section tacitly assumes that a representation of form (24.33) holds in a disc of radius 1 around $z = 1$. Convergence is improved further if additional information about the asymptotics of sums like (24.32) is used to improve the ansatz (24.35).

24.3.2 Analytical continuation by integral transformations

We will now introduce a method which provides an analytic continuation of sums of the form (24.32) without explicitly relying on an ansatz (24.35). The main idea is to rewrite the sum (24.32) as a sum over integrals with the help of the Poisson summation formula and find an analytic continuation of each integral by contour deformation. In order to do so, we need to know the n dependence of the coefficients $h_n \equiv h(n)$ explicitly for all n . If the coefficients are not known analytically, one may proceed by approximating the large n behavior in the form

$$h(n) = n^{-\alpha}(C_1 + C_2 n^{-1} + \dots), \quad n \neq 0,$$

and determine the constants C_i numerically from periodic orbit data. By using the Poisson resummation identity

$$\sum_{n=-\infty}^{\infty} \delta(x - n) = \sum_{m=-\infty}^{\infty} \exp(2\pi i m x), \quad (24.37)$$

we may write the sum as (24.32)

$$f(z) = \frac{1}{2}h(0) + \sum_{m=-\infty}^{\infty} \int_0^{\infty} dx e^{2\pi i m x} h(x) z^x. \quad (24.38)$$

The continuous variable x corresponds to the discrete summation index n and it is convenient to write $z = r \exp(i\sigma)$ from now on. The integrals are still not convergent for $r > 0$, but an analytical continuation can be found by considering the contour integral, where the contour goes out along the real axis, makes a quarter circle to either the positive or negative imaginary axis and goes back to zero. By letting the radius of the circle go to infinity, we essentially rotate the line of integration from the real onto the imaginary axis. For the $m = 0$ term in (24.38), we transform $x \rightarrow ix$ and the integral takes on the form

$$\int_0^{\infty} dx h(x) r^x e^{ix\sigma} = i \int_0^{\infty} dx h(ix) r^{ix} e^{-x\sigma}.$$

The integrand is now exponentially decreasing for all $r > 0$ and $\sigma \neq 0$ or 2π . The last condition reminds us again of the existence of a branch cut at $\text{Re } z \geq 1$. By the same technique, we find the analytic continuation for all the other integrals in (24.38). The real axis is then rotated according to $x \rightarrow \text{sign}(m)ix$ where $\text{sign}(m)$ refers to the sign of m .

$$\int_0^\infty dx e^{\pm 2\pi i |m|x} h(x) r^x e^{ix\sigma} = \pm i \int_0^\infty dx h(\pm ix) r^{\pm ix} e^{-x(2\pi |m| \pm \sigma)}.$$

Changing summation and integration, we can carry out the sum over $|m|$ explicitly and one finally obtains the compact expression

$$\begin{aligned} f(z) &= \frac{1}{2}h(0) + i \int_0^\infty dx h(ix) r^{ix} e^{-x\sigma} \\ &+ i \int_0^\infty dx \frac{e^{-2\pi x}}{1 - e^{-2\pi x}} [h(ix)r^{ix}e^{-x\sigma} - h(-ix)r^{-ix}e^{x\sigma}]. \end{aligned} \quad (24.39)$$

The transformation from the original sum to the two integrals in (24.39) is exact for $r \leq 1$, and provides an analytic continuation for $r > 0$. The expression (24.39) is especially useful for an efficient numerical calculations of a dynamical zeta function for $|z| > 1$, which is essential when searching for its zeros and poles.

24.3.3 Curvature contributions

So far, we have discussed only the fundamental term $\sum_{n=1}^\infty t_n$ in (24.31), and showed how to deal with such power series with algebraically decreasing coefficients. The fundamental term determines the main structure of the zeta function in terms of the leading order branch cut. Corrections to both the zeros and poles of the dynamical zeta function as well as the leading and subleading order terms in expansions like (24.33) are contained in the curvature terms in (24.31). The first curvature correction is the 2-cycle sum

$$\sum_{m=1}^\infty \sum_{n=1}^\infty \frac{1}{2}(t_{mn} - t_m t_n),$$

with algebraically decaying coefficients which again diverge for $|z| > 1$. The analytically continued curvature terms have as usual branch cuts along the positive real z axis. Our ability to calculate the higher order curvature terms depends on how much we know about the cycle weights t_{mn} . The form of the cycle stability (24.5) suggests that t_{mn} decrease asymptotically as

$$t_{mn} \sim \frac{1}{(nm)^{1+1/s}} \quad (24.40)$$

for 2-cycles, and in general for n -cycles as

$$t_{m_1 m_2 \dots m_n} \sim \frac{1}{(m_1 m_2 \dots m_n)^{1+1/s}}.$$

If we happen to know the cycle weights $t_{m_1 m_2 \dots m_n}$ analytically, we may proceed as in sect. 24.3.2, transform the multiple sums into multiple integrals and rotate the integration contours.

We have reached the edge of what has been accomplished so far in computing and what is worth the dynamical zeta functions from periodic orbit data. In the next section, we describe a probabilistic method applicable to intermittent maps which does not rely on periodic orbits.

24.4 BER zeta functions



So far we have focused on 1-d models as the simplest setting in which to investigate dynamical implications of marginal fixed points. We now take an altogether different track and describe how probabilistic methods may be employed in order to write down approximate dynamical zeta functions for intermittent systems.

We will discuss the method in a very general setting, for a flow in arbitrary dimension. The key idea is to introduce a surface of section \mathcal{P} such that all trajectories traversing this section will have spent some time both near the marginal stable fixed point and in the chaotic phase. An important quantity in what follows is (3.5), the *first return time* $\tau(x)$, or the time of flight of a trajectory starting in x to the next return to the surface of section \mathcal{P} . The period of a periodic orbit p intersecting the \mathcal{P} section n_p times is

$$T_p = \sum_{k=0}^{n_p-1} \tau(f^k(x_p)),$$

where $f(x)$ is the Poincaré map, and $x_p \in \mathcal{P}$ is a periodic point. The dynamical zeta function (19.15)

$$1/\zeta(z, s, \beta) = \prod_p \left(1 - \frac{z^{n_p} e^{\beta A_p - s T_p}}{|\Lambda_p|} \right), \quad A_p = \sum_{k=0}^{n_p-1} a(f^k(x_p)), \quad (24.41)$$

chapter 17

associated with the observable $a(x)$ captures the dynamics of both the flow *and* the Poincaré map. The dynamical zeta function for the flow is obtained as $1/\zeta(s, \beta) = 1/\zeta(1, s, \beta)$, and the dynamical zeta function for the discrete time Poincaré map is $1/\zeta(z, \beta) = 1/\zeta(z, 0, \beta)$.

Our basic assumption will be *probabilistic*. We assume that the chaotic interludes render the consecutive *return (or recurrence) times* $T(x_i), T(x_{i+1})$ and observables $a(x_i), a(x_{i+1})$ effectively uncorrelated. Consider the quantity $e^{\beta A(x_0,n) - sT(x_0,n)}$ averaged over the surface of section \mathcal{P} . With the above probabilistic assumption the large n behavior is

$$\langle e^{\beta A(x_0,n) - sT(x_0,n)} \rangle_{\mathcal{P}} \sim \left(\int_{\mathcal{P}} e^{\beta a(x) - s\tau} \rho(x) dx \right)^n,$$

where $\rho(x)$ is the invariant density of the Poincaré map. This type of behavior is equivalent to there being only one zero $\bar{z}_0(s, \beta) = \int_{\mathcal{P}} e^{\beta a(x) - s\tau(x)} \rho(x) dx$ of $1/\zeta(z, s, \beta)$ in the z - β plane. In the language of Ruelle-Pollicott resonances this means that there is an infinite gap to the first resonance. This in turn implies that $1/\zeta(z, s, \beta)$ may be written as

remark 17.1

$$1/\zeta(z, s, \beta) = z - \int_{\mathcal{P}} e^{\beta a(x) - s\tau(x)} \rho(x) dx, \quad (24.42)$$

where we have neglected a possible analytic and non-zero prefactor. The dynamical zeta function of the flow is now

$$1/\zeta(s, \beta) = 1/\zeta(1, s, \beta) = 1 - \int_{\mathcal{P}} e^{\beta a(x)} \rho(x) e^{-s\tau(x)} dx. \quad (24.43)$$

Normally, the best one can hope for is a finite gap to the leading resonance of the Poincaré map. with the above dynamical zeta function only approximately valid. As it is derived from an approximation due to Baladi, Eckmann, and Ruelle, we shall refer to it as the BER zeta function $1/\zeta_{\text{BER}}(s, \beta)$ in what follows.

A central role is played by the probability distribution of return times

$$\psi(\tau) = \int_{\mathcal{P}} \delta(\tau - \tau(x)) \rho(x) dx \quad (24.44)$$

exercise 25.6

The BER zeta function at $\beta = 0$ is then given in terms of the Laplace transform of this distribution

$$1/\zeta_{\text{BER}}(s) = 1 - \int_0^\infty \psi(\tau) e^{-s\tau} d\tau.$$

exercise 24.5

Example 24.1 Return times for the Bernoulli map. For the Bernoulli shift map (23.6)

$$x \mapsto f(x) = 2x \text{ mod } 1,$$

one easily derives the distribution of return times

$$\psi_n = \frac{1}{2^n} \quad n \geq 1.$$

The BER zeta function becomes (by the discrete Laplace transform (18.9))

$$\begin{aligned} 1/\zeta_{\text{BER}}(z) &= 1 - \sum_{n=1}^{\infty} \psi_n z^n = 1 - \sum_{n=1}^{\infty} \frac{z^n}{2^n} \\ &= \frac{1-z}{1-z/2} = \zeta^{-1}(z)/(1-z/\Lambda_0). \end{aligned} \quad (24.45)$$

Thanks to the uniformity of the piecewise linear map measure (17.19) the “approximate” zeta function is in this case the exact dynamical zeta function, with the periodic point $\bar{0}$ pruned.

Example 24.2 Return times for the model of sect. 24.2.1. For the toy model of sect. 24.2.1 one gets $\psi_1 = |\mathcal{M}_1|$, and $\psi_n = |\mathcal{M}_n|(1-b)/(1-a)$, for $n \geq 2$, leading to a BER zeta function

$$1/\zeta_{\text{BER}}(z) = 1 - z|\mathcal{M}_1| - \sum_{n=2}^{\infty} |\mathcal{M}_n|z^n,$$

which again coincides with the exact result, (24.10).

It may seem surprising that the BER approximation produces exact results in the two examples above. The reason for this peculiarity is that both these systems are piecewise linear and have complete Markov partitions. As long as the map is piecewise linear and complete, and the probabilistic approximation is exactly fulfilled, the cycle expansion curvature terms vanish. The BER zeta function and the fundamental part of a cycle expansion discussed in sect. 20.1.1 are indeed intricately related, but not identical in general. In particular, note that the BER zeta function obeys the flow conservation sum rule (22.11) by construction, whereas the fundamental part of a cycle expansion as a rule does not.

Résumé

The presence of marginally stable fixed points and cycles changes the analytic structure of dynamical zeta functions and the rules for constructing cycle expansions. The marginal orbits have to be omitted, and the cycle expansions now need to include families of infinitely many longer and longer unstable orbits which accumulate toward the marginally stable cycles. Correlations for such non-hyperbolic systems may decay algebraically with the decay rates controlled by the branch cuts of dynamical zeta functions. Compared to pure hyperbolic systems, the physical consequences are drastic: exponential decays are replaced by slow power-law decays, and transport properties, such as the diffusion may become anomalous.

Commentary

Remark 24.1 What about the evolution operator formalism? The main virtue of evolution operators was their semigroup property (17.25). This was natural for hyperbolic systems where instabilities grow exponentially, and evolution operators capture this behavior due to their multiplicative nature. Whether the evolution operator formalism is a good way to capture the slow, power law instabilities of intermittent dynamics is less clear. The approach taken here leads us to a formulation in terms of *dynamical zeta functions* rather than spectral determinants, circumventing evolution operators altogether. It is not known if the spectral determinants formulation would yield any benefits when applied to intermittent chaos. Some results on spectral determinants and intermittency can be found in [2]. A useful mathematical technique to deal with isolated marginally stable fixed point is that of *inducing*, that is, replacing the intermittent map by a completely hyperbolic map with infinite alphabet and redefining the discrete time; we have used this method implicitly by changing from a finite to an infinite alphabet. We refer to refs. [3, 20] for detailed discussions of this technique, as well as applications to 1-dimensional maps.

Remark 24.2 Intermittency. Intermittency was discovered by Manneville and Pomeau [1] in their study of the Lorenz system. They demonstrated that in neighborhood of parameter value $r_c = 166.07$ the mean duration of the periodic motion scales as $(r - r_c)^{1/2}$. In ref. [5] they explained this phenomenon in terms of a 1-dimensional map (such as (24.1)) near tangent bifurcation, and classified possible types of intermittency.

Piecewise linear models like the one considered here have been studied by Gaspard and Wang [6]. The escape problem has here been treated following ref. [7], resumptions following ref. [8]. The proof of the bound (24.27) can be found in P. Dahlqvist's notes on ChaosBook.org/PDahlqvistEscape.ps.gz.

Farey map (20.31) has been studied widely in the context of intermittent dynamics, for example in refs. [16, 17, 3, 18, 19, 15, 2]. The Fredholm determinant and the dynamical zeta functions for the Farey map (20.31) and the related Gauss shift map (16.46) have been studied by Mayer [16]. He relates the continued fraction transformation to the Riemann zeta function, and constructs a Hilbert space on which the evolution operator is self-adjoint, and its eigenvalues are exponentially spaced, just as for the dynamical zeta functions [24] for "Axiom A" hyperbolic systems.

Remark 24.3 Tauberian theorems. In this chapter we used Tauberian theorems for power series and Laplace transforms: Feller's monograph [9] is a highly recommended introduction to these methods.

Remark 24.4 Probabilistic methods, BER zeta functions. Probabilistic description of intermittent chaos was introduced by Geisel and Thomae [10]. The BER approximation studied here is inspired by Baladi, Eckmann and Ruelle [14], with further developments in refs. [13, 15].

Exercises

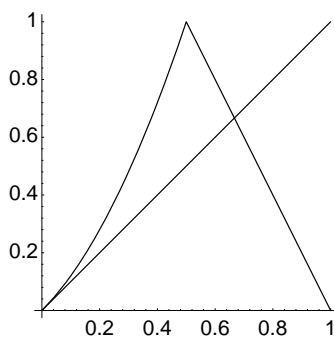
- 24.1. **Integral representation of Jonquière functions.** Check the integral representation

$$J(z, \alpha) = \frac{z}{\Gamma(\alpha)} \int_0^\infty d\xi \frac{\xi^{\alpha-1}}{e^\xi - z} \quad \text{for } \alpha > 0. \quad (24.46)$$

Note how the denominator is connected to Bose-Einstein distribution. Compute $J(x + i\epsilon) - J(x - i\epsilon)$ for a real $x > 1$.

- 24.2. **Power law correction to a power law.** Expand (24.20) further and derive the leading power law correction to (24.23).

- 24.3. **Power-law fall off.** In cycle expansions the stabilities of orbits do not always behave in a geometric fashion. Consider the map f



This map behaves as $f \rightarrow x$ as $x \rightarrow 0$. Define a symbolic dynamics for this map by assigning 0 to the points that land on the interval $[0, 1/2)$ and 1 to the points that land on $(1/2, 1]$. Show that the stability of orbits that spend a long time on the 0 side goes as n^2 . In particular, show that

$$\Lambda_{\underbrace{00\dots 0}_n} 1 \sim n^2$$

- 24.4. **Power law fall-off of Floquet multipliers in the stadium billiard**.** From the cycle expansions point of view, the most important consequence of the shear in \mathbf{J}^n for long sequences of rotation bounces n_k in (8.13) is that the Λ_n grows only as a power law in number of bounces:

$$\Lambda_n \propto n_k^2. \quad (24.47)$$

Check.

- 24.5. **Probabilistic zeta function for maps.** Derive the probabilistic zeta function for a map with recurrence distribution ψ_n .

- 24.6. **Accelerated diffusion.** Consider a map h , such that $\hat{h} = \hat{f}$, but now running branches are turned into standing branches and vice versa, so that 1, 2, 3, 4 are standing while 0 leads to both positive and negative jumps. Build the corresponding dynamical zeta function and show that

$$\sigma^{-2}(t) \sim \begin{cases} t & \text{for } \alpha > 2 \\ t \ln t & \text{for } \alpha = 2 \\ t^{3-\alpha} & \text{for } \alpha \in (1, 2) \\ t^2 / \ln t & \text{for } \alpha = 1 \\ t^2 & \text{for } \alpha \in (0, 1) \end{cases}$$

- 24.7. **Anomalous diffusion (hyperbolic maps).** Anomalous diffusive properties are associated to deviations from linearity of the variance of the phase variable we are looking at: this means the diffusion constant (17.13) either vanishes or diverges. We briefly illustrate in this exercise how the local local properties of a map are crucial to account for anomalous behavior even for hyperbolic systems.

Consider a class of piecewise linear maps, relevant to the problem of the onset of diffusion, defined by

$$f_\epsilon(x) = \begin{cases} \Lambda x & \text{for } x \in [0, x_1^+] \\ a - \Lambda_{\epsilon,\gamma}|x - x^+| & \text{for } x \in [x_1^+, x_2^+] \\ 1 - \Lambda'(x - x_2^+) & \text{for } x \in [x_2^+, x_1^-] \\ 1 - a + \Lambda_{\epsilon,\gamma}|x - x^-| & \text{for } x \in [x_1^-, x_2^-] \\ 1 + \Lambda(x - 1) & \text{for } x \in [x_2^-, 1] \end{cases} \quad (24.)$$

where $\Lambda = (1/3 - \epsilon^{1/\gamma})^{-1}$, $\Lambda' = (1/3 - 2\epsilon^{1/\gamma})^{-1}$, $\Lambda_{\epsilon,\gamma} = \epsilon^{1-1/\gamma}$, $a = 1 + \epsilon$, $x^+ = 1/3$, $x_1^+ = x^+ - \epsilon^{1/\gamma}$, $x_2^+ = x^+ + \epsilon^{1/\gamma}$, and the usual symmetry properties (25.11) are satisfied.

Thus this class of maps is characterized by two escaping windows (through which the diffusion process may take place) of size $2\epsilon^{1/\gamma}$: the exponent γ mimicks the order of the maximum for a continuous map, while piecewise linearity, besides making curvatures vanish and leading to finite cycle expansions, prevents the appearance of stable cycles. The symbolic dynamics is easily described once we consider a sequence of parameter values $\{\epsilon_m\}$, where $\epsilon_m = \Lambda^{-(m+1)}$: we then partition the unit interval through the sequence of points $0, x_1^+, x^+, x_2^+, x_1^-, x^-, x_2^-, 1$ and label the corresponding sub-intervals 1, $s_a, s_b, 2, d_b, d_a, 3$: symbolic dynamics is described by an unrestricted grammar over the following set of symbols

$$\{1, 2, 3, s_\# \cdot 1^i, d_\# \cdot 3^k\} \quad \# = a, b \quad i, k = m, m + 1, m$$

This leads to the following dynamical zeta function:

$$\zeta_0^{-1}(z, \alpha) = 1 - \frac{2z}{\Lambda} - \frac{z}{\Lambda'} - 4 \cosh(\alpha) \epsilon_m^{1/\gamma-1} \frac{z^{m+1}}{\Lambda^m} \left(1 - \frac{z}{\Lambda}\right)^{-1}$$

from which, by (25.8) we get

$$D = \frac{2\epsilon_m^{1/\gamma-1} \Lambda^{-m} (1 - 1/\Lambda)^{-1}}{1 - \frac{2}{\Lambda} - \frac{1}{\Lambda'} - 4\epsilon_m^{1/\gamma-1} \left(\frac{m+1}{\Lambda^m(1-1/\Lambda)} + \frac{1}{\Lambda^{m+1}(1-1/\Lambda)^2} \right)} \quad (24.49)$$

The main interest in this expression is that it allows exploring how D vanishes in the $\epsilon \mapsto 0$ ($m \mapsto \infty$) limit: as

a matter of fact, from (24.49) we get the asymptotic behavior $D \sim \epsilon^{1/\gamma}$, which shows how the onset of diffusion is governed by the order of the map at its maximum.

Remark 24.5 Onset of diffusion for continuous maps.

The zoology of behavior for continuous maps at the onset of diffusion is described in refs. [15, 16, 25]: our treatment for piecewise linear maps was introduced in ref. [26].

References

- [24.1] P. Manneville and Y. Pomeau, *Phys. Lett.* **75A**, 1 (1979).
- [24.2] H.H. Rugh, *Inv. Math.* **135**, 1 (1999).
- [24.3] T. Prellberg, *Maps of the interval with indifferent fixed points: thermodynamic formalism and phase transitions*, Ph.D. Thesis, Virginia Polytechnic Institute (1991); T. Prellberg and J. Slawny, "Maps of intervals with indifferent fixed points - thermodynamic formalism and phase transitions," *J. Stat. Phys.* **66**, 503 (1992).
- [24.4] T. Prellberg, *Towards a complete determination of the spectrum of a transfer operator associated with intermittency*, *J. Phys. A* **36**, 2455 (2003).
- [24.5] Y. Pomeau and P. Manneville, *Commun. Math. Phys.* **74**, 189 (1980).
- [24.6] P. Gaspard and X.-J. Wang, *Proc. Natl. Acad. Sci. U.S.A.* **85**, 4591 (1988); X.-J. Wang, *Phys. Rev.* **A40**, 6647 (1989); X.-J. Wang, *Phys. Rev.* **A39**, 3214 (1989).
- [24.7] P. Dahlqvist, *Phys. Rev. E* **60**, 6639 (1999).
- [24.8] P. Dahlqvist, *J. Phys. A* **30**, L351 (1997).
- [24.9] W. Feller, *An introduction to probability theory and applications, Vol. II* (Wiley, New York 1966).
- [24.10] T. Geisel and S. Thomaе, *Phys. Rev. Lett.* **52**, 1936 (1984).
- [24.11] T. Geisel, J. Nierwetberg and A. Zacherl, *Phys. Rev. Lett.* **54**, 616 (1985).
- [24.12] R. Artuso, G. Casati and R. Lombardi, *Phys. Rev. Lett.* **71**, 62 (1993).
- [24.13] P. Dahlqvist, *Nonlinearity* **8**, 11 (1995).
- [24.14] V. Baladi, J.-P. Eckmann and D. Ruelle, *Nonlinearity* **2**, 119 (1989).
- [24.15] P. Dahlqvist, *J. Phys. A* **27**, 763 (1994).
- [24.16] D.H. Mayer, *Bull. Soc. Math. France* **104**, 195 (1976).

- [24.17] D. Mayer and G. Roepstorff, *J. Stat. Phys.* **47**, 149 (1987).
- [24.18] D. H. Mayer, *Continued fractions and related transformations*, in ref. [2].
- [24.19] D. H. Mayer, *The Ruelle-Araki transfer operator in classical statistical mechanics* (Springer-Verlag, Berlin, 1980).
- [24.20] S. Isola, *J. Stat. Phys.* **97**, 263 (1999).
- [24.21] S. Isola, "On the spectrum of Farey and Gauss maps," mp-arc 01-280.
- [24.22] B. Fornberg and K.S. Kölbig, *Math. of Computation* **29**, 582 (1975).
- [24.23] A. Erdélyi, W. Magnus, F. Oberhettinger and F. G. Tricomi, *Higher transcendental functions, Vol. I* (McGraw-Hill, New York, 1953).
- [24.24] D. Ruelle, *Inventiones math.* **34**, 231 (1976)
- [24.25] S. Grossmann and H. Fujisaka, *Phys. Rev. A* **26**, 1779 (1982).
- [24.26] R. Lombardi, Laurea thesis, Università degli studi di Milano (1993).

Chapter 25

Deterministic diffusion

This is a bizzare and discordant situation.

—M.V. Berry

(R. Artuso and P. Cvitanović)

THE ADVANCES in the theory of dynamical systems have brought a new life to Boltzmann's mechanical formulation of statistical mechanics. Sinai, Ruelle and Bowen (SRB) have generalized Boltzmann's notion of ergodicity for a constant energy surface for a Hamiltonian system in equilibrium to dissipative systems in nonequilibrium stationary states. In this more general setting the attractor plays the role of a constant energy surface, and the SRB measure of sect. 16.1 is a generalization of the Liouville measure. Such measures are purely microscopic and indifferent to whether the system is at equilibrium, close to equilibrium or far from it. "Far from equilibrium" in this context refers to systems with large deviations from Maxwell's equilibrium velocity distribution. Furthermore, the theory of dynamical systems has yielded new sets of microscopic dynamics formulas for macroscopic observables such as diffusion constants and the pressure, to which we turn now.

We shall apply cycle expansions to the analysis of *transport* properties of chaotic systems.

The resulting formulas are exact; no probabilistic assumptions are made, and the all correlations are taken into account by the inclusion of cycles of all periods. The infinite extent systems for which the periodic orbit theory yields formulas for diffusion and other transport coefficients are spatially periodic, the global state space being tiled with copies of a elementary cell. The motivation are physical problems such as beam defocusing in particle accelerators or chaotic behavior of passive tracers in 2-dimensional rotating flows, problems which can be described as deterministic diffusion in periodic arrays.

In sect. 25.1 we derive the formulas for diffusion coefficients in a simple physical setting, the 2-dimensional periodic Lorentz gas. This system, however, is

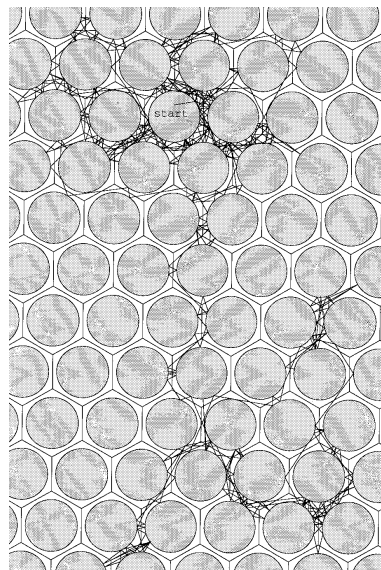


Figure 25.1: Deterministic diffusion in a finite horizon periodic Lorentz gas. (T. Schreiber)

not the best one to illustrate the theory, due to its complicated symbolic dynamics. Therefore we apply the theory first to diffusion induced by a 1 – *dimensional* maps in sect. 25.2.

25.1 Diffusion in periodic arrays

The 2 – *dimensional Lorentz gas* is an infinite scatterer array in which diffusion of a light molecule in a gas of heavy scatterers is modeled by the motion of a point particle in a plane bouncing off an array of reflecting disks. The Lorentz gas is called “gas” as one can equivalently think of it as consisting of any number of pointlike fast “light molecules” interacting only with the stationary “heavy molecules” and not among themselves. As the scatterer array is built up from only defocusing concave surfaces, it is a pure hyperbolic system, and one of the simplest nontrivial dynamical systems that exhibits deterministic diffusion, figure 25.1. We shall now show that the *periodic Lorentz gas* is amenable to a purely deterministic treatment. In this class of open dynamical systems quantities characterizing global dynamics, such as the Lyapunov exponent, pressure and diffusion constant, can be computed from the dynamics restricted to the elementary cell. The method applies to any hyperbolic dynamical system that is a periodic tiling $\hat{\mathcal{M}} = \bigcup_{\hat{n} \in T} \mathcal{M}_{\hat{n}}$ of the dynamical state space $\hat{\mathcal{M}}$ by translates $\mathcal{M}_{\hat{n}}$ of an *elementary cell* \mathcal{M} , with T the Abelian group of lattice translations. If the scattering array has further discrete symmetries, such as reflection symmetry, each elementary cell may be built from a *fundamental domain* $\tilde{\mathcal{M}}$ by the action of a discrete (not necessarily Abelian) group G . The symbol $\hat{\mathcal{M}}$ refers here to the full state space, i.e., both the spatial coordinates and the momenta. The spatial component of $\hat{\mathcal{M}}$ is the complement of the disks in the *whole* space.

We shall now relate the dynamics in \mathcal{M} to diffusive properties of the Lorentz gas in $\hat{\mathcal{M}}$.

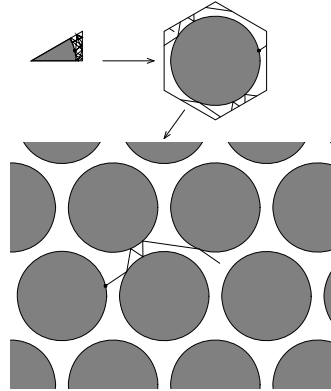


Figure 25.2: Tiling of $\hat{\mathcal{M}}$, a periodic lattice of reflecting disks, by the fundamental domain $\tilde{\mathcal{M}}$. Indicated is an example of a global trajectory $\hat{x}(t)$ together with the corresponding elementary cell trajectory $x(t)$ and the fundamental domain trajectory $\tilde{x}(t)$. (Courtesy of J.-P. Eckmann)

These concepts are best illustrated by a specific example, a Lorentz gas based on the hexagonal lattice Sinai billiard of figure 25.2. We distinguish two types of diffusive behavior; the *infinite horizon* case, which allows for infinite length flights, and the *finite horizon* case, where any free particle trajectory must hit a disk in finite time. In this chapter we shall restrict our consideration to the finite horizon case, with disks sufficiently large so that no infinite length free flight is possible. In this case the diffusion is normal, with $\hat{x}(t)^2$ growing like t . We shall discuss the anomalous diffusion case in sect. 25.3.

As we will work with three kinds of state spaces, good manners require that we repeat what tildes, nothings and hats atop symbols signify:

- ~ fundamental domain, triangle in figure 25.2
 - elementary cell, hexagon in figure 25.2
 - ^ full state space, lattice in figure 25.2
- (25.1)

It is convenient to define an evolution operator for each of the 3 cases of figure 25.2. $\hat{x}(t) = \hat{f}^t(\hat{x})$ denotes the point in the global space $\hat{\mathcal{M}}$ reached by the flow in time t . $x(t) = f^t(x_0)$ denotes the corresponding flow in the elementary cell; the two are related by

$$\hat{n}_t(x_0) = \hat{f}^t(x_0) - f^t(x_0) \in T, \tag{25.2}$$

the translation of the endpoint of the global path into the elementary cell \mathcal{M} . The quantity $\tilde{x}(t) = \tilde{f}^t(\tilde{x})$ denotes the flow in the fundamental domain $\tilde{\mathcal{M}}$; $\tilde{f}^t(\tilde{x})$ is related to $f^t(\tilde{x})$ by a discrete symmetry $g \in G$ which maps $\tilde{x}(t) \in \tilde{\mathcal{M}}$ to $x(t) \in \mathcal{M}$.

chapter 21

Fix a vector $\beta \in \mathbb{R}^d$, where d is the dimension of the state space. We will compute the diffusive properties of the Lorentz gas from the leading eigenvalue of the evolution operator (17.11)

$$s(\beta) = \lim_{t \rightarrow \infty} \frac{1}{t} \log \langle e^{\beta \cdot (\hat{x}(t) - x)} \rangle_{\mathcal{M}}, \tag{25.3}$$

where the average is over all initial points in the elementary cell, $x \in \mathcal{M}$.

If all odd derivatives vanish by symmetry, there is no drift and the second derivatives

$$2dD_{ij} = \left. \frac{\partial}{\partial \beta_i} \frac{\partial}{\partial \beta_j} s(\beta) \right|_{\beta=0} = \lim_{t \rightarrow \infty} \frac{1}{t} \langle (\hat{x}(t) - x)_i (\hat{x}(t) - x)_j \rangle_{\mathcal{M}},$$

yield a diffusion matrix. This symmetric matrix can, in general, be anisotropic (i.e., have d distinct eigenvalues and eigenvectors). The spatial diffusion constant is then given by the Einstein relation (17.13)

$$D = \frac{1}{2d} \sum_i \left. \frac{\partial^2}{\partial \beta_i^2} s(\beta) \right|_{\beta=0} = \lim_{t \rightarrow \infty} \frac{1}{2dt} \langle (\hat{q}(t) - q)^2 \rangle_{\mathcal{M}},$$

where the i sum is restricted to the spatial components q_i of the state space vectors $x = (q, p)$, i.e., if the dynamics is Hamiltonian, the sum is over the d the degrees of freedom.

We now turn to the connection between (25.3) and periodic orbits in the elementary cell. As the full $\hat{\mathcal{M}} \rightarrow \tilde{\mathcal{M}}$ reduction is complicated by the non-Abelian nature of G , we discuss only the Abelian $\hat{\mathcal{M}} \rightarrow \mathcal{M}$ reduction.

remark 25.5

25.1.1 Reduction from $\hat{\mathcal{M}}$ to \mathcal{M}

The key idea follows from inspection of the relation

$$\langle e^{\beta \cdot (\hat{x}(t) - x)} \rangle_{\mathcal{M}} = \frac{1}{|\mathcal{M}|} \int_{\substack{x \in \mathcal{M} \\ \hat{y} \in \hat{\mathcal{M}}} } dx d\hat{y} e^{\beta \cdot (\hat{y} - x)} \delta(\hat{y} - \hat{f}^t(x)).$$

$|\mathcal{M}| = \int_{\mathcal{M}} dx$ is the volume of the elementary cell \mathcal{M} . Due to translational symmetry, it suffices to start with a density of trajectories defined over a single elementary cell \mathcal{M} . As in sect. 17.2, we have used the identity $1 = \int_{\mathcal{M}} dy \delta(y - \hat{x}(t))$ to motivate the introduction of the evolution operator $\mathcal{L}(\hat{y}, x)$. There is a unique lattice translation \hat{n} such that $\hat{y} = y - \hat{n}$, with the endpoint $y \in \mathcal{M}$ translated back to the elementary cell, and $f^t(x)$ given by (25.2). The difference is a translation by a constant lattice vector \hat{n} , and the Jacobian for changing integration from $d\hat{y}$ to dy equals unity. Therefore, and this is the main point, translation invariance can be used to reduce this average to the elementary cell:

$$\langle e^{\beta \cdot (\hat{x}(t) - x)} \rangle_{\mathcal{M}} = \frac{1}{|\mathcal{M}|} \int_{x, y \in \mathcal{M}} dx dy e^{\beta \cdot (\hat{f}^t(x) - x)} \delta(y - f^t(x)). \quad (25.4)$$

As this is a translation, the Jacobian is $|\partial \hat{y} / \partial y| = 1$. In this way the global $\hat{f}^t(x)$ flow, infinite volume state space averages can be computed by following the flow

$f^t(x_0)$ restricted to the compact, finite volume elementary cell \mathcal{M} . The equation (25.4) suggests that we study the evolution operator

$$\mathcal{L}^t(y, x) = e^{\beta \cdot (\hat{x}(t) - x)} \delta(y - f^t(x)), \quad (25.5)$$

where $\hat{x}(t) = \hat{f}^t(x) \in \hat{\mathcal{M}}$ is the displacement in the full space, but $x, f^t(x), y \in \mathcal{M}$. It is straightforward to check that this operator satisfies the semigroup property (17.25),

$$\int_{\mathcal{M}} dz \mathcal{L}^{t_2}(y, z) \mathcal{L}^{t_1}(z, x) = \mathcal{L}^{t_2+t_1}(y, x) .$$

For $\beta = 0$, the operator (25.5) is the Perron-Frobenius operator (16.10), with the leading eigenvalue $e^{s_0} = 1$ because there is no escape from this system (see the flow conservation sum rule (22.11)).

The rest is old hat. The spectrum of \mathcal{L} is evaluated by taking the trace

section 18.2

$$\text{tr } \mathcal{L}^t = \int_{\mathcal{M}} dx e^{\beta \cdot \hat{n}_t(x)} \delta(x - x(t)) .$$

Here $\hat{n}_t(x)$ is the discrete lattice translation defined in (25.2). Two kinds of orbits periodic in the elementary cell contribute. A periodic orbit is called *standing* if it is also periodic orbit of the infinite state space dynamics, $\hat{f}^{T_p}(x) = x$, and it is called *running* if it corresponds to a lattice translation in the dynamics on the infinite state space, $\hat{f}^{T_p}(x) = x + \hat{n}_p$. We recognize the shortest repeating segment of a running orbit as our old ‘relative periodic orbit’ friend from chapter 9. In the theory of area-preserving maps such as the standard map of example 7.6 these orbits are called *accelerator modes*, as the diffusion takes place along the momentum rather than the position coordinate. The traveled distance $\hat{n}_p = \hat{n}_{T_p}(x_0)$ is independent of the starting point x_0 , as can be easily seen by continuing the path periodically in $\hat{\mathcal{M}}$.

The final result is the spectral determinant (19.6)

$$\det(s(\beta) - \mathcal{A}) = \prod_p \exp \left(- \sum_{r=1}^{\infty} \frac{1}{r} \frac{e^{(\beta \cdot \hat{n}_p - s T_p)r}}{|\det(\mathbf{1} - M_p^r)|} \right), \quad (25.6)$$

or the corresponding dynamical zeta function (19.15)

$$1/\zeta(\beta, s) = \prod_p \left(1 - \frac{e^{(\beta \cdot \hat{n}_p - s T_p)}}{|\Lambda_p|} \right). \quad (25.7)$$

The dynamical zeta function cycle averaging formula (20.21) for the diffusion constant (17.13), zero mean drift $\langle \hat{x}_i \rangle = 0$, is given by

$$D = \frac{1}{2d} \frac{\langle \hat{x}^2 \rangle_\zeta}{\langle T \rangle_\zeta} = \frac{1}{2d} \frac{1}{\langle T \rangle_\zeta} \sum' \frac{(-1)^{k+1} (\hat{n}_{p_1} + \dots + \hat{n}_{p_k})^2}{|\Lambda_{p_1} \dots \Lambda_{p_k}|}. \quad (25.8)$$

where the sum is over all distinct non-repeating combination of prime cycles. The derivation is standard, still the formula is strange. Diffusion is unbounded motion across an infinite lattice; nevertheless, the reduction to the elementary cell enables us to compute relevant quantities in the usual way, in terms of periodic orbits.

A sleepy reader might protest that $x(T_p) - x(0)$ is manifestly equal to zero for a periodic orbit. That is correct; \hat{n}_p in the above formula refers to a displacement $\hat{x}(T_p)$ on the *infinite* periodic lattice, while p refers to closed orbit of the dynamics $f^t(x)$ reduced to the elementary cell, with x_p a periodic point in the closed prime cycle p .

Even so, this is not an obvious formula. Globally periodic orbits have $\hat{x}_p^2 = 0$, and contribute only to the time normalization $\langle T \rangle_\zeta$. The mean square displacement $\langle \hat{x}^2 \rangle_\zeta$ gets contributions only from the periodic runaway trajectories; they are closed in the elementary cell, but on the periodic lattice each one grows like $\hat{x}(t)^2 = (\hat{n}_p/T_p)^2 t^2 = v_p^2 t^2$. So the orbits that contribute to the trace formulas and spectral determinants exhibit either ballistic transport or no transport at all: diffusion arises as a balance between the two kinds of motion, weighted by the $1/|\Lambda_p|$ measure. If the system is not hyperbolic such weights may be abnormally large, with $1/|\Lambda_p| \approx 1/T_p^\alpha$ rather than $1/|\Lambda_p| \approx e^{-T_p \lambda}$, where λ is the Lyapunov exponent, and they may lead to anomalous diffusion - accelerated or slowed down depending on whether the probabilities of the running or the standing orbits are enhanced.

section 25.3

We illustrate the main idea, tracking of a globally diffusing orbit by the associated confined orbit restricted to the elementary cell, with a class of simple 1 – *dimensional* dynamical systems where all transport coefficients can be evaluated analytically.

25.2 Diffusion induced by chains of 1 – *dimensional* maps

In a typical deterministic diffusive process, trajectories originating from a given scatterer reach a finite set of neighboring scatterers in one bounce, and then the process is repeated. As was shown in chapter 11, the essential part of this process is the stretching along the unstable directions of the flow, and in the crudest approximation the dynamics can be modeled by 1 – *dimensional* expanding maps. This observation motivates introduction of a class of particularly simple 1 – *dimensional* systems.

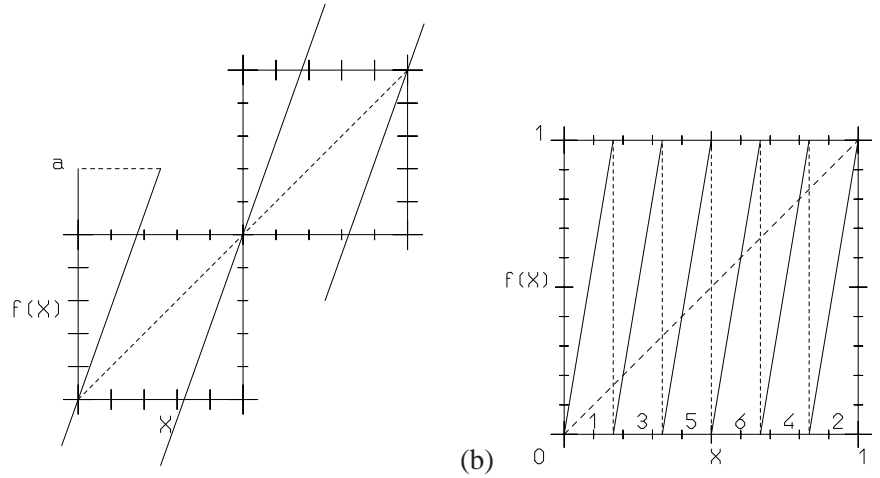


Figure 25.3: (a) $\hat{f}(\hat{x})$, the full space sawtooth map (25.9), $\Lambda > 2$. (b) $f(x)$, the sawtooth map restricted to the unit circle (25.12), $\Lambda = 6$.

Example 25.1 Chains of piecewise linear maps. We start by defining the map \hat{f} on the unit interval as

$$\hat{f}(\hat{x}) = \begin{cases} \Lambda \hat{x} & \hat{x} \in [0, 1/2) \\ \Lambda \hat{x} + 1 - \Lambda & \hat{x} \in (1/2, 1] \end{cases}, \quad \Lambda > 2, \tag{25.9}$$

and then extending the dynamics to the entire real line, by imposing the translation property

$$\hat{f}(\hat{x} + \hat{n}) = \hat{f}(\hat{x}) + \hat{n} \quad \hat{n} \in \mathbb{Z}. \tag{25.10}$$

As the map is discontinuous at $\hat{x} = 1/2$, $\hat{f}(1/2)$ is undefined, and the $x = 1/2$ point has to be excluded from the Markov partition. The map is antisymmetric under the \hat{x} -coordinate flip

$$\hat{f}(\hat{x}) = -\hat{f}(-\hat{x}), \tag{25.11}$$

so the dynamics will exhibit no mean drift; all odd derivatives of the generating function (17.11) with respect to β , evaluated at $\beta = 0$, will vanish.

The map (25.9) is sketched in figure 25.3 (a). Initial points sufficiently close to either of the fixed points in the initial unit interval remain in the elementary cell for one iteration; depending on the slope Λ , other points jump \hat{n} cells, either to the right or to the left. Repetition of this process generates a random walk for almost every initial condition.

The translational symmetry (25.10) relates the unbounded dynamics on the real line to dynamics restricted to the elementary cell - in the example at hand, the unit interval curled up into a circle. Associated to $\hat{f}(\hat{x})$ we thus also consider the circle map

$$f(x) = \hat{f}(\hat{x}) - [\hat{f}(\hat{x})], \quad x = \hat{x} - [\hat{x}] \in [0, 1] \tag{25.12}$$

figure 25.3 (b), where $[\dots]$ stands for the integer part (25.2). For the piecewise linear map of figure 25.3 we can evaluate the dynamical zeta function in closed form. Each branch has the same value of the slope, and the map can be parameterized by a single parameter, for example its critical value $a = \hat{f}(1/2)$, the absolute maximum on the interval $[0, 1]$ related to the slope of the map by $a = \Lambda/2$. The larger Λ is, the stronger is the stretching action of the map.

As noted in sect. 25.1.1, the elementary cell cycles correspond to either standing or running orbits for the map on the full line: we shall refer to $\hat{n}_p \in \mathbb{Z}$ as the *jumping number* of the p cycle, and take as the cycle weight

$$t_p = z^{n_p} e^{\beta \hat{n}_p} / |\Lambda_p|. \quad (25.13)$$

The diffusion constant formula (25.8) for 1 – dimensional maps is

$$D = \frac{1}{2} \frac{\langle \hat{n}^2 \rangle_\zeta}{\langle n \rangle_\zeta}, \quad (25.14)$$

where the “mean cycle time” is given by (20.22)

$$\langle n \rangle_\zeta = z \frac{\partial}{\partial z} \frac{1}{\zeta(0, z)} \Big|_{z=1} = - \sum' (-1)^k \frac{n_{p_1} + \dots + n_{p_k}}{|\Lambda_{p_1} \dots \Lambda_{p_k}|}, \quad (25.15)$$

and the “mean cycle displacement squared” by (20.25)

$$\langle \hat{n}^2 \rangle_\zeta = \frac{\partial^2}{\partial \beta^2} \frac{1}{\zeta(\beta, 1)} \Big|_{\beta=0} = - \sum' (-1)^k \frac{(\hat{n}_{p_1} + \dots + \hat{n}_{p_k})^2}{|\Lambda_{p_1} \dots \Lambda_{p_k}|}, \quad (25.16)$$

the primed sum indicating all distinct non-repeating combinations of prime cycles. The evaluation of these formulas for the simple system of example 25.1 will require nothing more than pencil and paper.

Example 25.2 Unrestricted symbolic dynamics. Whenever Λ is an integer number, the symbolic dynamics is exceedingly simple. For example, for the case $\Lambda = 6$ illustrated in figure 25.3 (b), the elementary cell map consists of 6 full branches, with uniform stretching factor $\Lambda = 6$. The branches have different jumping numbers: for branches 1 and 2 we have $\hat{n} = 0$, for branch 3 we have $\hat{n} = +1$, for branch 4 $\hat{n} = -1$, and finally for branches 5 and 6 we have respectively $\hat{n} = +2$ and $\hat{n} = -2$. The same structure reappears whenever Λ is an even integer $\Lambda = 2a$: all branches are mapped onto the whole unit interval and we have two $\hat{n} = 0$ branches, one branch for which $\hat{n} = +1$ and one for which $\hat{n} = -1$, and so on, up to the maximal jump $|\hat{n}| = a - 1$. The symbolic dynamics is thus full, unrestricted shift in $2a$ symbols $\{0_+, 1_+, \dots, (a-1)_+, (a-1)_-, \dots, 1_-, 0_-\}$, where the symbol indicates both the length and the direction of the corresponding jump.

For the piecewise linear maps with uniform stretching the weight associated with a given symbol sequence is a product of weights for individual steps, $t_{sq} = t_s t_q$. For the map of figure 25.3 there are 6 distinct weights (25.13):

$$\begin{aligned} t_1 &= t_2 = z/\Lambda \\ t_3 &= e^\beta z/\Lambda, \quad t_4 = e^{-\beta} z/\Lambda, \quad t_5 = e^{2\beta} z/\Lambda, \quad t_6 = e^{-2\beta} z/\Lambda. \end{aligned}$$

The piecewise linearity and the simple symbolic dynamics lead to the full cancelation of all curvature corrections in (20.7). The exact dynamical zeta function (15.15) is given by the fixed point contributions:

$$\begin{aligned} 1/\zeta(\beta, z) &= 1 - t_{0+} - t_{0-} - \dots - t_{(a-1)+} - t_{(a-1)-} \\ &= 1 - \frac{z}{a} \left(1 + \sum_{j=1}^{a-1} \cosh(\beta j) \right). \end{aligned} \quad (25.17)$$

The leading (and only) eigenvalue of the evolution operator (25.5) is

$$s(\beta) = \log \left\{ \frac{1}{a} \left(1 + \sum_{j=1}^{a-1} \cosh(\beta j) \right) \right\}, \quad \Lambda = 2a, \quad a \text{ integer}. \quad (25.18)$$

The flow conservation (22.11) sum rule is manifestly satisfied, so $s(0) = 0$. The first derivative $s(0)'$ vanishes as well by the left/right symmetry of the dynamics, implying vanishing mean drift $\langle \hat{x} \rangle = 0$. The second derivative $s(\beta)''$ yields the diffusion constant (25.14):

$$\langle n \rangle_{\zeta} = 2a \frac{1}{\Lambda} = 1, \quad \langle \hat{x}^2 \rangle_{\zeta} = 2 \frac{0^2}{\Lambda} + 2 \frac{1^2}{\Lambda} + 2 \frac{2^2}{\Lambda} + \dots + 2 \frac{(a-1)^2}{\Lambda} \quad (25.19)$$

Using the identity $\sum_{k=1}^n k^2 = n(n+1)(2n+1)/6$ we obtain

$$D = \frac{1}{24}(\Lambda - 1)(\Lambda - 2), \quad \Lambda \text{ even integer}. \quad (25.20)$$

Similar calculation for odd integer $\Lambda = 2k - 1$ yields

$$D = \frac{1}{24}(\Lambda^2 - 1), \quad \Lambda \text{ odd integer}. \quad (25.21)$$

exercise 25.1

25.2.1 Higher order transport coefficients

The same approach yields higher order transport coefficients

$$\mathcal{B}_k = \frac{1}{k!} \frac{d^k}{d\beta^k} s(\beta) \Big|_{\beta=0}, \quad \mathcal{B}_2 = D, \quad (25.22)$$

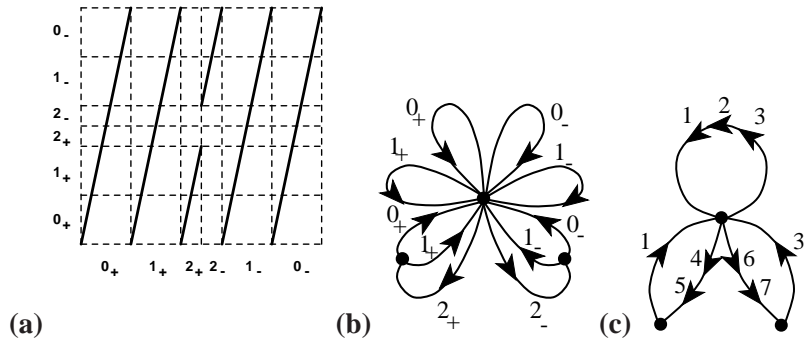
known for $k > 2$ as the Burnett coefficients. The behavior of the higher order coefficients yields information on the relaxation to the asymptotic distribution function generated by the diffusive process. Here \hat{x}_t is the relevant dynamical variable and \mathcal{B}_k 's are related to moments $\langle \hat{x}_t^k \rangle$ of arbitrary order.

Were the diffusive process purely Gaussian

$$e^{ts(\beta)} = \frac{1}{\sqrt{4\pi Dt}} \int_{-\infty}^{+\infty} d\hat{x} e^{\beta \hat{x}} e^{-\hat{x}^2/(4Dt)} = e^{\beta^2 Dt} \quad (25.23)$$

the only \mathcal{B}_k coefficient different from zero would be $\mathcal{B}_2 = D$. Hence, nonvanishing higher order coefficients signal deviations of deterministic diffusion from a Gaussian stochastic process.

Figure 25.4: (a) A partition of the unit interval into six intervals, labeled by the jumping number $\hat{n}(x)$ $I = \{0_+, 1_+, 2_+, 2_-, 1_-, 0_-\}$. The partition is Markov, as the critical point is mapped onto the right border of \mathcal{M}_{1_+} . (b) The transition graph for this partition. (c) The transition graph in the compact notation of (25.26) (introduced by Vadim Moroz).



Example 25.3 \mathcal{B}_4 Burnett coefficient. For the map under consideration the first Burnett coefficient \mathcal{B}_4 is easily evaluated. For example, using (25.18) in the case of even integer slope $\Lambda = 2a$ we obtain

$$\mathcal{B}_4 = -\frac{1}{4! \cdot 60}(a-1)(2a-1)(4a^2-9a+7). \tag{25.24}$$

exercise 25.2

We see that deterministic diffusion is not a Gaussian stochastic process. Higher order even coefficients may be calculated along the same lines.

25.2.2 Finite Markov partitions

For piecewise-linear maps exact results may be obtained whenever the critical points are mapped in finite numbers of iterations onto partition boundary points, or onto unstable periodic orbits. We will work out here an example for which this occurs in two iterations, leaving other cases as exercises. The key idea is to construct a *Markov partition* (11.2), with intervals mapped *onto* unions of intervals.

Example 25.4 A finite Markov partition. As an example we determine a value of the parameter $4 \leq \Lambda \leq 6$ for which $f(f(1/2)) = 0$. As in the integer Λ case, we partition the unit interval into six intervals, labeled by the jumping number $\hat{n}(x) \in \{\mathcal{M}_{0_+}, \mathcal{M}_{1_+}, \mathcal{M}_{2_+}, \mathcal{M}_{2_-}, \mathcal{M}_{1_-}, \mathcal{M}_{0_-}\}$, ordered by their placement along the unit interval, figure 25.4 (a).

In general the critical value $a = \hat{f}(1/2)$ will not correspond to an interval border, but now we choose a such that the critical point is mapped onto the right border of \mathcal{M}_{1_+} . Equating $f(1/2)$ with the right border of \mathcal{M}_{1_+} , $x = 1/\Lambda$, we obtain a quadratic equation with the expanding solution $\Lambda = 2(\sqrt{2}+1)$. For this parameter value $f(\mathcal{M}_{1_+}) = \mathcal{M}_{0_+} \cup \mathcal{M}_{1_+}$, $f(\mathcal{M}_{2_-}) = \mathcal{M}_{0_-} \cup \mathcal{M}_{1_-}$, while the remaining intervals map onto the whole unit interval \mathcal{M} . The transition matrix (14.1) is given by

$$\phi' = T\phi = \begin{pmatrix} 1 & 1 & 1 & 0 & 1 & 1 \\ 1 & 1 & 1 & 0 & 1 & 1 \\ 1 & 1 & 0 & 0 & 1 & 1 \\ 1 & 1 & 0 & 0 & 1 & 1 \\ 1 & 1 & 0 & 1 & 1 & 1 \\ 1 & 1 & 0 & 1 & 1 & 1 \end{pmatrix} \begin{pmatrix} \phi_{0_+} \\ \phi_{1_+} \\ \phi_{2_+} \\ \phi_{2_-} \\ \phi_{1_-} \\ \phi_{0_-} \end{pmatrix}. \tag{25.25}$$

One could diagonalize (25.25) on a computer, but, as we saw in chapter 14, the transition graph of figure 25.4 (b) corresponding to map figure 25.4 (a) offers more insight into the dynamics. Figure 25.4 (b) can be redrawn more compactly as transition graph figure 25.4 (c) by replacing parallel lines in a graph by their sum

$$\begin{array}{c} \curvearrowright \\ \text{1} \\ \text{2} \\ \text{3} \\ \curvearrowleft \end{array} = \bullet \xrightarrow{1+2+3} \bullet = t_1 + t_2 + t_3. \tag{25.26}$$

The dynamics is unrestricted in the alphabet

$$\mathcal{A} = \{0_+, 1_+, 2_+0_+, 2_+1_+, 2_-1_-, 2_-0_-, 1_-, 0_-\}.$$

Applying the loop expansion (15.15) of sect. 15.3, we are led to the dynamical zeta function

$$\begin{aligned} 1/\zeta(\beta, z) &= 1 - t_{0_+} - t_{1_+} - t_{2_+0_+} - t_{2_+1_+} - t_{2_-1_-} - t_{2_-0_-} - t_{1_-} - t_{0_-} \\ &= 1 - \frac{2z}{\Lambda} (1 + \cosh(\beta)) - \frac{2z^2}{\Lambda^2} (\cosh(2\beta) + \cosh(3\beta)). \end{aligned} \tag{25.27}$$

For grammar as simple as this one, the dynamical zeta function is the sum over fixed points of the unrestricted alphabet. As the first check of this expression for the dynamical zeta function we verify that

$$1/\zeta(0, 1) = 1 - \frac{4}{\Lambda} - \frac{4}{\Lambda^2} = 0,$$

as required by the flow conservation (22.11). Conversely, we could have started by picking the desired Markov partition, writing down the corresponding dynamical zeta function, and then fixing Λ by the $1/\zeta(0, 1) = 0$ condition. For more complicated transition graphs this approach, together with the factorization (25.35), is helpful in reducing the order of the polynomial condition that fixes Λ .

The diffusion constant follows from (25.14)

exercise 25.3

$$\begin{aligned} \langle n \rangle_\zeta &= 4 \frac{1}{\Lambda} + 4 \frac{2}{\Lambda^2}, & \langle \hat{n}^2 \rangle_\zeta &= 2 \frac{1^2}{\Lambda} + 2 \frac{2^2}{\Lambda^2} + 2 \frac{3^2}{\Lambda^2} \\ D &= \frac{15 + 2\sqrt{2}}{16 + 8\sqrt{2}}. \end{aligned} \tag{25.28}$$

It is by now clear how to build an infinite hierarchy of finite Markov partitions: tune the slope in such a way that the critical value $f(1/2)$ is mapped into the fixed point at the origin in a finite number of iterations $f^p(1/2) = 0$. By taking higher and higher values of p one constructs a dense set of Markov parameter values, organized into a hierarchy that resembles the way in which rationals are densely embedded in the unit interval. For example, each of the 6 primary intervals can be subdivided into 6 intervals obtained by the 2-nd iterate of the map, and for the critical point mapping into any of those in 2 steps the grammar (and the corresponding cycle expansion) is finite. So, if we can prove continuity of $D = D(\Lambda)$, we can apply the periodic orbit theory to the sawtooth map (25.9) for a random “generic” value of the parameter Λ , for example $\Lambda = 4.5$. The idea is to bracket this value of Λ by a sequence of nearby Markov values, compute the exact diffusion constant for each such Markov partition, and study their convergence toward

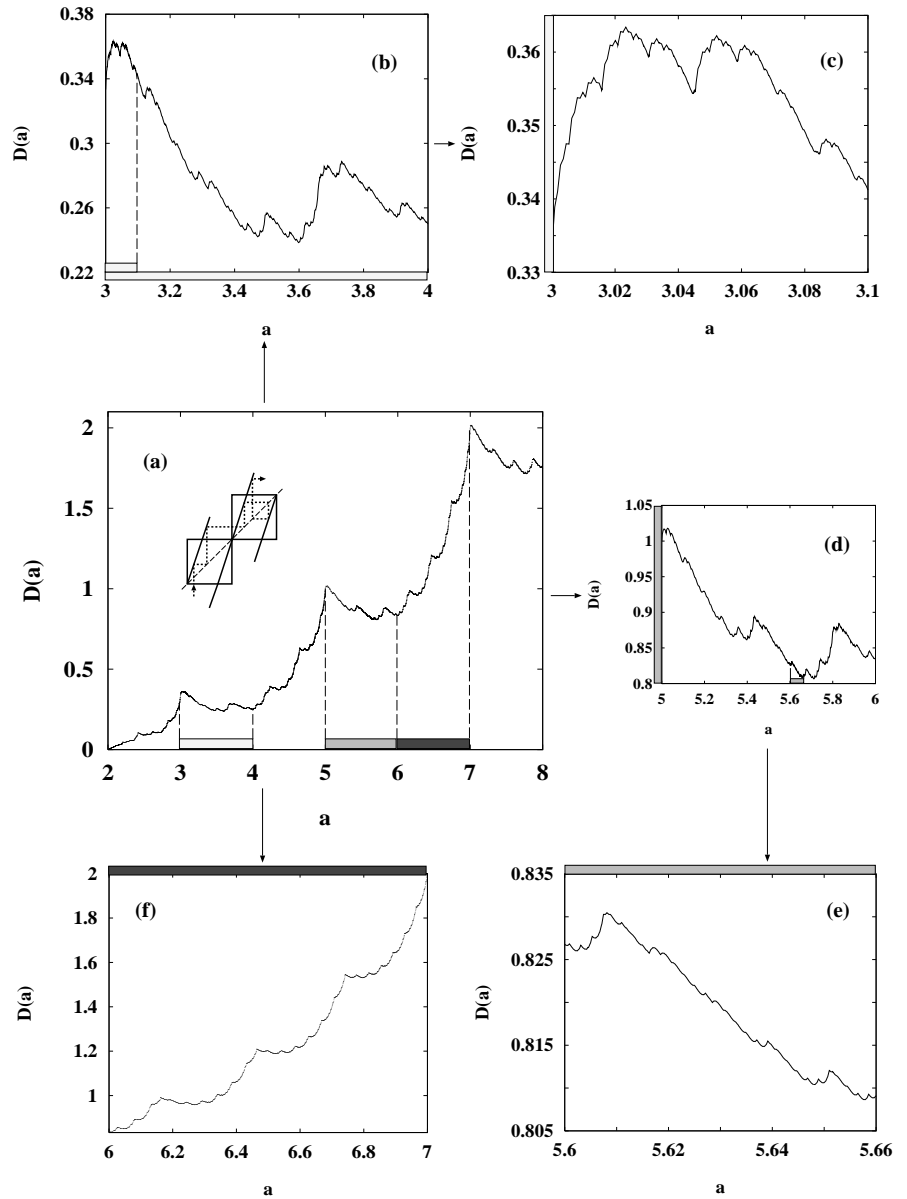


Figure 25.5: The dependence of D on the map parameter a is continuous, but not monotone. Here a stands for the slope Λ in (25.9). (From ref. [9].)

the value of D for $\Lambda = 4.5$. Judging how difficult such problem is already for a tent map (see sect. 15.5), this is not likely to take only a week of work.

Expressions like (25.20) may lead to an expectation that the diffusion coefficient (and thus transport properties) are smooth functions of parameters controlling the chaoticity of the system. For example, one might expect that the diffusion coefficient increases smoothly and monotonically as the slope Λ of the map (25.9) is increased, or, perhaps more physically, that the diffusion coefficient is a smooth function of the Lyapunov exponent λ . This turns out not to be true: D as a function of Λ is a fractal, nowhere differentiable curve illustrated in figure 25.5. The dependence of D on the map parameter Λ is rather unexpected - even though for larger Λ more points are mapped outside the unit cell in one iteration, the diffusion constant does not necessarily grow.

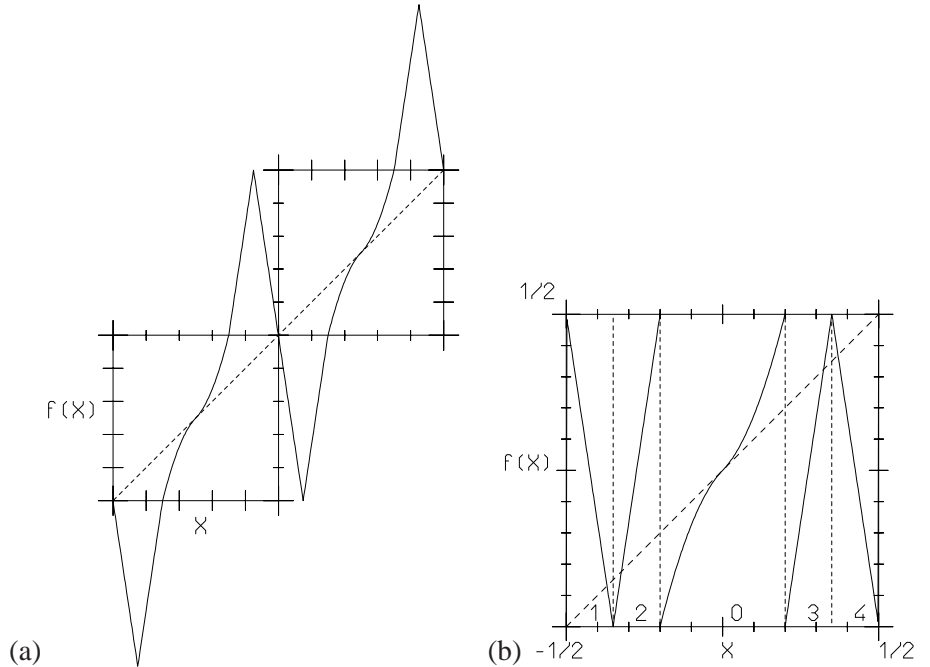


Figure 25.6: (a) A map with marginal fixed point.
 (b) The map restricted to the unit circle.

This is a consequence of the lack of structural stability, even of purely hyperbolic systems such as the Lozi map and the 1 – dimensional diffusion map (25.9). The trouble arises due to non-smooth dependence of the topological entropy on system parameters - any parameter change, no matter how small, leads to creation and destruction of infinitely many periodic orbits. As far as diffusion is concerned this means that even though local expansion rate is a smooth function of Λ , the number of ways in which the trajectory can re-enter the initial cell is an irregular function of Λ .

The lesson is that lack of structural stability implies lack of spectral stability, and no global observable is expected to depend smoothly on the system parameters. If you want to master the material, working through one of the deterministic diffusion projects on ChaosBook.org/pages is strongly recommended.

25.3 Marginal stability and anomalous diffusion

What effect does the intermittency of chapter 24 have on transport properties? A marginal fixed point affects the balance between the running and standing orbits, thus generating a mechanism that may result in anomalous diffusion.

Example 25.5 Anomalous diffusion. Consider a 1 – dimensional map of the real line on itself shown in figure 25.6 (a), with the same properties as in sect. 25.2, except for a marginal fixed point at $x = 0$. The corresponding circle map is given in figure 25.6 (b). As in sect. 24.2.1, a branch with support in M_i , $i = 1, 2, 3, 4$ has constant slope Λ_i , while $f|_{M_0}$ is of intermittent form. To keep you nimble, this time we take a slightly different choice of slopes. The toy example of sect. 24.2.1 was cooked up so that the

$1/s$ branch cut in dynamical zeta function was the whole answer. Here we shall take a slightly different route, and pick piecewise constant slopes such that the dynamical zeta function for intermittent system can be expressed in terms of the Jonquière function remark 25.7

$$J(z, s) = \sum_{k=1}^{\infty} z^k / k^s. \tag{25.29}$$

Once the $\bar{0}$ fixed point is pruned away, the symbolic dynamics is given by the infinite alphabet $\{1, 2, 3, 4, 0^i 1, 0^j 2, 0^k 3, 0^l 4\}$, $i, j, k, l = 1, 2, \dots$ (compare with table 24.1). The partitioning of the subinterval \mathcal{M}_0 is induced by $\mathcal{M}_{0^k(\text{right})} = \hat{f}_{(\text{right})}^{-k}(\mathcal{M}_3 \cup \mathcal{M}_4)$ (where $\hat{f}_{(\text{right})}^{-1}$ denotes the inverse of the right branch of $\hat{f}|_{\mathcal{M}_0}$) and the same reasoning applies to the leftmost branch. These are regions over which the slope of $\hat{f}|_{\mathcal{M}_0}$ is constant. Thus we have the following stabilities and jumping numbers associated to letters:

$$\begin{array}{lll} 0^k 3, 0^k 4 & \Lambda_p = \frac{k^{1+\alpha}}{q/2} & \hat{n}_p = 1 \\ 0^l 1, 0^l 2 & \Lambda_p = \frac{l^{1+\alpha}}{q/2} & \hat{n}_p = -1 \\ 3, 4 & \Lambda_p = \pm \Lambda & \hat{n}_p = 1 \\ 2, 1 & \Lambda_p = \pm \Lambda & \hat{n}_p = -1, \end{array} \tag{25.30}$$

where $\alpha = 1/s$ is determined by the intermittency exponent (24.1), while q is to be determined by the flow conservation (22.11) for \hat{f} :

$$\frac{4}{\Lambda} + 2q\zeta(\alpha + 1) = 1$$

(where ζ is the Riemann zeta function), so that $q = (\Lambda - 4)/(2\Lambda\zeta(\alpha + 1))$. The dynamical zeta function picks up contributions just by the alphabet's letters, as we have imposed piecewise linearity, and can be expressed in terms of a Jonquière function (25.29):

$$1/\zeta_0(z, \beta) = 1 - \frac{4}{\Lambda} z \cosh \beta - \frac{\Lambda - 4}{\Lambda\zeta(1 + \alpha)} z \cosh \beta \cdot J(z, \alpha + 1). \tag{25.31}$$

Its first zero $z(\beta)$ is determined by

$$\frac{4}{\Lambda} z + \frac{\Lambda - 4}{\Lambda\zeta(1 + \alpha)} z \cdot J(z, \alpha + 1) = \frac{1}{\cosh \beta}.$$

D vanishes by the implicit function theorem, $z'(\beta)|_{\beta=1} = 0$ when $\alpha \leq 1$. The physical interpretation is that a typical orbit will stick for long times near the $\bar{0}$ marginal fixed point, and the ‘trapping time’ will be larger for higher values of the intermittency parameter s (recall $\alpha = 1/s$). As always, we need to look more closely at the behavior of traces of high powers of the transfer operator.

The evaluation of transport coefficient requires one more derivative with respect to expectation values of state space observables (see sect. 25.1): if we use the diffusion dynamical zeta function (25.7), we may write the diffusion coefficient as an inverse Laplace transform, in such a way that the distinction between

maps and flows has vanished. In the case of 1 – dimensional diffusion we thus have

$$D = \lim_{t \rightarrow \infty} \frac{d^2}{d\beta^2} \frac{1}{2\pi i} \int_{a-i\infty}^{a+i\infty} ds e^{st} \frac{\zeta'(\beta, s)}{\zeta(\beta, s)} \Big|_{\beta=0} \quad (25.32)$$

where the ζ' refers to the derivative with respect to s .

The evaluation of inverse Laplace transforms for high values of the argument is most conveniently performed using Tauberian theorems. We shall take

$$\omega(\lambda) = \int_0^\infty dx e^{-\lambda x} u(x),$$

with $u(x)$ monotone as $x \rightarrow \infty$; then, as $\lambda \mapsto 0$ and $x \mapsto \infty$ respectively (and $\rho \in (0, \infty)$),

$$\omega(\lambda) \sim \frac{1}{\lambda^\rho} L\left(\frac{1}{\lambda}\right)$$

if and only if

$$u(x) \sim \frac{1}{\Gamma(\rho)} x^{\rho-1} L(x),$$

where L denotes any slowly varying function with $\lim_{t \rightarrow \infty} L(ty)/L(t) = 1$. Now

$$\frac{1/\zeta_0'(e^{-s}, \beta)}{1/\zeta_0(e^{-s}, \beta)} = \frac{\left(\frac{4}{\Lambda} + \frac{\Lambda-4}{\Lambda \zeta'(1+\alpha)} (J(e^{-s}, \alpha + 1) + J(e^{-s}, \alpha))\right) \cosh \beta}{1 - \frac{4}{\Lambda} e^{-s} \cosh \beta - \frac{\Lambda-4}{\Lambda \zeta'(1+\alpha)} e^{-s} (e^{-s}, \alpha + 1) \cosh \beta J}.$$

Taking the second derivative with respect to β we obtain

$$\begin{aligned} & \frac{d^2}{d\beta^2} \left(1/\zeta_0'(e^{-s}, \beta)/\zeta^{-1}(e^{-s}, \beta)\right)_{\beta=0} \\ &= \frac{\frac{4}{\Lambda} + \frac{\Lambda-4}{\Lambda \zeta'(1+\alpha)} (J(e^{-s}, \alpha + 1) + J(e^{-s}, \alpha))}{\left(1 - \frac{4}{\Lambda} e^{-s} - \frac{\Lambda-4}{\Lambda \zeta'(1+\alpha)} e^{-s} J(e^{-s}, \alpha + 1)\right)^2} = g_\alpha(s). \end{aligned} \quad (25.33)$$

The asymptotic behavior of the inverse Laplace transform (25.32) may then be evaluated via Tauberian theorems, once we use our estimate for the behavior of Jonquière functions near $z = 1$. The deviations from normal behavior correspond

to an explicit dependence of D on time. Omitting prefactors (which can be calculated by the same procedure) we have

$$g_\alpha(s) \sim \begin{cases} s^{-2} & \text{for } \alpha > 1 \\ s^{-(\alpha+1)} & \text{for } \alpha \in (0, 1) \\ 1/(s^2 \ln s) & \text{for } \alpha = 1. \end{cases}$$

The anomalous diffusion exponents follow:

exercise 25.6

$$\langle (x - x_0)^2 \rangle_t \sim \begin{cases} t^\alpha & \text{for } \alpha \in (0, 1) \\ t / \ln t & \text{for } \alpha = 1 \\ t & \text{for } \alpha > 1. \end{cases} \quad (25.34)$$

Résumé

With initial data accuracy $\delta x = |\delta \mathbf{x}(0)|$ and system size L , a trajectory is predictable only to the finite Lyapunov time $T_{\text{Lyap}} \approx \lambda^{-1} \ln |L/\delta x|$. Beyond that, chaos rules. We have discussed the implications in sect. 1.8: chaos is good news for prediction of long term observables such as transport in statistical mechanics.

The classical Boltzmann equation for evolution of 1-particle density is based on *stosszahlansatz*, neglect of particle correlations prior to, or after a 2-particle collision. It is a very good approximate description of dilute gas dynamics, but a difficult starting point for inclusion of systematic corrections. In the theory developed here, no correlations are neglected - they are all included in the cycle averaging formula such as the cycle expansion for the diffusion constant

$$D = \frac{1}{2d} \frac{1}{\langle T \rangle_\zeta} \sum' (-1)^{k+1} \frac{(\hat{n}_{p_1} + \dots + \hat{n}_{p_k})^2}{|\Lambda_{p_1} \dots \Lambda_{p_k}|}.$$

Such formulas are *exact*; the issue in their applications is what are the most effective schemes of estimating the infinite cycle sums required for their evaluation. Unlike most statistical mechanics, here there are no phenomenological macroscopic parameters; quantities such as transport coefficients are calculable to any desired accuracy from the microscopic dynamics.

For systems of a few degrees of freedom these results are on rigorous footing, but there are indications that they capture the essential dynamics of systems of many degrees of freedom as well.

Though superficially indistinguishable from the probabilistic random walk diffusion, deterministic diffusion is quite recognizable, at least in low dimensional settings, through fractal dependence of the diffusion constant on the system parameters, and through non-Gaussian relaxation to equilibrium (non-vanishing Burnett coefficients).

That Smale's "structural stability" conjecture turned out to be wrong is not a bane of chaotic dynamics - it is actually a virtue, perhaps the most dramatic experimentally measurable prediction of chaotic dynamics. As long as microscopic periodicity is exact, the prediction is counterintuitive for a physicist - transport coefficients are *not* smooth functions of system parameters, rather they are non-monotonic, *nowhere differentiable* functions.

Actual evaluation of transport coefficients is a test of the techniques developed above in physical settings. In cases of severe pruning the trace formulas and ergodic sampling of dominant cycles might be more effective strategy than the cycle expansions of dynamical zeta functions and systematic enumeration of all cycles.

Commentary

Remark 25.1 Lorentz gas. The original pinball model proposed by Lorentz [4] consisted of randomly, rather than regularly placed scatterers.

Remark 25.2 Who's dunnit? Cycle expansions for the diffusion constant of a particle moving in a periodic array have been introduced by R. Artuso [5] (exact dynamical zeta function for 1 – dimensional chains of maps (25.8)), by W.N. Vance [6], and by P. Cvitanović, J.-P. Eckmann, and P. Gaspard [7] (the dynamical zeta function cycle expansion (25.8) applied to the Lorentz gas).

Remark 25.3 Lack of structural stability for D. Expressions like (25.20) may lead to an expectation that the diffusion coefficient (and thus transport properties) are smooth functions of the chaoticity of the system (parameterized, for example, by the Lyapunov exponent $\lambda = \ln \Lambda$). This turns out not to be true: D as a function of Λ is a fractal, nowhere differentiable curve shown in figure 25.5. The dependence of D on the map parameter Λ is rather unexpected - even though for larger Λ more points are mapped outside the unit cell in one iteration, the diffusion constant does not necessarily grow. We refer the reader to refs. [15, 16] for early work on the deterministic diffusion induced by 1-dimensional maps. The sawtooth map (25.9) was introduced by Grossmann and Fujisaka [17] who derived the integer slope formulas (25.20) for the diffusion constant. The sawtooth map is also discussed in refs. [18]. The fractal dependence of diffusion constant on the map parameter is discussed in refs. [9, 8, 10]. Sect. 1.8 gives a brief summary of the experimental implications; for the the current state of the art of fractal transport coefficients consult the first part of Klage's monograph [12]. Would be nice if someone would eventually check these predictions in experiments... Statistical mechanics tend to believe that such complicated behavior is not to be expected in systems with very many degrees of freedom, as the addition to a large integer dimension of a number smaller than 1 should be as unnoticeable as a microscopic perturbation of a macroscopic quantity. No fractal-like behavior of the conductivity for the Lorentz gas has been detected so far [14]. (P. Cvitanović and L. Rondoni)

Remark 25.4 Symmetry factorization in one dimension. In the $\beta = 0$ limit the dynamics (25.11) is symmetric under $x \rightarrow -x$, and the zeta functions factorize into prod-

length	# cycles	$\zeta(0,0)$	λ
1	5	-1.216975	-
2	10	-0.024823	1.745407
3	32	-0.021694	1.719617
4	104	0.000329	1.743494
5	351	0.002527	1.760581
6	1243	0.000034	1.756546

Table 25.1: Fundamental domain, $w=0.3$.

ucts of zeta functions for the symmetric and antisymmetric subspaces, as described in sect. 21.1.1:

$$\begin{aligned} \frac{1}{\zeta(0, z)} &= \frac{1}{\zeta_s(0, z)} \frac{1}{\zeta_a(0, z)} \\ \frac{\partial}{\partial z} \frac{1}{\zeta} &= \frac{1}{\zeta_s} \frac{\partial}{\partial z} \frac{1}{\zeta_a} + \frac{1}{\zeta_a} \frac{\partial}{\partial z} \frac{1}{\zeta_s}. \end{aligned} \tag{25.35}$$

The leading (material flow conserving) eigenvalue $z = 1$ belongs to the symmetric subspace $1/\zeta_s(0, 1) = 0$, so the derivatives (25.15) also depend only on the symmetric subspace:

$$\begin{aligned} \langle n \rangle_\zeta &= z \frac{\partial}{\partial z} \frac{1}{\zeta(0, z)} \Big|_{z=1} \\ &= \frac{1}{\zeta_a(0, z)} z \frac{\partial}{\partial z} \frac{1}{\zeta_s(0, z)} \Big|_{z=1}. \end{aligned} \tag{25.36}$$

Implementing the symmetry factorization is convenient, but not essential, at this level of computation.

Remark 25.5 Lorentz gas in the fundamental domain. The vector valued nature of the generating function (25.3) in the case under consideration makes it difficult to perform a calculation of the diffusion constant within the fundamental domain. Yet we point out that, at least as regards scalar quantities, the full reduction to $\tilde{\mathcal{M}}$ leads to better estimates. A proper symbolic dynamics in the fundamental domain has been introduced in ref. [19].

In order to perform the full reduction for diffusion one should express the dynamical zeta function (25.7) in terms of the prime cycles of the fundamental domain $\tilde{\mathcal{M}}$ of the lattice (see figure 25.2) rather than those of the elementary (Wigner-Seitz) cell \mathcal{M} . This problem is complicated by the breaking of the rotational symmetry by the auxiliary vector β , or, in other words, the non-commutativity of translations and rotations: see ref. [7].

Remark 25.6 Anomalous diffusion. Anomalous diffusion for 1 – dimensional intermittent maps was studied in the continuous time random walk approach in refs. [10, 11]. The first approach within the framework of cycle expansions (based on truncated dynamical zeta functions) was proposed in ref. [12]. Our treatment follows methods introduced in ref. [13], applied there to investigate the behavior of the Lorentz gas with unbounded horizon.

Remark 25.7 Jonquière functions. In statistical mechanics Jonquière function (25.29) appears in the theory of free Bose-Einstein gas, see refs. [22, 23].

Exercises

25.1. **Diffusion for odd integer Λ .** Show that when the slope $\Lambda = 2k - 1$ in (25.9) is an odd integer, the diffusion constant is given by $D = (\Lambda^2 - 1)/24$, as stated in (25.21).

25.2. **Fourth-order transport coefficient.** Verify (25.24). You will need the identity

$$\sum_{k=1}^n k^4 = \frac{1}{30}n(n+1)(2n+1)(3n^2+3n-1).$$

25.3. **Finite Markov partitions.** Verify (25.28).

25.4. **Maps with variable peak shape:** Consider the following piecewise linear map

$$f_\delta(x) = \begin{cases} \frac{3x}{1-\delta} & x \in \mathcal{M}_1 \\ \frac{3}{2} - \left(\frac{2}{\delta} \left| \frac{4-\delta}{12} - x \right| \right) & x \in \mathcal{M}_2 \\ 1 - \frac{3}{1-\delta} \left(x - \frac{1}{6}(2+\delta) \right) & x \in \mathcal{M}_3 \end{cases} \quad (25.37)$$

where $\mathcal{M}_1 = [0, \frac{1}{3}(1-\delta)]$, $\mathcal{M}_2 = [\frac{1}{3}(1-\delta), \frac{1}{6}(2+\delta)]$, $\mathcal{M}_3 = [\frac{1}{6}(2+\delta), \frac{1}{2}]$, and the map in $[1/2, 1]$ is obtained by antisymmetry with respect to $x = 1/2, y = 1/2$. Write the corresponding dynamical zeta function relevant to diffusion and then show that

$$D = \frac{\delta(2+\delta)}{4(1-\delta)}$$

See refs. [21, 22] for further details.

25.5. **Two-symbol cycles for the Lorentz gas.** Write down all cycles labeled by two symbols, such as (0 6), (1 7), (1 5) and (0 5).

ChaosBook.org/pages offers several project-length deterministic diffusion exercises.

25.6. **Accelerated diffusion.** (medium difficulty) Consider a map h , such that $\hat{h} = \hat{f}$ of figure 25.6 (b), but now running branches are turned into standing branches and vice

versa, so that 1, 2, 3, 4 are standing while 0 leads to both positive and negative jumps. Build the corresponding dynamical zeta function and show that

$$\sigma^{-2}(t) \sim \begin{cases} t & \text{for } \alpha > 2 \\ t \ln t & \text{for } \alpha = 2 \\ t^{3-\alpha} & \text{for } \alpha \in (1, 2) \\ t^2 / \ln t & \text{for } \alpha = 1 \\ t^2 & \text{for } \alpha \in (0, 1) \end{cases}$$

25.7. **Recurrence times for Lorentz gas with infinite horizon.** Consider the Lorentz gas with unbounded horizon with a square lattice geometry, with disk radius R and unit lattice spacing. Label disks according to the (integer) coordinates of their center: the sequence of recurrence times $\{t_j\}$ is given by the set of collision times. Consider orbits that leave the disk sitting at the origin and hit a disk far away after a free flight (along the horizontal corridor). Initial conditions are characterized by coordinates (ϕ, α) (ϕ determines the initial position along the disk, while α gives the angle of the initial velocity with respect to the outward normal: the appropriate measure is then $d\phi \cos \alpha d\alpha$ ($\phi \in [0, 2\pi)$, $\alpha \in [-\pi/2, \pi/2]$). Find how $\phi(T)$ scales for large values of T : this is equivalent to investigating the scaling of portions of the state space that lead to a first collision with disk $(n, 1)$, for large values of n (as $n \mapsto \infty, n \simeq T$).

25.8. **Diffusion reduced to the fundamental domain.**



Maps such as figure 25.3 are antisymmetric. Reduce such antisymmetric maps as in example 9.3, and write down the formula (25.14) for the diffusion constant D in terms of the fundamental domain cycles (relative periodic orbits) alone (P. Gaspard says it cannot be done [7]).

References

- [25.1] J. Machta and R. Zwanzig, *Phys. Rev. Lett.* **50**, 1959 (1983).
 [25.2] G.P. Morriss and L. Rondoni, *J. Stat. Phys.* **75**, 553 (1994).

- [25.3] L. Rondoni and G.P. Morriss, “Stationary nonequilibrium ensembles for thermostated systems,” *Phys. Rev. E* **53**, 2143 (1996).
- [25.4] H.A. Lorentz, *Proc. Amst. Acad.* **7**, 438 (1905).
- [25.5] R. Artuso, *Phys. Lett. A* **160**, 528 (1991).
- [25.6] W.N. Vance, *Phys. Rev. Lett.* **96**, 1356 (1992).
- [25.7] P. Cvitanović, J.-P. Eckmann, and P. Gaspard, *Chaos, Solitons and Fractals* **6**, 113 (1995).
- [25.8] R. Klages and J.R. Dorfman, “Simple Maps with Fractal Diffusion Coefficients,” *Phys. Rev. Lett.* **74**, 387 (1995);
[arXiv:chao-dyn/9407018](https://arxiv.org/abs/chao-dyn/9407018).
- [25.9] R. Klages, *Deterministic diffusion in one-dimensional chaotic dynamical systems* (Wissenschaft & Technik-Verlag, Berlin, 1996);
www.mpipks-dresden.mpg.de/~rklages/publ/phd.html.
- [25.10] R. Klages and J.R. Dorfman, “Dynamical crossover in deterministic diffusion,” *Phys. Rev. E* **55**, R1247 (1997).
- [25.11] R. Klages and J.R. Dorfman, “Simple deterministic dynamical systems with fractal diffusion coefficients,” *Phys. Rev. E* **59**, 5361 (1999).
- [25.12] R. Klages, *Microscopic Chaos, Fractals and Transport in Nonequilibrium Statistical Mechanics*, (World Scientific, Singapore 2007).
- [25.13] G. Keller, P. Howard and R. Klages, “Continuity properties of transport coefficients in simple maps,” *Nonlinearity* **21**, 1719 (2008).
- [25.14] J. Lloyd, M. Niemeyer, L. Rondoni and G.P. Morriss, *CHAOS* **5**, 536 (1995).
- [25.15] T. Geisel and J. Nierwetberg, *Phys. Rev. Lett.* **48**, 7 (1982).
- [25.16] M. Schell, S. Fraser and R. Kapral, *Phys. Rev. A* **26**, 504 (1982).
- [25.17] S. Grossmann, H. Fujisaka, *Phys. Rev. A* **26**, 1179 (1982); H. Fujisaka and S. Grossmann, *Z. Phys. B* **48**, 261 (1982).
- [25.18] P. Gaspard and F. Baras, in M. Mareschal and B.L. Holian, eds., *Microscopic simulations of Complex Hydrodynamic Phenomena* (Plenum, NY 1992).
- [25.19] F. Christiansen, Master’s Thesis, Univ. of Copenhagen (June 1989).
- [25.20] P. Cvitanović, P. Gaspard, and T. Schreiber, “Investigation of the Lorentz Gas in terms of periodic orbits,” *CHAOS* **2**, 85 (1992).
- [25.21] S. Grossmann and S. Thomae, *Phys. Lett. A* **97**, 263 (1983).
- [25.22] R. Artuso, G. Casati and R. Lombardi, *Physica A* **205**, 412 (1994).
- [25.23] I. Dana and V.E. Chernov, “Periodic orbits and chaotic-diffusion probability distributions,” *Physica A* **332**, 219 (2004).

Chapter 26

Turbulence?

I am an old man now, and when I die and go to Heaven there are two matters on which I hope enlightenment. One is quantum electro-dynamics and the other is turbulence of fluids. About the former, I am rather optimistic.

—Sir Horace Lamb

THERE IS ONLY ONE honorable cause that would justify sweating through so much formalism - this is but the sharpening of a pencil in order that we may attack the Navier-Stokes equation,



$$\rho \left(\frac{\partial \mathbf{u}}{\partial t} + \mathbf{u} \cdot \nabla \mathbf{u} \right) = -\nabla p + \nu \nabla^2 \mathbf{u} + \mathbf{f}, \quad (26.1)$$

and solve the problem of turbulence.

Flows described by partial differential equations [PDEs] are said to be ‘infinite dimensional’ because if one writes them down as a set of ordinary differential equations [ODEs], one needs infinitely many of them to represent the dynamics of one partial differential equation. Even though the state space is infinite-dimensional, the long-time dynamics of many systems of physical interest is finite-dimensional, contained within an *inertial manifold*.

Being realistic, we are not so foolhardy to immediately plunge into *the* problem – there are too many dimensions and indices. Instead, we start small, in one spatial dimension, $\mathbf{u} \rightarrow u$, $\mathbf{u} \cdot \nabla \mathbf{u} \rightarrow u \partial_x$, assume constant ρ , forget about the pressure p , and so on. This line of reasoning, as well as many other equally sensible threads of thought, such as the amplitude equations obtained via weakly nonlinear stability analysis of steady flows, leads to a small set of frequently studied nonlinear PDEs, like the one that we turn to now.

26.1 Fluttering flame front

Romeo: ‘Misshapen chaos of well seeming forms!’

—W. Shakespeare, *Romeo and Julliet*, Act I, Scene I

The Kuramoto-Sivashinsky [KS] system describes the flame front flutter of gas burning on your kitchen stove, figure 26.1 (a), and many other problems of greater import, is one of the simplest nonlinear systems that exhibit ‘turbulence’ (in this context often referred to more modestly as ‘spatiotemporally chaotic behavior’). The time evolution of the ‘flame front velocity’ $u = u(x, t)$ on a periodic domain $u(x, t) = u(x + L, t)$ is given by

$$u_t + \frac{1}{2}(u^2)_x + u_{xx} + u_{xxxx} = 0, \quad x \in [0, L]. \quad (26.2)$$

In this equation t is the time and x is the spatial coordinate. The subscripts x and t denote partial derivatives with respect to x and t : $u_t = \partial u / \partial t$, u_{xxxx} stands for the 4th spatial derivative of $u = u(x, t)$ at position x and time t . In what follows we use interchangeably the “dimensionless system size” \tilde{L} , or the periodic domain size $L = 2\pi\tilde{L}$, as the system parameter. We take note, as in the Navier-Stokes equation (26.1), of the “inertial” term $u\partial_x u$, the “anti-diffusive” term $\partial_x^2 u$ (with a “wrong” sign), etc..

The term $(u^2)_x$ makes this a *nonlinear system*. This is one of the simplest conceivable nonlinear PDE, playing the role in the theory of spatially extended systems a bit like the role that the x^2 nonlinearity plays in the dynamics of iterated mappings. The time evolution of a typical solution of the Kuramoto-Sivashinsky system is illustrated by figure 26.1 (b).

section 3.3

remark 26.1

Spatial periodicity $u(x, t) = u(x + L, t)$ makes it convenient to work in the Fourier space,

$$u(x, t) = \sum_{k=-\infty}^{+\infty} a_k(t) e^{ikx/\tilde{L}}, \quad (26.3)$$

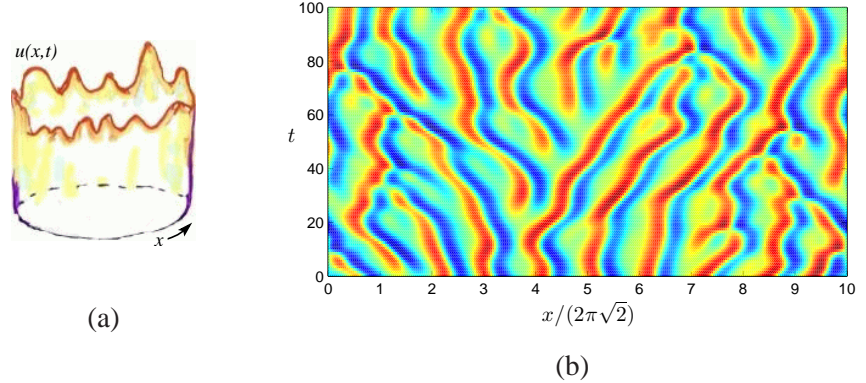
with the 1-dimensional PDE (26.2) replaced by an infinite set of ODEs for the complex Fourier coefficients $a_k(t)$:

$$\dot{a}_k = v_k(a) = ((k/\tilde{L})^2 - (k/\tilde{L})^4) a_k - i \frac{k}{2\tilde{L}} \sum_{m=-\infty}^{+\infty} a_m a_{k-m}. \quad (26.4)$$

Since $u(x, t)$ is real, $a_k = a_{-k}^*$, and we can replace the sum in (26.10) by a sum over $k > 0$.

Due to the hyperviscous damping u_{xxxx} , long time solutions of Kuramoto-Sivashinsky equation are smooth, a_k drop off fast with k , and truncations of (26.10)

Figure 26.1: (a) Kuramoto-Sivashinsky dynamics visualized as the Bunsen burner flame flutter, with $u = u(x, t)$ the “velocity of the flame front” at position x and time t . (b) A typical “turbulent” solution of the Kuramoto-Sivashinsky equation, system size $L = 88.86$. The color (gray scale) indicates the value of u at a given position and instant in time. The x coordinate is scaled with the most unstable wavelength $2\pi\sqrt{2}$, which is approximately also the mean wavelength of the turbulent flow. The dynamics is typical of a large system, in this case approximately 10 mean wavelengths wide. (from ref. [14])



to N terms, $16 \leq N \leq 128$, yield highly accurate solutions for system sizes considered here. Robustness of the Fourier representation of KS as a function of the number of modes kept in truncations of (26.10) is, however, a subtle issue. Adding an extra mode to a truncation of the system introduces a small perturbation. However, this can (and often will) throw the dynamics into a different asymptotic state. A chaotic attractor for $N = 15$ can collapse into an attractive period-3 cycle for $N = 16$, and so on. If we compute, for example, the Lyapunov exponent $\lambda(\tilde{L}, N)$ for a strange attractor of the system (26.10), there is no reason to expect $\lambda(\tilde{L}, N)$ to smoothly converge to a limit value $\lambda(\tilde{L}, \infty)$ as $N \rightarrow \infty$, because of the lack of structural stability both as a function of truncation N , and the system size \tilde{L} . The topology is more robust for \tilde{L} windows of transient turbulence, where the system can be structurally stable, and it makes sense to compute Lyapunov exponents, escape rates, etc., for the repeller, i.e., the closure of the set of all unstable periodic orbits.

Spatial representations of PDEs (such as the 3d snapshots of velocity and vorticity fields in Navier-Stokes) offer little insight into detailed dynamics of low- Re flows. Much more illuminating are the state space representations.

The objects explored in this paper: equilibria and short periodic orbits, are robust both under mode truncations and small system parameter \tilde{L} changes.

26.1.1 Scaling and symmetries

The Kuramoto-Sivashinsky equation (26.2) is space translationally invariant, time translationally invariant, and invariant under reflection $x \rightarrow -x$, $u \rightarrow -u$.

Comparing u_t and $(u^2)_x$ terms we note that u has dimensions of $[x]/[t]$, hence u is the “velocity,” rather than the “height” of the flame front. Indeed, the Kuramoto-Sivashinsky equation is Galilean invariant: if $u(x, t)$ is a solution, then $v + u(x +$

$2vt, t)$, with v an arbitrary constant velocity, is also a solution. Without loss of generality, in our calculations we shall work in the mean zero velocity frame

$$\int dx u = 0. \quad (26.5)$$

In terms of the system size L , the only length scale available, the dimensions of terms in (26.2) are $[x] = L$, $[t] = L^2$, $[u] = L^{-1}$, $[v] = L^2$. Scaling out the “viscosity” ν

$$x \rightarrow x\nu^{\frac{1}{2}}, \quad t \rightarrow t\nu, \quad u \rightarrow u\nu^{-\frac{1}{2}},$$

brings the Kuramoto-Sivashinsky equation (26.2) to a non-dimensional form

$$u_t = (u^2)_x - u_{xx} - u_{xxxx}, \quad x \in [0, L\nu^{-\frac{1}{2}}] = [0, 2\pi\tilde{L}]. \quad (26.6)$$

In this way we trade in the “viscosity” ν and the system size L for a single dimensionless system size parameter

$$\tilde{L} = L/(2\pi\sqrt{\nu}) \quad (26.7)$$

which plays the role of a “Reynolds number” for the Kuramoto-Sivashinsky system.

In the literature sometimes L is used as the system parameter, with ν fixed to 1, and at other times ν is varied with L fixed to either 1 or 2π . To minimize confusion, in what follows we shall state results of all calculations in units of dimensionless system size \tilde{L} . Note that the time units also have to be rescaled; for example, if T_p^* is a period of a periodic solution of (26.2) with a given ν and $L = 2\pi$, then the corresponding solution of the non-dimensionalized (26.6) has period

$$T_p = T_p^*/\nu. \quad (26.8)$$

26.1.2 Fourier space representation

Spatial periodic boundary condition $u(x, t) = u(x + 2\pi\tilde{L}, t)$ makes it convenient to work in the Fourier space,

$$u(x, t) = \sum_{k=-\infty}^{+\infty} b_k(t) e^{ikx/\tilde{L}}. \quad (26.9)$$

with (26.6) replaced by an infinite tower of ODEs for the Fourier coefficients:

$$\dot{b}_k = (k/\tilde{L})^2 \left(1 - (k/\tilde{L})^2\right) b_k + i(k/\tilde{L}) \sum_{m=-\infty}^{+\infty} b_m b_{k-m}. \quad (26.10)$$

This is the infinite set of ordinary differential equations promised in this chapter's introduction.

Since $u(x, t)$ is real, $b_k = b_{-k}^*$, so we can replace the sum over m in (26.10) by a sum over $m > 0$. As $\dot{b}_0 = 0$, b_0 is a conserved quantity, in our calculations fixed to $b_0 = 0$ by the vanishing mean $\langle u \rangle$ condition (26.5) for the front velocity.

Example 26.1 Kuramoto-Sivashinsky antisymmetric subspace: *The Fourier coefficients b_k are in general complex numbers. We can isolate the antisymmetric subspace $u(x, t) = -u(-x, t)$ by considering the case of b_k pure imaginary, $b_k = ia_k$, where $a_k = -a_{-k}$ are real, with the evolution equations*

$$\dot{a}_k = (k/\tilde{L})^2 \left(1 - (k/\tilde{L})^2\right) a_k - (k/\tilde{L}) \sum_{m=-\infty}^{+\infty} a_m a_{k-m}. \quad (26.11)$$

By picking this subspace we eliminate the continuous translational symmetry from our considerations; that is not an option for an experimentalist, but will do for our purposes. In the antisymmetric subspace the translational invariance of the full system reduces to the invariance under discrete translation by half a spatial period L . In the Fourier representation (26.11) this corresponds to invariance under

$$a_{2m} \rightarrow a_{2m}, a_{2m+1} \rightarrow -a_{2m+1}. \quad (26.12)$$

The antisymmetric condition amounts to imposing $u(0, t) = 0$ boundary condition.

26.2 Infinite-dimensional flows: Numerics

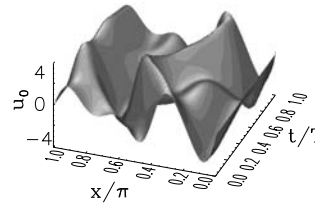
The computer is not a mere mathematical excrescence, useful for technological ends. Rather, I believe that it is a meta-development that might very well change what mathematics is considered to be.

— P. J. Davis [1]

The trivial solution $u(x, t) = 0$ is an equilibrium point of (26.2), but that is basically all we know as far as useful analytical solutions are concerned. To develop some intuition about the dynamics we turn to numerical simulations.

How are solutions such as figure 26.1 (b) computed? The salient feature of such partial differential equations is a theorem saying that for state space contracting flows, the asymptotic dynamics is describable by a *finite* set of “inertial

Figure 26.2: Spatiotemporally periodic solution $u_0(x, t)$, with period $T_0 = 30.0118$. The antisymmetric subspace, $u(x, t) = -u(-x, t)$, so we plot $x \in [0, L/2]$. System size $\tilde{L} = 2.89109$, $N = 16$ Fourier modes truncation. (From ref. [5])



manifold” ordinary differential equations. How you solve the equation (26.2) numerically is up to you. Here are some options:

Discrete mesh: You can divide the x interval into a sufficiently fine discrete grid of N points, replace space derivatives in (26.2) by approximate discrete derivatives, and integrate a finite set of first order differential equations for the discretized spatial components $u_j(t) = u(jL/N, t)$, by any integration routine you trust.

Fourier modes: You can integrate numerically the Fourier modes (26.10), truncating the ladder of equations to a finite number of modes N , i.e., set $a_k = 0$ for $k > N$. In the applied mathematics literature more sophisticated variants of such truncations are called *Galerkin truncations*, or *Galerkin projections*. You need to worry about “stiffness” of the equations and the stability of your integrator. For the parameter values explored in this chapter, truncations N in range 16 to 64 yields sufficient accuracy.

exercise 2.6

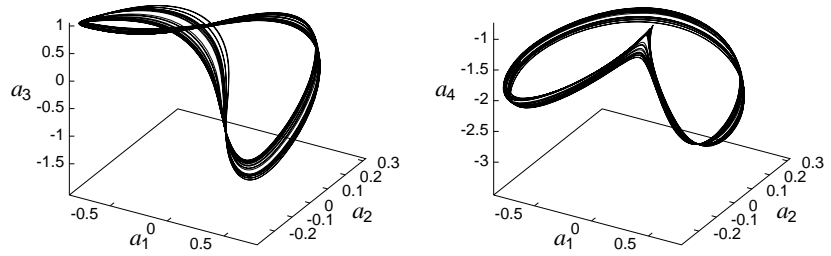
Pseudo-spectral methods: You can mix the two methods, exploiting the speed of Fast Fourier Transforms.

Example 26.2 Kuramoto-Sivashinsky simulation, antisymmetric subspace: To get started, we set $\nu = 0.029910$, $L = 2\pi$ in the Kuramoto-Sivashinsky equation (26.2), or, equivalently, $\nu = 1$, $L = 36.33052$ in the non-dimensionalized (26.6). Consider the antisymmetric subspace (26.11), so the non-dimensionalized system size is $\tilde{L} = L/4\pi = 2.89109$. Truncate (26.11) to $0 \leq k \leq 16$, and integrate an arbitrary initial condition. Let the transient behavior settle down.

Why this \tilde{L} ? For this system size \tilde{L} the dynamics appears to be chaotic, as far as can be determined numerically. Why $N = 16$? In practice one repeats the same calculation at different truncation cutoffs N , and makes sure that the inclusion of additional modes has no effect within the desired accuracy. For this system size $N = 16$ suffices.

Once a trajectory is computed in Fourier space, we can recover and plot the corresponding spatiotemporal pattern $u(x, t)$ over the configuration space using (26.9), as in figure 26.1 (b) and figure 26.2. Such patterns give us a qualitative picture of the flow, but no detailed dynamical information; for that, tracking the evolution in a high-dimensional state space, such as the space of Fourier modes, is much more informative.

Figure 26.3: Projections of a typical 16-dimensional trajectory onto different 3-dimensional subspaces, coordinates (a) $\{a_1, a_2, a_3\}$, (b) $\{a_1, a_2, a_4\}$. System size $\tilde{L} = 2.89109$, $N = 16$ Fourier modes truncation. (From ref. [5].)



26.3 Visualization

The ultimate goal, however, must be a rational theory of statistical hydrodynamics where $[\cdot \cdot \cdot]$ properties of turbulent flow can be mathematically deduced from the fundamental equations of hydromechanics.

—E. Hopf

The problem with high-dimensional representations, such as truncations of the infinite tower of equations (26.10), is that the dynamics is difficult to visualize. The best we can do without much programming is to examine the trajectory's projections onto any three axes a_i, a_j, a_k , as in figure 26.3.

section 26.3

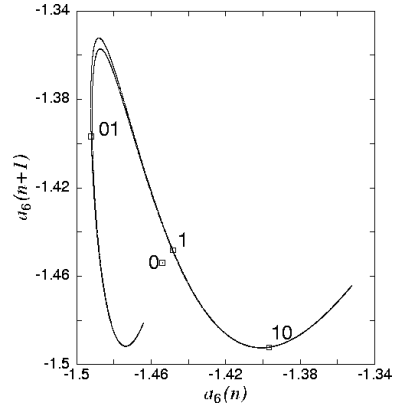
The question is: how is one to look at such a flow? It is not clear that restricting the dynamics to a Poincaré section necessarily helps - after all, a section reduces a $(d + 1)$ -dimensional flow to a d -dimensional map, and how much is gained by replacing a continuous flow in 16 dimensions by a set of points in 15 dimensions? The next example illustrates the utility of visualization of dynamics by means of Poincaré sections.

Example 26.3 Kuramoto-Sivashinsky Poincaré return maps: Consider the Kuramoto-Sivashinsky equation in the N Fourier modes representation. We pick (arbitrarily) the hyperplane $a_1 = 0$ as the Poincaré section, and integrate (26.10) with $a_1 = 0$, and an arbitrary initial point (a_2, \dots, a_N) . When the flow crosses the $a_1 = 0$ hyperplane in the same direction as initially, the initial point is mapped into $(a'_2, \dots, a'_N) = P(a_2, \dots, a_N)$. This defines P , the Poincaré return map (3.1) of the $(N - 1)$ -dimensional $a_1 = 0$ hyperplane into itself.

Figure 26.4 is a typical result. We have picked - again arbitrarily - a subspace such as $a_6(n + 1)$ vs. $a_6(n)$ in order to visualize the dynamics. While the topology of the attractor is still obscure, one thing is clear: even though the flow state space is infinite dimensional, the attractor is finite and thin, barely thicker than a line.

The above example illustrates why a Poincaré section gives a more informative snapshot of the flow than the full flow portrait. While no fine structure is discernible in the full state space flow portraits of the Kuramoto-Sivashinsky dynamics, figure 26.3, the Poincaré return map figure 26.4 reveals the fractal structure in the asymptotic attractor.

Figure 26.4: The attractor of the Kuramoto-Sivashinsky system (26.10), plotted as the a_6 component of the $a_1 = 0$ Poincaré section return map. Here 10,000 Poincaré section returns of a typical trajectory are plotted. Also indicated are the periodic points 0, 1, 01 and 10. System size $\tilde{L} = 2.89109$, $N = 16$ Fourier modes truncation. (From ref. [5].)



In order to find a better representation of the dynamics, we now turn to its topological invariants.

26.4 Equilibria of equilibria

(Y. Lan and P. Cvitanović)

The set of equilibria and their stable / unstable manifolds form the coarsest topological framework for organizing state space orbits.

The equilibrium condition $u_t = 0$ for the Kuramoto-Sivashinsky equation PDE (26.6) is the ODE

$$(u^2)_x - u_{xx} - u_{xxx} = 0$$

which can be analyzed as a dynamical system in its own right. Integrating once we get

$$u^2 - u_x - u_{xxx} = c, \tag{26.13}$$

where c is an integration constant whose value strongly influences the nature of the solutions. Written as a 3-dimensional dynamical system with spatial coordinate x playing the role of “time,” this is a volume preserving flow

$$u_x = v, \quad v_x = w, \quad w_x = u^2 - v - c, \tag{26.14}$$

with the “time” reversal symmetry,

$$x \rightarrow -x, \quad u \rightarrow -u, \quad v \rightarrow v, \quad w \rightarrow -w.$$

From (26.14) we see that

$$(u + w)_x = u^2 - c.$$

If $c < 0$, $u + w$ increases without bound with $x \rightarrow \infty$, and every solution escapes to infinity. If $c = 0$, the origin $(0, 0, 0)$ is the only bounded solution.

For $c > 0$ there is much c -dependent interesting dynamics, with complicated fractal sets of bounded solutions. The sets of the solutions of the equilibrium condition (26.14) are themselves in turn organized by the equilibria of the equilibrium condition, and the connections between them. For $c > 0$ the equilibrium points of (26.14) are $c_+ = (\sqrt{c}, 0, 0)$ and $c_- = (-\sqrt{c}, 0, 0)$. Linearization of the flow around c_+ yields Floquet multipliers $[2\lambda, -\lambda \pm i\theta]$ with

$$\lambda = \frac{1}{\sqrt{3}} \sinh \phi, \quad \theta = \cosh \phi,$$

and ϕ fixed by $\sinh 3\phi = 3\sqrt{3c}$. Hence c_+ has a 1-dimensional unstable manifold and a 2-dimensional stable manifold along which solutions spiral in. By the $x \rightarrow -x$ “time reversal” symmetry, the invariant manifolds of c_- have reversed stability properties.

The non-wandering set for this dynamical system is quite pretty, and surprisingly hard to analyze. However, we do not need to explore the fractal set of the Kuramoto-Sivashinsky equilibria for infinite size system here; for a fixed system size L with periodic boundary condition, the only surviving equilibria are those with periodicity L . They satisfy the equilibrium condition for (26.10)

$$(k/\tilde{L})^2 \left(1 - (k/\tilde{L})^2\right) b_k + i(k/\tilde{L}) \sum_{m=-\infty}^{+\infty} b_m b_{k-m} = 0. \quad (26.15)$$

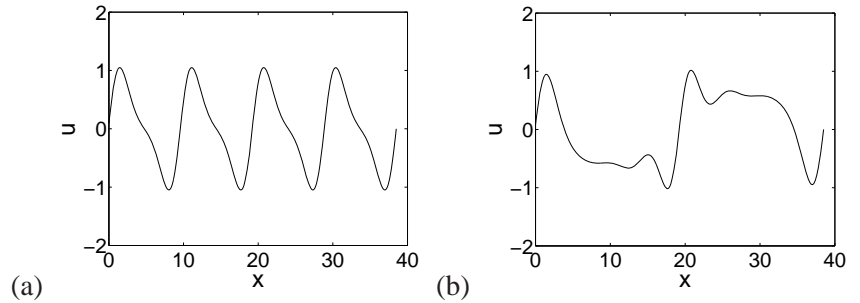
Periods of spatially periodic equilibria are multiples of L . Every time \tilde{L} crosses an integer value $\tilde{L} = n$, n -cell states are generated through pitchfork bifurcations. In the full state space they form an invariant circle due to the translational invariance of (26.6). In the antisymmetric subspace considered here, they correspond to two points, half-period translates of each other of the form

$$u(x, t) = -2 \sum_k b_{kn} \sin(knx),$$

where $b_{kn} \in \mathbb{R}$.

For any fixed period L the number of spatially periodic solutions is finite up to a spatial translation. This observation can be heuristically motivated as follows.

Figure 26.5: The non-wandering set under study appears to consist of three patches: the left part (S_L), the center part (S_C) and the right part (S_R), each centered around an unstable equilibrium: (a) central C_1 equilibrium, (b) side R_1 equilibrium on the interval $[0, L]$.



Finite dimensionality of the inertial manifold bounds the size of Fourier components of all solutions. On a finite-dimensional compact manifold, an analytic function can only have a finite number of zeros. So, the equilibria, i.e., the zeros of a smooth velocity field on the inertial manifold, are finitely many.

For a sufficiently small L the number of equilibria is small, mostly concentrated on the low wave number end of the Fourier spectrum. These solutions may be obtained by solving the truncated versions of (26.15).

Example 26.4 Some Kuramoto-Sivashinsky equilibria:

26.5 Why does a flame front flutter?

I understood every word.
—Fritz Haake

section 18.2

We start by considering the case where a_q is an equilibrium point (2.8). Expanding around the equilibrium point a_q , and using the fact that the matrix $\mathbf{A} = \mathbf{A}(a_q)$ in (4.2) is constant, we can apply the simple formula (4.31) also to the Jacobian matrix of an equilibrium point of a PDE,

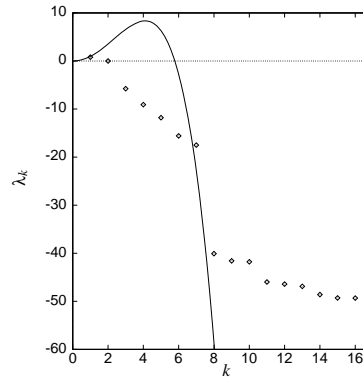
$$J^t(a_q) = e^{\mathbf{A}t} \quad \mathbf{A} = \mathbf{A}(a_q).$$

Example 26.5 Stability matrix, antisymmetric subspace: The Kuramoto-Sivashinsky flat flame front $u(x, t) = 0$ is an equilibrium point of (26.2). The stability matrix (4.3) follows from (26.10)

$$A_{kj}(a) = \frac{\partial v_k(a)}{\partial a_j} = ((k/\tilde{L})^2 - (k/\tilde{L})^4)\delta_{kj} - 2(k/\tilde{L})a_{k-j}. \tag{26.16}$$

For the $u(x, t) = 0$ equilibrium solution the stability matrix is diagonal, and – as in (4.16) – so is the Jacobian matrix $J_{kj}^t(0) = \delta_{kj}e^{((k/\tilde{L})^2 - (k/\tilde{L})^4)t}$.

Figure 26.6: Lyapunov exponents $\lambda_{\Gamma,k}$ versus k for the least unstable spatio-temporally periodic orbit $\bar{\Gamma}$ of the Kuramoto-Sivashinsky system, compared with the Floquet exponents of the $u(x, t) = 0$ stationary solution, $\lambda_k = k^2 - \nu k^4$. The eigenvalue $\lambda_{\Gamma,k}$ for $k \geq 8$ falls below the numerical accuracy of integration and are not meaningful. The cycle $\bar{\Gamma}$ was computed using methods of chapter 13. System size $\tilde{L} = 2.89109$, $N = 16$ Fourier modes truncation. (From ref. [5])



For $\tilde{L} < 1$, $u(x, t) = 0$ is the globally attractive stable equilibrium. As the system size \tilde{L} is increased, the “flame front” becomes increasingly unstable and turbulent, the dynamics goes through a rich sequence of bifurcations on which we shall not dwell here.

The long wavelength perturbations of the flat-front equilibrium are linearly unstable, while all short wavelength perturbations are strongly contractive. The high k eigenvalues, corresponding to rapid variations of the flame front, decay so fast that the corresponding eigen-directions are physically irrelevant. To illustrate the rapid contraction in the non-leading eigen-directions we plot in figure 26.6 the eigenvalues of the equilibrium in the unstable regime, for relatively small system size, and compare them with the Floquet multipliers of the least unstable cycle for the same system size. The equilibrium solution is very unstable, in 5 eigen-directions, the least unstable cycle only in one. Note that for $k > 7$ the rate of contraction is so strong that higher eigen-directions are numerically meaningless for either solution; even though the flow is infinite-dimensional, the attracting set must be rather thin.

While in general for \tilde{L} sufficiently large one expects many coexisting attractors in the state space, in numerical studies most random initial conditions settle converge to the same chaotic attractor.

From (26.10) we see that the origin $u(x, t) = 0$ has Fourier modes as the linear stability eigenvectors. When $|k| \in (0, \tilde{L})$, the corresponding Fourier modes are unstable. The most unstable modes has $|k| = \tilde{L}/\sqrt{2}$ and defines the scale of basic building blocks of the spatiotemporal dynamics of the Kuramoto-Sivashinsky equation in large system size limit.

Consider now the case of initial a_k sufficiently small that the bilinear $a_m a_{k-m}$ terms in (26.10) can be neglected. Then we have a set of decoupled linear equations for a_k whose solutions are exponentials, at most a finite number for which $k^2 > \nu k^4$ is growing with time, and infinitely many with $\nu k^4 > k^2$ decaying in time. The growth of the unstable long wavelengths (low $|k|$) excites the short wavelengths through the $a_m a_{k-m}$ nonlinear term in (26.10). The excitations thus transferred are dissipated by the strongly damped short wavelengths, and a “chaotic equilibrium” can emerge. The very short wavelengths $|k| \gg 1/\sqrt{\nu}$ remain small for all times, but the intermediate wavelengths of order $|k| \sim 1/\sqrt{\nu}$ play an important role in maintaining the dynamical equilibrium. As the damping parameter

Table 26.1: Important Kuramoto-Sivashinsky equilibria: the first few Floquet exponents

S	$\mu^{(1)} \pm i\omega^{(1)}$	$\mu^{(2)} \pm i\omega^{(2)}$	$\mu^{(3)} \pm i\omega^{(3)}$
C_1	$0.04422 \pm i0.26160$	$-0.255 \pm i0.431$	$-0.347 \pm i0.463$
R_1	$0.01135 \pm i0.79651$	$-0.215 \pm i0.549$	$-0.358 \pm i0.262$
T	0.25480	$-0.07 \pm i0.645$	-0.264

decreases, the solutions increasingly take on shock front character poorly represented by the Fourier basis, and many higher harmonics may need to be kept in truncations of (26.10).

Hence, while one may truncate the high modes in the expansion (26.10), care has to be exercised to ensure that no modes essential to the dynamics are chopped away.

In other words, even though our starting point (26.2) is an infinite-dimensional dynamical system, the asymptotic dynamics unfolds on a finite-dimensional attracting manifold, and so we are back on the familiar territory of sect. 2.2: the theory of a finite number of ODEs applies to this infinite-dimensional PDE as well.

We can now start to understand the remark on page 42 that for infinite dimensional systems time reversibility is not an option: evolution forward in time strongly damps the higher Fourier modes. There is no turning back: if we reverse the time, the infinity of high modes that contract strongly forward in time now explodes, instantly rendering evolution backward in time meaningless. As so much you are told about dynamics, this claim is also wrong, in a subtle way: if the initial $u(x, 0)$ is in the non-wandering set (2.2), the trajectory is well defined both forward and backward in time. For practical purposes, this subtlety is not of much use, as any time-reversed numerical trajectory in a finite-mode truncation will explode very quickly, unless special precautions are taken.

When is an equilibrium important? There are two kinds of roles equilibria play:

“Hole” in the natural measure. The more unstable eigen-directions it has (for example, the $u = 0$ solution), the more unlikely it is that an orbit will recur in its neighborhood.

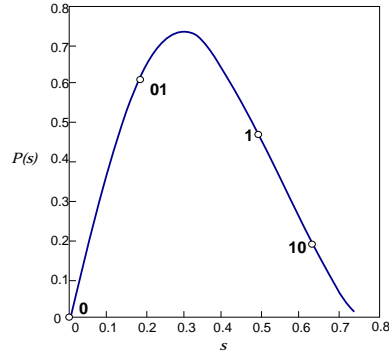
unstable manifold of a “least unstable” equilibrium. Asymptotic dynamics spends a large fraction of time in neighborhoods of a few equilibria with only a few unstable eigen-directions.

Example 26.6 Stability of Kuramoto-Sivashinsky equilibria:

spiraling out in a plane, all other directions contracting

Stability of “center” equilibrium

Figure 26.7: The Poincaré return map of the Kuramoto-Sivashinsky system (26.10) figure 26.4, from the unstable manifold of the $\bar{1}$ fixed point to the (neighborhood of) the unstable manifold. Also indicated are the periodic points $\bar{0}$ and $\bar{01}$.



linearized Floquet exponents:

$$(\mu^{(1)} \pm i\omega^{(1)}, \mu^{(2)} \pm i\omega^{(2)}, \dots) = (0.044 \pm i0.262, -0.255 \pm i0.431, \dots)$$

The plane spanned by $\mu^{(1)} \pm i\omega^{(1)}$ eigenvectors rotates with angular period $T \approx 2\pi/\omega^{(1)} = 24.02$.

a trajectory that starts near the C_1 equilibrium point spirals away per one rotation with multiplier $\Lambda_{radial} \approx \exp(\mu^{(1)}T) = 2.9$.

each Poincaré section return, contracted into the stable manifold by factor of $\Lambda_2 \approx \exp(\mu^{(2)}T) = 0.002$

The local Poincaré return map is in practice 1 – dimensional

26.6 Periodic orbits

expanding eigenvalue of the least unstable spatio-temporally periodic orbit $\bar{1}$:
 $\Lambda_1 = -2.0\dots$

very thin Poincaré section

thickness \propto least contracting eigenvalue $\Lambda_2 = 0.007\dots$

15 – dimensional \rightarrow 15 – dimensional Poincaré return map projection on the $[a_6 \rightarrow a_6]$ Fourier component is not even $1 \rightarrow 1$.

26.7 Intrinsic parametrization

Both in the Rössler flow of example 3.4, and in the Kuramoto-Sivashinsky system of example 26.3 we have learned that the attractor is very thin, but otherwise the return maps that we found were disquieting – neither figure 3.6 nor figure 26.4 appeared to be one-to-one maps. This apparent loss of invertibility is an artifact of projection of higher-dimensional return maps onto lower-dimensional subspaces. As the choice of lower-dimensional subspace is arbitrary, the resulting snapshots of return maps look rather arbitrary, too. Other projections might look even less suggestive.

Such observations beg a question: Does there exist a “natural,” intrinsically optimal coordinate system in which we should plot of a return map?

As we shall now argue (see also sect. 13.1), the answer is yes: The intrinsic coordinates are given by the stable/unstable manifolds, and a return map should be plotted as a map from the unstable manifold back onto the immediate neighborhood of the unstable manifold.

Examination of numerical plots such as figure 26.3 suggests that a more thoughtful approach would be to find a coordinate transformation $y = h(x)$ to a “center manifold,” such that in the new, curvilinear coordinates large-scale dynamics takes place in (y_1, y_2) coordinates, with exponentially small dynamics in $y_3, y_4 \dots$. But - thinking is extra price - we do not know how to actually accomplish this.

Both in the example of the Rössler flow and of the Kuramoto-Sivashinsky system we sketched the attractors by running a long chaotic trajectory, and noted that the attractors are very thin, but otherwise the return maps that we plotted were disquieting – neither figure 3.6 nor figure 26.4 appeared to be 1-to-1 maps. In this section we show how to use such information to approximately locate cycles.

26.8 Energy budget

The space average of a function $a = a(x, t)$ on the interval L ,

$$\langle a \rangle = \frac{1}{L} \int_0^L dx a(x, t), \quad (26.17)$$

is in general time dependent. Its mean value is given by the time average

$$\bar{a} = \lim_{t \rightarrow \infty} \frac{1}{t} \int_0^t d\tau \langle a \rangle = \lim_{t \rightarrow \infty} \frac{1}{tL} \int_0^t \int_0^L d\tau dx a(x, \tau). \quad (26.18)$$

The mean value \bar{a} , $a = a(u)$ evaluated on an equilibrium or relative equilibrium $u(x, t) = u_q(x - ct)$ is

$$a_q = \langle a \rangle_q. \quad (26.19)$$

Evaluation of the infinite time average (26.18) on a function of a period T_p periodic orbit or relative periodic orbit $u_p(x, t)$ requires only a single traversal of the periodic solution,

$$a_p = \frac{1}{T_p} \int_0^{T_p} d\tau \langle a \rangle. \quad (26.20)$$

Equation (26.2) can be written as

$$u_t = -V_x, \quad V(x, t) = \frac{1}{2}u^2 + u_x + u_{xxx}. \quad (26.21)$$

u is related to the “flame-front height” $h(x, t)$ by $u = h_x$, so E can be interpreted as the mean energy density (26.22). So, even though KS is a phenomenological small-amplitude equation, the time-dependent quantity

$$E = \frac{1}{L} \int_0^L dx V(x, t) = \frac{1}{L} \int_0^L dx \frac{u^2}{2} \quad (26.22)$$

has a physical interpretation as the average “energy” density of the flame front. This analogy to the corresponding definition of the mean kinetic energy density for the Navier-Stokes will be useful in what follows.

The energy (26.22) is also the quadratic norm in the Fourier space,

$$E = \sum_{k=1}^{\infty} E_k, \quad E_k = \frac{1}{2}|a_k|^2. \quad (26.23)$$

Take time derivative of the energy density (26.22), substitute (26.2) and integrate by parts. Total derivatives vanish by the spatial periodicity on the L domain:

$$\begin{aligned} \dot{E} &= \langle u_t u \rangle = - \left\langle \left(\frac{u^2}{2} + u u_x + u u_{xxx} \right)_x u \right\rangle \\ &= \left\langle +u_x \frac{u^2}{2} + (u_x)^2 + u_x u_{xxx} \right\rangle. \end{aligned} \quad (26.24)$$

For an equilibrium E is constant:

$$\dot{E} = \left\langle \left(\frac{u^2}{2} + u_x + u_{xxx} \right) u_x \right\rangle = E \langle u_x \rangle = 0.$$

The first term in (26.24) vanishes by integration by parts, $\langle (u^3)_x \rangle = 3 \langle u_x u^2 \rangle = 0$, and integrating the third term by parts yet again we get that the energy variation

$$\dot{E} = \langle (u_x)^2 \rangle - \langle (u_{xx})^2 \rangle \quad (26.25)$$

balances the KS equation (26.2) power pumped in by the anti-diffusion u_{xx} against energy dissipated by the hyperviscosity u_{xxx} .

In figure 26.8 we plot the power input $\langle (u_x)^2 \rangle$ vs. dissipation $\langle (u_{xx})^2 \rangle$ for all $L = 22$ equilibria and relative equilibria determined so far, several periodic orbits

Figure 26.8: Power input $\langle (u_x)^2 \rangle$ vs. dissipation $\langle (u_{xx})^2 \rangle$ for $L = 22$ equilibria and relative equilibria, for several periodic orbits and relative periodic orbits, and for a typical “turbulent” state. Note that $\overline{(u_{p,x})^2}$ of the $(T_p, d_p) = (32.8, 10.96)$ relative periodic orbit which appears well embedded within the turbulent state, is close to the turbulent expectation $\overline{(u_x)^2}$ [temporary Japanese heresy].

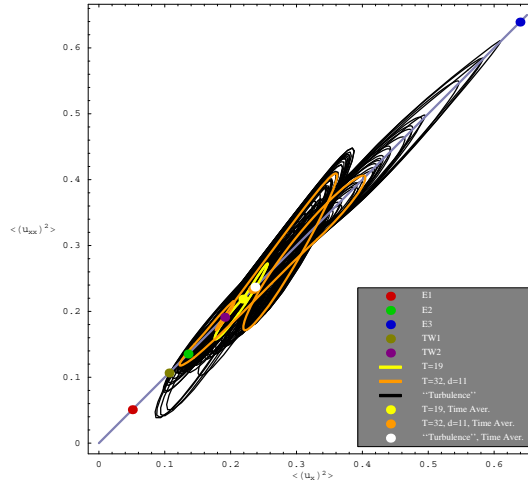
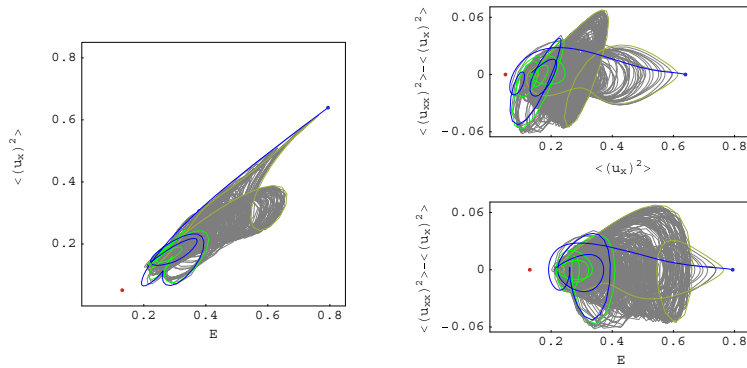


Figure 26.9: EQ_1 (red), EQ_2 (green), EQ_3 (blue), connections from EQ_1 to $A(L/4)EQ_1$ (green), from $A(L/4)EQ_1$ to EQ_1 (yellow-green) and from EQ_3 to $A(L/4)EQ_1$ (blue), along with a generic long-time “turbulent” evolution (grey) for $L = 22$. Three different projections of the $(E, \langle (u_x)^2 \rangle, \langle (u_{xx})^2 \rangle - \langle (u_x)^2 \rangle)$ representation are shown.



and relative periodic orbits, and for a typical “turbulent” evolution. The time averaged energy density \overline{E} computed on a typical orbit goes to a constant, so the expectation values (26.26) of drive and dissipation exactly balance each out:

$$\overline{E} = \lim_{t \rightarrow \infty} \frac{1}{t} \int_0^t d\tau \dot{E} = \overline{(u_x)^2} - \overline{(u_{xx})^2} = 0. \quad (26.26)$$

In particular, the equilibria and relative equilibria sit on the diagonal in figure 26.8, and so do time averages computed on periodic orbits and relative periodic orbits:

$$\begin{aligned} \overline{E}_p &= \frac{1}{T_p} \int_0^{T_p} d\tau E(\tau) \\ \overline{(u_x)^2}_p &= \frac{1}{T_p} \int_0^{T_p} d\tau \langle (u_x)^2 \rangle = \overline{(u_{xx})^2}_p. \end{aligned} \quad (26.27)$$

In the Fourier basis (26.23) the conservation of energy on average takes form

$$0 = \sum_{k=1}^{+\infty} ((k/\tilde{L})^2 - (k/\tilde{L})^4) \overline{E}_k, \quad E_k(t) = |a_k(t)|^2. \quad (26.28)$$

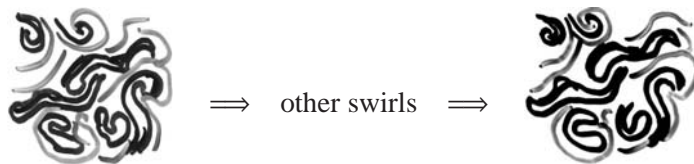
The large k convergence of this series is insensitive to the system size L ; $\overline{E_k}$ have to decrease much faster than $1/(k/L)^4$. Deviation of E_k from this bound for small k determines the active modes. This may be useful to bound the number of equilibria, with the upper bound given by zeros of a small number of long wavelength modes.

Résumé

Turbulence is the graveyard of theories
— Hans W. Liepmann

We have learned that an instanton is an analytic solution of Yang-Mills equations of motion, but shouldn't a strongly nonlinear field theory dynamics be dominated by turbulent solutions? How are we to think about systems where every spatiotemporal solution is unstable?

Here we think of turbulence in spatially extended systems in terms of recurrent spatiotemporal patterns. Pictorially, dynamics drives a given spatially extended system through a repertoire of unstable patterns; as we watch a turbulent system evolve, every so often we catch a glimpse of a familiar pattern:



For any finite spatial resolution, the system follows approximately for a finite time a pattern belonging to a finite alphabet of admissible patterns, and the long term dynamics can be thought of as a walk through the space of such patterns. Recasting this image into mathematics is the subject of this book.

The problem one faces with high-dimensional flows is that their topology is hard to visualize, and that even with a decent starting guess for a point on a periodic orbit, methods like the Newton-Raphson method are likely to fail. Methods that start with initial guesses for a number of points along the cycle, such as the multipoint shooting method of sect. 13.3, are more robust. The relaxation (or variational) methods take this strategy to its logical extreme, and start by a guess of not a few points along a periodic orbit, but a guess of the entire orbit. As these methods are intimately related to variational principles and path integrals, we postpone their introduction to chapter 29.

chapter 29

At present the theory is in practice applicable only to systems with a low intrinsic *dimension* – the minimum number of coordinates necessary to capture its essential dynamics. If the system is very turbulent (a description of its long time dynamics requires a space of very high intrinsic dimension) we are out of luck.

Commentary

Remark 26.1 Model PDE systems. The theorem on finite dimensionality of inertial manifolds of state space contracting PDE flows is proven in ref. [2]. The Kuramoto-Sivashinsky equation was introduced in refs. [3, 4]. Holmes, Lumley and Berkooz [6] offer a delightful discussion of why this system deserves study as a staging ground for studying turbulence in full-fledged Navier-Stokes equation. How good a description of a flame front this equation is not a concern here; suffice it to say that such model amplitude equations for interfacial instabilities arise in a variety of contexts - see e.g. ref. [7] - and this one is perhaps the simplest physically interesting spatially extended nonlinear system.

For equilibria the L -independent bound on E is given by Michelson [8]. The best current bound [9, 10] on the long-time limit of E as a function of the system size L scales as $E \propto L^{3/2}$.

The work described in this chapter was initiated by Putkaradze's 1996 term project (see ChaosBook.org/extras), and continued by Christiansen Cvitanović, Davidchack, Gibson, Halcrow, Lan, and Siminos [5, 11, 12, 16, 15, 14, 15, 13].

Exercises

26.1. Galilean invariance of the Kuramoto-Sivashinsky equation.


- (a) Verify that the Kuramoto-Sivashinsky equation is Galilean invariant: if $u(x, t)$ is a solution, then $v + u(x + 2vt, t)$, with v an arbitrary constant velocity, is also a solution.

- (b) Verify that mean

$$\langle u \rangle = \frac{1}{L} \int_L dx u$$

is conserved by the flow.

- (c) Argue that the choice (26.5) of the vanishing mean velocity, $\langle u \rangle = 0$ leads to no loss of generality in calculations that follow.

- (d)  [thinking is extra cost] Inspection of various “turbulent” solutions of Kuramoto-Sivashinsky equation reveals subregions of “traveling waves” with locally nonzero $\langle u \rangle$. Is there a way to use Galilean invariance locally, even though we eliminated it by the $\langle u \rangle = 0$ condition?

26.2. Infinite dimensional dynamical systems are not smooth.

Many of the operations we consider natural

for finite dimensional systems do not have smooth behavior in infinite dimensional vector spaces. Consider, as an example, a concentration ϕ diffusing on \mathbb{R} according to the diffusion equation

$$\partial_t \phi = \frac{1}{2} \nabla^2 \phi.$$

- (a) Interpret the partial differential equation as an infinite dimensional dynamical system. That is, write it as $\dot{x} = F(x)$ and find the velocity field.

- (b) Show by examining the norm

$$\|\phi\|^2 = \int_{\mathbb{R}} dx \phi^2(x)$$

that the vector field F is not continuous.

- (c) Try the norm

$$\|\phi\| = \sup_{x \in \mathbb{R}} |\phi(x)|.$$

Is F continuous?

- (d) Argue that the semi-flow nature of the problem is not the cause of our difficulties.

- (e) Do you see a way of generalizing these results?

References

- [26.1] P. J. Davis, “Spanning multiple worlds,” *SIAM News* **41** (Dec. 2008).
- [26.2] C. Foias, B. Nicolaenko, G.R. Sell, and R. Témam, “Kuramoto-Sivashinsky equation,” *J. Math. Pures et Appl.* **67**, 197 (1988).
- [26.3] Y. Kuramoto and T. Tsuzuki, “Persistent propagation of concentration waves in dissipative media far from thermal equilibrium,” *Progr. Theor. Physics* **55**, 365 (1976).
- [26.4] G.I. Sivashinsky, “Nonlinear analysis of hydrodynamical instability in laminar flames - I. Derivation of basic equations,” *Acta Astr.* **4**, 1177 (1977).
- [26.5] F. Christiansen, P. Cvitanović and V. Putkaradze, “Spatiotemporal chaos in terms of unstable recurrent patterns,” *Nonlinearity* **10**, 55 (1997); [arXiv:chao-dyn/9606016](#).
- [26.6] P. Holmes, J.L. Lumley and G. Berkooz, *Turbulence, Coherent Structures, Dynamical Systems and Symmetry* (Cambridge U. Press, Cambridge 1996).
- [26.7] I.G. Kevrekidis, B. Nicolaenko and J.C. Scovel, “Back in the saddle again: a computer assisted study of the Kuramoto-Sivashinsky equation,” *SIAM J. Applied Math.* **50**, 760 (1990).
- [26.8] D. Michelson, Steady solutions of the Kuramoto-Sivashinsky equation, *Physica D* **19**, 89 (1986).
- [26.9] L. Giacomelli and F. Otto, New bounds for the Kuramoto-Sivashinsky equation, *Comm. Pure Appl. Math.* **58**, 297 (2005).
- [26.10] J. C. Bronski and T. N. Gambill, Uncertainty estimates and L_2 bounds for the Kuramoto-Sivashinsky equation, *Nonlinearity* **19**, 2023–2039 (2006); [arXiv:math/0508481](#).
- [26.11] “Chaotic field theory: a sketch,” *Physica A* **288**, 61 (2000); [arXiv:nlin.CD/0001034](#).
- [26.12] Y. Lan, *Dynamical systems approach to 1-d spatiotemporal chaos – A cyclist’s view*, Ph.D. thesis, Georgia Inst. of Tech. (2004).
- [26.13] Y. Lan and P. Cvitanović, “Unstable recurrent patterns in Kuramoto-Sivashinsky dynamics,” *Phys. Rev. E* **78**, 026208 (2004); [arXiv:0804.2474](#).
- [26.14] P. Cvitanović, R. L. Davidchack and E. Siminos, “State space geometry of a spatio-temporally chaotic Kuramoto-Sivashinsky flow,” *SIAM J. Applied Dynam. Systems* (2009); [arXiv:0709.2944](#).
- [26.15] J. F. Gibson, J. Halcrow, and P. Cvitanović, “Visualizing the geometry of state-space in plane Couette flow,” *J. Fluid Mech.* **611**, 107 (2008); [arXiv:0705.3957](#).

- [26.16] J. F. Gibson, *Movies of plane Couette* (Georgia Tech, 2009); ChaosBook.org/tutorials.
- [26.17] A. K. Kassam and L. N. Trefethen, "Fourth-order time stepping for stiff PDEs," *SIAM J. Sci. Comp.*, (2004).
- [26.18] Poul Martin Møller, *En dansk Students Eventyr [The Adventures of a Danish Student]* (Copenhagen 1824).

Chapter 27

Irrationally winding

I don't care for islands, especially very small ones.

—D.H. Lawrence

(R. Artuso and P. Cvitanović)

THIS CHAPTER is concerned with the mode locking problems for circle maps: besides its physical relevance it nicely illustrates the use of cycle expansions away from the dynamical setting, in the realm of renormalization theory at the transition to chaos.

The physical significance of circle maps is connected with their ability to model the two-frequencies mode-locking route to chaos for dissipative systems. In the context of *dissipative* dynamical systems one of the most common and experimentally well explored routes to chaos is the two-frequency mode-locking route. Interaction of pairs of frequencies is of deep theoretical interest due to the generality of this phenomenon; as the energy input into a dissipative dynamical system (for example, a Couette flow) is increased, typically first one and then two of intrinsic modes of the system are excited. After two Hopf bifurcations (a fixed point with inward spiralling stability has become unstable and outward spirals to a limit cycle) a system lives on a two-torus. Such systems tend to mode-lock: the system adjusts its internal frequencies slightly so that they fall in step and minimize the internal dissipation. In such case the ratio of the two frequencies is a rational number. An irrational frequency ratio corresponds to a quasiperiodic motion - a curve that never quite repeats itself. If the mode-locked states overlap, chaos sets in. The likelihood that a mode-locking occurs depends on the strength of the coupling of the two frequencies.

Our main concern in this chapter is to illustrate the “global” theory of circle maps, connected with universality properties of the whole irrational winding set. We shall see that critical global properties may be expressed via cycle expansions involving “local” renormalization critical exponents. The renormalization theory of critical circle maps demands rather tedious numerical computations, and our

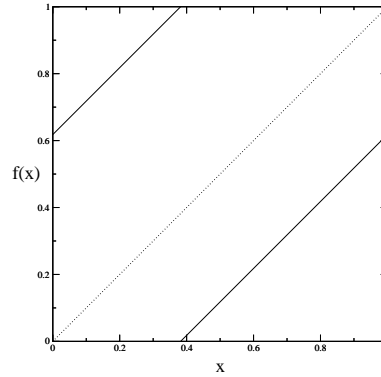


Figure 27.1: Unperturbed circle map ($k = 0$ in (27.1)) with golden mean rotation number.

intuition is much facilitated by approximating circle maps by number-theoretic models. The models that arise in this way are by no means mathematically trivial, they turn out to be related to number-theoretic abysses such as the Riemann conjecture, already in the context of the “trivial” models.

27.1 Mode locking

The simplest way of modeling a nonlinearly perturbed rotation on a circle is by 1-dimensional circle maps $x \rightarrow x' = f(x)$, restricted to the one dimensional torus, such as the *sine map*

$$x_{n+1} = f(x_n) = x_n + \Omega - \frac{k}{2\pi} \sin(2\pi x_n) \quad \text{mod } 1 . \tag{27.1}$$

$f(x)$ is assumed to be continuous, have a continuous first derivative, and a continuous second derivative at the inflection point (where the second derivative vanishes). For the generic, physically relevant case (the only one considered here) the inflection is cubic. Here k parametrizes the strength of the nonlinear interaction, and Ω is the *bare* frequency.

The state space of this map, the unit interval, can be thought of as the elementary cell of the map

$$\hat{x}_{n+1} = \hat{f}(\hat{x}_n) = \hat{x}_n + \Omega - \frac{k}{2\pi} \sin(2\pi \hat{x}_n) . \tag{27.2}$$

where $\hat{\cdot}$ is used in the same sense as in chapter 25.

The winding number is defined as

$$W(k, \Omega) = \lim_{n \rightarrow \infty} (\hat{x}_n - \hat{x}_0)/n. \tag{27.3}$$

and can be shown to be independent of the initial value \hat{x}_0 .

For $k = 0$, the map is a simple rotation (the *shift map*) see figure 27.1

$$x_{n+1} = x_n + \Omega \pmod{1}, \tag{27.4}$$

and the rotation number is given by the parameter Ω .

$$W(k = 0, \Omega) = \Omega .$$

For given values of Ω and k the winding number can be either rational or irrational. For invertible maps and rational winding numbers $W = P/Q$ the asymptotic iterates of the map converge to a unique attractor, a stable periodic orbit of period Q

$$\hat{f}^Q(\hat{x}_i) = \hat{x}_i + P, \quad i = 0, 1, 2, \dots, Q - 1 .$$

This is a consequence of the independence of \hat{x}_0 previously mentioned. There is also an unstable cycle, repelling the trajectory. For any rational winding number, there is a finite interval of values of Ω values for which the iterates of the circle map are attracted to the P/Q cycle. This interval is called the *P/Q mode-locked* (or *stability*) interval, and its width is given by

exercise 27.1

$$\Delta_{P/Q} = Q^{-2\mu_{P/Q}} = \Omega_{P/Q}^{right} - \Omega_{P/Q}^{left} . \tag{27.5}$$

where $\Omega_{P/Q}^{right}$ ($\Omega_{P/Q}^{left}$) denote the biggest (smallest) value of Ω for which $W(k, \Omega) = P/Q$. Parametrizing mode lockings by the exponent μ rather than the width Δ will be convenient for description of the distribution of the mode-locking widths, as the exponents μ turn out to be of bounded variation. The stability of the P/Q cycle is

$$\Lambda_{P/Q} = \frac{\partial x_Q}{\partial x_0} = f'(x_0)f'(x_1) \cdots f'(x_{Q-1})$$

For a stable cycle $|\Lambda_{P/Q}|$ lies between 0 (the superstable value, the “center” of the stability interval) and 1 (the $\Omega_{P/Q}^{right}$, $\Omega_{P/Q}^{left}$ endpoints of (27.5)). For the shift map (27.4), the stability intervals are shrunk to points. As Ω is varied from 0 to 1, the iterates of a circle map either mode-lock, with the winding number given by a rational number $P/Q \in (0, 1)$, or do not mode-lock, in which case the winding number is irrational. A plot of the winding number W as a function of the shift parameter Ω is a convenient visualization of the mode-locking structure of circle maps. It yields a monotonic “devil’s staircase” of figure 27.2 whose self-similar structure we are to unravel. Circle maps with zero slope at the inflection point x_c (see figure 27.3)

$$f'(x_c) = 0, \quad f''(x_c) = 0$$

Figure 27.2: The critical circle map ($k = 1$ in (27.1)) devil's staircase [3]; the winding number W as function of the parameter Ω .

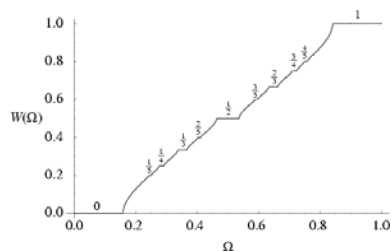
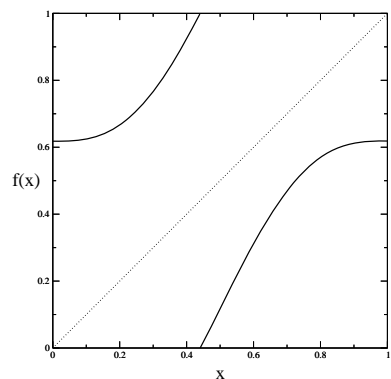


Figure 27.3: Critical circle map ($k = 1$ in (27.1)) with golden mean bare rotation number.



($k = 1$, $x_c = 0$ in (27.1)) are called *critical*: they delineate the borderline of chaos in this scenario. As the nonlinearity parameter k increases, the mode-locked intervals become wider, and for the critical circle maps ($k = 1$) they fill out the whole interval. A critical map has a superstable P/Q cycle for any rational P/Q , as the stability of any cycle that includes the inflection point equals zero. If the map is non-invertible ($k > 1$), it is called supercritical; the bifurcation structure of this regime is extremely rich and beyond the scope of this exposition.

The physically relevant transition to chaos is connected with the critical case, however the apparently simple “free” shift map limit is quite instructive: in essence it involves the problem of ordering rationals embedded in the unit interval on a hierarchical structure. From a physical point of view, the main problem is to identify a (number-theoretically) consistent hierarchy susceptible of experimental verification. We will now describe a few ways of organizing rationals along the unit interval: each has its own advantages as well as its drawbacks, when analyzed from both mathematical and physical perspective.

27.1.1 Hierarchical partitions of the rationals

Intuitively, the longer the cycle, the finer the tuning of the parameter Ω required to attain it; given finite time and resolution, we expect to be able to resolve cycles up to some maximal length Q . This is the physical motivation for partitioning mode lockings into sets of cycle length up to Q . In number theory such sets of rationals are called *Farey series*. They are denoted by \mathcal{F}_Q and defined as follows. The Farey series of order Q is the monotonically increasing sequence of all irreducible rationals between 0 and 1 whose denominators do not exceed Q . Thus P_i/Q_i

belongs to \mathcal{F}_Q if $0 < P_i \leq Q_i \leq Q$ and $(P_i|Q_i) = 1$. For example

$$\mathcal{F}_5 = \left\{ \frac{1}{5}, \frac{1}{4}, \frac{1}{3}, \frac{2}{5}, \frac{1}{2}, \frac{3}{5}, \frac{2}{3}, \frac{3}{4}, \frac{4}{5}, \frac{1}{1} \right\}$$

A Farey series is characterized by the property that if P_{i-1}/Q_{i-1} and P_i/Q_i are consecutive terms of \mathcal{F}_Q , then

$$P_i Q_{i-1} - P_{i-1} Q_i = 1.$$

The number of terms in the Farey series F_Q is given by

$$\Phi(Q) = \sum_{n=1}^Q \phi(n) = \frac{3Q^2}{\pi^2} + O(Q \ln Q). \tag{27.6}$$

Here the Euler function $\phi(Q)$ is the number of integers not exceeding and relatively prime to Q . For example, $\phi(1) = 1$, $\phi(2) = 1$, $\phi(3) = 2$, ..., $\phi(12) = 4$, $\phi(13) = 12$, ...

From a number-theorist's point of view, the *continued fraction partitioning* of the unit interval is the most venerable organization of rationals, preferred already by Gauss. The continued fraction partitioning is obtained by ordering rationals corresponding to continued fractions of increasing length. If we turn this ordering into a way of covering the complementary set to mode-lockings in a circle map, then the first level is obtained by deleting $\Delta_{[1]}$, $\Delta_{[2]}$, ..., $\Delta_{[a_1]}$, ... mode-lockings; their complement are the *covering* intervals $\ell_1, \ell_2, \dots, \ell_{a_1}, \dots$ which contain all windings, rational and irrational, whose continued fraction expansion starts with $[a_1, \dots]$ and is of length at least 2. The second level is obtained by deleting $\Delta_{[1,2]}$, $\Delta_{[1,3]}$, ..., $\Delta_{[2,2]}$, $\Delta_{[2,3]}$, ..., $\Delta_{[n,m]}$, ... and so on.

The n th level continued fraction partition $\mathcal{S}_n = \{a_1 a_2 \dots a_n\}$ is defined as the monotonically increasing sequence of all rationals P_i/Q_i between 0 and 1 whose continued fraction expansion is of length n :

$$\frac{P_i}{Q_i} = [a_1, a_2, \dots, a_n] = \frac{1}{a_1 + \frac{1}{a_2 + \dots + \frac{1}{a_n}}}$$

The object of interest, the set of the irrational winding numbers, is in this partitioning labeled by $\mathcal{S}_\infty = \{a_1 a_2 a_3 \dots\}$, $a_k \in \mathbb{Z}^+$, i.e., the set of winding numbers with infinite continued fraction expansions. The continued fraction labeling is particularly appealing in the present context because of the close connection of the Gauss

shift to the renormalization transformation R , discussed below. The Gauss map

$$T(x) = \begin{cases} \frac{1}{x} - \left[\frac{1}{x} \right] & x \neq 0 \\ 0 & x = 0 \end{cases} \quad (27.7)$$

($[\cdot \cdot \cdot]$ denotes the integer part) acts as a shift on the continued fraction representation of numbers on the unit interval

$$x = [a_1, a_2, a_3, \dots] \rightarrow T(x) = [a_2, a_3, \dots] . \quad (27.8)$$

into the “mother” interval $\ell_{a_2 a_3 \dots}$.

However natural the continued fractions partitioning might seem to a number theorist, it is problematic in practice, as it requires measuring infinity of mode-lockings even at the first step of the partitioning. Thus numerical and experimental use of continued fraction partitioning requires at least some understanding of the asymptotics of mode-lockings with large continued fraction entries.

The *Farey tree partitioning* is a systematic bisection of rationals: it is based on the observation that roughly halfway between any two large stability intervals (such as $1/2$ and $1/3$) in the devil’s staircase of figure 27.2 there is the next largest stability interval (such as $2/5$). The winding number of this interval is given by the Farey mediant $(P+P')/(Q+Q')$ of the parent mode-lockings P/Q and P'/Q' . This kind of cycle “gluing” is rather general and by no means restricted to circle maps; it can be attained whenever it is possible to arrange that the Q th iterate deviation caused by shifting a parameter from the correct value for the Q -cycle is exactly compensated by the Q' th iterate deviation from closing the Q' -cycle; in this way the two near cycles can be glued together into an exact cycle of length $Q+Q'$. The Farey tree is obtained by starting with the ends of the unit interval written as $0/1$ and $1/1$, and then recursively bisecting intervals by means of Farey mediants.

We define the n th *Farey tree level* T_n as the monotonically increasing sequence of those continued fractions $[a_1, a_2, \dots, a_k]$ whose entries $a_i \geq 1, i = 1, 2, \dots, k - 1, a_k \geq 2$, add up to $\sum_{i=1}^k a_i = n + 2$. For example

$$T_2 = \{[4], [2, 2], [1, 1, 2], [1, 3]\} = \left(\frac{1}{4}, \frac{1}{5}, \frac{3}{5}, \frac{3}{4} \right). \quad (27.9)$$

The number of terms in T_n is 2^n . Each rational in T_{n-1} has two “daughters” in T_n , given by

$$\begin{matrix} & & [\dots, a] & & \\ [\dots, a-1, 2] & & & & [\dots, a+1] \end{matrix}$$

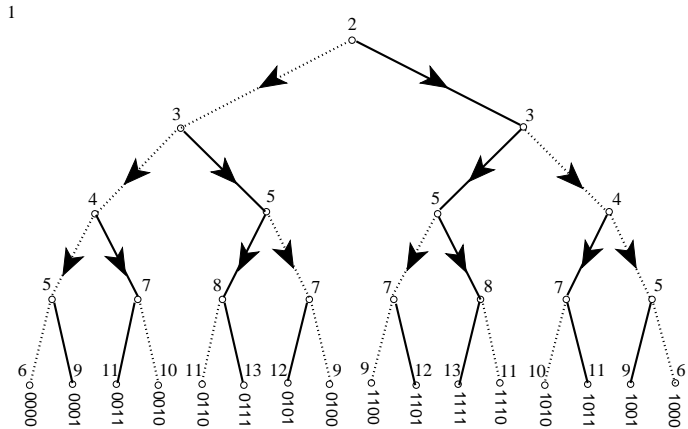


Figure 27.4: Farey tree: alternating binary ordered labeling of all Farey denominators on the n th Farey tree level.

Iteration of this rule places all rationals on a binary tree, labeling each by a unique binary label, figure 27.4.

The smallest and the largest denominator in T_n are respectively given by

$$[n - 2] = \frac{1}{n - 2}, \quad [1, 1, \dots, 1, 2] = \frac{F_{n+1}}{F_{n+2}} \propto \rho^n, \quad (27.10)$$

where the Fibonacci numbers F_n are defined by $F_{n+1} = F_n + F_{n-1}$; $F_0 = 0$, $F_1 = 1$, and ρ is the golden mean ratio

$$\rho = \frac{1 + \sqrt{5}}{2} = 1.61803\dots \quad (27.11)$$

Note the enormous spread in the cycle lengths on the same level of the Farey tree: $n \leq Q \leq \rho^n$. The cycles whose length grows only as a power of the Farey tree level will cause strong non-hyperbolic effects in the evaluation of various averages.

Having defined the partitioning schemes of interest here, we now briefly summarize the results of the circle-map renormalization theory.

27.2 Local theory: “Golden mean” renormalization



The way to pinpoint a point on the border of order is to recursively adjust the parameters so that at the recurrence times $t = n_1, n_2, n_3, \dots$ the trajectory passes through a region of contraction sufficiently strong to compensate for the accumulated expansion of the preceding n_i steps, but not so strong as to force the trajectory into a stable attracting orbit. The *renormalization operation* R implements this procedure by recursively magnifying the neighborhood of a point on the border in the dynamical space (by rescaling by a factor α), in the parameter space (by shifting the parameter origin onto the border and rescaling by a factor δ),

and by replacing the initial map f by the n th iterate f^n restricted to the magnified neighborhood

$$f_p(x) \rightarrow Rf_p(x) = \alpha f_p^n(x/\alpha)$$

There are by now many examples of such renormalizations in which the new function, framed in a smaller box, is a rescaling of the original function, i.e., the fixed point function of the renormalization operator R . The best known is the period doubling renormalization, with the recurrence times $n_k = 2^k$. The simplest circle map example is the golden mean renormalization, with recurrence times $n_k = F_k$ given by the Fibonacci numbers (27.10). Intuitively, in this context a metric self-similarity arises because iterates of critical maps are themselves critical, i.e., they also have cubic inflection points with vanishing derivatives.

The renormalization operator appropriate to circle maps acts as a generalization of the Gauss shift (27.38); it maps a circle map (represented as a pair of functions (g, f) , of winding number $[a, b, c, \dots]$ into a rescaled map of winding number $[b, c, \dots]$:

$$R_a \begin{pmatrix} g \\ f \end{pmatrix} = \begin{pmatrix} \alpha g^{a-1} \circ f \circ \alpha^{-1} \\ \alpha g^{a-1} \circ f \circ g \circ \alpha^{-1} \end{pmatrix}, \quad (27.12)$$

Acting on a map with winding number $[a, a, a, \dots]$, R_a returns a map with the same winding number $[a, a, \dots]$, so the fixed point of R_a has a quadratic irrational winding number $W = [a, a, a, \dots]$. This fixed point has a single expanding eigenvalue δ_a . Similarly, the renormalization transformation $R_{a_p} \dots R_{a_2} R_{a_1} \equiv R_{a_1 a_2 \dots a_p}$ has a fixed point of winding number $W_p = [a_1, a_2, \dots, a_{n_p}, a_1, a_2, \dots]$, with a single expanding eigenvalue δ_p .

For short repeating blocks, δ can be estimated numerically by comparing successive continued fraction approximants to W . Consider the P_r/Q_r rational approximation to a quadratic irrational winding number W_p whose continued fraction expansion consists of r repeats of a block p . Let Ω_r be the parameter for which the map (27.1) has a superstable cycle of rotation number $P_r/Q_r = [p, p, \dots, p]$. The δ_p can then be estimated by extrapolating from

$$\Omega_r - \Omega_{r+1} \propto \delta_p^{-r}. \quad (27.13)$$

What this means is that the “devil’s staircase” of figure 27.2 is self-similar under magnification by factor δ_p around any quadratic irrational W_p .

The fundamental result of the renormalization theory (and the reason why all this is so interesting) is that the ratios of successive P_r/Q_r mode-locked intervals converge to *universal* limits. The simplest example of (27.13) is the sequence of Fibonacci number continued fraction approximants to the golden mean winding number $W = [1, 1, 1, \dots] = (\sqrt{5} - 1)/2$.

When global problems are considered, it is useful to have at least an idea on external scaling laws for mode-lockings. This is achieved, in a first analysis, by fixing the cycle length Q and describing the range of possible asymptotics.

For a given cycle length Q , it is found that the *narrowest* interval shrinks with a power law

$$\Delta_{1/Q} \propto Q^{-3} \quad (27.14)$$

For fixed Q the *widest* interval is bounded by $P/Q = F_{n-1}/F_n$, the n th continued fraction approximant to the *golden mean*. The intuitive reason is that the golden mean winding sits as far as possible from any short cycle mode-locking.

The golden mean interval shrinks with a universal exponent

$$\Delta_{P/Q} \propto Q^{-2\mu_1} \quad (27.15)$$

where $P = F_{n-1}$, $Q = F_n$ and μ_1 is related to the universal Shenker number δ_1 (27.13) and the golden mean (27.11) by

$$\mu_1 = \frac{\ln |\delta_1|}{2 \ln \rho} = 1.08218\dots \quad (27.16)$$

The closeness of μ_1 to 1 indicates that the golden mean approximant mode-lockings barely feel the fact that the map is critical (in the $k=0$ limit this exponent is $\mu = 1$).

To summarize: for critical maps the spectrum of exponents arising from the circle maps renormalization theory is bounded from above by the harmonic scaling, and from below by the geometric golden-mean scaling:

$$3/2 > \mu_{m/n} \geq 1.08218\dots \quad (27.17)$$

27.3 Global theory: Thermodynamic averaging

Consider the following average over mode-locking intervals (27.5):

$$\Omega(\tau) = \sum_{Q=1}^{\infty} \sum_{(P/Q)=1} \Delta_{P/Q}^{-\tau} \quad (27.18)$$

The sum is over all irreducible rationals P/Q , $P < Q$, and $\Delta_{P/Q}$ is the width of the parameter interval for which the iterates of a critical circle map lock onto a cycle of length Q , with winding number P/Q .

The qualitative behavior of (27.18) is easy to pin down. For sufficiently negative τ , the sum is convergent; in particular, for $\tau = -1$, $\Omega(-1) = 1$, as for the critical circle maps the mode-lockings fill the entire Ω range [11]. However, as τ increases, the contributions of the narrow (large Q) mode-locked intervals $\Delta_{P/Q}$ get blown up to $1/\Delta_{P/Q}^\tau$, and at some critical value of τ the sum diverges. This occurs for $\tau < 0$, as $\Omega(0)$ equals the number of all rationals and is clearly divergent.

The sum (27.18) is infinite, but in practice the experimental or numerical mode-locked intervals are available only for small finite Q . Hence it is necessary to split up the sum into subsets $\mathcal{S}_n = \{i\}$ of rational winding numbers P_i/Q_i on the “level” n , and present the set of mode-lockings hierarchically, with resolution increasing with the level:

$$\bar{Z}_n(\tau) = \sum_{i \in \mathcal{S}_n} \Delta_i^{-\tau}. \tag{27.19}$$

The original sum (27.18) can now be recovered as the $z = 1$ value of a “generating” function $\Omega(z, \tau) = \sum_n z^n \bar{Z}_n(\tau)$. As z is anyway a formal parameter, and n is a rather arbitrary “level” in some *ad hoc* partitioning of rational numbers, we bravely introduce a still more general, P/Q weighted generating function for (27.18):

$$\Omega(q, \tau) = \sum_{Q=1}^{\infty} \sum_{(P|Q)=1} e^{-q\nu_{P/Q}} Q^{2\tau\mu_{P/Q}}. \tag{27.20}$$

The sum (27.18) corresponds to $q = 0$. Exponents $\nu_{P/Q}$ will reflect the importance we assign to the P/Q mode-locking, i.e., the *measure* used in the averaging over all mode-lockings. Three choices of of the $\nu_{P/Q}$ hierarchy that we consider here correspond respectively to the Farey series partitioning

$$\Omega(q, \tau) = \sum_{Q=1}^{\infty} \Phi(Q)^{-q} \sum_{(P|Q)=1} Q^{2\tau\mu_{P/Q}}, \tag{27.21}$$

the continued fraction partitioning

$$\Omega(q, \tau) = \sum_{n=1}^{\infty} e^{-qn} \sum_{[a_1, \dots, a_n]} Q^{2\tau\mu_{[a_1, \dots, a_n]}}, \tag{27.22}$$

and the Farey tree partitioning

$$\Omega(q, \tau) = \sum_{k=n}^{\infty} 2^{-qn} \sum_{i=1}^{2^n} Q_i^{2\tau\mu_i}, \quad Q_i/P_i \in T_n. \tag{27.23}$$

We remark that we are investigating a set arising in the analysis of the parameter space of a dynamical system: there is no “natural measure” dictated by dynamics, and the choice of weights reflects only the choice of hierarchical presentation.

27.4 Hausdorff dimension of irrational windings

A finite cover of the set irrational windings at the “ n th level of resolution” is obtained by deleting the parameter values corresponding to the mode-lockings in the subset \mathcal{S}_n ; left behind is the set of complement *covering* intervals of widths

$$\ell_i = \Omega_{P_r/Q_r}^{min} - \Omega_{P_l/Q_l}^{max} \tag{27.24}$$

Here Ω_{P_r/Q_r}^{min} (Ω_{P_l/Q_l}^{max}) are respectively the lower (upper) edges of the mode-locking intervals Δ_{P_r/Q_r} (Δ_{P_l/Q_l}) bounding ℓ_i and i is a symbolic dynamics label, for example the entries of the continued fraction representation $P/Q = [a_1, a_2, \dots, a_n]$ of one of the boundary mode-lockings, $i = a_1 a_2 \dots a_n$. ℓ_i provide a finite cover for the irrational winding set, so one may consider the sum

$$Z_n(\tau) = \sum_{i \in \mathcal{S}_n} \ell_i^{-\tau} \tag{27.25}$$

The value of $-\tau$ for which the $n \rightarrow \infty$ limit of the sum (27.25) is finite is the *Hausdorff dimension* D_H of the irrational winding set. Strictly speaking, this is the Hausdorff dimension only if the choice of covering intervals ℓ_i is optimal; otherwise it provides an upper bound to D_H . As by construction the ℓ_i intervals cover the set of irrational winding with no slack, we expect that this limit yields the Hausdorff dimension. This is supported by all numerical evidence, but a proof that would satisfy mathematicians is lacking.

The physically relevant statement is that for critical circle maps $D_H = 0.870\dots$ is a (global) universal number.

exercise 27.2

27.4.1 The Hausdorff dimension in terms of cycles

Estimating the $n \rightarrow \infty$ limit of (27.25) from finite numbers of covering intervals ℓ_i is a rather unilluminating chore. Fortunately, there exist considerably more elegant ways of extracting D_H . We have noted that in the case of the “trivial” mode-locking problem (27.4), the covering intervals are generated by iterations of the Farey map (27.37) or the Gauss shift (27.38). The n th level sum (27.25) can be approximated by \mathcal{L}_τ^n , where

$$\mathcal{L}_\tau(y, x) = \delta(x - f^{-1}(y)) |f'(y)|^\tau$$

This amounts to approximating each cover width ℓ_i by $|df^n/dx|$ evaluated on the i th interval. We are thus led to the following determinant

$$\det(1 - z\mathcal{L}_\tau) = \exp\left(-\sum_p \sum_{r=1}^{\infty} \frac{z^{rn_p}}{r} \frac{|\Lambda_p^r|^\tau}{1 - 1/\Lambda_p^r}\right)$$

$$= \prod_p \prod_{k=0}^{\infty} \left(1 - z^{n_p} |\Lambda_p|^\tau / \Lambda_p^k\right) . \tag{27.26}$$

The sum (27.25) is dominated by the leading eigenvalue of \mathcal{L}_τ ; the Hausdorff dimension condition $Z_n(-D_H) = O(1)$ means that $\tau = -D_H$ should be such that the leading eigenvalue is $z = 1$. The leading eigenvalue is determined by the $k = 0$ part of (27.26); putting all these pieces together, we obtain a pretty formula relating the Hausdorff dimension to the prime cycles of the map $f(x)$:

$$0 = \prod_p \left(1 - 1/|\Lambda_p|^{D_H}\right) . \tag{27.27}$$

For the Gauss shift (27.38) the stabilities of periodic cycles are available analytically, as roots of quadratic equations: For example, the x_a fixed points (quadratic irrationals with $x_a = [a, a, a \dots]$ infinitely repeating continued fraction expansion) are given by

$$x_a = \frac{-a + \sqrt{a^2 + 4}}{2}, \quad \Lambda_a = -\left(\frac{a + \sqrt{a^2 + 4}}{2}\right)^2 \tag{27.28}$$

and the $x_{ab} = [a, b, a, b, a, b, \dots]$ 2-cycles are given by

$$\begin{aligned} x_{ab} &= \frac{-ab + \sqrt{(ab)^2 + 4ab}}{2b} \\ \Lambda_{ab} &= (x_{ab}x_{ba})^{-2} = \left(\frac{ab + 2 + \sqrt{ab(ab + 4)}}{2}\right)^2 \end{aligned} \tag{27.29}$$

We happen to know beforehand that $D_H = 1$ (the irrationals take the full measure on the unit interval, or, from another point of view, the Gauss map is not a repeller), so is the infinite product (27.27) merely a very convoluted way to compute the number 1? Possibly so, but once the meaning of (27.27) has been grasped, the corresponding formula for the *critical* circle maps follows immediately:

$$0 = \prod_p \left(1 - 1/|\delta_p|^{D_H}\right) . \tag{27.30}$$

The importance of this formula relies on the fact that it expresses D_H in terms of *universal* quantities, thus providing a nice connection from local universal exponents to global scaling quantities: actual computations using (27.30) are rather involved, as they require a heavy computational effort to extract Shenker’s scaling δ_p for periodic continued fractions, and moreover dealing with an infinite alphabet requires control over tail summation if an accurate estimate is to be sought. In table 27.1 we give a small selection of computed Shenker’s scalings.

Table 27.1: Shenker’s δ_p for a few periodic continued fractions, from ref. [1].

p	δ_p
[1 1 1 1 ...]	-2.833612
[2 2 2 2 ...]	-6.7992410
[3 3 3 3 ...]	-13.760499
[4 4 4 4 ...]	-24.62160
[5 5 5 5 ...]	-40.38625
[6 6 6 6 ...]	-62.140
[1 2 1 2 ...]	17.66549
[1 3 1 3 ...]	31.62973
[1 4 1 4 ...]	50.80988
[1 5 1 5 ...]	76.01299
[2 3 2 3 ...]	91.29055

27.5 Thermodynamics of Farey tree: Farey model



We end this chapter by giving an example of a number theoretical model motivated by the mode-locking phenomenology. We will consider it by means of the thermodynamic formalism of chapter K, by looking at the free energy.

Consider the Farey tree partition sum (27.23): the narrowest mode-locked interval (27.15) at the n th level of the Farey tree partition sum (27.23) is the golden mean interval

$$\Delta_{F_{n-1}/F_n} \propto |\delta_1|^{-n}. \tag{27.31}$$

It shrinks exponentially, and for τ positive and large it dominates $q(\tau)$ and bounds $dq(\tau)/d\tau$:

$$q'_{max} = \frac{\ln |\delta_1|}{\ln 2} = 1.502642\dots \tag{27.32}$$

However, for τ large and negative, $q(\tau)$ is dominated by the interval (27.14) which shrinks only harmonically, and $q(\tau)$ approaches 0 as

$$\frac{q(\tau)}{\tau} = \frac{3 \ln n}{n \ln 2} \rightarrow 0. \tag{27.33}$$

So for finite n , $q_n(\tau)$ crosses the τ axis at $-\tau = D_n$, but in the $n \rightarrow \infty$ limit, the $q(\tau)$ function exhibits a phase transition; $q(\tau) = 0$ for $\tau < -D_H$, but is a non-trivial function of τ for $-D_H \leq \tau$. This non-analyticity is rather severe - to get a clearer picture, we illustrate it by a few number-theoretic models (the critical circle maps case is qualitatively the same).

An approximation to the “trivial” Farey level thermodynamics is given by the “Farey model,” in which the intervals $\ell_{P/Q}$ are replaced by Q^{-2} :

$$Z_n(\tau) = \sum_{i=1}^{2^n} Q_i^{2\tau}. \tag{27.34}$$

Here Q_i is the denominator of the i th Farey rational P_i/Q_i . For example (see figure 27.4),

$$Z_2(1/2) = 4 + 5 + 5 + 4.$$

By the annihilation property (27.38) of the Gauss shift on rationals, the n th Farey level sum $Z_n(-1)$ can be written as the integral

$$Z_n(-1) = \int dx \delta(f^n(x)) = \sum 1/|f'_{a_1 \dots a_k}(0)|,$$

and in general

$$Z_n(\tau) = \int dx \mathcal{L}_\tau^n(0, x),$$

with the sum restricted to the Farey level $a_1 + \dots + a_k = n + 2$. It is easily checked that $f'_{a_1 \dots a_k}(0) = (-1)^k Q_{[a_1, \dots, a_k]}^2$, so the Farey model sum is a partition generated by the Gauss map preimages of $x = 0$, i.e., by rationals, rather than by the quadratic irrationals as in (27.26). The sums are generated by the same transfer operator, so the eigenvalue spectrum should be the same as for the periodic orbit expansion, but in this variant of the finite level sums we can evaluate $q(\tau)$ exactly for $\tau = k/2$, k a nonnegative integer. First, one observes that $Z_n(0) = 2^n$. It is also easy to check that $Z_n(1/2) = \sum_i Q_i = 2 \cdot 3^n$. More surprisingly, $Z_n(3/2) = \sum_i Q_i^3 = 54 \cdot 7^{n-1}$. A few of these “sum rules” are listed in the table 27.2, they are consequence of the fact that the denominators on a given level are Farey sums of denominators on preceding levels.

exercise 27.3

A bound on D_H can be obtained by approximating (27.34) by

$$Z_n(\tau) = n^{2\tau} + 2^n \rho^{2n\tau}. \tag{27.35}$$

In this approximation we have replaced all $\ell_{P/Q}$, except the widest interval $\ell_{1/n}$, by the narrowest interval ℓ_{F_{n-1}/F_n} (see (27.15)). The crossover from the harmonic dominated to the golden mean dominated behavior occurs at the τ value for which the two terms in (27.35) contribute equally:

$$D_n = \hat{D} + O\left(\frac{\ln n}{n}\right), \quad \hat{D} = \frac{\ln 2}{2 \ln \rho} = .72\dots \tag{27.36}$$

For negative τ the sum (27.35) is the lower bound on the sum (27.25), so \hat{D} is a lower bound on D_H .

From a general perspective the analysis of circle maps thermodynamics has revealed the fact that physically interesting dynamical systems often exhibit mixtures of hyperbolic and marginal stabilities. In such systems there are orbits that

$\tau/2$	$Z_n(\tau/2)/Z_{n-1}(\tau/2)$
0	2
1	3
2	$(5 + \sqrt{17})/2$
3	7
4	$(5 + \sqrt{17})/2$
5	$7 + 4\sqrt{6}$
6	26.20249...

Table 27.2: Partition function sum rules for the Farey model.

stay ‘glued’ arbitrarily close to stable regions for arbitrarily long times. This is a generic phenomenon for Hamiltonian systems, where elliptic islands of stability coexist with hyperbolic homoclinic webs. Thus the considerations of chapter 24 are important also in the analysis of renormalization at the onset of chaos.

Résumé

The mode locking problem, and the quasiperiodic transition to chaos offer an opportunity to use cycle expansions on hierarchical structures in parameter space: this is not just an application of the conventional thermodynamic formalism, but offers a clue on how to extend universality theory from local scalings to global quantities.

Commentary

Remark 27.1 The physics of circle maps. Mode-locking phenomenology is reviewed in ref. [5], a more theoretically oriented discussion is contained in ref. [3]. While representative of dissipative systems we may also consider circle maps as a crude approximation to Hamiltonian local dynamics: a typical island of stability in a Hamiltonian 2-dimensional map is an infinite sequence of concentric KAM tori and chaotic regions. In the crudest approximation, the radius can here be treated as an external parameter Ω , and the angular motion can be modeled by a map periodic in the angular variable [8, 9]. By losing all of the ‘island-within-island’ structure of real systems, circle map models skirt the problems of determining the symbolic dynamics for a realistic Hamiltonian system, but they do retain some of the essential features of such systems, such as the golden mean renormalization [5, 8] and non-hyperbolicity in form of sequences of cycles accumulating toward the borders of stability. In particular, in such systems there are orbits that stay “glued” arbitrarily close to stable regions for arbitrarily long times. As this is a generic phenomenon in physically interesting dynamical systems, such as the Hamiltonian systems with coexisting elliptic islands of stability and hyperbolic homoclinic webs, development of good computational techniques is here of utmost practical importance.

Remark 27.2 Critical mode-locking set The fact that mode-lockings completely fill the unit interval at the critical point has been proposed in refs. [3, 10]. The proof that the

set of irrational windings is of zero Lebesgue measure in given in ref. [11].

Remark 27.3 Counting noise for Farey series. The number of rationals in the Farey series of order Q is $\phi(Q)$, which is a highly irregular function of Q : incrementing Q by 1 increases $\Phi(Q)$ by anything from 2 to Q terms. We refer to this fact as the “Euler noise.”

The Euler noise poses a serious obstacle for numerical calculations with the Farey series partitionings; it blocks smooth extrapolations to $Q \rightarrow \infty$ limits from finite Q data. While this in practice renders inaccurate most Farey-sequence partitioned averages, the finite Q Hausdorff dimension estimates exhibit (for reasons that we do not understand) surprising numerical stability, and the Farey series partitioning actually yields the *best* numerical value of the Hausdorff dimension (27.25) of any methods used so far; for example the computation in ref. [12] for critical sine map (27.1), based on $240 \leq Q \leq 250$ Farey series partitions, yields $D_H = .87012 \pm .00001$. The quoted error refers to the variation of D_H over this range of Q ; as the computation is not asymptotic, such numerical stability can underestimate the actual error by a large factor.

Remark 27.4 Farey tree presentation function. The Farey tree rationals can be generated by backward iterates of $1/2$ by the Farey presentation function [13]:

$$\begin{aligned} f_0(x) &= x/(1-x) & 0 \leq x < 1/2 \\ f_1(x) &= (1-x)/x & 1/2 < x \leq 1. \end{aligned} \tag{27.37}$$

The Gauss shift (27.7) corresponds to replacing the binary Farey presentation function branch f_0 in (27.37) by an infinity of branches

$$\begin{aligned} f_a(x) &= f_1 \circ f_0^{(a-1)}(x) = \frac{1}{x} - a, & \frac{1}{a-1} < x \leq \frac{1}{a}, \\ f_{ab\dots c}(x) &= f_c \circ \dots \circ f_b \circ f_a(x). \end{aligned} \tag{27.38}$$

A rational $x = [a_1, a_2, \dots, a_k]$ is annihilated by the k th iterate of the Gauss shift, $f_{a_1 a_2 \dots a_k}(x) = 0$. The above maps look innocent enough, but note that what is being partitioned is not the dynamical space, but the parameter space. The flow described by (27.37) and by its non-trivial circle-map generalizations will turn out to be a *renormalization group* flow in the function space of dynamical systems, not an ordinary flow in the state space of a particular dynamical system.

The Farey tree has a variety of interesting symmetries (such as “flipping heads and tails” relations obtained by reversing the order of the continued-fraction entries) with as yet unexploited implications for the renormalization theory: some of these are discussed in ref. [4].

An alternative labeling of Farey denominators has been introduced by Knauf [6] in context of number-theoretical modeling of ferromagnetic spin chains: it allows for a number of elegant manipulations in thermodynamic averages connected to the Farey tree hierarchy.

Remark 27.5 Circle map renormalization The idea underlying golden mean renormalization goes back to Shenker [9]. A renormalization group procedure was formulated

in refs. [7, 14], where moreover the uniqueness of the relevant eigenvalue is claimed. This statement has been confirmed by a computer-assisted proof [15], and in the following we will always assume it. There are a number of experimental evidences for local universality, see refs. [16, 17].

On the other side of the scaling tale, the power law scaling for harmonic fractions (discussed in refs. [2, 4]) is derived by methods akin to those used in describing intermittency [21]: $1/Q$ cycles accumulate toward the edge of 0/1 mode-locked interval, and as the successive mode-locked intervals $1/Q$, $1/(Q-1)$ lie on a parabola, their differences are of order Q^{-3} .

Remark 27.6 Farey series and the Riemann hypothesis The Farey series thermodynamics is of a number theoretical interest, because the Farey series provide uniform coverings of the unit interval with rationals, and because they are closely related to the deepest problems in number theory, such as the Riemann hypothesis [22, 23]. The distribution of the Farey series rationals across the unit interval is surprisingly uniform - indeed, so uniform that in the pre-computer days it has motivated a compilation of an entire handbook of Farey series [24]. A quantitative measure of the non-uniformity of the distribution of Farey rationals is given by displacements of Farey rationals for $P_i/Q_i \in \mathcal{F}_Q$ from uniform spacing:

$$\delta_i = \frac{i}{\Phi(Q)} - \frac{P_i}{Q_i}, \quad i = 1, 2, \dots, \Phi(Q)$$

The Riemann hypothesis states that the zeros of the Riemann zeta function lie on the $s = 1/2 + i\tau$ line in the complex s plane, and would seem to have nothing to do with physicists' real mode-locking widths that we are interested in here. However, there is a real-line version of the Riemann hypothesis that lies very close to the mode-locking problem. According to the theorem of Franel and Landau [25, 22, 23], the Riemann hypothesis is equivalent to the statement that

$$\sum_{Q_i \leq Q} |\delta_i| = o(Q^{\frac{1}{2} + \epsilon})$$

for all ϵ as $Q \rightarrow \infty$. The mode-lockings $\Delta_{P/Q}$ contain the necessary information for constructing the partition of the unit interval into the ℓ_i covers, and therefore implicitly contain the δ_i information. The implications of this for the circle-map scaling theory have not been worked out, and is not known whether some conjecture about the thermodynamics of irrational windings is equivalent to (or harder than) the Riemann hypothesis, but the danger lurks.

Remark 27.7 Farey tree partitioning. The Farey tree partitioning was introduced in refs. [26, 27, 4] and its thermodynamics is discussed in detail in refs. [12, 13]. The Farey tree hierarchy of rationals is rather new, and, as far as we are aware, not previously studied by number theorists. It is appealing both from the experimental and from the golden-mean renormalization point of view, but it has a serious drawback of lumping together mode-locking intervals of wildly different sizes on the same level of the Farey tree.

Remark 27.8 Local and global universality. Numerical evidences for global universal behavior have been presented in ref. [3]. The question was reexamined in ref. [12], where it was pointed out how a high-precision numerical estimate is in practice very hard to obtain. It is not at all clear whether this is the optimal global quantity to test but at least the Hausdorff dimension has the virtue of being independent of how one partitions mode-lockings and should thus be the same for the variety of thermodynamic averages in the literature.

The formula (27.30), linking local to global behavior, was proposed in ref. [1].

The derivation of (27.30) relies only on the following aspects of the “hyperbolicity conjecture” of refs. [4, 18, 19, 20]:

1. *limits* for Shenker δ 's exist and are universal. This should follow from the renormalization theory developed in refs. [7, 14, 15], though a general proof is still lacking.
2. δ_p grow exponentially with n_p , the length of the continued fraction block p .
3. δ_p for $p = a_1 a_2 \dots n$ with a large continued fraction entry n grows as a power of n . According to (27.14), $\lim_{n \rightarrow \infty} \delta_p \propto n^3$. In the calculation of ref. [1] the explicit values of the asymptotic exponents and prefactors were not used, only the assumption that the growth of δ_p with n is not slower than a power of n .

Remark 27.9 Farey model. The Farey model (27.33) has been proposed in ref. [12]; though it might seem to have been pulled out of a hat, the Farey model is as sensible description of the distribution of rationals as the periodic orbit expansion (27.26).

Remark 27.10 Symbolic dynamics for Hamiltonian rotational orbits. The rotational codes of ref. [37] are closely related to those for maps with a natural angle variable, for example for circle maps [34, 36] and cat maps [38]. Ref. [37] also offers a systematic rule for obtaining the symbolic codes of “islands around islands” rotational orbits [40]. These correspond, for example, to orbits that rotate around orbits that rotate around the elliptic fixed point; thus they are defined by a sequence of rotation numbers.

A different method for constructing symbolic codes for “islands around islands” was given in refs. [43, 41]; however in these cases the entire set of orbits in an island was assigned the same sequence and the motivation was to study the transport implications for chaotic orbits outside the islands [40, 42].

Exercises

27.1. **Mode-locked intervals.** Check that when $k \neq 0$ the interval $\Delta_{P/Q}$ have a non-zero width (look for instance at simple fractions, and consider k small). Show that for

small k the width of $\Delta_{0/1}$ is an increasing function of k .

- 27.2. **Bounds on Hausdorff dimension.** By making use of the bounds (27.17) show that the Hausdorff dimension for critical mode lockings may be bounded by

$$2/3 \leq D_H \leq .9240 \dots$$

- 27.3. **Farey model sum rules.** Verify the sum rules reported in table 27.2. An elegant way to get a number of sum rules for the Farey model is by taking into account an lexical ordering introduced by Contucci and Knauf, see ref. [28].

- 27.4. **Metric entropy of the Gauss shift.** Check that the Lyapunov exponent of the Gauss map (27.7) is given by $\pi^2/6 \ln 2$. This result has been claimed to be relevant in the discussion of “mixmaster” cosmologies, see ref. [30].

- 27.5. **Refined expansions.** Show that the above estimates can be refined as follows:

$$F(z, 2) \sim \zeta(2) + (1 - z) \log(1 - z) - (1 - z)$$

and

$$F(z, s) \sim \zeta(s) + \Gamma(1 - s)(1 - z)^{s-1} - S(s)(1 - z)$$

for $s \in (1, 2)$ ($S(s)$ being expressed by a converging sum). You may use either more detailed estimate for $\zeta(s, a)$ (via Euler summation formula) or keep on subtracting leading contributions [31].

- 27.6. j_n and α_{cr} . Look at the integration region and how it scales by plotting it for increasing values of n .

- 27.7. **Estimates of the Riemann zeta function.** Try to approximate numerically the Riemann zeta function for $s = 2, 4, 6$ using different acceleration algorithms: check your results with refs. [32, 33].

- 27.8. **Farey tree and continued fractions I.** Consider the Farey tree presentation function $f : [0, 1] \mapsto [0, 1]$, such that if $I = [0, 1/2)$ and $J = [1/2, 1]$, $f|_I = x/(1 - x)$ and $f|_J = (1 - x)/x$. Show that the corresponding induced map is the Gauss map $g(x) = 1/x - [1/x]$.

- 27.9. **Farey tree and continued fraction II. (Lethal weapon II).** Build the simplest piecewise linear approximation to the Farey tree presentation function (hint: substitute first the rightmost, hyperbolic branch with a linear one): consider then the spectral determinant of the induced map \hat{g} , and calculate the first two eigenvalues besides the probability conservation one. Compare the results with the rigorous bound deduced in ref. [17].

References

- [27.1] P. Cvitanović, G.H. Gunaratne and M. Vinson, *Nonlinearity* **3** (1990)
- [27.2] K. Kaneko, *Prog. Theor. Phys.* **68**, 669 (1982); **69**, 403 (1983); **69**, 1427 (1983)
- [27.3] M.H. Jensen, P. Bak, T. Bohr, *Phys. Rev. Lett.* **50**, 1637 (1983); *Phys. Rev.* **A 30**, 1960 (1984); P. Bak, T. Bohr and M.H. Jensen, *Physica Scripta* **T9**, 50 (1985)
- [27.4] P. Cvitanović, B. Shraiman and B. Söderberg, *Physica Scripta* **32**, 263 (1985).
- [27.5] J.A. Glazier and A. Libchaber, *IEEE Trans. Circ. Syst.*, **35**, 790 (1988)
- [27.6] A. Knauf, “On a ferromagnetic spin chain,” *Commun. Math. Phys.* **153**, 77 (1993).
- [27.7] M.J. Feigenbaum, L.P. Kadanoff, S.J. Shenker, *Physica* **5D**, 370 (1982)
- [27.8] S.J. Shenker and L.P. Kadanoff, *J. Stat. Phys.* **27**, 631 (1982)
- [27.9] S.J. Shenker, *Physica* **5D**, 405 (1982)
- [27.10] O.E. Lanford, *Physica* **14D**, 403 (1985)

- [27.11] G. Swiatek, *Commun. Math. Phys.* **119**, 109 (1988)
- [27.12] R. Artuso, P. Cvitanović and B.G. Kenny, *Phys. Rev.* **A39**, 268 (1989); P. Cvitanović, in R. Gilmore (ed), *Proceedings of the XV International Colloquium on Group Theoretical Methods in Physics*, (World Scientific, Singapore, 1987)
- [27.13] M.J. Feigenbaum, *J.Stat.Phys.* **52**, 527 (1988)
- [27.14] S. Ostlund, D.A. Rand, J. Sethna and E. Siggia, *Physica* **D 8**, 303 (1983).
- [27.15] B.D. Mestel, Ph.D. Thesis (U. of Warwick 1985).
- [27.16] J. Stavans, F. Heslot and A. Libchaber, *Phys. Rev. Lett.* **55**, 569 (1985)
- [27.17] E.G. Gwinn and R.M. Westervelt, *Phys. Rev. Lett.* **59**, 157 (1987)
- [27.18] O.E. Lanford, in M. Mebkhout and R. S en eor, eds., *Proc. 1986 IAMP Conference in Mathematical Physics* (World Scientific, Singapore 1987); D.A. Rand, *Proc. R. Soc. London A* **413**, 45 (1987); *Nonlinearity* **1**, 78 (1988)
- [27.19] S.-H. Kim and S. Ostlund, *Physica* **D 39**, 365, (1989)
- [27.20] M.J. Feigenbaum, *Nonlinearity* **1**, 577 (1988)
- [27.21] Y. Pomeau and P. Manneville, *Commun. Math. Phys.* **74**, 189 (1980); P. Manneville, *J. Phys.* (Paris) **41**, 1235 (1980)
- [27.22] H.M. Edwards, *Riemann's Zeta Function* (Academic, New York 1974)
- [27.23] E.C. Titchmarsh, *The Theory of Riemann Zeta Function* (Oxford Univ. Press, Oxford 1951); chapter XIV.
- [27.24] E.H. Neville, *Roy. Soc. Mathematical Tables* (Cambridge Univ. Press, Cambridge 1950)
- [27.25] J. Franel and E. Landau, *G ottinger Nachr.* 198 (1924)
- [27.26] G. T. Williams and D. H. Browne, *Amer. Math. Monthly* **54**, 534 (1947)
- [27.27] P. Cvitanović and J. Myrheim, *Phys. Lett.* **A94**, 329 (1983); *Commun. Math. Phys.* **121**, 225 (1989)
- [27.28] P. Contucci and A. Knauf, *Forum Math.* **9**, 547 (1997)
- [27.29] G.H. Hardy and E.M. Wright, *Theory of Numbers* (Oxford Univ. Press, Oxford 1938)
- [27.30] A. Csord as and P. Sz epfalusy, *Phys. Rev. A* **40**, 2221 (1989) and references therein.
- [27.31] P. Dahlqvist, unpublished notes.
- [27.32] D. Levin, *Inter. J. Computer Math.* **B3**, 371 (1973).

- [27.33] N. Osada, *SIAM J. Numer. Anal.* **27**, 178 (1990).
- [27.34] P. Veerman, “Symbolic dynamics and rotation numbers,” *Phys. A* **134**, 543 (1986).
- [27.35] J.J.P. Veerman and F.M. Tangerman. “Intersection properties of invariant manifolds in certain twist maps,” *Comm. Math. Phys.* **139**, 245 (1991).
- [27.36] W.-M. Zheng, “Symbolic dynamics for the circle map,” *Int. J. Mod. Phys. B* **5**, 481 (1991).
- [27.37] H.R. Dullin, J.D. Meiss and D.G. Sterling, “Symbolic codes for rotational orbits,”
[arXiv:nlin.CD/0408015](https://arxiv.org/abs/nlin.CD/0408015).
- [27.38] I.C. Percival and F. Vivaldi. “A linear code for the sawtooth and cat maps,” *Physica D* **27**, 373 (1987).
- [27.39] I.C. Percival and F. Vivaldi. “Arithmetical properties of strongly chaotic motion,” *Physica D* **25**, 105 (1987).
- [27.40] J.D. Meiss, “Class renormalization: Islands around islands,” *Phys. Rev. A* **34**, 2375 (1986).
- [27.41] V. Afraimovich, A. Maass, and J. Uras. “Symbolic dynamics for sticky sets in Hamiltonian systems,” *Nonlinearity* **13**, 617 (2000).
- [27.42] J.D. Meiss and E. Ott. “Markov tree model of transport in area preserving maps,” *Physica D* **20**, 387 (1986).
- [27.43] Y. Aizawa. “Symbolic dynamics approach to the two-D chaos in area-preserving maps,” *Prog. Theor. Phys.* **71**, 1419 (1984).
- [27.44] M. Yampolsky, “On the eigenvalues of a renormalization operator,” *Nonlinearity* **16**, 1565 (2003).

Part IV

The rest is noise

QUNADRY: all these cycles, but how many do I need?. Any physical system suffers background noise, any numerical prediction suffers computational roundoff noise, and any set of equations models nature up to a given accuracy, since degrees of freedom are always neglected. If the noise is weak, the short-time dynamics is not altered significantly: short periodic orbits of the deterministic flow still partition coarsely the state space.

Chapter 28

Noise

He who establishes his argument by noise and command shows that his reason is weak.

—M. de Montaigne

(G. Vattay and P. Cvitanović)

THIS CHAPTER (which reader can safely skip on the first reading) is about noise, how it affects classical dynamics, and the ways it mimics quantum dynamics.



Why - in a monograph on deterministic and quantum chaos - start discussing noise? First, in physical settings any dynamics takes place against a noisy background, and whatever prediction we might have, we have to check its robustness to noise. Second, as we show in this chapter, to the leading order in noise strength, the semiclassical Hamilton-Jacobi formalism applies to weakly stochastic flows in toto. As classical noisy dynamics is more intuitive than quantum dynamics, understanding effects of noise helps demystify some of the formal machinery of semiclassical quantization. Surprisingly, symplectic structure emerges here not as a deep principle of mechanics, but an artifact of the leading approximation to quantum/noisy dynamics, not respected by higher order corrections. The same is true of semiclassical quantum dynamics; higher corrections do not respect canonical invariance. Third, the variational principle derived here turns out to be a powerful tool for determining periodic orbits, see chapter 29. And, last but not least, upon some reflection, the whole enterprise of replacing deterministic trajectories by deterministic evolution operators, chapters 16 to 20, seems fatally flawed; if we have given up infinite precision in specifying initial conditions, why do we allow ourselves the infinite precision in the specification of evolution laws, i.e., define the evolution operator by means of the Dirac delta function $\delta(y - f(x))$? It will be comforting to learn that the deterministic evolution operators survive unscathed, as the leading approximation to the noisy ones in the limit of weak noise.

We start by deriving the continuity equation for purely deterministic, noiseless

flow, and then incorporate noise in stages: diffusion equation, Langevin equation, Fokker-Planck equation, Hamilton-Jacobi formulation, stochastic path integrals.

28.1 Deterministic transport

(E.A. Spiegel and P. Cvitanović)

The large body of accrued wisdom on the subject of flows called fluid dynamics is about physical flows of media with continuous densities. On the other hand, the flows in state spaces of dynamical systems frequently require more abstract tools. To sharpen our intuition about those, it is helpful to outline the more tangible fluid dynamical vision.

Consider first the simplest property of a fluid flow called *material invariant*. A material invariant $I(x)$ is a property attached to each point x that is preserved by the flow, $I(x) = I(f^t(x))$; for example, at point $x(t) = f^t(x)$ a green particle (more formally: a *passive scalar*) is embedded into the fluid. As $I(x)$ is invariant, its total time derivative vanishes, $\dot{I}(x) = 0$. Written in terms of partial derivatives this is the *conservation equation* for the material invariant

$$\partial_t I + v \cdot \partial I = 0. \quad (28.1)$$

Let the *density* of representative points be $\rho(x, t)$. The manner in which the flow redistributes $I(x)$ is governed by a partial differential equation whose form is relatively simple because the representative points are neither created nor destroyed. This conservation property is expressed in the integral statement

$$\partial_t \int_V dx \rho I = - \int_{\partial V} d\sigma \hat{n}_i v_i \rho I,$$

where V is an arbitrary volume in the state space \mathcal{M} , ∂V is its surface, \hat{n} is its outward normal, and repeated indices are summed over throughout. The divergence theorem turns the surface integral into a volume integral,

$$\int_V [\partial_t(\rho I) + \partial_i(v_i \rho I)] dx = 0,$$

where ∂_i is the partial derivative operator with respect to x_i . Since the integration is over an arbitrary volume, we conclude that

$$\partial_t(\rho I) + \partial_i(\rho I v_i) = 0. \quad (28.2)$$

The choice $I \equiv 1$ yields the *continuity equation* for the density:

$$\partial_t \rho + \partial_i(\rho v_i) = 0. \quad (28.3)$$

We have used here the language of fluid mechanics to ease the visualization, but, as we already saw in (16.25), our previous derivation of the continuity equation, any deterministic state space flow satisfies the continuity equation.

28.2 Brownian diffusion

Consider tracer molecules, let us say big, laggardly green molecules, embedded in a denser gas of light molecules. Assume that the density of tracer molecules ρ compared to the background gas density is low, so we can neglect green-green collisions. Each green molecule, jostled by frequent collisions with the background gas, executes its own Brownian motion. The molecules are neither created nor destroyed, so their number within an arbitrary volume V changes with time only by the current density j_i flow through its surface ∂V (with \hat{n} its outward normal):

$$\partial_t \int_V dx \rho = - \int_{\partial V} d\sigma \hat{n}_i j_i. \quad (28.4)$$

The divergence theorem turns this into the conservation law for tracer density:

$$\partial_t \rho + \partial_i j_i = 0. \quad (28.5)$$

The tracer density ρ is defined as the average density of a ‘material particle,’ averaged over a subvolume large enough to contain many green (and still many more background) molecules, but small compared to the macroscopic observational scales. What is j ? If the density is constant, on the average as many molecules leave the material particle volume as they enter it, so a reasonable phenomenological assumption is that the *average* current density (*not* the individual particle current density ρv_i in (28.3)) is driven by the density gradient

$$j_i = -D \frac{\partial \rho}{\partial x_i}. \quad (28.6)$$

This is the *Fick law*, with the diffusion constant D a phenomenological parameter. For simplicity here we assume that D is a scalar; in general $D \rightarrow D_{ij}(x, t)$ is a space- and time-dependent tensor. Substituting this j into (28.5) yields the *diffusion equation*

$$\frac{\partial}{\partial t} \rho(x, t) = D \frac{\partial^2}{\partial x^2} \rho(x, t). \quad (28.7)$$

This linear equation has an exact solution in terms of an initial Dirac delta density distribution, $\rho(x, 0) = \delta(x - x_0)$,

$$\rho(x, t) = \frac{1}{(4\pi Dt)^{d/2}} e^{-\frac{(x-x_0)^2}{4Dt}} = \frac{1}{(4\pi Dt)^{d/2}} e^{-\frac{x^2}{4Dt}}. \quad (28.8)$$

The average distance covered in time t obeys the Einstein diffusion formula

$$\langle (x - x_0)^2 \rangle_t = \int dx \rho(x, t) (x - x_0)^2 = 2dDt. \quad (28.9)$$

28.3 Weak noise

The connection between path integration and Brownian motion is so close that they are nearly indistinguishable. Unfortunately though, like a body and its mirror image, the sum over paths for Brownian motion is a theory having substance, while its path integral image exists mainly in the eye of the beholder.

—L. S. Schulman

So far we have considered tracer molecule dynamics which is purely Brownian, with no deterministic “drift.” Consider next a deterministic flow $\dot{x} = v(x)$ perturbed by a stochastic term $\xi(t)$,

$$\dot{x} = v(x) + \xi(t). \quad (28.10)$$

We shall refer to equations of this type as *Langevin equations*. Assume that $\xi(t)$ ’s fluctuate around $[\dot{x} - v(x)]$ with a Gaussian probability density

$$P(\xi, \delta t) = \left(\frac{\delta t}{4\pi D} \right)^{d/2} e^{-\frac{\xi^2}{4D} \delta t}, \quad (28.11)$$

and are uncorrelated in time (white noise)

$$\langle \xi(t) \xi(t') \rangle = 2dD \delta(t - t'). \quad (28.12)$$

The normalization factors in (28.8) and (28.11) differ, as $p(\xi, \delta t)$ is a probability density for velocity ξ , and $\rho(x, t)$ is a probability density for position x . The material particle now drifts along the trajectory $x(t)$, so the velocity diffusion follows (28.8) for infinitesimal time δt only. As $D \rightarrow 0$, the distribution tends to the (noiseless, deterministic) Dirac delta function.

The phenomenological Fick law current (28.6) is now a sum of two components, the material particle center-of-mass deterministic drift $v(x)$ and the weak noise term

$$j_i = \rho v_i - D \frac{\partial \rho}{\partial x_i}, \quad (28.13)$$

Substituting this j into (28.5) yields the *Fokker-Planck equation*

$$\partial_t \rho + \partial_i(\rho v_i) = D \partial^2 \rho. \quad (28.14)$$

The left hand side, $d\rho/dt = \partial_t \rho + \partial \cdot (\rho v)$, is deterministic, with the continuity equation (28.3) recovered in the weak noise limit $D \rightarrow 0$. The right hand side describes the diffusive transport in or out of the material particle volume. If the density is lower than in the immediate neighborhood, the local curvature is positive, $\partial^2 \rho > 0$, and the density grows. Conversely, for negative curvature diffusion lowers the local density, thus smoothing the variability of ρ . Where is the density going globally?

If the system is bound, the probability density vanishes sufficiently fast outside the central region, $\rho(x, t) \rightarrow 0$ as $|x| \rightarrow \infty$, and the total probability is conserved

$$\int dx \rho(x, t) = 1.$$

Any initial density $\rho(x, 0)$ is smoothed by diffusion and with time tends to the invariant density

$$\rho_0(x) = \lim_{t \rightarrow \infty} \rho(x, t), \quad (28.15)$$

an eigenfunction $\rho(x, t) = e^{st} \rho_0(x)$ of the time-independent Fokker-Planck equation

$$\left(\partial_i v_i - D \partial^2 + s_\alpha \right) \rho_\alpha = 0, \quad (28.16)$$

with vanishing eigenvalue $s_0 = 0$. Provided the noiseless classical flow is hyperbolic, in the vanishing noise limit the leading eigenfunction of the Fokker-Planck equation tends to natural measure (16.17) of the corresponding deterministic flow, the leading eigenvector of the Perron-Frobenius operator.

If the system is open, there is a continuous outflow of probability from the region under study, the leading eigenvalue is contracting, $s_0 < 0$, and the density of the system tends to zero. In this case the leading eigenvalue s_0 of the time-independent Fokker-Planck equation (28.16) can be interpreted by saying that a finite density can be maintained by pumping back probability into the system at a constant rate $\gamma = -s_0$. The value of γ for which any initial probability density converges to a finite equilibrium density is called the *escape rate*. In the noiseless limit this coincides with the deterministic escape rate (17.15).

We have introduced noise phenomenologically, and used the weak noise assumption in retaining only the first derivative of ρ in formulating the Fick law (28.6) and including noise additively in (28.13). A full theory of stochastic ODEs is much subtler, but this will do for our purposes.

28.4 Weak noise approximation

In the spirit of the WKB approximation, we shall now study the evolution of the probability distribution by rewriting it as

$$\rho(x, t) = e^{\frac{1}{2D}R(x,t)}. \quad (28.17)$$

The time evolution of R is given by

$$\partial_t R + v\partial R + (\partial R)^2 = D\partial v + D\partial^2 R.$$

Consider now the weak noise limit and drop the terms proportional to D . The remaining equation

$$\partial_t R + H(x, \partial R) = 0$$

is known as the Hamilton-Jacobi equation. The function R can be interpreted as the Hamilton's principal function, corresponding to the Hamiltonian

$$H(x, p) = p v(x) + p^2/2,$$

with the Hamilton's equations of motion

$$\begin{aligned} \dot{x} &= \partial_p H = v + p \\ \dot{p} &= -\partial_x H = -A^T p, \end{aligned} \quad (28.18)$$

where A is the stability matrix (4.3)

$$A_{ij}(x) = \frac{\partial v_i(x)}{\partial x_j}.$$

The noise Lagrangian is then

$$L(x, \dot{x}) = \dot{x} \cdot p - H = \frac{1}{2} [\dot{x} - v(x)]^2. \quad (28.19)$$

We have come the full circle - the Lagrangian is the exponent of our assumed Gaussian distribution (28.11) for noise $\xi^2 = [\dot{x} - v(x)]^2$. What is the meaning of this Hamiltonian, Lagrangian? Consider two points x_0 and x . Which noisy path is the most probable path that connects them in time t ? The probability of a given path \mathcal{P} is given by the probability of the noise sequence $\xi(t)$ which generates

the path. This probability is proportional to the product of the noise probability functions (28.11) along the path, and the total probability for reaching x from x_0 in time t is given by the sum over all paths, or the stochastic path integral (Wiener integral)

$$\begin{aligned} P(x, x_0, t) &\sim \sum_{\mathcal{P}} \prod_j p(\xi(\tau_j), \delta\tau_j) = \int \prod_j d\xi_j \left(\frac{\delta\tau_j}{4\pi D} \right)^{d/2} e^{-\frac{\xi(\tau_j)^2}{4D} \delta\tau_j} \\ &\rightarrow \frac{1}{Z} \sum_{\mathcal{P}} \exp\left(-\frac{1}{4D} \int_0^t d\tau \xi^2(\tau)\right), \end{aligned} \quad (28.20)$$

where $\delta\tau_i = \tau_i - \tau_{i-1}$, and the normalization constant is

$$\frac{1}{Z} = \lim \prod_i \left(\frac{\delta\tau_i}{2\pi D} \right)^{d/2}.$$

The most probable path is the one maximizing the integral inside the exponential. If we express the noise (28.10) as

$$\xi(t) = \dot{x}(t) - v(x(t)),$$

the probability is maximized by the variational principle

$$\min \int_0^t d\tau [\dot{x}(\tau) - v(x(\tau))]^2 = \min \int_0^t L(x(\tau), \dot{x}(\tau)) d\tau.$$

By the standard arguments, for a given x, x' and t the probability is maximized by a solution of Hamilton's equations (28.18) that connects the two points $x_0 \rightarrow x'$ in time t .

Résumé

When a deterministic trajectory is smeared out under the influence of Gaussian noise of strength D , the deterministic dynamics is recovered in the weak noise limit $D \rightarrow 0$. The effect of the noise can be taken into account by adding noise corrections to the classical trace formula.

Commentary

Remark 28.1 Literature. The theory of stochastic processes is a vast subject, spanning over centuries and over disciplines ranging from pure mathematics to impure finance. We

enjoyed reading van Kampen classic [1], especially his railings against those who blunder carelessly into nonlinear landscapes. Having committed this careless chapter to print, we shall no doubt be cast to a special place on the long list of van Kampen's sinners (and not for the first time, either). A more specialized monograph like Risken's [2] will do just as well. The standard Langevin equation is a stochastic equation for a Brownian particle, in which one replaces the Newton's equation for force by two counter-balancing forces: random accelerations $\xi(t)$ which tend to smear out a particle trajectory, and a damping term which drives the velocity to zero. Here we denote by 'Langevin equation' a more general family of stochastic differential equations (28.10) with additive weak noise limit.

If a flow is linear (in Hamiltonian case, with harmonic oscillator potential) with an attractive fixed point, \mathcal{L}_D^t describes a version of the Ornstein-Uhlenbeck process [20], (introduced already by Laplace in 1810, see ref. [21]). Gaussians are often rediscovered, so Onsager-Machlup seminal paper [18], which studies the same attractive linear fixed point is in literature often credited for being the first to introduce a variational method - the "principle of least dissipation" - based on the Lagrangian of form (28.19). They, in turn, credit Rayleigh [19] with introducing the least dissipation principle in hydrodynamics. Onsager-Machlup paper deals only with a finite set of linearly damped thermodynamic variables, and not with a nonlinear flow or unstable periodic orbits. In our exposition the setting is much more general: we study fluctuations over a state space varying velocity field $v(x)$. Schulman's monograph [11] contains a very readable summary of Kac's [12] exposition of Wiener's integral over stochastic paths.

Exercises

28.1. **Who ordered $\sqrt{\pi}$?** Derive the Gaussian integral

$$\frac{1}{\sqrt{2\pi}} \int_{-\infty}^{\infty} dx e^{-\frac{x^2}{2a}} = \sqrt{a}, \quad a > 0.$$

assuming only that you know to integrate the exponential function e^{-x} . Hint, hint: x^2 is a radius-squared of something. π is related to the area or circumference of something.

28.2. ***D*-dimensional Gaussian integrals.** Show that the Gaussian integral in *D*-dimensions is given by

$$\frac{1}{(2\pi)^{d/2}} \int d^d \phi e^{-\frac{1}{2} \phi^T \cdot M^{-1} \cdot \phi + \phi \cdot J} = |\det M|^{\frac{1}{2}} e^{\frac{1}{2} J^T \cdot M \cdot J}$$

where *M* is a real positive definite [*d* × *d*] matrix, i.e., a matrix with strictly positive eigenvalues. *x*, *J* are *D*-dimensional vectors, and *x*^{*T*} is the transpose of *x*.

28.3. **Convolution of Gaussians.** Show that the Fourier transform of convolution

$$[f * g](x) = \int d^d y f(x - y)g(y)$$

of two Gaussians

$$f(x) = e^{-\frac{1}{2} x^T \cdot \frac{1}{\Delta_1} \cdot x}, \quad g(x) = e^{-\frac{1}{2} x^T \cdot \frac{1}{\Delta_2} \cdot x}$$

factorizes as

$$[f * g](x) = \frac{1}{(2\pi)^d} \int dk F(k)G(k)e^{ik \cdot x}, \quad (28.22)$$

where

$$F(k) = \frac{1}{(2\pi)^d} \int d^d x f(x)e^{-ik \cdot x} = |\det \Delta_1|^{1/2} e^{\frac{1}{2} k^T \cdot \Delta_1 \cdot k}$$

$$G(k) = \frac{1}{(2\pi)^d} \int d^d x g(x)e^{-ik \cdot x} = |\det \Delta_2|^{1/2} e^{\frac{1}{2} k^T \cdot \Delta_2 \cdot k}$$

Hence

$$\begin{aligned} [f * g](x) &= \frac{1}{(2\pi)^d} |\det \Delta_1 \det \Delta_2|^{1/2} \int d^d p e^{\frac{1}{2} p^T \cdot (\Delta_1 + \Delta_2) \cdot p} e^{-ip \cdot x} \\ &= \frac{|\det \Delta_1 \det \Delta_2|^{1/2}}{|\det (\Delta_1 + \Delta_2)|} e^{-\frac{1}{2} x^T \cdot (\Delta_1 + \Delta_2)^{-1} \cdot x} \end{aligned}$$

References

[28.1] N. G. van Kampen, *Stochastic Processes in Physics and Chemistry* (North Holland, Amsterdam 1992).

[28.2] H. Risken, *The Fokker-Planck equation: Methods of solution and applications* (Springer-Verlag, New York, 1989).

[28.3] W. Dittrich and M. Reuter, *Classical and Quantum Dynamics: From Classical Paths to Path Integrals* (Springer-Verlag, Berlin 1994).

[28.4] E. M. Lifshitz and L. P. Pitaevskii, *Physical Kinetics* (Pergamon, London 1981).

[28.5] C. Itzykson and J.-M. Drouffe, *Statistical field theory* (Cambridge U. Press, 1991).

[28.6] V. Ambegaokar, *Reasoning about luck; probability and its uses in physics* (Cambridge Univ. Press, Cambridge 1996).

[28.7] B. Sakita, *Quantum theory of many variable systems and fields* (World Scientific, Singapore 1985).

- [28.8] G. E. Uhlenbeck, G. W. Ford and E. W. Montroll, *Lectures in Statistical Mechanics* (Amer. Math. Soc., Providence R.I., 1963).
- [28.9] M. Kac, "Random walk and the theory of Brownian motion," (1946), reprinted in ref. [10].
- [28.10] N. Wax, ed., *Selected Papers on Noise and Stochastic Processes* (Dover, New York 1954).
- [28.11] L. S. Schulman, *Techniques and Applications of Path Integration* (Wiley-Interscience, New York 1981).
- [28.12] M. Kac, *Probability and Related Topics in Physical Sciences* (Wiley-Interscience, New York 1959).
- [28.13] E. Nelson, *Quantum Fluctuations* (Princeton Univ. Press 1985).
- [28.14] H. Kunita, *Stochastic Flows and Stochastic Differential Equations* (Cambridge Univ. Press, Cambridge 1990).
- [28.15] H. Haken and G. Mayer-Kress, *Z. f. Physik* **B 43**, 185 (1981).
- [28.16] M. Roncadelli, *Phys. Rev.* **E 52**, 4661 (1995).
- [28.17] G. Ryskin, *Phys. Rev.* **E 56**, 5123 (1997).
- [28.18] L. Onsager and S. Machlup, *Phys. Rev.* **91**, 1505, 1512 (1953).
- [28.19] Lord Rayleigh, *Phil. Mag.* **26**, 776 (1913).
- [28.20] G. E. Uhlenbeck and L. S. Ornstein, *Phys. Rev.* **36**, 823 (1930).
- [28.21] M. Jacobsen, *Bernoulli J. of Math. Stat. and Prob.* **2**, 271 (1997).
- [28.22] P. Gaspard, "Trace Formula for Noisy Flows," *J. Stat. Phys.* **106**, 57 (2002).
- [28.23] M. I. Freidlin and A. D. Wentzel, *Random Perturbations of Dynamical Systems*, (Springer, New York 1998).
- [28.24] E. Gozzi, M. Reuter and W. D. Thacker, *Phys. Rev.* **D 40**, 3363 (1989).
- [28.25] E. Gozzi and M. Reuter, *Phys. Lett.* **233B**, 383 (1989); **238B**, 451 (1990); **240B**, 137 (1990).
- [28.26] E. Gozzi, M. Reuter and W. D. Thacker, *Phys. Rev.* **D 46**, 757 (1992).
- [28.27] E. Gozzi, M. Reuter and W. D. Thacker, *Chaos, Solitons and Fractals* **2**, 441 (1992).
- [28.28] R. Benzi, G. Paladin, G. Parisi and A. Vulpiani, *J. Phys.* **A 18**, 2157 (1985).
- [28.29] R. Graham, *Europhys. Lett.* **5**, 101 (1988).
- [28.30] R. Graham and T. Tél, *Phys. Rev. A* **35**, 1382 (1987).

- [28.31] L. Arnold and V. Wihstutz, *Lyapunov exponents, Lecture Notes in Math.* **1186** (Springer-Verlag, New York 1986).
- [28.32] M. V. Feigelman and A. M. Tsvetik, *Sov. Phys. JETP* **56**, 823 (1982).
- [28.33] G. Parisi and N. Sourlas, *Nucl. Phys.* **B206**, 321 (1982).
- [28.34] F. Langouche et al., *Functional integration and semiclassical expansion* (Reidel, Dordrecht 1982).
- [28.35] O. Cepas and J. Kurchan, “Canonically invariant formulation of Langevin and Fokker-Planck equations,” *European Phys. J. B* **2**, 221 (1998); [arXiv:cond-mat/9706296](https://arxiv.org/abs/cond-mat/9706296).
- [28.36] S. Tanase-Nicola and J. Kurchan, “Statistical-mechanical formulation of Lyapunov exponents;” [arXiv:cond-mat/0210380](https://arxiv.org/abs/cond-mat/0210380).

Chapter 29

Relaxation for cyclists

CYCLES, i.e., solutions of the periodic orbit condition (13.1)

$$f^{t+T}(x) = f^t(x), \quad T > 0 \quad (29.1)$$

are prerequisite to chapters 18 and 19 evaluation of spectra of classical evolution operators. Chapter 13 offered an introductory, hands-on guide to extraction of periodic orbits by means of the Newton-Raphson method. Here we take a very different tack, drawing inspiration from variational principles of classical mechanics, and path integrals of quantum mechanics.

In sect. 13.2.1 we converted orbits unstable forward in time into orbits stable backwards in time. Indeed, all methods for finding unstable cycles are based on the idea of constructing a new dynamical system such that (i) the position of the cycle is the same for the original system and the transformed one, (ii) the unstable cycle in the original system is a stable cycle of the transformed system.

The Newton-Raphson method for determining a fixed point x_* for a map $x' = f(x)$ is an example. The method replaces iteration of $f(x)$ by iteration of the Newton-Raphson map (13.5)

$$x'_i = g_i(x) = x_i - \left(\frac{1}{M(x) - \mathbf{1}} \right)_{ij} (f(x) - x)_j. \quad (29.2)$$

A fixed point x_* for a map $f(x)$ is also a fixed point of $g(x)$, indeed a superstable fixed point since $\partial g_i(x_*)/\partial x_j = 0$. This makes the convergence to the fixed point super-exponential.

We also learned in chapter 13 that methods that start with initial guesses for a number of points along a cycle are considerably more robust and safer than

searches based on direct solution of the fixed-point condition (29.1). The relaxation (or variational) methods that we shall now describe take this multipoint approach to its logical extreme, and start by a guess of not a few points along a periodic orbit, but a guess of the entire orbit.

The idea is to make an informed rough guess of what the desired periodic orbit looks like globally, and then use variational methods to drive the initial guess toward the exact solution. Sacrificing computer memory for robustness of the method, we replace a guess that a *point* is on the periodic orbit by a guess of the *entire orbit*. And, sacrificing speed for safety, in sect. 29.1 we replace the Newton-Raphson *iteration* by a fictitious time *flow* that minimizes a cost function computed as deviation of the approximate flow from the true flow along a loop approximation to a periodic orbit.

If you have some insight into the topology of the flow and its symbolic dynamics, or have already found a set of short cycles, you might be able to construct an initial approximation to a longer cycle p as a sequence of N points $(\tilde{x}_1^{(0)}, \tilde{x}_2^{(0)}, \dots, \tilde{x}_N^{(0)})$ with the periodic boundary condition $\tilde{x}_{N+1} = \tilde{x}_1$. Suppose you have an iterative method for improving your guess; after k iterations the cost function

$$F^2(\tilde{x}^{(k)}) = \sum_i^N (\tilde{x}_{i+1}^{(k)} - f(\tilde{x}_i^{(k)}))^2 \quad (29.3)$$

or some other more cleverly constructed function (for classical mechanics - action) is a measure of the deviation of the k th approximate cycle from the true cycle. This observation motivates variational approaches to determining cycles.

We give here three examples of such methods, two for maps, and one for billiards. In sect. 29.1 we start out by converting a problem of finding an unstable fixed point of a map into a problem of constructing a differential flow for which the desired fixed point is an attracting equilibrium point. Solving differential equations can be time intensive, so in sect. 29.2 we replace such flows by discrete iterations. In sect. 29.3 we show that for $2D$ -dimensional billiard flows variation of D coordinates (where D is the number of Hamiltonian degrees of freedom) suffices to determine cycles in the full $2D$ -dimensional phase space.

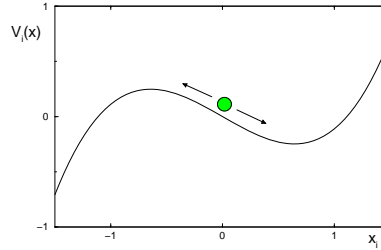
29.1 Fictitious time relaxation

(O. Biham, C. Chandre and P. Cvitanović)

The relaxation (or gradient) algorithm for finding cycles is based on the observation that a trajectory of a map such as the Hénon map (3.19),

$$\begin{aligned} x_{i+1} &= 1 - ax_i^2 + by_i \\ y_{i+1} &= x_i, \end{aligned} \quad (29.4)$$

Figure 29.1: “Potential” $V_i(x)$ (29.7) for a typical point along an initial guess trajectory. For $\sigma_i = +1$ the flow is toward the local maximum of $V_i(x)$, and for $\sigma_i = -1$ toward the local minimum. A large deviation of x_i ’s is needed to destabilize a trajectory passing through such local extremum of $V_i(x)$, hence the basin of attraction is expected to be large.



is a stationary solution of the relaxation dynamics defined by the flow

$$\frac{dx_i}{d\tau} = v_i, \quad i = 1, \dots, n \tag{29.5}$$

for any vector field $v_i = v_i(x)$ which vanishes on the trajectory. Here τ is a “fictitious time” variable, unrelated to the dynamical time (in this example, the discrete time of map iteration). As the simplest example, take v_i to be the deviation of an approximate trajectory from the exact 2-step recurrence form of the Hénon map (3.20)

$$v_i = x_{i+1} - 1 + ax_i^2 - bx_{i-1}. \tag{29.6}$$

For fixed x_{i-1}, x_{i+1} there are two values of x_i satisfying $v_i = 0$. These solutions are the two extremal points of a local “potential” function (no sum on i)

$$v_i = \frac{\partial}{\partial x_i} V_i(x), \quad V_i(x) = x_i(x_{i+1} - bx_{i-1} - 1) + \frac{a}{3}x_i^3. \tag{29.7}$$

Assuming that the two extremal points are real, one is a local minimum of $V_i(x)$ and the other is a local maximum. Now here is the idea; replace (29.5) by

$$\frac{dx_i}{d\tau} = \sigma_i v_i, \quad i = 1, \dots, n, \tag{29.8}$$

where $\sigma_i = \pm 1$.

The modified flow will be in the direction of the extremal point given by the local maximum of $V_i(x)$ if $\sigma_i = +1$ is chosen, or in the direction of the one corresponding to the local minimum if we take $\sigma_i = -1$. This is not quite what happens in solving (29.8) - all x_i and $V_i(x)$ change at each integration step - but this is the observation that motivates the method. The differential equations (29.8) then drive an approximate initial guess toward the exact trajectory. A sketch of the landscape in which x_i converges towards the proper fixed point is given in figure 29.1. As the “potential” function (29.7) is not bounded for a large $|x_i|$, the flow diverges for initial guesses which are too distant from the true trajectory. However, the basin of attraction of initial guesses that converge to a given cycle is nevertheless very large, with the spread in acceptable initial guesses for figure 29.1 of order 1, in contrast to the exponential precision required of initial guesses by the Newton-Raphson method.

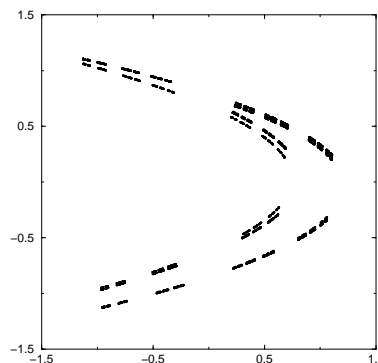


Figure 29.2: The repeller for the Hénon map at $a = 1.8$, $b = 0.3$.

Example 29.1 Hénon map cycles. Our aim in this calculation is to find all periodic orbits of period n for the Hénon map (29.4), in principle at most 2^n orbits. We start by choosing an initial guess trajectory (x_1, x_2, \dots, x_n) and impose the periodic boundary condition $x_{n+1} = x_1$. The simplest and a rather crude choice of the initial condition in the Hénon map example is $x_i = 0$ for all i . In order to find a given orbit one sets $\sigma_i = -1$ for all iterates i which are local minima of $V_i(x)$, and $\sigma_i = 1$ for iterates which are local maxima. In practice one runs through a complete list of prime cycles, such as the table 15.1. The real issue for all searches for periodic orbits, this one included, is how large is the basin of attraction of the desired periodic orbit? There is no easy answer to this question, but empirically it turns out that for the Hénon map such initial guess almost always converges to the desired trajectory as long as the initial $|x|$ is not too large compared to $1/\sqrt{a}$. Figure 29.1 gives some indication of a typical basin of attraction of the method (see also figure 29.3).

The calculation is carried out by solving the set of n ordinary differential equations (29.8) using a simple Runge-Kutta method with a relatively large step size ($h = 0.1$) until $|v|$ becomes smaller than a given value ε (in a typical calculation $\varepsilon \sim 10^{-7}$). Empirically, in the case that an orbit corresponding to the desired itinerary does not exist, the initial guess escapes to infinity since the “potential” $V_i(x)$ grows without bound.

exercise 29.3

Applied to the Hénon map at the Hénon’s parameters choice $a = 1.4$, $b = 0.3$, the method has yielded all periodic orbits to periods as long as $n = 28$, as well as selected orbits up to period $n = 1000$. All prime cycles up to period 10 for the Hénon map, $a = 1.4$ and $b = 0.3$, are listed in table 29.1. The number of unstable periodic orbits for periods $n \leq 28$ is given in table 29.2. Comparing this with the list of all possible 2-symbol alphabet prime cycles, table 15.1, we see that the pruning is quite extensive, with the number of periodic points of period n growing as $e^{0.4645 \cdot n} = (1.592)^n$ rather than as 2^n .

As another example we plot all unstable periodic points up to period $n = 14$ for $a = 1.8$, $b = 0.3$ in figure 29.2. Comparing this repelling set with the strange attractor for the Hénon’s parameters figure 3.9, we note the existence of gaps in the set, cut out by the preimages of the escaping regions.

remark 29.2

In practice, the relaxation flow (29.8) finds (almost) all periodic orbits which exist and indicates which ones do not. For the Hénon map the method enables us to calculate almost all unstable cycles of essentially any desired length and accuracy.

The idea of the relaxation algorithm illustrated by the above Hénon map example is that instead of searching for an unstable periodic orbit of a map, one searches for a stable attractor of a vector field. More generally, consider a d -dimensional map $x' = f(x)$ with a hyperbolic fixed point x_* . Any fixed point x_* is

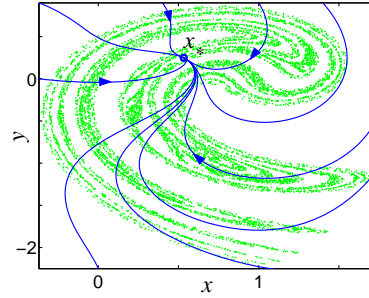
Table 29.1: All prime cycles up to period 10 for the Hénon map, $a = 1.4$ and $b = 0.3$. The columns list the period n_p , the itinerary (defined in remark 29.4), a periodic point (y_p, x_p) , and the cycle Lyapunov exponent $\lambda_p = \ln |\Lambda_p|/n_p$. While most of the cycles have $\lambda_p \approx 0.5$, several significantly do not. The $\bar{0}$ periodic point is very unstable, isolated and transient fixed point, with no other cycles returning close to it. At period 13 one finds a pair of cycles with exceptionally low Lyapunov exponents. The cycles are close for most of the trajectory, differing only in the one symbol corresponding to two periodic points straddle the (partition) fold of the attractor. As the system is not hyperbolic, there is no known lower bound on cycle Lyapunov exponents, and the Hénon's strange "attractor" might some day turn out to be nothing but a transient on the way to a periodic attractor of some long period.

n	p	(y_p, x_p)	λ_p
1	0	(-1.13135447, -1.13135447)	1.18167262
	1	(0.63135447, 0.63135447)	0.65427061
2	01	(0.97580005, -0.47580005)	0.55098676
4	0111	(-0.70676677, 0.63819399)	0.53908457
6	010111	(-0.41515894, 1.07011813)	0.55610982
	011111	(-0.80421990, 0.44190995)	0.55245341
7	00111101	(-1.04667757, -0.17877958)	0.40998559
	00111111	(-1.08728604, -0.28539206)	0.46539757
	01011111	(-0.34267842, 1.14123046)	0.41283650
	01111111	(-0.88050537, 0.26827759)	0.51090634
8	000111101	(-1.25487963, -0.82745422)	0.43876727
	000111111	(-1.25872451, -0.83714168)	0.43942101
	001111101	(-1.14931330, -0.48368863)	0.47834615
	001111111	(-1.14078564, -0.44837319)	0.49353764
	01010111	(-0.52309999, 0.93830866)	0.54805453
	01011111	(-0.38817041, 1.09945313)	0.55972495
	01111111	(-0.83680827, 0.36978609)	0.56236493
9	0001111101	(-1.27793296, -0.90626780)	0.38732115
	0001111111	(-1.27771933, -0.90378859)	0.39621864
	0011111101	(-1.10392601, -0.34524675)	0.51112950
	0011111111	(-1.11352304, -0.36427104)	0.51757012
	0101111111	(-0.36894919, 1.11803210)	0.54264571
	0111111111	(-0.85789748, 0.32147653)	0.56016658
10	00011111101	(-1.26640530, -0.86684837)	0.47738235
	00011111111	(-1.26782752, -0.86878943)	0.47745508
	001111111101	(-1.12796804, -0.41787432)	0.52544529
	001111111111	(-1.12760083, -0.40742737)	0.53063973
	0101010111	(-0.48815908, 0.98458725)	0.54989554
	0101011111	(-0.53496022, 0.92336925)	0.54960607
	0101110111	(-0.42726915, 1.05695851)	0.54836764
	0101111111	(-0.37947780, 1.10801373)	0.56915950
	0111011111	(-0.69555680, 0.66088560)	0.54443884
	0111111111	(-0.84660200, 0.34750875)	0.57591048
13	1110011101000	(-1.2085766485, -0.6729999948)	0.19882434
	1110011101001	(-1.0598110494, -0.2056310390)	0.21072511

Table 29.2: The number of unstable periodic orbits of the Hénon map for $a = 1.4$, $b = 0.3$, of all periods $n \leq 28$. M_n is the number of prime cycles of length n , and N_n is the total number of periodic points of period n (including repeats of shorter prime cycles).

n	M_n	N_n	n	M_n	N_n	n	M_n	N_n
11	14	156	17	166	2824	23	1930	44392
12	19	248	18	233	4264	24	2902	69952
13	32	418	19	364	6918	25	4498	112452
14	44	648	20	535	10808	26	6806	177376
15	72	1082	21	834	17544	27	10518	284042
16	102	1696	22	1225	27108	28	16031	449520

Figure 29.3: Typical trajectories of the vector field (29.9) for the stabilization of a hyperbolic fixed point of the Ikeda map (29.11) located at $(x, y) \approx (0.53275, 0.24689)$. The circle indicates the position of the fixed point. Note that the basin of attraction of this fixed point is large, larger than the entire Ikeda attractor.



by construction an equilibrium point of the fictitious time flow

$$\frac{dx}{d\tau} = f(x) - x. \tag{29.9}$$

If all eigenvalues of the Jacobian matrix $J(x_*) = Df(x_*)$ have real parts smaller than unity, then x_* is a stable equilibrium point of the flow.

If some of the eigenvalues have real parts larger than unity, then one needs to modify the vector field so that the corresponding directions of the flow are turned into stable directions in a neighborhood of the fixed point. In the spirit of (29.8), modify the flow by

$$\frac{dx}{d\tau} = \mathbf{C} (f(x) - x) , \tag{29.10}$$

where \mathbf{C} is a $[d \times d]$ invertible matrix. The aim is to turn x_* into a stable equilibrium point of the flow by an appropriate choice of \mathbf{C} . It can be shown that a set of permutation / reflection matrices with one and only one non-vanishing entry ± 1 per row or column (for d -dimensional systems, there are $d!2^d$ such matrices) suffices to stabilize any fixed point. In practice, one chooses a particular matrix \mathbf{C} , and the flow is integrated. For each choice of \mathbf{C} , one or more hyperbolic fixed points of the map may turn into stable equilibria of the flow.

Example 29.2 Ikeda map: We illustrate the method with the determination of the periodic orbits of the Ikeda map:

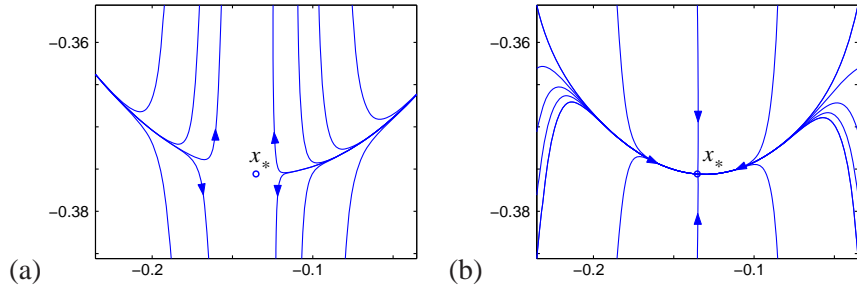
$$\begin{aligned} x' &= 1 + a(x \cos w - y \sin w) \\ y' &= a(x \sin w + y \cos w) \end{aligned} \tag{29.11}$$

where $w = b - \frac{c}{1 + x^2 + y^2}$,

with $a = 0.9, b = 0.4, c = 6$. The fixed point x_* is located at $(x, y) \approx (0.53275, 0.24689)$, with eigenvalues of the Jacobian matrix $(\Lambda_1, \Lambda_2) \approx (-2.3897, -0.3389)$, so the flow is already stabilized with $\mathbf{C} = \mathbf{1}$. Figure 29.3 depicts the flow of the vector field around the fixed point x_* .

In order to determine x_* , one needs to integrate the vector field (29.9) forward in time (the convergence is exponential in time), using a fourth order Runge-Kutta or any other integration routine.

Figure 29.4: Typical trajectories of the vector field (29.10) for a hyperbolic fixed point $(x, y) \approx (-0.13529, -0.37559)$ of f^3 , where f is the Ikeda map (29.11). The circle indicates the position of the fixed point. For the vector field corresponding to (a) $\mathbf{C} = \mathbf{1}$, x_* is a hyperbolic equilibrium point of the flow, while for (b) $\mathbf{C} = \begin{pmatrix} 1 & 0 \\ 0 & -1 \end{pmatrix}$, x_* is an attracting equilibrium point.



In contrast, determination of the 3-cycles of the Ikeda map requires nontrivial \mathbf{C} matrices, different from the identity. Consider for example the hyperbolic fixed point $(x, y) \approx (-0.13529, -0.37559)$ of the third iterate f^3 of the Ikeda map. The flow of the vector field for $\mathbf{C} = \mathbf{1}$, Figure 29.4 (a), indicates a hyperbolic equilibrium point, while for $\mathbf{C} = \begin{pmatrix} 1 & 0 \\ 0 & -1 \end{pmatrix}$ the flow of the vector field, figure 29.4 (b) indicates that x_ is an attracting equilibrium point, reached at exponential speed by integration forward in time.*

The generalization from searches for fixed points to searches for cycles is straightforward. In order to determine a prime cycle $x = (x_1, x_2, \dots, x_n)$ of a d -dimensional map $x' = f(x)$, we modify the multipoint shooting method of sect. 13.3, and consider the nd -dimensional vector field

$$\frac{dx}{d\tau} = \mathbf{C}(f(x) - x), \tag{29.12}$$

where $f(x) = (f(x_n), f(x_1), f(x_2), \dots, f(x_{n-1}))$, and \mathbf{C} is an invertible $[nd \times nd]$ matrix. For the Hénon map, it is sufficient to consider a set of 2^n diagonal matrices with eigenvalues ± 1 . Risking a bit of confusion, we denote by $x, f(x)$ both the d -dimensional vectors in (29.10), and nd -dimensional vectors in (29.12), as the structure of the equations is the same.

29.2 Discrete iteration relaxation method

(C. Chandre, F.K. Diakonov and P. Schmelcher)

The problem with the Newton-Raphson iteration (29.2) is that it requires very precise initial guesses. For example, the n th iterate of a unimodal map has as many as 2^n periodic points crammed into the unit interval, so determination of all cycles of length n requires that the initial guess for each one of them has to be accurate to roughly 2^{-n} . This is not much of a problem for 1-dimensional maps, but making a good initial guess for where a cycle might lie in a d -dimensional state space can be a challenge.

Emboldened by the success of the cyclist relaxation trick (29.8) of manually turning instability into stability by a sign change, we now (i) abandon the Newton-Raphson method altogether, (ii) abandon the continuous fictitious time flow (29.9) with its time-consuming integration, replacing it by a map g with a larger basin

of attraction (not restricted to a linear neighborhood of the fixed point). The idea is to construct a very simple map g , a linear transformation of the original f , for which the fixed point is stable. We replace the Jacobian matrix prefactor in (29.2) (whose inversion can be time-consuming) by a constant matrix prefactor

$$x' = g(x) = x + \Delta\tau \mathbf{C}(f(x) - x), \quad (29.13)$$

where $\Delta\tau$ is a positive real number, and \mathbf{C} is a $[d \times d]$ permutation and reflection matrix with one and only one non-vanishing entry ± 1 per row or column. A fixed point of f is also a fixed point of g . Since \mathbf{C} is invertible, the inverse is also true.

This construction is motivated by the observation that for small $\Delta\tau \rightarrow d\tau$ the map (29.13) is the Euler method for integrating the modified flow (29.10), with the integration step $\Delta\tau$.

The argument why a suitable choice of matrix \mathbf{C} can lead to the stabilization of an unstable periodic orbit is similar to the one used to motivate the construction of the modified vector field in sect. 29.1. Indeed, the flow (29.8) is the simplest example of this method, with the infinitesimal fictitious time increment $\Delta\tau \rightarrow d\tau$, the infinitesimal coordinate correction $(x - x') \rightarrow dx_i$, and the $[n \times n]$ diagonal matrix $\mathbf{C} \rightarrow \sigma_i = \pm 1$.

For a given fixed point of $f(x)$ we again chose a \mathbf{C} such that the flow in the expanding directions of $M(x_*)$ is turned into a contracting flow. The aim is to stabilize x_* by a suitable choice of \mathbf{C} . In the case where the map has multiple fixed points, the set of fixed points is obtained by changing the matrix \mathbf{C} (in general different for each unstable fixed point) and varying initial conditions for the map g . For example, for 2-dimensional dissipative maps it can be shown that the 3 matrices

remark 29.3

$$\mathbf{C} \in \left\{ \begin{pmatrix} 1 & 0 \\ 0 & 1 \end{pmatrix}, \begin{pmatrix} -1 & 0 \\ 0 & 1 \end{pmatrix}, \begin{pmatrix} 1 & 0 \\ 0 & -1 \end{pmatrix} \right\}$$

suffice to stabilize all kinds of possible hyperbolic fixed points.

If $\Delta\tau$ is chosen sufficiently small, the magnitude of the eigenvalues of the fixed point x_* in the transformed system are smaller than one, and one has a stable fixed point. However, $\Delta\tau$ should not be chosen too small: Since the convergence is geometrical with a ratio $1 - \alpha\Delta\tau$ (where the value of constant α depends on the stability of the fixed point in the original system), small $\Delta\tau$ can slow down the speed of convergence. The critical value of $\Delta\tau$, which just suffices to make the fixed point stable, can be read off from the quadratic equations relating the stability coefficients of the original system and those of the transformed system. In practice, one can find the optimal $\Delta\tau$ by iterating the dynamical system stabilized with a given \mathbf{C} and $\Delta\tau$. In general, all starting points converge on the attractor provided $\Delta\tau$ is small enough. If this is not the case, the trajectory either diverges (if $\Delta\tau$ is far too large) or it oscillates in a small section of the state space (if $\Delta\tau$ is close to its stabilizing value).

The search for the fixed points is now straightforward: A starting point chosen in the global neighborhood of the fixed point iterated with the transformed dynamical system g converges to the fixed point due to its stability. Numerical investigations show that the domain of attraction of a stabilized fixed point is a rather extended connected area, by no means confined to a linear neighborhood. At times the basin of attraction encompasses the complete state space of the attractor, so one can be sure to be within the attracting basin of a fixed point regardless of where on the attractor one picks the initial condition.

The step size $|g(x) - x|$ decreases exponentially when the trajectory approaches the fixed point. To get the coordinates of the fixed points with a high precision, one therefore needs a large number of iterations for the trajectory which is already in the linear neighborhood of the fixed point. To speed up the convergence of the final part of the approach to a fixed point we recommend a combination of the above approach with the Newton-Raphson method (29.2).

The fixed points of the n th iterate f^n are periodic points of a cycle of period n . If we consider the map

$$x' = g(x) = x + \Delta\tau \mathbf{C}(f^n(x) - x), \quad (29.14)$$

the iterates of g converge to a fixed point provided that $\Delta\tau$ is sufficiently small and \mathbf{C} is a $[d \times d]$ constant matrix chosen such that it stabilizes the flow. As n grows, $\Delta\tau$ has to be chosen smaller and smaller. In the case of the Ikeda map example 29.2 the method works well for $n \leq 20$. As in (29.12), the multipoint shooting method is the method of preference for determining longer cycles. Consider $x = (x_1, x_2, \dots, x_n)$ and the nd -dimensional map

$$x' = f(x) = (f(x_n), f(x_1), \dots, f(x_{n-1})).$$

Determining cycles with period n for the d -dimensional f is equivalent to determining fixed points of the multipoint dn -dimensional f . The idea is to construct a matrix \mathbf{C} such that the fixed point of f becomes stable for the map:

$$x' = x + \Delta\tau \mathbf{C}(f(x) - x),$$

where \mathbf{C} is now a $[nd \times nd]$ permutation/reflection matrix with only one non-zero matrix element ± 1 per row or column. For any given matrix \mathbf{C} , a certain fraction of the cycles becomes stable and can be found by iterating the transformed map which is now a nd dimensional map.

From a practical point of view, the main advantage of this method compared to the Newton-Raphson method is twofold: (i) the Jacobian matrix of the flow need not be computed, so there is no large matrix to invert, simplifying considerably the implementation, and (ii) empirical basins of attractions for individual \mathbf{C} are much larger than for the Newton-Raphson method. The price is a reduction in the speed of convergence.

Table 29.3: All prime cycles up to 6 bounces for the 3-disk fundamental domain, center-to-center separation $R = 6$, disk radius $a = 1$. The columns list the cycle itinerary, its expanding eigenvalue Λ_p , and the length of the orbit (if the velocity=1 this is the same as its period or the action). Note that the two 6 cycles 001011 and 001101 are degenerate due to the time reversal symmetry, but are not related by any discrete spatial symmetry. (Computed by P.E. Rosenqvist.)

p	Λ_p	T_p
0	9.898979485566	4.000000000000
1	$-1.177145519638 \times 10^1$	4.267949192431
01	$-1.240948019921 \times 10^2$	8.316529485168
001	$-1.240542557041 \times 10^3$	12.321746616182
011	$1.449545074956 \times 10^3$	12.580807741032
0001	$-1.229570686196 \times 10^4$	16.322276474382
0011	$1.445997591902 \times 10^4$	16.585242906081
0111	$-1.707901900894 \times 10^4$	16.849071859224
00001	$-1.217338387051 \times 10^5$	20.322330025739
00011	$1.432820951544 \times 10^5$	20.585689671758
00101	$1.539257907420 \times 10^5$	20.638238386018
00111	$-1.704107155425 \times 10^5$	20.853571517227
01011	$-1.799019479426 \times 10^5$	20.897369388186
01111	$2.010247347433 \times 10^5$	21.116994322373
000001	$-1.205062923819 \times 10^6$	24.322335435738
000011	$1.418521622814 \times 10^6$	24.585734788507
000101	$1.52597448217 \times 10^6$	24.638760250323
000111	$-1.688624934257 \times 10^6$	24.854025100071
001011	$-1.796354939785 \times 10^6$	24.902167001066
001101	$-1.796354939785 \times 10^6$	24.902167001066
001111	$2.005733106218 \times 10^6$	25.121488488111
010111	$2.119615015369 \times 10^6$	25.165628236279
011111	$-2.366378254801 \times 10^6$	25.384945785676

29.3 Least action method

(P. Dahlqvist)

The methods of sects. 29.1 and 29.2 are somewhat *ad hoc*, as for general flows and iterated maps there is no fundamental principle to guide us in choosing the cost function, such as (29.3), to vary.

For Hamiltonian dynamics, we are on much firmer ground; Maupertuis least action principle. You yawn your way through it in every mechanics course—but as we shall now see, it is a very hands-on numerical method for finding cycles.

Indeed, the simplest and numerically most robust method for determining cycles of planar billiards is given by the principle of least action, or equivalently, by extremizing the length of an approximate orbit that visits a given sequence of disks. In contrast to the multipoint shooting method of sect. 13.3 which requires variation of $2n$ phase space points, extremization of a cycle length requires variation of only n bounce positions s_i .

The problem is to find the extremum values of cycle length $L(s)$ where $s = (s_1, \dots, s_n)$, that is find the roots of $\partial_i L(s) = 0$. Expand to first order

$$\partial_i L(s_0 + \delta s) = \partial_i L(s_0) + \sum_j \partial_i \partial_j L(s_0) \delta s_j + \dots$$

exercise 29.1

and use $M_{ij}(s_0) = \partial_i \partial_j L(s_0)$ in the n -dimensional Newton-Raphson iteration scheme of sect. 13.2.2

$$s_i \mapsto s_i - \sum_j \left(\frac{1}{M(s)} \right)_{ij} \partial_j L(s) \quad (29.15)$$

The extremization is achieved by recursive implementation of the above algorithm, with proviso that if the dynamics is pruned, one also has to check that the final extremal length orbit does not penetrate a billiard wall.

exercise 29.2
exercise 13.13

As an example, the short periods and stabilities of 3-disk cycles computed this way are listed table 29.3.

Résumé

Unlike the Newton-Raphson method, variational methods are very robust. As each step around a cycle is short, they do not suffer from exponential instabilities, and with rather coarse initial guesses one can determine cycles of arbitrary length.

Commentary

Remark 29.1 Piecewise linear maps. The Lozi map (3.21) is linear, and 100,000's of cycles can be easily computed by [2x2] matrix multiplication and inversion.

Remark 29.2 Relaxation method. The relaxation (or gradient) algorithm is one of the methods for solving extremal problems [13]. The method described above was introduced by Biham and Wenzel [1], who have also generalized it (in the case of the Hénon map) to determination of *all* 2^n cycles of period n , real or complex [2]. The applicability and reliability of the method is discussed in detail by Grassberger, Kantz and Moening [5], who give examples of the ways in which the method fails: (a) it might reach a limit cycle rather than an equilibrium saddle point (that can be remedied by the complex Biham-Wenzel algorithm [2]) (b) different symbol sequences can converge to the same cycle (i.e., more refined initial conditions might be needed). Furthermore, Hansen (ref. [7] and chapter 4. of ref. [20]) has pointed out that the method cannot find certain cycles for specific values of the Hénon map parameters. In practice, the relaxation method for determining periodic orbits of maps appears to be effective almost always, but not always. It is much slower than the multipoint shooting method of sect. 13.3, but also much quicker to program, as it does not require evaluation of stability matrices and their inversion. If the complete set of cycles is required, the method has to be supplemented by other methods.

Remark 29.3 Hybrid Newton-Raphson/relaxation methods. The method discussed in sect. 29.2 was introduced by Schmelcher *et al* [9]. The method was extended to flows by means of the Poincaré surface of section technique in ref. [10]. It is also possible to combine the Newton-Raphson method and (29.13) in the construction of a transformed map [14]. In this approach, each step of the iteration scheme is a linear superposition of a step of the stability transformed system and a step of the Newton-Raphson algorithm. Far from the linear neighborhood the weight is dominantly on the globally acting stability transformation algorithm. Close to the fixed point, the steps of the iteration are dominated by the Newton-Raphson procedure.

Remark 29.4 Relation to the Smale horseshoe symbolic dynamics. For a complete horseshoe Hénon repeller (a sufficiently large), such as the one given in figure 29.2, the signs $\sigma_i \in \{1, -1\}$ are in a 1-to-1 correspondence with the Smale horseshoe symbolic dynamics $s_i \in \{0, 1\}$:

$$s_i = \begin{cases} 0 & \text{if } \sigma_i = -1, \quad x_i < 0 \\ 1 & \text{if } \sigma_i = +1, \quad x_i > 0 \end{cases} \quad (29.16)$$

For arbitrary parameter values with a finite subshift symbolic dynamics or with arbitrarily complicated pruning, the relation of sign sequences $\{\sigma_1, \sigma_2, \dots, \sigma_n\}$ to the itineraries $\{s_1, s_2, \dots, s_n\}$ can be much subtler; this is discussed in ref. [5].

Remark 29.5 Ikeda map. Ikeda map (29.11) was introduced in ref. [12] is a model which exhibits complex dynamics observed in nonlinear optical ring cavities.

Remark 29.6 Relaxation for continuous time flows. For a d -dimensional flow $\dot{x} = v(x)$, the method described above can be extended by considering a Poincaré surface of section. The Poincaré section yields a map f with dimension $d-1$, and the above discrete iterative maps procedures can be carried out. A method that keeps the trial orbit continuous throughout the calculation is the Newton descent, a variational method for finding periodic orbits of continuous time flows, is described in refs. [15, 16].

Remark 29.7 Stability ordering. The parameter $\Delta\tau$ in (29.13) is a key quantity here. It is related to the stability of the desired cycle in the transformed system: The more unstable a fixed point is, the smaller $\Delta\tau$ has to be to stabilize it. With increasing cycle periods, the unstable eigenvalue of the Jacobian matrix increases and therefore $\Delta\tau$ has to be reduced to achieve stabilization of all fixed points. In many cases the least unstable cycles of a given period n are of physically most important [11]. In this context $\Delta\tau$ operates as a stability filter. It allows the selective stabilization of only those cycles which possess Lyapunov exponents smaller than a cut-off value. If one starts the search for cycles within a given period n with a value $\Delta\tau \approx O(10^{-1})$, and gradually lowers $\Delta\tau$ one obtains the sequence of all unstable orbits of order n sorted with increasing values of their Lyapunov exponents. For the specific choice of \mathbf{C} the relation between $\Delta\tau$ and the stability coefficients of the fixed points of the original system is strictly monotonous. Transformed dynamical systems with other \mathbf{C} 's do not obey such a strict behavior but show a rough ordering of the sequence of Floquet multipliers of the fixed points stabilized in the course of decreasing values for $\Delta\tau$. As explained in sect. 20.5, stability ordered cycles are needed to order cycle expansions of dynamical quantities of chaotic systems for which a symbolic dynamics is not known. For such systems, an ordering of cycles with respect to their stability has been proposed [14, 15, 13], and shown to yield good results in practical applications.

section 20.5

Remark 29.8 Action extremization method. The action extremization (sect. 29.3) as a numerical method for finding cycles has been introduced independently by many people. We have learned it from G. Russberg, and from M. Sieber's and F. Steiner's hyperbola billiard computations [17, 18]. The convergence rate is really impressive, for the Sinai billiard some 5000 cycles are computed within CPU seconds with rather bad initial guesses.

Variational methods are the key ingredient of the Aubry-Mather theory of area-preserving twist maps (known in the condensed matter literature as the Frenkel-Kontorova models of 1-dimensional crystals), discrete-time Hamiltonian dynamical systems particularly suited to explorations of the K.A.M. theorem. Proofs of the Aubry-Mather theorem [20] on existence of quasi-periodic solutions are variational. It was quickly realized that the variational methods can also yield reliable, high precision computations of long periodic orbits of twist map models in 2 or more dimensions, needed for K.A.M. renormalization studies [19].

A fictitious time gradient flow similar to the one discussed here in sect. 29.1 was introduced by Anegent [21] for twist maps, and used by Gole [22] in his proof of the Aubry-Mather theorem. Mathematical bounds on the regions of stability of K.A.M. tori are notoriously restrictive compared to the numerical indications, and de la Llave, Falcolini and Tompaidis [23, 24] have found the gradient flow formulation advantageous both in studies of the analyticity domains of the K.A.M. stability, as well as proving the Aubry-Mather theorem for extended systems (for a pedagogical introduction, see the lattice dynamics section of ref. [25]).

All of the twist-maps work is based on extremizing the discrete dynamics version of the action S (in this context sometimes called a “generating function”). However, in their investigations in the complex plane, Falcolini and de la Llave [23] do find it useful to minimize instead $S\bar{S}$, analogous to our cost function (29.3).

Exercises

29.1. Evaluation of billiard cycles by minimization*.

Given a symbol sequence, you can construct a guess trajectory by taking a point on the boundary of each disk in the sequence, and connecting them by straight lines. If this were a rubber band wrapped through 3 rings, it would shrink into the physical trajectory, which minimizes the action (in this case, the length) of the trajectory.

Write a program to find the periodic orbits for your billiard simulator. Use the least action principle to extremize the length of the periodic orbit, and reproduce the periods and stabilities of 3-disk cycles, table 29.3. (One such method is given in sect. 29.3.) After that check the accuracy of the computed orbits by iterating them forward with your simulator. What is your error $|f^{T_p}(x) - x|$?

29.2. **Tracking cycles adiabatically***. Once a cycle has been found, orbits for different system parameters values may

be obtained by varying slowly (adiabatically) the parameters, and using the old orbit points as starting guesses in the Newton method. Try this method out on the 3-disk system. It works well for $R : a$ sufficiently large. For smaller values, some orbits change rather quickly and require very small step sizes. In addition, for ratios below $R : a = 2.04821419 \dots$ families of cycles are pruned, i.e. some of the minimal length trajectories are blocked by intervening disks.

29.3. **Cycles of the Hénon map.** Apply the method of sect. 29.1 to the Hénon map at the Hénon's parameters choice $a = 1.4, b = 0.3$, and compute all prime cycles for at least $n \leq 6$. Estimate the topological entropy, either from the definition (15.1), or as the zero of a truncated topological zeta function (15.27). Do your cycles agree with the cycles listed in table 29.1?

References

- [29.1] O. Biham and W. Wenzel, "Characterization of unstable periodic orbits in chaotic attractors and repellers," *Phys. Rev. Lett.* **63**, 819 (1989).
- [29.2] O. Biham and W. Wenzel, *Phys. Rev. A* **42**, 4639 (1990).
- [29.3] P. Grassberger and H. Kantz, "Generating partitions for the dissipative Hénon map," *Phys. Lett. A* **113**, 235 (1985).
- [29.4] H. Kantz and P. Grassberger, *Physica* **17D**, 75 (1985).
- [29.5] P. Grassberger, H. Kantz, and U. Moenig. "On the symbolic dynamics of the Hénon map," *J. Phys. A* **43**, 5217 (1989).
- [29.6] M. Eisele, "Comparison of several generating partitions of the Hnon map," *J. Phys. A* **32**, 1533 (1999).
- [29.7] K.T. Hansen, "Remarks on the symbolic dynamics for the Hénon map," *Phys. Lett. A* **165**, 100 (1992).
- [29.8] D. Sterling and J.D. Meiss, "Computing periodic orbits using the anti-integrable limit," *Phys. Lett. A* **241**, 46 (1998); [arXiv:chaos-dyn/9802014](https://arxiv.org/abs/chaos-dyn/9802014).

- [29.9] P. Schmelcher and F.K. Diakonov, *Phys. Rev. Lett.* **78**, 4733 (1997); *Phys. Rev. E* **57**, 2739 (1998).
- [29.10] D. Pingel, P. Schmelcher and F.K. Diakonov, O. Biham, *Phys. Rev. E* **64**, 026214 (2001).
- [29.11] F. K. Diakonov, P. Schmelcher, O. Biham, *Phys. Rev. Lett.* **81**, 4349 (1998).
- [29.12] K. Ikeda, *Opt. Commun.* **30**, 257 (1979).
- [29.13] F. Stummel and K. Hainer, *Praktische Mathematik* (Teubner, Stuttgart 1982).
- [29.14] R.L. Davidchack and Y.C. Lai, *Phys. Rev. E* **60**, 6172 (1999).
- [29.15] P. Cvitanović and Y. Lan, “Turbulent fields and their recurrences,” in N. Antoniou, ed., *Proceed. of 10. Intern. Workshop on Multiparticle Production: Correlations and Fluctuations in QCD* (World Scientific, Singapore 2003); [arXiv:nlin.CD/0308006](https://arxiv.org/abs/nlin.CD/0308006)
- [29.16] Y. Lan and P. Cvitanović, “Variational method for finding periodic orbits in a general flow,” *Phys. Rev. E* **69** 016217 (2004); [arXiv:nlin.CD/0308008](https://arxiv.org/abs/nlin.CD/0308008)
- [29.17] M. Sieber and F. Steiner, “Quantum Chaos in the Hyperbola Billiard,” *Phys. Lett. A* **148**, 415 (1990).
- [29.18] M. Sieber, *The Hyperbola Billiard: A Model for the Semiclassical Quantization of Chaotic Systems*, Ph.D. thesis (Hamburg 1991); DESY report 91-030.
- [29.19] H. T. Kook and J. D. Meiss, “Periodic orbits for reversible symplectic mappings,” *Physica D* **35**, 65 (1989).
- [29.20] J.N. Mather, “Variational construction of orbits of twist diffeomorphisms,” *J. Amer. Math. Soc.* **4** 207 (1991).
- [29.21] S. B. Angenent, “The periodic orbits of an area preserving twist-map,” *Comm. Math. Phys.* **115**, 353 (1988).
- [29.22] C. Golé, “A new proof of the Aubry-Mather’s theorem,” *Math. Z.* **210**, 441 (1992).
- [29.23] C. Falcolini and R. de la Llave, “Numerical calculation of domains of analyticity for perturbation theories in the presence of small divisors,” *J. Stat. Phys.* **67**, 645 (1992).
- [29.24] S. Tompaids, “Numerical Study of Invariant Sets of a Quasi-periodic Perturbation of a Symplectic Map,” *Experimental Mathematics* **5**, 211 (1996).
- [29.25] R. de la Llave, *Variational methods for quasiperiodic solutions of partial differential equations*, mp_arc **00-56**.

- [29.26] H. B. Keller, Numerical solution of bifurcation and nonlinear eigenvalue problems, in *Applications of Bifurcation Theory*, edited by P. H. Rabinowitz, pp. 359–384, New York, 1977, Academic Press.
- [29.27] H. B. Keller, Global homotopies and Newton methods, in *Recent advances in numerical analysis*, edited by C. de Boor and G. H. Golub, pp. 73–94, New York, 1979, Academic Press.
- [29.28] G. M. Shroff and H. B. Keller, Stabilization of unstable procedures: The recursive projection method, *SIAM Journal on Numerical Analysis* **30**, 1099 (1993).
- [29.29] E. L. Allgower and K. Georg, Numerically stable homotopy methods without an extra dimension, *Lect. Appl. Math.* **26**, 1 (1990), www.math.colostate.edu/emeriti/georg/homExtra.pdf.

Part V

Quantum chaos

Q^{UNADRY:}

Semiclassical Chaos



Predrag Cvitanović – Roberto Artuso – Per Dahlqvist – Ronnie Mainieri – Gregor Tanner – Gábor Vattay – Niall Whelan – Andreas Wirzba

ChaosBook.org version13, Dec 31 2009
ChaosBook.org

printed October 6, 2010
comments to: [predrag \[snail\] nbi.dk](mailto:predrag@snail.nbi.dk)

Chapter 30

Prologue

Anyone who uses words “quantum” and “chaos” in the same sentence should be hung by his thumbs on a tree in the park behind the Niels Bohr Institute.

—Joseph Ford

(G. Vattay, G. Tanner and P. Cvitanović)

YOU HAVE READ the first volume of this book. So far, so good – anyone can play a game of classical pinball, and a skilled neuroscientist can poke rat brains. We learned that information about chaotic dynamics can be obtained by calculating spectra of linear operators such as the evolution operator of sect. 17.2 or the associated partial differential equations such as the Liouville equation (16.37). The spectra of these operators can be expressed in terms of periodic orbits of the deterministic dynamics by means of trace formulas and cycle expansions.

But what happens quantum mechanically, i.e., if we scatter waves rather than point-like pinballs? Can we turn the problem round and study linear PDE’s in terms of the underlying deterministic dynamics? And, is there a link between structures in the spectrum or the eigenfunctions of a PDE and the dynamical properties of the underlying classical flow? The answer is yes, but . . . things are becoming somewhat more complicated when studying 2nd or higher order linear PDE’s. We can find classical dynamics associated with a linear PDE, just take geometric optics as a familiar example. Propagation of light follows a second order wave equation but may in certain limits be well described in terms of geometric rays. A theory in terms of properties of the classical dynamics alone, referred to here as the *semiclassical theory*, will not be exact, in contrast to the classical periodic orbit formulas obtained so far. Waves exhibit new phenomena, such as interference, diffraction, and higher \hbar corrections which will only be partially incorporated into the periodic orbit theory.

chapter 38

30.1 Quantum pinball

In what follows, we will restrict the discussion to the non-relativistic Schrödinger equation. The approach will be very much in the spirit of the early days of quantum mechanics, before its wave character has been fully uncovered by Schrödinger in the mid 1920's. Indeed, were physicists of the period as familiar with classical chaos as we are today, this theory could have been developed 80 years ago. It was the discrete nature of the hydrogen spectrum which inspired the Bohr - de Broglie picture of the old quantum theory: one places a wave instead of a particle on a Keplerian orbit around the hydrogen nucleus. The quantization condition is that only those orbits contribute for which this wave is stationary; from this followed the Balmer spectrum and the Bohr-Sommerfeld quantization which eventually led to the more sophisticated theory of Heisenberg, Schrödinger and others. Today we are very aware of the fact that elliptic orbits are an idiosyncrasy of the Kepler problem, and that chaos is the rule; so can the Bohr quantization be generalized to chaotic systems?

The question was answered affirmatively by M. Gutzwiller, as late as 1971: a chaotic system can indeed be quantized by placing a wave on each of the *infinity* of unstable periodic orbits. Due to the instability of the orbits the wave does not stay localized but leaks into neighborhoods of other periodic orbits. Contributions of different periodic orbits interfere and the quantization condition can no longer be attributed to a single periodic orbit: A coherent summation over the infinity of periodic orbit contributions gives the desired spectrum.

The pleasant surprise is that the zeros of the dynamical zeta function (1.10) derived in the context of classical chaotic dynamics,

chapter 19

$$1/\zeta(z) = \prod_p (1 - t_p),$$

also yield excellent estimates of *quantum* resonances, with the quantum amplitude associated with a given cycle approximated semiclassically by the weight

$$t_p = \frac{1}{|\Lambda_p|^{1/2}} e^{\frac{i}{\hbar} S_p - i\pi m_p/2}, \quad (30.1)$$

whose magnitude is the square root of the classical weight (19.10)

$$t_p = \frac{1}{|\Lambda_p|} e^{\beta \cdot A_p - s T_p},$$

and the phase is given by the Bohr-Sommerfeld action integral S_p , together with an additional topological phase m_p , the number of caustics along the periodic trajectory, points where the naive semiclassical approximation fails.

chapter 33

In this approach, the quantal spectra of classically chaotic dynamical systems are determined from the zeros of dynamical zeta functions, defined by cycle expansions of infinite products of form

$$1/\zeta = \prod_p (1 - t_p) = 1 - \sum_f t_f - \sum_k c_k \quad (30.2)$$

with weight t_p associated to every prime (non-repeating) periodic orbit (or *cycle*) p .

The key observation is that the chaotic dynamics is often organized around a few *fundamental* cycles. These short cycles capture the skeletal topology of the motion in the sense that any long orbit can approximately be pieced together from the fundamental cycles. In chapter 20 it was shown that for this reason the cycle expansion (30.2) is a highly convergent expansion dominated by short cycles grouped into *fundamental* contributions, with longer cycles contributing rapidly decreasing *curvature* corrections. Computations with dynamical zeta functions are rather straightforward; typically one determines lengths and stabilities of a finite number of shortest periodic orbits, substitutes them into (30.2), and estimates the zeros of $1/\zeta$ from such polynomial approximations.

From the vantage point of the dynamical systems theory, the trace formulas (both the exact Selberg and the semiclassical Gutzwiller trace formula) fit into a general framework of replacing phase space averages by sums over periodic orbits. For classical hyperbolic systems this is possible since the invariant density can be represented by sum over all periodic orbits, with weights related to their instability. The semiclassical periodic orbit sums differ from the classical ones only in phase factors and stability weights; such differences may be traced back to the fact that in quantum mechanics the amplitudes rather than the probabilities are added. chapter 34

The type of dynamics has a strong influence on the convergence of cycle expansions and the properties of quantal spectra; this necessitates development of different approaches for different types of dynamical behavior such as, on one hand, the strongly hyperbolic and, on the other hand, the intermittent dynamics of chapters 20 and 24. For generic nonhyperbolic systems (which we shall not discuss here), with mixed phase space and marginally stable orbits, periodic orbit summations are hard to control, and it is still not clear that the periodic orbit sums should necessarily be the computational method of choice.

Where is all this taking us? The goal of this part of the book is to demonstrate that the cycle expansions, developed so far in classical settings, are also a powerful tool for evaluation of *quantum* resonances of classically chaotic systems.

First, we shall warm up playing our game of pinball, this time in a quantum version. Were the game of pinball a closed system, quantum mechanically one would determine its stationary eigenfunctions and eigenenergies. For open systems one seeks instead complex resonances, where the imaginary part of the

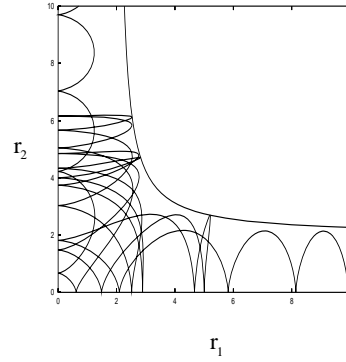


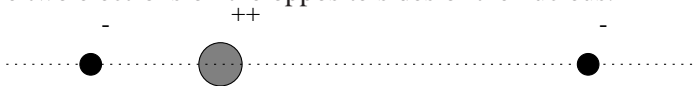
Figure 30.1: A typical collinear helium trajectory in the $r_1 - r_2$ plane; the trajectory enters along the r_1 axis and escapes to infinity along the r_2 axis.

eigenenergy describes the rate at which the quantum wave function leaks out of the central scattering region. This will turn out to work well, except who truly wants to know accurately the resonances of a quantum pinball?

chapter 35

30.2 Quantization of helium

Once we have derived the semiclassical weight associated with the periodic orbit p (30.1), we will finally be in position to accomplish something altogether remarkable. We are now able to put together all ingredients that make the game of pinball unpredictable, and compute a “chaotic” part of the helium spectrum to shocking accuracy. From the classical dynamics point of view, helium is an example of Poincaré’s dreaded and intractable 3-body problem. Undaunted, we forge ahead and consider the *collinear* helium, with zero total angular momentum, and the two electrons on the opposite sides of the nucleus.



We set the electron mass to 1, the nucleus mass to ∞ , the helium nucleus charge to 2, the electron charges to -1. The Hamiltonian is

chapter 37

$$H = \frac{1}{2}p_1^2 + \frac{1}{2}p_2^2 - \frac{2}{r_1} - \frac{2}{r_2} + \frac{1}{r_1 + r_2}. \tag{30.3}$$

Due to the energy conservation, only three of the phase space coordinates (r_1, r_2, p_1, p_2) are independent. The dynamics can be visualized as a motion in the $(r_1, r_2), r_i \geq 0$ quadrant, figure 30.1, or, better still, by a well chosen 2-dimensional Poincaré section.

The motion in the (r_1, r_2) plane is topologically similar to the pinball motion in a 3-disk system, except that the motion is not free, but in the Coulomb potential. The classical collinear helium is also a repeller; almost all of the classical trajectories escape. Miraculously, the symbolic dynamics for the survivors turns out to be binary, just as in the 3-disk game of pinball, so we know what cycles need to be computed for the cycle expansion (1.11). A set of shortest cycles up to

a given symbol string length then yields an estimate of the helium spectrum. This simple calculation yields surprisingly accurate eigenvalues; even though the cycle expansion was based on the *semiclassical approximation* (30.1) which is expected to be good only in the classical large energy limit, the eigenenergies are good to 1% all the way down to the ground state. chapter 37

Before we can get to this point, we first have to recapitulate some basic notions of quantum mechanics; after having defined the main quantum objects of interest, the quantum propagator and the Green's function, we will relate the quantum propagation to the classical flow of the underlying dynamical system. We will then proceed to construct semiclassical approximations to the quantum propagator and the Green's function. A rederivation of classical Hamiltonian dynamics starting from the Hamilton-Jacobi equation will be offered along the way. The derivation of the Gutzwiller trace formula and the semiclassical zeta function as a sum and as a product over periodic orbits will be given in chapter 34. In subsequent chapters we buttress our case by applying and extending the theory: a cycle expansion calculation of scattering resonances in a 3-disk billiard in chapter 35, the spectrum of helium in chapter 37, and the incorporation of diffraction effects in chapter 38.

Commentary

Remark 30.1 Guide to literature. A key prerequisite to developing any theory of “quantum chaos” is solid understanding of Hamiltonian mechanics. For that, Arnol'd monograph [5] is the essential reference. Ozorio de Almeida's monograph [9] offers a compact introduction to the aspects of Hamiltonian dynamics required for the quantization of integrable and nearly integrable systems, with emphasis on periodic orbits, normal forms, catastrophe theory and torus quantization. The book by Brack and Bhaduri [1] is an excellent introduction to the semiclassical methods. Gutzwiller's monograph [2] is an advanced introduction focusing on chaotic dynamics both in classical Hamiltonian settings and in the semiclassical quantization. This book is worth browsing through for its many insights and erudite comments on quantum and celestial mechanics even if one is not working on problems of quantum chaos. More suitable as a graduate course text is Reichl's exposition [3].

This book does not discuss the random matrix theory approach to chaos in quantal spectra; no randomness assumptions are made here, rather the goal is to milk the deterministic chaotic dynamics for its full worth. The book concentrates on the periodic orbit theory. For an introduction to “quantum chaos” that focuses on the random matrix theory the reader is referred to the excellent monograph by Haake [4], among others.

Remark 30.2 The dates. Schrödinger's first wave mechanics paper [3] (hydrogen spectrum) was submitted 27 January 1926. Submission date for Madelung's ‘quantum theory in hydrodynamical form’ paper [2] was 25 October 1926.

References

- [30.1] M. Brack and R.K. Bhaduri, *Semiclassical Physics* (Addison-Wesley, New York 1997).
- [30.2] M.C. Gutzwiller, *Chaos in Classical and Quantum Mechanics* (Springer, New York 1990).
- [30.3] L.E. Reichl, *The Transition to Chaos in Conservative Classical Systems: Quantum Manifestations* (Springer-Verlag, New York 1992).
- [30.4] F. Haake, *Quantum Signatures of Chaos*, 2. edition (Springer-Verlag, New York 2001).
- [30.5] V.I. Arnold, *Mathematical Methods in Classical Mechanics* (Springer-Verlag, Berlin 1978).

Chapter 31

Quantum mechanics, briefly

WE START WITH a review of standard quantum mechanical concepts prerequisite to the derivation of the semiclassical trace formula.

In coordinate representation the time evolution of a quantum mechanical wave function is governed by the Schrödinger equation

$$i\hbar \frac{\partial}{\partial t} \psi(q, t) = \hat{H}(q, \frac{\hbar}{i} \frac{\partial}{\partial q}) \psi(q, t), \quad (31.1)$$

where the Hamilton operator $\hat{H}(q, -i\hbar\partial_q)$ is obtained from the classical Hamiltonian by substitution $p \rightarrow -i\hbar\partial_q$. Most of the Hamiltonians we shall consider here are of form

$$H(q, p) = T(p) + V(q), \quad T(p) = p^2/2m, \quad (31.2)$$

describing dynamics of a particle in a D -dimensional potential $V(q)$. For time independent Hamiltonians we are interested in finding stationary solutions of the Schrödinger equation of the form

$$\psi_n(q, t) = e^{-iE_n t/\hbar} \phi_n(q), \quad (31.3)$$

where E_n are the eigenenergies of the time-independent Schrödinger equation

$$\hat{H}\phi(q) = E\phi(q). \quad (31.4)$$

If the kinetic term can be separated out as in (31.2), the time-independent Schrödinger equation

$$-\frac{\hbar^2}{2m} \partial^2 \phi(q) + V(q)\phi(q) = E\phi(q) \quad (31.5)$$

can be rewritten in terms of a local wavenumber

$$(\partial^2 + k^2(q))\phi = 0, \quad \hbar k(q) = \sqrt{2m(E - V(q))}. \quad (31.6)$$

For bound systems the spectrum is discrete and the eigenfunctions form an orthonormal,

$$\int dq \phi_n(q) \phi_m^*(q) = \delta_{nm}, \quad (31.7)$$

and complete,

$$\sum_n \phi_n(q) \phi_n^*(q') = \delta(q - q'), \quad (31.8)$$

set of functions in a Hilbert space. Here and throughout the text,

$$\int dq = \int dq_1 dq_2 \dots dq_D. \quad (31.9)$$

For simplicity we will assume that the system is bound, although most of the results will be applicable to open systems, where one has complex resonances instead of real energies, and the spectrum has continuous components. chapter 35

A given wave function can be expanded in the energy eigenbasis

$$\psi(q, t) = \sum_n c_n e^{-iE_n t/\hbar} \phi_n(q), \quad (31.10)$$

where the expansion coefficient c_n is given by the projection of the initial wave function $\psi(q, 0)$ onto the n th eigenstate

$$c_n = \int dq \phi_n^*(q) \psi(q, 0). \quad (31.11)$$

By substituting (31.11) into (31.10), we can cast the evolution of a wave function into a multiplicative form

$$\psi(q, t) = \int dq' K(q, q', t) \psi(q', 0),$$

with the kernel

$$K(q, q', t) = \sum_n \phi_n(q) e^{-iE_n t/\hbar} \phi_n^*(q') \quad (31.12)$$

called the quantum evolution operator, or the *propagator*. Applied twice, first for time t_1 and then for time t_2 , it propagates the initial wave function from q' to q'' , and then from q'' to q

$$K(q, q', t_1 + t_2) = \int dq'' K(q, q'', t_2) K(q'', q', t_1) \quad (31.13)$$

forward in time, hence the name “propagator.” In non-relativistic quantum mechanics the range of q'' is infinite, meaning that the wave can propagate at any speed; in relativistic quantum mechanics this is rectified by restricting the propagation to the forward light cone.

Since the propagator is a linear combination of the eigenfunctions of the Schrödinger equation, it also satisfies the Schrödinger equation

$$i\hbar \frac{\partial}{\partial t} K(q, q', t) = \hat{H}(q, \frac{i}{\hbar} \frac{\partial}{\partial q}) K(q, q', t), \quad (31.14)$$

and is thus a wave function defined for $t \geq 0$; from the completeness relation (31.8) we obtain the boundary condition at $t = 0$:

$$\lim_{t \rightarrow 0^+} K(q, q', t) = \delta(q - q'). \quad (31.15)$$

The propagator thus represents the time evolution of a wave packet which starts out as a configuration space delta-function localized in the point q' at the initial time $t = 0$.

For time independent Hamiltonians the time dependence of the wave functions is known as soon as the eigenenergies E_n and eigenfunctions ϕ_n have been determined. With time dependence rendered “trivial,” it makes sense to focus on the *Green’s function*, the Laplace transformation of the propagator

$$G(q, q', E + i\epsilon) = \frac{1}{i\hbar} \int_0^\infty dt e^{iEt - \frac{\epsilon}{\hbar}t} K(q, q', t) = \sum_n \frac{\phi_n(q)\phi_n^*(q')}{E - E_n + i\epsilon}. \quad (31.16)$$

Here ϵ is a small positive number, ensuring the existence of the integral. The eigenenergies show up as poles in the Green’s function with residues corresponding to the wave function amplitudes. If one is only interested in the spectrum, one may restrict the considerations to the (formal) trace of the Green’s function,

$$\text{tr} G(q, q', E) = \int dq G(q, q, E) = \sum_n \frac{1}{E - E_n}, \quad (31.17)$$

where E is complex, with a positive imaginary part, and we have used the eigenfunction orthonormality (31.7). This trace is formal, since as it stands, the sum

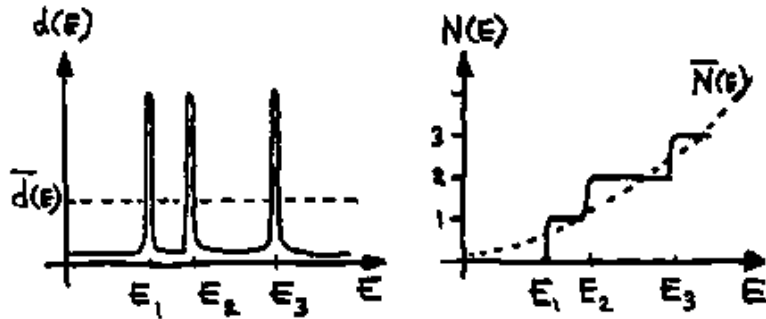


Figure 31.1: Schematic picture of **a)** the density of states $d(E)$, and **b)** the spectral staircase function $N(E)$. The dashed lines denote the mean density of states $\bar{d}(E)$ and the average number of states $\bar{N}(E)$ discussed in more detail in sect. 34.1.1.

in (31.17) is often divergent. We shall return to this point in sects. 34.1.1 and 34.1.2.

A useful characterization of the set of eigenvalues is given in terms of the *density of states*, with a delta function peak at each eigenenergy, figure 31.1 (a),

$$d(E) = \sum_n \delta(E - E_n). \quad (31.18)$$

Using the identity

exercise 31.1

$$\delta(E - E_n) = - \lim_{\epsilon \rightarrow +0} \frac{1}{\pi} \text{Im} \frac{1}{E - E_n + i\epsilon} \quad (31.19)$$

we can express the density of states in terms of the trace of the Green's function, that is

$$d(E) = \sum_n \delta(E - E_n) = - \lim_{\epsilon \rightarrow 0} \frac{1}{\pi} \text{Im} \text{tr} G(q, q', E + i\epsilon). \quad (31.20)$$

section 34.1.1

As we shall see after "some" work, a semiclassical formula for right hand side of this relation will yield the quantum spectrum in terms of periodic orbits.

The density of states can be written as the derivative $d(E) = dN(E)/dE$ of the *spectral staircase* function

$$N(E) = \sum_n \Theta(E - E_n) \quad (31.21)$$

which counts the number of eigenenergies below E , figure 31.1 (b). Here Θ is the Heaviside function

$$\Theta(x) = 1 \quad \text{if } x > 0; \quad \Theta(x) = 0 \quad \text{if } x < 0. \quad (31.22)$$

The spectral staircase is a useful quantity in many contexts, both experimental and theoretical. This completes our lightning review of quantum mechanics.

Exercises

- 31.1. **Dirac delta function, Lorentzian representation.**
Derive the representation (31.19)

$$\delta(E - E_n) = - \lim_{\epsilon \rightarrow +0} \frac{1}{\pi} \text{Im} \frac{1}{E - E_n + i\epsilon}$$

of a delta function as imaginary part of $1/x$.

(Hint: read up on principal parts, positive and negative frequency part of the delta function, the Cauchy theorem in a good quantum mechanics textbook).

- 31.2. **Green's function.** Verify Green's function Laplace transform (31.16),

$$\begin{aligned} G(q, q', E + i\epsilon) &= \frac{1}{i\hbar} \int_0^\infty dt e^{\frac{i}{\hbar}Et - \frac{\epsilon}{\hbar}t} K(q, q', t) \\ &= \sum \frac{\phi_n(q)\phi_n^*(q')}{E - E_n + i\epsilon} \end{aligned}$$

argue that positive ϵ is needed (hint: read a good quantum mechanics textbook).

Chapter 32

WKB quantization

THE WAVE FUNCTION for a particle of energy E moving in a constant potential V is

$$\psi = Ae^{\frac{i}{\hbar}pq} \quad (32.1)$$

with a constant amplitude A , and constant wavelength $\lambda = 2\pi/k$, $k = p/\hbar$, and $p = \pm\sqrt{2m(E-V)}$ is the momentum. Here we generalize this solution to the case where the potential varies slowly over many wavelengths. This semiclassical (or WKB) approximate solution of the Schrödinger equation fails at classical turning points, configuration space points where the particle momentum vanishes. In such neighborhoods, where the semiclassical approximation fails, one needs to solve locally the exact quantum problem, in order to compute connection coefficients which patch up semiclassical segments into an approximate global wave function.

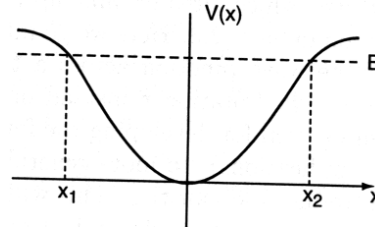
Two lessons follow. First, semiclassical methods can be very powerful - classical mechanics computations yield surprisingly accurate estimates of quantal spectra, without solving the Schrödinger equation. Second, semiclassical quantization does depend on a purely wave-mechanical phenomena, the coherent addition of phases accrued by all fixed energy phase space trajectories that connect pairs of coordinate points, and the topological phase loss at every turning point, a topological property of the classical flow that plays no role in classical mechanics.

32.1 WKB ansatz

Consider a time-independent Schrödinger equation in 1 spatial dimension:

$$-\frac{\hbar^2}{2m}\psi''(q) + V(q)\psi(q) = E\psi(q), \quad (32.2)$$

Figure 32.1: A 1-dimensional potential, location of the two turning points at fixed energy E .



with potential $V(q)$ growing sufficiently fast as $q \rightarrow \pm\infty$ so that the classical particle motion is confined for any E . Define the local momentum $p(q)$ and the local wavenumber $k(q)$ by

$$p(q) = \pm \sqrt{2m(E - V(q))}, \quad p(q) = \hbar k(q). \quad (32.3)$$

The variable wavenumber form of the Schrödinger equation

$$\psi'' + k^2(q)\psi = 0 \quad (32.4)$$

suggests that the wave function be written as $\psi = Ae^{\frac{i}{\hbar}S}$, A and S real functions of q . Substitution yields two equations, one for the real and other for the imaginary part:

$$(S')^2 = p^2 + \hbar^2 \frac{A''}{A} \quad (32.5)$$

$$S''A + 2S'A' = \frac{1}{A} \frac{d}{dq}(S'A^2) = 0. \quad (32.6)$$

The Wentzel-Kramers-Brillouin (*WKB*) or *semiclassical* approximation consists of dropping the \hbar^2 term in (32.5). Recalling that $p = \hbar k$, this amounts to assuming that $k^2 \gg \frac{A''}{A}$, which in turn implies that the phase of the wave function is changing much faster than its overall amplitude. So the WKB approximation can be interpreted either as a short wavelength/high frequency approximation to a wave-mechanical problem, or as the semiclassical, $\hbar \ll 1$ approximation to quantum mechanics.

Setting $\hbar = 0$ and integrating (32.5) we obtain the phase increment of a wave function initially at q' , at energy E

$$S(q, q', E) = \int_{q'}^q dq'' p(q''). \quad (32.7)$$

This integral over a particle trajectory of constant energy, called the *action*, will play a key role in all that follows. The integration of (32.6) is even easier

$$A(q) = \frac{C}{|p(q)|^{\frac{1}{2}}}, \quad C = |p(q')|^{\frac{1}{2}} \psi(q'), \quad (32.8)$$

where the integration constant C is fixed by the value of the wave function at the initial point q' . The *WKB* (or *semiclassical*) *ansatz* wave function is given by

$$\psi_{sc}(q, q', E) = \frac{C}{|p(q)|^{\frac{1}{2}}} e^{\frac{i}{\hbar} S(q, q', E)}. \quad (32.9)$$

In what follows we shall suppress dependence on the initial point and energy in such formulas, $(q, q', E) \rightarrow (q)$.

The WKB ansatz generalizes the free motion wave function (32.1), with the probability density $|A(q)|^2$ for finding a particle at q now inversely proportional to the velocity at that point, and the phase $\frac{1}{\hbar} q p$ replaced by $\frac{1}{\hbar} \int dq p(q)$, the integrated action along the trajectory. This is fine, except at any turning point q_0 , figure 32.1, where all energy is potential, and

$$p(q) \rightarrow 0 \quad \text{as} \quad q \rightarrow q_0, \quad (32.10)$$

so that the assumption that $k^2 \gg \frac{A''}{A}$ fails. What can one do in this case?

For the task at hand, a simple physical picture, due to Maslov, does the job. In the q coordinate, the turning points are defined by the zero kinetic energy condition (see figure 32.1), and the motion appears singular. This is not so in the full phase space: the trajectory in a smooth confining 1-dimensional potential is always a smooth loop, with the “special” role of the turning points q_L, q_R seen to be an artifact of a particular choice of the (q, p) coordinate frame. Maslov’s idea was to proceed from the initial point (q', p') to a point (q_A, p_A) preceding the turning point in the $\psi(q)$ representation, then switch to the momentum representation

$$\tilde{\psi}(p) = \frac{1}{\sqrt{2\pi\hbar}} \int dq e^{-\frac{i}{\hbar} qp} \psi(q), \quad (32.11)$$

continue from (q_A, p_A) to (q_B, p_B) , switch back to the coordinate representation,

$$\psi(q) = \frac{1}{\sqrt{2\pi\hbar}} \int dp e^{\frac{i}{\hbar} qp} \tilde{\psi}(p), \quad (32.12)$$

and so on.

The only rub is that one usually cannot evaluate these transforms exactly. But, as the WKB wave function (32.9) is approximate anyway, it suffices to estimate these transforms to leading order in \hbar accuracy. This is accomplished by the method of stationary phase.

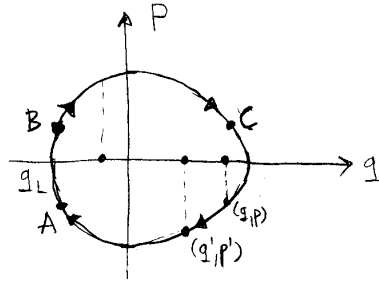


Figure 32.2: A 1-dof phase space trajectory of a particle moving in a bound potential.

32.2 Method of stationary phase

All “semiclassical” approximations are based on saddle point evaluations of integrals of the type

$$I = \int dx A(x) e^{is\Phi(x)}, \quad x, \Phi(x) \in \mathbb{R}, \tag{32.13}$$

where s is assumed to be a large, real parameter, and $\Phi(x)$ is a real-valued function. In our applications $s = 1/\hbar$ will always be assumed large.

For large s , the phase oscillates rapidly and “averages to zero” everywhere except at the *extremal points* $\Phi'(x_0) = 0$. The method of approximating an integral by its values at extremal points is called the *method of stationary phase*. Consider first the case of a 1-dimensional integral, and expand $\Phi(x_0 + \delta x)$ around x_0 to second order in δx ,

$$I = \int dx A(x) e^{is(\Phi(x_0) + \frac{1}{2}\Phi''(x_0)\delta x^2 + \dots)}. \tag{32.14}$$

Assume (for time being) that $\Phi''(x_0) \neq 0$, with either sign, $\text{sgn}[\Phi''] = \Phi''/|\Phi''| = \pm 1$. If in the neighborhood of x_0 the amplitude $A(x)$ varies slowly over many oscillations of the exponential function, we may retain the leading term in the Taylor expansion of the amplitude, and approximate the integral up to quadratic terms in the phase by

$$I \approx A(x_0)e^{is\Phi(x_0)} \int dx e^{\frac{1}{2}is\Phi''(x_0)(x-x_0)^2}. \tag{32.15}$$

Using the *Fresnel integral formula*

exercise 32.1

$$\frac{1}{\sqrt{2\pi}} \int_{-\infty}^{\infty} dx e^{-\frac{x^2}{2ia}} = \sqrt{ia} = |a|^{1/2} e^{i\frac{\pi}{4} \frac{a}{|a|}} \tag{32.16}$$

we obtain

$$I \approx A(x_0) \left| \frac{2\pi}{s\Phi''(x_0)} \right|^{1/2} e^{is\Phi(x_0) \pm i\frac{\pi}{4}}, \tag{32.17}$$

where \pm corresponds to the positive/negative sign of $s\Phi''(x_0)$.

32.3 WKB quantization

We can now evaluate the Fourier transforms (32.11), (32.12) to the same order in \hbar as the WKB wave function using the stationary phase method,

$$\begin{aligned}\tilde{\psi}_{sc}(p) &= \frac{C}{\sqrt{2\pi\hbar}} \int \frac{dq}{|p(q)|^{\frac{1}{2}}} e^{\frac{i}{\hbar}(S(q)-qp)} \\ &\approx \frac{C}{\sqrt{2\pi\hbar}} \frac{e^{\frac{i}{\hbar}(S(q^*)-q^*p)}}{|p(q^*)|^{\frac{1}{2}}} \int dq e^{\frac{i}{2\hbar}S''(q^*)(q-q^*)^2},\end{aligned}\quad (32.18)$$

where q^* is given implicitly by the stationary phase condition

$$0 = S'(q^*) - p = p(q^*) - p$$

and the sign of $S''(q^*) = p'(q^*)$ determines the phase of the Fresnel integral (32.16)

$$\tilde{\psi}_{sc}(p) = \frac{C}{|p(q^*)p'(q^*)|^{\frac{1}{2}}} e^{\frac{i}{\hbar}[S(q^*)-q^*p] + \frac{i\pi}{4}\text{sgn}[S''(q^*)]}.\quad (32.19)$$

As we continue from (q_A, p_A) to (q_B, p_B) , nothing problematic occurs - $p(q^*)$ is finite, and so is the acceleration $p'(q^*)$. Otherwise, the trajectory would take infinitely long to get across. We recognize the exponent as the Legendre transform

$$\tilde{S}(p) = S(q(p)) - q(p)p$$

which can be used to express everything in terms of the p variable,

$$q^* = q(p), \quad \frac{d}{dq}q = 1 = \frac{dp}{dq} \frac{dq(p)}{dp} = q'(p)p'(q^*).\quad (32.20)$$

As the classical trajectory crosses q_L , the weight in (32.19),

$$\frac{d}{dq}p^2(q_L) = 2p(q_L)p'(q_L) = -2mV'(q),\quad (32.21)$$

is finite, and $S''(q^*) = p'(q^*) < 0$ for any point in the lower left quadrant, including (q_A, p_A) . Hence, the phase loss in (32.19) is $-\frac{\pi}{4}$. To go back from the p to the q representation, just turn figure 32.2 90° anticlockwise. Everything is the same if you replace $(q, p) \rightarrow (-p, q)$; so, without much ado we get the semiclassical wave function at the point (q_B, p_B) ,

$$\psi_{sc}(q) = \frac{e^{\frac{i}{\hbar}(\tilde{S}(p^*)+qp^*)-\frac{i\pi}{4}}}{|q^*(p^*)|^{\frac{1}{2}}} \tilde{\psi}_{sc}(p^*) = \frac{C}{|p(q)|^{\frac{1}{2}}} e^{\frac{i}{\hbar}S(q)-\frac{i\pi}{2}}.\quad (32.22)$$

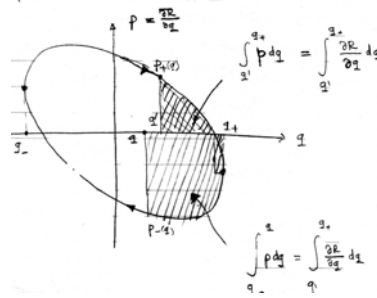


Figure 32.3: $S_p(E)$, the action of a periodic orbit p at energy E , equals the area in the phase space traced out by the 1-dof trajectory.

The extra $|p'(q^*)|^{1/2}$ weight in (32.19) is cancelled by the $|q'(p^*)|^{1/2}$ term, by the Legendre relation (32.20).

The message is that going through a smooth potential turning point the WKB wave function phase slips by $-\frac{\pi}{2}$. This is equally true for the right and the left turning points, as can be seen by rotating figure 32.2 by 180° , and flipping coordinates $(q, p) \rightarrow (-q, -p)$. While a turning point is not an invariant concept (for a sufficiently short trajectory segment, it can be undone by a 45° turn), for a complete period $(q, p) = (q', p')$ the total phase slip is always $-2 \cdot \pi/2$, as a loop always has $m = 2$ turning points.

The *WKB quantization condition* follows by demanding that the wave function computed after a complete period be single-valued. With the normalization (32.8), we obtain

$$\psi(q') = \psi(q) = \left| \frac{p(q')}{p(q)} \right|^{\frac{1}{2}} e^{i(\frac{1}{\hbar} \oint p(q) dq - \pi)} \psi(q').$$

The prefactor is 1 by the periodic orbit condition $q = q'$, so the phase must be a multiple of 2π ,

$$\frac{1}{\hbar} \oint p(q) dq = 2\pi \left(n + \frac{m}{4} \right), \tag{32.23}$$

where m is the number of turning points along the trajectory - for this 1-dof problem, $m = 2$.

The action integral in (32.23) is the area (see figure 32.3) enclosed by the classical phase space loop of figure 32.2, and the quantization condition says that eigen-energies correspond to loops whose action is an integer multiple of the unit quantum of action, Planck's constant \hbar . The extra topological phase, which, although it had been discovered many times in centuries past, had to wait for its most recent quantum chaotic (re)birth until the 1970's. Despite its derivation in a noninvariant coordinate frame, the final result involves only canonically invariant classical quantities, the periodic orbit action S , and the topological index m .

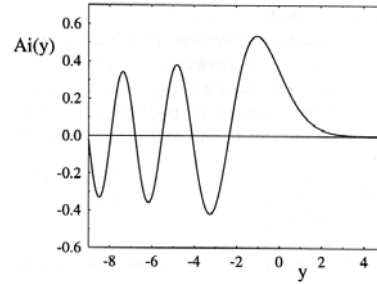


Figure 32.4: Airy function $Ai(q)$.

32.3.1 Harmonic oscillator quantization

Let us check the WKB quantization for one case (the only case?) whose quantum mechanics we fully understand: the harmonic oscillator

$$E = \frac{1}{2m} (p^2 + (m\omega q)^2).$$

The loop in figure 32.2 is now a circle in the $(m\omega q, p)$ plane, the action is its area $S = 2\pi E/\omega$, and the spectrum in the WKB approximation

$$E_n = \hbar\omega(n + 1/2) \quad (32.24)$$

turns out to be the *exact* harmonic oscillator spectrum. The stationary phase condition (32.18) keeps $V(q)$ accurate to order q^2 , which in this case is the whole answer (but we were simply lucky, really). For many 1-dof problems the WKB spectrum turns out to be very accurate all the way down to the ground state. Surprisingly accurate, if one interprets dropping the \hbar^2 term in (32.5) as a short wavelength approximation.

32.4 Beyond the quadratic saddle point

We showed, with a bit of Fresnel/Maslov voodoo, that in a smoothly varying potential the phase of the WKB wave function slips by a $\pi/2$ for each turning point. This $\pi/2$ came from a \sqrt{i} in the Fresnel integral (32.16), one such factor for every time we switched representation from the configuration space to the momentum space, or back. Good, but what does this mean?

The stationary phase approximation (32.14) fails whenever $\Phi'(x) = 0$, or, in our case the WKB ansatz (32.18), whenever the momentum $p'(q) = S''(q)$ vanishes. In that case we have to go beyond the quadratic approximation (32.15) to the first nonvanishing term in the Taylor expansion of the exponent. If $\Phi'''(x_0) \neq 0$, then

$$I \approx A(x_0)e^{iS\Phi(x_0)} \int_{-\infty}^{\infty} dx e^{iS\Phi'''(x_0)\frac{(x-x_0)^3}{6}}. \quad (32.25)$$

Airy functions can be represented by integrals of the form

$$Ai(x) = \frac{1}{2\pi} \int_{-\infty}^{+\infty} dy e^{i(xy - \frac{y^3}{3})}. \quad (32.26)$$

Derivations of the WKB quantization condition given in standard quantum mechanics textbooks rely on expanding the potential close to the turning point

$$V(q) = V(q_0) + (q - q_0)V'(q_0) + \dots,$$

solving the Airy equation

$$\psi'' = q\psi, \quad (32.27)$$

and matching the oscillatory and the exponentially decaying “forbidden” region wave function pieces by means of the *WKB connection formulas*. That requires staring at Airy functions and learning about their asymptotics - a challenge that we will have to eventually overcome, in order to incorporate diffraction phenomena into semiclassical quantization.

The physical origin of the topological phase is illustrated by the shape of the Airy function, figure 32.4. For a potential with a finite slope $V'(q)$ the wave function penetrates into the forbidden region, and accommodates a bit more of a stationary wavelength than what one would expect from the classical trajectory alone. For infinite walls (i.e., billiards) a different argument applies: the wave function must vanish at the wall, and the phase slip due to a specular reflection is $-\pi$, rather than $-\pi/2$.

Résumé

The WKB ansatz wave function for 1-degree of freedom problems fails at the turning points of the classical trajectory. While in the q -representation the WKB ansatz a turning point is singular, along the p direction the classical trajectory in the same neighborhood is smooth, as for any smooth bound potential the classical motion is topologically a circle around the origin in the (q, p) space. The simplest way to deal with such singularities is as follows; follow the classical trajectory in q -space until the WKB approximation fails close to the turning point; then insert $\int dp |p\rangle\langle p|$ and follow the classical trajectory in the p -space until you encounter the next p -space turning point; go back to the q -space representation, and so on. Each matching involves a Fresnel integral, yielding an extra $e^{-i\pi/4}$ phase shift, for a total of $e^{-i\pi}$ phase shift for a full period of a semiclassical particle moving in a soft potential. The condition that the wave-function be single-valued then leads to the 1-dimensional WKB quantization, and its lucky cousin, the Bohr-Sommerfeld quantization.

Alternatively, one can linearize the potential around the turning point a , $V(q) = V(a) + (q-a)V'(a) + \dots$, and solve the quantum mechanical constant linear potential $V(q) = qF$ problem exactly, in terms of an Airy function. An approximate wave function is then patched together from an Airy function at each turning point, and the WKB ansatz wave-function segments in-between via the WKB connection formulas. The single-valuedness condition again yields the 1-dimensional WKB quantization. This a bit more work than tracking the classical trajectory in the full phase space, but it gives us a better feeling for shapes of quantum eigenfunctions, and exemplifies the general strategy for dealing with other singularities, such as wedges, bifurcation points, creeping and tunneling: patch together the WKB segments by means of exact QM solutions to local approximations to singular points.


Commentary

Remark 32.1 Airy function. The stationary phase approximation is all that is needed for the semiclassical approximation, with the proviso that D in (33.36) has no zero eigenvalues. The zero eigenvalue case would require going beyond the Gaussian saddle-point approximation, which typically leads to approximations of the integrals in terms of Airy functions [10].

exercise 32.4

Remark 32.2 Bohr-Sommerfeld quantization. Bohr-Sommerfeld quantization condition was the key result of the old quantum theory, in which the electron trajectories were purely classical. They were lucky - the symmetries of the Kepler problem work out in such a way that the total topological index $m = 4$ amount effectively to numbering the energy levels starting with $n = 1$. They were unlucky - because the hydrogen $m = 4$ masked the topological index, they could never get the helium spectrum right - the semi-classical calculation had to wait for until 1980, when Leopold and Percival [5] added the topological indices.

Exercises


32.1. **WKB ansatz.**  Try to show that no other ansatz other than (33.1) gives a meaningful definition of the momentum in the $\hbar \rightarrow 0$ limit.

32.2. **Fresnel integral.** Derive the Fresnel integral

$$\frac{1}{\sqrt{2\pi}} \int_{-\infty}^{\infty} dx e^{-\frac{x^2}{2ia}} = \sqrt{ia} = |a|^{1/2} e^{i\frac{\pi}{4} \frac{a}{|a|}}.$$

32.3. **Stirling formula for $n!$.** Compute an approximate

value of $n!$ for large n using the stationary phase approximation. Hint: $n! = \int_0^{\infty} dt t^n e^{-t}$.

32.4. **Airy function for large arguments.**  Important contributions as stationary phase points may arise from extremal points where the first non-zero term in a Taylor expansion of the phase is of third or higher order. Such situations occur, for example, at bifurcation points or in diffraction effects, (such as waves near sharp cor-

ners, waves creeping around obstacles, etc.). In such calculations, one meets Airy functions integrals of the form

$$Ai(x) = \frac{1}{2\pi} \int_{-\infty}^{+\infty} dy e^{i(xy - \frac{y^3}{3})}. \quad (32.28)$$

Calculate the Airy function $Ai(x)$ using the stationary phase approximation. What happens when considering the limit $x \rightarrow 0$. Estimate for which value of x the stationary phase approximation breaks down.

References

- [32.1] D. J. Griffiths, *Introduction to Quantum Mechanics* (Prentice-Hall, Englewood Cliffs, New Jersey, 1994).
- [32.2] J.W.S. Rayleigh, *The Theory of Sound* (Macmillan, London 1896; reprinted by Dover, New York 1945).
- [32.3] J.B. Keller, "Corrected Bohr-Sommerfeld quantum conditions for nonseparable systems," *Ann. Phys. (N.Y.)* **4**, 180 (1958).
- [32.4] J.B. Keller and S.I. Rubinow, *Ann. Phys. (N.Y.)* **9**, 24 (1960).
- [32.5] J.B. Keller, "A geometrical theory of diffraction," in *Calculus of variations and its applications, Proc. of Symposia in appl. math.* **8**, (McGraw-Hill, New York, 1958).
- [32.6] J. B. Keller, *Calculus of Variations* **27**, (1958).
- [32.7] V. P. Maslov, *Théorie des Perturbations et Méthodes Asymptotiques* (Dunod, Paris, 1972).
- [32.8] V. P. Maslov and M.V. Fedoriuk, *Semi-Classical Approximation in Quantum Mechanics* (Reidel, Boston 1981).
- [32.9] V.I. Arnold, *Functional Anal. Appl.* **1**, 1 (1967).
- [32.10] N. Bleistein and R.A. Handelsman, *Asymptotic Expansions of Integrals* (Dover, New York 1986).
- [32.11] I.C. Percival, *Adv. Chem. Phys.* **36**, 1 (1977).

Chapter 33

Semiclassical evolution

William Rowan Hamilton was born in 1805. At three he could read English; by four he began to read Latin, Greek and Hebrew, by ten he read Sanskrit, Persian, Arabic, Chaldee, Syrian and sundry Indian dialects. At age seventeen he began to think about optics, and worked out his great principle of “Characteristic Function.”

— Turnbull, *Lives of Mathematicians*

(G. Vattay, G. Tanner and P. Cvitanović)

SEMICLASSICAL APPROXIMATIONS to quantum mechanics are valid in the regime where the de Broglie wavelength $\lambda \sim \hbar/p$ of a particle with momentum p is much shorter than the length scales across which the potential of the system changes significantly. In the short wavelength approximation the particle is a point-like object bouncing off potential walls, the same way it does in the classical mechanics. The novelty of quantum mechanics is the interference of the point-like particle with other versions of itself traveling along different classical trajectories, a feat impossible in classical mechanics. The short wavelength – or semiclassical – formalism is developed by formally taking the limit $\hbar \rightarrow 0$ in quantum mechanics in such a way that quantum quantities go to their classical counterparts.

remark 33.1

33.1 Hamilton-Jacobi theory

We saw in chapter 32 that for a 1-dof particle moving in a slowly varying potential, it makes sense to generalize the free particle wave function (32.1) to a wave function

$$\psi(q, t) = A(q, t)e^{iR(q, t)/\hbar}, \quad (33.1)$$

with slowly varying (real) amplitude $A(q, t)$ and rapidly varying (real) phase $R(q, t)$. its phase and magnitude. The time evolution of the phase and the magnitude of ψ follows from the Schrödinger equation (31.1)

exercise 32.1

$$\left(i\hbar \frac{\partial}{\partial t} + \frac{\hbar^2}{2m} \frac{\partial^2}{\partial q^2} - V(q) \right) \psi(q, t) = 0. \quad (33.2)$$

Assume $A \neq 0$, and separate out the real and the imaginary parts. We get two equations: The real part governs the time evolution of the phase

$$\frac{\partial R}{\partial t} + \frac{1}{2m} \left(\frac{\partial R}{\partial q} \right)^2 + V(q) - \frac{\hbar^2}{2m} \frac{1}{A} \frac{\partial^2}{\partial q^2} A = 0, \quad (33.3)$$

and the imaginary part the time evolution of the amplitude

exercise 33.6

exercise 33.7

$$\frac{\partial A}{\partial t} + \frac{1}{m} \sum_{i=1}^D \frac{\partial A}{\partial q_i} \frac{\partial R}{\partial q_i} + \frac{1}{2m} A \frac{\partial^2 R}{\partial q^2} = 0. \quad (33.4)$$

exercise 33.8

In this way a linear PDE for a complex wave function is converted into a set of coupled non-linear PDE's for real-valued functions R and A . The coupling term in (33.3) is, however, of order \hbar^2 and thus small in the semiclassical limit $\hbar \rightarrow 0$.

Now we generalize the *Wentzel-Kramers-Brillouin* (WKB) *ansatz* for 1-dof dynamics to the Van Vleck *ansatz* in arbitrary dimension: we assume the magnitude $A(q, t)$ varies slowly compared to the phase $R(q, t)/\hbar$, so we drop the \hbar -dependent term. In this approximation the phase $R(q, t)$ and the corresponding “momentum field” $\frac{\partial R}{\partial q}(q, t)$ can be determined from the amplitude independent equation

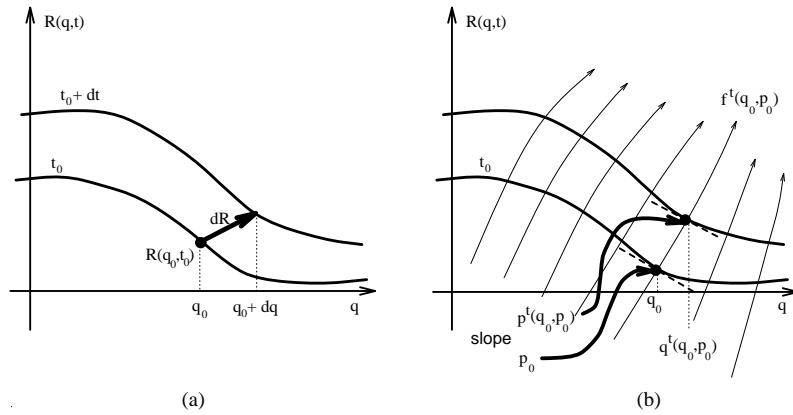
$$\frac{\partial R}{\partial t} + H\left(q, \frac{\partial R}{\partial q}\right) = 0. \quad (33.5)$$

In classical mechanics this equation is known as the *Hamilton-Jacobi equation*. We will refer to this step (as well as all leading order in \hbar approximations to follow) as the *semiclassical approximation* to wave mechanics, and from now on work only within this approximation.

33.1.1 Hamilton's equations

We now solve the nonlinear partial differential equation (33.5) in a way the 17 year old Hamilton might have solved it. The main step is the step leading from the nonlinear PDE (33.9) to Hamilton's ODEs (33.10). If you already understand the Hamilton-Jacobi theory, you can safely skip this section.

Figure 33.1: (a) A phase $R(q, t)$ plotted as a function of the position q for two infinitesimally close times. (b) The phase $R(q, t)$ transported by a swarm of “particles”; The Hamilton’s equations (33.10) construct $R(q, t)$ by transporting $q_0 \rightarrow q(t)$ and the slope of $R(q_0, t_0)$, that is $p_0 \rightarrow p(t)$.



fast track:
sect. 33.1.3, p. 605

The wave equation (31.1) describes how the wave function ψ evolves with time, and if you think of ψ as an (infinite dimensional) vector, position q plays a role of an index. In one spatial dimension the phase R plotted as a function of the position q for two different times looks something like figure 33.1 (a): The phase $R(q, t_0)$ deforms smoothly with time into the phase $R(q, t)$ at time t . Hamilton’s idea was to let a swarm of particles transport R and its slope $\partial R/\partial q$ at q at initial time $t = t_0$ to a corresponding $R(q, t)$ and its slope at time t , figure 33.1 (b). For notational convenience, define

$$p_i = p_i(q, t) := \frac{\partial R}{\partial q_i}, \quad i = 1, 2, \dots, D. \quad (33.6)$$

We saw earlier that (33.3) reduces in the semiclassical approximation to the Hamilton-Jacobi equation (33.5). To make life simple, we shall assume throughout this chapter that the Hamilton’s function $H(q, p)$ does not depend explicitly on time t , i.e., the energy is conserved.

To start with, we also assume that the function $R(q, t)$ is smooth and well defined for every q at the initial time t . This is true for sufficiently short times; as we will see later, R develops folds and becomes multi-valued as t progresses. Consider now the variation of the function $R(q, t)$ with respect to independent infinitesimal variations of the time and space coordinates dt and dq , figure 33.1 (a)

$$dR = \frac{\partial R}{\partial t} dt + \frac{\partial R}{\partial q} dq. \quad (33.7)$$

Dividing through by dt and substituting (33.5) we obtain the total derivative of $R(q, t)$ with respect to time *along the as yet arbitrary direction* \dot{q} , that is,

$$\frac{dR}{dt}(q, \dot{q}, t) = -H(q, p) + \dot{q} \cdot p. \quad (33.8)$$

Note that the “momentum” $p = \partial R/\partial q$ is a well defined function of q and t . In order to integrate $R(q, t)$ with the help of (33.8) we also need to know how $p = \partial R/\partial q$ changes along \dot{q} . Varying p with respect to independent infinitesimal variations dt and dq and substituting the Hamilton-Jacobi equation (33.5) yields

$$d\frac{\partial R}{\partial q} = \frac{\partial^2 R}{\partial q \partial t} dt + \frac{\partial^2 R}{\partial q^2} dq = -\left(\frac{\partial H}{\partial q} + \frac{\partial H}{\partial p} \frac{\partial p}{\partial q}\right) dt + \frac{\partial p}{\partial q} dq.$$

Note that $H(q, p)$ depends on q also through $p(q, t) = \partial R/\partial q$, hence the $\frac{\partial H}{\partial p}$ term in the above equation. Dividing again through by dt we get the time derivative of $\partial R/\partial q$, that is,

$$\dot{p}(q, \dot{q}, t) + \frac{\partial H}{\partial q} = \left(\dot{q} - \frac{\partial H}{\partial p}\right) \frac{\partial p}{\partial q}. \quad (33.9)$$

Time variation of p depends not only on the yet unknown \dot{q} , but also on the second derivatives of R with respect to q with yet unknown time dependence. However, if we *choose* \dot{q} (which was arbitrary, so far) such that the right hand side of the above equation vanishes, we can calculate the function $R(q, t)$ along a specific trajectory $(q(t), p(t))$ given by integrating the ordinary differential equations

$$\dot{q} = \frac{\partial H(q, p)}{\partial p}, \quad \dot{p} = -\frac{\partial H(q, p)}{\partial q} \quad (33.10)$$

with initial conditions

$$q(t_0) = q', \quad p(t_0) = p' = \frac{\partial R}{\partial q}(q', t_0). \quad (33.11)$$

section 7.1

We recognize (33.10) as Hamilton’s equations of motion of classical mechanics. The miracle happens in the step leading from (33.5) to (33.9) – if you missed it, you have missed the point. Hamilton derived his equations contemplating optics - it took him three more years to realize that all of Newtonian dynamics can be profitably recast in this form.

\dot{q} is no longer an independent function, and the phase $R(q, t)$ can now be computed by integrating equation (33.8) along the trajectory $(q(t), p(t))$

$$\begin{aligned} R(q, t) &= R(q', t_0) + R(q, t; q', t_0) \\ R(q, t; q', t_0) &= \int_{t_0}^t d\tau [\dot{q}(\tau) \cdot p(\tau) - H(q(\tau), p(\tau))] , \end{aligned} \quad (33.12)$$

with the initial conditions (33.11). In this way the Hamilton-Jacobi *partial* differential equation (33.3) is solved by integrating a set of *ordinary* differential equations, Hamilton’s equations. In order to determine $R(q, t)$ for arbitrary q and t we

have to find a q' such that the trajectory starting in $(q', p' = \partial_q R(q', t_0))$ reaches q in time t and then compute R along this trajectory, see figure 33.1 (b). The integrand of (33.12) is known as the *Lagrangian*,

$$L(q, \dot{q}, t) = \dot{q} \cdot p - H(q, p, t). \quad (33.13)$$

A variational principle lurks here, but we shall not make much fuss about it as yet.

Throughout this chapter we assume that the energy is conserved, and that the only time dependence of $H(q, p)$ is through $(q(\tau), p(\tau))$, so the value of $R(q, t; q', t_0)$ does not depend on t_0 , but only on the elapsed time $t - t_0$. To simplify notation we will set $t_0 = 0$ and write

$$R(q, q', t) = R(q, t; q', 0).$$

The initial momentum of the particle must coincide with the initial momentum of the trajectory connecting q' and q :

$$p' = \frac{\partial}{\partial q'} R(q', 0) = -\frac{\partial}{\partial q'} R(q, q', t). \quad (33.14)$$

exercise 33.5

The function $R(q, q', t)$ is known as *Hamilton's principal function*.

exercise 33.9

To summarize: Hamilton's achievement was to trade in the Hamilton-Jacobi *partial* differential equation (33.5) describing the evolution of a wave front for a finite number of *ordinary* differential equations of motion, with the initial phase $R(q, 0)$ incremented by the integral (33.12) evaluated along the phase space trajectory $(q(\tau), p(\tau))$.

33.1.2 Action

Before proceeding, we note in passing a few facts about Hamiltonian dynamics that will be needed for the construction of semiclassical Green's functions. If the energy is conserved, the $\int H(q, p) d\tau$ integral in (33.12) is simply Et . The first term, or the *action*

$$S(q, q', E) = \int_0^t d\tau \dot{q}(\tau) \cdot p(\tau) = \int_{q'}^q dq \cdot p \quad (33.15)$$

is integrated along a trajectory from q' to q with a fixed energy E . By (33.12) the action is a Legendre transform of Hamilton's principal function

$$S(q, q', E) = R(q, q', t) + Et. \quad (33.16)$$

The time of flight t along the trajectory connecting $q' \rightarrow q$ with fixed energy E is given by

$$\frac{\partial}{\partial E} S(q, q', E) = t. \quad (33.17)$$

The way to think about the formula (33.16) for action is that the time of flight is a function of the energy, $t = t(q, q', E)$. The left hand side is explicitly a function of E ; the right hand side is an implicit function of E through energy dependence of the flight time t .

Going in the opposite direction, the energy of a trajectory $E = E(q, q', t)$ connecting $q' \rightarrow q$ with a given time of flight t is given by the derivative of Hamilton's principal function

$$\frac{\partial}{\partial t} R(q, q', t) = -E, \quad (33.18)$$

and the second variations of R and S are related in the standard way of Legendre transforms:

$$\frac{\partial^2}{\partial t^2} R(q, q', t) \frac{\partial^2}{\partial E^2} S(q, q', E) = -1. \quad (33.19)$$

A geometric visualization of what the phase evolution looks like is very helpful in understanding the origin of topological indices to be introduced in what follows. Given an initial phase $R(q, t_0)$, the gradient $\partial_q R$ defines a D -dimensional *Lagrangian manifold* ($q, p = \partial_q R(q)$) in the full $2d$ dimensional phase space (q, p) . The defining property of this manifold is that any contractible loop γ in it has zero action, section 33.1.4

$$0 = \oint_{\gamma} dq \cdot p,$$

a fact that follows from the definition of p as a gradient, and the Stokes theorem. Hamilton's equations of motion preserve this property and map a Lagrangian manifold into a Lagrangian manifold at a later time. t

Returning back to the main line of our argument: so far we have determined the wave function phase $R(q, t)$. Next we show that the velocity field given by the Hamilton's equations together with the continuity equation determines the amplitude of the wave function.

33.1.3 Density evolution

To obtain the full solution of the Schrödinger equation (31.1), we also have to integrate (33.4).

$$\rho(q, t) := A^2 = \psi^* \psi$$

plays the role of a density. To the leading order in \hbar , the gradient of R may be interpreted as the semiclassical momentum density

$$\psi(q, t)^* (-i\hbar \frac{\partial}{\partial q}) \psi(q, t) = -i\hbar A \frac{\partial A}{\partial q} + \rho \frac{\partial R}{\partial q}.$$

Evaluated along the trajectory $(q(t), p(t))$, the amplitude equation (33.4) is equivalent to the continuity equation (16.36) after multiplying (33.4) by $2A$, that is

$$\frac{\partial \rho}{\partial t} + \frac{\partial}{\partial q_i} (\rho v_i) = 0. \quad (33.20)$$

Here, $v_i = \dot{q}_i = p_i/m$ denotes a velocity field, which is in turn determined by the gradient of $R(q, t)$, or the *Lagrangian manifold* $(q(t), p(t) = \partial_q R(q, t))$,

$$v = \frac{1}{m} \frac{\partial}{\partial q} R(q, t).$$

As we already know how to solve the Hamilton-Jacobi equation (33.5), we can also solve for the density evolution as follows:

The density $\rho(q)$ can be visualized as the density of a configuration space flow $q(t)$ of a swarm of hypothetical particles; the trajectories $q(t)$ are solutions of Hamilton's equations with initial conditions given by $(q(0) = q', p(0) = p' = \partial_q R(q', 0))$.

If we take a small configuration space volume $d^D q$ around some point q at time t , then the number of particles in it is $\rho(q, t) d^D q$. They started initially in a small volume $d^D q'$ around the point q' of the configuration space. For the moment, we assume that there is only one solution, the case of several paths will be considered below. The number of particles at time t in the volume is the same as the number of particles in the initial volume at $t = 0$,

$$\rho(q(t), t) d^D q = \rho(q', 0) d^D q',$$

see figure 33.2. The ratio of the initial and the final volumes can be expressed as

$$\rho(q(t), t) = \left| \det \frac{\partial q'}{\partial q} \right| \rho(q', 0). \quad (33.21)$$

section 16.2

As we know how to compute trajectories $(q(t), p(t))$, we know how to compute this Jacobian and, by (33.21), the density $\rho(q(t), t)$ at time t .

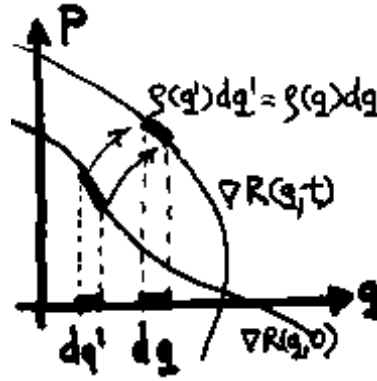


Figure 33.2: Density evolution of an initial surface $(q', p' = \partial_q R(q', 0))$ into $(q(t), p(t))$ surface time t later, sketched in 1 dimension. While the number of trajectories and the phase space Liouville volume are conserved, the density of trajectories projected on the q coordinate varies; trajectories which started in dq' at time zero end up in the interval dq .

33.1.4 Semiclassical wave function

Now we have all ingredients to write down the semiclassical wave function at time t . Consider first the case when our initial wave function can be written in terms of single-valued functions $A(q', 0)$ and $R(q', 0)$. For sufficiently short times, $R(q, t)$ will remain a single-valued function of q , and every $d^D q$ configuration space volume element keeps its orientation. The evolved wave function in the semiclassical approximation then given by

$$\begin{aligned} \psi_{sc}(q, t) &= A(q, t)e^{iR(q,t)/\hbar} = \sqrt{\det \frac{\partial q'}{\partial q}} A(q', 0)e^{i(R(q', 0)+R(q, q', t))/\hbar} \\ &= \sqrt{\det \frac{\partial q'}{\partial q}} e^{iR(q, q', t)/\hbar} \psi(q', 0). \end{aligned}$$

As the time progresses the Lagrangian manifold $\partial_q R(q, t)$ can develop folds, so for longer times the value of the phase $R(q, t)$ is not necessarily unique; in general more than one trajectory will connect points q and q' with different phases $R(q, q', t)$ accumulated along these paths, see figure 33.3.

We thus expect in general a collection of different trajectories from q' to q which we will index by j , with different phase increments $R_j(q, q', t)$. The hypothetical particles of the density flow at a given configuration space point can move with different momenta $p = \partial_q R_j(q, t)$. This is not an ambiguity, since in the full (q, p) phase space each particle follows its own trajectory with a unique momentum.

Whenever the Lagrangian manifold develops a fold, the density of the phase space trajectories in the fold projected on the configuration coordinates diverges. As illustrated in figure 33.3, when the Lagrangian manifold develops a fold at $q = q_1$; the volume element dq_1 in the neighborhood of the folding point is proportional to $\sqrt{dq'}$ instead of dq' . The Jacobian $\partial q' / \partial q$ diverges like $1/\sqrt{q_1 - q(t)}$ when computed along the trajectory going through the folding point at q_1 . After the folding the orientation of the interval dq has changed when being mapped into dq_2 ; in addition the function R , as well as its derivative which defines the

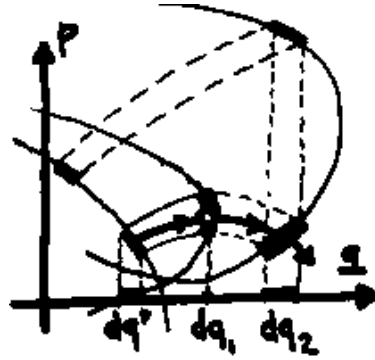


Figure 33.3: Folding of the Lagrangian surface $(q, \partial_q R(q, t))$.

Lagrangian manifold, becomes multi-valued. Distinct trajectories starting from different initial points q' can now reach the same final point q_2 . (That is, the point q' may have more than one pre-image.) The projection of a simple fold, or of an envelope of a family of phase space trajectories, is called a *caustic*; this expression comes from the Greek word for “capable of burning,” evoking the luminous patterns that one observes swirling across the bottom of a swimming pool.

The folding also changes the orientation of the pieces of the Lagrangian manifold $(q, \partial_q R(q, t))$ with respect to the initial manifold, so the eigenvalues of the Jacobian determinant change sign at each fold crossing. We can keep track of the signs by writing the Jacobian determinant as

$$\det \frac{\partial q'}{\partial q} \Big|_j = e^{-i\pi m_j(q, q', t)} \left| \det \frac{\partial q'}{\partial q} \right|_j,$$

where $m_j(q, q', t)$ counts the number of sign changes of the Jacobian determinant on the way from q' to q along the trajectory indexed with j , see figure 33.3. We shall refer to the integer $m_j(q, q', t)$ as the *topological* of the trajectory. So in general the semiclassical approximation to the wave function is thus a sum over possible trajectories that start at any initial q' and end in q in time t

$$\psi_{sc}(q, t) = \int dq' \sum_j \left| \det \frac{\partial q'}{\partial q} \right|_j^{1/2} e^{iR_j(q, q', t)/\hbar - i\pi m_j(q, q', t)/2} \psi(q'_j, 0), \quad (33.22)$$

each contribution weighted by corresponding density, phase increment and the topological index.

That the correct topological index is obtained by simply counting the number of eigenvalue sign changes and taking the square root is not obvious - the careful argument requires that quantum wave functions evaluated across the folds remain single valued.

33.2 Semiclassical propagator

We saw in chapter 31 that the evolution of an initial wave function $\psi(q, 0)$ is completely determined by the propagator (31.12). As $K(q, q', t)$ itself satisfies the Schrödinger equation (31.14), we can treat it as a wave function parameterized by the configuration point q' . In order to obtain a semiclassical approximation to the propagator we follow now the ideas developed in the last section. There is, however, one small complication: the initial condition (31.15) demands that the propagator at $t = 0$ is a δ -function at $q = q'$, that is, the amplitude is infinite at $q = q'$ and the phase is not well defined. Our hypothetical cloud of particles is thus initially localized at $q = q'$ with *any* initial velocity. This is in contrast to the situation in the previous section where we assumed that the particles at a given point q have well defined velocity (or a discrete set of velocities) given by $\dot{q} = \partial_p H(q, p)$. We will now derive a semiclassical expression for $K(q, q', t)$ by considering the propagator for short times first, and extrapolating from there to arbitrary times t .

33.2.1 Short time propagator

For infinitesimally short times δt away from the singular point $t = 0$ we assume that it is again possible to write the propagator in terms of a well defined phase and amplitude, that is

$$K(q, q', \delta t) = A(q, q', \delta t) e^{\frac{i}{\hbar} R(q, q', \delta t)}.$$

As all particles start at $q = q'$, $R(q, q', \delta t)$ will be of the form (33.12), that is

$$R(q, q', \delta t) = p\dot{q}\delta t - H(q, p)\delta t, \quad (33.23)$$

with $\dot{q} \approx (q - q')/\delta t$. For Hamiltonians of the form (31.2) we have $\dot{q} = p/m$, which leads to

$$R(q, q', \delta t) = \frac{m(q - q')^2}{2\delta t} - V(q)\delta t.$$

Here V can be evaluated any place along the trajectory from q to q' , for example at the midway point $V((q + q')/2)$. Inserting this into our ansatz for the propagator we obtain

$$K_{sc}(q, q', \delta t) \approx A(q, q', \delta t) e^{\frac{i}{\hbar} \left(\frac{m}{2\delta t} (q - q')^2 - V(q)\delta t \right)}. \quad (33.24)$$

For infinitesimal times we can neglect the term $V(q)\delta t$, so $K_{sc}(q, q', \delta t)$ is a d -dimensional Gaussian with width $\sigma^2 = i\hbar\delta t/m$. This Gaussian is a finite width approximation to the Dirac delta function

$$\delta(z) = \lim_{\sigma \rightarrow 0} \frac{1}{\sqrt{2\pi\sigma^2}} e^{-z^2/2\sigma^2} \quad (33.25)$$

if $A = (m/2\pi i\hbar\delta t)^{D/2}$, with $A(q, q', \delta t)$ fixed by the Dirac delta function normalization condition. The correctly normalized propagator for infinitesimal times δt is therefore

exercise 33.1

$$K_{sc}(q, q', \delta t) \approx \left(\frac{m}{2\pi i\hbar\delta t}\right)^{D/2} e^{i\hbar^{-1}\left(\frac{m(q-q')^2}{2\delta t} - V(q)\delta t\right)}. \quad (33.26)$$

The short time dynamics of the Lagrangian manifold $(q, \partial_q R)$ which corresponds to the quantum propagator can now be deduced from (33.23); one obtains

$$\frac{\partial R}{\partial q} = p \approx \frac{m}{\delta t}(q - q'),$$

i.e., is the particles start for short times on a Lagrangian manifold which is a plane in phase space, see figure 33.4. Note, that for $\delta t \rightarrow 0$, this plane is given by the condition $q = q'$, that is, particles start on a plane parallel to the momentum axis. As we have already noted, all particles start at $q = q'$ but with different velocities for $t = 0$. The initial surface $(q', p' = \partial_q R(q', 0))$ is mapped into the surface $(q(t), p(t))$ some time t later. The slope of the Lagrangian plane for a short finite time is given as

$$\frac{\partial p_i}{\partial q_j} = -\frac{\partial^2 R}{\partial q_j \partial q'_i} = -\frac{\partial p'_i}{\partial q_j} = \frac{m}{\delta t} \delta_{ij}.$$

The prefactor $(m/\delta t)^{D/2}$ in (33.26) can therefore be interpreted as the determinant of the Jacobian of the transformation from final position coordinates q to initial momentum coordinates p' , that is

$$K_{sc}(q, q', \delta t) = \frac{1}{(2\pi i\hbar)^{D/2}} \left(\det \frac{\partial p'}{\partial q}\right)^{1/2} e^{iR(q, q', \delta t)/\hbar}, \quad (33.27)$$

where

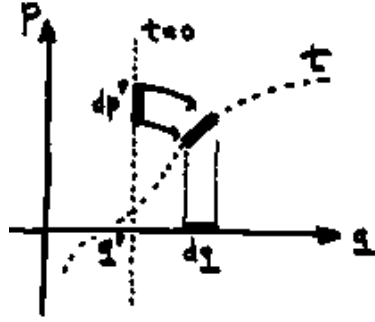
$$\left.\frac{\partial p'_i}{\partial q_j}\right|_{t, q'} = \frac{\partial^2 R(q, q', \delta t)}{\partial q_j \partial q'_i} \quad (33.28)$$

The subscript $\cdots|_{t, q'}$ indicates that the partial derivatives are to be evaluated with t, q' fixed.

The propagator in (33.27) has been obtained for short times. It is, however, already more or less in its final form. We only have to evolve our short time approximation of the propagator according to (33.22)

$$K_{sc}(q'', q', t' + \delta t) = \sum_j \left|\det \frac{\partial q}{\partial q''}\right|_j^{1/2} e^{iR_j(q'', q, t')/\hbar - i\pi m_j(q'', q, t')/2} K(q, q'_j, \delta t),$$

Figure 33.4: Evolution of the semiclassical propagator. The configuration which corresponds to the initial conditions of the propagator is a Lagrangian manifold $q = q'$, that is, a plane parallel to the p axis. The hypothetical particles are thus initially all placed at q' but take on all possible momenta p' . The Jacobian matrix C (33.29) relates an initial volume element in momentum space dp' to a final configuration space volume dq .



and we included here already the possibility that the phase becomes multi-valued, that is, that there is more than one path from q to q'' . The topological index $m_j = m_j(q'', q', t)$ is the number of singularities in the Jacobian along the trajectory j from q' to q'' . We can write $K_{sc}(q'', q', t + \delta t)$ in closed form using the fact that $R(q'', q, t') + R(q, q', \delta t) = R(q'', q', t' + \delta t)$ and the multiplicativity of Jacobian determinants, that is

$$\det \frac{\partial q}{\partial q''} \Big|_t \det \frac{\partial p'}{\partial q} \Big|_{q', \delta t} = \det \frac{\partial p'}{\partial q''} \Big|_{q', t' + \delta t} . \quad (33.29)$$

The final form of the semiclassical or *Van Vleck propagator*, is thus

$$K_{sc}(q, q', t) = \sum_j \frac{1}{(2\pi i \hbar)^{D/2}} \left| \det \frac{\partial p'}{\partial q} \right|^{1/2} e^{iR_j(q, q', t)/\hbar - im_j \pi/2} . \quad (33.30)$$

This Van Vleck propagator is the essential ingredient of the semiclassical quantization to follow.

The apparent simplicity of the semiclassical propagator is deceptive. The wave function is not evolved simply by multiplying by a complex number of magnitude $\sqrt{\det \partial p' / \partial q}$ and phase $R(q, q', t)$; the more difficult task in general is to find the trajectories connecting q and q in a given time t .

In addition, we have to treat the approximate propagator (33.30) with some care. Unlike the full quantum propagator, which satisfies the group property (31.13) exactly, the semiclassical propagator performs this only approximately, that is

$$K_{sc}(q, q', t_1 + t_2) \approx \int dq'' K_{sc}(q, q'', t_2) K_{sc}(q'', q', t_1) . \quad (33.31)$$

The connection can be made explicit by the stationary phase approximation, sect.32.2. Approximating the integral in (33.31) by integrating only over regions near points q'' at which the phase is stationary, leads to the stationary phase condition

$$\frac{\partial R(q, q'', t_2)}{\partial q''_i} + \frac{\partial R(q'', q', t_1)}{\partial q''_i} = 0 . \quad (33.32)$$

Classical trajectories contribute whenever the final momentum for a path from q' to q'' and the initial momentum for a path from q'' to q coincide. Unlike the classical evolution of sect. 17.2, the semiclassical evolution is not an evolution by linear operator multiplication, but evolution supplemented by a stationary phase condition $p_{out} = p_{in}$ that matches up the classical momenta at each evolution step.

33.2.2 Free particle propagator

To develop some intuition about the above formalism, consider the case of a free particle. For a free particle the potential energy vanishes, the kinetic energy is $\frac{m}{2}\dot{q}^2$, and the Hamilton's principal function (33.12) is

$$R(q, q', t) = \frac{m(q - q')^2}{2t}. \quad (33.33)$$

The weight $\det \frac{\partial p'}{\partial q}$ from (33.28) can be evaluated explicitly, and the Van Vleck propagator is

$$K_{sc}(q, q', t) = \left(\frac{m}{2\pi i \hbar t} \right)^{D/2} e^{im(q-q')^2/2\hbar t}, \quad (33.34)$$

identical to the short time propagator (33.26), with $V(q) = 0$. This case is rather exceptional: for a free particle the semiclassical propagator turns out to be the exact quantum propagator $K(q, q', t)$, as can be checked by substitution in the Schrödinger equation (33.2). The Feynman path integral formalism uses this fact to construct an exact quantum propagator by integrating the free particle propagator (with $V(q)$ treated as constant for short times) along all possible (not necessarily classical) paths from q' to q .

remark 33.3

exercise 33.10

exercise 33.11

exercise 33.12

33.3 Semiclassical Green's function

So far we have derived semiclassical formulas for the time evolution of wave functions, that is, we obtained approximate solutions to the time dependent Schrödinger equation (31.1). Even though we assumed in the calculation a time independent Hamiltonian of the special form (31.2), the derivation would lead to the same final result (33.30) were one to consider more complicated or explicitly time dependent Hamiltonians. The propagator is thus important when we are interested in finite time quantum mechanical effects. For time independent Hamiltonians, the time dependence of the propagator as well as of wave functions is, however, essentially given in terms of the energy eigen-spectrum of the system, as in (31.10). It is therefore advantageous to switch from a time representation to an energy representation, that is from the propagator (31.12) to the energy dependent Green's function (31.16). A semiclassical approximation of the Green's

function $G_{sc}(q, q', E)$ is given by the Laplace transform (31.16) of the Van Vleck propagator $K_{sc}(q, q', t)$:

$$G_{sc}(q, q', E) = \frac{1}{i\hbar} \int_0^\infty dt e^{iEt/\hbar} K_{sc}(q, q', t). \quad (33.35)$$

The expression as it stands is not very useful; in order to evaluate the integral, at least to the leading order in \hbar , we need to turn to the method of stationary phase again.

33.3.1 Stationary phase in higher dimensions

exercise 32.1

Generalizing the method of sect. 32.2 to d dimensions, consider stationary phase points fulfilling

$$\left. \frac{d}{dx_i} \Phi(x) \right|_{x=x_0} = 0 \quad \forall i = 1, \dots, d.$$

An expansion of the phase up to second order involves now the symmetric matrix of second derivatives of $\Phi(x)$, that is

$$D_{ij}(x_0) = \left. \frac{\partial^2}{\partial x_i \partial x_j} \Phi(x) \right|_{x=x_0}.$$

After choosing a suitable coordinate system which diagonalizes D , we can approximate the d -dimensional integral by d 1-dimensional Fresnel integrals; the stationary phase estimate of (32.13) is then

$$I \approx \sum_{x_0} (2\pi i/s)^{d/2} |\det D(x_0)|^{-1/2} A(x_0) e^{is\Phi(x_0) - \frac{i\pi}{2}m(x_0)}, \quad (33.36)$$

where the sum runs over all stationary phase points x_0 of $\Phi(x)$ and $m(x_0)$ counts the number of negative eigenvalues of $D(x_0)$.

exercise 28.2

exercise 33.2

exercise 32.3

The stationary phase approximation is all that is needed for the semiclassical approximation, with the proviso that D in (33.36) has no zero eigenvalues.

33.3.2 Long trajectories

When evaluating the integral (33.35) approximately we have to distinguish between two types of contributions: those coming from stationary points of the phase and those coming from infinitesimally short times. The first type of contributions

can be obtained by the stationary phase approximation and will be treated in this section. The latter originate from the singular behavior of the propagator for $t \rightarrow 0$ where the assumption that the amplitude changes slowly compared to the phase is not valid. The short time contributions therefore have to be treated separately, which we will do in sect. 33.3.3.

The stationary phase points t^* of the integrand in (33.35) are given by the condition

$$\frac{\partial}{\partial t} R(q, q', t^*) + E = 0. \quad (33.37)$$

We recognize this condition as the solution of (33.18), the time $t^* = t^*(q, q', E)$ in which a particle of energy E starting out in q' reaches q . Taking into account the second derivative of the phase evaluated at the stationary phase point,

$$R(q, q', t) + Et = R(q, q', t^*) + Et^* + \frac{1}{2}(t - t^*)^2 \frac{\partial^2}{\partial t^2} R(q, q', t^*) + \dots$$

the stationary phase approximation of the integral corresponding to a classical trajectory j in the Van Vleck propagator sum (33.30) yields

$$G_j(q, q', E) = \frac{1}{i\hbar(2i\pi\hbar)^{(D-1)/2}} \left| \det C_j \left(\frac{\partial^2 R_j}{\partial t^2} \right)^{-1} \right|^{1/2} e^{i\hbar S_j - \frac{i\pi}{2} m_j}, \quad (33.38)$$

where $m_j = m_j(q, q', E)$ now includes a possible additional phase arising from the time stationary phase integration (32.16), and $C_j = C_j(q, q', t^*)$, $R_j = R_j(q, q', t^*)$ are evaluated at the transit time t^* . We re-express the phase in terms of the energy dependent action (33.16)

$$S(q, q', E) = R(q, q', t^*) + Et^*, \quad \text{with } t^* = t^*(q, q', E), \quad (33.39)$$

the Legendre transform of Hamilton's principal function. Note that the partial derivative of the action (33.39) with respect to q_i

$$\frac{\partial S(q, q', E)}{\partial q_i} = \frac{\partial R(q, q', t^*)}{\partial q_i} + \left(\frac{\partial R(q, q', t)}{\partial t^*} + E \right) \frac{\partial t}{\partial q_i}.$$

is equal to

$$\frac{\partial S(q, q', E)}{\partial q_i} = \frac{\partial R(q, q', t^*)}{\partial q_i}, \quad (33.40)$$

due to the stationary phase condition (33.37), so the definition of momentum as a partial derivative with respect to q remains unaltered by the Legendre transform from time to energy domain.

exercise 33.13

Next we will simplify the amplitude term in (33.38) and rewrite it as an explicit function of the energy. Consider the $[(D + 1) \times (D + 1)]$ matrix

$$D(q, q', E) = \begin{pmatrix} \frac{\partial^2 S}{\partial q' \partial q} & \frac{\partial^2 S}{\partial q' \partial E} \\ \frac{\partial^2 S}{\partial q \partial E} & \frac{\partial^2 S}{\partial E^2} \end{pmatrix} = \begin{pmatrix} -\frac{\partial p'}{\partial q} & -\frac{\partial p'}{\partial E} \\ \frac{\partial t}{\partial q} & \frac{\partial t}{\partial E} \end{pmatrix}, \quad (33.41)$$

where $S = S(q, q', E)$ and we used (33.14–33.17) here to obtain the left hand side of (33.41). The minus signs follow from observing from the definition of (33.15) that $S(q, q', E) = -S(q', q, E)$. Note that D is nothing but the Jacobian matrix of the coordinate transformation $(q, E) \rightarrow (p', t)$ for fixed q' . We can therefore use the multiplication rules of determinants of Jacobians, which are just ratios of volume elements, to obtain

$$\begin{aligned} \det D &= (-1)^{D+1} \left(\det \frac{\partial(p', t)}{\partial(q, E)} \right)_{q'} = (-1)^{D+1} \left(\det \frac{\partial(p', t)}{\partial(q, t)} \frac{\partial(q, t)}{\partial(q, E)} \right)_{q'} \\ &= (-1)^{D+1} \left(\det \frac{\partial p'}{\partial q} \right)_{t, q'} \left(\det \frac{\partial t}{\partial E} \right)_{q', q} = \det C \left(\frac{\partial^2 R}{\partial t^2} \right)^{-1}. \end{aligned}$$

We use here the notation $(\det \cdot)_{q', t}$ for a Jacobian determinant with partial derivatives evaluated at t, q' fixed, and likewise for other subscripts. Using the relation (33.19) which relates the term $\frac{\partial t}{\partial E}$ to $\partial_t^2 R$ we can write the determinant of D as a product of the Van Vleck determinant (33.28) and the amplitude factor arising from the stationary phase approximation. The amplitude in (33.38) can thus be interpreted as the determinant of a Jacobian of a coordinate transformation which includes time and energy as independent coordinates. This causes the increase in the dimensionality of the matrix D relative to the Van Vleck determinant (33.28).

We can now write down the semiclassical approximation of the contribution of the j th trajectory to the Green's function (33.38) in explicitly energy dependent form:

$$G_j(q, q', E) = \frac{1}{i\hbar(2i\pi\hbar)^{(D-1)/2}} \left| \det D_j \right|^{1/2} e^{\frac{i}{\hbar} S_j - \frac{i\pi}{2} m_j}. \quad (33.42)$$

However, this is still not the most convenient form of the Green's function.

The trajectory contributing to $G_j(q, q', E)$ is constrained to a given energy E , and will therefore be on a phase space manifold of constant energy, that is $H(q, p) = E$. Writing this condition as a partial differential equation for $S(q, q', E)$, that is

$$H\left(q, \frac{\partial S}{\partial q}\right) = E,$$

one obtains

$$\begin{aligned}\frac{\partial}{\partial q'_i} H(q, p) &= 0 = \frac{\partial H}{\partial p_j} \frac{\partial p_j}{\partial q'_i} = \dot{q}_j \frac{\partial^2 S}{\partial q_j \partial q'_i} \\ \frac{\partial}{\partial q_i} H(q', p') &= 0 = \frac{\partial^2 S}{\partial q_i \partial q'_j} \dot{q}'_j,\end{aligned}\quad (33.43)$$

that is the sub-matrix $\partial^2 S / \partial q_i \partial q'_j$ has (left- and right-) eigenvectors corresponding to an eigenvalue 0. Rotate the local coordinate system at the either end of the trajectory

$$(q_1, q_2, q_3, \dots, q_d) \rightarrow (q_{\parallel}, q_{\perp 1}, q_{\perp 2}, \dots, q_{\perp (D-1)})$$

so that one axis points along the trajectory and all others are perpendicular to it

$$(\dot{q}_1, \dot{q}_2, \dot{q}_3, \dots, \dot{q}_d) \rightarrow (\dot{q}, 0, 0, \dots, 0).$$

With such local coordinate systems at both ends, with the longitudinal coordinate axis q_{\parallel} pointing along the velocity vector of magnitude \dot{q} , the stability matrix of $S(q, q', E)$ has a column and a row of zeros as (33.43) takes form

$$\dot{q} \frac{\partial^2 S}{\partial q_{\parallel} \partial q'_i} = \frac{\partial^2 S}{\partial q_i \partial q'_{\parallel}} \dot{q}' = 0.$$

The initial and final velocities are non-vanishing except for points $|\dot{q}| = 0$. These are the turning points (where all energy is potential), and we assume that neither q nor q' is a turning point (in our application - periodic orbits - we can always chose $q = q'$ not a turning point). In the local coordinate system with one axis along the trajectory and all other perpendicular to it the determinant of (33.41) is of the form

$$\det D(q, q', E) = (-1)^{D+1} \begin{pmatrix} 0 & 0 & \frac{\partial^2 S}{\partial E \partial q'_{\parallel}} \\ \det & 0 & \frac{\partial^2 S}{\partial q_{\perp} \partial q'_{\perp}} & * \\ \frac{\partial^2 S}{\partial q_{\parallel} \partial E} & * & * \end{pmatrix}. \quad (33.44)$$

The corner entries can be evaluated using (33.17)

$$\frac{\partial^2 S}{\partial q_{\parallel} \partial E} = \frac{\partial}{\partial q_{\parallel}} t = \frac{1}{\dot{q}}, \quad \frac{\partial^2 S}{\partial E \partial q'_{\parallel}} = \frac{1}{\dot{q}'}$$

As the q_{\parallel} axis points along the velocity direction, velocities \dot{q}, \dot{q}' are by construction almost always positive non-vanishing numbers. In this way the determinant

of the $[(D + 1) \times (D + 1)]$ dimensional matrix $D(q, q', E)$ can be reduced to the determinant of a $[(D - 1) \times (D - 1)]$ dimensional *transverse* matrix $D_{\perp}(q, q', E)$

$$\begin{aligned} \det D(q, q', E) &= \frac{1}{\dot{q}\dot{q}'} \det D_{\perp}(q, q', E) \\ D_{\perp}(q, q', E)_{ik} &= -\frac{\partial^2 S(q, q', E)}{\partial q_{\perp i} \partial q'_{\perp k}}. \end{aligned} \quad (33.45)$$

Putting everything together we obtain the j th trajectory contribution to the semiclassical Green's function

exercise 33.15

$$G_j(q, q', E) = \frac{1}{i\hbar(2\pi i\hbar)^{(D-1)/2}} \frac{1}{|\dot{q}\dot{q}'|^{1/2}} \left| \det D_{\perp}^j \right|^{1/2} e^{\frac{i}{\hbar} S_j - \frac{i\pi}{2} m_j}, \quad (33.46)$$

where the topological index $m_j = m_j(q, q', E)$ now counts the number of changes of sign of $\det D_{\perp}^j$ along the trajectory j which connects q' to q at energy E .

The endpoint velocities \dot{q}, \dot{q}' also depend on (q, q', E) and the trajectory j .

33.3.3 Short trajectories

The stationary phase method cannot be used when t^* is small, both because we cannot extend the integration in (32.16) to $-\infty$, and because the amplitude of $K(q, q', t)$ is divergent. In this case we have to evaluate the integral involving the short time form of the exact quantum mechanical propagator (33.26)

$$G_0(q, q', E) = \frac{1}{i\hbar} \int_0^{\infty} dt \left(\frac{m}{2\pi i\hbar t} \right)^{D/2} e^{\frac{i}{\hbar} \left(\frac{m(q-q')^2}{2t} - V(q)t + Et \right)}. \quad (33.47)$$

By introducing a dimensionless variable $\tau = t\sqrt{2m(E - V(q))}/m|q - q'|$, the integral can be rewritten as

$$G_0(q, q', E) = \frac{m}{i\hbar^2(2\pi i)^{D/2}} \left(\frac{\sqrt{2m(E - V)}}{\hbar|q - q'|} \right)^{\frac{D}{2}-1} \int_0^{\infty} \frac{d\tau}{\tau^{D/2}} e^{\frac{i}{2\hbar} S_0(q, q', E)(\tau+1/\tau)},$$

where $S_0(q, q', E) = \sqrt{2m(E - V)}|q - q'|$ is the short distance form of the action. Using the integral representation of the Hankel function of first kind

$$H_{\nu}^+(z) = -\frac{i}{\pi} e^{-i\nu\pi/2} \int_0^{\infty} e^{\frac{1}{2}iz(\tau+1/\tau)} \tau^{-\nu-1} d\tau$$

we can write the short distance form of the Green's function as

$$G_0(q, q', E) \approx -\frac{im}{2\hbar^2} \left(\frac{\sqrt{2m(E-V)}}{2\pi\hbar|q-q'|} \right)^{\frac{D-2}{2}} H_{\frac{D-2}{2}}^+(S_0(q, q', E)/\hbar). \quad (33.48)$$

Hankel functions are standard, and their the short wavelength asymptotics is described in standard reference books. The short distance Green's function approximation is valid when $S_0(q, q', E) \leq \hbar$.

Résumé

The aim of the semiclassical or short-wavelength methods is to approximate a solution of the Schrödinger equation with a semiclassical wave function

$$\psi_{sc}(q, t) = \sum_j A_j(q, t) e^{iR_j(q,t)/\hbar},$$

accurate to the leading order in \hbar . Here the sum is over all classical trajectories that connect the initial point q' to the final point q in time t . “Semi-” refers to \hbar , the quantum unit of phase in the exponent. The quantum mechanics enters only through this atomic scale, in units of which the variation of the phase across the classical potential is assumed to be large. “-classical” refers to the rest - both the amplitudes $A_j(q, t)$ and the phases $R_j(q, t)$ - which are determined by the classical Hamilton-Jacobi equations.

In the semiclassical approximation the quantum time evolution operator is given by the *semiclassical propagator*

$$K_{sc}(q, q', t) = \frac{1}{(2\pi i\hbar)^{D/2}} \sum_j \left| \det \frac{\partial p'}{\partial q} \right|_j^{1/2} e^{iR_j - \frac{i\pi}{2} m_j},$$

where the topological index $m_j(q, q', t)$ counts the number of the direction reversal along the j th classical trajectory that connects $q' \rightarrow q$ in time t . Until very recently it was not possible to resolve quantum evolution on quantum time scales (such as one revolution of electron around a nucleus) - physical measurements are almost always done at time scales asymptotically large compared to the intrinsic quantum time scale. Formally this information is extracted by means of a Laplace transform of the propagator which yields the energy dependent *semiclassical Green's function*

$$\begin{aligned} G_{sc}(q, q', E) &= G_0(q, q', E) + \sum_j G_j(q, q', E) \\ G_j(q, q', E) &= \frac{1}{i\hbar(2\pi i\hbar)^{\frac{(D-1)}{2}}} \left| \frac{1}{\dot{q}q'} \det \frac{\partial p'_\perp}{\partial q_\perp} \right|_j^{1/2} e^{iS_j - \frac{i\pi}{2} m_j} \end{aligned} \quad (33.49)$$

where $G_0(q, q', E)$ is the contribution of short trajectories with $S_0(q, q', E) \leq \hbar$, while the sum is over the contributions of long trajectories (33.46) going from q' to q with fixed energy E , with $S_j(q, q', E) \gg \hbar$.

Commentary

Remark 33.1 Limit $\hbar \rightarrow 0$. The semiclassical limit “ $\hbar \rightarrow 0$ ” discussed in sect. 33.1 is a shorthand notation for the limit in which typical quantities like the actions R or S in semiclassical expressions for the propagator or the Green’s function become large compared to \hbar . In the world that we live in the quantity \hbar is a fixed physical constant whose value [8] is $1.054571596(82) \cdot 10^{-34}$ Js.

Remark 33.2 Madelung’s fluid dynamics. Already Schrödinger [3] noted that

$$\rho = \rho(q, t) := A^2 = \psi^* \psi$$

plays the role of a density, and that the gradient of R may be interpreted as a local semiclassical momentum, as the momentum density is

$$\psi(q, t)^* (-i\hbar \frac{\partial}{\partial q}) \psi(q, t) = -i\hbar A \frac{\partial A}{\partial q} + \rho \frac{\partial R}{\partial q}.$$

A very different interpretation of (33.3–33.4) has been given by Madelung [2], and then built upon by Bohm [6] and others [3, 7]. Keeping the \hbar dependent term in (33.3), the ordinary differential equations driving the flow (33.10) have to be altered; if the Hamiltonian can be written as kinetic plus potential term $V(q)$ as in (31.2), the \hbar^2 term modifies the p equation of motion as

$$\dot{p}_i = -\frac{\partial}{\partial q_i} (V(q) + Q(q, t)), \tag{33.50}$$

where, for the example at hand,

$$Q(q, t) = -\frac{\hbar^2}{2m} \frac{1}{\sqrt{\rho}} \frac{\partial^2}{\partial q^2} \sqrt{\rho} \tag{33.51}$$

interpreted by Bohm [6] as the “quantum potential.” Madelung observed that Hamilton’s equation for the momentum (33.50) can be rewritten as

$$\frac{\partial v_i}{\partial t} + \left(v \cdot \frac{\partial}{\partial q} \right) v_i = -\frac{1}{m} \frac{\partial V}{\partial q_i} - \frac{1}{m\rho} \frac{\partial}{\partial q_j} \sigma_{ij}, \tag{33.52}$$

where $\sigma_{ij} = \frac{\hbar^2 \rho}{4m} \frac{\partial^2 \ln \rho}{\partial q_i \partial q_j}$ is the “pressure” stress tensor, $v_i = p_i/m$, and $\rho = A^2$ as defined [3] in sect. 33.1.3. We recall that the Eulerian $\frac{\partial}{\partial t} + \frac{\partial q_i}{\partial t} \frac{\partial}{\partial q_i}$ is the ordinary derivative

of Lagrangian mechanics, that is $\frac{d}{dt}$. For comparison, the Euler equation for classical hydrodynamics is

$$\frac{\partial v_i}{\partial t} + \left(v \cdot \frac{\partial}{\partial q} \right) v_i = -\frac{1}{m} \frac{\partial V}{\partial q_i} - \frac{1}{m\rho} \frac{\partial}{\partial q_j} (p\delta_{ij}),$$

where $p\delta_{ij}$ is the pressure tensor.

The classical dynamics corresponding to quantum evolution is thus that of an “hypothetical fluid” experiencing \hbar and ρ dependent stresses. The “hydrodynamic” interpretation of quantum mechanics has, however, not been very fruitful in practice.

Remark 33.3 Path integrals. The semiclassical propagator (33.30) can also be derived from Feynman’s path integral formalism. Dirac was the first to discover that in the short-time limit the quantum propagator (33.34) is exact. Feynman noted in 1946 that one can construct the exact propagator of the quantum Schrödinger equation by formally summing over all possible (and emphatically not classical) paths from q' to q .

Gutzwiller started from the path integral to rederive Van Vleck’s semiclassical expression for the propagator; Van Vleck’s original derivation is very much in the spirit of what has presented in this chapter. He did, however, not consider the possibility of the formation of caustics or folds of Lagrangian manifolds and thus did not include the topological phases in his semiclassical expression for the propagator. Some 40 years later Gutzwiller [4] added the topological indices when deriving the semiclassical propagator from Feynman’s path integral by stationary phase conditions.

Remark 33.4 Applications of the semiclassical Green’s function. The semiclassical Green’s function is the starting point of the semiclassical approximation in many applications. The generic semiclassical strategy is to express physical quantities (for example scattering amplitudes and cross section in scattering theory, oscillator strength in spectroscopy, and conductance in mesoscopic physics) in terms of the exact Green’s function and then replace it with the semiclassical formula.

Remark 33.5 The quasiclassical approximation The *quasiclassical* approximation was introduced by Maslov [8]. The term ‘quasiclassical’ is more appropriate than semiclassical since the Maslov type description leads to a pure classical evolution operator in a natural way. Following mostly ref. [9], we give a summary of the quasiclassical approximation, which was worked out by Maslov [8] in this form. One additional advantage of this description is that the wave function evolves along one single classical trajectory and we do not have to compute sums over increasing numbers of classical trajectories as in computations involving Van Vleck formula [27].

Exercises

33.1. Dirac delta function, Gaussian representation.

Consider the Gaussian distribution function

$$\delta_\sigma(z) = \frac{1}{\sqrt{2\pi\sigma^2}} e^{-z^2/2\sigma^2}.$$

Show that in $\sigma \rightarrow 0$ limit this is the Dirac delta function

$$\int_{\mathcal{M}} dx \delta(x) = 1 \text{ if } 0 \in \mathcal{M}, \text{ zero otherwise.}$$

33.2. Stationary phase approximation in higher dimensions.

All semiclassical approximations are based on saddle point evaluations of integrals of type

$$I = \int d^D x A(x) e^{i\Phi(x)/\hbar} \quad (33.53)$$

for small values of \hbar . Obtain the stationary phase estimate

$$I \approx \sum_n A(x_n) e^{i\Phi(x_n)/\hbar} \frac{(2\pi i \hbar)^{D/2}}{\sqrt{\det \mathbf{D}^2 \Phi(x_n)}},$$

where $\mathbf{D}^2 \Phi(x_n)$ denotes the second derivative matrix.

33.3. Schrödinger equation in the Madelung form.

Verify the decomposition of Schrödinger equation into real and imaginary parts, eqs. (33.3) and (33.4).

33.4. Transport equations.

Write the wave-function in the asymptotic form

$$\psi(q, t) = e^{\frac{i}{\hbar} R(x, t) + \frac{i}{\hbar} \epsilon t} \sum_{n \geq 0} (i\hbar)^n A_n(x, t).$$

Derive the transport equations for the A_n by substituting this into the Schrödinger equation and then collecting terms by orders of \hbar . Note that equation for A_n only requires knowledge of A_{n-1} and R .

33.5. Easy examples of the Hamilton's principal function.

Calculate $R(q, q', t)$ for

- a D -dimensional free particle
- a 3-dimensional particle in constant magnetic field
- a 1-dimensional harmonic oscillator.

(continuation: exercise 33.13.)

33.6. 1-dimensional harmonic oscillator.

Take a 1-dimensional harmonic oscillator $U(q) = \frac{1}{2}kq^2$. Take a WKB wave function of form $A(q, t) = a(t)$ and $R(q, t) = r(t) + b(t)q + c(t)q^2$, where $r(t), a(t), b(t)$ and $c(t)$ are time dependent coefficients. Derive ordinary differential equations by using (33.3) and (33.4) and solve them. (continuation: exercise 33.9.)

33.7. 1-dimensional linear potential.

Take a 1-dimensional linear potential $U(q) = -Fq$. Take a WKB wave function of form $A(q, t) = a(t)$ and $R(q, t) = r(t) + b(t)q + c(t)q^2$, where $r(t), a(t), b(t)$ and $c(t)$ are time dependent coefficients. Derive and solve the ordinary differential equations from (33.3) and (33.4).

33.8. D-dimensional quadratic potentials.

Generalize the above method to general D -dimensional quadratic potentials.

33.9. Time evolution of R.

(continuation of exercise 33.6). Calculate the time evolution of $R(q, 0) = a + bq + cq^2$ for a 1-dimensional harmonic oscillator using (33.12) and (33.14).

33.10. D-dimensional free particle propagator.

Verify the results in sect. 33.2.2; show explicitly that (33.34), the semiclassical Van Vleck propagator in D dimensions, solves the Schrödinger's equation.

33.11. Propagator, charged particle in constant magnetic field.

Calculate the semiclassical propagator for a charged particle in constant magnetic field in 3 dimensions. Verify that the semiclassical expression coincides with the exact solution.

33.12. 1-dimensional harmonic oscillator propagator.

Calculate the semiclassical propagator for a 1-dimensional harmonic oscillator and verify that it is identical to the exact quantum propagator.

33.13. Free particle action.

Calculate the energy dependent action for a free particle, a charged particle in a constant magnetic field and for the harmonic oscillator.

33.14. Zero length orbits.

Derive the classical trace (18.1) rigorously and either add the $t \rightarrow 0_+$ zero length contribution to the trace formula, or show that it vanishes. Send us a reprint of *Phys. Rev. Lett.* with the correct derivation.

33.15. Free particle semiclassical Green's functions.

Calculate the semiclassical Green's functions for the systems of exercise 33.13.

References

- [33.1] A. Einstein, “On the Quantum Theorem of Sommerfeld and Epstein,” p. 443, English translation of “Zum Quantensatz von Sommerfeld und Epstein,” *Verh. Deutsch. Phys. Ges.* **19**, 82 (1917), in *The Collected Papers of Albert Einstein*, Volume **6: The Berlin Years: Writings, 1914-1917**, A. Engel, transl. and E. Schucking, (Princeton Univ. Press, Princeton NJ 1997).
- [33.2] E. Madelung, *Zeitschr. fr Physik* **40**, 332 (1926).
- [33.3] E. Schrödinger, *Annalen der Physik* **79**, 361, 489; **80**, 437, **81**, 109 (1926).
- [33.4] J. H. van Vleck, *Quantum Principles and the Line Spectra*, Bull. Natl. Res. Council **10**, 1 (1926).
- [33.5] J. H. van Vleck, *Proc. Natl. Acad. Sci.* **14**, 178 (1928).
- [33.6] D. Bohm, *Phys. Rev.* **85**, 166 (1952).
- [33.7] P.R. Holland, *The quantum theory of motion - An account of the de Broglie-Bohm casual interpretation of quantum mechanics* (Cambridge Univ. Press, Cambridge 1993).
- [33.8] physics.nist.gov/cgi-bin/cuu

Chapter 34

Semiclassical quantization

(G. Vattay, G. Tanner and P. Cvitanović)

WE DERIVE HERE the Gutzwiller trace formula and the semiclassical zeta function, the central results of the semiclassical quantization of classically chaotic systems. In chapter 35 we will rederive these formulas for the case of scattering in open systems. Quintessential wave mechanics effects such as creeping, diffraction and tunneling will be taken up in chapter 38.

34.1 Trace formula

Our next task is to evaluate the Green's function trace (31.17) in the semiclassical approximation. The trace

$$\text{tr } G_{sc}(E) = \int d^D q G_{sc}(q, q, E) = \text{tr } G_0(E) + \sum_j \int d^D q G_j(q, q, E)$$

receives contributions from “long” classical trajectories labeled by j which start and end in q after finite time, and the “zero length” trajectories whose lengths approach zero as $q' \rightarrow q$.

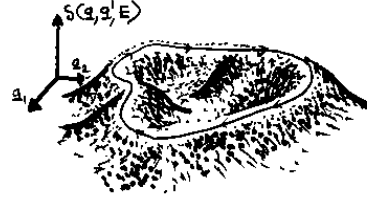
First, we work out the contributions coming from the finite time *returning* classical orbits, i.e., trajectories that originate and end at a given configuration point q . As we are identifying q with q' , taking of a trace involves (still another!) stationary phase condition in the $q' \rightarrow q$ limit,

$$\left. \frac{\partial S_j(q, q', E)}{\partial q_i} \right|_{q'=q} + \left. \frac{\partial S_j(q, q', E)}{\partial q'_i} \right|_{q'=q} = 0,$$

Figure 34.1: A returning trajectory in the configuration space. The orbit is periodic in the full phase space only if the initial and the final momenta of a returning trajectory coincide as well.



Figure 34.2: A romanticized sketch of $S_p(E) = S(q, q, E) = \oint p(q, E) dq$ landscape orbit. Unstable periodic orbits traverse isolated ridges and saddles of the mountainous landscape of the action $S(q_{\parallel}, q_{\perp}, E)$. Along a periodic orbit $S_p(E)$ is constant; in the transverse directions it generically changes quadratically.



meaning that the initial and final momenta (33.40) of contributing trajectories should coincide

$$p_i(q, q, E) - p'_i(q, q, E) = 0, \quad q \in j\text{th periodic orbit}, \quad (34.1)$$

so the trace receives contributions only from those long classical trajectories which are *periodic* in the full phase space.

For a periodic orbit the natural coordinate system is the intrinsic one, with q_{\parallel} axis pointing in the \dot{q} direction along the orbit, and q_{\perp} , the rest of the coordinates transverse to \dot{q} . The j th periodic orbit contribution to the trace of the semiclassical Green's function in the intrinsic coordinates is

$$\text{tr } G_j(E) = \frac{1}{i\hbar(2\pi\hbar)^{(d-1)/2}} \oint_j \frac{dq_{\parallel}}{\dot{q}} \int_j d^{d-1} q_{\perp} |\det D_{\perp}^j|^{1/2} e^{\frac{i}{\hbar} S_j - \frac{i\pi}{2} m_j},$$

where the integration in q_{\parallel} goes from 0 to L_j , the geometric length of small tube around the orbit in the configuration space. As always, in the stationary phase approximation we worry only about the fast variations in the phase $S_j(q_{\parallel}, q_{\perp}, E)$, and assume that the density varies smoothly and is well approximated by its value $D_{\perp}^j(q_{\parallel}, 0, E)$ on the classical trajectory, $q_{\perp} = 0$. The topological index $m_j(q_{\parallel}, q_{\perp}, E)$ is an integer which does not depend on the initial point q and not change in the infinitesimal neighborhood of an isolated periodic orbit, so we set $m_j(E) = m_j(q_{\parallel}, q_{\perp}, E)$.

The transverse integration is again carried out by the stationary phase method, with the phase stationary on the periodic orbit, $q_{\perp} = 0$. The result of the transverse integration can depend only on the parallel coordinate

$$\text{tr } G_j(E) = \frac{1}{i\hbar} \oint \frac{dq_{\parallel}}{\dot{q}} \left| \frac{\det D_{\perp j}(q_{\parallel}, 0, E)}{\det D'_{\perp j}(q_{\parallel}, 0, E)} \right|^{1/2} e^{\frac{i}{\hbar} S_j - \frac{i\pi}{2} m_j},$$

where the new determinant in the denominator, $\det D'_{\perp j} =$

$$\det \left(\frac{\partial^2 S(q, q', E)}{\partial q_{\perp i} \partial q_{\perp j}} + \frac{\partial^2 S(q, q', E)}{\partial q'_{\perp i} \partial q_{\perp j}} + \frac{\partial^2 S(q, q', E)}{\partial q_{\perp i} \partial q'_{\perp j}} + \frac{\partial^2 S(q, q', E)}{\partial q'_{\perp i} \partial q'_{\perp j}} \right),$$

is the determinant of the second derivative matrix coming from the stationary phase integral in transverse directions.

The ratio $\det D_{\perp j} / \det D'_{\perp j}$ is here to enforce the periodic boundary condition for the semiclassical Green's function evaluated on a periodic orbit. It can be given a meaning in terms of the monodromy matrix of the periodic orbit by following observations

$$\begin{aligned} \det D_{\perp} &= \left\| \frac{\partial p'_{\perp}}{\partial q_{\perp}} \right\| = \left\| \frac{\partial(q'_{\perp}, p'_{\perp})}{\partial(q_{\perp}, q'_{\perp})} \right\| \\ \det D'_{\perp} &= \left\| \frac{\partial p_{\perp}}{\partial q_{\perp}} - \frac{\partial p'_{\perp}}{\partial q_{\perp}} + \frac{\partial p_{\perp}}{\partial q'_{\perp}} - \frac{\partial p'_{\perp}}{\partial q'_{\perp}} \right\| = \left\| \frac{\partial(p_{\perp} - p'_{\perp}, q_{\perp} - q'_{\perp})}{\partial(q_{\perp}, q'_{\perp})} \right\|. \end{aligned}$$

Defining the $2(D - 1)$ -dimensional transverse vector $x_{\perp} = (q_{\perp}, p_{\perp})$ in the full phase space we can express the ratio

$$\begin{aligned} \frac{\det D'_{\perp}}{\det D_{\perp}} &= \left\| \frac{\partial(p_{\perp} - p'_{\perp}, q_{\perp} - q'_{\perp})}{\partial(q'_{\perp}, p'_{\perp})} \right\| = \left\| \frac{\partial(x_{\perp} - x'_{\perp})}{\partial x'_{\perp}} \right\| \\ &= \det(M - \mathbf{1}), \end{aligned} \quad (34.2)$$

in terms of the monodromy matrix M for a surface of section transverse to the orbit within the constant energy $E = H(q, p)$ shell.

The classical periodic orbit action $S_j(E) = \oint p(q_{\parallel}, E) dq_{\parallel}$ is an integral around a loop defined by the periodic orbit, and does not depend on the starting point q along the orbit, see figure 34.2. The eigenvalues of the monodromy matrix are also independent of where M_j is evaluated along the orbit, so $\det(1 - M_j)$ can also be taken out of the q_{\parallel} integral

$$\text{tr } G_j(E) = \frac{1}{i\hbar} \sum_j \frac{1}{|\det(1 - M_j)|^{1/2}} e^{r(\frac{i}{\hbar} S_j - \frac{i\pi}{2} m_j)} \oint \frac{dq_{\parallel}}{\dot{q}_{\parallel}}.$$

Here we have assumed that M_j has no marginal eigenvalues. The determinant of the monodromy matrix, the action $S_p(E) = \oint p(q_{\parallel}, E) dq_{\parallel}$ and the topological index are all classical invariants of the periodic orbit. The integral in the parallel direction we now do exactly.

First, we take into account the fact that any repeat of a periodic orbit is also a periodic orbit. The action and the topological index are additive along the trajectory, so for r th repeat they simply get multiplied by r . The monodromy matrix of

the r th repeat of a prime cycle p is (by the chain rule for derivatives) M_p^r , where M_p is the prime cycle monodromy matrix. Let us denote the time period of the prime cycle p , the single, shortest traversal of a periodic orbit by T_p . The remaining integral can be carried out by change of variables $dt = dq_{\parallel}/\dot{q}(t)$

$$\int_0^{L_p} \frac{dq_{\parallel}}{\dot{q}(t)} = \int_0^{T_p} dt = T_p.$$

Note that the spatial integral corresponds to a *single* traversal. If you do not see why this is so, rethink the derivation of the classical trace formula (18.23) - that derivation takes only three pages of text. Regrettably, in the quantum case we do not know of an honest derivation that takes less than 30 pages. The final result, the *Gutzwiller trace formula*

$$\text{tr } G_{sc}(E) = \text{tr } G_0(E) + \frac{1}{i\hbar} \sum_p T_p \sum_{r=1}^{\infty} \frac{1}{|\det(1 - M_p^r)|^{1/2}} e^{r(\frac{i}{\hbar} S_p - \frac{i\pi}{2} m_p)}, \quad (34.3)$$

an expression for the trace of the semiclassical Green's function in terms of periodic orbits, is beautiful in its simplicity and elegance.

The topological index $m_p(E)$ counts the number of changes of sign of the matrix of second derivatives evaluated along the prime periodic orbit p . By now we have gone through so many stationary phase approximations that you have surely lost track of what the total $m_p(E)$ actually is. The rule is this: The topological index of a closed curve in a $2D$ phase space is the sum of the number of times the partial derivatives $\frac{\partial p_i}{\partial q_i}$ for each dual pair (q_i, p_i) , $i = 1, 2, \dots, D$ (no sum on i) change their signs as one goes once around the curve.

34.1.1 Average density of states

We still have to evaluate $\text{tr } G_0(E)$, the contribution coming from the infinitesimal trajectories. The real part of $\text{tr } G_0(E)$ is infinite in the $q' \rightarrow q$ limit, so it makes no sense to write it down explicitly here. However, the imaginary part is finite, and plays an important role in the density of states formula, which we derive next.

The semiclassical contribution to the density of states (31.17) is given by the imaginary part of the Gutzwiller trace formula (34.3) multiplied with $-1/\pi$. The contribution coming from the zero length trajectories is the imaginary part of (33.48) for $q' \rightarrow q$ integrated over the configuration space

$$d_0(E) = -\frac{1}{\pi} \int d^D q \text{Im } G_0(q, q, E),$$

The resulting formula has a pretty interpretation; it estimates the number of quantum states that can be accommodated up to the energy E by counting the

available quantum cells in the phase space. This number is given by the *Weyl rule*, as the ratio of the phase space volume bounded by energy E divided by h^D , the volume of a quantum cell,

$$N_{sc}(E) = \frac{1}{h^D} \int d^D p d^D q \Theta(E - H(q, p)). \quad (34.4)$$

where $\Theta(x)$ is the Heaviside function (31.22). $N_{sc}(E)$ is an estimate of the spectral staircase (31.21), so its derivative yields the average density of states

$$d_0(E) = \frac{d}{dE} N_{sc}(E) = \frac{1}{h^D} \int d^D p d^D q \delta(E - H(q, p)), \quad (34.5)$$

precisely the semiclassical result (34.6). For Hamiltonians of type $p^2/2m + V(q)$, the energy shell volume in (34.5) is a sphere of radius $\sqrt{2m(E - V(q))}$. The surface of a d -dimensional sphere of radius r is $\pi^{d/2} r^{d-1} / \Gamma(d/2)$, so the average density of states is given by

exercise 34.2

$$d_0(E) = \frac{2m}{\hbar^D 2^d \pi^{D/2} \Gamma(D/2)} \int_{V(q) < E} d^D q [2m(E - V(q))]^{D/2-1}, \quad (34.6)$$

and

$$N_{sc}(E) = \frac{1}{h^D} \frac{\pi^{D/2}}{\Gamma(1 + D/2)} \int_{V(q) < E} d^D q [2m(E - V(q))]^{D/2}. \quad (34.7)$$

Physically this means that at a fixed energy the phase space can support $N_{sc}(E)$ distinct eigenfunctions; anything finer than the quantum cell h^D cannot be resolved, so the quantum phase space is effectively finite dimensional. The average density of states is of a particularly simple form in one spatial dimension

exercise 34.3

$$d_0(E) = \frac{T(E)}{2\pi\hbar}, \quad (34.8)$$

where $T(E)$ is the period of the periodic orbit of fixed energy E . In two spatial dimensions the average density of states is

$$d_0(E) = \frac{m\mathcal{A}(E)}{2\pi\hbar^2}, \quad (34.9)$$

where $\mathcal{A}(E)$ is the classically allowed area of configuration space for which $V(q) < E$.

exercise 34.4

The semiclassical density of states is a sum of the average density of states and the oscillation of the density of states around the average, $d_{sc}(E) = d_0(E) + d_{osc}(E)$, where

$$d_{osc}(E) = \frac{1}{\pi\hbar} \sum_p T_p \sum_{r=1}^{\infty} \frac{\cos(rS_p(E)/\hbar - rm_p\pi/2)}{|\det(1 - M_p^r)|^{1/2}} \quad (34.10)$$

follows from the trace formula (34.3).

34.1.2 Regularization of the trace

The real part of the $q' \rightarrow q$ zero length Green's function (33.48) is ultraviolet divergent in dimensions $d > 1$, and so is its formal trace (31.17). The short distance behavior of the real part of the Green's function can be extracted from the real part of (33.48) by using the Bessel function expansion for small z

$$Y_\nu(z) \approx \begin{cases} -\frac{1}{\pi}\Gamma(\nu)\left(\frac{z}{2}\right)^{-\nu} & \text{for } \nu \neq 0 \\ \frac{2}{\pi}(\ln(z/2) + \gamma) & \text{for } \nu = 0 \end{cases},$$

where $\gamma = 0.577\dots$ is the Euler constant. The real part of the Green's function for short distance is dominated by the singular part

$$G_{sing}(|q - q'|, E) = \begin{cases} -\frac{m}{2\hbar^2\pi^{\frac{d}{2}}}\Gamma((d-2)/2)\frac{1}{|q - q'|^{d-2}} & \text{for } d \neq 2 \\ \frac{m}{2\pi\hbar^2}(\ln(2m(E - V)|q - q'|/2\hbar) + \gamma) & \text{for } d = 2 \end{cases}.$$

The *regularized* Green's function

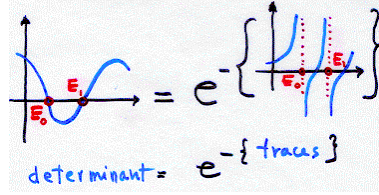
$$G_{reg}(q, q', E) = G(q, q', E) - G_{sing}(|q - q'|, E)$$

is obtained by subtracting the $q' \rightarrow q$ ultraviolet divergence. For the regularized Green's function the Gutzwiller trace formula is

$$\text{tr } G_{reg}(E) = -i\pi d_0(E) + \frac{1}{i\hbar} \sum_p T_p \sum_{r=1}^{\infty} \frac{e^{r(\frac{i}{\hbar}S_p(E) - \frac{i\pi}{2}m_p(E))}}{|\det(1 - M_p^r)|^{1/2}}. \quad (34.11)$$

Now you stand where Gutzwiller stood in 1990. You hold the trace formula in your hands. You have no clue how good is the $\hbar \rightarrow 0$ approximation, how to take care of the sum over an infinity of periodic orbits, and whether the formula converges at all.

Figure 34.3: A sketch of how spectral determinants convert poles into zeroes: The trace shows $1/(E - E_n)$ type singularities at the eigenenergies while the spectral determinant goes smoothly through zeroes.



34.2 Semiclassical spectral determinant

The problem with trace formulas is that they diverge where we need them, at the individual energy eigenvalues. What to do? Much of the quantum chaos literature responds to the challenge of wrestling the trace formulas by replacing the delta functions in the density of states (31.18) by Gaussians. But there is no need to do this - we can compute the eigenenergies without any further ado by remembering that the smart way to determine the eigenvalues of linear operators is by determining zeroes of their spectral determinants.

A sensible way to compute energy levels is to construct the spectral determinant whose zeroes yield the eigenenergies, $\det(\hat{H} - E)_{sc} = 0$. A first guess might be that the spectral determinant is the Hadamard product of form

$$\det(\hat{H} - E) = \prod_n (E - E_n),$$

but this product is not well defined, since for fixed E we multiply larger and larger numbers $(E - E_n)$. This problem is dealt with by *regularization*, discussed below in appendix 34.1.2. Here we offer an impressionistic sketch of regularization.

The logarithmic derivative of $\det(\hat{H} - E)$ is the (formal) trace of the Green's function

$$-\frac{d}{dE} \ln \det(\hat{H} - E) = \sum_n \frac{1}{E - E_n} = \text{tr} G(E).$$

This quantity, not surprisingly, is divergent again. The relation, however, opens a way to derive a convergent version of $\det(\hat{H} - E)_{sc}$, by replacing the trace with the regularized trace

$$-\frac{d}{dE} \ln \det(\hat{H} - E)_{sc} = \text{tr} G_{reg}(E).$$

The regularized trace still has $1/(E - E_n)$ poles at the semiclassical eigenenergies, poles which can be generated only if $\det(\hat{H} - E)_{sc}$ has a zero at $E = E_n$, see figure 34.3. By integrating and exponentiating we obtain

$$\det(\hat{H} - E)_{sc} = \exp\left(-\int^E dE' \text{tr} G_{reg}(E')\right)$$

Now we can use (34.11) and integrate the terms coming from periodic orbits, using the relation (33.17) between the action and the period of a periodic orbit, $dS_p(E) = T_p(E)dE$, and the relation (31.21) between the density of states and the spectral staircase, $dN_{sc}(E) = d_0(E)dE$. We obtain the *semiclassical zeta function*

$$\det(\hat{H} - E)_{sc} = e^{i\pi N_{sc}(E)} \exp\left(-\sum_p \sum_{r=1}^{\infty} \frac{1}{r} \frac{e^{ir(S_p/\hbar - m_p\pi/2)}}{|\det(1 - M_p^r)|^{1/2}}\right). \quad (34.12)$$

chapter 20

We already know from the study of classical evolution operator spectra of chapter 19 that this can be evaluated by means of cycle expansions. The beauty of this formula is that everything on the right side – the cycle action S_p , the topological index m_p and monodromy matrix M_p determinant – is intrinsic, coordinate-choice independent property of the cycle p .

34.3 One-dof systems

It has been a long trek, a stationary phase upon stationary phase. Let us check whether the result makes sense even in the simplest case, for quantum mechanics in one spatial dimension.

In one dimension the average density of states follows from the 1-dof form of the oscillating density (34.10) and of the average density (34.8)

$$d(E) = \frac{T_p(E)}{2\pi\hbar} + \sum_r \frac{T_p(E)}{\pi\hbar} \cos(rS_p(E)/\hbar - rm_p(E)\pi/2). \quad (34.13)$$

The classical particle oscillates in a single potential well with period $T_p(E)$. There is no monodromy matrix to evaluate, as in one dimension there is only the parallel coordinate, and no transverse directions. The r repetition sum in (34.13) can be rewritten by using the Fourier series expansion of a delta spike train

$$\sum_{n=-\infty}^{\infty} \delta(x - n) = \sum_{k=-\infty}^{\infty} e^{i2\pi kx} = 1 + \sum_{k=1}^{\infty} 2 \cos(2\pi kx).$$

We obtain

$$d(E) = \frac{T_p(E)}{2\pi\hbar} \sum_n \delta(S_p(E)/2\pi\hbar - m_p(E)/4 - n). \quad (34.14)$$

This expression can be simplified by using the relation (33.17) between T_p and S_p , and the identity (16.7) $\delta(x - x^*) = |f'(x)|\delta(f(x))$, where x^* is the only zero of the function $f(x^*) = 0$ in the interval under consideration. We obtain

$$d(E) = \sum_n \delta(E - E_n),$$

where the energies E_n are the zeroes of the arguments of delta functions in (34.14)

$$S_p(E_n)/2\pi\hbar = n - m_p(E)/4,$$

where $m_p(E) = m_p = 2$ for smooth potential at both turning points, and $m_p(E) = m_p = 4$ for two billiard (infinite potential) walls. These are precisely the *Bohr-Sommerfeld quantized energies* E_n , defined by the condition

$$\oint p(q, E_n) dq = h \left(n - \frac{m_p}{4} \right). \quad (34.15)$$

In this way the trace formula recovers the well known 1-dof quantization rule. In one dimension, the average of states can be expressed from the quantization condition. At $E = E_n$ the exact number of states is n , while the average number of states is $n - 1/2$ since the staircase function $N(E)$ has a unit jump in this point

$$N_{sc}(E) = n - 1/2 = S_p(E)/2\pi\hbar - m_p(E)/4 - 1/2. \quad (34.16)$$

The 1-dof spectral determinant follows from (34.12) by dropping the monodromy matrix part and using (34.16)

$$\det(\hat{H} - E)_{sc} = \exp\left(-\frac{i}{2\hbar}S_p + \frac{i\pi}{2}m_p\right) \exp\left(-\sum_r \frac{1}{r} e^{\frac{i}{\hbar}rS_p - \frac{i\pi}{2}rm_p}\right). \quad (34.17)$$

Summation yields a logarithm by $\sum_r t^r/r = -\ln(1-t)$ and we get

$$\begin{aligned} \det(\hat{H} - E)_{sc} &= e^{-\frac{i}{2\hbar}S_p + \frac{i\pi}{4} + \frac{i\pi}{2}} (1 - e^{\frac{i}{\hbar}S_p - i\frac{m_p}{2}}) \\ &= 2 \sin\left(S_p(E)/\hbar - m_p(E)/4\right). \end{aligned}$$

So in one dimension, where there is only one periodic orbit for a given energy E , nothing is gained by going from the trace formula to the spectral determinant. The spectral determinant is a real function for real energies, and its zeros are again the Bohr-Sommerfeld quantized eigenenergies (34.15).

34.4 Two-dof systems

For flows in two configuration dimensions the monodromy matrix M_p has two eigenvalues Λ_p and $1/\Lambda_p$, as explained in sect. 7.2. Isolated periodic orbits can be elliptic or hyperbolic. Here we discuss only the hyperbolic case, when the eigenvalues are real and their absolute value is not equal to one. The determinant

appearing in the trace formulas can be written in terms of the expanding eigenvalue as

$$|\det(1 - M_p^r)|^{1/2} = |\Lambda_p^r|^{1/2} \left(1 - 1/\Lambda_p^r\right),$$

and its inverse can be expanded as a geometric series

$$\frac{1}{|\det(1 - M_p^r)|^{1/2}} = \sum_{k=0}^{\infty} \frac{1}{|\Lambda_p^r|^{1/2} \Lambda_p^{kr}}.$$

With the 2-dof expression for the average density of states (34.9) the spectral determinant becomes

$$\begin{aligned} \det(\hat{H} - E)_{sc} &= e^{i\frac{m_p A E}{2\hbar^2}} \exp\left(-\sum_p \sum_{r=1}^{\infty} \sum_{k=0}^{\infty} \frac{e^{ir(S_p/\hbar - m_p\pi/2)}}{r|\Lambda_p^r|^{1/2} \Lambda_p^{kr}}\right) \\ &= e^{i\frac{m_p A E}{2\hbar^2}} \prod_p \prod_{k=0}^{\infty} \left(1 - \frac{e^{iS_p/\hbar - \frac{i\pi}{2}m_p}}{|\Lambda_p|^{1/2} \Lambda_p^k}\right). \end{aligned} \quad (34.18)$$

Résumé

Spectral determinants and dynamical zeta functions arise both in classical and quantum mechanics because in both the dynamical evolution can be described by the action of linear evolution operators on infinite-dimensional vector spaces. In quantum mechanics the periodic orbit theory arose from studies of semi-conductors, and the unstable periodic orbits have been measured in experiments on the very paradigm of Bohr's atom, the hydrogen atom, this time in strong external fields.

In practice, most “quantum chaos” calculations take the stationary phase approximation to quantum mechanics (the Gutzwiller trace formula, possibly improved by including tunneling periodic trajectories, diffraction corrections, etc.) as the point of departure. Once the stationary phase approximation is made, what follows is *classical* in the sense that all quantities used in periodic orbit calculations - actions, stabilities, geometrical phases - are classical quantities. The problem is then to understand and control the convergence of classical periodic orbit formulas.

While various periodic orbit formulas are formally equivalent, practice shows that some are preferable to others. Three classes of periodic orbit formulas are frequently used:

Trace formulas. The trace of the semiclassical Green's function

$$\text{tr } G_{sc}(E) = \int dq G_{sc}(q, q, E)$$

is given by a sum over the periodic orbits (34.11). While easiest to derive, in calculations the trace formulas are inconvenient for anything other than the leading eigenvalue estimates, as they tend to be divergent in the region of physical interest. In classical dynamics trace formulas hide under a variety of appellations such as the f - α or multifractal formalism; in quantum mechanics they are known as the Gutzwiller trace formulas.

Zeros of Ruelle or dynamical zeta functions

$$1/\zeta(s) = \prod_p (1 - t_p), \quad t_p = \frac{1}{|\Lambda_p|^{1/2}} e^{iS_p/\hbar - i\pi m_p/2}$$

yield, in combination with cycle expansions, the semiclassical estimates of *quantum* resonances. For hyperbolic systems the dynamical zeta functions have good convergence and are a useful tool for determination of classical and quantum mechanical averages.

Spectral determinants, Selberg-type zeta functions, Fredholm determinants, functional determinants are the natural objects for spectral calculations, with convergence better than for dynamical zeta functions, but with less transparent cycle expansions. The 2-dof semiclassical spectral determinant (34.18)

$$\det(\hat{H} - E)_{sc} = e^{i\pi N_{sc}(E)} \prod_p \prod_{k=0}^{\infty} \left(1 - \frac{e^{iS_p/\hbar - i\pi m_p/2}}{|\Lambda_p|^{1/2} \Lambda_p^k} \right)$$

is a typical example. Most periodic orbit calculations are based on cycle expansions of such determinants.

As we have assumed repeatedly during the derivation of the trace formula that the periodic orbits are isolated, and do not form families (as is the case for integrable systems or in KAM tori of systems with mixed phase space), the formulas discussed so far are valid only for hyperbolic and elliptic periodic orbits.

For deterministic dynamical flows and number theory, spectral determinants and zeta functions are exact. The quantum-mechanical ones, derived by the Gutzwiller approach, are at best only the stationary phase approximations to the exact quantum spectral determinants, and for quantum mechanics an important conceptual problem arises already at the level of derivation of the semiclassical formulas; how accurate are they, and can the periodic orbit theory be systematically improved?

Commentary

Remark 34.1 Gutzwiller quantization of classically chaotic systems. The derivation given here and in sects. 33.3 and 34.1 follows closely the excellent exposition [2] by Martin Gutzwiller, the inventor of the trace formula. The derivation presented here is self contained, but refs. [3, 1] might also be of help to the student.

Remark 34.2 Zeta functions. For “zeta function” nomenclature, see remark 19.4 on page 373.

Exercises

- 34.1. **Monodromy matrix from second variations of the action.** Show that

$$D_{\perp j}/D'_{\perp j} = (1 - M) \quad (34.19)$$

- 34.2. **Volume of d -dimensional sphere.** Show that the volume of a d -dimensional sphere of radius r equals $\pi^{d/2} r^d / \Gamma(1 + d/2)$. Show that $\Gamma(1 + d/2) = \Gamma(d/2)d/2$.

- 34.3. **Average density of states in 1 dimension.** Show that in one dimension the average density of states is given by (34.8)

$$\bar{d}(E) = \frac{T(E)}{2\pi\hbar},$$

where $T(E)$ is the time period of the 1-dimensional motion and show that

$$\bar{N}(E) = \frac{S(E)}{2\pi\hbar}, \quad (34.20)$$

where $S(E) = \oint p(q, E) dq$ is the action of the orbit.

- 34.4. **Average density of states in 2 dimensions.** Show that in 2 dimensions the average density of states is given by (34.9)

$$\bar{d}(E) = \frac{m\mathcal{A}(E)}{2\pi\hbar^2},$$

where $\mathcal{A}(E)$ is the classically allowed area of configuration space for which $U(q) < E$.

References

- [34.1] R.G. Littlejohn, *J. Stat. Phys.* **68**, 7 (1992).
- [34.2] L.D. Landau and E.M. Lifshitz, *Mechanics* (Pergamon, London, 1959).
- [34.3] R.G. Littlejohn, "Semiclassical structure of trace formulas," in G. Casati and B. Chirikov, eds., *Quantum Chaos*, (Cambridge Univ. Press, Cambridge 1994).
- [34.4] M.C. Gutzwiller, *J. Math. Phys.* **8**, 1979 (1967); **10**, 1004 (1969); **11**, 1791 (1970); **12**, 343 (1971).
- [34.5] M.C. Gutzwiller, *J. Math. Phys.* **12**, 343 (1971)
- [34.6] M.C. Gutzwiller, *J. Phys. Chem.* **92**, 3154 (1984).
- [34.7] A. Voros, *J. Phys. A* **21**, 685 (1988).
- [34.8] A. Voros, *Aspects of semiclassical theory in the presence of classical chaos*, *Prog. Theor. Phys. Suppl.* **116**, 17 (1994).
- [34.9] P. Cvitanović and P.E. Rosenqvist, in G.F. Dell'Antonio, S. Fantoni and V.R. Manfredi, eds., *From Classical to Quantum Chaos*, *Soc. Italiana di Fisica Conf. Proceed.* **41**, pp. 57-64 (Ed. Compositori, Bologna 1993).
- [34.10] A. Wirzba, "Validity of the semiclassical periodic orbit approximation in the 2-and 3-disk problems," *CHAOS* **2**, 77 (1992).

- [34.11] P. Cvitanović, G. Vattay and A. Wirzba, ‘Quantum fluids and classical determinants,’ in H. Friedrich and B. Eckhardt., eds., *Classical, Semiclassical and Quantum Dynamics in Atoms – in Memory of Dieter Wintgen, Lecture Notes in Physics* **485** (Springer, New York 1997), chao-dyn/9608012.
- [34.12] E.B. Bogomolny, *CHAOS* **2**, 5 (1992).
- [34.13] E.B. Bogomolny, *Nonlinearity* **5**, 805 (1992).
- [34.14] M. Kline, *Mathematical Thought from Ancient to Modern Times* (Oxford Univ. Press, Oxford 1972); on Monge and theory of characteristics - chapter 22.7.
- [34.15] E.T. Bell, *Men of Mathematics* (Penguin, London 1937).
- [34.16] R.P. Feynman, *Statistical Physics* (Addison Wesley, New York 1990).
- [34.17] H. Goldstein, *Classical Mechanics* (Addison-Wesley, Reading, 1980); chapter 9.
- [34.18] G. Tanner and D. Wintgen, *CHAOS* **2**, 53 (1992).
- [34.19] P. Cvitanović and F. Christiansen, *CHAOS* **2**, 61 (1992).
- [34.20] M.V. Berry and J.P. Keating, *J. Phys. A* **23**, 4839 (1990).
- [34.21] H.H. Rugh, ‘Generalized Fredholm determinants and Selberg zeta functions for Axiom A dynamical systems,’ *Ergodic Theory Dynamical Systems* **16**, 805 (1996).
- [34.22] B. Eckhard and G. Russberg, *Phys. Rev. E* **47**, 1578 (1993).
- [34.23] D. Ruelle, *Statistical Mechanics, Thermodynamical Formalism* (Addison-Wesley, Reading MA, 1987).
- [34.24] P. Szépfalusy, T. Tél, A. Csordás and Z. Kovács, *Phys. Rev. A* **36**, 3525 (1987).
- [34.25] H.H. Rugh, *Nonlinearity* **5**, 1237 (1992) and H.H. Rugh, *Ph.D. Thesis* (Niels Bohr Institute, 1993).
- [34.26] P. Cvitanović, P.E. Rosenqvist, H.H. Rugh and G. Vattay, *Scattering Theory - special issue*, *CHAOS* (1993).
- [34.27] E.J. Heller, S. Tomsovic and A. Sepúlveda *CHAOS* **2**, *Periodic Orbit Theory - special issue*, 105, (1992).
- [34.28] V.I. Arnold, *Geometrical Methods in the Theory of Ordinary Differential Equations*, (Springer, New York 1983).
- [34.29] R. Dashen, B. Hasslacher and A. Neveu, ‘Nonperturbative methods and extended hadron models in field theory. 1. Semiclassical functional methods,’ *Phys. Rev. D* **10**, 4114 (1974).
- [34.30] V.I. Arnold, *Geometrical Methods in the Theory of Ordinary Differential Equations* (Springer, New York 1983).

Chapter 35

Quantum scattering

Scattering is easier than gathering.

—Irish proverb

(A. Wirzba, P. Cvitanović and N. Whelan)

SO FAR the trace formulas have been derived assuming that the system under consideration is bound. As we shall now see, we are in luck - the semiclassics of bound systems is all we need to understand the semiclassics for open, scattering systems as well. We start by a brief review of the quantum theory of elastic scattering of a point particle from a (repulsive) potential, and then develop the connection to the standard Gutzwiller theory for bound systems. We do this in two steps - first, a heuristic derivation which helps us understand in what sense density of states is “density,” and then we sketch a general derivation of the central result of the spectral theory of quantum scattering, the Krein-Friedel-Lloyd formula. The end result is that we establish a connection between the scattering resonances (both positions and widths) of an open quantum system and the poles of the trace of the Green function, which we learned to analyze in earlier chapters.

35.1 Density of states

For a scattering problem the density of states (31.18) appear ill defined since formulas such as (34.6) involve integration over infinite spatial extent. What we will now show is that a quantity that makes sense physically is the difference of two densities - the first with the scatterer present and the second with the scatterer absent.

In non-relativistic dynamics the relative motion can be separated from the center-of-mass motion. Therefore the elastic scattering of two particles can be treated as the scattering of one particle from a static potential $V(q)$. We will study the scattering of a point-particle of (reduced) mass m by a short-range potential

$V(q)$, excluding *inter alia* the Coulomb potential. (The Coulomb potential decays slowly as a function of q so that various asymptotic approximations which apply to general potentials fail for it.) Although we can choose the spatial coordinate frame freely, it is advisable to place its origin somewhere near the geometrical center of the potential. The scattering problem is solved, if a scattering solution to the time-independent Schrödinger equation (31.5)

$$\left(-\frac{\hbar^2}{2m} \frac{\partial^2}{\partial q^2} + V(q)\right) \phi_{\vec{k}}(q) = E \phi_{\vec{k}}(q) \quad (35.1)$$

can be constructed. Here E is the energy, $\vec{p} = \hbar \vec{k}$ the initial momentum of the particle, and \vec{k} the corresponding wave vector.

When the argument $r = |q|$ of the wave function is large compared to the typical size a of the scattering region, the Schrödinger equation effectively becomes a free particle equation because of the short-range nature of the potential. In the asymptotic domain $r \gg a$, the solution $\phi_{\vec{k}}(q)$ of (35.1) can be written as superposition of ingoing and outgoing solutions of the free particle Schrödinger equation for fixed angular momentum:

$$\phi(q) = A\phi^{(-)}(q) + B\phi^{(+)}(q), \quad (+ \text{ boundary conditions}),$$

where in 1-dimensional problems $\phi^{(-)}(q)$, $\phi^{(+)}(q)$ are the “left,” “right” moving plane waves, and in higher-dimensional scattering problems the “incoming,” “outgoing” radial waves, with the constant matrices A , B fixed by the boundary conditions. What are the boundary conditions? The scatterer can modify only the outgoing waves (see figure 35.1), since the incoming ones, by definition, have yet to encounter the scattering region. This defines the quantum mechanical scattering matrix, or the S matrix

$$\phi_m(r) = \phi_m^{(-)}(r) + S_{mm'} \phi_{m'}^{(+)}(r). \quad (35.2)$$

All scattering effects are incorporated in the deviation of \mathbf{S} from the unit matrix, the transition matrix \mathbf{T}

$$\mathbf{S} = \mathbf{1} - i\mathbf{T}. \quad (35.3)$$

For concreteness, we have specialized to two dimensions, although the final formula is true for arbitrary dimensions. The indices m and m' are the angular momenta quantum numbers for the incoming and outgoing state of the scattering wave function, labeling the S -matrix elements $S_{mm'}$. More generally, given a set of quantum numbers β , γ , the S matrix is a collection $S_{\beta\gamma}$ of transition amplitudes $\beta \rightarrow \gamma$ normalized such that $|S_{\beta\gamma}|^2$ is the probability of the $\beta \rightarrow \gamma$ transition. The

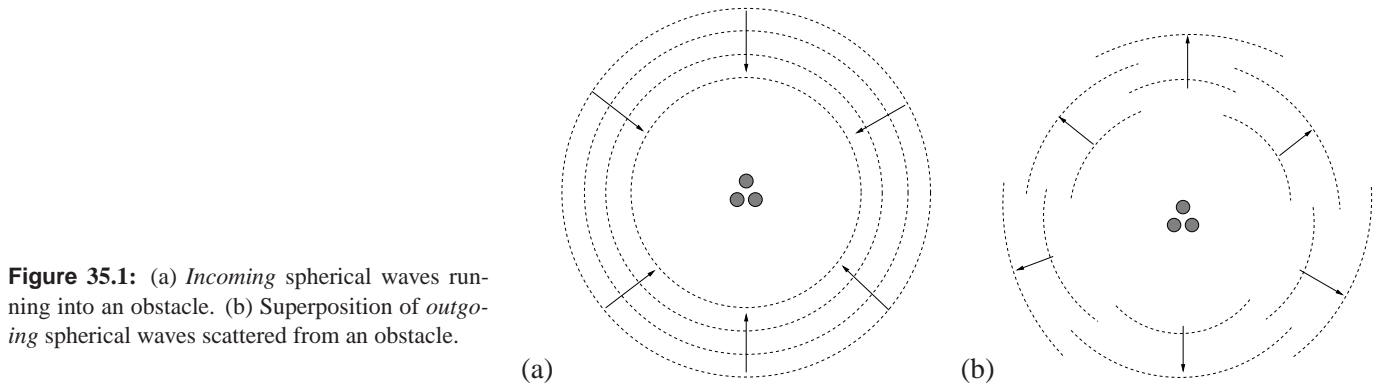


Figure 35.1: (a) *Incoming* spherical waves running into an obstacle. (b) Superposition of *outgoing* spherical waves scattered from an obstacle.

total probability that the ingoing state β ends up in some outgoing state must add up to unity

$$\sum_{\gamma} |S_{\beta\gamma}|^2 = 1, \quad (35.4)$$

so the S matrix is unitary: $\mathbf{S}^\dagger \mathbf{S} = \mathbf{S} \mathbf{S}^\dagger = \mathbf{1}$.

We have already encountered a solution to the 2-dimensional problem; free particle propagation Green's function (33.48) is a radial solution, given in terms of the Hankel function

$$G_0(r, 0, E) = -\frac{im}{2\hbar^2} H_0^{(+)}(kr),$$

where we have used $S_0(r, 0, E)/\hbar = kr$ for the action. The m th angular momentum eigenfunction is proportional to $\phi_m^{(\pm)}(q) \propto H_m^{(\pm)}(kr)$, and given a potential $V(q)$ we can in principle compute the infinity of matrix elements $S_{mm'}$. We will not need much information about $H_m^{(\pm)}(kr)$, other than that for large r its asymptotic form is

$$H^\pm \propto e^{\pm ikr}$$

In general, the potential $V(q)$ is not radially symmetric and (35.1) has to be solved numerically, by explicit integration, or by diagonalizing a large matrix in a specific basis. To simplify things a bit, we assume for the time being that a radially symmetric scatterer is centered at the origin; the final formula will be true for arbitrary asymmetric potentials. Then the solutions of the Schrödinger equation (31.5) are separable, $\phi_m(q) = \phi(r)e^{im\theta}$, $r = |q|$, the scattering matrix cannot mix different angular momentum eigenstates, and S is diagonal in the radial basis (35.2) with matrix elements given by

$$S_m(k) = e^{2i\delta_m(k)}. \quad (35.5)$$

The matrix is unitary so in a diagonal basis all entries are pure phases. This means that an incoming state of the form $H_m^{(-)}(kr)e^{im\theta}$ gets scattered into an outgoing state of the form $S_m(k)H_m^{(+)}(kr)e^{im\theta}$, where $H_m^{(\mp)}(z)$ are incoming and outgoing Hankel functions respectively. We now embed the scatterer in a infinite cylindrical well of radius R , and will later take $R \rightarrow \infty$. Angular momentum is still conserved so that each eigenstate of this (now bound) problem corresponds to some value of m . For large $r \gg a$ each eigenstate is of the asymptotically free form

$$\begin{aligned} \phi_m(r) &\approx e^{im\theta} \left(S_m(k)H_m^{(+)}(kr) + H_m^{(-)}(kr) \right) \\ &\approx \dots \cos(kr + \delta_m(k) - \chi_m), \end{aligned} \quad (35.6)$$

where \dots is a common prefactor, and $\chi_m = m\pi/2 + \pi/4$ is an annoying phase factor from the asymptotic expansion of the Hankel functions that will play no role in what follows.

The state (35.6) must satisfy the external boundary condition that it vanish at $r = R$. This implies the quantization condition

$$k_n R + \delta_m(k_n) - \chi_m = \pi(n + 1/2).$$

We now ask for the difference in the eigenvalues of two consecutive states of fixed m . Since R is large, the density of states is high, and the phase $\delta_m(k)$ does not change much over such a small interval. Therefore, to leading order we can include the effect of the change of the phase on state $n + 1$ by Taylor expanding. is

$$k_{n+1}R + \delta_m(k_{n+1}) + (k_{n+1} - k_n)\delta'_m(k_n) - \chi_m \approx \pi + \pi(n + 1/2).$$

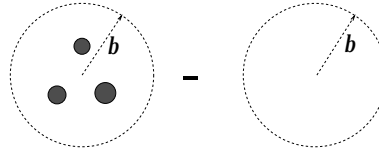
Taking the difference of the two equations we obtain $\Delta k \approx \pi(R + \delta'_m(k))^{-1}$. This is the eigenvalue spacing which we now interpret as the inverse of the density of states within m angular momentum subspace

$$d_m(k) \approx \frac{1}{\pi} (R + \delta'_m(k)).$$

The R term is essentially the $1 - d$ Weyl term (34.8), appropriate to $1 - d$ radial quantization. For large R , the dominant behavior is given by the size of the circular enclosure with a correction in terms of the derivative of the scattering phase shift, approximation accurate to order $1/R$. However, not all is well: the area under consideration tends to infinity. We regularize this by subtracting from the result from the free particle density of states $d_0(k)$, for the same size container, but this time without any scatterer, figure 35.2. We also sum over all m values so that

$$\begin{aligned} d(k) - d_0(k) &= \frac{1}{\pi} \sum_m \delta'_m(k) = \frac{1}{2\pi i} \sum_m \frac{d}{dk} \log S_m \\ &= \frac{1}{2\pi i} \text{Tr} \left(S^\dagger \frac{dS}{dk} \right). \end{aligned} \quad (35.7)$$

Figure 35.2: The “difference” of two bounded reference systems, one with and one without the scattering system.



The first line follows from the definition of the phase shifts (35.5) while the second line follows from the unitarity of S so that $S^{-1} = S^\dagger$. We can now take the limit $R \rightarrow \infty$ since the R dependence has been cancelled away.

This is essentially what we want to prove since for the left hand side we already have the semiclassical theory for the trace of the difference of Green’s functions,

$$d(k) - d_0(k) = -\frac{1}{2\pi k} \text{Im}(\text{tr}(G(k) - G_0(k))). \quad (35.8)$$

There are a number of generalizations. This can be done in any number of dimensions. It is also more common to do this as a function of energy and not wave number k . However, as the asymptotic dynamics is free wave dynamics labeled by the wavenumber k , we have adapted k as the natural variable in the above discussion.

Finally, we state without proof that the relation (35.7) applies even when there is no circular symmetry. The proof is more difficult since one cannot appeal to the phase shifts δ_m but must work directly with a non-diagonal S matrix.

35.2 Quantum mechanical scattering matrix

The results of the previous section indicate that there is a connection between the scattering matrix and the trace of the quantum Green’s function (more formally between the difference of the Green’s function with and without the scattering center.) We now show how this connection can be derived in a more rigorous manner. We will also work in terms of the energy E rather than the wavenumber k , since this is the more usual exposition. Suppose particles interact via forces of sufficiently short range, so that in the remote past they were in a free particle state labeled β , and in the distant future they will likewise be free, in a state labeled γ . In the Heisenberg picture the S -matrix is defined as $\mathbf{S} = \Omega_- \Omega_+^\dagger$ in terms of the Møller operators

$$\Omega_\pm = \lim_{t \rightarrow \pm\infty} e^{iHt/\hbar} e^{-iH_0t/\hbar}, \quad (35.9)$$

where H is the full Hamiltonian, whereas H_0 is the free Hamiltonian. In the interaction picture the S -matrix is given by

$$\mathbf{S} = \Omega_+^\dagger \Omega_- = \lim_{t \rightarrow \infty} e^{iH_0t/\hbar} e^{-2iHt/\hbar} e^{iH_0t/\hbar}$$

$$= T \exp \left(-i \int_{-\infty}^{+\infty} dt H'(t) \right), \quad (35.10)$$

where $H' = V = H - H_0$ is the interaction Hamiltonian and T is the time-ordering operator. In stationary scattering theory the S matrix has the following spectral representation

$$\begin{aligned} S &= \int_0^\infty dE S(E) \delta(H_0 - E) \\ S(E) &= Q_+(E) Q_-^{-1}(E), \quad Q_\pm(E) = \mathbf{1} + (H_0 - E \pm i\epsilon)^{-1} V, \end{aligned} \quad (35.11)$$

such that

$$\text{Tr} \left[S^\dagger(E) \frac{d}{dE} S(E) \right] = \text{Tr} \left[\frac{1}{H_0 - E - i\epsilon} - \frac{1}{H - E - i\epsilon} - (\epsilon \leftrightarrow -\epsilon) \right]. \quad (35.12)$$

The manipulations leading to (35.12) are justified if the operators $Q_\pm(E)$ can be linked to trace-class operators. appendix J

We can now use this result to derive the Krein-Lloyd formula which is the central result of this chapter. The Krein-Lloyd formula provides the connection between the trace of the Green's function and the poles of the scattering matrix, implicit in all of the trace formulas for open quantum systems which will be presented in the subsequent chapters.

35.3 Krein-Friedel-Lloyd formula

The link between quantum mechanics and semiclassics for scattering problems is provided by the semiclassical limit of the Krein-Friedel-Lloyd sum for the spectral density which we now derive. This derivation builds on the results of the last section and extends the discussion of the opening section.

In chapter 33 we linked the spectral density (see (31.18)) of a bounded system

$$d(E) \equiv \sum_n \delta(E_n - E) \quad (35.13)$$

via the identity

$$\begin{aligned} \delta(E_n - E) &= -\lim_{\epsilon \rightarrow 0} \frac{1}{\pi} \text{Im} \frac{1}{E - E_n + i\epsilon} \\ &= -\lim_{\epsilon \rightarrow 0} \frac{1}{\pi} \text{Im} \langle E_n | \frac{1}{E - H + i\epsilon} | E_n \rangle \\ &= \frac{1}{2\pi i} \lim_{\epsilon \rightarrow 0} \left\langle E_n \left| \frac{1}{E - H - i\epsilon} - \frac{1}{E - H + i\epsilon} \right| E_n \right\rangle \end{aligned} \quad (35.14)$$

to the trace of the Green's function (34.1.1). Furthermore, in the semiclassical approximation, the trace of the Green's function is given by the Gutzwiller trace formula (34.11) in terms of a smooth Weyl term and an oscillating contribution of periodic orbits.

Therefore, the task of constructing the semiclassics of a scattering system is completed, if we can find a connection between the spectral density $d(E)$ and the scattering matrix S . We will see that (35.12) provides the clue. Note that the right hand side of (35.12) has nearly the structure of (35.14) when the latter is inserted into (35.13). The principal difference between these two types of equations is that the S matrix refers to *outgoing* scattering wave functions which are not normalizable and which have a *continuous* spectrum, whereas the spectral density $d(E)$ refers to a bound system with normalizable wave functions with a discrete spectrum. Furthermore, the bound system is characterized by a *hermitian* operator, the Hamiltonian H , whereas the scattering system is characterized by a *unitary* operator, the S -matrix. How can we reconcile these completely different classes of wave functions, operators and spectra? The trick is to put our scattering system into a finite box as in the opening section. We choose a spherical container with radius R and with its center at the center of our finite scattering system. Our scattering potential $V(\vec{r})$ will be unaltered within the box, whereas at the box walls we will choose an infinitely high potential, with the Dirichlet boundary conditions at the outside of the box:

$$\phi(\vec{r})|_{r=R} = 0 . \quad (35.15)$$

In this way, for any finite value of the radius R of the box, we have mapped our scattering system into a bound system with a spectral density $d(E; R)$ over discrete eigenenergies $E_n(R)$. It is therefore important that our scattering potential was chosen to be short-ranged to start with. (Which explains why the Coulomb potential requires special care.) The hope is that in the limit $R \rightarrow \infty$ we will recover the scattering system. But some care is required in implementing this. The smooth Weyl term $\bar{d}(E; R)$ belonging to our box with the enclosed potential V diverges for a spherical 2-dimensional box of radius R quadratically, as $\pi R^2/(4\pi)$ or as R^3 in the 3-dimensional case. This problem can easily be cured if the spectral density of an empty reference box of the *same* size (radius R) is subtracted (see figure 35.2). Then all the divergences linked to the increasing radius R in the limit $R \rightarrow \infty$ drop out of the difference. Furthermore, in the limit $R \rightarrow \infty$ the energy-eigenfunctions of the box are only normalizable as a delta distribution, similarly to a plane wave. So we seem to recover a continuous spectrum. Still the problem remains that the wave functions do not discriminate between incoming and outgoing waves, whereas this symmetry, namely the hermiticity, is broken in the scattering problem. The last problem can be tackled if we replace the spectral density over discrete delta distributions by a smoothed spectral density with a small finite imaginary part η in the energy E :

$$d(E + i\eta; R) \equiv \frac{1}{i2\pi} \sum_n \left\{ \frac{1}{E - E_n(R) - i\eta} - \frac{1}{E - E_n(R) + i\eta} \right\} . \quad (35.16)$$

Note that $d(E + i\eta; R) \neq d(E - i\eta; R) = -d(E + i\eta; R)$. By the introduction of the positive *finite* imaginary part η the time-dependent behavior of the wave function has effectively been altered from an oscillating one to a decaying one and the hermiticity of the Hamiltonian is removed. Finally the limit $\eta \rightarrow 0$ can be carried out, respecting the order of the limiting procedures. First, the limit $R \rightarrow \infty$ has to be performed for a *finite* value of η , only then the limit $\eta \rightarrow 0$ is allowed. In practice, one can try to work with a finite value of R , but then it will turn out (see below) that the scattering system is only recovered if $R\sqrt{\eta} \gg 1$.

Let us summarize the relation between the smoothed spectral densities $d(E + i\eta; R)$ of the boxed potential and $d^{(0)}(E + i\eta; R)$ of the empty reference system and the S matrix of the corresponding scattering system:

$$\begin{aligned} \lim_{\eta \rightarrow +0} \lim_{R \rightarrow \infty} \left(d(E + i\eta; R) - d^{(0)}(E + i\eta; R) \right) &= \frac{1}{2\pi i} \text{Tr} \left[S^\dagger(E) \frac{d}{dE} S(E) \right] \\ &= \frac{1}{2\pi i} \text{Tr} \frac{d}{dE} \ln S(E) = \frac{1}{2\pi i} \frac{d}{dE} \ln \det S(E). \quad (35.17) \end{aligned}$$

This is the *Krein-Friedel-Lloyd formula*. It replaces the scattering problem by the difference of two bounded reference billiards of the same radius R which finally will be taken to infinity. The first billiard contains the scattering region or potentials, whereas the other does not (see figure 35.2). Here $d(E + i\eta; R)$ and $d^{(0)}(E + i\eta; R)$ are the *smoothed* spectral densities in the presence or in the absence of the scatterers, respectively. In the semiclassical approximation, they are replaced by a Weyl term (34.10) and an oscillating sum over periodic orbits. As in (34.2), the trace formula (35.17) can be integrated to give a relation between the smoothed staircase functions and the determinant of the S -matrix:

$$\lim_{\eta \rightarrow +0} \lim_{R \rightarrow \infty} \left(N(E + i\eta; R) - N^{(0)}(E + i\eta; R) \right) = \frac{1}{2\pi i} \ln \det S(E). \quad (35.18)$$

Furthermore, in both versions of the Krein-Friedel-Lloyd formulas the energy argument $E + i\eta$ can be replaced by the wavenumber argument $k + i\eta'$. These expressions only make sense for wavenumbers on or above the real k -axis. In particular, if k is chosen to be real, η' must be greater than zero. Otherwise, the exact left hand sides (35.18) and (35.17) would give discontinuous staircase or even delta function sums, respectively, whereas the right hand sides are continuous to start with, since they can be expressed by continuous phase shifts. Thus the order of the two limits in (35.18) and (35.17) is essential.

The necessity of the $+i\eta$ prescription can also be understood by purely phenomenological considerations in the semiclassical approximation: Without the $i\eta$ term there is no reason why one should be able to neglect spurious periodic orbits which are there solely because of the introduction of the confining boundary. The subtraction of the second (empty) reference system removes those spurious periodic orbits which never encounter the scattering region – in addition to the removal of the divergent Weyl term contributions in the limit $R \rightarrow \infty$. The periodic orbits that encounter both the scattering region and the external wall would still

survive the first limit $R \rightarrow \infty$, if they were not exponentially suppressed by the $+i\eta$ term because of their

$$e^{iL(R)\sqrt{2m(E+i\eta)}} = e^{iL(R)k} e^{-L(R)\eta'}$$

behavior. As the length $L(R)$ of a spurious periodic orbit grows linearly with the radius R . The bound $R\eta' \gg 1$ is an essential precondition on the suppression of the unwanted spurious contributions of the container if the Krein-Friedel-Lloyd formulas (35.17) and (35.18) are evaluated at a finite value of R .

exercise 35.1

Finally, the semiclassical approximation can also help us in the interpretation of the Weyl term contributions for scattering problems. In scattering problems the Weyl term appears with a negative sign. The reason is the subtraction of the empty container from the container with the potential. If the potential is a dispersing billiard system (or a finite collection of dispersing billiards), we expect an excluded volume (or the sum of excluded volumes) relative to the empty container. In other words, the Weyl term contribution of the empty container is larger than of the filled one and therefore a negative net contribution is left over. Second, if the scattering potential is a collection of a finite number of non-overlapping scattering regions, the Krein-Friedel-Lloyd formulas show that the corresponding Weyl contributions are completely independent of the position of the single scatterers, as long as these do not overlap.

35.4 Wigner time delay

The term $\frac{d}{dE} \ln \det S$ in the density formula (35.17) is dimensionally time. This suggests another, physically important interpretation of such formulas for scattering systems, the Wigner delay, defined as

$$\begin{aligned} d(k) &= \frac{d}{dk} \text{Argdet}(\mathbf{S}(k)) \\ &= -i \frac{d}{dk} \log \det(\mathbf{S}(k)) \\ &= -i \text{tr} \left(\mathbf{S}^\dagger(k) \frac{d\mathbf{S}}{dk}(k) \right) \end{aligned} \quad (35.19)$$

and can be shown to equal the total delay of a wave packet in a scattering system. We now review this fact.

A related quantity is the total scattering *phase shift* $\Theta(k)$ defined as

$$\det \mathbf{S}(k) = e^{+i\Theta(k)},$$

so that $d(k) = \frac{d}{dk} \Theta(k)$.

The time delay may be both positive and negative, reflecting attractive respectively repulsive features of the scattering system. To elucidate the connection between the scattering determinant and the time delay we study a plane wave:

The phase of a wave packet will have the form:

$$\phi = \vec{k} \cdot \vec{x} - \omega t + \Theta.$$

Here the term in the parenthesis refers to the phase shift that will occur if scattering is present. The center of the wave packet will be determined by the principle of stationary phase:

$$0 = d\phi = d\vec{k} \cdot \vec{x} - d\omega t + d\Theta.$$

Hence the packet is located at

$$\vec{x} = \frac{\partial \omega}{\partial \vec{k}} t - \frac{\partial \Theta}{\partial \vec{k}}.$$

The first term is just the group velocity times the given time t . Thus the packet is retarded by a length given by the derivative of the phase shift with respect to the wave vector \vec{k} . The arrival of the wave packet at the position \vec{x} will therefore be delayed. This *time delay* can similarly be found as

$$\tau(\omega) = \frac{\partial \Theta(\omega)}{\partial \omega}.$$

To show this we introduce the *slowness* of the phase $\vec{s} = \vec{k}/\omega$ for which $\vec{s} \cdot \vec{v}_g = 1$, where \vec{v}_g is the group velocity to get

$$d\vec{k} \cdot \vec{x} = \vec{s} \cdot \vec{x} d\omega = \frac{x}{v_g} d\omega,$$

since we may assume \vec{x} is parallel to the group velocity (consistent with the above). Hence the arrival time becomes

$$t = \frac{x}{v_g} + \frac{\partial \Theta(\omega)}{\partial \omega}.$$

If the scattering matrix is not diagonal, one interprets

$$\Delta t_{ij} = \text{Re} \left(-i S_{ij}^{-1} \frac{\partial S_{ij}}{\partial \omega} \right) = \text{Re} \left(\frac{\partial \Theta_{ij}}{\partial \omega} \right)$$

as the delay in the j th scattering channel after an injection in the i th. The probability for appearing in channel j goes as $|S_{ij}|^2$ and therefore the average delay for the incoming states in channel i is

$$\begin{aligned}\langle \Delta t_i \rangle &= \sum_j |S_{ij}|^2 \Delta t_{ij} = \operatorname{Re} \left(-i \sum_j S_{ij}^* \frac{\partial S_{ij}}{\partial \omega} \right) = \operatorname{Re} \left(-i \mathbf{S}^\dagger \cdot \frac{\partial \mathbf{S}}{\partial \omega} \right)_{ii} \\ &= -i \left(\mathbf{S}^\dagger \cdot \frac{\partial \mathbf{S}}{\partial \omega} \right)_{ii},\end{aligned}$$

where we have used the derivative, $\partial/\partial\omega$, of the unitarity relation $\mathbf{S} \cdot \mathbf{S}^\dagger = \mathbf{1}$ valid for real frequencies. This discussion can in particular be made for wave packets related to partial waves and superpositions of these like an incoming plane wave corresponding to free motion. The total Wigner delay therefore corresponds to the sum over all channel delays (35.19).

Commentary

Remark 35.1 Krein-Friedel-Lloyd formula. The third volume of Thirring [1], sections 3.6.14 (Levison Theorem) and 3.6.15 (the proof), or P. Scherer's thesis [15] (appendix) discusses the Levison Theorem.

It helps to start with a toy example or simplified example instead of the general theorem, namely for the radially symmetric potential in a symmetric cavity. Have a look at the book of K. Huang, chapter 10 (on the "second virial coefficient"), or Beth and Uhlenbeck [5], or Friedel [7]. These results for the correction to the density of states are particular cases of the Krein formula [3]. The Krein-Friedel-Lloyd formula (35.17) was derived in refs. [3, 7, 8, 9], see also refs. [11, 14, 15, 17, 18]. The original papers are by Krein and Birman [3, 4] but beware, they are mathematicians.

Also, have a look at pages 15-18 of Wirzba's talk on the Casimir effect [16]. Page 16 discusses the Beth-Uhlenbeck formula [5], the predecessor of the more general Krein formula for spherical cases.

Remark 35.2 Weyl term for empty container. For a discussion of why the Weyl term contribution of the empty container is larger than of the filled one and therefore a negative net contribution is left over, see ref. [15].

Remark 35.3 Wigner time delay. Wigner time delay and the Wigner-Smith time delay matrix, are powerful concepts for a statistical description of scattering. The diagonal elements Q_{aa} of the lifetime matrix $\mathbf{Q} = -i\mathbf{S}^{-1}\partial\mathbf{S}/\partial\omega$, where \mathbf{S} is the $[2N \times 2N]$ scattering matrix, are interpreted in terms of the time spent in the scattering region by a wave packet incident in one channel. As shown by Smith [26], they are the sum over all output channels (both in reflection and transmission) of $\Delta t_{ab} = \operatorname{Re} [(-i/S_{ab})(\partial S_{ab}/\partial\omega)]$ weighted by the probability of emerging from that channel. The sum of the Q_{aa} over all $2N$ channels is the Wigner time delay $\tau_W = \sum_a Q_{aa}$, which is the trace of the lifetime matrix and is proportional to the density of states.

Exercises

- 35.1. **Spurious orbits under the Krein-Friedel-Lloyd construction.** Draw examples for the three types of period orbits under the Krein-Friedel-Lloyd construction: (a) the genuine periodic orbits of the scattering region, (b) spurious periodic orbits which can be removed by the subtraction of the reference system, (c) spurious periodic orbits which cannot be removed by this subtraction. What is the role of the double limit $\eta \rightarrow 0$, container size $b \rightarrow \infty$?

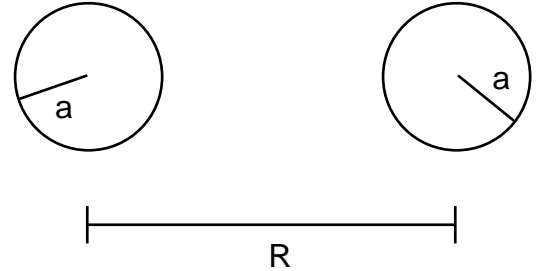
- 35.2. **The one-disk scattering wave function.** Derive the one-disk scattering wave function.

(Andreas Wirzba)

- 35.3. **Quantum two-disk scattering.** Compute the quasi-classical spectral determinant

$$Z(\varepsilon) = \prod_{p,j,l} \left(1 - \frac{t_p}{\Lambda_p^{j+2l}} \right)^{j+1}$$

for the two disk problem. Use the geometry



The full quantum mechanical version of this problem can be solved by finding the zeros in k for the determinant of the matrix

$$M_{m,n} = \delta_{m,n} + \frac{(-1)^n}{2} \frac{J_m(ka)}{H_n^{(1)}(ka)} \left(H_{m-n}^{(1)}(kR) + (-1)^n H_{m+n}^{(1)}(kR) \right)$$

where J_n is the n th Bessel function and $H_n^{(1)}$ is the Hankel function of the first kind. Find the zeros of the determinant closest to the origin by solving $\det M(k) = 0$. (Hints: note the structure $M = I + A$ to approximate the determinant; or read *Chaos* **2**, 79 (1992))

- 35.4. **Pinball topological index.** Upgrade your pinball simulator so that it computes the topological index for each orbit it finds.

References

- [35.1] W. Thirring, *Quantum mechanics of atoms and molecules, A course in mathematical physics* Vol. **3** (Springer, New York, 1979). (Springer, Wien 1979).
- [35.2] A. Messiah, *Quantum Mechanics, Vol. I* (North-Holland, Amsterdam, 1961).
- [35.3] M.G. Krein, *On the Trace Formula in Perturbation Theory*, Mat. Sborn. (N.S.) **33**, 597 (1953); *Perturbation Determinants and Formula for Traces of Unitary and Self-adjoint Operators*, Sov. Math.-Dokl. **3**, 707 (1962).
- [35.4] M.Sh. Birman and M.G. Krein, *On the Theory of Wave Operators and Scattering Operators*, Sov. Math.-Dokl. **3**, 740 (1962); M.Sh. Birman and D.R. Yafaev, *St. Petersburg Math. J.* **4**, 833 (1993).
- [35.5] E. Beth and G.E. Uhlenbeck, *Physica* **4**, 915 (1937).

- [35.6] K. Huang, *Statistical Mechanics* (John Wiley & Sons, New York (1987).
- [35.7] J. Friedel, *Phil. Mag.* **43**, 153 (1952); *Nuovo Cim. Ser. 10 Suppl.* **7**, 287 (1958).
- [35.8] P. Lloyd, Wave propagation through an assembly of spheres. II. The density of single-particle eigenstates, *Proc. Phys. Soc.* **90**, 207 (1967).
- [35.9] P. Lloyd and P.V. Smith, Multiple-scattering theory in condensed materials, *Adv. Phys.* **21**, 69 (1972), and references therein.
- [35.10] R. Balian and C. Bloch, *Ann. Phys. (N.Y.)* **63**, 592 (1971)
- [35.11] R. Balian and C. Bloch, *Solution of the Schrödinger Equation in Terms of Classical Paths Ann. Phys. (NY)* **85**, 514 (1974).
- [35.12] R. Balian and C. Bloch, *Distribution of eigenfrequencies for the wave equation in a finite domain: III. Eigenfrequency density oscillations*, *Ann. Phys. (N.Y.)* **69**,76 (1972).
- [35.13] J.S. Faulkner, "Scattering theory and cluster calculations," *J. Phys. C* **10**, 4661 (1977).
- [35.14] P. Gaspard and S.A. Rice, Semiclassical quantization of the scattering from a classically chaotic repeller, *J. Chem. Phys.* **90**, 2242 (1989).
- [35.15] P. Scherer, *Quantenzustände eines klassisch chaotischen Billards*, Ph.D. thesis, Univ. Köln (Berichte des Forschungszentrums Jülich 2554, ISSN 0366-0885, Jülich, Nov. 1991).
- [35.16] A. Wirzba, "A force from nothing into nothing: Casimir interactions," ChaosBook.org/projects/Wirzba/openfull.ps.gz overheads (2003).
- [35.17] P. Gaspard, Scattering Resonances: Classical and Quantum Dynamics, in: *Proceedings of the Int. School of Physics "Enrico Fermi"*, Course CXIX, Varena, 23 July - 2 August 1991, eds G. Casati, I. Guarneri and U. Smilansky (North-Holland, Amsterdam, 1993).
- [35.18] A. Norcliffe and I. C. Percival, *J. Phys. B* **1**, 774 (1968); L. Schulman, *Phys. Rev.* **176**, 1558 (1968).
- [35.19] W. Franz, *Theorie der Beugung Elektromagnetischer Wellen* (Springer, Berlin 1957); "Über die Greenschen Funktionen des Zylinders und der Kugel," *Z. Naturforschung* **9a**, 705 (1954).
- [35.20] G.N. Watson, *Proc. Roy. Soc. London Ser. A* **95**, 83 (1918).
- [35.21] M. Abramowitz and I.A. Stegun, *Handbook of Mathematical Functions with Formulas, Graphs and Mathematical Tables*, (Dover, New York, 1964).
- [35.22] W. Franz and R. Galle, "Semiasymptotische Reihen für die Beugung einer ebenen Welle am Zylinder," *Z. Naturforschung* **10a**, 374 (1955).

- [35.23] A. Wirzba, "Validity of the semiclassical periodic orbit approximation in the 2- and 3-disk problems," *CHAOS* **2**, 77 (1992).
- [35.24] M.V. Berry, "Quantizing a Classically Ergodic System: Sinai's Billiard and the KKR Method," *Ann. Phys. (N.Y.)* **131**, 163 (1981).
- [35.25] E.P. Wigner, *Phys. Rev.* **98**, 145 (1955).
- [35.26] F.T. Smith, *Phys. Rev.* **118**, 349 (1960).
- [35.27] A. Wirzba, *Quantum Mechanics and Semiclassics of Hyperbolic n -Disk Scattering*, *Physics Reports* **309**, 1-116 (1999); [chao-dyn/9712015](#).
- [35.28] V. A. Gopar, P. A. Mello, and M. Buttiker, *Phys. Rev. Lett.* **77**, 3005 (1996).
- [35.29] P. W. Brouwer, K. M. Frahm, and C. W. J. Beenakker, *Phys. Rev. Lett.* **78**, 4737 (1997).
- [35.30] Following the thesis of Eisenbud, the local delay time D_{tab} is defined in ref. [26] as the appearance of the peak in the outgoing signal in channel b after the injection of a wave packet in channel a . Our definition of the local delay time τ_{ab} in Eq. (1) coincides with the definition of D_{tab} in the limit of narrow bandwidth pulses, as shown in Eq. (3).
- [35.31] E. Doron and U. Smilansky, *Phys. Rev. Lett.* **68**, 1255 (1992).
- [35.32] G. Iannaccone, *Phys. Rev. B* **51**, 4727 (1995).
- [35.33] V. Gasparian, T. Christen, and M. Büttiker, *Phys. Rev. A* **54**, 4022 (1996).
- [35.34] For a complete and insightful review see Y. V. Fyodorov and H.-J. Sommers, *J. Math. Phys.* **38**, 1918 (1997).
- [35.35] R. Landauer and Th. Martin, *Rev. Mod. Phys.* **66**, 217 (1994). j
- [35.36] E. H. Hauge and J. A. Støveng, *Rev. Mod. Phys.* **61**, 917 (1989).

Chapter 36

Chaotic multiscattering

(A. Wirzba and P. Cvitanović)

WE DISCUSS HERE the semiclassics of scattering in open systems with a finite number of non-overlapping finite scattering regions. Why is this interesting at all? The semiclassics of scattering systems has five advantages compared to the bound-state problems such as the helium quantization discussed in chapter 37.

- For bound-state problem the semiclassical approximation does not respect quantum-mechanical unitarity, and the semi-classical eigenenergies are not real. Here we construct a *manifestly unitary* semiclassical scattering matrix.
- The Weyl-term contributions decouple from the multi-scattering system.
- The close relation to the classical escape processes discussed in chapter 1.
- For scattering systems the derivation of cycle expansions is more direct and controlled than in the bound-state case: the semiclassical cycle expansion is the saddle point approximation to the cumulant expansion of the determinant of the exact quantum-mechanical multi-scattering matrix.
- The region of convergence of the semiclassical spectral function is larger than is the case for the bound-state case.

We start by a brief review of the elastic scattering of a point particle from finite collection of non-overlapping scattering regions in terms of the standard textbook scattering theory, and then develop the semiclassical scattering trace formulas and spectral determinants for scattering off N disks in a plane.

36.1 Quantum mechanical scattering matrix

We now specialize to the elastic scattering of a point particle from finite collection of N non-overlapping reflecting disks in a 2-dimensional plane. As the point particle moves freely between the static scatterers, the time independent Schrödinger equation outside the scattering regions is the Helmholtz equation:

$$\left(\vec{\nabla}_r^2 + \vec{k}^2\right)\psi(\vec{r}) = 0, \quad \vec{r} \text{ outside the scattering regions.} \quad (36.1)$$

Here $\psi(\vec{r})$ is the wave function of the point particle at spatial position \vec{r} and $E = \hbar^2 \vec{k}^2 / 2m$ is its energy written in terms of its mass m and the wave vector \vec{k} of the incident wave. For reflecting wall billiards the scattering problem is a boundary value problem with Dirichlet boundary conditions:

$$\psi(\vec{r}) = 0, \quad \vec{r} \text{ on the billiard perimeter} \quad (36.2)$$

As usual for scattering problems, we expand the wave function $\psi(\vec{r})$ in the (2-dimensional) angular momentum eigenfunctions basis

$$\psi(\vec{r}) = \sum_{m=-\infty}^{\infty} \psi_m^k(\vec{r}) e^{-im\Phi_k}, \quad (36.3)$$

where k and Φ_k are the length and angle of the wave vector, respectively. A plane wave in two dimensions expanded in the angular momentum basis is

$$e^{i\vec{k}\cdot\vec{r}} = e^{ikr \cos(\Phi_r - \Phi_k)} = \sum_{m=-\infty}^{\infty} J_m(kr) e^{im(\Phi_r - \Phi_k)}, \quad (36.4)$$

where r and Φ_r denote the distance and angle of the spatial vector \vec{r} as measured in the global 2-dimensional coordinate system.

The m th angular component $J_m(kr) e^{im\Phi_r}$ of a plane wave is split into a superposition of incoming and outgoing 2-dimensional spherical waves by decomposing the ordinary Bessel function $J_m(z)$ into the sum

$$J_m(z) = \frac{1}{2} \left(H_m^{(1)}(z) + H_m^{(2)}(z) \right) \quad (36.5)$$

of the Hankel functions $H_m^{(1)}(z)$ and $H_m^{(2)}(z)$ of the first and second kind. For $|z| \gg 1$ the Hankel functions behave asymptotically as:

$$\begin{aligned} H_m^{(2)}(z) &\sim \sqrt{\frac{2}{\pi z}} e^{-i(z - \frac{\pi}{2}m - \frac{\pi}{4})} \quad \text{incoming,} \\ H_m^{(1)}(z) &\sim \sqrt{\frac{2}{\pi z}} e^{+i(z - \frac{\pi}{2}m - \frac{\pi}{4})} \quad \text{outgoing.} \end{aligned} \quad (36.6)$$

Thus for $r \rightarrow \infty$ and k fixed, the m th angular component $J_m(kr)e^{im\Phi_r}$ of the plane wave can be written as superposition of incoming and outgoing 2-dimensional spherical waves:

$$J_m(kr)e^{im\Phi_r} \sim \frac{1}{\sqrt{2\pi kr}} \left[e^{-i(kr - \frac{\pi}{2}m - \frac{\pi}{4})} + e^{i(kr - \frac{\pi}{2}m - \frac{\pi}{4})} \right] e^{im\Phi_r}. \quad (36.7)$$

In terms of the asymptotic (angular momentum) components ψ_m^k of the wave function $\psi(\vec{r})$, the scattering matrix (35.3) is defined as

$$\psi_m^k \sim \frac{1}{\sqrt{2\pi kr}} \sum_{m'=-\infty}^{\infty} \left[\delta_{mm'} e^{-i(kr - \frac{\pi}{2}m' - \frac{\pi}{4})} + S_{mm'} e^{i(kr - \frac{\pi}{2}m' - \frac{\pi}{4})} \right] e^{im'\Phi_r}. \quad (36.8)$$

The matrix element $S_{mm'}$ describes the scattering of an incoming wave with angular momentum m into an outgoing wave with angular momentum m' . If there are no scatterers, then $\mathbf{S} = \mathbf{1}$ and the asymptotic expression of the plane wave $e^{i\vec{k}\cdot\vec{r}}$ in two dimensions is recovered from $\psi(\vec{r})$.

36.1.1 1-disk scattering matrix

In general, \mathbf{S} is nondiagonal and nonseparable. An exception is the 1-disk scatterer. If the origin of the coordinate system is placed at the center of the disk, by (36.5) the m th angular component of the time-independent scattering wave function is a superposition of incoming and outgoing 2-dimensional spherical waves

exercise 35.2

$$\begin{aligned} \psi_m^k &= \frac{1}{2} \left(H_m^{(2)}(kr) + S_{mm} H_m^{(1)}(kr) \right) e^{im\Phi_r} \\ &= \left(J_m(kr) - \frac{i}{2} T_{mm} H_m^{(1)}(kr) \right) e^{im\Phi_r}. \end{aligned}$$

The vanishing (36.2) of the wave function on the disk perimeter

$$0 = J_m(ka) - \frac{i}{2} T_{mm} H_m^{(1)}(ka)$$

yields the 1-disk scattering matrix in analytic form:

$$S_{mm'}^s(k) = \left(1 - \frac{2J_m(ka_s)}{H_m^{(1)}(ka_s)} \right) \delta_{mm'} = -\frac{H_m^{(2)}(ka_s)}{H_m^{(1)}(ka_s)} \delta_{mm'}, \quad (36.9)$$

where $a = a_s$ is radius of the disk and the suffix s indicates that we are dealing with a disk whose label is s . We shall derive a semiclassical approximation to this 1-disk \mathbf{S} -matrix in sect. 36.3.

36.1.2 Multi-scattering matrix

Consider next a scattering region consisting of N non-overlapping disks labeled $s \in \{1, 2, \dots, N\}$, following the notational conventions of sect. 11.6. The strategy is to construct the full \mathbf{T} -matrix (35.3) from the exact 1-disk scattering matrix (36.9) by a succession of coordinate rotations and translations such that at each step the coordinate system is centered at the origin of a disk. Then the \mathbf{T} -matrix in $S_{mm'} = \delta_{mm'} - iT_{mm'}$ can be split into a product over three kinds of matrices,

$$T_{mm'}(k) = \sum_{s,s'=1}^N \sum_{l_s, l_{s'}=-\infty}^{\infty} C_{ml_s}^s(k) \mathbf{M}^{-1}(k)_{l_s l_{s'}}^{s s'} D_{l_{s'} m'}^{s'}(k).$$

The outgoing spherical wave scattered by the disk s is obtained by shifting the global coordinates origin distance R_s to the center of the disk s , and measuring the angle Φ_s with respect to direction \mathbf{k} of the outgoing spherical wave. As in (36.9), the matrix \mathbf{C}^s takes form

$$C_{ml_s}^s = \frac{2i}{\pi a_s} \frac{J_{m-l_s}(kR_s)}{H_{l_s}^{(1)}(ka_s)} e^{im\Phi_s}. \quad (36.10)$$

If we now describe the ingoing spherical wave in the disk s' coordinate frame by the matrix $\mathbf{D}^{s'}$

$$D_{l_{s'} m'}^{s'} = -\pi a_{s'} J_{m'-l_{s'}}(kR_{s'}) J_{l_{s'}}(ka_{s'}) e^{-im'\Phi_{s'}}, \quad (36.11)$$

and apply the Bessel function addition theorem

$$J_m(y+z) = \sum_{\ell=-\infty}^{\infty} J_{m-\ell}(y) J_{\ell}(z),$$

we recover the \mathbf{T} -matrix (36.9) for the single disk $s = s'$, $M = 1$ scattering. The Bessel function sum is a statement of the completeness of the spherical wave basis; as we shift the origin from the disk s to the disk s' by distance $R_{s'}$, we have to reexpand all basis functions in the new coordinate frame.

The labels m and m' refer to the angular momentum quantum numbers of the ingoing and outgoing waves in the global coordinate system, and $l_s, l_{s'}$ refer to the (angular momentum) basis fixed at the s th and s' th scatterer, respectively. Thus, \mathbf{C}^s and $\mathbf{D}^{s'}$ depend on the origin and orientation of the global coordinate system of the 2-dimensional plane as well as on the internal coordinates of the scatterers. As they can be made separable in the scatterer label s , they describe the single scatterer aspects of what, in general, is a multi-scattering problem.

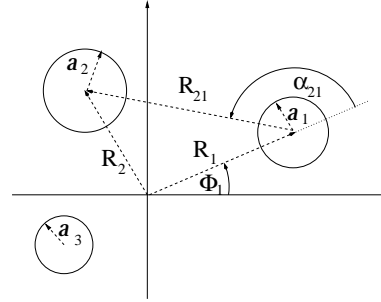


Figure 36.1: Global and local coordinates for a general 3-disk problem.

The matrix \mathbf{M} is called the *multi-scattering matrix*. If the scattering problem consists only of one scatterer, \mathbf{M} is simply the unit matrix $M_{l_s l_{s'}}^{s s'} = \delta^{s s'} \delta_{l_s l_{s'}}$. For scattering from more than one scatterer we separate out a “single traversal” matrix \mathbf{A} which transports the scattered wave from a scattering region \mathcal{M}_s to the scattering region $\mathcal{M}_{s'}$,

$$M_{l_s l_{s'}}^{s s'} = \delta^{s s'} \delta_{l_s l_{s'}} - A_{l_s l_{s'}}^{s s'} . \quad (36.12)$$

The matrix $\mathbf{A}^{s s'}$ reads:

$$A_{l_s l_{s'}}^{s s'} = -(1 - \delta^{s s'}) \frac{a_s}{a_{s'}} \frac{J_{l_s}(ka_s)}{H_{l_{s'}}^{(1)}(ka_{s'})} H_{l_s - l_{s'}}^{(1)}(kR_{s s'}) e^{i(l_s \alpha_{s' s} - l_{s'}(\alpha_{s s'} - \pi))} . \quad (36.13)$$

Here, a_s is the radius of the s th disk. R_s and Φ_s are the distance and angle, respectively, of the ray from the origin in the 2-dimensional plane to the center of disk s as measured in the global coordinate system. Furthermore, $R_{s s'} = R_{s' s}$ is the separation between the centers of the s th and s' th disk and $\alpha_{s' s}$ of the ray from the center of disk s to the center of disk s' as measured in the local (body-fixed) coordinate system of disk s (see figure 36.1).

Expanded as a geometrical series about the unit matrix $\mathbf{1}$, the inverse matrix \mathbf{M}^{-1} generates a multi-scattering series in powers of the single-traversal matrix \mathbf{A} . All genuine multi-scattering dynamics is contained in the matrix \mathbf{A} ; by construction \mathbf{A} vanishes for a single-scatterer system.

36.2 N -scatterer spectral determinant

In the following we limit ourselves to a study of the spectral properties of the \mathbf{S} -matrix: resonances, time delays and phase shifts. The resonances are given by the poles of the \mathbf{S} -matrix in the lower complex wave number (k) plane; more precisely, by the poles of the \mathbf{S} on the second Riemann sheet of the complex energy plane. As the \mathbf{S} -matrix is unitary, it is also natural to focus on its total phase shift $\eta(k)$ defined by $\det \mathbf{S} = \exp^{2i\eta(k)}$. The time-delay is proportional to the derivative of the phase shift with respect to the wave number k .

As we are only interested in spectral properties of the scattering problem, it suffices to study $\det \mathbf{S}$. This determinant is basis and coordinate-system independent, whereas the \mathbf{S} -matrix itself depends on the global coordinate system and on the choice of basis for the point particle wave function.

As the \mathbf{S} -matrix is, in general, an infinite dimensional matrix, it is not clear whether the corresponding determinant exists at all. If \mathbf{T} -matrix is trace-class, the determinant does exist. What does this mean?

36.2.1 Trace-class operators

An operator (an infinite-dimensional matrix) is called *trace-class* if and only if, for any choice of orthonormal basis, the sum of the diagonal matrix elements converges absolutely; it is called “Hilbert-Schmidt,” if the sum of the absolute squared diagonal matrix elements converges. Once an operator is diagnosed as trace-class, we are allowed to manipulate it as we manipulate finite-dimensional matrices. We review the theory of trace-class operators in appendix J; here we will assume that the \mathbf{T} -matrix (35.3) is trace-class, and draw the conclusions.

If \mathbf{A} is trace-class, the determinant $\det(\mathbf{1} - z\mathbf{A})$, as defined by the cumulant expansion, exists and is an entire function of z . Furthermore, the determinant is invariant under any unitary transformation.

The cumulant expansion is the analytical continuation (as Taylor expansion in the book-keeping variable z) of the determinant

$$\det(\mathbf{1} - z\mathbf{A}) = \exp[\text{tr} \ln(\mathbf{1} - z\mathbf{A})] = \exp\left(-\sum_{n=1}^{\infty} \frac{z^n}{n} \text{tr}(\mathbf{A}^n)\right).$$

That means

$$\det(\mathbf{1} - z\mathbf{A}) := \sum_{m=0}^{\infty} z^m Q_m(\mathbf{A}), \quad (36.14)$$

where the cumulants $Q_m(\mathbf{A})$ satisfy the Plemelj-Smithies recursion formula (J.19), a generalization of Newton’s formula to determinants of infinite-dimensional matrices,

$$\begin{aligned} Q_0(\mathbf{A}) &= 1 \\ Q_m(\mathbf{A}) &= -\frac{1}{m} \sum_{j=1}^m Q_{m-j}(\mathbf{A}) \text{tr}(\mathbf{A}^j) \quad \text{for } m \geq 1, \end{aligned} \quad (36.15)$$

in terms of cumulants of order $n < m$ and traces of order $n \leq m$. Because of the trace-class property of \mathbf{A} , all cumulants and traces exist separately.

For the general case of $N < \infty$ non-overlapping scatterers, the \mathbf{T} -matrix can be shown to be trace-class, so the determinant of the \mathbf{S} -matrix is well defined. What does trace-class property mean for the corresponding matrices \mathbf{C} , \mathbf{D}^s and $\mathbf{A}^{s s'}$? Manipulating the operators as though they were finite matrices, we can perform the following transformations:

$$\begin{aligned} \det \mathbf{S} &= \det (\mathbf{1} - i\mathbf{C}\mathbf{M}^{-1}\mathbf{D}) \\ &= \text{Det} (\mathbf{1} - i\mathbf{M}^{-1}\mathbf{D}\mathbf{C}) = \text{Det} (\mathbf{M}^{-1}(\mathbf{M} - i\mathbf{D}\mathbf{C})) \\ &= \frac{\text{Det} (\mathbf{M} - i\mathbf{D}\mathbf{C})}{\text{Det} (\mathbf{M})} \dots \end{aligned} \quad (36.16)$$

In the first line of (36.16) the determinant is taken over small ℓ (the angular momentum with respect to the global system). In the remainder of (36.16) the determinant is evaluated over the multiple indices $L_s = (s, l_s)$. In order to signal this difference we use the following notation: $\det \dots$ and $\text{tr} \dots$ refer to the $|\ell\rangle$ space, $\text{Det} \dots$ and $\text{Tr} \dots$ refer to the multiple index space. The matrices in the multiple index space are expanded in the complete basis $\{|L_s\rangle\} = \{|s, \ell_s\rangle\}$ which refers for fixed index s to the origin of the s th scatterer and not any longer to the origin of the 2-dimensional plane.

Let us explicitly extract the product of the determinants of the subsystems from the determinant of the total system (36.16):

$$\begin{aligned} \det \mathbf{S} &= \frac{\text{Det} (\mathbf{M} - i\mathbf{D}\mathbf{C})}{\text{Det} (\mathbf{M})} \\ &= \frac{\text{Det} (\mathbf{M} - i\mathbf{D}\mathbf{C})}{\text{Det} \mathbf{M}} \frac{\prod_{s=1}^N \det \mathbf{S}^s}{\prod_{s=1}^N \det \mathbf{S}^s} \\ &= \left(\prod_{s=1}^N \det \mathbf{S}^s \right) \frac{\text{Det} (\mathbf{M} - i\mathbf{D}\mathbf{C}) / \prod_{s=1}^N \det \mathbf{S}^s}{\text{Det} \mathbf{M}}. \end{aligned} \quad (36.17)$$

The final step in the reformulation of the determinant of the \mathbf{S} -matrix of the N -scatterer problem follows from the unitarity of the \mathbf{S} -matrix. The unitarity of $\mathbf{S}^\dagger(k^*)$ implies for the determinant

$$\det (\mathbf{S}(k^*)^\dagger) = 1/\det \mathbf{S}(k), \quad (36.18)$$

where this manipulation is allowed because the \mathbf{T} -matrix is trace-class. The unitarity condition should apply for the \mathbf{S} -matrix of the total system, \mathbf{S} , as for the each of the single subsystems, \mathbf{S}^s , $s = 1, \dots, N$. In terms of the result of (36.17), this implies

$$\frac{\text{Det} (\mathbf{M}(k) - i\mathbf{D}(k)\mathbf{C}(k))}{\prod_{s=1}^N \det \mathbf{S}^s} = \text{Det} (\mathbf{M}(k^*)^\dagger)$$

since all determinants in (36.17) exist separately and since the determinants $\det \mathbf{S}^s$ respect unitarity by themselves. Thus, we finally have

$$\det \mathbf{S}(k) = \left\{ \prod_{s=1}^N (\det \mathbf{S}^s(k)) \right\} \frac{\text{Det } \mathbf{M}(k^*)^\dagger}{\text{Det } \mathbf{M}(k)}, \quad (36.19)$$

where all determinants exist separately.

In summary: We assumed a scattering system of a *finite* number of *non-overlapping* scatterers which can be of different shape and size, but are all of finite extent. We assumed the trace-class character of the \mathbf{T} -matrix belonging to the total system and of the single-traversal matrix \mathbf{A} and finally unitarity of the \mathbf{S} -matrices of the complete and all subsystems.

What can one say about the point-particle scattering from a finite number of scatterers of arbitrary shape and size? As long as each of $N < \infty$ single scatterers has a finite spatial extent, i.e., can be covered by a finite disk, the total system has a finite spatial extent as well. Therefore, it too can be put inside a circular domain of finite radius b , e.g., inside a single disk. If the impact parameter of the point particle measured with respect to the origin of this disk is larger than the disk size (actually larger than $(e/2) \times b$), then the \mathbf{T} matrix elements of the N -scatterer problem become very small. If the wave number k is kept fixed, the modulus of the *diagonal* matrix elements, $|T_{mm}|$ with the angular momentum $m > (e/2)kb$, is bounded by the corresponding quantity of the covering disk.

36.2.2 Quantum cycle expansions

In formula (36.19) the genuine multi-scattering terms are separated from the single-scattering ones. We focus on the multi-scattering terms, i.e., on the ratio of the determinants of the multi-scattering matrix $\mathbf{M} = \mathbf{1} - \mathbf{A}$ in (36.19), since they are the origin of the periodic orbit sums in the semiclassical reduction. The resonances of the multi-scattering system are given by the zeros of $\text{Det } \mathbf{M}(k)$ in the lower complex wave number plane.

In order to set up the problem for the semiclassical reduction, we express the determinant of the multi-scattering matrix in terms of the traces of the powers of the matrix \mathbf{A} , by means of the cumulant expansion (36.14). Because of the finite number $N \geq 2$ of scatterers $\text{tr}(\mathbf{A}^n)$ receives contributions corresponding to all periodic itineraries $s_1 s_2 s_3 \cdots s_{n-1} s_n$ of total symbol length n with an alphabet $s_i \in \{1, 2, \dots, N\}$. of N symbols,

$$\begin{aligned} \text{tr } \mathbf{A}^{s_1 s_2} \mathbf{A}^{s_2 s_3} \cdots \mathbf{A}^{s_{n-1} s_n} \mathbf{A}^{s_n s_1} \\ = \sum_{l_{s_1} = -\infty}^{+\infty} \sum_{l_{s_2} = -\infty}^{+\infty} \cdots \sum_{l_{s_n} = -\infty}^{+\infty} A_{l_{s_1} l_{s_2}}^{s_1 s_2} A_{l_{s_2} l_{s_3}}^{s_2 s_3} \cdots A_{l_{s_{n-1}} l_{s_n}}^{s_{n-1} s_n} A_{l_{s_n} l_{s_1}}^{s_n s_1}. \end{aligned} \quad (36.20)$$

Remember our notation that the trace $\text{tr}(\cdot \cdot \cdot)$ refers only to the $|l\rangle$ space. By construction \mathbf{A} describes only scatterer-to-scatterer transitions, so the symbolic dynamics has to respect the no-self-reflection pruning rule: for admissible itineraries the successive symbols have to be different. This rule is implemented by the factor $1 - \delta^{s s'}$ in (36.13).

The trace $\text{tr} \mathbf{A}^n$ is the sum of all itineraries of length n ,

$$\text{tr} \mathbf{A}^n = \sum_{\{s_1 s_2 \dots s_n\}} \text{tr} \mathbf{A}^{s_1 s_2} \mathbf{A}^{s_2 s_3} \dots \mathbf{A}^{s_{n-1} s_n} \mathbf{A}^{s_n s_1} . \quad (36.21)$$

We will show for the N -disk problem that these periodic itineraries correspond in the semiclassical limit, $ka_{s_i} \gg 1$, to *geometrical* periodic orbits with the same symbolic dynamics.

For periodic orbits with creeping sections the symbolic alphabet has to be extended, see sect. 36.3.1. Furthermore, depending on the geometry, there might be nontrivial pruning rules based on the so called ghost orbits, see sect. 36.4.1.

36.2.3 Symmetry reductions

The determinants over the multi-scattering matrices run over the multiple index L of the multiple index space. This is the proper form for the symmetry reduction (in the multiple index space), e.g., if the scatterer configuration is characterized by a discrete symmetry group G , we have

$$\text{Det} \mathbf{M} = \prod_{\alpha} (\det \mathbf{M}_{D_{\alpha}}(k))^{d_{\alpha}} ,$$

where the index α runs over all conjugate classes of the symmetry group G and D_{α} is the α th representation of dimension d_{α} . The symmetry reduction on the exact quantum mechanical level is the same as for the classical evolution operators spectral determinant factorization (21.17) of sect. 21.4.2.

36.3 Semiclassical 1-disk scattering

We start by focusing on the single-scatterer problem. In order to be concrete, we will consider the semiclassical reduction of the scattering of a single disk in plane.

Instead of calculating the semiclassical approximation to the determinant of the one-disk system scattering matrix (36.9), we do so for

$$\mathbf{d}(k) \equiv \frac{1}{2\pi i} \frac{d}{dk} \ln \det \mathbf{S}^1(ka) = \frac{1}{2\pi i} \frac{d}{dk} \text{tr} \left(\ln \mathbf{S}^1(ka) \right) \quad (36.22)$$

the so called *time delay*.

$$\begin{aligned} \mathbf{d}(k) &= \frac{1}{2\pi i} \frac{d}{dk} \text{tr} \left(\ln \det \mathbf{S}^1(ka) \right) = \frac{1}{2\pi i} \sum_m \left(\frac{H_m^{(1)}(ka)}{H_m^{(2)}(ka)} \frac{d}{dk} \frac{H_m^{(2)}(ka)}{H_m^{(1)}(ka)} \right) \\ &= \frac{a}{2\pi i} \sum_m \left(\frac{H_m^{(2)'}(ka)}{H_m^{(2)}(ka)} - \frac{H_m^{(1)'}(ka)}{H_m^{(1)}(ka)} \right). \end{aligned} \quad (36.23)$$

Here the prime denotes the derivative with respect to the argument of the Hankel functions. Let us introduce the abbreviation

$$\chi_\nu = \frac{H_\nu^{(2)'}(ka)}{H_\nu^{(2)}(ka)} - \frac{H_\nu^{(1)'}(ka)}{H_\nu^{(1)}(ka)}. \quad (36.24)$$

We apply the Watson contour method to (36.23)

$$\mathbf{d}(k) = \frac{a_j}{2\pi i} \sum_{m=-\infty}^{+\infty} \chi_m = \frac{a_j}{2\pi i} \frac{1}{2i} \oint_C d\nu \frac{e^{-i\nu\pi}}{\sin(\nu\pi)} \chi_\nu. \quad (36.25)$$

Here the contour C encircles in a counter-clockwise manner a small semiinfinite strip D which completely covers the real ν -axis but which only has a small finite extent into the positive and negative imaginary ν direction. The contour C is then split up in the path above and below the real ν -axis such that

$$\mathbf{d}(k) = \frac{a}{4\pi i} \left\{ \int_{-\infty+i\epsilon}^{+\infty+i\epsilon} d\nu \frac{e^{-i\nu\pi}}{\sin(\nu\pi)} \chi_\nu - \int_{-\infty-i\epsilon}^{+\infty-i\epsilon} d\nu \frac{e^{-i\nu\pi}}{\sin(\nu\pi)} \chi_\nu \right\}.$$

Then, we perform the substitution $\nu \rightarrow -\nu$ in the second integral so as to get

$$\begin{aligned} \mathbf{d}(k) &= \frac{a}{4\pi} \left\{ \int_{-\infty+i\epsilon}^{+\infty+i\epsilon} d\nu \frac{e^{-i\nu\pi}}{\sin(\nu\pi)} \chi_\nu + \int_{-\infty-i\epsilon}^{+\infty-i\epsilon} d\nu \frac{e^{+i\nu\pi}}{\sin(\nu\pi)} \chi_{-\nu} \right\} \\ &= \frac{a}{2\pi i} \left\{ 2 \int_{-\infty+i\epsilon}^{+\infty+i\epsilon} d\nu \frac{e^{2i\nu\pi}}{1 - e^{2i\nu\pi}} \chi_\nu + \int_{-\infty}^{+\infty} d\nu \chi_\nu \right\}, \end{aligned} \quad (36.26)$$

where we used the fact that $\chi_{-\nu} = \chi_\nu$. The contour in the last integral can be deformed to pass over the real ν -axis since its integrand has no Watson denominator.

We will now approximate the last expression semiclassically, i.e., under the assumption $ka \gg 1$. As the two contributions in the last line of (36.26) differ by the presence or absence of the Watson denominator, they will have to be handled semiclassically in different ways: the first will be closed in the upper complex

plane and evaluated at the poles of χ_ν , the second integral will be evaluated on the real ν -axis under the Debye approximation for Hankel functions.

We will now work out the first term. The poles of χ_ν in the upper complex plane are given by the zeros of $H_\nu^{(1)}(ka)$ which will be denoted by $\nu_\ell(ka)$ and by the zeros of $H_\nu^{(2)}(ka)$ which we will denote by $-\bar{\nu}_\ell(ka)$, $\ell = 1, 2, 3, \dots$. In the Airy approximation to the Hankel functions they are given by

$$\nu_\ell(ka) = ka + i\alpha_\ell(ka), \quad (36.27)$$

$$-\bar{\nu}_\ell(ka) = -ka + i(\alpha_\ell(k^*a))^* = -(\nu_\ell(k^*a))^*, \quad (36.28)$$

with

$$\begin{aligned} i\alpha_\ell(ka) &= e^{i\frac{\pi}{3}} \left(\frac{ka}{6}\right)^{1/3} q_\ell - e^{-i\frac{\pi}{3}} \left(\frac{6}{ka}\right)^{1/3} \frac{q_\ell^2}{180} - \frac{1}{70ka} \left(1 - \frac{q_\ell^3}{30}\right) \\ &+ e^{i\frac{\pi}{3}} \left(\frac{6}{ka}\right)^{\frac{5}{3}} \frac{1}{3150} \left(\frac{29q_\ell}{6^2} - \frac{281q_\ell^4}{180 \cdot 6^3}\right) + \dots \end{aligned} \quad (36.29)$$

Here q_ℓ labels the zeros of the Airy integral

$$A(q) \equiv \int_0^\infty d\tau \cos(q\tau - \tau^3) = 3^{-1/3} \pi \text{Ai}(-3^{-1/3}q),$$

with $\text{Ai}(z)$ being the standard Airy function; approximately, $q_\ell \approx 6^{1/3} [3\pi(\ell - 1/4)]^{2/3}/2$. In order to keep the notation simple, we will abbreviate $\nu_\ell \equiv \nu_\ell(ka)$ and $\bar{\nu}_\ell \equiv \bar{\nu}_\ell(ka)$. Thus the first term of (36.26) becomes finally

$$\frac{a}{2\pi i} \left\{ 2 \int_{-\infty+i\epsilon}^{+\infty+i\epsilon} d\nu \frac{e^{2i\nu\pi}}{1 - e^{2i\nu\pi}} \chi_\nu \right\} = 2a \sum_{\ell=1}^{\infty} \left(\frac{e^{2i\nu_\ell\pi}}{1 - e^{2i\nu_\ell\pi}} + \frac{e^{-2i\bar{\nu}_\ell\pi}}{1 - e^{-2i\bar{\nu}_\ell\pi}} \right).$$

In the second term of (36.26) we will insert the Debye approximations for the Hankel functions:

$$H_\nu^{(1/2)}(x) \sim \sqrt{\frac{2}{\pi \sqrt{x^2 - \nu^2}}} \exp\left(\pm i \sqrt{x^2 - \nu^2} \mp i\nu \arccos \frac{\nu}{x} \mp i \frac{\pi}{4}\right) \quad \text{for } |x| > \nu \quad (36.30)$$

$$H_\nu^{(1/2)}(x) \sim \mp i \sqrt{\frac{2}{\pi \sqrt{\nu^2 - x^2}}} \exp\left(-\sqrt{\nu^2 - x^2} + \nu \text{ArcCosh} \frac{\nu}{x}\right) \quad \text{for } |x| < \nu.$$

Note that for $\nu > ka$ the contributions in χ_ν cancel. Thus the second integral of (36.26) becomes

$$\begin{aligned} \frac{a}{2\pi i} \int_{-\infty}^{+\infty} d\nu \chi_\nu &= \frac{a}{2\pi i} \int_{-ka}^{+ka} d\nu \frac{(-2i)}{a} \frac{d}{dk} \left(\sqrt{k^2 a^2 - \nu^2} - \nu \arccos \frac{\nu}{ka} \right) + \dots \\ &= -\frac{1}{k\pi} \int_{-ka}^{ka} d\nu \sqrt{k^2 a^2 - \nu^2} + \dots = -\frac{a^2}{2} k + \dots, \end{aligned} \quad (36.31)$$

where \dots takes care of the polynomial corrections in the Debye approximation and the boundary correction terms in the ν integration.

In summary, the semiclassical approximation to $\mathbf{d}(k)$ reads

$$\mathbf{d}(k) = 2a \sum_{\ell=1}^{\infty} \left(\frac{e^{2i\nu_{\ell}\pi}}{1 - e^{2i\nu_{\ell}\pi}} + \frac{e^{-2i\bar{\nu}_{\ell}\pi}}{1 - e^{-2i\bar{\nu}_{\ell}\pi}} \right) - \frac{a^2}{2}k + \dots$$

Using the definition of the time delay (36.22), we get the following expression for $\det \mathbf{S}^1(ka)$:

$$\begin{aligned} \ln \det \mathbf{S}^1(ka) - \lim_{k_0 \rightarrow 0} \ln \det \mathbf{S}^1(k_0a) & \quad (36.32) \\ &= 2\pi i a \int_0^k d\tilde{k} \left(-\frac{a\tilde{k}}{2} + 2 \sum_{\ell=1}^{\infty} \left(\frac{e^{i2\pi\nu_{\ell}(\tilde{k}a)}}{1 - e^{i2\pi\nu_{\ell}(\tilde{k}a)}} + \frac{e^{-i2\pi\bar{\nu}_{\ell}(\tilde{k}a)}}{1 - e^{-i2\pi\bar{\nu}_{\ell}(\tilde{k}a)}} \right) \right) + \dots \\ &\sim -2\pi i N(k) + 2 \sum_{\ell=1}^{\infty} \int_0^k d\tilde{k} \frac{d}{d\tilde{k}} \left\{ -\ln(1 - e^{i2\pi\nu_{\ell}(\tilde{k}a)}) + \ln(1 - e^{-i2\pi\bar{\nu}_{\ell}(\tilde{k}a)}) \right\} + \dots, \end{aligned}$$

where in the last expression it has been used that semiclassically $\frac{d}{dk}\nu_{\ell}(ka) \sim \frac{d}{dk}\bar{\nu}_{\ell}(ka) \sim a$ and that the Weyl term for a single disk of radius a goes like $N(k) = \pi a^2 k^2 / (4\pi) + \dots$ (the next terms come from the boundary terms in the ν -integration in (36.31)). Note that for the lower limit, $k_0 \rightarrow 0$, we have two simplifications: First,

$$\begin{aligned} \lim_{k_0 \rightarrow 0} S_{mm'}^1(k_0a) &= \lim_{k_0 \rightarrow 0} \frac{-H_m^{(2)}(k_0a)}{H_m^{(1)}(k_0a)} \delta_{mm'} = 1 \times \delta_{mm'} \quad \forall m, m' \\ &\rightarrow \lim_{k_0 \rightarrow 0} \det \mathbf{S}^1(k_0a) = 1. \end{aligned}$$

Secondly, for $k_0 \rightarrow 0$, the two terms in the curly bracket of (36.32) cancel.

36.3.1 1-disk spectrum interpreted; pure creeping

To summarize: the semiclassical approximation to the determinant $\mathbf{S}^1(ka)$ is given by

$$\det \mathbf{S}^1(ka) \sim e^{-i2\pi N(k)} \frac{\prod_{\ell=1}^{\infty} (1 - e^{-2i\pi\bar{\nu}_{\ell}(ka)})^2}{\prod_{\ell=1}^{\infty} (1 - e^{2i\pi\nu_{\ell}(ka)})^2}, \quad (36.33)$$

with

$$\begin{aligned} \nu_{\ell}(ka) &= ka + i\alpha_{\ell}(ka) &= ka + e^{+i\pi/3}(ka/6)^{1/3}q_{\ell} + \dots \\ \bar{\nu}_{\ell}(ka) &= ka - i(\alpha_{\ell}(k^*a))^* &= ka + e^{-i\pi/3}(ka/6)^{1/3}q_{\ell} + \dots \\ &= (\nu_{\ell}(k^*a))^* \end{aligned}$$

Figure 36.2: Right- and left-handed diffractive creeping paths of increasing mode number ℓ for a single disk.



and $N(ka) = (\pi a^2 k^2)/4\pi + \dots$ the leading term in the Weyl approximation for the staircase function of the wavenumber eigenvalues in the disk interior. From the point of view of the scattering particle, the interior domains of the disks are excluded relatively to the free evolution without scattering obstacles. Therefore the negative sign in front of the Weyl term. For the same reason, the subleading boundary term has here a Neumann structure, although the disks have Dirichlet boundary conditions.

Let us abbreviate the r.h.s. of (36.33) for a disk s as

$$\det \mathbf{S}^s(ka_s) \sim \left(e^{-i\pi N(ka_s)} \right)^2 \frac{\widetilde{Z}_\ell^s(k^* a_s)^* \widetilde{Z}_r^s(k^* a_s)^*}{\widetilde{Z}_\ell^s(ka_s) \widetilde{Z}_r^s(ka_s)}, \quad (36.34)$$

where $\widetilde{Z}_\ell^s(ka_s)$ and $\widetilde{Z}_r^s(ka_s)$ are the *diffractive* zeta functions (here and in the following we will label semiclassical zeta functions *with* diffractive corrections by a tilde) for creeping orbits around the s th disk in the left-handed sense and the right-handed sense, respectively (see figure 36.2). The two orientations of the creeping orbits are the reason for the exponents 2 in (36.33). Equation (36.33) describes the semiclassical approximation to the incoherent part (= the curly bracket on the r.h.s.) of the exact expression (36.19) for the case that the scatterers are disks.

In the following we will discuss the semiclassical resonances in the 1-disk scattering problem with Dirichlet boundary conditions, i.e. the so-called shape resonances. The quantum mechanical resonances are the poles of the S -matrix in the complex k -plane. As the 1-disk scattering problem is separable, the S -matrix is already diagonalized in the angular momentum eigenbasis and takes the simple form (36.9). The exact quantummechanical poles of the scattering matrix are therefore given by the zeros k_{nm}^{res} of the Hankel functions $H_m^{(1)}(ka)$ in the lower complex k plane which can be labeled by two indices, m and n , where m denotes the angular quantum number of the Hankel function and n is a radial quantum number. As the Hankel functions have to vanish at specific k values, one cannot use the usual Debye approximation as semiclassical approximation for the Hankel function, since this approximation only works in case the Hankel function is dominated by only one saddle. However, for the vanishing of the Hankel function, one has to have the interplay of two saddles, thus an Airy approximation is needed as in the case of the creeping poles discussed above. The Airy approximation of the

Hankel function $H_\nu^{(1)}(ka)$ of complex-valued index ν reads

$$H_\nu^{(1)}(ka) \sim \frac{2}{\pi} e^{-i\frac{\pi}{3}} \left(\frac{6}{ka}\right)^{1/3} A(q^{(1)}),$$

with

$$q^{(1)} = e^{-i\frac{\pi}{3}} \left(\frac{6}{ka}\right)^{1/3} (\nu - ka) + O((ka)^{-1}).$$

Hence the zeros ν_ℓ of the Hankel function in the complex ν plane follow from the zeros q_ℓ of the Airy integral $A(q)$ (see (36.3)). Thus if we set $\nu_\ell = m$ (with m integer), we have the following semiclassical condition on k^{res}

$$\begin{aligned} m &\sim k^{\text{res}} a + i\alpha_\ell (k^{\text{res}} a) \\ &= e^{i\frac{\pi}{3}} \left(\frac{k^{\text{res}} a}{6}\right)^{1/3} q_\ell - e^{-i\frac{\pi}{3}} \left(\frac{6}{k^{\text{res}} a}\right)^{1/3} \frac{q_\ell^2}{180} - \frac{1}{70k^{\text{res}} a} \left(1 - \frac{q_\ell^3}{30}\right) \\ &\quad + e^{i\frac{\pi}{3}} \left(\frac{6}{k^{\text{res}} a}\right)^{\frac{5}{3}} \frac{1}{3150} \left(\frac{29q_\ell}{6^2} - \frac{281q_\ell^4}{180 \cdot 6^3}\right) + \dots, \end{aligned}$$

$$\text{with } l = 1, 2, 3, \dots \tag{36.35}$$

For a given index l this is equivalent to

$$0 \sim 1 - e^{(ik^{\text{res}} - \alpha_\ell)2\pi a},$$

the de-Broglie condition on the wave function that encircles the disk. Thus the semiclassical resonances of the 1-disk problem are given by the zeros of the following product

$$\prod_{l=1}^{\infty} \left(1 - e^{(ik - \alpha_\ell)2\pi a}\right),$$

which is of course nothing else than $\widetilde{Z}_{1\text{-disk}}(k)$, the semiclassical diffraction zeta function of the 1-disk scattering problem, see (36.34). Note that this expression includes just the pure creeping contribution and no genuine geometrical parts. Because of

$$H_{-m}^{(1)}(ka) = (-1)^m H_m^{(1)}(ka),$$

the zeros are doubly degenerate if $m \neq 0$, corresponding to right- and left handed creeping turns. The case $m = 0$ is unphysical, since all zeros of the Hankel function $H_0^{(1)}(ka)$ have negative real value.

Figure 36.3: The shape resonances of the 1-disk system in the complex k plane in units of the disk radius a . The boxes label the exact quantum mechanical resonances (given by the zeros of $H_m^{(1)}(ka)$ for $m = 0, 1, 2$), the crosses label the diffractive semiclassical resonances (given by the zeros of the creeping formula in the Airy approximation (36.35) up to the order $\mathcal{O}([ka]^{1/3})$).

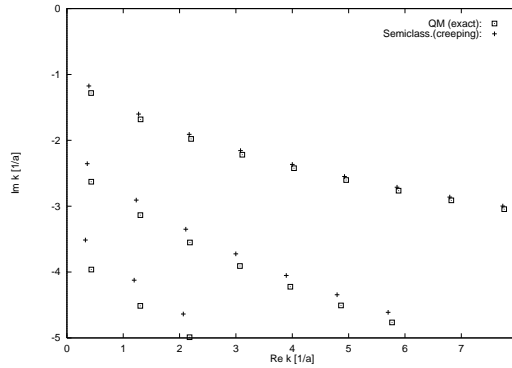
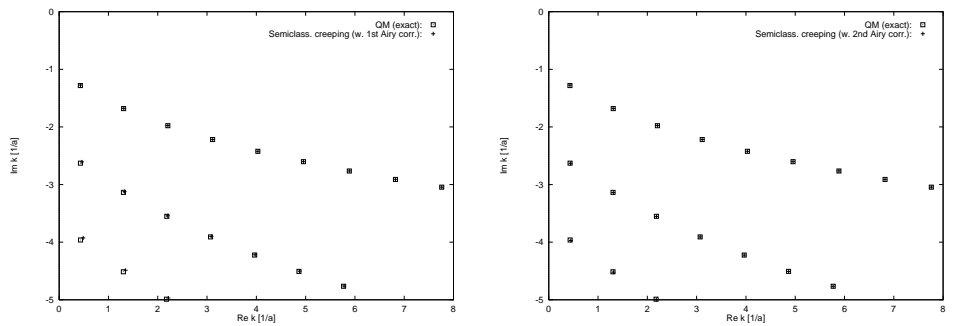


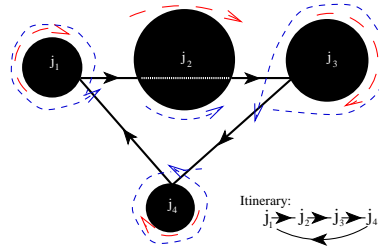
Figure 36.4: Same as in figure 36.3. However, the subleading terms in the Airy approximation (36.35) are taken into account up to the order $\mathcal{O}([ka]^{-1/3})$ (upper panel) and up to order $\mathcal{O}([ka]^{-1})$ (lower panel).



From figure 36.3 one notes that the creeping terms in the Airy order $\mathcal{O}([ka]^{1/3})$, which are used in the Keller construction, systematically underestimate the magnitude of the imaginary parts of the exact data. However, the creeping data become better for increasing $\text{Re } k$ and decreasing $|\text{Im } k|$, as they should as semiclassical approximations.

In the upper panel of figure 36.4 one sees the change, when the next order in the Airy approximation (36.35) is taken into account. The approximation is nearly perfect, especially for the leading row of resonances. The second Airy approximation using (36.35) up to order $\mathcal{O}([ka]^{-1})$ is perfect up to the drawing scale of figure 36.4 (lower panel).

Figure 36.5: A 4-disk problem with three specular reflections, one ghost tunneling, and distinct creeping segments from which all associated creeping paths can be constructed.



36.4 From quantum cycle to semiclassical cycle

The procedure for the semiclassical approximation of a general periodic itinerary (36.20) of length \$n\$ is somewhat laborious, and we will only sketch the procedure here. It follows, in fact, rather closely the methods developed for the semiclassical reduction of the determinant of the 1-disk system.

The quantum cycle

$$\text{tr } \mathbf{A}^{s_1 s_2} \dots \mathbf{A}^{s_m s_1} = \sum_{l_{s_1}=-\infty}^{\infty} \dots \sum_{l_{s_m}=-\infty}^{\infty} A_{l_{s_1} l_{s_2}}^{s_1 s_2} \dots A_{l_{s_m} l_{s_1}}^{s_m s_1}$$

still has the structure of a “multi-trace” with respect to angular momentum.

Each of the sums \$\sum_{l_{s_i}=-\infty}^{\infty}\$ – as in the 1-disk case – is replaced by a *Watson contour* resummation in terms of complex angular momentum \$\nu_{s_i}\$. Then the paths below the real \$\nu_{s_i}\$-axes are transformed to paths above these axes, and the integrals split into expressions *with* and *without* an explicit Watson \$\sin(\nu_{s_i}\pi)\$ denominator.

1. In the \$\sin(\nu_{s_i}\pi)\$-independent integrals we replace all Hankel and Bessel functions by Debye approximations. Then we evaluate the expression in the saddle point approximation: either left or right *specular reflection* at disk \$s_i\$ or *ghost tunneling* through disk \$s_i\$ result.
2. For the \$\sin(\nu_{s_i}\pi)\$-dependent integrals, we close the contour in the upper \$\nu_{s_i}\$ plane and evaluate the integral at the residua \$H_{\nu_{s_i}}^{(1)}(ka_{s_i})=0\$. Then we use the Airy approximation for \$J_{\nu_{s_i}}(ka_{s_i})\$ and \$H_{\nu_{s_i}}^{(1)}(ka_{s_i})\$: left and right *creeping paths* around disk \$s_i\$ result.

In the above we have assumed that no grazing geometrical paths appear. If they do show up, the analysis has to be extended to the case of coinciding saddles between the geometrical paths with \$\pi/2\$ angle reflection from the disk surface and paths with direct ghost tunneling through the disk.

There are three possibilities of “semiclassical” contact of the point particle with the disk \$s_i\$:

1. either geometrical which in turn splits into three alternatives

- (a) *specular reflection* to the right,
 - (b) *specular reflection* to the left,
 - (c) or ‘*ghost tunneling*’ where the latter induce the nontrivial pruning rules (as discussed above)
2. or *right-handed creeping turns*
 3. or *left-handed creeping turns*,

see figure 36.5. The specular reflection to the right is linked to left-handed creeping paths with at least one knot. The specular reflection to the left matches a right-handed creeping paths with at least one knot, whereas the shortest left- and right-handed creeping paths in the ghost tunneling case are topologically trivial. In fact, the topology of the creeping paths encodes the choice between the three alternatives for the geometrical contact with the disk. This is the case for the simple reason that creeping sections have to be positive definite in length: the creeping amplitude has to decrease during the creeping process, as tangential rays are constantly emitted. In mathematical terms, it means that the creeping angle has to be positive. Thus, the positivity of the *two* creeping angles for the shortest left *and* right turn uniquely specifies the topology of the creeping sections which in turn specifies which of the three alternatives, either specular reflection to the right or to the left or straight “ghost” tunneling through disk j , is realized for the semiclassical geometrical path. Hence, the existence of a unique saddle point is guaranteed.

In order to be concrete, we will restrict ourselves in the following to the scattering from $N < \infty$ non-overlapping *disks* fixed in the 2-dimensional plane. The semiclassical approximation of the periodic itinerary

$$\text{tr } \mathbf{A}^{s_1 s_2} \mathbf{A}^{s_2 s_3} \dots \mathbf{A}^{s_{n-1} s_n} \mathbf{A}^{s_n s_1}$$

becomes a standard periodic orbit labeled by the symbol sequence $s_1 s_2 \dots s_n$. Depending on the geometry, the individual legs $s_{i-1} \rightarrow s_i \rightarrow s_{i+1}$ result either from a standard specular reflection at disk s_i or from a ghost path passing straight through disk s_i . If furthermore creeping contributions are taken into account, the symbolic dynamics has to be generalized from single-letter symbols $\{s\}$ to triple-letter symbols $\{s_i, \sigma_i \times \ell_i\}$ with $\ell_i \geq 1$ integer valued and $\sigma_i = 0, \pm 1$.¹ By definition, the value $\sigma_i = 0$ represents the non-creeping case, such that $\{s_i, 0 \times \ell_i\} = \{s_i, 0\} = \{s_i\}$ reduces to the old single-letter symbol. The magnitude of a nonzero ℓ_i corresponds to creeping sections of mode number $|\ell_i|$, whereas the sign $\sigma_i = \pm 1$ signals whether the creeping path turns around the disk s_i in the positive or negative sense. Additional full creeping turns around a disk s_i can be summed up as a geometrical series; therefore they do not lead to the introduction of a further symbol.

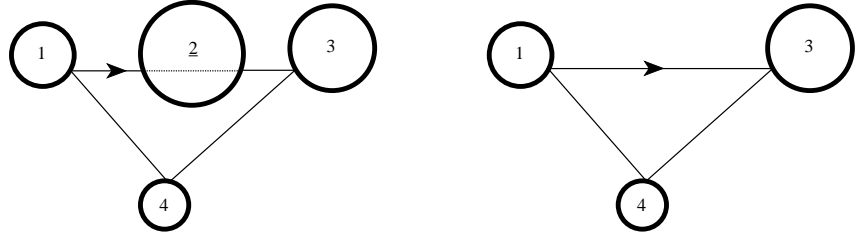


Figure 36.6: (a) The ghost itinerary (1, 2, 3, 4). (b) The parent itinerary (1, 3, 4).

36.4.1 Ghost contributions

An itinerary with a semiclassical ghost section at, say, disk s can be shown to have the same weight as the corresponding itinerary without the s th symbol. Thus, semiclassically, they cancel each other in the $\text{tr} \ln(\mathbf{1} - \mathbf{A})$ expansion, where they are multiplied by the permutation factor n/r with the integer r counting the repeats. For example, let (1, 2, 3, 4) be a non-repeated periodic itinerary with a ghost section at disk 2 stemming from the 4th-order trace $\text{tr} \mathbf{A}^4$. By convention, an underlined disk index signals a ghost passage (as in figure 36.6a), with corresponding semiclassical ghost traversal matrices also underlined, $\underline{\mathbf{A}}^{i,i+1} \underline{\mathbf{A}}^{i+1,i+2}$. Then its semiclassical, geometrical contribution to $\text{tr} \ln(\mathbf{1} - \mathbf{A})$ cancels exactly against the one of its “parent” itinerary (1, 3, 4) (see figure 36.6b) resulting from the 3rd-order trace:

$$\begin{aligned} & -\frac{1}{4} \left(4 \underline{\mathbf{A}}^{1,2} \underline{\mathbf{A}}^{2,3} \mathbf{A}^{3,4} \mathbf{A}^{4,1} \right) - \frac{1}{3} \left(3 \mathbf{A}^{1,3} \mathbf{A}^{3,4} \mathbf{A}^{4,1} \right) \\ & = (+1 - 1) \mathbf{A}^{1,3} \mathbf{A}^{3,4} \mathbf{A}^{4,1} = 0. \end{aligned}$$

The prefactors $-1/3$ and $-1/4$ are due to the expansion of the logarithm, the factors 3 and 4 inside the brackets result from the cyclic permutation of the periodic itineraries, and the cancellation stems from the rule

$$\dots \underline{\mathbf{A}}^{i,i+1} \underline{\mathbf{A}}^{i+1,i+2} \dots = \dots \left(-\mathbf{A}^{i,i+2} \right) \dots \quad (36.36)$$

The reader might study more complicated examples and convince herself that the rule (36.36) is sufficient to cancel any primary or repeated periodic orbit with one or more ghost sections completely out of the expansion of $\text{tr} \ln(\mathbf{1} - \mathbf{A})$ and therefore also out of the cumulant expansion in the semiclassical limit: Any periodic orbit of length m with $n (< m)$ ghost sections is cancelled by the sum of all ‘parent’ periodic orbits of length $m - i$ (with $1 \leq i \leq n$ and i ghost sections removed) weighted by their cyclic permutation factor and by the prefactor resulting from the *trace-log* expansion. This is the way in which the nontrivial pruning for the N -disk billiards can be derived from the exact quantum mechanical expressions in the semiclassical limit. Note that there must exist at least one index i in any given *periodic* itinerary which corresponds to a non-ghost section, since otherwise the itinerary in the semiclassical limit could only be straight and therefore nonperiodic. Furthermore, the series in the ghost cancelation has to stop at the 2nd-order trace, $\text{tr} \mathbf{A}^2$, as $\text{tr} \mathbf{A}$ itself vanishes identically in the full domain which is considered here.

¹Actually, these are double-letter symbols as σ_i and l_i are only counted as a product.

36.5 Heisenberg uncertainty

Where is the boundary $ka \approx 2^{m-1}\bar{L}/a$ coming from?

This boundary follows from a combination of the uncertainty principle with ray optics and the non-vanishing value for the topological entropy of the 3-disk repeller. When the wave number k is fixed, quantum mechanics can only resolve the classical repelling set up to the critical topological order n . The quantum wave packet which explores the repelling set has to disentangle 2^n different sections of size $d \sim a/2^n$ on the “visible” part of the disk surface (which is of order a) between any two successive disk collisions. Successive collisions are separated spatially by the mean flight length \bar{L} , and the flux spreads with a factor \bar{L}/a . In other words, the uncertainty principle bounds the maximal sensible truncation in the cycle expansion order by the highest quantum resolution attainable for a given wavenumber k .

Commentary

Remark 36.1 Sources. This chapter is based in its entirety on ref. [1]; the reader is referred to the full exposition for the proofs and discussion of details omitted here. sect. 36.3 is based on appendix E of ref. [1]. We follow Franz [19] in applying the Watson contour method [20] to (36.23). The Airy and Debye approximations to the Hankel functions are given in ref. [21], the Airy expansion of the 1-disk zeros can be found in ref. [22]. For details see refs. [19, 22, 23, 1]. That the interior domains of the disks are excluded relatively to the free evolution without scattering obstacles was noted in refs. [24, 15].

The procedure for the semiclassical approximation of a general periodic itinerary (36.20) of length n can be found in ref. [1] for the case of the N -disk systems. The reader interested in the details of the semiclassical reduction is advised to consult this reference.

The ghost orbits were introduced in refs. [12, 24].

Remark 36.2 Krein-Friedel-Lloyd formula. In the literature (see, e.g., refs. [14, 15] based on ref. [11] or ref. [1]) the transition from the quantum mechanics to the semiclassical of scattering problems has been performed via the semiclassical limit of the left hand sides of the Krein-Friedel-Lloyd sum for the (integrated) spectral density [5, 6, 8, 9]. See also ref. [13] for a modern discussion of the Krein-Friedel-Lloyd formula and refs. [1, 17] for the connection of (35.17) to the Wigner time delay.

The order of the two limits in (35.18) and (35.17) is essential, see e.g. Balian and Bloch [11] who stress that smoothed level densities should be inserted into the Friedel sums.

The necessity of the $+i\epsilon$ in the semiclassical calculation can be understood by purely phenomenological considerations: Without the $i\epsilon$ term there is no reason why one should be able to neglect spurious periodic orbits which solely are there because of the introduction of the confining boundary. The subtraction of the second (empty) reference system

helps just in the removal of those spurious periodic orbits which never encounter the scattering region. The ones that do would still survive the first limit $b \rightarrow \infty$, if they were not damped out by the $+i\epsilon$ term.

exercise 35.1

Remark 36.3 \mathbf{T} , \mathbf{C}^s , \mathbf{D}^s and $\mathbf{A}^{ss'}$ matrices are trace-class In refs. [1] it has explicitly been shown that the \mathbf{T} -matrix as well as the \mathbf{C}^s , \mathbf{D}^s and $\mathbf{A}^{ss'}$ -matrices of the scattering problem from $N < \infty$ non-overlapping finite disks are all trace-class. The corresponding properties for the single-disk systems is particularly easy to prove.

References

- [36.1] S. Müller, S. Heusler, A. Altland, P. Braun and F. Haake, “Periodic-orbit theory of universal level repulsion,” [arXiv:0906.1960](#).
- [36.2] J. Kuipers, “Semiclassics for chaotic systems with tunnel barriers,” [arXiv:0906.1964](#).

Chapter 37

Helium atom

“But,” Bohr protested, “nobody will believe me unless I can explain every atom and every molecule.” Rutherford was quick to reply, “Bohr, you explain hydrogen and you explain helium and everybody will believe the rest.”

—John Archibald Wheeler (1986)

(G. Tanner)

SO FAR much has been said about 1-dimensional maps, game of pinball and other curious but rather idealized dynamical systems. If you have become impatient and started wondering what good are the methods learned so far in solving real physical problems, we have good news for you. We will show in this chapter that the concepts of symbolic dynamics, unstable periodic orbits, and cycle expansions are essential tools to understand and calculate classical and quantum mechanical properties of nothing less than the helium, a dreaded three-body Coulomb problem.

This sounds almost like one step too much at a time; we all know how rich and complicated the dynamics of the three-body problem is – can we really jump from three static disks directly to three charged particles moving under the influence of their mutually attracting or repelling forces? It turns out, we can, but we have to do it with care. The full problem is indeed not accessible in all its detail, but we are able to analyze a somewhat simpler subsystem – collinear helium. This system plays an important role in the classical dynamics of the full three-body problem and its quantum spectrum.

The main work in reducing the quantum mechanics of helium to a semiclassical treatment of collinear helium lies in understanding why we are allowed to do so. We will not worry about this too much in the beginning; after all, 80 years and many failed attempts separate Heisenberg, Bohr and others in the 1920ties from the insights we have today on the role chaos plays for helium and its quantum spectrum. We have introduced collinear helium and learned how to integrate its

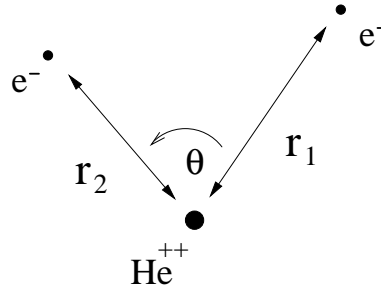


Figure 37.1: Coordinates for the helium three body problem in the plane.

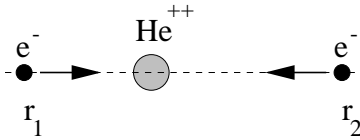


Figure 37.2: Collinear helium, with the two electrons on opposite sides of the nucleus.

trajectories in sect. 6.3. Here we will find periodic orbits and determine the relevant eigenvalues of the Jacobian matrix in sect. 37.1. We will explain in sect. 37.5 why a quantization of the collinear dynamics in helium will enable us to find parts of the full helium spectrum; we then set up the semiclassical spectral determinant and evaluate its cycle expansion. A full quantum justification of this treatment of helium is briefly discussed in sect. 37.5.1.

37.1 Classical dynamics of collinear helium

Recapitulating briefly what we learned in sect. 6.3: the collinear helium system consists of two electrons of mass m_e and charge $-e$ moving on a line with respect to a fixed positively charged nucleus of charge $+2e$, as in figure 37.2.

The Hamiltonian can be brought to a non-dimensionalized form

$$H = \frac{p_1^2}{2} + \frac{p_2^2}{2} - \frac{2}{r_1} - \frac{2}{r_2} + \frac{1}{r_1 + r_2} = -1. \tag{37.1}$$

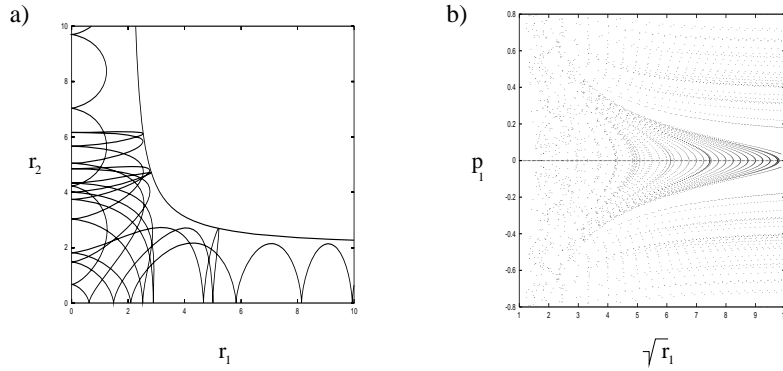
The case of negative energies chosen here is the most interesting one for us. It exhibits chaos, unstable periodic orbits and is responsible for the bound states and resonances of the quantum problem treated in sect. 37.5.

There is another classical quantity important for a semiclassical treatment of quantum mechanics, and which will also feature prominently in the discussion in the next section; this is the classical action (33.15) which scales with energy as

$$S(E) = \oint d\mathbf{q}(E) \cdot \mathbf{p}(E) = \frac{e^2 m_e^{1/2}}{(-E)^{1/2}} S, \tag{37.2}$$

with S being the action obtained from (37.1) for $E = -1$, and coordinates $\mathbf{q} = (r_1, r_2)$, $\mathbf{p} = (p_1, p_2)$. For the Hamiltonian (37.1), the period of a cycle and its action are related by (33.17), $T_p = \frac{1}{2} S_p$.

Figure 37.3: (a) A typical trajectory in the $r_1 - r_2$ plane; the trajectory enters here along the r_1 axis and escapes to infinity along the r_2 axis; (b) Poincaré map ($r_2=0$) for collinear helium. Strong chaos prevails for small r_1 near the nucleus.



After a Kustaanheimo–Stiefel transformation

$$r_1 = Q_1^2, \quad r_2 = Q_2^2, \quad p_1 = \frac{P_1}{2Q_1}, \quad p_2 = \frac{P_2}{2Q_2}, \quad (37.3)$$

and reparametrization of time by $d\tau = dt/r_1 r_2$, the equations of motion take form (6.19)

exercise 37.1

$$\begin{aligned} \dot{P}_1 &= 2Q_1 \left[2 - \frac{P_2^2}{8} - Q_2^2 \left(1 + \frac{Q_2^2}{R_{12}^4} \right) \right]; & \dot{Q}_1 &= \frac{1}{4} P_1 Q_2^2 \\ \dot{P}_2 &= 2Q_2 \left[2 - \frac{P_1^2}{8} - Q_1^2 \left(1 + \frac{Q_1^2}{R_{12}^4} \right) \right]; & \dot{Q}_2 &= \frac{1}{4} P_2 Q_1^2. \end{aligned} \quad (37.4)$$

Individual electron–nucleus collisions at $r_1 = Q_1^2 = 0$ or $r_2 = Q_2^2 = 0$ no longer pose a problem to a numerical integration routine. The equations (6.19) are singular only at the triple collision $R_{12} = 0$, i.e., when both electrons hit the nucleus at the same time.

The new coordinates and the Hamiltonian (6.18) are very useful when calculating trajectories for collinear helium; they are, however, less intuitive as a visualization of the three-body dynamics. We will therefore refer to the old coordinates r_1, r_2 when discussing the dynamics and the periodic orbits.

37.2 Chaos, symbolic dynamics and periodic orbits

Let us have a closer look at the dynamics in collinear helium. The electrons are attracted by the nucleus. During an electron–nucleus collision momentum is transferred between the inner and outer electron. The inner electron has a maximal screening effect on the charge of the nucleus, diminishing the attractive force on the outer electron. This electron – electron interaction is negligible if the outer electron is far from the nucleus at a collision and the overall dynamics is regular like in the 1-dimensional Kepler problem.

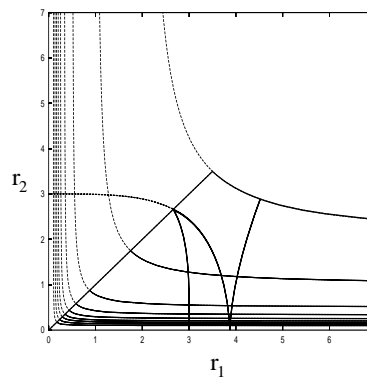


Figure 37.4: The cycle 011 in the fundamental domain $r_1 \geq r_2$ (full line) and in the full domain (dashed line).

Things change drastically if both electrons approach the nucleus nearly simultaneously. The momentum transfer between the electrons depends now sensitively on how the particles approach the origin. Intuitively, these nearly missed triple collisions render the dynamics chaotic. A typical trajectory is plotted in figure 37.3 (a) where we used r_1 and r_2 as the relevant axis. The dynamics can also be visualized in a Poincaré surface of section, see figure 37.3 (b). We plot here the coordinate and momentum of the outer electron whenever the inner particle hits the nucleus, i.e., r_1 or $r_2 = 0$. As the unstructured gray region of the Poincaré section for small r_1 illustrates, the dynamics is chaotic whenever the outer electron is close to the origin during a collision. Conversely, regular motions dominate whenever the outer electron is far from the nucleus. As one of the electrons escapes for almost any starting condition, the system is unbounded: one electron (say electron 1) can escape, with an arbitrary amount of kinetic energy taken by the fugitive. The remaining electron is trapped in a Kepler ellipse with total energy in the range $[-1, -\infty]$. There is no energy barrier which would separate the bound from the unbound regions of the phase space. From general kinematic arguments one deduces that the outer electron will not return when $p_1 > 0$, $r_2 \leq 2$ at $p_2 = 0$, the turning point of the inner electron. Only if the two electrons approach the nucleus almost symmetrically along the line $r_1 = r_2$, and pass close to the triple collision can the momentum transfer between the electrons be large enough to kick one of the particles out completely. In other words, the electron escape originates from the near triple collisions.

The collinear helium dynamics has some important properties which we now list.

37.2.1 Reflection symmetry

The Hamiltonian (6.10) is invariant with respect to electron–electron exchange; this symmetry corresponds to the mirror symmetry of the potential along the line $r_1 = r_2$, figure 37.4. As a consequence, we can restrict ourselves to the dynamics in the *fundamental domain* $r_1 \geq r_2$ and treat a crossing of the diagonal $r_1 = r_2$ as a hard wall reflection. The dynamics in the full domain can then be reconstructed by unfolding the trajectory through back-reflections. As explained in chapter 21, the dynamics in the fundamental domain is the key to the factorization of spectral

determinants, to be implemented here in (37.15). Note also the similarity between the fundamental domain of the collinear potential figure 37.4, and the fundamental domain figure 12.12 (b) in the 3-disk system, a simpler problem with the same binary symbolic dynamics.



in depth:
sect. 21.6, p. 410

37.2.2 Symbolic dynamics

We have already made the claim that the triple collisions render the collinear helium fully chaotic. We have no proof of the assertion, but the analysis of the symbolic dynamics lends further credence to the claim.

The potential in (37.1) forms a ridge along the line $r_1 = r_2$. One can show that a trajectory passing the ridge must go through at least one two-body collision $r_1 = 0$ or $r_2 = 0$ before coming back to the diagonal $r_1 = r_2$. This suggests a *binary* symbolic dynamics corresponding to the dynamics in the fundamental domain $r_1 \geq r_2$; the symbolic dynamics is linked to the Poincaré map $r_2 = 0$ and the symbols 0 and 1 are defined as

- 0: if the trajectory is not reflected from the line $r_1 = r_2$ between two collisions with the nucleus $r_2 = 0$;
- 1: if a trajectory is reflected from the line $r_1 = r_2$ between two collisions with the nucleus $r_2 = 0$.

Empirically, the symbolic dynamics is complete for a Poincaré map in the fundamental domain, i.e., there exists a one-to-one correspondence between binary symbol sequences and collinear trajectories in the fundamental domain, with exception of the $\bar{0}$ cycle.

37.2.3 Periodic orbits

The existence of a binary symbolic dynamics makes it easy to count the number of periodic orbits in the fundamental domain, as in sect. 15.7.2. However, mere existence of these cycles does not suffice to calculate semiclassical spectral determinants. We need to determine their phase space trajectories and calculate their periods, topological indices and stabilities. A restriction of the periodic orbit search to a suitable Poincaré surface of section, e.g. $r_2 = 0$ or $r_1 = r_2$, leaves us in general with a 2-dimensional search. Methods to find periodic orbits in multi-dimensional spaces have been described in chapter 13. They depend sensitively on good starting guesses. A systematic search for all orbits can be achieved only after combining multi-dimensional Newton methods with interpolation algorithms

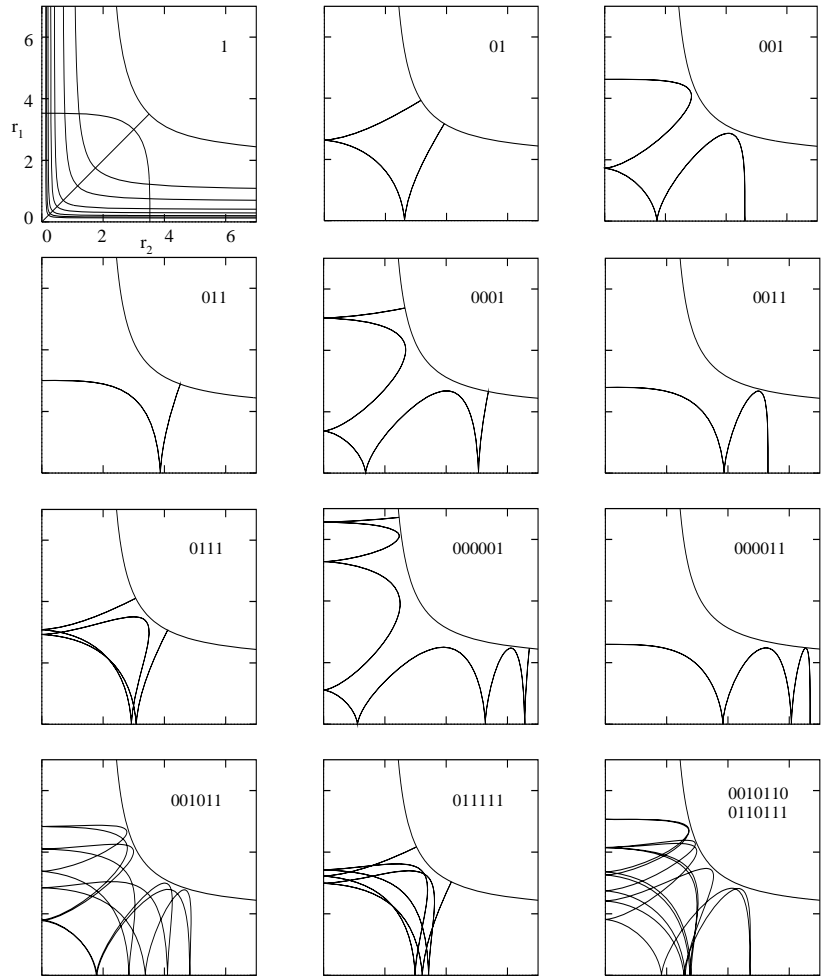


Figure 37.5: Some of the shortest cycles in collinear helium. The classical collinear electron motion is bounded by the potential barrier $-1 = -2/r_1 - 2/r_2 + 1/(r_1 + r_2)$ and the condition $r_i \geq 0$. The orbits are shown in the full r_1 - r_2 domain, the itineraries refers to the dynamics in the $r_1 \geq r_2$ fundamental domain. The last figure, the 14-cycle 00101100110111, is an example of a typical cycle with no symmetry.

based on the binary symbolic dynamics phase space partitioning. All cycles up to symbol length 16 (some 8000 prime cycles) have been computed by such methods, with some examples shown in figure 37.5. All numerical evidence indicates that the dynamics of collinear helium is hyperbolic, and that all periodic orbits are unstable.

Note that the fixed point $\bar{0}$ cycle is not in this list. The $\bar{0}$ cycle would correspond to the situation where the outer electron sits at rest infinitely far from the nucleus while the inner electron bounces back and forth into the nucleus. The orbit is the limiting case of an electron escaping to infinity with zero kinetic energy. The orbit is in the regular (i.e., separable) limit of the dynamics and is thus marginally stable. The existence of this orbit is also related to intermittent behavior generating the quasi-regular dynamics for large η that we have already noted in figure 37.3 (b).

Search algorithm for an arbitrary periodic orbit is quite cumbersome to program. There is, however, a class of periodic orbits, orbits with symmetries, which can be easily found by a one-parameter search. The only symmetry left for the dynamics in the fundamental domain is time reversal symmetry; a time reversal

symmetric periodic orbit is an orbit whose trajectory in phase space is mapped onto itself when changing $(p_1, p_2) \rightarrow (-p_1, -p_2)$, by reversing the direction of the momentum of the orbit. Such an orbit must be a “libration” or self-retracing cycle, an orbit that runs back and forth along the same path in the (r_1, r_2) plane. The cycles $\overline{1}$, $\overline{01}$ and $\overline{001}$ in figure 37.5 are examples of self-retracing cycles. Luckily, the shortest cycles that we desire most ardently have this symmetry.

Why is this observation helpful? A self-retracing cycle must start perpendicular to the boundary of the fundamental domain, that is, on either of the axis $r_2 = 0$ or $r_1 = r_2$, or on the potential boundary $-\frac{2}{r_1} - \frac{2}{r_2} + \frac{1}{r_1+r_2} = -1$. By shooting off trajectories perpendicular to the boundaries and monitoring the orbits returning to the boundary with the right symbol length we will find time reversal symmetric cycles by varying the starting point on the boundary as the only parameter. But how can we tell whether a given cycle is self-retracing or not? All the relevant information is contained in the itineraries; a cycle is self-retracing if its itinerary is invariant under time reversal symmetry (i.e., read backwards) and a suitable number of cyclic permutations. All binary strings up to length 5 fulfill this condition. The symbolic dynamics contains even more information; we can tell at which boundary the total reflection occurs. One finds that an orbit starts out perpendicular

- to the diagonal $r_1 = r_2$ if the itinerary is time reversal invariant and has an odd number of 1's; an example is the cycle $\overline{001}$ in figure 37.5;
- to the axis $r_2 = 0$ if the itinerary is time reversal invariant and has an even number of symbols; an example is the cycle $\overline{0011}$ in figure 37.5;
- to the potential boundary if the itinerary is time reversal invariant and has an odd number of symbols; an example is the cycle $\overline{011}$ in figure 37.5.

All cycles up to symbol length 5 are time reversal invariant, the first two non-time reversal symmetric cycles are cycles $\overline{001011}$ and $\overline{001101}$ in figure 37.5. Their determination would require a two-parameter search. The two cycles are mapped onto each other by time reversal symmetry, i.e., they have the same trace in the r_1-r_2 plane, but they trace out distinct cycles in the full phase space.

We are ready to integrate trajectories for classical collinear helium with the help of the equations of motions (6.19) and to find all cycles up to length 5. There is only one thing not yet in place; we need the governing equations for the matrix elements of the Jacobian matrix along a trajectory in order to calculate stability indices. We will provide the main equations in the next section, with the details of the derivation relegated to the appendix B.5.

exercise 37.5

37.3 Local coordinates, Jacobian matrix

In this section, we will derive the equations of motion for the Jacobian matrix along a collinear helium trajectory. The Jacobian matrix is 4-dimensional; the

two trivial eigenvectors corresponding to the conservation of energy and displacements along a trajectory can, however, be projected out by suitable orthogonal coordinates transformations, see appendix B. We will give the transformation to local coordinates explicitly, here for the regularized coordinates (6.17), and state the resulting equations of motion for the reduced $[2 \times 2]$ Jacobian matrix.

The vector locally parallel to the trajectory is pointing in the direction of the phase space velocity (7.7)

$$v_m = \dot{x}_m(t) = \omega_{mn} \frac{\partial H}{\partial x_n} = (H_{P_1}, H_{P_2}, -H_{Q_1}, -H_{Q_2})^T,$$

with $H_{Q_i} = \frac{\partial H}{\partial Q_i}$, and $H_{P_i} = \frac{\partial H}{\partial P_i}$, $i = 1, 2$. The vector perpendicular to a trajectory $x(t) = (Q_1(t), Q_2(t), P_1(t), P_2(t))$ and to the energy manifold is given by the gradient of the Hamiltonian (6.18)

$$\gamma = \nabla H = (H_{Q_1}, H_{Q_2}, H_{P_1}, H_{P_2})^T.$$

By symmetry $v_m \gamma_m = \omega_{mn} \frac{\partial H}{\partial x_n} \frac{\partial H}{\partial x_m} = 0$, so the two vectors are orthogonal.

Next, we consider the orthogonal matrix

$$\begin{aligned} \mathbf{O} &= (\gamma_1, \gamma_2, \gamma/R, v) \\ &= \begin{pmatrix} -H_{P_2}/R & H_{Q_2} & H_{Q_1}/R & H_{P_1} \\ H_{P_1}/R & -H_{Q_1} & H_{Q_2}/R & H_{P_2} \\ -H_{Q_2}/R & -H_{P_2} & H_{P_1}/R & -H_{Q_1} \\ H_{Q_1}/R & H_{P_1} & H_{P_2}/R & -H_{Q_2} \end{pmatrix} \end{aligned} \quad (37.5)$$

with $R = |\nabla H|^2 = (H_{Q_1}^2 + H_{Q_2}^2 + H_{P_1}^2 + H_{P_2}^2)$, which provides a transformation to local phase space coordinates centered on the trajectory $x(t)$ along the two vectors (γ, v) . The vectors $\gamma_{1,2}$ are phase space vectors perpendicular to the trajectory and to the energy manifold in the 4-dimensional phase space of collinear helium. The Jacobian matrix (4.6) rotated to the local coordinate system by \mathbf{O} then has the form

exercise 37.6

$$\mathbf{m} = \begin{pmatrix} m_{11} & m_{12} & * & 0 \\ m_{21} & m_{22} & * & 0 \\ 0 & 0 & 1 & 0 \\ * & * & * & 1 \end{pmatrix}, \quad M = \mathbf{O}^T \mathbf{m} \mathbf{O}$$

The linearized motion perpendicular to the trajectory on the energy manifold is described by the $[2 \times 2]$ matrix \mathbf{m} ; the ‘trivial’ directions correspond to unit eigenvalues on the diagonal in the 3rd and 4th column and row.

The equations of motion for the reduced Jacobian matrix \mathbf{m} are given by

$$\dot{\mathbf{m}} = \mathbf{l}(t)\mathbf{m}(t), \quad (37.6)$$

with $\mathbf{m}(0) = \mathbf{1}$. The matrix \mathbf{I} depends on the trajectory in phase space and has the form

$$\mathbf{I} = \begin{pmatrix} l_{11} & l_{12} & * & 0 \\ l_{21} & l_{22} & * & 0 \\ 0 & 0 & 0 & 0 \\ * & * & * & 0 \end{pmatrix},$$

where the relevant matrix elements l_{ij} are given by

$$\begin{aligned} l_{11} &= \frac{1}{R} [2H_{Q_1Q_2}(H_{Q_2}H_{P_1} + H_{Q_1}H_{P_2}) \\ &\quad + (H_{Q_1}H_{P_1} - H_{Q_2}H_{P_2})(H_{Q_1Q_1} - H_{Q_2Q_2} - H_{P_1P_1} + H_{P_2P_2})] \\ l_{12} &= -2H_{Q_1Q_2}(H_{Q_1}H_{Q_2} - H_{P_1}H_{P_2}) \\ &\quad + (H_{Q_1}^2 + H_{P_2}^2)(H_{Q_2Q_2} + H_{P_1P_1}) + (H_{Q_2}^2 + H_{P_1}^2)(H_{Q_1Q_1} + H_{P_2P_2}) \\ l_{21} &= \frac{1}{R^2} [2(H_{Q_1P_2} + H_{Q_2P_1})(H_{Q_2}H_{P_1} + H_{Q_1}H_{P_2}) \\ &\quad - (H_{P_1}^2 + H_{P_2}^2)(H_{Q_1Q_1} + H_{Q_2Q_2}) - (H_{Q_1}^2 + H_{Q_2}^2)(H_{P_1P_1} + H_{P_2P_2})] \\ l_{22} &= -l_{11}. \end{aligned} \tag{37.7}$$

Here $H_{Q_iQ_j}$, $H_{P_iP_j}$, $i, j = 1, 2$ are the second partial derivatives of H with respect to the coordinates Q_i , P_i , evaluated at the phase space coordinate of the classical trajectory.

37.4 Getting ready

Now everything is in place: the regularized equations of motion can be implemented in a Runge–Kutta or any other integration scheme to calculate trajectories. We have a symbolic dynamics and know how many cycles there are and how to find them (at least up to symbol length 5). We know how to compute the Jacobian matrix whose eigenvalues enter the semiclassical spectral determinant (34.12). By (33.17) the action S_p is proportional to the period of the orbit, $S_p = 2T_p$.

There is, however, still a slight complication. Collinear helium is an invariant 4-dimensional subspace of the full helium phase space. If we restrict the dynamics to angular momentum equal zero, we are left with 6 phase space coordinates. That is not a problem when computing periodic orbits, they are oblivious to the other dimensions. However, the Jacobian matrix does pick up extra contributions. When we calculate the Jacobian matrix for the full problem, we must also allow for displacements out of the collinear plane, so the full Jacobian matrix for dynamics for $L = 0$ angular momentum is 6 dimensional. Fortunately, the linearized dynamics in and off the collinear helium subspace decouple, and the Jacobian matrix can be written in terms of two distinct $[2 \times 2]$ matrices, with trivial eigen-directions providing the remaining two dimensions. The submatrix related to displacements

Table 37.1: Action S_p (in units of 2π), Lyapunov exponent $|\Lambda_p|/T_p$ for the motion in the collinear plane, winding number σ_p for the motion perpendicular to the collinear plane, and the topological index m_p for all fundamental domain cycles up to topological length 6.

p	$S_p/2\pi$	$\ln \Lambda_p $	σ_p	m_p
1	1.82900	0.6012	0.5393	2
01	3.61825	1.8622	1.0918	4
001	5.32615	3.4287	1.6402	6
011	5.39451	1.8603	1.6117	6
0001	6.96677	4.4378	2.1710	8
0011	7.04134	2.3417	2.1327	8
0111	7.25849	3.1124	2.1705	8
00001	8.56618	5.1100	2.6919	10
00011	8.64306	2.7207	2.6478	10
00101	8.93700	5.1562	2.7291	10
00111	8.94619	4.5932	2.7173	10
01011	9.02689	4.1765	2.7140	10
01111	9.07179	3.3424	2.6989	10
000001	10.13872	5.6047	3.2073	12
000011	10.21673	3.0323	3.1594	12
000101	10.57067	6.1393	3.2591	12
000111	10.57628	5.6766	3.2495	12
001011	10.70698	5.3251	3.2519	12
001101	10.70698	5.3251	3.2519	12
001111	10.74303	4.3317	3.2332	12
010111	10.87855	5.0002	3.2626	12
011111	10.91015	4.2408	3.2467	12

off the linear configuration characterizes the linearized dynamics in the additional degree of freedom, the Θ -coordinate in figure 37.1. It turns out that the linearized dynamics in the Θ coordinate is stable, corresponding to a bending type motion of the two electrons. We will need the Floquet exponents for all degrees of freedom in evaluating the semiclassical spectral determinant in sect. 37.5.

The numerical values of the actions, Floquet exponents, stability angles, and topological indices for the shortest cycles are listed in table 37.1. These numbers, needed for the semiclassical quantization implemented in the next section, are also helpful in checking your own calculations.

37.5 Semiclassical quantization of collinear helium

Before we get down to a serious calculation of the helium quantum energy levels let us have a brief look at the overall structure of the spectrum. This will give us a preliminary feel for which parts of the helium spectrum are accessible with the help of our collinear model – and which are not. In order to keep the discussion as simple as possible and to concentrate on the semiclassical aspects of our calculations we offer here only a rough overview. For a guide to more detailed accounts see remark 37.4.

37.5.1 Structure of helium spectrum

We start by recalling Bohr's formula for the spectrum of hydrogen like one-electron atoms. The eigenenergies form a Rydberg series

$$E_N = -\frac{e^4 m_e}{\hbar^2} \frac{Z^2}{2N^2}, \quad (37.8)$$

where Ze is the charge of the nucleus and m_e is the mass of the electron. Through the rest of this chapter we adopt the atomic units $e = m_e = \hbar = 1$.

The simplest model for the helium spectrum is obtained by treating the two electrons as independent particles moving in the potential of the nucleus neglecting the electron–electron interaction. Both electrons are then bound in hydrogen like states; the inner electron will see a charge $Z = 2$, screening at the same time the nucleus, the outer electron will move in a Coulomb potential with effective charge $Z - 1 = 1$. In this way obtain a first estimate for the total energy

$$E_{N,n} = -\frac{2}{N^2} - \frac{1}{2n^2} \quad \text{with } n > N. \quad (37.9)$$

This double Rydberg formula contains already most of the information we need to understand the basic structure of the spectrum. The (correct) ionizations thresholds $E_N = -\frac{2}{N^2}$ are obtained in the limit $n \rightarrow \infty$, yielding the ground and excited

states of the helium ion He^+ . We will therefore refer to N as the principal quantum number. We also see that all states $E_{N,n}$ with $N \geq 2$ lie above the first ionization threshold for $N = 1$. As soon as we switch on electron-electron interaction these states are no longer bound states; they turn into resonant states which decay into a bound state of the helium ion and a free outer electron. This might not come as a big surprise if we have the classical analysis of the previous section in mind: we already found that one of the classical electrons will almost always escape after some finite time. More remarkable is the fact that the first, $N = 1$ series consists of true bound states for all n , an effect which can only be understood by quantum arguments.

The hydrogen-like quantum energies (37.8) are highly degenerate; states with different angular momentum but the same principal quantum number N share the same energy. We recall from basic quantum mechanics of hydrogen atom that the possible angular momenta for a given N span $l = 0, 1 \dots N - 1$. How does that affect the helium case? Total angular momentum L for the helium three-body problem is conserved. The collinear helium is a subspace of the classical phase space for $L = 0$; we thus expect that we can only quantize helium states corresponding to the total angular momentum zero, a subspectrum of the full helium spectrum. Going back to our crude estimate (37.9) we may now attribute angular momenta to the two independent electrons, l_1 and l_2 say. In order to obtain total angular momentum $L = 0$ we need $l_1 = l_2 = l$ and $l_{z1} = -l_{z2}$, that is, there are N different states corresponding to $L = 0$ for fixed quantum numbers N, n . That means that we expect N different Rydberg series converging to each ionization threshold $E_N = -2/N^2$. This is indeed the case and the N different series can be identified also in the exact helium quantum spectrum, see figure 37.6. The degeneracies between the different N Rydberg series corresponding to the same principal quantum number N , are removed by the electron-electron interaction. We thus already have a rather good idea of the coarse structure of the spectrum.

In the next step, we may even speculate which parts of the $L = 0$ spectrum can be reproduced by the semiclassical quantization of collinear helium. In the collinear helium, both classical electrons move back and forth along a common axis through the nucleus, so each has zero angular momentum. We therefore expect that collinear helium describes the Rydberg series with $l = l_1 = l_2 = 0$. These series are the energetically lowest states for fixed (N, n) , corresponding to the Rydberg series on the outermost left side of the spectrum in figure 37.6. We will see in the next section that this is indeed the case and that the collinear model holds down to the $N = 1$ bound state series, including even the ground state of helium! We will also find a semiclassical quantum number corresponding to the angular momentum l and show that the collinear model describes states for moderate angular momentum l as long as $l \ll N$.

remark 37.4

37.5.2 Semiclassical spectral determinant for collinear helium

Nothing but lassitude can stop us now from calculating our first semiclassical eigenvalues. The only thing left to do is to set up the spectral determinant in terms

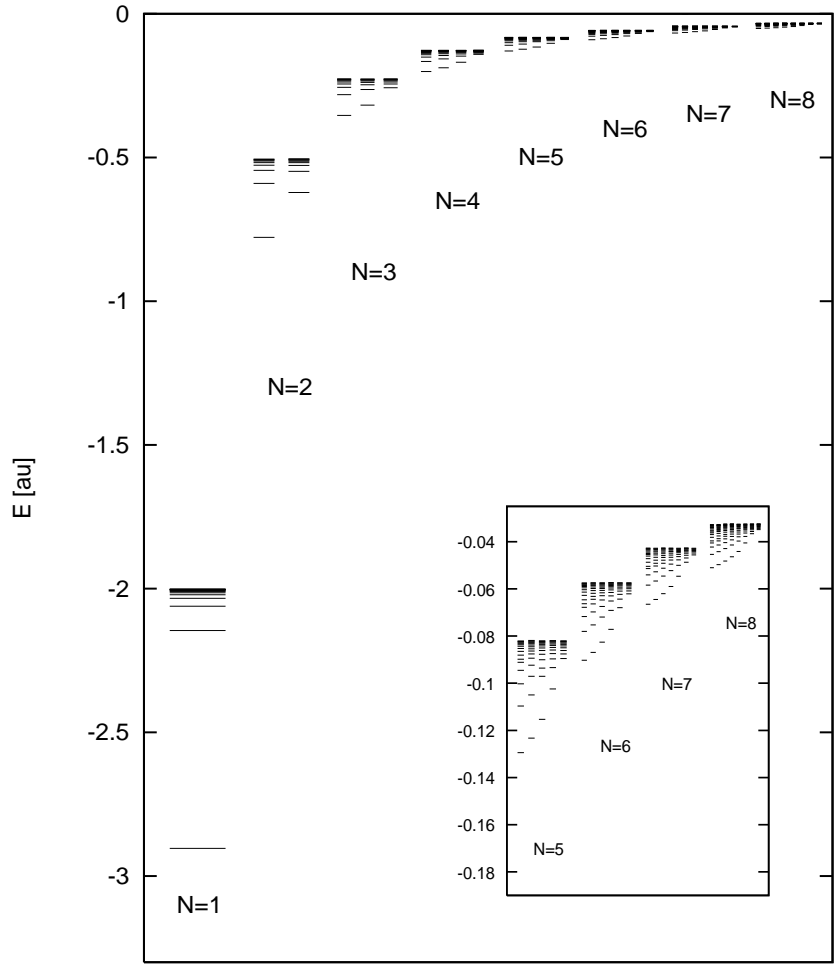


Figure 37.6: The exact quantum helium spectrum for $L = 0$. The energy levels denoted by bars have been obtained from full 3-dimensional quantum calculations [3].

of the periodic orbits of collinear helium and to write out the first few terms of its cycle expansion with the help of the binary symbolic dynamics. The semiclassical spectral determinant (34.12) has been written as product over all cycles of the classical systems. The energy dependence in collinear helium enters the classical dynamics only through simple scaling transformations described in sect. 6.3.1 which makes it possible to write the semiclassical spectral determinant in the form

$$\det(\hat{H}-E)_{sc} = \exp\left(-\sum_p \sum_{r=1}^{\infty} \frac{1}{r} \frac{e^{ir(sS_p - m_p \frac{\pi}{2})}}{(-\det(1 - M_{p\perp}^r))^{1/2} |\det(1 - M_{p\parallel}^r)|^{1/2}}\right), \quad (37.10)$$

with the energy dependence absorbed into the variable

$$s = \frac{e^2}{\hbar} \sqrt{\frac{m_e}{-E}},$$

obtained by using the scaling relation (37.2) for the action. As explained in sect. 37.3, the fact that the $[4 \times 4]$ Jacobian matrix decouples into two $[2 \times 2]$

submatrices corresponding to the dynamics *in* the collinear space and *perpendicular* to it makes it possible to write the denominator in terms of a product of two determinants. Stable and unstable degrees of freedom enter the trace formula in different ways, reflected by the absence of the modulus sign and the minus sign in front of $\det(1 - M_{\perp})$. The topological index m_p corresponds to the unstable dynamics in the collinear plane. Note that the factor $e^{j\pi\tilde{N}(E)}$ present in (34.12) is absent in (37.10). Collinear helium is an open system, i.e., the eigenenergies are resonances corresponding to the complex zeros of the semiclassical spectral determinant and the mean energy staircase $\tilde{N}(E)$ not defined. In order to obtain a spectral determinant as an infinite product of the form (34.18) we may proceed as in (19.9) by expanding the determinants in (37.10) in terms of the eigenvalues of the corresponding Jacobian matrices. The matrix representing displacements perpendicular to the collinear space has eigenvalues of the form $\exp(\pm 2\pi i\sigma)$, reflecting stable linearized dynamics. σ is the full winding number along the orbit in the stable degree of freedom, multiplicative under multiple repetitions of this orbit. The eigenvalues corresponding to the unstable dynamics along the collinear axis are paired as $\{\Lambda, 1/\Lambda\}$ with $|\Lambda| > 1$ and real. As in (19.9) and (34.18) we may thus write

$$\begin{aligned} & \left[-\det(1 - M'_{\perp}) |\det(1 - M'_{\parallel})| \right]^{-1/2} \\ &= \left[-(1 - \Lambda^r)(1 - \Lambda^{-r}) (1 - e^{2\pi i r \sigma})(1 - e^{-2\pi i r \sigma}) \right]^{-1/2} \\ &= \sum_{k, \ell=0}^{\infty} \frac{1}{|\Lambda^r|^{1/2} \Lambda^{rk}} e^{-ir(\ell+1/2)\sigma}. \end{aligned} \quad (37.11)$$

The \pm sign corresponds to the hyperbolic/inverse hyperbolic periodic orbits with positive/negative eigenvalues Λ . Using the relation (37.12) we see that the sum over r in (37.10) is the expansion of the logarithm, so the semiclassical spectral determinant can be rewritten as a product over dynamical zeta functions, as in (19.9):

$$\det(\hat{H} - E)_{sc} = \prod_{k=0}^{\infty} \prod_{m=0}^{\infty} \zeta_{k,m}^{-1} = \prod_{k=0}^{\infty} \prod_{m=0}^{\infty} \prod_p (1 - t_p^{(k,m)}), \quad (37.12)$$

where the cycle weights are given by

$$t_p^{(k,m)} = \frac{1}{|\Lambda|^{1/2} \Lambda^k} e^{i(sS_p - m_p \frac{\pi}{2} - 4\pi(\ell+1/2)\sigma_p)}, \quad (37.13)$$

and m_p is the topological index for the motion in the collinear plane which equals twice the topological length of the cycle. The two independent directions perpendicular to the collinear axis lead to a twofold degeneracy in this degree of freedom which accounts for an additional factor 2 in front of the winding number σ . The values for the actions, winding numbers and stability indices of the shortest cycles in collinear helium are listed in table 37.1.

The integer indices ℓ and k play very different roles in the semiclassical spectral determinant (37.12). A linearized approximation of the flow along a cycle corresponds to a harmonic approximation of the potential in the vicinity of the trajectory. Stable motion corresponds to a harmonic oscillator potential, unstable motion to an inverted harmonic oscillator. The index ℓ which contributes as a phase to the cycle weights in the dynamical zeta functions can therefore be interpreted as a harmonic oscillator quantum number; it corresponds to vibrational modes in the Θ coordinate and can in our simplified picture developed in sect. 37.5.1 be related to the quantum number $l = l_1 = l_2$ representing the single particle angular momenta. Every distinct ℓ value corresponds to a full spectrum which we obtain from the zeros of the semiclassical spectral determinant $1/\zeta$ keeping ℓ fixed. The harmonic oscillator approximation will eventually break down with increasing off-line excitations and thus increasing ℓ . The index k corresponds to ‘excitations’ along the unstable direction and can be identified with local resonances of the inverted harmonic oscillator centered on the given orbit. The cycle contributions $t_p^{(k,m)}$ decrease exponentially with increasing k . Higher k terms in an expansion of the determinant give corrections which become important only for large negative imaginary s values. As we are interested only in the leading zeros of (37.12), i.e., the zeros closest to the real energy axis, it is sufficient to take only the $k = 0$ terms into account.

Next, let us have a look at the discrete symmetries discussed in sect. 37.2. Collinear helium has a C_2 symmetry as it is invariant under reflection across the $r_1 = r_2$ line corresponding to the electron-electron exchange symmetry. As explained in sects. 21.1.1 and 21.5, we may use this symmetry to factorize the semiclassical spectral determinant. The spectrum corresponding to the states symmetric or antisymmetric with respect to reflection can be obtained by writing the dynamical zeta functions in the symmetry factorized form

$$1/\zeta^{(\ell)} = \prod_a (1 - t_a)^2 \prod_{\bar{s}} (1 - t_{\bar{s}}^2). \quad (37.14)$$

Here, the first product is taken over all asymmetric prime cycles, i.e., cycles that are not self-dual under the C_2 symmetry. Such cycles come in pairs, as two equivalent orbits are mapped into each other by the symmetry transformation. The second product runs over all self-dual cycles; these orbits cross the axis $r_1 = r_2$ twice at a right angle. The self-dual cycles close in the fundamental domain $r_1 \leq r_2$ already at half the period compared to the orbit in the full domain, and the cycle weights $t_{\bar{s}}$ in (37.14) are the weights of fundamental domain cycles. The C_2 symmetry now leads to the factorization of (37.14) $1/\zeta = \zeta_+^{-1} \zeta_-^{-1}$, with

$$\begin{aligned} 1/\zeta_+^{(\ell)} &= \prod_a (1 - t_a) \prod_{\bar{s}} (1 - t_{\bar{s}}), \\ 1/\zeta_-^{(\ell)} &= \prod_a (1 - t_a) \prod_{\bar{s}} (1 + t_{\bar{s}}), \end{aligned} \quad (37.15)$$

setting $k = 0$ in what follows. The symmetric subspace resonances are given by the zeros of $1/\zeta_+^{(\ell)}$, antisymmetric resonances by the zeros of $1/\zeta_-^{(\ell)}$, with the

two dynamical zeta functions defined as products over orbits in the fundamental domain. The symmetry properties of an orbit can be read off directly from its symbol sequence, as explained in sect. 37.2. An orbit with an odd number of 1's in the itinerary is self-dual under the C_2 symmetry and enters the spectral determinant in (37.15) with a negative or a positive sign, depending on the symmetry subspace under consideration.

37.5.3 Cycle expansion results

So far we have established a factorized form of the semiclassical spectral determinant and have thereby picked up two *good quantum numbers*; the quantum number m has been identified with an excitation of the bending vibrations, the exchange symmetry quantum number ± 1 corresponds to states being symmetric or antisymmetric with respect to the electron-electron exchange. We may now start writing down the binary cycle expansion (20.7) and determine the zeros of spectral determinant. There is, however, still another problem: there is no cycle $\bar{0}$ in the collinear helium. The symbol sequence $\bar{0}$ corresponds to the limit of an outer electron fixed with zero kinetic energy at $r_1 = \infty$, the inner electron bouncing back and forth into the singularity at the origin. This introduces intermittency in our system, a problem discussed in chapter 24. We note that the behavior of cycles going far out in the channel r_1 or $r_2 \rightarrow \infty$ is very different from those staying in the near core region. A cycle expansion using the binary alphabet reproduces states where both electrons are localized in the near core regions: these are the lowest states in each Rydberg series. The states converging to the various ionization thresholds $E_N = -2/N^2$ correspond to eigenfunctions where the wave function of the outer electron is stretched far out into the ionization channel $r_1, r_2 \rightarrow \infty$. To include those states, we have to deal with the dynamics in the limit of large r_1, r_2 . This turns out to be equivalent to switching to a symbolic dynamics with an infinite alphabet. With this observation in mind, we may write the cycle expansion (...) for a binary alphabet without the $\bar{0}$ cycle as

remark 37.5

$$1/\zeta^\ell(s) = 1 - t_1^{(\ell)} - t_{01}^{(\ell)} - [t_{001}^{(\ell)} + t_{011}^{(\ell)} - t_{01}^{(\ell)}t_1^{(\ell)}] - [t_{0001}^{(\ell)} + t_{0011}^{(\ell)} - t_{001}^{(\ell)}t_1^{(\ell)} + t_{0111}^{(\ell)} - t_{011}^{(\ell)}t_1^{(\ell)}] - \dots \quad (37.16)$$

The weights $t_p^{(\ell)}$ are given in (37.12), with contributions of orbits and composite orbits of the same total symbol length collected within square brackets. The cycle expansion depends only on the classical actions, stability indices and winding numbers, given for orbits up to length 6 in table 37.1. To get reacquainted with the cycle expansion formula (37.16), consider a truncation of the series after the first term

$$1/\zeta^\ell(s) \approx 1 - t_1.$$

Table 37.2: Collinear helium, real part of the symmetric subspace resonances obtained by a cycle expansion (37.16) up to cycle length j . The exact quantum energies [3] are in the last column. The states are labeled by their principal quantum numbers. A dash as an entry indicates a missing zero at that level of approximation.

N	n	$j = 1$	$j = 4$	$j = 8$	$j = 12$	$j = 16$	$-E_{\text{qm}}$
1	1	3.0970	2.9692	2.9001	2.9390	2.9248	2.9037
2	2	0.8044	0.7714	0.7744	0.7730	0.7727	0.7779
2	3	—	0.5698	0.5906	0.5916	0.5902	0.5899
2	4	—	—	—	0.5383	0.5429	0.5449
3	3	0.3622	0.3472	0.3543	0.3535	0.3503	0.3535
3	4	—	—	0.2812	0.2808	0.2808	0.2811
3	5	—	—	0.2550	0.2561	0.2559	0.2560
3	6	—	—	—	0.2416	0.2433	0.2438
4	4	0.2050	0.1962	0.1980	0.2004	0.2012	0.2010
4	5	—	0.1655	0.1650	0.1654	0.1657	0.1657
4	6	—	—	0.1508	0.1505	0.1507	0.1508
4	7	—	—	0.1413	0.1426	0.1426	0.1426

The quantization condition $1/\zeta^{(\ell)}(s) = 0$ leads to

$$E_{m,N} = -\frac{(S_1/2\pi)^2}{[m + \frac{1}{2} + 2(N + \frac{1}{2})\sigma_1]^2}, \quad m, N = 0, 1, 2, \dots, \quad (37.17)$$

with $S_1/2\pi = 1.8290$ for the action and $\sigma_1 = 0.5393$ for the winding number, see table 37.1, the 1 cycle in the fundamental domain. This cycle can be described as the *asymmetric stretch* orbit, see figure 37.5. The additional quantum number N in (37.17) corresponds to the principal quantum number defined in sect. 37.5.1. The states described by the quantization condition (37.17) are those centered closest to the nucleus and correspond therefore to the lowest states in each Rydberg series (for a fixed m and N values), in figure 37.6. The simple formula (37.17) gives already a rather good estimate for the ground state of helium! Results obtained from (37.17) are tabulated in table 37.2, see the 3rd column under $j = 1$ and the comparison with the full quantum calculations.

In order to obtain higher excited quantum states, we need to include more orbits in the cycle expansion (37.16), covering more of the phase space dynamics further away from the center. Taking longer and longer cycles into account, we indeed reveal more and more states in each N -series for fixed m . This is illustrated by the data listed in table 37.2 for symmetric states obtained from truncations of the cycle expansion of $1/\zeta_+$.

exercise 37.7

Results of the same quality are obtained for antisymmetric states by calculating the zeros of $1/\zeta_-^{(\ell)}$. Repeating the calculation with $\ell = 1$ or higher in (37.15) reveals states in the Rydberg series which are to the right of the energetically lowest series in figure 37.6.

Résumé

We have covered a lot of ground starting with considerations of the classical properties of a three-body Coulomb problem, and ending with the semiclassical helium spectrum. We saw that the three-body problem restricted to the dynamics on a collinear appears to be fully chaotic; this implies that traditional semiclassical methods such as *WKB* quantization will not work and that we needed the full periodic orbit theory to obtain leads to the semiclassical spectrum of helium. As a piece of unexpected luck the symbolic dynamics is simple, and the semiclassical quantization of the collinear dynamics yields an important part of the helium spectrum, including the ground state, to a reasonable accuracy. A sceptic might say: “Why bother with all the semiclassical considerations? A straightforward numerical quantum calculation achieves the same goal with better precision.” While this is true, the semiclassical analysis offers new insights into the *structure* of the spectrum. We discovered that the dynamics perpendicular to the collinear plane was stable, giving rise to an additional (approximate) quantum number ℓ . We thus understood the origin of the different Rydberg series depicted in figure 37.6, a fact which is not at all obvious from a numerical solution of the quantum problem.

Having traversed the long road from the classical game of pinball all the way to a credible helium spectrum computation, we could declare victory and fold down this enterprise. Nevertheless, there is still much to think about - what about such quintessentially quantum effects as diffraction, tunnelling, ...? As we shall now see, the periodic orbit theory has still much of interest to offer.

Commentary

Remark 37.1 Sources. The full 3-dimensional Hamiltonian after elimination of the center of mass coordinates, and an account of the finite nucleus mass effects is given in ref. [2]. The general two-body collision regularizing Kustaanheimo–Stiefel transformation [5], a generalization of Levi-Civita’s [13] Pauli matrix two-body collision regularization for motion in a plane, is due to Kustaanheimo [12] who realized that the correct higher-dimensional generalization of the “square root removal” trick (6.15), by introducing a vector Q with property $r = |Q|^2$, is the same as Dirac’s trick of getting linear equation for spin 1/2 fermions by means of spinors. Vector spaces equipped with a product and a known satisfy $|Q \cdot Q| = |Q|^2$ define *normed algebras*. They appear in various physical applications - as quaternions, octonions, spinors. The technique was originally developed in celestial mechanics [6] to obtain numerically stable solutions for planetary motions. The basic idea was in place as early as 1931, when H. Hopf [14] used a KS transformation in order to illustrate a Hopf’s invariant. The KS transformation for the collinear helium was introduced in ref. [2].

Remark 37.2 Complete binary symbolic dynamics. No stable periodic orbit and no exception to the binary symbolic dynamics of the collinear helium cycles have been found in numerical investigations. A proof that all cycles are unstable, that they are uniquely

labeled by the binary symbolic dynamics, and that this dynamics is complete is, however, still missing. The conjectured Markov partition of the phase space is given by the triple collision manifold, i.e., by those trajectories which start in or end at the singular point $r_1 = r_2 = 0$. See also ref. [2].

Remark 37.3 Spin and particle exchange symmetry. In our presentation of collinear helium we have completely ignored all dynamical effects due to the spin of the particles involved, such as the electronic spin-orbit coupling. Electrons are fermions and that determines the symmetry properties of the quantum states. The total wave function, including the spin degrees of freedom, must be antisymmetric under the electron-electron exchange transformation. That means that a quantum state symmetric in the position variables must have an antisymmetric spin wave function, i.e., the spins are antiparallel and the total spin is zero (singletstate). Antisymmetric states have symmetric spin wave function with total spin 1 (tripletstates). The threefold degeneracy of spin 1 states is lifted by the spin-orbit coupling.

Remark 37.4 Helium quantum numbers. The classification of the helium states in terms of single electron quantum numbers, sketched in sect. 37.5.1, prevailed until the 1960's; a growing discrepancy between experimental results and theoretical predictions made it necessary to refine this picture. In particular, the different Rydberg series sharing a given N -quantum number correspond, roughly speaking, to a quantization of the inter electronic angle Θ , see figure 37.1, and can not be described in terms of single electron quantum numbers l_1, l_2 . The fact that something is slightly wrong with the single electron picture laid out in sect. 37.5.1 is highlighted when considering the collinear configuration where both electrons are on the *same* side of the nucleus. As both electrons again have angular momentum equal to zero, the corresponding quantum states should also belong to single electron quantum numbers $(l_1, l_2) = (0, 0)$. However, the single electron picture breaks down completely in the limit $\Theta = 0$ where electron-electron interaction becomes the dominant effect. The quantum states corresponding to this classical configuration are distinctively different from those obtained from the collinear dynamics with electrons on different sides of the nucleus. The Rydberg series related to the classical $\Theta = 0$ dynamics are on the outermost right side in each N subspectrum in figure 37.6, and contain the energetically highest states for given N, n quantum numbers, see also remark 37.5. A detailed account of the historical development as well as a modern interpretation of the spectrum can be found in ref. [1].

Remark 37.5 Beyond the unstable collinear helium subspace. The semiclassical quantization of the chaotic collinear helium subspace is discussed in refs. [7, 8, 9]. Classical and semiclassical considerations beyond what has been discussed in sect. 37.5 follow several other directions, all outside the main of this book.

A classical study of the dynamics of collinear helium where both electrons are on the same side of the nucleus reveals that this configuration is fully stable both in the collinear plane and perpendicular to it. The corresponding quantum states can be obtained with the help of an approximate EBK-quantization which reveals helium resonances with extremely long lifetimes (quasi - bound states in the continuum). These states form the energetically highest Rydberg series for a given principal quantum number N , see figure 37.6. Details can be found in refs. [10, 11].

In order to obtain the Rydberg series structure of the spectrum, i.e., the succession of states converging to various ionization thresholds, we need to take into account the dynamics of orbits which make large excursions along the r_1 or r_2 axis. In the chaotic collinear subspace these orbits are characterized by symbol sequences of form $(a0^n)$ where a stands for an arbitrary binary symbol sequence and 0^n is a succession of n 0's in a row. A summation of the form $\sum_{n=0}^{\infty} t_a 0^n$, where t_p are the cycle weights in (37.12), and cycle expansion of indeed yield all Rydberg states up the various ionization thresholds, see ref. [4]. For a comprehensive overview on spectra of two-electron atoms and semiclassical treatments ref. [1].

Exercises

- 37.1. **Kustaanheimo–Stiefel transformation.** Check the Kustaanheimo–Stiefel regularization for collinear helium; derive the Hamiltonian (6.18) and the collinear helium equations of motion (6.19).
- 37.2. **Helium in the plane.** Starting with the helium Hamiltonian in the infinite nucleus mass approximation $m_{he} = \infty$, and angular momentum $L = 0$, show that the three body problem can be written in terms of three independent coordinates only, the electron-nucleus distances r_1 and r_2 and the inter-electron angle Θ , see figure 6.1.
- 37.3. **Helium trajectories.** Do some trial integrations of the collinear helium equations of motion (6.19). Due to the energy conservation, only three of the phase space coordinates (Q_1, Q_2, P_1, P_2) are independent. Alternatively, you can integrate in 4 dimensions and use the energy conservation as a check on the quality of your integrator.
- The dynamics can be visualized as a motion in the original configuration space (r_1, r_2) , $r_i \geq 0$ quadrant, or, better still, by an appropriately chosen 2 – dimensional Poincaré section, exercise 37.4. Most trajectories will run away, do not be surprised - the classical collinear helium is unbound. Try to guess approximately the shortest cycle of figure 37.4.
- 37.4. **A Poincaré section for collinear Helium.** Construct a Poincaré section of figure 37.3b that reduces the helium flow to a map. Try to delineate regions which correspond to finite symbol sequences, i.e. initial conditions that follow the same topological itinerary in figure 37.3a space for a finite number of bounces. Such rough partition can be used to initiate 2–dimensional Newton-Raphson method searches for helium cycles, exercise 37.5.
- 37.5. **Collinear helium cycles.** The motion in the (r_1, r_2) plane is topologically similar to the pinball motion in a 3-disk system, except that the motion is in the Coulomb potential.
- Just as in the 3-disk system the dynamics is simplified if viewed in the *fundamental domain*, in this case the region between r_1 axis and the $r_1 = r_2$ diagonal. Modify your integration routine so the trajectory bounces off the diagonal as off a mirror. Miraculously, the symbolic dynamics for the survivors again turns out to be binary, with 0 symbol signifying a bounce off the r_1 axis, and 1 symbol for a bounce off the diagonal. Just as in the 3-disk game of pinball, we thus know what cycles need to be computed for the cycle expansion (37.16).
- Guess some short cycles by requiring that topologically they correspond to sequences of bounces either returning to the same r_i axis or reflecting off the diagonal. Now either Use special symmetries of orbits such as self-retracing to find all orbits up to length 5 by a 1-dimensional Newton search.
- 37.6. **Collinear helium cycle stabilities.** Compute the eigenvalues for the cycles you found in exercise 37.5, as described in sect. 37.3. You may either integrate the reduced 2×2 matrix using equations (37.6) together with the generating function \mathbf{I} given in local coordinates by (37.7) or integrate the full 4×4 Jacobian matrix, see sect. K.1. Integration in 4 dimensions should give eigenvalues of the form $(1, 1, \Lambda_p, 1/\Lambda_p)$; The unit eigenvalues are due to the usual periodic orbit invariances; displacements along the orbit as well as perpendicular to the energy manifold are conserved; the latter one provides a check of the accuracy of your computation. Compare with table 37.1; you should get the actions and

Lyapunov exponents right, but topological indices and stability angles we take on faith.

- 37.7. **Helium eigenenergies.** Compute the lowest eigenenergies of singlet and triplet states of helium by substituting cycle data into the cycle expansion (37.16) for the symmetric and antisymmetric zeta functions (37.15). Probably the quickest way is to plot the magnitude of the

zeta function as function of real energy and look for the minima. As the eigenenergies in general have a small imaginary part, a contour plot such as figure 20.1, can yield informed guesses. Better way would be to find the zeros by Newton method, sect. 20.2.3. How close are you to the cycle expansion and quantum results listed in table 37.2? You can find more quantum data in ref. [3].

References

- [37.1] G. Tanner, J-M. Rost and K. Richter, *Rev. Mod. Phys.* **72**, 497 (2000).
- [37.2] K. Richter, G. Tanner, and D. Wintgen, *Phys. Rev. A* **48**, 4182 (1993).
- [37.3] Bürgers A., Wintgen D. and Rost J. M., *J. Phys. B* **28**, 3163 (1995).
- [37.4] G. Tanner and D. Wintgen *Phys. Rev. Lett.* **75** 2928 (1995).
- [37.5] P. Kustaanheimo and E. Stiefel, *J. Reine Angew. Math.* **218**, 204 (1965).
- [37.6] E.L. Steifel and G. Scheifele, *Linear and regular celestial mechanics* (Springer, New York 1971).
- [37.7] G.S. Ezra, K. Richter, G. Tanner and D. Wintgen, *J. Phys. B* **24**, L413 (1991).
- [37.8] D. Wintgen, K. Richter and G. Tanner, *CHAOS* **2**, 19 (1992).
- [37.9] R. Blümel and W. P. Reinhardt, *Directions in Chaos Vol 4*, eds. D. H. Feng and J.-M. Yuan (World Scientific, Hongkong), 245 (1992).
- [37.10] K. Richter and D. Wintgen, *J. Phys. B* **24**, L565 (1991).
- [37.11] D. Wintgen and K. Richter, *Comments At. Mol. Phys.* **29**, 261 (1994).
- [37.12] P. Kustaanheimo, *Ann. Univ. Turku, Ser. AI.*, **73** (1964).
- [37.13] T. Levi-Civita, *Opere matematiche* **2** (1956).
- [37.14] H. Hopf, *Math. Ann.* **104** (1931).

Chapter 38

Diffraction distraction

(N. Whelan)

DIFFRACTION EFFECTS characteristic to scattering off wedges are incorporated into the periodic orbit theory.

38.1 Quantum eavesdropping

As noted in chapter 37, the classical mechanics of the helium atom is undefined at the instant of a triple collision. This is a common phenomenon - there is often some singularity or discontinuity in the classical mechanics of physical systems. This discontinuity can even be helpful in classifying the dynamics. The points in phase space which have a past or future at the discontinuity form manifolds which divide the phase space and provide the symbolic dynamics. The general rule is that quantum mechanics smoothes over these discontinuities in a process we interpret as diffraction. We solve the local diffraction problem quantum mechanically and then incorporate this into our global solution. By doing so, we reconfirm the central leitmotif of this treatise: think locally - act globally.

While being a well-motivated physical example, the helium atom is somewhat involved. In fact, so involved that we do not have a clue how to do it. In its place we illustrate the concept of diffractive effects with a pinball game. There are various classes of discontinuities which a billiard can have. There may be a grazing condition such that some trajectories hit a smooth surface while others are unaffected - this leads to the creeping described in chapter 35. There may be a vertex such that trajectories to one side bounce differently from those to the other side. There may be a point scatterer or a magnetic flux line such that we do not know how to continue classical mechanics through the discontinuities. In what follows, we specialize the discussion to the second example - that of vertices or wedges. To further simplify the discussion, we consider the special case of a half line which can be thought of as a wedge of angle zero.

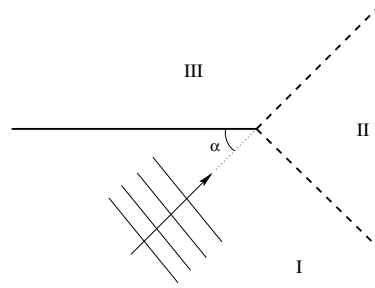


Figure 38.1: Scattering of a plane wave off a half line.

We start by solving the problem of the scattering of a plane wave off a half line (see figure 38.1). This is the local problem whose solution we will use to construct a global solution of more complicated geometries. We define the vertex to be the origin and launch a plane wave at it from an angle α . What is the total field? This is a problem solved by Sommerfeld in 1896 and our discussion closely follows his.

The total field consists of three parts - the incident field, the reflected field and the diffractive field. Ignoring the third of these for the moment, we see that the space is divided into three regions. In region I there is both an incident and a reflected wave. In region II there is only an incident field. In region III there is nothing so we call this the shadowed region. However, because of diffraction the field does enter this region. This accounts for why you can overhear a conversation if you are on the opposite side of a thick wall but with a door a few meters away. Traditionally such effects have been ignored in semiclassical calculations because they are relatively weak. However, they can be significant.

To solve this problem Sommerfeld worked by analogy with the full line case, so let us briefly consider that much simpler problem. There we know that the problem can be solved by images. An incident wave of amplitude A is of the form

$$v(r, \psi) = Ae^{-ikr \cos \psi} \tag{38.1}$$

where $\psi = \phi - \alpha$ and ϕ is the angular coordinate. The total field is then given by the method of images as

$$v_{\text{tot}} = v(r, \phi - \alpha) - v(r, \phi + \alpha), \tag{38.2}$$

where the negative sign ensures that the boundary condition of zero field on the line is satisfied.

Sommerfeld then argued that $v(r, \psi)$ can also be given a complex integral representation

$$v(r, \psi) = A \int_C d\beta f(\beta, \psi) e^{-ikr \cos \beta}. \tag{38.3}$$

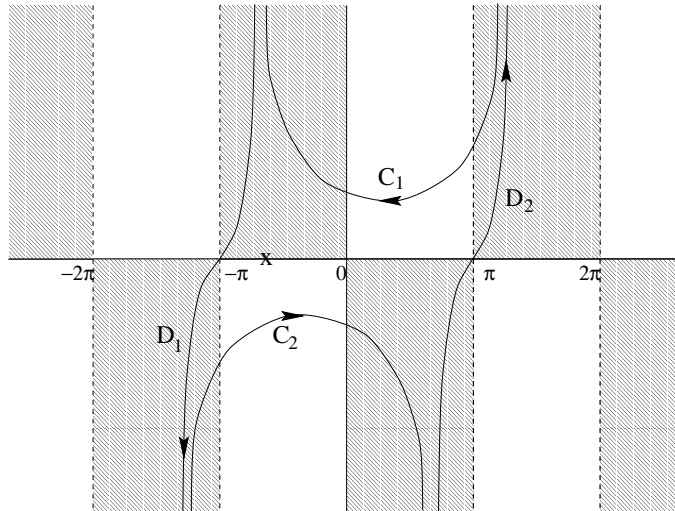


Figure 38.2: The contour in the complex β plane. The pole is at $\beta = -\psi$ (marked by \times in the figure) and the integrand approaches zero in the shaded regions as the magnitude of the imaginary part of β approaches infinity.

This is certainly correct if the function $f(\beta, \psi)$ has a pole of residue $1/2\pi i$ at $\beta = -\psi$ and if the contour C encloses that pole. One choice is

$$f(\beta, \psi) = \frac{1}{2\pi} \frac{e^{i\beta}}{e^{i\beta} - e^{-i\psi}}. \tag{38.4}$$

(We choose the pole to be at $\beta = -\psi$ rather than $\beta = \psi$ for reasons discussed later.) One valid choice for the contour is shown in figure 38.2. This encloses the pole and vanishes as $|\text{Im}\beta| \rightarrow \infty$ (as denoted by the shading). The sections D_1 and D_2 are congruent because they are displaced by 2π . However, they are traversed in an opposite sense and cancel, so our contour consists of just the sections C_1 and C_2 . The motivation for expressing the solution in this complicated manner should become clear soon.

What have we done? We extended the space under consideration by a factor of two and then constructed a solution by assuming that there is also a source in the unphysical space. We superimpose the solutions from the two sources and at the end only consider the solution in the physical space to be meaningful. Furthermore, we expressed the solution as a contour integral which reflects the 2π periodicity of the problem. The half line scattering problem follows by analogy.

Whereas for the full line the field is periodic in 2π , for the half line it is periodic in 4π . This can be seen by the fact that the field can be expanded in a series of the form $\{\sin(\phi/2), \sin(\phi), \sin(3\phi/2), \dots\}$. As above, we extend the space by thinking of it as two sheeted. The physical sheet is as shown in figure 38.1 and the unphysical sheet is congruent to it. The sheets are glued together along the half line so that a curve in the physical space which intersects the half line is continued in the unphysical space and vice-versa. The boundary conditions are that the total field is zero on both faces of the half line (which are physically distinct boundary conditions) and that as $r \rightarrow \infty$ the field is composed solely of plane waves and outgoing circular waves of the form $g(\phi) \exp(ikr)/\sqrt{kr}$. This last condition is a result of Huygens' principle.

We assume that the complete solution is also given by the method of images as

$$v_{\text{tot}} = u(r, \phi - \alpha) - u(r, \phi + \alpha). \quad (38.5)$$

where $u(r, \psi)$ is a 4π -periodic function to be determined. The second term is interpreted as an incident field from the unphysical space and the negative sign guarantees that the solution vanishes on both faces of the half line. Sommerfeld then made the ansatz that u is as given in equation (38.3) with the same contour $C_1 + C_2$ but with the 4π periodicity accounted for by replacing equation (38.4) with

$$f(\beta, \psi) = \frac{1}{4\pi} \frac{e^{i\beta/2}}{e^{i\beta/2} - e^{-i\psi/2}}. \quad (38.6)$$

(We divide by 4π rather than 2π so that the residue is properly normalized.) The integral (38.3) can be thought of as a linear superposition of an infinity of plane waves each of which satisfies the Helmholtz equation $(\nabla^2 + k^2)v = 0$, and so their combination also satisfies the Helmholtz equation. We will see that the diffracted field is an outgoing circular wave; this being a result of choosing the pole at $\beta = -\psi$ rather than $\beta = \psi$ in equation (38.4). Therefore, this ansatz is a solution of the equation and satisfies all boundary conditions and therefore constitutes a valid solution. By uniqueness this is the only solution.

In order to further understand this solution, it is useful to massage the contour. Depending on ϕ there may or may not be a pole between $\beta = -\pi$ and $\beta = \pi$. In region I, both functions $u(r, \phi \pm \alpha)$ have poles which correspond to the incident and reflected waves. In region II, only $u(r, \phi - \alpha)$ has a pole corresponding to the incident wave. In region III there are no poles because of the shadow. Once we have accounted for the geometrical waves (i.e., the poles), we extract the diffracted waves by saddle point analysis at $\beta = \pm\pi$. We do this by deforming the contours C so that they go through the saddles as shown in figure 38.2.

Contour C_1 becomes $E_2 + F$ while contour C_2 becomes $E_1 - F$ where the minus sign indicates that it is traversed in a negative sense. As a result, F has no net contribution and the contour consists of just E_1 and E_2 .

As a result of these machinations, the curves E are simply the curves D of figure 38.2 but with a reversed sense. Since the integrand is no longer 2π periodic, the contributions from these curves no longer cancel. We evaluate both stationary phase integrals to obtain

$$u(r, \psi) \approx -A \frac{e^{i\pi/4}}{\sqrt{8\pi}} \sec(\psi/2) \frac{e^{ikr}}{\sqrt{kr}} \quad (38.7)$$

so that the total diffracted field is

$$v_{\text{diff}} = -A \frac{e^{i\pi/4}}{\sqrt{8\pi}} \left(\sec\left(\frac{\phi - \alpha}{2}\right) - \sec\left(\frac{\phi + \alpha}{2}\right) \right) \frac{e^{ikr}}{\sqrt{kr}}. \quad (38.8)$$

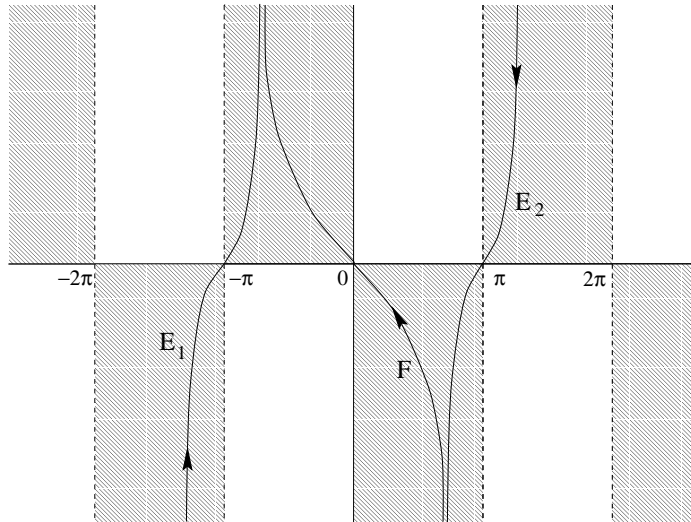


Figure 38.3: The contour used to evaluate the diffractive field after the contribution of possible poles has been explicitly evaluated. The curve F is traversed twice in opposite directions and has no net contribution.

Note that this expression breaks down when $\phi \pm \alpha = \pi$. These angles correspond to the borders among the three regions of figure 38.1 and must be handled more carefully - we can not do a stationary phase integral in the vicinity of a pole. However, the integral representation (38.3) and (38.6) is uniformly valid.

exercise 38.1

We now turn to the simple task of translating this result into the language of semiclassical Green's functions. Instead of an incident plane wave, we assume a source at point x' and then compute the resulting field at the receiver position x . If x is in region I, there is both a direct term, and a reflected term, if x is in region II there is only a direct term and if x is in region III there is neither. In any event these contributions to the semiclassical Green's function are known since the free space Green's function between two points x_2 and x_1 is

$$G_f(x_2, x_1, k) = -\frac{i}{4}H_0^{(+)}(kd) \approx -\frac{1}{\sqrt{8\pi kd}} \exp\{i(kd + \pi/4)\}, \quad (38.9)$$

where d is the distance between the points. For a reflection, we need to multiply by -1 and the distance is the length of the path via the reflection point. Most interesting for us, there is also a diffractive contribution to the Green's function. In equation (38.8), we recognize that the coefficient A is simply the intensity at the origin if there were no scatterer. This is therefore replaced by the Green's function to go from the source to the vertex which we label x_V . Furthermore, we recognize that $\exp(ikr)/\sqrt{kr}$ is, within a proportionality constant, the semiclassical Green's function to go from the vertex to the receiver.

Collecting these facts, we say

$$G_{\text{diff}}(x, x', k) = G_f(x, x_V, k)d(\theta, \theta')G_f(x_V, x', k), \quad (38.10)$$

where, by comparison with equations (38.8) and (38.9), we have

$$d(\theta, \theta') = \sec\left(\frac{\theta - \theta'}{2}\right) - \sec\left(\frac{\theta + \theta'}{2}\right). \quad (38.11)$$

Here θ' is the angle to the source as measured from the vertex and θ is the angle to the receiver. They were denoted as α and ϕ previously. Note that there is a symmetry between the source and receiver as we expect for a time-reversal invariant process. Also the diffraction coefficient d does not depend on which face of the half line we use to measure the angles. As we will see, a very important property of G_{diff} is that it is a simple multiplicative combination of other semiclassical Green's functions.

exercise 38.2

We now recover our classical perspective by realizing that we can still think of classical trajectories. In calculating the quantum Green's function, we sum over the contributions of various paths. These include the classical trajectories which connect the points and also paths which connect the points via the vertex. These have different weights as given by equations (38.9) and (38.10) but the concept of summing over classical paths is preserved.

For completeness, we remark that there is an exact integral representation for the Green's function in the presence of a wedge of arbitrary opening angle [15]. It can be written as

$$G(x, x', k) = g(r, r', k, \theta' - \theta) - g(r, r', k, \theta' + \theta) \tag{38.12}$$

where (r, θ) and (r', θ') are the polar coordinates of the points x and x' as measured from the vertex and the angles are measured from either face of the wedge. The function g is given by

$$g(r, r', k, \psi) = \frac{i}{8\pi\nu} \int_{C_1+C_2} d\beta \frac{H_0^+(k \sqrt{r^2 + r'^2 - 2rr' \cos \beta})}{1 - \exp(i\frac{\beta+\psi}{\nu})} \tag{38.13}$$

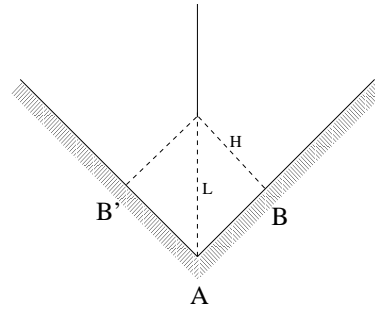
where $\nu = \gamma/\pi$ and γ is the opening angle of the wedge. (ie $\gamma = 2\pi$ in the case of the half plane). The contour $C_1 + C_2$ is the same as shown in figure 38.2.

The poles of this integral give contributions which can be identified with the geometric paths connecting x and x' . The saddle points at $\beta = \pm\pi$ give contributions which can be identified with the diffractive path connecting x and x' . The saddle point analysis allows us to identify the diffraction constant as

$$d(\theta, \theta') = -\frac{4 \sin \frac{\pi}{\nu}}{\nu} \frac{\sin \frac{\theta}{\nu} \sin \frac{\theta'}{\nu}}{\left(\cos \frac{\pi}{\nu} - \cos \frac{\theta+\theta'}{\nu}\right) \left(\cos \frac{\pi}{\nu} - \cos \frac{\theta-\theta'}{\nu}\right)}, \tag{38.14}$$

which reduces to (38.11) when $\nu = 2$. Note that the diffraction coefficient vanishes identically if $\nu = 1/n$ where n is any integer. This corresponds to wedge angles of $\gamma = \pi/n$ (eg. $n=1$ corresponds to a full line and $n=2$ corresponds to a right angle). This demonstration is limited by the fact that it came from a leading order asymptotic expansion but the result is quite general. For such wedge angles, we can use the method of images (we will require $2n - 1$ images in addition to

Figure 38.4: The billiard considered here. The dynamics consists of free motion followed by specular reflections off the faces. The top vertex induces diffraction while the bottom one is a right angle and induces two specular geometric reflections.



the actual source point) to obtain the Green's function and there is no diffractive contribution to any order. Classically this corresponds to the fact that for such angles, there is no discontinuity in the dynamics. Trajectories going into the vertex can be continued out of them unambiguously. This meshes with the discussion in the introduction where we argued that diffractive effects are intimately linked with classical discontinuities.

The integral representation is also useful because it allows us to consider geometries such that the angles are near the optical boundaries or the wedge angle is close to π/n . For these geometries the saddle point analysis leading to (38.14) is invalid due to the existence of a nearby pole. In that event, we require a more sophisticated asymptotic analysis of the full integral representation.

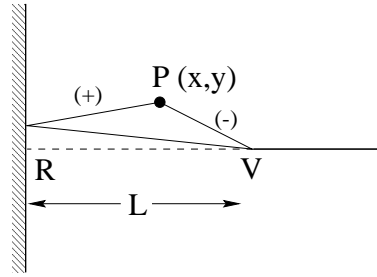
38.2 An application

Although we introduced diffraction as a correction to the purely classical effects; it is instructive to consider a system which can be quantized solely in terms of periodic diffractive orbits. Consider the geometry shown in figure 38.4. The classical mechanics consists of free motion followed by specular reflections off faces. The upper vertex is a source of diffraction while the lower one is a right angle and induces no diffraction. This is an open system, there are no bound states - only scattering resonances. However, we can still test the effectiveness of the theory in predicting them. Formally, scattering resonances are the poles of the scattering S matrix and by an identity of Balian and Bloch are also poles of the quantum Green's function. We demonstrate this fact in chapter 35 for 2-dimensional scatterers. The poles have complex wavenumber k , as for the 3-disk problem.

Let us first consider how diffractive orbits arise in evaluating the trace of G which we call $g(k)$. Specifying the trace means that we must consider all paths which close on themselves in the configuration space while stationary phase arguments for large wavenumber k extract those which are periodic - just as for classical trajectories. In general, $g(k)$ is given by the sum over all diffractive and geometric orbits. The contribution of the simple diffractive orbit labeled γ shown in figure 38.5 to $g(k)$ is determined as follows.

We consider a point P just a little off the path and determine the semiclassical Green's function to return to P via the vertex using (38.9) and (38.10). To leading

Figure 38.5: The dashed line shows a simple periodic diffractive orbit γ . Between the vertex V and a point P close to the orbit there are two geometric legs labeled \pm . The origin of the coordinate system is chosen to be at R .



order in y the lengths of the two geometric paths connecting P and V are $d_{\pm} = (L \pm x) + y^2 / (L \pm x)^2 / 2$ so that the phase factor $ik(d_+ + d_-)$ equals $2ikL +iky^2 / (L^2 - x^2)$. The trace integral involves integrating over all points P and is

$$g_{\gamma}(k) \approx -2d_{\gamma} \frac{e^{i(2kL+\pi/2)}}{8\pi k} \int_0^L \frac{dx}{\sqrt{L^2 - x^2}} \int_{-\infty}^{\infty} dy e^{i(ky^2 \frac{L}{L^2 - x^2})}. \quad (38.15)$$

We introduced an overall negative sign to account for the reflection at the hard wall and multiplied by 2 to account for the two traversal senses, $VRPV$ and $VPRV$. In the spirit of stationary phase integrals, we have neglected the y dependence everywhere except in the exponential. The diffraction constant d_{γ} is the one corresponding to the diffractive periodic orbit. To evaluate the y integral, we use the identity

$$\int_{-\infty}^{\infty} d\xi e^{ia\xi^2} = e^{i\pi/4} \sqrt{\frac{\pi}{a}}, \quad (38.16)$$

and thus obtain a factor which precisely cancels the x dependence in the x integral. This leads to the rather simple result

$$g_{\gamma} \approx -\frac{il_{\gamma}}{2k} \left\{ \frac{d_{\gamma}}{\sqrt{8\pi k l_{\gamma}}} \right\} e^{i(kl_{\gamma} + \pi/4)} \quad (38.17)$$

where $l_{\gamma} = 2L$ is the length of the periodic diffractive orbit. A more sophisticated analysis of the trace integral has been done [6] using the integral representation (38.13). It is valid in the vicinity of an optical boundary and also for wedges with opening angles close to π/n .

Consider a periodic diffractive orbit with n_{γ} reflections off straight hard walls and μ_{γ} diffractions each with a diffraction constant $d_{\gamma,j}$. The total length of the orbit $L_{\gamma} = \sum l_{\gamma,j}$ is the sum of the various diffractive legs and l_{γ} is the length of the corresponding prime orbit. For such an orbit, (38.17) generalizes to

$$g_{\gamma}(k) = -\frac{il_{\gamma}}{2k} \left\{ \prod_{j=1}^{\mu_{\gamma}} \frac{d_{\gamma,j}}{\sqrt{8\pi k l_{\gamma,j}}} \right\} \exp \{i(kL_{\gamma} + n_{\gamma}\pi - 3\mu_{\gamma}\pi/4)\}. \quad (38.18)$$

Each diffraction introduces a factor of $1/\sqrt{k}$ and multi-diffractive orbits are thereby suppressed.

If the orbit γ is prime then $L_\gamma = l_\gamma$. If γ is the r 'th repeat of a prime orbit β we have $L_\gamma = rl_\beta$, $n_\gamma = rp_\beta$ and $\mu_\gamma = r\sigma_\beta$, where l_β , p_β and σ_β all refer to the prime orbit. We can then write

$$g_\gamma = g_{\beta,r} = -\frac{il_\beta}{2k} t_\beta^r \quad (38.19)$$

where

$$t_\beta = \left\{ \prod_{j=1}^{\sigma_\beta} \frac{d_{\beta,j}}{\sqrt{8\pi k l_{\beta,j}}} \right\} \exp \{i(kl_\beta + p_\beta\pi - 3\sigma_\beta\pi/4)\}. \quad (38.20)$$

It then makes sense to organize the sum over diffractive orbits as a sum over the prime diffractive orbits and a sum over the repetitions

$$g_{\text{diff}}(k) = \sum_{\beta} \sum_{r=1}^{\infty} g_{\beta,r} = -\frac{i}{2k} \sum_{\beta} l_\beta \frac{t_\beta}{1-t_\beta}. \quad (38.21)$$

We cast this as a logarithmic derivative (19.7) by noting that $\frac{dt_\beta}{dk} = il_\beta t_\beta - \sigma_\beta t_\beta/2k$ and recognizing that the first term dominates in the semiclassical limit. It follows that

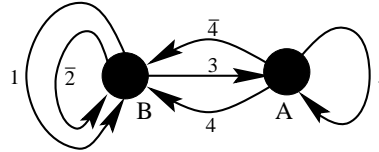
$$g_{\text{diff}}(k) \approx \frac{1}{2k} \frac{d}{dk} \left\{ \ln \prod_{\beta} (1-t_\beta) \right\}. \quad (38.22)$$

In the case that there are only diffractive periodic orbits - as in the geometry of figure 38.4 - the poles of $g(k)$ are the zeros of a dynamical zeta function

$$1/\zeta(k) = \prod_{\beta} (1-t_\beta). \quad (38.23)$$

For geometric orbits, this function would be evaluated with a cycle expansion as discussed in chapter 20. However, here we can use the multiplicative nature of the weights t_β to find a closed form representation of the function using a transition graph, as in chapter 14. This multiplicative property of the weights follows from the fact that the diffractive Green's function (38.10) is multiplicative in segment semiclassical Green's functions, unlike the geometric case.

Figure 38.6: The two-node transition graph with all the diffractive processes connecting the nodes.



There is a reflection symmetry in the problem which means that all resonances can be classified as even or odd. Because of this, the dynamical zeta function factorizes as $1/\zeta = 1/\zeta_+\zeta_-$ (as explained in sects. 21.5 and 21.1.1) and we determine $1/\zeta_+$ and $1/\zeta_-$ separately using the ideas of symmetry decomposition of chapter 21.

In the transition graph shown in figure 38.6, we enumerate all processes. We start by identifying the fundamental domain as just the right half of figure 38.4. There are two nodes which we call A and B . To get to another node from B , we can diffract (always via the vertex) in one of three directions. We can diffract back to B which we denote as process 1. We can diffract to B 's image point B' and then follow this by a reflection. This process we denote as $\bar{2}$ where the bar indicates that it involves a reflection. Third, we can diffract to node A . Starting at A we can also diffract to a node in three ways. We can diffract to B which we denote as 4. We can diffract to B' followed by a reflection which we denote as $\bar{4}$. Finally, we can diffract back to A which we denote as process 5. Each of these processes has its own weight which we can determine from the earlier discussion. First though, we construct the dynamical zeta functions.

The dynamical zeta functions are determined by enumerating all closed loops which do not intersect themselves in figure 38.6. We do it first for $1/\zeta_+$ because that is simpler. In that case, the processes with bars are treated on an equal footing as the others. Appealing back to sect. 21.5 we find

$$\begin{aligned} 1/\zeta_+ &= 1 - t_1 - t_2 - t_5 - t_3t_4 - t_3t_{\bar{4}} + t_5t_1 + t_5t_2, \\ &= 1 - (t_1 + t_2 + t_5) - 2t_3t_4 + t_5(t_1 + t_2) \end{aligned} \tag{38.24}$$

where we have used the fact that $t_4 = t_{\bar{4}}$ by symmetry. The last term has a positive sign because it involves the product of shorter closed loops. To calculate $1/\zeta_-$, we note that the processes with bars have a relative negative sign due to the group theoretic weight. Furthermore, process 5 is a boundary orbit (see sect. 21.3.1) and only affects the even resonances - the terms involving t_5 are absent from $1/\zeta_-$. The result is

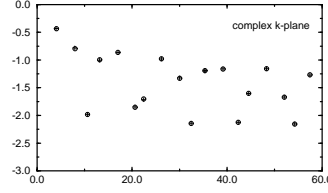
$$\begin{aligned} 1/\zeta_- &= 1 - t_1 + t_2 - t_3t_4 + t_3t_{\bar{4}}, \\ &= 1 - (t_1 - t_2). \end{aligned} \tag{38.25}$$

Note that these expressions have a finite number of terms and are not in the form of a curvature expansion, as for the 3-disk problem.

exercise 38.4

It now just remains to fix the weights. We use equation (38.20) but note that

Figure 38.7: The even resonances of the wedge scatterer of figure 38.4 plotted in the complex k -plane, with $L = 1$. The exact resonances are represented as circles and their semiclassical approximations as crosses.



each weight involves just one diffraction constant. It is then convenient to define the quantities

$$u_A^2 = \frac{\exp\{i(2kL + 2\pi)\}}{\sqrt{16\pi kL}} \quad u_B^2 = \frac{\exp\{i(2kH + \pi)\}}{\sqrt{16\pi kH}}. \quad (38.26)$$

The lengths L and $H = L/\sqrt{2}$ are defined in figure 38.4; we set $L = 1$ throughout. Bouncing inside the right angle at A corresponds to two specular reflections so that $p = 2$. We therefore explicitly include the factor $\exp(i2\pi)$ in (38.26) although it is trivially equal to one. Similarly, there is one specular reflection at point B giving $p = 1$ and therefore a factor of $\exp(i\pi)$. We have defined u_A and u_B because, together with some diffraction constants, they can be used to construct all of the weights. Altogether we define four diffraction coefficients: d_{AB} is the constant corresponding to diffracting from B to A and is found from (38.11) with $\theta' = 3\pi/4$ and $\theta = \pi$ and equals $2 \sec(\pi/8) \approx 2.165$. With analogous notation, we have d_{AA} and $d_{BB} = d_{B'B}$ which equal 2 and $1 + \sqrt{2}$ respectively. $d_{ij} = d_{ji}$ due to the Green's function symmetry between source and receiver referred to earlier. Finally, there is the diffractive phase factor $s = \exp(-i3\pi/4)$ each time there is a diffraction. The weights are then as follows:

$$\begin{aligned} t_1 = sd_{BB}u_B^2 & \quad t_2 = sd_{B'B}u_B^2 & \quad t_3 = t_4 = t_4 = sd_{AB}u_Au_B \\ t_5 = sd_{AA}u_A^2. & \end{aligned} \quad (38.27)$$

Each weight involves two u 's and one d . The u 's represent the contribution to the weight from the paths connecting the nodes to the vertex and the d gives the diffraction constant connecting the two paths.

The equality of d_{BB} and $d_{B'B}$ implies that $t_1 = t_2$. From (38.25) this means that there are no odd resonances because 1 can never equal 0. For the even resonances equation (38.24) is an implicit equation for k which has zeros shown in figure 38.7.

For comparison we also show the result from an exact quantum calculation. The agreement is very good right down to the ground state - as is so often the case with semiclassical calculations. In addition we can use our dynamical zeta function to find arbitrarily high resonances and the results actually improve in that limit. In the same limit, the exact numerical solution becomes more difficult to find so the dynamical zeta function approximation is particularly useful in that case.

exercise 38.5

In general a system will consist of both geometric and diffractive orbits. In that case, the full dynamical zeta function is the product of the geometric zeta

function and the diffractive one. The diffractive weights are typically smaller by order $O(1/\sqrt{k})$ but for small k they can be numerically competitive so that there is a significant diffractive effect on the low-lying spectrum. It might be expected that higher in the spectrum, the effect of diffraction is weaker due to the decreasing weights. However, it should be pointed out that an analysis of the situation for creeping diffraction [7] concluded that the diffraction is actually *more* important higher in the spectrum due to the fact that an ever greater fraction of the orbits need to be corrected for diffractive effects. The equivalent analysis has not been done for edge diffraction but a similar conclusion can probably be expected.

To conclude this chapter, we return to the opening paragraph and discuss the possibility of doing such an analysis for helium. The important point which allowed us to successfully analyze the geometry of figure 38.4 is that when a trajectory is near the vertex, we can extract its diffraction constant without reference to the other facets of the problem. We say, therefore, that this is a “local” analysis for the purposes of which we have “turned off” the other aspects of the problem, namely sides AB and AB' . By analogy, for helium, we would look for some simpler description of the problem which applies near the three body collision. However, there is nothing to “turn off.” The local problem is just as difficult as the global one since they are precisely the same problem, just related by scaling. Therefore, it is not at all clear that such an analysis is possible for helium.

Résumé

In this chapter we have discovered new types of periodic orbits contributing to the semiclassical traces and determinants. Unlike the periodic orbits we had seen so far, these are not true classical orbits. They are generated by singularities of the scattering potential. In these singular points the classical dynamics has no unique definition, and the classical orbits hitting the singularities can be continued in many different directions. While the classical mechanics does not know which way to go, quantum mechanics solves the dilemma by allowing us to continue in all possible directions. The likelihoods of different paths are given by the quantum mechanical weights called diffraction constants. The total contribution to a trace from such orbit is given by the product of transmission amplitudes between singularities and diffraction constants of singularities. The weights of diffractive periodic orbits are at least of order $1/\sqrt{k}$ weaker than the weights associated with classically realizable orbits, and their contribution at large energies is therefore negligible. Nevertheless, they can strongly influence the low lying resonances or energy levels. In some systems, such as the N disk scattering the diffraction effects do not only perturb semiclassical resonances, but can also create new low energy resonances. Therefore it is always important to include the contributions of diffractive periodic orbits when semiclassical methods are applied at low energies.

Commentary

Remark 38.1 Classical discontinuities. Various classes of discontinuities for billiard and potential problems discussed in the literature:

- a grazing condition such that some trajectories hit a smooth surface while others are unaffected, refs. [1, 2, 3, 7]
- a vertex such that trajectories to one side bounce differently from those to the other side, refs. [2, 4, 5, 8, 9].
- a point scatterer [10, 11] or a magnetic flux line [12, 13] such that we do not know how to continue classical mechanics through the discontinuities.

Remark 38.2 Geometrical theory of diffraction. In the above discussion we borrowed heavily from the ideas of Keller who was interested in extending the geometrical ray picture of optics to cases where there is a discontinuity. He maintained that we could hang onto that ray-tracing picture by allowing rays to strike the vertex and then leave at any angle with amplitude (38.8). Both he and Sommerfeld were thinking of optics and not quantum mechanics and they did not phrase the results in terms of semiclassical Green's functions but the essential idea is the same.

Remark 38.3 Generalizations Consider the effect of replacing our half line by a wedge of angle γ_1 and the right angle by an arbitrary angle γ_2 . If $\gamma_2 > \gamma_1$ and $\gamma_2 \geq \pi/2$ this is an open problem whose solution is given by equations (38.24) and (38.25) (there will then be odd resonances) but with modified weights reflecting the changed geometry [8]. (For $\gamma_2 < \pi/2$, more diffractive periodic orbits appear and the dynamical zeta functions are more complicated but can be calculated with the same machinery.) When $\gamma_2 = \gamma_1$, the problem in fact has bound states [21, 22]. This last case has been of interest in studying electron transport in mesoscopic devices and in microwave waveguides. However we can not use our formalism as it stands because the diffractive periodic orbits for this geometry lie right on the border between illuminated and shadowed regions so that equation (38.7) is invalid. Even the more uniform derivation of [6] fails for that particular geometry, the problem being that the diffractive orbit actually lives on the edge of a family of geometric orbits and this makes the analysis still more difficult.

Remark 38.4 Diffractive Green's functions. The result (38.17) is proportional to the length of the orbit times the semiclassical Green's function (38.9) to go from the vertex back to itself along the classical path. The multi-diffractive formula (38.18) is proportional to the total length of the orbit times the product of the semiclassical Green's functions to go from one vertex to the next along classical paths. This result generalizes to any system — either a pinball or a potential — which contains point singularities such that we can define a diffraction constant as above. The contribution to the trace of the semiclassical Green's function coming from a diffractive orbit which hits the singularities is proportional to the total length (or period) of the orbit times the product of semiclassical Green's functions in going from one singularity to the next. This result first appeared in reference [2] and a derivation can be found in reference [9]. A similar structure also exists for creeping [2].

Remark 38.5 Diffractive orbits for hydrogenic atoms. An analysis in terms of diffractive orbits has been made in a different atomic physics system, the response of hydrogenic atoms to strong magnetic fields [23]. In these systems, a single electron is highly excited and takes long traversals far from the nucleus. Upon returning to a hydrogen nucleus, it is re-ejected with the reversed momentum as discussed in chapter 37. However, if the atom is not hydrogen but sodium or some other atom with one valence electron, the returning electron feels the charge distribution of the core electrons and not just the charge of the nucleus. This so-called quantum defect induces scattering in addition to the classical re-ejection present in the hydrogen atom. (In this case the local analysis consists of neglecting the magnetic field when the trajectory is near the nucleus.) This is formally similar to the vertex which causes both specular reflection and diffraction. There is then additional structure in the Fourier transform of the quantum spectrum corresponding to the induced diffractive orbits, and this has been observed experimentally [24].

Exercises

- 38.1. **Stationary phase integral.** Evaluate the two stationary phase integrals corresponding to contours E_1 and E_2 of figure 38.3 and thereby verify (38.7).

(N. Whelan)

- 38.2. **Scattering from a small disk** Imagine that instead of a wedge, we have a disk whose radius a is much smaller than the typical wavelengths we are considering. In that limit, solve the quantum scattering problem - find the scattered wave which result from an incident plane wave. You can do this by the method of partial waves - the analogous three dimensional problem is discussed in most quantum textbooks. You should find that only the $m = 0$ partial wave contributes for small a . Following the discussion above, show that the diffraction constant is

$$d = \frac{2\pi}{\log\left(\frac{2}{ka}\right) - \gamma_e + i\frac{\pi}{2}} \quad (38.28)$$

where $\gamma_e = 0.577 \dots$ is Euler's constant. Note that in this limit d depends weakly on k but not on the scattering angle.

(N. Whelan)

- 38.3. **Several diffractive legs.** Derive equation (38.18). The calculation involves considering slight variations of the diffractive orbit as in the simple case discussed above. Here it is more complicated because there are more diffractive arcs - however you should convince yourself

that a slight variation of the diffractive orbit only affects one leg at a time.

(N. Whelan)

- 38.4. **Unsymmetrized dynamical zeta function.** Assume you know nothing about symmetry decomposition. Construct the 3-node transition graph for figure 38.1 by considering A , B and B' to be physically distinct. Write down the corresponding dynamical zeta function and check explicitly that for $B = B'$ it factorizes into the product of the even and odd dynamical zeta functions. Why is there no term t_2 in the full dynamical zeta function?

(N. Whelan)

- 38.5. **Three point scatterers.**

Consider the limiting case of the three disk game of pin-ball of figure 1.1 where the disks are very much smaller than their spacing R . Use the results of exercise 38.2 to construct the desymmetrized dynamical zeta functions, as in sect. 21.6. You should find $1/\zeta_{A_1} = 1 - 2t$ where $t = de^{i(kR-3\pi/4)}/\sqrt{8\pi kR}$. Compare this formula with that from chapter 11. By assuming that the real part of k is much greater than the imaginary part show that the positions of the resonances are $k_n R = \alpha_n - i\beta_n$ where $\alpha_n = 2\pi n + 3\pi/4$, $\beta_n = \log(\sqrt{2\pi\alpha_n}/d)$ and n is a non-negative integer. (See also reference [11].)

(N. Whelan)

References

- [38.1] A. Wirzba, *CHAOS* **2**, 77 (1992);
- [38.2] G. Vattay, A. Wirzba and P. E. Rosenqvist, *Phys. Rev. Lett.* **73**, 2304 (1994); G. Vattay, A. Wirzba and P. E. Rosenqvist in *Proceedings of the International Conference on Dynamical Systems and Chaos: vol. 2*, edited by Y. Aizawa, S. Saito and K. Shiraiwa (World Scientific, Singapore, 1994).
- [38.3] H. Primack, H. Schanz, U. Smilansky and I. Ussishkin, *Phys. Rev. Lett.* **76**, 1615 (1996).
- [38.4] N. D. Whelan, *Phys. Rev. E* **51**, 3778 (1995).
- [38.5] N. Pavloff and C. Schmit, *Phys. Rev. Lett.* **75**, 61 (1995).
- [38.6] M. Sieber, N. Pavloff, C. Schmit, *Phys. Rev. E* **55**, 2279 (1997).
- [38.7] H. Primack et. al., *J. Phys. A* **30**, 6693 (1997).
- [38.8] N. D. Whelan, *Phys. Rev. Lett.* **76**, 2605 (1996).
- [38.9] H. Bruus and N. D. Whelan, *Nonlinearity*, **9**, 1 (1996).
- [38.10] P. Seba, *Phys. Rev. Lett.* **64**, 1855 (1990).
- [38.11] P. E. Rosenqvist, N. D. Whelan and A. Wirzba, *J. Phys. A* **29**, 5441 (1996).
- [38.12] M. Brack et. al., *Chaos* **5**, 317 (1995).
- [38.13] S. M. Reimann et. al., *Phys. Rev. A* **53**, 39 (1996).
- [38.14] A. Sommerfeld, *Mathem. Ann.* **47**, 317 (1896); *Optics* (Academic Press, New York 1954).
- [38.15] H. S. Carslaw, *Proc. London Math. Soc. (Ser. 1)* **30**, 121 (1989); H. S. Carslaw, *Proc. London Math. Soc. (Ser. 2)* **18**, 291 (1920).
- [38.16] J. B. Keller, *J. Appl. Phys.* **28**, 426 (1957).
- [38.17] A. Voros, *J. Phys. A* **21**, 685 (1988).
- [38.18] see for example, D. Ruelle, *Statistical Mechanics, Thermodynamic Formalism* (Addison-Wesley, Reading MA, 1978).
- [38.19] see for example, P. Grassberger, *Z. Naturforsch.* **43a**, 671 (1988).
- [38.20] P. Cvitanović and B. Eckhardt, *Nonlinearity* **6**, 277 (1993).
- [38.21] P. Exner, P. Seba and P. Stovicek, *Czech J. Phys* **B39**, 1181 (1989).
- [38.22] Hua Wu and D. W. L. Sprung, *J. Appl. Phys.* **72**, 151 (1992).
- [38.23] P. A. Dando, T. S. Monteiro, D. Delande and K. T. Taylor, *Phys. Rev. Lett.* **74**, 1099 (1995). P. A. Dando, T. S. Monteiro and S. M. Owen, preprint (1997).

- [38.24] D. Delande et. al., J. Phys. B **27**, 2771 (1994); G. Raithel et. al., J. Phys. B **27**, 2849 (1994); M. Courtney et. al., Phys. Rev. Lett., **73**, 1340 (1994).

Epilogue

Nowadays, whatever the truth of the matter may be (and we will probably never know), the simplest solution is no longer emotionally satisfying. Everything we know about the world militates against it. The concepts of indeterminacy and chaos have filtered down to us from the higher sciences to confirm our nagging suspicions.

—L. Sante, “Review of ‘American Tabloid’ by James Ellroy,” *New York Review of Books* (May 11, 1995)

A MOTION on a strange attractor can be approximated by shadowing long orbits by sequences of nearby shorter periodic orbits. This notion has here been made precise by approximating orbits by prime cycles, and evaluating associated curvatures. A curvature measures the deviation of a long cycle from its approximation by shorter cycles; the smoothness of the dynamical system implies exponential fall-off for (almost) all curvatures. We propose that the theoretical and experimental non-wandering sets be expressed in terms of the symbol sequences of short cycles (a topological characterization of the spatial layout of the non-wandering set) and their eigenvalues (metric structure)

Cycles as the skeleton of chaos

We wind down this all-too-long treatise by asking: why cycle?

We tend to think of a dynamical system as a smooth system whose evolution can be followed by integrating a set of differential equations. Traditionally one used integrable motions as zeroth-order approximations to physical systems, and accounted for weak nonlinearities perturbatively. However, when the evolution is actually followed through to asymptotic times, one discovers that the strongly nonlinear systems show an amazingly rich structure which is not at all apparent in their formulation in terms of differential equations. In particular, the periodic orbits are important because they form the *skeleton* onto which all trajectories trapped for long times cling. This was already appreciated century ago by H. Poincaré, who, describing in *Les méthodes nouvelles de la mécanique céleste* his discovery of homoclinic tangles, mused that “the complexity of this figure will be striking, and I shall not even try to draw it.” Today such drawings are cheap and

plentiful; but Poincaré went a step further and, noting that hidden in this apparent chaos is a rigid skeleton, a tree of *cycles* (periodic orbits) of increasing lengths and self-similar structure, suggested that the cycles should be the key to chaotic dynamics.

The zeroth-order approximations to harshly chaotic dynamics are very different from those for the nearly integrable systems: a good starting approximation here is the stretching and kneading of a baker's map, rather than the winding of a harmonic oscillator.

For low dimensional deterministic dynamical systems description in terms of cycles has many virtues:

1. cycle symbol sequences are *topological* invariants: they give the spatial layout of a non-wandering set
2. cycle eigenvalues are *metric* invariants: they give the scale of each piece of a non-wandering set
3. cycles are *dense* on the asymptotic non-wandering set
4. cycles are ordered *hierarchically*: short cycles give good approximations to a non-wandering set, longer cycles only refinements. Errors due to neglecting long cycles can be bounded, and typically fall off exponentially or super-exponentially with the cutoff cycle length
5. cycles are *structurally robust*: for smooth flows eigenvalues of short cycles vary slowly with smooth parameter changes
6. asymptotic averages (such as correlations, escape rates, quantum mechanical eigenstates and other "thermodynamic" averages) can be efficiently computed from short cycles by means of *cycle expansions*

Points 1, 2: That the cycle topology and eigenvalues are invariant properties of dynamical systems follows from elementary considerations. If the same dynamics is given by a map f in one set of coordinates, and a map g in the next, then f and g (or any other good representation) are related by a reparametrization and a coordinate transformation $f = h^{-1} \circ g \circ h$. As both f and g are arbitrary representations of the dynamical system, the explicit form of the conjugacy h is of no interest, only the properties invariant under any transformation h are of general import. The most obvious invariant properties are topological; a fixed point must be a fixed point in any representation, a trajectory which exactly returns to the initial point (a cycle) must do so in any representation. Furthermore, a good representation should not mutilate the data; h must be a smooth transformation which maps nearby periodic points of f into nearby periodic points of g . This smoothness guarantees that the cycles are not only topological invariants, but that their linearized neighborhoods are also metrically invariant. In particular, the cycle eigenvalues (eigenvalues of the Jacobian matrix $df^n(x)/dx$ of periodic orbits $f^n(x) = x$) are invariant.

Point 5: An important virtue of cycles is their *structural robustness*. Many quantities customarily associated with dynamical systems depend on the notion of “structural stability,” i.e., robustness of non-wandering set to small parameter variations.

Still, the sufficiently short unstable cycles are structurally robust in the sense that they are only slightly distorted by such parameter changes, and averages computed using them as a skeleton are insensitive to small deformations of the non-wandering set. In contrast, lack of structural stability wreaks havoc with long time averages such as Lyapunov exponents, for which there is no guarantee that they converge to the correct asymptotic value in any finite time numerical computation.

The main recent theoretical advance is **point 4:** we now know how to control the errors due to neglecting longer cycles. As we seen above, even though the number of invariants is infinite (unlike, for example, the number of Casimir invariants for a compact Lie group) the dynamics can be well approximated to any finite accuracy by a small finite set of invariants. The origin of this convergence is geometrical, as we shall see in appendix I.1.2, and for smooth flows the convergence of cycle expansions can even be super-exponential.

The cycle expansions such as (20.7) outperform the pedestrian methods such as extrapolations from the finite cover sums (22.2) for a number of reasons. The cycle expansion is a better averaging procedure than the naive box counting algorithms because the strange attractor is here pieced together in a topologically invariant way from neighborhoods (“space average”) rather than explored by a long ergodic trajectory (“time average”). The cycle expansion is co-ordinate and reparametrization invariant - a finite n th level sum (22.2) is not. Cycles are of finite period but infinite duration, so the cycle eigenvalues are already evaluated in the $n \rightarrow \infty$ limit, but for the sum (22.2) the limit has to be estimated by numerical extrapolations. And, crucially, the higher terms in the cycle expansion (20.7) are deviations of longer prime cycles from their approximations by shorter cycles. Such combinations vanish exactly in piecewise linear approximations and fall off exponentially for smooth dynamical flows.

In the above we have reviewed the general properties of the cycle expansions; those have been applied to a series of examples of low-dimensional chaos: 1-d strange attractors, the period-doubling repeller, the Hénon-type maps and the mode locking intervals for circle maps. The cycle expansions have also been applied to the irrational windings set of critical circle maps, to the Hamiltonian period-doubling repeller, to a Hamiltonian three-disk game of pinball, to the three-disk quantum scattering resonances and to the extraction of correlation exponents. Feasibility of analysis of experimental non-wandering set in terms of cycles is discussed in ref. [1].

Homework assignment

“Lo! thy dread empire Chaos is restor’d, Light dies before
thy uncreating word; Thy hand, great Anarch, lets the cur-
tain fall, And universal darkness buries all.”

—Alexander Pope, *The Dunciad*

We conclude cautiously with a homework assignment posed May 22, 1990
(the original due date was May 22, 2000, but alas...):

1. **Topology** Develop optimal sequences (“continued fraction approximants”) of finite subshift approximations to generic dynamical systems. Apply to (a) the Hénon map, (b) the Lorenz flow and (c) the Hamiltonian standard map.
2. **Non-hyperbolicity** Incorporate power-law (marginal stability orbits, “intermittency”) corrections into cycle expansions. Apply to long-time tails in the Hamiltonian diffusion problem.
3. **Phenomenology** Carry through a convincing analysis of a genuine experimentally extracted data set in terms of periodic orbits.
4. **Invariants** Prove that the scaling functions, or the cycles, or the spectrum of a transfer operator are the maximal set of invariants of an (physically interesting) dynamically generated non-wandering set.
5. **Field theory** Develop a periodic orbit theory of systems with many unstable degrees of freedom. Apply to (a) coupled lattices, (b) cellular automata, (c) neural networks.
6. **Tunneling** Add complex time orbits to quantum mechanical cycle expansions (WKB theory for chaotic systems).
7. **Unitarity** Evaluate corrections to the Gutzwiller semiclassical periodic orbit sums. (a) Show that the zeros (energy eigenvalues) of the appropriate Selberg products are real. (b) Find physically realistic systems for which the “semiclassical” periodic orbit expansions yield the exact quantization.
8. **Atomic spectra** Compute the helium spectrum from periodic orbit expansions (already accomplished by Wintgen and Tanner!).
9. **Symmetries** Include fermions, gauge fields into the periodic orbit theory.
10. **Quantum field theory** Develop quantum theory of systems with infinitely many classically unstable degrees of freedom. Apply to (a) quark confinement (b) early universe (c) the brain.

Conclusion

Good-bye. I am leaving because I am bored.

—George Saunders' dying words

Nadie puede escribir un libro. Para Que un libro sea verdaderamente, Se requieren la aurora y el poniente Siglos, armas y el mar que une y separa.

—Jorge Luis Borges El Hacedor, *Ariosto y los arabes*

The butler did it.

Index

- abscissa
 - absolute conv., 392
 - conditional conv., 392
- accelerator mode, 489
- action, 329, 591, 604, 614
 - helium, 672
 - relation to period, 679
- adjacency matrix, 271, 291, *see* transition matrix
- admissible
 - periodic points, 288
 - trajectories, number of, 284
- Airy
 - equation, 597
 - function, 597
- Airy function, 598, 661, 664, 669
 - at a bifurcation, 598
- Airy integral, 597
- algebra, 753
 - associative, 753
 - Lie, 753
- allowable itinerary, *see* admissible
- alphabet, 201
- alternating binary tree, 219
- analyticity
 - domain, 360
- anomalous diffusion, 497
- Anosov flows, 241
- anti-hermitian
 - generator, 172, 173
- antiharmonic extension, 775
- arc, 273
- area preserving
 - Hénon map, 126
 - map, 829
- Artin-Mazur zeta function, 294
- associative algebra, 753
- attractor
 - basin, 41
 - Hénon, 344
 - strange, 41, 46, 338
- Aubry-Mather theory, 572
- autonomous flow, 43
- average
 - chaotic, 470
 - space, 316, 331
 - time, 316, 329
- averaging, 29
- Axiom A, 446, 453
- baker's map, 139, 233
- Balmer spectrum, 580
- basin of attraction, 41
- basis vector, 752
- BER
 - approximation, 481
- Bernoulli, 733
 - polynomials, 433
 - shift, 210, 428, 433, 441, 452, 454, 461, 479, 496, 736, 737, 882, 939
 - shift eigenfunctions, 448
 - shift return times, 479
- Berry-Keating conjecture, 747
- Bessel function, 652
 - addition theorem, 654
- bi-infinite itinerary, 216
- bifurcation
 - Airy function approximation, 598
 - bizarre, 775
 - generic, 139
 - Hopf, 526
 - saddle-node, 66
- billiard, 134–139
 - map, 135
 - stability, 99, 136
 - stadium, 134, 140, 162, 482, 827, 829, 865
- billiards, 925
- binary
 - prime cycles, 230, 239, 288
 - symbolic dynamics
 - collinear helium, 675
 - tree, alternating, 219
- Birkhoff
 - coordinates, 58, 135, 140
 - ergodic theorem, 317
- Birkhoff coordinates, 925
- block
 - finite sequence, 216
- block, pruning, 218

- Bohr
 - de Broglie picture, 580
 - Sommerfeld quantization, 580, 631, 744
 - helium, 671, 681
 - Uetli Schwur, 744
- Bohr-Sommerfeld quantization, 598
- Boltzmann
 - equation, 24, 500
 - stosszahlansatz, 24
- Boltzmann, L., 24, 735
- boredom, 712, 859
- Borges, J.L., 712
- boundary orbits, 406
- bounded operators, 845
- Bourbaki, N., 65
- Bowen, R., 31
- brain, rat, 5, 32
- branch cut, 465
 - singularity, 466
- Bunimovich
 - stadium, *see* stadium billiard
- Burnett coefficient, 494
- butterfly effect, 66
- $C_{3v} = D_3$ symmetry, 239
- $C_{3v} = D_3$ symmetry, 410
- canonical transformation, 124, 125, 763
- Cartwright, M.L., 162, 736
- Cauchy criterion, 843
- caustic, 608
- ceiling function, 358, 453
- center, 76
- center manifold, 519
- center of mass, 265
- centralizer, 149
- chain rule
 - matrix, 841
- change
 - of coordinates, 106
- chaology, *see* chaos
- chaos, 7, 9
 - caveats, 10
 - deterministic, 30
 - diagnostics, 48
 - quantum, 31
 - skeleton of, 13, 14
 - spatiotemporal, 507
 - successes, 10
- character
 - representation, 809
- characteristic
 - equation, 758
 - exponent, 77, 97
 - function, 309
 - polynomial, 290, 759, 810
 - value, 77
- chicken heart palpitations, 7
- circle map, 210, 274, 305, 491, 497, 526–528, 533, 540, 543, 710, 879, 1003, 1009
 - critical, 529, 534
- class, 147
- class algebra, 829
- Clebsch-Gordan
 - coefficients, 755
- co-moving frame, 99
- coarse-graining, 309
- coding, *see* symbolic dynamics
- collinear helium, 582
 - symbolic dynamics, 675
- combinatorics
 - teaching, 211
- compact group, 151
- compact invariant sets, 148
- complete
 - N -ary dynamics, 273
 - symbolic dynamics, 273
- completeness
 - relation, 78, 754, 759, 811
- complex eigenvalues, 79, 766, 993
- Complex Lorenz equations, 192
- complex Lorenz equations, 167
- complex Lorenz flow
 - equivariance, 175
 - relative periodic orbit, 179
- complexity
 - algorithmic, 303
- confession
 - C.N. Yang, 315
 - Kepler, 733
 - St. Augustine, 309
- configuration space, 48
- conjugacy, 108
 - invariant, 116
 - smooth, 106, 116, 119, 923
 - topological, 212
- conjugate, hermitian, 807
- connection formulas, 597
- conservation
 - equation, 550
 - phase space volume, 123, 125, 126, 129, 321
- continuity equation, 319, 321, 550, 553, 606
- contour integral, 366
- contracting
 - Floquet multipliers, 97, 349
 - flow, 41, 46, 85

- map, 91, 221
- contraction
 - state space
 - Rössler, 91, 397, 918
- convergence
 - abscissa of, 392
 - mediocre, 837
 - radius, 360
 - super-exponential, 438, 560
- convexity, 343
- coordinate
 - change, 106, 108, 921
 - longitudinal, 616
 - transformations, 119
- Copenhagen School, xi, 744
- correlation
 - decay
 - power law, 460
 - function, 448
 - spectrum, 448
 - time, 423
- coset, 147
- cost function, 561
- covariant Lyapunov vector, 95
- covering
 - symbolic dynamics, 216
- creeping
 - 1-disk, 662
- critical
 - point, 98, 208, 213, *see* equilibrium point
 - value, 209, 491
- cross section, 182
- cross-section, 192
- cumulant
 - expansion, 289, 293, 382
 - Plemelj-Smithies, 849
- curvature
 - correction, 379
 - expansion, 28, 379
- cycle, *see* periodic orbit
 - expansion, 19, 379, 630
 - 3-disk, 395
 - finite subshift, 387
 - Lyapunov exponent, 387
 - stability ordered, 388
 - fundamental, 290, 379, 835
 - limit, 338
 - Lyapunov exponent, 97
 - marginal stability, 72, 100, 181
 - prime, 217, 249, 304, 351
 - 3-disk, 249, 570
 - Hénon map, 563
 - pruning, 301
- Rössler
 - flow, 252
 - stability, 94–102
 - Gauss map, 537
 - stable, 98
 - superstable, 98
 - weight, 363
- cycle point, *see* periodic point
- cycles
 - Rössler flow, 264
- cyclic
 - invariance, 249
 - symmetry, 286
- cyclic group, 804, 805
- cyclist
 - Lie groups, 173
- damped Newton method, 254
- Danish pastry, *see* symbol plane
- danish pastry, 234
- de Broglie wavelength, 600
- Debye approximation, 669
- decay
 - rate, 370
 - rate of correlations, 449
- decomposition
 - irreducible, 813
- defining
 - rep, 807
 - vector space, 806
- degenerate
 - eigenvalues, 757
- degree of freedom, 10, 122, 522, 592
- delta function
 - Dirac, 311, 587, 949, 978
- density, 309, 550
 - evolution, 24
 - phase space, 321
- density of states
 - average, 626
 - Green's function, 588
 - quantum, 588
- desymmetrization, 182
 - 3-disk, 414, 961
- desymmetrized
 - state space, 182
- determinant
 - for flows, 362
 - Fredholm, 852
 - graph, 303
 - Hadamard, 360
 - spectral, 23, 289, 360
 - trace relation, 289
 - trace-class operator, 846
- deterministic dynamics, 7, 38, 318

- diagonalizing matrix, 810
- differential equations
 - almost ordinary, 50
 - ordinary
 - almost, 914
- diffraction
 - Green's function, 696
 - Keller, 704
 - Sommerfeld, 704
- diffusion
 - anomalous, 497
 - constant, 333
 - equation, 551
 - limited aggregates, 32
- digraph, *see* transition graph
- dihedral group, 804, 805
- dike map, 214, 221
- dimension
 - box counting, 862
 - fractal, 862
 - generalized, 11
 - information, 862, 863
 - intrinsic, 10, 522
- Dirac delta, 21, 23, 295, 311, 324, 336, 351, 358, 371, 442, 551
 - derivatives, 325
 - Jacobian, 319
- Dirac delta function, 311, 589, 609, 621, 949, 978
- Dirac path integral, 620
- Dirichlet series, 391
- dissipative
 - map, 91, 221
- divergence rate
 - local, 341
- divergence ultraviolet, 628
- DLA, 32
- dof, *see* degree of freedom
- dot product, 171
- doubling map, 210, 445
- dual
 - rep, 752, 806, 807
 - space, 752, 806
 - vector space, 806
- Duffing oscillator, 43, 48, 58, 122
- dynamical
 - system
 - gradient, 914
 - transitivity, 271
 - zeta function, 18, 364
 - Euler product rep., 364
- dynamical system, 37, 38
 - deterministic, 38
 - equivalent, 117
 - gradient, 50
 - infinite, 523
 - smooth, 20, 21, 28, 39, 297, 736, 882, 885, 887
- dynamics
 - deterministic, 7
 - hyperbolic, 273
 - irreversible, 42
 - reversible, 42
 - spatiotemporal, 31
 - stochastic, 7
 - symbolic, 12, 200, 215
 - symmetry, 145, 167
 - topological, 200, 215, 217, 272
- edge, 273
- eigendirection, 71
- eigenfunction
 - Perron-Frobenius operator, 431
 - energy, 585
 - Perron-Frobenius, 431
- eigenstate, *see* eigenfunction
- eigenvalue, 370
 - Perron-Frobenius operator, 431
 - complex, 79, 766
 - degenerate, 757
 - exponential spacing, 361
 - zero, 598, 613
- eigenvalues
 - complex, 993
- Einstein
 - diffusion formula, 552
- Einstein, A, 747
- elastic
 - scattering, 637
- elliptic
 - stability, 127
- enemy
 - thy, 461
- English
 - plain, 216
- ensemble
 - microcanonical, 343
- entire function, 431
- entropy
 - barrier, 394
 - Gauss map, 544
 - Kolmogorov, 139, 303, 857, 859, 864, 865, 913, 967
 - topological, 8, 284, 295, 303
- equation
 - of variations, 70
- equilibria
 - Kuramoto-Sivashinsky, 515
- equilibrium, 176

- Lorenz flow, 44, 60
- point, 43, 80, 315, 515, 563
- Rössler flow, 46, 50, 80, 204
- Rössler system, 915
- relative, 176
- stability, 921
- equilibrium measure, *see* natural measure
- equivalence
 - of dynamical systems, 117
- equivariance, 145
 - complex Lorenz flow, 175
- equivariant, 145, *see* relative
- ergodic
 - average, 317
 - theorem
 - multiplicative, 343
 - theory, 317
- error correlation matrix, 757
- escape rate, 14, 15, 325, 334, 335, 366, 368, 373, 382, 387, 395, 420, 427, 434, 454, 553, 801, 834, 859, 863, 864, 913, 952, 955, 958, 967, 998, 1001
- 3-disk, 386, 395, 418
- intermittency, 469
- vanishing, 325, 385, 773
- essential
 - spectral radius, 441, 450
 - spectrum, 441
- Euler
 - formula, 74, 433, 964
 - limit, 83
 - MacLaurin formula, 449
 - product, 83, 368
 - product rep.
 - dynamical zeta function, 364
 - totient function, 530
- Eulerian
 - coordinates, 72
- evolution
 - group, 50, 914
 - kernel probabilistic, 318
 - operator, 21, 337
 - quantum, 587
 - semigroup, 337
- expanding
 - Floquet multipliers, 97, 349
- expectation value, 331, 344
- exponent
 - characteristic, 97
 - Floquet, 97
- exponential
 - convergence, 360, 438
 - decay rate of correlations, 449
 - of a matrix, 75
 - proliferation, 303
- exponential proliferation, 22
- extremal point, 593
- factor group, 147
- false zeros, 368
- Farey
 - map, 203, 459, 481
 - mediant, 531
 - series, 529
 - tree, 531
- Feigenbaum
 - constant, 358
- Feynman path integral, 612, 620
- Fick law, 551
- finite group, 804
- finite subshift
 - cycle expansion, 387
- first return function, 54
- first return time, 478
- fixed point, 249
 - maps, 67
 - marginally stable, 459
 - under G , 149, 151
- fixed-point subspace, 149
- Floquet
 - exponent, 85, 97, 126
 - multiplier, 77, 84, 95, 97, 224, 349
 - multiplier, metric invariant, 115
 - theorem, 96
 - theory, 97, 103
 - vector, 95
- flow, 37–47
 - autonomous, 43
 - contracting, 41, 46, 85
 - deterministic, 318
 - elliptic, 98
 - generator of, 319, 786
 - Hamiltonian, 122, 829
 - hyperbolic, 98, 127, 370
 - incompressible, 85, 321
 - infinite-dimensional, 506–523
 - invariant subspace, 150
 - inverse hyperbolic, 127
 - linear, 73, 90
 - linearized, 71
 - nonhyperbolic, 98
 - spectral determinant, 362
 - stability, 79
 - stationary, 43
 - stochastic, 318
 - stretch & fold, 208
- Fokker-Planck equation, 553

- form, normal, 114
- Fourier
 - mode
 - truncation, 509
- Fréchet derivative, 71
- fractal, 32, 860
 - aggregates, 11
 - dimension, 862
 - geometry of nature, 11
 - probabilistic, 11
 - science, 11
- Fredholm
 - determinant, 852
- Fredholm theory, 438, 439
- Frenkel-Kontorova model, 572
- frequency analysis, 48
- Fresnel integral, 593, 598
- full shift, 273
- function
 - L^2 square-integrable, 450
 - analytic, 449
 - space, piecewise constant, 352
- functional, 316
 - composition, 42
 - Lyapunov, 41
- fundamental
 - cycle, 290
 - cycles, 835
 - domain, 239
 - collinear helium, 674
 - matrix, 71, 755
- fundamental matrix, 789
- G -equivariant, 170
- G -fixed, 149, 151
- G -invariant
 - basis, *see* invariant polynomial basis
 - polynomial basis, 151, 187
- G -invariant
 - polynomial basis, 150, 162, 163, 192
- G_p -symmetric, 152
- Gählerkin truncation, 511
- Galilean invariance, 509, 523
- Gatto Nero
 - professor, 209
- gauge fixing, 60
- Gauss map, 325, 481, 530, 531, 541
 - cycle stability, 537
 - metric entropy, 544
- Gauss shift, *see* Gauss map
- Gaussian
 - integral, 324, 493, 557, 621
 - integral, d -dimensional, 557, 609
 - noise, 892
 - probability density, 552
- generating function, 351, 573
- generating partition, 217
- generator
 - anti-hermitian, 172, 173
 - Lie algebra, 171
 - of flow, 319, 786
- Gilmore, R., 162
- $GL(n, \mathbb{F})$, 805
- golden mean, 274, 305
 - pruning, 221, 274, 291, 305, 373, 773, 937, 946, 955, 1007
 - renormalization, 533, 541
- good taste, 219
- gradient
 - algorithm, 561
 - system, 50, 914
- grammar
 - symbolic dynamics, 218
- graph
 - irreducible, 273
 - strongly connected, 273
 - transition, 270
- Gray codes, 219
- Green's function, 589
 - analogue of, 790
 - density of states, 588
 - diffraction, 696
 - energy dependent, 587
 - regularized, 628
 - scattering, 643
 - semiclassical, 618, 620, 621
 - short distance, 617, 618
 - trace, 587
 - long orbits, 617
- group, 804
 - S^1 , 804
 - compact, 151
 - cyclic, 804, 805
 - dihedral, 804, 805
 - dynamical, 42
 - evolution, 50, 914
 - finite, 144, 804
 - general linear, 805
 - Lie, 169, 170, 804
 - matrix, 808
 - not a, 830, 997
 - orbit, 148, 160, 170, 176
 - orbit, equilibrium, 194
 - orbit, marginal eigenvalue, 181
 - orbit, reduction, 182
 - orbit, slice, 177, 183, 186, 189
 - orbit, velocity, 761
 - order of, 144, 804

- representation, 808
- semi-, 319, 786
- symmetric, 804
- tangent field, 171, 174
- Gutzwiller
 - trace formula, 626
- Gutzwiller path integral, 620
- Gutzwiller, M., 739
- Hadamard determinant, 360
- Hadamard product, 629
- Hamilton
 - Jacobi equation, 554, 601, 618, 900
 - equations, 601
 - principal function, 554, 604
- Hamilton-Cayley theorem, 754, 759
- Hamiltonian, 585, 602
 - dynamics, 121–130
 - flow, 829
 - spectral determinant, 364
 - stability, 123, 764
 - flows, stability, 762
 - Hénon map, 126
 - repeller, periodic orbits, 265, 942
- Hankel function, 617, 652, 669
- harmonic oscillator, 119
- Harter, W. G., 829
- Heaviside function, 588
- Heisenberg, 744, 745
 - picture, 843
- Heisenberg, W., 785
- Helfand moments, 493
- helium, 671, 744
 - collinear, 51, 67, 123, 582, 690, 916
 - cycles, 265, 690
 - eigenenergies, 691
 - fundamental domain, 674
 - Poincaré section, 690
 - stabilities, 690
 - stability, 265
- Helmholtz equation, 652
- Hénon map, 64, 66, 127
 - attractor, 318, 344
 - cycles, 265, 561
 - fixed points, 67, 231
 - Hamiltonian, 126
 - horseshoe, 231
 - inverse, 231
 - Lyapunov exponent, 344, 953
 - natural measure, 315
 - prime cycles, 563, 574
 - pruning, 838
 - pruning front, 242
 - stability, 87, 98
 - structural stability, 243
 - symmetries, 829
 - time delay map, 257
 - transient, 563
- Hénon, M., 66
- Hénon-Heiles
 - symbolic dynamics, 162
- hermitian
 - conjugation, 807
 - matrix, 807
- heroes
 - unsung, xi, xvi
- Hessian matrix, 124
- heteroclinic orbit, 205, 211, 220
- Hilbert
 - basis, *see* invariant polynomial basis
 - space, 586
- Hilbert basis
 - SO(2), 187
- Hilbert-Schmidt
 - operators, 845
- Hilbert-Schmidt condition, 439
- Hilbert-Weyl theorem, 151
- Holmes, P., 523
- homoclinic orbit, 205
- Hopf
 - bifurcation, 526
 - Hopf's last hope, 742
- Hopf, E., 741
- Hopf, Ebehardt, 526
- Hopf, Eberhard, 740
- Hopf, Heinz, 688
- horseshoe, 230
 - complete, 233
- hydrodynamical
 - interpretation of QM, 620
- hyperbolic
 - flow, 98, 127, 370
 - non-, 25
- hyperbolic orbit
 - partially, 98
- hyperbolicity assumption, 17, 350
- image, 187
- image space, 182
- in/out nodes, 76
- inadmissible symbol sequence, 217
- incommensurate, 40
- incompressible flow, 85
- indecomposability, 271
 - metric, 202
- index
 - Maslov, *see* topological index
- index summation, repeated, 805
- indifferent

- stability, 71
- induced map, 473
- inertial manifold, 511, 523
- infinite-dimensional flows, 506–523
- inflection point, 527
- information
 - dimension, 862
- information dimension, 863
- initial
 - conditions
 - sensitivity to, 8
 - point x_0 , 16, 39, 71
 - state x_0 , 16, 39
- injective, 65
- integrable system, 105, 123
- integrated observable, 329, 330, 337, 341, 351, 365, 378, 836
- integration
 - Runge-Kutta, 50
- intermittency, 139, 444, 458
 - escape rate, 469
 - piecewise linear model, 461
 - resummation, 475
 - stability ordering, 390
- invariance
 - cyclic, 249
 - Galilean, 509, 523
 - of flows, 100
 - symplectic, 124, 130, 762
- invariant, 808
 - density, *see* natural measure
 - matrix, 807
 - measure, 315
 - measure, Gauss map, 325
 - metric, 95, 116
 - points, 149
 - polynomial basis, 150, 151, 162, 163, 182, 187–190, 192
 - polynomials, 926
 - set, compact, 148
 - subgroup, 147
 - subspace, 150
 - tensor, 174
 - topological, 95
 - tori, 190
 - vector, 807
- inverse
 - hyperbolic, 96, 127
 - iteration, 253
 - iteration, Hamiltonian repeller, 265, 942
- inversion, 144
- involution, 805
- inward/outward spirals, 76
- irreducible
 - decomposition, 813
 - graph, 273
 - matrix, 271
 - segment, 155
- irrep, 813
- irreversibility, 24, 42
- Ising model, 238, 409, 414, 870, 872, 883, 884, 889, 890
- isotropy, 151, 160, 161
- isotropy subgroup, 148
- isotypic decomposition, 161
- iteration, 39
 - inverse, 253
 - Hamiltonian repeller, 265, 942
 - map, 63
- itinerary, 12, 14, 58, 201, 250
 - bi-infinite, 203, 216
 - future, 209, 215
 - past, 216
- Jacobi, C.G.J., 90
- Jacobian, 84, 310
 - matrix, 16, 71, 756
- Jonquière function, 463, 482, 498, 500, 502
- Jordan form, 758
- Jordan normal form, 760
- KAM
 - tori, 458
- Karhunen-Loève, 228
- Keller
 - diffraction, 704
- Keller, J.B., 739
- Keplerian orbit, 580
- kernel
 - resolving, 440
- kneading
 - determinant, 219
 - sequence, 213, 221
 - theory, 213
 - value, 213, 221
- Kolmogorov entropy, 139, 303, 857, 859, 864, 865, 913, 967
- Koopman operator, 785, 790
- Kraichnan, R., 741
- Kramers, 744
- Krein-Friedel-Lloyd formula, 644
- Kronecker delta, 752, 806
- KS, *see* Kustaanheimo-Stiefel
- Kuramoto, Y., 523
- Kuramoto-Sivashinsky
 - equilibria, 515, 517
 - system, 512, 515, 518, 523

- kurtosis, 344, 493
- Kustaanheimo-Stiefel transformation, 111, 672
- L^2 function space, 450
- Lagrangian, 604
 - coordinates, 72
 - frame, 99
 - manifold, 605
- laminar states, 458
- Langevin equation, 552, 556
- Laplace
 - transform, 23, 295, 320, 353, 354, 358, 587, 618, 787
 - transform, discrete, 288, 351, 480
- Laplace, Pierre-Simon de, 6
- Laplacian
 - diagonalization, 831
 - non-local, 831
- last hope, Hopf's, 742
- least action principle, 249, 570
- Legendre transform, 604
- Leibniz, Gottfried Wilhelm, 6
- Letellier, C., 162
- level set, 122
- libration orbit, 677, *see* self-retracing
- Lie
 - algebra, 170, 174, 753
 - bracket, 175
 - derivative, 175
 - group, 169, 170, 804
 - product, 753
- Lie algebra, 171
- lifetime, 15
- lifetime matrix, 647
- limit
 - cycle, 338
- limit cycle
 - stability, 921
- linear
 - flow, 73, 90
 - space, 751
 - stability, 69, 94, 515
- linearized
 - flow, 71
- link, 273
- Liouville
 - equation, 321
 - operator, 322
 - theorem, 123, 125, 126, 129, 321
- Littlewood, J.E., 736
- local
 - divergence rate, 341
 - stability, 69, 94, 515
- logistic map, *see* unimodal
- longitudinal
 - coordinate, 616
- loop
 - intersecting, 290
- Lorentz gas, 458, 481
- Lorentzian, 589, 978
- Lorenz
 - complex, 167
- Lorenz flow, 44, 60, 81, 83, 85, 153, 156, 164, 205, 926, 997
 - polar coordinates, 163, 830
 - proto-Lorenz, 164, 926
 - symmetry, 146, 163
- Lorenz, E.N., 66, 162
- loxodromic, 764
- loxodromic quartet, 126, 131
- Lozi map, 65, 66
- Lyapunov
 - covariant vector, 95
 - exponent, 8, 85, 117, 338
 - exponent, cycle, 97
 - exponent, cycle expansion, 387
 - exponent, equilibrium, 516
 - exponent, natural measure, 341
 - exponent, numerical, 343
 - exponent, numerically, 340
 - functional, 41
 - time, 8, 10, 25, 42, 329
- \mathcal{M} state space volume, 334
- manifold
 - unstable, 225
- map, 39, 62–65
 - area preserving, 829
 - contracting, 91, 221
 - dike, 214, 221
 - dissipative, 91, 221
 - expanding, 203
 - fixed point, 67
 - Hénon, 64, 561, 829
 - Hamiltonian, 126
 - prime cycles, 563
 - Hamiltonian
 - Hénon, 126
 - iteration, 63
 - logistic, *see* unimodal
 - Lozi, 65, 66
 - once-folding, 230
 - order preserving, 212
 - orientation preserving, 829
 - orientation reversing, 829
 - quadratic, 65
 - return, 16, 54–56, 58, 204, 205, 215, 227, 231
 - sawtooth, 146, 152, 400

- stability, 86
- stroboscopic, 921
- tent, 208
- unimodal, 208
- marginal
 - stability, 16, 71, 97, 181, 349, 444, 458
 - cycle, 72, 100, 181
 - fixed point, 459
- Markov
 - chain, 216
 - graph, *see* transition graph
 - matrix, 271, 312, 387
 - partition, 494
 - finite, 203, 273
 - infinite, 280
 - not unique, 225
- Maslov index, *see* topological index
- material invariant, 550
- Mather, *see* Aubry-Mather theory
- matrix
 - diagonalizing, 810
 - exponential, 75, 788
 - group, 808
 - hermitian, 807
 - invariant, 807
 - irreducible, 271
 - of variations, *see* stability matrix
 - product, 753
 - rep, 753
 - stability, 70, 554
- matrix representation, 145
- Maupertuis, P.L.M. de, 249, 570
- measure, 309
 - continuous, 117
 - invariant, 315
 - natural, 66, 316, 323, 331, 424, 426, 485, 741, 746
- mechanics
 - quantum, 585
 - statistical, 24
- mediocre
 - convergence, 837
- memory
 - m -step, 201
 - finite, 275
- metric
 - indecomposability, 202, 839
 - invariant, 95, 116
 - Floquet multiplier, 115
 - transitivity, 839
- metric entropy
 - Gauss map, 544
- microcanonical ensemble, 343
- Mira, C., 66
- Misiurewicz, M., 66
- mixing, 8, 9, 17, 317
- mode
 - normal, 830
- Moebius inversion, 300
- monodromy matrix, 86, 101, 349, 763
- Morse index, *see* topological index
- moving frame, 183
 - SO(2), 184
- moving frames, 182
- multi-scattering matrix, 655
- multifractals, 879
- multiplicative ergodic theorem, 343
- multiplier
 - Floquet, 77, 97, 224
- multipoint shooting method, 255
- N -disk
 - transition matrix, 273
- natural density, *see* natural measure
- natural invariant, *see* natural measure
- natural measure, 66, 262, 316, 323, 331, 341, 424, 426, 447, 485, 741, 746
- nature
 - geometry of, 11
- Navier-Stokes equation, 506
- neighborhood, 69, 102
- Nero, G., 209
- neutral, *see* marginal
- New York subway map, 225
- Newton method, 254
 - convergence, 254
 - damped, 254
 - flows, 257
 - optimal surface of section, 769
- Newtonian dynamics, 121
- node, 273
- noise
 - Gaussian, 552, 555, 892
 - white, 552
- non-wandering set, 41, 232
- nonequilibrium, 485
- nonhyperbolic
 - flow, 98, 100
- norm, 843
- normal
 - divisor, 147
 - form, 114
 - mode, 830
 - washing machine, 144
- normal modes, 997
- obscure

- foundations, 744
- jargon, 200
- topology, 512, 517
- observable, 316, 323, 329, 349, 423, 470, 478, 485, 497, 739, 785, 867, 872, 889, 890
- integrated, 329, 330, 337, 341, 351, 365, 378, 836
- vector, 344
- observables, simultaneous, 812
- ODEs, 506
- $O(n)$ group, 804
- 1-disk
 - creeping, 662
 - scattering, 653
 - semiclassical scattering, 659
- Onsager-Machlup, 556
- open systems, 14, 333
- operator
 - evolution, 337
 - Hilbert-Schmidt, 845
 - Koopman, 785, 790
 - Liouville, 322
 - norm, 843
 - Perron-Frobenius, 311, 343
 - positive, 845
 - regularization, 851
 - resolvent, 288, 320, 787
 - semigroup
 - bounded, 320, 787
 - shift, 214, 216
 - trace-class, 844
- orbit, 39, 63, 148
 - inadmissible, 213
 - Keplerian, 580
 - periodic, 40, 217, 378, 624, 625
 - returning, 623
- orbit space, 182
- order preserving map, 212
- ordering
 - spatial, 210, 233
- ordinary differential equations, *see* ODEs
 - almost, 50, 914
- partial differential equations, 506
- orientation
 - preserving map, 829
 - reversing map, 829
- orthogonality
 - relation, 78, 754, 759, 811
- Oseledec multiplicative ergodic theorem, 343
- palpitations, chicken heart, 7
- paradise
 - this side of, 418
- partial differential equations, *see* PDEs
- partial differential equations, 506
- partially hyperbolic invariant tori, 190
- partially hyperbolic orbit, 98
- partition, 201, 217
 - state space, 309
 - generating, 217
 - infinite, 221, 295, 304
 - Markov, 203
- partition function, 342
- passive scalar, 550
- past topological coordinate, 235
- path integral
 - stochastic, *see* Wiener integral
- PDEs, 38, 506
- period
 - relation to action, 679
- periodic
 - orbit, 13, 40, 177, 217, 378, 624, 625
 - condition, 248, 262, 560
 - extraction, 248–262, 560–570
 - Hamiltonian repeller, 265
 - inverse iteration, 253
 - multipoint shooting, 255
 - Newton method, 254
 - relative, 178
 - relaxation algorithm, 561
 - orbit extraction
 - Hamiltonian repeller, 942
 - orbit, short, 155, 161
 - point, 13, 16, 21, 22, 40, 212, 217, 777
 - admissible, 288
 - count, 298
 - unstable, 14
- periodic orbit
 - unstable, 98
- Perron-Frobenius
 - matrix, 271
 - operator, 311, 343, 431
 - theorem, 447, 453, 882
- Peter-Weyl theorem, 169
- phase space, 38, 130, *see* state space
 - 3-disk, 839
 - density, 321
 - vs. state space, 48
- piecewise constant function, 352
- piecewise linear map, 481
 - intermittency, 461
 - repeller, 335
- pinball, *see* 3-disk
 - simulator, 140, 925
- plain English, 216

- plane Couette flow
 - energy, 523
 - relative solutions, 180
 - stability, 761
 - symmetries, 147, 151, 162, 169
 - unstable manifold, 227
- Plemelj-Smithies cumulants, 849
- POD, 228
- Poincaré invariants, 129
- Poincaré return map, 54, 55
 - cycle, 101
 - polynomial, 63
 - stability, 87
- Poincaré section, 13, 54–62, 231
 - 3-disk, 135
 - Hénon trick, 66
 - hyperplane, 56, 227
- Poincaré, H., 5, 9, 15
- point
 - non-wandering, 41
 - periodic, 13, 217
 - scatterer, 705
 - wandering, 40
- point-wise invariant, *see* G -fixed
- Poisson
 - bracket, 321, 322, 324, 762
 - resummation, 23, 476
- Poisson bracket, 175
- polar coordinates, 119
- Pollicott, M, 479
- Pollicott, M., 343
- polylogarithm, 463
- polynomial
 - characteristic, 290
 - topological, 294
- Pomeau, Y., 66
- positive operators, 845
- post-processing, 183, 190
- potential
 - problems, 50
- power law
 - correlation decay, 460
- pressure, 342
 - thermodynamic, 342
- prime cycle, 217, 249, 304, 351
 - 3-disk, 230, 304, 570
 - binary, 230, 239, 288
 - count, 300
 - Hénon map, 563, 574
 - ternary, 238
- primitive cycle, *see* prime cycle
- probabilistic zeta function, 479
- probability
 - matrix, 271
- probability density
 - Gaussian, 552
- product
 - Lie, 753
 - matrix, 753
- profile
 - spatial, 39
- projection operator, 759, 810
- propagator, 587
 - semiclassical, 609
 - short time, 610, 617
 - Van Vleck, 611
- pruning, 12, 458
 - block, 218
 - front, 236
 - golden mean, 221, 274, 291, 305, 373, 773, 937, 946, 955, 1007
 - individual cycles, 301
 - primary interval, 214
 - rules, 273
 - symbolic dynamics, 217
- pruning front
 - 3-disk, 203, 244
- pseudocycle, 378
- quadratic map, 65
- quantization
 - Bohr-Sommerfeld, 580
 - semiclassical, 623
 - WKB, 590, 594
- quantum
 - chaos, 583, 629
 - evolution, 587
 - interference, 600
 - mechanics, 585
 - potential, 619
 - propagator, 587
 - resonances, 580
 - theory, old, 744
- quantum chaology, *see* chaos, quantum
- quasiperiodicity, 40
- quotient
 - state space, 60
- quotient group, 147
- quotient space, 148, 182
- quotienting, 182
- radius
 - of convergence, 360
- random matrix theory, 583
- Rayleigh-Benard flow, 44
- recoding, 218, 230, 238
- rectangle, 234
- rectification
 - flows, 107

- maps, 113
- recurrence, 41, 200
 - time, *see* return time
- reduced
 - state space, 182
- reduced state space, 148, 181
- reducible representation, 169
- reflection, 144
- regularization, 110, 629
 - Green's function, 628
 - operator, 851
- relative
 - periodic orbit, 178
 - solutions, 354
- relative equilibrium, 176
- relaxation algorithm, 561
- renormalization, 139
 - golden mean, 533, 541
- rep
 - defining, 807
 - dual, 752, 806, 807
 - matrix, 753
 - standard, 805
- repeated index summation, 805
- repeller, 14, 41, 334, 582
 - piecewise-linear, 335
 - single fixed point, 431
- representation
 - character, 809
 - equivalent, 809
 - faithful, 809
 - linear, 169
 - matrix, 808
 - reducible, 169
 - regular, 809
- representation space, 805
- representative point, 38
- residue, 129
 - stability, 127, 131
- resolvent
 - kernel, 440
 - operator, 288, 320, 787
- resonances
 - complex, 582
 - quantum, 580
 - Ruelle-Pollicott, 343, 479
- resummation
 - intermittency, 475
- return map, 16, 56, 58, 231
 - Rössler flow, 204
- return time, 479
 - distribution, 479
- returning orbit, 623
- reversible
 - dynamics, 42
- Riemann zeta function, 391, 481, 498
- Rössler
 - attractor, 58
 - cycles, 252, 264
 - equilibria, 50, 80, 204
 - flow, 45, 48, 50, 58, 67, 91, 340
 - Lyapunov exponent, 344
 - return map, 204
 - web diagram, 215
- Rössler system, 915
 - equilibria, 915
- rotating wave, 176
- Roux
 - Henri, 30
- Roux, Henri, 85
- Ruelle
 - Pollicott resonances, 343, 479
 - zeta function, *see* dynamical zeta function
- Ruelle, D., 31, 343, 479
- Runge-Kutta integration, 50
- running orbit
 - Lorentz gas, 489
- Rutherford, 671
- Rydberg series, 681
- S^1 group, 804
- saddle, 76
- saddle point, *see* stationary phase
- saddle-node bifurcation, 66
- sausage, $(N+1)$ -dimensional, 168
- sawtooth map, 146, 152, 400
- scalar multiplication, 751
- scattering
 - 3-dimensional spheres, 139
 - elastic, 637
 - Green's function, 643
 - matrix, 638
 - phase shift, 645
 - point, 705
- schmactals, *see* fractal
- Schrödinger
 - equation, 585
 - time independent, 585
 - picture, 843
- Schrödinger, E, 785
- Schwartzian derivative, 117
- section
 - Poincaré, 13, 54, 56, 58, 135
- secular equation, 758, 759, 810
- self-retracing cycle, 677
- self-similar, 22
- semiclassical
 - approximation, 601

- Green's function, 618, 621
- propagator, 609
- quantization, 623
- spectral determinant
 - collinear helium, 682
 - wave function, 607
 - semiclassical zeta function, 630
- semiclassical resonances
 - 3-disk, 905
- semigroup, 319, 786
 - dynamical, 42
 - evolution, 337
 - operator, 320, 787
- Sensitivity
 - initial conditions, 911
- sensitivity to initial conditions, 8, 34, 66, 338
- set
 - non-wandering, 232
- shadowing, 19, 20, 297
 - 3-disk, 386
- shift, 216
 - Bernoulli, 210, 433, 479, 939
 - finite type, 218
 - full, 216, 273
 - map, 528
 - operator, 214, 216
 - sub-, 217
- short periodic orbit, 155, 161
- similarity transformation, 116
- simultaneous observables, 812
- Sinai, Ya., 31
- Sinai-Bowen-Ruelle measure, *see* natural measure
- single fixed point
 - repeller, 431
 - spectral determinant, 432
- singular value decomposition, 75, 90
- singular values, 76
- singularity
 - branch cut, 466
- Sivashinsky, G.I., 523
- skeleton of chaos, 13, 14
- slice, 182, 183, 192
 - condition, 183
- Smale
 - wild idea, 362, 372
- Smale, S., 11, 31, 224, 241, 303, 372, 736
- small divisor problem, 350
- S-matrix, 638
- smooth, 171
 - conjugacy, 106, 116, 119, 923
 - dynamical system, 523
 - dynamics, 20, 21, 28, 39, 297, 736, 882, 885, 887
 - Spectral determinant, 452
 - approximated, 834
 - interaction, 889
 - potential, 139
 - smooth conjugacy, 115
 - SO(2), 171, 184
 - SO(2), 80, 119, 169, 172, 175, 187, 193–195, 756
 - irreducible representation, 172
 - SO(3), 171, 743
 - solution
 - symmetry, 175
 - Sommerfeld
 - diffraction, 704
 - space
 - analytic functions, 449
 - average, 316
 - averaging, 331
 - configuration, 48
 - defining vector, 806
 - density functions, 352
 - dual, 752, 806
 - linear, 751
 - phase, 48
 - state, 48
 - vector, 751
 - span, 752
 - spatial
 - profile, 39
 - spatiotemporal chaos, 507
 - spatiotemporal dynamics, 31
 - spectral
 - determinant, 23, 289, 360
 - 1 – dimensional maps, 363
 - 2–dimensional hyperbolic Hamiltonian flow, 364
 - entire, 361, 438
 - for flows, 362
 - infinite product rep., 362
 - single fixed point, 432
 - weighted, 369
 - spectral determinant
 - 1-dof, 631
 - 2-dof, 632
 - radius, 432, 441
 - essential, 450
 - staircase, 588
- spectral decomposition, 78, 755, 759, 803, 812
- spectral stability, 497
- spectrum
 - Balmer, 580

- specular reflection, 134
- Spiegel, E.A., 741
- SRB measure, *see* natural measure
- St. Augustine, 309
- stability, 69–89
 - billiards, 99, 136
 - continuous symmetry, 181
 - eigenvalue, *see* Floquet multiplier
 - elliptic, 350
 - exact, 104, 921
 - exponent, *see* Floquet exponent
 - flow, 79
 - Hamiltonian flow, 764
 - Hamiltonian flows, 123, 762
 - indifferent, 71
 - linear, 69, 94, 515
 - maps, 86
 - marginal, 71, 181
 - matrix, 70, 554
 - multiplier, *see* Floquet multiplier
 - neutral, *see* marginal
 - ordering
 - cycle expansions, 388
 - intermittent flows, 390
 - Poincaré map cycle, 101
 - Poincaré return map, 87
 - residue, 127, 131
 - spectral, 497
 - structural, 232, 233, 241, 298, 497
 - window, 98
- stabilizer, 149, 151, 161
- stabilizer subgroup, *see* isotropy subgroup
- stable
 - cycle, 98
 - manifold, 16, 225–227, 231
- stadium billiard, 134, 140, 162, 482, 827, 829, 865
- stagnation point, *see* equilibrium point
- staircase
 - mean eigenvalue density, 684
 - spectral, 588
- standard map, 127, 131, 458
- standard representation space, 805
- standing orbit
 - Lorentz gas, 489
- standing wave, 43, 180
- state, 200, 273
 - set, 201
- state space, 38
 - discretization, 343
 - partition, 309
 - reduced, 148, 181
 - volume \mathcal{M} , 334
 - vs. phase space, 48
- stationary
 - flow, 43
 - phase approximation, 593, 598, 611, 624, 696, 705, 983, 984, 988
 - point, *see* equilibrium point
 - state, 315
- stationary phase, 318, 571, 593, 596, 598, 613, 621, 651, 666, 695, 697, 899, 973
- statistical mechanics, 24
- steady state, *see* equilibrium point
- Sterling formula, 598
- stochastic
 - dynamics, 7, 318
 - matrix, 271
 - path integral, *see* Wiener integral
- Stokes theorem, 130, 605
- stosszahlansatz, 24, 500
- strange
 - attractor, 41, 46
- strange attractor, 338
- Rössler flow, 58
- stretch & fold, 64, 208
- strobe method, 54
- stroboscopic map, 921
- strongly connected graph, 273
- structural stability, 27, 232, 233, 241, 298, 497, 501, 508, 710, 746
 - Hénon map, 243
- structure constant, 753
- structure constants, 174
- subgroup
 - isotropy, 148
- subshift, 217
 - finite type, 218, 241, 272–274, 276
- $SU(n)$ group, 804
- super-exponential
 - convergence, 560
- superstable cycle, 98
- superstable fixed point, 560
- surface of section
 - optimal, 769
- surjective, 65
- survival probability, 15, *see* escape rate
- symbol
 - sequence
 - inadmissible, 217
 - square, 234
 - symbol square, 233, 234
 - symbolic dynamics, 12, 200–218, 771–779
 - 3-disk, 34, 203, 244, 926
 - at a bifurcation, 139
 - binary

- collinear helium, 675
- coding, 218
 - transition graph, 387
- complete, 208, 219, 232, 273
- complete N -ary, 273
- covering, 216
- grammar, 218
- Hénon-Heiles, 162
- pruned, 217
- recoding, 218, 230, 238
- unimodal, 209
- symmetric group, 804
- symmetric, under G_p , 152
- symmetry
 - D_3 , 239, 410
 - 3-disk, 156, 159, 239, 410, 414, 961
 - cyclic, 286
 - discrete, 230, 237
 - dynamical system, 145, 167
 - Hénon map, 829
 - solution, 175
- symmetry, continuous, 167–189
- symmetry, discrete, 143–159
- symplectic
 - form, 124
 - group $Sp(2D)$, 763
 - Hénon map, 126
 - integrator, 789
 - invariance, 124, 130, 762
 - map, 125
 - transformation, 124, 230, 322
- systems
 - open, 333
- syzygy, 150, 163, 187, 188, 926
- tangent
 - bundle, 43, 70
 - space, 70
- tangent field, 171
 - group, 174
- Tauberian theorem, 481
- teaching
 - combinatorics, 211
- template, 204, 253
- tensor
 - invariant, 174
- tent map, 117, 119, 208
- ternary
 - prime cycles, 238
- tessalation
 - smooth dynamics, 834
- thermodynamical
 - pressure, 342
- 3-body problem, 108, 582, 671, 733, 745
- 3-dimensional sphere
 - scattering, 139
- 3-disk
 - boundary orbits, 406
 - convergence, 443, 834
 - cycle
 - analytically, 264
 - count, 160, 412, 784
 - expansion, 395
 - escape rate, 344, 386, 395, 418
 - fractal dimension, 860
 - geometry, 135
 - hyperbolicity, 350
 - phase space, 839
 - pinball, 6, 136, 139
 - point scatterer, 705
 - prime cycles, 18, 230, 249, 304, 570
 - pruning front, 203, 244
 - semiclassical resonances, 905
 - shadowing, 386
 - simulator, 140
 - state space, 14, 58, 860
 - symbolic dynamics, 12, 34, 203, 244, 926
 - symmetry, 156, 159, 239, 410, 414, 961
- time
 - arrow of, 24
 - as parametrization, 107
 - average, 316, 329, 340
 - ceiling function, *see* ceiling function
 - ordered integration, 84, 89
 - turnover, 80, 82, 757
- time delay
 - Wigner, 645
- time- t forward map, 48, 175
- topological
 - conjugacy, 212
 - dynamics, 200, 215, 217, 218, 272
 - entropy, 8, 284, 295
 - future coordinate, 212
 - index, 608
 - topological index, 745
 - invariant, 95
 - parameter, 215
 - polynomial, 294
 - trace formula, 288
 - transitivity, 271
 - zeta function, 294, 295
- topological index, 626
- topological Markov chain, 216
- torus, 40
- totient function, 530
- t_p cycle weight, 363

- trace
 - class operators, 656
 - formula
 - classical, 23
 - flows, 353
 - Gutzwiller, 626
 - maps, 351, 432
 - topological, 288, 295
 - local, 286
- trace-class operator, 844
 - determinant, 846
- trajectory, 39, 74
 - discrete, 63
- transfer
 - matrix, 312, 335
 - operator, 372
 - spectrum, 361
- transformation
 - canonical, 230
 - coordinate, 119
 - symplectic, 230
- transient, 40, 202, 279
- transition
 - graph, 270–280
 - infinite, 293
- transition matrix, 270, 284, 286
 - N -disk, 273
- transversality
 - condition, 55
- transverse
 - stability, 617
- traveling wave, 176, *see* relative equilibrium
- Trotter product formula, 843
- truncation
 - Galerkin, 511
- truncations
 - Fourier, 509
- turbulence, 9, 10, 522
 - problem of, 506
- turnback point, 229
- turnover time, 80, 82, 757
- Ulam map, 117, 119, 208, 264, 265
 - skew, 312, 428, 952
 - tent, 325, 374
- ultraviolet divergence, 628
- unimodal
 - kneading value, 221
 - well ordered symbols, 221
- unimodal map, 208
 - symbolic dynamics, 209
- unstable
 - cycle, 98
 - manifold, 16, 225–227, 231
 - periodic orbit, 98
 - periodic point, 14
- unsung
 - heroes, xi, xvi
- UPO (Unstable Periodic Orbit), *see* periodic orbit
- van Kampen, N. G., 556
- Van Vleck
 - propagator, 611
- variational principle, 555
- vector
 - basis, 752
 - field, 42
 - field, singularities, 107
 - invariant, 807
 - observable, 344
 - space, 751
 - defining, 806
 - dual, 806
- velocity gradients matrix, 70
- vertex, 273
- visitation frequency, 316
- visitation sequence, *see* itinerary
- volume preservation, 138
- von Neumann
 - ergodicity, 790
- Waleffe, F., 742
- walk, *see* itinerary
- wandering point, 40
- wave
 - standing, 43, 180
- wave function
 - semiclassical, 607
 - WKB, 608
- web diagram
 - Rössler flow, 215
- weight
 - multiplicative, 29
- well ordered symbols
 - unimodal, 221
- Wentzel-Kramers-Brillouin, *see* WKB
- Weyl
 - Peter-Weyl theorem, 169
- Weyl rule, 627
- Weyl, H., 810
- white noise, 552
- Wiener integral, 555
- Wigner delay time, 645
- winding number, 129, 527, 528
- WKB, 590, 601
 - connection formulas, 597
 - quantization, 590, 594
 - wave function, 608

Yang, C.N., 315

Young, L.-S., 66

zero eigenvalue, 598, 613

zeros

 false, 368

zeta function

 Artin-Mazur, 294

 dynamical, 18, 364

 probabilistic, 479

 Ruelle, *see* dynamical

 topological, 294, 295

Chaos: Classical and Quantum

**Volume www: Material available
on**

ChaosBook.org

Appendix A

A brief history of chaos

Laws of attribution

1. **Arnol'd's Law:** everything that is discovered is named after someone else (including Arnol'd's law)
2. **Berry's Law:** sometimes, the sequence of antecedents seems endless. So, nothing is discovered for the first time.
3. **Whiteheads's Law:** Everything of importance has been said before by someone who did not discover it.

— M.V. Berry

A.1 Chaos is born

(R. Mainieri and P. Cvitanović)

TRYING TO PREDICT the motion of the Moon has preoccupied astronomers since antiquity. Accurate understanding of its motion was important for determining the longitude of ships while traversing open seas.

Kepler's Rudolphine tables had been a great improvement over previous tables, and Kepler was justly proud of his achievements. He wrote in the introduction to the announcement of Kepler's third law, *Harmonice Mundi* (Linz, 1619) in a style that would not fly with the contemporary *Physical Review Letters* editors:

What I prophesied two-and-twenty years ago, as soon as I discovered the five solids among the heavenly orbits—what I firmly believed long before I had seen Ptolemy's *Harmonics*—what I had promised my friends in the title of this book, which I named before I was sure of my discovery—what sixteen

years ago, I urged as the thing to be sought—that for which I joined Tycho Brahé, for which I settled in Prague, for which I have devoted the best part of my life to astronomical contemplations, at length I have brought to light, and recognized its truth beyond my most sanguine expectations. It is not eighteen months since I got the first glimpse of light, three months since the dawn, very few days since the unveiled sun, most admirable to gaze upon, burst upon me. Nothing holds me; I will indulge my sacred fury; I will triumph over mankind by the honest confession that I have stolen the golden vases of the Egyptians to build up a tabernacle for my God far away from the confines of Egypt. If you forgive me, I rejoice; if you are angry, I can bear it; the die is cast, the book is written, to be read either now or in posterity, I care not which; it may well wait a century for a reader, as God has waited six thousand years for an observer.

Then came Newton. Classical mechanics has not stood still since Newton. The formalism that we use today was developed by Euler and Lagrange. By the end of the 1800's the three problems that would lead to the notion of chaotic dynamics were already known: the three-body problem, the ergodic hypothesis, and nonlinear oscillators.

A.1.1 Three-body problem

Bernoulli used Newton's work on mechanics to derive the elliptic orbits of Kepler and set an example of how equations of motion could be solved by integrating. But the motion of the Moon is not well approximated by an ellipse with the Earth at a focus; at least the effects of the Sun have to be taken into account if one wants to reproduce the data the classical Greeks already possessed. To do that one has to consider the motion of three bodies: the Moon, the Earth, and the Sun. When the planets are replaced by point particles of arbitrary masses, the problem to be solved is known as the three-body problem. The three-body problem was also a model to another concern in astronomy. In the Newtonian model of the solar system it is possible for one of the planets to go from an elliptic orbit around the Sun to an orbit that escaped its dominion or that plunged right into it. Knowing if any of the planets would do so became the problem of the stability of the solar system. A planet would not meet this terrible end if solar system consisted of two celestial bodies, but whether such fate could befall in the three-body case remained unclear.

After many failed attempts to solve the three-body problem, natural philosophers started to suspect that it was impossible to integrate. The usual technique for integrating problems was to find the conserved quantities, quantities that do not change with time and allow one to relate the momenta and positions at different times. The first sign on the impossibility of integrating the three-body problem came from a result of Burns that showed that there were no conserved quantities that were polynomial in the momenta and positions. Burns' result did not preclude the possibility of more complicated conserved quantities. This problem was settled by Poincaré and Sundman in two very different ways.

In an attempt to promote the journal *Acta Mathematica*, Mittag-Leffler got the permission of the King Oscar II of Sweden and Norway to establish a mathematical competition. Several questions were posed (although the king would have preferred only one), and the prize of 2500 kroner would go to the best submission. One of the questions was formulated by Weierstrass:

Given a system of arbitrary mass points that attract each other according to Newton's laws, under the assumption that no two points ever collide, try to find a representation of the coordinates of each point as a series in a variable that is some known function of time and for all of whose values the series converges uniformly.

This problem, whose solution would considerably extend our understanding of the solar system, . . .

Poincaré's submission won the prize. He showed that conserved quantities that were analytic in the momenta and positions could not exist. To show that he introduced methods that were very geometrical in spirit: the importance of state space flow, the role of periodic orbits and their cross sections, the homoclinic points.

The interesting thing about Poincaré's work was that it did not solve the problem posed. He did not find a function that would give the coordinates as a function of time for all times. He did not show that it was impossible either, but rather that it could not be done with the Bernoulli technique of finding a conserved quantity and trying to integrate. Integration would seem unlikely from Poincaré's prize-winning memoir, but it was accomplished by the Finnish-born Swedish mathematician Sundman. Sundman showed that to integrate the three-body problem one had to confront the two-body collisions. He did that by making them go away through a trick known as regularization of the collision manifold. The trick is not to expand the coordinates as a function of time t , but rather as a function of $\sqrt[3]{t}$. To solve the problem for all times he used a conformal map into a strip. This allowed Sundman to obtain a series expansion for the coordinates valid for all times, solving the problem that was proposed by Weierstrass in the King Oscar II's competition.

The Sundman's series are not used today to compute the trajectories of any three-body system. That is more simply accomplished by numerical methods or through series that, although divergent, produce better numerical results. The conformal map and the collision regularization mean that the series are effectively in the variable $1 - e^{-\sqrt[3]{t}}$. Quite rapidly this gets exponentially close to one, the radius of convergence of the series. Many terms, more terms than any one has ever wanted to compute, are needed to achieve numerical convergence. Though Sundman's work deserves better credit than it gets, it did not live up to Weierstrass's expectations, and the series solution did not "considerably extend our understanding of the solar system." The work that followed from Poincaré did.

A.1.2 Ergodic hypothesis

The second problem that played a key role in development of chaotic dynamics was the ergodic hypothesis of Boltzmann. Maxwell and Boltzmann had combined the mechanics of Newton with notions of probability in order to create statistical mechanics, deriving thermodynamics from the equations of mechanics. To evaluate the heat capacity of even a simple system, Boltzmann had to make a great simplifying assumption of ergodicity: that the dynamical system would visit every part of the phase space allowed by conservation laws equally often. This hypothesis was extended to other averages used in statistical mechanics and was called the ergodic hypothesis. It was reformulated by Poincaré to say that a trajectory comes as close as desired to any phase space point.

Proving the ergodic hypothesis turned out to be very difficult. By the end of twentieth century it has only been shown true for a few systems and wrong for quite a few others. Early on, as a mathematical necessity, the proof of the hypothesis was broken down into two parts. First one would show that the mechanical system was ergodic (it would go near any point) and then one would show that it would go near each point equally often and regularly so that the computed averages made mathematical sense. Koopman took the first step in proving the ergodic hypothesis when he realized that it was possible to reformulate it using the recently developed methods of Hilbert spaces. This was an important step that showed that it was possible to take a finite-dimensional nonlinear problem and reformulate it as a infinite-dimensional linear problem. This does not make the problem easier, but it does allow one to use a different set of mathematical tools on the problem. Shortly after Koopman started lecturing on his method, von Neumann proved a version of the ergodic hypothesis, giving it the status of a theorem. He proved that if the mechanical system was ergodic, then the computed averages would make sense. Soon afterwards Birkhoff published a much stronger version of the theorem.

A.1.3 Nonlinear oscillators

The third problem that was very influential in the development of the theory of chaotic dynamical systems was the work on the nonlinear oscillators. The problem is to construct mechanical models that would aid our understanding of physical systems. Lord Rayleigh came to the problem through his interest in understanding how musical instruments generate sound. In the first approximation one can construct a model of a musical instrument as a linear oscillator. But real instruments do not produce a simple tone forever as the linear oscillator does, so Lord Rayleigh modified this simple model by adding friction and more realistic models for the spring. By a clever use of negative friction he created two basic models for the musical instruments. These models have more than a pure tone and decay with time when not stroked. In his book *The Theory of Sound* Lord Rayleigh introduced a series of methods that would prove quite general, such as the notion of a limit cycle, a periodic motion a system goes to regardless of the initial conditions.

A.1.4 Chaos grows up

(R. Mainieri)

The theorems of von Neumann and Birkhoff on the ergodic hypothesis were published in 1912 and 1913. This line of enquiry developed in two directions. One direction took an abstract approach and considered dynamical systems as transformations of measurable spaces into themselves. Could we classify these transformations in a meaningful way? This led Kolmogorov to the introduction of the concept of entropy for dynamical systems. With entropy as a dynamical invariant it became possible to classify a set of abstract dynamical systems known as the Bernoulli systems. The other line that developed from the ergodic hypothesis was in trying to find mechanical systems that are ergodic. An ergodic system could not have stable orbits, as these would break ergodicity. So in 1898 Hadamard published a paper with a playful title of ‘... billiards ...,’ where he showed that the motion of balls on surfaces of constant negative curvature is everywhere unstable. This dynamical system was to prove very useful and it was taken up by Birkhoff. Morse in 1923 showed that it was possible to enumerate the orbits of a ball on a surface of constant negative curvature. He did this by introducing a symbolic code to each orbit and showed that the number of possible codes grew exponentially with the length of the code. With contributions by Artin, Hedlund, and H. Hopf it was eventually proven that the motion of a ball on a surface of constant negative curvature was ergodic. The importance of this result escaped most physicists, one exception being Krylov, who understood that a physical billiard was a dynamical system on a surface of negative curvature, but with the curvature concentrated along the lines of collision. Sinai, who was the first to show that a physical billiard can be ergodic, knew Krylov’s work well.

The work of Lord Rayleigh also received vigorous development. It prompted many experiments and some theoretical development by van der Pol, Duffing, and Hayashi. They found other systems in which the nonlinear oscillator played a role and classified the possible motions of these systems. This concreteness of experiments, and the possibility of analysis was too much of a temptation for **Mary Lucy Cartwright** and J.E. Littlewood [18], who set out to prove that many of the structures conjectured by the experimentalists and theoretical physicists did indeed follow from the equations of motion. Birkhoff had found a ‘remarkable curve’ in a two dimensional map; it appeared to be non-differentiable and it would be nice to see if a smooth flow could generate such a curve. The work of Cartwright and Littlewood led to the work of Levinson, which in turn provided the basis for the horseshoe construction of S. Smale.

chapter 12

In Russia, Lyapunov paralleled the methods of Poincaré and initiated the strong Russian dynamical systems school. Andronov carried on with the study of nonlinear oscillators and in 1937 introduced together with Pontryagin the notion of coarse systems. They were formalizing the understanding garnered from the study of nonlinear oscillators, the understanding that many of the details on how these oscillators work do not affect the overall picture of the state space: there will still be limit cycles if one changes the dissipation or spring force function by a little bit. And changing the system a little bit has the great advantage of eliminating

exceptional cases in the mathematical analysis. Coarse systems were the concept that caught Smale's attention and enticed him to study dynamical systems.

A.2 Chaos with us

(R. Mainieri)

In the fall of 1961 Steven Smale was invited to Kiev where he met Arnol'd, Anosov, Sinai, and Novikov. He lectured there, and spent a lot of time with Anosov. He suggested a series of conjectures, most of which Anosov proved within a year. It was Anosov who showed that there are dynamical systems for which all points (as opposed to a non-wandering set) admit the hyperbolic structure, and it was in honor of this result that Smale named these systems Axiom-A. In Kiev Smale found a receptive audience that had been thinking about these problems. Smale's result catalyzed their thoughts and initiated a chain of developments that persisted into the 1970's.

Smale collected his results and their development in the 1967 review article on dynamical systems, entitled "Differentiable dynamical systems." There are many great ideas in this paper: the global foliation of invariant sets of the map into disjoint stable and unstable parts; the existence of a horseshoe and enumeration and ordering of all its orbits; the use of zeta functions to study dynamical systems. The emphasis of the paper is on the global properties of the dynamical system, on how to understand the topology of the orbits. Smale's account takes you from a local differential equation (in the form of vector fields) to the global topological description in terms of horseshoes.

chapter 12

The path traversed from ergodicity to entropy is a little more confusing. The general character of entropy was understood by Weiner, who seemed to have spoken to Shannon. In 1948 Shannon published his results on information theory, where he discusses the entropy of the shift transformation. Kolmogorov went far beyond and suggested a definition of the metric entropy of an area preserving transformation in order to classify Bernoulli shifts. The suggestion was taken by his student Sinai and the results published in 1959. In 1960 Rohlin connected these results to measure-theoretical notions of entropy. The next step was published in 1965 by Adler and Palis, and also Adler, Konheim, McAndrew; these papers showed that one could define the notion of topological entropy and use it as an invariant to classify continuous maps. In 1967 Anosov and Sinai applied the notion of entropy to the study of dynamical systems. It was in the context of studying the entropy associated to a dynamical system that Sinai introduced Markov partitions in 1968.

Markov partitions allow one to relate dynamical systems and statistical mechanics; this has been a very fruitful relationship. It adds measure notions to the topological framework laid down in Smale's paper. Markov partitions divide the state space of the dynamical system into nice little boxes that map into each other. Each box is labeled by a code and the dynamics on the state space maps the codes

around, inducing a symbolic dynamics. From the number of boxes needed to cover all the space, Sinai was able to define the notion of entropy of a dynamical system. In 1970 Bowen came up independently with the same ideas, although there was presumably some flow of information back and forth before these papers got published. Bowen also introduced the important concept of shadowing of chaotic orbits. We do not know whether at this point the relations with statistical mechanics were clear to everyone. They became explicit in the work of Ruelle. Ruelle understood that the topology of the orbits could be specified by a symbolic code, and that one could associate an ‘energy’ to each orbit. The energies could be formally combined in a ‘partition function’ to generate the invariant measure of the system.

After Smale, Sinai, Bowen, and Ruelle had laid the foundations of the statistical mechanics approach to chaotic systems, research turned to studying particular cases. The simplest case to consider is 1-dimensional maps. The topology of the orbits for parabola-like maps was worked out in 1973 by Metropolis, Stein, and Stein. The more general 1-dimensional case was worked out in 1976 by Milnor and Thurston in a widely circulated preprint, whose extended version eventually got published in 1988.

A lecture of Smale and the results of Metropolis, Stein, and Stein inspired Feigenbaum to study simple maps. This led him to the discovery of the universality in quadratic maps and the application of ideas from field-theory to dynamical systems. Feigenbaum’s work was the culmination in the study of 1-dimensional systems; a complete analysis of a nontrivial transition to chaos. Feigenbaum introduced many new ideas into the field: the use of the renormalization group which led him to introduce functional equations in the study of dynamical systems, the scaling function which completed the link between dynamical systems and statistical mechanics, and the presentation functions which describe the dynamics of scaling functions.

The work in more than one dimension progressed very slowly and is still far from completed. The first result in trying to understand the topology of the orbits in two dimensions (the equivalent of Metropolis, Stein, and Stein, or Milnor and Thurston’s work) was obtained by Thurston. Around 1975 Thurston was giving lectures “On the geometry and dynamics of diffeomorphisms of surfaces.” Thurston’s techniques exposed in that lecture have not been applied in physics, but much of the classification that Thurston developed can be obtained from the notion of a ‘pruning front’ formulated independently by Cvitanović.

Once one develops an understanding of the topology of the orbits of a dynamical system, one needs to be able to compute its properties. Ruelle had already generalized the zeta function introduced by Artin and Mazur so that it could be used to compute the average value of observables. The difficulty with Ruelle’s zeta function is that it does not converge very well. Starting out from Smale’s observation that a chaotic dynamical system is dense with a set of periodic orbits, Cvitanović used these orbits as a skeleton on which to evaluate the averages of observables, and organized such calculations in terms of rapidly converging cycle expansions. This convergence is attained by using the shorter orbits used as a

basis for shadowing the longer orbits.

This account is far from complete, but we hope that it will help get a sense of perspective on the field. It is not a fad and it will not die anytime soon.

A.2.1 Periodic orbit theory

Pure mathematics is a branch of applied mathematics.

— Joe Keller, after being asked to define applied mathematics

The history of the periodic orbit theory is rich and curious, and the recent advances are to equal degree inspired by a century of separate development of three disparate subjects; 1. *classical chaotic dynamics*, initiated by Poincaré and put on its modern footing by Smale [27], Ruelle [32], and many others; 2. *quantum theory* initiated by Bohr, with the modern ‘chaotic’ formulation by Gutzwiller [13, 28]; and 3. *analytic number theory* initiated by Riemann and formulated as a spectral problem by Selberg [31, 32]. Following totally different lines of reasoning and driven by very different motivations, the three separate roads all arrive at formally nearly identical *trace formulas*, *zeta functions* and *spectral determinants*.

That these topics should be related is far from obvious. Connection between dynamics and number theory arises from Selberg’s observation that description of geodesic motion and wave mechanics on spaces of constant negative curvature is essentially a number-theoretic problem. *A posteriori*, one can say that zeta functions arise in both classical and quantum mechanics because in both the dynamical evolution can be described by the action of linear evolution (or transfer) operators on infinite-dimensional vector spaces. The spectra of these operators are given by the zeros of appropriate determinants. One way to evaluate determinants is to expand them in terms of traces, $\log \det = \text{tr} \log$, and in this way the spectrum of an evolution operator becomes related to its traces, i.e., periodic orbits. A perhaps deeper way of restating this is to observe that the trace formulas perform the same service in all of the above problems; they relate the spectrum of lengths (local dynamics) to the spectrum of eigenvalues (global averages), and for nonlinear geometries they play a role analogous to that the Fourier transform plays for the circle.

section 19.1

exercise 4.1

In Gutzwiller’s words:

“The classical periodic orbits are a crucial stepping stone in the understanding of quantum mechanics, in particular when then classical system is chaotic. This situation is very satisfying when one thinks of Poincaré who emphasized the importance of periodic orbits in classical mechanics, but could not have had any idea of what they could mean for quantum mechanics. The set of energy levels and the set of periodic orbits are complementary to each other since they are essentially related through a Fourier transform. Such a relation had been found earlier by the mathematicians in the study

of the Laplacian operator on Riemannian surfaces with constant negative curvature. This led to Selberg’s trace formula in 1956 which has exactly the same form, but happens to be exact. The mathematical proof, however, is based on the high degree of symmetry of these surfaces which can be compared to the sphere, although the negative curvature allows for many more different shapes.”

A.2.2 Dynamicist’s vision of turbulence

The key theoretical concepts that form the basis of the turbulence chapter 26 are rooted in the work of Poincaré, Hopf, Smale, Ruelle and Gutzwiller. In his 1889 analysis of the three-body problem [22] Poincaré introduced the geometric approach to dynamical systems and methods that lie at the core of the theory developed here: qualitative topology of state space flows, Poincaré sections, the key roles played by equilibria, periodic orbits, heteroclinic connections, and their stable/unstable manifolds. Poincaré’s work and parallel work by Lyapunov’s school in Russia was followed up by steady development of dynamical systems theory through the 20th century.

In a seminal 1948 paper [11], Hopf visualized the function space of allowable Navier-Stokes velocity fields as an infinite-dimensional phase space, parameterized by viscosity, boundary conditions and external forces, with instantaneous state of a flow represented by a point in this state space. Laminar flows correspond to equilibrium points, globally stable for sufficiently large viscosity. As the viscosity decreases (as the Reynolds number increases), ‘turbulent’ states set in, represented by chaotic state space trajectories.

Hopf’s observation that viscosity causes a contraction of state space volumes under the action of dynamics led to his key conjecture: that long-term, typically observed solutions of the Navier-Stokes equations lie on finite-dimensional manifolds embedded in the infinite-dimensional state space of allowed states. Hopf’s manifold, known today as the ‘inertial manifold,’ is well-studied in the mathematics of spatio-temporal PDEs. Its finite dimensionality for non-vanishing ‘viscosity’ parameter has been rigorously established in certain settings by Foias and collaborators [39].

Hopf noted “[t]he great mathematical difficulties of these important problems are well known and at present the way to a successful attack on them seems hopelessly barred. There is no doubt, however, that many characteristic features of the hydrodynamical phase flow occur in a much larger class of similar problems governed by non-linear space-time systems. In order to gain insight into the nature of hydrodynamical phase flows we are, at present, forced to find and to treat simplified examples within that class.”

Hopf’s call for geometric state space analysis of simplified models first came to fulfillment with the influential Lorenz’s truncation [8] of the Rayleigh-Bénard convection state space (see example 2.2), and was brought a bit closer to true hydrodynamics with the Cornell group’s POD models of boundary-layer turbulence [19, 12]. Further significant progress has proved possible for systems such

as the 1-spatial dimension Kuramoto-Sivashinsky flow [13, 14], a paradigmatic model of turbulent dynamics, and one of the most extensively studied spatially extended dynamical systems.

Today, as we hope to have convinced the reader, with modern computation and experimental insights, the way to a successful attack on the full Navier-Stokes problem is no longer “hopelessly barred.” We address the challenge in a way Hopf could not divine, employing methodology developed only within the past two decades, explained in depth in this book. Hopf presciently noted that “the geometrical picture of the phase flow is, however, not the most important problem of the theory of turbulence. Of greater importance is the determination of the probability distributions associated with the phase flow”. Hopf’s call for understanding of probability distributions under phase flow has indeed proven to be a key challenge, the one in which dynamical systems theory has made the greatest progress in the last half century, namely, the Sinai-Ruelle-Bowen ergodic theory of ‘natural’ or SRB measures for far-from-equilibrium systems [27, 28, 29, 32].

The story so far goes like this: in 1960 Edward A. Spiegel was Robert Kraichnan’s research associate. Kraichnan told him: “Flow follows a regular solution for a while, then another one, then switches to another one; that’s turbulence.” It was not too clear, but Kraichnan’s vision of turbulence moved Ed. In 1962 Spiegel and Derek Moore investigated a set of 3rd order convection equations which seemed to follow one periodic solution, then another, and continued going from periodic solution to periodic solution. Ed told Derek: “This is turbulence!” and Derek said “This is wonderful!” and was moved. He went to give a lecture at Caltech sometime in 1964 and came back angry as hell. They pilloried him there: “Why is this turbulence?” they kept asking and he could not answer, so he expunged the word ‘turbulence’ from their 1966 article[15] on periodic solutions. In 1970 Spiegel met Kraichnan and told him: “This vision of turbulence of yours has been very useful to me.” Kraichnan said: “That wasn’t my vision, that was Hopf’s vision.” What Hopf *actually* said and where he said it remains deeply obscure to this very day. There are papers that lump him together with Landau, as the ‘Landau-Hopf’s incorrect theory of turbulence,’ but he did not seem to propose incommensurate frequencies as building blocks of turbulence, which is what Landau’s guess was.

Starting with the introduction of ‘cycle expansions’ [1] in 1988, the classical, mathematically rigorous SRB, and the closely related semiclassical Gutzwiller theory, were refashioned into effective tools for computing long time averages of quantities measured in chaotic dynamics. The idea that chaotic dynamics is built upon unstable periodic orbits first arose in Ruelle’s work on hyperbolic systems, with ergodic averages associated with natural invariant measures expressed as weighted summations of the corresponding averages about the infinite set of unstable periodic orbits embedded in the underlying chaotic set. For a long time the convergence of such sums bedeviled the practitioners, until the periodic orbit theory was recast in terms of highly convergent *cycle expansions* [2] for which relatively few short periodic orbits led to highly accurate transport rates for classical systems, and quantal spectra for quantum systems. The idea, in nutshell, is that long orbits are shadowed by shorter orbits, and the n th term in a cycle expansion

is the difference between the shorter cycles estimate of the period n -cycles' contribution from the exact n -cycles sum. For hyperbolic, everywhere unstable flows, this difference falls off exponentially or super-exponentially. Implementing the cycle expansions theory, the group of Wintgen soon obtained a surprisingly accurate helium spectrum [20] from a small set of shortest cycles, 50 years after failure of the old quantum theory to do so, and 20 years after Gutzwiller first introduced his quantization of chaotic systems.

In 1996 Christiansen *et al.* [40] proposed (in what is now the gold standard for an exemplary ChaosBook.org project) that the periodic orbit theory be applied to infinite-dimensional flows, such as the Navier-Stokes, using the Kuramoto-Sivashinsky model as a laboratory for exploring the dynamics close to the onset of spatiotemporal chaos. The main conceptual advance in this initial foray was the demonstration that the high-dimensional (16-64 mode Galérkin truncations) dynamics of this dissipative flow can be reduced to an approximately 1-dimensional Poincaré return map $s \rightarrow f(s)$, by choosing the unstable manifold of the shortest periodic orbit as the intrinsic curvilinear coordinate from which to measure near recurrences. For the first time for any nonlinear PDE, some 1,000 unstable periodic orbits were determined numerically.

What was novel about this work? First, dynamics on a strange attractor embedded in a high-dimensional space was reduced to an *intrinsic* nearly 1-dimensional dynamics, an approximate 1 – *dimensional* map from the segment of the unstable manifold bracketed by the primary turning points onto itself. Second, the solutions found provided both a *qualitative description*, and highly accurate *quantitative predictions* for the given PDE with the given boundary conditions and the given system parameter values.

The 1996 project went as far as one could with methods and computation resources available, until 2002, when new variational methods were introduced [15, 41, 12]. Considerably more unstable, higher-dimensional regimes have become accessible [14], and the full Navier-Stokes analysis of wall-bounded flows has become feasible [42].

A.2.3 Gruppenpest

How many Tylenols should I take with this?... (never took group theory, still need to be convinced that there is any use to this beyond mind-numbing formalizations.)

— Fabian Waleffe, forced to read a version of chapter 9.

If you are not fan of chapter 9 “World in a mirror,” and its elaborations, you are not alone. Or, at least, you were not alone in 1930s. That is when the articles by two young mathematical physicists, Eugene Wigner and Johann von Neumann [23], and Wigner’s 1931 Gruppentheorie [24] started *Die Gruppenpest* that plagues us to this very day.

According to John Baez [25], the American physicist John Slater, inventor of the ‘Slater determinant,’ is famous for having dismissed groups as unnecessary to physics. He wrote:

“It was at this point that Wigner, Hund, Heitler, and Weyl entered the picture with their ‘Gruppenpest:’ the pest of the group theory [actually, the correct translation is ‘the group plague’] ... The authors of the ‘Gruppenpest’ wrote papers which were incomprehensible to those like me who had not studied group theory... The practical consequences appeared to be negligible, but everyone felt that to be in the mainstream one had to learn about it. I had what I can only describe as a feeling of outrage at the turn which the subject had taken ... it was obvious that a great many other physicists were disgusted as I had been with the group-theoretical approach to the problem. As I heard later, there were remarks made such as ‘Slater has slain the ‘Gruppenpest’’. I believe that no other piece of work I have done was so universally popular.”

A. John Coleman writes in *Groups and Physics - Dogmatic Opinions of a Senior Citizen* [26]: “The mathematical elegance and profundity of Weyl’s book [Theory of Groups and QM] was somewhat traumatic for the English-speaking physics community. In the preface of the second edition in 1930, after a visit to the USA, Weyl wrote, “It has been rumored that the ‘group pest’ is gradually being cut out of quantum physics. This is certainly not true in so far as the rotation and Lorentz groups are concerned; ...” In the autobiography of J. C. Slater, published in 1975, the famous MIT physicist described the “feeling of outrage” he and other physicists felt at the incursion of group theory into physics at the hands of Wigner, Weyl et al. In 1935, when Condon and Shortley published their highly influential treatise on the “Theory of Atomic Spectra”, Slater was widely heralded as having “slain the Gruppenpest”. Pages 10 and 11 of Condon and Shortley’s treatise are fascinating reading in this context. They devote three paragraphs to the role of group theory in their book. First they say, “We manage to get along without it.” This is followed by a lovely anecdote. In 1928 Dirac gave a seminar, at the end of which Weyl protested that Dirac had said he would make no use of group theory but that in fact most of his arguments were applications of group theory. Dirac replied, “I said that I would obtain the results without previous knowledge of group theory!” Mackey, in the article referred to previously, argues that what Slater and Condon and Shortley did was to rename the generators of the Lie algebra of $SO(3)$ as “angular momenta” and create the feeling that what they were doing was physics and not esoteric mathematics.”

From [AIP Wigner interview](#): AIP: “In that circle of people you were working with in Berlin, was there much interest in group theory at this time?” WIGNER: “No. On the opposite. Schrödinger coined the expression, ‘Gruppenpest’ must be abolished.” “It is interesting, and representative of the relations between mathematics and physics, that Wigner’s paper was originally submitted to a Springer physics journal. It was rejected, and Wigner was seeking a physics journal that might take it when von Neumann told him not to worry, he would get it into the Annals of Mathematics. Wigner was happy to accept his offer [27].”

A.3 Death of the Old Quantum Theory

In 1913 Otto Stern and Max Theodor Felix von Laue went up for a walk up the Uetliberg. On the top they sat down and talked about physics. In particular they talked about the new atom model of Bohr. There and then they made the ‘Uetli Schwur:’ If that crazy model of Bohr turned out to be right, then they would leave physics. It did and they didn’t.

— A. Pais, *Inward Bound: of Matter and Forces in the Physical World*

In an afternoon of May 1991 Dieter Wintgen is sitting in his office at the Niels Bohr Institute beaming with the unparalleled glee of a boy who has just committed a major mischief. The starting words of the manuscript he has just penned are

The failure of the Copenhagen School to obtain a reasonable . . .

34 years old at the time, Dieter was a scruffy kind of guy, always in sandals and holed out jeans, the German flavor of a 90’s left winger and a mountain climber, working around the clock with his students Gregor and Klaus to complete the work that Bohr himself would have loved to see done back in 1916: a ‘planetary’ calculation of the helium spectrum.

Never mind that the ‘Copenhagen School’ refers not to the old quantum theory, but to something else. The old quantum theory was no theory at all; it was a set of rules bringing some order to a set of phenomena which defied logic of classical theory. The electrons were supposed to describe planetary orbits around the nucleus; their wave aspects were yet to be discovered. The foundations seemed obscure, but Bohr’s answer for the once-ionized helium to hydrogen ratio was correct to five significant figures and hard to ignore. The old quantum theory marched on, until by 1924 it reached an impasse: the helium spectrum and the Zeeman effect were its death knell.

Since the late 1890’s it had been known that the helium spectrum consists of the orthohelium and parahelium lines. In 1915 Bohr suggested that the two kinds of helium lines might be associated with two distinct shapes of orbits (a suggestion that turned out to be wrong). In 1916 he got Kramers to work on the problem, and wrote to Rutherford: “I have used all my spare time in the last months to make a serious attempt to solve the problem of ordinary helium spectrum . . . I think really that at last I have a clue to the problem.” To other colleagues he wrote that “the theory was worked out in the fall of 1916” and of having obtained a “partial agreement with the measurements.” Nevertheless, the Bohr-Sommerfeld theory, while by and large successful for hydrogen, was a disaster for neutral helium. Heroic efforts of the young generation, including Kramers and Heisenberg, were of no avail.

For a while Heisenberg thought that he had the ionization potential for helium, which he had obtained by a simple perturbative scheme. He wrote enthusiastic

letters to Sommerfeld and was drawn into a collaboration with Max Born to compute the spectrum of helium using Born's systematic perturbative scheme. In first approximation, they reproduced the earlier calculations. The next level of corrections turned out to be larger than the computed effect. The concluding paragraph of Max Born's classic "Vorlesungen über Atommechanik" from 1925 sums it up in a somber tone:

(...) the systematic application of the principles of the quantum theory (...) gives results in agreement with experiment only in those cases where the motion of a single electron is considered; it fails even in the treatment of the motion of the two electrons in the helium atom.

This is not surprising, for the principles used are not really consistent. (...) A complete systematic transformation of the classical mechanics into a discontinuous mechanics is the goal towards which the quantum theory strives.

That year Heisenberg suffered a bout of hay fever, and the old quantum theory was dead. In 1926 he gave the first quantitative explanation of the helium spectrum. He used wave mechanics, electron spin and the Pauli exclusion principle, none of which belonged to the old quantum theory, and planetary orbits of electrons were cast away for nearly half a century.

Why did Pauli and Heisenberg fail with the helium atom? It was not the fault of the old quantum mechanics, but rather it reflected their lack of understanding of the subtleties of classical mechanics. Today we know what they missed in 1913-24: the role of conjugate points (topological indices) along classical trajectories was not accounted for, and they had no idea of the importance of periodic orbits in nonintegrable systems.

Since then the calculation for helium using the methods of the old quantum mechanics has been fixed. Leopold and Percival [5] added the topological indices in 1980, and in 1991 Wintgen and collaborators [8, 9] understood the role of periodic orbits. Dieter had good reasons to gloat; while the rest of us were preparing to sharpen our pencils and supercomputers in order to approach the dreaded 3-body problem, they just went ahead and did it. What it took—and much else—is described in this book.

One is also free to ponder what quantum theory would look like today if all this was worked out in 1917. In 1994 Predrag Cvitanović gave a talk in Seattle about helium and cycle expansions to—inter alia—Hans Bethe, who loved it so much that after the talk he pulled Predrag aside and they trotted over to Hans' secret place: the best lunch on campus (Business School). Predrag asked: "Would quantum mechanics look different if in 1917 Bohr and Kramers *et al.* figured out how to use the helium classical 3-body dynamics to quantize helium?"

Bethe was very annoyed. He responded with an exasperated look - in Bethe Deutschinglish (if you have ever talked to him, you can do the voice over yourself):

"It would not matter at all!"

Commentary

Remark A.1 Notion of global foliations. For each paper cited in dynamical systems literature, there are many results that went into its development. As an example, take the notion of global foliations that we attribute to Smale. As far as we can trace the idea, it goes back to René Thom; local foliations were already used by Hadamard. Smale attended a seminar of Thom in 1958 or 1959. In that seminar Thom was explaining his notion of transversality. One of Thom's disciples introduced Smale to Brazilian mathematician Peixoto. Peixoto (who had learned the results of the Andronov-Pontryagin school from Lefschetz) was the closest Smale had ever come until then to the Andronov-Pontryagin school. It was from Peixoto that Smale learned about structural stability, a notion that got him enthusiastic about dynamical systems, as it blended well with his topological background. It was from discussions with Peixoto that Smale got the problems in dynamical systems that lead him to his 1960 paper on Morse inequalities. The next year Smale published his result on the hyperbolic structure of the non-wandering set. Smale was not the first to consider a hyperbolic point, Poincaré had already done that; but Smale was the first to introduce a global hyperbolic structure. By 1960 Smale was already lecturing on the horseshoe as a structurally stable dynamical system with an infinity of periodic points and promoting his global viewpoint. (R. Mainieri)

Remark A.2 Levels of ergodicity. In the mid 1970's A. Katok and Ya.B. Pesin tried to use geometry to establish positive Lyapunov exponents. A. Katok and J.-M. Strelcyn carried out the program and developed a theory of general dynamical systems with singularities. They studied uniformly hyperbolic systems (as strong as Anosov's), but with sets of singularities. Under iterations a dense set of points hits the singularities. Even more important are the points that never hit the singularity set. In order to establish some control over how they approach the set, one looks at trajectories that approach the set by some given ϵ^n , or faster.

Ya.G. Sinai, L. Bunimovich and N.I. Chernov studied the geometry of billiards in a very detailed way. A. Katok and Ya.B. Pesin's idea was much more robust: look at the discontinuity set, take an ϵ neighborhood around it. Given that the Lebesgue measure is ϵ^α and the stability grows not faster than $(\text{distance})^n$. A. Katok and J.-M. Strelcyn proved that the Lyapunov exponent is non-zero.

In mid 1980's Ya.B. Pesin studied the dissipative case. Now the problem has no invariant Lebesgue measure. Assuming uniform hyperbolicity, with singularities, and tying together Lebesgue measure and discontinuities, and given that the stability grows not faster than $(\text{distance})^n$, Ya.B. Pesin proved that the Lyapunov exponent is non-zero, and that SRB measure exists. He also proved that the Lorenz, Lozi and Byelikh attractors satisfy these conditions.

In the systems that are uniformly hyperbolic, all trouble is in differentials. For the Hénon attractor, already the differentials are nonhyperbolic. The points do not separate uniformly, but the analogue of the singularity set can be obtained by excising the regions that do not separate. Hence there are 3 levels of ergodic systems:

1. Anosov flow

2. Anosov flow + singularity set: For the Hamiltonian systems the general case is studied by A. Katok and J.-M. Strelcyn, and the billiards case by Ya.G. Sinai and L. Bunimovich. The dissipative case is studied by Ya.B. Pesin.
3. Hénon case: The first proof was given by M. Benedicks and L. Carleson [28]. A more readable proof is given in M. Benedicks and L.-S. Young [21].

(based on Ya.B. Pesin's comments)

Remark A.3 Einstein did it? The first hint that chaos is afoot in quantum mechanics was given in a note by A. Einstein [22]. The total discussion is a one sentence remark. Einstein being Einstein, this one sentence has been deemed sufficient to give him the credit for being the pioneer of quantum chaos [28, 29]. We asked about the paper two people from that era, Sir Rudolf Peierls and Abraham Pais; neither had any recollection of the 1917 article. However, Theo Geisel has unearthed a reference that shows that in early 20s Born did have a study group meeting in his house that studied Poincaré's *Méchanique Céleste* [22]. In 1954 Fritz Reiche, who had previously followed Einstein as professor of physics in Breslau (now Wroclaw, Poland), pointed out to J.B. Keller that Keller's geometrical semiclassical quantization was anticipated by the long forgotten paper by A. Einstein [22]. In this way an important paper written by the physicist who at the time was the president of German Physical Society, and the most famous scientist of his time, came to be referred to for the first time by Keller [30], 41 years later. But before Ian Percival included the topological phase, and Wintgen and students recycled the Helium atom, knowing *Méchanique Céleste* was not enough to complete Bohr's original program.

Remark A.4 Berry-Keating conjecture. A very appealing proposal in the context of semiclassical quantization is due to M. Berry and J. Keating [33]. The idea is to improve cycle expansions by imposing unitarity as a functional equation ansatz. The cycle expansions that they use are the same as the original ones [2, 1] described above, but the philosophy is quite different; the claim is that the optimal estimate for low eigenvalues of classically chaotic quantum systems is obtained by taking the real part of the cycle expansion of the semiclassical zeta function, cut off at the appropriate cycle length. M. Sieber, G. Tanner and D. Wintgen, and P. Dahlqvist find that their numerical results support this claim; F. Christiansen and P. Cvitanović do not find any evidence in their numerical results. The usual Riemann-Siegel formulas exploit the self-duality of the Riemann and other zeta functions, but there is no evidence of such symmetry for generic Hamiltonian flows. Also from the point of hyperbolic dynamics discussed above, proposal in its current form belongs to the category of crude cycle expansions; the cycles are cut off by a single external criterion, such as the maximal cycle time, with no regard for the topology and the curvature corrections. While the functional equation conjecture is not in its final form yet, it is very intriguing and fruitful research inspiration.

The real life challenge are generic dynamical flows, which fit neither of extreme idealized settings, Smale horseshoe on one end, and the Riemann zeta function on the other.

Remark A.5 Sources. The tale of appendix A.3, aside from a few personal recollections, is in large part lifted from Abraham Pais' accounts of the demise of the old quantum theory [6, 7], as well as Jammer's account [2]. In August 1994 Dieter Wintgen died in a climbing accident in the Swiss Alps.

References

- [A.1] F. Diacu and P. Holmes, *Celestial Encounters, The Origins of Chaos and Stability* (Princeton Univ. Press, Princeton NJ 1996).
- [A.2] M. Jammer, *The Conceptual Development of Quantum mechanics* (McGraw-Hill, New York 1966).
- [A.3] J. Mehra and H. Rechtenberg, *The Historical Development of the Quantum Theory* (Springer, New York 1982).
- [A.4] M. Born, *Vorlesungen über Atommechanik* (Springer, Berlin 1925). English translation: *The Mechanics of the Atom*, (F. Ungar Publishing Co., New York 1927).
- [A.5] J. G. Leopold and I. Percival, *J. Phys. B*, **13**, 1037 (1980).
- [A.6] A. Pais, *Inward Bound: of Matter and Forces in the Physical World* (Oxford Univ. Press, Oxford 1986).
- [A.7] A. Pais, *Niels Bohr's Times, in Physics, Philosophy and Polity* (Oxford Univ. Press, Oxford 1991).
- [A.8] G.S. Ezra, K. Richter, G. Tanner and D. Wintgen, "Semiclassical cycle expansion for the helium atom," *J. Phys. B* **24**, L413 (1991).
- [A.9] D. Wintgen, K. Richter and G. Tanner, "The semiclassical helium atom," *CHAOS* **2**, 19 (1992).
- [A.10] E. Hopf, "Abzweigung einer periodischen Lösung," *Bereich. Sächs. Acad. Wiss. Leipzig, Math. Phys. Kl.* **94**, 15 (1942); "Bifurcation of a periodic solution from a stationary solution of a system of differential equations," transl. by L. N. Howard and N. Kopell, in *The Hopf bifurcation and its applications*, J. E. Marsden and M. McCracken, eds., pp. 163-193, (Springer-Verlag, New York 1976).
- [A.11] E. Hopf, "A mathematical example displaying features of turbulence," *Commun. Appl. Math.* **1**, 303 (1948).
- [A.12] P. Holmes, J.L. Lumley and G. Berkooz, *Turbulence, Coherent Structures, Dynamical Systems and Symmetry* (Cambridge Univ. Press, Cambridge 1996).
- [A.13] Y. Kuramoto and T. Tsuzuki, "Persistent propagation of concentration waves in dissipative media far from thermal equilibrium," *Progr. Theor. Physics* **55**, 365 (1976).
- [A.14] G.I. Sivashinsky, "Nonlinear analysis of hydrodynamical instability in laminar flames - I. Derivation of basic equations," *Acta Astr.* **4**, 1177 (1977).
- [A.15] D.W. Moore and E.A. Spiegel, "A thermally excited nonlinear oscillator," *Astrophys. J.*, **143**, 871 (1966).

- [A.16] N.H. Baker, D.W. Moore and E.A. Spiegel, *Quar. J. Mech. and Appl. Math.* **24**, 391 (1971).
- [A.17] E.A. Spiegel, *Chaos: a mixed metaphor for turbulence*, *Proc. Roy. Soc.* **A413**, 87 (1987).
- [A.18] M.L. Cartwright and J.E. Littlewood, "On nonlinear differential equations of the second order,"
- [A.19] N. Aubry, P. Holmes, J. L. Lumley and E. Stone, "The dynamics of coherent structures in the wall region of turbulent boundary layer," *J. Fluid Mech.* **192**, 115 (1988).
- [A.20] G.S. Ezra, K. Richter, G. Tanner and D. Wintgen, *J. Phys. B* **24**, L413 (1991).
- [A.21] M. Benedicks and L.-S. Young, "Absolutely continuous invariant measures and random perturbations for certain one-dimensional maps," *Ergod. Theor. Dynam. Syst.* **12**, 13 (1992).
- [A.22] A. Einstein, "On the Quantum Theorem of Sommerfeld and Epstein," p. 443, English translation of "Zum Quantensatz von Sommerfeld und Epstein," *Verh. Deutsch. Phys. Ges.* **19**, 82 (1917), in *The Collected Papers of Albert Einstein*, Volume **6: The Berlin Years: Writings, 1914-1917**, A. Engel, transl. and E. Schucking, (Princeton Univ. Press, Princeton NJ 1997).
- [A.23] J. von Neumann and E. P. Wigner, *Phys. Zeit.* **30**, 467 (1929).
- [A.24] E. P. Wigner, *Group Theory and Its Application to the Quantum Mechanics of Atomic Spectra* (Academic Press, New York 1959).
- [A.25] J. Baez, "[This Week's Finds in Mathematical Physics Week 236.](#)"
- [A.26] A. John Coleman, "Groups and physics – Dogmatic opinions of a senior citizen," *Notices of the AMS* **44**, 8 (1997).
- [A.27] I. Segal, *Bull. Amer. Math. Soc.* **33**, 459 (1996).
- [A.28] M.C. Gutzwiller, *Chaos in Classical and Quantum Mechanics* (Springer, New York 1990).
- [A.29] D. Stone, "1917 Einstein paper," *Physics Today* (15 Sep 2005)
- [A.30] J.B. Keller, "Corrected Bohr-Sommerfeld quantum conditions for nonseparable systems," *Ann. Phys. (N.Y.)* **4**, 180 (1958).
- [A.31] A. Selberg, *J. Ind. Math. Soc.* **20**, 47 (1956).
- [A.32] H.P. McKean, *Comm. Pure and Appl. Math.* **25**, 225 (1972); **27**, 134 (1974).
- [A.33] M.V. Berry and J.P. Keating, *J. Phys. A* **23**, 4839 (1990).

- [A.34] M. V. Berry, “Stokes’ phenomenon; smoothing a Victorian discontinuity,” *Publ. Math. of the Institut des Hautes Études Scientifique* **68**, 211 (1989). MR 90j:58019.
- [A.35] M. V. Berry, “**Exuberant interference: Rainbows, tides, edges, (de)coherence,**” *Phil. Trans. Roy. Soc. Lond. A* **360**, 1023 (2002).
- [A.36] T. Young, “The Bakerian Lecture: On the theory of light and colours,” *Phil. Trans. Roy. Soc.* **92**, 12 (1802).
- [A.37] G. B. Airy, “On the intensity of light in the neighbourhood of a caustic,” *Trans. Camb. Phil. Soc.* **6**, 379 (1838).
- [A.38] G. G. Stokes, “On the numerical calculation of a class of definite integrals and infinite series,” *Trans. Camb. Phil. Soc.* **9**, 379 (1847).
- [A.39] C. Foias, B. Nicolaenko, G.R. Sell, and R. Témam, “Kuramoto-Sivashinsky equation,” *J. Math. Pures et Appl.* **67**, 197 (1988).
- [A.40] F. Christiansen, P. Cvitanović and V. Putkaradze, “Hopf’s last hope: spatiotemporal chaos in terms of unstable recurrent patterns,” *Nonlinearity* **10**, 55 (1997); [arXiv:chao-dyn/9606016](#).
- [A.41] Y. Lan and P. Cvitanović, “Variational method for finding periodic orbits in a general flow,” *Phys. Rev. E* **69** 016217 (2004); [arXiv:nlin.CD/0308008](#)
- [A.42] J. F. Gibson, *Movies of plane Couette* (Georgia Tech, 2009); [ChaosBook.orgtutorials](#).

Appendix B

Linear stability

Mopping up operations are the activities that engage most scientists throughout their careers.

— Thomas Kuhn, *The Structure of Scientific Revolutions*

THE SUBJECT OF LINEAR ALGEBRA generates innumerable tomes of its own, and is way beyond what we can exhaustively cover. Here we recapitulate a few essential concepts that ChaosBook relies on. The punch line is Eq. (B.25):

Hamilton-Cayley equation $\prod(\mathbf{M} - \lambda_i \mathbf{1}) = 0$ associates with each distinct root λ_i of a matrix \mathbf{M} a projection onto i th vector subspace

$$\mathbf{P}_i = \prod_{j \neq i} \frac{\mathbf{M} - \lambda_j \mathbf{1}}{\lambda_i - \lambda_j}.$$

B.1 Linear algebra

In this section we collect a few basic definitions. The reader might prefer going straight to sect. B.2.

Vector space. A set V of elements $\mathbf{x}, \mathbf{y}, \mathbf{z}, \dots$ is called a *vector* (or *linear*) *space* over a field \mathbb{F} if

- (a) *vector addition* “+” is defined in V such that V is an Abelian group under addition, with identity element $\mathbf{0}$;
- (b) the set is *closed* with respect to *scalar multiplication* and vector addition

$$a(\mathbf{x} + \mathbf{y}) = a\mathbf{x} + a\mathbf{y}, \quad a, b \in \mathbb{F}, \quad \mathbf{x}, \mathbf{y} \in V$$

$$\begin{aligned}
(a + b)\mathbf{x} &= a\mathbf{x} + b\mathbf{x} \\
a(b\mathbf{x}) &= (ab)\mathbf{x} \\
1\mathbf{x} &= \mathbf{x}, \quad 0\mathbf{x} = \mathbf{0}.
\end{aligned} \tag{B.1}$$

Here the field \mathbb{F} is either \mathbb{R} , the field of reals numbers, or \mathbb{C} , the field of complex numbers. Given a subset $V_0 \subset V$, the set of all linear combinations of elements of V_0 , or the *span* of V_0 , is also a vector space.

A basis. $\{\mathbf{e}^{(1)}, \dots, \mathbf{e}^{(d)}\}$ is any linearly independent subset of V whose span is V . The number of basis elements d is the *dimension* of the vector space V .

Dual space, dual basis. Under a general linear transformation $g \in GL(n, \mathbb{F})$, the row of basis vectors transforms by right multiplication as $\mathbf{e}^{(j)} = \sum_k (\mathbf{g}^{-1})^j_k \mathbf{e}^{(k)}$, and the column of x_a 's transforms by left multiplication as $x' = \mathbf{g}x$. Under left multiplication the column (row transposed) of basis vectors $\mathbf{e}_{(k)}$ transforms as $\mathbf{e}_{(j)} = (\mathbf{g}^\dagger)^j_k \mathbf{e}_{(k)}$, where the *dual rep* $\mathbf{g}^\dagger = (\mathbf{g}^{-1})^T$ is the transpose of the inverse of \mathbf{g} . This observation motivates introduction of a *dual* representation space \bar{V} , the space on which $GL(n, \mathbb{F})$ acts via the dual rep \mathbf{g}^\dagger .

Definition. If V is a vector representation space, then the *dual space* \bar{V} is the set of all linear forms on V over the field \mathbb{F} .

If $\{\mathbf{e}^{(1)}, \dots, \mathbf{e}^{(d)}\}$ is a basis of V , then \bar{V} is spanned by the *dual basis* $\{\mathbf{e}_{(1)}, \dots, \mathbf{e}_{(d)}\}$, the set of d linear forms $\mathbf{e}_{(k)}$ such that

$$\mathbf{e}_{(j)} \cdot \mathbf{e}^{(k)} = \delta_j^k,$$

where δ_j^k is the Kronecker symbol, $\delta_j^k = 1$ if $j = k$, and zero otherwise. The components of dual representation space vectors $\bar{y} \in \bar{V}$ will here be distinguished by upper indices

$$(y^1, y^2, \dots, y^n). \tag{B.2}$$

They transform under $GL(n, \mathbb{F})$ as

$$y'^a = (\mathbf{g}^\dagger)^a_b y^b. \tag{B.3}$$

For $GL(n, \mathbb{F})$ no complex conjugation is implied by the \dagger notation; that interpretation applies only to unitary subgroups $U(n) \subset GL(n, \mathbb{C})$. In the index notation, \mathbf{g} can be distinguished from \mathbf{g}^\dagger by keeping track of the relative ordering of the indices,

$$(\mathbf{g})^b_a \rightarrow g_a^b, \quad (\mathbf{g}^\dagger)^b_a \rightarrow g^b_a. \tag{B.4}$$

Algebra. A set of r elements \mathbf{t}_α of a vector space \mathcal{T} forms an algebra if, in addition to the vector addition and scalar multiplication,

- (a) the set is *closed* with respect to multiplication $\mathcal{T} \cdot \mathcal{T} \rightarrow \mathcal{T}$, so that for any two elements $\mathbf{t}_\alpha, \mathbf{t}_\beta \in \mathcal{T}$, the product $\mathbf{t}_\alpha \cdot \mathbf{t}_\beta$ also belongs to \mathcal{T} :

$$\mathbf{t}_\alpha \cdot \mathbf{t}_\beta = \sum_{\gamma=0}^{r-1} \tau_{\alpha\beta}^\gamma \mathbf{t}_\gamma, \quad \tau_{\alpha\beta}^\gamma \in \mathbb{C}; \quad (\text{B.5})$$

- (b) the multiplication operation is *distributive*:

$$\begin{aligned} (\mathbf{t}_\alpha + \mathbf{t}_\beta) \cdot \mathbf{t}_\gamma &= \mathbf{t}_\alpha \cdot \mathbf{t}_\gamma + \mathbf{t}_\beta \cdot \mathbf{t}_\gamma \\ \mathbf{t}_\alpha \cdot (\mathbf{t}_\beta + \mathbf{t}_\gamma) &= \mathbf{t}_\alpha \cdot \mathbf{t}_\beta + \mathbf{t}_\alpha \cdot \mathbf{t}_\gamma. \end{aligned}$$

The set of numbers $\tau_{\alpha\beta}^\gamma$ are called the *structure constants*. They form a matrix rep of the algebra,

$$(\mathbf{t}_\alpha)_\beta^\gamma \equiv \tau_{\alpha\beta}^\gamma, \quad (\text{B.6})$$

whose dimension is the dimension r of the algebra itself.

Depending on what further assumptions one makes on the multiplication, one obtains different types of algebras. For example, if the multiplication is associative

$$(\mathbf{t}_\alpha \cdot \mathbf{t}_\beta) \cdot \mathbf{t}_\gamma = \mathbf{t}_\alpha \cdot (\mathbf{t}_\beta \cdot \mathbf{t}_\gamma),$$

the algebra is *associative*. Typical examples of products are the *matrix product*

$$(\mathbf{t}_\alpha \cdot \mathbf{t}_\beta)_a^c = (t_\alpha)_a^b (t_\beta)_b^c, \quad \mathbf{t}_\alpha \in V \otimes \bar{V}, \quad (\text{B.7})$$

and the *Lie product*

$$(\mathbf{t}_\alpha \cdot \mathbf{t}_\beta)_a^c = (t_\alpha)_a^b (t_\beta)_b^c - (t_\alpha)_c^b (t_\beta)_b^a, \quad \mathbf{t}_\alpha \in V \otimes \bar{V} \quad (\text{B.8})$$

which defines a *Lie algebra*.

B.2 Eigenvalues and eigenvectors

Eigenvalues of a $[d \times d]$ matrix \mathbf{M} are the roots of its characteristic polynomial

$$\det(\mathbf{M} - \lambda \mathbf{1}) = \prod (\lambda_i - \lambda) = 0. \quad (\text{B.9})$$

Given a nonsingular matrix \mathbf{M} , with all $\lambda_i \neq 0$, acting on d -dimensional vectors \mathbf{x} , we would like to determine *eigenvectors* $\mathbf{e}^{(i)}$ of \mathbf{M} on which \mathbf{M} acts by scalar multiplication by eigenvalue λ_i

$$\mathbf{M}\mathbf{e}^{(i)} = \lambda_i\mathbf{e}^{(i)}. \quad (\text{B.10})$$

If $\lambda_i \neq \lambda_j$, $\mathbf{e}^{(i)}$ and $\mathbf{e}^{(j)}$ are linearly independent. There are at most d distinct eigenvalues and eigenspaces, which we assume have been computed by some method, and ordered by their real parts, $\text{Re } \lambda_i \geq \text{Re } \lambda_{i+1}$.

If all eigenvalues are distinct $\mathbf{e}^{(j)}$ are d linearly independent vectors which can be used as a (non-orthogonal) basis for any d -dimensional vector $\mathbf{x} \in \mathbb{R}^d$

$$\mathbf{x} = x_1 \mathbf{e}^{(1)} + x_2 \mathbf{e}^{(2)} + \cdots + x_d \mathbf{e}^{(d)}. \quad (\text{B.11})$$

From (B.10) it follows that

$$(\mathbf{M} - \lambda_i \mathbf{1}) \mathbf{e}^{(j)} = (\lambda_j - \lambda_i) \mathbf{e}^{(j)},$$

matrix $(\mathbf{M} - \lambda_i \mathbf{1})$ annihilates $\mathbf{e}^{(i)}$, the product of all such factors annihilates any vector, and the matrix \mathbf{M} satisfies its characteristic equation (B.9),

$$\prod_{i=1}^d (\mathbf{M} - \lambda_i \mathbf{1}) = 0. \quad (\text{B.12})$$

This humble fact has a name: the Hamilton-Cayley theorem. If we delete one term from this product, we find that the remainder projects \mathbf{x} onto the corresponding eigenspace:

$$\prod_{j \neq i} (\mathbf{M} - \lambda_j \mathbf{1}) \mathbf{x} = \prod_{j \neq i} (\lambda_i - \lambda_j) x_i \mathbf{e}^{(i)}.$$

Dividing through by the $(\lambda_i - \lambda_j)$ factors yields the *projection operators*

$$\mathbf{P}_i = \prod_{j \neq i} \frac{\mathbf{M} - \lambda_j \mathbf{1}}{\lambda_i - \lambda_j}, \quad (\text{B.13})$$

which are *orthogonal* and *complete*:

$$\mathbf{P}_i \mathbf{P}_j = \delta_{ij} \mathbf{P}_j, \quad (\text{no sum on } j), \quad \sum_{i=1}^r \mathbf{P}_i = \mathbf{1}. \quad (\text{B.14})$$

It follows from the characteristic equation (B.12) that λ_i is the eigenvalue of \mathbf{M} on \mathbf{P}_i subspace:

$$\mathbf{M}\mathbf{P}_i = \lambda_i\mathbf{P}_i \quad (\text{no sum on } i). \quad (\text{B.15})$$

Using $\mathbf{M} = \mathbf{M}\mathbf{1}$ and completeness relation (B.14) we can rewrite \mathbf{M} as

$$\mathbf{M} = \lambda_1\mathbf{P}_1 + \lambda_2\mathbf{P}_2 + \cdots + \lambda_d\mathbf{P}_d. \quad (\text{B.16})$$

Any matrix function $f(\mathbf{M})$ takes the scalar value $f(\lambda_i)$ on the \mathbf{P}_i subspace, $f(\mathbf{M})\mathbf{P}_i = f(\lambda_i)\mathbf{P}_i$, and is thus easily evaluated through its *spectral decomposition*

$$f(\mathbf{M}) = \sum_i f(\lambda_i)\mathbf{P}_i. \quad (\text{B.17})$$

This, of course, is the reason why anyone but a fool works with irreducible reps: they reduce matrix (AKA “operator”) evaluations to manipulations with numbers.

By (B.10) every column of \mathbf{P}_i is proportional to a right eigenvector $\mathbf{e}^{(i)}$, and its every row to a left eigenvector $\mathbf{e}_{(i)}$. In general, neither set is orthogonal, but by the idempotence condition (B.14), they are mutually orthogonal,

$$\mathbf{e}_{(i)} \cdot \mathbf{e}^{(j)} = c \delta_i^j. \quad (\text{B.18})$$

The non-zero constant c is convention dependent and not worth fixing, unless you feel nostalgic about Clebsch-Gordan coefficients. We shall set $c = 1$. Then it is convenient to collect all left and right eigenvectors into a single matrix as follows.

Fundamental matrix. The set of solutions $x(t) = J^t(x_0)x_0$ for a system of homogeneous linear differential equations $\dot{x}(t) = A(t)x(t)$ of order 1 and dimension d forms a d -dimensional vector space. A basis $\{\mathbf{e}^{(1)}(t), \dots, \mathbf{e}^{(d)}(t)\}$ for this vector space is called a *fundamental system*. Every solution $x(t)$ can be written as

$$x(t) = \sum_{i=1}^d c_i \mathbf{e}^{(i)}(t).$$

The $[d \times d]$ matrix $\mathbf{F}_{ij}^{-1} = \mathbf{e}_i^{(j)}$ whose columns are the right eigenvectors of J

$$\mathbf{F}(t)^{-1} = (\mathbf{e}^{(1)}(t), \dots, \mathbf{e}^{(d)}(t)), \quad \mathbf{F}(t)^T = (\mathbf{e}_{(1)}(t), \dots, \mathbf{e}_{(d)}(t)) \quad (\text{B.19})$$

is the inverse of a *fundamental matrix*.

Jacobian matrix. The Jacobian matrix $J^f(x_0)$ is the linear approximation to a differentiable function $f^f(x_0)$, describing the orientation of a tangent plane to the function at a given point and the amount of local rotation and shearing caused by the transformation. The inverse of the Jacobian matrix of a function is the Jacobian matrix of the inverse function. If f is a map from d -dimensional space to itself, the Jacobian matrix is a square matrix, whose determinant we refer to as the ‘Jacobian.’

The Jacobian matrix can be written as transformation from basis at time t_0 to the basis at time t_1 ,

$$J^{t_1-t_0}(x_0) = \mathbf{F}(t_1)\mathbf{F}(t_0)^{-1}. \tag{B.20}$$

Then the matrix form of (B.18) is $\mathbf{F}(t)\mathbf{F}(t)^{-1} = \mathbf{1}$, i.e., for zero time the Jacobian matrix is the identity.

exercise B.1

Example B.1 Fundamental matrix. If A is constant in time, the system (4.2) is autonomous, and the solution is

$$x(t) = e^{At}x(0),$$

where $\exp(At)$ is defined by the Taylor series for $\exp(x)$. As the system is linear, the sum of any two solutions is also a solution. Therefore, given d independent initial conditions, $x_1(0), x_2(0), \dots, x_d(0)$ we can write the solution for an arbitrary initial condition based on its projection on to this set,

$$x(t) = \mathbf{F}(t)\mathbf{F}(0)^{-1}x(0) = e^{At},$$

where $\mathbf{F}(t) = (x_1(t), x_2(t), \dots, x_d(t))$ is a fundamental matrix of the system. (J. Halcrow)

exercise B.1

Example B.2 Complex eigenvalues. As \mathbf{M} has only real entries, it will in general have either real eigenvalues, or complex conjugate pairs of eigenvalues. That is not surprising, but also the corresponding eigenvectors can be either real or complex. All coordinates used in defining a dynamical flow are real numbers, so what is the meaning of a complex eigenvector?

If λ_k, λ_{k+1} eigenvalues that lie within a diagonal $[2 \times 2]$ sub-block $\mathbf{M}' \subset \mathbf{M}$ form a complex conjugate pair, $\{\lambda_k, \lambda_{k+1}\} = \{\mu + i\omega, \mu - i\omega\}$, the corresponding complex eigenvectors can be replaced by their real and imaginary parts, $\{\mathbf{e}^{(k)}, \mathbf{e}^{(k+1)}\} \rightarrow \{\text{Re } \mathbf{e}^{(k)}, \text{Im } \mathbf{e}^{(k)}\}$. In this 2-dimensional real representation, $\mathbf{M}' \rightarrow \mathbf{N}$, the block \mathbf{N} is a sum of the rescaling \times identity and the generator of $SO(2)$ rotations

$$\mathbf{N} = \begin{pmatrix} \mu & -\omega \\ \omega & \mu \end{pmatrix} = \mu \begin{pmatrix} 1 & 0 \\ 0 & 1 \end{pmatrix} + \omega \begin{pmatrix} 0 & -1 \\ 1 & 0 \end{pmatrix}.$$

Trajectories of $\dot{\mathbf{x}} = \mathbf{N}\mathbf{x}$, given by $\mathbf{x}(t) = J^t \mathbf{x}(0)$, where

$$J^t = e^{t\mathbf{N}} = e^{t\mu} \begin{pmatrix} \cos \omega t & -\sin \omega t \\ \sin \omega t & \cos \omega t \end{pmatrix}, \tag{B.21}$$

spiral in/out around $(x, y) = (0, 0)$, see figure 4.4, with the rotation period T and the radial expansion /contraction multiplier along the $\mathbf{e}^{(j)}$ eigen-direction per a turn of the spiral:

$$T = 2\pi/\omega, \quad \Lambda_{\text{radial}} = e^{T\mu}. \quad (\text{B.22})$$

We learn that the typical turnover time scale in the neighborhood of the equilibrium $(x, y) = (0, 0)$ is of order $\approx T$ (and not, let us say, $1000 T$, or $10^{-2}T$).

Error correlation matrix. In the sect. 17.3 calculation of Lyapunov exponents we do not care about the orientation of the vector between a trajectory and its perturbation, but only its magnitude. This magnitude is given by the *error correlation matrix*

$$|J^t(x_0)\delta x_0|^2 = \delta x_0^T (J^t)^T J^t \delta x_0. \quad (\text{B.23})$$

As J is in general not symmetric and not diagonalizable, it is sometimes more convenient to work with the symmetric and diagonalizable matrix $\mathbf{M} = (J^t)^T J^t$, with real positive eigenvalues $\{|\Lambda_1|^2 \geq \dots \geq |\Lambda_d|^2\}$, and a complete orthonormal set of eigenvectors of $\{u_1, \dots, u_d\}$.

Degenerate eigenvalues. While for a matrix with generic real elements all eigenvalues are distinct with probability 1, that is not true in presence of symmetries, or spacial parameter values (bifurcation points). What can one say about situation where d_α eigenvalues are degenerate, $\lambda_\alpha = \lambda_i = \lambda_{i+1} = \dots = \lambda_{i+d_\alpha-1}$? Hamilton-Cayley (B.12) now takes form

$$\prod_{\alpha=1}^r (\mathbf{M} - \lambda_\alpha \mathbf{1})^{d_\alpha} = 0, \quad \sum_{\alpha} d_\alpha = d. \quad (\text{B.24})$$

We distinguish two cases:

M can be brought to diagonal form. The characteristic equation (B.24) can be replaced by the minimal polynomial,

$$\prod_{\alpha=1}^r (\mathbf{M} - \lambda_\alpha \mathbf{1}) = 0, \quad (\text{B.25})$$

where the product includes each distinct eigenvalue only once. Matrix \mathbf{M} acts multiplicatively

$$\mathbf{M} \mathbf{e}^{(\alpha,k)} = \lambda_i \mathbf{e}^{(\alpha,k)}, \quad (\text{B.26})$$

on a d_α -dimensional subspace spanned by a linearly independent set of basis eigenvectors $\{\mathbf{e}^{(\alpha,1)}, \mathbf{e}^{(\alpha,2)}, \dots, \mathbf{e}^{(\alpha,d_\alpha)}\}$. This is the easy case whose discussion we continue in appendix H.2.1. Luckily, if the degeneracy is due to a finite or compact symmetry group, relevant \mathbf{M} matrices can always be brought to such Hermitian, diagonalizable form.

M can only be brought to upper-triangular, Jordan form. This is the messy case, so we only illustrate the key idea in example B.3.

Example B.3 Decomposition of 2-dimensional vector spaces: Enumeration of every possible kind of linear algebra eigenvalue / eigenvector combination is beyond what we can reasonably undertake here. However, enumerating solutions for the simplest case, a general $[2 \times 2]$ non-singular matrix

$$\mathbf{M} = \begin{pmatrix} M_{11} & M_{12} \\ M_{21} & M_{22} \end{pmatrix}.$$

takes us a long way toward developing intuition about arbitrary finite-dimensional matrices. The eigenvalues

$$\lambda_{1,2} = \frac{1}{2} \text{tr} \mathbf{M} \pm \frac{1}{2} \sqrt{(\text{tr} \mathbf{M})^2 - 4 \det \mathbf{M}} \quad (\text{B.27})$$

are the roots of the characteristic (secular) equation (B.9):

$$\begin{aligned} \det(\mathbf{M} - \lambda \mathbf{1}) &= (\lambda_1 - \lambda)(\lambda_2 - \lambda) \\ &= \lambda^2 - \text{tr} \mathbf{M} \lambda + \det \mathbf{M} = 0. \end{aligned}$$

Distinct eigenvalues case has already been described in full generality. The left/right eigenvectors are the rows/columns of projection operators

$$P_1 = \frac{\mathbf{M} - \lambda_2 \mathbf{1}}{\lambda_1 - \lambda_2}, \quad P_2 = \frac{\mathbf{M} - \lambda_1 \mathbf{1}}{\lambda_2 - \lambda_1}, \quad \lambda_1 \neq \lambda_2. \quad (\text{B.28})$$

Degenerate eigenvalues. If $\lambda_1 = \lambda_2 = \lambda$, we distinguish two cases: (a) \mathbf{M} can be brought to diagonal form. This is the easy case whose discussion in any dimension we continue in appendix H.2.1. (b) \mathbf{M} can be brought to Jordan form, with zeros everywhere except for the diagonal, and some 1's directly above it; for a $[2 \times 2]$ matrix the Jordan form is

$$\mathbf{M} = \begin{pmatrix} \lambda & 1 \\ 0 & \lambda \end{pmatrix}, \quad \mathbf{e}^{(1)} = \begin{pmatrix} 1 \\ 0 \end{pmatrix}, \quad \mathbf{v}^{(2)} = \begin{pmatrix} 0 \\ 1 \end{pmatrix}.$$

$\mathbf{v}^{(2)}$ helps span the 2-dimensional space, $(\mathbf{M} - \lambda)^2 \mathbf{v}^{(2)} = 0$, but is not an eigenvector, as $\mathbf{M} \mathbf{v}^{(2)} = \lambda \mathbf{v}^{(2)} + \mathbf{e}^{(1)}$. For every such Jordan $[d_\alpha \times d_\alpha]$ block there is only one eigenvector per block. Noting that

$$\mathbf{M}^m = \begin{pmatrix} \lambda^m & m\lambda^{m-1} \\ 0 & \lambda^m \end{pmatrix},$$

we see that instead of acting multiplicatively on \mathbb{R}^2 , Jacobian matrix $J^t = \exp(t\mathbf{M})$

$$e^{t\mathbf{M}} \begin{pmatrix} u \\ v \end{pmatrix} = e^{t\lambda} \begin{pmatrix} u + tv \\ v \end{pmatrix} \tag{B.29}$$

picks up a power-law correction. That spells trouble (logarithmic term $\ln t$ if we bring the extra term into the exponent).

Example B.4 Projection operator decomposition in 2 dimensions: Let's illustrate how the distinct eigenvalues case works with the $[2 \times 2]$ matrix

$$\mathbf{M} = \begin{pmatrix} 4 & 1 \\ 3 & 2 \end{pmatrix}.$$

Its eigenvalues $\{\lambda_1, \lambda_2\} = \{5, 1\}$ are the roots of (B.27):

$$\det(\mathbf{M} - \lambda\mathbf{1}) = \lambda^2 - 6\lambda + 5 = (\lambda - 5)(\lambda - 1) = 0.$$

That \mathbf{M} satisfies its secular equation (Hamilton-Cayley theorem) can be verified by explicit calculation:

$$\begin{pmatrix} 4 & 1 \\ 3 & 2 \end{pmatrix}^2 - 6 \begin{pmatrix} 4 & 1 \\ 3 & 2 \end{pmatrix} + 5 \begin{pmatrix} 1 & 0 \\ 0 & 1 \end{pmatrix} = \begin{pmatrix} 0 & 0 \\ 0 & 0 \end{pmatrix}.$$

Associated with each root λ_i is the projection operator (B.28)

$$P_1 = \frac{1}{4}(\mathbf{M} - \mathbf{1}) = \frac{1}{4} \begin{pmatrix} 3 & 1 \\ 3 & 1 \end{pmatrix} \tag{B.30}$$

$$P_2 = \frac{1}{4}(\mathbf{M} - 5 \cdot \mathbf{1}) = \frac{1}{4} \begin{pmatrix} 1 & -1 \\ -3 & 3 \end{pmatrix}. \tag{B.31}$$

Matrices \mathbf{P}_i are orthonormal and complete, The dimension of the i th subspace is given by $d_i = \text{tr } \mathbf{P}_i$; in case at hand both subspaces are 1-dimensional. From the characteristic equation it follows that \mathbf{P}_i satisfies the eigenvalue equation $\mathbf{M}\mathbf{P}_i = \lambda_i\mathbf{P}_i$. Two consequences are immediate. First, we can easily evaluate any function of \mathbf{M} by spectral decomposition, for example

$$\mathbf{M}^7 - 3 \cdot \mathbf{1} = (5^7 - 3)\mathbf{P}_1 + (1 - 3)\mathbf{P}_2 = \begin{pmatrix} 58591 & 19531 \\ 58593 & 19529 \end{pmatrix}.$$

Second, as \mathbf{P}_i satisfies the eigenvalue equation, its every column is a right eigenvector, and every row a left eigenvector. Picking first row/column we get the eigenvectors:

$$\begin{aligned} \{\mathbf{e}^{(1)}, \mathbf{e}^{(2)}\} &= \left\{ \begin{pmatrix} 1 \\ 1 \end{pmatrix}, \begin{pmatrix} 1 \\ -3 \end{pmatrix} \right\} \\ \{\mathbf{e}_{(1)}, \mathbf{e}_{(2)}\} &= \{(3 \ 1), (1 \ -1)\}, \end{aligned}$$

with overall scale arbitrary. The matrix is not hermitian, so $\{\mathbf{e}^{(j)}\}$ do not form an orthogonal basis. The left-right eigenvector dot products $\mathbf{e}_{(j)} \cdot \mathbf{e}^{(k)}$, however, are orthogonal as in (B.18), by inspection.

Example B.5 Computing matrix exponentials. If A is diagonal (the system is uncoupled), then e^{tA} is given by

$$\exp \begin{pmatrix} \lambda_1 t & & & \\ & \lambda_2 t & & \\ & & \ddots & \\ & & & \lambda_d t \end{pmatrix} = \begin{pmatrix} e^{\lambda_1 t} & & & \\ & e^{\lambda_2 t} & & \\ & & \ddots & \\ & & & e^{\lambda_d t} \end{pmatrix}.$$

If A is diagonalizable, $A = FDF^{-1}$, where D is the diagonal matrix of the eigenvalues of A and F is the matrix of corresponding eigenvectors, the result is simple: $A^n = (FDF^{-1})(FDF^{-1}) \dots (FDF^{-1}) = FD^n F^{-1}$. Inserting this into the Taylor series for e^x gives $e^{At} = F e^{Dt} F^{-1}$.

But A may not have d linearly independent eigenvectors, making F singular and forcing us to take a different route. To illustrate this, consider $[2 \times 2]$ matrices. For any linear system in \mathbb{R}^2 , there is a similarity transformation

$$B = U^{-1}AU,$$

where the columns of U consist of the generalized eigenvectors of A such that B has one of the following forms:

$$B = \begin{pmatrix} \lambda & 0 \\ 0 & \mu \end{pmatrix}, \quad B = \begin{pmatrix} \lambda & 1 \\ 0 & \lambda \end{pmatrix}, \quad B = \begin{pmatrix} \mu & -\omega \\ \omega & \mu \end{pmatrix}.$$

These three cases, called normal forms, correspond to A having (1) distinct real eigenvalues, (2) degenerate real eigenvalues, or (3) a complex pair of eigenvalues. It follows that

$$e^{Bt} = \begin{pmatrix} e^{\lambda t} & 0 \\ 0 & e^{\mu t} \end{pmatrix}, \quad e^{Bt} = e^{\lambda t} \begin{pmatrix} 1 & t \\ 0 & 1 \end{pmatrix}, \quad e^{Bt} = e^{\mu t} \begin{pmatrix} \cos bt & -\sin bt \\ \sin bt & \cos bt \end{pmatrix},$$

and $e^{At} = U e^{Bt} U^{-1}$. What we have done is classify all $[2 \times 2]$ matrices as belonging to one of three classes of geometrical transformations. The first case is scaling, the second is a shear, and the third is a combination of rotation and scaling. The generalization of these normal forms to \mathbb{R}^d is called the Jordan normal form. (J. Halcrow)

B.3 Eigenspectra: what to make out of them?

Well Mack the Finger said to Louie the King
 I got forty red white and blue shoe strings
 And a thousand telephones that don't ring
 Do you know where I can get rid of these things?
 — Bob Dylan, Highway 61 Revisited

Table B.1, taken from ref. [1], is an example of how to tabulate the leading Floquet eigenvalues of the stability matrix of an equilibrium or relative equilibrium. The isotropy subgroup $G_{EQ}^{(j)}$ of the corresponding eigenfunction should be indicated. If the isotropy is trivial, $G_{EQ}^{(j)} = \{e\}$, it is omitted from the table. The isotropy subgroup G_{EQ} of the solution itself needs to be noted, and for relative

Table B.1: The first 27 least stable Floquet exponents $\lambda = \mu \pm i\omega$ of equilibrium EQ_5 for plane Couette flow, $Re = 400$. The exponents are ordered by the decreasing real part. The two zero exponents, to the numerical precision of our computation, arise from the two translational symmetries. For details, see ref. [1].

j	$\mu_{EQ_5}^{(j)}$	$\omega_{EQ_5}^{(j)}$	$s_1 s_2 s_3$
1,2	0.07212161	0.04074989	S S S
3	0.06209526		S A A
4	0.06162059		A S A
5,6	0.02073075	0.07355143	S S S
7	0.009925378		S A A
8,9	0.009654012	0.04551274	A A S
10,11	0.009600794	0.2302166	S A A
12,13	1.460798e-06	1.542103e-06	- - A
14,15	-0.0001343539	0.231129	A A S
16	-0.006178861		A S A
17,18	-0.007785718	0.1372092	A A S
19	-0.01064716		S A A
20,21	-0.01220116	0.2774336	S S S
22,23	-0.01539667	0.2775381	S A A
24,25	-0.03451081	0.08674062	A S A
26,27	-0.03719139	0.215319	S A A

equilibrium (10.30) the velocity c along the group orbit. In addition, if the least stable (i.e., the most unstable) eigenvalue is complex, it is helpful to state the period of the spiral-out motion (or spiral-in, if stable), $T_{EQ} = 2\pi/\omega_{EQ}^{(1)}$.

Table B.2, taken from ref. [3], is an example of how to tabulate the leading Floquet exponents of the monodromy matrix of an periodic orbit or relative periodic orbit. For a periodic orbit one states the period T_p , $\Lambda_p = \prod \Lambda_{p,e}$, and the isotropy group G_p of the orbit; for a relative periodic orbit (10.35) one states in addition the shift parameters $\theta = (\theta_1, \theta_2, \dots, \theta_N)$. Λ_p , the product of expanding Floquet multipliers (5.7) is useful, as $1/|\Lambda_p|$ is the geometric weight of cycle p in a cycle expansion (remember that each complex eigenvalue contributes twice). We often do care about $\sigma_p^{(j)} = \Lambda_{p,j}/|\Lambda_{p,j}| \in \{+1, -1\}$, the sign of the j th Floquet multiplier, or, if $\Lambda_{p,j}$ is complex, its phase $T_p \omega_p^{(j)}$.

Surveying this multitude of equilibrium and Floquet exponents is aided by a plot of the complex exponent plane (μ, ω) . An example are the eigenvalues of equilibrium EQ_8 from ref. [2], plotted in figure B.1. To decide how many of the these are “physical” in the PDE case (where number of exponents is always infinite, in principle), it is useful to look at the $(j, \mu^{(j)})$ plot. However, intelligent choice of the j -axis units can be tricky for high-dimensional problems. For Kuramoto-Sivashinsky system the correct choice are the wave-numbers which, due to the $O(2)$ symmetry, come in pairs. For plane Couette flow the good choice is not known as yet; one needs to group $O(2) \times O(2)$ wave-numbers, as well as take care of the wall-normal node counting.

Figure B.1: Eigenvalues of the plane Couette flow equilibrium EQ_8 , plotted according to their isotropy groups: ● + + +, the S -invariant subspace, ► + - -, ◀ - + -, and ▲ - - +, where \pm symbols stand for symmetric/antisymmetric under symmetry operation s_1, s_2 , and s_3 respectively, defined in ref. [2]. For tables of numerical values of stability eigenvalues see Channelflow.org.

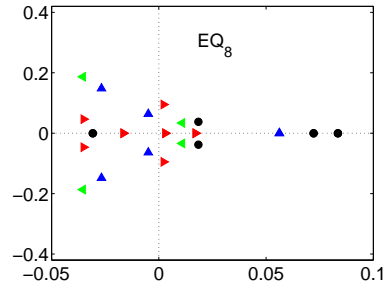


Table B.2: The first 13 least stable Floquet exponents $\lambda = \mu \pm i\omega$ of periodic orbit $p = P59.77$ for plane Couette flow, $Re = 400$, together with the symmetries of corresponding eigenvectors. The eigenvalues are ordered by the decreasing real part. The one zero eigenvalue, to the numerical precision of our computation, arises from the spanwise translational $SO(2)$ symmetry of this periodic orbit. For details, see ref. [3].

j	$\sigma_p^{(j)}$	$\mu_p^{(j)}$	$\omega_p^{(j)}$	$G_p^{(j)}$
1,2		0.07212161	0.04074989	D_1
3	1	0.06209526		?
4	-1	0.06162059		
5,6		0.02073075	0.07355143	
7	-1	0.009925378		
8,9		0.009654012	0.04551274	
10,11		0.009600794	0.2302166	

B.4 Stability of Hamiltonian flows



(M.J. Feigenbaum and P. Cvitanović)

The symplectic structure of Hamilton’s equations buys us much more than the incompressibility, or the phase space volume conservation alluded to in sect.7.1. The evolution equations for any p, q dependent quantity $Q = Q(q, p)$ are given by (16.32).

In terms of the Poisson brackets, the time evolution equation for $Q = Q(q, p)$ is given by (16.34). We now recast the symplectic condition (7.11) in a form convenient for using the symplectic constraints on M . Writing $x(t) = \mathcal{X} = [p', q']$ and the Jacobian matrix and its inverse

$$M = \begin{pmatrix} \frac{\partial q'}{\partial q} & \frac{\partial q'}{\partial p} \\ \frac{\partial p'}{\partial q} & \frac{\partial p'}{\partial p} \end{pmatrix}, \quad M^{-1} = \begin{pmatrix} \frac{\partial q}{\partial q'} & \frac{\partial q}{\partial p'} \\ \frac{\partial p}{\partial q'} & \frac{\partial p}{\partial p'} \end{pmatrix}, \quad (\text{B.32})$$

we can spell out the symplectic invariance condition (7.11):

$$\begin{aligned} \frac{\partial q'_k}{\partial q_i} \frac{\partial p'_k}{\partial q_j} - \frac{\partial p'_k}{\partial q_i} \frac{\partial q'_k}{\partial q_j} &= 0 \\ \frac{\partial q'_k}{\partial p_i} \frac{\partial p'_k}{\partial p_j} - \frac{\partial p'_k}{\partial p_i} \frac{\partial q'_k}{\partial p_j} &= 0 \\ \frac{\partial q'_k}{\partial q_i} \frac{\partial p'_k}{\partial p_j} - \frac{\partial p'_k}{\partial q_i} \frac{\partial q'_k}{\partial p_j} &= \delta_{ij}. \end{aligned} \quad (\text{B.33})$$

From (7.18) we obtain

$$\frac{\partial q_i}{\partial q'_j} = \frac{\partial p'_j}{\partial p_i}, \quad \frac{\partial p_i}{\partial p'_j} = \frac{\partial q'_j}{\partial q_i}, \quad \frac{\partial q_i}{\partial p'_j} = -\frac{\partial q'_j}{\partial p_i}, \quad \frac{\partial p_i}{\partial q'_j} = -\frac{\partial p'_j}{\partial q_i}. \quad (\text{B.34})$$

Taken together, (B.34) and (B.33) imply that the flow conserves the $\{p, q\}$ Poisson brackets

$$\begin{aligned} \{q_i, q_j\} &= \frac{\partial q_i}{\partial p'_k} \frac{\partial q_j}{\partial q'_k} - \frac{\partial q_j}{\partial p'_k} \frac{\partial q_i}{\partial q'_k} = 0 \\ \{p_i, p_j\} &= 0, \quad \{p_i, q_j\} = \delta_{ij}, \end{aligned} \quad (\text{B.35})$$

i.e., the transformations induced by a Hamiltonian flow are *canonical*, preserving the form of the equations of motion. The first two relations are symmetric under i, j interchange and yield $D(D-1)/2$ constraints each; the last relation yields D^2 constraints. Hence only $(2D)^2 - 2D(D-1)/2 - D^2 = d(2D+1)$ elements of M are linearly independent, as it behooves group elements of the symplectic group $Sp(2D)$.

B.5 Monodromy matrix for Hamiltonian flows



(G. Tanner)

It is not the Jacobian matrix J of the flow (4.6), but the *monodromy matrix* M , which enters the trace formula. This matrix gives the time dependence of a displacement perpendicular to the flow on the energy manifold. Indeed, we discover some trivial parts in the Jacobian matrix J . An initial displacement in the direction of the flow $x = \omega \nabla H(x)$ transfers according to $\delta x(t) = x(t) \delta t$ with δt time independent. The projection of any displacement on δx on $\nabla H(x)$ is constant, i.e., $\nabla H(x(t)) \delta x(t) = \delta E$. We get the equations of motion for the monodromy matrix directly choosing a suitable local coordinate system on the orbit $x(t)$ in form of the (non singular) transformation $\mathbf{U}(x(t))$:

$$\tilde{J}(x(t)) = \mathbf{U}^{-1}(x(t)) J(x(t)) \mathbf{U}(x(0)) \quad (\text{B.36})$$

These lead to

$$\begin{aligned} \dot{\tilde{J}} &= \tilde{\mathbf{L}} \tilde{J} \\ \text{with } \tilde{\mathbf{L}} &= \mathbf{U}^{-1}(\mathbf{L}\mathbf{U} - \dot{\mathbf{U}}) \end{aligned} \quad (\text{B.37})$$

Note that the properties a) – c) are only fulfilled for \tilde{J} and $\tilde{\mathbf{L}}$ if \mathbf{U} itself is symplectic.

Choosing $x_E = \nabla H(t)/|\nabla H(t)|^2$ and x_t as local coordinates uncovers the two trivial eigenvalues 1 of the transformed matrix in (B.36) at any time t . Setting $\mathbf{U} = (x_t^T, x_E^T, x_1^T, \dots, x_{2d-2}^T)$ gives

$$\tilde{\mathbf{J}} = \begin{pmatrix} 1 & * & * & \dots & * \\ 0 & 1 & 0 & \dots & 0 \\ 0 & * & & & \\ \vdots & \vdots & & \mathbf{M} & \\ 0 & * & & & \end{pmatrix}; \quad \tilde{\mathbf{L}} = \begin{pmatrix} 0 & * & * & \dots & * \\ 0 & 0 & 0 & \dots & 0 \\ 0 & * & & & \\ \vdots & \vdots & & \mathbf{I} & \\ 0 & * & & & \end{pmatrix}, \quad (\text{B.38})$$

The matrix \mathbf{M} is now the monodromy matrix and the equation of motion are given by

$$\dot{\mathbf{M}} = \mathbf{I} \mathbf{M}. \quad (\text{B.39})$$

The vectors x_1, \dots, x_{2d-2} must span the space perpendicular to the flow on the energy manifold.

For a system with two degrees of freedom, the matrix $\mathbf{U}(\mathbf{t})$ can be written down explicitly, i.e.,

$$\mathbf{U}(t) = (x_t, x_1, x_E, x_2) = \begin{pmatrix} \dot{x} & -\dot{y} & -\dot{u}/q^2 & -\dot{v}/q^2 \\ \dot{y} & \dot{x} & -\dot{v}/q^2 & \dot{u}/q^2 \\ \dot{u} & \dot{v} & \dot{x}/q^2 & -\dot{y}/q^2 \\ \dot{v} & -\dot{u} & \dot{y}/q^2 & \dot{x}/q^2 \end{pmatrix} \quad (\text{B.40})$$

with $x^T = (x, y, u, v)$ and $q = |\nabla H| = |\dot{x}|$. The matrix \mathbf{U} is non singular and symplectic at every phase space point x , except the equilibrium points $\dot{x} = 0$. The matrix elements for \mathbf{I} are given (B.42). One distinguishes 4 classes of eigenvalues of \mathbf{M} .

- *stable or elliptic*, if $\Lambda = e^{\pm i\pi\nu}$ and $\nu \in]0, 1[$.
- *marginal*, if $\Lambda = \pm 1$.
- *hyperbolic, inverse hyperbolic*, if $\Lambda = e^{\pm\lambda}$, $\Lambda = -e^{\pm\lambda}$.
- *loxodromic*, if $\Lambda = e^{\pm\mu \pm i\omega}$ with μ and ω real. This is the most general case, possible only in systems with 3 or more degree of freedoms.

For 2 degrees of freedom, i.e., \mathbf{M} is a $[2 \times 2]$ matrix, the eigenvalues are determined by

$$\lambda = \frac{\text{tr}(\mathbf{M}) \pm \sqrt{\text{tr}(\mathbf{M})^2 - 4}}{2}, \quad (\text{B.41})$$

i.e., $\text{tr}(\mathbf{M}) = 2$ separates stable and unstable behavior.

The \mathbf{I} matrix elements for the local transformation (B.40) are

$$\begin{aligned}
\tilde{\mathbf{I}}_{11} &= \frac{1}{q} [(h_x^2 - h_y^2 - h_u^2 + h_v^2)(h_{xu} - h_{yv}) + 2(h_x h_y - h_u h_v)(h_{xv} + h_{yu}) \\
&\quad - (h_x h_u + h_y h_v)(h_{xx} + h_{yy} - h_{uu} - h_{vv})] \\
\tilde{\mathbf{I}}_{12} &= \frac{1}{q^2} [(h_x^2 + h_v^2)(h_{yy} + h_{uu}) + (h_y^2 + h_u^2)(h_{xx} + h_{vv}) \\
&\quad - 2(h_x h_u + h_y h_v)(h_{xu} + h_{yv}) - 2(h_x h_y - h_u h_v)(h_{xy} - h_{uv})] \\
\tilde{\mathbf{I}}_{21} &= -(h_x^2 + h_y^2)(h_{uu} + h_{vv}) - (h_u^2 + h_v^2)(h_{xx} + h_{yy}) \\
&\quad + 2(h_x h_u - h_y h_v)(h_{xu} - h_{yv}) + 2(h_x h_v + h_y h_u)(h_{xv} + h_{yu}) \\
\tilde{\mathbf{I}}_{22} &= -\tilde{\mathbf{I}}_{11},
\end{aligned} \tag{B.42}$$

with h_i, h_{ij} is the derivative of the Hamiltonian H with respect to the phase space coordinates and $q = |\nabla H|^2$.

Exercises

B.1. **Real representation of complex eigenvalues.** (Verification of example B.2.) λ_k, λ_{k+1} eigenvalues form a complex conjugate pair, $\{\lambda_k, \lambda_{k+1}\} = \{\mu + i\omega, \mu - i\omega\}$. Show that

- (a) corresponding projection operators are complex conjugates of each other,

$$\mathbf{P} = \mathbf{P}_k, \quad \mathbf{P}^* = \mathbf{P}_{k+1},$$

where we denote \mathbf{P}_k by \mathbf{P} for notational brevity.

- (b) \mathbf{P} can be written as

$$\mathbf{P} = \frac{1}{2}(\mathbf{R} + i\mathbf{Q}),$$

where $\mathbf{R} = \mathbf{P}_k + \mathbf{P}_{k+1}$ and \mathbf{Q} are matrices with real elements.

$$(c) \quad \begin{pmatrix} \mathbf{P}_k \\ \mathbf{P}_{k+1} \end{pmatrix} = \frac{1}{2} \begin{pmatrix} 1 & i \\ 1 & -i \end{pmatrix} \begin{pmatrix} \mathbf{R} \\ \mathbf{Q} \end{pmatrix}.$$

- (d) $\dots + \lambda_k \mathbf{P}_k + \lambda_k^* \mathbf{P}_{k+1} + \dots$ complex eigenvalue pair in the spectral decomposition (B.16) is now replaced by a real $[2 \times 2]$ matrix

$$\dots + \begin{pmatrix} \mu & -\omega \\ \omega & \mu \end{pmatrix} \begin{pmatrix} \mathbf{R} \\ \mathbf{Q} \end{pmatrix} + \dots$$

or whatever you find the clearest way to write this real representation.

References

- [B.1] J. Halcrow, *Geometry of turbulence: An exploration of the state-space of plane Couette flow*, School of Physics, Georgia Inst. of Technology, (Atlanta, 2008);
ChaosBook.org/projects/theses.html.
- [B.2] J.F. Gibson, J. Halcrow and P. Cvitanović, "Equilibrium and traveling-wave solutions of plane Couette flow," *J. Fluid Mech.* **638**, 243 (2009);
[arXiv:0808.3375](https://arxiv.org/abs/0808.3375)
- [B.3] D. W. Spieker, *Gone fishin' - a blog*, School of Physics, Georgia Inst. of Technology, (Atlanta, 2009);
ChaosBook.org/projects/Spieker.

Appendix C

Finding cycles

(C. Chandre)

C.1 Newton-Raphson method

C.1.1 Contraction rate

CONSIDER A d -DIMENSIONAL MAP $x' = f(x)$ with an unstable fixed point x_* . The Newton-Raphson algorithm is obtained by iterating the following map

$$x' = g(x) = x - (J(x) - \mathbf{1})^{-1} (f(x) - x).$$

The linearization of g near x_* leads to

$$x_* + \epsilon' = x_* + \epsilon - (J(x_*) - \mathbf{1})^{-1} (f(x_*) + J(x_*)\epsilon - x_* - \epsilon) + O(\|\epsilon\|^2),$$

where $\epsilon = x - x_*$. Therefore,

$$x' - x_* = O((x - x_*)^2).$$

After n steps and if the initial guess x_0 is close to x_* , the error decreases super-exponentially

$$g^n(x_0) - x_* = O((x_0 - x_*)^{2^n}).$$

C.1.2 Computation of the inverse

The Newton-Raphson method for finding n -cycles of d -dimensional mappings using the multi-shooting method reduces to the following equation

$$\begin{pmatrix} \mathbf{1} & & & -Df(x_n) \\ -Df(x_1) & \mathbf{1} & & \\ & \cdots & \mathbf{1} & \\ & & -Df(x_{n-1}) & \mathbf{1} \end{pmatrix} \begin{pmatrix} \delta_1 \\ \delta_2 \\ \cdots \\ \delta_n \end{pmatrix} = - \begin{pmatrix} F_1 \\ F_2 \\ \cdots \\ F_n \end{pmatrix}, \quad (\text{C.1})$$

where $Df(x)$ is the $[d \times d]$ Jacobian matrix of the map evaluated at the point x , and $\delta_m = x'_m - x_m$ and $F_m = x_m - f(x_{m-1})$ are d -dimensional vectors. By some straightforward algebra, the vectors δ_m are expressed as functions of the vectors F_m :

$$\delta_m = - \sum_{k=1}^m \beta_{k,m-1} F_k - \beta_{1,m-1} (\mathbf{1} - \beta_{1,n})^{-1} \left(\sum_{k=1}^n \beta_{k,n} F_k \right), \quad (\text{C.2})$$

for $m = 1, \dots, n$, where $\beta_{k,m} = Df(x_m)Df(x_{m-1}) \cdots Df(x_k)$ for $k < m$ and $\beta_{k,m} = \mathbf{1}$ for $k \geq m$. Therefore, finding n -cycles by a Newton-Raphson method with multiple shooting requires the inverting of a $[d \times d]$ matrix $\mathbf{1} - Df(x_n)Df(x_{n-1}) \cdots Df(x_1)$.

C.2 Hybrid Newton-Raphson / relaxation method



Consider a d -dimensional map $x' = f(x)$ with an unstable fixed point x_* . The transformed map is the following one:

$$x' = g(x) = x + \gamma C(f(x) - x),$$

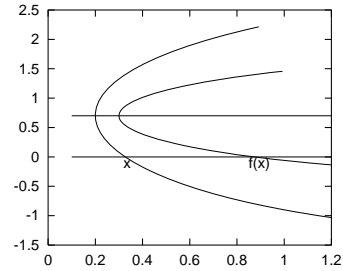
where $\gamma > 0$ and C is a $d \times d$ invertible constant matrix. We note that x_* is also a fixed point of g . Consider the stability matrix at the fixed point x_*

$$A_g = \left. \frac{dg}{dx} \right|_{x=x_*} = \mathbf{1} + \gamma C(A_f - \mathbf{1}).$$

The matrix C is constructed such that the eigenvalues of A_g are of modulus less than one. Assume that A_f is diagonalizable: In the basis of diagonalization, the matrix writes:

$$\tilde{A}_g = \mathbf{1} + \gamma \tilde{C}(\tilde{A}_f - \mathbf{1}),$$

Figure C.1: Illustration of the optimal Poincaré surface. The original surface $y = 0$ yields a large distance $x - f(x)$ for the Newton iteration. A much better choice is $y = 0.7$.



where \tilde{A}_f is diagonal with elements μ_i . We restrict the set of matrices \tilde{C} to diagonal matrices with $\tilde{C}_{ii} = \epsilon_i$ where $\epsilon_i = \pm 1$. Thus \tilde{A}_g is diagonal with eigenvalues $\gamma_i = 1 + \gamma\epsilon_i(\mu_i - 1)$. The choice of γ and ϵ_i is such that $|\gamma_i| < 1$. It is easy to see that if $\text{Re}(\mu_i) < 1$ one has to choose $\epsilon_i = 1$, and if $\text{Re}(\mu_i) > 1$, $\epsilon_i = -1$. If λ is chosen such that

$$0 < \gamma < \min_{i=1,\dots,d} \frac{2|\text{Re}(\mu_i) - 1|}{|\mu_i - 1|^2},$$

all the eigenvalues of A_g have modulus less than one. The contraction rate at the fixed point for the map g is then $\max_i |1 + \gamma\epsilon_i(\mu_i - 1)|$. If $\text{Re}(\mu_i) = 1$, it is not possible to stabilize x_* by the set of matrices γC .

From the construction of C , we see that 2^d choices of matrices are possible. For example, for 2-dimensional systems, these matrices are

$$C \in \left\{ \begin{pmatrix} 1 & 0 \\ 0 & 1 \end{pmatrix}, \begin{pmatrix} -1 & 0 \\ 0 & 1 \end{pmatrix}, \begin{pmatrix} 1 & 0 \\ 0 & -1 \end{pmatrix}, \begin{pmatrix} -1 & 0 \\ 0 & -1 \end{pmatrix} \right\}.$$

For 2-dimensional dissipative maps, the eigenvalues satisfy $\text{Re}(\mu_1)\text{Re}(\mu_2) \leq \det Df < 1$. The case $(\text{Re}(\mu_1) > 1, \text{Re}(\mu_2) > 1)$ which is stabilized by $\begin{pmatrix} -1 & 0 \\ 0 & -1 \end{pmatrix}$ has to be discarded. The minimal set is reduced to three matrices.

C.2.1 Newton method with optimal surface of section



(F. Christiansen)

In some systems it might be hard to find a good starting guess for a fixed point, something that could happen if the topology and/or the symbolic dynamics of the flow is not well understood. By changing the Poincaré section one might get a better initial guess in the sense that x and $f(x)$ are closer together. In figure C.1 there is an illustration of this. The figure shows a Poincaré section, $y = 0$, an initial guess x , the corresponding $f(x)$ and pieces of the trajectory near these two points.

If the Newton iteration does not converge for the initial guess x we might have to work very hard to find a better guess, particularly if this is in a high-dimensional system (high-dimensional might in this context mean a Hamiltonian system with

3 degrees of freedom.) But clearly we could easily have a much better guess by simply shifting the Poincaré section to $y = 0.7$ where the distance $x - f(x)$ would be much smaller. Naturally, one cannot see by eye the best surface in higher dimensional systems. The way to proceed is as follows: We want to have a minimal distance between our initial guess x and the image of this $f(x)$. We therefore integrate the flow looking for a minimum in the distance $d(t) = |f^t(x) - x|$. $d(t)$ is now a minimum with respect to variations in $f^t(x)$, but not necessarily with respect to x . We therefore integrate x either forward or backward in time. Doing this we minimize d with respect to x , but now it is no longer minimal with respect to $f^t(x)$. We therefore repeat the steps, alternating between correcting x and $f^t(x)$. In most cases this process converges quite rapidly. The result is a trajectory for which the vector $(f(x) - x)$ connecting the two end points is perpendicular to the flow at both points. We can now choose to define a Poincaré surface of section as the hyper-plane that goes through x and is normal to the flow at x . In other words the surface of section is determined by

$$(x' - x) \cdot v(x) = 0. \quad (\text{C.3})$$

Note that $f(x)$ lies on this surface. This surface of section is optimal in the sense that a close return on the surface is a local minimum of the distance between x and $f^t(x)$. But more importantly, the part of the stability matrix that describes linearization perpendicular to the flow is exactly the stability of the flow in the surface of section when $f(x)$ is close to x . In this method, the Poincaré surface changes with each iteration of the Newton scheme. Should we later want to put the fixed point on a specific Poincaré surface it will only be a matter of moving along the trajectory.


Appendix D

Symbolic dynamics techniques

THE KNEADING THEORY for unimodal mappings is developed in sect. **D.1**. The prime factorization for dynamical itineraries of sect. **D.2** illustrates the sense in which prime cycles are “prime” - the product structure of zeta functions is a consequence of the unique factorization property of symbol sequences.

D.1 Topological zeta functions for infinite subshifts

(P. Dahlqvist)

 The transition graph methods outlined in chapter **11** are well suited for symbolic dynamics of finite subshift type. A sequence of well defined rules leads to the answer, the topological zeta function, which turns out to be a polynomial. For infinite subshifts one would have to go through an infinite sequence of graph constructions and it is of course very difficult to make any asymptotic statements about the outcome. Luckily, for some simple systems the goal can be reached by much simpler means. This is the case for unimodal maps.

We will restrict our attention to the topological zeta function for unimodal maps with one external parameter $f_\lambda(x) = \Lambda g(x)$. As usual, symbolic dynamics is introduced by mapping a time series $\dots x_{i-1}x_ix_{i+1}\dots$ onto a sequence of symbols $\dots s_{i-1}s_is_{i+1}\dots$ where

$$\begin{aligned} s_i &= 0 & x_i < x_c \\ s_i &= C & x_i = x_c \\ s_i &= 1 & x_i > x_c \end{aligned} \tag{D.1}$$

and x_c is the critical point of the map (i.e., maximum of g). In addition to the usual binary alphabet we have added a symbol C for the critical point. The kneading

$I(C)$	$\zeta_{top}^{-1}(z)/(1-z)$	$I(C)$	$\zeta_{top}^{-1}(z)/(1-z)$
1C		1001C	
101C		100111C	
1011101C		10011C	
$H^\infty(1)$	$\prod_{n=0}^\infty (1-z^{2^n})$	100110C	
10111C		100C	
1011111C		100010C	
101^∞	$(1-2z^2)/(1+z)$	10001C	
10111111C		100011C	
101111C		1000C	
1011C		100001C	
101101C		10000C	
10C	$(1-z-z^2)$	100000C	
10010C		10^∞	$(1-2z)/(1-z)$
100101C			

Table D.1: All ordered kneading sequences up to length seven, as well as some longer kneading sequences. Harmonic extension $H^\infty(1)$ is defined below.

sequence K_Λ is the itinerary of the critical point (11.13). The crucial observation is that no periodic orbit can have a topological coordinate (see sect.D.1.1) beyond that of the kneading sequence. The kneading sequence thus inserts a border in the list of periodic orbits (ordered according to maximal topological coordinate), cycles up to this limit are allowed, all beyond are pruned. All unimodal maps (obeying some further constraints) with the same kneading sequence thus have the same set of periodic orbits and the same topological zeta function. The topological coordinate of the kneading sequence increases with increasing Λ .

The kneading sequence can be of one of three types

1. It maps to the critical point again, after n iterations. If so, we adopt the convention to terminate the kneading sequence with a C , and refer to the kneading sequence as finite.
2. Preperiodic, i.e., it is infinite but with a periodic tail.
3. Aperiodic.

As an archetype unimodal map we will choose the *tent map*

$$x \mapsto f(x) = \begin{cases} \Lambda x & x \in [0, 1/2] \\ \Lambda(1-x) & x \in (1/2, 1] \end{cases}, \tag{D.2}$$

where the parameter $\Lambda \in (1, 2]$. The topological entropy is $h = \log \Lambda$. This follows from the fact any trajectory of the map is bounded, the escape rate is strictly zero, and so the dynamical zeta function

$$1/\zeta(z) = \prod_p \left(1 - \frac{z^{n_p}}{|\Lambda_p|}\right) = \prod_p \left(1 - \left(\frac{z}{\Lambda}\right)^{n_p}\right) = 1/\zeta_{top}(z/\Lambda)$$

has its leading zero at $z = 1$.

The set of periodic points of the tent map is countable. A consequence of this fact is that the set of parameter values for which the kneading sequence (1.13) is periodic or preperiodic are countable and thus of measure zero and consequently *the kneading sequence is aperiodic for almost all Λ* . For general unimodal maps the corresponding statement is that the kneading sequence is aperiodic for almost all topological entropies.

For a given periodic kneading sequence of period n , $\underline{K}_\Lambda = PC = s_1 s_2 \dots s_{n-1} C$ there is a simple expansion for the topological zeta function. Then the expanded zeta function is a polynomial of degree n

$$1/\zeta_{\text{top}}(z) = \prod_p (1 - z_p^n) = (1 - z) \sum_{i=0}^{n-1} a_i z^i, \quad a_i = \prod_{j=1}^i (-1)^{s_j} \quad (\text{D.3})$$

and $a_0 = 1$.

Aperiodic and preperiodic kneading sequences are accounted for by simply replacing n by ∞ .

Example. Consider as an example the kneading sequence $K_\Lambda = 10C$. From (D.3) we get the topological zeta function $1/\zeta_{\text{top}}(z) = (1 - z)(1 - z - z^2)$, see table D.1. This can also be realized by redefining the alphabet. The only forbidden subsequence is 100. All allowed periodic orbits, except $\bar{0}$, can be built from an alphabet with letters $\underline{10}$ and $\underline{1}$. We write this alphabet as $\{\underline{10}, \underline{1}; \bar{0}\}$, yielding the topological zeta function $1/\zeta_{\text{top}}(z) = (1 - z)(1 - z - z^2)$. The leading zero is the inverse golden mean $z_0 = (\sqrt{5} - 1)/2$.

Example. As another example we consider the preperiodic kneading sequence $K_\Lambda = 101^\infty$. From (D.3) we get the topological zeta function $1/\zeta_{\text{top}}(z) = (1 - z)(1 - 2z^2)/(1 + z)$, see table D.1. This can again be realized by redefining the alphabet. There are now an infinite number of forbidden subsequences, namely $101^{2n}0$ where $n \geq 0$. These pruning rules are respected by the alphabet $\{\underline{01}^{2n+1}; \bar{1}, \bar{0}\}$, yielding the topological zeta function above. The pole in the zeta function $\zeta_{\text{top}}^{-1}(z)$ is a consequence of the infinite alphabet.

An important consequence of (D.3) is that the sequence $\{a_i\}$ has a periodic tail if and only if the kneading sequence has one (however, their period may differ by a factor of two). We know already that the kneading sequence is aperiodic for almost all Λ .

The analytic structure of the function represented by the infinite series $\sum a_i z^i$ with unity as radius of convergence, depends on whether the tail of $\{a_i\}$ is periodic or not. If the period of the tail is N we can write

$$1/\zeta_{\text{top}}(z) = p(z) + q(z)(1 + z^N + z^{2N} \dots) = p(z) + \frac{q(z)}{1 - z^N},$$

for some polynomials $p(z)$ and $q(z)$. The result is a set of poles spread out along the unit circle. This applies to the preperiodic case. An aperiodic sequence of coefficients would formally correspond to infinite N and it is natural to assume that the singularities will fill the unit circle. There is indeed a theorem ensuring that this is the case [58], provided the a_i 's can only take on a finite number of values. The unit circle becomes a *natural boundary*, already apparent in a finite polynomial approximations to the topological zeta function, as in figure 15.2. A function with a natural boundary lacks an analytic continuation outside it.

To conclude: The topological zeta function $1/\zeta_{top}$ for unimodal maps has the unit circle as a natural boundary for almost all topological entropies and for the tent map (D.2), for almost all Λ .

Let us now focus on the relation between the analytic structure of the topological zeta function and the number of periodic orbits, or rather (15.8), the number N_n of fixed points of $f^n(x)$. The trace formula is (see sect. 15.4)

$$N_n = \text{tr } T^n = \frac{1}{2\pi i} \oint_{\gamma_r} dz z^{-n} \frac{d}{dz} \log \zeta_{top}^{-1}$$

where γ_r is a (circular) contour encircling the origin $z = 0$ in clockwise direction. Residue calculus turns this into a sum over zeros z_0 and poles z_p of ζ_{top}^{-1}

$$N_n = \sum_{z_0: r < |z_0| < R} z_0^{-n} - \sum_{z_p: r < |z_p| < R} z_p^{-n} + \frac{1}{2\pi i} \oint_{\gamma_R} dz z^{-n} \frac{d}{dz} \log \zeta_{top}^{-1}$$

and a contribution from a large circle γ_R . For meromorphic topological zeta functions one may let $R \rightarrow \infty$ with vanishing contribution from γ_R , and N_n will be a sum of exponentials.

The leading zero is associated with the topological entropy, as discussed in chapter 15.

We have also seen that for preperiodic kneading there will be poles on the unit circle.

To appreciate the role of natural boundaries we will consider a (very) special example. Cascades of period doublings is a central concept for the description of unimodal maps. This motivates a close study of the function

$$\Xi(z) = \prod_{n=0}^{\infty} (1 - z^{2^n}) . \tag{D.4}$$

This function will appear again when we derive (D.3).

The expansion of $\Xi(z)$ begins as $\Xi(z) = 1 - z - z^2 + z^3 - z^4 + z^5 \dots$. The radius of convergence is obviously unity. The simple rule governing the expansion will

effectively prohibit any periodicity among the coefficients making the unit circle a natural boundary.

It is easy to see that $\Xi(z) = 0$ if $z = \exp(2\pi m/2^n)$ for any integer m and n . (Strictly speaking we mean that $\Xi(z) \rightarrow 0$ when $z \rightarrow \exp(2\pi m/2^n)$ from inside). Consequently, zeros are dense on the unit circle. One can also show that singular points are dense on the unit circle, for instance $|\Xi(z)| \rightarrow \infty$ when $z \rightarrow \exp(2\pi m/3^l)$ for any integer m and n .

As an example, the topological zeta function at the accumulation point of the first Feigenbaum cascade is $\zeta_{top}^{-1}(z) = (1-z)\Xi(z)$. Then $N_n = 2^{l+1}$ if $n = 2^l$, otherwise $N_n = 0$. The growth rate in the number of cycles is anything but exponential. It is clear that N_n cannot be a sum of exponentials, the contour γ_R cannot be pushed away to infinity, R is restricted to $R \leq 1$ and N_n is entirely determined by \int_{γ_R} which picks up its contribution from the natural boundary.

We have so far studied the analytic structure for some special cases and we know that the unit circle is a natural boundary for almost all Λ . But how does it look out there in the complex plane for some typical parameter values? To explore that we will imagine a journey from the origin $z = 0$ out towards the unit circle. While traveling we let the parameter Λ change slowly. The trip will have a distinct science fiction flavor. The first zero we encounter is the one connected to the topological entropy. Obviously it moves smoothly and slowly. When we move outward to the unit circle we encounter zeros in increasing densities. The closer to the unit circle they are, the wilder and stranger they move. They move from and back to the horizon, where they are created and destroyed through bizarre bifurcations. For some special values of the parameter the unit circle suddenly gets transparent and we get (infinitely) short glimpses of another world beyond the horizon.

We end this section by deriving eqs (D.5) and (D.6). The impenetrable prose is hopefully explained by the accompanying tables.

We know one thing from chapter 11, namely for that finite kneading sequence of length n the topological polynomial is of degree n . The graph contains a node which is connected to itself only via the symbol 0. This implies that a factor $(1-z)$ may be factored out and $\zeta_{top}(z) = (1-z)\sum_{i=0}^{n-1} a_i z^i$. The problem is to find the coefficients a_i .

The ordered list of (finite) kneading sequences table D.1 and the ordered list of periodic orbits (on maximal form) are intimately related. In table D.2 we indicate how they are nested during a period doubling cascade. Every finite kneading sequence PC is bracketed by two periodic orbits, $\overline{P1}$ and $\overline{P0}$. We have $\overline{P1} < PC < \overline{P0}$ if P contains an odd number of 1's, and $\overline{P0} < PC < \overline{P1}$ otherwise. From now on we will assume that P contains an odd number of 1's. The other case can be worked out in complete analogy. The first and second harmonic of PC are displayed in table D.2. The periodic orbit $\overline{P1}$ (and the corresponding infinite kneading sequence) is sometimes referred to as the antiharmonic extension of PC (denoted $A^\infty(P)$) and the accumulation point of the cascade is called the harmonic extension of PC [8] (denoted $H^\infty(P)$).

periodic orbits	finite kneading sequences
$\overline{P1} = A^\infty(P)$	PC
$\overline{P0}$	$P0PC$
$\overline{P0P1}$	$P0P1P0PC$
\downarrow	\downarrow
$H^\infty(P)$	$H^\infty(P)$

Table D.2: Relation between periodic orbits and finite kneading sequences in a harmonic cascade. The string P is assumed to contain an odd number of 1's.

A central result is the fact that a period doubling cascade of PC is not interfered by any other sequence. Another way to express this is that a kneading sequence PC and its harmonic are adjacent in the list of kneading sequences to any order.

$I(C)$	$\zeta_{stop}^{-1}(z)/(1-z)$
$P_1 = 100C$	$1 - z - z^2 - z^3$
$H^\infty(P_1) = 10001001100\dots$	$1 - z - z^2 - z^3 - z^4 + z^5 + z^6 + z^7 - z^8 \dots$
$P' = 10001C$	$1 - z - z^2 - z^3 - z^4 + z^5$
$A^\infty(P_2) = 1000110001\dots$	$1 - z - z^2 - z^3 - z^4 + z^5 - z^6 - z^7 - z^8 \dots$
$P_2 = 1000C$	$1 - z - z^2 - z^3 - z^4$

Table D.3: Example of a step in the iterative construction of the list of kneading sequences PC .

Table D.3 illustrates another central result in the combinatorics of kneading sequences. We suppose that P_1C and P_2C are neighbors in the list of order 5 (meaning that the shortest finite kneading sequence $P'C$ between P_1C and P_2C is longer than 5.) The important result is that P' (of length $n' = 6$) has to coincide with the first $n' - 1$ letters of both $H^\infty(P_1)$ and $A^\infty(P_2)$. This is exemplified in the left column of table D.3. This fact makes it possible to generate the list of kneading sequences in an iterative way.

The zeta function at the accumulation point $H^\infty(P_1)$ is

$$\zeta_{P_1}^{-1}(z)\Xi(z^{n_1}) \ , \tag{D.5}$$

and just before $A^\infty(P_2)$

$$\zeta_{P_2}^{-1}(z)/(1 - z^{n_2}) \ . \tag{D.6}$$

A short calculation shows that this is exactly what one would obtain by applying (D.3) to the antiharmonic and harmonic extensions directly, provided that it applies to $\zeta_{P_1}^{-1}(z)$ and $\zeta_{P_2}^{-1}(z)$. This is the key observation.

Recall now the product representation of the zeta function $\zeta^{-1} = \prod_p(1 - z^{n_p})$. We will now make use of the fact that the zeta function associated with

$P'C$ is a polynomial of order n' . There is no periodic orbit of length shorter than $n' + 1$ between $H^\infty(P_1)$ and $A^\infty(P_2)$. It thus follows that the coefficients of this polynomial coincides with those of (D.5) and (D.6), see Table D.3. We can thus conclude that our rule can be applied directly to $P'C$.

This can be used as an induction step in proving that the rule can be applied to every finite and infinite kneading sequences.

Remark D.1 How to prove things. The explicit relation between the kneading sequence and the coefficients of the topological zeta function is not commonly seen in the literature. The result can proven by combining some theorems of Milnor and Thurston [14]. That approach is hardly instructive in the present context. Our derivation was inspired by Metropolis, Stein and Stein classical paper [8]. For further detail, consult [14].

D.1.1 Periodic orbits of unimodal maps

A *periodic point* (*cycle point*) x_k belonging to a cycle of period n is a real solution of

$$f^n(x_k) = f(f(\dots f(x_k)\dots)) = x_k, \quad k = 0, 1, 2, \dots, n-1. \quad (\text{D.7})$$

The n th iterate of a unimodal map has at most 2^n monotone segments, and therefore there will be 2^n or fewer periodic points of length n . Similarly, the backward and the forward Smale horseshoes intersect at most 2^n times, and therefore there will be 2^n or fewer periodic points of length n . A periodic orbit of length n corresponds to an infinite repetition of a length $n = n_p$ symbol string, customarily indicated by a line over the string:

$$S_p = (s_1 s_2 s_3 \dots s_n)^\infty = \overline{s_1 s_2 s_3 \dots s_n}.$$

As all itineraries are infinite, we shall adopt convention that a finite string itinerary $S_p = s_1 s_2 s_3 \dots s_n$ stands for infinite repetition of a finite block, and routinely omit the overline. x_0 , its cyclic permutation $\overline{s_k s_{k+1} \dots s_n s_1 \dots s_{k-1}}$ corresponds to the point x_{k-1} in the same cycle. A cycle p is called *prime* if its itinerary S cannot be written as a repetition of a shorter block S' .

Each cycle p is a set of n_p rational-valued full tent map periodic points γ . It follows from (11.9) that if the repeating string $s_1 s_2 \dots s_n$ contains an odd number "1"s, the string of well ordered symbols $w_1 w_2 \dots w_{2n}$ has to be of the double length before it repeats itself. The cycle-point γ is a geometrical sum which we can rewrite as the fraction

$$\gamma(\overline{s_1 s_2 \dots s_n}) = \frac{2^{2n}}{2^{2n} - 1} \sum_{t=1}^{2n} w_t / 2^t \quad (\text{D.8})$$

Using this we can calculate the $\hat{\gamma}(S)$ for all short cycles. For orbits up to length 5 this is done in table 11.1.

Here we give explicit formulas for the topological coordinate of a periodic point, given its itinerary. For the purpose of what follows it is convenient to compactify the itineraries by replacing the binary alphabet $\mathfrak{s} = \{0, 1\}$ by the infinite alphabet

$$\{a_1, a_2, a_3, a_4, \dots; \bar{0}\} = \{1, 10, 100, 1000, \dots; \bar{0}\}. \tag{D.9}$$

In this notation the itinerary $S = a_i a_j a_k a_l \dots$ and the corresponding topological coordinate (11.9) are related by $\gamma(S) = .1^i 0^j 1^k 0^l \dots$. For example:

$$\begin{aligned} S &= 111011101001000\dots = a_1 a_1 a_2 a_1 a_1 a_2 a_3 a_4 \dots \\ \gamma(S) &= .101101001110000\dots = .1^1 0^1 1^2 0^1 1^1 0^2 1^3 0^4 \dots \end{aligned}$$

Cycle points whose itineraries start with $w_1 = w_2 = \dots = w_i = 0, w_{i+1} = 1$ remain on the left branch of the tent map for i iterations, and satisfy $\gamma(0 \dots 0S) = \gamma(S)/2^i$.

Periodic points correspond to rational values of γ , but we have to distinguish *even* and *odd* cycles. The even (odd) cycles contain even (odd) number of a in the repeating block, with periodic points given by

$$\gamma(a_i a_j \dots a_k a_\ell) = \begin{cases} \frac{2^n}{2^n - 1} \cdot 1^i 0^j \dots 1^k & \text{even} \\ \frac{1}{2^n + 1} (1 + 2^n \times 1^i 0^j \dots 1^\ell) & \text{odd} \end{cases}, \tag{D.10}$$

where $n = i + j + \dots + k + \ell$ is the cycle period. The maximal value periodic point is given by the cyclic permutation of S with the largest a_i as the first symbol, followed by the smallest available a_j as the next symbol, and so on. For example:

$$\begin{aligned} \hat{\gamma}(1) &= \gamma(a_1) = .10101\dots = \overline{.10} = 2/3 \\ \hat{\gamma}(10) &= \gamma(a_2) = .1^2 0^2 \dots = \overline{.1100} = 4/5 \\ \hat{\gamma}(100) &= \gamma(a_3) = .1^3 0^3 \dots = \overline{.111000} = 8/9 \\ \hat{\gamma}(101) &= \gamma(a_2 a_1) = .1^2 0^1 \dots = \overline{.110} = 6/7 \end{aligned}$$

An example of a cycle where only the third symbol determines the maximal value periodic point is

$$\hat{\gamma}(1101110) = \gamma(a_2 a_1 a_2 a_1 a_1) = \overline{.11011010010010} = 100/129.$$

Maximal values of all cycles up to length 5 are given in table!?

D.2 Prime factorization for dynamical itineraries



The Möbius function is not only a number-theoretic function, but can be used to manipulate ordered sets of noncommuting objects such as symbol strings. Let $\mathbf{P} = \{p_1, p_2, p_3, \dots\}$ be an ordered set of *prime* strings, and

$$\mathcal{N} = \{n\} = \left\{ p_1^{k_1} p_2^{k_2} p_3^{k_3} \cdots p_j^{k_j} \right\},$$

$j \in \mathbb{N}, k_i \in \mathbb{Z}_+$, be the set of all strings n obtained by the ordered concatenation of the “primes” p_i . By construction, every string n has a unique prime factorization. We say that a string has a divisor d if it contains d as a substring, and define the string division n/d as n with the substring d deleted. Now we can do things like this: defining $t_n := t_{p_1}^{k_1} t_{p_2}^{k_2} \cdots t_{p_j}^{k_j}$ we can write the inverse dynamical zeta function (20.2) as

$$\prod_p (1 - t_p) = \sum_n \mu(n) t_n,$$

and, if we care (we do in the case of the Riemann zeta function), the dynamical zeta function as .

$$\prod_p \frac{1}{1 - t_p} = \sum_n t_n \tag{D.11}$$

A striking aspect of this formula is its resemblance to the factorization of natural numbers into primes: the relation of the cycle expansion (D.11) to the product over prime cycles is analogous to the Riemann zeta (exercise 19.10) represented as a sum over natural numbers vs. its Euler product representation.

We now implement this factorization explicitly by decomposing recursively binary strings into ordered concatenations of prime strings. There are 2 strings of length 1, both prime: $p_1 = 0, p_2 = 1$. There are 4 strings of length 2: 00, 01, 11, 10. The first three are ordered concatenations of primes: $00 = p_1^2, 01 = p_1 p_2, 11 = p_2^2$; by ordered concatenations we mean that $p_1 p_2$ is legal, but $p_2 p_1$ is not. The remaining string is the only prime of length 2, $p_3 = 10$. Proceeding by discarding the strings which are concatenations of shorter primes $p_1^{k_1} p_2^{k_2} \cdots p_j^{k_j}$, with primes lexically ordered, we generate the standard list of primes, in agreement with table 15.1: 0, 1, 10, 101, 100, 1000, 1001, 1011, 10000, 10001, 10010, 10011, 10110, 10111, 100000, 100001, 100010, 100011, 100110, 100111, 101100, 101110, 101111, . . . This factorization is illustrated in table D.4.

factors	string	factors	string	factors	string	factors	string
p_1	0	p_1^4	0000	p_1^5	00000	$p_1^2 p_5$	00101
p_2	1	$p_1^3 p_2$	0001	$p_1^4 p_2$	00001	$p_1 p_2 p_5$	01101
		$p_1^2 p_2^2$	0011	$p_1^3 p_2^2$	00011	$p_2^2 p_5$	11101
p_1^2	00	$p_1 p_2^3$	0111	$p_1^2 p_2^3$	00111	$p_3 p_5$	10101
$p_1 p_2$	01	p_2^4	1111	$p_1 p_2^4$	01111	$p_1 p_6$	01000
p_2^2	11	$p_1^2 p_3$	0010	p_2^5	11111	$p_2 p_6$	11000
p_3	10	$p_1 p_2 p_3$	0110	p_3^2	00010	$p_1 p_7$	01001
		$p_2^2 p_3$	1110	$p_1^3 p_3$	00110	$p_2 p_7$	11001
p_1^3	000	$p_2^3 p_3$	1010	$p_1^2 p_2 p_3$	00110	$p_1 p_8$	01011
$p_1^2 p_2$	001	p_2^2	1010	$p_1 p_2^2 p_3$	01110	$p_2 p_8$	11011
$p_1 p_2^2$	011	$p_1 p_4$	0100	$p_2^3 p_3$	11110	p_9	10000
p_2^3	111	$p_2 p_4$	1100	$p_1 p_2^3$	01010	p_{10}	10001
$p_1 p_3$	010	$p_1 p_5$	0101	$p_2 p_3^2$	11010	p_{11}	10010
$p_2 p_3$	110	$p_2 p_5$	1101	$p_1^2 p_4$	00100	p_{12}	10011
p_4	100	p_6	1000	$p_1 p_2 p_4$	01100	p_{13}	10110
p_5	101	p_7	1001	$p_2^2 p_4$	11100	p_{14}	10111
		p_8	1011	$p_3 p_4$	10100		

Table D.4: Factorization of all periodic points strings up to length 5 into ordered concatenations $p_1^{k_1} p_2^{k_2} \dots p_n^{k_n}$ of prime strings $p_1 = 0, p_2 = 1, p_3 = 10, p_4 = 100, \dots, p_{14} = 10111$.

D.2.1 Prime factorization for spectral determinants



Following sect. D.2, the spectral determinant cycle expansions is obtained by expanding F as a multinomial in prime cycle weights t_p

$$F = \prod_p \sum_{k=0}^{\infty} C_{p^k} t_p^k = \sum_{k_1 k_2 k_3 \dots = 0}^{\infty} \tau_{p_1^{k_1} p_2^{k_2} p_3^{k_3} \dots} \quad (\text{D.12})$$

where the sum goes over all pseudocycles. In the above we have defined

$$\tau_{p_1^{k_1} p_2^{k_2} p_3^{k_3} \dots} = \prod_{i=1}^{\infty} C_{p_i^{k_i}} t_{p_i}^{k_i} . \quad (\text{D.13})$$

exercise 19.10

A striking aspect of the spectral determinant cycle expansion is its resemblance to the factorization of natural numbers into primes: as we already noted in sect. D.2, the relation of the cycle expansion (D.12) to the product formula (19.9) is analogous to the Riemann zeta represented as a sum over natural numbers vs. its Euler product representation.

This is somewhat unexpected, as the cycle weights factorize exactly with respect to r repetitions of a prime cycle, $t_{pp\dots p} = t_p^r$, but only approximately (*shadowing*) with respect to subdividing a string into prime substrings, $t_{p_1 p_2} \approx t_{p_1} t_{p_2}$.

The coefficients C_{p^k} have a simple form only in 1 – dimensional, given by the Euler formula (23.5). In higher dimensions C_{p^k} can be evaluated by expanding (19.9), $F(z) = \prod_p F_p$, where

$$F_p = 1 - \left(\sum_{r=1}^{\infty} \frac{t_p^r}{rd_{p,r}} \right) + \frac{1}{2} \left(\sum_{r=1}^{\infty} \frac{t_p^r}{rd_{p,r}} \right)^2 - \dots$$

Expanding and recollecting terms, and suppressing the p cycle label for the moment, we obtain

$$\begin{aligned} F_p &= \sum_{r=1}^{\infty} C_k t^k, \quad C_k = (-)^k c_k / D_k, \\ D_k &= \prod_{r=1}^k d_r = \prod_{a=1}^d \prod_{r=1}^k (1 - u_a^r) \end{aligned} \tag{D.14}$$

where evaluation of c_k requires a certain amount of not too luminous algebra:

$$\begin{aligned} c_0 &= 1 \\ c_1 &= 1 \\ c_2 &= \frac{1}{2} \left(\frac{d_2}{d_1} - d_1 \right) = \frac{1}{2} \left(\prod_{a=1}^d (1 + u_a) - \prod_{a=1}^d (1 - u_a) \right) \\ c_3 &= \frac{1}{3!} \left(\frac{d_2 d_3}{d_1^2} + 2d_1 d_2 - 3d_3 \right) \\ &= \frac{1}{6} \left(\prod_{a=1}^d (1 + 2u_a + 2u_a^2 + u_a^3) \right. \\ &\quad \left. + 2 \prod_{a=1}^d (1 - u_a - u_a^2 + u_a^3) - 3 \prod_{a=1}^d (1 - u_a^3) \right) \end{aligned}$$

etc.. For example, for a general 2-dimensional map we have

$$F_p = 1 - \frac{1}{D_1} t + \frac{u_1 + u_2}{D_2} t^2 - \frac{u_1 u_2 (1 + u_1)(1 + u_2) + u_1^3 + u_2^3}{D_3} t^3 + \dots \tag{D.15}$$

We discuss the convergence of such cycle expansions in sect.I.4.

With $\tau_{p_1^{k_1} p_2^{k_2} \dots p_n^{k_n}}$ defined as above, the prime factorization of symbol strings is unique in the sense that *each symbol string can be written as a unique concatenation of prime strings*, up to a convention on ordering of primes. This factorization is a nontrivial example of the utility of generalized Möbius inversion, sect.D.2.

How is the factorization of sect. D.2 used in practice? Suppose we have computed (or perhaps even measured in an experiment) all prime cycles up to length

n , i.e., we have a list of t_p 's and the corresponding Jacobian matrix eigenvalues $\Lambda_{p,1}, \Lambda_{p,2}, \dots, \Lambda_{p,d}$. A cycle expansion of the Selberg product is obtained by generating all strings in order of increasing length j allowed by the symbolic dynamics and constructing the multinomial

$$F = \sum_n \tau_n \tag{D.16}$$

where $n = s_1 s_2 \dots s_j$, s_i range over the alphabet, in the present case $\{0, 1\}$. Factorizing every string $n = s_1 s_2 \dots s_j = p_1^{k_1} p_2^{k_2} \dots p_j^{k_j}$ as in table D.4, and substituting $\tau_{p_1^{k_1} p_2^{k_2} \dots}$ we obtain a multinomial approximation to F . For example, $\tau_{001001010101} = \tau_{001001010101} = \tau_{001^2} \tau_{01^3}$, and $\tau_{01^3}, \tau_{001^2}$ are known functions of the corresponding cycle eigenvalues. The zeros of F can now be easily determined by standard numerical methods. The fact that as far as the symbolic dynamics is concerned, the cycle expansion of a Selberg product is simply an average over all symbolic strings makes Selberg products rather pretty.

To be more explicit, we illustrate the above by expressing binary strings as concatenations of prime factors. We start by computing N_n , the number of terms in the expansion (D.12) of the total cycle length n . Setting $C_{p^k} t_p^k = z^{n_p k}$ in (D.12), we obtain

$$\sum_{n=0}^{\infty} N_n z^n = \prod_p \sum_{k=0}^{\infty} z^{n_p k} = \frac{1}{\prod_p (1 - z^{n_p})} .$$

So the generating function for the number of terms in the Selberg product is the topological zeta function. For the complete binary dynamics we have $N_n = 2^n$ contributing terms of length n :

$$\zeta_{top} = \frac{1}{\prod_p (1 - z^{n_p})} = \frac{1}{1 - 2z} = \sum_{n=0}^{\infty} 2^n z^n$$

Hence the number of distinct terms in the expansion (D.12) is the same as the number of binary strings, and conversely, the set of binary strings of length n suffices to label all terms of the total cycle length n in the expansion (D.12).

Appendix E

Counting itineraries

E.1 Counting curvatures

ONE CONSEQUENCE of the finiteness of topological polynomials is that the contributions to curvatures at every order are even in number, half with positive and half with negative sign. For instance, for complete binary labeling (20.7),



$$c_4 = -t_{0001} - t_{0011} - t_{0111} - t_0 t_{01} t_1 + t_0 t_{001} + t_0 t_{011} + t_{001} t_1 + t_{011} t_1. \quad (\text{E.1})$$

We see that 2^3 terms contribute to c_4 , and exactly half of them appear with a negative sign - hence if all binary strings are admissible, this term vanishes in the counting expression.

exercise E.2

Such counting rules arise from the identity

$$\prod_p (1 + t_p) = \prod_p \frac{1 - t_p^2}{1 - t_p}. \quad (\text{E.2})$$

Substituting $t_p = z^{np}$ and using (15.18) we obtain for unrestricted symbol dynamics with N letters

$$\prod_p (1 + z^{np}) = \frac{1 - Nz^2}{1 - Nz} = 1 + Nz + \sum_{k=2}^{\infty} z^k (N^k - N^{k-1})$$

The z^n coefficient in the above expansion is the number of terms contributing to c_n curvature, so we find that for a complete symbolic dynamics of N symbols and

$n > 1$, the number of terms contributing to c_n is $(N - 1)N^{k-1}$ (of which half carry a minus sign).

exercise E.4

We find that for complete symbolic dynamics of N symbols and $n > 1$, the number of terms contributing to c_n is $(N - 1)N^{n-1}$. So, superficially, not much is gained by going from periodic orbits trace sums which get N^n contributions of n to the curvature expansions with $N^n(1 - 1/N)$. However, the point is not the number of the terms, but the cancelations between them.



Exercises

E.1. **Lefschetz zeta function.** Elucidate the relation between the topological zeta function and the Lefschetz zeta function.

Substituting into the identity

$$\prod_p (1 + t_p) = \prod_p \frac{1 - t_p^2}{1 - t_p}$$

E.2. **Counting the 3-disk pinball counterterms.** Verify that the number of terms in the 3-disk pinball curvature expansion (20.35) is given by

we obtain

$$\begin{aligned} \prod_p (1 + t_p) &= \frac{1 - 3z^4 - 2z^6}{1 - 3z^2 - 2z^3} = 1 + 3z^2 + 2z^3 + \frac{z^4(6 + 12z + 2z^2)}{1 - 3z^2 - 2z^3} \\ &= 1 + 3z^2 + 2z^3 + 6z^4 + 12z^5 + 20z^6 + 48z^7 + 84z^8 + 184z^9 + \dots \end{aligned} \tag{E.3}$$

$$= 1 + t_0 + t_1 + \sum_{n=2}^{\infty} \sum_{k=1}^{n-1} 2 \binom{n-2}{k-1} t_0^k t_1^{n-k} \tag{E.5}$$

This means that, for example, c_6 has a total of 20 terms, in agreement with the explicit 3-disk cycle expansion (20.36).

Hence for $n \geq 2$ the number of terms in the expansion ?! with k 0's and $n - k$ 1's in their symbol sequences is $2 \binom{n-2}{k-1}$. This is the degeneracy of distinct cycle eigenvalues in fig.?!; for systems with non-uniform hyperbolicity this degeneracy is lifted (see fig. ?!).

E.3. **Cycle expansion denominators**.** Prove that the denominator of c_k is indeed D_k , as asserted (D.14).

In order to count the number of prime cycles in each such subset we denote with $M_{n,k}$ ($n = 1, 2, \dots$; $k = \{0, 1\}$ for $n = 1$; $k = 1, \dots, n - 1$ for $n \geq 2$) the number of prime n -cycles whose labels contain k zeros, use binomial string counting and Möbius inversion and obtain

E.4. **Counting subsets of cycles.** The techniques developed above can be generalized to counting subsets of cycles. Consider the simplest example of a dynamical system with a complete binary tree, a repeller map (11.4) with two straight branches, which we label 0 and 1. Every cycle weight for such map factorizes, with a factor t_0 for each 0, and factor t_1 for each 1 in its symbol string. The transition matrix traces (15.7) collapse to $tr(T^k) = (t_0 + t_1)^k$, and $1/\zeta$ is simply

$$\prod_p (1 - t_p) = 1 - t_0 - t_1 \tag{E.4}$$

$$\begin{aligned} M_{1,0} &= M_{1,1} = 1 \\ nM_{n,k} &= \sum_{m|\frac{n}{k}} \mu(m) \binom{n/m}{k/m}, \quad n \geq 2, k = 1, \dots, n-1 \end{aligned}$$

where the sum is over all m which divide both n and k .

Appendix F

Implementing evolution

F.1 Koopmania

THE WAY in which time evolution acts on observables may be rephrased in the language of functional analysis, by introducing the *Koopman operator*, whose action on a state space function $a(x)$ is to replace it by its downstream value time t later, $a(x) \rightarrow a(x(t))$ evaluated at the trajectory point $x(t)$:

$$\mathcal{K}^t a(x) = a(f^t(x)). \quad (\text{F.1})$$

Observable $a(x)$ has no explicit time dependence; all the time dependence comes from its evaluation at $x(t)$ rather than at $x = x(0)$.

Suppose we are starting with an initial density of representative points $\rho(x)$: then the average value of $a(x)$ evolves as

$$\langle a \rangle(t) = \frac{1}{|\rho_{\mathcal{M}}|} \int_{\mathcal{M}} dx a(f^t(x)) \rho(x) = \frac{1}{|\rho_{\mathcal{M}}|} \int_{\mathcal{M}} dx [\mathcal{K}^t a(x)] \rho(x).$$

An alternative point of view (analogous to the shift from the Heisenberg to the Schrödinger picture in quantum mechanics) is to push dynamical effects into the density. In contrast to the Koopman operator which advances the trajectory by time t , the Perron-Frobenius operator (16.10) depends on the trajectory point time t in the past, so the Perron-Frobenius operator is the adjoint of the Koopman operator

$$\int_{\mathcal{M}} dx [\mathcal{K}^t a(x)] \rho(x) = \int_{\mathcal{M}} dx a(x) [\mathcal{L}^t \rho(x)]. \quad (\text{F.2})$$

Checking this is an easy change of variables exercise. For finite dimensional deterministic invertible flows the Koopman operator (F.1) is simply the inverse of the

Perron-Frobenius operator (16.6), so in what follows we shall not distinguish the two. However, for infinite dimensional flows contracting forward in time and for stochastic flows such inverses do not exist, and there you need to be more careful.

The family of Koopman’s operators $\{\mathcal{K}^t\}_{t \in \mathbb{R}_+}$ forms a semigroup parameterized by time

- (a) $\mathcal{K}^0 = \mathbf{1}$
- (b) $\mathcal{K}^t \mathcal{K}^{t'} = \mathcal{K}^{t+t'} \quad t, t' \geq 0$ (semigroup property) ,

with the *generator* of the semigroup, the generator of infinitesimal time translations defined by

$$\mathcal{A} = \lim_{t \rightarrow 0^+} \frac{1}{t} (\mathcal{K}^t - \mathbf{1}) .$$

(If the flow is finite-dimensional and invertible, \mathcal{A} is a generator of a group). The explicit form of \mathcal{A} follows from expanding dynamical evolution up to first order, as in (2.5):

$$\mathcal{A} a(x) = \lim_{t \rightarrow 0^+} \frac{1}{t} (a(f^t(x)) - a(x)) = v_i(x) \partial_i a(x) . \tag{F.3}$$

Of course, that is nothing but the definition of the time derivative, so the equation of motion for $a(x)$ is

$$\left(\frac{d}{dt} - \mathcal{A} \right) a(x) = 0 . \tag{F.4}$$

appendix F.2

The finite time Koopman operator (F.1) can be formally expressed by exponentiating the time evolution generator \mathcal{A} as

$$\mathcal{K}^t = e^{t\mathcal{A}} . \tag{F.5}$$

exercise F.1

The generator \mathcal{A} looks very much like the generator of translations. Indeed, for a constant velocity field dynamical evolution is nothing but a translation by time \times velocity:

exercise 16.10

$$e^{tv \frac{\partial}{\partial x}} a(x) = a(x + tv) . \tag{F.6}$$

As we will not need to implement a computational formula for general $e^{t\mathcal{A}}$ in what follows, we relegate making sense of such operators to appendix F.2. Here

appendix F.2

we limit ourselves to a brief remark about the notion of “spectrum” of a linear operator.

The Koopman operator \mathcal{K} acts multiplicatively in time, so it is reasonable to suppose that there exist constants $M > 0, \beta \geq 0$ such that $\|\mathcal{K}^t\| \leq Me^{t\beta}$ for all $t \geq 0$. What does that mean? The operator norm is define in the same spirit in which we defined the matrix norms in sect. J.2: We are assuming that no value of $\mathcal{K}^t \rho(x)$ grows faster than exponentially for any choice of function $\rho(x)$, so that the fastest possible growth can be bounded by $e^{t\beta}$, a reasonable expectation in the light of the simplest example studied so far, the exact escape rate (17.20). If that is so, multiplying \mathcal{K}^t by $e^{-t\beta}$ we construct a new operator $e^{-t\beta} \mathcal{K}^t = e^{t(\mathcal{A}-\beta)}$ which decays exponentially for large $t, \|e^{t(\mathcal{A}-\beta)}\| \leq M$. We say that $e^{-t\beta} \mathcal{K}^t$ is an element of a *bounded* semigroup with generator $\mathcal{A} - \beta \mathbf{1}$. Given this bound, it follows by the Laplace transform

$$\int_0^\infty dt e^{-st} \mathcal{K}^t = \frac{1}{s - \mathcal{A}}, \quad \text{Re } s > \beta, \tag{F.7}$$

that the *resolvent* operator $(s - \mathcal{A})^{-1}$ is bounded (“resolvent” = able to cause separation into constituents)

section J.2

$$\left\| \frac{1}{s - \mathcal{A}} \right\| \leq \int_0^\infty dt e^{-st} M e^{t\beta} = \frac{M}{s - \beta}.$$

If one is interested in the spectrum of \mathcal{K} , as we will be, the resolvent operator is a natural object to study. The main lesson of this brief aside is that for the continuous time flows the Laplace transform is the tool that brings down the generator in (16.29) into the resolvent form (16.31) and enables us to study its spectrum.

F.2 Implementing evolution

(R. Artuso and P. Cvitanović)



We now come back to the semigroup of operators \mathcal{K}^t . We have introduced the generator of the semigroup (16.27) as

$$\mathcal{A} = \left. \frac{d}{dt} \mathcal{K}^t \right|_{t=0}.$$

If we now take the derivative at arbitrary times we get

$$\begin{aligned} \left(\frac{d}{dt} \mathcal{K}^t \psi \right) (x) &= \lim_{\eta \rightarrow 0} \frac{\psi(f^{t+\eta}(x)) - \psi(f^t(x))}{\eta} \\ &= v_i(f^t(x)) \left. \frac{\partial}{\partial \tilde{x}_i} \psi(\tilde{x}) \right|_{\tilde{x}=f^t(x)} \\ &= (\mathcal{K}^t \mathcal{A} \psi) (x) \end{aligned}$$

which can be formally integrated like an ordinary differential equation yielding exercise F.1

$$\mathcal{K}^t = e^{t\mathcal{A}}. \quad (\text{F.8})$$

This guarantees that the Laplace transform manipulations in sect. 16.5 are correct. Though the formal expression of the semigroup (F.8) is quite simple one has to take care in implementing its action. If we express the exponential through the power series

$$\mathcal{K}^t = \sum_{k=0}^{\infty} \frac{t^k}{k!} \mathcal{A}^k, \quad (\text{F.9})$$

we encounter the problem that the infinitesimal generator (16.27) contains non-commuting pieces, i.e., there are i, j combinations for which the commutator does not satisfy

$$\left[\frac{\partial}{\partial x_i}, v_j(x) \right] = 0.$$

To derive a more useful representation, we follow the strategy used for finite-dimensional matrix operators in sects. 4.2 and 4.3 and use the semigroup property to write

$$\mathcal{K}^t = \prod_{m=1}^{t/\delta\tau} \mathcal{K}^{\delta\tau}$$

as the starting point for a discretized approximation to the continuous time dynamics, with time step $\delta\tau$. Omitting terms from the second order onwards in the expansion of $\mathcal{K}^{\delta\tau}$ yields an error of order $O(\delta\tau^2)$. This might be acceptable if the time step $\delta\tau$ is sufficiently small. In practice we write the Euler product

$$\mathcal{K}^t = \prod_{m=1}^{t/\delta\tau} (1 + \delta\tau \mathcal{A}_{(m)}) + O(\delta\tau^2) \quad (\text{F.10})$$

where

$$(\mathcal{A}_{(m)}\psi)(x) = v_i(f^{m\delta\tau}(x)) \left. \frac{\partial\psi}{\partial \tilde{x}_i} \right|_{\tilde{x}=f^{m\delta\tau}(x)}$$

As far as the x dependence is concerned, $e^{\delta\tau \mathcal{A}_i}$ acts as

$$e^{\delta\tau \mathcal{A}_i} \begin{Bmatrix} x_1 \\ \cdot \\ x_i \\ \cdot \\ x_d \end{Bmatrix} \rightarrow \begin{Bmatrix} x_1 \\ \cdot \\ x_i + \delta\tau v_i(x) \\ \cdot \\ x_d \end{Bmatrix}. \quad (\text{F.11})$$

exercise 2.6

We see that the product form (F.10) of the operator is nothing else but a prescription for finite time step integration of the equations of motion - in this case the simplest Euler type integrator which advances the trajectory by $\delta\tau \times$ velocity at each time step.

F.2.1 A symplectic integrator



The procedure we described above is only a starting point for more sophisticated approximations. As an example on how to get a sharper bound on the error term consider the Hamiltonian flow $\mathcal{A} = \mathcal{B} + \mathcal{C}$, $\mathcal{B} = p_i \frac{\partial}{\partial q_i}$, $\mathcal{C} = -\partial_i V(q) \frac{\partial}{\partial p_i}$. Clearly the potential and the kinetic parts do not commute. We make sense of the formal solution (F.10) by splitting it into infinitesimal steps and keeping terms up to $\delta\tau^2$ in

exercise F.2

$$\mathcal{K}^{\delta\tau} = \hat{\mathcal{K}}^{\delta\tau} + \frac{1}{24}(\delta\tau)^3[\mathcal{B} + 2\mathcal{C}, [\mathcal{B}, \mathcal{C}]] + \dots, \tag{F.12}$$

where

$$\hat{\mathcal{K}}^{\delta\tau} = e^{\frac{1}{2}\delta\tau\mathcal{B}} e^{\delta\tau\mathcal{C}} e^{\frac{1}{2}\delta\tau\mathcal{B}}. \tag{F.13}$$

The approximate infinitesimal Liouville operator $\hat{\mathcal{K}}^{\delta\tau}$ is of the form that now generates evolution as a sequence of mappings induced by (16.30), a free flight by $\frac{1}{2}\delta\tau\mathcal{B}$, scattering by $\delta\tau\partial V(q')$, followed again by $\frac{1}{2}\delta\tau\mathcal{B}$ free flight:

$$\begin{aligned} e^{\frac{1}{2}\delta\tau\mathcal{B}} \begin{Bmatrix} q \\ p \end{Bmatrix} &\rightarrow \begin{Bmatrix} q' \\ p' \end{Bmatrix} = \begin{Bmatrix} q - \frac{\delta\tau}{2}p \\ p \end{Bmatrix} \\ e^{\delta\tau\mathcal{C}} \begin{Bmatrix} q' \\ p' \end{Bmatrix} &\rightarrow \begin{Bmatrix} q'' \\ p'' \end{Bmatrix} = \begin{Bmatrix} q' \\ p' + \delta\tau\partial V(q') \end{Bmatrix} \\ e^{\frac{1}{2}\delta\tau\mathcal{B}} \begin{Bmatrix} q'' \\ p'' \end{Bmatrix} &\rightarrow \begin{Bmatrix} q''' \\ p''' \end{Bmatrix} = \begin{Bmatrix} q' - \frac{\delta\tau}{2}p'' \\ p'' \end{Bmatrix} \end{aligned} \tag{F.14}$$

Collecting the terms we obtain an integration rule for this type of symplectic flow which is better than the straight Euler integration (F.11) as it is accurate up to order $\delta\tau^2$:

$$\begin{aligned} q_{n+1} &= q_n - \delta\tau p_n - \frac{(\delta\tau)^2}{2}\partial V(q_n - \delta\tau p_n/2) \\ p_{n+1} &= p_n + \delta\tau\partial V(q_n - \delta\tau p_n/2) \end{aligned} \tag{F.15}$$

The Jacobian matrix of one integration step is given by

$$M = \begin{pmatrix} 1 & -\delta\tau/2 \\ 0 & 1 \end{pmatrix} \begin{pmatrix} 1 & 0 \\ \delta\tau\partial V(q') & 1 \end{pmatrix} \begin{pmatrix} 1 & -\delta\tau/2 \\ 0 & 1 \end{pmatrix}. \tag{F.16}$$

Note that the billiard flow (8.11) is an example of such symplectic integrator. In that case the free flight is interrupted by instantaneous wall reflections, and can be integrated out.

Commentary

Remark F.1 Koopman operators. The “Heisenberg picture” in dynamical systems theory has been introduced by Koopman and Von Neumann [1, 2], see also ref. [12]. Inspired by the contemporary advances in quantum mechanics, Koopman [1] observed in 1931 that \mathcal{K}^t is unitary on $L^2(\mu)$ Hilbert spaces. The Koopman operator is the classical analogue of the quantum evolution operator $\exp(i\hat{H}t/\hbar)$ – the kernel of $\mathcal{L}^t(y, x)$ introduced in (16.16) (see also sect. 17.2) is the analogue of the Green’s function discussed here in chapter 31. The relation between the spectrum of the Koopman operator and classical ergodicity was formalized by von Neumann [2]. We shall not use Hilbert spaces here and the operators that we shall study *will not* be unitary. For a discussion of the relation between the Perron-Frobenius operators and the Koopman operators for finite dimensional deterministic invertible flows, infinite dimensional contracting flows, and stochastic flows, see Lasota-Mackey [12] and Gaspard [8].

Remark F.2 Symplectic integration. The reviews [12] and [13] offer a good starting point for exploring the symplectic integrators literature. For a higher order integrators of type (F.13), check ref. [18].

Exercises

F.1. **Exponential form of semigroup elements.** Check that the Koopman operator and the evolution generator commute, $\mathcal{K}^t \mathcal{A} = \mathcal{A} \mathcal{K}^t$, by considering the action of both operators on an arbitrary state space function $a(x)$.

F.2. **Non-commutativity.** Check that the commutators in

(F.12) are not vanishing by showing that

$$[\mathcal{B}, \mathcal{C}] = -p \left(v'' \frac{\partial}{\partial p} - v' \frac{\partial}{\partial q} \right).$$

F.3. **Symplectic leapfrog integrator.** Implement (F.15) for 2-dimensional Hamiltonian flows; compare it with Runge-Kutta integrator by integrating trajectories in some (chaotic) Hamiltonian flow.

References

[F.1] B. O. Koopman, *Proc. Nat. Acad. Sci. USA* **17**, 315 (1931).

- [F.2] J. von Neumann, *Ann. Math.* **33**, 587 (1932).
- [F.3] M. Axenides and E. Floratos, “Strange Attractors in Dissipative Nambu Mechanics: Classical and Quantum Aspects,” [arXiv:0910.3881](https://arxiv.org/abs/0910.3881).
- [F.4] G. Levine and M. Tabor, “Integrating the Nonintegrable: Analytic Structure of the Lorenz Model Revisited,” *Physica* **33**, 189 (1988).
- [F.5] M. Tabor, *Chaos and Integrability in Nonlinear Dynamics: An Introduction* (Wiley, New York, 1989).
- [F.6] H. P. F. Swinnerton-Dyer, “The Invariant Algebraic Surfaces of the Lorenz System,” *Math. Proc. Cambridge Philos. Soc.* **132**, 385 (2002).
- [F.7] M. Kuš, “Integrals of Motion for the Lorenz System,” *J. Phys. A* **16**, L689 (1983).
- [F.8] B. A. Shadwick, J. C. Bowman, and P. J. Morrison, *Exactly Conservative Integrators*, chao-dyn/9507012, Submitted to *SIAM J. Sci. Comput.*
- [F.9] D. J. D. Earn, *Symplectic integration without roundoff error*, astro-ph/9408024.
- [F.10] P. E. Zadunaiski, “On the estimation of errors propagated in the numerical integration of ordinary differential equations,” *Numer. Math.* **27**, 21 (1976).
- [F.11] K. Feng, “Difference schemes for Hamiltonian formalism and symplectic geometry,” *J. Comput. Math.* **4**, 279 (1986).
- [F.12] P. J. Channell and C. Scovel, “Symplectic integration of Hamiltonian systems,” *Nonlinearity* **3**, 231 (1990).
- [F.13] J. M. Sanz-Serna and M. P. Calvo, *Numerical Hamiltonian problems* (Chapman and Hall, London, 1994).
- [F.14] J. M. Sanz-Serna, “Geometric integration,” pp. 121-143, in *The State of the Art in Numerical Analysis*, I. S. Duff and G. A. Watson, eds., (Clarendon Press, Oxford, 1997).
- [F.15] K. W. Morton, “Book Review: Simulating Hamiltonian Dynamics,” *SIAM Review* **48**, 621 (2006).
- [F.16] B. Leimkuhler and S. Reich, *Simulating Hamiltonian Dynamics* (Cambridge Univ. Press, Cambridge 2005).
- [F.17] E. Hairer, Ch. Lubich, and G. Wanner, *Geometric Numerical Integration* (Springer-Verlag, Berlin 2002).
- [F.18] M. Suzuki, “General theory of fractal path integrals with applications to many-body theories and statistical physics,” *J. Math. Phys.* **32**, 400 (1991).

Appendix G

Transport of vector fields

Man who says it cannot be done should not interrupt man doing it.

—Sayings of Vattay Gábor

IN THIS APPENDIX we show that the multidimensional Lyapunov exponents and relaxation exponents (dynamo rates) of vector fields can be expressed in terms of leading eigenvalues of appropriate evolution operators.

G.1 Evolution operator for Lyapunov exponents



Lyapunov exponents were introduced and computed for 1 – *dimensional* maps in sect. 17.3.2. For higher-dimensional flows only the Jacobian matrices are multiplicative, not individual eigenvalues, and the construction of the evolution operator for evaluation of the Lyapunov spectra requires the extension of evolution equations to the flow in the tangent space. We now develop the requisite theory.

Here we construct a multiplicative evolution operator (G.4) whose spectral determinant (G.8) yields the leading Lyapunov exponent of a d -dimensional flow (and is entire for Axiom A flows).

The key idea is to extend the dynamical system by the tangent space of the flow, suggested by the standard numerical methods for evaluation of Lyapunov exponents: start at x_0 with an initial infinitesimal tangent space vector in the d -dimensional tangent space $\eta(0) \in T\mathcal{M}_{x_0}$, and let the flow transport it along the trajectory $x(t) = f^t(x_0)$.

The dynamics in the tangent bundle $(x, \delta x) \in \mathbf{T}\mathcal{M}$ is governed by the system of equations of variations (4.2):

$$\dot{x} = v(x), \quad \dot{\eta} = A(x)\eta.$$

Here $A(x)$ is (4.3), the stability matrix (velocity gradients matrix) of the flow. We write the solution as

$$x(t) = f^t(x_0), \quad \eta(t) = J^t(x_0)\eta_0, \quad (\text{G.1})$$

with the tangent space vector η transported by the Jacobian matrix $J(x_0) = \partial x(t)/\partial x_0$ (4.6).

As explained in sect. 4.1, the growth rate of this vector is multiplicative along the trajectory and can be represented as $\eta(t) = |\eta(t)|/|\eta(0)|u(t)$ where $u(t)$ is a “unit” vector in some norm $\|\cdot\|$. For asymptotic times and for almost every initial $(x_0, \eta(0))$, this factor converges to the leading eigenvalue of the linearized stability matrix of the flow.

We implement this multiplicative evaluation of Floquet multipliers by adjoining the d -dimensional transverse tangent space $\eta \in \mathbf{T}\mathcal{M}_x$; $\eta(x) \cdot v(x) = 0$ to the $(d+1)$ -dimensional dynamical evolution space $x \in \mathcal{M} \subset \mathbb{R}^{d+1}$. In order to determine the length of the vector η we introduce a homogeneous differentiable scalar function $g(\eta) = \|\eta\|$. It has the property $g(\Lambda\eta) = |\Lambda|g(\eta)$ for any Λ . An example is the projection of a vector to its d th component

$$g \begin{pmatrix} \eta_1 \\ \eta_2 \\ \dots \\ \eta_d \end{pmatrix} = |\eta_d|.$$

Any vector $\eta(0) \in \mathbf{T}\mathcal{M}_x$ can now be represented by the product $\eta = \Lambda u$, where u is a “unit” vector in the sense that its norm is $\|u\| = 1$, and the factor

$$\Lambda^t(x_0, u_0) = g(\eta(t)) = g(J^t(x_0)u_0) \quad (\text{G.2})$$

is the multiplicative “stretching” factor.

Unlike the leading eigenvalue of the Jacobian the stretching factor is multiplicative along the trajectory:

$$\Lambda^{t'+t}(x_0, u_0) = \Lambda^{t'}(x(t), u(t)) \Lambda^t(x_0, u_0).$$

exercise G.1

The u evolution constrained to $E\mathbf{T}_{g,x}$, the space of unit transverse tangent vectors, is given by rescaling of (G.1):

$$u' = R^t(x, u) = \frac{1}{\Lambda^t(x, u)} J^t(x)u. \quad (\text{G.3})$$

Eqs. (G.1), (G.2) and (G.3) enable us to define a *multiplicative* evolution operator on the extended space $U \times E\mathbf{T}_{g,x}$

$$\mathcal{L}^t(x', u'; x, u) = \delta(x' - f^t(x)) \frac{\delta(u' - R^t(x, u))}{|\Lambda^t(x, u)|^{\beta-1}}, \quad (\text{G.4})$$

where β is a variable.

To evaluate the expectation value of $\log |\Lambda^t(x, u)|$ which is the Lyapunov exponent we again have to take the proper derivative of the leading eigenvalue of (G.4). In order to derive the trace formula for the operator (G.4) we need to evaluate $\text{Tr } \mathcal{L}^t = \int dx du \mathcal{L}^t(u, x; u, x)$. The $\int dx$ integral yields a weighted sum over prime periodic orbits p and their repetitions r :

$$\begin{aligned} \text{Tr } \mathcal{L}^t &= \sum_p T_p \sum_{r=1}^{\infty} \frac{\delta(t - rT_p)}{|\det(1 - M_p^r)|} \Delta_{p,r}, \\ \Delta_{p,r} &= \int_g du \frac{\delta(u - R^{T_p r}(x_p, u))}{|\Lambda^{T_p r}(x_p, u)|^{\beta-1}}, \end{aligned} \quad (\text{G.5})$$

where M_p is the prime cycle p transverse stability matrix. As we shall see below, $\Delta_{p,r}$ is intrinsic to cycle p , and independent of any particular periodic point x_p .

We note next that if the trajectory $f^t(x)$ is periodic with period T , the tangent space contains d periodic solutions

$$\mathbf{e}^{(i)}(x(T+t)) = \mathbf{e}^{(i)}(x(t)), \quad i = 1, \dots, d,$$

corresponding to the d unit eigenvectors $\{\mathbf{e}^{(1)}, \mathbf{e}^{(2)}, \dots, \mathbf{e}^{(d)}\}$ of the transverse stability matrix, with “stretching” factors (G.2) given by its eigenvalues

$$M_p(x)\mathbf{e}^{(i)}(x) = \Lambda_{p,i}\mathbf{e}^{(i)}(x), \quad i = 1, \dots, d. \quad (\text{no summation on } i)$$

The $\int du$ integral in (G.5) picks up contributions from these periodic solutions. In order to compute the stability of the i th eigen-direction solution, it is convenient to expand the variation around the eigenvector $\mathbf{e}^{(i)}$ in the stability matrix eigenbasis $\delta u = \sum \delta u_\ell \mathbf{e}^{(\ell)}$. The variation of the map (G.3) at a complete period $t = T$ is then given by

$$\begin{aligned} \delta R^T(\mathbf{e}^{(i)}) &= \frac{M\delta u}{g(M\mathbf{e}^{(i)})} - \frac{M\mathbf{e}^{(i)}}{g(M\mathbf{e}^{(i)})^2} \left(\frac{\partial g(\mathbf{e}^{(i)})}{\partial u} M\delta u \right) \\ &= \sum_{k \neq i} \frac{\Lambda_{p,k}}{\Lambda_{p,i}} \left(\mathbf{e}^{(k)} - \mathbf{e}^{(i)} \frac{\partial g(\mathbf{e}^{(i)})}{\partial u_k} \right) \delta u_k. \end{aligned} \quad (\text{G.6})$$

The δu_i component does not contribute to this sum since $g(\mathbf{e}^{(i)} + du; \mathbf{e}^{(i)}) = 1 + du_i$ implies $\partial g(\mathbf{e}^{(i)})/\partial u_i = 1$. Indeed, infinitesimal variations δu must satisfy

$$g(u + \delta u) = g(u) = 1 \implies \sum_{\ell=1}^d \delta u_\ell \frac{\partial g(u)}{\partial u_\ell} = 0,$$

so the allowed variations are of form

$$\delta u = \sum_{k \neq i} \left(\mathbf{e}^{(k)} - \mathbf{e}^{(i)} \frac{\partial g(\mathbf{e}^{(i)})}{\partial u_k} \right) c_k, \quad |c_k| \ll 1,$$

and in the neighborhood of the $\mathbf{e}^{(i)}$ eigenvector the $\int du$ integral can be expressed as

$$\int_g du = \int \prod_{k \neq i} dc_k.$$

Inserting these variations into the $\int du$ integral we obtain

$$\begin{aligned} \int_g du & \delta(\mathbf{e}^{(i)} + \delta u - R^T(\mathbf{e}^{(i)}) - \delta R^T(\mathbf{e}^{(i)}) + \dots) \\ &= \int \prod_{k \neq i} dc_k \delta((1 - \Lambda_k/\Lambda_i)c_k + \dots) \\ &= \prod_{k \neq i} \frac{1}{|1 - \Lambda_k/\Lambda_i|}, \end{aligned}$$

and the $\int du$ trace (G.5) becomes

$$\Delta_{p,r} = \sum_{i=1}^d \frac{1}{|\Lambda_{p,i}^r|^{\beta-1}} \prod_{k \neq i} \frac{1}{|1 - \Lambda_{p,k}^r/\Lambda_{p,i}^r|}. \tag{G.7}$$

The corresponding spectral determinant is obtained by observing that the Laplace transform of the trace (18.23) is a logarithmic derivative $\text{Tr } \mathcal{L}(s) = -\frac{d}{ds} \log F(s)$ of the spectral determinant:

$$F(\beta, s) = \exp \left(- \sum_{p,r} \frac{e^{sT_{p,r}}}{r |\det(1 - M_p^r)|} \Delta_{p,r}(\beta) \right). \tag{G.8}$$

This determinant is the central result of this section. Its zeros correspond to the eigenvalues of the evolution operator (G.4), and can be evaluated by the cycle expansion methods.

The leading zero of (G.8) is called “pressure” (or free energy)

$$P(\beta) = s_0(\beta). \quad (\text{G.9})$$

The average Lyapunov exponent is then given by the first derivative of the pressure at $\beta = 1$:

$$\bar{\lambda} = P'(1). \quad (\text{G.10})$$

The simplest application of (G.8) is to 2-dimensional hyperbolic Hamiltonian maps. The Floquet multipliers are related by $\Lambda_1 = 1/\Lambda_2 = \Lambda$, and the spectral determinant is given by

$$\begin{aligned} F(\beta, z) &= \exp\left(-\sum_{p,r} \frac{z^{rn_p}}{r|\Lambda_p^r|} \frac{1}{(1-1/\Lambda_p^r)^2} \Delta_{p,r}(\beta)\right) \\ \Delta_{p,r}(\beta) &= \frac{|\Lambda_p^r|^{1-\beta}}{1-1/\Lambda_p^{2r}} + \frac{|\Lambda_p^r|^{\beta-3}}{1-1/\Lambda_p^{2r}}. \end{aligned} \quad (\text{G.11})$$

The dynamics (G.3) can be restricted to a u unit eigenvector neighborhood corresponding to the largest eigenvalue of the Jacobi matrix. On this neighborhood the largest eigenvalue of the Jacobi matrix is the only fixed point, and the spectral determinant obtained by keeping only the largest term the $\Delta_{p,r}$ sum in (G.7) is also entire.

In case of maps it is practical to introduce the logarithm of the leading zero and to call it “pressure”

$$P(\beta) = \log z_0(\beta).$$

The average of the Lyapunov exponent of the map is then given by the first derivative of the pressure at $\beta = 1$:

$$\bar{\lambda} = P'(1).$$

By factorizing the determinant (G.11) into products of zeta functions we can conclude that the leading zero of the (G.4) can also be recovered from the leading zeta function

$$1/\zeta_0(\beta, z) = \exp\left(-\sum_{p,r} \frac{z^{rn_p}}{r|\Lambda_p^r|^\beta}\right). \quad (\text{G.12})$$

This zeta function plays a key role in thermodynamic applications, see chapter K.

G.2 Advection of vector fields by chaotic flows

Fluid motions can move embedded vector fields around. An example is the magnetic field of the Sun which is “frozen” in the fluid motion. A passively evolving vector field \mathbf{V} is governed by an equation of the form

$$\partial_t \mathbf{V} + \mathbf{u} \cdot \nabla \mathbf{V} - \mathbf{V} \cdot \nabla \mathbf{u} = 0, \quad (\text{G.13})$$

where $u(x, t)$ represents the velocity field of the fluid. The strength of the vector field can grow or decay during its time evolution. The amplification of the vector field in such a process is called the “dynamo effect.” In a strongly chaotic fluid motion we can characterize the asymptotic behavior of the field with an exponent

$$\mathbf{V}(x, t) \sim \mathbf{V}(x) e^{\nu t}, \quad (\text{G.14})$$

where ν is called the fast dynamo rate. The goal of this section is to show that periodic orbit theory can be developed for such a highly non-trivial system as well.

We can write the solution of (G.13) formally, as shown by Cauchy. Let $\mathbf{x}(t, \mathbf{a})$ be the position of the fluid particle that was at the point \mathbf{a} at $t = 0$. Then the field evolves according to

$$\mathbf{V}(\mathbf{x}, t) = \mathbf{J}(\mathbf{a}, t) \mathbf{V}(\mathbf{a}, 0) \quad , \quad (\text{G.15})$$

where $\mathbf{J}(\mathbf{a}, t) = \partial(\mathbf{x})/\partial(\mathbf{a})$ is the Jacobian matrix of the transformation that moves the fluid into itself $\mathbf{x} = \mathbf{x}(\mathbf{a}, t)$.

We write $\mathbf{x} = f^t(\mathbf{a})$, where f^t is the flow that maps the initial positions of the fluid particles into their positions at time t . Its inverse, $\mathbf{a} = f^{-t}(\mathbf{x})$, maps particles at time t and position \mathbf{x} back to their initial positions. Then we can write (G.15)

$$V_i(\mathbf{x}, t) = \sum_j \int d^3 \mathbf{a} \mathcal{L}_{ij}^t(\mathbf{x}, \mathbf{a}) V_j(\mathbf{a}, 0) \quad , \quad (\text{G.16})$$

with

$$\mathcal{L}_{ij}^t(\mathbf{x}, \mathbf{a}) = \delta(\mathbf{a} - f^{-t}(\mathbf{x})) \frac{\partial x_i}{\partial a_j} \quad . \quad (\text{G.17})$$

For large times, the effect of \mathcal{L}^t is dominated by its leading eigenvalue, $e^{\nu_0 t}$ with $Re(\nu_0) > Re(\nu_i)$, $i = 1, 2, 3, \dots$. In this way the transfer operator furnishes the fast dynamo rate, $\nu := \nu_0$.

The trace of the transfer operator is the sum over all periodic orbit contributions, with each cycle weighted by its intrinsic stability

$$\text{Tr} \mathcal{L}^t = \sum_p T_p \sum_{r=1}^{\infty} \frac{\text{tr} M_p^r}{|\det(\mathbf{1} - M_p^{-r})|} \delta(t - rT_p). \quad (\text{G.18})$$

We can construct the corresponding spectral determinant as usual

$$F(s) = \exp \left[- \sum_p \sum_{r=1}^{\infty} \frac{1}{r} \frac{\text{tr} M_p^r}{|\det(\mathbf{1} - M_p^{-r})|} e^{srT_p} \right]. \quad (\text{G.19})$$

Note that in this formuli we have omitted a term arising from the Jacobian transformation along the orbit which would give $1 + \text{tr} M_p^r$ in the numerator rather than just the trace of M_p^r . Since the extra term corresponds to advection along the orbit, and this does not evolve the magnetic field, we have chosen to ignore it. It is also interesting to note that the negative powers of the Jacobian occur in the denominator, since we have f^{-t} in (G.17).

In order to simplify $F(s)$, we factor the denominator cycle stability determinants into products of expanding and contracting eigenvalues. For a 3-dimensional fluid flow with cycles possessing one expanding eigenvalue Λ_p (with $|\Lambda_p| > 1$), and one contracting eigenvalue λ_p (with $|\lambda_p| < 1$) the determinant may be expanded as follows:

$$|\det(\mathbf{1} - M_p^{-r})|^{-1} = |(1 - \Lambda_p^{-r})(1 - \lambda_p^{-r})|^{-1} = |\lambda_p|^r \sum_{j=0}^{\infty} \sum_{k=0}^{\infty} \Lambda_p^{-jr} \lambda_p^{kr}. \quad (\text{G.20})$$

With this decomposition we can rewrite the exponent in (G.19) as

$$\sum_p \sum_{r=1}^{\infty} \frac{1}{r} \frac{(\lambda_p^r + \Lambda_p^r) e^{srT_p}}{|\det(\mathbf{1} - M_p^{-r})|} = \sum_p \sum_{j,k=0}^{\infty} \sum_{r=1}^{\infty} \frac{1}{r} (|\lambda_p| \Lambda_p^{-j} \lambda_p^k e^{sT_p})^r (\lambda_p^r + \Lambda_p^r), \quad (\text{G.21})$$

which has the form of the expansion of a logarithm:

$$\sum_p \sum_{j,k} \left[\log(1 - e^{sT_p} |\lambda_p| \Lambda_p^{1-j} \lambda_p^k) + \log(1 - e^{sT_p} |\lambda_p| \Lambda_p^{-j} \lambda_p^{1+k}) \right]. \quad (\text{G.22})$$

The spectral determinant is therefore of the form,

$$F(s) = F_e(s) F_c(s), \quad (\text{G.23})$$

where

$$F_e(s) = \prod_p \prod_{j,k=0}^{\infty} \left(1 - t_p^{(jk)} \Lambda_p\right) \quad , \quad (G.24)$$

$$F_c(s) = \prod_p \prod_{j,k=0}^{\infty} \left(1 - t_p^{(jk)} \lambda_p\right), \quad (G.25)$$

with

$$t_p^{(jk)} = e^{sT_p} |\lambda_p| \frac{\lambda_p^k}{\Lambda_p^j} \quad . \quad (G.26)$$

The two factors present in $F(s)$ correspond to the expanding and contracting exponents. (Had we not neglected a term in (G.19), there would be a third factor corresponding to the translation.)

For 2 – dimensional Hamiltonian volume preserving systems, $\lambda = 1/\Lambda$ and (G.24) reduces to

$$F_e(s) = \prod_p \prod_{k=0}^{\infty} \left(1 - \frac{t_p}{\Lambda_p^{k-1}}\right)^{k+1} \quad , \quad t_p = \frac{e^{sT_p}}{|\Lambda_p|} \quad . \quad (G.27)$$

With $\sigma_p = \Lambda_p/|\Lambda_p|$, the Hamiltonian zeta function (the $j = k = 0$ part of the product (G.25)) is given by

$$1/\zeta_{dyn}(s) = \prod_p \left(1 - \sigma_p e^{sT_p}\right) \quad . \quad (G.28)$$

This is a curious formula — the zeta function depends only on the return times, not on the eigenvalues of the cycles. Furthermore, the identity,

$$\frac{\Lambda + 1/\Lambda}{|(1 - \Lambda)(1 - 1/\Lambda)|} = \sigma + \frac{2}{|(1 - \Lambda)(1 - 1/\Lambda)|} \quad ,$$

when substituted into (G.23), leads to a relation between the vector and scalar advection spectral determinants:

$$F_{dyn}(s) = F_0^2(s)/\zeta_{dyn}(s) \quad . \quad (G.29)$$

The spectral determinants in this equation are entire for hyperbolic (axiom A) systems, since both of them correspond to multiplicative operators.

In the case of a flow governed by a map, we can adapt the formulas (G.27) and (G.28) for the dynamo determinants by simply making the substitution

$$z^{n_p} = e^{sT_p} \quad , \quad (\text{G.30})$$

where n_p is the integer order of the cycle. Then we find the spectral determinant $F_e(z)$ given by equation (G.27) but with

$$t_p = \frac{z^{n_p}}{|\Lambda_p|} \quad (\text{G.31})$$

for the weights, and

$$1/\zeta_{\text{dyn}}(z) = \prod_p (1 - \sigma_p z^{n_p}) \quad (\text{G.32})$$

for the zeta-function

For *maps* with finite Markov partition the inverse zeta function (G.32) reduces to a polynomial for z since curvature terms in the cycle expansion vanish. For example, for maps with complete binary partition, and with the fixed point stabilities of opposite signs, the cycle expansion reduces to

$$1/\zeta_{\text{dyn}}(s) = 1. \quad (\text{G.33})$$

For such *maps* the dynamo spectral determinant is simply the square of the scalar advection spectral determinant, and therefore all its zeros are double. In other words, for flows governed by such discrete maps, the fast dynamo rate equals the scalar advection rate.

In contrast, for 3-dimensional *flows*, the dynamo effect is distinct from the scalar advection. For example, for flows with finite symbolic dynamical grammars, (G.29) implies that the dynamo zeta function is a ratio of two entire determinants:

$$1/\zeta_{\text{dyn}}(s) = F_{\text{dyn}}(s)/F_0^2(s). \quad (\text{G.34})$$

This relation implies that for *flows* the zeta function has double poles at the zeros of the scalar advection spectral determinant, with zeros of the dynamo spectral determinant no longer coinciding with the zeros of the scalar advection spectral determinant; Usually the leading zero of the dynamo spectral determinant is larger than the scalar advection rate, and the rate of decay of the magnetic field is no longer governed by the scalar advection.

exercise G.2

Commentary

Remark G.1 Lyapunov exponents. Sect. G.1 is based on ref. [1].

Remark G.2 Dynamo zeta. The dynamo zeta (G.32) has been introduced by Aurell and Gilbert [3] and reviewed in ref. [4]. Our exposition follows ref. [21].

Exercises

G.1. **Stretching factor.** Prove the multiplicative property of the stretching factor (G.2). Why should we extend the phase space with the tangent space?

G.2. **Dynamo rate.** Suppose that the fluid dynamics is highly dissipative and can be well approximated by the piecewise linear map

$$f(x) = \begin{cases} 1 + ax & \text{if } x < 0, \\ 1 - bx & \text{if } x > 0, \end{cases} \quad (\text{G.35})$$

on an appropriate surface of section ($a, b > 2$). Suppose also that the return time is constant T_a for $x < 0$ and T_b

for $x > 0$. Show that the dynamo zeta is

$$1/\zeta_{\text{dyn}}(s) = 1 - e^{sT_a} + e^{sT_b}. \quad (\text{G.36})$$

Show also that the escape rate is the leading zero of

$$1/\zeta_0(s) = 1 - e^{sT_a}/a - e^{sT_b}/b. \quad (\text{G.37})$$

Calculate the dynamo and the escape rates analytically if $b = a^2$ and $T_b = 2T_a$. Do the calculation for the case when you reverse the signs of the slopes of the map. What is the difference?

References

- [G.1] P. Cvitanović and G. Vattay, *Entire Fredholm determinants for evaluation of semi-classical and thermodynamical spectra*, *Phys. Rev. Lett.* **71**, 4138 (1993); [arXiv:chao-dyn/9307012](https://arxiv.org/abs/chao-dyn/9307012).
- [G.2] Ya.B. Pesin, *Uspekhi Mat. Nauk* **32**, 55 (1977), [*Russian Math. Surveys* **32**, 55 (1977)].
- [G.3] E. Aurell and A. Gilbert, *Geophys. & Astrophys. Fluid Dynamics* (1993).
- [G.4] S. Childress and A.D. Gilbert *Stretch, Twist, Fold: The Fast Dynamo, Lecture Notes in Physics* **37** (Springer Verlag, Berlin 1995).
- [G.5] J. Balatoni and A. Renyi, *Publi. Math. Inst. Hung. Acad. Sci.* **1**, 9 (1956); english translation **1**, 588 (Akademia Budapest, 1976).
- [G.6] R. Benzi, G. Paladin, G. Parisi and A. Vulpiani, *J. Phys.* **A17**, 3521 (1984).

- [G.7] Even though the thermodynamic formalism is of older vintage (we refer the reader to ref. [32] for a comprehensive, and incomprehensible overview), we adhere here to the notational conventions of ref. [8], more frequently employed in the physics literature.
- [G.8] T.C. Halsey, M.H. Jensen, L.P. Kadanoff, I. Procaccia and B.I. Shraiman, *Phys. Rev.* **A107**, 1141 (1986).
- [G.9] P. Grassberger, *Phys. Lett.* **97A**, 227 (1983); **107A**, 101 (1985); H.G.E. Hentschel and I. Procaccia, *Physica* **8D**, 435 (1983); R. Benzi, G. Paladin, G. Parisi and A. Vulpiani, *em J. Phys.* **A17**, 3521 (1984).
- [G.10] P. Grassberger and I. Procaccia, *Phys. Rev. A* **31**, 1872 (1985).
- [G.11] C. Shannon, *Bell System Technical Journal*, **27**, 379 (1948).
- [G.12] H. Fujisaka, *Progr. Theor. Phys* **70**, 1264 (1983).
- [G.13] M. Barnsley, *Fractals Everywhere*, (Academic Press, New York 1988).
- [G.14] A.S. Pikovsky, unpublished.
- [G.15] C. Beck, "Higher correlation functions of chaotic dynamical systems - a graph theoretical approach," *Nonlinearity* **4**, 1131 (1991); to be published.
- [G.16] The 4-point correlation function is given in ref. [15].
- [G.17] G. Hackenbroich and F. von Oppen, "Semiclassical theory of transport in antidot lattices," *Z. Phys.* **B 97**, 157 (1995).
- [G.18] M.J. Feigenbaum, *J. Stat. Phys.* **21**, 669 (1979); reprinted in ref. [5].
- [G.19] P. Szépfalussy, T. Tél, A. Csordás and Z. Kovács, *Phys. Rev. A* **36**, 3525 (1987).

Appendix H

Discrete symmetries of dynamics

BASIC GROUP-THEORETIC NOTIONS are recapitulated here: groups, irreducible representations, invariants. Our notation follows birdtracks.eu.

The key result is the construction of projection operators from invariant matrices. The basic idea is simple: a hermitian matrix can be diagonalized. If this matrix is an invariant matrix, it decomposes the reps of the group into direct sums of lower-dimensional reps. Most of computations to follow implement the spectral decomposition

$$\mathbf{M} = \lambda_1 \mathbf{P}_1 + \lambda_2 \mathbf{P}_2 + \cdots + \lambda_r \mathbf{P}_r,$$

which associates with each distinct root λ_i of invariant matrix \mathbf{M} a projection operator (H.17):

$$\mathbf{P}_i = \prod_{j \neq i} \frac{\mathbf{M} - \lambda_j \mathbf{1}}{\lambda_i - \lambda_j}.$$

Sects. H.3 and H.4 develop Fourier analysis as an application of the general theory of invariance groups and their representations.

H.1 Preliminaries and definitions

(A. Wirzba and P. Cvitanović)

We define *group*, *representation*, *symmetry of a dynamical system*, and *invariance*.

Group axioms. A group G is a set of elements g_1, g_2, g_3, \dots for which *composition* or *group multiplication* $g_2 \circ g_1$ (which we often abbreviate as $g_2 g_1$) of any two elements satisfies the following conditions:

1. If $g_1, g_2 \in G$, then $g_2 \circ g_1 \in G$.
2. The group multiplication is associative: $g_3 \circ (g_2 \circ g_1) = (g_3 \circ g_2) \circ g_1$.
3. The group G contains *identity* element e such that $g \circ e = e \circ g = g$ for every element $g \in G$.
4. For every element $g \in G$, there exists a unique $h = g^{-1} \in G$ such that $h \circ g = g \circ h = e$.

A *finite* group is a group with a finite number of elements

$$G = \{e, g_2, \dots, g_{|G|}\},$$

where $|G|$, the number of elements, is the *order* of the group.

Example H.1 Finite groups: Some finite groups that frequently arise in applications:

- C_n (also denoted Z_n): the cyclic group of order n .
- D_n : the dihedral group of order $2n$, rotations and reflections in plane that preserve a regular n -gon.
- S_n : the symmetric group of all permutations of n symbols, order $n!$.

Example H.2 Lie groups: Some compact continuous groups that arise in dynamical systems applications:

- S^1 (also denoted T^1): circle group of dimension 1.
- $T_m = S^1 \times S^1 \cdots \times S^1$: m -torus, of dimension m .
- $SO(2)$: rotations in the plane, dimension 1. Isomorphic to S^1 .
- $O(2) = SO(2) \times D_1$: group of rotations and reflections in the plane, of dimension 1.
- $U(1)$: group of phase rotations in the complex plane, of dimension 1. Isomorphic to $SO(2)$.
- $SO(3)$: rotation group of dimension 3.
- $SU(2)$: unitary group of dimension 3. Isomorphic to $SO(3)$.
- $GL(n)$: general linear group of invertible matrix transformations, dimension n^2 .
- $SO(n)$: special orthogonal group of dimension $n(n-1)/2$.
- $O(n) = SO(n) \times D_1$: orthogonal group of dimension $n(n-1)/2$.
- $Sp(n)$: symplectic group of dimension $n(n+1)/2$.
- $SU(n)$: special unitary group of dimension $n^2 - 1$.

Example H.3 Cyclic and dihedral groups: The cyclic group $C_n \subset SO(2)$ of order n is generated by one element. For example, this element can be rotation through $2\pi/n$. The dihedral group $D_n \subset O(2)$, $n > 2$, can be generated by two elements one at least of which must reverse orientation. For example, take σ corresponding to reflection in the x -axis. $\sigma^2 = e$; such operation σ is called an involution. C to rotation through $2\pi/n$, then $D_n = \langle \sigma, C \rangle$, and the defining relations are $\sigma^2 = C^n = e$, $(C\sigma)^2 = e$.

Groups are defined and classified as abstract objects by their multiplication tables (for finite groups) or Lie algebras (for Lie groups). What concerns us in applications is their *action* as groups of transformations on a given space, usually a vector space (see appendix B.1), but sometimes an affine space, or a more general manifold \mathcal{M} .

Repeated index summation. Throughout this text, the repeated pairs of upper/lower indices are always summed over

$$G_a{}^b x_b \equiv \sum_{b=1}^n G_a{}^b x_b, \quad (\text{H.1})$$

unless explicitly stated otherwise.

General linear transformations. Let $GL(n, \mathbb{F})$ be the group of general linear transformations,

$$GL(n, \mathbb{F}) = \{g : \mathbb{F}^n \rightarrow \mathbb{F}^n \mid \det(g) \neq 0\}. \quad (\text{H.2})$$

Under $GL(n, \mathbb{F})$ a basis set of V is mapped into another basis set by multiplication with a $[n \times n]$ matrix g with entries in field \mathbb{F} (\mathbb{F} is either \mathbb{R} or \mathbb{C}),

$$\mathbf{e}'^a = \mathbf{e}^b (g^{-1})_b{}^a.$$

As the vector \mathbf{x} is what it is, regardless of a particular choice of basis, under this transformation its coordinates must transform as

$$x'_a = g_a{}^b x_b.$$

Standard rep. We shall refer to the set of $[n \times n]$ matrices g as a *standard rep* of $GL(n, \mathbb{F})$, and the space of all n -tuples $(x_1, x_2, \dots, x_n)^T$, $x_i \in \mathbb{F}$ on which these matrices act as the *standard representation space* V .

Under a general linear transformation $g \in GL(n, \mathbb{F})$, the row of basis vectors transforms by right multiplication as $\mathbf{e}' = \mathbf{e} g^{-1}$, and the column of x_a 's transforms by left multiplication as $x' = g x$. Under left multiplication the column

(row transposed) of basis vectors \mathbf{e}^T transforms as $\mathbf{e}'^T = g^\dagger \mathbf{e}^T$, where the *dual rep* $g^\dagger = (g^{-1})^T$ is the transpose of the inverse of g . This observation motivates introduction of a *dual* representation space \bar{V} , the space on which $GL(n, \mathbb{F})$ acts via the dual rep g^\dagger .

Dual space. If V is a vector representation space, then the *dual space* \bar{V} is the set of all linear forms on V over the field \mathbb{F} .

If $\{\mathbf{e}^{(1)}, \dots, \mathbf{e}^{(d)}\}$ is a (right) basis of V , then \bar{V} is spanned by the *dual basis* (left basis) $\{\mathbf{e}_{(1)}, \dots, \mathbf{e}_{(d)}\}$, the set of n linear forms $\mathbf{e}_{(j)}$ such that

$$\mathbf{e}_{(i)} \cdot \mathbf{e}^{(j)} = \delta_i^j,$$

where δ_a^b is the Kronecker symbol, $\delta_a^b = 1$ if $a = b$, and zero otherwise. The components of dual representation space vectors will here be distinguished by upper indices

$$(y^1, y^2, \dots, y^n). \quad (\text{H.3})$$

They transform under $GL(n, \mathbb{F})$ as

$$y'^a = (g^\dagger)_b^a y^b. \quad (\text{H.4})$$

For $GL(n, \mathbb{F})$ no complex conjugation is implied by the \dagger notation; that interpretation applies only to unitary subgroups of $GL(n, \mathbb{C})$. g can be distinguished from g^\dagger by meticulously keeping track of the relative ordering of the indices,

$$g_a^b \rightarrow g_a^b, \quad (g^\dagger)_a^b \rightarrow g^b_a. \quad (\text{H.5})$$

Defining space, dual space. In what follows V will always denote the *defining* n -dimensional complex vector representation space, that is to say the initial, “elementary multiplet” space within which we commence our deliberations. Along with the defining vector representation space V comes the *dual* n -dimensional vector representation space \bar{V} . We shall denote the corresponding element of \bar{V} by raising the index, as in (H.3), so the components of defining space vectors, resp. dual vectors, are distinguished by lower, resp. upper indices:

$$\begin{aligned} x &= (x_1, x_2, \dots, x_n), & \mathbf{x} &\in V \\ \bar{x} &= (x^1, x^2, \dots, x^n), & \bar{\mathbf{x}} &\in \bar{V}. \end{aligned} \quad (\text{H.6})$$

Defining rep. Let G be a group of transformations acting linearly on V , with the action of a group element $g \in G$ on a vector $x \in V$ given by an $[n \times n]$ matrix g

$$x'_a = g_a{}^b x_b \quad a, b = 1, 2, \dots, n. \quad (\text{H.7})$$

We shall refer to $g_a{}^b$ as the *defining rep* of the group G . The action of $g \in G$ on a vector $\bar{q} \in \bar{V}$ is given by the *dual rep* $[n \times n]$ matrix g^\dagger :

$$x'^a = x^b (g^\dagger)_b{}^a = g^a{}_b x^b. \quad (\text{H.8})$$

In the applications considered here, the group G will almost always be assumed to be a subgroup of the *unitary group*, in which case $g^{-1} = g^\dagger$, and \dagger indicates hermitian conjugation:

$$(g^\dagger)_a{}^b = (g_b{}^a)^* = g^b{}_a. \quad (\text{H.9})$$

Hermitian conjugation is effected by complex conjugation and index transposition: Complex conjugation interchanges upper and lower indices; transposition reverses their order. A matrix is *hermitian* if its elements satisfy

$$(\mathbf{M}^\dagger)_b{}^a = M_b{}^a. \quad (\text{H.10})$$

For a hermitian matrix there is no need to keep track of the relative ordering of indices, as $M_b{}^a = (\mathbf{M}^\dagger)_b{}^a = M^a{}_b$.

Invariant vectors. The vector $q \in V$ is an *invariant vector* if for any transformation $g \in G$

$$q = gq. \quad (\text{H.11})$$

If a bilinear form $\mathbf{M}(\bar{x}, y) = x^a M_a{}^b y_b$ is invariant for all $g \in G$, the matrix

$$M_a{}^b = g_a{}^c g^b{}_d M_c{}^d \quad (\text{H.12})$$

is an *invariant matrix*. Multiplying with $g_b{}^e$ and using the unitary condition (H.9), we find that the invariant matrices *commute* with all transformations $g \in G$:

$$[g, \mathbf{M}] = 0. \quad (\text{H.13})$$

Invariants. We shall refer to an invariant relation between p vectors in V and q vectors in \bar{V} , which can be written as a homogeneous polynomial in terms of vector components, such as

$$H(x, y, \bar{z}, \bar{r}, \bar{s}) = h^{ab}{}_{cde} x_b y_a s^e r^d z^c, \quad (\text{H.14})$$

as an *invariant* in $V^q \otimes \bar{V}^p$ (repeated indices, as always, summed over). In this example, the coefficients $h^{ab}{}_{cde}$ are components of invariant tensor $h \in V^3 \otimes \bar{V}^2$.

Matrix group on vector space. We will now apply these abstract group definitions to the set of $[d \times d]$ -dimensional non-singular matrices $\mathbf{A}, \mathbf{B}, \mathbf{C}, \dots \in GL(d)$ acting in a d -dimensional vector space $V \in \mathbb{R}^d$. The product of matrices \mathbf{A} and \mathbf{B} gives the matrix \mathbf{C} ,

$$\mathbf{C}x = \mathbf{B}(\mathbf{A}x) = (\mathbf{B}\mathbf{A})x \in V, \quad \forall x \in V.$$

The identity of the group is the unit matrix $\mathbf{1}$ which leaves all vectors in V unchanged. Every matrix in the group has a unique inverse.

Matrix representation of a group. Let us now map the abstract group G *homomorphically* on a group of matrices $\mathbf{D}(G)$ acting on the vector space V , i.e., in such a way that the group properties, especially the group multiplication, are preserved:

1. Any $g \in G$ is mapped to a matrix $\mathbf{D}(g) \in \mathbf{D}(G)$.
2. The group product $g_2 \circ g_1 \in G$ is mapped onto the matrix product $\mathbf{D}(g_2 \circ g_1) = \mathbf{D}(g_2)\mathbf{D}(g_1)$.
3. The associativity is preserved: $\mathbf{D}(g_3 \circ (g_2 \circ g_1)) = \mathbf{D}(g_3)(\mathbf{D}(g_2)\mathbf{D}(g_1)) = (\mathbf{D}(g_3)(\mathbf{D}(g_2))\mathbf{D}(g_1))$.
4. The identity element $e \in G$ is mapped onto the unit matrix $\mathbf{D}(e) = \mathbf{1}$ and the inverse element $g^{-1} \in G$ is mapped onto the inverse matrix $\mathbf{D}(g^{-1}) = [\mathbf{D}(g)]^{-1} \equiv \mathbf{D}^{-1}(g)$.

We call this matrix group $\mathbf{D}(G)$ a linear or matrix *representation* of the group G in the *representation space* V . We emphasize here ‘*linear*’ in order to distinguish the matrix representations from other representations that do not have to be linear, in general. Throughout this appendix we only consider linear representations.

If the dimensionality of V is d , we say the representation is an *d-dimensional representation*. We will often abbreviate the notation by writing matrices $\mathbf{D}(g) \in \mathbf{D}(G)$ as g , i.e., $x' = gx$ corresponds to the matrix operation $x'_i = \sum_{j=1}^d \mathbf{D}(g)_{ij} x_j$.

Character of a representation. The character of $\chi_\alpha(g)$ of a d -dimensional representation $\mathbf{D}(g)$ of the group element $g \in G$ is defined as trace

$$\chi_\alpha(g) = \text{tr } \mathbf{D}(g) = \sum_{i=1}^d \mathbf{D}_{ii}(g).$$

Note that $\chi(e) = d$, since $\mathbf{D}_{ij}(e) = \delta_{ij}$ for $1 \leq i, j \leq d$.

Faithful representations, factor group. If the mapping G on $\mathbf{D}(G)$ is an isomorphism, the representation is said to be *faithful*. In this case the order of the group of matrices $\mathbf{D}(G)$ is equal to the order $|G|$ of the group. In general, however, there will be several elements $h \in G$ that will be mapped on the unit matrix $\mathbf{D}(h) = \mathbf{1}$. This property can be used to define a subgroup $H \subset G$ of the group G consisting of all elements $h \in G$ that are mapped to the unit matrix of a given representation. Then the representation is a faithful representation of the *factor group* G/H .

Equivalent representations, equivalence classes. A representation of a group is by no means unique. If the basis in the d -dimensional vector space V is changed, the matrices $\mathbf{D}(g)$ have to be replaced by their transformations $\mathbf{D}'(g)$, with the new matrices $\mathbf{D}'(g)$ and the old matrices $\mathbf{D}(g)$ are related by an equivalence transformation through a non-singular matrix \mathbf{C}

$$\mathbf{D}'(g) = \mathbf{C} \mathbf{D}(g) \mathbf{C}^{-1}.$$

The group of matrices $\mathbf{D}'(g)$ form a representation $\mathbf{D}'(G)$ equivalent to the representation $\mathbf{D}(G)$ of the group G . The equivalent representations have the same structure, although the matrices look different. Because of the cyclic nature of the trace the character of equivalent representations is the same

$$\chi(g) = \sum_{i=1}^n \mathbf{D}'_{ii}(g) = \text{tr } \mathbf{D}'(g) = \text{tr}(\mathbf{C} \mathbf{D}(g) \mathbf{C}^{-1}).$$

Regular representation of a finite group. The *regular* representation of a group is a special representation that is defined as follows: Combine the elements of a finite group into a vector $\{g_1, g_2, \dots, g_{|G|}\}$. Multiplication by any element g_ν permutes $\{g_1, g_2, \dots, g_{|G|}\}$ entries. We can represent the element g_ν by the permutation it induces on the components of vector $\{g_1, g_2, \dots, g_{|G|}\}$. Thus for $i, j = 1, \dots, |G|$, we define the *regular representation*

$$\mathbf{D}_{ij}(g_\nu) = \begin{cases} \delta_{jl_i} & \text{if } g_\nu g_i = g_{l_i} \text{ with } l_i = 1, \dots, |G|, \\ 0 & \text{otherwise.} \end{cases}$$

In the regular representation the diagonal elements of all matrices are zero except for the identity element $g_\nu = e$ with $g_\nu g_i = g_i$. So in the regular representation the character is given by

$$\chi(g) = \begin{cases} |G| & \text{for } g = e, \\ 0 & \text{for } g \neq e. \end{cases}$$

H.2 Invariants and reducibility

What follows is a bit dry, so we start with a motivational quote from Hermann Weyl on the “so-called first main theorem of invariant theory”:

“All invariants are expressible in terms of a finite number among them. We cannot claim its validity for every group G ; rather, it will be our chief task to investigate for each particular group whether a finite integrity basis exists or not; the answer, to be sure, will turn out affirmative in the most important cases.”

It is easy to show that any rep of a finite group can be brought to unitary form, and the same is true of all compact Lie groups. Hence, in what follows, we specialize to unitary and hermitian matrices.

H.2.1 Projection operators

For \mathbf{M} a hermitian matrix, there exists a diagonalizing unitary matrix \mathbf{C} such that

$$\mathbf{CMC}^\dagger = \begin{pmatrix} \boxed{\begin{matrix} \lambda_1 & \dots & 0 \\ & \ddots & \\ 0 & \dots & \lambda_1 \end{matrix}} & & 0 & & 0 \\ & & & & \\ & & 0 & & \\ & & & \boxed{\begin{matrix} \lambda_2 & 0 & \dots & 0 \\ 0 & \lambda_2 & & \\ \vdots & & \ddots & \vdots \\ 0 & \dots & & \lambda_2 \end{matrix}} & & 0 \\ & & 0 & & 0 & & \boxed{\begin{matrix} \lambda_3 & \dots \\ \vdots & \ddots \end{matrix}} \end{pmatrix}. \quad (\text{H.15})$$

Here $\lambda_i \neq \lambda_j$ are the r distinct roots of the minimal *characteristic* (or *secular*) polynomial

$$\prod_{i=1}^r (\mathbf{M} - \lambda_i \mathbf{1}) = 0. \quad (\text{H.16})$$

In the matrix $\mathbf{C}(\mathbf{M} - \lambda_2\mathbf{1})\mathbf{C}^\dagger$ the eigenvalues corresponding to λ_2 are replaced by zeroes:

$$\left(\begin{array}{c|c|c} \lambda_1 - \lambda_2 & & \\ \hline & \begin{array}{c} 0 \\ \vdots \\ 0 \end{array} & \\ \hline & & \begin{array}{c} \lambda_3 - \lambda_2 \\ \lambda_3 - \lambda_2 \\ \vdots \end{array} \end{array} \right),$$

and so on, so the product over all factors $(\mathbf{M} - \lambda_2\mathbf{1})(\mathbf{M} - \lambda_3\mathbf{1}) \dots$, with exception of the $(\mathbf{M} - \lambda_1\mathbf{1})$ factor, has nonzero entries only in the subspace associated with λ_1 :

$$\mathbf{C} \prod_{j \neq 1} (\mathbf{M} - \lambda_j\mathbf{1})\mathbf{C}^\dagger = \prod_{j \neq 1} (\lambda_1 - \lambda_j) \left(\begin{array}{c|c} \begin{array}{ccc} 1 & 0 & 0 \\ 0 & 1 & 0 \\ 0 & 0 & 1 \end{array} & \begin{array}{c} 0 \\ \vdots \\ 0 \end{array} \\ \hline \begin{array}{c} 0 \\ \vdots \\ 0 \end{array} & \begin{array}{ccc} 0 & & \\ & 0 & \\ & & \ddots \end{array} \end{array} \right).$$

Thus we can associate with each distinct root λ_i a *projection operator* \mathbf{P}_i ,

$$\mathbf{P}_i = \prod_{j \neq i} \frac{\mathbf{M} - \lambda_j\mathbf{1}}{\lambda_i - \lambda_j}, \tag{H.17}$$

which acts as identity on the i th subspace, and zero elsewhere. For example, the projection operator onto the λ_1 subspace is

$$\mathbf{P}_1 = \mathbf{C}^\dagger \left(\begin{array}{c|c} \begin{array}{ccc} 1 & & \\ & \ddots & \\ & & 1 \end{array} & \\ \hline & \begin{array}{ccc} 0 & & \\ & 0 & \\ & & \ddots \\ & & & 0 \end{array} \end{array} \right) \mathbf{C}. \tag{H.18}$$

The diagonalization matrix \mathbf{C} is deployed in the above only as a pedagogical device. The whole point of the projector operator formalism is that we *never* need to carry such explicit diagonalization; all we need are whatever invariant matrices \mathbf{M} we find convenient, the algebraic relations they satisfy, and orthonormality and completeness of \mathbf{P}_i : The matrices \mathbf{P}_i are *orthogonal*

$$\mathbf{P}_i\mathbf{P}_j = \delta_{ij}\mathbf{P}_j, \quad (\text{no sum on } j), \tag{H.19}$$

and satisfy the *completeness relation*

$$\sum_{i=1}^r \mathbf{P}_i = \mathbf{1}. \quad (\text{H.20})$$

As $\text{tr}(\mathbf{C}\mathbf{P}_i\mathbf{C}^\dagger) = \text{tr}\mathbf{P}_i$, the dimension of the i th subspace is given by

$$d_i = \text{tr}\mathbf{P}_i. \quad (\text{H.21})$$

It follows from the characteristic equation (H.16) and the form of the projection operator (H.17) that λ_i is the eigenvalue of \mathbf{M} on \mathbf{P}_i subspace:

$$\mathbf{M}\mathbf{P}_i = \lambda_i\mathbf{P}_i, \quad (\text{no sum on } i). \quad (\text{H.22})$$

Hence, any matrix polynomial $f(\mathbf{M})$ takes the scalar value $f(\lambda_i)$ on the \mathbf{P}_i subspace

$$f(\mathbf{M})\mathbf{P}_i = f(\lambda_i)\mathbf{P}_i. \quad (\text{H.23})$$

This, of course, is the reason why one wants to work with irreducible reps: they reduce matrices and “operators” to pure numbers.

H.2.2 Irreducible representations

Suppose there exist several linearly independent invariant [$d \times d$] hermitian matrices $\mathbf{M}_1, \mathbf{M}_2, \dots$, and that we have used \mathbf{M}_1 to decompose the d -dimensional vector space $V = V_1 \oplus V_2 \oplus \dots$. Can $\mathbf{M}_2, \mathbf{M}_3, \dots$ be used to further decompose V_i ? Further decomposition is possible if, and only if, the invariant matrices commute:

$$[\mathbf{M}_1, \mathbf{M}_2] = 0, \quad (\text{H.24})$$

or, equivalently, if projection operators \mathbf{P}_j constructed from \mathbf{M}_2 commute with projection operators \mathbf{P}_i constructed from \mathbf{M}_1 ,

$$\mathbf{P}_i\mathbf{P}_j = \mathbf{P}_j\mathbf{P}_i. \quad (\text{H.25})$$

Usually the simplest choices of independent invariant matrices do not commute. In that case, the projection operators \mathbf{P}_i constructed from \mathbf{M}_1 can be used to project commuting pieces of \mathbf{M}_2 :

$$\mathbf{M}_2^{(i)} = \mathbf{P}_i\mathbf{M}_2\mathbf{P}_i, \quad (\text{no sum on } i).$$

That $\mathbf{M}_2^{(i)}$ commutes with \mathbf{M}_1 follows from the orthogonality of \mathbf{P}_i :

$$[\mathbf{M}_2^{(i)}, \mathbf{M}_1] = \sum_j \lambda_j [\mathbf{M}_2^{(i)}, \mathbf{P}_j] = 0. \quad (\text{H.26})$$

Now the characteristic equation for $\mathbf{M}_2^{(i)}$ (if nontrivial) can be used to decompose V_i subspace.

An invariant matrix \mathbf{M} induces a decomposition only if its diagonalized form (H.15) has more than one distinct eigenvalue; otherwise it is proportional to the unit matrix and commutes trivially with all group elements. A rep is said to be *irreducible* if all invariant matrices that can be constructed are proportional to the unit matrix.

According to (H.13), an invariant matrix \mathbf{M} commutes with group transformations $[G, \mathbf{M}] = 0$. Projection operators (H.17) constructed from \mathbf{M} are polynomials in \mathbf{M} , so they also commute with all $g \in \mathcal{G}$:

$$[G, \mathbf{P}_i] = 0 \quad (\text{H.27})$$

Hence, a $[d \times d]$ matrix rep can be written as a direct sum of $[d_i \times d_i]$ matrix reps:

$$G = \mathbf{1}G\mathbf{1} = \sum_{i,j} \mathbf{P}_i G \mathbf{P}_j = \sum_i \mathbf{P}_i G \mathbf{P}_i = \sum_i G_i. \quad (\text{H.28})$$

In the diagonalized rep (H.18), the matrix \mathbf{g} has a block diagonal form:

$$\mathbf{C}\mathbf{g}\mathbf{C}^\dagger = \begin{bmatrix} \mathbf{g}_1 & 0 & 0 \\ 0 & \mathbf{g}_2 & 0 \\ 0 & 0 & \ddots \end{bmatrix}, \quad \mathbf{g} = \sum_i \mathbf{C}^i \mathbf{g}_i \mathbf{C}_i. \quad (\text{H.29})$$

The rep \mathbf{g}_i acts only on the d_i -dimensional subspace V_i consisting of vectors $\mathbf{P}_i q$, $q \in V$. In this way an invariant $[d \times d]$ hermitian matrix \mathbf{M} with r distinct eigenvalues induces a decomposition of a d -dimensional vector space V into a direct sum of d_i -dimensional vector subspaces V_i :

$$V \xrightarrow{\mathbf{M}} V_1 \oplus V_2 \oplus \dots \oplus V_r. \quad (\text{H.30})$$

H.3 Lattice derivatives

Consider a smooth function $\phi(x)$ evaluated on a finite d -dimensional lattice

$$\phi_\ell = \phi(x), \quad x = a\ell = \text{lattice point}, \quad \ell \in \mathbf{Z}^d, \quad (\text{H.31})$$

where a is the lattice spacing and there are N^d points in all. A vector ϕ specifies a lattice configuration. Assume the lattice is hyper-cubic, and let $\hat{n}_\mu \in \{\hat{n}_1, \hat{n}_2, \dots, \hat{n}_d\}$ be the unit lattice cell vectors pointing along the d positive directions, $|\hat{n}_\mu| = 1$. The *lattice partial derivative* is then

$$(\partial_\mu \phi)_\ell = \frac{\phi(x + a\hat{n}_\mu) - \phi(x)}{a} = \frac{\phi_{\ell+\hat{n}_\mu} - \phi_\ell}{a}.$$

Anything else with the correct $a \rightarrow 0$ limit would do, but this is the simplest choice. We can rewrite the derivative as a linear operator, by introducing the *hopping operator* (or “shift,” or “step”) in the direction μ

$$(\mathbf{h}_\mu)_{\ell j} = \delta_{\ell+\hat{n}_\mu, j}. \quad (\text{H.32})$$

As \mathbf{h} will play a central role in what follows, it pays to understand what it does, so we write it out for the 1-dimensional case in its full $[N \times N]$ matrix glory:

$$\mathbf{h} = \begin{pmatrix} 0 & 1 & & & & \\ & 0 & 1 & & & \\ & & 0 & 1 & & \\ & & & & \ddots & \\ & & & & & 0 & 1 \\ 1 & & & & & & 0 \end{pmatrix}. \quad (\text{H.33})$$

We will assume throughout that the lattice is *periodic* in each \hat{n}_μ direction; this is the easiest boundary condition to work with if we are interested in large lattices where surface effects are negligible.

Applied on the lattice configuration $\phi = (\phi_1, \phi_2, \dots, \phi_N)$, the hopping operator shifts the lattice by one site, $\mathbf{h}\phi = (\phi_2, \phi_3, \dots, \phi_N, \phi_1)$. Its transpose shifts the entries the other way, so the transpose is also the inverse

$$\mathbf{h}^{-1} = \mathbf{h}^T. \quad (\text{H.34})$$

The lattice derivative can now be written as a multiplication by a matrix:

$$\partial_\mu \phi_\ell = \frac{1}{a} (\mathbf{h}_\mu - \mathbf{1})_{\ell j} \phi_j.$$

In the 1-dimensional case the $[N \times N]$ matrix representation of the lattice derivative is:

$$\partial = \frac{1}{a} \begin{pmatrix} -1 & 1 & & & & \\ & -1 & 1 & & & \\ & & -1 & 1 & & \\ & & & & \ddots & \\ & & & & & 1 & -1 \\ 1 & & & & & & -1 \end{pmatrix}. \quad (\text{H.35})$$

To belabor the obvious: On a finite lattice of N points a derivative is simply a finite $[N \times N]$ matrix. Continuum field theory is a world in which the lattice is so fine that it looks smooth to us. Whenever someone calls something an “operator,” think “matrix.” For finite-dimensional spaces a linear operator *is* a matrix; things get subtler for infinite-dimensional spaces.

H.3.1 Lattice Laplacian

In order to get rid of some of the lattice indices it is convenient to employ vector notation for the terms bilinear in ϕ , and keep the rest lumped into “interaction,”

$$S[\phi] = -\frac{M^2}{2} \phi^T \cdot \phi - \frac{C}{2} [(\mathbf{h}_\mu - \mathbf{1})\phi]^T \cdot (\mathbf{h}_\mu - \mathbf{1})\phi + S_I[\phi]. \quad (\text{H.36})$$

For example, for the discretized Landau Hamiltonian $M^2/2 = \beta m_0^2/2$, $C = \beta/a^2$, and the quartic term $S_I[\phi]$ is local site-by-site, $\gamma_{\ell_1 \ell_2 \ell_3 \ell_4} = -4! \beta u \delta_{\ell_1 \ell_2} \delta_{\ell_2 \ell_3} \delta_{\ell_3 \ell_4}$, so this general quartic coupling is a little bit of an overkill, but by the time we get to the Fourier-transformed theory, it will make sense as a momentum conserving vertex (H.62).

In the continuum integration by parts moves ∂_μ around; on a lattice this amounts to a matrix transposition

$$[(\mathbf{h}_\mu - \mathbf{1})\phi]^T \cdot [(\mathbf{h}_\mu - \mathbf{1})\phi] = \phi^T \cdot (\mathbf{h}_\mu^{-1} - \mathbf{1})(\mathbf{h}_\mu - \mathbf{1}) \cdot \phi.$$

If you are wondering where the “integration by parts” minus sign is, it is there in discrete case as well. It comes from the identity $\partial^T = -\mathbf{h}^{-1}\partial$. The combination $\Delta = \mathbf{h}^{-1}\partial^2$

$$\Delta = -\frac{1}{a^2} \sum_{\mu=1}^d (\mathbf{h}_\mu^{-1} - \mathbf{1})(\mathbf{h}_\mu - \mathbf{1}) = -\frac{2}{a^2} \sum_{\mu=1}^d \left(\mathbf{1} - \frac{1}{2}(\mathbf{h}_\mu^{-1} + \mathbf{h}_\mu) \right) \quad (\text{H.37})$$

is the *lattice Laplacian*. We shall show below that this Laplacian has the correct continuum limit. It is the simplest spatial derivative allowed for $x \rightarrow -x$ symmetric actions. In the 1-dimensional case the $[N \times N]$ matrix representation of the lattice Laplacian is:

$$\Delta = \frac{1}{a^2} \begin{pmatrix} -2 & 1 & & & 1 \\ 1 & -2 & 1 & & \\ & 1 & -2 & 1 & \\ & & 1 & \ddots & \\ 1 & & & 1 & -2 \end{pmatrix}. \quad (\text{H.38})$$

Consider the effect of a $\phi \rightarrow \mathbf{h}\phi$ translation on the action

$$S[\mathbf{h}\phi] = -\frac{1}{2}\phi^T \cdot \mathbf{h}^T M^{-1} \mathbf{h} \cdot \phi - \frac{\beta g_0}{4!} \sum_{\ell=1}^{N^d} (\mathbf{h}\phi)_\ell^4.$$

As M^{-1} is constructed from \mathbf{h} and its inverse, M^{-1} and \mathbf{h} commute, and the bilinear term is \mathbf{h} invariant. In the quartic term \mathbf{h} permutes cyclically the terms in the sum, so the total action is translationally invariant

$$S[\mathbf{h}\phi] = S[\phi] = -\frac{1}{2}\phi^T \cdot M^{-1} \cdot \phi - \frac{\beta g_0}{4!} \sum_{\ell=1}^{N^d} \phi_\ell^4. \quad (\text{H.41})$$

If a function (in this case, the action $S[\phi]$) defined on a vector space (in this case, the configuration ϕ) commutes with a linear operator \mathbf{h} , then the eigenvalues of \mathbf{h} can be used to decompose the ϕ vector space into invariant subspaces. For a hyper-cubic lattice the translations in different directions commute, $\mathbf{h}_\mu \mathbf{h}_\nu = \mathbf{h}_\nu \mathbf{h}_\mu$, so it is sufficient to understand the spectrum of the 1-dimensional shift operator (H.33). To develop a feeling for how this reduction to invariant subspaces works in practice, let us continue humbly, by expanding the scope of our deliberations to a lattice consisting of 2 points.

H.4.1 A 2-point lattice diagonalized

The action of the shift operator \mathbf{h} (H.33) on a 2-point lattice $\phi = (\phi_1, \phi_2)$ is to permute the two lattice sites

$$\mathbf{h} = \begin{pmatrix} 0 & 1 \\ 1 & 0 \end{pmatrix}.$$

As exchange repeated twice brings us back to the original configuration, $\mathbf{h}^2 = \mathbf{1}$, and the characteristic polynomial of \mathbf{h} is

$$(\mathbf{h} + \mathbf{1})(\mathbf{h} - \mathbf{1}) = 0,$$

with eigenvalues $\lambda_0 = 1, \lambda_1 = -1$. Construct now the symmetrization, antisymmetrization projection operators

$$P_0 = \frac{\mathbf{h} - \lambda_1 \mathbf{1}}{\lambda_0 - \lambda_1} = \frac{1}{2}(\mathbf{1} + \mathbf{h}) = \frac{1}{2} \begin{pmatrix} 1 & 1 \\ 1 & 1 \end{pmatrix} \quad (\text{H.42})$$

$$P_1 = \frac{\mathbf{h} - \lambda_0 \mathbf{1}}{\lambda_1 - \lambda_0} = \frac{1}{2}(\mathbf{1} - \mathbf{h}) = \frac{1}{2} \begin{pmatrix} 1 & -1 \\ -1 & 1 \end{pmatrix}. \quad (\text{H.43})$$

Noting that $P_0 + P_1 = \mathbf{1}$, we can project the lattice configuration ϕ onto the two eigenvectors of \mathbf{h} :

$$\begin{aligned} \phi &= \mathbf{1}\phi = P_0 \cdot \phi + P_1 \cdot \phi, \\ \begin{pmatrix} \phi_1 \\ \phi_2 \end{pmatrix} &= \frac{(\phi_1 + \phi_2)}{\sqrt{2}} \frac{1}{\sqrt{2}} \begin{pmatrix} 1 \\ 1 \end{pmatrix} + \frac{(\phi_1 - \phi_2)}{\sqrt{2}} \frac{1}{\sqrt{2}} \begin{pmatrix} 1 \\ -1 \end{pmatrix} \end{aligned} \tag{H.44}$$

$$= \tilde{\phi}_0 \hat{n}_0 + \tilde{\phi}_1 \hat{n}_1. \tag{H.45}$$

As $P_0 P_1 = 0$, the symmetric and the antisymmetric configurations transform separately under any linear transformation constructed from \mathbf{h} and its powers.

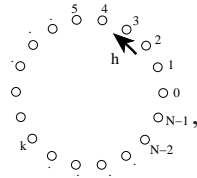
In this way the characteristic equation $\mathbf{h}^2 = \mathbf{1}$ enables us to reduce the 2-dimensional lattice configuration to two 1-dimensional ones, on which the value of the shift operator (shift matrix) \mathbf{h} is a number, $\lambda \in \{1, -1\}$, and the eigenvectors are $\hat{n}_0 = \frac{1}{\sqrt{2}}(1, 1)$, $\hat{n}_1 = \frac{1}{\sqrt{2}}(1, -1)$. We have inserted $\sqrt{2}$ factors only for convenience, in order that the eigenvectors be normalized unit vectors. As we shall now see, $(\tilde{\phi}_0, \tilde{\phi}_1)$ is the 2-site periodic lattice discrete Fourier transform of the field (ϕ_1, ϕ_2) .

H.5 Discrete Fourier transforms

Now let us generalize this reduction to a 1-dimensional periodic lattice with N sites.

Each application of \mathbf{h} translates the lattice one step; in N steps the lattice is back in the original configuration

$$\mathbf{h}^N = \mathbf{1}$$



so the eigenvalues of \mathbf{h} are the N distinct N -th roots of unity

$$\mathbf{h}^N - \mathbf{1} = \prod_{k=0}^{N-1} (\mathbf{h} - \omega^k \mathbf{1}) = 0, \quad \omega = e^{i\frac{2\pi}{N}}. \tag{H.46}$$

As the eigenvalues are all distinct and N in number, the space is decomposed into N 1-dimensional subspaces. The general theory (expounded in appendix H.2) associates with the k -th eigenvalue of \mathbf{h} a projection operator that projects a configuration ϕ onto k -th eigenvector of \mathbf{h} ,

$$P_k = \prod_{j \neq k} \frac{\mathbf{h} - \lambda_j \mathbf{1}}{\lambda_k - \lambda_j}. \tag{H.47}$$

A factor $(\mathbf{h} - \lambda_j \mathbf{1})$ kills the j -th eigenvector φ_j component of an arbitrary vector in expansion $\phi = \dots + \tilde{\phi}_j \varphi_j + \dots$. The above product kills everything but the eigen-direction φ_k , and the factor $\prod_{j \neq k} (\lambda_k - \lambda_j)$ ensures that P_k is normalized as a projection operator. The set of the projection operators is complete

$$\sum_k P_k = \mathbf{1} \tag{H.48}$$

and orthonormal

$$P_k P_j = \delta_{kj} P_k \quad (\text{no sum on } k). \tag{H.49}$$

Constructing explicit eigenvectors is usually not a the best way to fritter one's youth away, as choice of basis is largely arbitrary, and all of the content of the theory is in projection operators. However, in case at hand the eigenvectors are so simple that we can forget the general theory, and construct the solutions of the eigenvalue condition

$$\mathbf{h} \varphi_k = \omega^k \varphi_k \tag{H.50}$$

by hand:

$$\frac{1}{\sqrt{N}} \begin{pmatrix} 0 & 1 & & & \\ & 0 & 1 & & \\ & & 0 & 1 & \\ & & & \ddots & \ddots \\ & & & & 0 & 1 \\ 1 & & & & & 0 \end{pmatrix} \begin{pmatrix} 1 \\ \omega^k \\ \omega^{2k} \\ \omega^{3k} \\ \vdots \\ \omega^{(N-1)k} \end{pmatrix} = \omega^k \frac{1}{\sqrt{N}} \begin{pmatrix} 1 \\ \omega^k \\ \omega^{2k} \\ \omega^{3k} \\ \vdots \\ \omega^{(N-1)k} \end{pmatrix}$$

The $1/\sqrt{N}$ factor is chosen in order that φ_k be normalized unit vectors

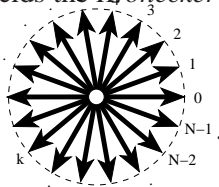
$$\begin{aligned} \varphi_k^\dagger \cdot \varphi_k &= \frac{1}{N} \sum_{k=0}^{N-1} 1 = 1, \quad (\text{no sum on } k) \\ \varphi_k^\dagger &= \frac{1}{\sqrt{N}} (1, \omega^{-k}, \omega^{-2k}, \dots, \omega^{-(N-1)k}). \end{aligned} \tag{H.51}$$

The eigenvectors are orthonormal

$$\varphi_k^\dagger \cdot \varphi_j = \delta_{kj}, \tag{H.52}$$

as the explicit evaluation of $\varphi_k^\dagger \cdot \varphi_j$ yields the *Kronecker delta function for a periodic lattice*

$$\delta_{kj} = \frac{1}{N} \sum_{\ell=0}^{N-1} e^{i \frac{2\pi}{N} (k-j)\ell} \tag{H.53}$$



The sum is over the N unit vectors pointing at a uniform distribution of points on the complex unit circle; they cancel each other unless $k = j \pmod{N}$, in which case each term in the sum equals 1.

The projection operators can be expressed in terms of the eigenvectors (H.50), (H.51) as

$$(P_k)_{\ell\ell'} = (\varphi_k)_\ell (\varphi_k^\dagger)_{\ell'} = \frac{1}{N} e^{i\frac{2\pi}{N}(\ell-\ell')k}, \quad (\text{no sum on } k). \quad (\text{H.54})$$

The completeness (H.48) follows from (H.53), and the orthonormality (H.49) from (H.52).

$\tilde{\phi}_k$, the projection of the ϕ configuration on the k -th subspace is given by

$$\begin{aligned} (P_k \cdot \phi)_\ell &= \tilde{\phi}_k (\varphi_k)_\ell, \quad (\text{no sum on } k) \\ \tilde{\phi}_k &= \varphi_k^\dagger \cdot \phi = \frac{1}{\sqrt{N}} \sum_{\ell=0}^{N-1} e^{-i\frac{2\pi}{N}k\ell} \phi_\ell \end{aligned} \quad (\text{H.55})$$

We recognize $\tilde{\phi}_k$ as the *discrete Fourier transform* of ϕ_ℓ . Hopefully rediscovering it this way helps you a little toward understanding why Fourier transforms are full of $e^{ix \cdot p}$ factors (they are eigenvalues of the generator of translations) and when are they the natural set of basis functions (only if the theory is translationally invariant).

H.5.1 Fourier transform of the propagator

Now insert the identity $\sum P_k = \mathbf{1}$ wherever profitable:

$$\mathbf{M} = \mathbf{1M1} = \sum_{kk'} P_k \mathbf{M} P_{k'} = \sum_{kk'} \varphi_k (\varphi_k^\dagger \cdot \mathbf{M} \cdot \varphi_{k'}) \varphi_{k'}^\dagger.$$

The matrix

$$\tilde{M}_{kk'} = (\varphi_k^\dagger \cdot \mathbf{M} \cdot \varphi_{k'}) \quad (\text{H.56})$$

is the Fourier space representation of \mathbf{M} . No need to stop here - the terms in the action (H.41) that couple four (and, in general, 3, 4, \dots) fields also have the Fourier space representations

$$\begin{aligned} \gamma_{\ell_1 \ell_2 \dots \ell_n} \phi_{\ell_1} \phi_{\ell_2} \dots \phi_{\ell_n} &= \tilde{\gamma}_{k_1 k_2 \dots k_n} \tilde{\phi}_{k_1} \tilde{\phi}_{k_2} \dots \tilde{\phi}_{k_n}, \\ \tilde{\gamma}_{k_1 k_2 \dots k_n} &= \gamma_{\ell_1 \ell_2 \dots \ell_n} (\varphi_{k_1})_{\ell_1} (\varphi_{k_2})_{\ell_2} \dots (\varphi_{k_n})_{\ell_n} \\ &= \frac{1}{N^{n/2}} \sum_{\ell_1 \dots \ell_n} \gamma_{\ell_1 \ell_2 \dots \ell_n} e^{-i\frac{2\pi}{N}(k_1 \ell_1 + \dots + k_n \ell_n)}. \end{aligned} \quad (\text{H.57})$$

According to (H.52) the matrix $U_{k\ell} = (\varphi_k)_\ell = \frac{1}{\sqrt{N}} e^{i\frac{2\pi}{N}k\ell}$ is a unitary matrix, and the Fourier transform is a linear, unitary transformation $UU^\dagger = \sum P_k = \mathbf{1}$ with Jacobian $\det U = 1$. The form of the action (H.41) does not change under $\phi \rightarrow \tilde{\phi}_k$ transformation, and from the formal point of view, it does not matter whether we compute in the Fourier space or in the configuration space that we started out with. For example, the trace of \mathbf{M} is the trace in either representation

$$\begin{aligned} \text{tr } \mathbf{M} &= \sum_{\ell} M_{\ell\ell} = \sum_{kk'} \sum_{\ell} (P_k \mathbf{M} P_{k'})_{\ell\ell} \\ &= \sum_{kk'} \sum_{\ell} (\varphi_k)_\ell (\varphi_k^\dagger \cdot \mathbf{M} \cdot \varphi_{k'})_\ell = \sum_{kk'} \delta_{kk'} \tilde{M}_{kk'} = \text{tr } \tilde{\mathbf{M}}. \end{aligned} \quad (\text{H.58})$$

From this it follows that $\text{tr } \mathbf{M}^n = \text{tr } \tilde{\mathbf{M}}^n$, and from the $\text{tr } \ln = \ln \text{tr}$ relation that $\det \mathbf{M} = \det \tilde{\mathbf{M}}$. In fact, any scalar combination of ϕ 's, J 's and couplings, such as the partition function $Z[J]$, has exactly the same form in the configuration and the Fourier space.

OK, a dizzying quantity of indices. But what's the pay-back?

H.5.2 Lattice Laplacian diagonalized

Now use the eigenvalue equation (H.50) to convert \mathbf{h} matrices into scalars. If \mathbf{M} commutes with \mathbf{h} , then $(\varphi_k^\dagger \cdot \mathbf{M} \cdot \varphi_{k'}) = \tilde{M}_k \delta_{kk'}$, and the matrix \mathbf{M} acts as a multiplication by the scalar \tilde{M}_k on the k -th subspace. For example, for the 1-dimensional version of the lattice Laplacian (H.37) the projection on the k -th subspace is

$$\begin{aligned} (\varphi_k^\dagger \cdot \Delta \cdot \varphi_{k'}) &= \frac{2}{a^2} \left(\frac{1}{2} (\omega^{-k} + \omega^k) - 1 \right) (\varphi_k^\dagger \cdot \varphi_{k'}) \\ &= \frac{2}{a^2} \left(\cos \left(\frac{2\pi}{N} k \right) - 1 \right) \delta_{kk'} \end{aligned} \quad (\text{H.59})$$

In the k -th subspace the bare propagator (H.59) is simply a number, and, in contrast to the mess generated by (H.39), there is nothing to inverting M^{-1} :

$$(\varphi_{\mathbf{k}}^\dagger \cdot M \cdot \varphi_{\mathbf{k}'}) = (\tilde{G}_0)_{\mathbf{k}} \delta_{\mathbf{k}\mathbf{k}'} = \frac{1}{\beta m_0^2 - \frac{2c}{a^2} \sum_{\mu=1}^d \left(\cos \left(\frac{2\pi}{N} k_\mu \right) - 1 \right)}, \quad (\text{H.60})$$

where $\mathbf{k} = (k_1, k_2, \dots, k_\mu)$ is a d -dimensional vector in the N^d -dimensional dual lattice.

Going back to the partition function (28.21) and sticking in the factors of $\mathbf{1}$ into the bilinear part of the interaction, we replace the spatial J_ℓ by its Fourier

transform \tilde{J}_k , and the spatial propagator $(M)_{\ell\ell'}$ by the diagonalized Fourier transformed $(\tilde{G}_0)_k$

$$J^T \cdot M \cdot J = \sum_{k,k'} (J^T \cdot \varphi_k)(\varphi_k^\dagger \cdot M \cdot \varphi_{k'})(\varphi_{k'}^\dagger \cdot J) = \sum_k \tilde{J}_k^\dagger (\tilde{G}_0)_k \tilde{J}_k. \quad (\text{H.61})$$

What's the price? The interaction term $S_I[\phi]$ (which in (28.21) was local in the configuration space) now has a more challenging k dependence in the Fourier transform version (H.57). For example, the locality of the quartic term leads to the 4-vertex *momentum conservation* in the Fourier space

$$\begin{aligned} S_I[\phi] &= \frac{1}{4!} \gamma_{\ell_1 \ell_2 \ell_3 \ell_4} \phi_{\ell_1} \phi_{\ell_2} \phi_{\ell_3} \phi_{\ell_4} = -\beta u \sum_{\ell=1}^{N^d} (\phi_\ell)^4 \Rightarrow \\ &= -\beta u \frac{1}{N^{3d/2}} \sum_{\{\mathbf{k}_i\}}^N \delta_{0, \mathbf{k}_1 + \mathbf{k}_2 + \mathbf{k}_3 + \mathbf{k}_4} \tilde{\phi}_{\mathbf{k}_1} \tilde{\phi}_{\mathbf{k}_2} \tilde{\phi}_{\mathbf{k}_3} \tilde{\phi}_{\mathbf{k}_4}. \end{aligned} \quad (\text{H.62})$$

H.6 C_{4v} factorization

If an N -disk arrangement has C_N symmetry, and the disk visitation sequence is given by disk labels $\{\epsilon_1 \epsilon_2 \epsilon_3 \dots\}$, only the relative increments $\rho_i = \epsilon_{i+1} - \epsilon_i \bmod N$ matter. Symmetries under reflections across axes increase the group to C_{Nv} and add relations between symbols: $\{\epsilon_i\}$ and $\{N - \epsilon_i\}$ differ only by a reflection. As a consequence of this reflection increments become decrements until the next reflection and vice versa. Consider four equal disks placed on the vertices of a square (figure H.1). The symmetry group consists of the identity \mathbf{e} , the two reflections σ_x, σ_y across x, y axes, the two diagonal reflections σ_{13}, σ_{24} , and the three rotations C_4, C_2 and C_4^3 by angles $\pi/2, \pi$ and $3\pi/2$. We start by exploiting the C_4 subgroup symmetry in order to replace the absolute labels $\epsilon_i \in \{1, 2, 3, 4\}$ by relative increments $\rho_i \in \{1, 2, 3\}$. By reflection across diagonals, an increment by 3 is equivalent to an increment by 1 and a reflection; this new symbol will be called $\underline{1}$. Our convention will be to first perform the increment and then to change the orientation due to the reflection. As an example, consider the fundamental domain cycle 112. Taking the disk $1 \rightarrow$ disk 2 segment as the starting segment, this symbol string is mapped into the disk visitation sequence $1_{+1}2_{+1}3_{+2}1 \dots = \overline{123}$, where the subscript indicates the increments (or decrements) between neighboring symbols; the period of the cycle $\overline{112}$ is thus 3 in both the fundamental domain and the full space. Similarly, the cycle $\underline{112}$ will be mapped into $1_{+1}2_{-1}1_{-2}3_{-1}2_{+1}3_{+2}1 = \overline{121323}$ (note that the fundamental domain symbol $\underline{1}$ corresponds to a flip in orientation after the second and fifth symbols); this time the period in the full space is twice that of the fundamental domain. In particular, the fundamental domain fixed points correspond to the following 4-disk cycles:

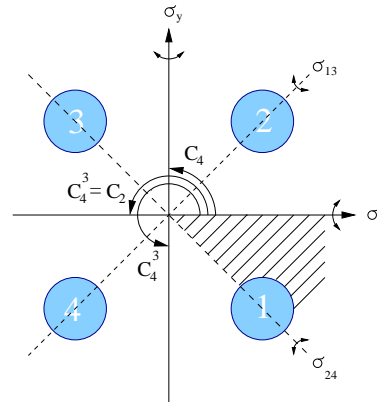


Figure H.1: Symmetries of four disks on a square. A fundamental domain indicated by the shaded wedge.

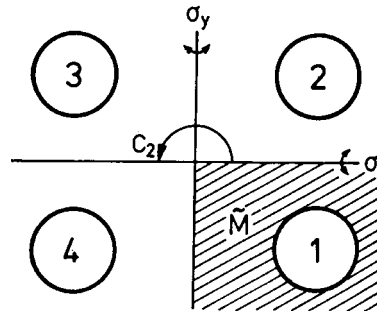


Figure H.2: Symmetries of four disks on a rectangle. A fundamental domain indicated by the shaded wedge.

4-disk		reduced
12	\leftrightarrow	$\frac{1}{1}$
1234	\leftrightarrow	$\frac{1}{1}$
13	\leftrightarrow	$\frac{1}{2}$

Conversions for all periodic orbits of reduced symbol period less than 5 are listed in table H.1.

This symbolic dynamics is closely related to the group-theoretic structure of the dynamics: the global 4-disk trajectory can be generated by mapping the fundamental domain trajectories onto the full 4-disk space by the accumulated product of the C_{4v} group elements $g_1 = C$, $g_2 = C^2$, $g_{\perp} = \sigma_{diag}C = \sigma_{axis}$, where C is a rotation by $\pi/2$. In the $\overline{112}$ example worked out above, this yields $g_{\perp 12} = g_2 g_1 g_{\perp} = C^2 C \sigma_{axis} = \sigma_{diag}$, listed in the last column of table H.1. Our convention is to multiply group elements in the reverse order with respect to the symbol sequence. We need these group elements for our next step, the dynamical zeta function factorizations.

The C_{4v} group has four 1-dimensional representations, either symmetric (A_1) or antisymmetric (A_2) under both types of reflections, or symmetric under one and antisymmetric under the other (B_1, B_2), and a degenerate pair of 2-dimensional representations E . Substituting the C_{4v} characters

Table H.1: C_{4v} correspondence between the ternary fundamental domain prime cycles \tilde{p} and the full 4-disk $\{1,2,3,4\}$ labeled cycles p , together with the C_{4v} transformation that maps the end point of the \tilde{p} cycle into an irreducible segment of the p cycle. For typographical convenience, the symbol $\underline{1}$ of sect. H.6 has been replaced by 0, so that the ternary alphabet is $\{0, 1, 2\}$. The degeneracy of the p cycle is $m_p = 8n_{\tilde{p}}/n_p$. Orbit $\bar{2}$ is the sole boundary orbit, invariant both under a rotation by π and a reflection across a diagonal. The two pairs of cycles marked by (a) and (b) are related by time reversal, but cannot be mapped into each other by C_{4v} transformations.

\tilde{p}	p	$\mathbf{h}_{\tilde{p}}$	\tilde{p}	p	$\mathbf{h}_{\tilde{p}}$
0	12	σ_x	0001	1212 1414	σ_{24}
1	1234	C_4	0002	12124343	σ_y
2	13	C_2, σ_{13}	0011	12123434	C_2
01	1214	σ_{24}	0012	12124141 34342323	C_4^3
02	1243	σ_y	0021 (a)	12134142 34312324	C_4^3
12	1241 3423	C_4^3	0022	1213	e
001	121232343414	C_4	0102 (a)	12142321 34324143	C_4
002	121343	C_2	0111	12143234	σ_{13}
011	121434	σ_y	0112 (b)	12142123	σ_x
012	121323	σ_{13}	0121 (b)	12132124	σ_x
021	124324	σ_{13}	0122	12131413	σ_{24}
022	124213	σ_x	0211	12432134	σ_x
112	123	e	0212	12431423	σ_{24}
122	124231342413	C_4	0221	12421424	σ_{24}
			0222	12424313	σ_y
			1112	12342341 34124123	C_4
			1122	12313413	C_2
			1222	12424131 34242313	C_4^3

C_{4v}	A_1	A_2	B_1	B_2	E
e	1	1	1	1	2
C_2	1	1	1	1	-2
C_4, C_4^3	1	1	-1	-1	0
σ_{axes}	1	-1	1	-1	0
σ_{diag}	1	-1	-1	1	0

into (21.15) we obtain:

$$\begin{array}{l}
 \mathbf{h}_{\tilde{p}} \\
 e: (1 - t_{\tilde{p}})^8 = (1 - t_{\tilde{p}}) (1 - t_{\tilde{p}}) (1 - t_{\tilde{p}}) (1 - t_{\tilde{p}}) (1 - t_{\tilde{p}}) (1 - t_{\tilde{p}}) (1 - t_{\tilde{p}}) (1 - t_{\tilde{p}}) \\
 C_2: (1 - t_{\tilde{p}}^2)^4 = (1 - t_{\tilde{p}}) (1 - t_{\tilde{p}}) (1 - t_{\tilde{p}}) (1 - t_{\tilde{p}}) (1 - t_{\tilde{p}}) (1 - t_{\tilde{p}}) (1 + t_{\tilde{p}})^4 \\
 C_4, C_4^3: (1 - t_{\tilde{p}}^4)^2 = (1 - t_{\tilde{p}}) (1 - t_{\tilde{p}}) (1 + t_{\tilde{p}}) (1 + t_{\tilde{p}}) (1 + t_{\tilde{p}}^2)^2 \\
 \sigma_{axes}: (1 - t_{\tilde{p}}^4)^4 = (1 - t_{\tilde{p}}) (1 + t_{\tilde{p}}) (1 - t_{\tilde{p}}) (1 + t_{\tilde{p}}) (1 - t_{\tilde{p}}^2)^2 \\
 \sigma_{diag}: (1 - t_{\tilde{p}}^2)^4 = (1 - t_{\tilde{p}}) (1 + t_{\tilde{p}}) (1 + t_{\tilde{p}}) (1 - t_{\tilde{p}}) (1 - t_{\tilde{p}}^2)^2
 \end{array}$$

The possible irreducible segment group elements $\mathbf{h}_{\tilde{p}}$ are listed in the first column; σ_{axes} denotes a reflection across either the x-axis or the y-axis, and σ_{diag} denotes a reflection across a diagonal (see figure H.1). In addition, degenerate pairs of boundary orbits can run along the symmetry lines in the full space, with the fundamental domain group theory weights $\mathbf{h}_p = (C_2 + \sigma_x)/2$ (axes) and

$\mathbf{h}_p = (C_2 + \sigma_{13})/2$ (diagonals) respectively:

$$\begin{array}{l} \text{axes:} \\ \text{diagonals:} \end{array} \quad \begin{array}{l} A_1 \quad A_2 \quad B_1 \quad B_2 \quad E \\ (1 - t_{\tilde{p}}^2)^2 = (1 - t_{\tilde{p}})(1 - 0t_{\tilde{p}})(1 - t_{\tilde{p}})(1 - 0t_{\tilde{p}})(1 + t_{\tilde{p}})^2 \\ (1 - t_{\tilde{p}}^2)^2 = (1 - t_{\tilde{p}})(1 - 0t_{\tilde{p}})(1 - 0t_{\tilde{p}})(1 - t_{\tilde{p}})(1 + t_{\tilde{p}})^2 \end{array} \quad (\text{H.63})$$

(we have assumed that $t_{\tilde{p}}$ does not change sign under reflections across symmetry axes). For the 4-disk arrangement considered here only the diagonal orbits $\overline{13}, \overline{24}$ occur; they correspond to the $\overline{2}$ fixed point in the fundamental domain.

The A_1 subspace in C_{4v} cycle expansion is given by

$$\begin{aligned} 1/\zeta_{A_1} &= (1 - t_0)(1 - t_1)(1 - t_2)(1 - t_{01})(1 - t_{02})(1 - t_{12}) \\ &\quad (1 - t_{001})(1 - t_{002})(1 - t_{011})(1 - t_{012})(1 - t_{021})(1 - t_{022})(1 - t_{112}) \\ &\quad (1 - t_{122})(1 - t_{0001})(1 - t_{0002})(1 - t_{0011})(1 - t_{0012})(1 - t_{0021}) \dots \\ &= 1 - t_0 - t_1 - t_2 - (t_{01} - t_0t_1) - (t_{02} - t_0t_2) - (t_{12} - t_1t_2) \\ &\quad - (t_{001} - t_0t_{01}) - (t_{002} - t_0t_{02}) - (t_{011} - t_1t_{01}) \\ &\quad - (t_{022} - t_2t_{02}) - (t_{112} - t_1t_{12}) - (t_{122} - t_2t_{12}) \\ &\quad - (t_{012} + t_{021} + t_0t_1t_2 - t_0t_{12} - t_1t_{02} - t_2t_{01}) \dots \end{aligned} \quad (\text{H.64})$$

(for typographical convenience, $\underline{1}$ is replaced by 0 in the remainder of this section). For 1-dimensional representations, the characters can be read off the symbol strings: $\chi_{A_2}(\mathbf{h}_{\tilde{p}}) = (-1)^{n_0}$, $\chi_{B_1}(\mathbf{h}_{\tilde{p}}) = (-1)^{n_1}$, $\chi_{B_2}(\mathbf{h}_{\tilde{p}}) = (-1)^{n_0+n_1}$, where n_0 and n_1 are the number of times symbols 0, 1 appear in the \tilde{p} symbol string. For B_2 all t_p with an odd total number of 0's and 1's change sign:

$$\begin{aligned} 1/\zeta_{B_2} &= (1 + t_0)(1 + t_1)(1 - t_2)(1 - t_{01})(1 + t_{02})(1 + t_{12}) \\ &\quad (1 + t_{001})(1 - t_{002})(1 + t_{011})(1 - t_{012})(1 - t_{021})(1 + t_{022})(1 - t_{112}) \\ &\quad (1 + t_{122})(1 - t_{0001})(1 + t_{0002})(1 - t_{0011})(1 + t_{0012})(1 + t_{0021}) \dots \\ &= 1 + t_0 + t_1 - t_2 - (t_{01} - t_0t_1) + (t_{02} - t_0t_2) + (t_{12} - t_1t_2) \\ &\quad + (t_{001} - t_0t_{01}) - (t_{002} - t_0t_{02}) + (t_{011} - t_1t_{01}) \\ &\quad + (t_{022} - t_2t_{02}) - (t_{112} - t_1t_{12}) + (t_{122} - t_2t_{12}) \\ &\quad - (t_{012} + t_{021} + t_0t_1t_2 - t_0t_{12} - t_1t_{02} - t_2t_{01}) \dots \end{aligned} \quad (\text{H.65})$$

The form of the remaining cycle expansions depends crucially on the special role played by the boundary orbits: by (H.63) the orbit t_2 does not contribute to A_2 and B_1 ,

$$\begin{aligned} 1/\zeta_{A_2} &= (1 + t_0)(1 - t_1)(1 + t_{01})(1 + t_{02})(1 - t_{12}) \\ &\quad (1 - t_{001})(1 - t_{002})(1 + t_{011})(1 + t_{012})(1 + t_{021})(1 + t_{022})(1 - t_{112}) \\ &\quad (1 - t_{122})(1 + t_{0001})(1 + t_{0002})(1 - t_{0011})(1 - t_{0012})(1 - t_{0021}) \dots \\ &= 1 + t_0 - t_1 + (t_{01} - t_0t_1) + t_{02} - t_{12} \\ &\quad - (t_{001} - t_0t_{01}) - (t_{002} - t_0t_{02}) + (t_{011} - t_1t_{01}) \\ &\quad + t_{022} - t_{122} - (t_{112} - t_1t_{12}) + (t_{012} + t_{021} - t_0t_{12} - t_1t_{02}) \dots \end{aligned} \quad (\text{H.66})$$

and

$$\begin{aligned}
 1/\zeta_{B_1} &= (1 - t_0)(1 + t_1)(1 + t_{01})(1 - t_{02})(1 + t_{12}) \\
 &\quad (1 + t_{001})(1 - t_{002})(1 - t_{011})(1 + t_{012})(1 + t_{021})(1 - t_{022})(1 - t_{112}) \\
 &\quad (1 + t_{122})(1 + t_{0001})(1 - t_{0002})(1 - t_{0011})(1 + t_{0012})(1 + t_{0021}) \dots \\
 &= 1 - t_0 + t_1 + (t_{01} - t_0 t_1) - t_{02} + t_{12} \\
 &\quad + (t_{001} - t_0 t_{01}) - (t_{002} - t_0 t_{02}) - (t_{011} - t_1 t_{01}) \\
 &\quad - t_{022} + t_{122} - (t_{112} - t_1 t_{12}) + (t_{012} + t_{021} - t_0 t_{12} - t_1 t_{02}) \dots \text{(H.67)}
 \end{aligned}$$

In the above we have assumed that t_2 does not change sign under C_{4v} reflections. For the mixed-symmetry subspace E the curvature expansion is given by

$$\begin{aligned}
 1/\zeta_E &= 1 + t_2 + (-t_0^2 + t_1^2) + (2t_{002} - t_2 t_0^2 - 2t_{112} + t_2 t_1^2) \\
 &\quad + (2t_{0011} - 2t_{0022} + 2t_2 t_{002} - t_{01}^2 - t_{02}^2 + 2t_{1122} - 2t_2 t_{112} \\
 &\quad + t_{12}^2 - t_0^2 t_1^2) + (2t_{00002} - 2t_{00112} + 2t_2 t_{0011} - 2t_{00121} - 2t_{00211} \\
 &\quad + 2t_{00222} - 2t_2 t_{0022} + 2t_{01012} + 2t_{01021} - 2t_{01102} - t_2 t_{01}^2 + 2t_{02022} \\
 &\quad - t_2 t_{02}^2 + 2t_{11112} - 2t_{11222} + 2t_2 t_{1122} - 2t_{12122} + t_2 t_{12}^2 - t_2 t_0^2 t_1^2 \\
 &\quad + 2t_{002}(-t_0^2 + t_1^2) - 2t_{112}(-t_0^2 + t_1^2)) \text{(H.68)}
 \end{aligned}$$

A quick test of the $\zeta = \zeta_{A_1} \zeta_{A_2} \zeta_{B_1} \zeta_{B_2} \zeta_E^2$ factorization is afforded by the topological polynomial; substituting $t_p = z^{n_p}$ into the expansion yields

$$1/\zeta_{A_1} = 1 - 3z, \quad 1/\zeta_{A_2} = 1/\zeta_{B_1} = 1, \quad 1/\zeta_{B_2} = 1/\zeta_E = 1 + z,$$

in agreement with (15.46).

exercise 20.9

H.7 C_{2v} factorization

An arrangement of four identical disks on the vertices of a rectangle has C_{2v} symmetry (figure H.2b). C_{2v} consists of $\{e, \sigma_x, \sigma_y, C_2\}$, i.e., the reflections across the symmetry axes and a rotation by π .

This system affords a rather easy visualization of the conversion of a 4-disk dynamics into a fundamental domain symbolic dynamics. An orbit leaving the fundamental domain through one of the axis may be folded back by a reflection on that axis; with these symmetry operations $g_0 = \sigma_x$ and $g_1 = \sigma_y$ we associate labels 1 and 0, respectively. Orbits going to the diagonally opposed disk cross the boundaries of the fundamental domain twice; the product of these two reflections is just $C_2 = \sigma_x \sigma_y$, to which we assign the label 2. For example, a ternary string 0010201... is converted into 12143123..., and the associated group-theory weight is given by ... $g_1 g_0 g_2 g_0 g_1 g_0 g_0$.

Table H.2: C_{2v} correspondence between the ternary $\{0, 1, 2\}$ fundamental domain prime cycles \tilde{p} and the full 4-disk $\{1,2,3,4\}$ cycles p , together with the C_{2v} transformation that maps the end point of the \tilde{p} cycle into an irreducible segment of the p cycle. The degeneracy of the p cycle is $m_p = 4n_{\tilde{p}}/n_p$. Note that the 012 and 021 cycles are related by time reversal, but cannot be mapped into each other by C_{2v} transformations. The full space orbit listed here is generated from the symmetry reduced code by the rules given in sect. H.7, starting from disk 1.

\tilde{p}	p	\mathbf{g}	\tilde{p}	p	\mathbf{g}
0	14	σ_y	0001	14143232	C_2
1	12	σ_x	0002	14142323	σ_x
2	13	C_2	0011	1412	e
01	1432	C_2	0012	14124143	σ_y
02	1423	σ_x	0021	14134142	σ_y
12	1243	σ_y	0022	1413	e
001	141232	σ_x	0102	14324123	σ_y
002	141323	C_2	0111	14343212	C_2
011	143412	σ_y	0112	14342343	σ_x
012	143	e	0121	14312342	σ_x
021	142	e	0122	14313213	C_2
022	142413	σ_y	0211	14212312	σ_x
112	121343	C_2	0212	14213243	C_2
122	124213	σ_x	0221	14243242	C_2
			0222	14242313	σ_x
			1112	12124343	σ_y
			1122	1213	e
			1222	12424313	σ_y

Short ternary cycles and the corresponding 4-disk cycles are listed in table H.2. Note that already at length three there is a pair of cycles (012 = 143 and 021 = 142) related by time reversal, but *not* by any C_{2v} symmetries.

The above is the complete description of the symbolic dynamics for 4 sufficiently separated equal disks placed at corners of a rectangle. However, if the fundamental domain requires further partitioning, the ternary description is insufficient. For example, in the stadium billiard fundamental domain one has to distinguish between bounces off the straight and the curved sections of the billiard wall; in that case five symbols suffice for constructing the covering symbolic dynamics.

The group C_{2v} has four 1-dimensional representations, distinguished by their behavior under axis reflections. The A_1 representation is symmetric with respect to both reflections; the A_2 representation is antisymmetric with respect to both. The B_1 and B_2 representations are symmetric under one and antisymmetric under the other reflection. The character table is

C_{2v}	A_1	A_2	B_1	B_2
e	1	1	1	1
C_2	1	1	-1	-1
σ_x	1	-1	1	-1
σ_y	1	-1	-1	1

Substituted into the factorized determinant (21.14), the contributions of peri-

odic orbits split as follows

$$\begin{array}{lcl}
 g_{\bar{p}} & & A_1 \quad A_2 \quad B_1 \quad B_2 \\
 e: & (1 - t_{\bar{p}})^4 = & (1 - t_{\bar{p}}) \quad (1 - t_{\bar{p}}) \quad (1 - t_{\bar{p}}) \quad (1 - t_{\bar{p}}) \\
 C_2: & (1 - t_{\bar{p}}^2)^2 = & (1 - t_{\bar{p}}) \quad (1 - t_{\bar{p}}) \quad (1 - t_{\bar{p}}) \quad (1 - t_{\bar{p}}) \\
 \sigma_x: & (1 - t_{\bar{p}}^2)^2 = & (1 - t_{\bar{p}}) \quad (1 + t_{\bar{p}}) \quad (1 - t_{\bar{p}}) \quad (1 + t_{\bar{p}}) \\
 \sigma_y: & (1 - t_{\bar{p}}^2)^2 = & (1 - t_{\bar{p}}) \quad (1 + t_{\bar{p}}) \quad (1 + t_{\bar{p}}) \quad (1 - t_{\bar{p}})
 \end{array}$$

Cycle expansions follow by substituting cycles and their group theory factors from table H.2. For A_1 all characters are +1, and the corresponding cycle expansion is given in (H.64). Similarly, the totally antisymmetric subspace factorization A_2 is given by (H.65), the B_2 factorization of C_{4v} . For B_1 all t_p with an odd total number of 0's and 2's change sign:

$$\begin{aligned}
 1/\zeta_{B_1} &= (1 + t_0)(1 - t_1)(1 + t_2)(1 + t_{01})(1 - t_{02})(1 + t_{12}) \\
 &\quad (1 - t_{001})(1 + t_{002})(1 + t_{011})(1 - t_{012})(1 - t_{021})(1 + t_{022})(1 + t_{112}) \\
 &\quad (1 - t_{122})(1 + t_{0001})(1 - t_{0002})(1 - t_{0011})(1 + t_{0012})(1 + t_{0021}) \dots \\
 &= 1 + t_0 - t_1 + t_2 + (t_{01} - t_0 t_1) - (t_{02} - t_0 t_2) + (t_{12} - t_1 t_2) \\
 &\quad - (t_{001} - t_0 t_{01}) + (t_{002} - t_0 t_{02}) + (t_{011} - t_1 t_{01}) \\
 &\quad + (t_{022} - t_2 t_{02}) + (t_{112} - t_1 t_{12}) - (t_{122} - t_2 t_{12}) \\
 &\quad - (t_{012} + t_{021} + t_0 t_1 t_2 - t_0 t_{12} - t_1 t_{02} - t_2 t_{01}) \dots \tag{H.69}
 \end{aligned}$$

For B_2 all t_p with an odd total number of 1's and 2's change sign:

$$\begin{aligned}
 1/\zeta_{B_2} &= (1 - t_0)(1 + t_1)(1 + t_2)(1 + t_{01})(1 + t_{02})(1 - t_{12}) \\
 &\quad (1 + t_{001})(1 + t_{002})(1 - t_{011})(1 - t_{012})(1 - t_{021})(1 - t_{022})(1 + t_{112}) \\
 &\quad (1 + t_{122})(1 + t_{0001})(1 + t_{0002})(1 - t_{0011})(1 - t_{0012})(1 - t_{0021}) \dots \\
 &= 1 - t_0 + t_1 + t_2 + (t_{01} - t_0 t_1) + (t_{02} - t_0 t_2) - (t_{12} - t_1 t_2) \\
 &\quad + (t_{001} - t_0 t_{01}) + (t_{002} - t_0 t_{02}) - (t_{011} - t_1 t_{01}) \\
 &\quad - (t_{022} - t_2 t_{02}) + (t_{112} - t_1 t_{12}) + (t_{122} - t_2 t_{12}) \\
 &\quad - (t_{012} + t_{021} + t_0 t_1 t_2 - t_0 t_{12} - t_1 t_{02} - t_2 t_{01}) \dots \tag{H.70}
 \end{aligned}$$

Note that all of the above cycle expansions group long orbits together with their pseudoorbit shadows, so that the shadowing arguments for convergence still apply.

The topological polynomial factorizes as

$$\frac{1}{\zeta_{A_1}} = 1 - 3z \quad , \quad \frac{1}{\zeta_{A_2}} = \frac{1}{\zeta_{B_1}} = \frac{1}{\zeta_{B_2}} = 1 + z,$$

consistent with the 4-disk factorization (15.46).

H.8 Hénon map symmetries

We note here a few simple symmetries of the Hénon map (3.19). For $b \neq 0$ the Hénon map is reversible: the backward iteration of (3.20) is given by

$$x_{n-1} = -\frac{1}{b}(1 - ax_n^2 - x_{n+1}). \quad (\text{H.71})$$

Hence the time reversal amounts to $b \rightarrow 1/b$, $a \rightarrow a/b^2$ symmetry in the parameter plane, together with $x \rightarrow -x/b$ in the coordinate plane, and there is no need to explore the (a, b) parameter plane outside the strip $b \in \{-1, 1\}$. For $b = -1$ the map is orientation and area preserving ,

$$x_{n-1} = 1 - ax_n^2 - x_{n+1}, \quad (\text{H.72})$$

the backward and the forward iteration are the same, and the non-wandering set is symmetric across the $x_{n+1} = x_n$ diagonal. This is one of the simplest models of a Poincaré return map for a Hamiltonian flow. For the orientation reversing $b = 1$ case we have

$$x_{n-1} = 1 - ax_n^2 + x_{n+1}, \quad (\text{H.73})$$

and the non-wandering set is symmetric across the $x_{n+1} = -x_n$ diagonal.

Commentary

Remark H.1 Literature This material is covered in any introduction to linear algebra [1, 2, 3] or group theory [15, 2]. The exposition given in sects. H.2.1 and H.2.2 is taken from refs. [9, 10, 4]. Who wrote this down first we do not know, but we like Harter's exposition [23, 24, 15] best. Harter's theory of class algebras offers a more elegant and systematic way of constructing the maximal set of commuting invariant matrices \mathbf{M}_i than the sketch offered in this section.

Remark H.2 Labeling conventions While there is a variety of labeling conventions [19, 23] for the reduced C_{4v} dynamics, we prefer the one introduced here because of its close relation to the group-theoretic structure of the dynamics: the global 4-disk trajectory can be generated by mapping the fundamental domain trajectories onto the full 4-disk space by the accumulated product of the C_{4v} group elements.

Remark H.3 C_{2v} symmetry C_{2v} is the symmetry of several systems studied in the literature, such as the stadium billiard [10], and the 2-dimensional anisotropic Kepler potential [3].

Exercises

H.1. **Am I a group?** Show that multiplication table

	<i>e</i>	<i>a</i>	<i>b</i>	<i>c</i>	<i>d</i>	<i>f</i>
<i>e</i>	<i>e</i>	<i>a</i>	<i>b</i>	<i>c</i>	<i>d</i>	<i>f</i>
<i>a</i>	<i>a</i>	<i>e</i>	<i>d</i>	<i>b</i>	<i>f</i>	<i>c</i>
<i>b</i>	<i>b</i>	<i>d</i>	<i>e</i>	<i>f</i>	<i>c</i>	<i>a</i>
<i>c</i>	<i>c</i>	<i>b</i>	<i>f</i>	<i>e</i>	<i>a</i>	<i>d</i>
<i>d</i>	<i>d</i>	<i>f</i>	<i>c</i>	<i>a</i>	<i>e</i>	<i>b</i>
<i>f</i>	<i>f</i>	<i>c</i>	<i>a</i>	<i>d</i>	<i>b</i>	<i>e</i>

describes a group. Or does it? (Hint: check whether this table satisfies the group axioms of appendix H.1.)

From W.G. Harter [15]

H.2. **Three coupled pendulums with a C_2 symmetry.**

Consider 3 pendulums in a row: the 2 outer ones of the same mass m and length l , the one midway of same length but different mass M , with the tip coupled to the tips of the outer ones with springs of stiffness k . Assume displacements are small, $x_i/l \ll 1$.

(a) Show that the acceleration matrix $\ddot{\mathbf{x}} = -\mathbf{a} \mathbf{x}$ is

$$\begin{bmatrix} \ddot{x}_1 \\ \ddot{x}_2 \\ \ddot{x}_3 \end{bmatrix} = - \begin{bmatrix} a+b & -a & 0 \\ -c & 2c+b & -c \\ 0 & -a & a+b \end{bmatrix} \begin{bmatrix} x_1 \\ x_2 \\ x_3 \end{bmatrix},$$

where $a = k/ml$, $c = k/Ml$ and $b = g/l$.

(b) Check that $[\mathbf{a}, \mathbf{R}] = 0$, i.e., that the dynamics is invariant under $C_2 = \{e, R\}$, where \mathbf{R} interchanges the outer pendulums,

$$\mathbf{R} = \begin{bmatrix} 0 & 0 & 1 \\ 0 & 1 & 0 \\ 1 & 0 & 0 \end{bmatrix}.$$

(c) Construct the corresponding projection operators \mathbf{P}_+ and \mathbf{P}_- , and show that the 3-pendulum system decomposes into a 1-dimensional subspace, with eigenvalue $(\omega^{(-)})^2 = a + b$, and a 2-dimensional subspace, with acceleration matrix (trust your own algebra, if it strays from what is stated here)

$$\mathbf{a}^{(+)} = \begin{bmatrix} a+b & -\sqrt{2}a \\ -\sqrt{2}c & c+b \end{bmatrix}.$$

The exercise is simple enough that you can do it without using the symmetry, so: construct \mathbf{P}_+ , \mathbf{P}_- first, use them to reduce \mathbf{a} to irreps, then proceed with computing remaining eigenvalues of \mathbf{a} .

(d) Does anything interesting happen if $M = m$?

The point of the above exercise is that almost always the symmetry reduction is only partial: a matrix representation of dimension d gets reduced to a set of subspaces whose dimensions $d^{(\alpha)}$ satisfy $\sum d^{(\alpha)} = d$. Beyond that, love many, trust few, and paddle your own canoe.

From W.G. Harter [15]

H.3. **Lorenz system in polar coordinates: dynamics.** (continuation of exercise 9.8.)

1. Show that (9.24) has two equilibria:

$$\begin{aligned} (r_0, z_0) &= (0, 0), \quad \theta_0 \text{ undefined} \\ (r_1, \theta_1, z_1) &= (\sqrt{2b(\rho-1)}, \pi/4, \rho) \text{ (H174)} \end{aligned}$$

2. Verify numerically that the eigenvalues and eigenvectors of the two equilibria are (we list here the precise numbers to help you check your programs):

$EQ_1 = (0, 12, 27)$ **equilibrium:** (and its $C^{1/2}$ -rotation EQ_2) has one stable real eigenvalue $\lambda^{(1)} = -13.854578$,

and the unstable complex conjugate pair $\lambda^{(2,3)} = \mu^{(2)} \pm i\omega^{(2)} = 0.093956 \pm i10.194505$.

The unstable eigenplane is defined by eigenvectors

$$\text{Re } \mathbf{e}^{(2)} = (-0.4955, -0.2010, -0.8450)$$

$$\text{Im } \mathbf{e}^{(2)} = (0.5325, -0.8464, 0)$$

with period $T = 2\pi/\omega^{(2)} = 0.6163306$,

radial expansion multiplier

$$\Lambda_r = \exp(2\pi\mu^{(2)}/\omega^{(2)}) = 1.059617,$$

and the contracting multiplier

$$\Lambda_c = \exp(2\pi\mu^{(1)}/\omega^{(2)}) \approx 1.95686 \times 10^{-4}$$

along the stable eigenvector of EQ_1 ,

$$\mathbf{e}^{(3)} = (0.8557, -0.3298, -0.3988).$$

$EQ_0 = (0, 0, 0)$ **equilibrium:** The stable eigenvector $\mathbf{e}^{(1)} = (0, 0, 1)$ of EQ_0 , has contraction rate $\lambda^{(2)} = -b = -2.666 \dots$

The other stable eigenvector is

$$\mathbf{e}^{(2)} = (-0.244001, -0.969775, 0), \text{ with contracting eigenvalue}$$

$$\lambda^{(2)} = -22.8277. \text{ The unstable eigenvector}$$

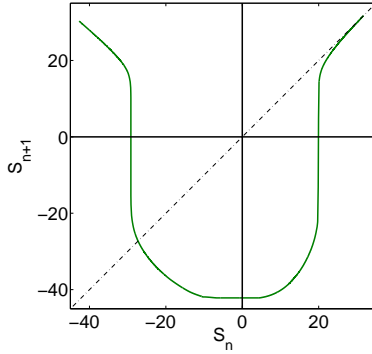
$$\mathbf{e}^{(3)} = (-0.653049, 0.757316, 0) \text{ has eigenvalue}$$

$$\lambda^{(3)} = 11.8277.$$

3. Plot the Lorenz strange attractor both in the Lorenz coordinates figure 2.5, and in the doubled-polar angle coordinates (9.20) for the Lorenz parameter values $\sigma = 10$, $b = 8/3$, $\rho = 28$. Topologically, does it resemble the Lorenz butterfly, the

Rössler attractor, or neither? The Poincaré section of the Lorenz flow fixed by the z -axis and the equilibrium in the doubled polar angle representation, and the corresponding Poincaré return map (s_n, s_{n+1}) are plotted in figure 11.8.

4. Construct the Poincaré return map (s_n, s_{n+1}) ,



where s is arc-length measured along the unstable manifold of E_{Q_0} , lower Poincaré section of figure 11.8 (b). Elucidate its relation to the Poincaré return map of figure 11.9. (plot by J. Halcrow)

5. Show that if a periodic orbit of the polar representation Lorenz is also periodic orbit of the Lorenz flow, their Floquet multipliers are the same. How do the Floquet multipliers of relative periodic orbits of the representations relate to each other?
6. What does the volume contraction formula (4.48) look like now? Interpret.

H.4. Laplacian is a non-local operator.

While the Laplacian is a simple tri-diagonal difference operator (H.38), its inverse (the “free” propagator of statistical mechanics and quantum field theory) is a messier object. A way to compute is to start expanding propagator as a power series in the Laplacian

$$\frac{1}{m^2 \mathbf{1} - \Delta} = \frac{1}{m^2} \sum_{n=0}^{\infty} \frac{1}{m^{2n}} \Delta^n. \tag{H.75}$$

As Δ is a finite matrix, the expansion is convergent for

sufficiently large m^2 . To get a feeling for what is involved in evaluating such series, show that Δ^2 is:

$$\Delta^2 = \frac{1}{a^4} \begin{pmatrix} 6 & -4 & 1 & & & 1 & -4 \\ -4 & 6 & -4 & 1 & & & \\ 1 & -4 & 6 & -4 & 1 & & \\ & & 1 & -4 & \ddots & & \\ & & & & & & 6 & -4 \\ -4 & 1 & & & & 1 & -4 & 6 \end{pmatrix}. \tag{H.76}$$

What $\Delta^3, \Delta^4, \dots$ contributions look like is now clear; as we include higher and higher powers of the Laplacian, the propagator matrix fills up; while the *inverse* propagator is differential operator connecting only the nearest neighbors, the propagator is integral operator, connecting every lattice site to any other lattice site.

This matrix can be evaluated as is, on the lattice, and sometime it is evaluated this way, but in case at hand a wonderful simplification follows from the observation that the lattice action is translationally invariant, exercise H.5.

- H.5. **Lattice Laplacian diagonalized.** Insert the identity $\sum \mathbf{P}^{(k)} = \mathbf{1}$ wherever you profitably can, and use the eigenvalue equation (H.50) to convert shift \mathbf{h} matrices into scalars. If \mathbf{M} commutes with \mathbf{h} , then $(\varphi_k^\dagger \cdot \mathbf{M} \cdot \varphi_{k'}) = \tilde{M}^{(k)} \delta_{kk'}$, and the matrix \mathbf{M} acts as a multiplication by the scalar $\tilde{M}^{(k)}$ on the k th subspace. Show that for the 1-dimensional version of the lattice Laplacian (H.38) the projection on the k th subspace is

$$(\varphi_k^\dagger \cdot \Delta \cdot \varphi_{k'}) = \frac{2}{a^2} \left(\cos \left(\frac{2\pi}{N} k \right) - 1 \right) \delta_{kk'}. \tag{H.77}$$

In the k th subspace the propagator is simply a number, and, in contrast to the mess generated by (H.75), there is nothing to evaluating:

$$\varphi_k^\dagger \cdot \frac{1}{m^2 \mathbf{1} - \Delta} \cdot \varphi_{k'} = \frac{\delta_{kk'}}{m^2 - \frac{2}{(ma)^2} (\cos 2\pi k/N - 1)}, \tag{H.78}$$

where k is a site in the N -dimensional dual lattice, and $a = L/N$ is the lattice spacing.

- H.6. **Fix Predrag’s lecture od Feb 5, 2008.** Are the C_3 frequencies on pp. 4,5 correct? If not, write the correct expression for the beat frequency.

References

[H.1] I. M. Gel’fand, *Lectures on Linear Algebra* (Dover, New York 1961).
 [H.2] S. Lang, *Linear Algebra* (Addison-Wesley, Reading, MA 1971).

- [H.3] K. Nomizu, *Fundamentals of Linear Algebra* (Chelsea Publ., New York 1979).
- [H.4] J. M. Robbins, S. C. Creagh and R. G. Littlejohn, *Phys. Rev.* **A39**, 2838 (1989); **A41**, 6052 (1990).
- [H.5] B. Eckhardt and G. Ott, "Periodic orbit analysis of the Lorenz attractor," *J. Zeitschr. Physik B* **93**, 259 (1994).
- [H.6] V. Franceschini, C. Giberti and Z.M. Zheng, "Characterization of the Lorenz attractor by unstable periodic orbits," *Nonlinearity* **6**, 251 (1993).
- [H.7] B. Lahme and R. Miranda, "Karhunen-Loève Decomposition in the Presence of Symmetry - Part I," *IEEE Trans. Image Processing* **8**, 1183 (1999)
- [H.8] C. Letellier, R. Gilmore and T. Jones, "Peeling bifurcations of toroidal chaotic attractors," [arXiv:0707.3975](https://arxiv.org/abs/0707.3975).
- [H.9] R. Gilmore, "Two-parameter families of strange attractors," *Chaos* **17**, 013104 (2007).
- [H.10] R. Gilmore and M. Lefranc, *The topology of chaos* (Wiley, New York 2002).
- [H.11] R. Gilmore and C. Letellier, "Dressed symbolic dynamics," *Phys. Rev.* **E67**, 036205 (2003).
- [H.12] C. Letellier and R. Gilmore "Symmetry groups for 3D dynamical systems," *J. Phys. A* **40**, 5597 (2007).
- [H.13] R. Gilmore, "Topological analysis of chaotic time series data," *Revs. Mod. Phys.* **70**, 1455 (1998).
- [H.14] J. S. Birman and R. F. Williams, "Knotted periodic orbits in dynamical systems I: Lorenz's equations," *Topology* **22**, 47 (1983).
- [H.15] J. Birman and R. F. Williams, "Knotted periodic orbits in dynamical systems II: Knot holders for fibered knots," *Cont. Math.* **20**, 1 (1983).
- [H.16] T. Tsankov and R. Gilmore, "Strange attractors are classified by bounding tori," *Phys. Rev. Lett.* **91**, 134104 (2003)
- [H.17] T. D. Tsankov and R. Gilmore, "Topological aspects of the structure of chaotic attractors in \mathbb{R}^3 ," *Phys. Rev.* **E69**, 056206 (2004).
- [H.18] O. E. Lanford, "Circle mappings," pp. 1-17 in H. Mitter and L. Pittner, eds., *Recent developments in mathematical physics* (Springer-Verlag, Berlin 1987).
- [H.19] C. Letellier, T. Tsankov, G. Byrne and R. Gilmore, "Large-scale structural reorganization of strange attractors," *Phys. Rev.* **E72**, 026212 (2005).
- [H.20] R. Shaw, "Strange attractors, chaotic behavior, and information flow," *Z. Naturf.* **36a**, 80 (1981).

- [H.21] D.J. Driebe and G.E. Ordnez, *Phys. Lett. A* **211**, 204 (1996).
- [H.22] G.E. Ordnez and D.J. Driebe, *J. Stat. Phys.* **84**, 269 (1996).
- [H.23] W. G. Harter, *J. Math. Phys.* **10**, 4 (1969).
- [H.24] W. G. Harter and N. Dos Santos, "Double-group theory on the half-shell and the two-level system. I. Rotation and half-integral spin states," *Am. J. Phys.* **46**, 251 (1978).

Appendix I

Convergence of spectral determinants

I.1 Curvature expansions: geometric picture

IF YOU HAS SOME EXPERIENCE with numerical estimates of fractal dimensions, you will note that the numerical convergence of cycle expansions for systems such as the 3-disk game of pinball, table 20.2, is very impressive; only three input numbers (the two fixed points $\underline{0}$, $\underline{1}$ and the 2-cycle $\underline{10}$) already yield the escape rate to 4 significant digits! We have omitted an infinity of unstable cycles; so why does approximating the dynamics by a finite number of cycles work so well?

Looking at the cycle expansions simply as sums of unrelated contributions is not specially encouraging: the cycle expansion (20.2) is not absolutely convergent in the sense of Dirichlet series of sect. 20.6, so what one makes of it depends on the way the terms are arranged.

The simplest estimate of the error introduced by approximating smooth flow by periodic orbits is to think of the approximation as a tessalation of a smooth curve by piecewise linear tiles, figure 1.11.

I.1.1 Tessalation of a smooth flow by cycles

One of the early high accuracy computations of π was due to Euler. Euler computed the circumference of the circee of unit radius by inscribing into it a regular polygon with N sides; the error of such computation is proportional to $1 - \cos(2\pi/N) \propto N^{-2}$. In a periodic orbit tessalation of a smooth flow, we cover the phase space by e^{hn} tiles at the n th level of resolution, where h is the topological entropy, the growth rate of the number of tiles. Hence we expect the error in approximating a smooth flow by e^{hn} linear segments to be exponentially small, of order $N^{-2} \propto e^{-2hn}$.

1.1.2 Shadowing and convergence of curvature expansions

We have shown in chapter 15 that if the symbolic dynamics is defined by a finite grammar, a finite number of cycles, let us say the first k terms in the cycle expansion are necessary to correctly count the pieces of the Cantor set generated by the dynamical system.

They are composed of products of non-intersecting loops on the transition graph, see (15.15). We refer to this set of non-intersecting loops as the *fundamental* cycles of the strange set. It is only after these terms have been included that the cycle expansion is expected to converge smoothly, i.e., only for $n > k$ are the curvatures c_n , a measure of the variation of the quality of a linearized covering of the dynamical Cantor set by the length n cycles, and expected to fall off rapidly with n .

The rate of fall-off of the cycle expansion coefficients can be estimated by observing that for subshifts of finite type the contributions from longer orbits in curvature expansions such as (20.7) can always be grouped into shadowing combinations of pseudo-cycles. For example, a cycle with itinerary $\overline{ab} = s_1 s_2 \cdots s_n$ will appear in combination of form

$$1/\zeta = 1 - \cdots - (t_{ab} - t_{a\bar{a}b}) - \cdots ,$$

with \overline{ab} shadowed by cycle \bar{a} followed by cycle \bar{b} , where $a = s_1 s_2 \cdots s_m$, $b = s_{m+1} \cdots s_{n-1} s_n$, and s_k labels the Markov partition \mathcal{M}_{s_k} (11.2) that the trajectory traverses at the k th return. If the two trajectories coincide in the first m symbols, at the m th return to a Poincaré section they can land anywhere in the phase space \mathcal{M}

$$|f^{T_a}(x_a) - f^{T_{a\dots}}(x_{a\dots})| \approx 1 ,$$

where we have assumed that the \mathcal{M} is compact, and that the maximal possible separation across \mathcal{M} is $O(1)$. Here x_a is a point on the \bar{a} cycle of period T_a , and $x_{a\dots}$ is a nearby point whose trajectory tracks the cycle \bar{a} for the first m Poincaré section returns completed at the time $T_{a\dots}$. An estimate of the maximal separation of the initial points of the two neighboring trajectories is achieved by Taylor expanding around $x_{a\dots} = x_{\bar{a}} + \delta x_{a\dots}$

$$f^{T_a}(x_{\bar{a}}) - f^{T_{a\dots}}(x_{a\dots}) \approx \frac{\partial f^{T_a}(x_{\bar{a}})}{\partial x} \cdot \delta x_{a\dots} = M_a \cdot \delta x_{a\dots} ,$$

hence the hyperbolicity of the flow forces the initial points of neighboring trajectories that track each other for at least m consecutive symbols to lie exponentially close

$$|\delta x_{a\dots}| \propto \frac{1}{|\Lambda_a|} .$$

Similarly, for any observable (17.1) integrated along the two nearby trajectories

$$A^{T_{a\dots}}(x_{a\dots}) \approx A^{T_a}(x_{\bar{a}}) + \left. \frac{\partial A^{T_a}}{\partial x} \right|_{x=x_{\bar{a}}} \cdot \delta x_{a\dots},$$

so

$$|A^{T_{a\dots}}(x_{a\dots}) - A^{T_a}(x_{\bar{a}})| \propto \frac{T_a \text{Const}}{|\Lambda_a|},$$

As the time of return is itself an integral along the trajectory, return times of nearby trajectories are exponentially close

$$|T_{a\dots} - T_a| \propto \frac{T_a \text{Const}}{|\Lambda_a|},$$

and so are the trajectory stabilities

$$|A^{T_{a\dots}}(x_{a\dots}) - A^{T_a}(x_{\bar{a}})| \propto \frac{T_a \text{Const}}{|\Lambda_a|},$$

Substituting t_{ab} one finds

$$\frac{t_{ab} - t_a t_b}{t_{ab}} = 1 - e^{-s(T_a + T_b - T_{ab})} \left| \frac{\Lambda_a \Lambda_b}{\Lambda_{ab}} \right|.$$

Since with increasing m segments of \overline{ab} come closer to \bar{a} , the differences in action and the ratio of the eigenvalues converge exponentially with the eigenvalue of the orbit \bar{a} ,

$$T_a + T_b - T_{ab} \approx \text{Const} \times \Lambda_a^{-j}, \quad |\Lambda_a \Lambda_b / \Lambda_{ab}| \approx \exp(-\text{Const} / \Lambda_{ab})$$

Expanding the exponentials one thus finds that this term in the cycle expansion is of the order of

$$t_{a^j b} - t_a t_{a^{j-1} b} \approx \text{Const} \times t_{a^j b} \Lambda_a^{-j}. \quad (\text{I.1})$$

Even though the number of terms in a cycle expansion grows exponentially, the shadowing cancellations improve the convergence by an exponential factor compared to trace formulas, and extend the radius of convergence of the periodic orbit sums. Table I.1 shows some examples of such compensations between long cycles and their pseudo-cycle shadows.

n	$t_{ab} - t_a t_b$	$T_{ab} - (T_a + T_b)$	$\log \frac{\Lambda_a \Lambda_b}{\Lambda_{ab}}$	$ab - a \cdot b$
2	$-5.23465150784 \times 10^4$	$4.85802927371 \times 10^2$	-6.3×10^2	01-0·1
3	$-7.96028600139 \times 10^6$	$5.21713101432 \times 10^3$	-9.8×10^3	001-0·01
4	$-1.03326529874 \times 10^7$	$5.29858199419 \times 10^4$	-1.3×10^3	0001-0·001
5	$-1.27481522016 \times 10^9$	$5.35513574697 \times 10^5$	-1.6×10^4	00001-0·0001
6	$-1.52544704823 \times 10^{11}$	$5.40999882625 \times 10^6$	-1.8×10^5	000001-0·00001
2	$-5.23465150784 \times 10^4$	$4.85802927371 \times 10^2$	-6.3×10^2	01-0·1
3	$5.30414752996 \times 10^6$	$-3.67093656690 \times 10^3$	7.7×10^3	011-01·1
4	$-5.40934261680 \times 10^8$	$3.14925761316 \times 10^4$	-9.2×10^4	0111-011·1
5	$4.99129508833 \times 10^{10}$	$-2.67292822795 \times 10^5$	1.0×10^4	01111-0111·1
6	$-4.39246000586 \times 10^{12}$	$2.27087116266 \times 10^6$	-1.0×10^5	011111-01111·1

Table I.1: Demonstration of shadowing in curvature combinations of cycle weights of form $t_{ab} - t_a t_b$, the 3-disk fundamental domain cycles at $R : d = 6$, table 29.3. The ratio $\Lambda_a \Lambda_b / \Lambda_{ab}$ is approaching unity exponentially fast.

It is crucial that the curvature expansion is grouped (and truncated) by topologically related cycles and pseudo-cycles; truncations that ignore topology, such as inclusion of all cycles with $T_p < T_{max}$, will contain orbits unmatched by shadowed orbits, and exhibit a mediocre convergence compared with the curvature expansions.

Note that the existence of a pole at $z = 1/c$ implies that the cycle expansions have a finite radius of convergence, and that analytic continuations will be required for extraction of the non-leading zeros of $1/\zeta$. Preferably, one should work with cycle expansions of Selberg products, as discussed in sect.20.2.2.

I.1.3 No shadowing, poorer convergence

Conversely, if the dynamics is not of a finite subshift type, there is no finite topological polynomial, there are no “curvature” corrections, and the convergence of the cycle expansions will be poor.

I.2 On importance of pruning

If the grammar is not finite and there is no finite topological polynomial, there will be no “curvature” expansions, and the convergence will be poor. That is the generic case, and one strategy for dealing with it is to find a good sequence of approximate but finite grammars; for each approximate grammar cycle expansions yield exponentially accurate eigenvalues, with successive approximate grammars converging toward the desired infinite grammar system.

When the dynamical system’s symbolic dynamics does not have a finite grammar, and we are not able to arrange its cycle expansion into curvature combinations (20.7), the series is truncated as in sect. 20.5, by including all pseudo-cycles such that $|\Lambda_{p_1} \cdots \Lambda_{p_k}| \leq |\Lambda_P|$, where P is the most unstable prime cycle included

into truncation. The truncation error should then be of order $O(e^{hT_P} T_P / |\Lambda_P|)$, with h the topological entropy, and e^{hT_P} roughly the number of pseudo-cycles of stability $\approx |\Lambda_P|$. In this case the cycle averaging formulas do not converge significantly better than the approximations such as the trace formula (22.18).

Numerical results (see for example the plots of the accuracy of the cycle expansion truncations for the Hénon map in ref. [3]) indicate that the truncation error of most averages tracks closely the fluctuations due to the irregular growth in the number of cycles. It is not known whether one can exploit the sum rules such as the mass flow conservation (22.11) to improve the accuracy of dynamical averaging.

I.3 Ma-the-matical caveats

“Lo duca e io per quel cammino ascoso intrammo a ritornar nel chiaro monde; e senza cura aver d’alcun riposa salimmo sù, el primo e io secondo, tanto ch’i’ vidi de le cose belle che porta ‘l ciel, per un perutgio tondo.”

—Dante



The periodic orbit theory is learned in stages. At first glance, it seems totally impenetrable. After basic exercises are gone through, it seems totally trivial; all that seems to be at stake are elementary manipulations with traces, determinants, derivatives. But if start thinking about you will get a more and more uncomfortable feeling that from the mathematical point of view, this is a perilous enterprise indeed. In chapter 23 we shall explain which parts of this enterprise are really solid; here you give a fortaste of what objections a mathematician might rise.

Birkhoff’s 1931 ergodic theorem states that the time average (17.4) exists almost everywhere, and, if the flow is ergodic, it implies that $\langle a(x) \rangle = \langle a \rangle$ is a constant for almost all x . The problem is that the above cycle averaging formulas implicitly rely on ergodic hypothesis: they are strictly correct only if the dynamical system is locally hyperbolic and globally mixing. If one takes a β derivative of both sides

$$\rho_\beta(y) e^{ts(\beta)} = \int_{\mathcal{M}} dx \delta(y - f^t(x)) e^{\beta \cdot A^t(x)} \rho_\beta(x),$$

and integrates over y

$$\int_{\mathcal{M}} dy \left. \frac{\partial}{\partial \beta} \rho_\beta(y) \right|_{\beta=0} + t \left. \frac{\partial s}{\partial \beta} \right|_{\beta=0} \int_{\mathcal{M}} dy \rho_0(y) = \int_{\mathcal{M}} dx A^t(x) \rho_0(x) + \int_{\mathcal{M}} dx \left. \frac{\partial}{\partial \beta} \rho_\beta(x) \right|_{\beta=0},$$

one obtains in the long time limit

$$\left. \frac{\partial s}{\partial \beta} \right|_{\beta=0} = \int_{\mathcal{M}} dy \rho_0(x) \langle a(x) \rangle . \quad (\text{I.2})$$

This is the expectation value (17.12) only if the time average (17.4) equals the space average (17.9), $\langle a(x) \rangle = \langle a \rangle$, for all x except a subset $x \in \mathcal{M}$ of zero measure; if the phase space is foliated into non-communicating subspaces $\mathcal{M} = \mathcal{M}_1 + \mathcal{M}_2$ of finite measure such that $f^t(\mathcal{M}_1) \cap \mathcal{M}_2 = \emptyset$ for all t , this fails. In other words, we have tacitly assumed metric indecomposability or transitivity. We have also glossed over the nature of the “phase space” \mathcal{M} . For example, if the dynamical system is open, such as the 3-disk game of pinball, \mathcal{M} in the expectation value integral (17.22) is a Cantor set, the closure of the union of all periodic orbits. Alternatively, \mathcal{M} can be considered continuous, but then the measure ρ_0 in (I.2) is highly singular. The beauty of the periodic orbit theory is that instead of using an arbitrary coordinatization of \mathcal{M} it partitions the phase space by the intrinsic topology of the dynamical flow and builds the correct measure from cycle invariants, the Floquet multipliers of periodic orbits.

Were we to restrict the applications of the formalism only to systems which have been rigorously proven to be ergodic, we might as well fold up the shop right now. For example, even for something as simple as the Hénon mapping we do not know whether the asymptotic time attractor is strange or periodic. Physics applications require a more pragmatic attitude. In the cycle expansions approach we construct the invariant set of the given dynamical system as a closure of the union of periodic orbits, and investigate how robust are the averages computed on this set. This turns out to depend very much on the observable being averaged over; dynamical averages exhibit “phase transitions”, and the above cycle averaging formulas apply in the “hyperbolic phase” where the average is dominated by exponentially many exponentially small contributions, but fail in a phase dominated by few marginally stable orbits. Here the noise - always present, no matter how weak - helps us by erasing an infinity of small traps that the deterministic dynamics might fall into.

exercise 17.1

Still, in spite of all the caveats, periodic orbit theory is a beautiful theory, and the cycle averaging formulas are the most elegant and powerful tool available today for evaluation of dynamical averages for low dimensional chaotic deterministic systems.

I.4 Estimate of the n th cumulant

An immediate consequence of the exponential spacing of the eigenvalues is that the convergence of the Selberg product expansion (D.12) as function of the topological cycle length, $F(z) = \sum_n C_n z^n$, is faster than exponential. Consider a d -dimensional cycle map for which all Jacobian matrix eigenvalues are equal: $u_p = \Lambda_{p,1} = \Lambda_{p,2} = \dots = \Lambda_{p,d}$. The Floquet multipliers are generally not isotropic;

however, to obtain qualitative bounds on the spectrum, we replace all Floquet multipliers with the least expanding one. In this case the p cycle contribution to the product (19.9) reduces to

$$\begin{aligned}
 F_p(z) &= \prod_{k_1 \dots k_d=0}^{\infty} (1 - t_p u_p^{k_1+k_2+\dots+k_d}) \\
 &= \prod_{k=0}^{\infty} (1 - t_p u_p^k)^{m_k}; \quad m_k = \binom{d-1+k}{d-1} = \frac{(k+d-1)!}{k!(d-1)!} \\
 &= \prod_{k=0}^{\infty} \sum_{\ell=0}^{m_k} \binom{m_k}{\ell} (-u_p^k t_p)^{\ell}
 \end{aligned} \tag{I.3}$$

In one dimension the expansion can be given in closed form (23.5), and the coefficients C_k in (D.12) are given by

$$\tau_{p^k} = (-1)^k \frac{u_p^{\frac{k(k-1)}{2}} t_p^k}{\prod_{j=1}^k (1 - u_p^j)} \tag{I.4}$$

Hence the coefficients in the $F(z) = \sum_n C_n z^n$ expansion of the spectral determinant (20.11) fall off faster than exponentially, as $|C_n| \approx u^{n(n-1)/2}$. In contrast, the cycle expansions of dynamical zeta functions fall of “only” exponentially; in numerical applications, the difference is dramatic.

In higher dimensions the expansions are not quite as compact. The leading power of u and its coefficient are easily evaluated by use of binomial expansions (I.3) of the $(1+tu^k)^{m_k}$ factors. More precisely, the leading u^l terms in t^k coefficients are of form

$$\begin{aligned}
 \prod_{k=0}^{\infty} (1 + tu^k)^{m_k} &= \dots + u^{m_1+2m_2+\dots+jm_j} t^{1+m_1+m_2+\dots+m_j} + \dots \\
 &= \dots + \left(u^{\frac{m_d}{d+1}} t \right)^{\binom{d+m}{m}} + \dots \approx \dots + u^{\frac{d\sqrt{d}}{(d-1)!} n} t^{\frac{d+1}{d}} t^n + \dots
 \end{aligned}$$

Hence the coefficients in the $F(z)$ expansion fall off faster than exponentially, as $u^{n^{1+1/d}}$. The Selberg products are entire functions in any dimension, provided that the symbolic dynamics is a finite subshift, and all cycle eigenvalues are sufficiently bounded away from 1.

The case of particular interest in many applications are the 2-d Hamiltonian mappings; their symplectic structure implies that $u_p = \Lambda_{p,1} = 1/\Lambda_{p,2}$, and the Selberg product (19.13) In this case the expansion corresponding to (23.5) is given in exercise 23.4 and the coefficients fall off asymptotically as $C_n \approx u^{n^{3/2}}$.

Appendix J

Infinite dimensional operators

(A. Wirzba)

THIS APPENDIX, taken from ref. [1], summarizes the definitions and properties of trace-class and Hilbert-Schmidt matrices, the determinants over infinite dimensional matrices and regularization schemes for matrices or operators which are not of trace-class.

J.1 Matrix-valued functions

(P. Cvitanović)

As a preliminary we summarize some of the properties of functions of finite-dimensional matrices.

The derivative of a matrix is a matrix with elements

$$A'(x) = \frac{dA(x)}{dx}, \quad A'_{ij}(x) = \frac{d}{dx}A_{ij}(x). \quad (\text{J.1})$$

Derivatives of products of matrices are evaluated by the chain rule

$$\frac{d}{dx}(A\mathbf{B}) = \frac{dA}{dx}\mathbf{B} + A\frac{d\mathbf{B}}{dx}. \quad (\text{J.2})$$

A matrix and its derivative matrix in general do not commute

$$\frac{d}{dx}A^2 = \frac{dA}{dx}A + A\frac{dA}{dx}. \quad (\text{J.3})$$

The derivative of the inverse of a matrix, follows from $\frac{d}{dx}(AA^{-1}) = 0$:

$$\frac{d}{dx}A^{-1} = -\frac{1}{A} \frac{dA}{dx} \frac{1}{A}. \quad (\text{J.4})$$

A function of a single variable that can be expressed in terms of additions and multiplications generalizes to a matrix-valued function by replacing the variable by the matrix.

In particular, the exponential of a constant matrix can be defined either by its series expansion, or as a limit of an infinite product:

$$e^A = \sum_{k=0}^{\infty} \frac{1}{k!} A^k, \quad A^0 = \mathbf{1} \quad (\text{J.5})$$

$$= \lim_{N \rightarrow \infty} \left(\mathbf{1} + \frac{1}{N} A \right)^N \quad (\text{J.6})$$

The first equation follows from the second one by the binomial theorem, so these indeed are equivalent definitions. That the terms of order $O(N^{-2})$ or smaller do not matter follows from the bound

$$\left(1 + \frac{x - \epsilon}{N} \right)^N < \left(1 + \frac{x + \delta x_N}{N} \right)^N < \left(1 + \frac{x + \epsilon}{N} \right)^N,$$

where $|\delta x_N| < \epsilon$. If $\lim \delta x_N \rightarrow 0$ as $N \rightarrow \infty$, the extra terms do not contribute.

Consider now the determinant

$$\det(e^A) = \lim_{N \rightarrow \infty} (\det(\mathbf{1} + A/N))^N.$$

To the leading order in $1/N$

$$\det(\mathbf{1} + A/N) = 1 + \frac{1}{N} \text{tr} A + O(N^{-2}).$$

hence

$$\det e^A = \lim_{N \rightarrow \infty} \left(1 + \frac{1}{N} \text{tr} A + O(N^{-2}) \right)^N = e^{\text{tr} A} \quad (\text{J.7})$$

Due to non-commutativity of matrices, generalization of a function of several variables to a function is not as straightforward. Expression involving several

matrices depend on their commutation relations. For example, the commutator expansion

$$e^{t\mathbf{A}}\mathbf{B}e^{-t\mathbf{A}} = \mathbf{B} + t[\mathbf{A}, \mathbf{B}] + \frac{t^2}{2}[\mathbf{A}, [\mathbf{A}, \mathbf{B}]] + \frac{t^3}{3!}[\mathbf{A}, [\mathbf{A}, [\mathbf{A}, \mathbf{B}]]] + \dots \quad (\text{J.8})$$

sometimes used to establish the equivalence of the Heisenberg and Schrödinger pictures of quantum mechanics follows by recursive evaluation of t derivatives

$$\frac{d}{dt} (e^{t\mathbf{A}}\mathbf{B}e^{-t\mathbf{A}}) = e^{t\mathbf{A}}[\mathbf{A}, \mathbf{B}]e^{-t\mathbf{A}}.$$

Manipulations of such ilk yield

$$e^{(\mathbf{A}+\mathbf{B})/N} = e^{\mathbf{A}/N}e^{\mathbf{B}/N} - \frac{1}{2N^2}[\mathbf{A}, \mathbf{B}] + O(N^{-3}),$$

and the Trotter product formula: if \mathbf{B} , \mathbf{C} and $\mathbf{A} = \mathbf{B} + \mathbf{C}$ are matrices, then

$$e^{\mathbf{A}} = \lim_{N \rightarrow \infty} (e^{\mathbf{B}/N}e^{\mathbf{C}/N})^N \quad (\text{J.9})$$

J.2 Operator norms

(R. Mainieri and P. Cvitanović)



The limit used in the above definition involves matrices - operators in vector spaces - rather than numbers, and its convergence can be checked using tools familiar from calculus. We briefly review those tools here, as throughout the text we will have to consider many different operators and how they converge.

The $n \rightarrow \infty$ convergence of partial products

$$\mathbf{E}_n = \prod_{0 \leq m < n} \left(\mathbf{1} + \frac{t}{m} \mathbf{A} \right)$$

can be verified using the Cauchy criterion, which states that the sequence $\{\mathbf{E}_n\}$ converges if the differences $\|\mathbf{E}_k - \mathbf{E}_j\| \rightarrow 0$ as $k, j \rightarrow \infty$. To make sense of this we need to define a sensible norm $\|\cdot\|$. Norm of a matrix is based on the Euclidean norm for a vector: the idea is to assign to a matrix \mathbf{M} a norm that is the largest possible change it can cause to the length of a unit vector \hat{n} :

$$\|\mathbf{M}\| = \sup_{\hat{n}} \|\mathbf{M}\hat{n}\|, \quad \|\hat{n}\| = 1. \quad (\text{J.10})$$

We say that $\|\cdot\|$ is the operator norm induced by the vector norm $\|\cdot\|$. Constructing a norm for a finite-dimensional matrix is easy, but had \mathbf{M} been an operator in an infinite-dimensional space, we would also have to specify the space \hat{n} belongs to. In the finite-dimensional case, the sum of the absolute values of the components of a vector is also a norm; the induced operator norm for a matrix \mathbf{M} with components M_{ij} in that case can be defined by

$$\|\mathbf{M}\| = \max_i \sum_j |M_{ij}|. \quad (\text{J.11})$$

The operator norm (J.11) and the vector norm (J.10) are only rarely distinguished by different notation, a bit of notational laziness that we shall uphold.

Now that we have learned how to make sense out of norms of operators, we can check that

$$\|e^{tA}\| \leq e^{t\|A\|}. \quad (\text{J.12})$$

exercise J.1

exercise 2.9

As $\|A\|$ is a number, the norm of e^{tA} is finite and therefore well defined. In particular, the exponential of a matrix is well defined for all values of t , and the linear differential equation (4.10) has a solution for all times.

J.3 Trace class and Hilbert-Schmidt class

This section is mainly an extract from ref. [9]. Refs. [7, 10, 11, 14] should be consulted for more details and proofs. The trace class and Hilbert-Schmidt property will be defined here for linear, in general non-hermitian operators $\mathbf{A} \in \mathcal{L}(\mathcal{H})$: $\mathcal{H} \rightarrow \mathcal{H}$ (where \mathcal{H} is a separable Hilbert space). The transcription to matrix elements (used in the prior chapters) is simply $\alpha_{ij} = \langle \phi_i, \mathbf{A}\phi_j \rangle$ where $\{\phi_n\}$ is an orthonormal basis of \mathcal{H} and $\langle \cdot, \cdot \rangle$ is the inner product in \mathcal{H} (see sect. J.5 where the theory of *von Koch matrices* of ref. [12] is discussed). So, the trace is the generalization of the usual notion of the sum of the diagonal elements of a matrix; but because infinite sums are involved, not all operators will have a trace:

Definition:

- (a) An operator \mathbf{A} is called **trace class**, $\mathbf{A} \in \mathcal{J}_1$, if and only if, for every orthonormal basis, $\{\phi_n\}$:

$$\sum_n |\langle \phi_n, \mathbf{A}\phi_n \rangle| < \infty. \quad (\text{J.13})$$

The family of all trace class operators is denoted by \mathcal{J}_1 .

- (b) An operator \mathbf{A} is called **Hilbert-Schmidt**, $\mathbf{A} \in \mathcal{J}_2$, if and only if, for every orthonormal basis, $\{\phi_n\}$:

$$\sum_n \|\mathbf{A}\phi_n\|^2 < \infty.$$

The family of all Hilbert-Schmidt operators is denoted by \mathcal{J}_2 .

Bounded operators are dual to trace class operators. They satisfy the following condition: $|\langle \psi, B\phi \rangle| \leq C\|\psi\|\|\phi\|$ with $C < \infty$ and $\psi, \phi \in \mathcal{H}$. If they have eigenvalues, these are bounded too. The family of bounded operators is denoted by $\mathcal{B}(\mathcal{H})$ with the norm $\|\mathbf{B}\| = \sup_{\phi \neq 0} \frac{\|\mathbf{B}\phi\|}{\|\phi\|}$ for $\phi \in \mathcal{H}$. Examples for bounded operators are unitary operators and especially the unit matrix. In fact, every bounded operator can be written as linear combination of four unitary operators.

A bounded operator \mathbf{C} is *compact*, if it is the norm limit of finite rank operators.

An operator \mathbf{A} is called *positive*, $\mathbf{A} \geq 0$, if $\langle \mathbf{A}\phi, \phi \rangle \geq 0 \forall \phi \in \mathcal{H}$. Note that $\mathbf{A}^\dagger \mathbf{A} \geq 0$. We define $|\mathbf{A}| = \sqrt{\mathbf{A}^\dagger \mathbf{A}}$.

The most important properties of the trace and Hilbert-Schmidt classes are summarized in (see refs. [7, 9]):

- (a) \mathcal{J}_1 and \mathcal{J}_2 are **ideals*., i.e., they are vector spaces closed under scalar multiplication, sums, adjoints, and multiplication with bounded operators.
- (b) $\mathbf{A} \in \mathcal{J}_1$ if and only if $\mathbf{A} = \mathbf{B}\mathbf{C}$ with $\mathbf{B}, \mathbf{C} \in \mathcal{J}_2$.
- (c) $\mathcal{J}_1 \subset \mathcal{J}_2 \subset \text{Compact operators}$.
- (d) For any operator \mathbf{A} , we have $\mathbf{A} \in \mathcal{J}_2$ if $\sum_n \|\mathbf{A}\phi_n\|^2 < \infty$ for a single basis. For any operator $\mathbf{A} \geq 0$ we have $\mathbf{A} \in \mathcal{J}_1$ if $\sum_n |\langle \phi_n, \mathbf{A}\phi_n \rangle| < \infty$ for a single basis.
- (e) If $\mathbf{A} \in \mathcal{J}_1$, $\text{Tr}(\mathbf{A}) = \sum \langle \phi_n, \mathbf{A}\phi_n \rangle$ is independent of the basis used.
- (f) Tr is linear and obeys $\text{Tr}(\mathbf{A}^\dagger) = \overline{\text{Tr}(\mathbf{A})}$; $\text{Tr}(\mathbf{A}\mathbf{B}) = \text{Tr}(\mathbf{B}\mathbf{A})$ if either $\mathbf{A} \in \mathcal{J}_1$ and \mathbf{B} bounded, \mathbf{A} bounded and $\mathbf{B} \in \mathcal{J}_1$ or both $\mathbf{A}, \mathbf{B} \in \mathcal{J}_2$.
- (g) \mathcal{J}_2 endowed with the inner product $\langle \mathbf{A}, \mathbf{B} \rangle_2 = \text{Tr}(\mathbf{A}^\dagger \mathbf{B})$ is a Hilbert space. If $\|\mathbf{A}\|_2 = [\text{Tr}(\mathbf{A}^\dagger \mathbf{A})]^{1/2}$, then $\|\mathbf{A}\|_2 \geq \|\mathbf{A}\|$ and \mathcal{J}_2 is the $\|\cdot\|_2$ -closure of the *finite* rank operators.
- (h) \mathcal{J}_1 endowed with the norm $\|\mathbf{A}\|_1 = \text{Tr}(\sqrt{\mathbf{A}^\dagger \mathbf{A}})$ is a Banach space. $\|\mathbf{A}\|_1 \geq \|\mathbf{A}\|_2 \geq \|\mathbf{A}\|$ and \mathcal{J}_1 is the $\|\cdot\|_1$ -norm closure of the *finite* rank operators. The dual space of \mathcal{J}_1 is $\mathcal{B}(\mathcal{H})$, the family of bounded operators with the duality $\langle \mathbf{B}, \mathbf{A} \rangle = \text{Tr}(\mathbf{B}\mathbf{A})$.
- (i) If $\mathbf{A}, \mathbf{B} \in \mathcal{J}_2$, then $\|\mathbf{A}\mathbf{B}\|_1 \leq \|\mathbf{A}\|_2 \|\mathbf{B}\|_2$. If $\mathbf{A} \in \mathcal{J}_2$ and $\mathbf{B} \in \mathcal{B}(\mathcal{H})$, then $\|\mathbf{A}\mathbf{B}\|_2 \leq \|\mathbf{A}\|_2 \|\mathbf{B}\|$. If $\mathbf{A} \in \mathcal{J}_1$ and $\mathbf{B} \in \mathcal{B}(\mathcal{H})$, then $\|\mathbf{A}\mathbf{B}\|_1 \leq \|\mathbf{A}\|_1 \|\mathbf{B}\|$.

Note the most important property for proving that an operator is trace class is the decomposition **(b)** into two Hilbert-Schmidt ones, as the Hilbert-Schmidt property can easily be verified in one single orthonormal basis (see **(d)**). Property **(e)** ensures then that the trace is the same in any basis. Properties **(a)** and **(f)** show that trace class operators behave in complete analogy to finite rank operators. The proof whether a matrix is trace-class (or Hilbert-Schmidt) or not simplifies enormously for diagonal matrices, as then the second part of property **(d)** is directly applicable: just the moduli of the eigenvalues (or – in case of Hilbert-Schmidt – the squares of the eigenvalues) have to be summed up in order to answer that question. A good strategy in checking the trace-class character of a general matrix **A** is therefore the decomposition of that matrix into two matrices **B** and **C** where one, say **C**, should be chosen to be diagonal and either just barely of Hilbert-Schmidt character leaving enough freedom for its partner **B** or of trace-class character such that one only has to show the boundedness for **B**.

J.4 Determinants of trace class operators

This section is mainly based on refs. [8, 10] which should be consulted for more details and proofs. See also refs. [11, 14].

Pre-definitions (Alternating algebra and Fock spaces):

Given a Hilbert space \mathcal{H} , $\otimes^n \mathcal{H}$ is defined as the vector space of multi-linear functionals on \mathcal{H} with $\phi_1 \otimes \cdots \otimes \phi_n \in \otimes^n \mathcal{H}$ in case $\phi_1, \dots, \phi_n \in \mathcal{H}$. $\wedge^n(\mathcal{H})$ is defined as the subspace of $\otimes^n \mathcal{H}$ spanned by the wedge-product

$$\phi_1 \wedge \cdots \wedge \phi_n = \frac{1}{\sqrt{n!}} \sum_{\pi \in \mathcal{P}_n} \epsilon(\pi) [\phi_{\pi(1)} \otimes \cdots \otimes \phi_{\pi(n)}]$$

where \mathcal{P}_n is the group of all permutations of n letters and $\epsilon(\pi) = \pm 1$ depending on whether π is an even or odd permutation, respectively. The inner product in $\wedge^n(\mathcal{H})$ is given by

$$(\phi_1 \wedge \cdots \wedge \phi_n, \eta_1 \wedge \cdots \wedge \eta_n) = \det \{(\phi_i, \eta_j)\}$$

where $\det\{a_{ij}\} = \sum_{\pi \in \mathcal{P}_n} \epsilon(\pi) a_{1\pi(1)} \cdots a_{n\pi(n)}$. $\wedge^n(\mathbf{A})$ is defined as functor (a functor satisfies $\wedge^n(\mathbf{AB}) = \wedge^n(\mathbf{A}) \wedge^n(\mathbf{B})$) on $\wedge^n(\mathcal{H})$ with

$$\wedge^n(\mathbf{A})(\phi_1 \wedge \cdots \wedge \phi_n) = \mathbf{A}\phi_1 \wedge \cdots \wedge \mathbf{A}\phi_n.$$

When $n = 0$, $\wedge^n(\mathcal{H})$ is defined to be C and $\wedge^n(\mathbf{A})$ as $1: C \rightarrow C$.

Properties: If **A** trace class, i.e., $\mathbf{A} \in \mathcal{J}_1$, then for any k , $\wedge^k(\mathbf{A})$ is trace class, and for any orthonormal basis $\{\phi_n\}$ the cumulant

$$\mathrm{Tr} \left(\wedge^k(\mathbf{A}) \right) = \sum_{i_1 < \cdots < i_k} ((\phi_{i_1} \wedge \cdots \wedge \phi_{i_k}), (\mathbf{A}\phi_{i_1} \wedge \cdots \wedge \mathbf{A}\phi_{i_k})) < \infty$$

is independent of the basis (with the understanding that $\text{Tr} \wedge^0(\mathbf{A}) \equiv 1$).

Definition: Let $\mathbf{A} \in \mathcal{J}_1$, then $\det(\mathbf{1} + \mathbf{A})$ is defined as

$$\det(\mathbf{1} + \mathbf{A}) = \sum_{k=0}^{\infty} \text{Tr} \left(\wedge^k(\mathbf{A}) \right) \quad (\text{J.14})$$

Properties:

Let \mathbf{A} be a linear operator on a separable Hilbert space \mathcal{H} and $\{\phi_j\}_1^{\infty}$ an orthonormal basis.

- (a) $\sum_{k=0}^{\infty} \text{Tr} \left(\wedge^k(\mathbf{A}) \right)$ converges for each $\mathbf{A} \in \mathcal{J}_1$.
- (b) $|\det(\mathbf{1} + \mathbf{A})| \leq \prod_{j=1}^{\infty} (1 + \mu_j(\mathbf{A}))$ where $\mu_j(\mathbf{A})$ are the *singular* values of \mathbf{A} , i.e., the eigenvalues of $|\mathbf{A}| = \sqrt{\mathbf{A}^\dagger \mathbf{A}}$.
- (c) $|\det(\mathbf{1} + \mathbf{A})| \leq \exp(\|\mathbf{A}\|_1)$.
- (d) For any $\mathbf{A}_1, \dots, \mathbf{A}_n \in \mathcal{J}_1$, $\langle z_1, \dots, z_n \rangle \mapsto \det(\mathbf{1} + \sum_{i=1}^n z_i \mathbf{A}_i)$ is an entire analytic function.
- (e) If $\mathbf{A}, \mathbf{B} \in \mathcal{J}_1$, then

$$\begin{aligned} \det(\mathbf{1} + \mathbf{A})\det(\mathbf{1} + \mathbf{B}) &= \det(\mathbf{1} + \mathbf{A} + \mathbf{B} + \mathbf{A}\mathbf{B}) \\ &= \det((\mathbf{1} + \mathbf{A})(\mathbf{1} + \mathbf{B})) \\ &= \det((\mathbf{1} + \mathbf{B})(\mathbf{1} + \mathbf{A})) . \end{aligned} \quad (\text{J.15})$$

If $\mathbf{A} \in \mathcal{J}_1$ and \mathbf{U} unitary, then

$$\det(\mathbf{U}^{-1}(\mathbf{1} + \mathbf{A})\mathbf{U}) = \det(\mathbf{1} + \mathbf{U}^{-1}\mathbf{A}\mathbf{U}) = \det(\mathbf{1} + \mathbf{A}) .$$

- (f) If $\mathbf{A} \in \mathcal{J}_1$, then $(\mathbf{1} + \mathbf{A})$ is invertible if and only if $\det(\mathbf{1} + \mathbf{A}) \neq 0$.
- (g) If $\lambda \neq 0$ is an n -times degenerate eigenvalue of $\mathbf{A} \in \mathcal{J}_1$, then $\det(\mathbf{1} + z\mathbf{A})$ has a zero of order n at $z = -1/\lambda$.
- (h) For any ϵ , there is a $C_\epsilon(\mathbf{A})$, depending on $\mathbf{A} \in \mathcal{J}_1$, so that $|\det(\mathbf{1} + z\mathbf{A})| \leq C_\epsilon(\mathbf{A}) \exp(\epsilon|z|)$.
- (i) For any $\mathbf{A} \in \mathcal{J}_1$,

$$\det(\mathbf{1} + \mathbf{A}) = \prod_{j=1}^{N(\mathbf{A})} (1 + \lambda_j(\mathbf{A})) \quad (\text{J.16})$$

where here and in the following $\{\lambda_j(\mathbf{A})\}_{j=1}^{N(\mathbf{A})}$ are the eigenvalues of \mathbf{A} counted with algebraic multiplicity .

(j) *Lidskii's theorem*: For any $\mathbf{A} \in \mathcal{J}_1$,

$$\text{Tr}(\mathbf{A}) = \sum_{j=1}^{N(\mathbf{A})} \lambda_j(\mathbf{A}) < \infty .$$

(k) If $\mathbf{A} \in \mathcal{J}_1$, then

$$\begin{aligned} \text{Tr}\left(\bigwedge^k(\mathbf{A})\right) &= \sum_{j=1}^{N(\bigwedge^k(\mathbf{A}))} \lambda_j\left(\bigwedge^k(\mathbf{A})\right) \\ &= \sum_{1 \leq j_1 < \dots < j_k \leq N(\mathbf{A})} \lambda_{j_1}(\mathbf{A}) \cdots \lambda_{j_k}(\mathbf{A}) < \infty . \end{aligned}$$

(l) If $\mathbf{A} \in \mathcal{J}_1$, then

$$\det(1 + z\mathbf{A}) = \sum_{k=0}^{\infty} z^k \sum_{1 \leq j_1 < \dots < j_k \leq N(\mathbf{A})} \lambda_{j_1}(\mathbf{A}) \cdots \lambda_{j_k}(\mathbf{A}) < \infty . \quad (\text{J.17})$$

(m) If $\mathbf{A} \in \mathcal{J}_1$, then for $|z|$ small (i.e., $|z| \max |\lambda_j(\mathbf{A})| < 1$) the series $\sum_{k=1}^{\infty} z^k \text{Tr}((- \mathbf{A})^k) / k$ converges and

$$\begin{aligned} \det(1 + z\mathbf{A}) &= \exp\left(- \sum_{k=1}^{\infty} \frac{z^k}{k} \text{Tr}((- \mathbf{A})^k)\right) \\ &= \exp(\text{Tr} \ln(\mathbf{1} + z\mathbf{A})) . \end{aligned} \quad (\text{J.18})$$

(n) *The Plemelj-Smithies formula*: Define $\alpha_m(\mathbf{A})$ for $\mathbf{A} \in \mathcal{J}_1$ by

$$\det(\mathbf{1} + z\mathbf{A}) = \sum_{m=0}^{\infty} z^m \frac{\alpha_m(\mathbf{A})}{m!} . \quad (\text{J.19})$$

Then $\alpha_m(\mathbf{A})$ is given by the $m \times m$ determinant:

$$\alpha_m(\mathbf{A}) = \begin{vmatrix} \text{Tr}(\mathbf{A}) & m-1 & 0 & \cdots & 0 \\ \text{Tr}(\mathbf{A}^2) & \text{Tr}(\mathbf{A}) & m-2 & \cdots & 0 \\ \text{Tr}(\mathbf{A}^3) & \text{Tr}(\mathbf{A}^2) & \text{Tr}(\mathbf{A}) & \cdots & 0 \\ \vdots & \vdots & \vdots & \vdots & \vdots \\ \text{Tr}(\mathbf{A}^m) & \text{Tr}(\mathbf{A}^{(m-1)}) & \text{Tr}(\mathbf{A}^{(m-2)}) & \cdots & \text{Tr}(\mathbf{A}) \end{vmatrix} \quad (\text{J.20})$$

with the understanding that $\alpha_0(\mathbf{A}) \equiv 1$ and $\alpha_1(\mathbf{A}) \equiv \text{Tr}(\mathbf{A})$. Thus the cumulants $c_m(\mathbf{A}) \equiv \alpha_m(\mathbf{A})/m!$ satisfy the following recursion relation

$$\begin{aligned} c_m(\mathbf{A}) &= \frac{1}{m} \sum_{k=1}^m (-1)^{k+1} c_{m-k}(\mathbf{A}) \text{Tr}(\mathbf{A}^k) \quad \text{for } m \geq 1 \\ c_0(\mathbf{A}) &\equiv 1 . \end{aligned} \quad (\text{J.21})$$

Note that in the context of quantum mechanics formula (J.19) is the quantum analog to the curvature expansion of the semiclassical zeta function with $\text{Tr}(\mathbf{A}^n)$ corresponding to the sum of all periodic orbits (prime and also repeated ones) of total topological length m , i.e., let $c_m(\text{s.c.})$ denote the m^{th} curvature term, then the curvature expansion of the semiclassical zeta function is given by the recursion relation

$$c_m(\text{s.c.}) = \frac{1}{m} \sum_{k=1}^m (-1)^{k+m+1} c_{m-k}(\text{s.c.}) \sum_{\substack{p:r>0 \\ \text{with } [p]_r=k}} [p] \frac{t_p(k)^r}{1 - \left(\frac{1}{\Lambda_p}\right)^r} \quad \text{for } m \geq 1$$

$$c_0(\text{s.c.}) \equiv 1. \tag{J.22}$$

In fact, in the cumulant expansion (J.19) as well as in the curvature expansion there are large cancelations involved. Let us order – without loss of generality – the eigenvalues of the operator $\mathbf{A} \in \mathcal{J}_1$ as follows:

$$|\lambda_1| \geq |\lambda_2| \geq \dots \geq |\lambda_{i-1}| \geq |\lambda_i| \geq |\lambda_{i+1}| \geq \dots$$

(This is always possible because of $\sum_{i=1}^{N(\mathbf{A})} |\lambda_i| < \infty$.) Then, in the standard (Plemelj-Smithies) cumulant evaluation of the determinant, eq. (J.19), we have enormous cancelations of big numbers, e.g. at the k^{th} cumulant order ($k > 3$), all the intrinsically large ‘numbers’ $\lambda_1^k, \lambda_1^{k-1}\lambda_2, \dots, \lambda_1^{k-2}\lambda_2\lambda_3, \dots$ and many more have to cancel out exactly until only $\sum_{1 \leq j_1 < \dots < j_k \leq N(\mathbf{A})} \lambda_{j_1} \dots \lambda_{j_k}$ is finally left over. Algebraically, the fact that there are these large cancelations is of course of no importance. However, if the determinant is calculated numerically, the big cancelations might spoil the result or even the convergence. Now, the curvature expansion of the semiclassical zeta function, as it is known today, is the semiclassical approximation to the curvature expansion (unfortunately) in the Plemelj-Smithies form. As the exact quantum mechanical result is approximated semiclassically, the errors introduced in the approximation might lead to big effects as they are done with respect to large quantities which eventually cancel out and not – as it would be of course better – with respect to the small surviving cumulants. Thus it would be very desirable to have a semiclassical analog to the reduced cumulant expansion (J.17) or even to (J.16) directly. It might not be possible to find a direct semiclassical analog for the individual eigenvalues λ_j . Thus the direct construction of the semiclassical equivalent to (J.16) is rather unlikely. However, in order to have a semiclassical “cumulant” summation without large cancelations – see (J.17) – it would be just sufficient to find the semiclassical analog of each complete cumulant (J.17) and not of the single eigenvalues. Whether this will eventually be possible is still an open question.

J.5 Von Koch matrices

Implicitly, many of the above properties are based on the theory of von Koch matrices [11, 12, 13]: An infinite matrix $\mathbf{1} - \mathbf{A} = \|\delta_{jk} - a_{jk}\|_1^\infty$, consisting of

complex numbers, is called a matrix with an *absolutely convergent determinant*, if the series $\sum |a_{j_1 k_1} a_{j_2 k_2} \cdots a_{j_n k_n}|$ converges, where the sum extends over all pairs of systems of indices (j_1, j_2, \dots, j_n) and (k_1, k_2, \dots, k_n) which differ from each other only by a permutation, and $j_1 < j_2 < \dots < j_n$ ($n = 1, 2, \dots$). Then the limit

$$\lim_{n \rightarrow \infty} \det \|\delta_{jk} - a_{jk}\|_1^n = \det(\mathbf{1} - \mathbf{A})$$

exists and is called the determinant of the matrix $\mathbf{1} - \mathbf{A}$. It can be represented in the form

$$\det(\mathbf{1} - \mathbf{A}) = 1 - \sum_{j=1}^{\infty} a_{jj} + \frac{1}{2!} \sum_{j,k=1}^{\infty} \begin{vmatrix} a_{jj} & a_{jk} \\ a_{kj} & a_{kk} \end{vmatrix} - \frac{1}{3!} \sum_{j,k,m=1}^{\infty} \begin{vmatrix} a_{jj} & a_{jk} & a_{jm} \\ a_{kj} & a_{kk} & a_{km} \\ a_{mj} & a_{mk} & a_{mm} \end{vmatrix} + \dots,$$

where the series on the r.h.s. will remain convergent even if the numbers a_{jk} ($j, k = 1, 2, \dots$) are replaced by their moduli and if all the terms obtained by expanding the determinants are taken with the plus sign. The matrix $\mathbf{1} - \mathbf{A}$ is called *von Koch matrix*, if both conditions

$$\sum_{j=1}^{\infty} |a_{jj}| < \infty, \tag{J.23}$$

$$\sum_{j,k=1}^{\infty} |a_{jk}|^2 < \infty \tag{J.24}$$

are fulfilled. Then the following holds (see ref. [11, 13]): (1) Every von Koch matrix has an absolutely convergent determinant. If the elements of a von Koch matrix are functions of some parameter μ ($a_{jk} = a_{jk}(\mu)$, $j, k = 1, 2, \dots$) and both series in the defining condition converge uniformly in the domain of the parameter μ , then as $n \rightarrow \infty$ the determinant $\det \|\delta_{jk} - a_{jk}(\mu)\|_1^n$ tends to the determinant $\det(\mathbf{1} + \mathbf{A}(\mu))$ uniformly with respect to μ , over the domain of μ . (2) If the matrices $\mathbf{1} - \mathbf{A}$ and $\mathbf{1} - \mathbf{B}$ are von Koch matrices, then their product $\mathbf{1} - \mathbf{C} = (\mathbf{1} - \mathbf{A})(\mathbf{1} - \mathbf{B})$ is a von Koch matrix, and

$$\det(\mathbf{1} - \mathbf{C}) = \det(\mathbf{1} - \mathbf{A}) \det(\mathbf{1} - \mathbf{B}).$$

Note that every trace-class matrix $\mathbf{A} \in \mathcal{J}_1$ is also a von Koch matrix (and that any matrix satisfying condition (J.24) is Hilbert-Schmidt and vice versa). The inverse implication, however, is not true: von Koch matrices are not automatically trace-class. The caveat is that the definition of von Koch matrices is basis-dependent, whereas the trace-class property is basis-independent. As the traces involve infinite sums, the basis-independence is not at all trivial. An example for an infinite matrix which is von Koch, but not trace-class is the following:

$$\mathbf{A}_{ij} = \begin{cases} 2/j & \text{for } i - j = -1 \text{ and } j \text{ even,} \\ 2/i & \text{for } i - j = +1 \text{ and } i \text{ even,} \\ 0 & \text{else,} \end{cases}$$

i.e.,

$$\mathbf{A} = \begin{pmatrix} 0 & 1 & 0 & 0 & 0 & 0 & \cdots \\ 1 & 0 & 0 & 0 & 0 & 0 & \cdots \\ 0 & 0 & 0 & 1/2 & 0 & 0 & \cdots \\ 0 & 0 & 1/2 & 0 & 0 & 0 & \cdots \\ 0 & 0 & 0 & 0 & 0 & 1/3 & \ddots \\ 0 & 0 & 0 & 0 & 1/3 & 0 & \ddots \\ \vdots & \vdots & \vdots & \vdots & \ddots & \ddots & \ddots \end{pmatrix}. \tag{J.25}$$

Obviously, condition (J.23) is fulfilled by definition. Second, the condition (J.24) is satisfied as $\sum_{n=1}^{\infty} 2/n^2 < \infty$. However, the sum over the moduli of the eigenvalues is just twice the harmonic series $\sum_{n=1}^{\infty} 1/n$ which does not converge. The matrix (J.25) violates the trace-class definition (J.13), as in its eigenbasis the sum over the moduli of its diagonal elements is infinite. Thus the *absolute* convergence is traded for a *conditional* convergence, since the sum over the eigenvalues themselves can be arranged to still be zero, if the eigenvalues with the same modulus are summed first. Absolute convergence is of course essential, if sums have to be rearranged or exchanged. Thus, the trace-class property is indispensable for any controlled unitary transformation of an infinite determinant, as then there will be necessarily a change of basis and in general also a re-ordering of the corresponding traces. Therefore the claim that a *Hilbert-Schmidt operator with a vanishing trace is automatically trace-class* is false. In general, such an operator has to be regularized in addition (see next chapter).

J.6 Regularization

Many interesting operators are not of trace class (although they might be in some \mathcal{J}_p with $p > 1$ - an operator A is in \mathcal{J}_p iff $\text{Tr}|A|^p < \infty$ in any orthonormal basis). In order to compute determinants of such operators, an extension of the cumulant expansion is needed which in fact corresponds to a regularization procedure [8, 10]:

E.g. let $\mathbf{A} \in \mathcal{J}_p$ with $p \leq n$. Define

$$R_n(z\mathbf{A}) = (\mathbf{1} + z\mathbf{A}) \exp \left(\sum_{k=1}^{n-1} \frac{(-z)^k}{k} \mathbf{A}^k \right) - \mathbf{1}$$

as the regulated version of the operator $z\mathbf{A}$. Then the regulated operator $R_n(z\mathbf{A})$ is trace class, i.e., $R_n(z\mathbf{A}) \in \mathcal{J}_1$. Define now $\det_n(\mathbf{1} + z\mathbf{A}) = \det(\mathbf{1} + R_n(z\mathbf{A}))$. Then the regulated determinant

$$\det_n(\mathbf{1} + z\mathbf{A}) = \prod_{j=1}^{N(z\mathbf{A})} \left[\left(1 + z\lambda_j(\mathbf{A}) \right) \exp \left(\sum_{k=1}^{n-1} \frac{(-z\lambda_j(\mathbf{A}))^k}{k} \right) \right] < \infty. \tag{J.26}$$

exists and is finite. The corresponding Plemelj-Smithies formula now reads [10]:

$$\det_n(\mathbf{1} + z\mathbf{A}) = \sum_{m=0}^{\infty} z^m \frac{\alpha_m^{(n)}(\mathbf{A})}{m!}. \tag{J.27}$$

with $\alpha_m^{(n)}(\mathbf{A})$ given by the $m \times m$ determinant:

$$\alpha_m^{(n)}(\mathbf{A}) = \begin{vmatrix} \sigma_1^{(n)} & m-1 & 0 & \cdots & 0 \\ \sigma_2^{(n)} & \sigma_1^{(n)} & m-2 & \cdots & 0 \\ \sigma_3^{(n)} & \sigma_2^{(n)} & \sigma_1^{(n)} & \cdots & 0 \\ \vdots & \vdots & \vdots & \vdots & \vdots \\ \sigma_m^{(n)} & \sigma_{m-1}^{(n)} & \sigma_{m-2}^{(n)} & \cdots & \sigma_1^{(n)} \end{vmatrix} \tag{J.28}$$

where

$$\sigma_k^{(n)} = \begin{cases} \text{Tr}(\mathbf{A}^k) & k \geq n \\ 0 & k \leq n-1 \end{cases}$$

As Simon [10] says simply, the beauty of (J.28) is that we get $\det_n(\mathbf{1} + \mathbf{A})$ from the standard Plemelj-Smithies formula (J.19) by simply setting $\text{Tr}(\mathbf{A}), \text{Tr}(\mathbf{A}^2), \dots, \text{Tr}(\mathbf{A}^{n-1})$ to zero.

See also ref. [15] where $\{\lambda_j\}$ are the eigenvalues of an elliptic (pseudo)-differential operator \mathbf{H} of order m on a compact or bounded manifold of dimension $d, 0 < \lambda_0 \leq \lambda_1 \leq \dots$ and $\lambda_k \uparrow +\infty$. and the Fredholm determinant

$$\Delta(\lambda) = \prod_{k=0}^{\infty} \left(1 - \frac{\lambda}{\lambda_k}\right)$$

is regulated in the case $\mu \equiv d/m > 1$ as Weierstrass product

$$\Delta(\lambda) = \prod_{k=0}^{\infty} \left[\left(1 - \frac{\lambda}{\lambda_k}\right) \exp\left(\frac{\lambda}{\lambda_k} + \frac{\lambda^2}{2\lambda_k^2} + \cdots + \frac{\lambda^{[\mu]}}{[\mu]\lambda_k^{[\mu]}}\right) \right] \tag{J.29}$$

where $[\mu]$ denotes the integer part of μ . This is, see ref. [15], the unique entire function of order μ having zeros at $\{\lambda_k\}$ and subject to the normalization conditions

$$\ln \Delta(0) = \frac{d}{d\lambda} \ln \Delta(0) = \cdots = \frac{d^{[\mu]}}{d\lambda^{[\mu]}} \ln \Delta(0) = 0.$$

Clearly (J.29) is the same as (J.26); one just has to identify $z = -\lambda, \mathbf{A} = 1/\mathbf{H}$ and $n-1 = [\mu]$. An example is the regularization of the spectral determinant

$$\Delta(E) = \det[(E - \mathbf{H})] \tag{J.30}$$

which – as it stands – would only make sense for a finite dimensional basis (or finite dimensional matrices). In ref. [16] the regulated spectral determinant for the example of the hyperbola billiard in two dimensions (thus $d = 2$, $m = 2$ and hence $\mu = 1$) is given as

$$\Delta(E) = \det [(E - \mathbf{H})\Omega(E, \mathbf{H})]$$

where

$$\Omega(E, \mathbf{H}) = -\mathbf{H}^{-1} e^{E\mathbf{H}^{-1}}$$

such that the spectral determinant in the eigenbasis of \mathbf{H} (with eigenvalues $E_n \neq 0$) reads

$$\Delta(E) = \prod_n \left(1 - \frac{E}{E_n}\right) e^{E/E_n} < \infty.$$

Note that \mathbf{H}^{-1} is for this example of Hilbert-Schmidt character.

Exercises

- J.1. **Norm of exponential of an operator.** Verify inequality (J.12):

$$\|e^{tA}\| \leq e^{t\|A\|}.$$

References

- [J.1] A. Wirzba, *Quantum Mechanics and Semiclassics of Hyperbolic n-Disk Scattering*, Habilitationsschrift, Technische Universität, Germany, 1997, HAB, chaos-dyn/9712015, *Physics Reports* in press.
- [J.2] A. Grothendieck, “La théorie de Fredholm,” *Bull. Soc. Math. France*, **84**, 319 (1956).
- [J.3] A. Grothendieck, *Produits tensoriels topologiques et espaces nucléaires*, Amer. Meth. Soc. **16**, Providence R. I. (1955).
- [J.4] C.A. Tracy and H. Widom, CHECK THIS!: *Fredholm Determinants, Differential Equations and Matrix Models*, hep-th/9306042.

- [J.5] M.G. Krein, *On the Trace Formula in Perturbation Theory* Mat. Sborn. (N.S.) **33** (1953) 597-626; *Perturbation Determinants and Formula for Traces of Unitary and Self-adjoint Operators* Sov. Math.-Dokl. **3** (1962) 707-710. M.S. Birman and M.G. Krein, *On the Theory of Wave Operators and Scattering Operators*, Sov. Math.-Dokl. **3** (1962) 740-744.
- [J.6] J. Friedel, *Nuovo Cim. Suppl.* **7** (1958) 287-301.
- [J.7] M. Reed and B. Simon, *Methods of Modern Mathematical Physics*, Vol. I: *Functional Analysis*, Chap. VI, Academic Press (New York), 1972.
- [J.8] M. Reed and B. Simon, *Methods of Modern Mathematical Physics*, Vol. IV: *Analysis of Operators*, Chap. XIII.17, Academic Press (New York), 1976.
- [J.9] B. Simon, *Quantum Mechanics for Hamiltonians defined as Quadratic Forms*, Princeton Series in Physics, 1971, Appendix.
- [J.10] B. Simon, *Notes on Infinite Determinants of Hilbert Space Operators*, *Adv. Math.* **24** (1977) 244-273.
- [J.11] I.C. Gohberg and M.G. Krein, *Introduction to the theory of linear non-selfadjoint operators*, Translations of Mathematical Monographs **18**, Amer. Math. Soc. (1969).
- [J.12] H. von Koch, *Sur quelques points de la théorie des déterminants infinis*, *Acta. Math.* **24** (1900) 89-122; *Sur la convergence des déterminants infinis*, *Rend. Circ. Mat. Palermo* **28** (1909) 255-266.
- [J.13] E. Hille and J.D. Tamarkin, *On the characteristic values of linear integral equations*, *Acta Math.* **57** (1931) 1-76.
- [J.14] T. Kato, *Perturbation Theory of Linear Operators* (Springer, New York, 1966), Chap. X, § 1.3 and § 1.4.
- [J.15] A. Voros, *Spectral Functions, Special Functions and the Selberg Zeta Function*, *Comm. Math Phys.* **110**, 439 (1987).
- [J.16] J.P. Keating and M. Sieber, "Calculation of spectral determinants," preprint (1994).

Appendix K

Thermodynamic formalism

Being Hungarian is not sufficient. You also must be talented.

— Zsa Zsa Gabor

(G. Vattay)

IN THE PRECEDING CHAPTERS we characterized chaotic systems via global quantities such as averages. It turned out that these are closely related to very fine details of the dynamics like stabilities and time periods of individual periodic orbits. In statistical mechanics a similar duality exists. Macroscopic systems are characterized with thermodynamic quantities (pressure, temperature and chemical potential) which are averages over fine details of the system called microstates. One of the greatest achievements of the theory of dynamical systems was when in the sixties and seventies Bowen, Ruelle and Sinai made the analogy between these two subjects explicit. Later this “Thermodynamic Formalism” of dynamical systems became widely used making it possible to calculate various fractal dimensions. We sketch the main ideas of this theory and show how periodic orbit theory helps to carry out calculations.

K.1 Rényi entropies

As we have already seen trajectories in a dynamical system can be characterized by their symbolic sequences from a generating Markov partition. We can locate the set of starting points $\mathcal{M}_{s_1 s_2 \dots s_n}$ of trajectories whose symbol sequence starts with a given set of n symbols $s_1 s_2 \dots s_n$. We can associate many different quantities to these sets. There are geometric measures such as the volume $V(s_1 s_2 \dots s_n)$, the area $A(s_1 s_2 \dots s_n)$ or the length $l(s_1 s_2 \dots s_n)$ of this set. Or in general we can have some measure $\mu(\mathcal{M}_{s_1 s_2 \dots s_n}) = \mu(s_1 s_2 \dots s_n)$ of this set. As we have seen in (22.10) the most important is the natural measure, which is the probability that an ergodic trajectory visits the set $\mu(s_1 s_2 \dots s_n) = P(s_1 s_2 \dots s_n)$. The natural measure is additive.

Summed up for all possible symbol sequences of length n it gives the measure of the whole state space:

$$\sum_{s_1 s_2 \dots s_n} \mu(s_1 s_2 \dots s_n) = 1 \quad (\text{K.1})$$

expresses probability conservation. Also, summing up for the last symbol we get the measure of a one step shorter sequence

$$\sum_{s_n} \mu(s_1 s_2 \dots s_n) = \mu(s_1 s_2 \dots s_{n-1}).$$

As we increase the length (n) of the sequence the measure associated with it decreases typically with an exponential rate. It is then useful to introduce the exponents

$$\lambda(s_1 s_2 \dots s_n) = -\frac{1}{n} \log \mu(s_1 s_2 \dots s_n). \quad (\text{K.2})$$

To get full information on the distribution of the natural measure in the symbolic space we can study the distribution of exponents. Let the number of symbol sequences of length n with exponents between λ and $\lambda + d\lambda$ be given by $N_n(\lambda)d\lambda$. For large n the number of such sequences increases exponentially. The rate of this exponential growth can be characterized by $g(\lambda)$ such that

$$N_n(\lambda) \sim \exp(ng(\lambda)).$$

The knowledge of the distribution $N_n(\lambda)$ or its essential part $g(\lambda)$ fully characterizes the microscopic structure of our dynamical system.

As a natural next step we would like to calculate this distribution. However it is very time consuming to calculate the distribution directly by making statistics for millions of symbolic sequences. Instead, we introduce auxiliary quantities which are easier to calculate and to handle. These are called partition sums

$$Z_n(\beta) = \sum_{s_1 s_2 \dots s_n} \mu^\beta(s_1 s_2 \dots s_n), \quad (\text{K.3})$$

as they are obviously motivated by Gibbs type partition sums of statistical mechanics. The parameter β plays the role of inverse temperature $1/k_B T$ and $E(s_1 s_2 \dots s_n) = -\log \mu(s_1 s_2 \dots s_n)$ is the energy associated with the microstate labeled by $s_1 s_2 \dots s_n$. We are tempted also to introduce something analogous with the Free energy. In dynamical systems this is called the Rényi entropy [5] defined by the growth rate of the partition sum

$$K_\beta = \lim_{n \rightarrow \infty} \frac{1}{n} \frac{1}{1 - \beta} \log \left(\sum_{s_1 s_2 \dots s_n} \mu^\beta(s_1 s_2 \dots s_n) \right). \quad (\text{K.4})$$

In the special case $\beta \rightarrow 1$ we get Kolmogorov entropy

$$K_1 = \lim_{n \rightarrow \infty} \frac{1}{n} \sum_{s_1 s_2 \dots s_n} -\mu(s_1 s_2 \dots s_n) \log \mu(s_1 s_2 \dots s_n),$$

while for $\beta = 0$ we recover the topological entropy

$$h_{top} = K_0 = \lim_{n \rightarrow \infty} \frac{1}{n} \log N(n),$$

where $N(n)$ is the number of existing length n sequences. To connect the partition sums with the distribution of the exponents, we can write them as averages over the exponents

$$Z_n(\beta) = \int d\lambda N_n(\lambda) \exp(-n\lambda\beta),$$

where we used the definition (K.2). For large n we can replace $N_n(\lambda)$ with its asymptotic form

$$Z_n(\beta) \sim \int d\lambda \exp(ng(\lambda)) \exp(-n\lambda\beta).$$

For large n this integral is dominated by contributions from those λ^* which maximize the exponent

$$g(\lambda) - \lambda\beta.$$

The exponent is maximal when the derivative of the exponent vanishes

$$g'(\lambda^*) = \beta. \tag{K.5}$$

From this equation we can determine $\lambda^*(\beta)$. Finally the partition sum is

$$Z_n(\beta) \sim \exp(n[g(\lambda^*(\beta)) - \lambda^*(\beta)\beta]).$$

Using the definition (K.4) we can now connect the Rényi entropies and $g(\lambda)$

$$(\beta - 1)K_\beta = \lambda^*(\beta)\beta - g(\lambda^*(\beta)). \tag{K.6}$$

Equations (K.5) and (K.6) define the Legendre transform of $g(\lambda)$. This equation is analogous with the thermodynamic equation connecting the entropy and the

free energy. As we know from thermodynamics we can invert the Legendre transform. In our case we can express $g(\lambda)$ from the Rényi entropies via the Legendre transformation

$$g(\lambda) = \lambda\beta^*(\lambda) - (\beta^*(\lambda) - 1)K_{\beta^*(\lambda)}, \quad (\text{K.7})$$

where now $\beta^*(\lambda)$ can be determined from

$$\frac{d}{d\beta^*}[(\beta^* - 1)K_{\beta^*}] = \lambda. \quad (\text{K.8})$$

Obviously, if we can determine the Rényi entropies we can recover the distribution of probabilities from (K.7) and (K.8).

The periodic orbit calculation of the Rényi entropies can be carried out by approximating the natural measure corresponding to a symbol sequence by the expression (22.10)

$$\mu(s_1, \dots, s_n) \approx \frac{e^{n\gamma}}{|\Lambda_{s_1 s_2 \dots s_n}|}. \quad (\text{K.9})$$

The partition sum (K.3) now reads

$$Z_n(\beta) \approx \sum_i \frac{e^{n\beta\gamma}}{|\Lambda_i|^\beta}, \quad (\text{K.10})$$

where the summation goes for periodic orbits of length n . We can define the characteristic function

$$\Omega(z, \beta) = \exp\left(-\sum_n \frac{z^n}{n} Z_n(\beta)\right). \quad (\text{K.11})$$

According to (K.4) for large n the partition sum behaves as

$$Z_n(\beta) \sim e^{-n(\beta-1)K_\beta}. \quad (\text{K.12})$$

Substituting this into (K.11) we can see that the leading zero of the characteristic function is

$$z_0(\beta) = e^{(\beta-1)K_\beta}.$$

On the other hand substituting the periodic orbit approximation (K.10) into (K.11) and introducing prime and repeated periodic orbits as usual we get

$$\Omega(z, \beta) = \exp \left(- \sum_{p,r} \frac{z^{n_{pr}} e^{\beta \gamma n_{pr}}}{r |\Lambda_p^r|^\beta} \right).$$

We can see that the characteristic function is the same as the zeta function we introduced for Lyapunov exponents (G.12) except we have $ze^{\beta\gamma}$ instead of z . Then we can conclude that the Rényi entropies can be expressed with the pressure function directly as

$$P(\beta) = (\beta - 1)K_\beta + \beta\gamma, \quad (\text{K.13})$$

since the leading zero of the zeta function is the pressure. The Rényi entropies K_β , hence the distribution of the exponents $g(\lambda)$ as well, can be calculated via finding the leading eigenvalue of the operator (G.4).

From (K.13) we can get all the important quantities of the thermodynamic formalism. For $\beta = 0$ we get the topological entropy

$$P(0) = -K_0 = -h_{top}. \quad (\text{K.14})$$

For $\beta = 1$ we get the escape rate

$$P(1) = \gamma. \quad (\text{K.15})$$

Taking the derivative of (K.13) in $\beta = 1$ we get Pesin's formula [2] connecting Kolmogorov entropy and the Lyapunov exponent

$$P'(1) = \bar{\lambda} = K_1 + \gamma. \quad (\text{K.16})$$

exercise K.1

It is important to note that, as always, these formulas are strictly valid for nice hyperbolic systems only. At the end of this Chapter we discuss the important problems we are facing in non-hyperbolic cases.

On figure K.2 we show a typical pressure and $g(\lambda)$ curve computed for the two scale tent map of Exercise K.4. We have to mention, that all typical hyperbolic dynamical system produces a similar parabola like curve. Although this is somewhat boring we can interpret it like a sign of a high level of universality: The exponents λ have a sharp distribution around the most probable value. The most probable value is $\lambda = P'(0)$ and $g(\lambda) = h_{top}$ is the topological entropy. The average value in closed systems is where $g(\lambda)$ touches the diagonal: $\bar{\lambda} = g(\bar{\lambda})$ and $1 = g'(\bar{\lambda})$.

Next, we are looking at the distribution of trajectories in real space.

Figure K.1

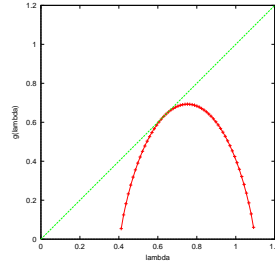
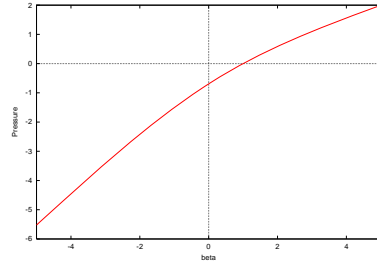


Figure K.2: $g(\lambda)$ and $P(\beta)$ for the map of exercise K.4 at $a = 3$ and $b = 3/2$.



K.2 Fractal dimensions

By looking at the repeller we can recognize an interesting spatial structure. In the 3-disk case the starting points of trajectories not leaving the system after the first bounce form two strips. Then these strips are subdivided into an infinite hierarchy of substrings as we follow trajectories which do not leave the system after more and more bounces. The finer strips are similar to strips on a larger scale. Objects with such self similar properties are called *fractals*.

We can characterize fractals via their local scaling properties. The first step is to draw a uniform grid on the surface of section. We can look at various measures in the square boxes of the grid. The most interesting measure is again the natural measure located in the box. By decreasing the size of the grid ϵ the measure in a given box will decrease. If the distribution of the measure is smooth then we expect that the measure of the i th box is proportional with the dimension of the section

$$\mu_i \sim \epsilon^d.$$

If the measure is distributed on a hairy object like the repeller we can observe unusual scaling behavior of type

$$\mu_i \sim \epsilon^{\alpha_i},$$

where α_i is the local “dimension” or Hölder exponent of the object. As α is not necessarily an integer here we are dealing with objects with fractional dimensions. We can study the distribution of the measure on the surface of section by looking at the distribution of these local exponents. We can define

$$\alpha_i = \frac{\log \mu_i}{\log \epsilon},$$

the local Hölder exponent and then we can count how many of them are between α and $\alpha + d\alpha$. This is $N_\epsilon(\alpha)d\alpha$. Again, in smooth objects this function scales simply with the dimension of the system

$$N_\epsilon(\alpha) \sim \epsilon^{-d},$$

while for hairy objects we expect an α dependent scaling exponent

$$N_\epsilon(\alpha) \sim \epsilon^{-f(\alpha)}.$$

$f(\alpha)$ can be interpreted [7] as the dimension of the points on the surface of section with scaling exponent α . We can calculate $f(\alpha)$ with the help of partition sums as we did for $g(\lambda)$ in the previous section. First, we define

$$Z_\epsilon(q) = \sum_i \mu_i^q. \quad (\text{K.17})$$

Then we would like to determine the asymptotic behavior of the partition sum characterized by the $\tau(q)$ exponent

$$Z_\epsilon(q) \sim \epsilon^{-\tau(q)}.$$

The partition sum can be written in terms of the distribution function of α -s

$$Z_\epsilon(q) = \int d\alpha N_\epsilon(\alpha) \epsilon^{q\alpha}.$$

Using the asymptotic form of the distribution we get

$$Z_\epsilon(q) \sim \int d\alpha \epsilon^{q\alpha - f(\alpha)}.$$

As ϵ goes to zero the integral is dominated by the term maximizing the exponent. This α^* can be determined from the equation

$$\frac{d}{d\alpha^*} (q\alpha^* - f(\alpha^*)) = 0,$$

leading to

$$q = f'(\alpha^*).$$

Finally we can read off the scaling exponent of the partition sum

$$\tau(q) = \alpha^* q - f(\alpha^*).$$

In a uniform fractal characterized by a single dimension both α and $f(\alpha)$ collapse to $\alpha = f(\alpha) = D$. The scaling exponent then has the form $\tau(q) = (q - 1)D$. In case of non uniform fractals we can introduce generalized dimensions [9] D_q via the definition

$$D_q = \tau(q)/(q - 1).$$

Some of these dimensions have special names. For $q = 0$ the partition sum (K.17) counts the number of non empty boxes \bar{N}_ϵ . Consequently

$$D_0 = - \lim_{\epsilon \rightarrow 0} \frac{\log \bar{N}_\epsilon}{\log \epsilon},$$

is called the box counting dimension. For $q = 1$ the dimension can be determined as the limit of the formulas for $q \rightarrow 1$ leading to

$$D_1 = \lim_{\epsilon \rightarrow 0} \sum_i \mu_i \log \mu_i / \log \epsilon.$$

This is the scaling exponent of the Shannon information entropy [11] of the distribution, hence its name is *information dimension*.

Using equisize grids is impractical in most of the applications. Instead, we can rewrite (K.17) into the more convenient form

$$\sum_i \frac{\mu_i^q}{\epsilon^{\tau(q)}} \sim 1. \quad (\text{K.18})$$

If we cover the i th branch of the fractal with a grid of size l_i instead of ϵ we can use the relation [5]

$$\sum_i \frac{\mu_i^q}{l_i^{\tau(q)}} \sim 1, \quad (\text{K.19})$$

the non-uniform grid generalization of K.18. Next we show how can we use the periodic orbit formalism to calculate fractal dimensions. We have already seen that the width of the strips of the repeller can be approximated with the stabilities of the periodic orbits placed within them

$$l_i \sim \frac{1}{|\Lambda_i|}.$$

Then using this relation and the periodic orbit expression of the natural measure we can write (K.19) into the form

$$\sum_i \frac{e^{q\gamma n}}{|\Lambda_i|^{q-\tau(q)}} \sim 1, \quad (\text{K.20})$$

where the summation goes for periodic orbits of length n . The sum for stabilities can be expressed with the pressure function again

$$\sum_i \frac{1}{|\Lambda_i|^{q-\tau(q)}} \sim e^{-nP(q-\tau(q))},$$

and (K.20) can be written as

$$e^{q\gamma n} e^{-nP(q-\tau(q))} \sim 1,$$

for large n . Finally we get an implicit formula for the dimensions

$$P(q - (q - 1)D_q) = q\gamma. \quad (\text{K.21})$$

Solving this equation directly gives us the partial dimensions of the multifractal repeller along the stable direction. We can see again that the pressure function alone contains all the relevant information. Setting $q = 0$ in (K.21) we can prove that the zero of the pressure function is the box-counting dimension of the repeller

$$P(D_0) = 0.$$

Taking the derivative of (K.21) in $q = 1$ we get

$$P'(1)(1 - D_1) = \gamma.$$

This way we can express the information dimension with the escape rate and the Lyapunov exponent

$$D_1 = 1 - \gamma/\bar{\lambda}. \quad (\text{K.22})$$

If the system is bound ($\gamma = 0$) the information dimension and all other dimensions are $D_q = 1$. Also since $D_1 > 0$ is positive (K.22) proves that the Lyapunov exponent must be larger than the escape rate $\bar{\lambda} > \gamma$ in general.

exercise K.4
exercise K.5

Résumé

In this chapter we have shown that thermodynamic quantities and various fractal dimensions can be expressed in terms of the pressure function. The pressure function is the leading eigenvalue of the operator which generates the Lyapunov exponent. In the Lyapunov case β is just an auxiliary variable. In thermodynamics it plays an essential role. The good news of the chapter is that the distribution of locally fluctuating exponents should not be computed via making statistics. We can use cyclist formulas for determining the pressure. Then the pressure can be found using short cycles + curvatures. Here the head reaches the tail of the snake. We just argued that the statistics of long trajectories coded in $g(\lambda)$ and $P(\beta)$ can be calculated from short cycles. To use this intimate relation between long and short trajectories effectively is still a research level problem.

Commentary

Remark K.1 Mild phase transition. In non-hyperbolic systems the formulas derived in this chapter should be modified. As we mentioned in 22.1 in non-hyperbolic systems the periodic orbit expression of the measure can be

$$\mu_0 = e^{\gamma n} / |\Lambda_0|^\delta,$$

where δ can differ from 1. Usually it is 1/2. For sufficiently *negative* β the corresponding term $1/|\Lambda_0|^\beta$ can dominate (K.10) while in (K.3) $e^{\gamma n} / |\Lambda_0|^{\delta\beta}$ plays no dominant role. In this case the pressure as a function of β can have a kink at the critical point $\beta = \beta_c$ where $\beta_c \log |\Lambda_0| = (\beta_c - 1)K_{\beta_c} + \beta_c\gamma$. For $\beta < \beta_c$ the pressure and the Rényi entropies differ

$$P(\beta) \neq (\beta - 1)K_\beta + \beta\gamma.$$

This phenomena is called phase transition. This is however not a very deep problem. We can fix the relation between pressure and the entropies by replacing $1/|\Lambda_0|$ with $1/|\Lambda_0|^\delta$ in (K.10).

Remark K.2 Hard phase transition. The really deep trouble of thermodynamics is caused by intermittency. In that case we have periodic orbits with $|\Lambda_0| \rightarrow 1$ as $n \rightarrow \infty$. Then for $\beta > 1$ the contribution of these orbits dominate both (K.10) and (K.3). Consequently the partition sum scales as $Z_n(\beta) \rightarrow 1$ and both the pressure and the entropies are zero. In this case quantities connected with $\beta \leq 1$ make sense only. These are for example the topological entropy, Kolmogorov entropy, Lyapunov exponent, escape rate, D_0 and D_1 . This phase transition cannot be fixed. It is probably fair to say that quantities which depend on this phase transition are only of mathematical interest and not very useful for characterization of realistic dynamical systems.

Exercises

K.1. Thermodynamics in higher dimensions. Define Lyapunov exponents as the time averages of the eigen-exponents of the Jacobian matrix J

$$\mu^{(k)} = \lim_{t \rightarrow \infty} \frac{1}{t} \log |\Lambda_k^t(x_0)|, \tag{K.23}$$

as a generalization of (17.32).

Show that in d dimensions Pesin's formula is

$$K_1 = \sum_{k=1}^d \mu^{(k)} - \gamma, \tag{K.24}$$

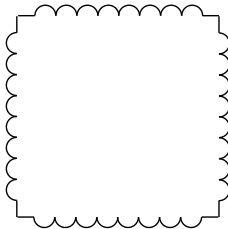
where the summation goes for the positive $\mu^{(k)}$ -s only. Hint: Use the d -dimensional generalization of (K.9)

$$\mu_p = e^{ny} / \left| \prod_k \Lambda_{p,k} \right|,$$

where the product goes for the expanding eigenvalues of the Jacobian matrix of p -cycle. (G. Vattay)

K.2. Stadium billiard Kolmogorov entropy. (continuation of exercise 8.4.) Take $a = 1.6$ and $d = 1$ in the stadium billiard figure 8.1, and estimate the Lyapunov exponent by averaging over a very long trajectory. Biham and Kvale [14] estimate the discrete time Lyapunov to $\lambda \approx 1.0 \pm .1$, the continuous time Lyapunov to $\lambda \approx 0.43 \pm .02$, the topological entropy (for their symbolic dynamics) $h \approx 1.15 \pm .03$.

K.3. Entropy of rugged-edge billiards. Take a semi-circle of diameter ε and replace the sides of a unit square by $\lfloor 1/\varepsilon \rfloor$ semi-circle arcs.



(a) Is the billiard ergodic as $\varepsilon \rightarrow 0$?

(b) (hard) Show that the entropy of the billiard map is

$$K_1 \rightarrow -\frac{2}{\pi} \ln \varepsilon + \text{const},$$

as $\varepsilon \rightarrow 0$. (Hint: do not write return maps.)

(c) (harder) Show that when the semi-circles of the stadium billiard are far apart, say L , the entropy for the flow decays as

$$K_1 \rightarrow \frac{2 \ln L}{\pi L}.$$

K.4. Two scale map. Compute all those quantities - dimensions, escape rate, entropies, etc. - for the repeller of the one dimensional map

$$f(x) = \begin{cases} 1 + ax & \text{if } x < 0, \\ 1 - bx & \text{if } x > 0. \end{cases} \tag{K.25}$$

where a and b are larger than 2. Compute the fractal dimension, plot the pressure and compute the $f(\alpha)$ spectrum of singularities.

K.5. Transfer matrix. Take the unimodal map $f(x) = \sin(\pi x)$ of the interval $I = [0, 1]$. Calculate the four preimages of the intervals $I_0 = [0, 1/2]$ and $I_1 = [1/2, 1]$. Extrapolate $f(x)$ with piecewise linear functions on these intervals. Find a_1, a_2 and b of the previous exercise. Calculate the pressure function of this linear extrapolation. Work out higher level approximations by linearly extrapolating the map on the 2^n -th preimages of I .

References

[K.1] J. Balatoni and A. Renyi, *Publi. Math. Inst. Hung. Acad.Sci.* **1**, 9 (1956); (english translation **1**, 588 (Akademia Budapest, 1976)).

[K.2] Ya.B. Pesin, *Uspekhi Mat. Nauk* **32**, 55 (1977), [*Russian Math. Surveys* **32**, 55 (1977)].

- [K.3] Even though the thermodynamic formalism is of older vintage (we refer the reader to ref. [4] for a comprehensive overview), we adhere here to the notational conventions of ref. [5] which are more current in the physics literature: we strongly recommend also ref. [6], dealing with period doubling universality.
- [K.4] D. Ruelle, *Statistical Mechanics, Thermodynamic Formalism*, (Addison-Wesley, Reading MA, 1978)
- [K.5] T.C. Halsey, M.H. Jensen, L.P. Kadanoff, I. Procaccia and B.I. Shraiman, *Phys. Rev.* **A107**, 1141 (1986).
- [K.6] E. B. Vul, Ya. G. Sinai, and K. M. Khanin, *Uspekhi Mat. Nauk.* **39**, 3 (1984).
- [K.7] C. Shannon, *Bell System Technical Journal*, **27**, 379 (1948).
- [K.8] V.I. Arnold and A. Avez, *Ergodic Problems of Classical Mechanics*, (Addison-Wesley, Redwood City 1989).
- [K.9] Ya.G. Sinai, *Topics in Ergodic Theory*, (Princeton Univ. Press, Princeton NJ 1994).
- [K.10] A.N. Kolmogorov, *Dokl.Akad.Nauk.* **124**, 754 (1959).
- [K.11] V.I. Arnold, *Mathematical Methods in Classical Mechanics* (Springer-Verlag, Berlin, 1978).
- [K.12] C.M. Bender and S.A. Orszag S.A, *Advanced Mathematical Methods for Scientists and Engineers* (McGraw-Hill, Singapore 1978)
- [K.13] J.-P. Eckmann and D. Ruelle, *Rev. Mod. Phys.* **57**, 617
- [K.14] O. Biham and M. Kvale, *Phys. Rev. A* **46**, 6334 (1992).

Appendix L

Statistical mechanics recycled

(R. Mainieri)

A SPIN SYSTEM with long-range interactions can be converted into a chaotic dynamical system that is differentiable and low-dimensional. The thermodynamic limit quantities of the spin system are then equivalent to long time averages of the dynamical system. In this way the spin system averages can be recast as the cycle expansions. If the resulting dynamical system is analytic, the convergence to the thermodynamic limit is faster than with the standard transfer matrix techniques.

L.1 The thermodynamic limit

There are two motivations to recycle statistical mechanics: one gets better control over the thermodynamic limit and one gets detailed information on how one is converging to it. From this information, most other quantities of physical interest can be computed.

In statistical mechanics one computes the averages of observables. These are functions that return a number for every state of the system; they are an abstraction of the process of measuring the pressure or temperature of a gas. The average of an observable is computed in the thermodynamic limit — the limit of system with an arbitrarily large number of particles. The thermodynamic limit is an essential step in the computation of averages, as it is only then that one observes the bulk properties of matter.

Without the thermodynamic limit many of the thermodynamic properties of matter could not be derived within the framework of statistical mechanics. There would be no extensive quantities, no equivalence of ensembles, and no phase transitions. From experiments it is known that certain quantities are extensive, that is,

they are proportional to the size of the system. This is not true for an interacting set of particles. If two systems interacting via pairwise potentials are brought close together, work will be required to join them, and the final total energy will not be the sum of the energies of each of the parts. To avoid the conflict between the experiments and the theory of Hamiltonian systems, one needs systems with an infinite number of particles. In the canonical ensemble the probability of a state is given by the Boltzmann factor which does not impose the conservation of energy; in the microcanonical ensemble energy is conserved but the Boltzmann factor is no longer exact. The equality between the ensembles only appears in the limit of the number of particles going to infinity at constant density. The phase transitions are interpreted as points of non-analyticity of the free energy in the thermodynamic limit. For a finite system the partition function cannot have a zero as a function of the inverse temperature β , as it is a finite sum of positive terms.

The thermodynamic limit is also of central importance in the study of field theories. A field theory can be first defined on a lattice and then the lattice spacing is taken to zero as the correlation length is kept fixed. This continuum limit corresponds to the thermodynamic limit. In lattice spacing units the correlation length is going to infinity, and the interacting field theory can be thought of as a statistical mechanics model at a phase transition.

For general systems the convergence towards the thermodynamic limit is slow. If the thermodynamic limit exists for an interaction, the convergence of the free energy per unit volume f is as an inverse power in the linear dimension of the system.

$$f(\beta) \rightarrow \frac{1}{n} \quad (\text{L.1})$$

where n is proportional to $V^{1/d}$, with V the volume of the d -dimensional system. Much better results can be obtained if the system can be described by a transfer matrix. A transfer matrix is concocted so that the trace of its n th power is exactly the partition function of the system with one of the dimensions proportional to n . When the system is described by a transfer matrix then the convergence is exponential,

$$f(\beta) \rightarrow e^{-\alpha n} \quad (\text{L.2})$$

and may only be faster than that if all long-range correlations of the system are zero — that is, when there are no interactions. The coefficient α depends only on the inverse correlation length of the system.

One of the difficulties in using the transfer matrix techniques is that they seem at first limited to systems with finite range interactions. Phase transitions can happen only when the interaction is long range. One can try to approximate the long range interaction with a series of finite range interactions that have an ever increasing range. The problem with this approach is that in a formally defined

transfer matrix, not all the eigenvalues of the matrix correspond to eigenvalues of the system (in the sense that the rate of decay of correlations is not the ratio of eigenvalues).

Knowledge of the correlations used in conjunction with finite size scaling to obtain accurate estimates of the parameters of systems with phase transitions. (Accurate critical exponents are obtained by series expansions or transfer matrices, and infrequently by renormalization group arguments or Monte Carlo.) In a phase transition the coefficient α of the exponential convergence goes to zero and the convergence to the thermodynamic limit is power-law.

The computation of the partition function is an example of a functional integral. For most interactions these integrals are ill-defined and require some form of normalization. In the spin models case the functional integral is very simple, as “space” has only two points and only “time” being infinite has to be dealt with. The same problem occurs in the computation of the trace of transfer matrices of systems with infinite range interactions. If one tries to compute the partition function Z_n

$$Z_n = \text{tr } T^n$$

when T is an infinite matrix, the result may be infinite for any n . This is not to say that Z_n is infinite, but that the relation between the trace of an operator and the partition function breaks down. We could try regularizing the expression, but as we shall see below, that is not necessary, as there is a better physical solution to this problem.

What will be described here solves both of these problems in a limited context: it regularizes the transfer operator in a physically meaningful way, and as a consequence, it allows for the faster than exponential convergence to the thermodynamic limit and complete determination of the spectrum. The steps to achieve this are:

- Redefine the transfer operator so that there are no limits involved except for the thermodynamic limit.
- Note that the divergences of this operator come from the fact that it acts on a very large space. All that is needed is the smallest subspace containing the eigenvector corresponding to the largest eigenvalue (the Gibbs state).
- Rewrite all observables as depending on a local effective field. The eigenvector is like that, and the operator restricted to this space is trace-class.
- Compute the spectrum of the transfer operator and observe the magic.

L.2 Ising models

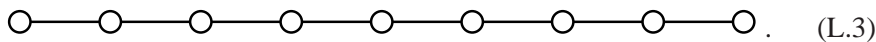
The Ising model is a simple model to study the cooperative effects of many small interacting magnetic dipoles. The dipoles are placed on a lattice and their interaction is greatly simplified. There can also be a field that includes the effects of an external magnetic field and the average effect of the dipoles among themselves. We will define a general class of Ising models (also called spin systems) where the dipoles can be in one of many possible states and the interactions extend beyond the nearest neighboring sites of the lattice. But before we extend the Ising model, we will examine the simplest model in that class.

L.2.1 Ising model

One of the simplest models in statistical mechanics is the Ising model. One imagines that one has a 1-dimensional lattice with small magnets at each site that can point either up or down.

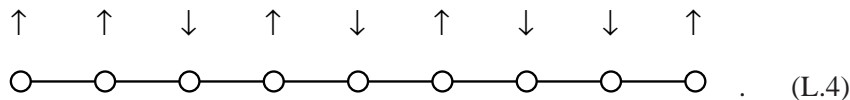


Each little magnet interacts only with its neighbors. If they both point in the same direction, then they contribute an energy $-J$ to the total energy of the system; and if they point in opposite directions, then they contribute $+J$. The signs are chosen so that they prefer to be aligned. Let us suppose that we have n small magnets arranged in a line: A line is drawn between two sites to indicate that there is an interaction between the small magnets that are located on that site



(L.3)

(This figure can be thought of as a graph, with sites being vertices and interacting magnets indicated by edges.) To each of the sites we associate a variable, that we call a spin, that can be in either of two states: up (\uparrow) or down (\downarrow). This represents the two states of the small magnet on that site, and in general we will use the notation Σ_0 to represent the set of possible values of a spin at any site; all sites assume the same set of values. A configuration consists of assigning a value to the spin at each site; a typical configuration is



(L.4)

The set of all configurations for a lattice with n sites is called Ω_0^n and is formed by the Cartesian product $\Omega_0 \times \Omega_0 \cdots \times \Omega_0$, the product repeated n times. Each configuration $\sigma \in \Omega^n$ is a string of n spins

$$\sigma = \{\sigma_0, \sigma_1, \dots, \sigma_n\}, \quad (\text{L.5})$$

In the example configuration (L.4) there are two pairs of spins that have the same orientation and six that have the opposite orientation. Therefore the total energy H of the configuration is $J \times 6 - J \times 2 = 4J$. In general we can associate an energy H to every configuration

$$H(\sigma) = \sum_i J\delta(\sigma_i, \sigma_{i+1}), \quad (\text{L.6})$$

where

$$\delta(\sigma_1, \sigma_2) = \begin{cases} +1 & \text{if } \sigma_1 = \sigma_2 \\ -1 & \text{if } \sigma_1 \neq \sigma_2 \end{cases}. \quad (\text{L.7})$$

One of the problems that was avoided when computing the energy was what to do at the boundaries of the 1-dimensional chain. Note that as written, (L.6) requires the interaction of spin n with spin $n + 1$. In the absence of phase transitions the boundaries do not matter much to the thermodynamic limit and we will connect the first site to the last, implementing periodic boundary conditions.

Thermodynamic quantities are computed from the partition function $Z^{(n)}$ as the size n of the system becomes very large. For example, the free energy per site f at inverse temperature β is given by

$$-\beta f(\beta) = \lim_{n \rightarrow \infty} \frac{1}{n} \ln Z^{(n)}. \quad (\text{L.8})$$

The partition function $Z^{(n)}$ is computed by a sum that runs over all the possible configurations on the 1-dimensional chain. Each configuration contributes with its Gibbs factor $\exp(-\beta H(\sigma))$ and the partition function $Z^{(n)}$ is

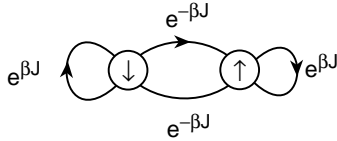
$$Z^{(n)}(\beta) = \sum_{\sigma \in \Omega_0^n} e^{-\beta H(\sigma)}. \quad (\text{L.9})$$

The partition function can be computed using transfer matrices. This is a method that generalizes to other models. At first, it is a little mysterious that matrices show up in the study of a sum. To see where they come from, we can try and build a configuration on the lattice site by site. The first thing to do is to expand out the sum for the energy of the configuration

$$Z^{(n)}(\beta) = \sum_{\sigma \in \Omega^n} e^{\beta J \delta(\sigma_1, \sigma_2)} e^{\beta J \delta(\sigma_2, \sigma_3)} \dots e^{\beta J \delta(\sigma_n, \sigma_1)}. \quad (\text{L.10})$$

Let us use the configuration in (L.4). The first site is $\sigma_1 = \uparrow$. As the second site is \uparrow , we know that the first term in (L.10) is a term $e^{\beta J}$. The third spin is \downarrow , so the second term in (L.10) is $e^{-\beta J}$. If the third spin had been \uparrow , then the term would

have been $e^{\beta J}$ but it would not depend on the value of the first spin σ_1 . This means that the configuration can be built site by site and that to compute the Gibbs factor for the configuration just requires knowing the last spin added. We can then think of the configuration as being a weighted random walk where each step of the walk contributes according to the last spin added. The random walk take place on the transition graph



Choose one of the two sites as a starting point. Walk along any allowed edge making your choices randomly and keep track of the accumulated weight as you perform the n steps. To implement the periodic boundary conditions make sure that you return to the starting node of the transition graph. If the walk is carried out in all possible 2^n ways then the sum of all the weights is the partition function. To perform the sum we consider the matrix

$$T(\beta) = \begin{bmatrix} e^{\beta J} & e^{-\beta J} \\ e^{-\beta J} & e^{\beta J} \end{bmatrix}. \quad (\text{L.11})$$

As in chapter 11 the sum of all closed walks is given by the trace of powers of the matrix. These powers can easily be re-expressed in terms of the two eigenvalues λ_1 and λ_2 of the transfer matrix:

$$Z^{(n)}(\beta) = \text{tr } T^n(\beta) = \lambda_1(\beta)^n + \lambda_2(\beta)^n. \quad (\text{L.12})$$

L.2.2 Averages of observables

Averages of observables can be re-expressed in terms of the eigenvectors of the transfer matrix. Alternatively, one can introduce a modified transfer matrix and compute the averages through derivatives. Sounds familiar?

L.2.3 General spin models

The more general version of the Ising model — the spin models — will be defined on a regular lattice, \mathbb{Z}^D . At each lattice site there will be a spin variable that can assume a finite number of states identified by the set Ω_0 .

The transfer operator \mathcal{T} was introduced by Kramers and Wannier [12] to study the Ising model on a strip and concocted so that the trace of its n th power is the

partition function Z_n of system when one of its dimensions is n . The method can be generalized to deal with any finite-range interaction. If the range of the interaction is L , then \mathcal{T} is a matrix of size $2^L \times 2^L$. The longer the range, the larger the matrix.

L.3 Fisher droplet model

In a series of articles [20], Fisher introduced the droplet model. It is a model for a system containing two phases: gas and liquid. At high temperatures, the typical state of the system consists of droplets of all sizes floating in the gas phase. As the temperature is lowered, the droplets coalesce, forming larger droplets, until at the transition temperature, all droplets form one large one. This is a first order phase transition.

Although Fisher formulated the model in 3-dimensions, the analytic solution of the model shows that it is equivalent to a 1-dimensional lattice gas model with long range interactions. Here we will show how the model can be solved for an arbitrary interaction, as the solution only depends on the asymptotic behavior of the interaction.

The interest of the model for the study of cycle expansions is its relation to intermittency. By having an interaction that behaves asymptotically as the scaling function for intermittency, one expects that the analytic structure (poles and cuts) will be same.

Fisher used the droplet model to study a first order phase transition [20]. Gallavotti [21] used it to show that the zeta functions cannot in general be extended to a meromorphic functions of the entire complex plane. The droplet model has also been used in dynamical systems to explain features of mode locking, see Artuso [22]. In computing the zeta function for the droplet model we will discover that at low temperatures the cycle expansion has a limited radius of convergence, but it is possible to factorize the expansion into the product of two functions, each of them with a better understood radius of convergence.

L.3.1 Solution

The droplet model is a 1-dimensional lattice gas where each site can have two states: empty or occupied. We will represent the empty state by 0 and the occupied state by 1. The configurations of the model in this notation are then strings of zeros and ones. Each configuration can be viewed as groups of contiguous ones separated by one or more zeros. The contiguous ones represent the droplets in the model. The droplets do not interact with each other, but the individual particles within each droplet do.

To determine the thermodynamics of the system we must assign an energy to every configuration. At very high temperatures we would expect a gaseous

phase where there are many small droplets, and as we decrease the temperature the droplets would be expected to coalesce into larger ones until at some point there is a phase transition and the configuration is dominated by one large drop. To construct a solvable model and yet one with a phase transition we need long range interaction among all the particles of a droplet. One choice is to assign a fixed energy θ_n for the interactions of the particles of a cluster of size n . In a given droplet one has to consider all the possible clusters formed by contiguous particles. Consider for example the configuration 0111010. It has two droplets, one of size three and another of size one. The droplet of size one has only one cluster of size one and therefore contributes to the energy of the configuration with θ_1 . The cluster of size three has one cluster of size three, two clusters of size two, and three clusters of size one; each cluster contributing a θ_i term to the energy. The total energy of the configuration is then

$$H(0111010) = 4\theta_1 + 2\theta_2 + 1\theta_3 . \quad (\text{L.13})$$

If there were more zeros around the droplets in the above configuration the energy would still be the same. The interaction of one site with the others is assumed to be finite, even in the ground state consisting of a single droplet, so there is a restriction on the sum of the cluster energies given by

$$a = \sum_{n>0} \theta_n < \infty . \quad (\text{L.14})$$

The configuration with all zeros does not contribute to the energy.

Once we specify the function θ_n we can compute the energy of any configuration, and from that determine the thermodynamics. Here we will evaluate the cycle expansion for the model by first computing the generating function

$$G(z, \beta) = \sum_{n>0} z^n \frac{Z_n(\beta)}{n} \quad (\text{L.15})$$

and then considering its exponential, the cycle expansion. Each partition function Z_n must be evaluated with periodic boundary conditions. So if we were computing Z_3 we must consider all eight binary sequences of three bits, and when computing the energy of a configuration, say 011, we should determine the energy per three sites of the long chain

...011011011011...

In this case the energy would be $\theta_2 + 2\theta_1$. If instead of 011 we had considered one of its rotated shifts, 110 or 101, the energy of the configuration would have been the same. To compute the partition function we only need to consider one of the configurations and multiply by the length of the configuration to obtain the

contribution of all its rotated shifts. The factor $1/n$ in the generating function cancels this multiplicative factor. This reduction will not hold if the configuration has a symmetry, as for example 0101 which has only two rotated shift configurations. To compensate this we replace the $1/n$ factor by a symmetry factor $1/s(b)$ for each configuration b . The evaluation of G is now reduced to summing over all configurations that are not rotated shift equivalent, and we call these the basic configurations and the set of all of them B . We now need to evaluate

$$G(z, \beta) = \sum_{b \in B} \frac{z^{|b|}}{s(b)} e^{-\beta H(b)}. \quad (\text{L.16})$$

The notation $|\cdot|$ represents the cardinality of the set.

Any basic configuration can be built by considering the set of droplets that form it. The smallest building block has size two, as we must also put a zero next to the one so that when two different blocks get put next to each other they do not coalesce. The first few building blocks are

size	droplets	
2	01	(L.17)
3	001 011	
4	0001 0011 0111	

Each droplet of size n contributes with energy

$$W_n = \sum_{1 \leq k \leq n} (n - k + 1) \theta_k. \quad (\text{L.18})$$

So if we consider the sum

$$\sum_{n \geq 1} \frac{1}{n} \left(z^2 e^{-\beta H(01)} + z^3 (e^{-\beta H(001)} + e^{-\beta H(011)}) + \right. \\ \left. + z^4 (e^{-\beta H(0001)} + e^{-\beta H(0011)} + e^{-\beta H(0111)}) + \dots \right)^n \quad (\text{L.19})$$

then the power in n will generate all the configurations that are made from many droplets, while the z will keep track of the size of the configuration. The factor $1/n$ is there to avoid the over-counting, as we only want the basic configurations and not its rotated shifts. The $1/n$ factor also gives the correct symmetry factor in the case the configuration has a symmetry. The sum can be simplified by noticing that it is a logarithmic series

$$- \ln \left(1 - (z^2 e^{-\beta W_1} + z^3 (e^{-\beta W_1} + e^{-\beta W_2}) + \dots) \right), \quad (\text{L.20})$$

where the $H(b)$ factors have been evaluated in terms of the droplet energies W_n . A proof of the equality of (L.19) and (L.20) can be given, but we there was not

enough space on the margin to write it down. The series that is subtracted from one can be written as a product of two series and the logarithm written as

$$-\ln\left(1 - (z^1 + z^2 + z^3 + \dots)(ze^{-\beta W_1} + z^2 e^{-\beta W_2} + \dots)\right) \quad (\text{L.21})$$

The product of the two series can be directly interpreted as the generating function for sequences of droplets. The first series adds one or more zeros to a configuration and the second series add a droplet.

There is a whole class of configurations that is not included in the above sum: the configurations formed from a single droplet and the vacuum configuration. The vacuum is the easiest, as it has zero energy it only contributes a z . The sum of all the null configurations of all sizes is

$$\sum_{n>0} \frac{z^n}{n}. \quad (\text{L.22})$$

The factor $1/n$ is here because the original G had them and the null configurations have no rotated shifts. The single droplet configurations also do not have rotated shifts so their sum is

$$\sum_{n>0} \frac{z^n e^{-\beta H(\overbrace{11 \dots 11}^n)}}{n}. \quad (\text{L.23})$$

Because there are no zeros in the above configuration clusters of all size exist and the energy of the configuration is $n \sum \theta_k$ which we denote by na .

From the three sums (L.21), (L.22), and (L.23) we can evaluate the generating function G to be

$$G(z, \beta) = -\ln(1 - z) - \ln(1 - ze^{-\beta a}) - \ln\left(1 - \frac{z}{1 - z} \sum_{n \geq 1} z^n e^{-\beta W_n}\right). \quad (\text{L.24})$$

The cycle expansion $\zeta^{-1}(z, \beta)$ is given by the exponential of the generating function e^{-G} and we obtain

$$\zeta^{-1}(z, \beta) = (1 - ze^{-\beta a})(1 - z(1 + \sum_{n \geq 1} z^n e^{-\beta W_n})) \quad (\text{L.25})$$

To pursue this model further we need to have some assumptions about the interaction strengths θ_n . We will assume that the interaction strength decreases with the inverse square of the size of the cluster, that is, $\theta_n = -1/n^2$. With this we can estimate that the energy of a droplet of size n is asymptotically

$$W_n \sim -n + \ln n + O\left(\frac{1}{n}\right). \quad (\text{L.26})$$

If the power chosen for the polynomially decaying interaction had been other than inverse square we would still have the droplet term proportional to n , but there would be no logarithmic term, and the O term would be of a different power. The term proportional to n survives even if the interactions falls off exponentially, and in this case the correction is exponentially small in the asymptotic formula. To simplify the calculations we are going to assume that the droplet energies are exactly

$$W_n = -n + \ln n \quad (\text{L.27})$$

in a system of units where the dimensional constants are one. To evaluate the cycle expansion (L.25) we need to evaluate the constant a , the sum of all the θ_n . One can write a recursion for the θ_n

$$\theta_n = W_n - \sum_{1 \leq k < n} (n - k + 1)\theta_k \quad (\text{L.28})$$

and with an initial choice for θ_1 evaluate all the others. It can be verified that independent of the choice of θ_1 the constant a is equal to the number that multiplies the n term in (L.27). In the units used

$$a = -1. \quad (\text{L.29})$$

For the choice of droplet energy (L.27) the sum in the cycle expansion can be expressed in terms of a special function: the Lerch transcendent ϕ_L . It is defined by

$$\phi_L(z, s, c) = \sum_{n \geq 0} \frac{z^n}{(n + c)^s}, \quad (\text{L.30})$$

excluding from the sum any term that has a zero denominator. The Lerch function converges for $|z| < 1$. The series can be analytically continued to the complex plane and it will have a branch point at $z = 1$ with a cut chosen along the positive real axis. In terms of Lerch transcendent function we can write the cycle expansion (L.25) using (L.27) as

$$\zeta^{-1}(z, \beta) = (1 - ze^\beta) \left(1 - z(1 + \phi_L(ze^\beta, \beta, 1)) \right) \quad (\text{L.31})$$

This serves as an example of a zeta function that cannot be extended to a meromorphic function of the complex plane as one could conjecture.

The thermodynamics for the droplet model comes from the smallest root of (L.31). The root can come from any of the two factors. For large value of β (low temperatures) the smallest root is determined from the $(1 - ze^\beta)$ factor, which gave

the contribution of a single large drop. For small β (large temperatures) the root is determined by the zero of the other factor, and it corresponds to the contribution from the gas phase of the droplet model. The transition occurs when the smallest root of each of the factors become numerically equal. This determines the critical temperature β_c through the equation

$$1 - e^{-\beta_c}(1 + \zeta_R(\beta_c)) = 0 \quad (\text{L.32})$$

which can be solved numerically. One finds that $\beta_c = 1.40495$. The phase transition occurs because the roots from two different factors get swapped in their roles as the smallest root. This in general leads to a first order phase transition. For large β the Lerch transcendental is being evaluated at the branch point, and therefore the cycle expansion cannot be an analytic function at low temperatures. For large temperatures the smallest root is within the radius of convergence of the series for the Lerch transcendental, and the cycle expansion has a domain of analyticity containing the smallest root.

As we approach the phase transition point as a function of β the smallest root and the branch point get closer together until at exactly the phase transition they collide. This is a sufficient condition for the existence of a first order phase transitions. In the literature of zeta functions [19] there have been speculations on how to characterize a phase transition within the formalism. The solution of the Fisher droplet model suggests that for first order phase transitions the factorized cycle expansion will have its smallest root within the radius of convergence of one of the series except at the phase transition when the root collides with a singularity. This does not seem to be the case for second order phase transitions.

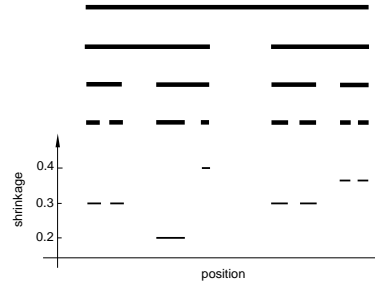
The analyticity of the cycle expansion can be restored if we consider separate cycle expansions for each of the phases of the system. If we separate the two terms of ζ^{-1} in (L.31), each of them is an analytic function and contains the smallest root within the radius of convergence of the series for the relevant β values.

L.4 Scaling functions

There is a relation between general spin models and dynamical system. If one thinks of the boxes of the Markov partition of a hyperbolic system as the states of a spin system, then computing averages in the dynamical system is carrying out a sum over all possible states. One can even construct the natural measure of the dynamical system from a translational invariant “interaction function” call the scaling function.

There are many routes that lead to an explanation of what a scaling function is and how to compute it. The shortest is by breaking away from the historical development and considering first the presentation function of a fractal. The presentation function is a simple chaotic dynamical system (hyperbolic, unlike the circle map) that generates the fractal and is closely related to the definition

Figure L.1: Construction of the steps of the scaling function from a Cantor set. From one level to the next in the construction of the Cantor set the covers are shrunk, each parent segment into two children segments. The shrinkage of the last level of the construction is plotted and by removing the gaps one has an approximation to the scaling function of the Cantor set.



of fractals of Hutchinson [24] and the iterated dynamical systems introduced by Barnsley and collaborators [13]. From the presentation function one can derive the scaling function, but we will not do it in the most elegant fashion, rather we will develop the formalism in a form that is directly applicable to the experimental data.

In the upper part of figure L.1 we have the successive steps of the construction similar to the middle third Cantor set. The construction is done in levels, each level being formed by a collection of segments. From one level to the next, each “parent” segment produces smaller “children” segments by removing the middle section. As the construction proceeds, the segments better approximate the Cantor set. In the figure not all the segments are the same size, some are larger and some are smaller, as is the case with multifractals. In the middle third Cantor set, the ratio between a segment and the one it was generated from is exactly 1/3, but in the case shown in the figure the ratios differ from 1/3. If we went through the last level of the construction and made a plot of the segment number and its ratio to its parent segment we would have a scaling function, as indicated in the figure. A function giving the ratios in the construction of a fractal is the basic idea for a scaling function. Much of the formalism that we will introduce is to be able to give precise names to every segments and to arrange the “lineage” of segments so that the children segments have the correct parent. If we do not take these precautions, the scaling function would be a “wild function,” varying rapidly and not approximated easily by simple functions.

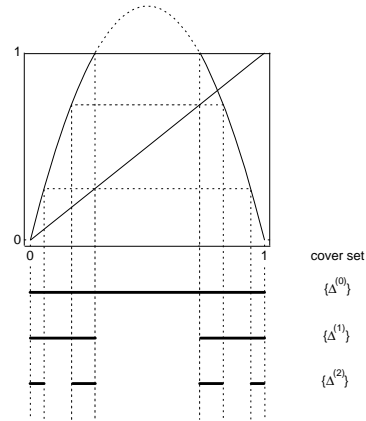
To describe the formalism we will use a variation on the quadratic map that appears in the theory of period doubling. This is because the combinatorial manipulations are much simpler for this map than they are for the circle map. The scaling function will be described for a one dimensional map F as shown in figure L.2. Drawn is the map

$$F(x) = 5x(1 - x) \tag{L.33}$$

restricted to the unit interval. We will see that this map is also a presentation function.

It has two branches separated by a gap: one over the left portion of the unit interval and one over the right. If we choose a point x at random in the unit interval and iterate it under the action of the map F , (L.33), it will hop between the branches and eventually get mapped to minus infinity. An orbit point is guaranteed

Figure L.2: A Cantor set presentation function. The Cantor set is the set of all points that under iteration do not leave the interval $[0, 1]$. This set can be found by backwards iterating the gap between the two branches of the map. The dotted lines can be used to find these backward images. At each step of the construction one is left with a set of segments that form a cover of the Cantor set.



to go to minus infinity if it lands in the gap. The hopping of the point defines the orbit of the initial point x : $x \mapsto x_1 \mapsto x_2 \mapsto \dots$. For each orbit of the map F we can associate a symbolic code. The code for this map is formed from 0s and 1s and is found from the orbit by associating a 0 if $x_t < 1/2$ and a 1 if $x_t > 1/2$, with $t = 0, 1, 2, \dots$

Most initial points will end up in the gap region between the two branches. We then say that the orbit point has escaped the unit interval. The points that do not escape form a Cantor set C (or Cantor dust) and remain trapped in the unit interval for all iterations. In the process of describing all the points that do not escape, the map F can be used as a presentation of the Cantor set C , and has been called a presentation function by Feigenbaum [13].

How does the map F “present” the Cantor set? The presentation is done in steps. First, we determine the points that do not escape the unit interval in one iteration of the map. These are the points that are not part of the gap. These points determine two segments, which are an approximation to the Cantor set. In the next step we determine the points that do not escape in two iterations. These are the points that get mapped into the gap in one iteration, as in the next iteration they will escape; these points form the two segments $\Delta_0^{(1)}$ and $\Delta_1^{(1)}$ at level 1 in figure L.2. The processes can be continued for any number of iterations. If we observe carefully what is being done, we discover that at each step the pre-images of the gap (backward iterates) are being removed from the unit interval. As the map has two branches, every point in the gap has two pre-images, and therefore the whole gap has two pre-images in the form of two smaller gaps. To generate all the gaps in the Cantor set one just has to iterate the gap backwards. Each iteration of the gap defines a set of segments, with the n th iterate defining the segments $\Delta_k^{(n)}$ at level n . For this map there will be 2^n segments at level n , with the first few drawn in figure L.2. As $n \rightarrow \infty$ the segments that remain for at least n iterates converge to the Cantor set C .

The segments at one level form a cover for the Cantor set and it is from a cover that all the invariant information about the set is extracted (the cover generated from the backward iterates of the gap form a Markov partition for the map as a dynamical system). The segments $\{\Delta_k^{(n)}\}$ at level n are a refinement of the cover formed by segments at level $n - 1$. From successive covers we can compute the

trajectory scaling function, the spectrum of scalings $f(\alpha)$, and the generalized dimensions.

To define the scaling function we must give labels (names) to the segments. The labels are chosen so that the definition of the scaling function allows for simple approximations. As each segment is generated from an inverse image of the unit interval, we will consider the inverse of the presentation function F . Because F does not have a unique inverse, we have to consider restrictions of F . Its restriction to the first half of the segment, from 0 to 1/2, has a unique inverse, which we will call F_0^{-1} , and its restriction to the second half, from 1/2 to 1, also has a unique inverse, which we will call F_1^{-1} . For example, the segment labeled $\Delta^{(2)}(0, 1)$ in figure L.2 is formed from the inverse image of the unit interval by mapping $\Delta^{(0)}$, the unit interval, with F_1^{-1} and then F_0^{-1} , so that the segment

$$\Delta^{(2)}(0, 1) = F_0^{-1} \left(F_1^{-1} \left(\Delta^{(0)} \right) \right). \quad (\text{L.34})$$

The mapping of the unit interval into a smaller interval is what determines its label. The sequence of the labels of the inverse maps is the label of the segment:

$$\Delta^{(n)}(\epsilon_1, \epsilon_2, \dots, \epsilon_n) = F_{\epsilon_1}^{-1} \circ F_{\epsilon_2}^{-1} \circ \dots \circ F_{\epsilon_n}^{-1} \left(\Delta^{(0)} \right).$$

The scaling function is formed from a set of ratios of segments length. We use $|\cdot|$ around a segment $\Delta^{(n)}(\epsilon)$ to denote its size (length), and define

$$\sigma^{(n)}(\epsilon_1, \epsilon_2, \dots, \epsilon_n) = \frac{|\Delta^{(n)}(\epsilon_1, \epsilon_2, \dots, \epsilon_n)|}{|\Delta^{(n-1)}(\epsilon_2, \dots, \epsilon_n)|}.$$

We can then arrange the ratios $\sigma^{(n)}(\epsilon_1, \epsilon_2, \dots, \epsilon_n)$ next to each other as piecewise constant segments in increasing order of their binary label $\epsilon_1, \epsilon_2, \dots, \epsilon_n$ so that the collection of steps scan the unit interval. As $n \rightarrow \infty$ this collection of steps will converge to the scaling function.

L.5 Geometrization

The \mathcal{L} operator is a generalization of the transfer matrix. It gets more by considering less of the matrix: instead of considering the whole matrix it is possible to consider just one of the rows of the matrix. The \mathcal{L} operator also makes explicit the vector space in which it acts: that of the observable functions. Observables are functions that to each configuration of the system associate a number: the energy, the average magnetization, the correlation between two sites. It is in the average of observables that one is interested in. Like the transfer matrix, the \mathcal{L} operator considers only semi-infinite systems, that is, only the part of the interaction between spins to the right is taken into account. This may sound un-symmetric, but

it is a simple way to count each interaction only once, even in cases where the interaction includes three or more spin couplings. To define the \mathcal{L} operator one needs the interaction energy between one spin and all the rest to its right, which is given by the function ϕ . The \mathcal{L} operators defined as

$$\mathcal{L}g(\sigma) = \sum_{\sigma_0 \in \Omega_0} g(\sigma_0\sigma) e^{-\beta\phi(\sigma_0\sigma)}.$$

To each possible value in Ω_0 that the spin σ_0 can assume, an average of the observable g is computed weighed by the Boltzmann factor $e^{-\beta\phi}$. The formal relations that stem from this definition are its relation to the free energy when applied to the observable ι that returns one for any configuration:

$$-\beta f(\beta) = \lim_{n \rightarrow \infty} \frac{1}{n} \ln \|\mathcal{L}^n \iota\|$$

and the thermodynamic average of an observable

$$\langle g \rangle = \lim_{n \rightarrow \infty} \frac{\|\mathcal{L}^n g\|}{\|\mathcal{L}^n \iota\|}.$$

Both relations hold for almost all configurations. These relations are part of the theorem of Ruelle that enlarges the domain of the Perron-Frobenius theorem and sharpens its results. The theorem shows that just as the transfer matrix, the largest eigenvalue of the \mathcal{L} operator is related to the free-energy of the spin system. It also shows that there is a formula for the eigenvector related to the largest eigenvalue. This eigenvector $|\rho\rangle$ (or the corresponding one for the adjoint \mathcal{L}^* of \mathcal{L}) is the Gibbs state of the system. From it all averages of interest in statistical mechanics can be computed from the formula

$$\langle g \rangle = \langle \rho | g | \rho \rangle.$$

The Gibbs state can be expressed in an explicit form in terms of the interactions, but it is of little computational value as it involves the Gibbs state for a related spin system. Even then it does have an enormous theoretical value. Later we will see how the formula can be used to manipulate the space of observables into a more convenient space.

The geometrization of a spin system converts the shift dynamics (necessary to define the Ruelle operator) into a smooth dynamics. This is equivalent to the mathematical problem in ergodic theory of finding a smooth embedding for a given Bernoulli map.

The basic idea for the dynamics is to establish the a set of maps F_{σ_k} such that

$$F_{\sigma_k}(0) = 0$$

and

$$F_{\sigma_1} \circ F_{\sigma_2} \circ \cdots \circ F_{\sigma_n}(0) = \phi(+, \sigma_1, \sigma_2, \dots, \sigma_n, -, -, \dots).$$

This is a formal relation that expresses how the interaction is to be converted into a dynamical systems. In most examples F_{σ_k} is a collection of maps from a subset of R^D to itself.

If the interaction is complicated, then the dimension of the set of maps may be infinite. If the resulting dynamical system is infinite have we gained anything from the transformation? The gain in this case is not in terms of added speed of convergence to the thermodynamic limit, but in the fact that the Ruelle operator is of trace-class and all eigenvalues are related to the spin system and not artifacts of the computation.

The construction of the higher dimensional system is done by borrowing the state space reconstruction technique from dynamical systems. State space reconstruction can be done in several ways: by using delay coordinates, by using derivatives of the position, or by considering the value of several independent observables of the system. All these may be used in the construction of the equivalent dynamics. Just as in the study of dynamical systems, the exact method does not matter for the determination of the thermodynamics ($f(\alpha)$ spectra, generalized dimension), also in the construction of the equivalent dynamics the exact choice of observable does not matter.

We will only consider configurations for the half line. This is because for translational invariant interactions the thermodynamic limit on half line is the same as in the whole line. One can prove this by considering the difference in a thermodynamic average in the line and in the semiline and compare the two as the size of the system goes to infinity.

When the interactions are long range in principle one has to specify the boundary conditions to be able to compute the interaction energy of a configuration in a finite box. If there are no phase transitions for the interaction, then which boundary conditions are chosen is irrelevant in the thermodynamic limit. When computing quantities with the transfer matrix, the long range interaction is truncated at some finite range and the truncated interaction is then use to evaluate the transfer matrix. With the Ruelle operator the interaction is never truncated, and the boundary must be specified.

The interaction $\phi(\sigma)$ is any function that returns a number on a configuration. In general it is formed from pairwise spin interactions

$$\phi(\sigma) = \sum_{n>0} \delta_{\sigma_0, \sigma_n} J(n)$$

with different choices of $J(n)$ leading to different models. If $J(n) = 1$ only if $n = 1$ and 0 otherwise, then one has the nearest neighbor Ising model. If $J(n) = n^{-2}$, then one has the inverse square model relevant in the study of the Kondo problem.

Let us say that each site of the lattice can assume two values $+, -$ and the set of all possible configurations of the semiline is the set Ω . Then an observable g is a function from the set of configurations Ω to the reals. Each configuration is indexed by the integers from 0 up, and it is useful to think of the configuration as a string of spins. One can append a spin η_0 to its beginning, $\eta \vee \sigma$, in which case η is at site 0, ω_0 at site 1, and so on.

The Ruelle operator \mathcal{L} is defined as

$$\mathcal{L}g(\eta) = \sum_{\omega_0 \in \Omega_0} g(\omega_0 \vee \eta) e^{-\beta\phi(\omega_0 \vee \eta)}.$$

This is a positive and bounded operator over the space of bounded observables. There is a generalization of the Perron-Frobenius theorem by Ruelle that establishes that the largest eigenvalue of \mathcal{L} is isolated from the rest of the spectrum and gives the thermodynamics of the spin system just as the largest eigenvalue of the transfer matrix does. Ruelle also gave a formula for the eigenvector related to the largest eigenvalue.

The difficulty with it is that the relation between the partition function and the trace of its n th power, $\text{tr } \mathcal{L}^n = Z_n$ no longer holds. The reason is that the trace of the Ruelle operator is ill-defined, it is infinite.

We now introduce a special set of observables $\{x_1(\sigma), \dots, x_l(\sigma)\}$. The idea is to choose the observables in such a way that from their values on a particular configuration σ the configuration can be reconstructed. We also introduce the interaction observables h_{σ_0} .

To geometrize spin systems, the interactions are assumed to be translationally invariant. The spins σ_k will only assume a finite number of values. For simplicity, we will take the interaction ϕ among the spins to depend only on pairwise interactions,

$$\phi(\sigma) = \phi(\sigma_0, \sigma_1, \sigma_2, \dots) = J_0\sigma_0 + \sum_{n>0} \delta_{\sigma_0, \sigma_n} J_1(n), \quad (\text{L.35})$$

and limit σ_k to be in $\{+, -\}$. For the 1-dimensional Ising model, J_0 is the external magnetic field and $J_1(n) = 1$ if $n = 1$ and 0 otherwise. For an exponentially decaying interaction $J_1(n) = e^{-\alpha n}$. Two- and 3-dimensional models can be considered in this framework. For example, a strip of spins of $L \times \infty$ with helical boundary conditions is modeled by the potential $J_1(n) = \delta_{n,1} + \delta_{n,L}$.

The transfer operator \mathcal{T} was introduced by Kramers and Wannier [12] to study the Ising model on a strip and concocted so that the trace of its n th power is the partition function Z_n of system when one of its dimensions is n . The method can be generalized to deal with any finite-range interaction. If the range of the interaction is L , then \mathcal{T} is a matrix of size $2^L \times 2^L$. The longer the range, the larger the matrix. When the range of the interaction is infinite one has to define the \mathcal{T} operator by

its action on an observable g . Just as the observables in quantum mechanics, g is a function that associates a number to every state (configuration of spins). The energy density and the average magnetization are examples of observables. From this equivalent definition one can recover the usual transfer matrix by making all quantities finite range. For a semi-infinite configuration $\sigma = \{\sigma_0, \sigma_1, \dots\}$:

$$\mathcal{T}g(\sigma) = g(+ \vee \sigma)e^{-\beta\phi(+ \vee \sigma)} + g(- \vee \sigma)e^{-\beta\phi(- \vee \sigma)}. \quad (\text{L.36})$$

By $+ \vee \sigma$ we mean the configuration obtained by prepending $+$ to the beginning of σ resulting in the configuration $\{+, \sigma_0, \sigma_1, \dots\}$. When the range becomes infinite, $\text{tr } \mathcal{T}^n$ is infinite and there is no longer a connection between the trace and the partition function for a system of size n (this is a case where matrices give the wrong intuition). Ruelle [13] generalized the Perron-Frobenius theorem and showed that even in the case of infinite range interactions the largest eigenvalue of the \mathcal{T} operator is related to the free-energy of the spin system and the corresponding eigenvector is related to the Gibbs state. By applying \mathcal{T} to the constant observable u , which returns 1 for any configuration, the free energy per site f is computed as

$$-\beta f(\beta) = \lim_{n \rightarrow \infty} \frac{1}{n} \ln \|\mathcal{T}^n u\|. \quad (\text{L.37})$$

To construct a smooth dynamical system that reproduces the properties of \mathcal{T} , one uses the phase space reconstruction technique of Packard *et al.* [6] and Takens [7], and introduces a vector of state observables $x(\sigma) = \{x_1(\sigma), \dots, x_D(\sigma)\}$. To avoid complicated notation we will limit the discussion to the example $x(\sigma) = \{x_+(\sigma), x_-(\sigma)\}$, with $x_+(\sigma) = \phi(+ \vee \sigma)$ and $x_-(\sigma) = \phi(- \vee \sigma)$; the more general case is similar and used in a later example. The observables are restricted to those g for which, for all configurations σ , there exist an analytic function G such that $G(x_1(\sigma), \dots, x_D(\sigma)) = g(\sigma)$. This at first seems a severe restriction as it may exclude the eigenvector corresponding to the Gibbs state. It can be checked that this is not the case by using the formula given by Ruelle [14] for this eigenvector. A simple example where this formalism can be carried out is for the interaction $\phi(\sigma)$ with pairwise exponentially decaying potential $J_1(n) = a^n$ (with $|a| < 1$). In this case $\phi(\sigma) = \sum_{n>0} \delta_{\sigma_0, \sigma_n} a^n$ and the state observables are $x_+(\sigma) = \sum_{n>0} \delta_{+, \sigma_n} a^n$ and $x_-(\sigma) = \sum_{n>0} \delta_{-, \sigma_n} a^n$. In this case the observable x_+ gives the energy of $+$ spin at the origin, and x_- the energy of a $-$ spin.

Using the observables x_+ and x_- , the transfer operator can be re-expressed as

$$\mathcal{T}G(x(\sigma)) = \sum_{\eta \in \{+, -\}} G(x_+(\eta \vee \sigma), x_-(\eta \vee \sigma)) e^{-\beta x_\eta(\sigma)}. \quad (\text{L.38})$$

In this equation the only reference to the configuration σ is when computing the new observable values $x_+(\eta \vee \sigma)$ and $x_-(\eta \vee \sigma)$. The iteration of the function that gives these values in terms of $x_+(\sigma)$ and $x_-(\sigma)$ is the dynamical system that will

reproduce the properties of the spin system. For the simple exponentially decaying potential this is given by two maps, F_+ and F_- . The map F_+ takes $\{x_+(\sigma), x_+(\sigma)\}$ into $\{x_+(\sigma + \nu), x_-(\sigma + \nu)\}$ which is $\{a(1 + x_+), ax_-\}$ and the map F_- takes $\{x_+, x_-\}$ into $\{ax_+, a(1 + x_-)\}$. In a more general case we have maps F_η that take $x(\sigma)$ to $x(\eta \vee \sigma)$.

We can now define a new operator \mathcal{L}

$$\mathcal{L}G(x) \stackrel{\text{def}}{=} \mathcal{T}G(x(\sigma)) = \sum_{\eta \in \{+, -\}} G(F_\eta(x)) e^{-\beta x_\eta}, \quad (\text{L.39})$$

where all dependencies on σ have disappeared — if we know the value of the state observables x , the action of \mathcal{L} on G can be computed.

A dynamical system is formed out of the maps F_η . They are chosen so that one of the state variables is the interaction energy. One can consider the two maps F_+ and F_- as the inverse branches of a hyperbolic map f , that is, $f^{-1}(x) = \{F_+(x), F_-(x)\}$. Studying the thermodynamics of the interaction ϕ is equivalent to studying the long term behavior of the orbits of the map f , achieving the transformation of the spin system into a dynamical system.

Unlike the original transfer operator, the \mathcal{L} operator — acting in the space of observables that depend only on the state variables — is of trace-class (its trace is finite). The finite trace gives us a chance to relate the trace of \mathcal{L}^n to the partition function of a system of size n . We can do better. As most properties of interest (thermodynamics, fall-off of correlations) are determined directly from its spectrum, we can study instead the zeros of the Fredholm determinant $\det(1 - z\mathcal{L})$ by the technique of cycle expansions developed for dynamical systems [2]. A cycle expansion consists of finding a power series expansion for the determinant by writing $\det(1 - z\mathcal{L}) = \exp(\text{tr} \ln(1 - z\mathcal{L}))$. The logarithm is expanded into a power series and one is left with terms of the form $\text{tr} \mathcal{L}^n$ to evaluate. For evaluating the trace, the \mathcal{L} operator is equivalent to

$$\mathcal{L}G(x) = \int_{\mathbf{R}^D} dy \delta(y - f(x)) e^{-\beta y} G(y) \quad (\text{L.40})$$

from which the trace can be computed:

$$\text{tr} \mathcal{L}^n = \sum_{x=f^{(on)}(x)} \frac{e^{-\beta H(x)}}{|\det(1 - \partial_x f^{(on)}(x))|} \quad (\text{L.41})$$

with the sum running over all the fixed points of $f^{(on)}$ (all spin configurations of a given length). Here $f^{(on)}$ is f composed with itself n times, and $H(x)$ is the energy of the configuration associated with the point x . In practice the map f is never constructed and the energies are obtained directly from the spin configurations.

To compute the value of $\text{tr } \mathcal{L}^n$ we must compute the value of $\partial_x f^{(on)}$; this involves a functional derivative. To any degree of accuracy a number x in the range of possible interaction energies can be represented by a finite string of spins ϵ , such as $x = \phi(+, \epsilon_0, \epsilon_1, \dots, -, -, \dots)$. By choosing the sequence ϵ to have a large sequence of spins $-$, the number x can be made as small as needed, so in particular we can represent a small variation by $\phi(\eta)$. As $x_+(\epsilon) = \phi(+ \vee \epsilon)$, from the definition of a derivative we have:

$$\partial_x f(x) = \lim_{m \rightarrow \infty} \frac{\phi(\epsilon \vee \eta^{(m)}) - \phi(\epsilon)}{\phi(\eta^{(m)})}, \quad (\text{L.42})$$

where $\eta^{(m)}$ is a sequence of spin strings that make $\phi(\eta^{(m)})$ smaller and smaller. By substituting the definition of ϕ in terms of its pairwise interaction $J(n) = n^s a^{n^\gamma}$ and taking the limit for the sequences $\eta^{(m)} = \{+, -, -, \dots, \eta_{m+1}, \eta_{m+2}, \dots\}$ one computes that the limit is a if $\gamma = 1$, 1 if $\gamma < 1$, and 0 if $\gamma > 1$. It does not depend on the positive value of s . When $\gamma < 1$ the resulting dynamical system is not hyperbolic and the construction for the operator \mathcal{L} fails, so one cannot apply it to potentials such as $(1/2)^{\sqrt{n}}$. One may solve this problem by investigating the behavior of the formal dynamical system as $\gamma \rightarrow 0$.

The manipulations have up to now assumed that the map f is smooth. If the dimension D of the embedding space is too small, f may not be smooth. Determining under which conditions the embedding is smooth is a complicated question [15]. But in the case of spin systems with pairwise interactions it is possible to give a simple rule. If the interaction is of the form

$$\phi(\sigma) = \sum_{n \geq 1} \delta_{\sigma_0, \sigma_n} \sum_k p_k(n) a_k^{n^\gamma} \quad (\text{L.43})$$

where p_k are polynomials and $|a_k| < 1$, then the state observables to use are $x_{s,k}(\sigma) = \sum \delta_{+, \sigma_n} n^s a_k^n$. For each k one uses $x_{0,k}, x_{1,k}, \dots$ up to the largest power in the polynomial p_k . An example is the interaction with $J_1(n) = n^2(3/10)^n$. It leads to a 3-dimensional system with variables $x_{0,0}, x_{1,0}$, and $x_{2,0}$. The action of the map F_+ for this interaction is illustrated figure L.3. Plotted are the pairs $\{\phi(+ \vee \sigma), \phi(+ \vee + \vee \sigma)\}$. This can be seen as the strange attractor of a chaotic system for which the variables $x_{0,0}, x_{1,0}$, and $x_{2,0}$ provide a good (analytic) embedding.

The added smoothness and trace-class of the \mathcal{L} operator translates into faster convergence towards the thermodynamic limit. As the reconstructed dynamics is analytic, the convergence towards the thermodynamic limit is faster than exponential [23, 16]. We will illustrate this with the polynomial-exponential interactions (L.43) with $\gamma = 1$, as the convergence is certainly faster than exponential if $\gamma > 1$, and the case of a^n has been studied in terms of another Fredholm determinant by Gutzwiller [17]. The convergence is illustrated in figure L.4 for the interaction $n^2(3/10)^n$. Plotted in the graph, to illustrate the transfer matrix convergence, are the number of decimal digits that remain unchanged as the range of the interaction is increased. Also in the graph are the number of decimal digits that

Figure L.3: The spin adding map F_+ for the potential $J(n) = \sum n^2 a^{n\ell}$. The action of the map takes the value of the interaction energy between + and the semi-infinite configuration $\{\sigma_1, \sigma_2, \sigma_3, \dots\}$ and returns the interaction energy between + and the configuration $\{+, \sigma_1, \sigma_2, \sigma_3, \dots\}$.

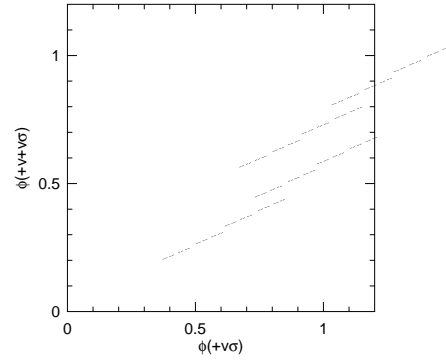
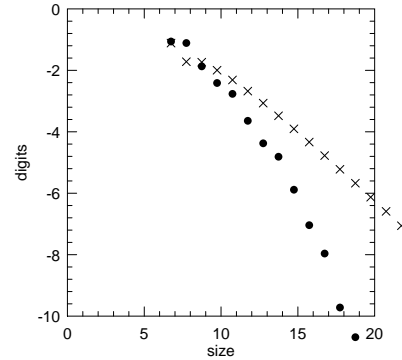


Figure L.4: Number of digits for the Fredholm method (●) and the transfer function method (×). The size refers to the largest cycle considered in the Fredholm expansions, and the truncation length in the case of the transfer matrix.



remain unchanged as the largest power of $\text{tr } \mathcal{L}^n$ considered. The plot is effectively a logarithmic plot and straight lines indicate exponentially fast convergence. The curvature indicates that the convergence is faster than exponential. By fitting, one can verify that the free energy is converging to its limiting value as $\exp(-n^{4/3})$. Cvitanović [23] has estimated that the Fredholm determinant of a map on a D dimensional space should converge as $\exp(-n^{1+1/D})$, which is confirmed by these numerical simulations.

Résumé

The geometrization of spin systems strengthens the connection between statistical mechanics and dynamical systems. It also further establishes the value of the Fredholm determinant of the \mathcal{L} operator as a practical computational tool with applications to chaotic dynamics, spin systems, and semiclassical mechanics. The example above emphasizes the high accuracy that can be obtained: by computing the shortest 14 periodic orbits of period 5 or less it is possible to obtain three digit accuracy for the free energy. For the same accuracy with a transfer matrix one has to consider a 256×256 matrix. This makes the method of cycle expansions practical for analytic calculations.

Commentary

Remark L.1 Presentation functions. The best place to read about Feigenbaum's work is in his review article published in *Los Alamos Science* (reproduced in various reprint collections and conference proceedings, such as ref. [5]). Feigenbaum's *Journal of Statistical Physics* article [13] is the easiest place to learn about presentation functions.

Remark L.2 Interactions are smooth In most computational schemes for thermodynamic quantities the translation invariance and the smoothness of the basic interaction are never used. In Monte Carlo schemes, aside from the periodic boundary conditions, the interaction can be arbitrary. In principle for each configuration it could be possible to have a different energy. Schemes such as the Swenson-Wang cluster flipping algorithm use the fact that interaction is local and are able to obtain dramatic speed-ups in the equilibration time for the dynamical Monte Carlo simulation. In the geometrization program for spin systems, the interactions are assumed translation invariant and smooth. The smoothness means that any interaction can be decomposed into a series of terms that depend only on the spin arrangement and the distance between spins:

$$\phi(\sigma_0, \sigma_1, \sigma_2, \dots) = J_0\sigma_0 + \sum \delta(\sigma_0, \sigma_n)J_1(n) + \sum \delta(\sigma_0, \sigma_{n_1}, \sigma_{n_2})J_2(n_1, n_2) + \dots$$

where the J_k are symmetric functions of their arguments and the δ are arbitrary discrete functions. This includes external constant fields (J_0), but it excludes site dependent fields such as a random external magnetic field.

Exercises

- L.1. **Not all Banach spaces are also Hilbert.** If we are given a norm $\|\cdot\|$ of a Banach space B , it may be possible to find an inner product $\langle \cdot, \cdot \rangle$ (so that B is also a Hilbert space H) such that for all vectors $f \in B$, we have

$$\|f\| = \langle f, f \rangle^{1/2}.$$

This is the norm induced by the scalar product. If we cannot find the inner product how do we know that we just are not being clever enough? By checking the parallelogram law for the norm. A Banach space can be made into a Hilbert space if and only if the norm satisfies the parallelogram law. The parallelogram law says that for any two vectors f and g the equality

$$\|f + g\|^2 + \|f - g\|^2 = 2\|f\|^2 + 2\|g\|^2,$$

must hold.

Consider the space of bounded observables with the norm given by $\|a\| = \sup_{\sigma \in \Omega^{\mathbb{N}}} |a(\sigma)|$. Show that there is no scalar product that will induce this norm.

- L.2. **Automaton for a droplet.** Find the transition graph and the weights on the edges so that the energies of configurations for the droplet model are correctly generated. For any string starting in zero and ending in zero your diagram should yield a configuration the weight $e^{H(\sigma)}$, with H computed along the lines of (L.13) and (L.18).

Hint: the transition graph is infinite.

- L.3. **Spectral determinant for a^n interactions.** Compute the spectral determinant for 1-dimensional Ising model with the interaction

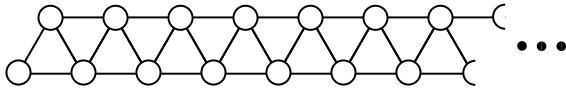
$$\phi(\sigma) = \sum_{k>0} a^k \delta(\sigma_0, \sigma_k).$$

Take a as a number smaller than $1/2$.

- (a) What is the dynamical system this generates? That is, find F_+ and F_- as used in (L.39).
- (b) Show that

$$\frac{d}{dx} F_{\{+ \text{ or } -\}} = \begin{bmatrix} a & 0 \\ 0 & a \end{bmatrix}$$

L.4. **Ising model on a thin strip.** Compute the transfer matrix for the Ising model defined on the graph



Assume that whenever there is a bond connecting two sites, there is a contribution $J\delta(\sigma_i, \sigma_j)$ to the energy.

L.5. **Infinite symbolic dynamics.** Let σ be a function that returns zero or one for every infinite binary string: $\sigma : \{0, 1\}^{\mathbb{N}} \rightarrow \{0, 1\}$. Its value is represented by $\sigma(\epsilon_1, \epsilon_2, \dots)$ where the ϵ_i are either 0 or 1. We will now define an operator \mathcal{T} that acts on observables on the space of binary strings. A function a is an observable if it has bounded variation, that is, if

$$\|a\| = \sup_{\{\epsilon_i\}} |a(\epsilon_1, \epsilon_2, \dots)| < \infty.$$

For these functions

$$\mathcal{T}a(\epsilon_1, \epsilon_2, \dots) = a(0, \epsilon_1, \epsilon_2, \dots)\sigma(0, \epsilon_1, \epsilon_2, \dots) + a(1, \epsilon_1, \epsilon_2, \dots)$$

The function σ is assumed such that any of \mathcal{T} 's "matrix representations" in (a) have the Markov property (the matrix, if read as an adjacency graph, corresponds to a graph where one can go from any node to any other node).

- (a) (easy) Consider a finite version T_n of the operator \mathcal{T} :

$$T_n a(\epsilon_1, \epsilon_2, \dots, \epsilon_n) = a(0, \epsilon_1, \epsilon_2, \dots, \epsilon_{n-1})\sigma(0, \epsilon_1, \epsilon_2, \dots, \epsilon_{n-1}) + a(1, \epsilon_1, \epsilon_2, \dots, \epsilon_{n-1})\sigma(1, \epsilon_1, \epsilon_2, \dots, \epsilon_{n-1}).$$

Show that T_n is a $2^n \times 2^n$ matrix. Show that its trace is bounded by a number independent of n .

- (b) (medium) With the operator norm induced by the function norm, show that \mathcal{T} is a bounded operator.
- (c) (hard) Show that \mathcal{T} is not trace-class. (Hint: check if \mathcal{T} is compact).

Classes of operators are nested; trace-class \leq compact \leq bounded.

References

[L.1] Ya. Sinai. Gibbs measures in ergodic theory. *Russ. Math. Surveys*, 166:21–69, 1972.

[L.2] R. Bowen. Periodic points and measure for axiom-A diffeomorphisms. *Transactions Amer. Math. Soc.*, 154:377–397, 1971.

[L.3] D. Ruelle. Statistical mechanics on a compound set with Z' action satisfying expansiveness and specification. *Transactions Amer. Math. Soc.*, 185:237–251, 1973.

[L.4] E. B. Vul, Ya. G. Sinai, and K. M. Khanin. Feigenbaum universality and the thermodynamic formalism. *Uspekhi Mat. Nauk.*, 39:3–37, 1984.

[L.5] M.J. Feigenbaum, M.H. Jensen, and I. Procaccia. Time ordering and the thermodynamics of strange sets: Theory and experimental tests. *Physical Review Letters*, 57:1503–1506, 1986.

[L.6] N. H. Packard, J. P. Crutchfield, J. D. Farmer, and R. S. Shaw. Geometry from a time series. *Physical Review Letters*, 45:712 – 716, 1980.

[L.7] F. Takens, Detecting strange attractors in turbulence. In *Lecture Notes in Mathematics 898*, pages 366–381. Springer, Berlin, 1981.

- [L.8] R. Mainieri. Thermodynamic zeta functions for Ising models with long range interactions. *Physical Review A*, 45:3580, 1992.
- [L.9] R. Mainieri. Zeta function for the Lyapunov exponent of a product of random matrices. *Physical Review Letters*, 68:1965–1968, March 1992.
- [L.10] D. Wintgen. Connection between long-range correlations in quantum spectra and classical periodic orbits. *Physical Review Letters*, 58(16):1589–1592, 1987.
- [L.11] G. S. Ezra, K. Richter, G. Tanner, and D. Wintgen. Semiclassical cycle expansion for the Helium atom. *Journal of Physics B*, 24(17):L413–L420, 1991.
- [L.12] H. A. Kramers and G. H. Wannier. Statistics of the two-dimensional ferromagnet. Part I. *Physical Review*, 60:252–262, 1941.
- [L.13] D. Ruelle. Statistical mechanics of a one-dimensional lattice gas. *Communications of Mathematical Physics*, 9:267–278, 1968.
- [L.14] David Ruelle. *Thermodynamic Formalism*. Addison-Wesley, Reading, 1978.
- [L.15] P. Walters, *An introduction to ergodic theory* (Springer, New York 1982).
- [L.16] H.H. Rugh. *Time evolution and correlations in chaotic dynamical systems*. PhD thesis (Niels Bohr Institute, 1992).
- [L.17] M. C. Gutzwiller, “The quantization of a classically ergodic system,” *Physica D* **5**, 183 (1982).
- [L.18] M. Feigenbaum. The universal metric properties of non-linear transformations. *Journal of Statistical Physics*, 19:669, 1979.
- [L.19] G.A. Baker. One-dimensional order-disorder model which approaches a second order phase transition. *Phys. Rev.*, 122:1477–1484, 1961.
- [L.20] M. E. Fisher. The theory of condensation and the critical point. *Physics*, 3:255–283, 1967.
- [L.21] G. Gallavotti. Funzioni zeta ed insiemi basilari. *Accad. Lincei. Rend. Sc. fis. mat. e nat.*, 61:309–317, 1976.
- [L.22] R. Artuso. Logarithmic strange sets. *J. Phys. A.*, 21:L923–L927, 1988.
- [L.23] P. Cvitanović, “Periodic orbits as the skeleton of classical and quantum chaos,” *Physica D* **51**, 138 (1991).
- [L.24] Hutchinson

Appendix M

Noise/quantum corrections

(G. Vattay)

THE GUTZWILLER TRACE FORMULA is only a good approximation to the quantum mechanics when \hbar is small. Can we improve the trace formula by adding quantum corrections to the semiclassical terms? A similar question can be posed when the classical deterministic dynamics is disturbed by some way Gaussian white noise with strength D . The deterministic dynamics then can be considered as the weak noise limit $D \rightarrow 0$. The effect of the noise can be taken into account by adding noise corrections to the classical trace formula. A formal analogy exists between the noise and the quantum problem. This analogy allows us to treat the noise and quantum corrections together.



M.1 Periodic orbits as integrable systems

From now on, we use the language of quantum mechanics, since it is more convenient to visualize the results there. Where it is necessary we will discuss the difference between noise and quantum cases.

First, we would like to introduce periodic orbits from an unusual point of view, which can convince you, that chaotic and integrable systems are in fact not as different from each other, than we might think. If we start orbits in the neighborhood of a periodic orbit and look at the picture on the Poincaré section we can see a regular picture. For stable periodic orbits the points form small ellipses around the center and for unstable orbits they form hyperbolas (See Fig. M.1).

Figure M.1: Poincaré section close to a stable and an unstable periodic orbit

The motion close to a periodic orbits is regular in both cases. This is due to the fact, that we can linearize the Hamiltonian close to an orbit, and linear systems are always integrable. The linearized Hamilton's equations close to the periodic orbit $(q_p(t) + q, p_p(t) + p)$ look like

$$\dot{q} = +\partial_{pq}^2 H(q_p(t), p_p(t))q + \partial_{pp}^2 H(q_p(t), p_p(t))p, \quad (\text{M.1})$$

$$\dot{p} = -\partial_{qq}^2 H(q_p(t), p_p(t))q - \partial_{qp}^2 H(q_p(t), p_p(t))p, \quad (\text{M.2})$$

where the new coordinates q and p are relative to a periodic orbit. This linearized equation can be regarded as a d dimensional oscillator with time periodic frequencies. These equations are representing the equation of motion in a redundant way since more than one combination of q, p and t determines the same point of the phase space. This can be cured by an extra restriction on the variables, a constraint the variables should fulfill. This constraint can be derived from the time independence or stationarity of the full Hamiltonian

$$\partial_t H(q_p(t) + q, p_p(t) + p) = 0. \quad (\text{M.3})$$

Using the linearized form of this constraint we can eliminate one of the linearized equations. It is very useful, although technically difficult, to do one more transformation and to introduce a coordinate, which is parallel with the Hamiltonian flow (x_{\parallel}) and others which are orthogonal. In the orthogonal directions we again get linear equations. These equations with x_{\parallel} dependent rescaling can be transformed into normal coordinates, so that we get tiny oscillators in the new coordinates with constant frequencies. This result has first been derived by Poincaré for equilibrium points and later it was extended for periodic orbits by V.I. Arnol'd and co-workers. In the new coordinates, the Hamiltonian reads as

$$H_0(x_{\parallel}, p_{\parallel}, x_n, p_n) = \frac{1}{2}p_{\parallel}^2 + U(x_{\parallel}) + \sum_{n=1}^{d-1} \frac{1}{2}(p_n^2 \pm \omega_n^2 x_n^2), \quad (\text{M.4})$$

which is the general form of the Hamiltonian in the neighborhood of a periodic orbit. The \pm sign denotes, that for stable modes the oscillator potential is positive while for an unstable mode it is negative. For the unstable modes, ω is the Lyapunov exponent of the orbit

$$\omega_n = \ln \Lambda_{p,n} / T_p, \quad (\text{M.5})$$

where $\Lambda_{p,n}$ is the expanding eigenvalue of the Jacobi matrix. For the stable directions the eigenvalues of the Jacobi matrix are connected with ω as

$$\Lambda_{p,n} = e^{-i\omega_n T_p}. \quad (\text{M.6})$$

The Hamiltonian close to the periodic orbit is integrable and can be quantized by the Bohr-Sommerfeld rules. The result of the Bohr-Sommerfeld quantization for the oscillators gives the energy spectra

$$\begin{aligned} E_n &= \hbar\omega_n \left(j_n + \frac{1}{2} \right) \text{ for stable modes,} \\ E_n &= -i\hbar\omega_n \left(j_n + \frac{1}{2} \right) \text{ for unstable modes,} \end{aligned} \quad (\text{M.7})$$

where $j_n = 0, 1, \dots$. It is convenient to introduce the index $s_n = 1$ for stable and $s_n = -i$ for unstable directions. The parallel mode can be quantized implicitly through the classical action function of the mode:

$$\frac{1}{2\pi} \oint p_{\parallel} dx_{\parallel} = \frac{1}{2\pi} S_{\parallel}(E_m) = \hbar \left(m + \frac{m_p \pi}{2} \right), \quad (\text{M.8})$$

where m_p is the topological index of the motion in the parallel direction. This latter condition can be rewritten by a very useful trick into the equivalent form

$$(1 - e^{iS_{\parallel}(E_m)/\hbar - im_p \pi/2}) = 0. \quad (\text{M.9})$$

The eigen-energies of a semiclassically quantized periodic orbit are all the possible energies

$$E = E_m + \sum_{n=1}^{d-1} E_n. \quad (\text{M.10})$$

This relation allows us to change in (M.9) E_m with the full energy minus the oscillator energies $E_m = E - \sum_n E_n$. All the possible eigenenergies of the periodic orbit then are the zeroes of the expression

$$\Delta_p(E) = \prod_{j_1, \dots, j_{d-1}} (1 - e^{iS_{\parallel}(E - \sum_n \hbar s_n \omega_n (j_n + 1/2))/\hbar - im_p \pi/2}). \quad (\text{M.11})$$

If we Taylor expand the action around E to first order

$$S_{\parallel}(E + \epsilon) \approx S_{\parallel}(E) + T(E)\epsilon, \quad (\text{M.12})$$

where $T(E)$ is the period of the orbit, and use the relations of ω and the eigenvalues of the Jacobi matrix, we get the expression of the Selberg product

$$\Delta_p(E) = \prod_{j_1, \dots, j_{d-1}} \left(1 - \frac{e^{iS_p(E)/\hbar - im_p \pi/2}}{\prod_n \Lambda_{p,n}^{(1/2 + j_n)}} \right). \quad (\text{M.13})$$

If we use the right convention for the square root we get exactly the d dimensional expression of the Selberg product formula we derived from the Gutzwiller trace formula in ? . Just here we derived it in a different way! The function $\Delta_p(E)$ is the semiclassical zeta function for one prime orbit.

Now, if we have many prime orbits and we would like to construct a function which is zero, whenever the energy coincides with the BS quantized energy of one of the periodic orbits, we have to take the product of these determinants:

$$\Delta(E) = \prod_p \Delta_p(E). \quad (\text{M.14})$$

The miracle of the semiclassical zeta function is, that if we take infinitely many periodic orbits, the infinite product will have zeroes not at these energies, but close to the eigen=energies of the whole system !

So we learned, that both stable and unstable orbits are integrable systems and can be individually quantized semiclassically by the old Bohr-Sommerfeld rules. So we almost completed the program of Sommerfeld to quantize general systems with the method of Bohr. *Let us have a remark here. In addition to the Bohr-Sommerfeld rules, we used the unjustified approximation (M.12). Sommerfeld would never do this ! At that point we loose some important precision compared to the BS rules and we get somewhat worse results than a semiclassical formula is able to do. We will come back to this point later when we discuss the quantum corrections.* To complete the program of full scale Bohr-Sommerfeld quantization of chaotic systems we have to go beyond the linear approximation around the periodic orbit.

The Hamiltonian close to a periodic orbit in the parallel and normal coordinates can be written as the ‘harmonic’ plus ‘anaharmonic’ perturbation

$$H(x_{\parallel}, p_{\parallel}, x_n, p_n) = H_0(x_{\parallel}, p_{\parallel}, x_n, p_n) + H_A(x_{\parallel}, x_n, p_n), \quad (\text{M.15})$$

where the anaharmonic part can be written as a sum of homogeneous polynomials of x_n and p_n with x_{\parallel} dependent coefficients:

$$H_A(x_{\parallel}, x_n, p_n) = \sum_{k=3} H^k(x_{\parallel}, x_n, p_n) \quad (\text{M.16})$$

$$H^k(x_{\parallel}, x_n, p_n) = \sum_{\sum l_n + m_n = k} H_{l_n, m_n}^k(x_{\parallel}) x_n^{l_n} p_n^{m_n} \quad (\text{M.17})$$

This classical Hamiltonian is hopeless from Sommerfeld’s point of view, since it is non integrable. However, Birkhoff in 1927³ introduced the concept of normal form, which helps us out from this problem by giving successive integrable approximation to a non-integrable problem. Let’s learn a bit more about it!

³It is really a pity, that in 1926 Schrödinger introduced the wave mechanics and blocked the development of Sommerfeld’s concept.

M.2 The Birkhoff normal form

Birkhoff studied the canonical perturbation theory close to an equilibrium point of a Hamiltonian. Equilibrium point is where the potential has a minimum $\nabla U = 0$ and small perturbations lead to oscillatory motion. We can linearize the problem and by introducing normal coordinates x_n and conjugate momentums p_n the quadratic part of the Hamiltonian will be a set of oscillators

$$H_0(x_n, p_n) = \sum_{n=1}^d \frac{1}{2}(p_n^2 + \omega_n^2 x_n^2). \quad (\text{M.18})$$

The full Hamiltonian can be rewritten with the new coordinates

$$H(x_n, p_n) = H_0(x_n, p_n) + H_A(x_n, p_n), \quad (\text{M.19})$$

where H_A is the anaharmonic part of the potential in the new coordinates. The anaharmonic part can be written as a series of homogeneous polynomials

$$H_A(x_n, p_n) = \sum_{j=3}^{\infty} H^j(x_n, p_n), \quad (\text{M.20})$$

$$H^j(x_n, p_n) = \sum_{||l||+|m|=j} h_{lm}^j x^l p^m, \quad (\text{M.21})$$

where h_{lm}^j are real constants and we used the multi-indices $l := (l_1, \dots, l_d)$ with definitions

$$||l|| = \sum l_n, \quad x^l := x_1^{l_1} x_2^{l_2} \dots x_d^{l_d}.$$

Birkhoff showed, that that by successive canonical transformations one can introduce new momentums and coordinates such, that in the new coordinates the anaharmonic part of the Hamiltonian up to any given n polynomial will depend only on the variable combination

$$\tau_n = \frac{1}{2}(p_n^2 + \omega_n^2 x_n^2), \quad (\text{M.22})$$

where x_n and p_n are the new coordinates and momentums, but ω_n is the original frequency. This is called the Birkhoff normal form of degree N :

$$H(x_n, p_n) = \sum_{j=2}^N H^j(\tau_1, \dots, \tau_d), \quad (\text{M.23})$$

where H^j are homogeneous degree j polynomials of τ -s. This is an integrable Hamiltonian, the non-integrability is pushed into the remainder, which consists of polynomials of degree higher than N . We run into trouble only when the oscillator frequencies are commensurate e.g. it is possible to find a set of integers m_n such that the linear combination

$$\sum_{n=1}^d \omega_n m_n,$$

vanishes. This extra problem has been solved by Gustavson in 1966 and we call the object Birkhoff-Gustavson normal form. The procedure of the successive canonical transformations can be computerized and can be carried out up to high orders (~ 20).

Of course, we pay a price for forcing the system to be integrable up to degree N . For a non-integrable system the high order terms behave quite wildly and the series is not convergent. Therefore we have to use this tool carefully. Now, we learned how to approximate a non-integrable system with a sequence of integrable systems and we can go back and carry out the BS quantization.

M.3 Bohr-Sommerfeld quantization of periodic orbits

There is some difference between equilibrium points and periodic orbits. The Hamiltonian (M.4) is not a sum of oscillators. One can transform the parallel part, describing circulation along the orbit, into an oscillator Hamiltonian, but this would make the problem extremely difficult. Therefore, we carry out the canonical transformations dictated by the Birkhoff procedure only in the orthogonal directions. The x_{\parallel} coordinate plays the role of a parameter. After the transformation up to order N the Hamiltonian (M.17) is

$$H(x_{\parallel}, p_{\parallel}, \tau_1, \dots, \tau_{d-1}) = H_0(x_{\parallel}, p_{\parallel}, \tau_1, \dots, \tau_{d-1}) + \sum_{j=2}^N U^j(x_{\parallel}, \tau_1, \dots, \tau_{d-1}), \quad (\text{M.24})$$

where U^j is a j th order homogeneous polynomial of τ -s with x_{\parallel} dependent coefficients. The orthogonal part can be BS quantized by quantizing the individual oscillators, replacing τ -s as we did in (M.8). This leads to a one dimensional effective potential indexed by j_1, \dots, j_{d-1}

$$H(x_{\parallel}, p_{\parallel}, j_1, \dots, j_{d-1}) = \frac{1}{2} p_{\parallel}^2 + U(x_{\parallel}) + \sum_{n=1}^{d-1} \hbar s_n \omega_n (j_n + 1/2) + \quad (\text{M.25})$$

$$+ \sum_{k=2}^N U^k(x_{\parallel}, \hbar s_1 \omega_1 (j_1 + 1/2), \hbar s_2 \omega_2 (j_2 + 1/2), \dots, \hbar s_{d-1} \omega_{d-1} (j_{d-1} + 1/2)),$$

where j_n can be any non-negative integer. The term with index k is proportional with \hbar^k due to the homogeneity of the polynomials.

The parallel mode now can be BS quantized for any given set of j -s

$$S_p(E, j_1, \dots, j_{d-1}) = \oint p_{\parallel} dx_{\parallel} = \tag{M.26}$$

$$= \oint dx_{\parallel} \sqrt{E - \sum_{n=1}^{d-1} \hbar s_n \omega_n (j_n + 1/2) - U(x_{\parallel}, j_1, \dots, j_{d-1}) = 2\pi\hbar(m + m_p/2)},$$

where U contains all the x_{\parallel} dependent terms of the Hamiltonian. The spectral determinant becomes

$$\Delta_p(E) = \prod_{j_1, \dots, j_{d-1}} (1 - e^{iS_p(E, j_1, \dots, j_{d-1})/\hbar - m_p\pi/2}). \tag{M.27}$$

This expression completes the Sommerfeld method and tells us how to quantize chaotic or general Hamiltonian systems. Unfortunately, quantum mechanics postponed this nice formula until our book.

This formula has been derived with the help of the semiclassical Bohr-Sommerfeld quantization rule and the classical normal form theory. Indeed, if we expand S_p in the exponent in the powers of \hbar

$$S_p = \sum_{k=0}^N \hbar^k S_k,$$

we get more than just a constant and a linear term. This formula already gives us corrections to the semiclassical zeta function in all powers of \hbar . There is a very attracting feature of this semiclassical expansion. \hbar in S_p shows up only in the combination $\hbar s_n \omega_n (j_n + 1/2)$. A term proportional with \hbar^k can only be a homogeneous expression of the oscillator energies $s_n \omega_n (j_n + 1/2)$. For example in two dimensions there is only one possibility of the functional form of the order k term

$$S_k = c_k(E) \cdot \omega_n^k (j + 1/2)^k,$$

where $c_k(E)$ is the only function to be determined.

The corrections derived sofar are *doubly* semiclassical, since they give semiclassical corrections to the semiclassical approximation. What can quantum mechanics add to this ? As we have stressed in the previous section, the exact quantum mechanics is not invariant under canonical transformations. In other context, this phenomenon is called the operator ordering problem. Since the operators \hat{x}

and \hat{p} do not commute, we run into problems, when we would like to write down operators for classical quantities like $x^2 p^2$. On the classical level the four possible orderings $xpxp$, $ppxx$, $pxpx$ and $xxpp$ are equivalent, but they are different in the quantum case. The expression for the energy (M.26) is not exact. We have to go back to the level of the Schrödinger equation if we would like to get the exact expression.

M.4 Quantum calculation of \hbar corrections

The Gutzwiller trace formula has originally been derived from the saddle point approximation of the Feynman path integral form of the propagator. The exact trace is a path-sum for all closed paths of the system

$$\text{Tr}G(x, x', t) = \int dx G(x, x, t) = \int \mathcal{D}x e^{iS(x,t)/\hbar}, \quad (\text{M.28})$$

where $\int \mathcal{D}x$ denotes the discretization and summation for all paths of time length t in the limit of the infinite refinement and $S(x, t)$ is the classical action calculated along the path. The trace in the saddle point calculation is a sum for classical periodic orbits and zero length orbits, since these are the extrema of the action $\delta S(x, t) = 0$ for closed paths:

$$\text{Tr}G(x, x', t) = g_0(t) + \sum_{p \in PO} \int \mathcal{D}\xi_p e^{iS(\xi_p + x_p(t), t)/\hbar}, \quad (\text{M.29})$$

where $g_0(t)$ is the zero length orbit contribution. We introduced the new coordinate ξ_p with respect to the periodic orbit $x_p(t)$, $x = \xi_p + x_p(t)$. Now, each path sum $\int \mathcal{D}\xi_p$ is computed in the vicinity of periodic orbits. Since the saddle points are taken in the configuration space, only spatially distinct periodic orbits, the so called prime periodic orbits, appear in the summation. So far nothing new has been invented. If we continue the standard textbook calculation scheme, we have to Taylor expand the action in ξ_p and keep the quadratic term in the exponent while treating the higher order terms as corrections. Then we can compute the path integrals with the help of Gaussian integrals. The key point here is that we don't compute the path sum directly. We use the correspondence between path integrals and partial differential equations. This idea comes from Maslov [5] and a good summary is in ref. [6]. We search for that Schrödinger equation, which leads to the path sum

$$\int \mathcal{D}\xi_p e^{iS(\xi_p + x_p(t), t)/\hbar}, \quad (\text{M.30})$$

where the action around the periodic orbit is in a multi-dimensional Taylor expanded form:

$$S(x, t) = \sum_{\mathbf{n}} s_{\mathbf{n}}(t)(x - x_p(t))^{\mathbf{n}}/\mathbf{n}!. \quad (\text{M.31})$$

The symbol $\mathbf{n} = (n_1, n_2, \dots, n_d)$ denotes the multi index in d dimensions, $\mathbf{n}! = \prod_{i=1}^d n_i!$ the multi factorial and $(x - x_p(t))^{\mathbf{n}} = \prod_{i=1}^d (x_i - x_{p,i}(t))^{n_i}$, respectively. The expansion coefficients of the action can be determined from the Hamilton-Jacobi equation

$$\partial_t S + \frac{1}{2}(\nabla S)^2 + U = 0, \quad (\text{M.32})$$

in which the potential is expanded in a multidimensional Taylor series around the orbit

$$U(x) = \sum_{\mathbf{n}} u_{\mathbf{n}}(t)(x - x_p(t))^{\mathbf{n}}/\mathbf{n}!. \quad (\text{M.33})$$

The Schrödinger equation

$$i\hbar\partial_t\psi = \hat{H}\psi = -\frac{\hbar^2}{2}\Delta\psi + U\psi, \quad (\text{M.34})$$

with this potential also can be expanded around the periodic orbit. Using the WKB ansatz

$$\psi = \varphi e^{iS/\hbar}, \quad (\text{M.35})$$

we can construct a Schrödinger equation corresponding to a given order of the Taylor expansion of the classical action. The Schrödinger equation induces the Hamilton-Jacobi equation (M.32) for the phase and the transport equation of Maslov and Fjedoriuk [7] for the amplitude:

$$\partial_t\varphi + \nabla\varphi\nabla S + \frac{1}{2}\varphi\Delta S - \frac{i\hbar}{2}\Delta\varphi = 0. \quad (\text{M.36})$$

This is the partial differential equation, solved in the neighborhood of a periodic orbit with the expanded action (M.31), which belongs to the local path-sum (M.30).

If we know the Green's function $G_p(\xi, \xi', t)$ corresponding to the local equation (M.36), then the local path sum can be converted back into a trace:

$$\int \mathcal{D}\xi_p e^{i/\hbar \sum_{\mathbf{n}} S_{\mathbf{n}}(x_p(t), t) \xi_p^{\mathbf{n}}/\mathbf{n}!} = \text{Tr}G_p(\xi, \xi', t). \quad (\text{M.37})$$

The saddle point expansion of the trace in terms of local traces then becomes

$$\text{Tr}G(x, x', t) = \text{Tr}G_W(x, x', t) + \sum_p \text{Tr}G_p(\xi, \xi', t), \quad (\text{M.38})$$

where $G_W(x, x', t)$ denotes formally the Green's function expanded around zero length (non moving) periodic orbits, known as the Weyl term [8]. Each Green's function can be Fourier-Laplace transformed independently and by definition we get in the energy domain:

$$\text{Tr}G(x, x', E) = g_0(E) + \sum_p \text{Tr}G_p(\xi, \xi', E). \quad (\text{M.39})$$

Note that we do not need here to take further saddle points in time, since we are dealing with exact time and energy domain Green's functions. indexGreen's function!energy dependent

The spectral determinant is a function which has zeroes at the eigen-energies E_n of the Hamilton operator \hat{H} . Formally it is

$$\Delta(E) = \det(E - \hat{H}) = \prod_n (E - E_n).$$

The logarithmic derivative of the spectral determinant is the trace of the energy domain Green's function:

$$\text{Tr}G(x, x', E) = \sum_n \frac{1}{E - E_n} = \frac{d}{dE} \log \Delta(E). \quad (\text{M.40})$$

We can define the spectral determinant $\Delta_p(E)$ also for the local operators and we can write

$$\text{Tr}G_p(\xi, \xi', E) = \frac{d}{dE} \log \Delta_p(E). \quad (\text{M.41})$$

Using (M.39) we can express the full spectral determinant as a product for the sub-determinants

$$\Delta(E) = e^{W(E)} \prod_p \Delta_p(E),$$

where $W(E) = \int^E g_0(E') dE'$ is the term coming from the Weyl expansion.

The construction of the local spectral determinants can be done easily. We have to consider the stationary eigenvalue problem of the local Schrödinger problem and keep in mind, that we are in a coordinate system moving together with

the periodic orbit. If the classical energy of the periodic orbit coincides with an eigen-energy E of the local Schrödinger equation around the periodic orbit, then the corresponding stationary eigenfunction fulfills

$$\psi_p(\xi, t + T_p) = \int d\xi' G_p(\xi, \xi', t + T_p) \psi_p(\xi', t) = e^{-iET_p/\hbar} \psi_p(\xi, t), \quad (\text{M.42})$$

where T_p is the period of the prime orbit p . If the classical energy of the periodic orbit is not an eigen-energy of the local Schrödinger equation, the non-stationary eigenfunctions fulfill

$$\psi_p^{\mathbf{l}}(\xi, t + T_p) = \int d\xi' G_p(\xi, \xi', t + T_p) \psi_p(\xi', t) = e^{-iET_p/\hbar} \lambda_p^{\mathbf{l}}(E) \psi_p^{\mathbf{l}}(t), \quad (\text{M.43})$$

where $\mathbf{l} = (l_1, l_2, \dots)$ is a multi-index of the possible quantum numbers of the local Schrödinger equation. If the eigenvalues $\lambda_p^{\mathbf{l}}(E)$ are known the local functional determinant can be written as

$$\Delta_p(E) = \prod_{\mathbf{l}} (1 - \lambda_p^{\mathbf{l}}(E)), \quad (\text{M.44})$$

since $\Delta_p(E)$ is zero at the eigen-energies of the local Schrödinger problem. We can insert the ansatz (M.35) and reformulate (M.43) as

$$e^{\frac{i}{\hbar}S(t+T_p)} \varphi_p^{\mathbf{l}}(t + T_p) = e^{-iET_p/\hbar} \lambda_p^{\mathbf{l}}(E) e^{\frac{i}{\hbar}S(t)} \varphi_p^{\mathbf{l}}(t). \quad (\text{M.45})$$

The phase change is given by the action integral for one period $S(t + T_p) - S(t) = \int_0^{T_p} L(t) dt$. Using this and the identity for the action $S_p(E)$ of the periodic orbit

$$S_p(E) = \oint p dq = \int_0^{T_p} L(t) dt + ET_p, \quad (\text{M.46})$$

we get

$$e^{\frac{i}{\hbar}S_p(E)} \varphi_p^{\mathbf{l}}(t + T_p) = \lambda_p^{\mathbf{l}}(E) \varphi_p^{\mathbf{l}}(t). \quad (\text{M.47})$$

Introducing the eigen-equation for the amplitude

$$\varphi_p^{\mathbf{l}}(t + T_p) = R_{\mathbf{l},p}(E) \varphi_p^{\mathbf{l}}(t), \quad (\text{M.48})$$

the local spectral determinant can be expressed as a product for the quantum numbers of the local problem:

$$\Delta_p(E) = \prod_{\mathbf{l}} (1 - R_{\mathbf{l},p}(E) e^{\frac{i}{\hbar}S_p(E)}). \quad (\text{M.49})$$

Since \hbar is a small parameter we can develop a perturbation series for the amplitudes $\varphi_p^{\mathbf{l}}(t) = \sum_{m=0}^{\infty} \left(\frac{i\hbar}{2}\right)^m \varphi_p^{\mathbf{l}(m)}(t)$ which can be inserted into the equation (M.36) and we get an iterative scheme starting with the semiclassical solution $\varphi^{\mathbf{l}(0)}$:

$$\begin{aligned} \partial_t \varphi^{\mathbf{l}(0)} + \nabla \varphi^{\mathbf{l}(0)} \nabla S + \frac{1}{2} \varphi^{\mathbf{l}(0)} \Delta S &= 0, \\ \partial_t \varphi^{\mathbf{l}(m+1)} + \nabla \varphi^{\mathbf{l}(m+1)} \nabla S + \frac{1}{2} \varphi^{\mathbf{l}(m+1)} \Delta S &= \Delta \varphi^{\mathbf{l}(m)}. \end{aligned} \quad (\text{M.50})$$

The eigenvalue can also be expanded in powers of $i\hbar/2$:

$$R_{\mathbf{l},p}(E) = \exp \left\{ \sum_{m=0}^{\infty} \left(\frac{i\hbar}{2}\right)^m C_{\mathbf{l},p}^{(m)} \right\} \quad (\text{M.51})$$

$$= \exp(C_{\mathbf{l},p}^{(0)}) \left\{ 1 + \frac{i\hbar}{2} C_{\mathbf{l},p}^{(1)} + \left(\frac{i\hbar}{2}\right)^2 \left(\frac{1}{2} (C_{\mathbf{l},p}^{(1)})^2 + C_{\mathbf{l},p}^{(2)} \right) + \dots \right\} \quad (\text{M.52})$$

The eigenvalue equation (M.48) in \hbar expanded form reads as

$$\begin{aligned} \varphi_p^{\mathbf{l}(0)}(t + T_p) &= \exp(C_{\mathbf{l},p}^{(0)}) \varphi_p^{\mathbf{l}(0)}(t), \\ \varphi_p^{\mathbf{l}(1)}(t + T_p) &= \exp(C_{\mathbf{l},p}^{(0)}) [\varphi_p^{\mathbf{l}(1)}(t) + C_{\mathbf{l},p}^{(1)} \varphi_p^{\mathbf{l}(0)}(t)], \\ \varphi_p^{\mathbf{l}(2)}(t + T_p) &= \exp(C_{\mathbf{l},p}^{(0)}) [\varphi_p^{\mathbf{l}(2)}(t) + C_{\mathbf{l},p}^{(1)} \varphi_p^{\mathbf{l}(1)}(t) + (C_{\mathbf{l},p}^{(2)} + \frac{1}{2} (C_{\mathbf{l},p}^{(1)})^2) \varphi_p^{\mathbf{l}(0)}(t)], \end{aligned} \quad (\text{M.53})$$

and so on. These equations are the conditions selecting the eigenvectors and eigenvalues and they hold for all t .

It is very convenient to expand the functions $\varphi_p^{\mathbf{l}(m)}(x, t)$ in Taylor series around the periodic orbit and to solve the equations (M.51) in this basis [10], since only a couple of coefficients should be computed to derive the first corrections. This technical part we are going to publish elsewhere [9]. One can derive in general the zero order term $C_{\mathbf{l}}^{(0)} = i\pi\nu_p + \sum_{i=1}^{d-1} \left(l_i + \frac{1}{2}\right) u_{p,i}$, where $u_{p,i} = \log \Lambda_{p,i}$ are the logarithms of the eigenvalues of the monodromy matrix M_p and ν_p is the topological index of the periodic orbit. The first correction is given by the integral

$$C_{\mathbf{l},p}^{(1)} = \int_0^{T_p} dt \frac{\Delta \varphi_p^{\mathbf{l}(0)}(t)}{\varphi_p^{\mathbf{l}(0)}(t)}.$$

When the theory is applied for billiard systems, the wave function should fulfill the Dirichlet boundary condition on hard walls, e.g. it should vanish on the wall. The wave function determined from (M.36) behaves discontinuously when the trajectory $x_p(t)$ hits the wall. For the simplicity we consider a two dimensional billiard system here. The wave function on the wall before the bounce (t_0) is given by

$$\psi_{in}(x, y(x), t) = \varphi(x, y(x), t_0) e^{iS(x, y(x), t_0)/\hbar}, \quad (\text{M.54})$$

where $y(x) = Y_2x^2/2! + Y_3x^3/3! + Y_4x^4/4! + \dots$ is the parametrization of the wall around the point of reflection (see Fig 1.). The wave function on the wall after the bounce (t_{+0}) is

$$\psi_{out}(x, y(x), t) = \varphi(x, y(x), t_{+0})e^{iS(x, y(x), t_{+0})/\hbar}. \quad (\text{M.55})$$

The sum of these wave functions should vanish on the hard wall. This implies that the incoming and the outgoing amplitudes and the phases are related as

$$S(x, y(x), t_{-0}) = S(x, y(x), t_{+0}), \quad (\text{M.56})$$

and

$$\varphi(x, y(x), t_{-0}) = -\varphi(x, y(x), t_{+0}). \quad (\text{M.57})$$

The minus sign can be interpreted as the topological phase coming from the hard wall.

Now we can reexpress the spectral determinant with the local eigenvalues:

$$\Delta(E) = e^{W(E)} \prod_p \prod_{\mathbf{l}} (1 - R_{\mathbf{l},p}(E)e^{iS_p(E)}). \quad (\text{M.58})$$

This expression is the quantum generalization of the semiclassical Selberg-product formula [11]. A similar decomposition has been found for quantum Baker maps in ref. [12]. The functions

$$\zeta_{\mathbf{l}}^{-1}(E) = \prod_p (1 - R_{\mathbf{l},p}(E)e^{iS_p(E)}) \quad (\text{M.59})$$

are the generalizations of the Ruelle type [23] zeta functions. The trace formula can be recovered from (M.40):

$$\text{Tr}G(E) = g_0(E) + \frac{1}{i\hbar} \sum_{p, \mathbf{l}} (T_p(E) - i\hbar \frac{d \log R_{\mathbf{l},p}(E)}{dE}) \frac{R_{\mathbf{l},p}(E)e^{iS_p(E)}}{1 - R_{\mathbf{l},p}(E)e^{iS_p(E)}}. \quad (\text{M.60})$$

We can rewrite the denominator as a sum of a geometric series and we get

$$\text{Tr}G(E) = g_0(E) + \frac{1}{i\hbar} \sum_{p, r, \mathbf{l}} (T_p(E) - i\hbar \frac{d \log R_{\mathbf{l},p}(E)}{dE}) (R_{\mathbf{l},p}(E))^r e^{i r S_p(E)}. \quad (\text{M.61})$$

The new index r can be interpreted as the repetition number of the prime orbit p . This expression is the generalization of the semiclassical trace formula for

the exact quantum mechanics. We would like to stress here, that the perturbation calculus introduced above is just one way to compute the eigenvalues of the local Schrödinger problems. Non-perturbative methods can be used to calculate the local eigenvalues for stable, unstable and marginal orbits. Therefore, our trace formula is not limited to integrable or hyperbolic systems, it can describe the most general case of systems with mixed phase space.

The semiclassical trace formula can be recovered by dropping the sub-leading term $-\hbar d \log R_{1,p}(E)/dE$ and using the semiclassical eigenvalue $R_{1,p}^{(0)}(E) = e^{C_p^{(0)}} = e^{-iv_p\pi} e^{-\sum_i (l_i+1/2)u_{p,i}}$. Summation for the indexes l_i yields the celebrated semiclassical amplitude

$$\sum_l (R_{1,p}^{(0)}(E))^l = \frac{e^{-iv_p\pi}}{|\det(\mathbf{1} - M_p^r)|^{1/2}}. \quad (\text{M.62})$$

To have an impression about the improvement caused by the quantum corrections we have developed a numerical code [13] which calculates the first correction $C_{p,l}^{(1)}$ for general two dimensional billiard systems. The first correction depends only on some basic data of the periodic orbit such as the lengths of the free flights between bounces, the angles of incidence and the first three Taylor expansion coefficients Y_2, Y_3, Y_4 of the wall in the point of incidence. To check that our new local method gives the same result as the direct calculation of the Feynman integral, we computed the first \hbar correction $C_{p,0}^{(1)}$ for the periodic orbits of the 3-disk scattering system [14] where the quantum corrections have been. We have found agreement up to the fifth decimal digit, while our method generates these numbers with any desired precision. Unfortunately, the $l \neq 0$ coefficients cannot be compared to ref. [15], since the l dependence was not realized there due to the lack of general formulas (M.58) and (M.59). However, the l dependence can be checked on the 2 disk scattering system [16]. On the standard example [14, 15, 16, 18], when the distance of the centers (R) is 6 times the disk radius (a), we got

$$C_l^{(1)} = \frac{1}{\sqrt{2E}} (-0.625l^3 - 0.3125l^2 + 1.4375l + 0.625).$$

For $l = 0$ and 1 this has been confirmed by A. Wirzba [17], who was able to compute $C_0^{(1)}$ from his exact quantum calculation. Our method makes it possible to utilize the symmetry reduction of Cvitanović and Eckhardt and to repeat the fundamental domain cycle expansion calculation of ref. [18] with the first quantum correction. We computed the correction to the leading 226 prime periodic orbits with 10 or less bounces in the fundamental domain. Table I. shows the numerical values of the exact quantum calculation [16], the semiclassical cycle expansion [10] and our corrected calculation. One can see, that the error of the corrected calculation vs. the error of the semiclassical calculation decreases with the wave-number. Besides the improved results, a fast convergence up to six decimal digits can be observed, which is just three decimal digits in the full domain calculation [15].

Figure M.2: A typical bounce on a billiard wall. The wall can be characterized by the local expansion $y(x) = Y_2x^2/2! + Y_3x^3/3! + Y_4x^4/4! + \dots$

Table M.1: Real part of the resonances ($\text{Re } k$) of the 3-disk scattering system at disk separation 6:1. Semiclassical and first corrected cycle expansion versus exact quantum calculation and the error of the semiclassical δ_{SC} divided by the error of the first correction δ_{Corr} . The magnitude of the error in the imaginary part of the resonances remains unchanged.

Quantum	Semiclassical	First correction	$\delta_{SC}/\delta_{Corr}$
0.697995	0.758313	0.585150	0.53
2.239601	2.274278	2.222930	2.08
3.762686	3.787876	3.756594	4.13
5.275666	5.296067	5.272627	6.71
6.776066	6.793636	6.774061	8.76
...
30.24130	30.24555	30.24125	92.3
31.72739	31.73148	31.72734	83.8
32.30110	32.30391	32.30095	20.0
33.21053	33.21446	33.21048	79.4
33.85222	33.85493	33.85211	25.2
34.69157	34.69534	34.69152	77.0

References

- [M.1] M. C. Gutzwiller, J. Math. Phys. **12**, 343 (1971); *Chaos in Classical and Quantum Mechanics* (Springer-Verlag, New York, 1990)
- [M.2] A. Selberg, J. Indian Math. Soc. **20**, 47 (1956)
- [M.3] See examples in : CHAOS **2** (1) Thematic Issue; E. Bogomolny and C. Schmit, Nonlinearity **6**, 523 (1993)
- [M.4] R. P. Feynman, Rev. Mod. Phys. **20**, 367 (1948)
- [M.5] We thank E. Bogomolny for bringing this reference to our attention.
- [M.6] V. M. Babić and V. S. Buldyrev, *Short Wavelength Diffraction Theory*, Springer Series on Wave Phenomena, Springer-Verlag (1990)
- [M.7] V. P. Maslov and M. V. Fjedoriuk, *Semiclassical Approximation in Quantum Mechanics*, Dordrecht-Reidel (1981)
- [M.8] R. B. Balian and C. Bloch, Ann. Phys. (New York) **60**, 81 (1970); *ibid.* **63**, 592 (1971); M.V. Berry, M.V., C.J. Howls, C.J. Proceedings of the Royal Society of London. **447**, 1931 (1994)
- [M.9] P. E. Rosenqvist and G. Vattay, in progress.
- [M.10] P. Cvitanović, P. E. Rosenqvist, G. Vattay and H. H. Rugh, CHAOS **3** (4), 619 (1993)
- [M.11] A. Voros, J. Phys. **A21**, 685 (1988)

- [M.12] A. Voros, Prog. Theor. Phys. Suppl. **116**,17 (1994); M. Saraceno and A. Voros, to appear in Physica D.
- [M.13] The FORTRAN code is available upon e-mail request to G. Vattay.
- [M.14] P. Gaspard and S. A. Rice, J. Chem. Phys. **90** 2225, 2242, 2255 (1989) **91** E3279 (1989)
- [M.15] D. Alonso and P. Gaspard, Chaos **3**, 601 (1993); P. Gaspard and D. Alonso, Phys. Rev. **A47**, R3468 (1993)
- [M.16] A. Wirzba, CHAOS **2**, 77 (1992); Nucl. Phys. **A560**, 136 (1993)
- [M.17] A. Wirzba, private communication.
- [M.18] P. Cvitanović and B. Eckhardt, Phys. Rev. Lett. **63**, 823 (1989)

Appendix S

Solutions

Chapter 1. Overture

Solution 1.1 - 3-disk symbolic dynamics. There are 2^k topologically different k -step trajectories starting from each disk, and the 3-disk pinball has $3 \cdot 2^{n-1}$ periodic points with length n itineraries composed of disk labels $\{1, 2, 3\}$.

As explained in sect. 1.4, each orbit segment can be characterized by either of the two symbols 0 and 1, differentiating topologically bouncing back or going onto the third disk.

Prime cycles in the 3-disk space (prime cycles in fundamental domain, respectively) are

- Of length 2: 12,13,32 (or 0).
- Of length 3: 123,321 (or 1).
- Of length 4: 1213,1232,1323 (or 01).
- Of length 5: 12123,12132,12313,12323,13132,13232 (or 00111).

Some of the cycles are listed in table 12.2 and drawn in figure ??.

(Y. Lan)

Solution 1.1 - 3-disk symbolic dynamics. Starting from a disk we cannot end up at the same disk in the next step, see figure S.1. We have 3 choices for the first disk and 2 choices for the next disk at each step, hence at most $3 \cdot 2^{n-1}$ itineraries of length n

Thus, it remains to show that any symbol sequence with the only constraint of no two identical consecutive symbols is realized. The most convenient way to do so is to work with the phase space representation of the pinball machine. Parametrize the state right after a reflection by the label of the disk, the arc length parameter corresponding to the point of reflection, and the $\sin \phi$ with ϕ being the angle of reflection relative to the normal vector, see figure S.1. Thus the Poincaré section consists of three cylinders, with the arc length parameter is cyclic on each disk, as shown in figure S.2.

Consider disk “1” as the starting point. Fixing the angle of reflection, by varying the position all the way around the disk we first escape, then hit disk “3”, then

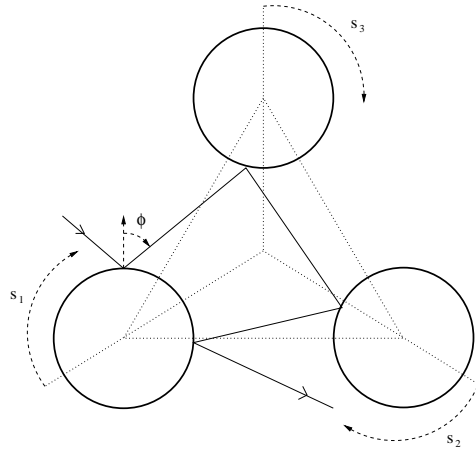


Figure S.1: Geometry of the 3-disk pinball.

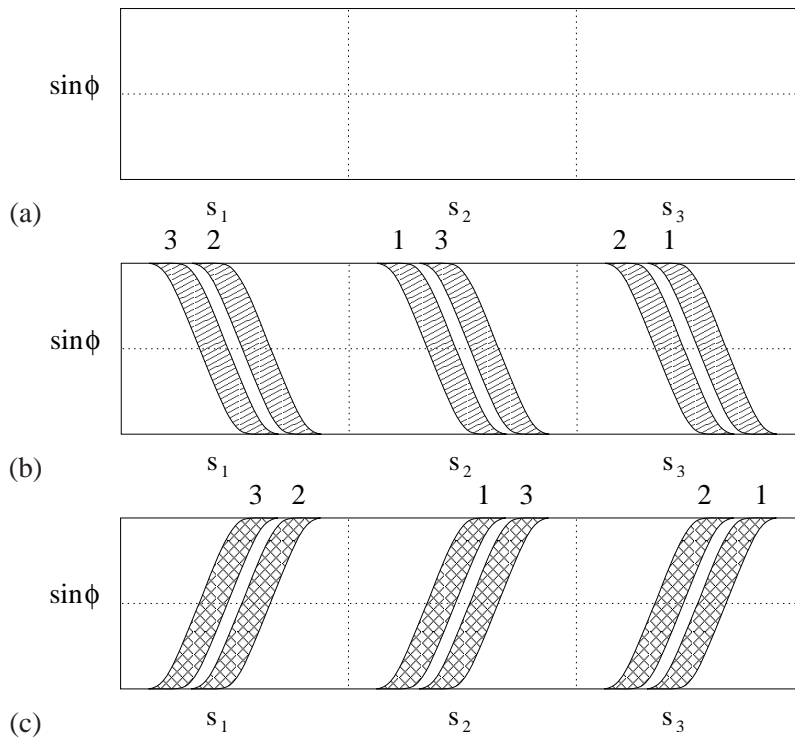


Figure S.2: (a) The phase space of the 3-disk pinball. (b) The part of phase space which remains on the table for one more iterate. (c) The images of the disks in one iteration.

escape, then hit disk “2”, and then escape again, when increasing the arc length parameter in the manner indicated in figure S.1 (a). Thus—if the disks are sufficiently well separated—there are two strips of initial conditions which do not escape. By symmetry this yields figure S.1 (b) where the numbers indicate onto which disk these initial trajectories are going to end up on. By time reversal Figure S.1 (c) shows the strips labeled by disk where the pinball came from.

Combining figure S.1 (b) and (c) we obtain three sections, which are the same except for the labeling of the disks. One of such section is shown in figure S.3.

The billiard map enjoys a certain monotonicity, as depicted in figure S.4, which

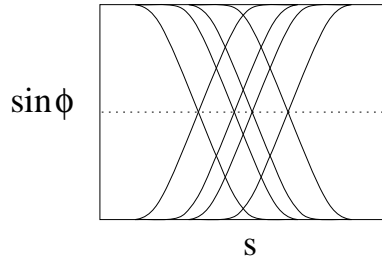


Figure S.3: The intersection of one iterate images and preimages.

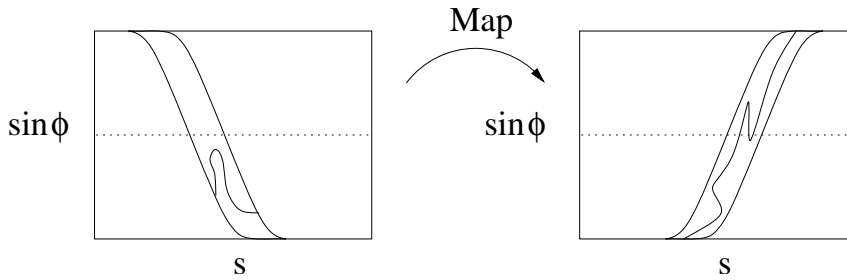


Figure S.4: Monotonicity of the billiard map.

easily verified by inspecting figure S.1. It says that any curve connecting the two boundaries of one of the strips gets mapped to a curve within the image of that strip running all the way across from top to bottom.

This, in particular, means that the intersections of the image of the previous disk and the initial conditions to land onto the next disk, see figure S.3, will map onto (thin) strips running across from top to bottom, as shown in figure S.5.

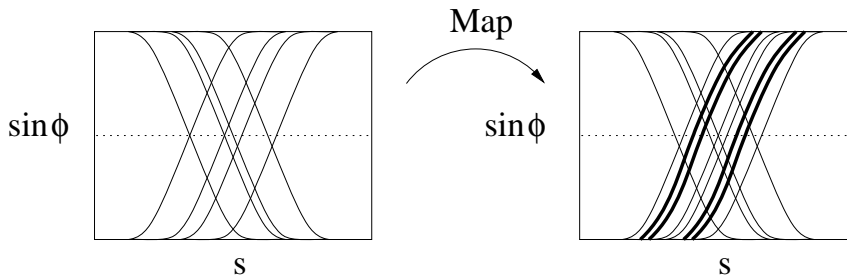


Figure S.5: Images in the second iterate. This is, of course, schematically, because we dropped the labels of the disks; in fact, the two intersection regions get mapped onto two different disks.

Finally, since the images of the intersection regions run all the way across in the vertical direction, we can iterate the argument. Every time the number of strips doubles, and we find regions of states which can go to either of the two neighboring disks at every step. Hence any symbol sequence with no repeat of consecutive symbols can be realized.

The itineraries of periodic points of period 2, 3, 4, 5 are

n	all periodic cycles
2	12 13 21 23 31 32
3	123 132 213 231 312 321
4	1212 1213 1232 1312 1313 1323 2121 2123 2131 2313 2321 2323 3121 3131 3132 3212 3231 3232
5	12123 12132 12312 12313 12323 13123 13132 13212 13213 13232 21213 21231 21313 21321 21323 23121 23123 23131 23213 23231 31212 31231 31232 31312 31321 32121 32131 32132 32312 32321 .

The prime cycles (lexically lowest periodic point itinerary within a non-repeating cycle) are indicated in bold, and the ones given in the exercise are sketched in figure S.6.

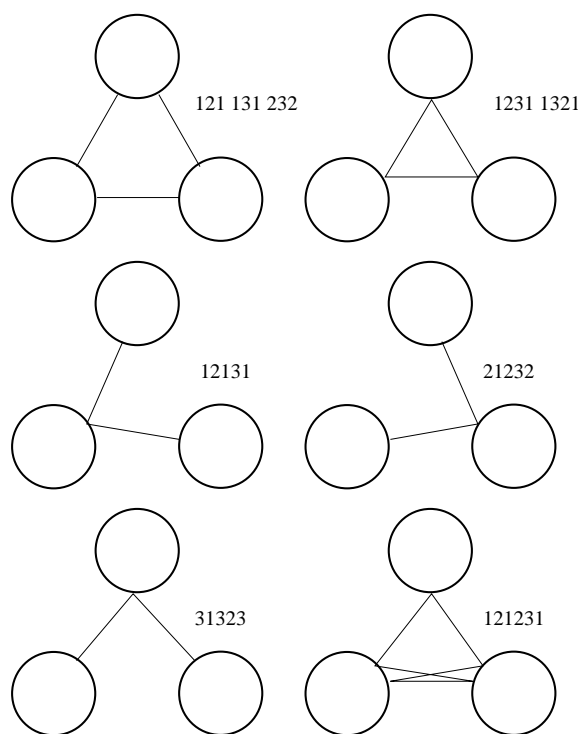


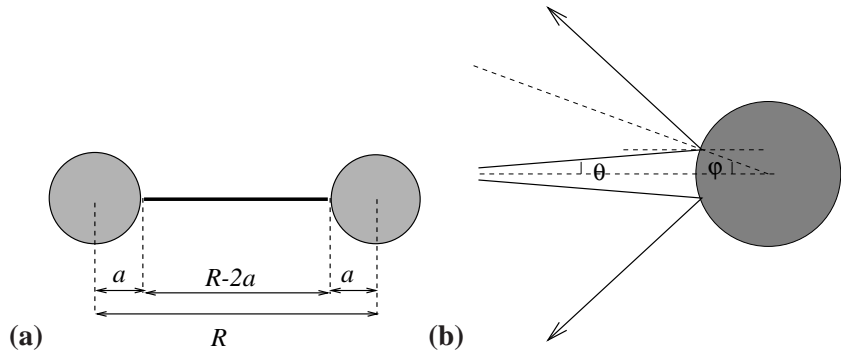
Figure S.6: Sketch of the indicated prime cycles.

(Alexander Grigo)

Solution 1.2 - Sensitivity to initial conditions. To estimate the pinball sensitivity we consider a narrow beam of point particles bouncing between two disks, figure S.7 (a). Or if you find this easier to visualize, think of a narrow ray of light. We assume that the ray of light is focused along the axis between the two points. This is where the least unstable periodic orbit lies, so its stability should give us an upper bound on the number of bounces we can expect to achieve. To estimate the stability we assume that the ray of light has a width $w(t)$ and a “dispersion angle” $\theta(t)$ (we assume both are small), figure S.7 (b). Between bounces the dispersion angle stays constant while the width increases as

$$w(t) \approx w(t') + (t - t')\theta$$

Figure S.7: The 2-disk pinball (a) geometry, (b) defocusing of scattered rays.



At each bounce the width stays constant while the angle increases by

$$\theta_{n+1} = \theta_n + 2\phi \approx \theta_n + w(t)/a.$$

where θ_n denotes the angle after bounce n . Denoting the width of the ray at the n th bounce by w_n then we obtain the pair of coupled equations

$$w_{n+1} = w_n + (R - 2a)\theta_n \tag{S.1}$$

$$\theta_n = \theta_{n-1} + \frac{w_n}{a} \tag{S.2}$$

where we ignore corrections of order w_n^2 and θ_n^2 . Solving for θ_n we find

$$\theta_n = \theta_0 + \frac{1}{a} \sum_{j=1}^n w_j.$$

Assuming $\theta_0 = 0$ then

$$w_{n+1} = w_n + \frac{R - 2a}{a} \sum_{j=1}^n w_j$$

Plugging in the values in the question we find the width at each bounce in Ångströms grows as 1, 5, 29, 169, 985, etc. To find the asymptotic behavior for a large number of bounces we try an solution of the form $w_n = ax^n$. Substituting this into the equation above and ignoring terms that do not grow exponentially we find solutions

$$w_n \approx aw_n^{asym} = a(3 \pm 2\sqrt{2})^n$$

The solution with the positive sign will clearly dominate. The constant a we cannot determine by this local analysis although it is clearly proportional to w_0 . However, the asymptotic solution is a good approximation even for quite a small number of bounces. To find an estimate of a we see that w_n/w_n^{asym} very rapidly converges to 0.146447, thus

$$w_n \approx 0.146447w_0(3 + 2\sqrt{2})^n \approx 0.1 \times w_0 \times 5.83^n$$

The outside edges of the ray of light will miss the disk when the width of the ray exceeds 2 cm; this occurs after 11 bounces.

(Adam Prügel-Bennett)

Solution 1.2 - Sensitivity to initial conditions, another try. Adam's estimate is not very good - do you have a better one? The first problem with it is that the instability is very underestimated. As we shall check in exercise 13.7, the exact formula for the 2-cycle stability is $\Lambda = R - 1 + R\sqrt{1 - 2/R}$. For $R = 6$, $a = 1$ this yields $w_n/w_0 \approx (5 + 2\sqrt{6})^n = 9.898979^n$, so if that were the whole story, the pinball would be not likely to make it much beyond 8 bounces.

The second problem is that local instability overestimates the escape rate from an enclosure; trajectories are reinjected by scatterers. In the 3-disk pinball the particle leaving a disk can be reinjected by hitting either of other 2 disks, hence $w_n/w_0 \approx (9.9/2)^n$. This interplay between local instability and global reinjection will be cast into the exact formula involving "Lyapunov exponent" and "Kolmogorov entropy." In order to relate this estimate to our best continuous time escape rate estimate $\gamma = 0.4103\dots$ (see table 20.2), we will have to also compute the mean free flight time (20.24). As a crude estimate, we take the shortest disk-to-disk distance, $\langle T \rangle = R - 2 = 4$. The continuous time escape rate result implies that $w_n/w_0 \approx e^{(R-2)\gamma n} = (5.16)^n$, in the same ballpark as the above expansion-reinjection estimate. (P. Cvitanović)

Chapter 2. Go with the flow

Solution 2.1 - Trajectories do not intersect. Suppose that two trajectories C_x and C_y intersect at some point z . We claim that any points \tilde{x} on C_x is also a point on C_y and vice versa. We only need to prove the first part of the statement.

According to the definition of C_x , there exist $t_x, t_y, t_1 \in \mathbb{R}$ such that $f^{t_x}(x) = z, f^{t_y}(y) = z, f^{t_1}(x) = \tilde{x}$. It is easy to check that $f^{t_y - t_x + t_1}(y) = \tilde{x}$. So, $\tilde{x} \in C_y$. Therefore, if two trajectories intersect, then they are the same trajectory. (Y. Lan)

Solution 2.2 - Evolution as a group. Let's check the basic defining properties of a group. The members of the set are $f^t, t \in \mathbb{R}$ and the "product law" is given by 'o'.

- As $f^{t+s} = f^t \circ f^s$, the set is closed, i.e., the product of any two members generates another member of the set.
- It is associative, as $(f^t \circ f^s) \circ f^r = f^{t+s+r} = f^t \circ (f^s \circ f^r)$.
- $I = f^0$ is the identity, as $f^t \circ f^0 = f^t$.
- f^{-t} is the inverse of f^t , as $f^{-t} \circ f^t = I$.

So, $\{f^t, \circ\}_{t \in \mathbb{R}}$ forms a group. As $f^t \circ f^s = f^{t+s} = f^s \circ f^t$, it is a commutative (Abelian) group.

Any Abelian group can replace the continuous time. For example, \mathbb{R} can be replaced by \mathbb{Z}_6 . To mess things up try a non-commutative group. (Y. Lan)

Solution 2.3 - Almost ODE's. What is an ODE on \mathbb{R} ? An ODE is an equality which reveals explicitly the relation between function $x(t)$ and its time derivatives \dot{x}, \ddot{x}, \dots , i.e., $F(t, x, \dot{x}, \ddot{x}, \dots) = 0$ for some given function F . Let's check the equations given in the exercise.

(a) $\dot{x} = \exp(\dot{x})$ is an ODE.

(b) $\dot{x} = x(x(t))$ is not an ODE, as $x(x(t))$ is not a known function acting on $x(t)$.

(c) $\dot{x} = x(t+1)$ is not an ODE, as $x(t+1)$ is not a value at current time. Actually, it is a difference-differential equation. (Y. Lan)

Solution 2.4 - All equilibrium points are fixed points. Given a vector field $v(x)$, the state space dynamics is defined by

$$\frac{d}{dt}x(t) = v(x(t)). \quad (\text{S.3})$$

An equilibrium point a of v is defined by $v(a) = 0$, so $x(t) = a$ is a constant solution of (S.3). For the flow f^t defined by (S.3), this solution satisfies $f^t(a) = a, t \in \mathbb{R}$. So, it is a fixed point of the dynamics f^t . (Y. Lan)

Solution 2.5 - Gradient systems.

1. The directional derivative

$$\frac{d}{dn}\phi = n \cdot \nabla\phi$$

produces the increasing rate along the unit vector n . So, along the gradient direction $\nabla\phi/|\nabla\phi|$, ϕ has the largest increasing rate. The velocity of the particle has the opposite direction to the gradient, so ϕ decreases most rapidly in the velocity direction.

2. An extremum a of ϕ satisfies $\nabla\phi(a) = 0$. According to exercise 2.4, a is a fixed point of the flow.
3. Two arguments lead to the same conclusion here.

First, near an equilibrium point, the equation is always linearizable. For gradient system, after orthogonal transformation it is even possible to write the linearized equation in diagonal form so that we need only to consider one eigen-direction. The corresponding scalar equation is $\dot{x} = \lambda x$. Note that we moved the origin to the equilibrium point. The solution of this equation is $x(t) = x(0) \exp(\lambda t)$, for $\lambda \neq 0$. if $x(0) \neq 0$, it will take infinite amount of time (positive or negative) for $x(t) \rightarrow 0$. For $\lambda = 0$, the approach to zero is even slower as then only higher orders of x take effect.

The second argument seems easier. We know that the solution curve through an equilibrium point is the point itself. According to exercise 2.1, no other solution curve will intersect it, which means that if not starting from the equilibrium point itself, other point can never reach it.

4. On a periodic orbit, the velocity is bounded away from zero. So ϕ is always decreasing on a periodic orbit, but in view of the periodicity, we know that this can not happen (at each point, there is only one value of ϕ). So, there is no periodic orbit in a gradient system.

(Y. Lan)

Solution 2.7 - Rössler system. You will probably want the matlab function ode45 to do this. There are several others which perform better in different situations (for example ode23 for stiff ODEs), but ode45 seems to be the best for general use.

To use ode45 you must create a function, say 'rossler', which will take in a time and a vector of $[x, y, z]$ and return $[x\dot{,} y\dot{,} z\dot{]}$. Then the command would be something like

```
ode45([tmin, tmax], [x0 y0 z0], @rossler)
```

(Jonathan Halcrow)

Solution 2.8 - Equilibria of the Rössler system.

1. Solve $\dot{x} = \dot{y} = \dot{z} = 0$, to get $x = az$, $y = -z$ and $x^2 - cx + ab = 0$. There are two solutions of a quadratic equation, hence there are two equilibrium points:

$$x^\pm = az^\pm = -ay^\pm = (c \pm \sqrt{c^2 - 4ab})/2.$$

2. The above expressions are exact. However, it pays to think of $\epsilon = a/c$ as a small parameter in the problem. By substitution from exercise 2.8,

$$x^\pm = cp^\pm, \quad y^\pm = -p^\pm/\epsilon, \quad z^\pm = p^\pm/\epsilon. \quad (\text{S.4})$$

Expanding \sqrt{D} in ϵ yields $p^- = \epsilon^2 + o(\epsilon^3)$, and $p^+ = 1 - \epsilon^2 + o(\epsilon^3)$. Hence

$$\begin{aligned} x^- &= a^2/c + o(\epsilon^3), & x^+ &= c - a^2/c + o(\epsilon^3), \\ y^- &= -a/c + o(\epsilon^2), & z^+ &= c/a + a/c + o(\epsilon^2), \\ z^- &= a/c + o(\epsilon^2), & z^+ &= c/a - a/c + o(\epsilon^2). \end{aligned} \quad (\text{S.5})$$

For $a = b = 0.2$, $c = 5.7$ in (2.17), $\epsilon \approx 0.035$, so

$$\begin{aligned}(x^-, y^-, z^-) &= (0.0070, -0.0351, 0.0351), \\(x^+, y^+, z^+) &= (5.6929, -28.464, 28.464).\end{aligned}\tag{S.6}$$

(R. Paškauskas)

Solution 2.10 - Classical collinear helium dynamics. An example of a solution are A. Prügel-Bennett's programs, available at ChaosBook.org/extras.

Chapter 3. Discrete time dynamics

(No solutions available.)

Chapter 4. Local stability

Solution 4.1 - Trace-log of a matrix. 1) Consider $M = \exp A$.

$$\det M = \det \lim_{n \rightarrow \infty} \left(\mathbf{1} + \frac{1}{n}A \right)^n = \lim_{n \rightarrow \infty} \left(\mathbf{1} + \frac{1}{n} \text{tr} A + \dots \right)^n = \exp(\text{tr}(\ln M))$$

2) A rephrasing of the solution 1): evaluate $\frac{d}{dt} \det(e^{t \ln M})$ by definition of derivative in terms of infinitesimals. (Kasper Juel Eriksen)

3) Here is an example of wrong/incomplete answer, hiding behind fancier notation: This identity makes sense for a matrix $M \in \mathbb{C}^{n \times n}$, if $|\prod_{i=1}^n \lambda_i| < \infty$ and $\{|\lambda_i| > 0, \forall i\}$, where $\{\lambda_i\}$ is a set of eigenvalues of M . Under these conditions there exist a nonsingular $O : M = ODO^{-1}$, $D = \text{diag}\{\lambda_i, i = 1, \dots, n\}$. If $f(M)$ is a matrix valued function defined in terms of power series then $f(M) = Of(D)O^{-1}$, and $f(D) = \text{diag}\{f(\lambda_i)\}$. Using these properties and cyclic property of the trace we obtain

$$\exp(\text{tr}(\ln M)) = \exp\left(\sum_i \ln \lambda_i\right) = \prod_i \lambda_i = \det(M)$$

What's wrong about it? If a matrix with degenerate eigenvalues, $\lambda_i = \lambda_j$ is of Jordan type, it cannot be diagonalized, so a bit more of discussion is needed to show that the identity is satisfied by upper-triangular matrices.

4) First check that this is true for any Hermitian matrix M . Then write an arbitrary complex matrix as sum $M = A + zB$, A, B Hermitian, Taylor expand in z and prove by analytic continuation that the identity applies to arbitrary M . (David Mermin)

5) check appendix J.1

Solution 4.2 - Stability, diagonal case. The relation (4.17) can be verified by noting that the defining product (4.13) can be rewritten as

$$\begin{aligned} e^{tA} &= \left(\mathbf{U}\mathbf{U}^{-1} + \frac{t\mathbf{U}\mathbf{A}_D\mathbf{U}^{-1}}{m} \right) \left(\mathbf{U}\mathbf{U}^{-1} + \frac{t\mathbf{U}\mathbf{A}_D\mathbf{U}^{-1}}{m} \right) \dots \\ &= \mathbf{U} \left(\mathbf{I} + \frac{t\mathbf{A}_D}{m} \right) \mathbf{U}^{-1} \mathbf{U} \left(\mathbf{I} + \frac{t\mathbf{A}_D}{m} \right) \mathbf{U}^{-1} \dots = \mathbf{U} e^{t\mathbf{A}_D} \mathbf{U}^{-1}. \end{aligned} \tag{S.7}$$

Solution 4.3 - State space volume contraction.

- (a) The Rössler flow volume contraction rate at the equilibria follows from $\partial_i v_i = x + a - c = x - 5.5$; $\partial \cdot v|_- = -5.493$, $\partial \cdot v|_+ = +0.1929$.
- (b,c) The result is obvious and uninteresting. The point of the exercise is that the instantaneous velocity gradients matrix velocity gradients matrix gives no information about recurrent dynamics, what you want to color code are the eigenvalues of the finite time J^t at Poincaré section returns.

- (d) The average contraction rate (4.47) along a typical trajectory on the Rössler attractor is something like $\langle \partial \cdot v \rangle = -5.3$ (Li, after 10^5 iterations); -5.319 (Ding, after ? iterations); -5.3302 (Daniel, after 10^4 iterations); -5.36545648709 (Nah, unexplained procedure). Its plot as a function of time illustrates one problem of time-averaging in chaotic flows - it varies widely across each recurrence to a given Poincaré section. Even if it were worth your while to know its numerical value, the contraction rate cannot be linked to a computable fractal dimension. The relation goes through expanding eigenvalues, sect. 5.4. As the contraction is of order of 10^{-15} , there is no numerical algorithm that would give you any fractal dimension other than $D_H = 1$ for this attractor.
- (e) (any argument tends to be good enough).
- (f) The average contraction on the escape side of the outer equilibrium: not available.

Solution 4.4 - Topology of the Rössler flow.

1. The characteristic determinant of the stability matrix that yields the equilibrium point stability (4.31) yields

$$\begin{vmatrix} -\lambda & -1 & -1 \\ 1 & a - \lambda & 0 \\ z^\pm & 0 & x^\pm - c - \lambda \end{vmatrix} = 0$$

$$\lambda^3 + \lambda^2(-a - x^\pm + c) + \lambda(a(x^\pm - c) + 1 + x^\pm/a) + c - 2x^\pm = 0.$$

Equation (4.59) follows after noting that $x^\pm - c = c(p^\pm - 1) = -cp^\mp$ and $2x^\pm - c = c(2p^\pm - 1) = \pm c\sqrt{D}$, see (2.8).

2. Approximate solutions of (4.59) are obtained by expanding p^\pm and \sqrt{D} and substituting into this equation. Namely,

$$\begin{aligned} \sqrt{D} &= 1 - 2\epsilon^2 - 2\epsilon^4 - 4\epsilon^6 - \dots \\ p^- &= \epsilon^2 + \epsilon^4 + 2\epsilon^6 + \dots \\ p^+ &= 1 - \epsilon^2 - \epsilon^4 - 2\epsilon^6 + \dots \end{aligned}$$

In case of the equilibrium “-”, close to the origin expansion of (4.59) results in

$$(\lambda^2 + 1)(\lambda + c) = -\epsilon\lambda(1 - c^2 - c\lambda) + \epsilon^2c(\lambda^2 + 2) + o(\epsilon^2)$$

The term on the left-hand side suggests the expansion for eigenvalues as

$$\lambda_1 = -c + \epsilon a_1 + \dots, \quad \lambda_2 + i\theta_2 = \epsilon b_1 + i + \dots$$

after some algebra one finds the first order correction coefficients $a_1 = c/(c^2 + 1)$ and $b_1 = (c^3 + i)/(2(c^2 + 1))$. Numerical values are $\lambda_1 \approx -5.694$, $\lambda_2 + i\theta_2 \approx 0.0970 + i1.0005$.

In case of p^+ , the leading order term in (4.59) is $1/\epsilon$. Set $x = \lambda/\epsilon$, then expansion of (4.59) results in

$$x = c - \epsilon x - \epsilon^2(2c - x) - \epsilon^3(x^3 - cx^2) - \epsilon^4(2c - x(1 + c^2) + cx^2) + o(\epsilon^4)$$

Solve for real eigenvalue first. Set $x = c + \epsilon a_1 + \epsilon^2 a_2 + \epsilon^3 a_3 + \epsilon^4 a_4 + \dots$. The subtle point here is that leading order correction term of the real eigenvalue is ϵa_1 , but to determine leading order of the real part of complex eigenvalue, one needs all terms a_1 through a_4 .

Collecting powers of ϵ results in

$$\begin{aligned} \epsilon : a_1 + c &= 0 & a_1 &= -c \\ \epsilon^2 : c + a_1 + a_2 &= 0 & a_2 &= 0 \\ \epsilon^3 : a_1 - a_2 - a_3 &= 0 & a_3 &= -c \\ \epsilon^4 : c + c^2 a_1 - a_2 + a_3 + a_4 &= 0 & a_4 &= c^3. \end{aligned}$$

hence

$$\mu^{(1)} = \epsilon x = a - a^2/c + o(\epsilon^3) \approx 0.192982.$$

To calculate the complex eigenvalue, one can make use of identities $\det A = \prod \lambda = 2x^+ - c$, and $\text{tr} A = \sum \lambda = a + x^+ - c$. Namely,

$$\lambda_2 = \frac{1}{2}(a - cp^- - \lambda_1) = -\frac{a^5}{2c^2} + o(\epsilon^5) \approx -0.49 \times 10^{-6},$$

$$\theta_2 = \sqrt{\frac{2x^+ - c}{\lambda_1} - \lambda_2^2} = \sqrt{\frac{a+c}{a}}(1 + o(\epsilon)) \approx 5.431.$$

(R. Paškauskas)

Chapter 5. Cycle stability

Solution 5.1 - A limit cycle with analytic Floquet exponent. The 2 – dimensional flow is cooked up so that $x(t) = (q(t), p(t))$ is separable (check!) in polar coordinates $q = r \cos \phi$, $p = r \sin \phi$:

$$\dot{r} = r(1 - r^2), \quad \dot{\phi} = 1. \quad (\text{S.8})$$

In the (r, ϕ) coordinates the flow starting at any $r > 0$ is attracted to the $r = 1$ limit cycle, with the angular coordinate ϕ wrapping around with a constant angular velocity $\omega = 1$. The non-wandering set of this flow consists of the $r = 0$ equilibrium and the $r = 1$ limit cycle.

Equilibrium stability: As the change of coordinates is defined everywhere except at the equilibrium point ($r = 0$, any ϕ), the equilibrium stability matrix (4.31) has to be computed in the original (q, p) coordinates,

$$A = \begin{bmatrix} 1 & 1 \\ -1 & 1 \end{bmatrix}. \quad (\text{S.9})$$

The eigenvalues are $\lambda = \mu \pm i\omega = 1 \pm i$, indicating that the origin is linearly unstable, with nearby trajectories spiralling out with the constant angular velocity $\omega = 1$. The Poincaré section ($p = 0$, for example) return map is in this case also a stroboscopic map, strobed at the period (Poincaré section return time) $T = 2\pi/\omega = 2\pi$. The radial Floquet multiplier per one Poincaré return is $|\Lambda| = e^{\mu T} = e^{2\pi}$.

Limit cycle stability: From (S.8) the stability matrix is diagonal in the (r, ϕ) coordinates,

$$A = \begin{bmatrix} 1 - 3r^2 & 0 \\ 0 & 0 \end{bmatrix}. \quad (\text{S.10})$$

The vanishing of the angular $\lambda^{(\theta)} = 0$ eigenvalue is due to the rotational invariance of the equations of motion along ϕ direction. The expanding $\lambda^{(r)} = 1$ radial eigenvalue of the equilibrium $r = 0$ confirms the above equilibrium stability calculation. The contracting $\lambda^{(r)} = -2$ eigenvalue at $r = 1$ decreases the radial deviations from $r = 1$ with the radial Floquet multiplier $\Lambda_r = e^{\mu T} = e^{-4\pi}$ per one Poincaré return. This limit cycle is very attracting.

Stability of a trajectory segment: Multiply (S.8) by r to obtain $\frac{1}{2}\dot{r}^2 = r^2 - r^4$, set $r^2 = 1/u$, separate variables $du/(1-u) = 2 dt$, and integrate: $\ln(1-u) - \ln(1-u_0) = -2t$. Hence the $r(r_0, t)$ trajectory is

$$r(t)^{-2} = 1 + (r_0^{-2} - 1)e^{-2t}. \quad (\text{S.11})$$

The $[1 \times 1]$ Jacobian matrix

$$J(r_0, t) = \left. \frac{\partial r(t)}{\partial r_0} \right|_{r_0=r(0)}. \quad (\text{S.12})$$

satisfies (4.9)

$$\frac{d}{dt}J(r, t) = A(r)J(r, t) = (1 - 3r(t)^2)J(r, t), \quad J(r_0, 0) = 1.$$

This too can be solved by separating variables $d(\ln J(r, t)) = dt - 3r(t)^2 dt$, substituting (S.11) and integrating. The stability of any finite trajectory segment is:

$$J(r_0, t) = (r_0^2 + (1 - r_0^2)e^{-2t})^{-3/2} e^{-2t}. \quad (\text{S.13})$$

On the $r = 1$ limit cycle this agrees with the limit cycle multiplier $\Lambda_r(1, t) = e^{-2t}$, and with the radial part of the equilibrium instability $\Lambda_r(r_0, t) = e^t$ for $r_0 \ll 1$. (P. Cvitanović)

Solution 5.2 - The other example of a limit cycle with analytic Floquet exponent.
Email your solution to ChaosBook.org and G.B. Ermentrout.

Solution 5.3 - Yet another example of a limit cycle with analytic Floquet exponent.
Email your solution to ChaosBook.org and G.B. Ermentrout.

Chapter 6. Get straight

Solution 6.1 - Harmonic oscillator in polar coordinates. *Harmonic oscillator equations in Cartesian coordinates are*

$$\dot{p} = -q, \quad \dot{q} = p. \quad (\text{S.14})$$

In polar form, we write

$$q = r \cos \theta, \quad p = r \sin \theta. \quad (\text{S.15})$$

The inverse of the Jacobian $\frac{\partial\{q,p\}}{\partial\{r,\theta\}}$ of this transformation is

$$\frac{\partial\{r,\theta\}}{\partial\{q,p\}} = \begin{pmatrix} \cos \theta & \sin \theta \\ -\frac{1}{r} \sin \theta & \frac{1}{r} \cos \theta \end{pmatrix}, \quad (\text{S.16})$$

leading to

$$\begin{pmatrix} \dot{r} \\ \dot{\theta} \end{pmatrix} = \begin{pmatrix} \cos \theta & \sin \theta \\ -\frac{1}{r} \sin \theta & \frac{1}{r} \cos \theta \end{pmatrix} \cdot \begin{pmatrix} \dot{q} \\ \dot{p} \end{pmatrix} = \begin{pmatrix} 0 \\ -1 \end{pmatrix} \quad (\text{S.17})$$

(R. Wilczak)

Solution 6.2 - Coordinate transformations. *(No solution available.)*

Solution 6.3 - Linearization for maps. *(difficulty: medium) The first few terms of the map h that conjugates f to αz*

$$f(z) = h^{-1}(\alpha h(z)).$$

are determined many places, for example in ref. [9].

There are conditions on the derivative of f at the origin to assure that the conjugation is always possible. These conditions are formulated in ref. [26], among others.

Solution 6.4 - Ulam and tent maps. *This conjugacy is derived in many introductory chaos textbooks: see, for example, ref. [11] for a detailed discussion.*

Chapter 7. Newtonian dynamics

(No solutions available.)

Chapter 8. Billiards

Solution 8.1 - A pinball simulator. *Examples of pretty pinballs are A. Prügel-Bennett's `xpinball.c` and W. Benfold's java programs, available at ChaosBook.org/extras*

Solution 8.4 - Billiard exercises. *Korsch and Jodl [16] have a whole book of numerical exercises with billiards, including 3-disks.*

Solution 8.6 - Birkhoff coordinates. *Hint: compute the determinant of (8.11).*

Chapter 9. World in a mirror

Solution 9.1 - Polynomials invariant under discrete operations on \mathbb{R}^3 . See Gilmore and Letellier [13], Sect. 2.1.

Solution 9.2 - $G_x \subset G$. Keep in mind that the representation of $g_j \circ g_i$ is $\mathbf{g}_j \mathbf{g}_i$.

1. Closure: If $g_i, g_j \in G_x$, then $(\mathbf{g}_j \mathbf{g}_i)x = \mathbf{g}_j(\mathbf{g}_i x) = \mathbf{g}_j x = x$ and thus $g_j \circ g_i \in G_x$.
2. Associativity: Trivial.
3. Identity e : $e x = x$ for any x and thus $e \in G_x$.
4. Inverse g^{-1} : For every $g \in G_x$, there exists a unique element $h = g^{-1} \in G$ such that $h \circ g = g \circ h = e$. We need to show $g^{-1} \in G_x$. Multiply $\mathbf{g} x = x$ from the left with \mathbf{g}^{-1} to get $\mathbf{g}^{-1} \mathbf{g} x = \mathbf{g}^{-1} x$ or $\mathbf{g}^{-1} x = x$ and thus $g^{-1} \in G_x$.

(Evangelos Siminos)

Solution 9.4 - Isotropy subgroup of $\mathbf{g}x$. For every $h \in G_{\mathbf{g}x}$ we have

$$\mathbf{h}(\mathbf{g}x) = \mathbf{g}x$$

Multiplying from the left with \mathbf{g}^{-1} and using associativity we get $(\mathbf{g}^{-1} \mathbf{h} \mathbf{g})x = x$ and thus $\mathbf{g}^{-1} \circ \mathbf{h} \circ \mathbf{g} \in G_x$ for every $h \in G_{\mathbf{g}x}$. Therefore x and $\mathbf{g}x$ have conjugate isotropy subgroups.

(Evangelos Siminos)

Solution 9.6 - Reduction of 3-disk symbolic dynamics. The answer is given in sect. 21.6, see figure 9.6, figure 9.9, figure 12.12. Some remarks concerning part (c):

If an orbit does not have any spatial symmetry, its length in the fundamental domain is equal to that in the full space. One fundamental domain orbit corresponds to six copies of the orbit in the full space related to each other by symmetries. If a periodic orbit does have a spatial symmetry, then its fundamental domain image is a fraction of that in the whole space, and the orbit (and its symmetry partners) in the full space is tiled by copies of the relative periodic orbit, corresponding to an orbit in the fundamental domain. The higher symmetry an orbit has, the shorter the relative periodic orbit.

Another way to visualize a fundamental domain orbit: put a periodic orbit and all its spatial symmetry relatives simultaneously in the full space. The segments that fall into a fundamental domain constitute the orbit in the fundamental domain. (Y. Lan)

Solution 12.6 - 3-disk fundamental domain symbolic dynamics. Read sect. 1.4.

Solution 9.8 - Lorenz system in polar coordinates: group theory. No solution available.

Solution 9.9 - Proto-Lorenz system. This exercise is based on Miranda and Stone [11]; their paper gives a detailed discussion.

1. The proto-Lorenz equation, (2.12), in terms of variables $(u, v, z) = (x^2 - y^2, 2xy, z)$:

$$\begin{aligned} \begin{bmatrix} \dot{u} \\ \dot{v} \\ \dot{z} \end{bmatrix} &= \begin{bmatrix} -(\sigma + 1)u + (\sigma - r)v + (1 - \sigma)N + vz \\ (r - \sigma)u - (\sigma + 1)v + (r + \sigma)N - uz - uN \\ v/2 - bz \end{bmatrix} \\ N &= \sqrt{u^2 + v^2}. \end{aligned} \tag{S.18}$$

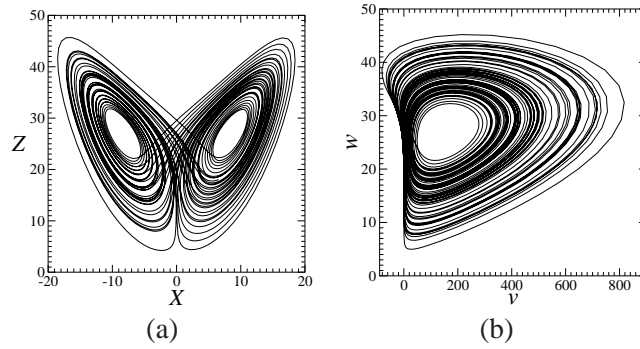


Figure S.8: (a) The Lorenz attractor. (b) The Rössler-like proto-Lorenz attractor, with points related by rotation symmetry about the z -axis identified. (From ref. [8].)

4. The equilibria of proto-Lorenz: origin the same, $(u, v, z) = (0, 0, 0)$. The R -symmetric pair (2.13) is now a single equilibrium at

$$u_{EQ_1} = (0, 2b(r-1), r-1). \quad (\text{S.19})$$

Chapter 10. Continuous symmetries

Solution 10.1 - Visualizations of the 5-dimensional complex Lorenz flow. A numerical solution of the set of ODEs (10.2) is obtained by using the *Mathematica* `NDSolve` function, for t from 0 to 100 and setting the initial (x_1, x_2, y_1, y_2, z) to some arbitrary value. We set `MaxSteps` \rightarrow `Infinity` in order to resolve the fine structure of the flow. The solution is then plotted by means of `ParametricPlot3D`, in any three of the five $\{x_1, x_2, y_1, y_2, z\}$ axes. Figure 10.1 illustrates the shape of the attractor projected onto the $\{x_1, x_2, z\}$ subspace, with (10.2) parameter values. Projections onto $\{y_1, y_2, z\}$ and other subspaces are visually similar, and seem not to offer additional insights into dynamics of this system.

Here is a *Mathematica* program that generates a long-time plot of complex Lorenz equations, such as figure 10.1, initiated from a point on the attractor (after this integration, the initial condition `ic` is the final point of the preceding integration):

```
v[t_]={-σ x1[t] + σ y1[t], -σ x2[t] + σ y2[t],
(r1 - z[t])x1[t] - r2x2[t] - y1[t] - ey2[t],
r2x1[t] + (r1 - z[t])x2[t] + ey1[t] - y2[t],
-b z[t] + x1[t]y1[t] + x2[t]y2[t]};
x[t_] = {x1[t], x2[t], y1[t], y2[t], z[t]};
d=Length[x[t]];
eqns=Table[D[x[t][[i]],t]==v[t][[i]],{i,1,d}];
xde={x1, x2, y1, y2, z};

r1= 28; r2=0; b=8/3; e=1/10; σ=10;
tf= 80;
ic={x1[0]==0.867, x2[0]==-0.455, y1[0]==-0.552, y2[0]==0.453,
z[0]==22.4};

sol=NDSolve[{eqns,ic}, xde, {t,0,tf}, MaxSteps  $\rightarrow$  ∞]//Flatten;
traj[t_]=x[t]/.sol;
p1=ParametricPlot3D[{traj[t][[1]], traj[t][[2]], traj[t][[5]]},
{t,0,tf}, PlotPoints  $\rightarrow$  400, PlotRange  $\rightarrow$  All]
ic=Table[x[0][[i]]==traj[tf][[i]], {i,1,d}];
(R. Wilczak)
```

Solution 10.2 - A flow with two Fourier modes. (Solution not available.)

Solution 10.3 - SO(2) rotations in a plane. Expand $\exp(\theta \mathbf{T})$ as a power series, noting that

$$\mathbf{T}^2 = \begin{pmatrix} 0 & 1 \\ -1 & 0 \end{pmatrix}^2 = -\mathbf{1}.$$

See also example 4.5.

(P. Cvitanović)

Solution 10.5 - U(1) equivariance of complex Lorenz equations for finite angles. Multiply the coordinates by a complex phase: $x \rightarrow e^\theta x$, $y \rightarrow e^\theta y$. Equivariance of (10.1) follows by inspection. If all coefficients are real, there is also a discrete C_1 symmetry under complex conjugation of the three equations. However, we consider here the cases where one or both of the parameters r and a are complex, breaking this discrete symmetry.

(P. Cvitanović)

Solution 10.6 - SO(2) equivariance of complex Lorenz equations for finite angles. For this problem, the operation is rotation and $v(x)$ is given by (10.2). Rotation can be defined using the matrix $g(\theta)$ defined in (10.18), where θ is the angle of rotation. We need to verify that

$$v(x) = g^{-1}v(gx). \tag{S.20}$$

First, the system is rotated as

$$\begin{pmatrix} \cos(\theta) & \sin(\theta) & 0 & 0 & 0 \\ -\sin(\theta) & \cos(\theta) & 0 & 0 & 0 \\ 0 & 0 & \cos(\theta) & \sin(\theta) & 0 \\ 0 & 0 & -\sin(\theta) & \cos(\theta) & 0 \\ 0 & 0 & 0 & 0 & 1 \end{pmatrix} \cdot \begin{pmatrix} x_1(t) \\ x_2(t) \\ y_1(t) \\ y_2(t) \\ z(t) \end{pmatrix}. \tag{S.21}$$

The time derivative of the resulting matrix is taken, and then it is multiplied on the left by the inverse of the rotation matrix, giving

$$g^{-1}v(gx) = \begin{pmatrix} \sigma y_1(t) - \sigma x_1(t) \\ \sigma y_2(t) - \sigma x_2(t) \\ -r_2 x_2(t) - y_1(t) - e y_2(t) + x_1(t)(r_1 - z(t)) \\ r_2 x_1(t) + e y_1(t) - y_2(t) + x_2(t)(r_1 - z(t)) \\ x_1(t)y_1(t) + x_2(t)y_2(t) - bz(t) \end{pmatrix}, \tag{S.22}$$

which is the same as the original system of ODEs, so that the system is rotationally equivariant for all finite angle rotations. (R. Wilczak)

Solution 10.7 - Stability matrix of complex Lorenz flow. The stability matrix (10.26), defined in (4.3), for complex Lorenz flow (10.2) can be computed by Mathematica program

$$\begin{aligned} v[t] &= \{x1'[t], x2'[t], y1'[t], y2'[t], z'[t]\}; \\ x[t] &= \{x1[t], x2[t], y1[t], y2[t], z[t]\}; \\ A &= D[v[t], \{x[t], 1\}] \end{aligned}$$

(R. Wilczak and P. Cvitanović)

Solution 10.8 - Rotational equivariance of complex Lorenz equations for infinitesimal angles. Now that we have the stability matrix (10.26), we can check the equivariance condition (10.24), $0 = -T v(x) + A T x$, where A is the stability matrix (4.3), by explicit substitution. The matrix T is (10.17). Plugging these into (10.24), as well as using (10.2) for $v(x)$, the result is indeed 0, as expected. Then the system is rotationally equivariant for infinitesimal angles. (R. Wilczak)

Solution 10.9 - Discover the equivariance of a given flow? If M is in the Lie algebra, by the equivariance condition (10.24) the Lie derivative $M v(x) - A M x$ vanishes. You have $v(x)$ and the stability matrix A , hence try finding whether a M can be found such that the Lie derivative vanishes. You know that if the symmetry group is a subgroup of $SO(d)$, the Lie algebra elements M can be taken antisymmetric. (Have not tried to solve this problem, so let us know if you succeed) (P. Cvitanović)

Solution 10.10 - Equilibria of complex Lorenz equations. To find these points for complex Lorenz equations, I used the `Solve` function in *Mathematica*, with

$$\begin{pmatrix} \dot{x}_1(t) \\ \dot{x}_2(t) \\ \dot{y}_1(t) \\ \dot{y}_2(t) \\ \dot{z}(t) \end{pmatrix} = \begin{pmatrix} \sigma y_1(t) - \sigma x_1(t) \\ \sigma y_2(t) - \sigma x_2(t) \\ -r_2 x_2(t) - y_1(t) - e y_2(t) + x_1(t)(r_1 - z(t)) \\ r_2 x_1(t) + e y_1(t) - y_2(t) + x_2(t)(r_1 - z(t)) \\ x_1(t)y_1(t) + x_2(t)y_2(t) - b z(t) \end{pmatrix} = \begin{pmatrix} 0 \\ 0 \\ 0 \\ 0 \\ 0 \end{pmatrix}$$

as the equations defining the system, and then solved for $(x_1(t), x_2(t), y_1(t), y_2(t), z(t))$. *Mathematica* returns the point $(0, 0, 0, 0, 0)$ as the only solution, and thus (I hope, have no proof) the only equilibrium point. (R. Wilczak)

Solution 10.11 - Equilibria of complex Lorenz equations. See *Siminos thesis* [29].

Solution 10.12 - Complex Lorenz equations in polar coordinates. We use the same method here as in exercise 6.1. The Jacobian of this transformation can be written as

$$\frac{\partial\{r_1, \theta_1, r_2, \theta_2, z\}}{\partial\{x_1, x_2, y_1, y_2, z\}} = \begin{pmatrix} \cos(\theta_1) & \sin(\theta_1) & 0 & 0 & 0 \\ -\frac{\sin(\theta_1)}{r_1} & \frac{\cos(\theta_1)}{r_1} & 0 & 0 & 0 \\ 0 & 0 & \cos(\theta_2) & \sin(\theta_2) & 0 \\ 0 & 0 & -\frac{\sin(\theta_2)}{r_2} & \frac{\cos(\theta_2)}{r_2} & 0 \\ 0 & 0 & 0 & 0 & 1 \end{pmatrix}. \tag{S.23}$$

Multiplying the velocity matrix on the left by the Jacobian (S.23), we get

$$\begin{pmatrix} \dot{r}_1 \\ \dot{\theta}_1 \\ \dot{r}_2 \\ \dot{\theta}_2 \\ \dot{z} \end{pmatrix} = \begin{pmatrix} -\sigma(r_1 - r_2 \cos \theta) \\ -\sigma \frac{r_2}{r_1} \sin \theta \\ -r_2 + r_1((\rho_1 - z) \cos \theta - \rho_2 \sin \theta) \\ e + \frac{r_1}{r_2}((\rho_1 - z) \sin \theta + \rho_2 \cos \theta) \\ -b z + r_1 r_2 \cos \theta \end{pmatrix},$$

where $\theta = \theta_1 - \theta_2$. Following ref. [29], we set $\rho_2 = 0$ in what follows. We rewrite this as 4 coupled equations (10.58), and two driven ones for the two angles,

$$\begin{pmatrix} \dot{\theta}_1 \\ \dot{\theta}_2 \end{pmatrix} = \begin{pmatrix} -\sigma \frac{r_2}{r_1} \sin \theta \\ e + (\rho_1 - z) \frac{r_1}{r_2} \sin \theta \end{pmatrix}. \tag{S.24}$$

Our result confirms formulas stated in ref. [29]. (R. Wilczak and P. Cvitanović)

Solution 10.13 - Visualizations of the complex Lorenz flow in polar coordinates. (solution not available)

Solution 10.14 - Computing the relative equilibrium TW_1 . A relative equilibrium point occurs when the derivatives (10.58) are equal to zero (so that the difference between the two angles θ_1 and θ_2 is constant, but the angles themselves are not constant). We use the `Solve` function (or the `Reduce` function) in *Mathematica* to find these points.

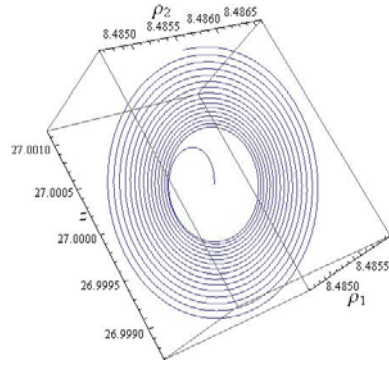


Figure S.9: $\{r_1, r_2, z\}$ plot of the complex Lorenz flow, with initial point close to TW_1 (note the scales).

We define the system in *Solve* by setting all time derivatives in (10.58) to zero. *Mathematica* returns eight solutions of the form

$$\begin{aligned}
 z(t) &\rightarrow \rho_1 - 1 - \frac{e^2}{(\sigma + 1)^2} \\
 r_2(t) &\rightarrow \pm \frac{\sqrt{e^2 + (\sigma + 1)^2} \sqrt{-b(e^2 - (\rho_1 - 1)(\sigma + 1)^2)}}{(\sigma + 1)^2} \\
 r_1(t) &\rightarrow \pm \frac{\sqrt{-b(e^2 - (\rho_1 - 1)(\sigma + 1)^2)}}{|\sigma + 1|} \\
 \theta(t) &\rightarrow \pm \cos^{-1} \left(\pm \frac{\sqrt{(\sigma + 1)^2}}{\sqrt{e^2 + (\sigma + 1)^2}} \right)
 \end{aligned} \tag{S.25}$$

The solutions differ by combinations of negative and positive r_1, r_2, θ . A negative r_i solution corresponds to the same group orbit of solutions, related to the positive r_i solution by a rotation by π . The $r_1 \geq 0, r_2 \geq 0$ condition in (10.57) reduces these solutions to two, differing by the sign of \cos^{-1} term. As will be further shown in exercise 10.16, the two $\pm \cos^{-1}(\dots)$ solutions are equivalent. We can write the solution compactly as in (10.59), in agreement with ref. [29]. For the (10.2) parameter values, the relative equilibrium is at

$$x_{TW_1} = (r_1, r_2, \theta, z) = (8.48527, 8.48562, 0.00909066, 26.9999). \tag{S.26}$$

The angular velocity of relative equilibrium TW_1 follows from (S.24). Both angles move with the same velocity (10.60) and period $T_{TW_1} = 2\pi(\sigma + 1)/\sigma e$. $T_{TW_1} = 69.115\dots$ for the (10.2) parameter values. That implies that the simulation has to be run up to time of order of at least 70 for the strange attractor in figure 10.1 to start filling in. (R. Wilczak and P. Cvitanović)

Solution 10.15 - Relative equilibrium TW_1 in polar coordinates. The same method as in exercise (10.1) can be used here. First, a numerical solution is found with *NDSolve* for t going 0 to 10 and initial point TW_1 . We again set *MaxSteps* \rightarrow *Infinity* in order to resolve the structure of the flow. Using *ParametricPlot3D* to plot the flow in $\{r_1, r_2, z\}$ axes, Figure S.9 illustrates the shape of the flow with (10.2) parameter values. (R. Wilczak)

Solution 10.16 - Relative equilibrium TW_1 in Cartesian coordinates. Using the same method as in exercise 10.15 and in exercise 10.1, we can plot the relative equilibrium in Cartesian coordinates. However, the Cartesian system is five-dimensional

and our polar system has only four dimensions. To resolve this, we set θ_2 to an arbitrary value and set $\theta_1 = \theta + \theta_2$. With this and (10.57), we can verify the numerical value (10.61) of a point on the TW_1 orbit in Cartesian coordinates. Using *Mathematica* to plot the system with t going from 0 to 100, figure 10.4 shows the complex Lorenz flow at TW_1 projected onto the $\{x_1, x_2, z\}$ subspace.

Note that the for a relative equilibrium the flow is along a circle, i.e., the group-orbit of any point on it, but due to finite precision of the initial point and the integration, the trajectory eventually spirals away in a "horn" shape. This circle cuts through the middle of the complex Lorenz equations strange attractor, as shown in figure 10.1. (R. Wilczak)

Solution 10.17 - Eigenvalues and eigenvectors of TW_1 stability matrix. Using the *Mathematica* function *Eigensystem* and setting $(r_1, r_2, \theta, z)(0)$ to the values in (S.26) we obtain

$$(\lambda_{1,2}, \lambda_3, \lambda_4) = (0.0938179 \pm 10.1945i, -11.0009, -13.8534)$$

as the eigenvalues of the system with the associated eigenvectors:

$$\begin{aligned} \operatorname{Re} e_1 &= (0.266121, -0.0321133, 0.00034139, 0.719222) \\ \operatorname{Im} e_1 &= (0.295017, 0.569063, 0.000551886, 0) \\ e_3 &= (-0.0883591, -0.0851485, -0.989135, -0.0809553) \\ e_4 &= (-0.855586, -0.329912, -0.00273531, -0.398902) \end{aligned} \quad (\text{S.27})$$

(R. Wilczak and P. Cvitanović)

Solution 10.18 - The eigen-system of TW_1 stability matrix in polar coordinates. In order to plot the complex eigenvectors, we split them into their real and complex parts as in exercise 10.20. Using the same method as in exercise 10.1, exercise 10.16, and exercise 10.15, we can plot the flow in polar coordinates with an initial point very near to TW_1 along one of the eigenvectors. Figure S.10 shows just this. (R. Wilczak)

Solution 10.19 - Eigenvalues and eigenvectors of EQ_0 stability matrix. Using the *Mathematica* function *Eigensystem* and setting $(x_1, x_2, y_1, y_2, z) = (0, 0, 0, 0, 0)$ at $t = 0$ we obtain the eigenvalues, the associated eigenvectors:

$$\begin{aligned} (\lambda_{1,2}, \lambda_{3,4}, \lambda_5) &= (11.8277 \pm 0.062985i, -22.8277 \pm 0.037015i, -2.66667) \\ e_1 = e_2^* &= (0.00132196 + 0.458131i, 0.458131 - 0.00132196i, i, 1, 0) \\ e_3 = e_4^* &= (0.002249 - 0.77955i, -0.77955 - 0.002249i, 2.84217 + i, 1, 0) \\ e_5 &= (0, 0, 0, 0, 1). \end{aligned} \quad (\text{S.28})$$

(R. Wilczak)

Solution 10.20 - The eigen-system of the stability matrix at EQ_0 . In order to plot the complex eigenvectors, we split them into their real and complex parts and plot each separately (so that one complex eigenvector becomes two, defining a plane). By examining the eigensystem, we can get a sense of what happens to points near the equilibrium EQ_0 . The numerical values of the real parts of the eigenvalues determine

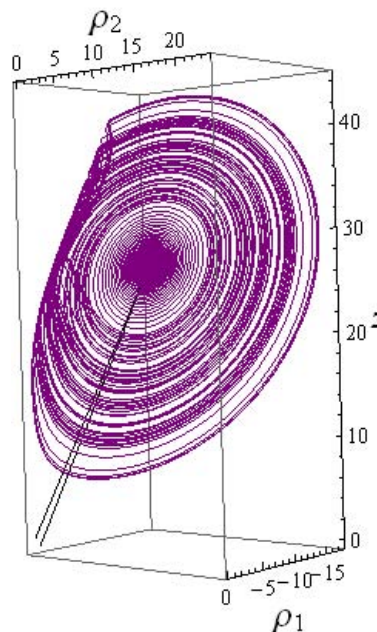


Figure S.10: $\{\rho_1, \rho_2, z\}$ plot of the eigenvector e_3 with initial point at $\frac{6}{100}e_3$ (violet), integrated for time t from 0 to 100.

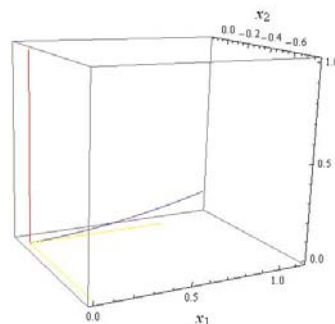


Figure S.11: $\{x_1, x_2, z\}$ plot of the expanding eigenvector e_1 (red) and the contracting eigenvector e_4 (yellow) of the equilibrium E_0 stability matrix of complex Lorenz flow, with initial point at $0.01 e_4$.

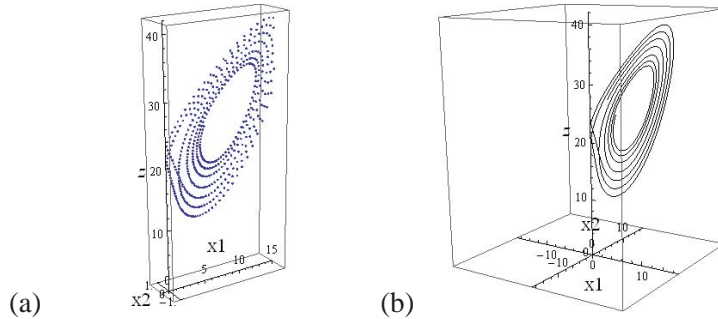
how quickly the flow will converge onto or diverge away from the equilibrium. For a positive real part the flow will diverge, and for a negative real part it will converge. Complex eigenvalues also indicate that the motion will be spiraling.

For the complex Lorenz equations equilibrium E_{Q_0} , the values (S.28) of the imaginary parts are orders of magnitude smaller than the real parts, so that there will be very little spiraling. The large values of the real parts tell us that the flow will diverge/converge from the equilibrium very quickly.

To illustrate this, we plot the eigenvectors (as real and imaginary parts) and the flow at initial points close to E_{Q_0} . The two real vectors (corresponding to a single complex eigenvector) define the plane in which the flow will spiral. We initiate the flow very close to E_{Q_0} at a point along one of these vectors. In figure S.11, we can see that for the vectors with a very small imaginary part and a positive real part, the flow does not spiral noticeably and that it diverges away from the equilibrium very quickly.

We arrive at figure S.11 using the same method as in the previous plotting exercises (exercise 10.1, exercise 10.15, exercise 10.16). As the eigenvalues are nearly real, the stable/unstable $2d$ manifolds barely spiral, and are not very illuminating. (R.

Figure S.12: (a) $\{x_1, x_2, z\}$ plot of the complex Lorenz flow as each point is rotated back to the plane. The time step used to make this plot was 0.01 and the integration went from $t = 0$ to $t = 50$. (b) With the points connected into a curve.



Wilczak)

Solution 10.21 - SO(2) or harmonic oscillator slice: We can now construct a moving frame as follows. We write out explicitly the group transformations:

$$\begin{aligned} \bar{x} &= x \cos \theta - y \sin \theta \\ \bar{y} &= x \sin \theta + y \cos \theta. \end{aligned}$$

Then set $\bar{x} = 0$ and solve (S.29) for the group parameter to obtain the moving frame

$$\theta = \tan^{-1} x/y \tag{S.29}$$

which brings any point back to the slice. Substituting (S.29) in the remaining equation, we get the SO(2)-invariant expression $\bar{y} = \sqrt{x^2 + y^2}$. (E. Siminos)

Solution 10.22 - State space reduction by a slice. We start by setting the initial point and the time step that will be used during the integration. Using *Mathematica*, we first remove the z component of the initial point so that we have $x(0) = x(0) \cdot \hat{z} = \{x_1(0), x_2(0), y_1(0), y_2(0), 0\}$. In order to rotate each of the points, we must construct the group representation matrix (10.18), where θ is the angle between the new point (minus the z component) and the positive x_1 axis ($\hat{x}_1 = \{1, 0, 0, 0, 0\}$). From exercise 10.5, we know that the complex Lorenz equations are invariant for this kind of rotation, so that when we reduce the complex Lorenz flow it contains the same information as the 5-dimensional system. We do not need to determine the angles themselves, we need only their cosines and sines. The cosine is found by a dot product as $\cos(\theta) = x \cdot \hat{x}_1 / |x|$.

Sines can be found by rotating each point by $\pi/2$ and then taking the dot product as with cosine. Taking the first point, we first rotate it with g , and starting with this rotated point, we integrate over the defined time step. We then take the last point from the integration, find its g and rotate it, then use it at the beginning of the next integration from $t = \text{timestep}$ to $t = 2 \cdot \text{timestep}$. This process continues (using a *For* loop in *Mathematica*) until the end of the integration (at an arbitrary time). The resulting list of rotated points is then plotted. Using this method, we produced figure S.12. (R. Wilczak)

Solution 10.23 - State space reduction by a slice, ODE formulation: Infinitesimal time version of the moving frames symmetry reduction is attained by taking small time steps in figure 10.11 and dropping the higher order terms, as in sect. 10.4.2:

$$dx^{(n)} = dt v(x^{(n)}) + d\theta_1^{(n)} \mathbf{T}x^{(n)}.$$

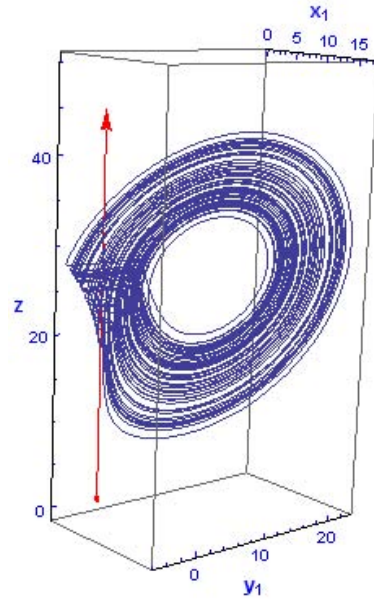


Figure S.13: Method of moving frames, continuous time version, for the polar coordinates motivated $x^* = (0, 1, 0, 0)$, $x_1 = 0$, $x_2 > 0$, slice. The strange attractor of figure 10.1 in the reduced state space, $\{x_2, y_2, z\}$ projection exhibits a discontinuity at $x_2 = 0$.

The infinitesimal angle is proportional to the time step,

$$\theta_1^{(n)} \approx \sin \theta_1^{(n)} = -dt \frac{\hat{\mathbf{e}}_1 \cdot v(x^{(n)})}{r_1^{(n)}} \approx -dt v_1(x^{(n)})/x_2^{(n)},$$

where (r_1, θ_1) are polar coordinates, $r_1 = (x_1^2 + x_2^2)^{1/2}$, see (10.57). Our slice condition is $x_1 = 0$, $x_2 > 0$, so the reduced state space equations are given by

$$\dot{x} = v - \frac{v_1}{x_2} \mathbf{T}x. \tag{S.30}$$

The motion stays in the $(d-1)$ -slice, as $\dot{x}_1 = 0$ due to the orthogonal action of \mathbf{T} to the direction x . Moving frames symmetry reduced complex Lorenz equations are a 4-dimensional first order ODE system

$$\begin{aligned} \dot{x}_2 &= -\sigma(x_2 - y_2) \\ \dot{y}_1 &= -y_1 + r_2 x_2 - (e + \sigma y_1/x_2) y_2 \\ \dot{y}_2 &= -y_2 + (\rho_1 - z)x_2 + (e + \sigma y_1/x_2) y_1 \\ \dot{z} &= -bz + x_2 y_2. \end{aligned} \tag{S.31}$$

The resulting trajectory is illustrated in figure S.13. It agrees with trajectories reported by Siminos (there the simulation is in the full state space, and the reduced state space dynamics is obtained by a coordinate change).

- Checked that it agrees with finite step + rotation of figure 10.11
- x_2 and y_2 seem locked, oscillate the same way with amplitude up to 20
- y_1 is very small, mostly below 0.1
- (x_2, y_2, z) plot looks discontinuous in y_2 whenever x_2 small, across the z -axis (indicated in red). (R. Wilczak)

Solution 10.24 - Accumulated phase shift in slice reduced state space: (not available)

Solution 10.25 - The moving frame flow stays in the reduced state space: The motion stays in the $(d-1)$ -dimensional slice, as the flow along the group action direction vanishes,

$$\dot{x} \cdot \mathbf{T}y' = v \cdot \mathbf{T}y' - \frac{(v \cdot \mathbf{T}y')}{(x \cdot y')_4} (\mathbf{T}x) \cdot \mathbf{T}y' = 0.$$

(P. Cvitanović)

Solution 10.26 - State space reduction by a relative equilibrium TW_1 cross-section. We note that $x_{TW_1} \cdot t_{TW_1} = 0$ by the antisymmetry of \mathbf{T} , so (10.64) is a linear condition $\hat{x} \cdot \mathbf{T}x_{TW_1} = x \cdot g(\theta)^T \mathbf{T}x_{TW_1} = 0$ that determines θ . Substituting (10.55) and (10.17) yields a formula

$$\tan \theta = \frac{x_1 x_2^{TW_1} - x_1 x_2^{TW_1} + y_1 y_2^{TW_1} - y_1 y_2^{TW_1}}{x_1 x_1^{TW_1} + x_2 x_2^{TW_1} + y_1 y_1^{TW_1} + y_2 y_2^{TW_1}} \quad (\text{S.32})$$

for the rotation angle $\hat{x} = g(\theta)x$ (actually, there are two solutions, separated by π) that rotates x into the cross-section. In contrast to fixing one of the polar angles as in the method of moving frames of sect. 10.4.1, this cross-section introduces no singularities, as $x_1^2 + x_2^2 + y_1^2 + y_2^2 > 0$. To compute $\sin \theta$, $\cos \theta$ needed by $g(\theta)$ rewrite (S.32) as

$$\begin{aligned} \cos \theta &= (x_1 x_1^{TW_1} + x_2 x_2^{TW_1} + y_1 y_1^{TW_1} + y_2 y_2^{TW_1})/N \\ \sin \theta &= (x_1 x_2^{TW_1} - x_1 x_2^{TW_1} + y_1 y_2^{TW_1} - y_1 y_2^{TW_1})/N, \end{aligned} \quad (\text{S.33})$$

with N fixed by $\sin^2 + \cos^2 = 1$.

(P. Cvitanović)

Chapter 11. Qualitative dynamics, for pedestrians

Solution 11.1 - Binary symbolic dynamics. *Read the text.*

Solution 11.2 - Generating prime cycles. *(No solution available.)*

Solution 11.3 - A contracting baker's map. *(No solution available.)*

Solution 11.4 - Unimodal map symbolic dynamics. *Hint: write down an arbitrary binary number such as $\gamma = .1101001101000\dots$ and generate the future itinerary S^+ by checking whether $f^n(\gamma)$ is greater or less than $1/2$. Then verify that (11.9) recovers γ .*

Solution 11.4 - Unimodal map symbolic dynamics. *The easiest way to see this is to derive the itinerary from the binary expansion using the tent map as the prototypical example of a unimodal map. Let the binary expansion of x be $x = .\omega_1\omega_2\omega_3\omega_4\dots$ then $1 - x = .\bar{\omega}_1\bar{\omega}_2\bar{\omega}_3\bar{\omega}_4\dots$ with $\bar{\omega} = 1 - \omega$. Thus the tent map can be written as*

$$T.\omega_1\omega_2\omega_3\dots = \begin{cases} .\omega_2\omega_3\omega_4\dots & \text{if } \omega_1 = 0 \\ .\bar{\omega}_2\bar{\omega}_3\bar{\omega}_4\dots & \text{if } \omega_1 = 1 \end{cases} = \begin{cases} .\omega_2\omega_3\omega_4\dots & \text{if } \omega_1 = 0 \\ 1 - .\omega_2\omega_3\omega_4\dots & \text{if } \omega_1 = 1 \end{cases}$$

Since the symbol of x is simply ω_1 we can generate the symbolic sequence from the binary expansion of x via $s_n = (T^{n-1}x)_1$ for all $n \geq 1$.

Note that $T(1 - x) = Tx$ hence for all $n \geq 1$

$$T^n x = T\sigma^{n-1}x = \begin{cases} \sigma^n x & \text{if } (\sigma^{n-1}x)_1 = 0 \\ 1 - \sigma^n x & \text{if } (\sigma^{n-1}x)_1 = 1 \end{cases} = \begin{cases} \sigma^n x & \text{if } \omega_n = 0 \\ 1 - \sigma^n x & \text{if } \omega_n = 1 \end{cases}$$

with σ being the left shift. Therefore, given the symbol sequence s_n we have for $n \geq 1$

$$s_{n+1} = (T^n x)_1 = \begin{cases} (\sigma^n x)_1 & \text{if } \omega_n = 0 \\ (1 - \sigma^n x)_1 & \text{if } \omega_n = 1 \end{cases} = \begin{cases} \omega_{n+1} & \text{if } \omega_n = 0 \\ 1 - \omega_{n+1} & \text{if } \omega_n = 1 \end{cases}$$

which shows

$$\omega_{n+1} = \begin{cases} s_{n+1} & \text{if } \omega_n = 0 \\ 1 - s_{n+1} & \text{if } \omega_n = 1 \end{cases} \quad \text{with } \omega_1 = s_1$$

for all $n \geq 1$.

(Alexander Grigo)

Solution 11.5 - Unimodal map kneading value. *(No solution available.)*

Solution 11.6 - "Golden mean" pruned map.

(a) Consider the 3-cycle drawn in the figure. Denote the lengths of the two horizontal intervals by a and b . We have $a/b = b/(a + b)$, so the slope is given by the golden mean, $\Lambda = b/a = (1 + \sqrt{5})/2$, and the piecewise linear tent map is given by

$$f(x) = \begin{cases} \Lambda x, & x \in [0, 1/2] \\ \Lambda(1 - x), & x \in [1/2, 1] \end{cases}$$

Alternative derivation: 3-cycle periodic point at $x = 1/2$ is a fixed point of the 3rd iterate, $f^3(1/2) = \Lambda^2(1 - \Lambda/2) = 1/2$. $\Lambda = 1, (1 - \sqrt{5})/2$ solutions are no good, so $\Lambda = (1 + \sqrt{5})/2$.

(b) The 3-cycle periodic points are $\{x_{C10}, x_{10C}, x_{0C1}\} = \{1/2, \Lambda/2, 1/(2\Lambda)\}$. Once a point enters the region covered by the interval M of length $a + b$, bracketed by the 3-cycle, it will be trapped there forever. Outside M , all points on unit interval will be mapped to $(0, 1/2]$, except for 0. The points in the interval $(0, 1/(2\Lambda))$ approach M monotonically.

(c) It will land in $(\frac{1}{2}, \frac{\Lambda}{2})$.

(d) From (b), we know that except for $x_0 = 0$, all periodic orbits should be in M . By (c), we cannot have the substring 00 in a periodic orbit (except for the fixed point at 0). Hence $_00_$ is the only pruning block, and the symbolic dynamics is a finite subshift, with alphabet $\{0, 1\}$ and only one grammar rule: a consecutive repeat of symbol 0 is inadmissible.

(e) There are two exceptions. 0 is an isolated periodic orbit with itinerary $\bar{0}$. It is unstable and no point in its neighborhood returns to it, and it plays only an indirect role in the asymptotic dynamics. However, the 3-cycle in the figure is important, as it includes the critical point x_c and thus defines the attractor basin boundary. If it is labeled $\overline{010}$ (that is what it becomes if Λ is increased slightly) rather than $\overline{C10}$ (here 'C' is the symbol for the critical point), it also violates the $_00_$ pruning rule. (Y. Lan and P. Cvitanović)

Solution 11.7 - Binary 3-step transition matrix. (No solution available.)

Solution 11.8 - Full tent map periodic points. (a) For short cycles it is easy to solve the fixed point condition (11.11), with

$$f(\gamma) = \begin{cases} f_0(\gamma) = 2\gamma & \text{if } \gamma < 1/2 \\ f_1(\gamma) = 2(1 - \gamma) & \text{if } \gamma > 1/2 \end{cases} \quad (S.34)$$

directly. The 2-cycle periodic points satisfy $f_1 \circ f_0(\gamma_{01}) = 4(1 - \gamma_{01}) = \gamma_{01}$ the 3-cycle periodic points satisfy

$$\begin{aligned} f_1 \circ f_0 \circ f_0(\gamma_{001}) &= 2(1 - 4\gamma_{001}) = \gamma_{001} \\ f_1 \circ f_0 \circ f_0(\gamma_{011}) &= 2(1 - 2(1 - \gamma_{011})) = \gamma_{011}, \end{aligned}$$

etc., yielding periodic points $\{\gamma_{01}, \gamma_{01}\} = \{2/5, 4/5\}$, $\{\gamma_{001}, \gamma_{010}, \gamma_{100}\} = \{2/9, 4/9, 8/9\}$ $\{\gamma_{011}, \gamma_{110}, \gamma_{101}\} = \{2/7, 4/7, 6/7\}$. But this gets tedious quickly, while formula (11.12) is just a formula:

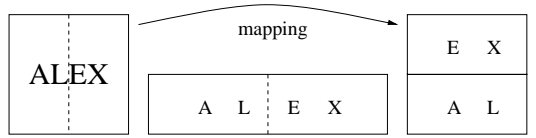
(b) $\{\gamma_{00111}, \gamma_{01110}, \gamma_{11100}, \gamma_{11001}, \gamma_{10011}\} = \{2/11, 4/11, 8/11, 6/11, 10/11\}$.

(c) $\{\gamma_{00001}, \gamma_{00010}, \gamma_{00100}, \gamma_{01000}, \gamma_{10000}\} = \{2/33, 4/33, 8/33, 16/33, 32/33\}$.

(d)

Chapter 12. Qualitative dynamics, for cyclists

Solution 12.3 - Slicing Danish without flipping. *The action of an orientation preserving baker map is given by*



with the right half sliced off and slid over the top of the left half. A formal way of writing the map is

$$T: [0, 1]^2 \rightarrow [0, 1]^2 \quad \text{with} \quad T(x, y) = \begin{cases} (2x, \frac{1}{2}y) & \text{if } x < \frac{1}{2} \\ (2x - 1, \frac{1}{2}y + \frac{1}{2}) & \text{if } \frac{1}{2} < x \end{cases} \pmod{0}.$$

It is immediate from the figure that a coding is obtained by symbols

$$0 \leftrightarrow \{x < 1/2\} \quad \text{and} \quad 1 \leftrightarrow \{x > 1/2\}$$

which correspond to the left and right half of the square, respectively. The corresponding symbolic dynamics is indicated in figure S.14, which shows the itineraries for up

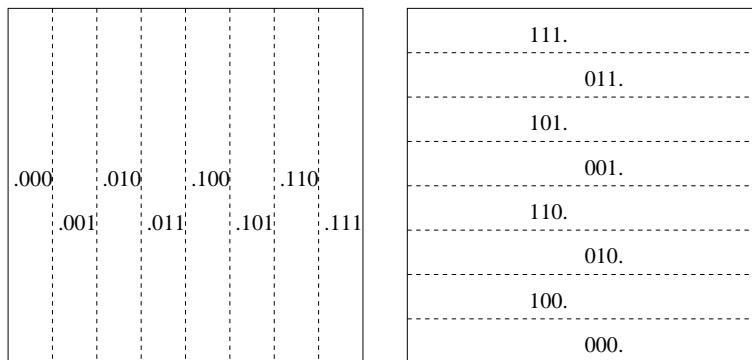


Figure S.14: Itineraries of three steps in forward (left figure) and backward (right figure) direction. The digits on the left of the decimal dot are the past, and the decimal on the right are the future starting with the current symbol.

to three steps in forward and backward direction. The slicing, orientation preserving baker map is simply a 2-dimensional version of the Bernoulli shift map (23.6), with the spatial ordering the same as the temporal ordering. (Alexander Grigo)

Solution 14.1 - Time reversibility. *A link between two nodes, say n_1 and n_2 , is present if and only if the map takes some points belonging to symbol n_1 to points with symbol n_2 . Thus for a fine enough partition there will be no symmetry between $n_1 \rightarrow n_2$ and $n_2 \rightarrow n_1$. As a simple example consider the rotation by a fixed angle α of the plane around the origin (which is a Hamiltonian map). If α is very small and positive,*

and if we partition the plane into three equal sectors about the origin, denoted by 1, 2, 3, then the corresponding transition graph has transition matrix

$$M = \begin{pmatrix} 1 & 1 & 0 \\ 0 & 1 & 1 \\ 1 & 0 & 1 \end{pmatrix}$$

which has no symmetry in forward/backward direction, i.e. $M \neq M^T$. Furthermore, the eigenvalues of M are $\Lambda = \{2, \frac{1}{2} \pm \frac{\sqrt{3}}{2}i\}$ hence are not all real.

To see that the transition matrices for Hamiltonian are not necessarily diagonalizable, consider the symplectic mappings of the plane $(x, y) \rightarrow (x, y - 1)$ or $(x, y) \rightarrow (2x, y/2)$. Choose two symbols, $1 \leftrightarrow \{y < 0\}$, $2 \leftrightarrow \{y > 0\}$, and $1 \leftrightarrow \{|x| > 1/4\}$, $2 \leftrightarrow \{|x| < 1/4\}$, respectively. Then in both cases the transition matrix reads

$$M = \begin{pmatrix} 1 & 1 \\ 0 & 1 \end{pmatrix}$$

which is not diagonalizable.

(Alexander Grigo)

Chapter 13. Fixed points, and how to get them

Solution 13.1 - Cycles of the Ulam map. *Minimizing (see chapter 29)*

$$F(x_1, \dots, x_n) = \frac{1}{n} \sum_{i=1}^n [f(x_i) - x_{i+1}]^2$$

using steepest decent

$$\begin{aligned} \nabla F &= \sum_{i=1}^N [f(x_i) - x_{i+1}] [f'(x_i) e_i - e_{i+1}] \\ &= \sum_{i=1}^N [f(x_i) - x_{i+1}] f'(x_i) e_i - \sum_{i=1}^N [f(x_{i-1}) - x_i] e_i \\ &= \sum_{i=1}^N [f(x_i) f'(x_i) - f(x_{i-1}) + x_i - x_{i+1} f'(x_i)] e_i \\ x^{(n+1)} &= x^{(n)} - \Delta\tau_n \frac{F(x^{(n)}) \nabla F(x^{(n)})}{\|\nabla F(x^{(n)})\|^2} \quad \text{with } \Delta\tau_n \in (0, 1], \end{aligned}$$

we can find periodic points of f of period N . The values of the Λ_n are chosen to be the least power of $1/2$ (including the power zero) such that the new point $x^{(n+1)}$ has all coordinates in the unit interval and has the same topological order with respect to the partition $\{(0, 1/2), (1/2, 1)\}$ as $x^{(n)}$.

p	x_1	Λ	p	x_1	x_2	Λ
0	0.0	2	01	0.3454915028	0.9045084972	-4
1	1.0	-2				
p	x_1	x_2	x_3	Λ		
001	0.1169777784	0.4131759111	0.9698463104	-8		
011	0.1882550991	0.611260467	0.9504844339	8		
p	x_1	x_2	x_3	x_4	Λ	
0001	0.03376388529	0.1304955414	0.4538658202	0.9914865498	-16	
0011	0.04322727119	0.1654346968	0.5522642317	0.9890738004	16	
0111	0.2771308221	0.8013173182	0.6368314951	0.9251085679	-16	

(Alexander Grigo)

Solution 13.2 - Cycles stabilities for the Ulam map, exact. *Since eigenvalues of the monodromy matrix corresponding to any periodic orbit are invariant under (reasonably smooth) change of coordinates we can use the following two observations to prove the claim. Let $U(x)$ denote the Ulam map, and let $T(x)$ denote the tent map.*

Firstly, note that the change of variables

$$x' = h(x) = \frac{1}{2} [1 + \sin(\pi (2x - 1))] = \frac{1 - \cos(\pi x)}{2}$$

satisfies

$$h(1 - |x|) = \frac{1 - \cos(\pi (1 - |x|))}{2} = \frac{1 + \cos(\pi |x|)}{2} = 1 - h(|x|) = 1 - h(x)$$

and therefore

$$\begin{aligned} U \circ h(x) &= 4h(x)[1-h(x)] = [1+\cos(\pi x)][1-\cos(\pi x)] = \sin(\pi x)^2 \\ h \circ T(x) &\equiv h(1-2|x-1/2|) = 1-h(2x-1) = 1 - \frac{1-\cos(\pi(2x-1))}{2} \\ &= \frac{1-\cos(2\pi x)}{2} = \sin(\pi x)^2, \end{aligned}$$

which shows that h conjugates T and U .

Secondly, the tent map $T(x) = 1-2|x-1/2|$ has derivative ± 2 everywhere (except, of course, at $x = 1/2$). The derivative is 2 on the left of $1/2$, i.e. on the symbol 0, and it is -2 on its right, i.e. on the symbol 1. Therefore the periodic orbit with symbolic representation $s_1 s_2 \dots s_N$ has the eigenvalue $\Lambda = (-1)^{\sum_{i=1}^N s_i} 2^N \equiv (-1)^{\#1} 2^N$, as was observed numerically. (Alexander Grigo)

Solution 13.3 - Stability of billiard cycles. The 2-cycle $\bar{0}$ stability (13.7) is the solution to both problems (provided you evaluate correctly the hyperbola curvature on the diagonal).

Solution 13.3 - Stability of billiard cycles. In both cases there is one periodic orbit, the 2-cycle along the shortest line segment connecting the two scatterers. The stability is given by the monodromy matrix

$$J = \left[- \begin{pmatrix} 1 & 0 \\ 2 & 1 \end{pmatrix} \begin{pmatrix} 1 & L \\ 0 & 1 \end{pmatrix} \right]^2 = \left[- \begin{pmatrix} 1 & L \\ 2 & 1+2L \end{pmatrix} \right]^2$$

with eigenvalues $\Lambda_u = [-(1+L+\sqrt{2L+L^2})]^2$ and $\Lambda_s = 1/\Lambda_u$.

For the billiard with the straight line and the hyperbola, the monodromy matrix reads

$$\begin{aligned} L &= \sqrt{2} \quad \text{and} \quad \kappa_{\text{hyperbola}} = \frac{y''(-1)}{\sqrt{1+y'(-1)^2}} = \frac{\sqrt{2}}{2} \\ \text{hence } J &= \begin{pmatrix} 1 & 0 \\ 2\kappa & 1 \end{pmatrix} \begin{pmatrix} 1 & 2L \\ 0 & 1 \end{pmatrix} = \begin{pmatrix} 1 & 0 \\ \sqrt{2} & 1 \end{pmatrix} \begin{pmatrix} 1 & 2\sqrt{2} \\ 0 & 1 \end{pmatrix} \\ &= \begin{pmatrix} 1 & 2\sqrt{2} \\ \sqrt{2} & 5 \end{pmatrix} \end{aligned}$$

with eigenvalues $\Lambda_u = 3+2\sqrt{2}$ and $\Lambda_s = 1/\Lambda_u$.

(Alexander Grigo)

Solution 13.4 - Numerical cycle routines. A number of sample Fortran programs for finding periodic orbits is available on ChaosBook.org/extras.

Solution 13.13 - Inverse iteration method for a Hamiltonian repeller. For the complete repeller case (all binary sequences are realized), the cycles can be evaluated variationally, as follows. According to (3.19), the coordinates of a periodic orbit of length n_p satisfy the equation

$$x_{p,i+1} + x_{p,i-1} = 1 - \alpha x_{p,i}^2, \quad i = 1, \dots, n_p, \quad (\text{S.35})$$

with the periodic boundary condition $x_{p,0} = x_{p,n_p}$.

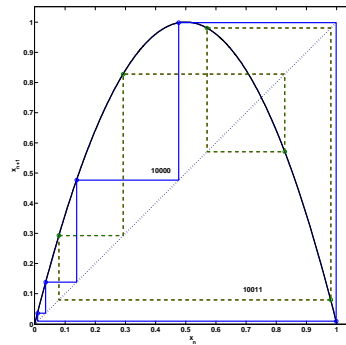
In the complete repeller case, the Hénon map is a realization of the Smale horseshoe, and the symbolic dynamics has a very simple description in terms of the binary alphabet $\epsilon \in \{0, 1\}$, $\epsilon_{p,i} = (1 + S_{p,i})/2$, where $S_{p,i}$ are the signs of the corresponding periodic point coordinates, $S_{p,i} = x_{p,i}/|x_{p,i}|$. We start with a preassigned sign sequence $S_{p,1}, S_{p,2}, \dots, S_{p,n_p}$, and a good initial guess for the coordinates $x'_{p,i}$. Using the inverse of the equation (13.26)

$$x''_{p,i} = S_{p,i} \sqrt{\frac{1 - x'_{p,i+1} - x'_{p,i-1}}{a}} \quad i = 1, \dots, n_p$$

we converge iteratively, at exponential rate, to the desired periodic points $x_{p,i}$. Given the periodic points, the cycle stabilities and periods are easily computed using (4.53). The itineraries and the stabilities of the short periodic orbits for the Hénon repeller (S.35) for $a = 6$ are listed in table ??; in actual calculations all prime cycles up to topological length $n = 20$ have been computed. (G. Vattay)

Solution 13.15 - Ulam map periodic points.

- (a) $\{x_{00111}, x_{01110}, x_{11100}, x_{11001}, x_{10011}\} = \{0.079373, 0.292292, 0.827430, 0.571157, 0.979746\}$
- (b) $\{x_{00001}, x_{00010}, x_{00100}, x_{01000}, x_{10000}\} = \{0.009036, 0.035816, 0.138132, 0.476209, 0.997736\}$
- (c)



D. Borrero

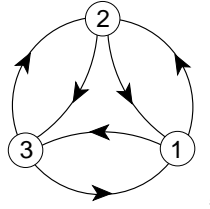
Chapter 14. Walkabout: Transition graphs

Solution 14.1 - Time reversibility.** *The answer is “no.” Work out a few simple Hamiltonian maps as counterexamples.*

Solution 14.2 - Alphabet {0,1}, prune $_1000_$, $_00100_$, $_01100_$ *This is worked out in the exercise itself.*

Chapter 15. Counting

Solution 15.1 - A transition matrix for 3-disk pinball. a) As the disk is convex, the transition to itself is forbidden. Therefore, the transition graph is



with the corresponding transition matrix

$$\mathbb{T} = \begin{pmatrix} 0 & 1 & 1 \\ 1 & 0 & 1 \\ 1 & 1 & 0 \end{pmatrix}.$$

Note that $\mathbb{T}^2 = \mathbb{T} + 2\mathbb{I}$. Suppose that $\mathbb{T}^n = a_n\mathbb{T} + b_n\mathbb{I}$, then

$$\mathbb{T}^{n+1} = a_n\mathbb{T}^2 + b_n\mathbb{T} = (a_n + b_n)\mathbb{T} + 2a_n\mathbb{I}.$$

So $a_{n+1} = a_n + b_n$, $b_{n+1} = 2a_n$ with $a_1 = 1$, $b_1 = 0$.

b) From a) we have $a_{n+1} = a_n + 2a_{n-1}$. Suppose that $a_n \propto \lambda^n$. Then $\lambda^2 = \lambda + 2$. Solving this equation and using the initial condition for $n = 1$, we obtain the general formula

$$\begin{aligned} a_n &= \frac{1}{3}(2^n - (-1)^n), \\ b_n &= \frac{2}{3}(2^{n-1} + (-1)^n). \end{aligned}$$

c) \mathbb{T} has eigenvalues $\{2, -1, -1\}$. So the topological entropy is $\ln 2$, the same as in the case of the binary symbolic dynamics. (Y. Lan)

Solution 15.3 - Sum of A_{ij} is like a trace. Suppose that $A\phi_k = \lambda_k\phi_k$, where λ_k, ϕ_k are eigenvalues and eigenvectors, respectively. Expressing the vector $v = (1, 1, \dots, 1)^t$ in terms of the eigenvectors ϕ_k , i.e., $v = \sum_k d_k\phi_k$, we have

$$\begin{aligned} \Gamma_n &= \sum_{ij}[A^n]_{ij} = v^t A^n v = \sum_k v^t A^n d_k\phi_k = \sum_k d_k \lambda_k^n (v^t\phi_k) \\ &= \sum_k c_k \lambda_k^n, \end{aligned}$$

where $c_k = (v^t\phi_k)d_k$ are constants.

a) As $\text{tr } A^n = \sum_k \lambda_k^n$, it is easy to see that both $\text{tr } A^n$ and Γ_n are dominated by the largest eigenvalue λ_0 . That is

$$\frac{\ln |\text{tr } A^n|}{\ln |\Gamma_n|} = \frac{n \ln |\lambda_0| + \ln |\sum_k (\frac{\lambda_k}{\lambda_0})^n|}{n \ln |\lambda_0| + \ln |\sum_k d_k (\frac{\lambda_k}{\lambda_0})^n|} \rightarrow 1 \text{ as } n \rightarrow \infty.$$

b) The nonleading eigenvalues do not need to be distinct, as the ratio in a) is controlled by the largest eigenvalues only. (Y. Lan)

Solution 15.5 - Transition matrix and cycle counting. a) According to the definition of \mathbb{T}_{ij} , the transition matrix is

$$\mathbb{T} = \begin{pmatrix} a & c \\ b & 0 \end{pmatrix}.$$

b) All walks of length three 0000, 0001, 0010, 0100, 0101, 1000, 1001, 1010 (four symbols!) with weights $aaa, aac, acb, cba, cbc, baa, bac, bcb$. Let's calculate \mathbb{T}^3 ,

$$\mathbb{T}^3 = \begin{pmatrix} a^3 + 2abc & a^2c + bc^2 \\ a^2b + b^2c & abc \end{pmatrix}.$$

There are altogether 8 terms, corresponding exactly to the terms in all the walks.

c) Let's look at the following equality

$$\mathbb{T}_{ij}^n = \sum_{k_1, k_2, \dots, k_{n-1}} \mathbb{T}_{ik_1} \mathbb{T}_{k_1 k_2} \cdots \mathbb{T}_{k_{n-1} j}.$$

Every term in the sum is a possible path from i to j , though the weight could be zero. The summation is over all possible intermediate points ($n - 1$ of them). So, \mathbb{T}_{ij}^n gives the total weight (probability or number) of all the walks from i to j in n steps.

d) We take $a = b = c = 1$ to just count the number of possible walks in n steps. This is the crudest description of the dynamics. Taking a, b, c as transition probabilities would give a more detailed description. The eigenvalues of \mathbb{T} is $(1 \pm \sqrt{5})/2$, so we get $N(n) \propto \left(\frac{1+\sqrt{5}}{2}\right)^n$.

e) The topological entropy is then $\ln \frac{1+\sqrt{5}}{2}$. (Y. Lan)

Solution 15.7 - "Golden mean" pruned map. It is easy to write the transition matrix \mathbb{T}

$$\mathbb{T} = \begin{pmatrix} 0 & 1 \\ 1 & 1 \end{pmatrix}.$$

The eigenvalues are $(1 \pm \sqrt{5})/2$. The number of periodic orbits of length n is the trace

$$\mathbb{T}^n = \frac{(1 + \sqrt{5})^n + (1 - \sqrt{5})^n}{2^n}.$$

(Y. Lan)

Solution 15.2 - 3-disk prime cycle counting. The formula for arbitrary length cycles is derived in sect. 15.4.

Solution 15.10 - Whence Möbius function? Written out $f(n)$ line-by-line for a few values of n , (15.43) yields

$$\begin{aligned}
 f(1) &= g(1) \\
 f(2) &= g(2) + g(1) \\
 f(3) &= g(3) + g(1) \\
 f(4) &= g(4) + g(2) + g(1) \\
 &\dots \\
 f(6) &= g(6) + g(3) + g(2) + g(1) \\
 &\dots
 \end{aligned}
 \tag{S.36}$$

Now invert recursively this infinite tower of equations to obtain

$$\begin{aligned}
 g(1) &= f(1) \\
 g(2) &= f(2) - f(1) \\
 g(3) &= f(3) - f(1) \\
 g(4) &= f(4) - [f(2) - f(1)] - f(1) = f(4) - f(2) \\
 &\dots \\
 g(6) &= f(6) - [f(3) - f(1)] - [f(2) - f(1)] - f(1) \\
 &\dots
 \end{aligned}$$

We see that $f(n)$ contributes with factor -1 if n prime, and not at all if n contains a prime factor to a higher power. This is precisely the *raison d'etre* for the Möbius function, with whose help the inverse of (15.43) can be written as the Möbius inversion formula [29] (15.44).

Solution 15.16 - Alphabet $\{a, b, c\}$, prune $_ab_$. This pruning rule implies that any string of “b”s must be preceded by a “c;” so one possible alphabet is $\{a, cb^k; \bar{b}\}$, $k=0,1,2,\dots$. As the rule does not prune the fixed point \bar{b} , it is explicitly included in the list. The cycle expansion (15.15) becomes

$$\begin{aligned}
 1/\zeta &= (1 - t_a)(1 - t_b)(1 - t_c) \times \\
 &\quad (1 - t_{cb})(1 - t_{ac})(1 - t_{cbb}) \dots \\
 &= 1 - t_a - t_b - t_c + t_a t_b - (t_{cb} - t_c t_b) \\
 &\quad - (t_{ac} - t_a t_c) - (t_{cbb} - t_{cb} t_b) \dots
 \end{aligned}$$

The effect of pruning $_ab_$ is to unbalance the 2-cycle curvature $t_{ab} - t_a t_b$; the remainder of the cycle expansion retains the curvature form.

Solution 15.18 - Alphabet $\{0,1\}$, prune $_1000_$, $_00100_$, $_01100_$.

step 1. $_1000_$ prunes all cycles with a $_000_$ subsequence with the exception of the fixed point $\bar{0}$; hence we factor out $(1 - t_0)$ explicitly, and prune $_000_$ from the rest. Physically this means that x_0 is an isolated fixed point - no cycle stays in its vicinity for more than 2 iterations. In the notation of exercise 15.17, the alphabet is $\{1, 2, 3; \bar{0}\}$, and the remaining pruning rules have to be rewritten in terms of symbols $2=10, 3=100$:

step 2. alphabet $\{1, 2, 3; \bar{0}\}$, prune $\underline{33}$, $\underline{213}$, $\underline{313}$. Physically, the 3-cycle $\bar{3} = 100$ is pruned and no long cycles stay close enough to it for a single $\underline{100}$ repeat. As in exercise 15.6, prohibition of $\underline{33}$ is implemented by dropping the symbol "3" and extending the alphabet by the allowed blocks 13, 23:

step 3. alphabet $\{1, 2, \underline{13}, \underline{23}; \bar{0}\}$, prune $\underline{213}$, $\underline{2313}$, $\underline{1313}$, where $\underline{13} = 13$, $\underline{23} = 23$ are now used as single letters. Pruning of the repetitions $\underline{1313}$ (the 4-cycle $\underline{13} = \underline{1100}$ is pruned) yields the

Result: alphabet $\{1, 2, \underline{23}, \underline{113}; \bar{0}\}$, unrestricted 4-ary dynamics. The other remaining possible blocks $\underline{213}$, $\underline{2313}$ are forbidden by the rules of step 3. The topological zeta function is given by

$$1/\zeta = (1 - t_0)(1 - t_1 - t_2 - t_{23} - t_{113}) \quad (\text{S.37})$$

for unrestricted 4-letter alphabet $\{1, 2, \underline{23}, \underline{113}\}$.

Chapter 16. Transporting densities

Solution 16.1 - Integrating over Dirac delta functions. (a) Whenever $h(x)$ crosses 0 with a nonzero velocity ($\det \partial_x h(x) \neq 0$), the delta function contributes to the integral. Let $x_0 \in h^{-1}(0)$. Consider a small neighborhood V_0 of x_0 so that $h : V_0 \rightarrow V_0$ is a one-to-one map, with the inverse function $x = x(h)$. By changing variable from x to h , we have

$$\begin{aligned} \int_{V_0} dx \delta(h(x)) &= \int_{h(V_0)} dh |\det \partial_x h| \delta(h) = \int_{h(V_0)} dh \frac{1}{|\det \partial_x h|} \delta(h) \\ &= \frac{1}{|\det \partial_x h|_{h=0}}. \end{aligned}$$

Here, the absolute value $|\cdot|$ is taken because delta function is always positive and we keep the orientation of the volume when the change of variables is made. Therefore all the contributions from each point in $h^{-1}(0)$ add up to the integral

$$\int_{\mathbb{R}^d} dx \delta(h(x)) = \sum_{x \in h^{-1}(0)} \frac{1}{|\det \partial_x h|}.$$

Note that if $\det \partial_x h = 0$, then the delta function integral is not well defined.

(b) The formal expression can be written as the limit

$$F := \int_{\mathbb{R}} dx \delta(x^2) = \lim_{\sigma \rightarrow 0} \int_{\mathbb{R}} dx \frac{e^{-\frac{x^4}{2\sigma}}}{\sqrt{2\pi\sigma}},$$

by invoking the approximation given in the exercise. The change of variable $y = x^2 / \sqrt{\sigma}$ gives

$$F = \lim_{\sigma \rightarrow 0} \sigma^{-3/4} \int_{\mathbb{R}^+} dy \frac{e^{-\frac{y^2}{2}}}{\sqrt{2\pi y}} = \infty,$$

where \mathbb{R}^+ represents the positive part of the real axis. So, the formal expression does not make sense. The zero derivative of x^2 at $x = 0$ invalidates the expression in (a). (Y. Lan)

Solution 16.2 - Derivatives of Dirac delta functions. We do this problem just by direct evaluation. We denote by Ω_y a sufficiently small neighborhood of y . (a)

$$\begin{aligned} \int_{\mathbb{R}} dx \delta'(y) &= \sum_{x \in y^{-1}(0)} \int_{\Omega_y} dy \det \left(\frac{dy}{dx} \right)^{-1} \delta'(y) \\ &= \sum_{x \in y^{-1}(0)} \frac{\delta(y)}{|y'|} \Big|_{-\epsilon}^{\epsilon} - \int_{\Omega_y} dy \frac{\delta(y)}{y'^2} (-y'') \frac{1}{y'} \\ &= \sum_{x \in y^{-1}(0)} \frac{y''}{|y'| y'^2}, \end{aligned}$$

where the absolute value is taken to take care of the sign of the volume.

(b)

$$\begin{aligned}
\int_{\mathbb{R}} dx \delta^{(2)}(y) &= \Sigma_{x \in y^{-1}(0)} \int_{\Omega_y} dy \frac{\delta^{(2)}(y)}{y'} \\
&= \Sigma_{x \in y^{-1}(0)} \frac{\delta'(y)}{|y'|} \Big|_{-\epsilon}^{\epsilon} - \int_{\Omega_y} dy \frac{\delta'(y)}{y'^2} (-y'') \frac{1}{y'} \\
&= \Sigma_{x \in y^{-1}(0)} \frac{y'' \delta(y)}{|y'| y'^2} \Big|_{-\epsilon}^{\epsilon} - \int_{\Omega_y} dy \delta(y) \frac{d}{dx} \left(\frac{y''}{y'^3} \right) \frac{1}{y'} \\
&= \Sigma_{x \in y^{-1}(0)} - \int_{\Omega_y} dy \delta(y) \left(\frac{y'''}{y'^3} - 3 \frac{y''^2}{y'^4} \right) \frac{1}{y'} \\
&= \Sigma_{x \in y^{-1}(0)} \left(3 \frac{y''^2}{y'^4} - \frac{y'''}{y'^3} \right) \frac{1}{|y'|}.
\end{aligned}$$

(c)

$$\begin{aligned}
\int_{\mathbb{R}} dx b(x) \delta^{(2)}(y) &= \Sigma_{x \in y^{-1}(0)} \int_{\Omega_y} dy b(x) \frac{\delta^{(2)}(y)}{y'} \\
&= \Sigma_{x \in y^{-1}(0)} \frac{b(x) \delta'(y)}{|y'|} \Big|_{-\epsilon}^{\epsilon} - \int_{\Omega_y} dy \delta'(y) \frac{d}{dx} \left(\frac{b}{y'} \right) \frac{1}{y'} \\
&= \Sigma_{x \in y^{-1}(0)} - \delta(y) \frac{d}{dx} \left(\frac{b}{y'} \right) \frac{1}{y'} \Big|_{-\epsilon}^{\epsilon} + \int_{\Omega_y} dy \delta(y) \frac{d}{dx} \left(\frac{d}{dx} \left(\frac{b}{y'} \right) \frac{1}{y'} \right) \\
&= \Sigma_{x \in y^{-1}(0)} \frac{1}{|y'|} \frac{d}{dx} \left(\frac{b'}{y'^2} - \frac{b y''}{y'^3} \right) \\
&= \Sigma_{x \in y^{-1}(0)} \frac{1}{|y'|} \left[\frac{b''}{y'^2} - \frac{b' y''}{y'^3} - 2 \frac{b' y''}{y'^3} + b \left(3 \frac{y''^2}{y'^4} - \frac{y'''}{y'^3} \right) \right] \\
&= \Sigma_{x \in y^{-1}(0)} \frac{1}{|y'|} \left[\frac{b''}{y'^2} - 3 \frac{b' y''}{y'^3} + b \left(3 \frac{y''^2}{y'^4} - \frac{y'''}{y'^3} \right) \right].
\end{aligned}$$

(Yueheng Lan)

Solution 16.3 - \mathcal{L}^t generates a semigroup. Every “sufficiently good” transformation f^t in state space M is associated with a Perron-Frobenius operator \mathcal{L}^t which is when acting on a function $\rho(x)$ in \mathcal{M}

$$\mathcal{L}^t \cdot \rho(x) = \int_{\mathcal{M}} dy \delta(x - f^t(y)) \rho(y).$$

In some proper function space \mathcal{F} on \mathcal{M} , the one parameter family of operators $\{\mathcal{L}^t\}_{t \in \mathbb{R}^+}$ generate a semigroup. Let's check this statement. For any $t_1, t_2 > 0$ and $\rho \in \mathcal{F}$, the product “ \circ ” of two operators is defined as usual

$$(\mathcal{L}^{t_1} \circ \mathcal{L}^{t_2}) \cdot \rho(y) = \mathcal{L}^{t_1} \cdot (\mathcal{L}^{t_2} \cdot \rho)(y).$$

So, we have

$$(\mathcal{L}^{t_1} \circ \mathcal{L}^{t_2})(y, x) = \int_{\mathcal{M}} dz \mathcal{L}^{t_1}(y, z) \mathcal{L}^{t_2}(z, x)$$

$$\begin{aligned}
&= \int_{\mathcal{M}} dz \delta(y - f^{t_1}(z)) \delta(z - f^{t_2}(x)) \\
&= \delta(y - f^{t_1}(f^{t_2}(x))) \\
&= \delta(y - f^{t_1+t_2}(x)) \\
&= \mathcal{L}^{t_1+t_2}(y, x),
\end{aligned}$$

where the semigroup property $f^{t_1}(f^{t_2}(x)) = f^{t_1+t_2}(x)$ of f^t has been used. This proves the claim in the title. (Y. Lan)

Solution 16.5 - Invariant measure. Hint: We do (a),(b),(c),(d) for the first map and (e) for the second.

(a) The partition point is in the middle of $[0, 1]$. If the density on the two pieces are two constants ρ_0^A and ρ_0^B , respectively, the Perron-Frobenius operator still leads to the piecewise constant density

$$\rho_1^A = \frac{1}{2}(\rho_0^A + \rho_0^B), \quad \rho_1^B = \frac{1}{2}(\rho_0^A + \rho_0^B).$$

In general, if a finite Markov partition exists and the map is linear on each partition cell, a finite-dimensional invariant subspace which is a piecewise constant function can always be identified in the function space.

(b) From the discussion of (a), any constant function on $[0, 1]$ is an invariant measure. If we consider the invariant probability measure, then the constant has to be 1.

(c) As the map is invariant in $[0, 1]$ (there is no escaping), the leading eigenvalue of \mathcal{L} is always 1 due to the “mass” conservation.

(d) Take a typical point on $[0, 1]$ and record its trajectory under the first map for some time (10^5 steps). Plot the histogram...ONLY 0 is left finally!! This happens because of the finite accuracy of the computer arithmetics. A small trick is to change the slope 2 to 1.999999999. You will find a constant measure on $[0, 1]$ which is the natural measure. Still, the finite precision of the computer will make every point eventually periodic and strictly speaking the measure is defined only on subsets of lattice points. But as the resolution improves, the computer-generated measure steadily approaches the natural measure. For the first map, any small deviation from the constant profile will be stretched and smeared out. So, the natural measure has to be constant.

(e) Simple calculation shows that α is the partition point. We may use A, B to mark the left and right part of the partition, respectively. A maps to B and B maps to the whole interval $[0, 1]$. As the magnitude of the slope $\Lambda = (\sqrt{5} + 1)/2$ is greater than 1, we may expect the natural measure is still piecewise constant with eigenvalue 1. The determining equation is

$$\begin{pmatrix} 0 & 1/\Lambda \\ 1/\Lambda & 1/\Lambda \end{pmatrix} \begin{pmatrix} \rho^A \\ \rho^B \end{pmatrix} = \begin{pmatrix} \rho^A \\ \rho^B \end{pmatrix},$$

which gives $\rho^B/\rho^A = \Lambda$.

For the second map, the construction of Exercise 15.7 is worth a look. (Y. Lan)

Solution 16.4 - The escape rate is the leading zero of the zeta function

$$0 = 1/\zeta(\gamma) = 1 - e^\gamma/2a - e^\gamma/2a = 1 - e^\gamma/a.$$

So, $\gamma = \log(a)$ if $a > a_c = 1$ and $\gamma = 0$ otherwise. For $a \approx a_c$ the escape rate behaves like

$$\gamma(a) \approx (a - a_c).$$

Solution 16.7 - Eigenvalues of the skew full tent map Perron-Frobenius operator. If we have density $\rho_n(x)$, the action of the Perron-Frobenius operator associated with $f(x)$ gives a new density

$$\rho_{n+1}(x) = \frac{1}{\Lambda_0} \rho_n(x/\Lambda_0) + \frac{1}{\Lambda_1} \rho_n(1 - x/\Lambda_1),$$

where $\Lambda_1 = \frac{\Lambda_0}{\Lambda_0 - 1}$. The eigenvalue equation is given by

$$\rho_{n+1}(x) = \lambda \rho_n(x). \tag{S.38}$$

We may solve it by assuming that the eigenfunctions are N -th order polynomials $P(N)$ (check it). Indeed, detailed calculation gives the following results:

- $P(0)$ gives $\lambda = 1$, corresponding to the expected leading eigenvalue.
- $P(1)$ gives $\lambda = \frac{1}{\Lambda_0^2} - \frac{1}{\Lambda_1^2} = \frac{2}{\Lambda_0} - 1$,
- $P(2)$ gives $\lambda = \frac{1}{\Lambda_0^3} + \frac{1}{\Lambda_1^3}$,
- $P(3)$ gives $\lambda = \frac{1}{\Lambda_0^4} - \frac{1}{\Lambda_1^4}$,
- The guess is that $P(N)$ gives $\lambda = \frac{1}{\Lambda_0^{N+1}} + (-1)^N \frac{1}{\Lambda_1^{N+1}}$.

The final solution is that the piecewise linear function $\rho^A = -\Lambda_0, \rho^B = \Lambda_1$ gives the eigenvalue 0. If only the continuous functions are considered, this kind of eigenfunction of course should not be included. (Y. Lan)

Solution 16.7 - Eigenvalues of the skew full tent map Perron-Frobenius operator. The first few eigenvalues are

$$\begin{aligned} e^{s_0} &= 1, & e^{s_1} &= \frac{2}{\Lambda_0} - 1 \\ e^{s_2} &= \frac{1}{4} + \frac{3}{4} \left(\frac{2}{\Lambda_0} - 1 \right)^2, & e^{s_3} &= \frac{1}{2} \left(\frac{2}{\Lambda_0} - 1 \right) + \frac{1}{2} \left(\frac{2}{\Lambda_0} - 1 \right)^3 \dots \end{aligned}$$

For eigenvectors (invariant densities for skew tent maps), see for example L. Billings and E.M. Bolt [14].

Solution 16.10 - \mathcal{A} as a generator of translations. If v is a constant in space, Taylor series expansion gives

$$a(x + tv) = \sum_{k=0}^{\infty} \frac{1}{k!} (tv \frac{\partial}{\partial x})^k a(x) = e^{tv \frac{\partial}{\partial x}} a(x).$$

(Y. Lan)

Chapter 17. Averaging

Solution 17.1 - How unstable is the Hénon attractor?

1. Evaluate numerically the Lyapunov exponent by iterating the Hénon map; For $a = 1.4$, $b = 0.3$ the answer should be close to $\lambda = 0.41922\dots$. If you have a good estimate and a plot of the convergence of your estimate with t , please send us your results for possible inclusion into this text.
2. Both Lyapunov exponents for $a = 1.39945219$, $b = 0.3$ are negative, roughly $\lambda_1 = -0.2712$, $\lambda_2 = -0.9328$ (check that these values respect the constant volume contraction condition (4.54) for the Hénon map). Why? Because after a long transient exploration of the Hénon map's non-wandering set, on average after some 11,000 iterates, almost every initial point falls into a stable 13-cycle. You can check its existence by starting at one of its periodic points $(x_p, y_p) = (-0.2061, -0.3181)$.

If you missed the stable 13-cycle (as all students in one of the courses did), you should treat your computer experiments with great deal of scepticism.

As the product of eigenvalues is the constant $-b$, you need to evaluate only the expanding eigenvalue. There are many ways to implement this calculation - here are a few:

1. The most naive way - take the log of distance of two nearby trajectories, iterate until you run out of accuracy. Try this many times, estimate an average.
2. Slightly smarter: as above, but keep rescaling the length of the vector connecting neighboring points so it remains small, average over the sum of logs of rescaling factors. You can run this forever.
3. Keep multiplying the $[2 \times 2]$ Jacobian stability matrix (4.53) until you run out of accuracy. Compute the log of the leading eigenvalue try this many times, estimate an average.
4. Slightly smarter still: as above, but start with an arbitrary initial tangent space vector, keep multiplying it with the Jacobian stability matrix, and rescaling the length of the vector so it remains small. You can run this forever.
5. There is probably no need to use the QR decomposition method or any other such numerical method for this 2-dimensional problem.

(Y. Lan and P. Cvitanović)

Solution 17.4 - Rössler attractor Lyapunov exponents. J. Sprott: $\{\lambda_1, \lambda_2, \lambda_3\} = \{0.0714, 0, -5.3943\}$

Chapter 18. Trace formulas

(No solutions available.)

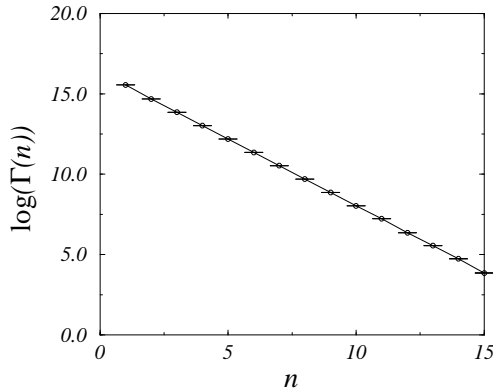


Figure S.15: Plot of $\log(\Gamma(n))$ versus n for the logistic map $x_{n+1} = 6x_n(1 - x_n)$. Error bars show estimated errors in the mean assuming a binomial distribution. 10 000 000 random initial starting points were used.

Chapter 19. Spectral determinants

Solution 19.1 - Numerical estimate of the escape rate for a 1-dimensional repeller

The logistic map is defined by $x_{n+1} = Ax_n(1 - x_n)$. For $A \leq 4$ any point in the unit interval $[0, 1]$ will remain in the interval forever. For $A > 4$ almost all points starting in the unit interval will eventually escape towards $-\infty$.

The rate of escape can be easily measured by numerical experiment. We define the fraction of initial conditions that leave the interval after n iterations to be Γ_n . Figure S.15 shows a plot of $\log(\Gamma_n)$ versus n , computed by starting with 10 000 000 random initial points. Asymptotically the escape rate falls off exponentially as

$$\Gamma(n) = Ce^{-\gamma n}.$$

Figure S.15 suggests that this formula is very accurate even for relatively small n . We estimate γ by measuring the slope of the curve in figure S.15. To avoid errors due to rounding and transients only the points $5 \leq n \leq 10$ were used. A linear regression fit yields the escape rate for $A = 6$:

$$\gamma = 0.8315 \pm 0.0001,$$

where the error is from statistical fluctuations (there may be systematic errors either due to rounding or because we are not in the true asymptotic regime).

(Adam Prügel-Bennet)

Solution 19.3 - Dynamical zeta functions

1. Work through section sect. 19.3.2.
2. Generalize the transition matrix (14.10) to a transfer operator.

Solution 19.2 - Spectrum of the “golden mean” pruned map.

1. The idea is that with the redefinition $2 = 10$, the alphabet $\{1, 2\}$ is unrestricted binary, and due to the piecewise linearity of the map, the stability weights factor in a way similar to (18.11).

2. As in (19.9), the spectral determinant for the Perron-Frobenius operator takes form (19.11)

$$\det(1 - z\mathcal{L}) = \prod_{k=0}^{\infty} \frac{1}{\zeta_k}, \quad \frac{1}{\zeta_k} = \prod_p \left(1 - \frac{z^{n_p}}{|\Lambda_p| \Lambda_p^k} \right).$$

The mapping is piecewise linear, so the form of the topological zeta function worked out in (15.19) already suggests the form of the answer. The alphabet $\{1,2\}$ is unrestricted binary, so the dynamical zeta functions receive contributions only from the two fixed points, with all other cycle contributions cancelled exactly. The $1/\zeta_0$ is the spectral determinant for the transfer operator like the one in (17.19) with the $T_{00} = 0$, and in general

$$\begin{aligned} \frac{1}{\zeta_k} &= \left(1 - \frac{z}{|\Lambda_1| \Lambda_1^k} \right) \left(1 - \frac{z^2}{|\Lambda_2| \Lambda_2^k} \right) \left(1 - \frac{z^3}{|\Lambda_{12}| \Lambda_{12}^k} \right) \cdots \\ &= 1 - (-1)^k \left(\frac{z}{\Lambda^{k+1}} + \frac{z^2}{\Lambda^{2k+2}} \right). \end{aligned} \quad (\text{S.39})$$

The factor $(-1)^k$ arises because both stabilities Λ_1 and Λ_2 include a factor $-\Lambda$ from the right branch of the map.

Solution 19.6 - Dynamical zeta functions as ratios of spectral determinants. Try inserting a factor equal to one in the zeta function and then expanding it. The problem is solved in sect. 19.5.

Solution 19.9 - Dynamical zeta functions for Hamiltonian maps. Read example 19.7.

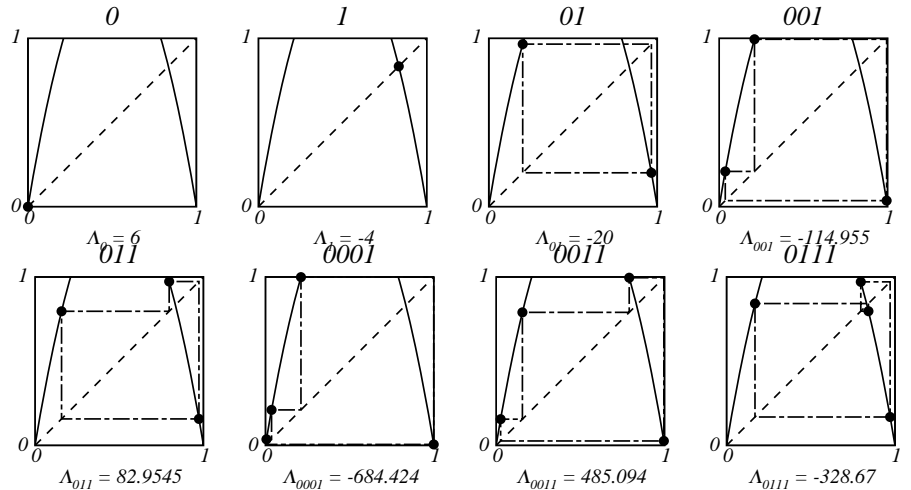


Figure S.16: Periodic orbits and stabilities for the logistics equation $x_{n+1} = 6x_n(1 - x_n)$.

Chapter 20. Cycle expansions

Solution 20.2 - Prime cycles for a 1 – dimensional repeller, analytic formulas. For the logistic map the prime cycles, ordered in terms of their symbolic dynamics, are listed in table 15.1

$$\mathbf{P} = \{0, 1, 01, 001, 011, 0001, 0011, 0111, \dots\}$$

The position of the prime cycles can be found by iterating the inverse mapping. If we wish to find the position of a prime orbit $p = b_1 b_2 \dots b_{n_p}$, where $b_i \in \{0, 1\}$, then starting from some initial point, $x = 1/2$ say, we apply one of the inverse mappings

$$f_{\pm}^{-1}(x) = \frac{1}{2} \pm \frac{1}{2} \sqrt{1 - x/4A}$$

where we choose f_-^{-1} if $b_1 = 0$ or f_+^{-1} if $b_1 = 1$. We then apply the inverse mapping again depending on the next element in the prime orbit. Repeating this procedure many times we converge onto the prime cycle. The stability Λ_p of a prime cycle p is given by the product of slopes of f around the cycle. The first eight prime cycles are shown in figure S.16.

The stabilities of the first five prime orbits can be calculated for arbitrary A . We find that $\Lambda_0 = A$, $\Lambda_1 = 2 - A$, $\Lambda_{01} = 4 + 2A - A^2$, and

$$\Lambda_{011} = 8 + 2A - A^2 \pm A(2 - A) \sqrt{A^2 - 2A - 7}. \tag{S.40}$$

There is probably a closed form expression for the 4-cycles as well.

For crosschecking purposes: if $A = 9/2$, $\Lambda_0 = 9/2$, $\Lambda_1 = -5/2$, $\Lambda_{01} = -7.25$, $\Lambda_{011} = 19.942461 \dots$

(Adam Prügel-Bennet)

Solution 20.2 - Dynamical zeta function for a 1 – dimensional repeller The escape rate can be estimated from the leading zero in the dynamical zeta function $1/\zeta(z)$, defined by

$$1/\zeta(z) = \prod_p (1 - z^{n_p}/|\Lambda_p|).$$

To compute the position of this pole we expand $1/\zeta(z)$ as a power series (20.7) in z .

$$1/\zeta(z) = 1 - \sum_{i=1} \hat{c}_i z^i$$

where

$$\begin{aligned} \hat{c}_1 &= |\Lambda_0|^{-1} + |\Lambda_1|^{-1}, & \hat{c}_2 &= |\Lambda_{01}|^{-1} - |\Lambda_1 \Lambda_0|^{-1} \\ \hat{c}_3 &= |\Lambda_{001}|^{-1} - |\Lambda_0 \Lambda_{01}|^{-1} + |\Lambda_{011}|^{-1} - |\Lambda_{01} \Lambda_1|^{-1} \end{aligned}$$

etc.. Using the cycles up to length 6 we get

$$\begin{aligned} 1/\zeta(z) &= 1 - 0.416667z - 0.00833333z^2 \\ &\quad + 0.000079446z^3 - 9.89291 \times 10^{-7}z^4 + \dots \end{aligned}$$

The leading zero of this Taylor series is an estimate of $\exp(\gamma)$. Using $n = 1, 2, 3$ and 4 we obtain the increasingly accurate estimates for γ : $0.875469, 0.830597, 0.831519$ and 0.831492 . In a hope to improve the convergence we can use the Padé approximates $P_M^N(z) = \sum_{i=1}^N p_i z^i / (1 + \sum_{j=1}^M q_j z^j)$. Using the Padé approximates $P_1^{n-1}(z)$ for $n = 2, 3$ and 4 we obtain the estimates $0.828585, 0.831499$ and 0.831493 .

The above results correspond to $A = 6$; in the $A = 9/2$ case the leading zero is $1/z = 1.43549\dots$ and $\gamma = 0.36150\dots$ (Adam Prügel-Bennet)

Solution 20.2 - Spectral determinant for a 1 – dimensional repeller We are told the correct expression for the escape rate is also given by the logarithm of the leading zero of the spectral determinant (19.11), expanded as the Taylor series (20.11). The coefficients c_i should fall off super-exponentially so that truncating the Taylor series is expected to give a far more accurate estimate of the escape rate than using the dynamical zeta function. How do we compute the c_i coefficients in (20.11)? One straightforward method is to first compute the Taylor expansion of $\log(F(z))$

$$\begin{aligned} \log(F(z)) &= \sum_p \sum_{k=0} \log\left(1 - \frac{t_p}{\Lambda_p^k}\right) = - \sum_p \sum_{k=0} \sum_{r=1} \frac{t_p^r}{\Lambda_p^{kr}} \\ &= - \sum_p \sum_{r=1} \frac{t_p^r}{1 - \Lambda_p^{-r}} = - \sum_p \sum_{r=1} B_p(r) z^{n_p r} \end{aligned}$$

where $B_p(r) = -1/r |\Lambda_p^r| (1 + \Lambda_p^{-r})$. Writing $\log(F(z))$ as a power series

$$\log(F(z)) = - \sum_{i=1} b_i z^i$$

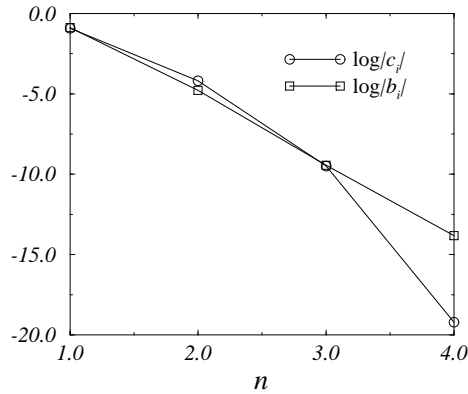


Figure S.17: Plot of the Taylor coefficients for the spectral determinant, c_i , and for the dynamical zeta function, b_i .

we obtain

$$\begin{aligned}
 b_1 &= B_0(1) + B_1(1) \\
 b_2 &= B_{01}(1) + B_0(2) + B_1(2) \\
 b_3 &= B_{001}(1) + B_{011}(1) + B_0(3) + B_1(3) \\
 b_3 &= B_{0001}(1) + B_{0011}(1) + B_{0111}(1) + B_{01}(2) + B_0(4) + B_1(4)
 \end{aligned} \tag{S.41}$$

etc.. To obtain the coefficients for the spectral determinant we solve

$$F(z) = 1 - \sum_{i=1} Q_i z^i = \exp\left(\sum_{i=1} b_i z^i\right)$$

for the Q_i 's. This gives

$$\begin{aligned}
 Q_1 &= b_1, \quad Q_2 = b_2 + b_1^2/2, \quad Q_3 = b_3 + b_1 b_2 + b_1^3/6 \\
 Q_4 &= b_4 + b_1 b_3 + b_2^2/2 + b_2 b_1^2/2 + b_1^4/24
 \end{aligned}$$

Using these formulas we find

$$F(z) = 1 - 0.4z - 0.0152381z^2 - 0.0000759784z^3 + 4.5311 \times 10^{-9}z^4 + \dots$$

The logarithm of the leading zero of $F(z)$ again gives the escape rate. Using the $n = 1, 2, 3,$ and 4 truncations we find the approximation to γ of $0.916291, 0.832345, 0.83149289$ and 0.8314929875 . As predicted, the convergence is much faster for the spectral determinant than for the dynamical zeta function.

In figure S.17 we show a plot of the logarithm of the coefficients for the spectral determinant and for the dynamical zeta function.

(Adam Prügel-Bennet)

The above results correspond to $A = 6$; in the $A = 9/2$ case all cycles up to length 10 yield $\gamma = 0.36150966984250926 \dots$
(Vadim Moroz)

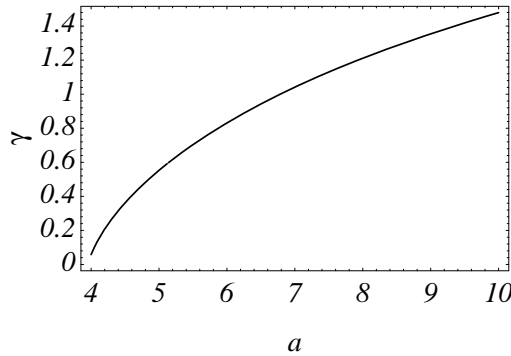


Figure S.18: Plot of the escape rate versus a for the logistic map $x_{n+1} = ax_n(1 - x_n)$ calculated from the first five periodic orbits.

Solution 20.2 - Escape rate for a 1 – dimensional repeller We can compute an approximate functional dependence of the escape rate on the parameter a using the stabilities of the first five prime orbits computed above, see (S.40). The spectral determinant (for $a > 4$) is

$$\begin{aligned}
 F = & 1 - \frac{2z}{a-1} - \frac{8z^2}{(a-3)(a-1)^2(a+1)} \\
 & + \left(\frac{2(32 - 18a + 17a^2 - 16a^3 + 14a^4 - 6a^5 + a^6)}{(a-3)(a-1)^3(1+a)(a^2 - 5a + 7)(a^2 + a + 1)} \right. \\
 & \left. - \frac{2a(a-2)\sqrt{a^2 - 2a - 7}}{(a^2 - 5a + 7)(a^2 - 2a - 7)(a^2 + a + 1)} \right) z^3
 \end{aligned} \tag{S.42}$$

The leading zero is plotted in figure S.18; it always remains real while the other two roots which are large and negative for $a > 5.13 \dots$ become imaginary below this critical value. The accuracy of this truncation is clearly worst for $a \rightarrow 4$, the value at which the hyperbolicity is lost and the escape rate goes to zero.

(Adam Prügel-Bennet)

Solution 20.3 - Escape rate for the Ulam map. The answer is worked out in Nonlinearity 3, 325; 3, 361 (1990).

Solution 20.11 - Escape rate for the Rössler system. No solution available as yet.

Chapter 21. Discrete symmetries factorize spectral determinants.

Solution 21.2 - Sawtooth map desymmetrization. *No solution available as yet.*

Solution 21.4 - 3-disk desymmetrization.

b) *The shortest cycle with no symmetries is $\overline{121213}$.*

c) *The shortest fundamental domain cycle cycle whose time reversal is not obtained by a discrete symmetry is $\overline{010011}$. It corresponds to $\overline{121313212323}$ in the full space.*

Ben Web

Solution 21.5 - C_2 factorizations: the Lorenz and Ising systems. *No solution available as yet.*

Solution 21.6 - Ising model. *No solution available as yet.*

Solution 21.7 - One orbit contribution. *No solution available as yet.*

Solution ?? - Characters. *No solution available as yet.*

Chapter 22. Why cycle?

Solution 22.1 - The escape is controlled by the size of the primary gap of the repeller. All subgaps in the repeller will be proportional to the main gap. The size of the main gap is $l = \sqrt{1 - 1/a}$. Near $a_c = 1$ the escape rate is

$$\gamma(a) \sim (a - a_c)^{1/2}.$$

We can generalize this and the previous result and conclude that

$$\gamma(a) \sim (a - a_c)^{1/z},$$

where z is the order of the maximum of the single humped map.

Solution 22.2 - By direct evaluation we can calculate the zeta functions and the Fredholm determinant of this map.

$$(a) \quad s_{01} = \frac{\Lambda_0}{\Lambda_0 - 1} \frac{b - 1}{b}, \quad s_{10} = -\frac{\Lambda_1 - 1}{\Lambda_1} \frac{b}{b - 1}, \quad c = b + \frac{b - 1}{\Lambda_1}.$$

(b) Show that the 2-cycle Floquet multiplier does not depend on b ,

$$\Lambda_{01} = s_{01} s_{10} = -\frac{\Lambda_0 \Lambda_1}{(\Lambda_0 - 1)(\Lambda_1 + 1)}.$$

$$(c) \quad \mathbf{L} = \begin{pmatrix} L_{00} & L_{01} \\ L_{10} & L_{11} \end{pmatrix},$$

where $L_{00} = 1/\Lambda_0$, $L_{01} = 1/s_{01}$, $L_{11} = 1/\Lambda_1$, $L_{10} = 1/s_{10}$ are inverses of the slopes of the map.

(e) $\det(1 - z\mathbf{L}) = 1 - ???$

(h) Yes.

The Fredholm determinant is the product of zeta functions

$$F(z) = \prod_{k=0}^{\infty} 1/\zeta_k(z).$$

The leading zeroes of the Fredholm determinant can come from the zeroes of the leading zeta functions.

The zeroes of $1/\zeta_0(z)$ are

$$\begin{aligned} 1/z_1 &= \frac{T_{00} + T_{11} + \sqrt{(T_{00} - T_{11})^2 + 4T_{01}T_{10}}}{2}, \\ 1/z_2 &= \frac{T_{00} + T_{11} - \sqrt{(T_{00} - T_{11})^2 + 4T_{01}T_{10}}}{2}. \end{aligned}$$

The zeroes of $1/\zeta_1(z)$ are

$$\begin{aligned} 1/z_3 &= \frac{T_{00}^2 + T_{11}^2 + \sqrt{(T_{00}^2 - T_{11}^2)^2 + 4T_{01}^2 T_{10}^2}}{2}, \\ 1/z_4 &= \frac{T_{00}^2 + T_{11}^2 - \sqrt{(T_{00}^2 - T_{11}^2)^2 + 4T_{01}^2 T_{10}^2}}{2}. \end{aligned}$$

By substituting the slopes we can show that $z_1 = 1$ is the leading eigenvalue. The next to leading eigenvalue, which is the correlation decay in discrete time, can be $1/z_3$ or $1/z_2$.

Solution 22.3 -

(d) In the $A = 9/2$ case all cycles up to length 9 yield $\lambda = 1.08569 \dots$ (Vadim Moroz)

Chapter 23. Why does it work?

Solution 23.3 - Euler formula. Let

$$P = \prod_{k=0}^{\infty} (1 + tu^k) = \sum_{n=0}^{\infty} P_n t^n$$

then

$$\begin{aligned} P_n &= \frac{1}{n!} \left. \frac{\partial^n P}{\partial t^n} \right|_{t=0} = \frac{1}{n!} \sum_{i_n \neq i_{n-1} \neq \dots \neq i_1} u^{i_n + i_{n-1} + \dots + i_1} \\ &= \sum_{i_n > i_{n-1} > \dots > i_1 \geq 0} u^{i_n + i_{n-1} + \dots + i_1} \end{aligned} \tag{S.43}$$

Clearly $P_0 = 1$, and

$$P_1 = \sum_{i=0} u^i$$

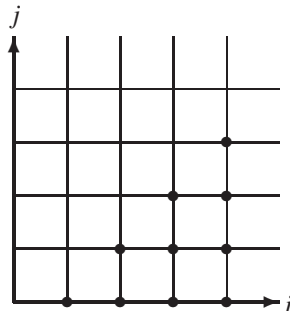
multiplying both sides by $1 - u$

$$(1 - u)P_1 = 1 + u + u^2 + \dots - (u + u^2 + \dots) = 1$$

(since, for $|u| < 1$, $\lim_{n \rightarrow \infty} u^n = 0$). Thus $P_1 = 1/(1 - u)$. Similarly

$$P_2 = \sum_{i > j \geq 0} u^{i+j}$$

Graphically the allowed values of i and j are



Performing the same trick as for P_1

$$(1 - u)P_2 = \sum_{i > j \geq 0} u^{i+j} - \sum_{i > j \geq 0} u^{i+(j+1)}$$

The only terms that survive are those for which $j = i - 1$ (that is the top diagonal in the figure) thus

$$(1 - u)P_2 = u^{-1} \sum_{i=1}^{\infty} u^{2i}$$

and

$$(1 - u)(1 - u^2)P_2 = u^{-1} (u^2 + u^4 + \dots - (u^4 + u^6 + \dots)) = u$$

Thus

$$P_2 = \frac{u}{(1 - u)(1 - u^2)}$$

In general

$$(1 - u)P_n = \sum_{i_n > i_{n-1} > \dots > i_1 \geq 0} u^{i_n + i_{n-1} + \dots + i_1} - \sum_{i_n > i_{n-1} > \dots > i_1 \geq 0} u^{i_n + i_{n-1} + \dots + (i_1 + 1)} \tag{S.44}$$

$$= u^{-1} \sum_{i_n > i_{n-1} > \dots > i_2 \geq 1} u^{i_n + i_{n-1} + \dots + 2i_2} \tag{S.45}$$

since only the term $i_1 = i_2 - 1$ survives. Repeating this trick

$$(1 - u)(1 - u^2)P_n = u^{-1-2} \sum_{i_n > i_{n-1} > \dots > i_3 \geq 2} u^{i_n + i_{n-1} + \dots + 3i_3}$$

and

$$\prod_{i=1}^n (1 - u^i) P_n = u^{-(1+2+\dots+n)} u^{n(n-1)} = u^{n(n-1)/2}$$

Thus

$$P_n = \frac{u^{n(n-1)/2}}{\prod_{i=1}^n (1 - u^i)}$$

(Adam Prügel-Bennet)

Solution 23.3 - Euler formula, 2nd method. The coefficients Q_k in (23.4) are given explicitly by the Euler formula

$$Q_k = \frac{1}{1 - \Lambda^{-1}} \frac{\Lambda^{-1}}{1 - \Lambda^{-2}} \dots \frac{\Lambda^{-k+1}}{1 - \Lambda^{-k}} \tag{S.46}$$

Such a formula is easily proved by considering the finite order product

$$\mathcal{W}_j(z, \gamma) = \prod_{l=0}^j (1 + z\gamma^l) = \sum_{l=0}^{j+1} \Gamma_l z^l$$

Since we have that

$$(1 + z\gamma^{j+1})\mathcal{W}_j(z, \gamma) = (1 + z)\mathcal{W}_j(\gamma z, \gamma),$$

we get the following identity for the coefficients

$$\Gamma_m + \Gamma_{m-1}\gamma^{j+1} = \Gamma_m\gamma^m + \Gamma_{m-1}\gamma^{m-1} \quad m = 1, \dots$$

Starting with $\Gamma_0 = 1$, we recursively get

$$\Gamma_1 = \frac{1 - \gamma^{j+1}}{1 - \gamma} \quad \Gamma_2 = \frac{(1 - \gamma^{j+1})(\gamma - \gamma^{j+1})}{(1 - \gamma)(1 - \gamma^2)} \dots$$

the Euler formula (23.5) follows once we take the $j \rightarrow \infty$ limit for $|\gamma| < 1$.

(Robert Artuso)

Solution 23.3 - Euler formula, 3rd method. First define

$$f(t, u) := \prod_{k=0}^{\infty} (1 + tu^k). \tag{S.47}$$

Note that

$$f(t, u) = (1 + t)f(tu, u), \tag{S.48}$$

by factoring out the first term in the product. Now make the ansatz

$$f(t, u) = \sum_{n=0}^{\infty} t^n g_n(u), \tag{S.49}$$

plug it into (S.48), compare the coefficients of t^n and get

$$g_n(u) = u^n g_n(u) + u^{n-1} g_{n-1}(u). \tag{S.50}$$

Of course $g_0(u) = 1$. Therefore by solving the recursion (S.50) and by noting that $\sum_{k=1}^{n-1} k = \frac{n(n-1)}{2}$ one finally arrives at

$$g_n(u) = \frac{u^{\frac{n(n-1)}{2}}}{\prod_{k=1}^n (1 - u^k)}. \tag{S.51}$$

Euler got this formula and he and Jacobi got many nice number theoretical results from it, most prominent the pentagonal number theorem, which says that in the series expansion of $\prod_{k=1}^{\infty} (1 - q^k)$ all terms cancel except those which have as an exponent the circumference of a regular pentagon with integer base length.

(Juri Rolf)

Solution 23.4 - 2 – dimensional product expansion. Now let us try to apply the same trick as above to the two dimensional situation

$$h(t, u) := \prod_{k=0}^{\infty} (1 + tu^k)^{k+1}. \quad (\text{S.52})$$

Write down the first terms and note that similar to (S.48)

$$h(t, u) = f(t, u)h(tu, u), \quad (\text{S.53})$$

where f is the Euler product (S.47). Now make the ansatz

$$h(t, u) = \sum_{n=0}^{\infty} t^n a_n(u) \quad (\text{S.54})$$

and use the series expansion for f in (S.53) to get the recursion

$$a_n(u) = \frac{1}{1 - u^n} \sum_{m=0}^{n-1} u^m a_m(u) g_{n-m}(u). \quad (\text{S.55})$$

With this one can at least compute the generalized Euler product effectively, but it would be nice if one could use it for a proof of the general behaviour of the coefficients a_n .

(Juri Rolf)

Chapter K. Thermodynamic formalism

Solution K.1 - In the higher dimensional case there is no change in the derivation except Λ_p should be replaced with the product of expanding eigenvalues $\prod_j |\Lambda_{p,j}|$. The logarithm of this product is $\sum_j \log |\Lambda_{p,j}|$. The average of $\log |\Lambda_{p,j}|$ is the j th Lyapunov exponent. (G. Vattay)

Solution K.4 - The zeta function for the two scale map is

$$1/\zeta(z, \beta) = 1 - z \left(\frac{1}{a^\beta} + \frac{1}{b^\beta} \right).$$

The pressure function is

$$P(\beta) = \log z_0(\beta) = -\log \left(\frac{1}{a^\beta} + \frac{1}{b^\beta} \right).$$

The escape rate is

$$\gamma = P(1) = -\log \left(\frac{1}{a} + \frac{1}{b} \right),$$

The topological entropy is

$$K_0 = h_{top} = -P(0) = \log 2.$$

The Lyapunov exponent is

$$\bar{\lambda} = P'(1) = \frac{\log a/a + \log b/b}{1/a + 1/b}.$$

The Kolmogorov entropy is

$$K_1 = \bar{\lambda} - \gamma = P'(1) - P(1) = \frac{\log a/a + \log b/b}{1/a + 1/b} + \log \left(\frac{1}{a} + \frac{1}{b} \right).$$

The Rényi entropies are

$$K_\beta = (P(\beta) - \beta\gamma)/(\beta - 1) = (\log \left(\frac{1}{a^\beta} + \frac{1}{b^\beta} \right) + \beta \log \left(\frac{1}{a} + \frac{1}{b} \right))/(\beta - 1).$$

The box counting dimension is the solution of the implicit equation $P(D_0) = 0$, which is

$$1 = \frac{1}{a_0^{D_0}} + \frac{1}{b_0^{D_0}}.$$

The information dimension is

$$D_1 = 1 - \gamma/\bar{\lambda}.$$

The rest of the dimensions can be determined from equation $P(q - (q - 1)D_q) = \gamma q$. Taking exp of both sides we get

$$\frac{1}{a^{q-(q-1)D_q}} + \frac{1}{b^{q-(q-1)D_q}} = \left(\frac{1}{a} + \frac{1}{b} \right)^q.$$

For a given q we can find D_q from this implicit equation.

Solution ?? - The zeta function is

$$1/\zeta(z, \beta) = \det(1 - \mathbf{T}_{\beta-1}),$$

where we replaced k with $\beta - 1$ in solution **S**. The pressure can be calculated from the leading zero which is (see solution **S**)

$$P(\beta) = \log z_0(\beta) = -\log \left(\frac{T_{00}^\beta + T_{11}^\beta + \sqrt{(T_{00}^\beta - T_{11}^\beta)^2 + 4T_{01}^\beta T_{10}^\beta}}{2} \right).$$

Solution K.5 - We can easily read off that $b = 1/2$, $a_1 = \arcsin(1/2)/2\pi$ and $a_2 = a_1$ and do the steps as before.

Chapter 24. Intermittency

(No solutions available.)

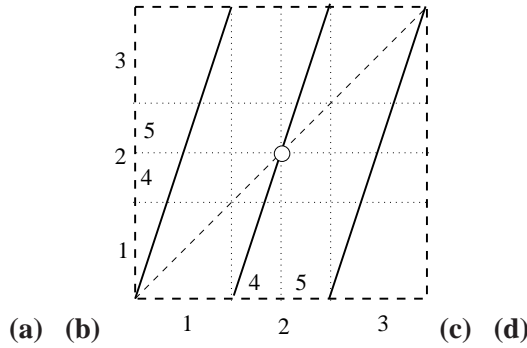
Chapter ??. Continuous symmetries

Solution ?? - To be constructed: Rotate coordinates $x' = \mathbf{g}x$:

$$\mathcal{L}(x', y') = \delta(\mathbf{g}y - f(\mathbf{g}x)) = |\det \mathbf{g}|^{-1} \delta(y - f(x)) = \mathcal{L}(x, y) = |\det \mathbf{g}| \mathcal{L}(\mathbf{g}x, \mathbf{g}y).$$

For a compact semisimple Lie group $|\det \mathbf{g}| = 1$, hence (??).

Figure S.19: (a) (b) A partition of the unit interval into three or five intervals, labeled by the order along the unit interval $\mathcal{A} = \{\mathcal{M}_1, \mathcal{M}_2 = \mathcal{M}_4 \cup (\frac{1}{2}) \cup \mathcal{M}_5, \mathcal{M}_3\}$. The partition is Markov, as the critical point is also a fixed point. (c) the transition graph for this Markov partition.



Chapter 25. Deterministic diffusion

Solution 25.1 - Diffusion for odd integer Λ . Consider first the case $\Lambda = 3$, illustrated in figure S.19. If $\beta = 0$, the dynamics in the elementary cell is simple enough; a partition can be constructed from three intervals, which we label $\{\mathcal{M}_1, \mathcal{M}_2, \mathcal{M}_3\}$, with the alphabet ordered as the intervals are laid out along the unit interval. The transition graph is figure S.19(c), and the dynamical zeta function is

$$1/\zeta|_{\beta=0} = 1 - (t_1 + t_2 + t_3) = 1 - 3z/\Lambda,$$

with eigenvalue $z = 1$ as required by the flow conservation.

However, description of global diffusion requires more care. As explained in the definition of the map (25.9), we have to split the partition $\mathcal{M}_2 = \mathcal{M}_4 \cup (\frac{1}{2}) \cup \mathcal{M}_5$, and exclude the fixed point $f(\frac{1}{2}) = \frac{1}{2}$, as the map $\hat{f}(\hat{x})$ is not defined at $\hat{f}(\frac{1}{2})$. (Are we to jump to the right or to the left at that point?) As we have $f(\mathcal{M}_4) = \mathcal{M}_1 \cup \mathcal{M}_4$, and similarly for $f(\mathcal{M}_5)$, the transition graph figure S.19(d) is infinite, and so is the dynamical zeta function:

$$1/\zeta = 1 - t_1 - t_{14} - t_{144} - t_{1444} \dots - t_3 - t_{35} - t_{355} - t_{3555} \dots$$

The infinite alphabet $\mathcal{A} = \{1, 14, 144, 1444 \dots 3, 35, 355, 3555 \dots\}$ is a consequence of the exclusion of the fixed point(s) x_4, x_5 . As is customary in such situations (see exercise 20.10, and chapter 24, inter alia), we deal with this by dividing out the undesired fixed point from the dynamical zeta function. We can factorize and resum the weights using the piecewise linearity of (25.9)

$$1/\zeta = 1 - \frac{t_1}{1 - t_4} - \frac{t_3}{1 - t_5}.$$

The diffusion constant is now most conveniently evaluated by evaluating the partial derivatives of $1/\zeta$ as in (20.19)

$$\begin{aligned} \langle T \rangle_\zeta &= -z \frac{\partial}{\partial z} \frac{1}{\zeta} = 2 \left(\frac{t_1}{1 - t_4} + \frac{t_1 t_4}{(1 - t_4)^2} \right) \Big|_{z=1, \beta=0} = \frac{3}{4} \\ \langle \hat{x}^2 \rangle_\zeta \Big|_{z=1, \beta=0} &= 2 \left(\frac{\hat{n}_1(\hat{n}_1 + \hat{n}_4)\Lambda^2}{(1 - 1/\Lambda)^2} + 2 \frac{\hat{n}_4^2/\Lambda^3}{(1 - 1/\Lambda)^3} \right) = \frac{1}{2} \end{aligned} \tag{S.56}$$

yielding $D = 1/3$, in agreement with in (25.21) for $\Lambda = 3$.

Solution 25.6 - Accelerated diffusion. SUGGESTED STEPS

1. Show that the condition assuring that a trajectory indexed by (ϕ, α) hits the (m, n) disk (all other disks being transparent) is written as

$$\left| \frac{d_{m,n}}{R} \sin(\phi - \alpha - \theta_{m,n}) + \sin \alpha \right| \leq 1 \quad (\text{S.57})$$

where $d_{m,n} = \sqrt{m^2 + n^2}$ and $\theta_{m,n} = \arctan(n/m)$. You can then use a small R expansion of (S.57).

2. Now call j_n the portion of the state space leading to a first collision with disk $(n, 1)$ (take into account screening by disks $(1, 0)$ or $(n-1, 1)$). Denote by $J_n = \bigcup_{k=n+1}^{\infty} j_k$ and show that $J_n \sim 1/n^2$, from which the result for the distribution function follows.

Chapter 28. Noise

Solution 28.2 - d -dimensional Gaussian integrals. We require that the matrix in the exponent is nondegenerate (i.e. has no zero eigenvalues.) The converse may happen when doing stationary phase approximations which requires going beyond the Gaussian saddle point approximation, typically to the Airy-function type stationary points [10]. We also assume that M is positive-definite, otherwise the integral is infinite.

Make a change of variables $y = Ax$ such that $A^T M^{-1} A = \text{Id}$. Then

$$I = \frac{1}{(2\pi)^{d/2}} \int_{\mathbf{R}^d} \exp\left[-\frac{1}{2} \sum_i (y_i^2 - 2(JA)_i y_i)\right] |\det A| dy$$

Complete each term under in the sum in the exponent to a full square

$$y_i^2 - 2(JA)_i y_i = (y_i - (JA)_i)^2 - (JA)_i^2$$

and shift the origin of integration to $JA/2$, so that

$$I = \frac{1}{(2\pi)^{d/2}} \exp\left(\frac{1}{2} J^T A A^T J\right) |\det A| \int_{\mathbf{R}^d} \exp\left[-\frac{1}{2} \sum_i y_i^2\right] dy$$

Note that $A A^T M^{-1} A A^T = A A^T$, therefore $A A^T = M$ and $|\det A| = \sqrt{\det M}$. The remaining integral is equal to a Poisson integral raised to the d -th power, i.e. $(2\pi)^{d/2}$.
Answer:

$$I = \sqrt{\det M} \exp\left[\frac{1}{2} J^T M J\right]$$

(R. Paškauskas)

Chapter 26. Turbulence?

(No solutions available.)

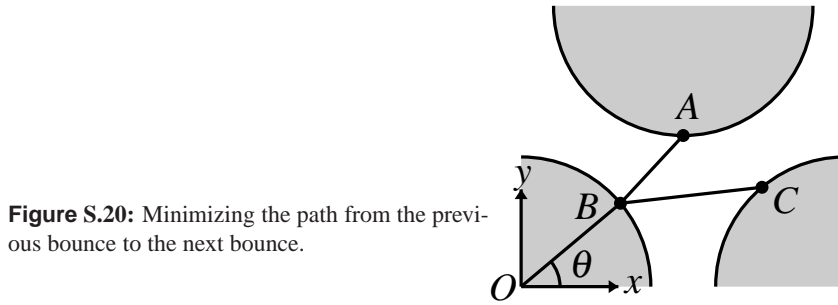


Figure S.20: Minimizing the path from the previous bounce to the next bounce.

Chapter 29. Relaxation for cyclists

Solution 29.1 - Evaluation of cycles by minimization. To start with a guess path where each bounce is given some arbitrary position on the correct disk and then iteratively improve on the guess. To accomplish this an improvement cycle is constructed whereby each bouncing point in the orbit is taken in turn and placed in a new position so that it minimizes the path. Since the positions of all the other bounces are kept constant this involves choosing the new bounce position which minimizes the path from the previous bounce to the next bounce. This problem is schematically represented in figure S.20

Finding the point B involves a one dimensional minimization. We define the vectors $\vec{A} = \vec{OA}$, $\vec{B} = \vec{OB}$ and $\vec{C} = \vec{OC}$. We wish to minimize the length L_{ABC} by varying \vec{B} subject to the constraint that $|\vec{B}| = a$. Clearly

$$\begin{aligned} L_{ABC} &= |\vec{A} - \vec{B}| + |\vec{C} - \vec{B}| \\ &= \sqrt{\vec{A}^2 + \vec{B}^2 - 2\vec{A} \cdot \vec{B}} + \sqrt{\vec{C}^2 + \vec{B}^2 - 2\vec{C} \cdot \vec{B}} \end{aligned}$$

writing

$$\vec{B}(\theta) = a(\cos \theta, \sin \theta)$$

then the minima is given by

$$\frac{dL_{ABC}}{d\theta} = - \left(\frac{\vec{A}}{\sqrt{\vec{A}^2 + \vec{B}^2 - 2\vec{A} \cdot \vec{B}}} + \frac{\vec{C}}{\sqrt{\vec{C}^2 + \vec{B}^2 - 2\vec{C} \cdot \vec{B}}} \right) \cdot \vec{B}'(\theta) = 0.$$

The minima can then be found using a bisection algorithm or using Newton-Raphson. A simpler way is to observe that $\vec{B}'(\theta)$ is orthogonal to $\vec{B}(\theta)$ so that the vector

$$\vec{D} = \frac{\vec{A}}{\sqrt{\vec{A}^2 + \vec{B}^2 - 2\vec{A} \cdot \vec{B}}} + \frac{\vec{C}}{\sqrt{\vec{C}^2 + \vec{B}^2 - 2\vec{C} \cdot \vec{B}}}$$

will be proportional to \vec{B} . This then provides an iterative sequence for finding \vec{B}

- Starting from your current guess for \vec{B} calculate \vec{D}

- Put $\vec{B} = a\vec{D}/|\vec{D}|$
- Repeat the first step until you converge.

At each iteration of the improvement cycle the total length of the orbit is measured. The minimization is complete when the path length stops improving. Although this algorithm is not as fast as the Newton-Raphson method, it nevertheless converges very rapidly.

(Adam Prügel-Bennet)

Chapter 27. Irrationally winding

(No solutions available.)

Chapter 31. Quantum mechanics, briefly

Solution 31.1 - Lorentzian representation of the Dirac delta function. *General hint: read up on principal parts, positive and negative frequency parts of the Dirac delta function, perhaps the Cauchy theorem, in any good quantum mechanics textbook.*

To see that (31.19) satisfies properties of the delta function,

$$\delta(E - E_n) = -\lim_{\epsilon \rightarrow 0} \frac{1}{\pi} \text{Im} \frac{1}{E - E_n + i\epsilon},$$

start by expressing explicitly the imaginary part:

$$\begin{aligned} -\text{Im} \frac{1}{E - E_n + i\epsilon} &= -\text{Im} \frac{E - E_n - i\epsilon}{(E - E_n + i\epsilon)(E - E_n - i\epsilon)} \\ &= \frac{\epsilon}{(E - E_n)^2 + \epsilon^2}. \end{aligned}$$

This is a Lorentzian of width ϵ , with a peak at $E = E_n$. It has the correct normalization for the delta function,

$$\begin{aligned} \frac{1}{\pi} \int_{-\infty}^{\infty} dE \frac{\epsilon}{(E - E_n)^2 + \epsilon^2} &= \frac{1}{\pi} \frac{\epsilon}{\epsilon} \arctan \frac{E - E_n}{\epsilon} \Big|_{-\infty}^{\infty} \\ &= \frac{1}{\pi} (\pi/2 - (-\pi/2)) = 1, \end{aligned}$$

so

$$\frac{1}{\pi} \int_{-\infty}^{\infty} dE \frac{\epsilon}{(E - E_n)^2 + \epsilon^2} = 1, \quad (\text{S.58})$$

independently of the width ϵ .

Next we show that in the $\epsilon \rightarrow \infty$ limit the support of the Lorentzian is concentrated at $E = E_n$. When $E = E_n$,

$$\lim_{\epsilon \rightarrow 0} \frac{1}{\pi} \left(\frac{\epsilon}{(E - E_n)^2 + \epsilon^2} \right) = \lim_{\epsilon \rightarrow 0} \frac{1}{\pi} \frac{1}{\epsilon} = \infty,$$

and when $E \neq E_n$,

$$\lim_{\epsilon \rightarrow 0} \frac{1}{\pi} \frac{\epsilon}{(E - E_n)^2 + \epsilon^2} = 0$$

Providing that a function convolved with $\delta(s)$, $\int f(E)\delta(E - E_n)dE$ has a continuous first derivative at $E = E_n$ and falls off sufficiently rapidly as $E \rightarrow \pm\infty$, this is a representation of the delta function.

(R. Paskauskas, Bo Li)

Solution 31.2 - Green's function. The Laplace transform of the (time-dependent) quantum propagator

$$K(q, q', t) = \sum_n \phi_n(q) e^{-iE_n t/\hbar} \phi_n^*(q')$$

is the (energy-dependent) Green's function

$$\begin{aligned} G(q, q', E + i\varepsilon) &= \frac{1}{i\hbar} \int_0^\infty dt e^{\frac{i}{\hbar}Et - \frac{\varepsilon}{\hbar}t} \sum_n \phi_n(q) e^{-iE_n t/\hbar} \phi_n^*(q') \\ &= \frac{1}{i\hbar} \sum_n \phi_n(q) \phi_n^*(q') \int_0^\infty dt e^{\frac{i}{\hbar}(E - E_n + i\varepsilon)t} \\ &= - \sum_n \phi_n(q) \phi_n^*(q') \frac{1}{E - E_n + i\varepsilon} e^{-\frac{\varepsilon}{\hbar}t} e^{i(E - E_n)t/\hbar} \Big|_{t=0}^{t=\infty}. \end{aligned}$$

When ε is positive, $e^{-\frac{\varepsilon}{\hbar}\infty} = 0$, so

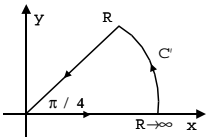
$$G(q, q', E + i\varepsilon) = \sum_n \frac{\phi_n(q) \phi_n^*(q')}{E - E_n + i\varepsilon}.$$

(Bo Li)

Chapter 32. WKB quantization

Solution 32.1 - Fresnel integral. Start by re-expressing the integral over the infinite half-line:

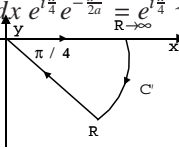
$$\frac{1}{\sqrt{2\pi}} \int_{-\infty}^{\infty} dx e^{-\frac{x^2}{2ia}} = \frac{2}{\sqrt{2\pi}} \int_0^{\infty} dx e^{-\frac{x^2}{2ia}}, \quad a \in \mathbb{R}, \quad a \neq 0.$$

When $a > 0$, the contour  vanishes, as it contains no pole:

$$\begin{aligned} \oint_C dz e^{-z^2/2ia} &= \int_0^{\infty} dx e^{-\frac{x^2}{2ia}} + \int_{C'} + \int_{\infty}^0 e^{i\frac{\pi}{4}} e^{-\frac{x^2}{2ia}} dx = 0 \\ \int_{C'} &= \int_0^{\frac{\pi}{4}} e^{iR^2 e^{i2\phi}/2a} Re^{i\phi} i d\phi = 0. \end{aligned} \tag{S.59}$$

So

$$\frac{2}{\sqrt{2\pi}} \int_0^{\infty} dx e^{-\frac{x^2}{2ia}} = \frac{2}{\sqrt{2\pi}} \int_0^{\infty} dx e^{i\frac{\pi}{4}} e^{-\frac{x^2}{2ia}} \stackrel{R \rightarrow \infty}{=} e^{i\frac{\pi}{4}} \sqrt{a} = \sqrt{ia}$$

In the $a < 0$ case take the contour 

$$\begin{aligned} \oint_C dz e^{-z^2/2ia} &= \int_0^{\infty} dx e^{-\frac{x^2}{2ia}} + \int_{C'} + \int_{\infty}^0 e^{-i\frac{\pi}{4}} e^{\frac{x^2}{2ia}} dx \\ &= \int_0^{\infty} dx e^{-\frac{x^2}{2ia}} - e^{-i\frac{\pi}{4}} \int_0^{\infty} dx e^{\frac{x^2}{2ia}} = 0. \end{aligned}$$

Again

$$\frac{2}{\sqrt{2\pi}} \int_0^{\infty} dx e^{-\frac{x^2}{2ia}} = e^{-i\frac{\pi}{4}} \sqrt{|a|},$$

and, as one should have perhaps intuited by analyticity arguments, for either sign of a we have the same Gaussian integral formula

$$\frac{1}{\sqrt{2\pi}} \int_{-\infty}^{\infty} dx e^{-\frac{x^2}{2ia}} = |a|^{1/2} e^{i\frac{\pi}{4} \frac{a}{|a|}} = \sqrt{ia}.$$

The vanishing of the C' contour segment (S.59) can be proven as follows: Substitute $z = Re^{i\phi}$ into the integral

$$I_R = \int_0^{\frac{\pi}{4}} e^{iR^2 e^{i2\phi}/2a} Re^{i\phi} i d\phi = \int_0^{\frac{\pi}{4}} e^{iR^2(\cos 2\phi + i \sin 2\phi)/2a} Re^{i\phi} i d\phi.$$

Then

$$|I_R| \leq R \int_0^{\frac{\pi}{4}} e^{-R^2 \sin 2\phi/2a} d\phi = \frac{R}{2} \int_0^{\frac{\pi}{2}} e^{-R^2 \sin \theta/2a} d\theta.$$

In the range $[0, \pi/2]$ we can replace $\frac{2}{\pi}\theta \leq \sin \theta$, obtain a bound

$$|I_R| \leq \frac{R}{2} \int_0^{\frac{\pi}{2}} e^{-R^2 \theta/\pi a} d\theta = \frac{R}{2} \frac{1 - e^{-R^2/2a}}{R^2/a\pi},$$

so

$$\lim_{R \rightarrow \infty} |I_R| = 0.$$

(Bo Li)

Chapter 33. Semiclassical evolution

Solution 33.5 - Free particle R -function. Calculate R from its definition

$$R(q', q, t) = \int_0^t \mathcal{L}(\dot{q}(t'), q(t'), t') dt'$$

where the solution of Lagrange equations of motion is substituted for $q(t)$.

a a D -dimensional free particle:

We have

$$\begin{aligned} \mathcal{L}(\dot{q}(t'), q(t'), t') &= \frac{m}{2} \sum_{i=1}^D [\dot{q}_i(t')]^2, \\ \dot{q}_i(t) &= \text{const} = \frac{q'_i - q_i}{t}. \end{aligned} \quad (\text{S.60})$$

The answer:

$$R(q', q, t) = \frac{m}{2} \sum_{i=1}^D \frac{[q'_i - q_i]^2}{t}.$$

b Using symmetric gauge for vector potential and denoting the Larmor frequency by $\omega = \frac{eB}{mc}$, we have

$$\mathcal{L} = \frac{m}{2} (\dot{x}^2 + \dot{y}^2 + \dot{z}^2 + \omega(x\dot{y} - y\dot{x}))$$

The equations of motion are

$$\ddot{x} - \omega\dot{y} = 0, \quad \ddot{y} + \omega\dot{x} = 0, \quad \ddot{z} = 0.$$

To calculate the expression for the principal function we do integration by parts on $\dot{x}^2 + \dot{y}^2$, and the result is

$$R = \int \mathcal{L} dt = \frac{m}{2} \left(x\dot{x}|_{t_0}^t + y\dot{y}|_{t_0}^t + \frac{(z' - z)^2}{t} + \int_{t_0}^t [x(-\ddot{x} + \omega\dot{y}) + y(-\ddot{y} - \omega\dot{x})] dt \right),$$

however terms inside the integral vanish by equations of motion. Denote $w(t) = x(t) + iy(t)$, then the first two equations of motion are equivalent to equation in complex $w(t)$:

$$\dot{w}(t) + i\omega\bar{w}(t) = 0,$$

solution to which is

$$w' \equiv \dot{w}(t) = w + \frac{\dot{w}(1 - e^{-i\omega t})}{i\omega}.$$

We must reexpress velocities in R in terms of time and initial and final coordinates. In terms of \dot{w} we have

$$\begin{aligned} \dot{w}_0 &= \frac{\omega e^{\frac{i\omega t}{2}} (w - w_0)}{2 \sin(\frac{\omega t}{2})} \\ \dot{w} &= \frac{\omega e^{-\frac{i\omega t}{2}} (w - w_0)}{2 \sin(\frac{\omega t}{2})} \end{aligned} \quad (\text{S.61})$$

Note that

$$\begin{aligned} x\dot{x} + y\dot{y} &= \operatorname{Re} w^* \dot{w} \\ \operatorname{Re} w^* \dot{w}'_0 &= \frac{\omega}{2 \sin \frac{\omega t}{2}} \left((|w|^2 + |w_0|^2) \cos \frac{\omega t}{2} - 2 \operatorname{Re} w_0 w^* e^{-\frac{i\omega t}{2}} \right) \\ &= \frac{\omega}{2} \left(\cot \left(\frac{\omega t}{2} \right) [(x - x_0)^2 + (y - y_0)^2] + 2(x_0 y - y_0 x) \right) \\ R &= \frac{m(z - z_0)^2}{2t} + \frac{m\omega}{4} \left(\cot \left(\frac{\omega t}{2} \right) [(x - x_0)^2 + (y - y_0)^2] + 2(x_0 y - y_0 x) \right) \end{aligned}$$

Solution 33.1 - Dirac delta function, Gaussian representation. To prove that δ_σ converges to a dirac delta function, it is enough to show that it has the following properties:

1. $\int_{-\infty}^{\infty} \delta_\sigma(x) dx = 1$
2. $\lim_{\sigma \rightarrow 0} \int_{-a}^a f(x) \delta_\sigma(x) dx = f(0)$

for arbitrary $f(x)$ continuous and positive a .

First property is satisfied by the choice of normalisation constant. Second property is verified by the change of variables $y = x / \sqrt{2\sigma^2}$:

$$\lim_{\sigma \rightarrow 0} \int_{-a}^a f(x) \delta_\sigma(x) dx = \lim_{\sigma \rightarrow 0} \frac{1}{\sqrt{\pi}} \int_{\frac{-a}{\sqrt{2\sigma^2}}}^{\frac{a}{\sqrt{2\sigma^2}}} f(\sqrt{2\sigma^2} y) e^{-y^2} dy = f(0)$$

(R. Paškauskas)

Solution 33.2 - Stationary phase approximation.

Main contribution to this integral come from critical points of $\Phi(x)$. Suppose that p is such a nondegenerate critical point, $p : D\Phi(p) = 0$, and $D^2\Phi(p)$ has full rank. Then there is a local coordinate system y in the neighbourhood of p such that $\Phi(p + y) = \Phi(p) - \sum_{i=1}^\lambda y_i^2 + \sum_{i=\lambda+1}^d y_i^2$, where λ is the number of negative eigenvalues of $D^2\Phi(p)$. Indeed, if we set $x - p = Ay$, then $\Phi(x) \approx \Phi(p) + \frac{1}{2} y A^T D^2\Phi(p) Ay$. There exist such A that $\frac{1}{2} A^T D^2\Phi(p) A = \operatorname{diag}[\underbrace{-1, \dots, -1}_\lambda, \underbrace{+1, \dots}_d]$. With this change of variables in mind,

we have

$$I = e^{\frac{i\Phi(p)}{\hbar}} \int_{\mathbb{R}^d} e^{\frac{i}{\hbar} (-\sum_{i=1}^\lambda y_i^2 + \sum_{i=\lambda+1}^d y_i^2)} |\det A| dy = e^{\frac{i\Phi(p)}{\hbar}} (\pi \hbar)^{d/2} e^{\frac{i\pi}{4} (-2\lambda + d)} |\det A|$$

Furthermore, $(\det A)^2 \det D^2\Phi(p) = 2^d \exp i\pi\lambda$, therefore

$$|\det A| = \frac{2^{d/2} \exp \frac{i\pi\lambda}{4}}{\sqrt{\det D^2\Phi(p)}}$$

Phase factors $\exp i\pi\lambda/2$ and $\exp -i\pi\lambda/2$ cancel out. Substitute $\exp i\pi d/2 = i^{d/2}$.

The result:

$$I = \frac{(2i\pi\hbar)^{d/2} e^{\frac{i\Phi(p)}{\hbar}}}{\sqrt{\det D^2\Phi(p)}}$$

Critical nondegenerate points are isolated. Therefore if Φ has more than one critical point, then equivalent local approximation can be made in the neighbourhoods of each critical point and the complete approximation to the integral made by adding contributions of all critical points.

Answer:

$$I = \sum_{p: D\Phi(p)=0} \frac{(2i\pi\hbar)^{d/2} e^{i\frac{\Phi(p)}{\hbar}} A(p)}{\sqrt{\det D^2\Phi(p)}}$$

Rytis Paškauskas

Solution 33.2 - Stationary phase approximation.

values of x of stationary phase, the points for which the gradient of the phase vanishes

$$\frac{\partial}{\partial x} \Phi(x) = 0.$$

Intuitively, these are the important contributions as for $\hbar \rightarrow 0$ the phase $\Phi(x)/\hbar$ grows large and the function $e^{i\Phi(x)/\hbar}$ oscillates rapidly as a function of x , with the negative and positive parts canceling each other. More precisely, if the stationary points are well separated local extrema of $\Phi(x)$, we can deform the integration contour and approximate $\Phi(x)/\hbar$ up to the second order in x by

$$I \approx \sum_n A(x_n) e^{i\Phi(x_n)/\hbar} \int d^d x e^{\frac{i}{2\hbar}(x-x_n)^T \mathbf{D}^2\Phi(x_n)(x-x_n)}.$$

The second derivative matrix is a real symmetric matrix, so we can transform it to a diagonal matrix by a similarity transformation

$$\text{Diag}(\lambda_1, \dots, \lambda_d) = \mathbf{O} \mathbf{D}^2 \Phi \mathbf{O}^+,$$

where \mathbf{O} is a matrix of an orthogonal transformation. In the rotated coordinate system $u = \mathbf{O}(x - x_n)$ and the integral takes form

$$I \approx \sum_n A(x_n) e^{i\Phi(x_n)/\hbar} \int d^d u e^{\sum_{k=1}^d i\lambda_k u_k^2 / 2\hbar},$$

where we used the fact that the Jacobi determinant of an orthogonal transformation is $\det \mathbf{O} = 1$. Carrying out the Gauss integrals

$$\int d^d u e^{i\lambda u^2 / 2\hbar} = \frac{(2\pi i\hbar)^{d/2}}{\sqrt{\lambda}} \quad (\text{S.63})$$

and using $\det \mathbf{D}^2\Phi(x_n) = \prod_{k=1}^d \lambda_k$ we obtain the stationary phase estimate of (33.53).

A nice exposition of the subject is given in ref. [10].

Solution 33.10 - D-dimensional free particle propagator. A free particle reaches q from q' by only one trajectory. Taking this into account the semiclassical Van Vleck propagator is

$$K_{sc}(q, q', t) = \frac{e^{iR/\hbar}}{(2\pi i\hbar)^{D/2}} \left| \det \frac{\partial^2 R}{\partial q_i \partial q'_j} \right|^{1/2}$$

The principal function of free motion in D -dimensions is

$$R(q, q', t) = \frac{m}{2t} \sum_{\mu=1}^D (q_{\mu} - q'_{\mu})^2$$

The derivative is

$$\frac{\partial^2 R}{\partial q_i \partial q'_j} = -\delta_{i,j} \frac{m}{t}$$

According to that determinant is

$$\left| \det \frac{\partial^2 R}{\partial q_i \partial q'_j} \right|^{1/2} = e^{i\pi D/2} \left(\frac{m}{t} \right)^{D/2},$$

and the Van Vleck propagator is

$$K_{sc}(q, q', t) = e^{i\pi D/4} \left(\frac{m}{2\pi\hbar t} \right)^{D/2} \prod_{\mu=1}^D \exp \left[\frac{im}{2\hbar t} (q_{\mu} - q'_{\mu})^2 \right]$$

The next step is to calculate the exact quantum propagator:

$$K(q, q', t) = \sum_n \phi_n(q) e^{-iE_n t/\hbar} \phi_n^*(q')$$

Taking that particle wave function in free space is

$$\phi_p(q) = \frac{1}{(2\pi\hbar)^{D/2}} e^{ipq/\hbar}$$

we derive that propagator K is

$$\frac{1}{(2\pi\hbar)^D} \int e^{-\frac{it}{2m\hbar} p^2 + ip(q-q')} d^D p$$

We can split multi-dimensional integral that stands here into a product of one dimensional integrals. Then we should change variables for purpose of reduction to Poisson-type integrals. We have omitted some straightforward algebra. The result is that the semiclassical Van Vleck propagator and the exact quantum propagator are identical:

$$K(q, q', t) = e^{i\pi D/4} \left(\frac{m}{2\pi\hbar t} \right)^{D/2} \prod_{\mu=1}^D \exp \left[\frac{im}{2\hbar t} (q_{\mu} - q'_{\mu})^2 \right] = K_{sc}(q, q', t)$$

This result could have been anticipated because approximate formula (??37) becomes exact for the free particle Lagrangian. (R. Paškauskas)

Chapter 34. Semiclassical quantization

Solution 34.1 - Monodromy matrix from second variations of the action. If we take two points in the configuration space q and q' connected with a trajectory with energy E and vary them in such a way that the variation of their initial and final points are transverse to the velocity of the orbit in that point, we can write the variations of the initial and final momenta as

$$\delta p_{\perp i} = \frac{\partial^2 S(q, q', E)}{\partial q_{\perp i} \partial q_{\perp k}} \delta q_{\perp k} + \frac{\partial^2 S(q, q', E)}{\partial q_{\perp i} \partial q'_{\perp k}} \delta q'_{\perp k} \quad (\text{S.64})$$

and

$$\delta p'_{\perp i} = -\frac{\partial^2 S(q, q', E)}{\partial q'_{\perp i} \partial q_{\perp k}} \delta q_{\perp k} - \frac{\partial^2 S(q, q', E)}{\partial q'_{\perp i} \partial q'_{\perp k}} \delta q'_{\perp k}. \quad (\text{S.65})$$

Next we express the variations of the final momenta and coordinates in terms of the initial ones. In the obvious shorthand we can write (S.65) as

$$\delta q_{\perp} = -S_{q'q}^{-1} S_{q'q'} \delta q'_{\perp} - S_{q'q}^{-1} \delta p'_{\perp},$$

From (S.64) it then follows that

$$\delta p_{\perp} = (S_{qq'} - S_{qq} S_{q'q}^{-1} S_{q'q'}) \delta q'_{\perp} - S_{qq} S_{q'q}^{-1} \delta p'_{\perp}. \quad (\text{S.66})$$

These relations remain valid in the $q' \rightarrow q$ limit, with q on the periodic orbit, and can also be expressed in terms of the monodromy matrix of the periodic orbit. The monodromy matrix for a surface of section transverse to the orbit within the constant energy $E = H(q, p)$ shell is

$$\begin{aligned} \delta q_{\perp} &= M_{qq} \delta q'_{\perp} + M_{qp} \delta p'_{\perp}, \\ \delta p_{\perp} &= M_{pq} \delta q'_{\perp} + M_{pp} \delta p'_{\perp}. \end{aligned} \quad (\text{S.67})$$

In terms of the second derivatives of the action the monodromy matrix is

$$\begin{aligned} M_{qq} &= -S_{q'q}^{-1} S_{q'q'}, & M_{qp} &= -S_{q'q}^{-1}, \\ M_{pq} &= (S_{qq'} - S_{qq} S_{q'q}^{-1} S_{q'q'}), & M_{pp} &= -S_{qq} S_{q'q}^{-1}, \end{aligned}$$

and vice versa

$$\begin{aligned} S_{qq} &= M_{pp} M_{qp}^{-1}, & S_{qq'} &= M_{pq} - M_{pp} M_{qp}^{-1} M_{qq}, \\ S_{q'q} &= -M_{qp}^{-1}, & S_{q'q'} &= -M_{qp}^{-1} M_{qq}. \end{aligned}$$

Now do exercise ??.

Solution ?? - Stationary phase approximation in higher dimensions. In this case $1/\hbar$ is assumed to be a very large number. parameter. The idea of this method is that we only evaluate part of integral I where $e^{i\varphi}$ is stationary i.e., $\varphi \approx \text{const}$. That means we need extrema (saddle points) of manifold Φ . In this case

$$\frac{\partial \Phi}{\partial x_{sp,\mu}} = 0$$

Introduce a new d -dimensional variable s such, that

$$i\Phi(x) = i\Phi(x_{sp,\mu}) - s^2$$

Integral I in terms of new variables is

$$I = \sum_n e^{i\Phi(x_n)/\hbar} \int e^{-s^2/\hbar} A(x_n(s)) \left| \frac{Dx}{Ds} \right| d^d s$$

Here n sums all stationary phase points which the path of integration (in complex plane!) meets. next, we need to calculate the Jacobian J :

$$J = 1 / \left| \frac{\partial s_i}{\partial x_k} \right|,$$

where

$$\frac{\partial s_i}{\partial x_k} = \frac{1}{2i s_i} \frac{\partial \Phi}{\partial x_k}.$$

This expression is undetermined at stationary phase points, because its right hand side becomes division zero by zero. However, by the chain rule

$$\frac{\partial s_i}{\partial x_k} = \frac{1}{2i} \frac{\frac{\partial \Phi^2}{\partial x_m}}{\frac{\partial s_i}{\partial x_m} \partial x_k \partial x_m}$$

where $x = x_{sp}$ are evaluated at the stationary phase point. From this expression we obtain that

$$\left[\left(\frac{\partial s}{\partial x} \right)^2 \right]_{i,k} = \frac{1}{2i} \frac{\partial \Phi^2}{\partial x_i \partial x_k}$$

So the Jacobian is (employing a standard notation for a second derivative)

$$J = \frac{(2i)^{d/2}}{\sqrt{\det D^2 \Phi}}.$$

Since the exponential factor $e^{-s^2/\hbar}$ cuts integration sharply because of a very large parameter $1/\hbar$, the function is evaluated only at the stationary point $s = 0$, and the integral is approximately

$$I \approx \sum_n e^{i\Phi(x_n)/\hbar} A(x_n) \frac{(2i)^{d/2}}{\sqrt{\det D^2\Phi(x_n)}} \int e^{-s^2/\hbar} d^d s$$

Limits of integration may depend on particular situation. If limits are infinite, then

$$\int e^{-s^2/\hbar} d^d s = \left(\int_{-\infty}^{\infty} e^{-s^2/\hbar} ds \right) = (\pi\hbar)^{d/2}$$

We substitute this into I and get the answer.

(R. Paškauskas)

Solution ?? - Jacobi gymnastics. We express the Jacobi matrix elements in $\det(\mathbf{1} - \mathbf{J})$ with the derivative matrices of S

$$\det(\mathbf{1} - \mathbf{J}) = \det \begin{pmatrix} I + S_{q'q'}^{-1} S_{q'q'} & S_{q'q}^{-1} \\ -S_{qq'} + S_{qq} S_{q'q}^{-1} S_{q'q'} & I + S_{qq} S_{q'q}^{-1} \end{pmatrix}.$$

We can multiply the second column with $S_{q'q}$ from the and subtract from the first column, leaving the determinant unchanged

$$\det(\mathbf{1} - \mathbf{J}) = \det \begin{pmatrix} I & S_{q'q}^{-1} \\ -S_{qq'} - S_{q'q'} & I + S_{qq} S_{q'q}^{-1} \end{pmatrix}.$$

Then, we multiply the second column with $S_{q'q}$ from the right and compensate this by dividing the determinant with $\det S_{q'q}$

$$\det(\mathbf{1} - \mathbf{J}) = \det \begin{pmatrix} I & I \\ -S_{qq'} - S_{q'q'} & S_{q'q} + S_{qq} \end{pmatrix} / \det S_{q'q}.$$

Finally we subtract the first column from the second one

$$\det(\mathbf{1} - \mathbf{J}_j) = \det \begin{pmatrix} I & 0 \\ S_{qq'} + S_{q'q'} & S_{qq'} + S_{q'q'} + S_{q'q} + S_{qq} \end{pmatrix} / \det S_{q'q}.$$

The last determinant can now be evaluated and yields the desired result (34.2)

$$\det(\mathbf{1} - \mathbf{J}_j) = \det(S_{qq'} + S_{q'q'} + S_{q'q} + S_{qq}) / \det S_{q'q}.$$

Chapter 35. Quantum scattering**Solution 35.2 - The one-disk scattering wave function.**

$$\psi(\vec{r}) = \frac{1}{2} \sum_{m=-\infty}^{\infty} \left(H_m^{(2)}(kr) - \frac{H_m^{(2)}(ka)}{H_m^{(1)}(ka)} H_m^{(1)}(kr) \right) e^{im(\Phi_r - \Phi_k)}. \quad (\text{S.68})$$

(For $r < a$, $\psi(\vec{r}) = 0$ of course.)

(Andreas Wirzba)

Chapter 37. Helium atom

(No solutions available.)

Chapter 38. Diffraction distraction

(No solutions available.)

Chapter B. Linear stability**Solution B.1 - Real representation of complex eigenvalues.**

$$\frac{1}{2} \begin{pmatrix} 1 & 1 \\ -i & i \end{pmatrix} \begin{pmatrix} \lambda & 0 \\ 0 & \lambda^* \end{pmatrix} \begin{pmatrix} 1 & i \\ 1 & -i \end{pmatrix} = \begin{pmatrix} \mu & -\omega \\ \omega & \mu \end{pmatrix}.$$

(P. Cvitanović)

Chapter F. Implementing evolution

(No solutions available.)

Chapter D. Symbolic dynamics techniques

(No solutions available.)

Chapter E. Counting itineraries

Solution E.1 - Lefschetz zeta function. *Starting with dynamical zeta function ref. [13] develops the Atiyah-Bott-Lefschetz fixed point formula and relates it to Weyl characters. Might be worth learning.*

Chapter H. Discrete symmetries of dynamics

Solution H.1 - Am I a group? *I'm no group because $(ab)c = a \neq a(bc) = c$ breaks the associativity requirement.*

W.G. Harter [15]

Solution H.2 - Three coupled pendulums with a C_2 symmetry. *Consider 3 pendulums in a row: the 2 outer ones of the same mass m and length l , the one midway of same length but different mass M , with the tip coupled to the tips of the outer ones with springs of stiffness k . Assume displacements are small, $x_i/l \ll 1$.*

(a) Show that the acceleration matrix $\ddot{\mathbf{x}} = -\mathbf{a}\mathbf{x}$ is ...: Just do it.

(b) Check that $[\mathbf{a}, \mathbf{R}] = 0$, i.e., that the dynamics is invariant under $C_2 = \{e, R\}$, where \mathbf{R} interchanges the outer pendulums: Just do it.

(c) Associated with roots $\{\lambda^{(+)}, \lambda^{(-)}\} = \{1, -1\}$ are the projection operators (B.28)

$$\mathbf{P}_+ = \frac{1}{2} \begin{pmatrix} 1 & 0 & 1 \\ 0 & 2 & 0 \\ 1 & 0 & 1 \end{pmatrix}, \quad \mathbf{P}_- = \frac{1}{2} \begin{pmatrix} 1 & 0 & -1 \\ 0 & 0 & 0 \\ -1 & 0 & 1 \end{pmatrix}.$$

The 3-pendulum system decomposes into a $\text{tr } \mathbf{P}_- = 1$ and $\text{tr } \mathbf{P}_+ = 2$ subspaces. On the 1-dimensional $\mathbf{P}_-\mathbf{a}$ yields eigenvalue $(\omega^{(-)})^2 = a + b$. On the 2-dimensional subspace the acceleration matrix is

$$\mathbf{a}^{(+)} = \begin{bmatrix} a + b & -\sqrt{2}a \\ -\sqrt{2}c & c + b \end{bmatrix}.$$

The exercise is simple enough that you can do it without using the symmetry, so: construct $\mathbf{P}^{(+)}, \mathbf{P}^{(-)}$ first, use them to reduce \mathbf{a} to irreps, then proceed with computing remaining eigenvalues of \mathbf{a} .

(d) Does anything interesting happen if $M = m$? No, no new symmetry or eigenvalue degeneracy arises from the equal masses case, for any other choice of (non-vanishing, positive) masses.

Solution H.3 - Lorenz system in polar coordinates: dynamics. *No solution available.*

Solution H.4 - Laplacian is a non-local operator. *none available*

Solution H.5 - Lattice Laplacian diagonalized. *none available*

Solution H.6 - Fix Predrag's lecture of Feb 5, 2008. *none available*

Chapter G. Applications

Solution G.1 - Using the multiplicative property of the Jacobi matrix we can write

$$\Lambda^{t+t}(x_0, \mathbf{u}_0) = \|\mathbf{J}^{t+t}(x_0)\mathbf{u}_0\| = \|\mathbf{J}^t(x(t))\mathbf{J}^t(x_0)\mathbf{u}_0\|.$$

We can introduce the time evolved unit vector

$$\mathbf{u}(t) = \mathbf{J}^t(x_0)\mathbf{u}_0 / \|\mathbf{J}^t(x_0)\mathbf{u}_0\|.$$

Then

$$\|\mathbf{J}^t(x(t))\mathbf{J}^t(x_0)\mathbf{u}_0\| = \|\mathbf{J}^t(x(t))\mathbf{u}(t)\| \|\mathbf{J}^t(x_0)\mathbf{u}_0\|,$$

which is the desired result.

We have to adjoin the tangent space, since the stretching factor depends on \mathbf{u} and not just on x . The stretching factor is multiplicative along the entire trajectory $(x(t), \mathbf{u}(t))$. However, it is not multiplicative along the state space trajectory $x(t)$ with a fixed \mathbf{u} .

Solution G.2 - If $b = a^2$ and $T_b = 2T_a$ we can introduce the variable $y = e^{sT_a}$. The dynamo rate equation then reads

$$0 = 1 - x + x^2.$$

The solutions of this are $x_{\pm} = (1 \pm i\sqrt{3})/2$. The dynamo rate is then a complex conjugate pair $\nu = \log x_{\pm}/T_a$.

The escape rate equation is

$$0 = 1 - x/a - x^2/a^2.$$

The solutions are $x_{\pm} = a(-1 \pm \sqrt{5})/2$. The escape rate is $\gamma = \log(x_+)/T_a$.

In the reverse case the escape rate remains unchanged, while the dynamo rate becomes $\nu = \log((\sqrt{5} + 1)/2)/T_a$. In this case the advected field grows with an exponential rate. In the previous case it shows oscillations in addition to the exponential growth due to the imaginary part of the rate.

Chapter J. Infinite dimensional operators

Solution J.1 - Norm of exponential of an operator. *No solution available.*

Chapter L. Statistical mechanics recycled

(No solutions available.)

Appendix T

Projects

YOU ARE URGED to work through the essential steps in a project that combines the techniques learned in the course with some application of interest to you for other reasons. It is OK to share computer programs and such, but otherwise each project should be distinct, not a group project. The essential steps are:

- **Dynamics**

1. construct a symbolic dynamics
2. count prime cycles
3. prune inadmissible itineraries, construct transition graphs if appropriate
4. implement a numerical simulator for your problem
5. compute a set of the shortest periodic orbits
6. compute cycle stabilities

- **Averaging, numerical**

1. estimate by numerical simulation some observable quantity, like the escape rate,
2. or check the flow conservation, compute something like the Lyapunov exponent

- **Averaging, periodic orbits**

1. implement the appropriate cycle expansions
2. check flow conservation as function of cycle length truncation, if the system is closed
3. implement desymmetrization, factorization of zeta functions, if dynamics possesses a discrete symmetry

4. compute a quantity like the escape rate as a leading zero of a spectral determinant or a dynamical zeta function.
5. or evaluate a sequence of truncated cycle expansions for averages, such as the Lyapunov exponent or/and diffusion coefficients
6. compute a physically interesting quantity, such as the conductance
7. compute some number of the classical and/or quantum eigenvalues, if appropriate

T.1 Deterministic diffusion, zig-zag map

To illustrate the main idea of chapter 25, tracking of a globally diffusing orbit by the associated confined orbit restricted to the fundamental cell, we consider a class of simple 1 – *dimensional* dynamical systems, chains of piecewise linear maps, where all transport coefficients can be evaluated analytically. The translational symmetry (25.10) relates the unbounded dynamics on the real line to the dynamics restricted to a “fundamental cell” - in the present example the unit interval curled up into a circle. An example of such map is the sawtooth map

$$\hat{f}(x) = \begin{cases} \Lambda x & x \in [0, 1/4 + 1/4\Lambda] \\ -\Lambda x + (\Lambda + 1)/2 & x \in [1/4 + 1/4\Lambda, 3/4 - 1/4\Lambda] \\ \Lambda x + (1 - \Lambda) & x \in [3/4 - 1/4\Lambda, 1] \end{cases} . \quad (\text{T.1})$$

The corresponding circle map $f(x)$ is obtained by modulo the integer part. The elementary cell map $f(x)$ is sketched in figure T.1. The map has the symmetry property

$$\hat{f}(\hat{x}) = -\hat{f}(-\hat{x}), \quad (\text{T.2})$$

so that the dynamics has no drift, and all odd derivatives of the generating function (25.3) with respect to β evaluated at $\beta = 0$ vanish.

The cycle weights are given by

$$t_p = z^{n_p} \frac{e^{\beta \hat{n}_p}}{|\Lambda_p|}. \quad (\text{T.3})$$

The diffusion constant formula for 1 – *dimensional* maps is

$$D = \frac{1}{2} \frac{\langle \hat{n}^2 \rangle_\zeta}{\langle n \rangle_\zeta} \quad (\text{T.4})$$

where the “mean cycle time” is given by

$$\langle n \rangle_\zeta = z \frac{\partial}{\partial z} \frac{1}{\zeta(0, z)} \Big|_{z=1} = - \sum' (-1)^k \frac{n_{p_1} + \dots + n_{p_k}}{|\Lambda_{p_1} \dots \Lambda_{p_k}|}, \quad (\text{T.5})$$

the mean cycle displacement squared by

$$\langle \hat{n}^2 \rangle_\zeta = \frac{\partial^2}{\partial \beta^2} \frac{1}{\zeta(\beta, 1)} \Big|_{\beta=0} = - \sum' (-1)^k \frac{(\hat{n}_{p_1} + \dots + \hat{n}_{p_k})^2}{|\Lambda_{p_1} \dots \Lambda_{p_k}|}, \quad (\text{T.6})$$

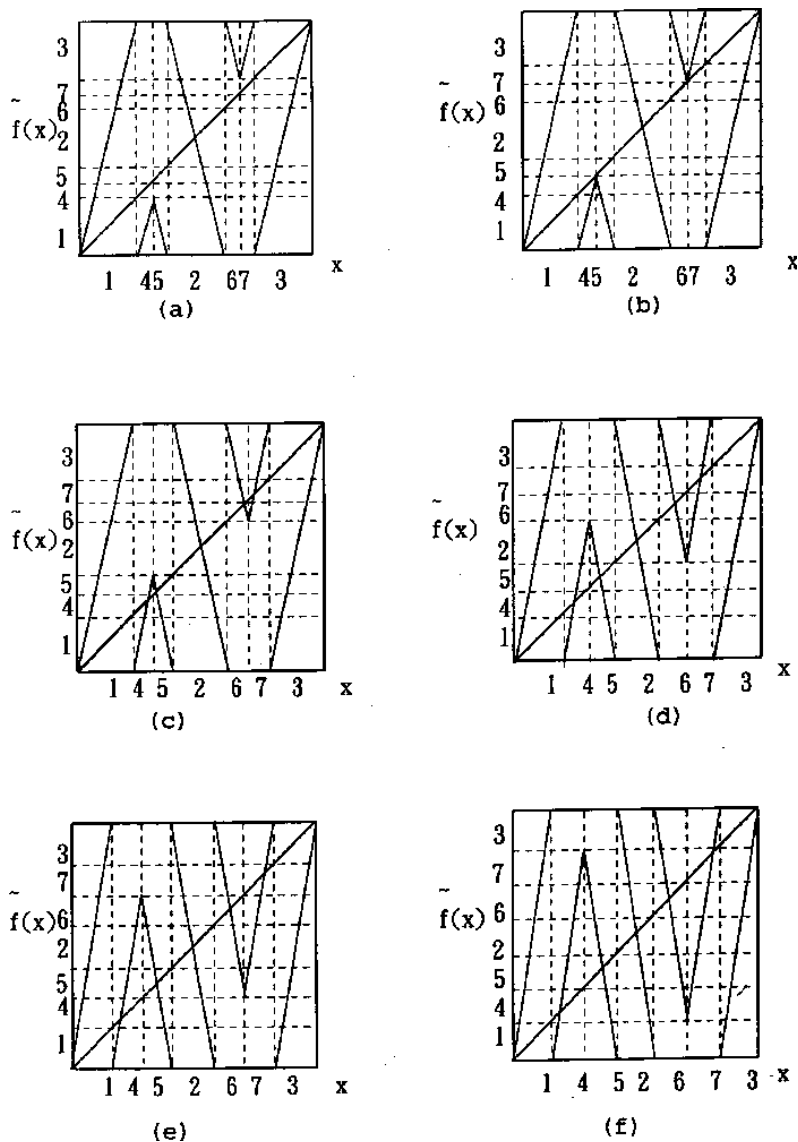


Figure T.1: (a)-(f) The sawtooth map (T.1) for the 6 values of parameter a for which the folding point of the map aligns with the endpoint of one of the 7 intervals and yields a finite Markov partition (from ref. [1]). The corresponding transition graphs are given in figure T.2.

and the sum is over all distinct non-repeating combinations of prime cycles. Most of results expected in this projects require no more than pencil and paper computations.

Implementing the symmetry factorization (25.35) is convenient, but not essential for this project, so if you find sect. 21.1.1 too long a read, skip the symmetrization.

T.1.1 The full shift

Take the map (T.1) and extend it to the real line. As in example of figure 25.3, denote by a the critical value of the map (the maximum height in the unit cell)

$$a = \hat{f}\left(\frac{1}{4} + \frac{1}{4\Lambda}\right) = \frac{\Lambda + 1}{4}. \tag{T.7}$$

Describe the symbolic dynamics that you obtain when a is an integer, and derive the formula for the diffusion constant:

$$D = \frac{(\Lambda^2 - 1)(\Lambda - 3)}{96\Lambda} \quad \text{for } \Lambda = 4a - 1, \quad a \in \mathbb{Z}. \quad (\text{T.8})$$

If you are going strong, derive also the formula for the half-integer $a = (2k + 1)/2$, $\Lambda = 4a + 1$ case and email it to DasBuch@nbi.dk. You will need to partition \mathcal{M}_2 into the left and right half, $\mathcal{M}_2 = \mathcal{M}_8 \cup \mathcal{M}_9$, as in the derivation of (25.21).

exercise 25.1

T.1.2 Subshifts of finite type

We now work out an example when the partition is Markov, although the slope is not an integer number. The key step is that of having a partition where intervals are mapped *onto* unions of intervals. Consider for example the case in which $\Lambda = 4a - 1$, where $1 \leq a \leq 2$. A first partition is constructed from seven intervals, which we label $\{\mathcal{M}_1, \mathcal{M}_4, \mathcal{M}_5, \mathcal{M}_2, \mathcal{M}_6, \mathcal{M}_7, \mathcal{M}_3\}$, with the alphabet ordered as the intervals are laid out along the unit interval. In general the critical value a will not correspond to an interval border, but now we choose a such that the critical point is mapped onto the right border of \mathcal{M}_1 , as in figure T.1 (a). The critical value of $f()$ is $f(\frac{\Lambda+1}{4\Lambda}) = a - 1 = (\Lambda - 3)/4$. Equating this with the right border of \mathcal{M}_1 , $x = 1/\Lambda$, we obtain a quadratic equation with the expanding solution $\Lambda = 4$. We have that $f(\mathcal{M}_4) = f(\mathcal{M}_5) = \mathcal{M}_1$, so the transition matrix (14.1) is given by

$$\phi' = T\phi = \begin{pmatrix} 1 & 1 & 1 & 1 & 0 & 0 & 1 \\ 1 & 0 & 0 & 1 & 0 & 0 & 1 \\ 1 & 0 & 0 & 1 & 0 & 0 & 1 \\ 1 & 0 & 0 & 1 & 0 & 0 & 1 \\ 1 & 0 & 0 & 1 & 0 & 0 & 1 \\ 1 & 0 & 0 & 1 & 1 & 1 & 1 \end{pmatrix} \begin{pmatrix} \phi_1 \\ \phi_4 \\ \phi_5 \\ \phi_2 \\ \phi_6 \\ \phi_7 \\ \phi_3 \end{pmatrix} \quad (\text{T.9})$$

and the dynamics is unrestricted in the alphabet

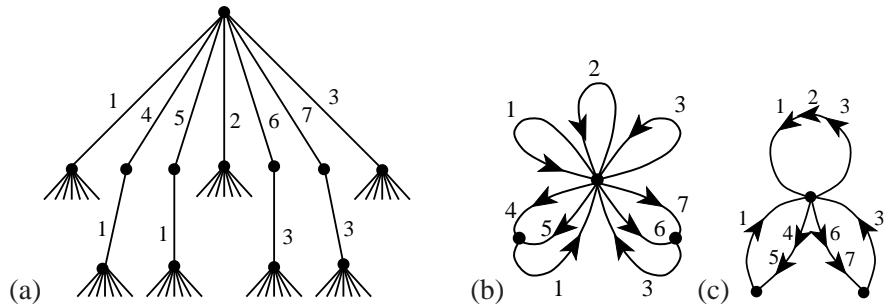
$$\{1, \underline{41}, \underline{51}, 2, \underline{63}, \underline{73}, 3, \}$$

One could diagonalize (T.9) on the computer, but, as we saw in chapter 14, the transition graph figure T.2 (b) corresponding to figure T.1 (a) offers more insight into the dynamics. The dynamical zeta function

$$\begin{aligned} 1/\zeta &= 1 - (t_1 + t_2 + t_3) - 2(t_{14} + t_{37}) \\ 1/\zeta &= 1 - 3\frac{z}{\Lambda} - 4 \cosh \beta \frac{z^2}{\Lambda^2}. \end{aligned} \quad (\text{T.10})$$

follows from the loop expansion (15.15) of sect. 15.3.

Figure T.2: (a) The sawtooth map (T.1) partition tree for figure T.1 (a); while intervals $\mathcal{M}_1, \mathcal{M}_2, \mathcal{M}_3$ map onto the whole unit interval, $f(\mathcal{M}_1) = f(\mathcal{M}_2) = f(\mathcal{M}_3) = \mathcal{M}$, intervals $\mathcal{M}_4, \mathcal{M}_5$ map onto \mathcal{M}_1 only, $f(\mathcal{M}_4) = f(\mathcal{M}_5) = \mathcal{M}_1$, and similarly for intervals $\mathcal{M}_6, \mathcal{M}_7$. An initial point starting out in the interval $\mathcal{M}_1, \mathcal{M}_2$ or \mathcal{M}_3 can land anywhere on the unit interval, so the subtrees originating from the corresponding nodes on the partition three are similar to the whole tree and can be identified (as, for example, in figure 14.5), yielding (b) the transition graph for the Markov partition of figure T.1 (a). (c) the transition graph in the compact notation of (25.26).



The material flow conservation sect. 22.3 and the symmetry factorization (25.35) yield

$$0 = \frac{1}{\zeta(0, 1)} = \left(1 + \frac{1}{\Lambda}\right) \left(1 - \frac{4}{\Lambda}\right)$$

which indeed is satisfied by the given value of Λ . Conversely, we can use the desired Markov partition topology to write down the corresponding dynamical zeta function, and use the $1/\zeta(0, 1) = 0$ condition to fix Λ . For more complicated transition matrices the factorization (25.35) is very helpful in reducing the order of the polynomial condition that fixes Λ .

The diffusion constant follows from (25.36) and (T.4)

$$\langle n \rangle_\zeta = -\left(1 + \frac{1}{\Lambda}\right) \left(-\frac{4}{\Lambda}\right), \quad \langle \hat{n}^2 \rangle_\zeta = \frac{4}{\Lambda^2}$$

$$D = \frac{1}{2} \frac{1}{\Lambda + 1} = \frac{1}{10}$$

Think up other non-integer values of the parameter for which the symbolic dynamics is given in terms of Markov partitions: in particular consider the cases illustrated in figure T.1 and determine for what value of the parameter a each of them is realized. Work out the transition graph, symmetrization factorization and the diffusion constant, and check the material flow conservation for each case. Derive the diffusion constants listed in table T.1. It is not clear why the final answers tend to be so simple. Numerically, the case of figure T.1 (c) appears to yield the maximal diffusion constant. Does it? Is there an argument that it should be so?

The seven cases considered here (see table T.1, figure T.1 and (T.8)) are the 7 simplest complete Markov partitions, the criterion being that the critical points map onto partition boundary points. This is, for example, what happens for unimodal tent map; if the critical point is preperiodic to an unstable cycle, the grammar is complete. The simplest example is the case in which the tent map critical

figure T.1	Λ	D
	3	0
(a)	4	$\frac{1}{10}$
(b)	$\sqrt{5} + 2$	$\frac{1}{2\sqrt{5}}$
(c)	$\frac{1}{2}(\sqrt{17} + 5)$	$\frac{2}{\sqrt{17}}$
(c')	5	$\frac{2}{5}$
(d)	$\frac{1}{2}(\sqrt{33} + 5)$	$\frac{1}{8} + \frac{5}{88}\sqrt{33}$
(e)	$2\sqrt{2} + 3$	$\frac{1}{2\sqrt{2}}$
(f)	$\frac{1}{2}(\sqrt{33} + 7)$	$\frac{1}{4} + \frac{1}{4\sqrt{33}}$
	7	$\frac{2}{7}$

Table T.1: The diffusion constant as function of the slope Λ for the $a = 1, 2$ values of (T.8) and the 6 Markov partitions of figure T.1

point is preperiodic to a unimodal map 3-cycle, in which case the grammar is of golden mean type, with `_00_` substring prohibited (see figure 14.5). In case at hand, the “critical” point is the junction of branches 4 and 5 (symmetry automatically takes care of the other critical point, at the junction of branches 6 and 7), and for the cases considered the critical point maps into the endpoint of each of the seven branches.

One can fill out parameter a axis arbitrarily densely with such points - each of the 7 primary intervals can be subdivided into 7 intervals obtained by 2-nd iterate of the map, and for the critical point mapping into any of those in 2 steps the grammar (and the corresponding cycle expansion) is finite, and so on.

T.1.3 Diffusion coefficient, numerically

(optional:)

Attempt a numerical evaluation of

$$D = \frac{1}{2} \lim_{n \rightarrow \infty} \frac{1}{n} \langle \hat{x}_n^2 \rangle. \tag{T.11}$$

Study the convergence by comparing your numerical results to the exact answers derived above. Is it better to use few initial \hat{x} and average for long times, or to use many initial \hat{x} for shorter times? Or should one fit the distribution of \hat{x}^2 with a Gaussian and get the D this way? Try to plot dependence of D on Λ ; perhaps blow up a small region to show that the dependence of D on the parameter Λ is fractal. Compare with figure 25.5 and figures in refs. [1, 2, 9, 8, 10].

T.1.4 D is a nonuniform function of the parameters

(optional:)

The dependence of D on the map parameter Λ is rather unexpected - even though

for larger Λ more points are mapped outside the unit cell in one iteration, the diffusion constant does not necessarily grow. An interpretation of this lack of monotonicity would be interesting.

You can also try applying periodic orbit theory to the sawtooth map (T.1) for a random “generic” value of the parameter Λ , for example $\Lambda = 6$. The idea is to bracket this value of Λ by the nearby ones, for which higher and higher iterates of the critical value $a = (\Lambda + 1)/4$ fall onto the partition boundaries, compute the exact diffusion constant for each such approximate Markov partition, and study their convergence toward the value of D for $\Lambda = 6$. Judging how difficult such problem is already for a tent map (see sect. 15.5 and appendix D.1), this is too ambitious for a week-long exam.

References

- [T.1] H.-C. Tseng, H.-J. Chen, P.-C. Li, W.-Y. Lai, C.-H. Chou and H.-W. Chen, “Some exact results for the diffusion coefficients of maps with pruned cycles,” *Phys. Lett. A* 195, 74 (1994).
- [T.2] C.-C. Chen, “Diffusion Coefficient of Piecewise Linear Maps,” *Phys. Rev.* **E51**, 2815 (1995).
- [T.3] H.-C. Tseng and H.-J. Chen, “Analytic results for the diffusion coefficient of a piecewise linear map,” *Int. J. Mod. Phys.* **B 10**, 1913 (1996).

T.2 Deterministic diffusion, sawtooth map

To illustrate the main idea of chapter 25, tracking of a globally diffusing orbit by the associated confined orbit restricted to the fundamental cell, we consider in more detail the class of simple 1 – *dimensional* dynamical systems, chains of piecewise linear maps (25.9). The translational symmetry (25.10) relates the unbounded dynamics on the real line to the dynamics restricted to a “fundamental cell” - in the present example the unit interval curled up into a circle. The corresponding circle map $f(x)$ is obtained by modulo the integer part. The elementary cell map $f(x)$ is sketched in figure 25.3. The map has the symmetry property

$$\hat{f}(\hat{x}) = -\hat{f}(-\hat{x}), \quad (\text{T.12})$$

so that the dynamics has no drift, and all odd derivatives of the generating function (25.3) with respect to β evaluated at $\beta = 0$ vanish.

The cycle weights are given by

$$t_p = z^{n_p} \frac{e^{\beta \hat{n}_p}}{|\Lambda_p|}. \quad (\text{T.13})$$

The diffusion constant formula for 1 – *dimensional* maps is

$$D = \frac{1}{2} \frac{\langle \hat{n}^2 \rangle_\zeta}{\langle n \rangle_\zeta} \quad (\text{T.14})$$

where the “mean cycle time” is given by

$$\langle n \rangle_\zeta = z \frac{\partial}{\partial z} \frac{1}{\zeta(0, z)} \Big|_{z=1} = - \sum' (-1)^k \frac{n_{p_1} + \dots + n_{p_k}}{|\Lambda_{p_1} \dots \Lambda_{p_k}|}, \quad (\text{T.15})$$

the mean cycle displacement squared by

$$\langle \hat{n}^2 \rangle_\zeta = \frac{\partial^2}{\partial \beta^2} \frac{1}{\zeta(\beta, 1)} \Big|_{\beta=0} = - \sum' (-1)^k \frac{(\hat{n}_{p_1} + \dots + \hat{n}_{p_k})^2}{|\Lambda_{p_1} \dots \Lambda_{p_k}|}, \quad (\text{T.16})$$

and the sum is over all distinct non-repeating combinations of prime cycles. Most of results expected in this projects require no more than pencil and paper computations.

T.2.1 The full shift

Reproduce the formulas of sect. 25.2 for the diffusion constant D for Λ both even and odd integer.

figure 25.4	Λ	D
	4	$\frac{1}{4}$
(a)	$2 + \sqrt{6}$	$1 - \frac{3}{4}\sqrt{6}$
(b)	$2\sqrt{2} + 2$	$\frac{15+2\sqrt{2}}{16+4\sqrt{2}}$
(c)	5	1
(d)	$3 + \sqrt{5}$	$\frac{5}{2} \frac{\Lambda-1}{3\Lambda-4}$
(e)	$3 + \sqrt{7}$	$\frac{5\Lambda-4}{3\Lambda-2}$
	6	$\frac{5}{6}$

Table T.2: The diffusion constant as function of the slope Λ for the $\Lambda = 4, 6$ values of (25.20) and the 5 Markov partitions like the one indicated in figure 25.4.

T.2.2 Subshifts of finite type

We now work out examples when the partition is Markov, although the slope is not an integer number. The key step is that of having a partition where intervals are mapped *onto* unions of intervals.

Start by reproducing the formula (25.28) of sect. 25.2.2 for the diffusion constant D for the Markov partition, the case where the critical point is mapped onto the right border of I_{1+} .

Think up other non-integer values of the parameter Λ for which the symbolic dynamics is given in terms of Markov partitions: in particular consider the remaining four cases for which the critical point is mapped onto a border of a partition in one iteration. Work out the transition graph symmetrization factorization and the diffusion constant, and check the material flow conservation for each case. Fill in the diffusion constants missing in table T.2. It is not clear why the final answers tend to be so simple. What value of Λ appears to yield the maximal diffusion constant?

The 7 cases considered here (see table T.2 and figure 25.4) are the 7 simplest complete Markov partitions in the $4 \leq \Lambda \leq 6$ interval, the criterion being that the critical points map onto partition boundary points. In case at hand, the “critical” point is the highest point of the left branch of the map (symmetry automatically takes care of the other critical point, the lowest point of the left branch), and for the cases considered the critical point maps into the endpoint of each of the seven branches.

One can fill out parameter a axis arbitrarily densely with such points - each of the 6 primary intervals can be subdivided into 6 intervals obtained by 2-nd iterate of the map, and for the critical point mapping into any of those in 2 steps the grammar (and the corresponding cycle expansion) is finite, and so on.

T.2.3 Diffusion coefficient, numerically

(optional:)

Attempt a numerical evaluation of

$$D = \frac{1}{2} \lim_{n \rightarrow \infty} \frac{1}{n} \langle \hat{x}_n^2 \rangle. \quad (\text{T.17})$$

Study the convergence by comparing your numerical results to the exact answers derived above. Is it better to use few initial \hat{x} and average for long times, or to use many initial \hat{x} for shorter times? Or should one fit the distribution of \hat{x}^2 with a Gaussian and get the D this way? Try to plot dependence of D on Λ ; perhaps blow up a small region to show that the dependence of D on the parameter Λ is fractal. Compare with figure 25.5 and figures in refs. [1, 2, 9, 8, 10].

T.2.4 D is a nonuniform function of the parameters

(optional:)

The dependence of D on the map parameter Λ is rather unexpected - even though for larger Λ more points are mapped outside the unit cell in one iteration, the diffusion constant does not necessarily grow. Figure 25.5 taken from ref. [9] illustrates the fractal dependence of diffusion constant on the map parameter. An interpretation of this lack of monotonicity would be interesting.

You can also try applying periodic orbit theory to the sawtooth map (25.9) for a random “generic” value of the parameter Λ , for example $\Lambda = 4.5$. The idea is to bracket this value of Λ by the nearby ones, for which higher and higher iterates of the critical value $a = \Lambda/2$ fall onto the partition boundaries, compute the exact diffusion constant for each such approximate Markov partition, and study their convergence toward the value of D for $\Lambda = 4.5$. Judging how difficult such problem is already for a tent map (see sect. 15.5 and appendix D.1), this is too ambitious for a week-long exam.